Changyou Gao *Editor*

Polymeric Biomaterials for Tissue Regeneration

From Surface/Interface Design to 3D Constructs

Second Edition

Springer

Polymeric Biomaterials for Tissue Regeneration

Changyou Gao
Editor

Polymeric Biomaterials for Tissue Regeneration

From Surface/Interface Design to 3D Constructs

Second Edition

Springer

Editor
Changyou Gao
MOE Key Laboratory of Macromolecular
Synthesis and Functionalization,
Department of Polymer Science and
Engineering
Zhejiang University
Hangzhou, China

ISBN 978-981-99-6947-0 ISBN 978-981-99-6948-7 (eBook)
https://doi.org/10.1007/978-981-99-6948-7

This Springer imprint is published by the registered company Springer Nature Singapore Pte Ltd.
The registered company address is: 152 Beach Road, #21-01/04 Gateway East, Singapore 189721, Singapore

Paper in this product is recyclable.

Preface

The biomaterials are a type of materials used in biology, pharmacology, medicine, diagnosis, etc. in vitro and/or in vivo. Among the various types of biomaterials, the biomedical polymers have been attracting much more attention for tissue regeneration because of their ease of design and synthesis, diverse chemical and physical structures and tailorable properties, formulation of different types of scaffolds, and thereby biological and medicinal performance. As the scaffolding materials to support tissue regeneration, the fundamental interplay between the scaffolds and cells/tissues is the key issue. In-depth understanding of the discipline and mechanism of this interplay is mandatory for the design and fabrication of bioactive and inducive scaffolds and constructs, leading to better tissue regeneration in a more rational manner.

With the major focuses on structural scaffolds and bio-activation, biomaterials surfaces/interfaces and bio-interactions, and regeneration of some clinic-targeted tissues, this book reviews the state-of-the-art of polymeric biomaterials for regenerative medicine and highlights advances in both fundamental science and clinical demand-driven applications. It summarizes the latest techniques in polymeric scaffold fabrication, delivery carriers, physiochemical property modulation, as well as their influences on adhesion and performance of biomolecules, cells, and tissues. It also describes methods for creating biofunctional surfaces/interfaces and subsequently modulating the host response to implantable materials. Lastly, it discusses the applications of biomaterials and constructs in soft-tissue regenerative medicine. It has to mention that the regeneration of tissues correlates to many factors such as cells, bioactive factors and cell growth factors etc. besides of the materials and scaffolds. Moreover, the polymers used for tissue regeneration, which are easily found in many books and review articles, are not deliberately enumerated in this book.

On the basis of success of the first edition of this book, the structure of this second edition is maintained with the update contents. Due to various reasons, some authors of the first edition could not update their contents. To keep the integrity and ensure the quality of this book, new authors are invited to contribute to Chaps. 3 and 12.

Moreover, Chap. 13 is newly added to meet the fast development and extreme importance of nerve regeneration, in particular for central nerve system.

We believe that this book is a valuable resource for materials scientists and engineers in the rational design of ideal scaffolds and constructs and for physicians in the therapy of some diseases that are not fully covered by the current approaches, as listed in the book. The book also offers engineering students a sense of the relevance of materials science in the development of novel therapeutic strategies.

All the authors for both the first edition and second edition are sincerely acknowledged for their excellent contribution and timely update of the contents. We also thank the editorial staff of Springer for their continuous support in every step of publishing this book. Lastly, it is my greatest pleasure to collaborate with so many excellent colleagues since my jumping in biomaterials for tissue engineering and regeneration in 1996. Many of the students and postdocs ever studying in our lab on biomedical polymers for tissue repair and regeneration have become the leading scientists or engineers in biomaterials and medicinal devices. It is expected that in the next decade more advanced devices and products based on regenerative biomaterials will be developed to meet the diverse demands on healthcare and disease therapy.

Hangzhou, Zhejiang, China Changyou Gao

Contents

Part III Regeneration of Some Clinic-Targeted Tissues

Chapter 1
An Introduction to Scaffolds, Biomaterial Surfaces, and Stem Cells

Jun Deng and Changyou Gao

Abstract *In situ* tissue regeneration utilizes the regenerative potential of the body to control cell behaviors for tissue repair. The design of scaffolding biomaterials for tissue engineering requires precise control of the biophysical and biochemical cues to guide endogenous cells to the injury site. These cues are required to induce regeneration by modulating the extracellular microenvironment or driving cellular reprogramming. Upon contact with the biological systems, the proteins will interact with the surface/interface of the biomaterials. The interactions between biomaterials and cells could be to a great extent directed through protein adsorption. Owing to their self-renewal and differentiation ability, stem cells are conducive for repairing injured tissues, making them a promising source of seed cells for tissue engineering. Biomaterial platform to control stem cell fate is an area of tissue engineering that has grown exponentially over the last decades. In this chapter, the scaffolds, biomaterial surfaces, and stem cells are briefly summarized, including biomaterials design, interfacial interactions, and application of stem cells for traditional tissue engineering and *in situ* tissue regeneration. Regeneration of some clinic-targeted tissues is introduced as well.

Keywords *In situ* tissue regeneration · Scaffolds · Biomaterial interface · Protein adsorption · Stem cells

J. Deng (✉)
MOE Key Laboratory of Macromolecular Synthesis and Functionalization, Department of Polymer Science and Engineering, Zhejiang University, Hangzhou, China

State Key Laboratory of Trauma and Chemical Poisoning, Institute of Burn Research, Southwest Hospital, Third Military Medical University (Army Medical University), Chongqing, China
e-mail: djun.123@163.com

C. Gao (✉)
MOE Key Laboratory of Macromolecular Synthesis and Functionalization, Department of Polymer Science and Engineering, Zhejiang University, Hangzhou, China
e-mail: cygao@zju.edu.cn

C. Gao (ed.), *Polymeric Biomaterials for Tissue Regeneration*,
https://doi.org/10.1007/978-981-99-6948-7_1

1.1 Introduction

With the quick development of global modernization and aging, the demand for biomaterials and medical devices has rapidly increased. Novel implant materials including drug-carrying stents for regenerative medicine, joint replacement materials, prostheses, and implantable detection sensors have sprung up with an estimated annual growth rate of 13.7%, reaching a net worth of $130 billion by the end of 2021 [1]. However, the rapid development of biomaterials is always accompanied with challenges such as excessive or insufficient immune response and uncontrolled cell regulation, etc.

Biomaterials play a critical role in the success of *in situ* tissue regeneration because they can support cell growth and extracellular matrix (ECM) formation. Thus, various formats of biomaterials such as porous scaffolds [2, 3], hydrogels [4, 5], membranes [6], tubes [7], and micro- and nanospheres [8] are available and can be fabricated specifically according to the requirements of different damaged tissues. Multiple technologies including freeze-drying [9], gas foaming [10], electrospinning [11], layer-by-layer (LbL) assembly [12], microfluidic technology, and three-dimension (3D) printing [13] are used to process biomaterials with organized structures and well-defined functions. Various types of biomaterials such as natural biomaterials [14], synthetic polymers [15], bioceramics [16], and ECM-based biomaterials [14] are employed for the *in situ* tissue regeneration.

Engineered biomaterials can be used to direct endogenous progenitors or stem cells to the injury intima and thereby promote tissue repair [17]. During this process, biomaterials provide a structural framework to facilitate the attachment and migration of host stem cells and progenitor cells, and drive the differentiation of these cells into tissue-specific cell types. Most studies believe that cell behaviors regulated by biomaterials are attributed to biomaterials' bulk mechanical and chemical properties [18, 19]. In fact, upon implantation into the living body, it is the biomaterial surface/interface that directly contacts with the biological systems [20]. Cells interact with the matrix through the cell–matrix interface, and thereby the "interfacial" properties such as energy, wettability, and surface topography play a pivotal role in regulating cell adhesion, proliferation, differentiation, and functions. In addition, the biological microenvironment is comprised of the aqueous milieu enriched with soluble proteins and sugars [18]. Upon contact with physiological fluids (e.g., blood), various types of proteins such as albumin, immunoglobulin (IgG), fibrinogen (Fg), fibronectin (Fn), and vitronectin (Vn) adsorb onto the implant surface from body fluids within seconds to minutes [21]. Thus, the cell–surface interaction is ultimately an interaction between cells and surface-bound proteins. The type, amount, conformation/orientation, and bioactivity of the adsorbed proteins subsequently influence the overall kinetics and thermodynamics of the binding events between cells and implant surface [21]. On the one hand, certain adsorbed adhesive proteins mediate the attachment and activation of platelets, macrophages, and other inflammatory cells, triggering clotting and immune responses in the host [20]. On the other hand, the adsorbed ECM proteins assist in specific cell adhesion and spreading through

integrin binding and regulate other subsequent signaling events (proliferation, differentiation, motility, gene expression, and survival) [22]. Therefore, the interfacial interactions are crucial in determining the success of implant devices.

Stem cells possess the ability to self-renew and produce progeny that differentiate into multiple functional cell lineages, which endows them with the ability to act as a seed cell source for various tissues/organs in regenerative medicine. Tissues that can now be engineered using stem cells comprise a diverse range from epithelial surfaces (skin, cornea, and mucosal membranes) to skeletal tissues [23]. Fabrication of substrates or 3D biomaterial scaffolds with biophysical cues that mimic ECM-like microenvironment can assist in reshaping cell phenotypes and behaviors. The biophysical cues include, but are not limited to, topography, matrix stiffness and elasticity, mechanical force, and external physical field stimuli. All these factors can modulate stem cells individually or synergistically by simulating the ECM microenvironment. In addition, the adhesion molecules (e.g., proteins and growth factors) on the ECM can regulate its interactions with stem cells [24]. Therefore, comprehensively and accurately understanding the molecular mechanism related to cellular response to biophysical stimuli remains challenging.

All these findings are increasingly directing the design of appropriate scaffolds for tissue repair and regeneration [25]. Considerable progress has been made in the design of bioactive and bioresorbable scaffolds that support tissue regeneration. ECM protein motifs, growth factors, and/or genes can be incorporated into the scaffolds by physical incorporation or chemical immobilization, which are used to regulate cell activity and functions by providing signals to stimulate or inhibit cellular adhesion, recruitment, migration, growth, differentiation, and gene expression [25, 26]. Therefore, utilizing more novel engineered biomaterials for tissue regeneration *in vivo* is full of challenges.

1.2 Scaffolds

The scaffolds are defined as 3D porous solid biomaterials designed to perform some or all the biological functions and play a unique role in tissue engineering and regenerative medicine. The major function of the scaffolds is to provide a temporary support to body structures, allowing the stress transfer overtime to the injured sites and facilitating tissue regeneration on the scaffolds. Scaffolds support cells with the reasonable surviving conditions, ideal oxygen and nutrient levels, successful supplement and waste transport in addition to providing adequate mechanical support. Therefore, the scaffolds should have some other functions, such as (1) sufficient transport of gases, nutrients, and regulatory factors to cell survival, (2) biodegradable at a controllable rate matching the tissue regeneration, and (3) without or with very low inflammation and toxicity. In fact, the performance of the scaffold is affected by numerous parameters, such as porosity, surface charge, degradability, physicomechanical characteristics, and cell preferences. Thus, it is very important to design scaffold materials according to the specific needs of tissue regeneration and

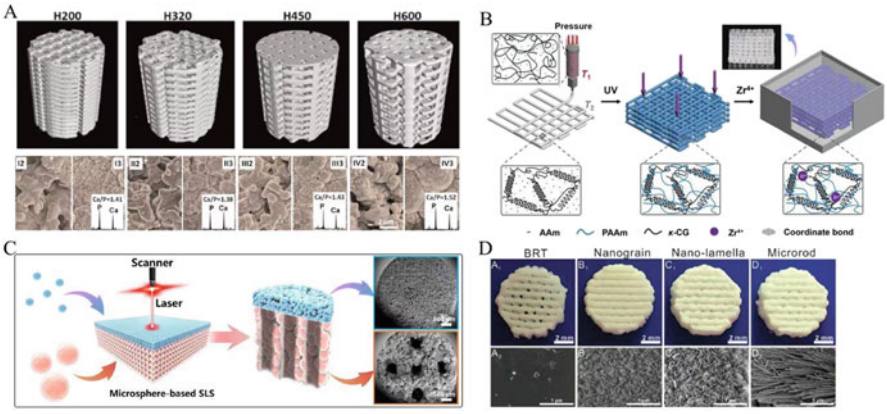

Fig. 1.1 Different types of scaffolds. (**a**) Images of porous scaffolds. (Reprinted from [27] with permission, copyright 2021 Elsevier). (**b**) Graphical representation of hydrogel scaffolds. (Reprinted from [28] with permission, copyright 2022 Royal Society of Chemistry). (**c**) Schematic of microsphere scaffolds. (Reprinted from [29] with permission, copyright 2022 Elsevier). (**d**) Images of micro/nanostructured scaffolds (Reprinted from [30] with permission, copyright 2019 Wiley-VCH Verlag)

repair. So far different types of scaffolds, including sponges (porous scaffolds), microsphere scaffolds, hydrogel scaffolds, and micro/nanostructured scaffolds, have been extensively developed (Fig. 1.1).

1.2.1 Porous Scaffolds

The 3D polymeric porous scaffolds with higher porosity and interconnected pore network are highly useful for tissue engineering and regeneration. The porous structure provides space for cell migration and proliferation. The interconnected voids allow cell infiltration before material degradation, which is conducive to cell recruitment and neovascularization, and avoid the restriction of the nonporous structure on the inward growth and proliferation of cells, as well as cell death caused by insufficient supply of nutrients and oxygen. Ideal pore size and porosity can be varied for different types of tissues and cells [31, 32]. The porosity, pore size, and pore distribution of the scaffolds govern their mechanical properties and play a pivotal role in cell proliferation, migration, and differentiation [32]. Ma et al. fabricated 3D poly(ethylene terephthalate) (PET) nonwoven fibrous scaffolds with variable pore size and porosity using thermal compression [33]. The high porosity (HP) matrices have a porosity of 0.896 and an average pore size of 39 μm, while the low porosity (LP) ones have a porosity of 0.849 and average pore size of 30 μm. Cells cultured in the LP matrix could spread across adjacent fibers more easily, leading to faster cell proliferation, while the smaller pore size of LP matrices limits the formation of large cell aggregates and reduces cell differentiation. Conversely,

cells cultured in HP matrices show a higher degree of cell aggregation and differentiation. The porosity and pore size significantly influence the mechanical properties as well. Although a higher porosity and pore size in scaffolds can enhance the nutrient and gas exchange, the mechanical properties of the scaffolds will be compromised due to the large amount of void volume [34]. In general, the mechanical strength of scaffolds should match that of the native tissue *in vivo* and remain intact until the tissue regenerates and offers sufficient space for cell proliferation and nutrient exchange. Therefore, the porosity and pore size of a scaffold should be optimized such that the mechanical properties are not compromised significantly. The porous scaffolds can be fabricated with a specific pore size, porosity, and structure using various methods, such as template leaching [35], phase separation [35], freeze-drying [36], electrospinning [37], selective laser sintering [38], and 3D/4D printing [39]. A variety of natural products (e.g., collagen, fibrinogen, chitosan, and acellular matrix) and synthetic biodegradable polymers (e.g., poly (L-lactic acid) (PLLA), poly(glutamic acid), poly(lactide-co-glycolide) (PLGA), poly(ε-caprolactone) (PCL), poly(D, L-lactic acid) (PDLLA), and poly(ethylene oxide) (PEO)) are widely used as the scaffolding materials [40]. For example, Nicole et al. described a technique that combines salt leaching with additive manufacturing to obtain a magnesium (Mg)-based porous scaffold with a controlled and ordered porosity. Specifically, a 3D-printed NaCl template with adjustable structured porosity was used to prepare the Mg-based porous scaffold by infiltrating the template with a Mg melt and then leaching in an NaOH aqueous solution to remove the NaCl template (Fig. 1.2a) [41]. Unlike the traditional template leaching techniques, this strategy can create scaffolds with complex morphology. Ilaria et al. also prepared novel, chitosan-based chitosan porous scaffolds with superior mechanical properties by combining stabilization processes. The chitosan solutions were thermally phase-separated to obtain a highly porous structure after freeze-drying. Then, the freeze-gelation and photo-crosslinking together could improve the mechanical resistance of chitosan scaffolds (Fig. 1.2b) [42]. This fabrication method generates the porous scaffolds without an external crosslinking agent or sophisticated instrumentation. Lian et al. combined single solution electrospinning writing (SEW) and solution electrospinning (SES) to create a multifunctional, bi-layered porous scaffold for guided bone regeneration. The Cu-loaded mesoporous silica nanoparticles (Cu@MSNs) were dispersed in a PLGA/gelatin (PLGA/Gel, denoted as PG) solution to obtain the electrospinning solution matrix, whose loose and porous SEW layer facilitated bone ingrowth. Its dense and compact SES layer resisted nonosteoblast interference (Fig. 1.2c) [43]. The superior mechanical properties and simple fabrication procedure of the multifunctional scaffold render its clinically promising. Hossain et al. 3D printed an *in situ* mullite ($3Al_2O_3{\cdot}2SiO_2$) porous scaffold. The inks contained an aqueous binder with α-alumina, two different silica sources (rice husk ash extracted biogenic nano-silica (NS) and commercial silica (CS)), 5 wt% poly(vinyl alcohol) solution, and 6 vol% glycerol. Unlike the CS, the NS (45 vol% solid-loading) showed excellent printability even through a tiny nozzle size (~500 μm) under low shear stress (~0.06 MPa) and could retain the

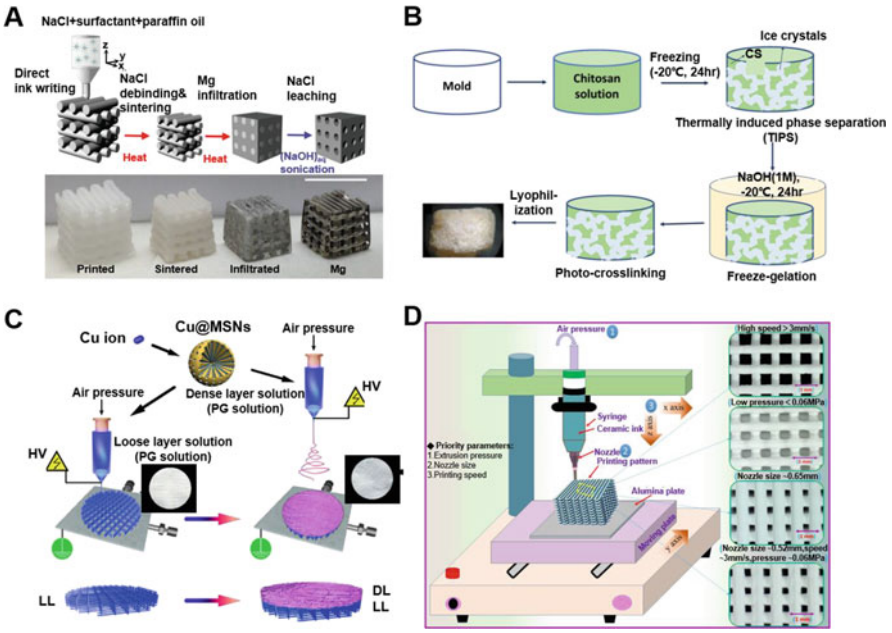

Fig. 1.2 Various methods to fabricate porous scaffolds. (**a**) A magnesium-based porous scaffold was prepared with the template leaching method. (Reprinted from [41] with permission, copyright 2019 Wiley-VCH Verlag). (**b**) A reinforced chitosan porous scaffold was fabricated by phase separation and freeze-drying. (Reprinted from [42] with permission, copyright 2021 Elsevier). (**c**) A bi-layered PG-Cu@MSNs porous scaffold was prepared by electrospinning. (Reprinted from [43] with permission, copyright 2020 Elsevier). (**d**) An *in situ* mullite ($3Al_2O_3{\cdot}2SiO_2$) porous scaffold was 3D printed (Reprinted from [44] with permission, copyright 2022 Elsevier)

original shape of the printing structure (high-aspect ratio) without deforming or slumping (Fig. 1.2d) [44].

1.2.2 Hydrogel Scaffolds

Hydrogels are defined as physically or chemically cross-linked polymer networks that can absorb and maintain large amount of water [45], which is from 10% to 20% (an arbitrary lower limit) up to thousands times of their dry weight [46]. The networks are formed by molecular entanglements, covalent bonding, and/or secondary forces including ionic, H-bonding, hydrophobic forces and etc. The networks can also be formed by biospecific recognitions such as the interactions between Concanavalin A and polysaccharide [47] and between avidin and biotin [48], respectively. Since the use of hydrophilic networks of cross-linked poly (2-hydroxyethyl methacrylate) (PHEMA) as soft contact lens material in 1960 [49], the hydrogels have gained increasing interest in biomedical applications

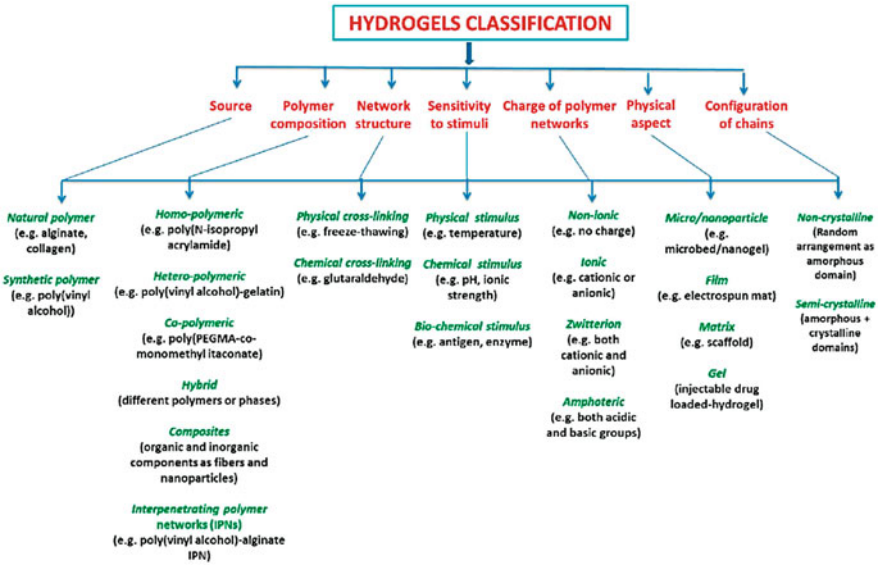

Fig. 1.3 The classification of hydrogel (Reprinted from [51] with permission, copyright 2020 MDPI)

[50]. So far, hydrogels have been widely used in soft tissue engineering of skin, blood vessel, muscle, and fat etc.

Hydrogels are classified into different categories that depend on various parameters including hydrogel network bonding, external stimuli, and chemical composition (Fig. 1.3). First, the hydrogel network bonding is divided into two categories: physical and chemical. The physical gel is formed by physical forces such as electrostatic interactions, hydrogen bonding, and entanglement of chains. The chemical gel is a 3D network of polymers formed by chemical crosslinking. The hydrogels can also be divided into another two categories according to how they respond to external stimuli: the traditional hydrogels that are insensitive to environmental changes such as temperature or pH, and the environmentally sensitive hydrogels including polymer gels that sense stimuli in the external environment (temperature, pH, light, electricity, and pressure) and respond by changing their physical or chemical properties, especially their swelling behavior. This response to stimuli can be exploited as a sensor or controlled-release switch. Finally, the hydrogels can be divided into synthetic gels and natural gels according to their material compositions. The natural polymers garner attention due to their better biocompatibility, environmental sensitivity, abundance, and low price. However, the natural polymer materials are unstable and degrade easily. Their counterparts can be prepared from synthetic materials with precisely controlled structures, mechanical properties, and functions, although their biocompatibility is limited. Overall, various types of hydrogels can be prepared by combining these two classes of materials to optimize biocompatibility and mechanical properties.

Because of their soft and rubbery consistence, they closely resemble the structures and properties of many types of living tissues. Meanwhile, the high water content of the hydrogels contributes largely to their excellent biocompatibility [50]. Therefore, the hydrogels are especially suitable for the applications in the revolutionary field of tissue engineering to guide the growth of new tissues, such as cartilage healing, bone regeneration, and wound care. They can act as carriers for drug delivery too [46]. By loading cell growth factors, they can more strongly support the proliferation [47], migration [52], and differentiation of cells [53] during tissue regeneration. Hydrogels in tissue engineering application should meet a number of design criteria including physical parameters (e.g., degradation rate and mechanics) and biological parameters. Therefore, the properties of hydrogels should be well defined and characterized with good reproducibility.

1.2.3 Micro-/Nanostructured Scaffolds

Nature structural materials are built at ambient temperature from a fairly limited selection of components and are usually comprised of hard and soft phases arranged in complex hierarchical architectures with the dimensions varying from nanoscale to macroscopic physiological scale. The nano−/microstructure of some natural materials such as bone, teeth, and antler has been well characterized [54]. For example, bone is composed of cells embedded in the bone ECM, which is an ordered network assembled from two major nanophases: collagen fibrils made of type I collagen molecules (~300 nm long, ~1.5 nm in diameter) and hydroxyapatite ($Ca_{10}(PO_4)_6(OH)_2$) nanocrystals (plate-shaped, 50 × 25 nm in size, 1.5–4 nm thick) distributing along the collagen fibrils [54]. These structures inspire the investigators to fabricate new micro/nanostructured scaffolds mimicking the nature materials in tissue regeneration application, such as fibrous scaffolds, microsphere scaffolds, and hybrid (polymer/bioceramic composite) scaffolds. For instance, the development of nanofibers has enhanced the scope for fabricating scaffolds that can potentially mimic the architecture of natural human tissues at the nanometer scale. Microsphere scaffolds have spatial extension and temporal duration control, providing the stiffness gradient for interfacial tissue engineering [55]. Reducing the dimensions of a material into the nanoscale range usually results in the change of its physiochemical properties especially reactivity. Meanwhile, the micro/nanostructured scaffolds possess a larger surface area, which provides much more adsorption sites for bioactive molecules. Surfaces characterized by submicron scale features have been used to study cells' response to nanometer-scale topographical cues that can influence a wide range of cellular functions such as morphology, adhesion, and migration. Therefore, the micro/nanostructured design is also proved to be a strategic method in improving the bioactivity and biological responses of the scaffolds.

Up to present, various technologies have been developed to fabricate the micro/nanostructured scaffolds, such as biomimetic mineralization [56, 57], micromachining, photolithography, layer-by-layer deposition [58], solution casting

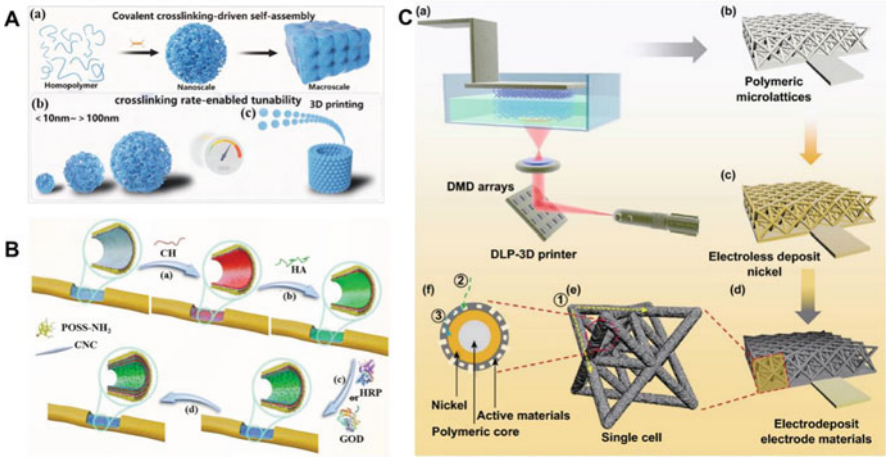

Fig. 1.4 (**a**) Schematic of the covalent crosslinking-driven self-assembly (COSA) of a homopolymer. Controlled covalent assembly of the homopolymer (blue) with a chemical crosslinker (orange) can be used to design nano- to macroscale hydrogels. (Reprinted from [64] with permission, copyright 2022 Wiley-VCH GmbH). (**b**) Schematic of the LbL assembly of chitosan (CH) and hyaluronic acid (HA) for enzyme immobilization in an all-liquid microfluidic chip. (Reprinted from [65] with permission, copyright 2021 Wiley-VCH GmbH). (**c**) Schematic of composite lattice fabrication (Reprinted from [66] with permission, copyright 2019 Springer)

[59], self-assembly [60], thin-film or tape deposition [54], freeze casting [61, 62], and additive manufacturing (e.g., 3D/4D inkjet printing, robocasting, stereolithography, or two-photon polymerization) [62, 63]. A self-assembled covalent polymer described by Bai et al. was used to synthesize multiscale hierarchical gel networks [64]. Unlike the noncovalent self-assembly, the covalent self-assembly is independent of and unaffected by solvent conditions and does not require additional agents. This method instead relies on new control mechanisms such as tunable rates of crosslinking, which can be used to fabricate nanogels whose unprecedented and precisely controlled dimensions range from less than 10 nm to above 100 nm (Fig. 1.4a). Liu et al. [65] exploited LbL assembly of two natural polysaccharides, chitosan (CH) and hyaluronic acid (HA), to fabricate biocompatible polysaccharide multilayers on the surface of a microchannel through the interfacial assembly of nanoparticle surfactants (NPSs) in a biphasic system. This method is based on a newly developed all-liquid microfluidic chip, which enhances the mechanical properties of the microchannel and offers a biocompatible microenvironment for enzyme immobilization (Fig. 1.4b). Xue et al. used stereolithography and electroless plating to fabricate metallic ocet-truss lattices from 3D hierarchically porous graphene [66]. The pore size of the quasisolid supercapacitor ranges from nanometers to millimeters and can be tuned to optimize the areal capacitance, rate capability, and lifespan (Fig. 1.4c).

1.3 Biomaterial Surface/Interface and Biointeractions

Upon contact with the biological systems, it is the biomaterial surface that interacts directly with biomacromolecules and living cells, and thereby the cell behaviors are significantly influenced by the surface properties (Fig. 1.5). Hence, the properties of biomaterial surface play a vital role in determining the biological identity and biocompatibility. So far much attention has been paid to understanding the bio-interactions of biomaterial surface and the living systems.

1.3.1 Interactions of Biomaterial Surfaces with Proteins and Cells

After being placed in a biological milieu containing cells, the first molecules reaching to the biomaterial surface are water and salt ions, followed by proteins, and eventually cells come into contact (Fig. 1.6) [68]. The adsorption of proteins on surfaces is a unique phenomenon of major physiological and toxicological

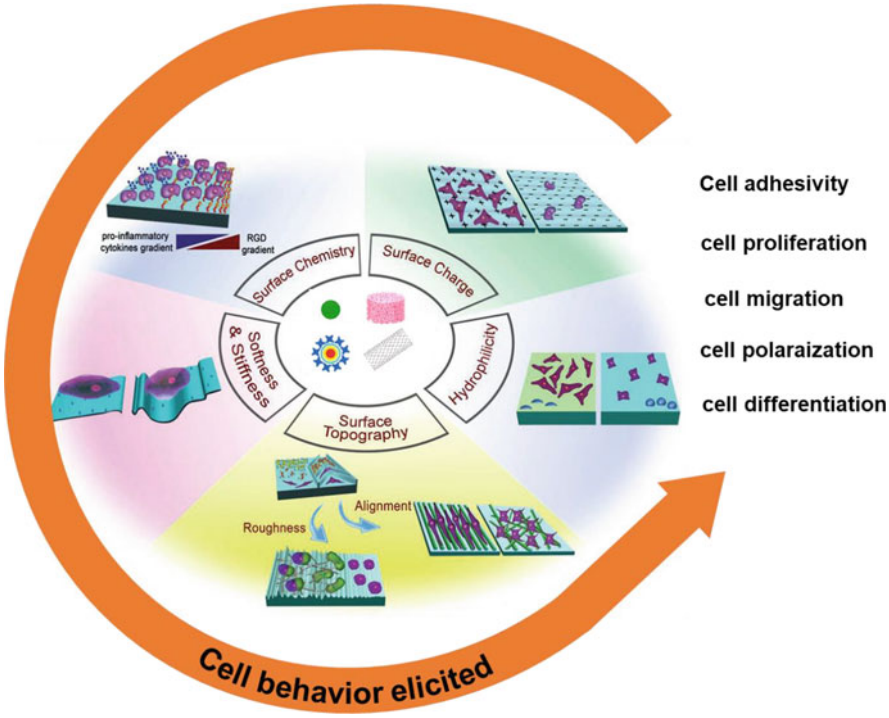

Fig. 1.5 Schematic of various biomaterial surface properties that determine cell behavior (Reprinted from [67] with permission, copyright 2019 Wiley-VCH GmbH)

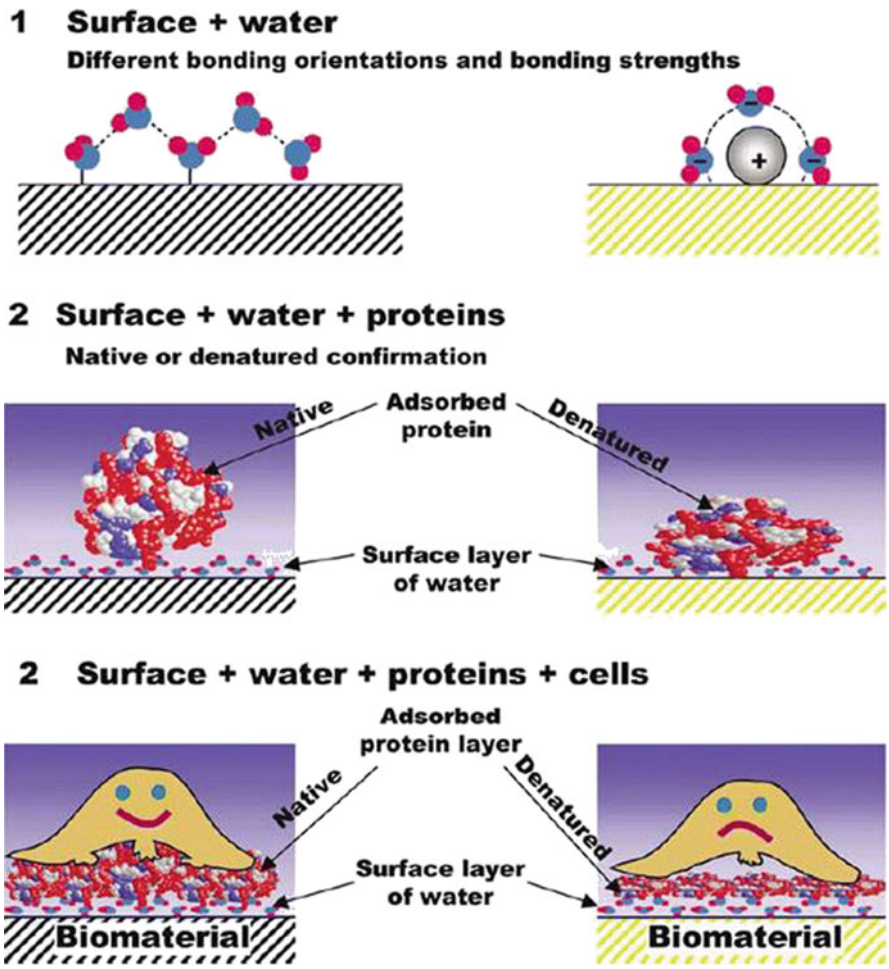

Fig. 1.6 Schematic illustration of the successive events after the implantation of a medical implant. The first molecules to reach the surface are water molecules (ns time scale). Then, protein adsorption starts on the micro- to millisecond time scale and continues for a much longer time. Eventually, cells reach the surface (Reprinted from [68] with permission. Copyright 1998 Elsevier)

significance. Besides macrophages and dendritic cells (DCS), the adsorbed proteins are the key factors for cells to start connecting with biomaterials. Furthermore, the anchoring and extracellular orientation of cells depend on the adsorption of specific proteins, including fibronectin (FN), fibrinogen (FG), complement C3 and albumin (ALB). It is generally believed that the action of the proteins is highly dependent on the physiochemical properties of the surface of biomaterials. In this way, the key proteins can lead to actual cellular reactions, including cell adhesion, migration and proliferation, which ultimately lead to tissue regeneration. However, it should be

mentioned that when the biomaterials are implanted into the body, the abnormal adsorbed proteins may cause serious foreign body reactions.

Proteins are complex biopolymers composed of 20 natural amino acids whose structures include four types: primary, secondary, tertiary, and quaternary. The local composition and complex structure of amino acids determine the surface affinity of each region of the proteins. The biomaterial can adsorb proteins through attractive Coulomb and van der Waals interactions, hydrogen bonding, or increased entropy of solvent molecules or release of counterions. Environmental factors such as pH, temperature, and ion concentration as well as protein types and biomaterial surface properties influence protein adsorption on the biomaterial surface [69, 70]. Generally, proteins direct their hydrophobic patches to the hydrophobic surfaces [71]. Analogously, positively or negatively charged regions of proteins are attracted to oppositely charged biomaterial surfaces/interfaces [72]. Thus, proteins prefer to adhere more strongly to high surface tension than to low surface tension, to nonpolar than to polar surfaces, and to charged than to uncharged substrates [69]. Experiments suggest that nonpolar surfaces destabilize proteins and thereby reorient their conformation to strengthen surface-protein interactions. Upon adsorption onto a solid surface/interface, a protein changes its conformation to minimize the free energy [69]. Conformational changes affect biological functions: some types of proteins or peptides reveal their functions only after adsorption [73, 74].

When cells arrive, they "see" a protein-covered surface. It is widely recognized that adsorbed extracellular matrix (ECM) proteins assist in specific cell adhesion and spreading through integrin binding and regulate other subsequent signaling events [75] including proliferation, differentiation [76], motility [77–79], gene expression, and survival. Liu et al. found that a piezoelectric PLLA nanofiber scaffold enhanced extracellular protein adsorption, which enhanced cell migration or recruitment as well as chondrogenesis and cartilage regeneration [80]. The structure of amphiphilic β-peptide polymers can be varied to tune the surface-adsorbed serum proteins and further affect the adhesion, proliferation, and migration of endothelial cells (EC) and smooth muscle cells (SMA) [81]. Surface topographic cues (e.g., geometry, roughness, and shape), mechanical properties (e.g., stiffness, elasticity, and collagen density), and surface chemical modifications (e.g., surface charging, hydrophilicity, and adhesion ligands) can also enhance cell adhesion, morphology, migration, differentiation, and metabolism [82].

1.3.2 Mediation of Cell Migration by Gradient Biomaterials

Cell migration is a widespread form of live cell activity during complex dynamic process, which plays an important role in tissue regeneration and repair. For example, during embryonic development in mammals, cells migrate beneath the ectoderm to create a different germ layer, and this targeted cell translocation is required for proper tissue formation [83]. Upon wound occurrence, the fibroblasts and inflammatory cells migrate into the temporarily formed clots. Meanwhile, the epidermal

cells migrate and proliferate to cover the surface [84]. Cells migrate *in vivo* in response to diverse gradients of stimuli including physical, chemical, and signal gradients. Physical gradients occur naturally in bone structure and are defined as the gradual change in a physical property such as porosity, stiffness, and topology [85]. The dense cortical bone is located at the outer layer of the bone, inside which is the low-density trabecular bone. The pore size decreases from inside to outside. These structures can provide excellent permeability and desired mechanical support [85]. The cell migration *in vivo* is widely recognized as the gradients of ECM proteins, growth factors, and other signaling molecules. Inspired by these natural phenomena, gradient biomaterials have been created to investigate the cell migration *in vitro*.

The recruitment and migration of cells assisted by biomaterials is very important for the process of tissue regeneration, because the directional migration of cells to the wound site is a key prerequisite for tissue regeneration. In the case of damaged tissues, unexpected cell migration and overgrowth can lead to serious diseases. Therefore, cell selective biomaterials have important significance in tissue regeneration and reconstruction. The design of cell selective biomaterials is based on the specific interaction between materials and cells by physical, chemical or biological cues, because they can directly affect cell migration s and further affect the process of tissue regeneration. Chemical and biological molecules (peptides, growth factors, and adhesion molecules), physical properties (hardness, morphology, and hydrophilicity), physiological signals (cell chemokines or cytokines) are all effective regulatory factors in the design of cell selective biomaterials (Fig. 1.7).

Therefore, various techniques including "top-down" and "bottom-up" have been developed to prepare gradient surfaces [87]. The "top-down" approach is usually used to introduce active sites for further functionalization on an inert surface without reactive groups. This method modifies the surface gradually via external sources such as corona discharge [88], ultraviolet irradiation [89, 90], plasma [91, 92], chemical degradation [93, 94], and so on to change the surface properties. Han et al. developed gradient poly(sodium 4-styrenesulfonate) (PSS)/poly (diallyldimethylammonium) chloride (PDADMAC) multilayers with a gradually changed swelling ratio by using a salt-etched method [95]. Wang et al. prepared Cys-Ala-Gly (CAG) peptide density gradient poly(2-hydroxyethyl methacrylate-co-glycidyl methacrylate) brushes through immersing in a complementary gradient solution of CAG and competitive mercapto-terminated methoxyl poly(ethylene glycol). The gradient brushes could inhibit the adhesion and spreading of smooth muscle cells and promote endothelial cells migration [96]. Xue et al. developed a novel preparation method to fabricate graded protein/poly(ethylene glycol) (PEG) nanopattern arrays by inclined reactive-ion etching based on colloidal lithography [97]. Another chemical gradient surface was prepared using a diffusion-controlled plasma polymerization technique, which possessed a gradient of aldehyde group density [98].

The "bottom-up" technology is mostly used to introduce species of functional molecules onto surfaces with an adjustable grafting density, chain length, and mobility [99–101]. The gradient surfaces of materials can be obtained by time and

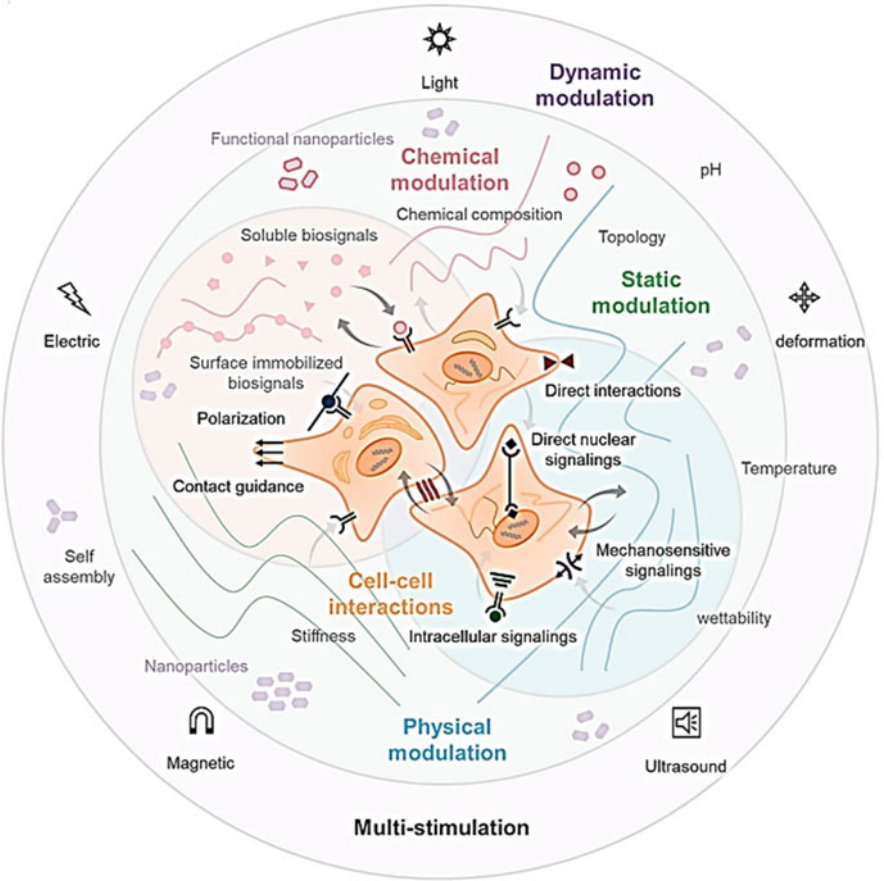

Fig. 1.7 Schematic of physical and chemical properties of the ECM that determine cell fates through mechanisms such as direct interaction, intracellular signaling, direct nuclear signaling, and mechanosensitivity signaling (Reprinted from [86] with permission. Copyright 2022 MPDI)

spatially controlled reactions or by reactions in a gradient concentration of molecules. For instance, Ren et al. fabricated a molecular weight gradient of poly (2-hydroxyethyl methacrylate) (PHEMA) brushes with a thickness ranging from 3 to 30 nm and slopes of 0.8–3.2 nm/mm by using surface-initiated atom transfer radical polymerization (ATRP) and a dynamically controlled reaction process [102]. Another group fabricated a poly(polyethyleneglycol methacrylate) (poly (PEGMA)) gradient surface whose thickness can be controlled at nanoscale [103].

Since they are more similar to the situation *in vivo* and also have the potential application of inducing cell migration in the tissue regeneration process, the gradients in a 3D matrix are more important. However, the "top-down" and "bottom-up" are only used for fabricating the gradient surface on 2D surface, but are not suitable in a 3D matrix owing to their relatively complicated structure. There are only a few

technologies that have been successfully applied in a 3D matrix (e.g., porous scaffolds and hydrogels) [104, 105]. For example, Woodfield et al. fabricated a pore-size gradient using a novel 3D fiber deposition technique [104]. DeLong et al. developed hydrogels with a basic fibroblast growth factor (bFGF) gradient by diffusing two types of hydrogel precursor solutions (PEG-conjugated bFGF solution and only PEG solution) in a gradient maker [48]. Cells were observed to align on the hydrogels modified with a bFGF gradient in the direction of increasing tethered bFGF concentration as early as 24 h after seeding [52]. Oh et al. fabricated a surface area gradient porous PCL/Pluronic F127 cylindrical scaffold by a centrifugation method (Fig. 1.8a) [106]. The cylindrical scaffolds exhibit gradually increasing surface areas along the longitudinal direction. Then, growth factors are immobilized via heparin binding to produce scaffolds with gradually increasing concentration of growth factors from the top position (near to rotation center) to the bottom position (bottom of the centrifuge tube, far to the rotation center) (Fig. 1.8b) [106]. The released amount of growth factor from the cylindrical scaffold gradually decreased along the longitudinal direction (from the bottom of the centrifuge tube to the top of the centrifuge tube) in a sustained manner for up to 35 days, which can allow for a minutely controlled spatial distribution of growth factors in a 3D environment (Fig. 1.8b) [106]. Motealleh et al. 3D printed a step-gradient nanocomposite hydrogel to direct cell migration toward highly concentrated, biopolymer-coated nanomaterials (NMs). The increased NM content in the gradient structure promotes the migration of human bone marrow-derived mesenchymal stem cells as well as Ca^{2+} deposition [108]. Another strong gradient hydrogel scaffold was 3D printed to recapitulate osteochondral tissue and its microenvironment. Transforming growth factor beta 1 (TGF-β1) and β-tricalciumphosphate (β-TCP) were distributed in distinct layers to regenerate cartilage in the upper hydrogel layers and bond with the host bone in the bottom layers (Fig. 1.8c) [107].

1.3.3 Influence of Biomaterial Surface on Stem Cell Fate

The promise of cellular therapy and tissue regeneration depends strongly on the cells used and the cell–biomaterial interaction *in vitro* and *in vivo* [109, 110]. However, the lack of available donor cell sources limits its ultimate clinical applicability. Stem cells (SCs) such as mesenchymal stem cells (MSCs) possess the potential to differentiate into different cell lineages and have gradually become the most versatile and valuable cell source for organ transplantation, disease treatment and cosmetology (Fig. 1.9). Control over their differentiation to a lineage of choice in an efficient and scalable manner is critical for the ultimate clinical success of cellular therapeutics [112, 113]. Surface modification to biomaterials can directly influence on stem cell behavior by altering surface interactions and microenvironment architecture and ultimately manipulating the signal transduction pathways in stem cells [114–116]. Diverse factors can contribute to overall stem cell fates (i.e., differentiation

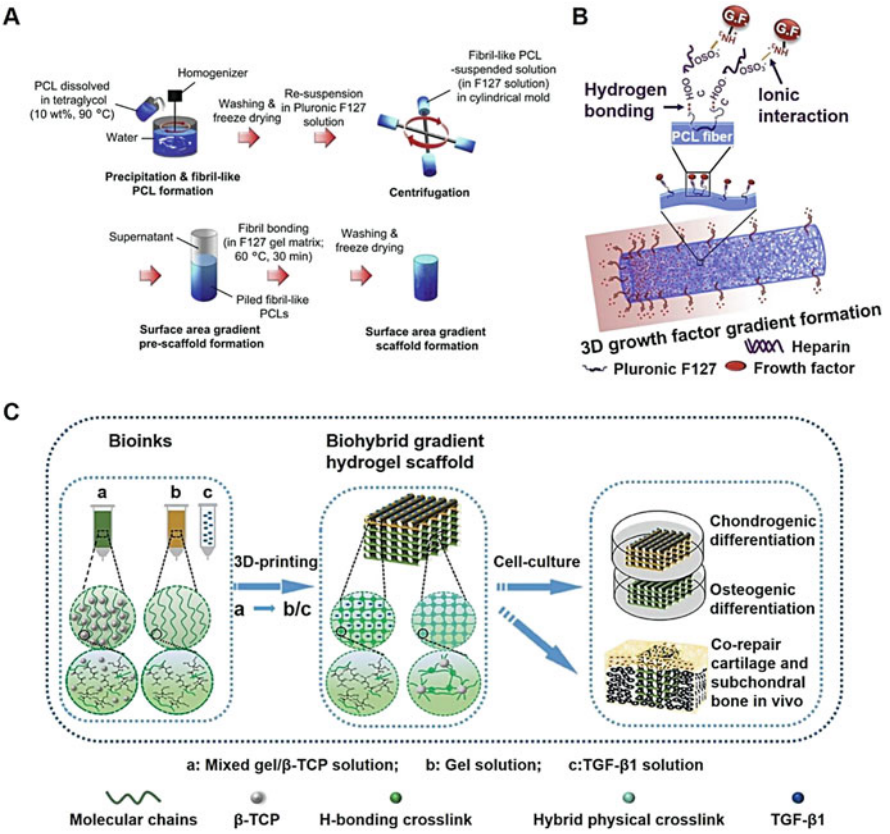

Fig. 1.8 (**a**) Schematic showing the fabrication of the surface area gradient porous scaffold using a centrifugation method. (**b**) Schematic of the successive binding of heparin and growth factor onto the fibril surface of a PCL/F127 cylindrical scaffold and the formation of a 3D growth factor gradient on the scaffold. (Reprinted from [106] with permission. Copyright 2011 Elsevier). (**c**) Procedure of thermal-assisted extrusion 3D printing of the biohybrid gradient scaffolds to repair osteochondral defects. (1) Gel region: the PNT hydrogel maintained a gelling state in a lower temperature region and underwent a gel–sol transition with increasing temperature; (2) shear-thinning region: the viscosity of PNT sol decreased markedly with the increasing shear rate so that it could be easily extruded from the nozzles under pressure; (3) sol–gel transition region for scaffold formation: the extruded filaments gelled quickly on the printing substrate at room temperature, and the mechanical properties and viscosity recovered rapidly (Reprinted from [107] with permission. Copyright 2018 Wiley-VCH Verlag)

into specific lineages), including the mechanical properties (e.g., elasticity or rigidity and stiffness), chemical and biological signals, and surface pattern [114–117].

The topography, elasticity, and surface roughness of a biomaterial orchestrate the physical interactions between SCs and the substrates, which can influence SC fates, although genetic or molecular mediators are considered as the primary factors [118, 119]. Micro- and nanoscale topography plays a crucial role in embryonic

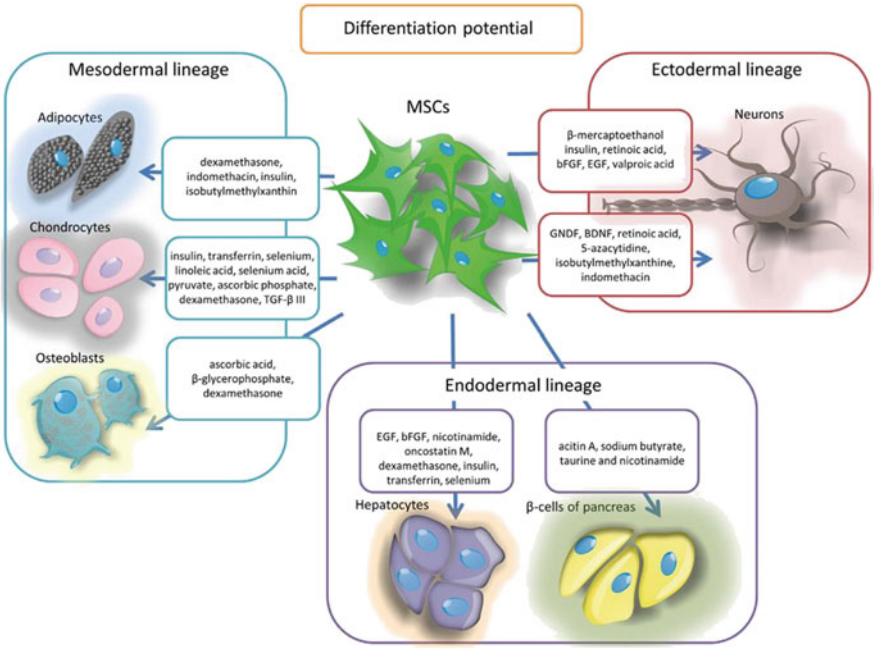

Fig. 1.9 The differentiation potential of mesenchymal stem cells (Reprinted from [111] with permission, copyright 2019 Oxford University Press)

development and SC differentiation [120–123]. For example, a rapid, single-step 3D printing method based on direct ink writing using agitated viscous polymer solutions has been used to manufacture polymer scaffolds consisting of microcolumns (ca. 60 μm) with micro/nanometer surface pores (0.2–2.4 μm). Pore density, size, and alignment can be modified by varying the degree of stirring or printing speed. 3D-printed scaffolds with microporous/nanopore scaffolds promote cartilaginous and osteogenic differentiation of MSCs without soluble differentiation factors. Depending on differentiation medium composition, varying topographies could be used to modify the adhesion, morphology, and differentiation of MSCs toward cartilage and osteogenic lineages (Fig. 1.10a) [127]. ECM stiffness can affect cell fate and affect a wide range of biological processes [128–131]. For example, the use of methacrylated hyaluronic acid hydrogels as an *in vitro* 3D microniche allows SC volume and matrix stiffness to be modified independently. This approach allows the decoupling of matrix stiffness and cell volume in 3D microenvironments. Single 3D microniches with varying volumes (2800, 3600, and 6000 μm^3) and stiffnesses (5, 12, and 23 kPa) were used to culture human mesenchymal stem cells (hMSCs). Cellular responses to matrix stiffness were shown to be affected by cell volume, with cells forming stress fibers and focal adhesions on matrices of all stiffnesses when cell volume was sufficient (Fig. 1.10b) [132]. Previous studies have reported that SCs are able to sense and respond to material interface roughness, thereby altering cell fate

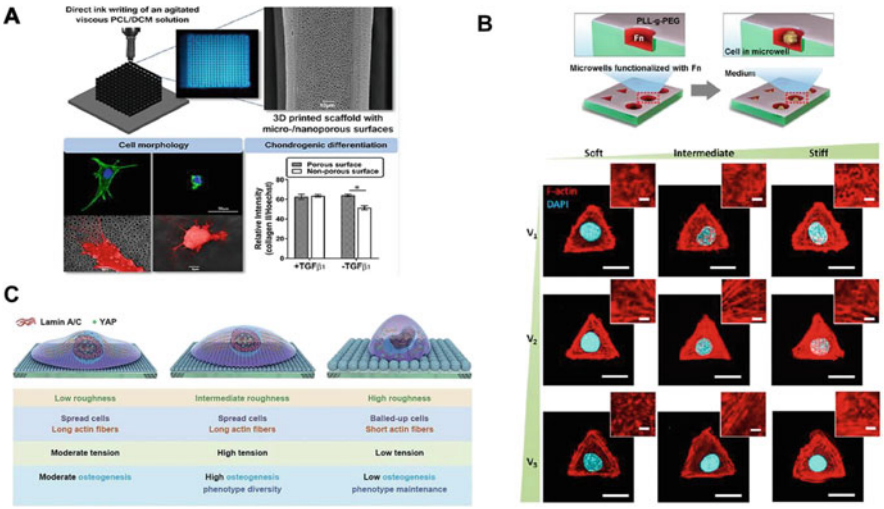

Fig. 1.10 Biomaterial designs that regulate stem cell differentiation. (**a**) Schematic of a 3D printing approach to fabricate nanoporous/microporous surfaces that influence chondrogenic differentiation. (Reprinted from [124] with permission. Copyright 2019 American Chemical Society). (**b**) Cells were cultured in 3D microniches with different hydrogel stiffness for 12 h and stained for F-actin (red) and nuclei (blue). Scale bars represent 10 μm. (Reprinted from [125] with permission. Copyright 2018 American Chemical Society). (**c**) MSCs cultured on a surface of intermediate roughness spread and exhibit high-cellular tension to enhance osteogenic differentiation and diversity of cell phenotype. The adhesion of MSCs to a very rough surface is limited, but the cells can maintain their phenotype (Reprinted from [126] with permission. Copyright 2020 Wiley-VCH GmbH)

[133–135] through mechanotransduction pathways such as FA formation, activation of signaling proteins, nuclear tension generation, chromatin remodeling, and transcriptional activity (Fig. 1.10c) [136].

1.4 Regenerations of Some Clinic-Targeted Tissues

Due to the poor regenerative capacity of tissues *in vivo*, the regeneration and repair of large-area defect tissue is a great challenge [137]. Tissue engineering applies the principles of cytology and engineering to research and develop biological substitutes for repairing or improving the structure and function of defective tissues and organs [138, 139]. Tissue engineering technology is to build natural and healthy autologous tissue through the basic unit of the human body cells, with the help of temporary 3D scaffolds and normal growth patterns. At present, the research of epithelial and bone tissue engineering has achieved preliminary results. Here, regeneration of some clinic-targeted tissues such as cartilage, skin, blood vessels, and cardiovascular is described briefly.

1.4.1 Cartilage Regeneration

Osteoarthritis (OA) is a degenerative joint disease that irreversibly and progressively breaks down the articular cartilage. Currently, 52.2 million Americans are diagnosed with arthritis, and this number is estimated to rise to 78.4 million by 2040. Symptomatic relief and eventual joint replacement remain the standard treatments because no intervention exists to inhibit disease progression. The limited capacity of damaged cartilage to regenerate and the potential morbidity associated with implanting or transferring bone and cartilage render cartilage regeneration an attractive alternative. Therefore, cartilage tissue engineering aims to create biologically compatible cartilage constructs that contain relevant certain cell types to help regenerate the avascular and aneural cartilage. Tissue-engineered cartilage includes various constituent cell types, biomimetic scaffolds, inductive bioactive factors, and genes.

The cells seeded into the scaffolds are responsible for the synthesis and metabolism of ECM. Initially, chondrocytes are used in cell-based therapy for repairing cartilage lesions, which is the principal cell type found in cartilage [140]. However, the availability of chondrocytes (e.g., adult chondrocytes and juvenile chondrocytes) is limited. The potential of stem cells to treat regenerated cartilage has aroused extensive interest. Most stem cell specific trials for the treatment of hip and knee osteoarthritis are pilot or feasibility studies that use plastic adhesion, culture and expansion of mesenchymal stem cells (MSCs). These MSCs are mainly derived from bone marrow or adipose tissue. However, these MSCs do not constitute validated stem-cell populations, and it is difficult to ascertain the degree of engraftment by the transplanted cells and their contribution to changes in functional outcomes.

Cells seeded on a 3D scaffold could retain the seeded cells and provide mechanical support to aid in the development of cartilage over time. Mainly four types of scaffolds including protein-based polymers, carbohydrate-based polymers, synthetic polymers, and composite polymers are applied in cartilage tissue engineering [40]. Inspired by nature, the protein-based polymers such as fibrin, gelatin, and collagen have been widely used in bioengineered scaffolds. For example, collagen is the major component of ECM and can be used as a scaffold that could retain cell phenotypes. Being seeded with autologous chondrocytes in collagen type I-based scaffold, the obtained construct was implanted in 21 patients with grade III chondral defects of the distal femur [141]. The patients treated with these scaffold materials have significantly lower pain scores [141]. Hyaluronan, alginate, chitosan, and agarose are typical examples of carbohydrates and have been used as hydrogel scaffolds. They have a strong ability to adsorb and maintain water, which is similar to the properties of cartilage ECM. In one study, significant improvement in function and relief of pain was seen in cartilage defect patients being treated with hyaluronic acid-based scaffolds [142]. Synthetic polymers such as PLA, PCL, and PLGA are the most common materials used in cartilage regeneration. Previous work has demonstrated that a synthetic polymer-based scaffold containing PLGA and calcium sulfate could enhance the growth of cartilage and bone [143].

In contrast to scaffolds and stem cells, growth factors are used to stimulate SC growth, enhance chondrogenesis, and augment the management of cartilage defects. The five main groups of growth factors used in cartilage regeneration are transforming growth factor-β superfamily, fibroblast growth factor family, insulin-like growth factor, platelet-derived growth factor, and platelet-rich plasma [144]. Recently, bone morphogenetic protein 4 (BMP-4) and transforming growth factor-β3 (TGFβ-3) were combined in the cartilage construct that was implanted in an established knee cartilage defect model. PLGA (50:50 PLA/PGA) microspheres (μS) were used to deliver these growth factors in hydrogel (Fig. 1.11a, b) [145], which can potentially regenerate cartilage *in situ*.

1.4.2 Skin Regeneration

Skin, the largest organ of human body, plays a significant role in protecting the body against outside environment. It mainly consists of the epidermis, dermis, and hypodermis [146]. Severe acute and chronic wounds on the skin such as burns, abrasions, lesions, and chronic ulcers may result in significant disability or even death. Because of the antigenicity of donor tissue and the limitation of donor sources, skin grafts have been a challenging task for surgeons, limiting their wide application [147, 148]. Therefore, various models for skin epidermis and dermis reconstruction have been developed to enhance skin cell growth during wound healing. The possibility of using biomaterials as a platform to generate stimuli can promote cell activities related to skin regeneration due to its versatility, which is receiving more attention.

Biomaterials are powerful tools to change the host microenvironment due to their characteristics obtained in the manufacturing process. Surface chemistry, topography, mechanical properties and degradation products can promote effective regeneration by combining or not combining with biological signals. They are multistimulatory and are not limited to biochemical signals. To simulate the *in vivo* environment, a series of natural materials including silk, collagen, fibrin, and sugar are preferred for tissue-engineering applications. For example, collagen is the main structural protein in vertebrates and the most useful biomaterial in bioengineering. Existing commercial leather brackets, such as Lando®, Integra®, PELNAC® Collagen, mainly composed of collagen, have two fatal defects: (1) they degrade too fast (< 1 month) and cannot meet the time required for tissue regeneration and repair (more than 3–6 months); (2) the single component has insufficient activity to induce tissue regeneration and repair. A 3D bionic short-fiber scaffold with the functions of early biofluid collection, response to coupled endogenous electric fields (EF), is constructed by guiding the short fibers into a 3D network structure and subsequent multifunctional modification, which serves as an ideal candidate for repairing different defective tissues by rapidly reversing water absorption and stabilizing electrical performances [149]. Synthetic polymers are also widely used in skin repair. For example, the hydrophilicity of reactive oxygen

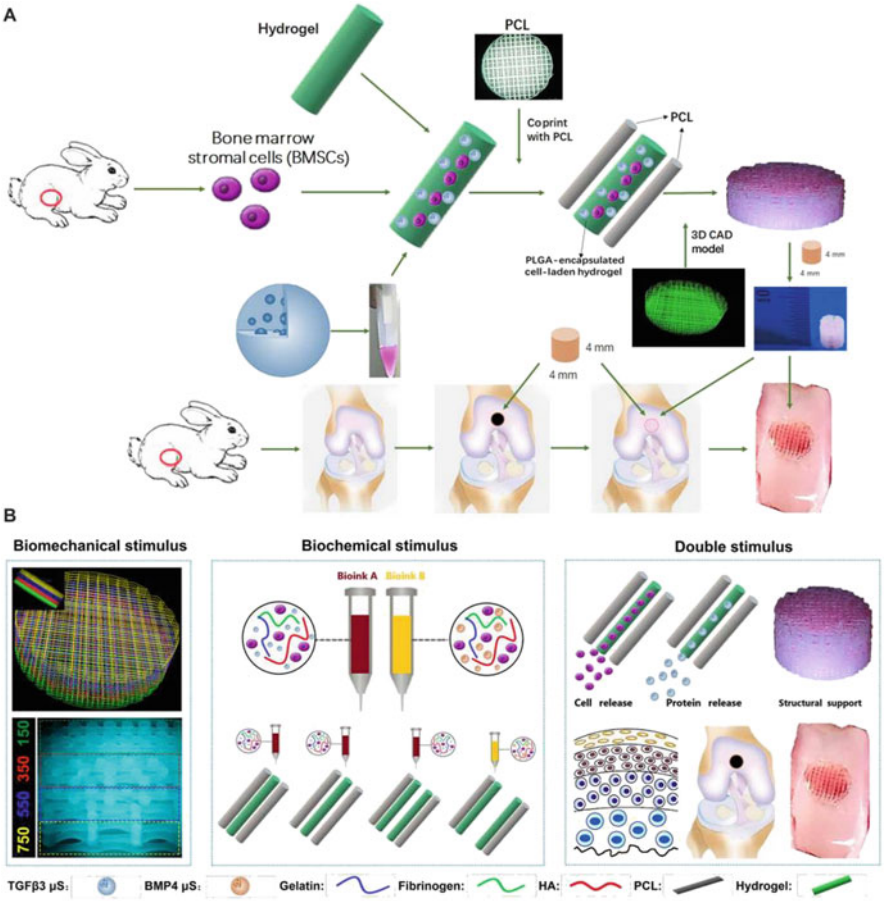

Fig. 1.11 (**a**) Schematic of 3D-bioprinted, dual-factor releasing, and gradient-structured MSC-laden constructs for articular cartilage regeneration in rabbits. (**b**) A computer-aided design (CAD) model was used to design the four-layer gradient PCL scaffold, which offers BMS for anisotropic chondrogenic differentiation and supplies nutrients in deep layers (left). A gradient anisotropic cartilage scaffold was fabricated from one-step 3D-bioprinted gradient polymeric scaffold and dual protein-releasing composite hydrogels whose bioinks encapsulated BMSCs with BMP-4 or TGF-β for chondrogenesis (middle). The anisotropic cartilage construct provides structural support and sustained release of BMSCs and differentiative proteins for biomimetic regeneration of the anisotropic articular cartilage when transplanted in an animal model (right) (Reprinted from [145] permission, copyright 2020 American Association for the Advancement of Science (AAAS))

species (ROS)-degradable polythioketal (PTK) urethane (UR) foams can be varied to heal skin wounds [150]. Moreover, a microfluidic blow-spinning strategy was used to fabricate a biodegradable sealant-loaded nanofiber scaffold composed of fibrinogen-loaded polycaprolactone/silk fibroin (PCL/SF) ultrafine core-shell nanofibers. Then the fibrin sealant gelled *in situ* between thrombin and fibrinogen

on a PCL/SF nanofiber surface to promote the migration and proliferation of fibroblasts, accelerating skin regeneration [151].

Biological scaffolding has broad applications in skin flap regeneration. Recently, a novel MX-ene-bonded hollow fiber (MX-HF) scaffold with dynamic response channels was shown to promote angiogenesis and skin flap regeneration using a microfluidic-assisted 3D printing strategy. MX-HF scaffolds shrink and expand in response to near infrared (NIR) light due to the photothermal conversion capability of MXene nanosheets and temperature responsiveness of poly (NIPAM) hydrogel, thereby facilitating the penetration of cells into scaffold channels from the surrounding environment [152]. Zunzhen et al. encapsulated *Lactobacillus reuteri* in hydrogel microspheres using emulsion polymerization and covalent crosslinking of methacrylic acid modified hyaluronic acid (Fig. 1.12a) [153]. A further study reported the fabrication of a novel biological hybrid scaffold for skin flap regeneration by combining the advantages of anisotropic fish scales and MSCs (Fig. 1.12b) [118].

1.4.3 Nerve Regeneration

Nerve regeneration remains a great challenge. The nervous system is a complex network composed of millions of neurons, which is one of the most complex systems in the human body. After injury or degenerative disease, the damage to the nervous system is overwhelming due to its complexity and limited regenerative capacity. According to statistics, in the United States alone, more than 50,000 patients receive surgical repair of peripheral nerve injury (PNI) every year. The incidence of PNI is between 13 and 23 per 100,000 persons per year in the developed countries, resulting in partial or total loss of motion, sensory, and autonomic function in the involved segments of the body [119]. The most common used methods for current clinical treatment involve the end-to-end anastomosis and utilization of autografts. However, both of these procedures have their drawbacks and are often ineffective because of the gap length between the injured nerves, formation of neuromas, and shortage of donor sources. Therefore, these ineffective therapies and limited availability of donor nerves motivate the development of artificial biodegradable nerve grafts.

Because the regeneration of injured nerves is a complex biological process, which requires a variety of signals to promote the survival of nerve cells and stimulate the growth of neurites, the artificial nerve grafts should ideally have multiple functions. These functions should include a favorable environment for regenerating axons and enhancing cellular growth and migration and offering the guidance and protection abilities from the surrounding tissues [120]. Furthermore, nerve grafts must possess sufficient mechanical strength for suturing to the nerve stumps and suitable biodegradation properties [121, 122]. Thus, natural biomaterials [123] (e.g., collagen, chitosan, fibrinogen, and alginate) and synthetic polymers [127, 128] (e.g., aliphatic polyesters) are common materials used for production of nerve grafts. To improve

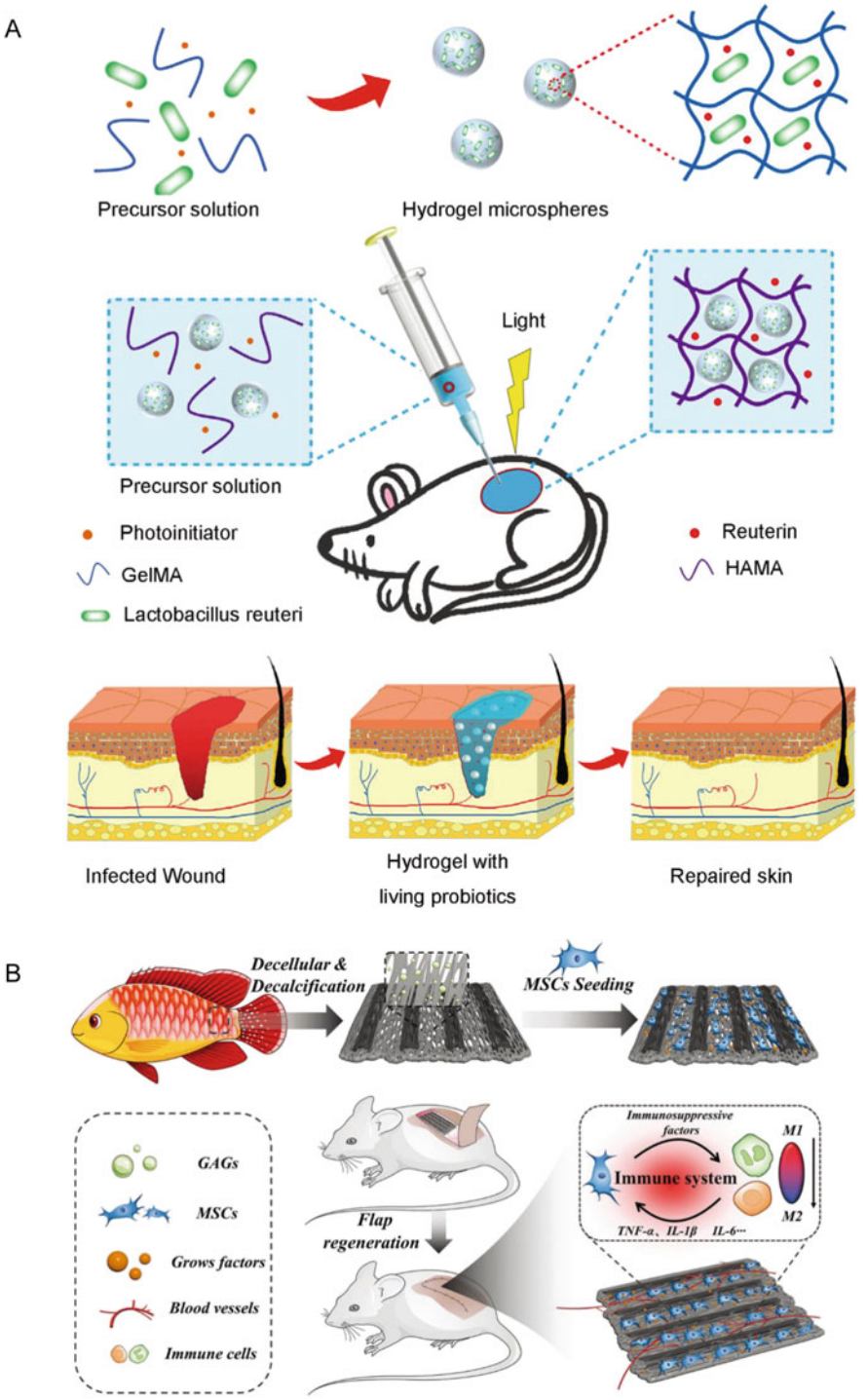

Fig. 1.12 (**a**) Schematic diagram of the preparation of active probiotic hydrogel and application in accelerating the wound healing process. (Reprinted from [153] with permission, copyright 2021

the biological performance of artificial grafts, several additional functionalities including topographical guidance, electrical activity, and neurotrophic activity have been introduced into the devices. Topography plays a fundamental role in nerve repair [129]. Electrospinning is widely used to develop aligned topography that supports cell adhesion and regulates the growth of neurons [130]. Besides, electrical stimulation is closely related to nerve regeneration as well [131]. Thus, electrically conducting polymers such as polypyrrole (PPY) and its derivatives are widely used in nerve repair [132]. Jin et al. designed and constructed a wearable neural invasive electrical stimulation (iES) system to regulate bionic nerves [133] and replace the autologous graft. Furthermore, trophic elements such as neurotrophic agents (e.g., acetylcholine [134], laminin-derived peptides including IKVAV and YIGSR [135, 136], and nerve growth factor (NGF) [154]) and Schwann cells [155] are often combined with artificial conduits. Chang et al. fabricated a neural conduit whose aligned electrospun nanofibers and neurotrophic gradients (MC/AN/NG) guide axon growth and degrade naturally. Gelatin-based conduits simulate the branching structure of natural neural ECM as shown by a mechanically stable multichannel (MC) scaffold crosslinked with microbial transglutaminase [156]. Additionally, the release profiles of double neurotrophic factors, nerve growth factor (NGF), and brain-derived neurotrophic factor in a MC conduit can be temporally controlled [156]. Zhang et al. fabricated a micropattern and a peptide gradient on the inner wall of poly(D, L-lactide-co-caprolactone) (PLCL) to regenerate peripheral nerves *in vivo* and *in vitro* (Fig. 1.13a) [157]. Schwann cells aligned well and migrated faster to the region of a higher peptide density. The micropattern and peptide gradient in a PLCL-based nerve conduit quickly recovered the microstructure and function of the sciatic nerve while reducing fibrosis in muscle tissue. The nerve conduit can also promote M2 macrophage polarization and angiogenesis (Fig. 1.13b) [157].

1.4.4 Regeneration of Blood Vessels

Vascular replacement and repair are the most commonly used surgical procedures to treat atherosclerotic diseases, infections, and trauma. Although there is a high clinical demand for engineered artery substitutes, they often pose challenges such as immune rejection, poor mechanical strength, and low thrombosis. The blood vessels are lined with ECs, which are covered by vascular smooth muscle cells followed by fibroblasts and matrix on the outermost layer of the vessel [158]. These layers of cells repair, remodel, and maintain the blood vessels following an injury.

Fig. 1.12 (continued) Wiley-VCH GmbH). (**b**) Fabrication of MSC-loaded fish scales and application in promoting skin flap survival (Reprinted from [118] with permission, copyright 2022 Wiley-VCH GmbH)

Current strategies to develop a functional blood vessel include tissue-engineered cell-seeded scaffolds and bioactive, cell-free approaches.

Tissue-engineered cell-seeded scaffolds can potentially replace veins and arteries if they achieve the following objectives: (1) the engineered artery should have an ECM that can stretch, retain sutures, and resist mechanical stress; (2) its matrix should be naturally-derived to better integrate with the immune system of the host and not elicit a foreign body reaction; (3) both active and inactive cells should be autologous to prevent immune recognition, degradation, and aneurysm in the implanted blood vessel; (4) the host should be able to remodel, refill, and revitalize the engineered artery postimplantation; and (5) a nonthrombogenic lumen surface may be required for small caliber or low-flow arterial bypass applications. This surface may be a cellular or biochemical surface, but blood coagulation contact activation, platelet adhesion and activation, and thrombosis in the arterial system should be avoided.

Both synthetic and natural biomaterials have been developed [159, 160]. Natural polymers, including collagen/gelatin and chitosan, are biocompatible and therefore promote cell adhesion and differentiation [161, 162]. Badhe et al. fabricated a bilayer scaffold by combining gelatin and chitosan, which supported cell growth and spreading [163]. Collagen itself can also be used to make vascular grafts [164] as shown by Zhu et al., who fabricated a vascular scaffold by combining HA and collagen that together matched the mechanical and biophysical properties of the natural ECM [165]. Decellularized scaffolds offer mechanical strength as well as cell adhesion sites [166] [167], although they degrade quickly, are not very accessible, and cannot change the content and structure of the ECM [168]. Large amounts of ECM implanted in the vascular system may also cause thrombosis [169].

Modified tissue-engineered scaffolds could alleviate intimal hyperplasia and thrombosis of unmodified grafts. Jennifer et al. showed that heparin or fluorosurfactant (FSP) modification can inhibit intimal hyperplasia and thrombosis of ePTFE vascular grafts [170]. Wo et al. also modified polyurethane (PU) vascular grafts with heparin and cell-adhesive peptides, which significantly increased the patency rate of the PU grafts compared to their unmodified counterparts at 9 weeks postimplantation [171]. Decellularized scaffolds coated with vascular endothelial growth factor (VEGF) and peptides also reduced intima formation and thrombus formation [172, 173]. Large-diameter tissue-engineered scaffolds are primarily fabricated with nondegradable synthetic materials that are not recommended for small-diameter scaffolds. Composite materials have garnered more attention because they offer the advantages of both synthetic and natural polymers. Indeed, studies have shown that composite materials enhance the graft's compatibility [174]. Decellularized scaffolds derived from a variety of sources can reduce host immune responses while promoting the growth, proliferation, and differentiation of inoculated cells.

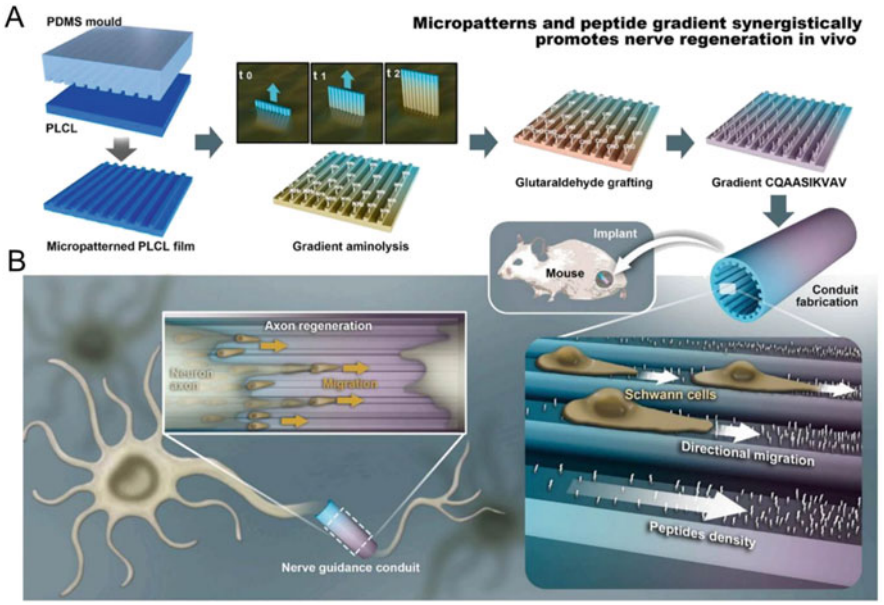

Fig. 1.13 (**a**) Schematic of micropatterned poly(D,L-lactide-co-caprolactone) (PLCL) film with a CQAASIKVAV peptide density gradient. The striped micropatterns with ridges and grooves are fabricated by thermally pressing a polydimethylsiloxane (PDMS) template onto a PLCL film. Gradient aminolysis leads to the density gradient of the amino groups, which are then transferred to the CQAASIKVAV gradient. (**b**) The micropatterned PLCL film and its peptide gradient synergistically enhance the directional migration of SCs toward the high-density region of the patterns *in vitro*. The resulting guidance conduit promotes the reconstruction and functional recovery of rat sciatic nerve *in vivo* (Reprinted from [157] with permission, copyright 2022 Elsevier)

1.4.5 Cardiovascular Engineering

Cardiovascular diseases (CVDs) including coronary heart disease, rheumatic heart disease, congenital heart disease, myocardial infarction, and strokes are major cause of morbidity and mortality worldwide [175]. According to the estimation of the World Health Organization, the number of deaths shows an increase from 17.3 million in 2008 to 23.3 million by 2030. Adult cardiovascular tissues cannot repair or renew themselves after injury due to the limited regenerative capacity of cardiomyocytes (CMS). In the late stage of cardiovascular disease, transplantation or replacement is usually the only treatment option. These clinical implants include autografts, allografts, xenografts, and prosthetics. The cardiac implantation methods are mainly limited by the shortage of available donors and immune rejection. In addition, coagulation, mechanical mismatch and limited durability are other major problems. As a promising alternative, cardiovascular tissue engineering is being

explored to restore cardiac function and replace abnormal or necrotic cardiovascular tissues.

One focus in the field of tissue engineering is the generation and development of functional biomaterials. These materials should be bioactive (e.g., releasing drugs, proteins, growth factors, and ECM components) and suitable mechanical functionality. Enormous efforts have been paid to generate and design biomaterials for cardiovascular tissue engineering (Fig. 1.14) [177, 178]. The biomimetic materials can mimic ECM architecture and provide potentially controllable *in vivo*-like microenvironments for cells [179]. Therefore, various biomimetic materials are developed for myocardial repair, cardiac patch generation, and heart valve tissue engineering [177, 180]. Hydrogels are commonly used in cardiovascular engineering, which can be made of PEG [181], chitosan [182, 183], fibrin [184], collagen [185], and alginate [186]. Zhong et al. reported a printed bilayer proteinaceous hydrogel patch for heart failure treatments based on genetically engineered multidomain proteins [187]. The intrinsic self-healing nature of hydrogels physically enable seamless interfacial integration of two disparate hydrogels, endowing the cardiac patches with the combinatorial advantages of each layer. Liu et al. constructed a paintable hydrogel based on simultaneous Fe^{3+}-triggered polymerization of covalently linked pyrrole and dopamine in the hyperbranched chains, whose conductive polypyrrole formed *in situ* also uniquely serves to crosslink network [188]. This conductive and adhesive hydrogel can be patched onto the heart without adverse liquid leakage. Electrospinning is another widely used method for creating fibrous and highly porous scaffolds for cardiovascular engineering [189].

Another focus in the field of tissue engineering is cell-based therapy, which has been clinically performed by the direct injection of dissociated cells [190]. This strategy avoids problems that may be related to synthetic materials, such as inflammation, stenosis, and infection, allowing for the complete graft integration and increase of the patency rate. The cell sources used for cardiovascular disease are mainly ESCs, induced pluripotent stem cells (iPSCs), and autologous cells [175, 177, 180]. ESCs and iPSCs are attractive for cardiovascular disease due to their ability to differentiate into beating cardiomyocytes easily by some certain methods [191, 192], while other human stem and progenitor cells can hardly do [177]. Autologous cells such as bone marrow- and peripheral blood-derived cells are under clinical trials for cardiovascular disease [193]. Although various cell injection therapies are now clinically performed and some therapies cause modest therapeutic effects, the efficacies are found to be unable to reach the level as clinicians expected [194–197]. Furthermore, it is a big issue for the cell injection therapy in terms of cell retention in the target tissue, since the injected cells are largely washed out or died [198, 199].

Some studies are focused on fabrication of completely biological tissue-engineered vascular grafts without the use of scaffolds. Thus, the cell-sheet-based technology have been developed, which consists of the *in vitro* growing of cells in the culture medium containing ascorbic acid to generate a large production of ECM [200]. After maturation, the cell sheets are detached from the culture flasks using various technologies [201–203]. For example, a temperature-responsive polymer

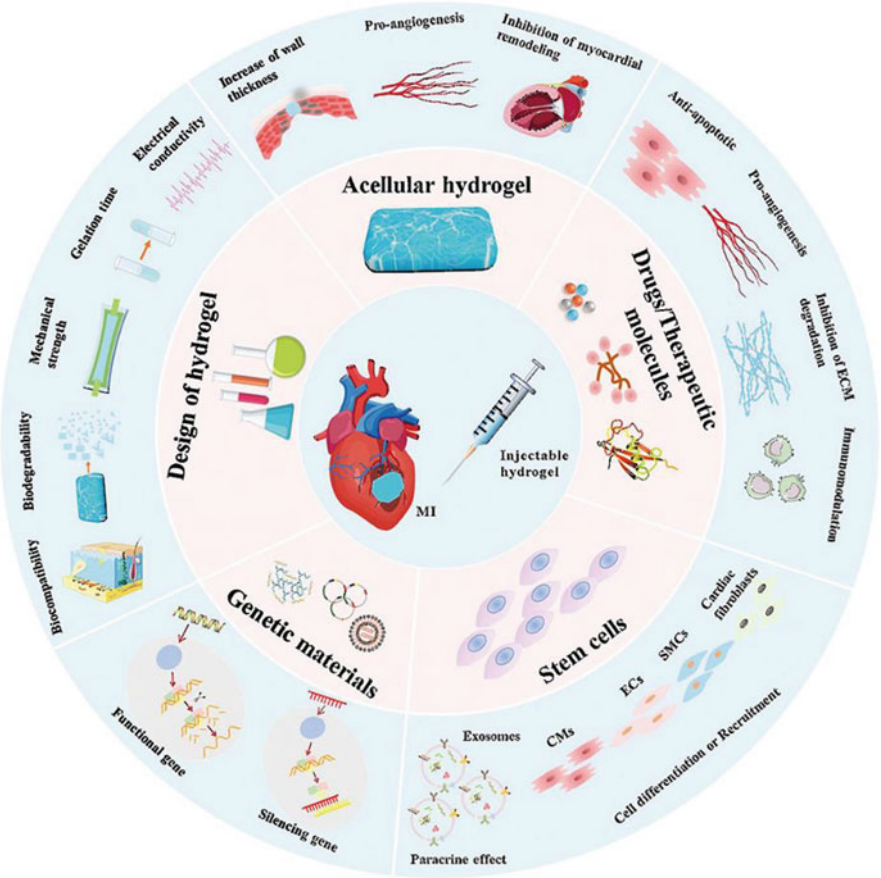

Fig. 1.14 Biomaterials for cardiovascular tissue engineering. Injectable hydrogels and/or cardiac patches are used to treat cardiac damage. Both materials can include cells and/or bioactive molecules such as RNA, small molecules, growth factors, or proteins (Reprinted from [176] with permission. Copyright 2021 Elsevier)

such as poly(N-isopropylacrylamide) (PNIPAm) can be grafted onto a culture plate surface [204]. Three-dimensional tissues can be easily prepared by layering cell sheets whose cells can be delivered without cell loss because the embedded cells preserve their own ECM [201, 202]. Araki et al. transplanted skeletal myoblasts embedded in cell sheets, which improved cardiac performance and lifespan in an animal model by reorganizating cytoskeletal proteins in the host's cardiac tissue and reducing myocardial fibrosis [205].

The use of bioreactors is advantageous when generating a tissue-engineered heart valve *in vitro*, which mimics the biophysical signals (e.g., various forces such as strain, pressure, torsion, or flow in tissues) presenting in the native organophysiological environment [175, 177]. For instance, the additional pulsatile

flow bioreactor in a porous scaffold improves ECM production by vascular cells [206]. The pulsatile flow bioreactor also shows an increased collagen and elastin production and a significantly improved recellularization of the heart valve [207, 208].

References

1. Zhang D, Chen Q, Shi C, Chen M, Ma K, Wan J, Liu R. Dealing with the foreign-body response to implanted biomaterials: strategies and applications of new materials. Adv Funct Mater. 2021;31:2007226.
2. Lin R-B, He Y, Li P, Wang H, Zhou W, Chen B. Multifunctional porous hydrogen-bonded organic framework materials. Chem Soc Rev. 2019;48:1362–89.
3. Chen W, Chen P, Zhang G, Xing G, Feng Y, Yang Y-W, Chen L. Macrocycle-derived hierarchical porous organic polymers: synthesis and applications. Chem Soc Rev. 2021;50: 11684–714.
4. Xue X, Hu Y, Deng Y, Su J. Recent advances in design of functional biocompatible hydrogels for bone tissue engineering. Adv Funct Mater. 2021;31:2009432.
5. Chimene D, Kaunas R, Gaharwar AK. Hydrogel bioink reinforcement for additive manufacturing: a focused review of emerging strategies. Adv Mater. 2020;32:1902026.
6. Hasani-Sadrabadi MM, Sarrion P, Nakatsuka N, Young TD, Taghdiri N, Ansari S, Aghaloo T, Li S, Khademhosseini A, Weiss PS, Moshaverinia A. Hierarchically patterned polydopamine-containing membranes for periodontal tissue engineering. ACS Nano. 2019;13:3830–8.
7. Liu Y, Dabrowska C, Mavousian A, Strauss B, Meng F, Mazzaglia C, Ouaras K, Macintosh C, Terentjev E, Lee J-H, Huang YYS. Bio-assembling macro-scale, lumenized airway tubes of defined shape via multi-organoid patterning and fusion. Adv Sci. 2021;8:2003332.
8. Limongi T, Tirinato L, Pagliari F, Giugni A, Allione M, Perozziello G, Candeloro P, Di Fabrizio E. Fabrication and applications of micro/nanostructured devices for tissue engineering. Nanomicro Lett. 2017;9:1–13.
9. Fereshteh Z. Freeze-drying technologies for 3D scaffold engineering. In: Functional 3D tissue engineering scaffolds; 2018. p. 151–74.
10. Costantini M, Barbetta A. Gas foaming technologies for 3D scaffold engineering. In: Functional 3D tissue engineering scaffolds; 2018. p. 127–49.
11. Rahmati M, Mills DK, Urbanska AM, Saeb M, Venugopal JR, Ramakrishna S, Mozafari M. Electrospinning for tissue engineering applications. Prog Mater Sci. 2021;117:100721.
12. Gelain F, Luo Z, Zhang S. Self-assembling peptide EAK16 and RADA16 nanofiber scaffold hydrogel. Chem Rev. 2020;120:13434–60.
13. Cui H, Miao S, Esworthy T, Zhou X, Lee S-J, Liu C, Yu Z-X, Fisher JP, Mohiuddin M, Zhang L. 3D bioprinting for cardiovascular regeneration and pharmacology. Adv Drug Deliv Rev. 2018;132:252–69.
14. Ajalloueian F, Lemon G, Hilborn J, Chronakis IS, Fossum M. Bladder biomechanics and the use of scaffolds for regenerative medicine in the urinary bladder. Nat Rev Urol. 2018;15:155–74.
15. Koons GL, Diba M, Mikos AG. Materials design for bone-tissue engineering. Nat Rev Mater. 2020;5:584–603.
16. Alizadeh-Osgouei M, Li Y, Wen C. A comprehensive review of biodegradable synthetic polymer-ceramic composites and their manufacture for biomedical applications. Bioact Mater. 2019;4:22–36.
17. Gaharwar AK, Singh I, Khademhosseini A. Engineered biomaterials for in situ tissue regeneration. Nat Rev Mater. 2020;5:686–705.

18. Tu Z, Zhong Y, Hu H, Shao D, Haag R, Schirner M, Lee J, Sullenger B, Leong KW. Design of therapeutic biomaterials to control inflammation. Nat Rev Mater. 2022;7:557–74.
19. Li C, Ouyang L, Armstrong JP, Stevens MM. Advances in the fabrication of biomaterials for gradient tissue engineering. Trends Biotechnol. 2021;39:150–64.
20. Whitaker R, Hernaez-Estrada B, Hernandez RM, Santos-Vizcaino E, Spiller KL. Immunomodulatory biomaterials for tissue repair. Chem Rev. 2021;121:11305–35.
21. Rahmati M, Mozafari M. Protein adsorption on polymers. Mater Today Commun. 2018;17: 527–40.
22. Ngandu Mpoyi E, Cantini M, Reynolds PM, Gadegaard N, Dalby MJ, Salmerón-Sánchez M. Protein adsorption as a key mediator in the nanotopographical control of cell behavior. ACS Nano. 2016;10:6638–47.
23. Bianco P, Robey PG. Stem cells in tissue engineering. Nature. 2001;414:118–21.
24. Williams CK, Segarra M, De La Luz SM, Sainson RC, Tosato G, Harris AL. Regulation of CXCR4 by the notch ligand delta-like 4 in endothelial cells. Cancer Res. 2008;68:1889–95.
25. Lu B, Atala A. Small molecules and small molecule drugs in regenerative medicine. Drug Discov Today. 2014;19:801–8.
26. Lampe KJ, Heilshorn SC. Building stem cell niches from the molecule up through engineered peptide materials. Neurosci Lett. 2012;519:138–46.
27. Wu R, Li Y, Shen M, Yang X, Zhang L, Ke X, Yang G, Gao C, Gou Z, Xu S. Bone tissue regeneration: the role of finely tuned pore architecture of bioactive scaffolds before clinical translation. Bioact Mater. 2021;6:1242–54.
28. Du C, Hu J, Wu X, Shi H, Yu H, Qian J, Yin J, Gao C, Wu Z, Zheng Q. 3D printing of a tough double-network hydrogel and its use as a scaffold to construct a tissue-like hydrogel composite. J Mater Chem B. 2022;10:468–76.
29. Xiang G, Zha Y, Li Y, Chen J, Liu S, Du Y, Zhang S, Wang J. Integrated polycaprolactone microsphere-based scaffolds with biomimetic hierarchy and tunable vascularization for osteochondral repair. Acta Biomater. 2022;141:190–7.
30. Deng C, Lin R, Zhang M, Qin C, Yao Q, Wang L, Chang J, Wu C. Micro/nanometer-structured scaffolds for regeneration of both cartilage and subchondral bone. Adv Funct Mater. 2019;29:1806068.
31. Wei G, Ma PX. Structure and properties of nano-hydroxyapatite/polymer composite scaffolds for bone tissue engineering. Biomaterials. 2004;25:4749–57.
32. Loh QL, Choong C. Three-dimensional scaffolds for tissue engineering applications: role of porosity and pore size. Tissue Eng Part B Rev. 2013;19:485–502.
33. Ma T, Li Y, Yang ST, Kniss DA. Effects of pore size in 3-D fibrous matrix on human trophoblast tissue development. Biotechnol Bioeng. 2000;70:606–18.
34. Ikeda R, Fujioka H, Nagura I, Kokubu T, Toyokawa N, Inui A, Makino T, Kaneko H, Doita M, Kurosaka M. The effect of porosity and mechanical property of a synthetic polymer scaffold on repair of osteochondral defects. Int Orthop. 2009;33:821–8.
35. Lee SB, Kim YH, Chong MS, Hong SH, Lee YM. Study of gelatin-containing artificial skin V: fabrication of gelatin scaffolds using a salt-leaching method. Biomaterials. 2005;26:1961–8.
36. Wu X, Liu Y, Li X, Wen P, Zhang Y, Long Y, Wang X, Guo Y, Xing F, Gao J. Preparation of aligned porous gelatin scaffolds by unidirectional freeze-drying method. Acta Biomater. 2010;6:1167–77.
37. Zhu X, Cui W, Li X, Jin Y. Electrospun fibrous mats with high porosity as potential scaffolds for skin tissue engineering. Biomacromolecules. 2008;9:1795–801.
38. Yeong WY, Sudarmadji N, Yu HY, Chua CK, Leong KF, Venkatraman SS, Boey YC, Tan LP. Porous polycaprolactone scaffold for cardiac tissue engineering fabricated by selective laser sintering. Acta Biomater. 2010;6:2028–34.
39. Cox SC, Thornby JA, Gibbons GJ, Williams MA, Mallick KK. 3D printing of porous hydroxyapatite scaffolds intended for use in bone tissue engineering applications. Mater Sci Eng C. 2015;47:237–47.

40. Dhandayuthapani B, Yoshida Y, Maekawa T, Kumar DS. Polymeric scaffolds in tissue engineering application: a review. Int J Polym Sci. 2011;2011:1–19.
41. Kleger N, Cihova M, Masania K, Studart AR, Lffler JF. 3D printing of salt as a template for magnesium with structured porosity. Adv Mater. 2019;31:1903783.
42. Silvestro I, Sergi R, Scotto d'Abusco A, Mariano A, Martinelli A, Piozzi A, Francolini I. Chitosan scaffolds with enhanced mechanical strength and elastic response by combination of freeze gelation, photo-crosslinking and freeze-drying. Carbohyd Polym. 2021;267:118156.
43. Lian M, Han Y, Sun B, Xu L, Zhang X. A multifunctional electrowritten bi-layered scaffold for guided bone regeneration. Acta Biomater. 2020;118:83–99.
44. Hossain SS, Baek IW, Son HJ, Park S, Bae CJ. 3D printing of porous low-temperature in-situ mullite ceramic using waste rice husk ash-derived silica. J Eur Ceram Soc. 2022;42:2408–19.
45. Peppas NA, Bures P, Leobandung W, Ichikawa H. Hydrogels in pharmaceutical formulations. Eur J Pharm Biopharm. 2000;50:27–46.
46. Hoffman AS. Hydrogels for biomedical applications. Adv Drug Deliv Rev. 2012;64:18–23.
47. Mahoney MJ, Anseth KS. Three-dimensional growth and function of neural tissue in degradable polyethylene glycol hydrogels. Biomaterials. 2006;27:2265–74.
48. Clapper JD, Pearce ME, Guymon CA, Salem AK. Biotinylated biodegradable nanotemplated hydrogel networks for cell interactive applications. Biomacromolecules. 2008;9:1188–94.
49. Wichterle O, Lim D. Hydrophilic gels for biological use. Nature. 1960;185:117–8.
50. Van Vlierberghe S, Dubruel P, Schacht E. Biopolymer-based hydrogels as scaffolds for tissue engineering applications: a review. Biomacromolecules. 2011;12:1387–408.
51. Vasile C, Pamfil D, Stoleru E, Baican M. New developments in medical applications of hybrid hydrogels containing natural polymers. Molecules. 2020;25:1539.
52. DeLong SA, Moon JJ, West JL. Covalently immobilized gradients of bFGF on hydrogel scaffolds for directed cell migration. Biomaterials. 2005;26:3227–34.
53. Anjum F, Lienemann PS, Metzger S, Biernaskie J, Kallos MS, Ehrbar M. Enzyme responsive GAG-based natural-synthetic hybrid hydrogel for tunable growth factor delivery and stem cell differentiation. Biomaterials. 2016;87:104–17.
54. Wegst UG, Bai H, Saiz E, Tomsia AP, Ritchie RO. Bioinspired structural materials. Nat Mater. 2015;14:23–36.
55. Singh M, Sandhu B, Scurto A, Berkland C, Detamore MS. Microsphere-based scaffolds for cartilage tissue engineering: using subcritical CO_2 as a sintering agent. Acta Biomater. 2010;6:137–43.
56. Schnepp ZA, Gonzalez-McQuire R, Mann S. Hybrid biocomposites based on calcium phosphate mineralization of self-assembled supramolecular hydrogels. Adv Mater. 2006;18:1869–72.
57. Watanabe J, Akashi M. Novel biomineralization for hydrogels: electrophoresis approach accelerates hydroxyapatite formation in hydrogels. Biomacromolecules. 2006;7:3008–11.
58. Kato T. Polymer/calcium carbonate layered thin-film composites. Adv Mater. 2000;12:1543–6.
59. Li YQ, Yu T, Yang TY, Zheng LX, Liao K. Bio-inspired nacre-like composite films based on graphene with superior mechanical, electrical, and biocompatible properties. Adv Mater. 2012;24:3426–31.
60. Hartgerink JD, Beniash E, Stupp SI. Self-assembly and mineralization of peptide-amphiphile nanofibers. Science. 2001;294:1684–8.
61. Deville S, Saiz E, Nalla RK, Tomsia AP. Freezing as a path to build complex composites. Science. 2006;311:515–8.
62. Lewis JA. Direct ink writing of 3D functional materials. Adv Funct Mater. 2006;16:2193–204.
63. Pham TA, Kim DP, Lim TW, Park SH, Yang DY, Lee KS. Three-dimensional SiCN ceramic microstructures via nano-stereolithography of inorganic polymer photoresists. Adv Funct Mater. 2006;16:1235–41.

64. Bai X, Sun Q, Cui H, Guerzoni LPB, Wuttke S, Kiessling F, De Laporte L, Lammers T, Shi Y. Controlled covalent self-assembly of a homopolymer for multiscale materials engineering. Adv Mater. 2022;34:2109701.
65. Liu T, Yin Y, Yang Y, Russell TP, Shi S. Layer-by-layer engineered all-liquid microfluidic chips for enzyme immobilization. Adv Mater. 2022;34:2105386.
66. Xue J, Gao L, Hu X, Cao K, Zhou W, Wang W, Lu Y. Stereolithographic 3D printing-based hierarchically cellular lattices for high-performance quasi-solid supercapacitor. Nanomicro Lett. 2019;11:46.
67. Amani H, Arzaghi H, Bayandori M, Dezfuli AS, Pazoki-Toroudi H, Shafiee A, Moradi L. Controlling cell behavior through the design of biomaterial surfaces: a focus on surface modification techniques. Adv Mater Interf. 2019;6:1900572.
68. Kasemo B. Biological surface science. Curr Opin Solid S T M. 1998;3:451–9.
69. Rabe M, Verdes D, Seeger S. Understanding protein adsorption phenomena at solid surfaces. Adv Colloid Interf Sci. 2011;162:87–106.
70. Vogler EA. Protein adsorption in three dimensions. Biomaterials. 2012;33:1201–37.
71. Means GE, Ampon K. Protein immobilization by adsorption of a hydrophobic amidine protein derivative to a hydrophobic surface. Google Patents; 1989.
72. Aramesh M, Shimoni O, Ostrikov K, Prawer S, Cervenka J. Surface charge effects in protein adsorption on nanodiamonds. Nanoscale. 2015;7:5726–36.
73. Hlady V, Buijs J. Protein adsorption on solid surfaces. Curr Opin Biotech. 1996;7:72–7.
74. Hollmann O, Steitz R, Czeslik C. Structure and dynamics of α-lactalbumin adsorbed at a charged brush interface. Phys Chem Chem Phys. 2008;10:1448–56.
75. Mazzucotelli J-P, Klein-Soyer C, Beretz A, Brisson C, Archipoff G, Cazenave J-P. Endothelial cell seeding: coating dacron and expanded polytetrafluoroethylene vascular grafts with a biological glue allows adhesion and growth of human saphenous vein endothelial cells. Int J Artif Organs. 1991;14:482–90.
76. Miron RJ, Bosshardt DD, Hedbom E, Zhang Y, Haenni B, Buser D, Sculean A. Adsorption of enamel matrix proteins to a bovine-derived bone grafting material and its regulation of cell adhesion, proliferation, and differentiation. J Periodontol. 2012;83:936–47.
77. Sun M, Deng J, Tang Z, Wu J, Li D, Chen H, Gao C. A correlation study of protein adsorption and cell behaviors on substrates with different densities of PEG chains. Colloids Surf B Biointerfaces. 2014;122:134–42.
78. Deng J, et al. Adsorption of fibronectin on salt-etched polyelectrolyte multilayers and its roles in mediating the adhesion and migration of vascular smooth muscle cells. Macromol Biosci. 2015;15:241–52.
79. Sun M, Deng J, Gao C. The correlation between fibronectin adsorption and attachment of vascular cells on heparinized polycaprolactone membrane. J Colloid Interface Sci. 2015;448: 231–7.
80. Liu Y, Dzidotor G, Le TT, Vinikoor T, Morgan K, Curry EJ, Das R, McClinton A, Eisenberg E, Apuzzo LN, Tran KTM, Prasad P, Flanagan TJ, Lee SW, Kan HM, Chorsi MT, Lo KWH, Laurencin CT, Nguyen TD. Exercise-induced piezoelectric stimulation for cartilage regeneration in rabbits. Sci Transl Med. 2022;14:eabi7282.
81. Zhou R, Wu Y, Chen K, Zhang D, Chen Q, Zhang D, She Y, Zhang W, Liu L, Zhu Y, Gao C, Liu R. A polymeric strategy empowering vascular cell selectivity and potential application superior to extracellular matrix peptides. Adv Mater. 2022;34:2200464.
82. Ma C, Kuzma ML, Bai X, Yang J. Biomaterial-based metabolic regulation in regenerative engineering. Adv Sci. 2019;6:1900819.
83. Gunawan RC, Silvestre J, Gaskins HR, Kenis PJ, Leckband DE. Cell migration and polarity on microfabricated gradients of extracellular matrix proteins. Langmuir. 2006;22:4250–8.
84. Martin P. Wound healing—aiming for perfect skin regeneration. Science. 1997;276:75–81.
85. Lin S, Sangaj N, Razafiarison T, Zhang C, Varghese S. Influence of physical properties of biomaterials on cellular behavior. Pharm Res. 2011;28:1422–30.

86. Park H-J, Park HJ, Hong H, Thangam R, Song M-G, Kim J-E, Jo E-H, Jang Y-J, Choi W-H, Lee M-Y, Kang H, Lee KB. Static and dynamic biomaterial engineering for cell modulation. Nanomaterials (Basel). 2022;12:1377.
87. Wu J, Mao Z, Tan H, Han L, Ren T, Gao C. Gradient biomaterials and their influences on cell migration. Interface Focus. 2012;2:337–55.
88. Shin YN, et al. Adhesion comparison of human bone marrow stem cells on a gradient wettable surface prepared by corona treatment. Appl Surf Sci. 2008;255:293–6.
89. Gijsman P, Meijers G, Vitarelli G. Comparison of the UV-degradation chemistry of polypropylene, polyethylene, polyamide 6 and polybutylene terephthalate. Polym Degrad Stabil. 1999;65:433–41.
90. Li B, Ma Y, Wang S, Moran PM. A technique for preparing protein gradients on polymeric surfaces: effects on PC12 pheochromocytoma cells. Biomaterials. 2005;26:1487–95.
91. Whittle JD, Barton D, Alexander MR, Short RD. A method for the deposition of controllable chemical gradients. Chem Commun. 2003;14:1766–7.
92. Spijker HT, Bos R, van Oeveren W, de Vries J, Busscher HJ. Protein adsorption on gradient surfaces on polyethylene prepared in a shielded gas plasma. Colloid Surf B Biointerfaces. 1999;15:89–97.
93. Zhu Y, Gao C, Liu X, He T, Shen J. Immobilization of biomacromolecules onto aminolyzed poly (L-lactic acid) toward acceleration of endothelium regeneration. Tissue Eng. 2004;10:53–61.
94. Zhu Y, Gao C, He T, Shen J. Endothelium regeneration on luminal surface of polyurethane vascular scaffold modified with diamine and covalently grafted with gelatin. Biomaterials. 2004;25:423–30.
95. Han L, Mao Z, Wu J, Guo Y, Ren T, Gao C. Directional cell migration through cell–cell interaction on polyelectrolyte multilayers with swelling gradients. Biomaterials. 2013;34:975–84.
96. Du W, Gao C. Selective adhesion and directional migration of endothelial cells guided by Cys-Ala-Gly peptide density gradient on antifouling polymer brushes. Macromol Biosci. 2019;19:1900292.
97. Xue P, Liu W, Gu Z, Chen X, Nan J, Zhang J, Sun H, Cui Z, Yang B. Graded protein/PEG nanopattern arrays: well-defined gradient biomaterials to induce basic cellular behaviors. ACS Appl Mater Interface. 2019;11:1595–603.
98. Rasi Ghaemi S, Delalat B, Cavallaro A, Mierczynska-Vasilev A, Vasilev K, Voelcker NH. Differentiation of rat mesenchymal stem cells toward osteogenic lineage on extracellular matrix protein gradients. Adv Healthc Mater. 2019;8:1900595.
99. Yu X, Wang Z, Jiang Y, Zhang X. Surface gradient material: from superhydrophobicity to superhydrophilicity. Langmuir. 2006;22:4483–6.
100. Li L, Zhu Y, Li B, Gao C. Fabrication of thermoresponsive polymer gradients for study of cell adhesion and detachment. Langmuir. 2008;24:13632–9.
101. Morgenthaler S, Lee S, Zürcher S, Spencer ND. A simple, reproducible approach to the preparation of surface-chemical gradients. Langmuir. 2003;19:10459–62.
102. Ren T, Mao Z, Guo J, Gao C. Directional migration of vascular smooth muscle cells guided by a molecule weight gradient of poly (2-hydroxyethyl methacrylate) brushes. Langmuir. 2013;29:6386–95.
103. Tu C, Zhou T, Deng L, Gao C. Fabrication of poly(PEGMA) surface with controllable thickness gradient and its mediation on the gradient adhesion of cells. J Appl Polym Sci. 2021;138:50463.
104. Woodfield T, Blitterswijk CV, Wijn JD, Sims T, Hollander A, Riesle J. Polymer scaffolds fabricated with pore-size gradients as a model for studying the zonal organization within tissue-engineered cartilage constructs. Tissue Eng. 2005;11:1297–311.
105. Oh SH, Park IK, Kim JM, Lee JH. In vitro and in vivo characteristics of PCL scaffolds with pore size gradient fabricated by a centrifugation method. Biomaterials. 2007;28:1664–71.

106. Oh SH, Kim TH, Lee JH. Creating growth factor gradients in three dimensional porous matrix by centrifugation and surface immobilization. Biomaterials. 2011;32:8254–60.
107. Gao F, Xu Z, Liang Q, Liu B, Li H, Wu Y, Zhang Y, Lin Z, Wu M, Ruan C, Liu W. Direct 3D printing of high strength biohybrid gradient hydrogel scaffolds for efficient repair of osteochondral defect. Adv Funct Mater. 2018;28:1706644.
108. Motealleh A, Çelebi-Saltik B, Ermis N, Nowak S, Khademhosseini A, Kehr NS. 3D printing of step-gradient nanocomposite hydrogels for controlled cell migration. Biofabrication. 2019;11:045015.
109. Wu KH, Liu YL, Zhou B, Han ZC. Cellular therapy and myocardial tissue engineering: the role of adult stem and progenitor cells. Eur J Cardiothorac Surg. 2006;30:770–81.
110. Wertheim JA, Baptista PM, Soto-Gutierrez A. Cellular therapy and bioartificial approaches to liver replacement. Curr Opin Organ Transplant. 2012;17:235.
111. Andrzejewska A, Lukomska B, Janowski M. Concise review: mesenchymal stem cells: from roots to boost. Stem Cells. 2019;37:855–64.
112. Wei X, Yang X, Han Z-p, Qu F-f, Shao L, Shi Y-f. Mesenchymal stem cells: a new trend for cell therapy. Acta Pharmacol Sin. 2013;34:747–54.
113. Robinton DA, Daley GQ. The promise of induced pluripotent stem cells in research and therapy. Nature. 2012;481:295–305.
114. Trappmann B, Gautrot JE, Connelly JT, Strange DG, Li Y, Oyen ML, Cohen Stuart MA, Boehm H, Li B, Vogel V, Spatz JP, Watt FM, Huck WT. Extracellular-matrix tethering regulates stem-cell fate. Nat Mater. 2012;11:642–9.
115. Dalby MJ, Gadegaard N, Oreffo RO. Harnessing nanotopography and integrin–matrix interactions to influence stem cell fate. Nature Mater. 2014;13:558–69.
116. Lee J, Abdeen AA, Zhang D, Kilian KA. Directing stem cell fate on hydrogel substrates by controlling cell geometry, matrix mechanics and adhesion ligand composition. Biomaterials. 2013;34:8140–8.
117. Khetan S, Guvendiren M, Legant WR, Cohen DM, Chen CS, Burdick JA. Degradation-mediated cellular traction directs stem cell fate in covalently crosslinked three-dimensional hydrogels. Nat Mater. 2013;12:458–65.
118. Lin X, Kong B, Zhu Y, Zhao Y. Bioactive fish scale scaffolds with MSCs-loading for skin flap regeneration. Adv Sci. 2022;9:2201226.
119. Li R, Liu Z, Pan Y, Chen L, Zhang Z, Lu L. Peripheral nerve injuries treatment: a systematic review. Cell Biochem Biophys. 2014;68:449–54.
120. Lundborg G. Alternatives to autologous nerve grafts. Handchir Mikrochir Plast Chir. 2004;37:1–7.
121. Huang YC, Huang YY. Biomaterials and strategies for nerve regeneration. Artif Organs. 2006;30:514–22.
122. Yoshii S, Oka M. Collagen filaments as a scaffold for nerve regeneration. J Biomed Mater Res. 2001;56:400–5.
123. Khaing ZZ, Schmidt CE. Advances in natural biomaterials for nerve tissue repair. Neurosci Lett. 2012;519:103–14.
124. Prasopthum A, Cooper M, Shakesheff KM, Yang J. Three-dimensional printed scaffolds with controlled micro−/nanoporous surface topography direct chondrogenic and osteogenic differentiation of mesenchymal stem cells. ACS Appl Mater Interface. 2019;11:18896–906.
125. Bao M, Bao M, Xie J, Katoele N, Hu X, Wang B, Piruska A, Huck WTS. Cellular volume and matrix stiffness direct stem cell behavior in a 3D microniche. ACS Appl Mater Interface. 2018;11:1754–9.
126. Hou Y, Xie W, Yu L, Camacho LC, Nie C, Zhang M, Haag R, Wei Q. Surface roughness gradients reveal topography-specific mechanosensitive responses in human mesenchymal stem cells. Small. 2020;16:e1905422.
127. Meek MF, Coert JH. US Food and Drug Administration/Conformit Europe-approved absorbable nerve conduits for clinical repair of peripheral and cranial nerves. Ann Plast Surg. 2008;60:110–6.

128. Kehoe S, Zhang X, Boyd D. FDA approved guidance conduits and wraps for peripheral nerve injury: a review of materials and efficacy. Injury. 2012;43:553–72.
129. Spivey EC, Khaing ZZ, Shear JB, Schmidt CE. The fundamental role of subcellular topography in peripheral nerve repair therapies. Biomaterials. 2012;33:4264–76.
130. Wang HB, Mullins ME, Cregg JM, Hurtado A, Oudega M, Trombley MT, Gilbert RJ. Creation of highly aligned electrospun poly-L-lactic acid fibers for nerve regeneration applications. J Neural Eng. 2008;6:016001.
131. Syed N, Jullien G. Electrically stimulating nerve regeneration. Google Patents; 2006.
132. Lee JY, Bashur CA, Goldstein AS, Schmidt CE. Polypyrrole-coated electrospun PLGA nanofibers for neural tissue applications. Biomaterials. 2009;30:4325–35.
133. Jin F, Li T, Wei Z, Xiong R, Qian L, Ma J, Yuan T, Wu Q, Lai C, Ma X, Wang F, Zhao Y, Sun F, Wang T, Feng ZQ. Biofeedback electrostimulation for bionic and long-lasting neural modulation. Nat Commun. 2022;13:5302.
134. Ferrati G, Bion G, Harris AJ, Greenfield S. Protective and reversal actions of a novel peptidomimetic against a pivotal toxin implicated in Alzheimer's disease. Biomed Pharmacother. 2019;109:1052–61.
135. Zhang D, Wu S, Feng J, Duan Y, Xing D, Gao C. Micropatterned biodegradable polyesters clicked with CQAASIKVAV promote cell alignment, directional migration, and neurite outgrowth. Acta Biomater. 2018;74:143–55.
136. Silantyeva EA, Nasir W, Carpenter J, Manahan O, Becker ML, Willits RK. Accelerated neural differentiation of mouse embryonic stem cells on aligned GYIGSR-functionalized nanofibers. Acta Biomater. 2018;75:129–39.
137. Jackson DW, Scheer MJ, Simon TM. Cartilage substitutes: overview of basic science and treatment options. J Am Acad Orthop Surg. 2001;9:37–52.
138. Langer R, Vacanti J. Advances in tissue engineering. J Pediatr Surg. 2016;51:8–12.
139. Vacanti CA. History of tissue engineering and a glimpse into its future. Tissue Eng. 2006;12:1137–42.
140. Johnson K, Zhu S, Tremblay MS, Payette JN, Wang J, Bouchez LC, Meeusen S, Althage A, Cho CY, Wu X, Schultz PG. A stem cell–based approach to cartilage repair. Science. 2012;336:717–21.
141. Crawford DC, Heveran CM, Cannon WD, Foo LF, Potter HG. An autologous cartilage tissue implant neo cart for treatment of grade III chondral injury to the distal femur: prospective clinical safety trial at 2 years. Am J Sport Med. 2009;37:1334–43.
142. Gobbi A, Kon E, Berruto M, Francisco R, Filardo G, Marcacci M. Patellofemoral full-thickness chondral defects treated with Hyalograft-C: a clinical, arthroscopic, and histologic review. Am J Sport Med. 2006;34:1763–73.
143. Li P, Fu L, Liao Z, Peng Y, Ning C, Gao C, Zhang D, Sui X, Lin Y, Liu S, Hao C, Guo Q. Chitosan hydrogel/3D-printed poly (ε-caprolactone) hybrid scaffold containing synovial mesenchymal stem cells for cartilage regeneration based on tetrahedral framework nucleic acid recruitment. Biomaterials. 2021;278:121131.
144. Tuan RS, Chen AF, Klatt BA. Cartilage regeneration. J Am Acad Orthop Surg. 2013;21:303.
145. Sun Y, You Y, Jiang W, Wang B, Wu Q, Dai K. 3D bioprinting dual-factor releasing and gradient-structured constructs ready to implant for anisotropic cartilage regeneration. Sci Adv. 2020;6:eaay1422.
146. Böttcher-Haberzeth S, Biedermann T, Reichmann E. Tissue engineering of skin. Burns. 2010;36:450–60.
147. Boyce ST. Design principles for composition and performance of cultured skin substitutes. Burns. 2001;27:523–33.
148. Ma L, Gao C, Mao Z, Zhou J, Shen J, Hu X, Han C. Collagen/chitosan porous scaffolds with improved biostability for skin tissue engineering. Biomaterials. 2003;24:4833–41.
149. Wang J, Lin J, Chen L, Deng L, Cui W. Endogenous electric-field-coupled electrospun short fiber via collecting wound exudation. Adv Mater. 2022;34:2108325.

150. Patil P, Russo KA, McCune JT, Pollins AC, Cottam MA, Dollinger BR, DeJulius CR, Gupta MK, D'Arcy R, Colazo JM, Yu F, Bezold MG, Martin JR, Cardwell NL, Davidson JM, Thompson CM, Barbul A, Hasty AH, Guelcher SA, Duvall CL. Reactive oxygen species–degradable polythioketal urethane foam dressings to promote porcine skin wound repair. Sci Transl Med. 2022;14:eabm6586.
151. Cui T, Yu J, Li Q, Wang CF, Chen S, Li W, Wang G. Large-scale fabrication of robust artificial skins from a biodegradable sealant-loaded nanofiber scaffold to skin tissue via microfluidic blow-spinning. Adv Mater. 2020;32:2000982.
152. Wang X, Yu Y, Yang C, Shang L, Zhao Y, Shen X. Dynamically responsive scaffolds from microfluidic 3D printing for skin flap regeneration. Adv Sci. 2022;9:e2201155.
153. Ming Z, Han L, Bao M, Zhu H, Qiang S, Xue S, Liu W. Living bacterial hydrogels for accelerated infected wound healing. Adv Sci. 2021;8:2102545.
154. Zhou G, Chang W, Zhou X, Chen Y, Dai F, Anwar A, Yu X. Nanofibrous nerve conduits with nerve growth factors and bone marrow stromal cells pre-cultured in bioreactors for peripheral nerve regeneration. ACS Appl Mater Interface. 2020;12:16168–77.
155. Li R, Li D, Wu C, Ye L, Wu Y, Yuan Y, Yang S, Xie L, Mao Y, Jiang T, Li Y, Wang J, Zhang H, Li X, Xiao J. Nerve growth factor activates autophagy in Schwann cells to enhance myelin debris clearance and to expedite nerve regeneration. Theranostics. 2020;10:1649–77.
156. Chang Y-C, Chen M-H, Liao S-Y, Wu H-C, Kuan C-H, Sun J-S, Wang T-W. Multichanneled nerve guidance conduit with spatial gradients of neurotrophic factors and oriented nanotopography for repairing the peripheral nervous system. ACS Appl Mater Interface. 2017;9:37623–36.
157. Zhang D, Li Z, Shi H, Yao Y, Du W, Lu P, Liang K, Hong L, Gao C. Micropatterns and peptide gradient on the inner surface of a guidance conduit synergistically promotes nerve regeneration in vivo. Bioact Mater. 2022;9:134–46.
158. Vara DS, Salacinski HJ, Kannan RY, Bordenave L, Hamilton G, Seifalian AM. Cardiovascular tissue engineering: state of the art. Pathol Biol. 2005;53:599–612.
159. Nemeno-Guanzon JG, Lee S, Berg JR, Jo YH, Yeo JE, Nam BM, Koh YG, Lee JI. Trends in tissue engineering for blood vessels. J Biomed Biotechnol. 2012;2012:956345.
160. He S, Xia T, Wang H, Wei L, Luo X, Li X. Multiple release of polyplexes of plasmids VEGF and bFGF from electrospun fibrous scaffolds towards regeneration of mature blood vessels. Acta Biomater. 2012;8:2659–69.
161. Quint C, Kondo Y, Manson RJ, Lawson JH, Dardik A, Niklason LE. Decellularized tissue-engineered blood vessel as an arterial conduit. Proc Natl Acad Sci. 2011;108:9214–9.
162. Simionescu DT, Lu Q, Song Y, Lee JS, Rosenbalm TN, Kelley C, Vyavahare NR. Biocompatibility and remodeling potential of pure arterial elastin and collagen scaffolds. Biomaterials. 2006;27:702–13.
163. Badhe RV, Bijukumar D, Chejara DR, Mabrouk M, Choonara YE, Kumar P, du Toit LC, Kondiah PPD, Pillay V. A composite chitosan-gelatin bi-layered, biomimetic macroporous scaffold for blood vessel tissue engineering. Carbohyd Polym. 2017;157:1215–25.
164. Wu H-C, Wang T-W, Kang P-L, Tsuang Y-H, Sun J-S, Lin F-H. Coculture of endothelial and smooth muscle cells on a collagen membrane in the development of a small-diameter vascular graft. Biomaterials. 2007;28:1385–92.
165. Zhu C, Fan D, Wang Y. Human-like collagen/hyaluronic acid 3D scaffolds for vascular tissue engineering. Mater Sci Eng C. 2014;34:393–401.
166. Lopera Higuita M, Griffiths LG. Small diameter xenogeneic extracellular matrix scaffolds for vascular applications. Tissue Eng Part B Rev. 2020;26:26–45.
167. Xing Q, Yates K, Tahtinen M, Shearier E, Qian Z, Zhao F. Decellularization of fibroblast cell sheets for natural extracellular matrix scaffold preparation. Tissue Eng Part C Methods. 2015;21:77–87.
168. Fernandez CE, Achneck HE, Reichert WM, Truskey GA. Biological and engineering design considerations for vascular tissue engineered blood vessels (TEBVs). Curr Opin Chem Eng. 2014;3:83–90.

169. Wang Y, Gallant RC, Ni H. Extracellular matrix proteins in the regulation of thrombus formation. Curr Opin Hematol. 2016;23:280–7.
170. Bastijanic JM, Kligman FL, Marchant RE, Kottke-Marchant K. Dual biofunctional polymer modifications to address endothelialization and smooth muscle cell integration of ePTFE vascular grafts. J Biomed Mater Res A. 2016;104:71–81.
171. Choi WS, Joung YK, Lee Y, Bae JW, Park HK, Park YH, Park JC, Park KD. Enhanced patency and endothelialization of small-caliber vascular grafts fabricated by coimmobilization of heparin and cell-adhesive peptides. ACS Appl Mater Interfaces. 2016;8:4336–46.
172. Tsai T-N, Kirton JP, Campagnolo P, Zhang L, Xiao Q, Zhang Z, Wang W, Hu Y, Xu Q. Contribution of stem cells to neointimal formation of decellularized vessel grafts in a novel mouse model. Am J Pathol. 2012;181:362–73.
173. Mahara A, Somekawa S, Kobayashi N, Hirano Y, Kimura Y, Fujisato T, Yamaoka T. Tissue-engineered acellular small diameter long-bypass grafts with neointima-inducing activity. Biomaterials. 2015;58:54–62.
174. Haghjooy Javanmard S, Anari J, Zargar Kharazi A, Vatankhah E. In vitro hemocompatibility and cytocompatibility of a three-layered vascular scaffold fabricated by sequential electrospinning of PCL, collagen, and PLLA nanofibers. J Biomater Appl. 2016;31:438–49.
175. Catto V, Farè S, Freddi G, Tanzi MC. Vascular tissue engineering: recent advances in small diameter blood vessel regeneration. Int Sch Res Notices. 2014;2014:1–27.
176. Zheng Z, Tan Y, Li Y, Liu Y, Yi G, Yu CY, Wei H. Biotherapeutic-loaded injectable hydrogels as a synergistic strategy to support myocardial repair after myocardial infarction. J Control Release. 2021;335:216–36.
177. Hinderer S, Brauchle E, Schenke-Layland K. Generation and assessment of functional biomaterial scaffolds for applications in cardiovascular tissue engineering and regenerative medicine. Adv Healthc Mater. 2015;4:2326–41.
178. Jaganathan SK, Supriyanto E, Murugesan S, Balaji A, Asokan MK. Biomaterials in cardiovascular research: applications and clinical implications. Bio Med Res Int. 2014;2014:1–11.
179. Kim TG, Shin H, Lim DW. Biomimetic scaffolds for tissue engineering. Adv Funct Mater. 2012;22:2446–68.
180. Haraguchi Y, Shimizu T, Yamato M, Okano T. Concise review: cell therapy and tissue engineering for cardiovascular disease. Stem Cells Transl Med. 2012;1:136–41.
181. Habib M, Shapira-Schweitzer K, Caspi O, Gepstein A, Arbel G, Aronson D, Seliktar D, Gepstein L. A combined cell therapy and in-situ tissue-engineering approach for myocardial repair. Biomaterials. 2011;32:7514–23.
182. Wang H, Shi J, Wang Y, Yin Y, Wang L, Liu J, Liu Z, Duan C, Zhu P, Wang C. Promotion of cardiac differentiation of brown adipose derived stem cells by chitosan hydrogel for repair after myocardial infarction. Biomaterials. 2014;35:3986–98.
183. Liu Z, Wang H, Wang Y, Lin Q, Yao A, Cao F, Li D, Zhou J, Duan C, Du Z, Wang Y, Wang C. The influence of chitosan hydrogel on stem cell engraftment, survival and homing in the ischemic myocardial microenvironment. Biomaterials. 2012;33:3093–106.
184. Zhang X, Wang H, Ma X, Adila A, Wang B, Liu F, Chen B, Wang C, Ma Y. Preservation of the cardiac function in infarcted rat hearts by the transplantation of adipose-derived stem cells with injectable fibrin scaffolds. Exp Biol Med. 2010;235:1505–15.
185. Parenteau-Bareil R, Gauvin R, Berthod F. Collagen-based biomaterials for tissue engineering applications. Materials. 2010;3:1863–87.
186. Leor J, Cohen S. Myocardial tissue engineering: creating a muscle patch for a wounded heart. Ann N Y Acad Sci. 2004;1015:312–9.
187. Jiang X, Feng T, An B, Ren S, Meng J, Li K, Liu S, Wu H, Zhang H, Zhong C. A bi-layer hydrogel cardiac patch made of recombinant functional proteins. Adv Mater. 2022;4:2201411.
188. Liang S, Zhang Y, Wang H, Xu Z, Chen J, Bao R, Tan B, Cui Y, Fan G, Wang W, Wang W, Liu W. Paintable and rapidly bondable conductive hydrogels as therapeutic cardiac patches. Adv Mater. 2018;30:1704235.

189. Khan M, Sridharan D, Kumar N, Palaniappan A, Dougherty JA, Isai DG, Czirok A, Powell H. 3d-engineered aligned co-axial nanofibrous cardiac patch for drug screening and cardiac repair applications. Circ Res. 2020;127:A396.
190. Menasché P, Hagège AA, Scorsin M, Pouzet B, Desnos M, Duboc D, Schwartz K, Vilquin JT, Marolleau JP. Myoblast transplantation for heart failure. Lancet. 2001;357:279–80.
191. Takahashi K, Tanabe K, Ohnuki M, Narita M, Ichisaka T, Tomoda K, Yamanaka S. Induction of pluripotent stem cells from adult human fibroblasts by defined factors. Cell. 2007;131:861–72.
192. Kehat I, Kenyagin-Karsenti D, Snir M, Segev H, Amit M, Gepstein A, Livne E, Binah O, Itskovitz-Eldor J, Gepstein L. Human embryonic stem cells can differentiate into myocytes with structural and functional properties of cardiomyocytes. J Clin Invest. 2001;108:407–14.
193. Alaiti MA, Ishikawa M, Costa MA. Bone marrow and circulating stem/progenitor cells for regenerative cardiovascular therapy. Transl Res. 2010;156:112–29.
194. Soejitno A, Wihandani DM, Kuswardhani R. Clinical applications of stem cell therapy for regenerating the heart. Acta Med Indones. 2010;42:243–57.
195. Abdel-Latif A, Bolli R, Tleyjeh IM, Montori VM, Perin EC, Hornung CA, Zuba-Surma EK, Al-Mallah M, Dawn B. Adult bone marrow–derived cells for cardiac repair: a systematic review and meta-analysis. Arch Int Med. 2007;167:989–97.
196. Lipinski MJ, Biondi-Zoccai GG, Abbate A, Khianey R, Sheiban I, Bartunek J, Vanderheyden M, Kim HS, Kang HJ, Strauer BE, Vetrovec GW. Impact of intracoronary cell therapy on left ventricular function in the setting of acute myocardial infarction: a collaborative systematic review and meta-analysis of controlled clinical trials. J Am Coll Cardiol. 2007;50:1761–7.
197. Martin-Rendon E, Brunskill SJ, Hyde CJ, Stanworth SJ, Mathur A, Watt SM. Autologous bone marrow stem cells to treat acute myocardial infarction: a systematic review. Eur Heart J. 2008;29:1807–18.
198. Zhang M, Methot D, Poppa V, Fujio Y, Walsh K, Murry CE. Cardiomyocyte grafting for cardiac repair: graft cell death and anti-death strategies. J Mol Cell Cardiol. 2001;33:907–21.
199. Hofmann M, Wollert KC, Meyer GP, Menke A, Arseniev L, Hertenstein B, Ganser A, Knapp WH, Drexler H. Monitoring of bone marrow cell homing into the infarcted human myocardium. Circulation. 2005;111:2198–202.
200. Peck M, Gebhart D, Dusserre N, McAllister TN, L'Heureux N. The evolution of vascular tissue engineering and current state of the art. Cells Tissues Organs. 2012;195:144–58.
201. Jiang Z, et al. Genetically modified cell sheets in regenerative medicine and tissue engineering. Biomaterials. 2021;275:120908.
202. Viola JM, Porter CM, Gupta A, Alibekova M, Prahl LS, Hughes AJ. Guiding cell network assembly using shape-morphing hydrogels. Adv Mater. 2020;32:2002195.
203. Wang H, Feng Z, Xu B. Intercellular instructed-assembly mimics protein dynamics to induce cell spheroids. J Am Chem Soc. 2019;141:7271–4.
204. Takahashi H, Okano T. Thermally-triggered fabrication of cell sheets for tissue engineering and regenerative medicine. Adv Drug Deliv Rev. 2019;138:276–92.
205. Araki K, Miyagawa S, Kawamura T, Ishii R, Harada A, Ueno T, Toda K, Sawa Y. Autologous skeletal myoblast patch remodeled swine pressure-overloaded right heart by amelioration in myocardial ischemia. Circulation. 2020;142:A13717.
206. Sodian R, Hoerstrup SP, Sperling JS, Daebritz SH, Martin DP, Schoen FJ, Vacanti JP, Mayer JE Jr. Tissue engineering of heart valves: in vitro experiences. Ann Thorac Surg. 2000;70:140–4.
207. Schenke-Layland K, et al. Complete dynamic repopulation of decellularized heart valves by application of defined physical signals—an in vitro study. Cardiovasc Res. 2003;60:497–509.
208. Berry JL, Steen JA, Koudy Williams J, Jordan JE, Atala A, Yoo JJ. Bioreactors for development of tissue engineered heart valves. Ann Biomed Eng. 2010;38:3272–9.

Part I
Structural Scaffolds and Bio-activation

Chapter 2
Polymeric and Biomimetic ECM Scaffolds for Tissue Engineering Applications

Guoping Chen and Naoki Kawazoe

Abstract Porous scaffolds can provide temporary biomimetic microenvironments to control cell functions and to guide new tissue regeneration. Many methods have been developed to prepare porous scaffolds of biodegradable polymers and acellular extracellular matrix (ECM) for tissue engineering applications. Ice particulate method and sacrificial template method have been used to prepared scaffolds with well-controlled pore structures such as open surface pores and interconnected bulk pores for easy cell seeding, migration, and distribution. Porous scaffolds with interconnected pore structure, funnel-like structure, and micropatterned structures have been prepared by these methods. Composite scaffolds of biodegradable synthetic polymers and naturally derived polymers have been prepared by hybridization method to combine the advantages of each type of polymers. Furthermore, cell-derived biomimetic ECM scaffolds have been prepared by cell culture method. Composition of the ECM scaffolds can be adjusted by using different type of cells or controlling the differentiation of stem cells. This chapter features and summarizes the details of these methods and scaffolds.

Keywords Polymer scaffold · Porous scaffold · Biodegradable polymer · Synthetic polymer · Naturally derived polymer · Pore structure · Funnel-like structure · ECM scaffold · Biomimetic · Micropatterned structure · Tissue engineering

2.1 Introduction

Polymeric and biomimetic scaffolds have been a broad application in tissue engineering to control cell functions and to provide temporary support for the regeneration of functional new tissues and organs [1–3]. The scaffolds can be prepared from biodegradable polymers, either synthetic or naturally derived. The most frequently

G. Chen (✉) · N. Kawazoe
Research Center for Macromolecules and Biomaterials, National Institute for Materials Science, Tsukuba, Ibaraki, Japan
e-mail: Guoping.CHEN@nims.go.jp

C. Gao (ed.), *Polymeric Biomaterials for Tissue Regeneration*,
https://doi.org/10.1007/978-981-99-6948-7_2

used biodegradable synthetic polymers for tissue engineering are aliphatic polyesters, such as poly(glycolic acid) (PGA), poly(lactic acid) (PLA), poly(lactic acid-*co*-glycolic acid) (PLGA), and poly(ε-caprolactone) (PCL). Naturally derived polymers are produced from living organisms and can be categorized as proteins, polysaccharides, polyhydroxyalkanoates, and polynucleotides. The first two categories are usually used to prepare porous scaffolds, which are usually modified or cross-linked to control their degradation to support cell culture and tissue formation. Acellular matrices are also very useful scaffolds for tissue engineering because of their similarity to the in vivo microenvironments [4, 5].

Scaffolds can be prepared by many methods, such as particle leaching, freeze-drying, phase separation, gas foaming, electrospinning, fiber bonding, and 3D printing [6]. The nano- and microstructures of scaffolds can be tailored for specific tissue engineering applications. The physical and biochemical properties of scaffolds can affect the functions of cells cultured in vitro or in vivo. Porous scaffolds with a variety of nano- and microstructure, mechanical property, and biochemical composition have been prepared by these methods.

Scaffold properties have diverse influences on cell functions. The pore structure of scaffolds can affect the cell behaviors, such as distribution, migration, assembly, and tissue formation [7, 8]. Open pore structure of scaffolds is the premise to enable homogeneous cell seeding and homogenous tissue formation. Scaffolds with isotropic and open pore structure enable a homogeneous distribution of cells and formation of a homogenous tissue.

Chemical composition of scaffolds can also greatly affect cell functions. Cell adhesion and spreading are usually more promoted by naturally derived polymer scaffolds compared with synthetic polymer scaffolds. Cells in normal tissue are surrounded with ECM which serves as a substrate to modulate cell behaviors. ECM of normal tissue has multiple components, such as collagen, laminin, aggrecan, hyaluronic acid, and fibronectin. Scaffolds with a similar composition to that of normal tissue ECM should benefit cell proliferation and tissue formation [9]. This chapter introduces the methods to prepare polymer porous scaffolds with well-controlled microporous structures, hybrid scaffolds of biodegradable synthetic polymers and naturally derived polymers, and cell-derived biomimetic ECM scaffolds.

2.2 Scaffolds Prepared with Free Ice Particulates

Scaffolds used for tissue engineering should have an adequate microporous structure for enabling cellular penetration into the construct to obtain a desirable cell distribution. Although many three-dimensional porous scaffolds have been developed from biodegradable polymers, their pore structures should be controlled to make their surface pores open and bulk pores interconnected. When porous scaffolds are used for cell seeding and 3D cell culture, cells are easily allocated and distributed in the peripheral areas which results in nonhomogeneous cell distribution and partial

tissue formation in the outermost peripheral layers of the scaffolds. Open pore structure is required to guarantee smooth entry of cells into the inner pores of the scaffolds during cell seeding. Meanwhile, pore interconnectivity is required to allow cells for free movement to reach all the pores throughout the scaffolds.

There are a few methods that have been developed for controlling various aspects of the pore structures, such as pore size, porosity, and interconnectivity of the scaffolds [10–13]. Among these methods, the porogen-leaching method offers many advantages for the easy manipulation and control of pore size and porosity. In this method, the porogen materials can leave replica pores after leaching. Selection of porogen materials is important to decide the pore structures. Isolated particles of porogen materials may result in the formation of isolated pores, a situation which is not desirable for tissue engineering scaffolds. To improve pore interconnectivity, the porogen materials are bonded before mixing them with polymer matrix [14, 15]. However, the bonded porogen materials require organic solvents for leaching and the residual solvents are toxic to cells. Mixing of polymer solution with the bonded porogen materials becomes difficult if the polymer solution has a high viscosity. To overcome these problems, an approach using free ice particulates as a porogen material has been developed [11, 16, 17]. Many porous scaffolds and their composites have been prepared by this method [18–27].

In the ice particulate method, free ice particulates are at first prepared. Free ice particulates can be easily prepared by spraying or injecting water into liquid nitrogen through a sprayer or capillary. Free ice particulates formed by spraying method are spherical. Their diameters can be controlled by the spraying speed. The ice particulates can be sieved by sieves with different mesh pores under low temperatures to obtain ice particulates with desired diameters. Subsequently, the free ice particulates are homogenously mixed with polymer solution. The mixing temperature is set at a temperature where the ice particulates do not melt and polymer solution does not freeze. Finally, the mixture is frozen and freeze-dried to form porous structures. Ice particulates can be easily and completely removed by freeze-drying. The porous scaffolds are cross-linked after freeze-drying if the polymers are water soluble. During the preparation procedures, the pre-prepared free ice particulates not only work as porogens to control the pore size and porosity, but also work as nuclei to initiate the formation of new ice crystals during freezing process if polymer aqueous solution is used. Pore structure is decided by both the free ice particulates and the newly formed ice crystals. The newly formed ice crystals can increase the pore interconnectivity if they grow and extend from the pre-prepared free ice particulates.

Collagen porous scaffolds have been prepared by this method [11]. Free ice particulates having diameters of 150–250, 250–355, 355–425, and 425–500 μm are used to control the bulk pore structures of collagen scaffolds. Gross appearance and microstructures of the collagen porous scaffolds prepared with 2 (w/v)% collagen and free ice particulates at a ratio of 50:50 (w/v, ice particulates/collagen solution) are shown in Fig. 2.1. The collagen porous scaffolds have large spherical pores and small pores. The small pores surround the large spherical pores, and are located on the walls of large pores. The large spherical pores are evenly distributed and well stacked. The small pores on the walls of large pores connect the large pores,

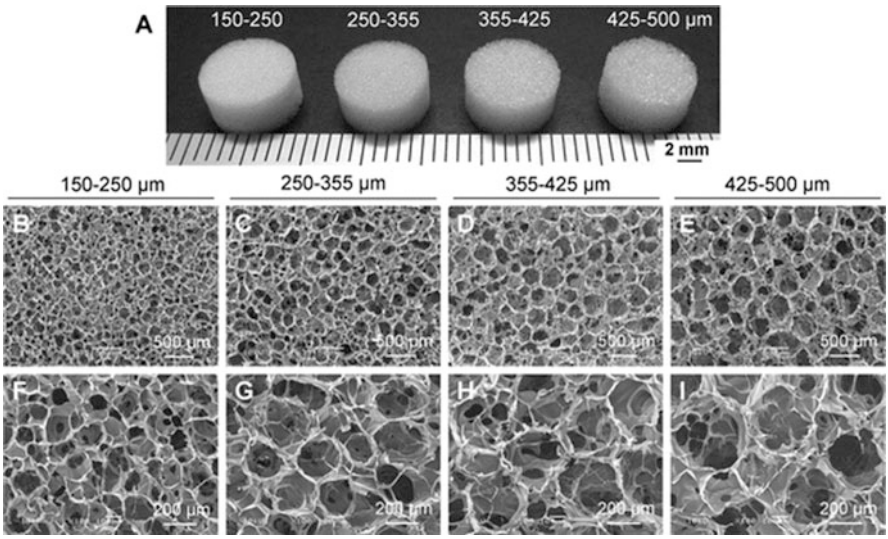

Fig. 2.1 Gross appearances (**a**) and SEM micrographs (**b**–**i**) of the cross-sections of four types of collagen porous scaffolds prepared with ice particulates having diameter ranges of 150–250 (**b**, **f**), 250–355 (**c**, **g**), 355–425 (**d**, **h**), and 425–500 μm (**e**, **i**) at low (**b**–**e**) and high (**f**–**i**) magnifications. (Adapted from Ref. [11] with permission from Elsevier)

making the scaffold well interconnected. The size and density of large pores are dependent on the size and ratio of free ice particulates used to prepare the scaffolds because they are the negative replicas of the free ice particulates. The small pores are the negative replicas of ice crystals that are formed during freezing, which size is dependent upon the freezing temperature. When the collagen porous scaffolds are used for culture of bovine articular chondrocytes, cells can be easily seeded and homogenously distributed throughout the scaffolds. The homogenous cell distribution in the four types of collagen porous scaffolds should be due to the good interconnectivity of the scaffolds. The interconnectivity among the spherical large pores facilitates the smooth delivery of cells in the scaffolds to each corner of the scaffolds.

The ratio of ice particulates and collagen concentration has some influence on the pore structure and mechanical property of collagen porous scaffolds. When collagen porous scaffolds prepared with 25, 50, and 75 (v/w)% ice particulates having a diameter from 335 to 425 μm are compared, the large spherical pores in the scaffolds prepared with 25 (v/w)% ice particulates are sparsely distributed. When 75% ice particulates are used, some collapsed large pores are observed. With a high ratio of ice particulates, the collagen aqueous solution filling the spaces between the spherical ice particulates decreases and the collagen matrix surrounding the large pores decreases. In addition, mixing of the ice particulates and the collagen aqueous solution becomes difficult when the ice particulate ratio is high. The collapsed large pores can be due to the less dense collagen matrix and incomplete mixing.

Collagen scaffolds prepared with 50 (w/v)% ice particulates have the most homogenous pore structure.

The effect of the collagen concentration on the pore structure is investigated by fixing the ice particulate ratio at 50% (w/v) and changing the collagen concentration from 1% to 3% (w/v). Collapsed large pores are observed in the collagen scaffolds prepared with 1% and 3% collagen aqueous solutions. The collapsed large pores in collagen scaffolds prepared with the 1% collagen aqueous solution may be because of the low concentration which results in a less dense collagen matrix surrounding the large pores. The case involving the 3% collagen aqueous solution may be due to incomplete mixing because the 3% collagen solution is too viscous. The collagen scaffold prepared with 2% collagen solution has the most homogeneous pore structure.

When collagen concentration is fixed at 2% and the ratio of ice particulates is changed, the Young's modulus of collagen porous scaffolds increases in the following order: $75\% < 25\% < 50\%$. The collagen porous scaffolds prepared with 50% ice particulates have the highest Young's modulus. The difference in the mechanical properties is mainly ascribed to the different pore structures. The spherical pores formed by ice particulates are thought to resist mechanical loading, therefore reinforcing the collagen scaffolds. The high mechanical strength of the collagen scaffolds prepared with 50% ice particulates should be due to the most appropriate packing of the large spherical pores and appropriate filling of the collagen matrix between the large spherical pores. The low mechanical strength of the collagen scaffold prepared with 75% ice particulates may be due to the partially collapsed large pore structure. When the ratio of ice particulates is fixed at 50 (w/v)%, the Young's modulus increases as the collagen concentration increases. A dense collagen matrix surrounding the large pores can be formed to reinforce the scaffolds when the collagen concentration increases.

The ice particulate method has also been used to prepare porous scaffolds of gelatin, and hyaluronic acid/collagen [19, 20]. This method is applicable for many naturally derived polymers. Most of the naturally derived polymers are water soluble. There are many advantages of free ice particulate method for scaffold preparation of naturally derived polymers because the method is proceeded at low temperature and no organic solvent is used. The method is good for incorporation of growth factors in the porous scaffolds, while maintaining their bioactivities.

The method can also be used for scaffold preparation of biodegradable synthetic polymers [18]. Synthetic polymers are dissolved in organic solvents that have a much lower freezing temperature than the melting temperature of the ice particulates. The temperature of biodegradable polymer solution can be decreased to avoid melting of ice particulates during mixing of synthetic polymer solution and the free ice particulates. Freezing of the mixture can induce phase separation of synthetic polymer solution among the ice particulates, resulting in the formation of microporous wall after freeze-drying. However, the mechanical property of biodegradable synthetic polymer scaffolds prepared by this method is much lower than the scaffolds prepared by normal porogen-leaching method using salt particles or sugar particles.

2.3 Funnel-Like Porous Scaffolds and Micropatterned Porous Scaffolds Prepared with Embossing Ice Particulates

To make the scaffold surface pores open, a method using embossing ice particulates has been used [28]. The method is similar to the free ice particulate method. The ice particulates are formed on a surface, and then used as a template to prepare porous scaffolds. As a general procedure, water droplets are at first formed on a thin film by spraying or injecting water, or applying moisture on a hydrophobic surface. The size of the water droplets can be controlled by the number of spraying times, injected water volume, or the moisture application time. Embossing ice particulates are formed after freezing the water droplets. And then, the embossing ice particulates are used as a template to prepare porous scaffolds. The freezing, freeze-drying, cross-linking, and washing steps during scaffold preparation are the same as those of the above-mentioned procedures of free ice particulate method. An aqueous solution of naturally derived polymers is eluted onto the embossing ice particulates, and the construct is frozen. The frozen construct is freeze-dried to remove the embossing ice particulates and ice crystals that are newly formed during freezing. Porous scaffolds having open surface pore structures are prepared after cross-linking and washing.

The method has been used to prepare porous scaffolds of collagen, chitosan, hyaluronic acid, and glycosaminoglycan that have open surface pore structures [29–31]. The porous scaffolds have large open pores on their surfaces and small pores underlying the large surface pores. Such a structure likes a funnel, and therefore the porous scaffolds are referred as funnel-like porous scaffolds. The morphology, size and density of large surface pores are dependent on the embossing ice particulates because they are the negative replicas of the embossing ice particulates. The small pores are the negative replicas of ice crystals that are newly formed during freezing. The size of small pores is dependent on the freezing temperature as mentioned above.

The embossing ice particulate method can be used to prepare micropatterned pore structures in porous scaffolds [32]. In such an application, the embossing ice particulates are micropatterned. Micropatterned ice particulates or ice lines are at first prepared, and used as templates to prepare the micropatterned porous scaffolds. The micropatterned ice particulates or ice lines are prepared by ejecting water droplets through a dispensing machine at a low temperature. By designing an ejection program, the micropatterns can be tailored. Figure 2.2a–h shows some micropatterns of ice particulates and the respective micropatterned collagen porous scaffolds. The micropatterned pore layers can be stacked to construct collagen porous scaffolds with 3D micropatterned pores (Fig. 2.2i, j).

To prepare the 3D micropattern pore structures, polymer solution is eluted on the micropatterned ice particulates that are formed on a film (first layer of ice particulates) and frozen. The frozen polymer solution on the first layer of micropatterned ice particulates is used to prepare the second layer of micropatterned ice particulates (second layer of ice particulates) instead of the film. Polymer solution is eluted on the

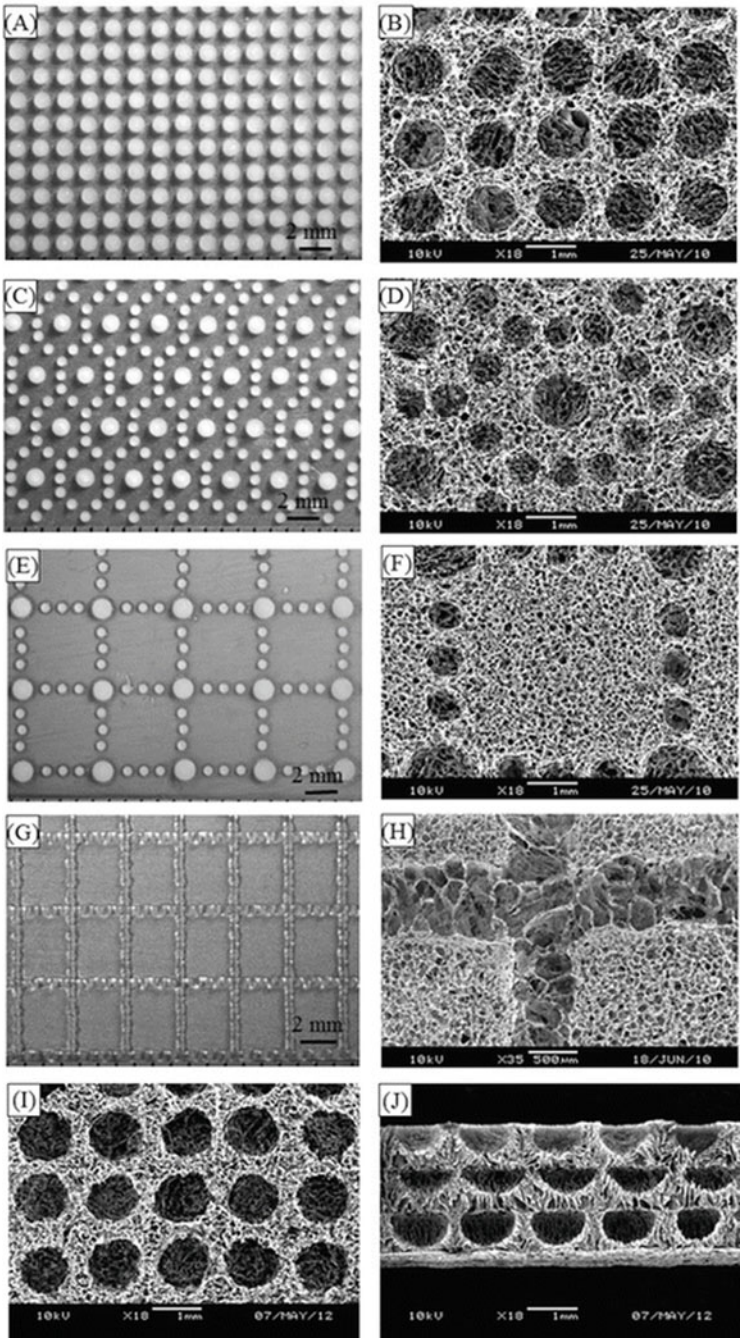

Fig. 2.2 Light microscopy micrographs of four types of ice micropattern templates (**a**, **c**, **e**, **g**) and SEM images of collagen porous scaffolds with one layer of micropatterned pores that are prepared with the respective ice micropattern templates (**b**, **d**, **f**, **h**), and a collagen sponge with three-

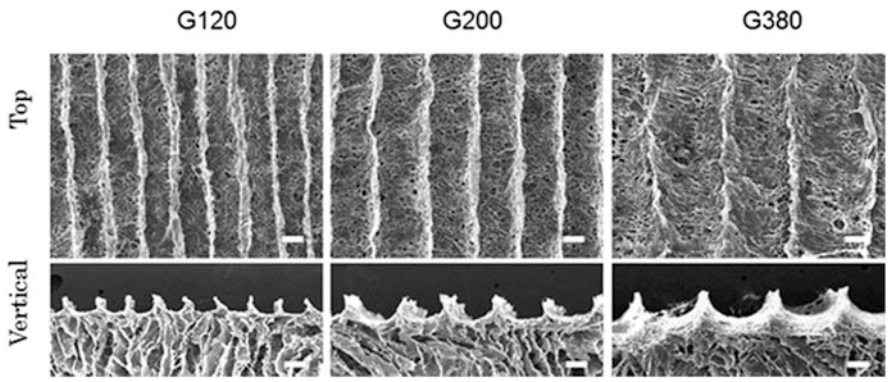

Fig. 2.3 SEM micrographs of microgroove collagen porous scaffolds with mean microgroove widths of 120, 200, and 380 μm. Upper images show the top view, and bottom images show the vertical cross-sectional view of the scaffolds. Scale bar = 100 μm. (Adapted from Ref. [33] with permission from Elsevier)

second layer of ice particulates and frozen. By repeating the procedure, polymer matrix embedded with multilayers of micropatterned ice particulates can be obtained. After freeze-drying, cross-linking, and washing, polymer porous scaffolds with 3D micropatterned pore structures are prepared. A collagen porous scaffold with 3D micropatterned pore structure is shown in Fig. 2.2i, j. The cross-section SEM image shows the stacked 3D pore structure.

Microgroove collagen porous scaffolds have been prepared with this method by using micropatterned ice lines as a template [33]. By controlling the width of ice lines, three types of collagen porous scaffolds with microgroove width of 120, 200 and 380 μm are prepared (Fig. 2.3). They are referred as G120, G200, and G380. The microgroove porous scaffolds have aligned concave microgrooves that exhibit semicircular shape in cross-sections.

The collagen microgroove porous scaffolds have been used for culture of L6 skeletal myoblasts for skeletal muscle tissue engineering. The myoblasts aggregate and form bundles in the microgroove scaffolds. The width of microgrooves has some effects on cell orientation and cell bundle formation. Scaffolds with wide microgrooves (G200 and G380) enable the formation of discrete cell bundles after 14 days of culture. Scaffolds with narrow microgrooves (G120) result in the formation of some cell bundles in microgrooves and mostly cellular flakes covering most of the area of scaffolds. Staining of myosin heavy chain (MHC) shows that well-aligned myotubes are formed in G200 and G380, while in G120 some myotubes are aligned in microgrooves and other myotubes in cellular flakes have random orientation.

Fig. 2.2 (continued) dimensional micropattern pores prepared with an ice micropattern template shown in **a** (**i** top surface, **j** cross-section). (Adapted from Ref. [32] with permission from John Wiley and Sons)

Furthermore, the embossing ice particulate method can be used to micropattern bioactive molecules in 3D porous polymer scaffolds. As an example, collagen porous scaffolds with micropatterned fibronectin, VEGF, and NGF have been prepared by the method [34, 35]. In this case, a collagen aqueous solution containing the bioactive molecules, other than pure water, is used to prepare the micropatterned ice lines. The ice micropatterns of the mixture of collagen/bioactive molecules are used to prepare collagen porous scaffolds having micropatterns of bioactive molecules. Not only single bioactive molecule, but also a few types of bioactive molecules can be co-micropatterned in the porous scaffolds. The bioactive molecules can be mixed and micropatterned together, or the bioactive molecules can be micropatterned separately to construct the porous scaffolds having co-micropatterns of a few types of bioactive molecules. Collagen porous scaffolds with micropatterned NGF and VEGF show stimulative effects on the regeneration of neural network and capillary network, respectively.

2.4 Scaffolds Prepared with Sacrificial Templates

Porous templating structures of biodegradable polymers have been used as sacrificial templates to generate interconnected pores in scaffolds [36–39]. PLGA sponges and PLGA meshes have been used as the sacrificial template because their degradation can be accelerated at a high pH. Unlike the ice particulates, PLGA sponges and PLGA meshes have integral, and continuous frame structures which negative replica form the interconnected pore structures in the scaffolds. Collagen scaffolds with interconnected pore structures prepared by this method are shown in Fig. 2.4 [36]. At first, PLGA sponge templates are prepared. Six types of PLGA sponges are prepared and used as the templates. A solvent casting/particulate leaching method is used to

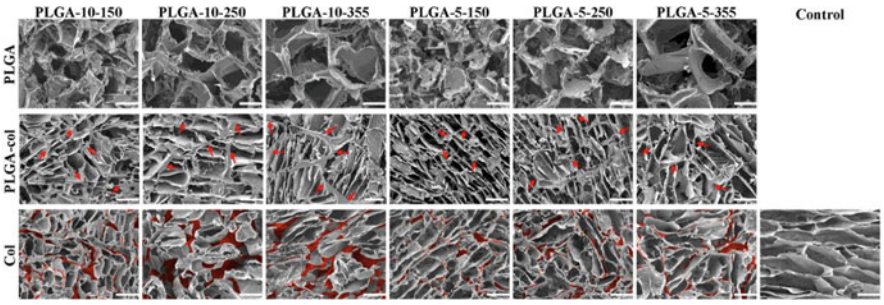

Fig. 2.4 SEM micrographs of the PLGA sponge templates, PLGA-collagen sponges (PLGA-col), and collagen sponges (Col). The central cross-sections of the sponges are used for SEM observation. The pore walls of the PLGA sponge templates are indicated by red arrows in the middle row micrographs (PLGA-col). The negative replica spaces of the PLGA sponge templates after their removal are indicated by the red marks in the bottom row micrographs (Col). Scale bar is 200 μm. (Adapted from Ref. [38] with permission from RSC)

the PLGA sponge templates by using NaCl particulates of three sizes (diameter of 150–250, 250–355, 355–500 μm). The ratio of PLGA/NaCl is 10:90 and 5:95. The PLGA sponge templates prepared with the different ratio of PLGA/NaCl and different size of NaCl particulates are designated as PLGA-10-150, PLGA-5-150, PLGA-10-250, PLGA-5-250, PLGA-10-355, and PLGA-5-355 (Fig. 2.4). The PLGA sponge templates have pore structures controlled by the NaCl particulate and PLGA/NaCl ratio. Their pore size is almost the same as that of the NaCl particulates. The PLGA-10-355 and PLGA-5-355 sponge templates prepared with 355–500 μm NaCl particulates have the largest pore size. Thickness of the pore walls increase with the PLGA/NaCl ratio.

And then, the PLGA sponge templates are immersed in 1 wt% collagen aqueous solution under vacuum to fill all the pores with collagen aqueous solution. After freeze-drying and crosslinking, PLGA-collagen sponges are prepared. 50 mM 1-ethyl-3-(3-dimethylaminopropyl) carbodiimide and 20 mM *N*-hydroxysuccinimide are used for the cross-linking, which is conducted in 95 (v/v)%, 90 (v/v)%, and 80 (v/v)% ethanol aqueous solutions, each for 3 h. SEM observation shows that hybridization with collagen results in the formation of collagen microsponges in the pores of the PLGA sponge templates (Fig. 2.4).

Finally, the PLGA sponge templates are selectively removed by accelerated degradation via immersion of the PLGA-collagen sponges in a 3 (wt/v)% ammonia hydroxide solution. The collagen component in the PLGA-collagen sponges remains intact during the accelerated degradation process. Collagen sponges with interconnected pore structures are formed after selectively removing the PLGA sponge templates. There are designated as Col-10-150, Col-5-150, Col-10-250, Col-5-250, Col-10-355, and Col-5-355. Collagen sponge prepared with direct freeze-drying of 1 wt% collagen aqueous solution without PLGA sponge templates is used as a comparison (control).

SEM observation shows the interconnected pore structures of the collagen scaffolds prepared with PLGA sponge templates (Fig. 2.4). The negative replica spaces of the PLGA sponge templates form the interconnecting channels among the pores of the collagen scaffolds. The character of the interconnecting channels is dependent on the frame structures of the PLGA sponge templates. The interconnecting channels become wider when the pore walls of the PLGA sponge templates are thick. The thickness of the interconnecting channels in the collagen scaffold prepared with PLGA-10-355 template was widest. The collagen sponges are used for culture of bovine articular chondrocytes and human bone marrow-derived mesenchymal stem cells (hMSCs). The cells can migrate into the pores through the interconnecting channels. The interconnecting channels in all the collagen sponges prepared with PLGA sponge templates facilitate cell migration and homogeneous distribution. Cell distribution in the collagen sponge prepared with PLGA-10-355 template is most homogeneous.

Besides the PLGA sponge templates, PLGA mesh has been used as sacrificial templates to fabricate mesh-like collagen scaffolds [39]. Mesh-like collagen scaffolds with large and small sizes are prepared by using PLGA mesh template (Fig. 2.5). The mesh-like collagen scaffold of large size is fabricated by forming a

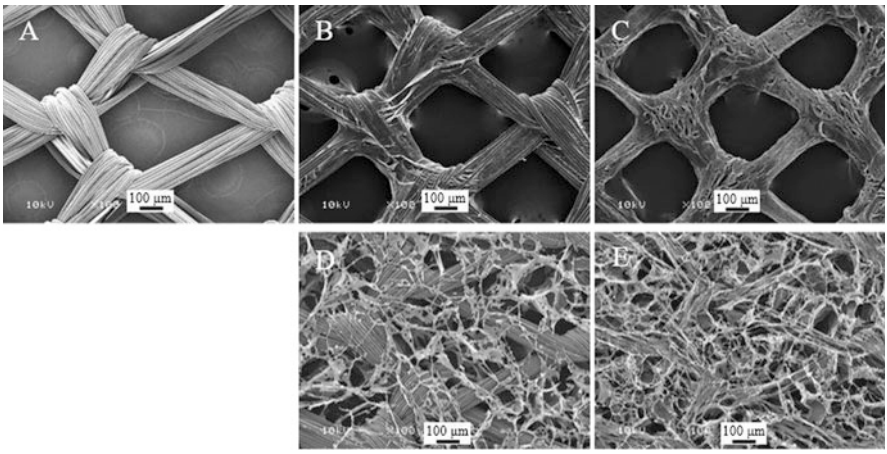

Fig. 2.5 SEM micrographs of PLGA mesh (**a**), collagen-coated PLGA mesh (**b**), mesh-like collagen scaffold of large size (**c**), PLGA-collagen composite mesh (**d**), and mesh-like collagen scaffold of small size (**e**). (Adapted from Ref. [36] with permission from RSC)

thin coating layer of collagen on the PLGA mesh template surface, followed by selective removal of the PLGA mesh template. Removal of PLGA mesh template is conducted by the accelerated degradation of PLGA, which is the same as above-mentioned. The mesh-like collagen scaffold of small size is fabricated by selective removal of PLGA mesh template from PLGA-collagen composite mesh which is fabricated by introducing collagen microsponges in the open spaces of the PLGA mesh template.

As shown in Fig. 2.5, the collagen-coated PLGA mesh has a similar pore structure to that of the PLGA mesh template. The mesh-like collagen scaffold of large size also has a similar pore structure. However, SEM observation of the cross-sections shows the cross-sections of the mesh-like collagen scaffold have microtubular structures. The microtubular structures are generated from the negative replica of PLGA fibers. The mesh-like collagen scaffold of small size has similar pore structure to that of the PLGA-collagen composite mesh, while its cross-sections have microtubular structures. Thickness of the mesh-like collagen scaffolds is controlled by the thickness of the PLGA mesh templates. The mesh-like collagen scaffolds can be used for tissue engineering of thin tissues. When human dermal fibroblasts are cultured in the mesh-like collagen scaffolds, they support cell adhesion and promote cell proliferation. The fibroblasts form layered structures more rapidly in the mesh-like collagen scaffold of small size than in the mesh-like collagen scaffold of large size.

The sacrificial PLGA meshes have also been used to prepare extracellular matrices (ECM) scaffolds [40, 41]. At first, cells are cultured in the PLGA meshes. The cells proliferate and excrete their own extracellular matrices. Subsequently, the cellular components are removed by decellularization after the cells have excreted enough amount of extracellular matrices. Finally, the templates are selectively

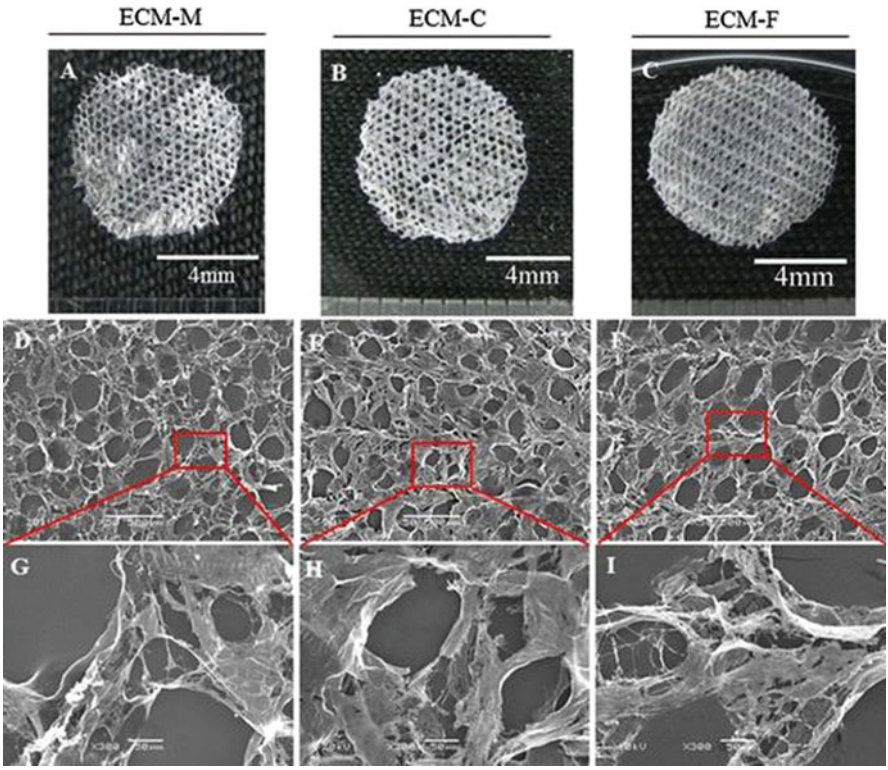

Fig. 2.6 Gross appearance (**a**–**c**) and SEM micrographs (**d**–**i**) of ECM porous scaffolds prepared from hMSCs (**a**, **d**, **g**), chondrocytes (**b**, **e**, **h**), and fibroblasts (**c**, **f**, **i**). Scale bar = 500 μm in (**d**–**f**), and 50 μm in (**g**–**i**). (Adapted from Ref. [40] with permission from Elsevier)

removed, while the extracellular matrices are remained. After cross-linking, ECM scaffolds are obtained. ECM scaffolds have been prepared from human bone marrow mesenchymal stem cells (hMSCs), human articular chondrocytes, and human dermal fibroblasts by the method. The ECM scaffolds from hMSCs (ECM-M), chondrocytes (ECM-C), and fibroblasts (ECM-F) have a mesh-like appearance similar to that of the PLGA mesh template (Fig. 2.6). The ECM scaffolds have different composition that is dependent on the cell type and culture condition.

2.5 Composite Porous Scaffolds

Porous scaffolds of biodegradable synthetic polymers, and naturally derived polymers have their respective advantages and problems. Porous scaffolds prepared from synthetic biodegradable polymers such as PGA, PLA, PLGA, and PCL have relatively strong mechanical strength. Their degradation can be controlled by

crystallinity, molecular weight, and copolymer ratio of the polymers. However, synthetic polymer scaffolds are devoid of cell recognition signals, and their hydrophobic surface property hinders smooth cell seeding. On the other hand, naturally derived polymers, such as collagen, gelatin, and hyaluronic acid, have the advantages of specific cell interactions and hydrophilicity, while their mechanical property is inferior to synthetic polymer scaffolds. Biodegradable synthetic polymers, and naturally derived polymers have hybridized to prepare their composite scaffolds to combine the advantageous properties of both types of polymers, and overcome their drawbacks [25, 42, 43]. One type of hybridization is to form microsponges of naturally derived polymers in the void spaces or opening of a porous skeleton of biodegradable synthetic polymers [44–47]. The void space or opening of biodegradable synthetic polymer porous skeleton is filled with microsponges of naturally derived polymers. The pore surface of biodegradable polymer porous skeleton is also coated with naturally derived polymers. When the composite scaffolds are used for 3D cell culture, cells only contact and interact with naturally derived polymers. The porous skeleton of biodegradable polymers serves as a mechanical skeleton to provide necessary mechanical strength to support the whole scaffolds. Another type of hybridization is to construct naturally derived polymer porous structures in the open space of a cup, cage, or cylinder of biodegradable synthetic polymers [48, 49]. All the composite porous scaffolds have high mechanical strength, good cell interaction and surface hydrophilicity.

As a typical example of composite scaffolds, PLGA-collagen composite mesh can be prepared by introducing collagen microsponges in the interstices of a PLGA knitted mesh [46, 47]. Collagen sponge can also be formed on one side of the PLGA knitted mesh or both sides of the PLGA knitted mesh to construct semi-type or sandwich-type PLGA-collagen composite scaffolds [50]. The semi-type and sandwich-type PLGA-collagen composite scaffolds have been used for culture of bovine articular chondrocytes for cartilage tissue engineering. Both composite scaffolds show a spatially even cell distribution, natural chondrocyte morphology, abundant cartilaginous extracellular matrix deposition, and excellent biodegradation in vivo. The histological structure and mechanical properties of the engineered cartilage using the semi-type and sandwich-type composite scaffolds match the native bovine articular cartilage. The composite scaffolds are useful for tissue engineering and regenerative medicine.

2.6 Biomimetic ECM Scaffolds

ECM are a complex network composed of a variety of proteins and proteoglycans. ECM play a very important role in regulation of cell functions. ECM derived from decellularized tissues have been widely explored as a source of biological scaffolds for tissue engineering. Acellular ECM has been prepared by decellularization of tissues and organs, such as the small intestinal submucosa, heart valve, blood vessel, skin, nerve, tendon, ligament, urinary bladder, vocal fold, amniotic membrane, heart,

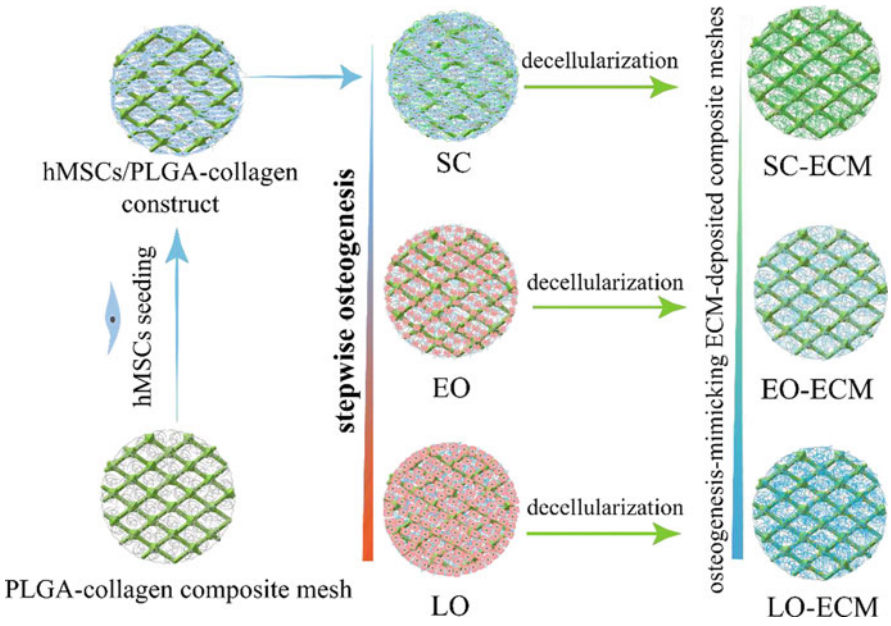

Fig. 2.7 Fabrication scheme of PLGA-collagen-ECM composite meshes mimicking the ECM composition of stepwise osteogenesis. (Adapted from Ref. [64] with permission from IOP Science)

liver, and lung [4]. The ECM scaffolds obtained from decellularized tissues and organs offer the advantage of maintaining the structures of the respective tissues and organs. However, they suffer from problems of autologous tissue/organ scarcity, host responses, and pathogen transfer when allogeneic and xenogeneic tissues and organs are used.

Cell culture method has been adopted as an alternate method to prepare the ECM scaffolds [51–58]. Cell-derived ECM have been used to fabricate various scaffolds for tissue engineering applications [59, 60]. Cultured cells offer several advantages of pathogen-free and availability over the decellularization of tissues and organs. The method can be adopted to fabricate ECM scaffolds mimicking the dynamically remodeled ECM compositions. Differentiation of stem cells to mature cells has been reported to pass through stepwise stages of maturation [61, 62]. ECM are dynamically changed and remodeled during the stepwise development process [63]. By controlling the stepwise differentiation of stem cells into different lineage, ECM scaffolds mimicking stepwise osteogenesis, stepwise adipogenesis, and stepwise chondrogenesis are fabricated.

As shown in Fig. 2.7, PLGA-collagen-ECM composite meshes that mimic the dynamically remodeled ECM composition of stepwise osteogenesis have been fabricated by controlling the differentiation stages during osteogenic differentiation of hMSCs in the PLGA-collagen composite meshes [64]. When hMSCs are cultured in the PLGA-collagen composite meshes, hMSCs secret their ECM that are

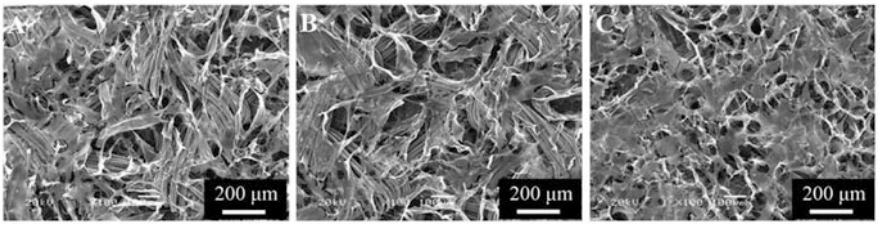

Fig. 2.8 SEM micrographs of PLGA-collagen-ECM scaffolds mimicking stem cell ECM (**a**), early osteogenesis stage ECM (**b**), and late osteogenesis stage ECM (**c**). (Adapted from Ref. [64] with permission from IOP Science)

deposited in the composite meshes. The osteogenic differentiation stages can be controlled at stem cell stage, early osteogenesis stage, and late osteogenesis stage by using proliferation medium or osteogenic differentiation medium, and by adjusting culture time. The stem cell stage ECM (SC-ECM) are deposited in the composite meshes by culturing hMSCs in basal medium for 7 days. The early osteogenesis stage ECM (EO-ECM) are deposited in the composite meshes by culturing hMSCs in osteogenic medium for 7 days. During 7 days culture in osteogenic differentiation medium, the cells express high level of early-stage osteogenesis marker, alkaline phosphatase (ALP), while no calcium deposition which is a late-stage marker of osteogenesis is detected. The late osteogenesis stage ECM (LO-ECM) are deposited in the composite meshes by culturing hMSCs in osteogenic medium for 21 days. The late osteogenesis stage is confirmed by high expression of ALP and calcium deposition.

After decellularization of the hMSCs/scaffold constructs, the three types of stepwise ECM scaffolds are obtained. The porous structures of the stepwise osteogenesis-mimicking ECM scaffolds are shown in Fig. 2.8. The ECM scaffolds have different compositions which are dependent on the osteogenic differentiation stage of hMSCs.

The stepwise osteogenesis-mimicking ECM scaffolds show different osteogenesis-induction effects on hMSCs. The EO-ECM scaffold shows a promotive effect on osteogenic differentiation of hMSCs, and the LO-ECM scaffold has a moderate effect on osteogenic differentiation of hMSCs. However, the SC-ECM scaffold exhibits an inhibitory effect on osteogenic differentiation of hMSCs. The varied effects of the ECM scaffold on osteogenic differentiation of hMSCs are related with the dynamically remodeling ECM components in the stepwise osteogenesis-mimicking ECM scaffolds.

By the same method, stepwise adipogenesis-mimicking ECM-deposited PLGA-collagen composite meshes have been prepared by controlling the adipogenic differentiation stages of hMSCs in the PLGA-collagen composite meshes [65]. The ECM components are dependent on the adipogenic differentiation stages. The stepwise adipogenesis-mimicking ECM scaffolds show different effects on adipogenic differentiation of hMSCs. The ECM scaffold fabricated from early stage of adipogenesis enhances the adipogenic differentiation, while the ECM

scaffold prepared from stem cell stage or late stage of adipogenesis show an inhibitive effect on adipogenic differentiation of hMSCs.

The method has also been used to prepare ECM scaffolds mimicking endochondral ossification-related ECM by depositing ECM secreted from stem cells (SC-ECM), chondrogenic (CH-ECM), hypertrophic (HY-ECM) and osteogenic (OS-ECM) stages of hMSCs in the PLGA-collagen composite mesh [66]. During bone tissue development, endochondral ossification (ECO) occurs. ECM play an important role in ECO. The SC-ECM, CH-ECM, HY-ECM and OS-ECM are adopted for culture of hMSCs to elucidate the effects of biomimetic ECM mimicking the ECO-related ECM on differentiation of hMSCs. Their effects on osteogenic differentiation of hMSCs are different. Their promotive effect on osteogenic differentiation of hMSCs is an order of HY-ECM scaffold > CH-ECM scaffold, OS-ECM scaffold > SC-ECM scaffold. Their effects on chondrogenic or adipogenic differentiation are almost the same. Therefore, the HY-ECM may be important for ECO.

Furthermore, ECM scaffolds mimicking the dynamically remodeling ECM during simultaneous osteogenic and adipogenic differentiation of hMSCs have been fabricated by simultaneously controlling osteogenic and adipogenic differentiation of hMSCs in the PLGA-collagen composite meshes [67]. The simultaneous osteogenic and adipogenic differentiation of hMSCs is controlled at four stages, early osteogenesis/early adipogenesis (EOEA-ECM), early osteogenesis/late adipogenesis (EOLA-ECM), late osteogenesis/early adipogenesis (LOEA-ECM), and late osteogenesis/late adipogenesis (LOLA-ECM). Mixtures of osteogenic induction medium and adipogenic induction medium at different ratios are adopted to control the simultaneous osteogenic and adipogenic differentiation. The compositions of the ECM scaffolds vary according the different stages of simultaneous differentiation stages. They also show different effects on adipogenic and osteogenic differentiation of hMSCs. The EOEA-ECM scaffold has a promotive effect on adipogenesis, while a suppressive effect on osteogenesis. The LOEA-ECM and LOLA-ECM scaffolds show a promotive effect on osteogenesis and a moderate effect on adipogenesis. The EOLA-ECM scaffold exhibits a suppressive effect on both osteogenesis and adipogenesis. The varied effects of the ECM scaffolds on hMSCs differentiation are dependent on their ECM compositions. These ECM scaffolds can be used as models for 3D cell culture for investigation of ECM-cell interaction and tissue engineering applications.

2.7 Summary

Porous scaffolds can be prepared from a number of biodegradable polymers and extracellular matrices. Their composition can be controlled by combining a few types of polymers and matrices. Biodegradable synthetic polymers and naturally derived polymers can also be hybridized to overcome the drawbacks of single polymers. Their porous structures can be controlled by using different fabrication methods. Free ice particulate method, embossing ice particulate method, and

sacrificial template method can well control the porous structures and introduce micropatterns in the scaffolds. Cell-derived ECM scaffolds not only mimic the cellular microenvironment, but also mimic the dynamics of ECM remolding during stem cell differentiation or tissue development. The polymer porous scaffolds and biomimetic ECM scaffolds can be widely used for engineering of various tissues and organs.

Acknowledgment This work was supported by JSPS KAKENHI 19H04475, 21H03830, and 22K19926.

References

1. Engelmayr GC, Cheng M, Bettinger CJ, Borenstein JT, Langer R, Freed LE. Accordion-like honeycombs for tissue engineering of cardiac anisotropy. Nat Mater. 2008;7(12):1003–10.
2. Lu H, Kawazoe N, Kitajima T, Myoken Y, Tomita M, Umezawa A, Chen G, Ito Y. Spatial immobilization of bone morphogenetic protein-4 in a collagen-PLGA hybrid scaffold for enhanced osteoinductivity. Biomaterials. 2012;33(26):6140–6.
3. Wang M, Xu P, Lei B. Engineering multifunctional bioactive citrate-based biomaterials for tissue engineering. Bioact Mater. 2023;19:511–37.
4. Hoshiba T, Lu H, Kawazoe N, Chen G. Decellularized matrices for tissue engineering. Expert Opin Biol Ther. 2010;10(12):1717–28.
5. Hussey GS, Dziki JL, Badylak SF. Extracellular matrix-based materials for regenerative medicine. Nat Rev Mater. 2018;3(7):159–73.
6. Bajaj P, Schweller RM, Khademhosseini A, West JL, Bashir R. 3D biofabrication strategies for tissue engineering and regenerative medicine. Annu Rev Biomed Eng. 2014;16:247–76.
7. Wu R, Li Y, Shen M, Yang X, Zhang L, Ke X, Yang G, Gao C, Gou Z, Xu S. Bone tissue regeneration: The role of finely tuned pore architecture of bioactive scaffolds before clinical translation. Bioact Mater. 2021;6(5):1242–54.
8. Li W, Bai Y, Cao J, Gao S, Xu P, Feng G, Wang H, Kong D, Fan M. Highly interconnected inverse opal extracellular matrix scaffolds enhance stem cell therapy in limb ischemia. Acta Biomater. 2021;128:209–21.
9. Lin K, Zhang D, Macedo MH, Cui W, Sarmento B, Shen G. Advanced collagen-based biomaterials for regenerative biomedicine. Adv Funct Mater. 2019;29(3):1804943.
10. Reed S, Lau G, Delattre B, Lopez DD, Tomsia AP, Wu BM. Macro- and micro-designed chitosan-alginate scaffold architecture by three-dimensional printing and directional freezing. Biofabrication. 2016;8(1):015003.
11. Zhang Q, Lu H, Kawazoe N, Chen G. Pore size effect of collagen scaffolds on cartilage regeneration. Acta Biomater. 2014;10(5):2005–13.
12. Sutrisno L, Chen H, Chen Y, Yoshitomi T, Kawazoe N, Yang Y, Chen G. Composite scaffolds of black phosphorus nanosheets and gelatin with controlled pore structures for photothermal cancer therapy and adipose tissue engineering. Biomaterials. 2021;275:120923.
13. Zhao P, Wang J, Li Y, Wang X, Chen C, Liu G. Microfluidic technology for the production of well-ordered porous polymer scaffolds. Polymers. 2020;12(9):1863.
14. Zhang YS, Zhu C, Xia Y. Inverse opal scaffolds and their biomedical applications. Adv Mater. 2017;29(33):1701115.
15. Huang D, Liu T, Liao J, Maharjan S, Xie X, Pérez M, Anaya I, Wang S, Mayer AT, Kang Z. Reversed-engineered human alveolar lung-on-a-chip model. Proc Natl Acad Sci U S A. 2021;118(19):e2016146118.

16. Zhang Q, Lu H, Kawazoe N, Chen G. Preparation of collagen scaffolds with controlled pore structures and improved mechanical property for cartilage tissue engineering. J Bioact Compat Polym. 2013;28(5):426–38.
17. Zhang Q, Lu H, Kawazoe N, Chen G. Preparation of collagen porous scaffolds with a gradient pore size structure using ice particulates. Mater Lett. 2013;107:280–3.
18. Chen G, Ushida T, Tateishi T. Preparation of poly(L-lactic acid) and poly(DL-lactic-co-glycolic acid) foams by use of ice microparticulates. Biomaterials. 2001;22(18):2563–7.
19. Chen S, Zhang Q, Kawazoe N, Chen G. Effect of high molecular weight hyaluronic acid on chondrocytes cultured in collagen/hyaluronic acid porous scaffolds. RSC Adv. 2015;5 (114):94405–10.
20. Chen S, Zhang Q, Nakamoto T, Kawazoe N, Chen G. Gelatin scaffolds with controlled pore structure and mechanical property for cartilage tissue engineering. Tissue Eng Part C Methods. 2016;22(3):189–98.
21. Zhang J, Li J, Chen S, Kawazoe N, Chen G. Preparation of gelatin/Fe_3O_4 composite scaffolds for enhanced and repeatable cancer cell ablation. J Mater Chem B. 2016;4(34):5664–72.
22. Wang X, Zhang J, Li J, Chen Y, Kawazoe N, Chen G. Bifunctional scaffolds for the photothermal therapy of breast tumor cells and adipose tissue regeneration. J Mater Chem B. 2018;6(46):7728–36.
23. Wang X, Kawazoe N, Chen G. Interaction of immune cells and tumor cells in gold nanorod-gelatin composite porous scaffolds. Nanomaterials. 2019;9(10):1367.
24. Chen H, Wang X, Sutrisno L, Zeng T, Kawazoe N, Yang Y, Chen G. Folic acid-functionalized composite scaffolds of gelatin and gold nanoparticles for photothermal ablation of breast cancer cells. Front Bioeng Biotechnol. 2020;8:589905.
25. Sutrisno L, Chen H, Yoshitomi T, Kawazoe N, Yang Y, Chen G. PLGA-collagen-BPNS Bifunctional composite mesh for photothermal therapy of melanoma and skin tissue engineering. J Mater Chem B. 2022;10(2):204–13.
26. Sutrisno L, Chen H, Yoshitomi T, Kawazoe N, Yang Y, Chen G. Preparation of composite scaffolds composed of gelatin and Au nanostar-deposited black phosphorus nanosheets for the photothermal ablation of cancer cells and adipogenic differentiation of stem cells. Biomater Adv. 2022;138:212938.
27. Chen H, Sun R, Zheng J, Kawazoe N, Yang Y, Chen G. Doxorubicin-encapsulated thermosensitive liposome-functionalized photothermal composite scaffolds for synergistic photothermal therapy and chemotherapy. J Mater Chem B. 2022;10(25):4771–82.
28. Ko Y-G, Kawazoe N, Tateishi T, Chen G. Preparation of chitosan scaffolds with a hierarchical porous structure. J Biomed Mater Res B Appl Biomater. 2010;93(2):341–50.
29. Ko Y-G, Kawazoe N, Tateishi T, Chen G. Preparation of novel collagen sponges using an ice particulate template. J Bioact Compat Polym. 2010;25(4):360–73.
30. Ko Y-G, Grice S, Kawazoe N, Tateishi T, Chen G. Preparation of collagen-glycosaminoglycan sponges with open surface porous structures using ice particulate template method. Macromol Biosci. 2010;10(8):860–71.
31. Forget A, Waibel M, Rojas-Canales DM, Chen S, Kawazoe N, Harding FJ, Loudovaris T, Coates PTH, Blencowe A, Chen G, Voelcker NH. IGF-2 coated porous collagen microwells for the culture of pancreatic islets. J Mater Chem B. 2017;5(2):220–5.
32. Oh HH, Ko Y-G, Lu H, Kawazoe N, Chen G. Preparation of porous collagen scaffolds with micropatterned structures. Adv Mater. 2012;24(31):4311–6.
33. Chen S, Nakamoto T, Kawazoe N, Chen G. Engineering multi-layered skeletal muscle tissue by using 3D microgrooved collagen scaffolds. Biomaterials. 2015;73:23–31.
34. Oh HH, Lu H, Kawazoe N, Chen G. Spatially guided angiogenesis by three-dimensional collagen scaffolds micropatterned with vascular endothelial growth factor. J Biomater Sci Polym Ed. 2012;23(17):2185–95.
35. Oh HH, Lu H, Kawazoe N, Chen G. Differentiation of PC_{12} cells in three-dimensional collagen sponges with micropatterned nerve growth factor. Biotechnol Prog. 2012;28(3):773–9.

36. Xie Y, Lee K, Wang X, Yoshitomi T, Kawazoe N, Yang Y, Chen G. Interconnected collagen porous scaffolds prepared with sacrificial PLGA sponge templates for cartilage tissue engineering. J Mater Chem B. 2021;9(40):8491–500.
37. Xie Y, Sutrisno L, Yoshitomi T, Kawazoe N, Yang Y, Chen G. Three-dimensional culture and chondrogenic differentiation of mesenchymal stem cells in interconnected collagen scaffolds. Biomed Mater Bristol Engl. 2022;17(3)
38. Zheng J, Xie Y, Yoshitomi T, Kawazoe N, Yang Y, Chen G. Stepwise proliferation and chondrogenic differentiation of mesenchymal stem cells in collagen sponges under different microenvironments. Int J Mol Sci. 2022;23(12):6406.
39. Xie Y, Kawazoe N, Yang Y, Chen G. Preparation of mesh-like collagen scaffolds for tissue engineering. Mater Adv. 2022;3(3):1556–64.
40. Lu H, Hoshiba T, Kawazoe N, Chen G. Autologous extracellular matrix scaffolds for tissue engineering. Biomaterials. 2011;32(10):2489–99.
41. Lu H, Hoshiba T, Kawazoe N, Koda I, Song MH, Chen G. Cultured cell-derived extracellular matrix scaffolds for tissue engineering. Biomaterials. 2011;32(36):9658–66.
42. Chen G, Ushida T, Tateishi T. Hybrid biomaterials for tissue engineering: a preparative method for PLA or PLGA–collagen hybrid sponges. Adv Mater. 2000;12(6):455–7.
43. Chen G, Ushida T, Tateishi T. Scaffold design for tissue engineering. Macromol Biosci. 2002;2 (2):67–77.
44. Chen G, Ushida T, Tateishi T. A hybrid network of synthetic polymer mesh and collagen sponge. Chem Commun. 2000;16:1505–6.
45. Chen G, Sato T, Ohgushi H, Ushida T, Tanaka J. Culturing of skin fibroblasts in a thin PLGA-collagen hybrid mesh. Biomaterials. 2005;26(15):2559–66.
46. Chen G, Sato T, Ushida T, Hirochika R, Shirasaki Y, Ochiai N, Tateishi T. The use of a novel PLGA fiber/collagen composite web as a scaffold for engineering of articular cartilage tissue with adjustable thickness. J Biomed Mater Res A. 2003;67(4):1170–80.
47. Chen G, Sato T, Ushida T, Ochiai N, Tateishi T. Tissue engineering of cartilage using a hybrid scaffold of synthetic polymer and collagen. Tissue Eng. 2004;10(3–4):323–30.
48. He X, Lu H, Kawazoe N, Tateishi T, Chen G. A novel cylinder-type poly(L-lactic acid)-collagen hybrid sponge for cartilage tissue engineering. Tissue Eng Part C Methods. 2010;16 (3):329–38.
49. Kawazoe N, Inoue C, Tateishi T, Chen G. A cell leakproof PLGA-collagen hybrid scaffold for cartilage tissue engineering. Biotechnol Prog. 2010;26(3):819–26.
50. Dai W, Kawazoe N, Lin X, Dong J, Chen G. The influence of structural design of PLGA/collagen hybrid scaffolds in cartilage tissue engineering. Biomaterials. 2010;31(8):2141–52.
51. Hoshiba T, Kawazoe N, Tateishi T, Chen G. Development of stepwise osteogenesis-mimicking matrices for the regulation of mesenchymal stem cell functions. J Biol Chem. 2009;284 (45):31164–73.
52. Hoshiba T, Lu H, Yamada T, Kawazoe N, Tateishi T, Chen G. Effects of extracellular matrices derived from different cell sources on chondrocyte functions. Biotechnol Prog. 2011;27 (3):788–95.
53. Hoshiba T, Kawazoe N, Chen G. The balance of osteogenic and adipogenic differentiation in human mesenchymal stem cells by matrices that mimic stepwise tissue development. Biomaterials. 2012;33(7):2025–31.
54. Hoshiba T, Lu H, Kawazoe N, Yamada T, Chen G. Effects of extracellular matrix proteins in chondrocyte-derived matrices on chondrocyte functions. Biotechnol Prog. 2013;29(5):1331–6.
55. Cai R, Nakamoto T, Kawazoe N, Chen G. Influence of stepwise chondrogenesis-mimicking 3D extracellular matrix on chondrogenic differentiation of mesenchymal stem cells. Biomaterials. 2015;52:199–207.
56. Cai R, Kawazoe N, Chen G. Influence of surfaces modified with biomimetic extracellular matrices on adhesion and proliferation of mesenchymal stem cells and osteosarcoma cells. Colloids Surf B Biointerfaces. 2015;126:381–6.

57. Cai R, Nakamoto T, Hoshiba T, Kawazoe N, Chen G. Matrices secreted during simultaneous osteogenesis and adipogenesis of mesenchymal stem cells affect stem cells differentiation. Acta Biomater. 2016;35:185–93.
58. Hoshiba T, Kawazoe N, Chen G. Preparation of cell-derived decellularized matrices mimicking native ecm during the osteogenesis and adipogenesis of mesenchymal stem cells. Methods Mol Biol. 2018;1577:71–86.
59. Liao JH, Guo XA, Grande-Allen KJ, Kasper FK, Mikos AG. Bioactive polymer/extracellular matrix scaffolds fabricated with a flow perfusion bioreactor for cartilage tissue engineering. Biomaterials. 2010;31(34):8911–20.
60. Wolchok JC, Tresco PA. The isolation of cell derived extracellular matrix constructs using sacrificial open-cell foams. Biomaterials. 2010;31(36):9595–603.
61. Ramani-Mohan R-K, Schwedhelm I, Finne-Wistrand A, Krug M, Schwarz T, Jakob F, Walles H, Hansmann J. Deformation strain is the main physical driver for skeletal precursors to undergo osteogenesis in earlier stages of osteogenic cell maturation. J Tissue Eng Regen Med. 2018;12(3):e1474–9.
62. Kanke K, Masaki H, Saito T, Komiyama Y, Hojo H, Nakauchi H, Lichtler AC, Takato T, Chung UI, Ohba S. Stepwise differentiation of pluripotent stem cells into osteoblasts using four small molecules under serum-free and feeder-free conditions. Stem Cell Rep. 2014;2(6):751–60.
63. Rosales AM, Anseth KS. The design of reversible hydrogels to capture extracellular matrix dynamics. Nat Rev Mater. 2016;1(2):1–15.
64. Chen Y, Lee K, Yang Y, Kawazoe N, Chen G. PLGA-collagen-ECM hybrid meshes mimicking stepwise osteogenesis and their influence on the osteogenic differentiation of hMSCs. Biofabrication. 2020;12(2):025027.
65. Chen Y, Lee K, Chen Y, Yang Y, Kawazoe N, Chen G. Preparation of stepwise adipogenesis-mimicking ECM-deposited PLGA-collagen hybrid meshes and their influence on adipogenic differentiation of hMSCs. ACS Biomater Sci Eng. 2019;5(11):6099–108.
66. Chen Y, Lee K, Kawazoe N, Yang Y, Chen G. ECM scaffolds mimicking extracellular matrices of endochondral ossification for the regulation of mesenchymal stem cell differentiation. Acta Biomater. 2020;114:158–69.
67. Chen Y, Lee K, Kawazoe N, Yang Y, Chen G. PLGA-collagen-ECM hybrid scaffolds functionalized with biomimetic extracellular matrices secreted by mesenchymal stem cells during stepwise osteogenesis-co-adipogenesis. J Mater Chem B. 2019;7(45):7195–206.

Chapter 3
Versatile Hydrogels in Regenerative Medicine

Yaping Li, Peipei Su, Yuqi Wang, Tingting Ye, Grzegorz Nowaczyk, and Wei Wang

Abstract Hydrogels, as the most typical polymer materials with three-dimensional network structures, have attracted wide attention owing to their outstanding features such as high-water content, tunable mechanical properties, excellent biodegradability, and biocompatibility. Advances in hydrogel design have revolutionized the way to address biomedical issues including tissue engineering, bioactive factor carriers, soft electronics, and actuators. Hydrogels with various structure diversities and excellent properties are emerging, and the development of hydrogels is very vigorous over the past decade. Especially for regenerative medicine, hydrogels are one of the most attractive materials due to their similarity to native extracellular matrix. This chapter focuses on development of hydrogels and state-of-the-art research, explores the main physical, chemical, and biological cross-linking methods to develop the diversity of hydrogels, and lists out several excellent properties inherent to hydrogels. Based on the recent achievements in nano- and microtechnologies, the interaction between hydrogels and bioactive factors (drug and cell) in biomimetic hydrogel materials are explored in detail. In addition, current injectable hydrogel-based regenerative medicine strategies for treating multiple tissues, such as cardiac tissue, bone tissue, nervous tissue, muscle tissue, and wound, are also covered. Clinical hydrogels that have been applied in regenerative medicine are also summarized. Broadened applications of hydrogels, however, require more advanced engineering technology and design in scientific research and mass production. Finally, this chapter is done with the promises and challenges for the future evolution of hydrogels and their applications, and discusses the avenues of improvement in terms of hydrogel application that will be faced in the future.

Y. Li · P. Su · Y. Wang · T. Ye · W. Wang (✉)
College of Chemical and Biological Engineering, Zhejiang University, Hangzhou, Zhejiang, China
e-mail: wwgfz@zju.edu.cn

G. Nowaczyk
NanoBioMedical Centre, Adam Mickiewicz University, Poznan, Poland

C. Gao (ed.), *Polymeric Biomaterials for Tissue Regeneration*,
https://doi.org/10.1007/978-981-99-6948-7_3

Keywords Regenerative medicine · Mechanical properties · Biodegradability · Biocompatibility · Drug delivery · Cell carrier · Injectable hydrogel

3.1 Introduction

The term "hydrogel" was initially introduced in 1894 to describe the gel-like formations of inorganic salts [1]. Over time, the definition of hydrogel has become more specific, referring to three-dimensional networks of polymer chains that are cross-linked and have the ability to absorb and retain significant amounts of water within the spaces between the networks [2, 3]. Hydrogels possess remarkable properties, leading to their application in various fields including chemical industry, environment engineering, and biological electronic. In 1949, the invention of the poly(vinyl alcohol) (PVA) sponge, commercially known as Ivalon, marked a significant development. From the 1950s onward, PVA hydrogel was extensively studied for its potential biomedical uses, ranging from skin replacement and scaffolds for articular cartilage regeneration to vascular prostheses, tuberculosis treatment, and even as an embolic material [4]. After that, many advanced hydrogels have been developed. For instance, in 1960, poly(2-hydroxyethyl methacrylate) (pHEMA) gels were introduced for soft contact lenses [5], while in 1989, hydrogels derived from collagen and shark fish cartilage emerged for tissue engineering purposes [6].

Since the concept of hydrogel was proposed, the studies of hydrogels are mainly focused on the fabrication, basic physicochemical properties and practical application. In recent decades, there has been a notable surge in research focusing on the functionalization and innovative applications of hydrogels. More specifically, the latest generations of hydrogels have demonstrated remarkable responsiveness to various stimuli such as pH, temperature, biological molecules, electric fields, magnetic fields, and ionic strength of the solution. This unique characteristic has transformed them into "smart" biomaterials, capable of adapting and reacting intelligently [7, 8]. Despite the recent progress in development and application of hydrogels, there are still many challenges to be undertaken in this field. For example, traditional hydrogels cannot afford shocks from the outside, which reduces the service life of materials. Drawing inspiration from the natural world, the incorporation of noncovalent cross-links through well-designed molecular and structural arrangements has the potential to confer a diverse set of desirable properties upon synthetic hydrogels. These properties encompass enhancements in strength, toughness, resilience, processability, and dynamic adaptability. Through the introduction of these noncovalent cross-links, synthetic hydrogels can acquire an array of appealing characteristics, mirroring and even surpassing those found in nature [9].

The aim of regenerative medicine is that convergence in the fields of life science, advanced material science, clinical medicine, computer science and engineering to replace, repair, reconstruct and regenerate complex tissues even organs of the human body. Hydrogels are one of the most attractive materials for regenerative medicine

due to their high-water content, biocompatibility and similarity to native extracellular matrix (ECM). In recent times, researchers have successfully developed a wide range of hydrogels with optimized physical and chemical properties, specifically tailored for applications in regenerative medicine. These hydrogels have been designed to effectively repair and regenerate various types of tissues in the body [10]. As an illustration, hydrogel scaffolds have been strategically engineered to incorporate diverse biophysical and chemical cues, such as toughness, porosity, and degradation. These cues are carefully controlled in terms of their spatial and temporal distribution, enabling systematic regulation of cellular behavior within the hydrogel scaffolds. This regulation encompasses crucial cellular processes such as migration, proliferation, and differentiation [11, 12]. Furthermore, numerous advanced chemical strategies have been proposed along with the integration of functional materials to enhance the functionality of hydrogels. These approaches aim to expand the capabilities and performance of hydrogels, enabling them to fulfill more diverse and sophisticated functions [3, 13].

In this chapter, we explore the frequently utilized hydrogel materials and the strategies employed for their fabrication (bonding modes), properties and applications in regenerative medicine. We emphasize the correlation between hydrogels and bioactive factors (including drugs and cells) in the design and engineering of biomimetic materials. We specifically focus on recent advancements in nano- and microtechnologies that have enabled the development of these materials. Furthermore, we delve into the realm of regenerative medicine and explore current strategies utilizing injectable hydrogels for the treatment of various tissues, such as the heart, bones, nervous system, muscles, and wounds. The intersection of various disciplines such as materials science, cell biology, and chemistry will continue to have a significant impact on the development of functional hydrogels for the regeneration of intricate tissues. The collaboration and integration of knowledge from these diverse fields will be crucial in designing hydrogels that possess the necessary properties and capabilities to successfully regenerate complex tissues. Lastly, we provide perspectives on the current challenges and clinical application prospect in the development of hydrogel-based biomaterials.

3.2 Hydrogel Design Strategy

Hydrogels are three-dimensional interconnected molecular structures, typically polymers, which have the ability to retain significant quantities of water. They contain distinctive functional groups that have the potential to amplify the effectiveness of active elements or cells in the field of regenerative medicine, including enhancing cell adhesion, promoting biodegradation, and facilitating chemical discharge. A range of synthetic polymers (e.g., polyacrylic acid (PAA), polyacrylamide (PAAm), PVA, and their derivatives) and natural polymers (e.g., polysaccharides, polypeptides, and DNA) have been widely explored to synthesize hydrogels with desirable characteristics [14–16].

Recently, different from the above hydrogels, there is a special class of small molecule hydrogels. Small molecule hydrogels are mostly formed by self-assembly of small molecules. Small molecules can form relatively stable aggregations with relatively regular structures by the interaction of nonchemical bonds (e. g. hydrogen bond and p-π phase interaction). Due to the excellent biocompatibility of self-assembled systems, small molecule hydrogels are widely used in life science and medicine. At present, small molecule hydrogels as 3D scaffolds for adherent cells have been relatively mature, which has shown remarkable properties in promoting stem cell-directed differentiation and cell proliferation. Small molecule hydrogels attached drug molecules to gelatinized network for targeted drug delivery by their environmental sensitivity have been reported as well. Several outstanding review papers summarized the development and applications of small molecule hydrogels [17]. In this chapter, we concentrated on the macromolecular hydrogels.

Hydrogel networks are formed either through covalent bonds or noncovalent interactions. Several methods of cross-linking to build polymer networks are subsequently examined, including: (1) physical cross-linking, involving structures like helices, microdomains, hydrogen bonds, electrostatic interactions, metal coordination, guest–host interactions, hydrophobic associations, and π–π stacking; (2) chemical cross-linking, such as the formation of carbon–carbon, carbon–nitrogen, carbon–oxygen, carbon–sulfide, silicon–oxygen, disulfide, hydrazone, oxime, boronate ester bonds, as well as Diels–Alder and Schiff's base reactions; and (3) biological cross-linking, which includes processes like enzyme-driven reactions and molecular recognition [15, 18]. These cross-linking methods exist alone or synergistically constitute to form the hydrogel system.

3.2.1 Physical Cross-Linking

Physical interactions are profoundly prevalent in biological entities and have been rigorously researched for their role in designing soft materials like hydrogels. The purpose of such studies often extends to obtaining superior mechanical properties, among other objectives. As indicated in Fig. 3.1 and Table 3.1, the process of physical cross-linking in hydrogels employs a variety of mechanisms, which include the formation of helical structures, microdomains, hydrogen bonds, electrostatic interactions, and metal coordination. It also involves guest–host interactions, hydrophobic associations, and π–π stacking. Different kinds of physical interactions occupy a considerable part in the preparation of hydrogels, especially in the design of multifunctions in hydrogels.

3.2.1.1 Microdomain

Microdomains are created when amorphous polymers undergo a reversible transition from liquid to glass as the temperature drops below their glass-transition points. This

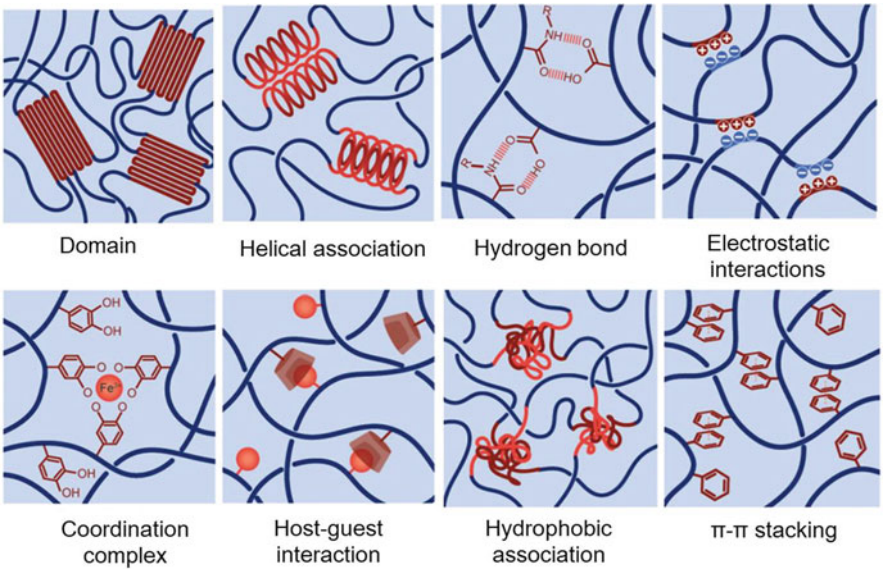

Fig. 3.1 Schematics of polymer network interactions of physical cross-linking [15] (Reprinted with permission from Ref. [15]. Copyright 2021, American Chemical Society)

transition essentially forms a cross-linking network by connecting neighboring polymer chains. An example of this is seen with the polystyrene segments in polystyrene-b-PNIPAm-b-polystyrene copolymers, which can create microdomains at room temperature, thereby cross-linking the block copolymer chains into a polymer network [19]. Microdomains function as high-efficiency cross-linking elements and intrinsically high-energy phases within polymer networks. This, in turn, bestows the resulting hydrogels with exceptional mechanical properties.

Regarding the mechanism of crystalline microdomains, a specific group of both synthetic and natural polymers can form these microdomains under the right conditions. These crystalline microdomains, ranging in size from nanometers to micrometers, can function as a robust physical cross-link for multiple amorphous polymer chains connected to it. For instance, Polyvinyl Alcohol (PVA) can generate crystalline microdomains through repeated freeze-thaw cycles or by annealing at temperatures above its glass transition temperature, enabling it to form a stable gel. Similarly, chitin and chitosan can create semicrystalline polymer networks with crystalline microdomains cross-linking amorphous chains. This is achieved by treating chitin and chitosan with strongly acidic or basic solutions to overcome interchain electrostatic repulsions. Cellulose is another example that can form highly crystallized nanofibers due to the strong interaction between glucose units. These cellulose nanofibers can further aggregate and form a stable network through alkaline treatments. It is important to note, however, that heating these semicrystalline polymer networks above their melting temperatures can dismantle the

Table 3.1 Typical examples of polymer network interactions of physical cross-linking [15] (Reprinted with permission from Ref. [15]. Copyright 2020, American Chemical Society)

Physical cross-linking	Typical examples
Microdomain	Polystyrene-b-poly(N-isopropylacrylamide)-b-polystyrene poly(methyl methacrylate)-b-poly(n-butyl acrylate)
Helical association	Self-assemble of type I collagen, linear agarose, gelatin, fibrinogen and elastin-like polypeptides
Crystalline domain	PVA treated by freeze-thawing or annealing Chitin and chitosan treated by strongly acidic or basic solutions Cellulose treated by alkaline
Hydrogen bond	Gelatin, agarose, amylose, amylopectin, and carrageenan in solutions PMA or PAA with PEG PVA solutions treated by repeated freezing and thawing PEG, PHMEA, and PNIPAm functionalized with amine triazine or diamino triazine groups PEG, PHMEA, PNIPAm, PAA, and PDMAA chains functionalized with UPy groups Polymer chains attached complementary DNA base pairs (A-T, C-G)
Electrostatic interaction	Alginate with Ca^{2+}, Ba^{2+}, Mg^{2+}, Zn^{2+} Chitosan with citrate and tripolyphosphate Cationic polyelectrolytes with anionic polyelectrolytes (anionic poly (L-glutamic acid) and cationic poly(L-lysine)) Poly(3-(methacryloylamino) propyl trimethylammonium chloride) and poly(sodium p-styrene sulfonate)
Coordination complex	Bisphosphonate, catechol, histidine, thiolate, carboxylate, pyridine, bipyridine, and iminodiacetate with metal ions (Cu^{2+}, Zn^{2+}, Fe^{3+}, Co^{2+}, and Ni^{2+}) Bisphosphonate-containing polymers with metal ions (Ca^{2+}, Mg^{2+}, or Ag^{+}) Catechol-containing polymers with metal ions (Cu^{2+}, Zn^{2+}, and Fe^{3+}) Histidine-containing polymers with metal ions (Cu^{2+}, Co^{2+}, and Ni^{2+})
Host–guest interaction	Polymers containing β-CD moieties with azobenzene group adamantly group ferrocene group, t-butyl group Cyclohexyl(ester) group cyclododecyl (amide group, benzyl) Group2-naphthylmethyl group1-pyrenylmethyl group Polymers containing a-CD moieties with n-butyl group, adamantly group, benzyl group trans-azobenzene group Polymers containing cucurbit[n]turil moieties with spermine, diamino hexane, viologens, naphthalenes
Hydrophobic association	PEG, PAAm, PNIPAm, PAM, PDMA, PVA containing hydrophobic moieties (octyl phenol-PEG acrylate, stearyl acrylate lauryl acrylate) Triblock amphiphilic copolymers with PEG, PAAm, PVA, PHEMA middle blocks, and n-alkyl acrylate end blocks
π–π stacking	Polymers modified with aromatic moieties or conjugated structures Hydrogels containing carbon nanotubes, polythiophene, and graphene-based nanomaterials

PMA polymethacrylic acid, *PEG* polyethylene glycol, *PHMEA* poly(2-hydroxethyl methacrylate), *PNIPAm* poly(N-isopropylacrylamide), *PDMA* poly(N,N-dimethylacrylamide), *β-CD* β-cyclodextrin, *α-CD* α-cyclodextrin, *UPy* ureido-pyrimidinone

crystalline microdomains in the networks, although most crystalline microdomains are stable at room and body temperatures.

Regarding the mechanism of crystalline microdomains, a specific group of both synthetic and natural polymers can form these microdomains under the right conditions. These crystalline microdomains, ranging in size from nanometers to micrometers, can function as a robust physical cross-link for multiple amorphous polymer chains connected to it. For instance, Polyvinyl Alcohol (PVA) can generate crystalline microdomains through repeated freeze-thaw cycles or by annealing at temperatures above its glass transition temperature, enabling it to form a stable gel [20]. Similarly, chitin and chitosan can create semicrystalline polymer networks with crystalline microdomains cross-linking amorphous chains. This is achieved by treating chitin and chitosan with strongly acidic or basic solutions to overcome interchain electrostatic repulsions [21]. Cellulose is another example that can form highly crystallized nanofibers due to the strong interaction between glucose units. These cellulose nanofibers can further aggregate and form a stable network through alkaline treatments [22, 23]. It is important to note, however, that heating these semicrystalline polymer networks above their melting temperatures can dismantle the crystalline microdomains in the networks, although most crystalline microdomains are stable at room and body temperatures.

3.2.1.2 Helical Association

Owing to their accurately controlled structures, many natural polymers can form nanometer-scale helical fibers (or fibrils). These can subsequently aggregate or intertwine to create a cross-linking network. As an example, the commonly recognized triple-helix structure of type I collagen is a result of the self-assembly of three peptide strands. These collagen triple helices can bundle together to produce collagen nanofibers, which further self-assemble to form an interconnected network within a hydrogel [24]. Here's another instance: linear agarose chains exhibit disordered coil-like structures in aqueous solutions at elevated temperatures. However, when the temperature is reduced to room or body temperature, they can arrange themselves into double helix strings or simple helical chains. These strings or chains can associate via hydrogen bonding to construct agarose fibers, which can then intertwine to form an interconnected hydrogel network [25].

3.2.1.3 Hydrogen Bond

Compared to these physical cross-linking mechanisms above, many other physical cross-linking mechanisms in polymer networks such as hydrogen bond are relatively weak, transient and reversible. Many natural polymers (such as gelatin, agarose, amylose, amylopectin, and carrageenan) and synthetic polymers (e.g., PVA) can form hydrogels by the intermolecular and intramolecular hydrogen bonds [15]. Another case in point, as shown in Fig. 3.2, Liu and his team developed

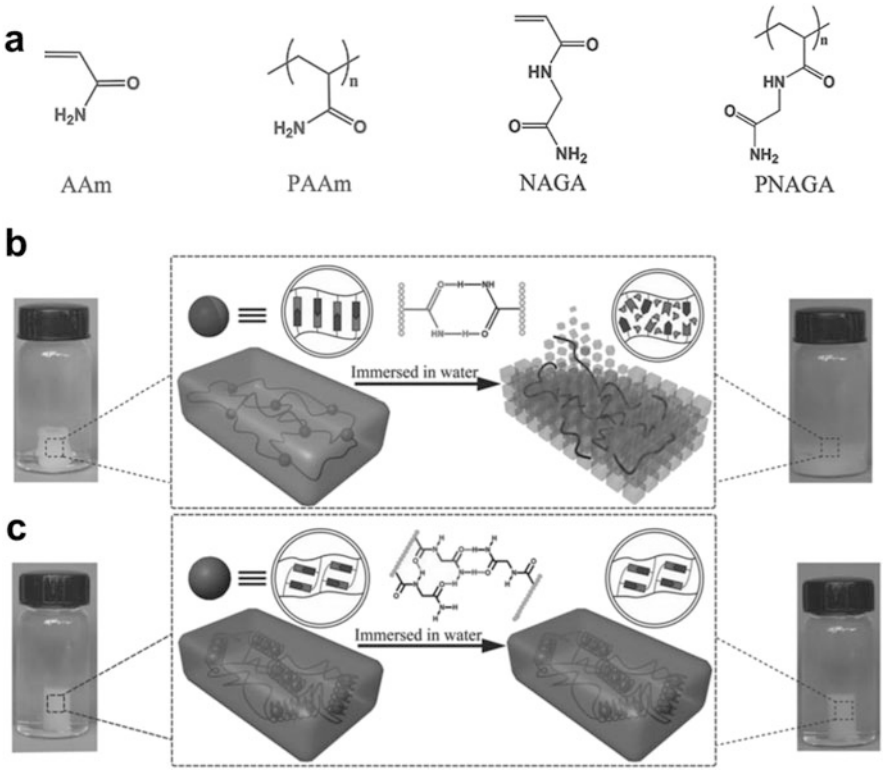

Fig. 3.2 (**a**) Molecular structures of N-acryloyl glycinamide, poly(N-acryloyl glycinamide), acrylamide, and PAAm; (**b**) instability of single amide hydrogen bonding cannot maintain the integrity of a PAAm hydrogel; (**c**) mechanisms underlying the reinforcement effect of dual amide hydrogen bonding microdomains and the high stability of the resultant hydrogels in water (Reprinted with permission from Ref. [26]. Copyright 2020, Wiley-VCH)

N-acryloyl glycinamide (NAGA) in an effort to replicate and intensify the hydrogen bonding interactions among amino acid residues in a polymer hydrogel. This approach was used to ultimately convert these interactions into the primary method of enhancing the mechanical properties of the hydrogel. The enhanced properties included high tensile and compressive strength (at MPa levels), over 1400% elongation at break, substantial toughness, and recoverable deformation [26]. Notably, the dynamic nature of hydrogen bonding rendered the PNAGA gel both thermoplastic and self-healing. This gifted the supramolecular polymer hydrogel with adaptable remolding capabilities, recyclability, and reusability.

3.2.1.4 Electrostatic Interaction

Polyelectrolytes, natural and synthetic polymers with fixed charges, can be physically cross-linked by electrostatic interactions. Chitosan, for instance, is a typical example of a cationic polyelectrolyte hydrogel. It can cross-link with multivalent anions like citrate and tri-polyphosphate. Similarly, electrostatic interactions between oppositely charged polyelectrolytes can also form physically cross-linked hydrogels. A case in point is the injectable hydrogel formed by simply mixing anionic poly(L-glutamic acid) and cationic poly(L-lysine) in phosphate buffered saline solutions. As illustrated in Fig. 3.3, Gong and his team have conducted extensive research on polyampholyte (PA) hydrogels. For instance, they created a PA hydrogel endowed with antifatigue properties [27]. It's important to mention that the creation of ionic cross-linking typically necessitates the use of solvents with a low ionic strength for the hydrogels. This is to prevent the occurrence of charge shielding.

3.2.1.5 Coordination Complex

Hydrogels cross-linked by coordination complexes are primarily created by incorporating chelating ligands into polymer backbones, which then form coordination

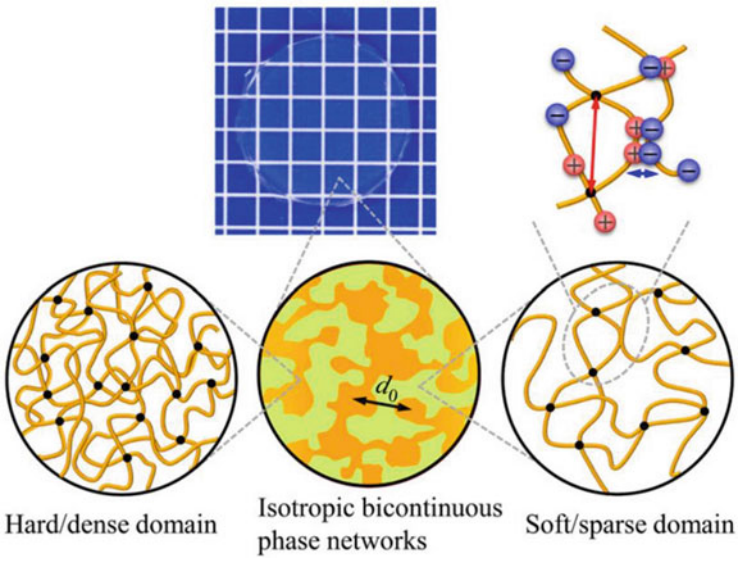

Fig. 3.3 Illustration for hierarchical structures in PA gels. PA gels are composed of hierarchical structures containing ionic bonds (sacrificial bond) at the 1-nm scale (indicated by blue arrow), cross-linked polymer network with mesh size at the 10-nm scale (indicated by red arrow), and bicontinuous hard/soft phase networks with mesh size at $d_0 \sim$ 100-nm scale (indicated by black arrow) (Reprinted with permission from Ref. [27]. Copyright 2020, American Chemical Society)

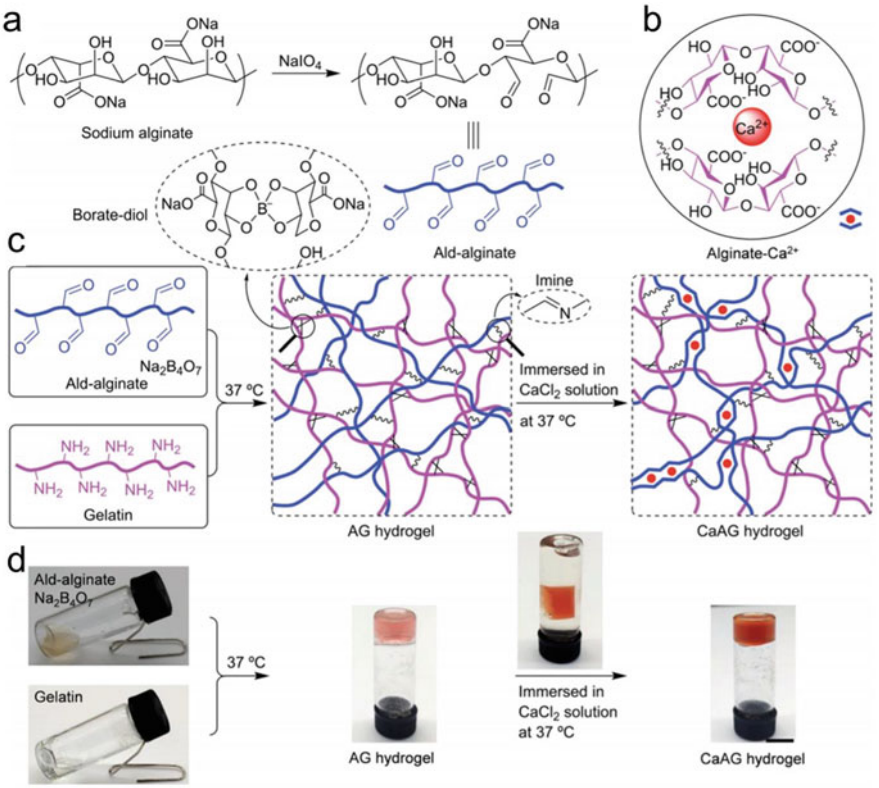

Fig. 3.4 Schematic representation of CaAG hydrogel preparation. (**a**) Synthesis of ald-alginate. The hydroxyl groups of alginate are oxidized by periodate into aldehyde groups; (**b**) Schematic illustration of the alginate-Ca^{2+} "egg-box" structure; (**c**) Preparation of the CaAG hydrogel. The AG hydrogel is formed by imine linkage between ald-alginate and gelatin. The CaAG hydrogel is formed by a combination of covalent cross-linking between gelatin and ald-alginate and ionic cross-linking between Ca^{2+} and ald-alginate; (**d**) Image of CaAG hydrogel preparation. The AG hydrogel is obtained by mixing ald-alginate, borax, and gelatin. The CaAG hydrogel is obtained by immersing the AG hydrogel in $CaCl_2$ solution. The wine red hydrogel becomes darker with increasing incubation time ascribed to the formation of imine linkage (-CH=N-) (Reprinted with permission from Ref. [28]. Copyright 2020, RSC)

complexes with metal ions. A classic example involves the amino acid histidine providing an imidazole ligand residue, which is one of the most crucial chelators in the human body. The mechanical attributes of hydrogels cross-linked by coordination complexes can be adjusted by altering the types of metal ions and/or chelating ligands used. For metal coordination, a typical case is alginate forms a hydrogel in the vicinity of divalent cations (such as Ca^{2+}, Ba^{2+}, Zn^{2+} and Mg^{2+}). In this context, the two carboxylic groups present on various polymer chains are linked together by divalent cations due to the electrostatic forces generated between the opposite charges. As demonstrated in Fig. 3.4, based on ion coordination complexes, Zhang

et al. prepared a highly Ca^{2+}-cross-linking ald-oalginate-gelatin imine (CaAG) hydrogel by diffusion method with high stretchability and flexibility [28].

3.2.1.6 Other Interactions

Host–Guest Interaction

Host–guest interactions describe the unique structural relationships between two or more molecules or ions, which are maintained by forces other than covalent bonds. The most prevalent host entities include Cyclodextrins (CDs) and Cucurbit[n]urils (CB[n]). For instance, α-CDs serve as host molecules for various hydrophobic guest molecules (such as azobenzene and ferrocene) that have suitable molecular sizes. They form a stable gel through hydrophobic and van der Waals interactions [29]. In another instance, Cucurbit[n]urils (CB[n]) can create stable complexes with either two molecules of 2,6-bis(4,5-dihydro-1H-imidazol-2-yl) naphthalene, or one molecule each of viologen (paraquat) and 2,6-dihydroxynaphthalene, resulting in the formation of hydrogels [30].

Hydrophobic Association

Hydrophobic domains can be incorporated either through postpolymerization modifications (for instance, using the grafting-to approach) or by copolymerizing hydrophobic monomers within the polymer chains, whether randomly or in blocks. These adjustments typically necessitate the use of nonaqueous solvents, mixed solvents, or micellar systems. A standard method of introducing hydrophobic domains is by copolymerizing hydrophobic stearyl acrylate monomers within PAAm chains [31]. Another instance of introducing hydrophobic domains is the creation of multiblock copolymers with hydrophobic alkyl acrylate end blocks and a substantial middle block composed of PEG, PAAm, PAA, or PHEMA polymers [32]. It's important to note that because a single hydrophobic association can link multiple polymer chains, hydrophobic associations have been employed as high-functionality cross-links in hydrogels. However, the energy of hydrophobic association is typically lower than that of crystalline domains and microdomains.

π–π Stacking Interaction

The π–π stacking interaction represents a specific type of noncovalent interaction, specifically involving the attractive forces between π electrons in aromatic groups. Natural amino acids possessing aromatic rings, such as phenylalanine, tyrosine, and tryptophan, along with other compounds featuring conjugated structures like fluorenylmethyloxycarbonyl (Fmoc), 1-pyrenebutyric acid, 2-naphthalene acetic acid, and nitrophenyl methacrylate, can be utilized in the design and production of

polymers with aromatic components. These can facilitate gelation through the π–π stacking interactions [33].

3.2.2 Chemical Cross-Linking

Chemically cross-linked hydrogels have significantly influenced research in recent years due to their advantageous mechanical attributes and the ability to fine-tune their structural and chemical properties. The formation of hydrogels through chemical cross-linking encompasses irreversible chemical cross-linking as well as dynamic reversible chemical cross-linking. In the past several decades, chemical bonds have been devised and synthesized for soft materials, including elastomers, hydrogels, and organ gels, with the aim of achieving exceptional properties.

3.2.2.1 Irreversible Chemical Cross-Linking

In the field of chemistry, the gelation process is defined as the gradual linking of polymer chains within the reaction system into one large-scale molecule of "infinite" size. Here, irreversible chemical bonds are the most typical, and numerous properties of hydrogels have been built on this principle. Standard instances of irreversible chemical cross-linking encompass carbon–carbon bonds, carbon–nitrogen bonds, carbon–oxygen bonds, carbon–sulfide bonds, and silicon–oxygen bonds. These bonds are the most frequently used techniques to construct traditional hydrogels.

Carbon–Carbon Bond

Hydrogels that are covalently cross-linked by carbon–carbon bonds typically form via the radical copolymerization of monomers and di−/multivinyl cross-linkers. These cross-linkers can either be small molecules with two double bonds (like N, N′-methylenebis-(acrylamide) (MBAA)) or macromolecules carrying multiple acrylate groups. For example, the integration of a photo initiator within the polymer framework, such as Gelatin Methacryloyl (GelMA) or hyaluronic acid methacryloyl (HAMA), under light exposure (like UV light) will produce free radicals via rearrangement, fragmentation, or energy transfer. This creation of free radicals is then followed by the polymerization propagation step, which aids in the formation of carbon–carbon bonds and the resultant hydrogel [34]. For instance, as shown in Fig. 3.5, Qiao et al. prepared developed an innovative osteogenic polypeptide hydrogel, termed GelMA-c-OGP. This was achieved by co-cross-linking a template photo-cross-linked GelMA with photo-cross-linkable osteogenic growth peptides (OGP) using ultraviolet radiation [35].

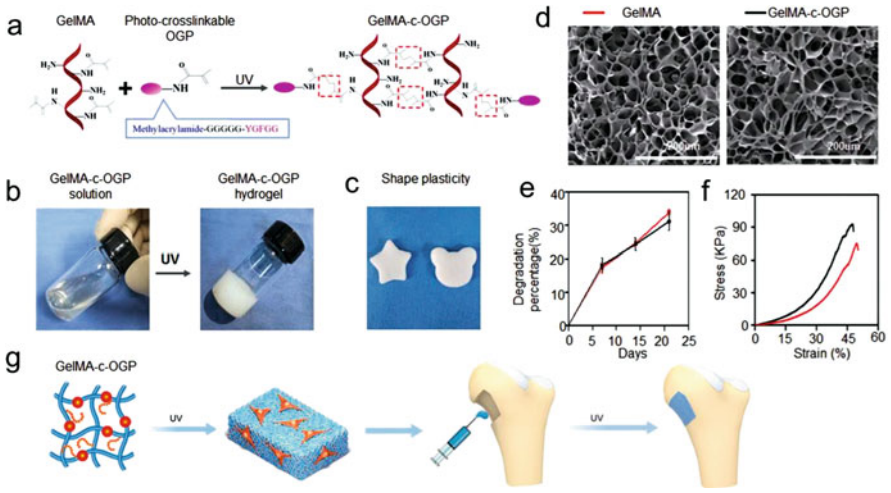

Fig. 3.5 Flow chart of GelMA-c-OGP hydrogel construction and its mechanical properties. (**a**) The chemical molecular structure of the methacrylate OGP polypeptide and gelatin (GelMA), and the structure of GelMA-c-OGP with ultraviolet (UV) light; (**b**) photograph of GelMA-c-OGP solution and GelMA-c-OGP hydrogel formation after UV light; (**c**) a fixed-shaped gel block after photo-cross-linking of GelMA-c-OGP hydrogel; (**d**) SEM images of GelMA and GelMA-c-OGP hydrogel; (**e**) degradation percentage of GelMA and GelMA-c-OGP hydrogel ($n = 3$); (**f**) stress of GelMA and GelMA-c-OGP hydrogel ($n = 3$); (**g**) the pipeline of GelMA-c-OGP applied for bone regeneration (Reprinted with permission from Ref. [35]. Copyright 2019, Wiley-VCH)

Carbon–Nitrogen Bond

Hydrogels that are covalently cross-linked through carbon–nitrogen bonds typically form via highly efficient chemical reactions involving complementary groups. For instance, amide bonds have been extensively utilized as the covalent cross-links for hydrogels, achieved by condensation reactions between amines and carboxylic acids or their derivatives. Facilitating agents like N-Hydroxysuccinimide (NHS) and N, N-(3-(dimethylamino) propyl)-N-ethyl carbodiimide (EDC) are often used to speed up the condensation reaction between amines and carboxylic acids. The carbon–nitrogen bonds can also be created via the addition reactions of amines with electrophiles, such as adipic acid dihydrazide and diisocyanate cross-linkers [36]. Another type of reaction that can produce carbon–nitrogen cross-links for hydrogels is the azide-alkyne cycloaddition reaction [37].

Carbon–Oxygen Bond

The ester bond, a prevalent form of the carbon–oxygen bond, is typically formed through reactions between hydroxyl groups and carboxylic acids or their derivatives. These ester cross-links can be easily hydrolyzed, making the hydrogels degradable under ambient temperature and physiological conditions [15, 18]. In addition to ester

cross-linking, carbon–oxygen bonds also occur in ether groups and urethane groups. These bonds can establish a polymer network due to the reactions between side groups on polymers, such as hydroxyl groups on polysaccharides and glutaraldehyde [38].

Carbon–Sulfide Bond

The formation of covalent cross-linking in hydrogels via carbon–sulfide bonds is primarily accomplished through thiol-click reactions. The substantial electron density of the sulfide atom predisposes thiols to engage in reactions with various functional groups via a catalyzed or radical process. Thiol groups can be readily transformed into electrophilic thiyl radicals or nucleophilic thiolates, which then proceed with radical chain processes or nucleophilic reactions to execute thiol-click reactions. Specifically, for radical thiol-click reactions, thiol groups can be stimulated by heat or UV light, generating radicals that initiate the radical-mediated thiol-yne or thiol-ene reactions [39]. In contrast, for nucleophilic thiol-click reactions triggered by strong bases, thiol groups can readily engage in reactions with electron-deficient end-functional compounds via Michael addition, with isocyanate derivatives via carbonyl addition, with halides via SN_2 nucleophilic substitution, and with epoxy motifs via SN_2 ring-opening reactions [40]. Thiol-click reactions are typically highly efficient and result in a high conversion rate without producing any side products, even in the presence of water, ions, and oxygen. These reactions have been widely utilized in the production of hydrogels for a variety of biomedical applications.

Silicon–Oxygen Bond

The silicon–oxygen bond is primarily employed in the creation of silicone-based hydrogels and generally boosts the mechanical characteristics of these hydrogels [41]. Furthermore, silicon–oxygen bonds have been extensively utilized for modifying the surfaces of materials, including hydrogels, to improve their specific performance characteristics [42].

3.2.2.2 Reversible Chemical Cross-Linking

Reversible chemical cross-linking method accounts for a large part of the latest research about hydrogels. Reversible chemical cross-linking mainly involves the incorporation of functional groups in the polymer chains such as disulfide bond, hydrazone bond, oxime bond, boronate ester bond, Diels–Alder reaction and Schiff's base reaction. Because of the introduction of dynamic reversible chemical bonds, hydrogels are designed to construct many excellent novel properties. These dynamic chemical bonds give hydrogels some special properties. As shown in the

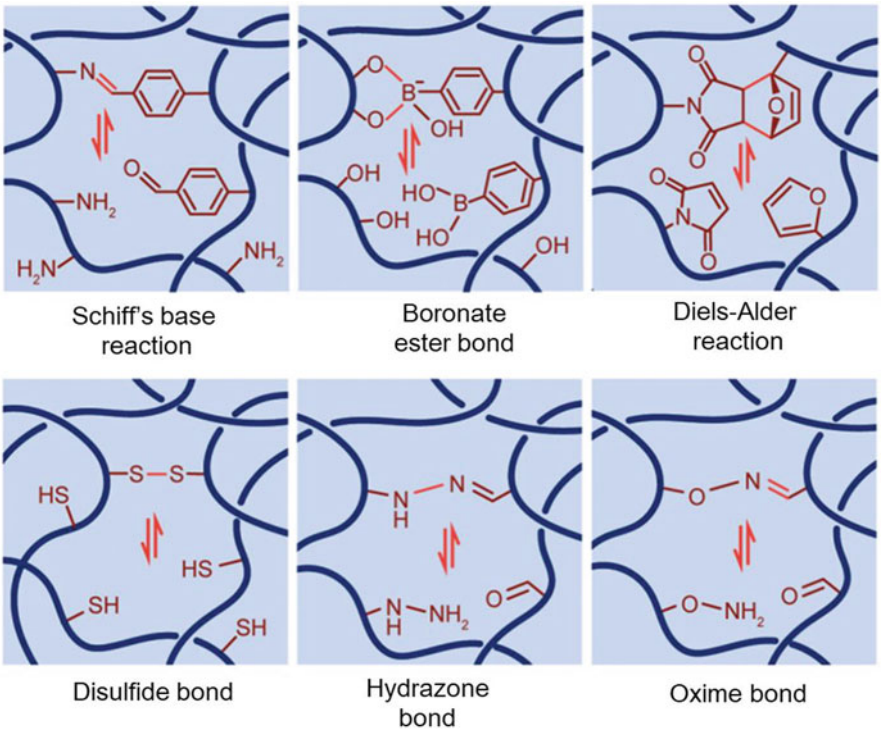

Fig. 3.6 Schematics of polymer network interactions of dynamic reversible chemical cross-linking [15] (Reprinted with permission from Ref. [15]. Copyright 2021, American Chemical Society)

Fig. 3.6 and Table 3.2, several reversible chemical cross-linking methods are outlined and their performance in biological systems is summarized.

Disulfide Bond

Disulfide bonds are dynamic covalent bonds that form based on thiol-thiol interactions under mildly alkaline or mildly oxidative conditions. The reaction between thiol groups occurs at a relatively quick pace and can be employed to manufacture dynamic hydrogels. Hydrogels that are cross-linked by disulfide bonds are ideal for encapsulating various types of cells due to the gentle reaction conditions. As illustrated in Fig. 3.7, hydrogels were created through the copolymerization of acrylamide (AAm), acrylic acid (AAc), and N, N′-bis(acryloyl)-(L)-cystine salt (BISS). BISS, which contains photo-exchangeable disulfide bonds, served as a dynamic covalent cross-linker to impart photoplasticity. The dynamic exchange potential of the disulfide bonds enables the hydrogel shapeshifter's form to be dictated by plasticity [43].

Table 3.2 Typical examples of polymer network interactions of chemical cross-links [15] (Reprinted with permission from Ref. [15]. Copyright 2021, American Chemical Society)

Chemical cross-linking	Typical examples
Carbon–carbon bond	Radical copolymerization of monomers and di-/multivinyl cross-linkers or macromolecules with several (acrylate groups) Monomers and cross-linkers with vinyl groups or acrylate groups high-energy radiation (gamma and electron beams) Polymers without unsaturated bonds under high-energy radiation (gamma and electron beams)
Carbon–nitrogen bond	Amines with carboxylic acids and derivatives Addition reactions of amines with electrophiles (adipic acid dihydrazide and diisocyanate cross-linkers) Azide-alkyne cycloaddition reaction between alkyne and azide
Carbon–oxygen bond	Hydroxyl groups and carboxylic acids or derivatives Ether groups and urethane groups (hydroxyl groups (polysaccharides and PVA) and reactive cross-linkers (glutaraldehyde, divinyl sulfone, dibromide, and diisocyanate))
Carbon–sulfide bond	Thiol-click reactions
Silicon–oxygen bond	Silicone-based hydrogels Hydrogels and diverse engineering materials with modified surfaces
Boronate ester bond	PVA, alginate, and cellulose solution and phenylboronic acid
Disulfide bond	Thioctic acid, bovine serum albumin (BSA) Other cysteine-containing proteins, peptides, or other thiolated polymers Pyridyl disulfide-modified HA with PEG-dithiols
Hydrazone bond	Oxidized HA-containing aldehyde groups (HA-CHO) and adipic acid dihydrazide-modified HA (HA-ADH)
Oxime bond	ODex and amine alkoxylate modified Pluronic F127 (AOP127)
Diels–Alder reaction	Hyaluronic acid/cellulose modified with diene groups and dienophile groups PNIPAM/PEG modified with diene groups and dienophile groups
Schiff's base reaction	Amino on gelatin and glutaraldehyde

Hydrazone Bond

Hydrazone bonds are the product of reactions between aldehyde and hydrazide groups. By simply combining aldehyde- and hydrazide-bearing polymers under physiological conditions, reversible hydrazone bonds can be formed. Due to the biocompatible nature and swift gelation kinetics of aldehyde and hydrazide coupling, hydrogels that are cross-linked by hydrazone bonds are suitable for *in situ* cell encapsulation. The mechanical properties of such hydrogels can be adjusted easily, allowing for the exploration of the correlations between cell behaviors and hydrogel mechanics, like stress–relaxation kinetics. Hydrazone bonds can also facilitate the creation of self-healing and injectable hydrogels, thanks to their reversibility in slightly acidic environments (pH 4.0–6.0). As demonstrated in Fig. 3.8, hyaluronic acid containing aldehyde groups (HA–CHO) and adipic acid dihydrazide-modified

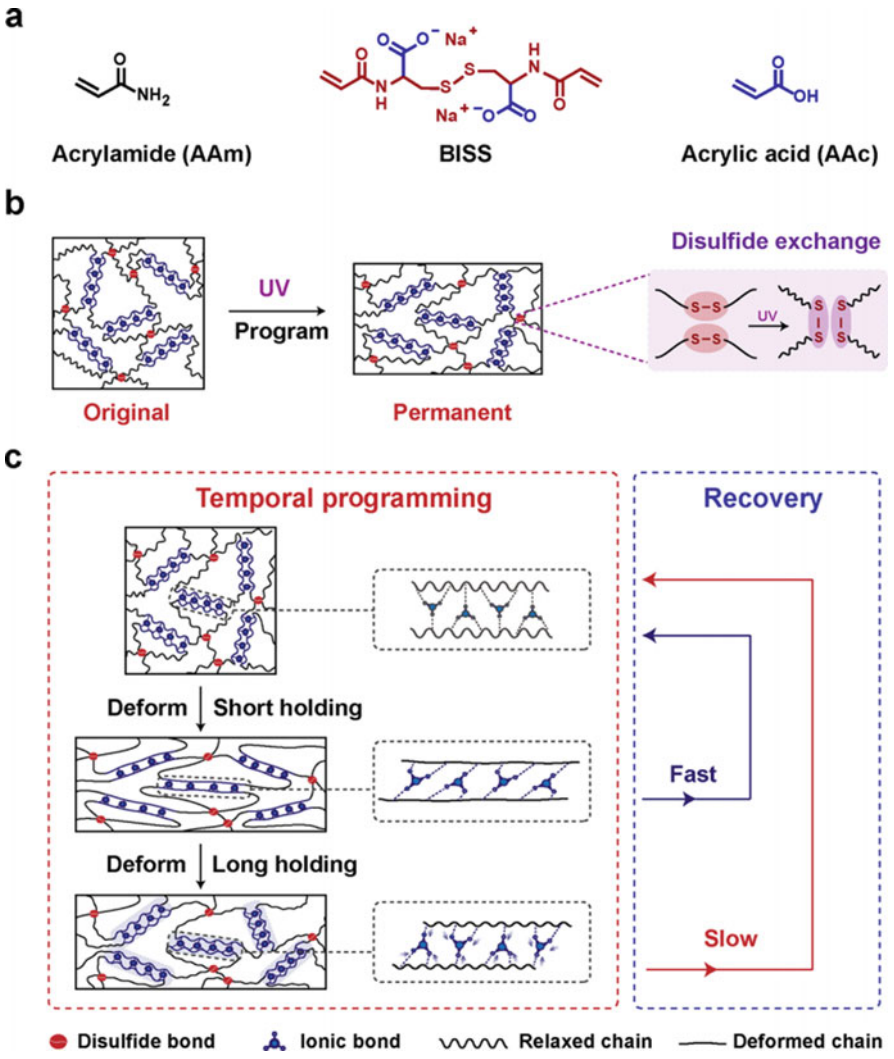

Fig. 3.7 Design of the orthogonal dynamic network and the molecular mechanism for programming its shapeshifting behaviors. (**a**) Molecular structures of the monomers and cross-linker; (**b**) Disulfide exchange for photo-plasticity; (**c**) Molecular mechanism for temporal programming via ion exchange (Reprinted with permission from Ref. [43]. Copyright 2021, American Chemical Society)

HA (HA–ADH) were synthesized through $NaIO_4$ oxidation and carbodiimide coupling reactions respectively. The hydrogel was then produced by combining aqueous solutions of HA-CHO and HA-ADH, capitalizing on the dynamic covalent hydrazone bond. This resulted in a self-healing and malleable hyaluronic acid (HA) hydrogel, which was used as an antiadhesion barrier around tendons [44].

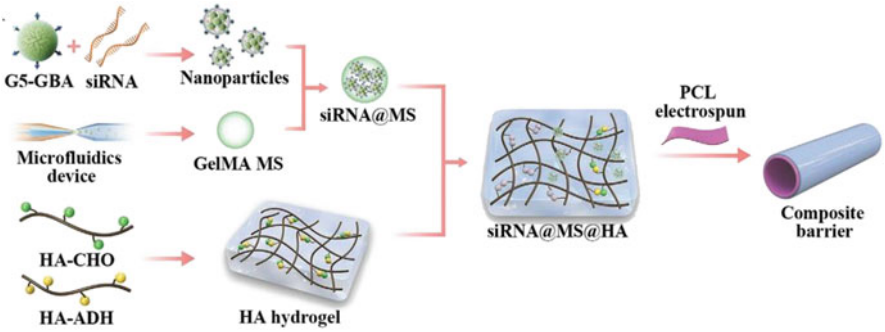

Fig. 3.8 Fabrication process of the siRNA@MS@HA hydrogel-electrospun antiadhesion barrier for peritendinous antiadhesion (Reprinted with permission from Ref. [44]. Copyright 2022, Wiley-VCH)

Schiff's Base Reaction

Schiff's base reactions occur when aldehyde and amine groups react. This condensation reaction, which involves the dehydration of a water molecule, results in the formation of a carbon–nitrogen double bond. The reversible characteristics of the Schiff's bond confer upon the resulting hydrogels qualities such as mechanical dissipation, self-healing capabilities, and response to stimuli. Schiff base bonds are particularly advantageous in the creation of biomedical hydrogels, as most biocompatible natural (like gelatin and protein) and synthetic polymers carry amino groups. As depicted in Fig. 3.9, a series of adhesive hydrogels with desirable properties were designed through a dual-dynamic bond cross-linking process involving Fe, protocatechualdehyde containing catechol and aldehyde groups, and quaternized chitosan (QCS). Firstly, the dual-cross-linking of a pH-sensitive coordinate bond (catechol-Fe) and dynamic Schiff base bonds, which can reversibly break and reform, enhances the mechanical characteristics of the hydrogel while also granting it injectability and self-healing attributes. Additionally, the catechol-Fe cross-linked matrix demonstrates excellent photothermal capacity. The hydrogel also shows remarkable antibacterial capability due to the inherent antibacterial activity of QCS. Furthermore, the catechol and aldehyde groups used for dynamic cross-linking give the hydrogel excellent adhesive properties. Most importantly, the pH-sensitive catechol-Fe bond, whose stability depends on the addition of an iron-chelating agent, allows for the controlled dissolution or removal of the adhesive hydrogel when a suitable stimulus is applied. These beneficial properties make the adhesive hydrogel a smart wound sealant and glue suitable for closing skin incisions, and promoting infected wound healing and tissue regeneration [45].

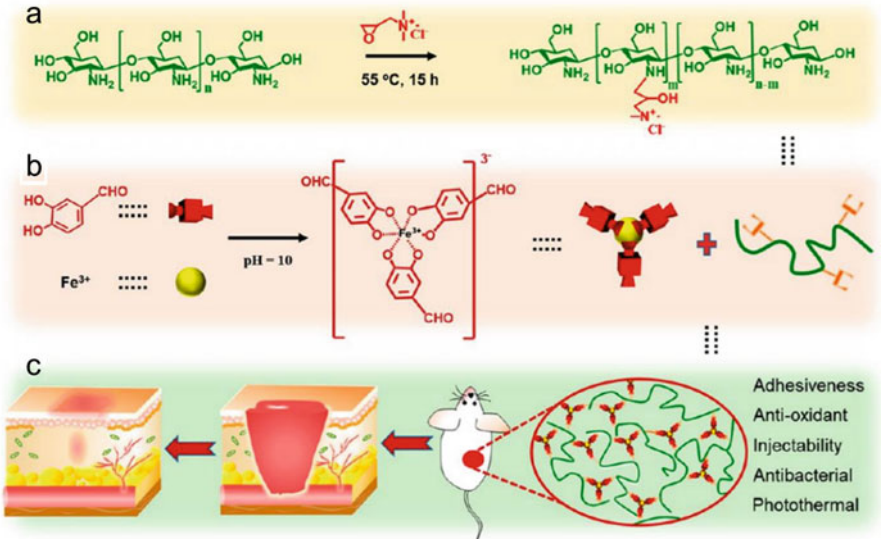

Fig. 3.9 Schematic illustration for the preparation and application of an adhesive hydrogel. (**a**) Synthesis of quaternized chitosan. The molar ratio of GTMAC to amino groups on the chitosan backbone was set as 2:1; (**b**) fabrication of a PA@Fe tricomplex molecule (pH 10); (**c**) dual-dynamic-bond cross-linked adhesive hydrogel shows applications in wound closure and postwound-closure care (Reprinted with permission from Ref. [45]. Copyright 2021, American Chemical Society)

Boronate Ester Bond

Dynamic boronate ester bonds are created through the reaction of diols and boronic acid. A characteristic example is that polyhydroxy polymers like PVA, alginate, and cellulose can be turned into dynamic hydrogels. This is achieved by combining these polyhydroxy polymers with boronic acid-containing polymers in aqueous solutions.

Oxime Bond

Oxime bonds are created when hydroxylamine reacts with aldehyde or ketone, a process that is highly efficient under gentle conditions. The aldehyde or ketone groups can be integrated onto polymers through radical polymerization or oxidation, while hydroxylamine motifs are primarily added to hydroxyl-rich polymers through a series of reactions involving N-hydroxyphthalimide-induced Mitsunobu reaction and hydrazine reduction. Oxime bonds are then formed by mixing the polymers containing aldehyde or ketone with those containing hydroxylamine in a neutral or slightly acidic water solution. This reaction is biocompatible, not yielding cytotoxic byproducts, and can be used to form hydrogels from biopolymers. Thanks to their dynamic nature, oxime bonds have been employed in the creation of self-healing and

injectable hydrogels. These gels display greater resistance to hydrolysis than hydrogels cross-linked by imines and hydrazones.

Diels–Alder Reaction

The Diels–Alder reaction is a click reaction that occurs between diene and dienophile groups. To leverage the dynamic Diels–Alder reaction for the reversible cross-linking of hydrogels, both natural polymers (like hyaluronic acid, cellulose, and other polysaccharides) and synthetic polymers (like PNIPAM and PEG) can be altered. This alteration involves the introduction of diene functional groups (like furan) and dienophile functional groups (such as maleimide) on the polymer backbones or chain ends.

3.2.3 Biological Cross-Linking

Biological cross-linking is one of preparation methods of hydrogels' network. Biological cross-linking typically engages enzyme-driven reactions and molecular identification processes, as well as the incorporation of bioactive particles. Biological cross-linking often has high reaction efficiency. But biological cross-linking tends to degrade due to their weak interaction.

3.2.3.1 Enzyme-Mediated Reaction

Enzyme-driven reactions serve as one of the methods for cross-linking in the creation of hydrogels, typically involving the use of enzymes. Comprehending the kinetics of these enzymes allows us to employ them to catalyze the gelation formation process. For example, horseradish peroxidase, a protein that in the presence of hydrogen peroxide, oxidizes phenols, thus initiating carbon–oxygen (C-O) or carbon–carbon (C-C) bonds between the two phenols. Another illustrative example is the cross-linking of layers by the monophenol residues [46]. Another illustrative example is utilizing the synergistic bridging of triazoles and metal ions to induce the formation of porous enzyme-assembled hydrogels with reusability and increased activity. The catalytic efficiency of the prepared enzyme-assembled hydrogels toward acetophenone reduction is 6.3 times higher than that of the free enzyme [47], as demonstrated in Fig. 3.10.

3.2.3.2 Molecular Recognition

Biomolecular recognition represents another significant approach in biological cross-linking. Essential molecules for recognition and signaling, such as

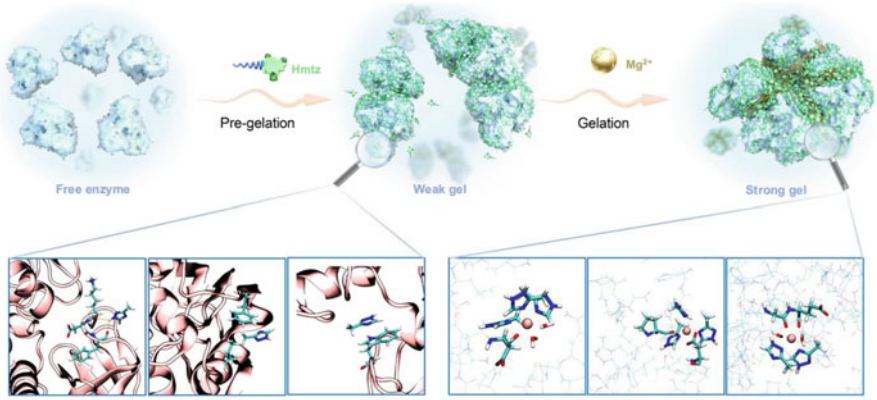

Fig. 3.10 Schematic of EAG preparation. 1H-3-methyl-1,2,4-triazole (Hmtz) and Mg^{2+} ions were added to the enzyme solution before the pregelation and gelation processes, respectively. The left three local structures show some potential interaction sites of Hmtz on the protein surface; the right three local structures show the possible coordination spheres of Mg^{2+} at the bridging interface (Reprinted with permission from Ref. [47]. Copyright 2023, Springer Nature)

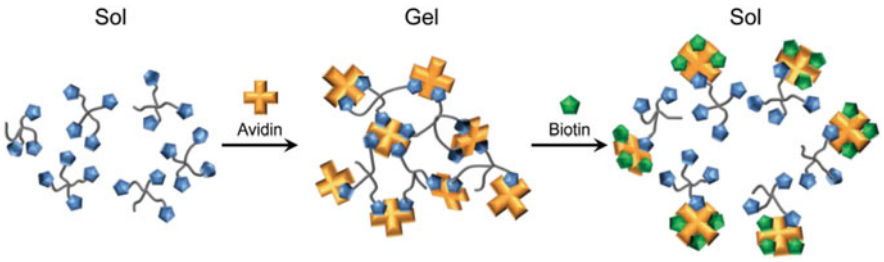

Fig. 3.11 Schematic representation of the sol-gel transition of a buffer solution with biotinylated Tetra-PEG in response to free avidin and biotin (Reprinted with permission from Ref. [49]. Copyright 2019, RSC)

antigen-antibody pairs and transmembrane proteins with their ligands, are prevalent in organisms, facilitating fundamental life functions. Miyata and his colleagues devised a number of hydrogels responsive to biomolecules. For example, they developed a structure incorporating immunoglobulin G (IgG) as both the antigen and antibody, wherein IgGs promote the coalescence of monomers, leading to the hydrogel's gelation [48]. As depicted in Fig. 3.11, a buffer solution featuring biotinylated Tetra-PEG undergoes a phase transition from a sol to a gel state in response to Avidin used as a target biomolecule. Upon the addition of Biotin, the solution instantaneously reverts to a sol state due to the formation of a biomolecular complex between Avidin and Biotin [49].

Every gelation system comes with its own set of advantages and disadvantages. For example, physical cross-linking methods, while convenient, typically result in weaker structures. On the other hand, chemically cross-linked systems have superior

mechanical strength. However, the chemical cross-linking process often involves substances that may have detrimental impacts on cells. When it comes to biological cross-linking, the use of bioactive particles can lead to instability, as these particles are susceptible to denaturation or degradation. The benefits and drawbacks of each gelation system are detailed in Table 3.3.

3.3 Properties of Hydrogels

Owing to their distinctive network structure, hydrogels exhibit a range of physical and chemical properties including high-water content, robustness, toughness, elasticity, extensibility, biodegradability, and biocompatibility. These properties can be meticulously controlled to align with the specific demands of applications in diverse areas such as tissue engineering, biomedicine, biosensors, and environmental engineering. This discussion explores inherent characteristics of hydrogels including their swelling/nonswelling behavior, mechanical attributes, degradation properties, and biocompatibility.

3.3.1 Swelling/Nonswelling Properties

Swelling property is an inherent property of hydrogels. Because of the interleaved three-dimensional network structure and high porosity inside hydrogels, they can store large amounts of water (up to 50% and above). The swelling capacity is usually measured by weighing method. Hydrogels were removed from solution, blotted with filter paper to eliminate excess medium from the surface and weighed at regular intervals. The swelling capacity is calculated as the following Eq. (3.1) at different time points [50, 51].

$$SC = \frac{w_s - w_d}{w_d} \times 100\% \tag{3.1}$$

where SC (%) is the swelling capacity, w_s is mass of the wet hydrogels, w_d is mass of the dried hydrogels.

Initially, PAA hydrogels improve the swelling capacity of hydrogels from several times to thousands of times. However, the biggest problem of PAA hydrogel is that it cannot be degraded. Therefore, many studies have been carried out on the degradability of superabsorbent hydrogels. Achieving the equilibrium between absorbability and degradability will also be the development trend of superabsorbent hydrogels in the future. High-water content makes hydrogels have the characteristics (such as permeability for various chemical and biological molecules) like the liquid. So, it has a broad application prospect in many fields such as biology and medicine. High-water content gives hydrogels these excellent properties and expands their

Table 3.3 Different cross-linking mechanisms and their respective advantages and disadvantages

Cross-linking mechanism		Pros	Cons
Physical cross-linking	Microdomain	Strong mechanical properties	–
	Helical association	Simple synthesis method	–
	Crystalline domain	Enhancing the mechanical properties of hydrogels to exhibit exceptional characteristics such as toughness, strength, resilience, and fatigue resistance	Raising the temperature of semicrystalline polymer networks beyond their melting points can lead to the disruption of their crystalline regions
	Hydrogen bond	Transient; reversible	–
	Electrostatic interaction	Simple synthesis method	Require low ionic strength of the solvents for the hydrogels to avoid charge shielding
	Coordination complex	Mechanical properties can be tuned	–
	Host–guest interaction	High efficiency; mild reaction conditions	Only specific groups
	Hydrophobic association	Transient; reversible	–
	π–π stacking	Transient; reversible	Only aromatic groups; weak mechanical properties
Chemical cross-linking	Carbon–carbon bond	High efficiency; high specificity	Need external energy (e.g., UV, gamma, and electron beams)
	Carbon–nitrogen bond	High reaction efficiency; mechanical properties can be regulated by adjusting the concentration and ratio of the polymers and cross-linking agents; Azide-alkyne cycloaddition reaction has good biocompatibility without side reactions	Small molecule residue
	Carbon–oxygen bond	High efficiency	Degradable under ambient temperature and physiological conditions
	Carbon–sulfide bond	High efficiency; conversion rate of the reaction is notably high, with no formation of side products	Heat and/or UV light
	Silicon–oxygen bond	High reaction efficiency	High-temperature/high-energy excitation
	Boronate ester bond	Usually can dynamically restructure after fracture, making the resultant hydrogels injectable and self-healable	–
	Disulfide bond	Have the ability to undergo dynamic restructuring following	Potentially toxic chemicals involved

(continued)

Table 3.3 (continued)

Cross-linking mechanism		Pros	Cons
		fracture, thereby enabling them to be injectable and self-healing in nature	
	Hydrazone bond	Simple synthesis method; high specificity; can be easily tuned	–
	Oxime bond	High efficiency; mild conditions	–
	Diels–Alder reaction	Biocompatible without cytotoxic side products; higher hydrolytic stability	–
	Schiff's base reaction	Sensitivity to a wide range of chemical and biological stimuli, such as pH, free amine, and free aldehydes. Makes them suitable for applications in biomedicine as self-healing materials and injectable scaffolds	–
Biological cross-linking	Enzymatic cross-linking	High specificity	Specific conditions; side effects
	Biomolecule recognition	–	Rapid degradation

applications. Since hydrogels directly exposure in air, which can remove water inside them, so the preservation of hydrogels becomes a major issue limiting their application.

However, how to control the swelling and response behavior of hydrogels to make them more widely used (such as pH response) is still a research hotspot. Si et al. developed highly elastic, cellular-structured nanofibrous hydrogels (NFHs) with adjustable water content, enabling them to monitor dynamic pressure over an extensive range (>50 Pa), and offering strong sensitivity (0.24 kPa^{-1}) and durability (100 cycles) [52]. Another noteworthy example is a hydrogel device designed to be swallowed like an ordinary pill, which expands into a large soft sphere once ingested [53] (Fig. 3.12).

Despite the exceptional qualities of hydrogels, their applicability can be limited due to a phenomenon known as "swelling," which is triggered by differences in osmotic pressure. Swelling can significantly reduce the mechanical toughness of the hydrogels. Additionally, if hydrogels show hysteresis during deformation, the equilibrium between osmotic and elastic energies is lost when part of the polymer network breaks, even if only temporarily. This leads to further swelling, and sustained mechanical stress can ultimately lead to the hydrogel's destruction [54]. To tackle this issue, the concept of nonswelling was introduced. A viable strategy involves incorporating thermoresponsive segments to control swelling and thus maintain the initial shape of a robust hydrogel that can function under physiological conditions [55].

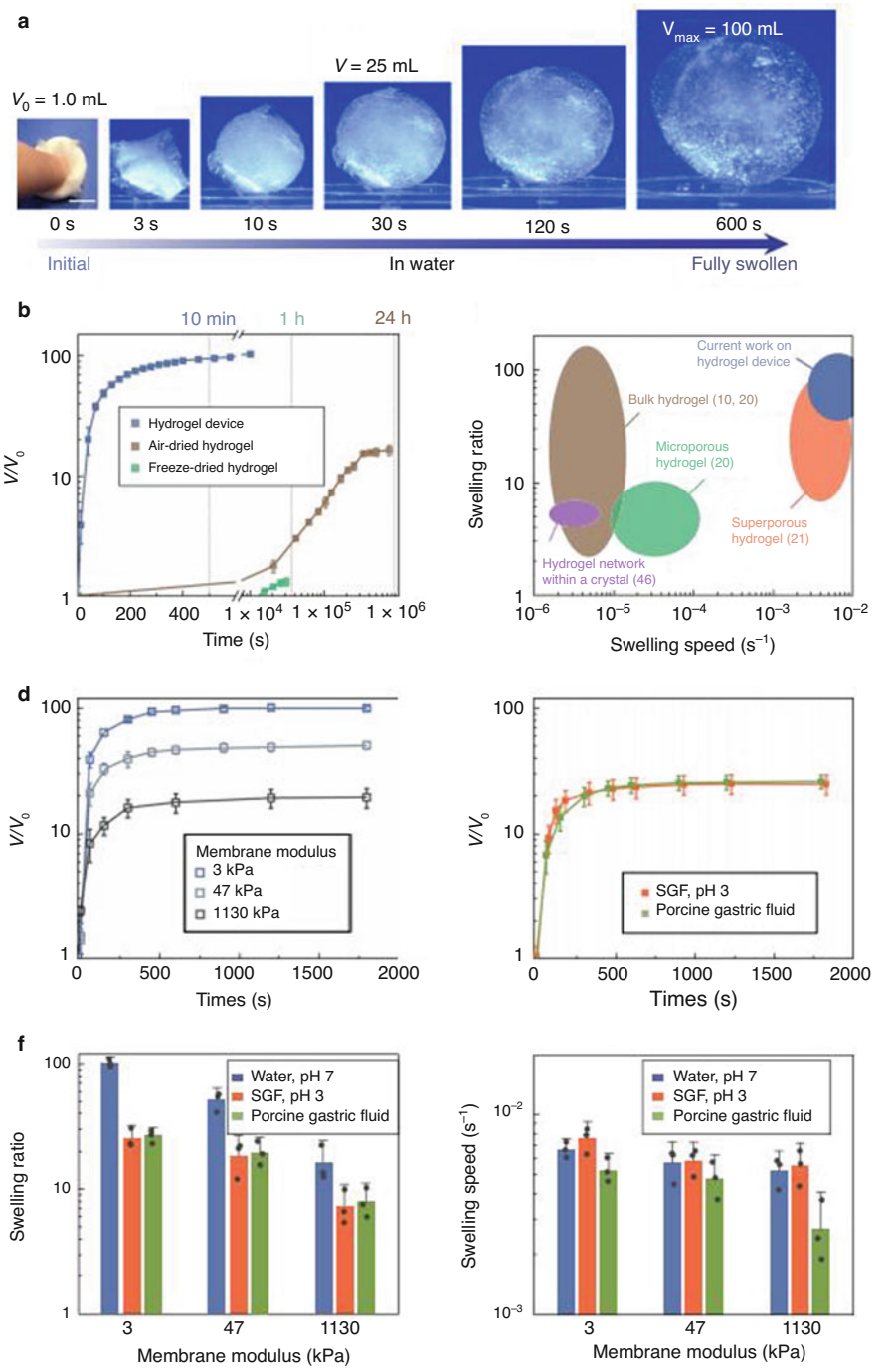

Fig. 3.12 High-speed and high-ratio swelling of the ingestible hydrogel device. (**a**) Time-lapse images of the hydrogel device swelling in water (pH = 7); (**b**) volume changes of the hydrogel device (membrane modulus 3 kPa), air-dried hydrogel, and freeze-dried hydrogel of the same size

3.3.2 Mechanical Properties

For the practical application of hydrogels, achieving requirements for specific mechanical properties is one of the most prominent issues. Due to the fragility of hydrogel, mechanical tests were usually conducted using a universal testing machine with a load speed of 5–10 mm/min using a 100–500 N load cell. Rectangular specimens (5–10 mm width, 40–50 mm length, and 3–10 mm thickness) were prepared for tensile testing ($n \geq 3$) [56, 57].

Hydrogels, depending on their preparation process and composite materials, can exhibit mechanical strengths varying from a few Pascals to several hundred MPa, opening up possibilities for their use across diverse fields [58]. Chemically bonded hydrogels generally demonstrate respectable mechanical strength and durability, and dual cross-linked network hydrogels exhibit enhanced mechanical characteristics [59]. Nanocomposite-based supramolecular networks can show superior stretchability and tensile strength, expanding the range of potential applications for hydrogels, such as in flexible wearable sensors [60]. Furthermore, the mechanical properties of hydrogels are a critical consideration in the development of devices using 3D printing technology [61]. A typical case is constructing dual-physical cross-linking networks based on PVA and chitosan to achieve varied mechanical strength hydrogels by 3D printing (Fig. 3.13).

3.3.3 Biodegradability

Biodegradability is one of the basic characteristic activities of hydrogel carriers (drug, protein, gene, and macromolecule) entering organisms. The organism consumes and absorbs the carrier by an enzyme or other active molecule, and the carrier also acts on the organism in turn, affecting the rate of its reaction. The degradation mechanism of hydrogels is attributed to the break of polymer molecular chains. There are three main degradation pathways: hydrolysis (such as synthetic hydrogels PEG and PLA), enzymatic hydrolysis (such as collagen, gelatin and HA) and dissolution (such as ion cross-linked sodium alginate hydrogels) [62]. According to the different degradation mechanisms of hydrogels, certain shape hydrogels were

Fig. 3.12 (continued) as a function of swelling time in water; (**c**) comparison of the swelling ratios and speeds in water between the hydrogel device in current work and previously reported hydrogels; (**d**) volume changes of the hydrogel devices with various membrane moduli as functions of swelling time in water. (**e**) volume changes of the hydrogel devices (membrane modulus 3 kPa) as functions of swelling time in porcine gastric fluid and SGF (pH = 3); (**f**) swelling ratios of the hydrogel devices with various membrane moduli in water, SGF (pH = 3), and porcine gastric fluid; (**g**) swelling speeds of the hydrogel devices with various membrane moduli in water, SGF (pH = 3), and porcine gastric fluid. Scale bar is 10 mm in (**a**). Data represent the mean ± s.d. ($N = 3$) (Reprinted with permission from Ref. [53]. Copyright 2019, Springer)

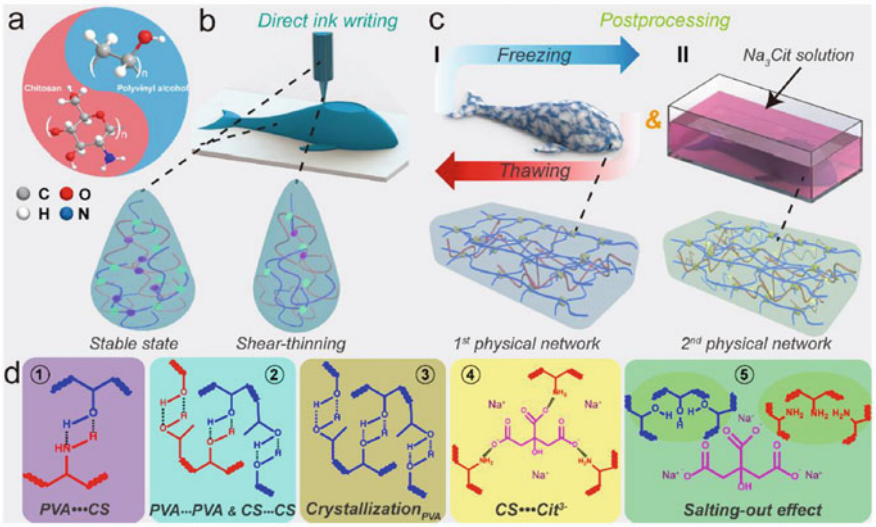

Fig. 3.13 (**a**, **b**) The hybrid hydrogel ink, consisting of PVA and chitosan, used to manufacture desirable complex structures by DIW relying on the rheology. (**c**) The dual-step post processing: cyclic freezing-thawing and soaking into Sodium citrate solution. (**d**) The dominant molecular interactions in the whole manufacturing steps (Reprinted with permission from Ref. [61]. Copyright 2017, American Chemical Society)

placed in the water environment/body fluid environment *in vitro* or *in vivo*. The mass changes before and after degradation was calculated and compared at regular intervals in laboratory. The degradation behavior (degradation rate or degradation percentage) of hydrogels could be obtained by the dry state weighing method [62]. More detailed terms are specified in ISO 10993-9-2019 (framework for identification and quantification of potential degradation) and ISO 10993-13-2010 (identification and quantification of degradation products from polymeric medical devices).

Due to the nonuniformity of hydrogels, they will degrade during practical application, especially in organisms. Through composition control and structure design, the time and rate of carriers' biodegradation can be controlled. A new self-healing hydrogel was created using chitosan-fibrin (CF) as the base material. As exhibited in Fig. 3.14, this hydrogel demonstrated injectability and underwent approximately 70% degradation within a span of 2 weeks. Notably, it successfully restored blood circulation in the ischemic hindlimb of mice, showcasing its potential therapeutic capabilities [62].

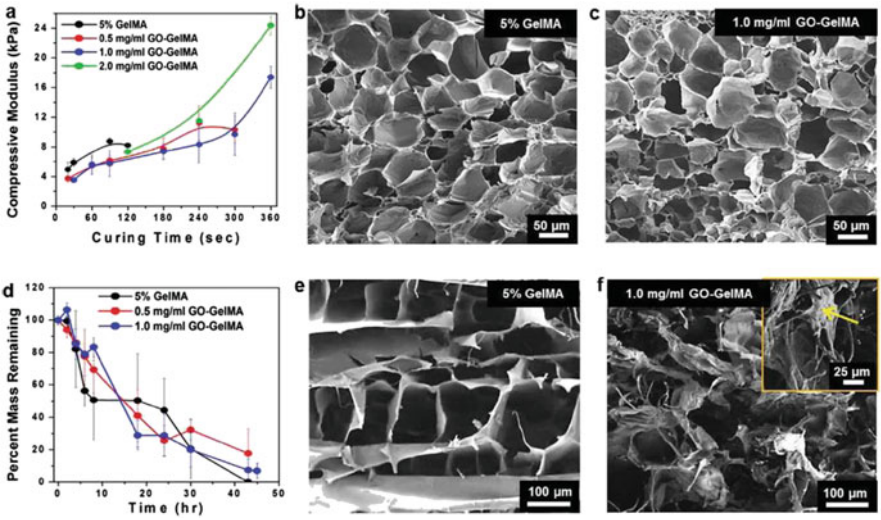

Fig. 3.14 Mechanical, porosity and degradation characteristics of GO-GelMA hybrid hydrogels. (**a**) Compressive modulus varies with the GO concentration and UV-exposure time. SEM cross-sectional images of hydrogels with (**b**) 5% GelMA (0 mg/mL GO, 120 s exposure) and (**c**) GO-GelMA hybrid (1.0 mg/mL GO, 360 s exposure) reveal similar porosity before collagenase degradation; (**d**) Degradation profiles of hydrogels with various GO concentrations when exposed to collagenase. SEM cross-sectional images of (**e**) GelMA and (**f**) GO-GelMA hydrogels reveal distinctively different gel morphologies after degradation with collagenase for 24 h. In the inset of (**f**), the yellow arrow indicates a folded GO sheet (Reprinted with permission from Ref. [62]. Copyright 2017, Wiley-VCH)

3.3.4 Biocompatibility

Biocompatibility refers to the performance of living tissues in response to inactive materials, generally refers to the compatibility between materials and hosts. After implanted into the organisms, the biological material will exert influence and effect on the specific biological tissue environment, and the biological tissue will also exert influence and effect on the biological material. The cyclic effect of the two will continue until the balance is reached or the implant is removed. Conventional biological assessment involves the examination of the interactions between materials and the body at the cellular and tissue levels, considering both short-term and long-term effects. This evaluation utilizes various morphological detection methods, including cytotoxicity, sensitization, stimulation, systemic toxicity (acute toxicity), subchronic toxicity (subacute toxicity), genotoxicity, implantation, chronic toxicity, carcinogenicity, reproductive and developmental toxicity, and biodegradation. ISO standards such as ISO 10993-5-2009, ISO 10993-3-2014, ISO 10993-4-2017, ISO 10993-10-2010, ISO 10993-23-2021, ISO 10993-11-2017, and ISO 10993-6-2016 outline specific tests for various aspects of biological evaluation. These include *in vitro* cytotoxicity tests, tests for genotoxicity, carcinogenicity, and reproductive

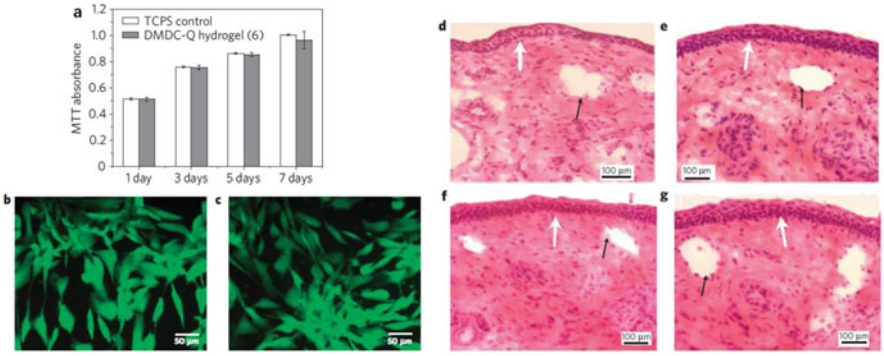

Fig. 3.15 *In vitro* and *in vivo* biocompatibility studies. (**a**) MTT activities (absorbance at 490 nm) of primary epidermal keratinocytes on tissue culture polystyrene dish (TCPS) control and DMDC-Q-g-EM hydrogel (entry 6). Error bars represent mean standard deviation of mean for $n = 3$; (**b**, **c**) LIVE/DEAD analysis of primary epidermal keratinocytes on TCPS control (**b**) and DMDC-Q-g-EM hydrogel (entry 6) (**c**) after 7 days of culture; (**d**–**g**) microscopic observations of hematoxylin–eosin-stained frozen sections of conjunctiva: (**d**) Normal conjunctiva epithelium showing normal epithelium and stromal blood vessels; (**e**) PO day 5 positive control, tissue overlying the surgically created pocket without a lens implant; (**f**) PO day 5, tissue overlying the pocket with an uncoated lens; (**g**) PO day 5, tissue overlying the pocket containing a DMDC-Q-g-EM hydrogel-coated lens (entry 9). White arrows indicate the conjunctival epithelium and black arrows indicate blood vessels [63] (Reprinted with permission from Ref. [63]. Copyright 2011, Springer)

toxicity, tests for interactions with blood, tests for irritation and skin sensitization, tests for irritation, tests for systemic toxicity, and tests for local effects after implantation.

Biocompatibility is an eternal theme throughout the research of biomaterials. At present, many studies have tried to reach equilibrium state of biocompatibility and other function to improve the efficiency of biomaterials utilization. For example, Li et al. have reported an antimicrobial hydrogel that incorporates dimethyldecylammonium chitosan with high quaternization, grafted with poly(ethylene glycol) methacrylate (DMDC-Q-g-EM), and poly(ethylene glycol) diacrylate. This innovative hydrogel effectively meets the demands for antibacterial and antifungal properties while also exhibiting biocompatibility [63] (Fig. 3.15).

3.3.5 Other Properties

Later, thanks to the abundance of groups in hydrogels, scientists developed more functions of hydrogels to meet the new needs in partial applications such as conductivity, adhesiveness, lubrication, luminescence, anisotropy, self-healing properties, antimicrobial ability, self-healing ability, antimicrobial properties and shape-memory capability. Or researchers are using more sophisticated methods to produce specific microstructure hydrogels with excellent properties, such as 3D

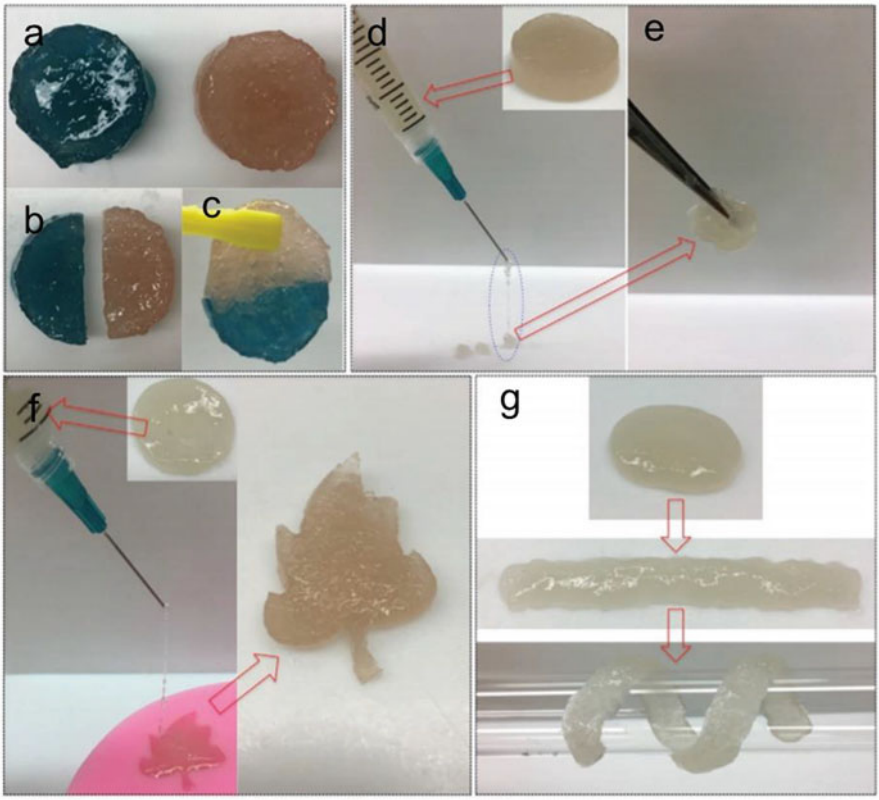

Fig. 3.16 Macroscopic self-healing behavior of the catechol-conjugated chitosan/aldehyde-modified cellulose nanocrystal (CHI-C/DACNC) hydrogel: (**a**) Two disk-shaped original hydrogels (one of the hydrogels is colored with a dye for better observation); (**b**) the hydrogels are cut in half and then put together; (**c**) the hydrogels healed completely into one block quickly at room temperature without any external stimuli. Injectable performance of the CHI-C/DACNC hydrogel; (**d**) the hydrogel is loaded into a syringe with a needle (23-gauge) and then is extruded directly through the needle without clogging; (**e**) the broken hydrogel fragments reformed an integrated hydrogel immediately at room temperature without any stimuli; (**f**–**g**) the CHI-C/DACNC adhesive self-healing hydrogel could be molded into various shapes (Reprinted with permission from Ref. [64]. Copyright 2021, American Chemical Society)

printing and 4D printing. As illustrated in Fig. 3.16, a multifunctional hydrogel based on catechol-conjugated chitosan (CHI-C) was developed, which exhibited adhesion, self-healing, cytocompatibility, hemocompatibility, and the ability to promote blood cell coagulation. The hydrogel was prepared by cross-linking aldehyde-modified cellulose nanocrystals (DACNC). The presence of abundant amine groups in CHI-C and aldehyde groups in DACNC facilitated the formation of strong hydrogels at room temperature through dynamic Schiff-base linkages. Additionally, the inclusion of DACNC nanofillers contributed to the reinforcement of the hydrogel structure. The hydrogel's role in the entire process of bone defect healing, from

hemostasis to tissue regeneration, was investigated, and it was found to promote tissue adhesion, facilitate hemostasis, and support bone regeneration [64].

3.4 Drug Delivery Hydrogels

Traditional dosing methods often require large doses or repeated dosing to achieve therapeutic effects, which will lead to reduced compliance of patients and also prone to large fluctuations in drug concentrations *in vivo* during treatment [55]. When the concentration of drugs is higher than the concentration required for treatment and the maximum safe level, it might be toxic and cause certain side effects to human body [65]. On the other hand, due to the poor targeting of traditional therapies, drug molecules must pass through multiple biological barriers and resist degradation in various chemical environments before finally acting on the target site [66]. Drug concentrations can decrease through diffusion, degradation, and metabolism, which limits their effectiveness. Therefore, controlling the quantitative release of drugs at specific sites in a certain way is in demand, which can maintain the stability of blood drug concentration, thereby improving the therapeutic effect of drugs, reducing dosing frequency [67].

As a particularly attractive new drug delivery system, hydrogels have made various achievements in the field of drug delivery in recent years. Various hydrogels are being developed, such as supramolecular hydrogels [68], DNA hydrogels [69], bio-inspired hydrogels [70], multifunctional hydrogels, stimuli-responsive hydrogels [71], and so on. Reported in many applications, the drug can be dispersed in hydrogels and delivered in a controlled and stable manner under specific conditions or for a long period [72]. To put it simply, the hydrogel is a kind of drug storage from which drugs slowly elute, maintaining a high local concentration of drug in the surrounding tissues over an extended period [65]. At the same time, hydrogels offer a merit that protects labile drug from degradation [72]. Therefore, it is a very efficient drug delivery system with a wide range of application prospects.

The research on drug loading and drug release of hydrogel in recent years are mainly introduced in this part, and an outlook on future directions of hydrogel-based drug delivery systems is provided at the end.

3.4.1 Various Drug Loading Strategies

Incorporation of drugs or bioactive molecules into hydrogels is a prerequisite before their release. By strategically designing the interactions between the drug and the polymer chain, the release of the drug from the hydrogel can be regulated. In this section, various drug loading strategies are introduced, such as physical incorporation, covalent tethering, and affinity interactions [67].

3.4.1.1 Physical Entrapment of Drugs in Hydrogels

To load small molecules, the most straightforward approach is immersing the fully formed hydrogel in a drug-saturated medium. The drug will gradually permeate the gel, influenced by factors such as gel porosity, the unique physical and chemical properties of each component, as well as the drug's size. Once applied *in vivo*, the drug can freely diffuse out of the hydrogel and into the neighboring tissue. This combination strategy enables the convenient physical incorporation of drugs into the hydrogel network. The physical capture and release of drugs by hydrogels were only affected by concentration gradient and cross-linking density of hydrogels [72].

3.4.1.2 Covalent Tethering of Drugs to Hydrogels

Nonetheless, when dealing with larger drugs, proteins, macromolecules, and biological ligands that cannot be easily contained through basic physical entrapment due to their size, the encapsulation and incorporation of these substances need to be achieved through methods such as encapsulation or covalent bonding during the gelation process. The drug and polymer are linked by covalent bonds with highly stable covalent binding, because of which the drug is retained in the hydrogel and released until the bond is subjected to environmental changes or cleaved over time. A variety of cleavable covalent connections exist, spanning from small-molecule connections like ester bonds, disulfide bonds, and linkages that can be cleaved through β-elimination, to larger, macromolecular connections such as those found in peptide sequences. The rate of drug release depends on the rate of cleavage of the linker [72].

As shown in Fig. 3.17, Sun et al. designed a dual-cross-linked hydrogel (DC-gel) with a unique nanoscale network topology, in which substantial mechanical stability provided by the permanent cross-linker can minimizes drug leakage under intrinsic mechanical stress, while the dynamic cross-linker effectively responds to external ultrasound stimuli [73]. The model drug tannic acid (TA) is linked to the hydrogel via dynamic covalent bonds to further reduce endogenous force-induced release. This novel drug delivery system, which can be reliably used under substantial mechanical loads and releases drugs on demand in response to external mechanical forces, could be used to treat diseases of load-bearing tissues such as muscle and cartilage.

3.4.1.3 Affinity Binding of Drugs with Hydrogels

Leveraging diverse physical attractions presents an effective strategy to maintain the containment of drugs within hydrogel networks. This approach benefits from the attraction between two molecules that results from opposing charges, hydrophobic interactions, hydrogen bonding, and/or van der Waals forces [72].

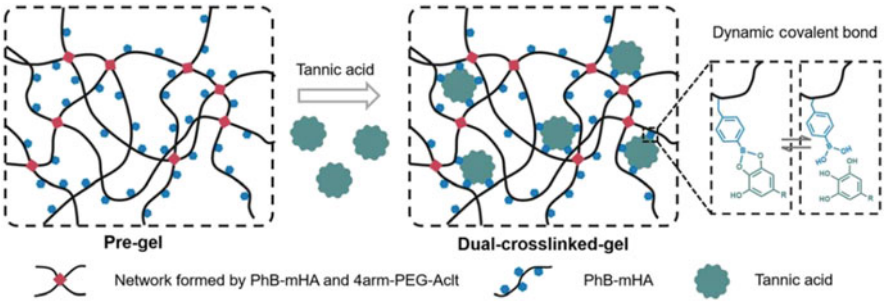

Fig. 3.17 Schematic illustration of a modular DC-gel network composed of dynamic covalent interactions (blue polygon) and permanent covalent cross-linking (red diamond) [73]. The compound 4-(aminomethyl) phenyl boronic acid (PhB) was bonded with hyaluronic acid (HA) to produce PhB-HA. Subsequently, this product was reacted with methacrylic anhydride to form PhB-mHA. Hydrogels were then synthesized through the copolymerization of PhB-mHA and four-armed polyethylene-glycol acrylate (4-arm-PEG-Aclt), creating a pregel only containing the permanently cross-linked network. This pregel was then submerged in a phosphate buffer saline (PBS, pH = 7.4) solution with various tannic acid (TA) concentrations, ultimately leading to the final DC-gel. The hydrogel backbone is connected with TA by dynamic covalent boronate ester linkages (Reprinted with permission from Ref. [73]. Copyright 2018, Springer)

Electrostatic Interactions

Many drugs and polymers that carry charges can be combined by electrostatic interaction and thus have a strong affinity. Drug release occurs either when the hydrogel undergoes degradation or when the electrostatic interactions are masked by the presence of mobile ions from the surrounding environment. For example, as shown in Fig. 3.18, Ding's team successfully engineered a pH-responsive DC-gel loaded with gentamicin (Gen) that boasts superior mechanical properties and sustained antibacterial activity. This was achieved by carrying out free radical polymerization of 2-hydroxyethyl methacrylate (HEMA) and acrylic acid (AA), with the antibiotic Gen serving as the dynamic physical cross-linker. Positively charged Gen binds to negatively charged acrylic monomers through electrostatic interactions, thus incorporating the drug into the hydrogel [74]. The electrostatic interaction between the two can be regulated by pH to control the release of the drug. The hydrogel infused with Gen demonstrated its efficacy in eradicating bacteria in wounds and notably hastening the wound healing process. As such, it could potentially serve as a superior substitute for anti-infective dressings in treating wounds afflicted by bacterial infection.

Hydrophobic Associations

Hydrophobic drugs are inherently incompatible with the hydrophilic hydrogel network. In order to improve load efficiency and sustained release of drugs, the hydrogels delivery system could be designed. For example, coating hydrophobic

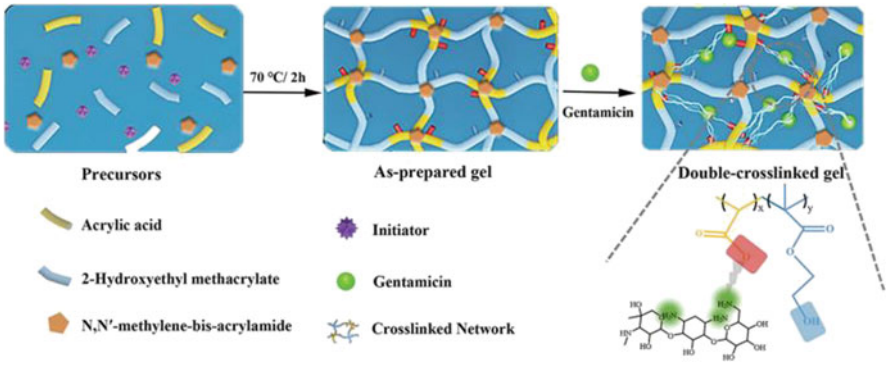

Fig. 3.18 Schematic illustration for the fabrication of DC-gel P(AA-co-HEMA) loaded with Gen [74]. P(AA-co-HEMA) hydrogels were synthesized through free radical polymerization of AA and HEMA, with ammonium persulfate (APS) employed as the initiator and cross-linked using MBAA in diverse compositions. Following this, the P(AA-co-HEMA) hydrogels were submerged in a Gen solution to establish the second network, leveraging the electrostatic interactions between the carboxyl groups of polyacrylic acid and the amino groups of Gen (Reprinted with permission from Ref. [74]. Copyright 2022, Wiley-VCH)

drugs with hydrophilic components prior to incorporation into hydrogels, or introducing hydrophobic domains into hydrogel networks [67], which can make hydrogels have hydrophobic properties, so that they are more suitable for loading hydrophobic drugs. As shown in Fig. 3.19, in Huong's study, physically/chemically DC-hydrogel was designed, utilizing norbornene-functionalized chitosan oligosaccharide (COS-Nb) and tetrazine-functionalized alginate (Alg-Tz) [75]. This design achieved exceptional hydrophobic drug loading efficiency. This accomplishment was made possible through Nb-Tz chemical cross-linking, employing a hydrophobic interaction mechanism that involved the drug, Nb-Tz cross-linkages, and Nb groups. This approach effectively addressed challenges such as premature drug release in gastric conditions, instability of a singular electrostatic network, and the limited drug loading capacity of hydrophobic drugs. This work opens a possible route to prepare hydrophilic hydrogels from natural polysaccharides for the delivery of hydrophobic drugs.

Hydrogen Bond Interaction

Hydrogen bonds represent feeble diatomic associations that occur between an electron-deficient hydrogen atom and an electron-rich atom, typically oxygen or nitrogen. Given their noncovalent and reversible nature, hydrogen bonds ensure the regulated release of the target drug in response to specific stimuli. Hydrogen bonding is also one of the drug loading strategies for hydrogels [76]. A case in point by Song's group, as shown in Fig. 3.20, hydrophilic PVA and certain hydrophobic compounds (luteolin (LUT), quercetin (QUE), and myricetin (MYR)) were swiftly

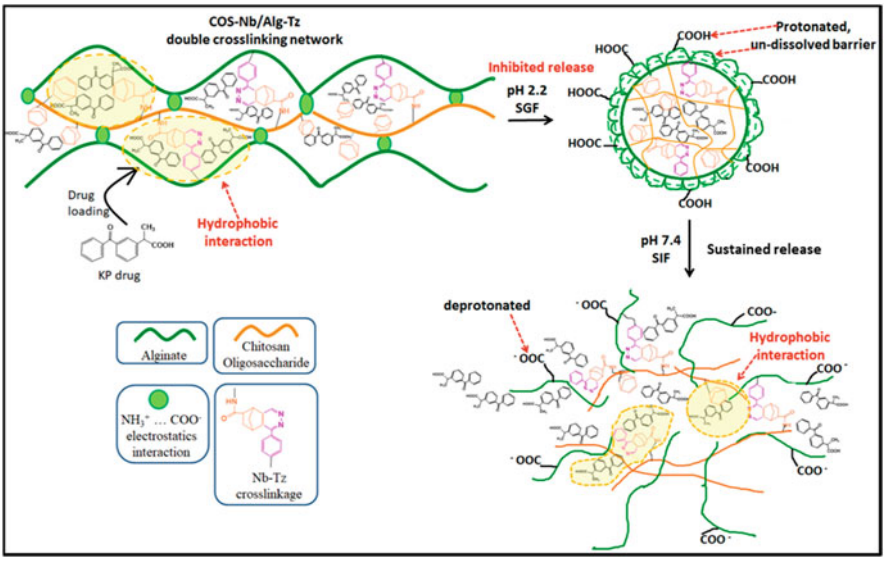

Fig. 3.19 Illustration of mechanism of hydrophobic drug loading and sustained release with the hydrophobic interaction between the drug and hydrogel matrix [75]. The double DC-hydrogels featuring the Nb-Tz hydrophobic linkages, can engage in hydrophobic interactions with the hydrophobic drug, thereby considerably enhancing the drug loading capacity. The discharge of Ketoprofen (KP) from the hydrogels is suppressed at a pH level of 2.2, whereas the release notably escalates at a pH level of 7.4 (Reprinted with permission from Ref. [75]. Copyright 2022, Elsevier)

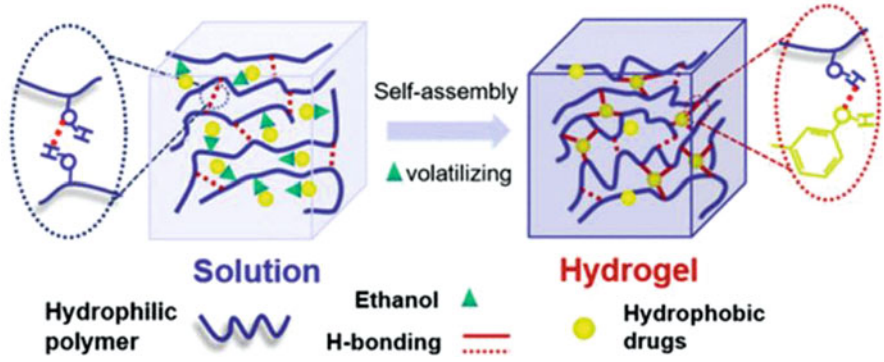

Fig. 3.20 Proposed formation mechanisms of ultra/microhydrophobic cross-linked self-assembled hydrogel [77]. Hydrophobic drugs were used as cross-linkers to produce drug delivery hydrogels. PVA and hydrophobic drugs were rapidly prepared into supramolecular hydrogels by evaporating ethanol to drive hydrogen bond formation. Reversible hydrogen bonds are formed between PVA and hydrophobic drugs through a simple supramolecular self-assembly process (Reprinted with permission from Ref. [77]. Copyright 2021, American Chemical Society)

transformed into a supramolecular hydrogel, which is accomplished by evaporating ethanol to stimulate the creation of hydrogen bonds [77]. In this drug delivery system, the intermolecular hydrogen bonds that form between the hydrophobic drug and the hydrophilic polymer serve to restrict the drug's aggregation, consequently enhancing its solubility within the gel. At the same time, since the hydrogen bond formed between PVA and the drug is noncovalent and reversible, the hydrogel exhibits excellent flexibility and self-healing attributes. Moreover, the release of drugs can be regulated by adjusting the output stimuli. This approach can be further employed to formulate hydrogels with other natural molecules that have poor solubility, broadening its potential for clinical applications.

Ionic Interactions

Ionic interactions, which naturally occur between two molecules of opposite charges, can also be utilized to manage drug delivery. Cationic polymers, characterized by a high density of positive charge groups, can be melded with negatively charged molecules to generate stable complexes [72]. The drug can be retained in the hydrogel by ion binding between the hydrogel and counterionic drug molecules, and the release of drug molecules can be triggered by the degradation of ionic hydrogel or the change of pH. As illustrated in Fig. 3.21, Olate-Moya et al. prepared a novel injectable hydrogel that is responsive to pH and controls the release of doxorubicin hydrochloride (DOX) [78]. This was achieved by incorporating graphene oxide (GO) into polysyringane (PPR) hydrogels, which are formed by inclusion complexes between PEG and α-CD. The supramolecular hydrogels could easily be loaded with DOX due to the attractive ionic interactions between DOX molecules and the carboxylate groups of GO sheets. The resulting nanocomposite displayed a potent pH-responsive drug release mechanism, which was especially quick in acidic conditions. This responsive behavior can be attributed to the protonation of GO carboxylate groups at such pH levels, which reduces the interactions with DOX and consequently initiates its release (Table 3.4).

Proteins in traditional hydrogels are physically retained, and methods to bind proteins in hydrogels by affinity through binding sites such as heparin, peptides and aptamers have also been developed [79]. Advantages and disadvantages of various methods are listed in Table 3.4. There are other affinity effects like host–guest interactions such as host–guest interaction [80], coordination bonds, π–π stacking, and so on.

3.4.2 Drug Release Mechanism in Hydrogel

Various processes are involved in the release of drugs from hydrogels. In many hydrogels, there isn't an immediate or notable swelling when they are transferred to a release environment [81]. In such cases, diffusion becomes the primary mode that

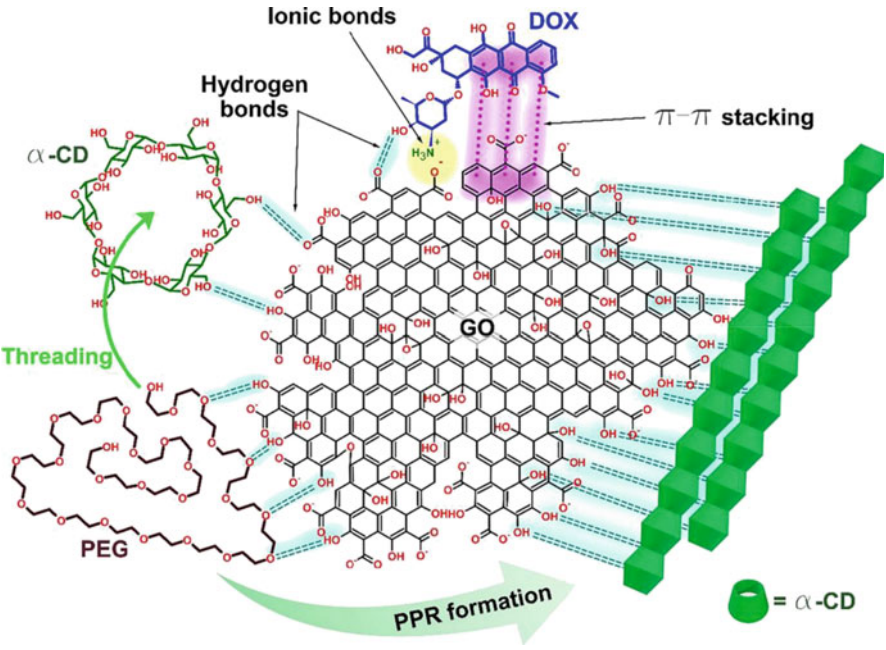

Fig. 3.21 Schematic representation of PPR formation and possible GO interactions with PEG chains, free α-CD, DOX molecules, and PPR structures [78]. PEG chains and α-CD molecules can adhere to GO sheets through hydrogen bonding, which in turn slows down the production of PPR. Additionally, PPR can engage with GO via hydrogen bonds formed between the outer hydroxyl groups of the inclusion complex and the hydrogen donor/acceptor groups present on GO. Furthermore, DOX molecules can form connections with GO via two means: ionic bonds (established between the ammonium group of DOX and the carboxylate groups of GO) and π–π interactions (between the aromatic rings of DOX and the basal plane of GO) (Reprinted with permission from Ref. [78]. Copyright 2021, Wiley-VCH)

regulates the release of drugs from hydrogels, often referred to as diffusion-controlled release [82]. The process of drug release can be effectively described using Fick's laws of diffusion. Yet, there are certain hydrogels that can experience rapid and substantial swelling upon exposure to an aqueous environment. Before the hydrogels begin to swell, the drugs are typically in a stationary state. When the hydrogels transition from a glassy to a rubbery phase during swelling, the drugs start to diffuse rapidly. The rate at which the entrapped drugs are released largely depends on the extent of swelling, a process known as swelling-controlled release. Besides physically enclosing drugs within the hydrogels, it's also possible to chemically attach drugs to the chains of hydrogels. The rate of drug or protein release from these hydrogels is primarily determined by the degradation rate of the hydrogel chains, any mechanical changes, and alterations in the interactions between the polymer and the drug, a process referred to as chemically controlled release [83].

Through network design and mathematical modeling, Chien-Chilin described several mechanisms of molecular release in polymer hydrogel system, including

Table 3.4 Release mechanisms, advantages, and disadvantages of hydrogels for protein delivery [79] (Reprinted with permission from Ref. [79]. Copyright 2021, Elsevier)

Type	Characteristics	Mechanism	Advantages	Disadvantages
Traditional Hydrogels	Proteins are physically retained in matrix No specific binding sites for protein drugs	Diffusion	Simple	Poor protein sequestration Significant burst release
Heparin-based Hydrogels	Heparins serve as binding sites for proteins Binding affinity can be adjusted by varying heparin concentration and sulfation pattern	Reaction-diffusion	Low burst release Promiscuous interaction With variety of proteins	Safety concern due to Derivation from animal tissues Low specificity
Peptide-based Hydrogels	Peptides serve as binding sites for proteins Binding affinity can be adjusted by varying Peptide affinity and concentration	Reaction-diffusion	Reduced burst release High biocompatibility	Low binding affinity High peptide: Protein ratio
Aptamer-based Hydrogels	Aptamers serve as binding sites for proteins Binding affinity can be adjusted by varying aptamer affinity and concentration	Reaction-diffusion	Low burst release High affinity and specificity High biocompatibility Spatiotemporal release Control	Limited availability of aptamers

Table. 3.5 Advantages and disadvantages of delivery approaches [72] (Reprinted with permission from Ref. [72]. Copyright 2014, Elsevier)

Delivery strategies	Advantages	Disadvantages
Physical incorporation-simple Diffusion	Straightforward and simple formulation	Initial burst release; limited control over release profile
Covalent tethering	Controlled release profiles upon degradation of polymer-therapeutic linkages or hydrogel backbone	Issues regarding maintaining therapeutics' stability and biological activity
Affinity binding	Controlled release kinetics; therapeutics Loading of lyophilized scaffolds can be Regulated via physical interactions	Potentially limited release of bioactive molecules possessing high affinity with biomaterials

diffusion, swelling and chemically controlled release [81]. He infers that the physicochemical properties of the hydrogel network and the choice of drug loading method will determine the mechanism of drug release. The advantages and disadvantages of different delivery strategies are summarized as shown in Table 3.5 [72].

3.4.2.1 Diffusion-Controlled Delivery Mechanism

For hydrogel systems containing physically incorporation drugs, the release curve is usually simple diffusion. In this system, the transport of drug molecules through a polymer network is driven by concentration gradients. If there's no interaction between the hydrogel matrix and the drug molecules, a rapid initial discharge typically occurs, which is later followed by a minor delayed release at a subsequent point in time. Here, the cross-linking density of the polymer network is an important design parameter for the release curve. The increase in cross-linking density decreases the average molecular distance between adjacent cross-links, thus reducing the mesh size of the hydrogel. As a result, the diffusivity of the drug factor is reduced. At the same time, it can act as a molecular confinement because the smaller mesh size increases the interaction of the molecule with the hydrogel network. Over time, the cross-linking density of volumetric degraded hydrogels decreases, which increases the pore size of the network and accelerates the transport of molecules (Fig. 3.22).

In Yasin's work, a local drug delivery system was developed, comprising of polycaprolactone (PCL) microspheres filled with methadone hydrochloride/PEG-based hydrogels [84]. The outcomes demonstrated that the drug release could be regulated by both the dual-barrier matrix (hydrogel/microsphere) and the cross-linking density within the hydrogels. In order to examine the impact of cross-linking density on the release pattern of the water-loving drug, methadone hydrochloride, two varieties of pure PEG-based hydrogels were created using two cross-linker agents of varying sizes. The cross-linking density of the hydrogel could be reduced by extending the spacer between functional groups involved in the click reaction. The findings suggested that the cross-linking density of hydrogels could play a significant role in modulating the drug release profiles.

As illustrated in Fig. 3.23, Preeti et al. used PEG as a cross-linking agent to graft polyacrylamide-acrylic acid hydrogel onto cotton fabric to form drug dressing composite [85]. Upon applying the drug release data to the Peppas model, as well as the first and second-order kinetic equations, it was observed that drug release is managed by diffusion and follows the Fickian diffusion mechanism when PEG is used as a cross-linker in the preparation of the composite.

In swelling-controlled drug delivery systems, the thermodynamic compatibility between the polymer chains and water triggers swelling of the polymer when it comes into contact with water-based solutions [86]. As water infiltrates the glassy network, the glass transition temperature of the polymer drops, causing the hydrogel to become rubbery. The drug that is encapsulated within the hydrogel then dissolves into the absorbed water and starts diffusing out of the network.

This occurrence is driven by three forces: the gradient of the penetrant concentration, gradients in polymer stress, and osmotic forces. In a nonswelling-controlled delivery system, the rate at which the polymer relaxes is much slower than the rate of water transport inside the hydrogel. Consequently, the transport mechanism of such systems follows Fickian diffusion. When the relaxation of the macromolecular

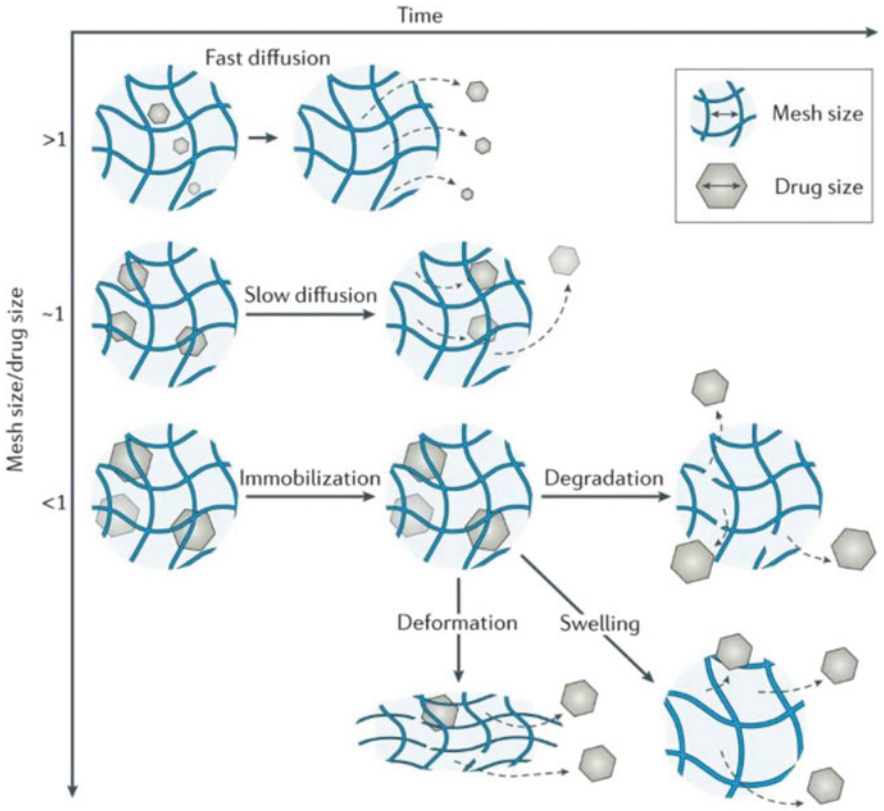

Fig. 3.22 A small drug relative to the mesh size diffuses rapidly through the hydrogel, resulting in a short release duration [67]. As the size of a drug nears the mesh size($r_{mesh}/r_{drug} \approx 1$), the drug's release significantly slows down. If the drug is larger than the mesh size ($r_{mesh}/r_{drug} < 1$), the drugs are physically trapped within the network. To facilitate the release of these initially immobilized drugs, the mesh size can be increased by either degrading the network, inducing swelling, or applying deformation to disrupt the network. The dashed lines represent the route taken by drugs as they diffuse (Reprinted with permission from Ref. [67]. Copyright 2016, Springer)

chains becomes the dominating force, Case II transport is seen. However, an anomalous transport mechanism, which is characterized by a combination of Fickian diffusion and Case II transport, has been noted in many swelling-controlled delivery systems, Fig. 3.24 depicts two typical drug diffusion mechanisms.

3.4.2.2 Stimuli-Responsive Delivery Mechanism

Besides the diffusion and swelling-controlled delivery systems previously mentioned, there exists a third type of molecule release mechanism, known as chemically controlled delivery. In this mechanism, drugs can be progressively released from

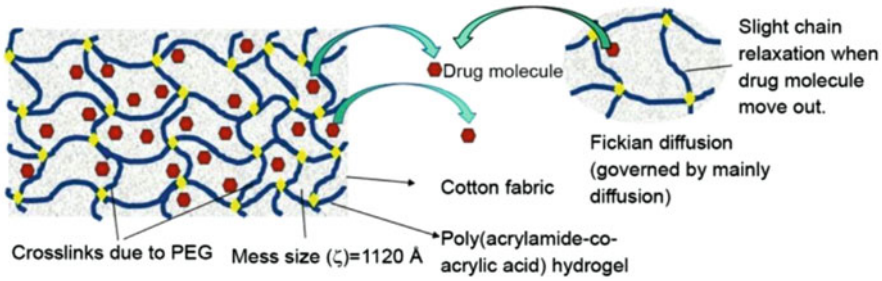

Fig. 3.23 Schematic diagram showing mechanism of drug release from sample [85]. The calculation of mesh size indicates a larger mesh size in the case of the hydrogel composite created with PEG. As it possesses a greater surface area, drug release is primarily controlled by diffusion rather than chain relaxation, a characteristic of Fickian diffusion (Reprinted with permission from Ref. [85]. Copyright 2021, Springer)

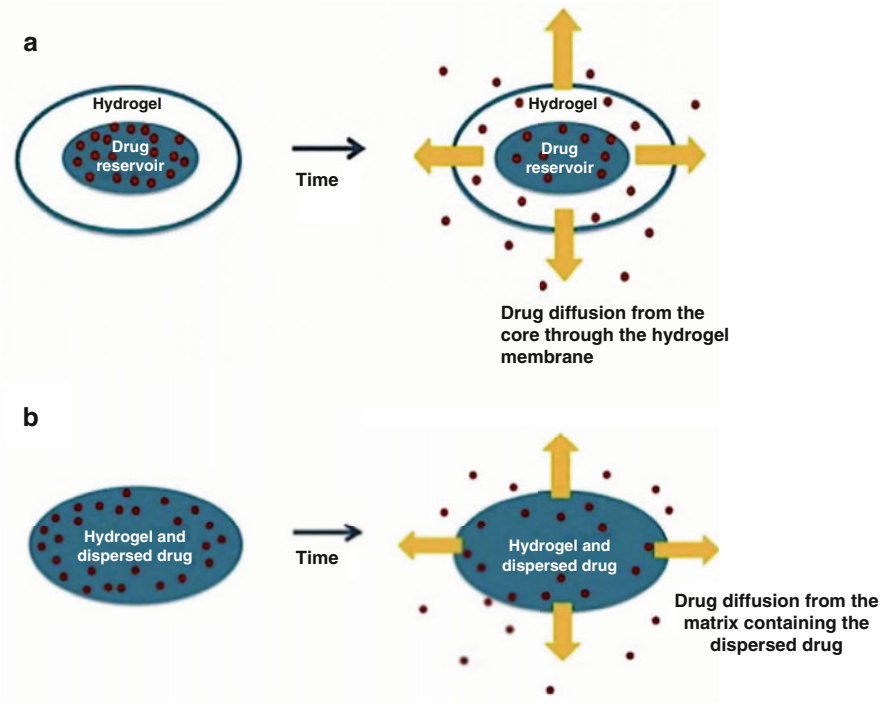

Fig. 3.24 (**a**) In a reservoir delivery system, the drug-containing core is coated with a hydrogel membrane, with the drug concentration being highest at the system's center. This arrangement facilitates a constant release rate of the drug; (**b**) In the case of matrix delivery, the drug is evenly dissolved or dispersed throughout the three-dimensional structure of the hydrogel [87] (Reprinted with permission from Ref. [87]. Copyright 2021, MDPI)

hydrogels through processes such as network degradation, mechanical deformation, and alterations in polymer–drug interactions. These interactions may include covalent conjugation, electrostatic interactions, and hydrophobic associations, for instance [81].

Stimuli-responsive hydrogels represent a new class of intelligent materials that respond to various stimuli. Physical and chemical properties of hydrogels as well as polymer–drug interactions can be meticulously controlled by applying different stimuli, so as to achieve the chemically controlled release of drugs [71]. Disease-affected cells or tissues have abnormal metabolism patterns, which can remodel their microenvironment and change the levels of pH, reactive oxygen species (ROS), and glucose. The degree of these changes is closely linked to the extent of disease progression. Therefore, designing hydrogels that respond to endogenous signaling stimuli associated with disease could allow the hydrogel to release drugs at the desired local zone [88].

pH-Response Release of Drug

The pH levels vary under different physiological and pathological conditions, with a range of 5.4 to 7.4 at wound sites, 6.5 to 7.2 in tumor cells, 7.34 to 7.45 in blood, and 4.8 to 8.2 in the upper small intestine [89]. pH-responsive hydrogels have been extensively utilized in local therapeutic treatments for these diverse diseases. A case in point is QCS/PF hydrogel in Fig. 3.25, which prepared by mixing quaternized chitosan (QCS) and benzaldehyde-terminated pluronic (center dot) F127 (PF127-CHO), was designed for wounds healing [88]. The QCS/PF hydrogel was used to carry curcumin and then subjected to a drug release test. As anticipated, the resulting

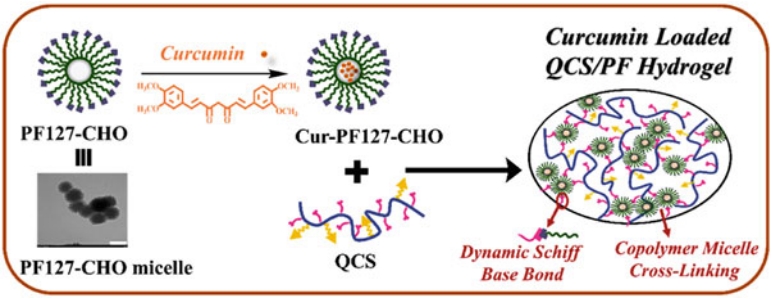

Fig. 3.25 Schematic illustration of Cur-QCS/PF hydrogel and TEM image of PF127-CHO micelles [88]. PF127 is a typical amphiphilic triblock copolymer, which self-assembles into micelles in water, acting as a dynamic microcross-linker to form the initial hydrogel network. Subsequently, Schiff base bonds were established between the amino groups from QCS and the aldehyde groups from the Cur-PF127-CHO polymer within the hydrogel network. This system forms hybrid physically-chemically cross-linked double network hydrogels through the combination of dynamic chemical bonds (Schiff base) and micelle cross-linking (Reprinted with permission from Ref. [88]. Copyright 2022, Wiley-VCH)

curcumin-loaded hydrogels (Cur-QCS/PF) released approximately 78% of the curcumin after remaining in PBS for 288 h at a pH level of 6.0. However, the release dropped to 61% and 28% at pH levels of 6.8 and 7.4, respectively, demonstrating its good acid-reactivity. Animal experiments indicated that the hydrogel promoted wound healing more effectively compared to commercial films and the hydrogel without the drug.

Redox-Response Release of Drug

Redox-sensitive hydrogels, known for their potential as intracellular drug delivery systems, have been developed and acknowledged for their ability to deliver various therapeutic agents. They are particularly suitable for gene delivery due to the unique and inherent redox gradients present in the body. A novel intelligent hydrogel with redox and temperature dual responsive properties for drug target delivery was proposed in Zong's work [90] (Fig. 3.26). The cellulose nanofiber (CNF) was incorporated into the NIPAM hydrogel system, becoming intertwined and interconnected through hydrogen bonds and van der Waals forces, thereby enhancing the strength of the NIPAM hydrogel. N,N′-bis(acryloyl) cystamine (BAC), which contains S-S bonds, was introduced as a cross-linker, allowing the resulting hydrogels to respond to reducing conditions due to the integration of disulfide bonds. The drug release profiles show that the release speed of DOX from the hydrogels increases with the rise in glutathione (GSH) concentration in the PBS solution. This

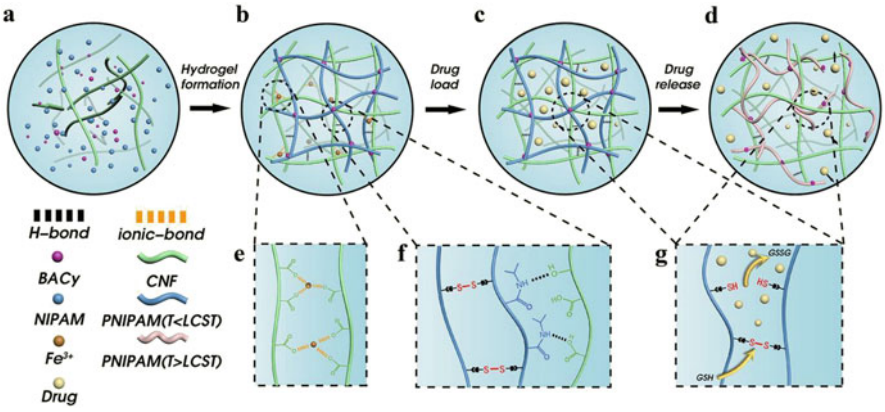

Fig. 3.26 The hydrogel formation and responsive release mechanism of hydrogels [90]. (**a**) Raw materials are collected for the preparation of hydrogels; (**b**) The CNF/NIPAM hydrogel forms a network structure through cross-linking; (**c**) The drug is loaded into the hydrogels; (**d**) The process of drug release from the hydrogel takes place; (**e**) An ionic bond is formed between the Fe^{3+} ion and the carboxyl group present on CNF; (**f**) PNIPAM is linked by BAC; NIPAM and CNF are connected through a hydrogen bond; (**g**) Under reductive conditions, the disulfide bonds break, leading to the release of the drug (Reprinted with permission from Ref. [90]. Copyright 2022, Elsevier)

can be explained by the gradual breaking of the disulfide bonds, which originally linked polymer chains, under reducing conditions. This leads to the degradation of the hydrogel network and facilitates the release of the drug from the interior of the hydrogels.

ROS-Response Release of Drug

An upward trend of ROS is observed in various prevalent pathologies, such as inflammation, cardiovascular and cerebrovascular diseases, neurodegenerative disorders, diabetes, and cancers [91]. In order to circumvent oxidative stress, cells boost their own reduction system. These redox dynamics in diseased tissues provide an additional stimulus for the release of drugs from loaded hydrogels. As illustrated in Fig. 3.27, Yu developed cartilage-targeting hydrogel microspheres KGN/Dex-TSPBA@WHMs with ROS-responsive ability, which was achieved by combining the microfluidic method and photopolymerization processes to incorporate cartilage-targeting peptides and ROS-responsive nanoparticles into the hydrogel matrix [92]. Notably, the ROS-responsive nanoparticles could interact with the osteoarthritis (OA)-induced intracellular ROS, resulting in the depolymerization of nanoparticles. This not only eliminated excess ROS and reduced inflammation but also facilitated the release of dexamethasone (Dex) and kartogenin (KGN) *in situ*, realizing effective OA therapy. It was shown that this hydrogel microsphere demonstrated favorable ROS-responsive ability and enhanced chondrogenic differentiation, as well as downregulating proinflammatory factors *in vitro*.

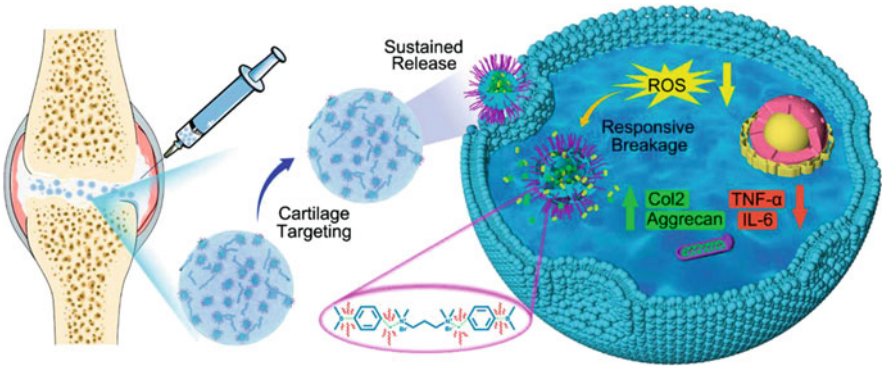

Fig. 3.27 The mechanism of KGN/Dex-TSPBA@WHMs in the treatment of OA [92]. KGN/Dex-TSPBA@WHMs showed favorable cartilage-targeting and ROS-responsive abilities, which could react with OA-induced intracellular ROS, resulting in the depolymerization of nanoparticles. After treated with the KGN/Dex-TSPBA@WHMs, the levels of tumor necrosis factor-α (TNF-α) and Interleukin-6 (IL-6), the indicators for the inflammation of activated ATDC5 cells, had significantly decreased. While the expression of collagen II and aggrecan, two major cartilage biomarkers, increased (Reprinted with permission from Ref. [92]. Copyright 2022, American Chemical Society)

Glucose-Response Release of Drug

The prevalence of diabetes makes it imperative to treat it. Insulin is a common and effective treatment for diabetes, but its repeated intravenous administration greatly reduces patient compliance. Hydrogel embedding allows long-term sustained release of insulin. Over the past few decades, glucose-response hydrogels have been developed to monitor blood glucose fluctuations and release insulin in real time on demand. As shown in Fig. 3.28, a pH/glucose dual responsive PEGS-PBA-BA/CS-DA-LAG (PC) hydrogel dressing was created for the specific release of the drug metformin. This hydrogel was prepared via the double dynamic bonds of a Schiff base and dynamic phenylboronate ester, which were formed between dihydrocaffeic acid and l-arginine cografted chitosan (CS-DA-LAG) and phenylboronic acid and benzaldehyde bifunctional polyethylene glycol-co-poly(glycerol sebacic acid) (PEGS-PBA-BA) [93]. Then added metformin (Met) and GO to better promote wound healing in the body. The amino group on Met reacted with the aldehyde group on PEGS-PBA-BA, which contributed to drug loading in hydrogel. The 1,2-diol structure in glucose can contend for the bond between catechol and phenylboronic acid, causing the network of the PC hydrogel to partially dissociate.

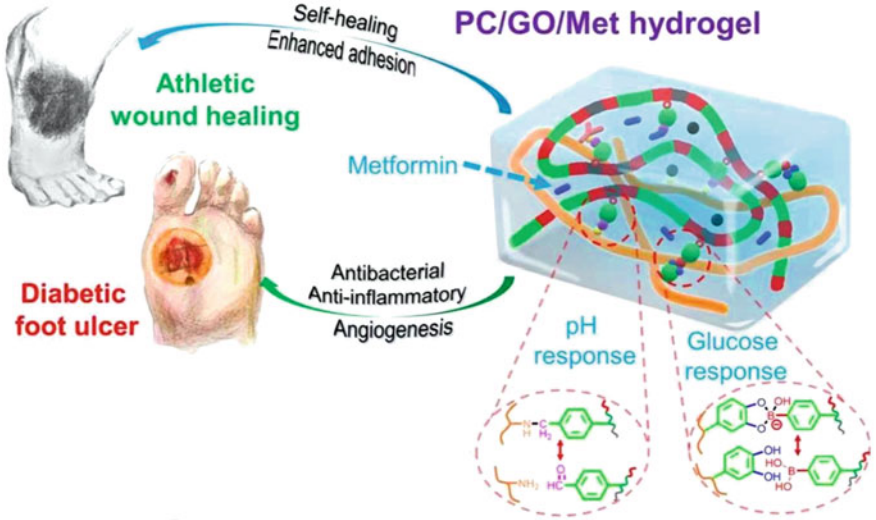

Fig. 3.28 The schematic diagram of structure, pH, and glucose-responsive mechanism of PC hydrogel and its application in diabetic foot ulcers and athletic wound healing [93]. The PC/GO/Met hydrogel was developed, boasting suitable mechanical properties, robust antioxidant ability, hemostasis and conductivity, pH/glucose dual responsive drug release capability, and biocompatibility. This hydrogel, designed with a double dynamic bond of Schiff-base and phenylboronate ester, was specifically used for the repair of athletic diabetic foot wounds. Because the Schiff base structure easily dissociates under acidic conditions, and glucose can competitively bind to phenylboronic acid, it causes the dissociation of the coordination structure between phenylboronic acid and catechol (Reprinted with permission from Ref. [93]. Copyright 2022, American Chemical Society)

This results in increased release of Met loaded into the PC/Met hydrogel. Testing confirmed the glucose-responsive Met release of the PC hydrogel, marking it as advantageous in the treatment of diabetic foot wounds.

In addition to endogenous signals, hydrogels have been designed to be responsive to various physical stimuli such as light, magnetic fields, electrical stimulation, and ultrasound. These stimuli have been incorporated into hydrogel systems for drug delivery and controlled release applications. By accurately manipulating the degree of response, it becomes possible to generate on-demand drug doses, thereby maximizing therapeutic efficacy. This manipulation is achieved by adjusting relevant parameters such as frequency, intensity, duration, and power of the applied stimuli. Photo-, magnetic-, and ultrasound stimulation all generate heat, which can intervene in the physical interactions of gelation molecules, such as host–guest and electrostatic interactions. This allows for the control of drug release from the hydrogel system [88].

Light-Triggered Release of Drug

Light radiation has gained popularity as a medical intervention approach due to its ease of acquisition, remote operation, and strong manageability. The use of photo stimulation to regulate gel formation and biodegradation has been an ongoing research focus. The light sensitivity of hydrogels is highly appealing as it allows for precise control of drug release within an endogenous environment. This control can be achieved by carefully designing parameters such as power density, wavelength, beam diameter, and exposure time, enabling the easy realization of precisely controlled drug release [94]. The conversion of light to heat is one of the main ways to cause gel structure and drug release. As demonstrated in Fig. 3.29, a highly stretchable, thermal-sensitive PNIPAm hydrogel that can be triggered by near-infrared (NIR) light was developed. This hydrogel is composed of a matrix of cellulose nanocrystals (CNCs) reinforced with PNIPAm, and it incorporates homogeneously dispersed magnetic Fe_3O_4 nanoparticles (NPs) throughout the network (Fe_3O_4/CNCs@PNIPAm) [95]. The CNCs, which are coupled with Fe_3O_4 NPs, serve as both a reinforcing phase and a photothermal agent within the hydrogel system. The photo-triggered release mechanism of hydrogel was studied using Vancomycin (VCM) as a model drug. All hydrogels demonstrated a rapid release of vancomycin upon irradiation with near-infrared (NIR) light. Subsequent research has indicated that this drug delivery system has the potential to enable more personalized therapy plans based on the progression of diseases by controlling the intensity and duration of NIR irradiation.

Magnetic-Triggered Release of Drug

Utilizing the localized heat generated on the surface of magnetic nanoparticles (MNPs) when subjected to an alternating magnetic field (AMF) has emerged as an

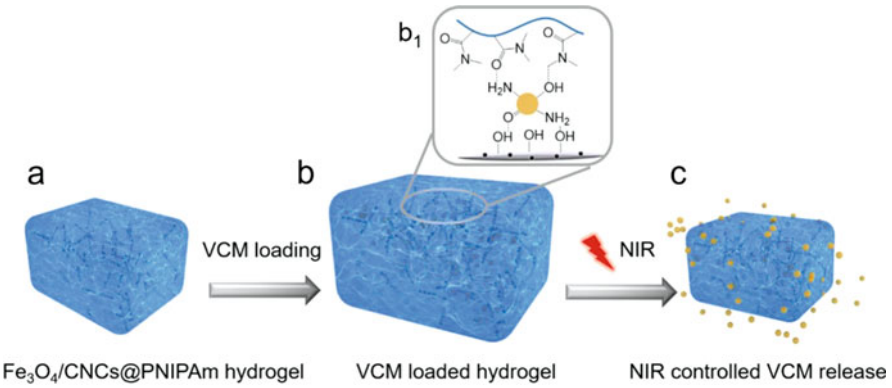

Fig. 3.29 NIR-controlled release of VCM [95]. (**a**, **b**) Vancomycin (VCM) was incorporated into the hydrogel through a swelling process, allowing it to be loaded within the hydrogel matrix; (b1) The presence of functional groups (-OH) on the surfaces of the Fe_3O_4/CNCs enables the formation of additional hydrogen bonding interactions with the drug, further enhancing its retention within the hydrogel; (**c**) Upon exposure to near-infrared (NIR) irradiation, the release of VCM from the hydrogel is triggered, resulting in controlled drug release (Reprinted with permission from Ref. [95]. Copyright 2021, Elsevier)

intriguing strategy for remotely triggered drug delivery. In this approach, the heat generated from MNPs during magnetic hyperthermia (MHT) is considered a promising stimulus for triggering the release of loaded molecules. In line with this concept, drug molecules are attached to the surface of MNPs through thermally sensitive bonds that can be disrupted upon either macroscopic or localized temperature changes [97]. As illustrated in Fig. 3.30, Mai et al. introduced a magnetic nanocarrier composed of iron oxide nanocubes (IONCs) and a multifunctional polymer capable of loading doxorubicin (DOX) through a retro Diels–Alder reaction. This loading process occurs under clinically relevant magnetic hyperthermia (MHT) field conditions. The DOX is conjugated to the ligand platform via a thermally labile Diels–Alder adduct, allowing for its release upon the local heat generated on the nanocube surface during MHT. This unique local release effect makes the magnetic nanoplatform a promising tool for drug delivery, enabling remote actuation through magnetic hyperthermia while maintaining a dose-independent action of the magnetic nanoparticles (MNPs) [96].

Electric-Triggered Release of Drug

The electrical activity observed in cells is a common phenomenon that plays a vital role in maintaining cell homeostasis and promoting intracellular development [99]. With its high level of controllability, electrical stimulation has emerged as a highly manageable approach for gel carriers to achieve precise and accurate control over drug release. Consequently, it has become an appealing method for enhancing the reactivity of hydrogel-based delivery systems. As indicated in Fig. 3.31, an

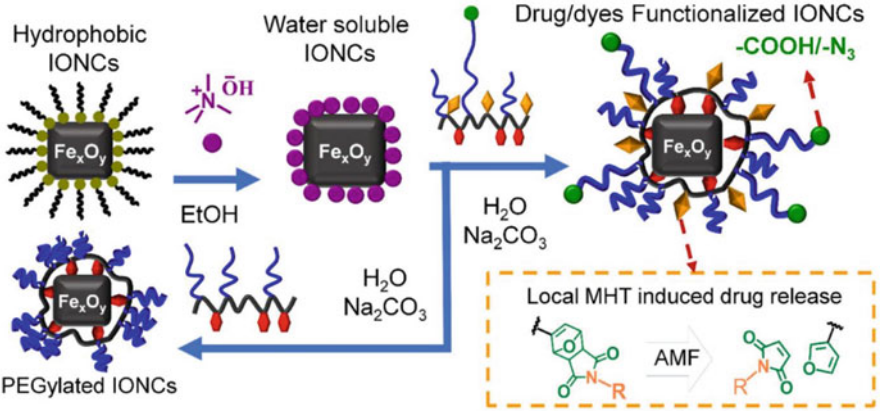

Fig. 3.30 The sketch illustrates a two-step phase transfer procedure [96]. In the first step, the transfer of iron oxide nanocubes (IONCs) from chloroform to water is achieved using tetramethylammonium hydroxide (TMAOH). In the second step, TMAOH is replaced with the developed ligands in a basic solution, resulting in the formation of physiologically stable IONCs. The inset demonstrates that the dye or drug, which is conjugated to the ligand platform through a thermally labile Diels–Alder adduct, can be released upon the local heat generated on the surface of the nanocubes during magnetic hyperthermia (MHT). This indicates the controlled release mechanism facilitated by the heat generated during MHT (Reprinted with permission from Ref. [96]. Copyright 2022, American Chemical Society)

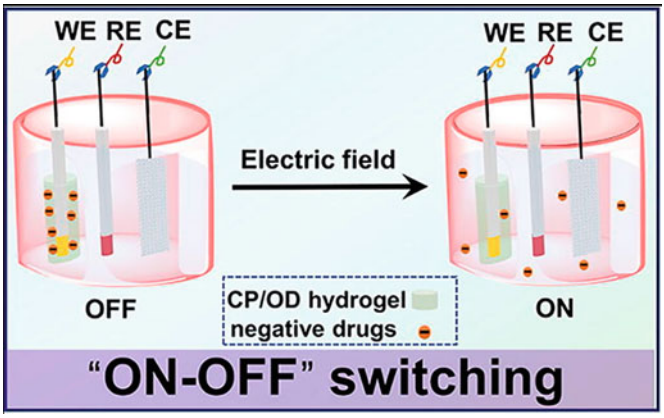

Fig. 3.31 Schematic illustration of pulse release of drug model from CP/OD conductive hydrogel [100]. The hydrogels with desirable electro-responsive properties demonstrated an "on-off" pulse release mechanism. When a voltage was applied to the hydrogels, a greater amount of the drug was released compared to when no voltage was applied, thus confirming the concept of "on-off" control of drug release (Reprinted with permission from Ref. [100]. Copyright 2018, Elsevier)

antibacterial conductive injectable hydrogel with the properties of electro-responsiveness was successfully synthesized based on the chitosan-graft-polyaniline (CP) copolymer and oxidize dextran (ODex) polymer [100]. In this study, the model drugs amoxicillin (hydrophilic) and ibuprofen (hydrophobic) were chosen. It was observed that as the applied voltage increased, the cumulative release of amoxicillin significantly increased. "On-off" pulse release experiments revealed that both drugs exhibited a higher release rate when the voltage was turned on, and a lower release rate when the voltage was turned off. This indicates that the released dose of the drugs could be controlled by applying an electric field, suggesting the potential of these systems as on-demand release vehicles.

Ultrasound-Triggered Release of Drug

Ultrasound waves possess several advantageous characteristics, including good directionality, strong reflection ability, the ability to concentrate acoustic energy, and long propagation distance in water. Ultrasound is particularly effective in penetrating tissues with high spatial and temporal resolution, making it a convenient stimulus for various applications [98]. As shown in Fig. 3.32, Sun et al. have developed a DC-hydrogel that incorporates boronate ester bonds between tannic acid (TA) and phenyl boronic acid as dynamic cross-linkers. The dynamic covalent boronate ester linkages enable effective ultrasound-triggered pulsatile release of TA [73]. Ultrasound treatment applies solvodynamic shear force to the bonds between TA, resulting in enhanced release of TA. The study demonstrated that by treating the hydrogel with ultrasound for varying durations (5, 10, and 20 min) every hour, there was a significant increase in the release of TA. Moreover, the longer the duration of

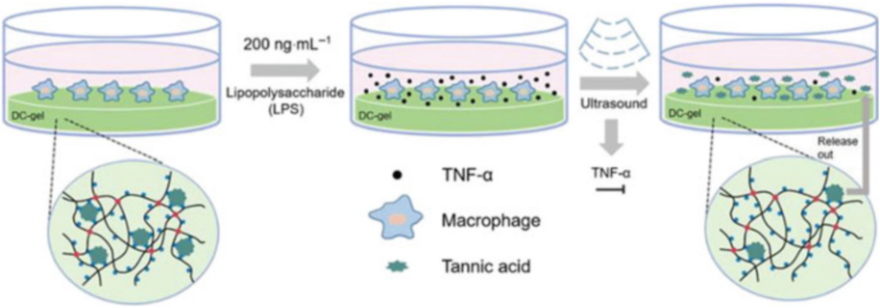

Fig. 3.32 TA released from the DC-gels by ultrasound [73]. The inflammatory response in RAW 264.7 cells was activated by treatment with lipopolysaccharide (LPS). These LPS-stimulated RAW 264.7 cells were then subjected to DC-gels and ultrasound cycles. Ultrasound is capable of triggering the dynamic covalent boronate ester linkages between the hydrogel backbone and tannic acid (TA), causing it to break. After the ultrasound prompted the release of TA from the DC gels, there was a noted reduction in the concentration of TNF-α, an inflammatory marker (Reprinted with permission from Ref. [73]. Copyright 2018, Springer)

ultrasound treatment, the faster the release of TA from the hydrogel. The release of TA was originated from the dynamic breakage.

Microwave-Triggered Release of Drug

Microwaves (MWs) are a type of electromagnetic wave with frequencies ranging from 300 MHz to 300 GHz. They are of particular interest as an external stimulus because of their capacity to deeply penetrate living tissue. In this regard, MW radiation has demonstrated its usefulness in applications such as transdermal drug transport and as a skin permeation enhancer [102]. Graphene, known for its exceptional microwave absorption properties, was integrated into diaminotriazine (DAT) hydrogels to strengthen the interaction between the hydrogel and the electromagnetic impulse, thereby facilitating the absorption of microwave radiation (Fig. 3.33) [101]. The drug release behavior was observed in both graphene diaminotriazine (G-DAT) and DAT hydrogel under microwaves. The findings support the notion that the enhancement in drug release seen with the 915 MHz microwave stimulus is likely due to the selective disruption of drug-hydrogel interactions, potentially from hydrogen bond disruption among DAT dipoles under microwave irradiation. This

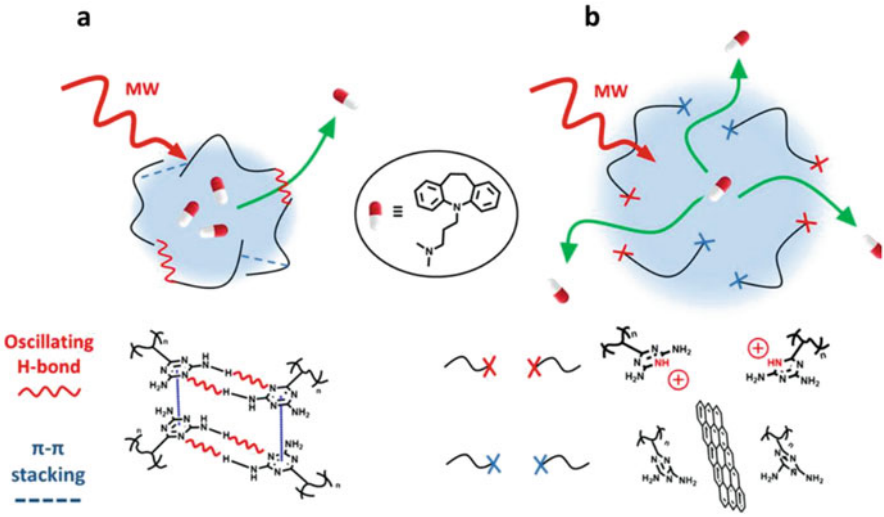

Fig. 3.33 Proposed mechanism for the interaction between 915 MHz MW [101]. (**a**) When DAT hydrogel is placed in PBS (pH 7.4), the hydrogen bonds that connect the DAT molecules start to disrupt. This disruption leads to the free oscillation of DAT, which opens up pathways for the release of the hydrophobic drug into the medium. The presence of graphene and SGF media disturbs the DAT-DAT π–π stacking and DAT-DAT hydrogen bonds; (**b**) When G-DAT hydrogel is in SGF (simulated gastric fluid; pH 1.2) media, both graphene and the external acidic pH work together to disrupt the hydrophobic interactions within the DAT. This cooperative disruption significantly increases the swelling capacity of the hydrogel (Reprinted with permission from Ref. [101]. Copyright 2020, MDPI)

characteristics positions these materials as promising drug reservoirs that can respond to an electromagnetic stimulus capable of penetrating tissue, thereby enabling on-demand drug release without inflicting harm on nearby organs.

3.4.3 Conclusions and Outlook

In summary, due to the unique advantages of functional hydrogels in biodegradability and biocompatibility, functional hydrogels hold substantial technological importance in drug delivery applications. Recent advancements in the realm of targeted drug delivery utilizing hydrogels have been remarkable [87]. These hydrogels are tailored with specific targeting ligands and a variety of polymer types that bestow upon them unique properties suitable for drug delivery. Consequently, the number of relevant studies being conducted in this area is increasing significantly [104]. Studies on hydrogels as drug carriers are emerging in an endless stream, and the mechanisms of drug loading and sustained release are also being studied [88]. However, many parameters in the model of the release mechanism of hydrogel drug molecules are still unknown and may change with the change of time or location, which cannot fully describe the coupling mechanism controlling the release of molecules in these systems [81]. At the same time, precise control of drug release rate and targeted release is still challenging.

Based on the current research status, the future research focus of drug delivery hydrogels lie in: combining and comprehensively using the release mechanism and preparation method of a variety of drugs to optimize the method design, so as to prepare a series of multifunctional carriers to achieve the expected drug release effect [105]; drug carrier matrix modification, targeted drug release; studying the metabolites and pathways of drug-loaded matrix *in vivo* to ensure its safety and effectiveness in clinical application [103].

It is anticipated that as research continues to evolve and deepen, hydrogel drug delivery systems are poised to significantly transform the size, effectiveness, and cost of therapeutic treatments. This progression will consequently continue to enhance healthcare and wellbeing for humans [106].

3.5 Cell Delivery Hydrogel

Hydrogels with high-water content have high biocompatibility and adjustability, such as permeability, resilience, rigidity and chemical reactivity, and can simulate the microenvironment of native ECM by controlling the time and space of biochemical and physical clues. The reported hydrogels have potential organ-like applications, including alginate, chitosan, hyaluronic acid and collagen from natural sources, and some synthetic polymer-based hydrogels (e.g., PEG, PAAm, and PVA) [107].

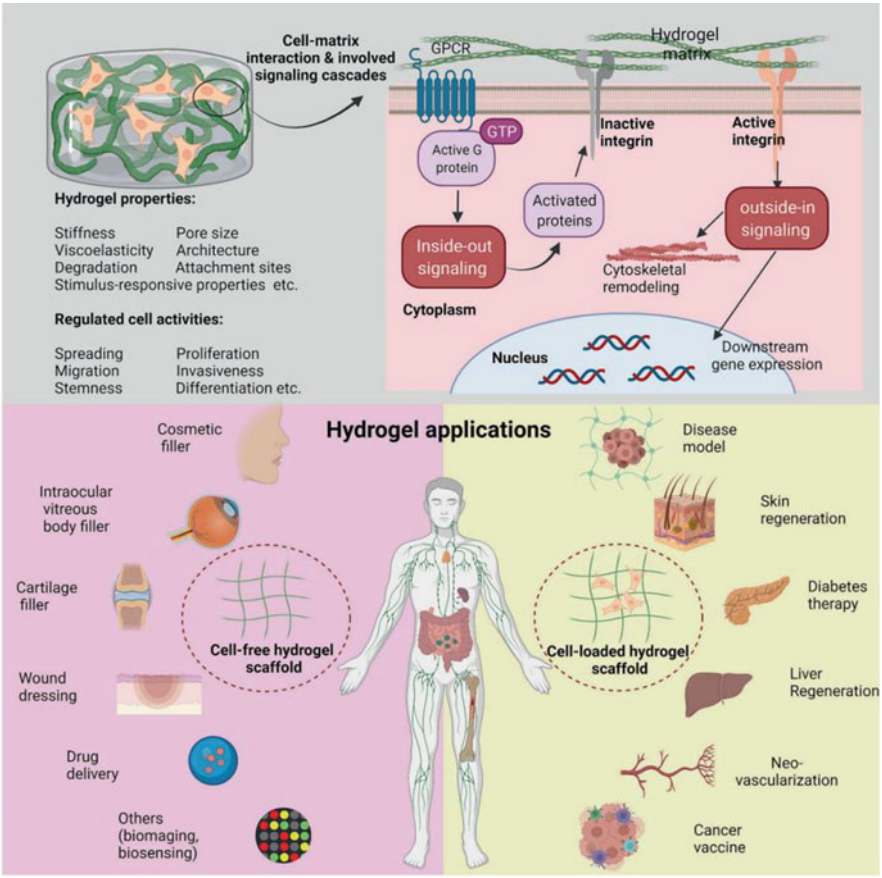

Fig. 3.34 A demonstration diagram showing how cells interact with hydrogel matrix. Hydrogels trigger cell signal cascade (e.g., signals from inside to outside and from outside to inside), reveal how the physical and chemical properties of hydrogels affect cell biology, and explain the biomedical applications of cell-free and cell-loaded hydrogels (Reprinted with permission from Ref. [112]. Copyright 2021 by Springer Nature)

Biohydrogel-based scaffolds are helpful for cell delivery. These vectors are usually used as a part of tissue engineering to deliver the right cells to the targeted place to recover the damage to tissues or organs. Different hydrogel properties have different effects upon cell behaviors and cell signaling, which include integrin clustering, accumulation and activation of focal adhesion (FA) complex, cytoskeleton rearrangement, protein nucleus shuttle and activation (such as yes-related protein (YAP), catenin, etc.), cell chamber recombination, gene expression, as well as further cell biological regulation (such as diffusion, migration, proliferation, lineage commitment, etc.) [11, 108–111] (Fig. 3.34). On this basis, the current applications of hydrogels *in vitro* and *in vivo* mainly include cell delivery in tissue

regeneration and disease treatment, intelligent drug carriers, biological imaging, biosensors, etc.

3.5.1 Hydrogels as Cell Carrier

Hydrogel can simulate the scaffold structure of cell survival matrix, so as to support the activities of contained cells and meet their physiological needs in a cell/tissue type dependent manner. In addition, in ECMs based on 2D and 3D hydrogels, the distribution and morphology of cells in hydrogel are also different. The expansion of cells in the 3D case is opposite to that in the 2D case. Specifically, in the 2D environment, the cells are diffused in a large area on the rigid collagen-based hydrogel and round on the soft gel. In contrast, in 3D environment, cells are aggregated into a circular shape in rigid collagen-based hydrogel, while they are shown as diffusion shapes in soft gel. Besides, the cellular distribution of 2D and 3D hydrogel ECMs is disparate, and the cytoskeleton structure at the molecular level is also different [112].

Due to the porous structure of hydrogel, it allows cells to attach and grow, and "intelligently" release biological agents at the damaged site. For example, Ballios et al. [113] developed a hydrogel based on HA and methylcellulose (HAMC) to deliver retinal progenitor cells to subretinal space. The hydrogel showed good biocompatibility and optimal biodegradability, so that the loaded cells could be accurately and evenly distributed at the target site.

Hydrogel can be used not only as a cell carrier, but also as a matrix for growth factor attachment and controlled release, providing high concentration and long-term growth factor exposure near transplanted cells. As indicated in Fig. 3.35, Geng et al. [114] loaded muscle-derived stem cells (MDSCs) in hydrogel scaffolds to express hypoxia inducible factor-1α (HIF-1α) to induce angiogenesis, and effectively repaired the injured cavernous body. Specifically, they deposited heparin onto the 3D-printed hydrogel scaffold by assembling poly-L-lysine (PLL) layer by layer (Fig. 3.35a, b). Through the adsorption of heparin, the angiogenic factors produced by HIF-1α overexpression MDSCs were enriched on the 3D-printed hydrogel scaffold surface, thus stimulating angiogenesis *in vivo* (Fig. 3.35c–e).

In addition, hydrogel can be used to support cells and guide the growth and differentiation of cells in organs. For example, Wu et al. [115] showed that methacrylate hyaluronic acid (MA-HA) hydrogel can effectively promote the differentiation of human-induced pluripotent stem cell-derived neural progenitor cells (hiPSC-NPCs) *in vitro*. The softer hydrogel with a stiffness of 0.51 ± 0.20 kPa can promote the neural differentiation of hiPSC-NPCs compared with the harder hydrogel with a stiffness of 1.41 ± 0.27 kPa [115]. In a word, combining stem cells and hydrogel can be considered as a promising method for tissue regeneration.

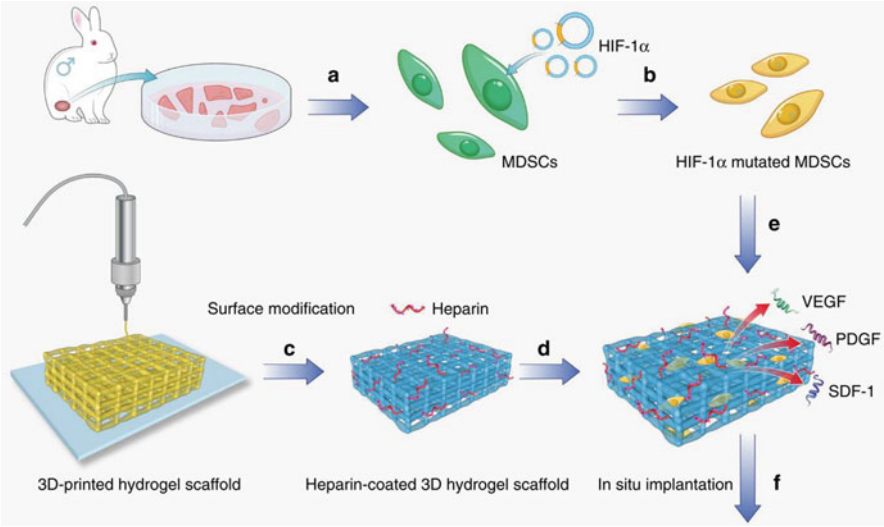

Fig. 3.35 Schematic diagram of repairing rabbit cavernous injury with hydrogel and MDSCs. (**a**) The MDSCs were extracted from rabbit leg muscles; (**b**) the HIF-1α-mutated MDSCs were gathered through lentiviral transfection; (**c**) obtained the 3D-printed hydrogel bracket through 3D printing; (**d**) deposited heparin on the surface of the 3D-printed hydrogel scaffold by layer-by-layer self-assembly technology in order to obtain a heparin-coated hydrogel scaffold; (**e**) inoculated MDSCs mutated by HIF-1α onto heparin-coated hydrogel scaffolds, and secreting angiogenesis-related factors (Reprinted with permission from Ref. [114]. Copyright 2020 by Springer Nature)

3.5.2 Various Microorganisms Combined with Hydrogels

Hydrogels can be combined with various microorganisms, including bacteria, fungi, algae and animal cells, and used as engineering living materials or biological hybrids to realize a series of applications. In active materials, living cells are combined with matrix or scaffold, and the active ingredients endow materials with unique functional characteristics. Based on the design of nonliving composite materials encapsulating living cells, active materials can be produced from living cells. Researchers designed polymer networks and chemical compositions of aqueous solutions to provide biochemical clues for living microbial cells [116]. The structure of hydrogels can be further improved, so that the structural features (such as geometry, porosity and size) of hydrogels prepared in different scales (nanometers to millimeters) by conventional manufacturing techniques can provide space constraints and mechanical forces for living cells [116].

Microorganisms are encapsulated in a polymeric matrix, usually in the form of microcapsules or fiber webs, to facilitate the transport of microorganisms to the application site or to isolate microorganisms after reaction. However, biomedical applications would require the use of Generally Recognized as Safe (GRAS) species of bacteria [117]. At present, adhesive bacterial matrix has been used to treat chronic

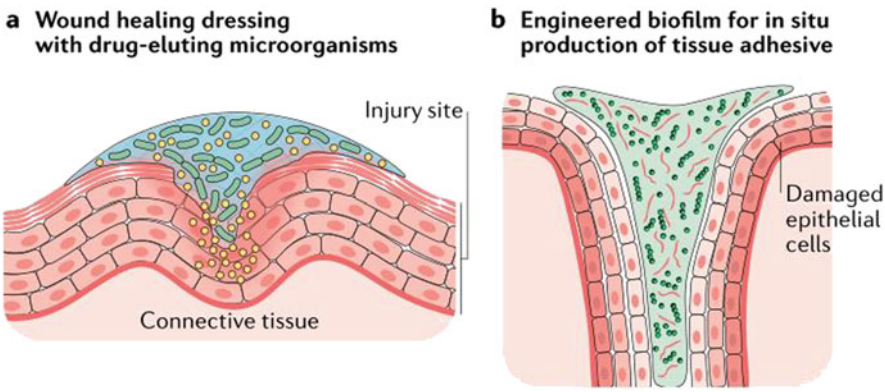

Fig. 3.36 Biomaterials as tissue adhesives. (**a**) Biomaterials loaded with engineering microorganisms can promote the healing of chronic wounds (such as burns and diabetic wounds) by producing and eluting recombinant proteins or small molecules *in situ*; For example, Escherichia coli Nissle 1917 strain produces recombinant CsgA curli fiber fused with trefoil factor to restore epithelial function; (**b**) engineering bacteria embedded in active materials can be edited to produce tissue adhesives, such as crimped fibers, to promote the recovery of injured tissues (Reprinted with permission from Ref. [119]. Copyright 2021 by Springer Nature)

intestinal inflammation or to seal blood leakage in vascular tissue, and self-replenishing drug bank for delivering antibiotics or therapeutic protein [118]. For example, in order to treat inflammatory bowel disease, as indicated in Fig. 3.36, Escherichia coli strain Nissle 1917 is programmed to secrete CsgA curli fiber proteins fused to trefoil factors [117], which promotes intestinal barrier function and epithelial recovery. Curli-based system can also sense heme B in the environment by bacteria and produce sticky curli fibers in the form of glue to repair damaged bleeding vascular tissue [120].

However, there are still challenges in developing active materials with dynamic characteristics and the ability to continuously perceive and respond to the environment. How to make bacteria-rich hydrogels secrete growth factors and cytokines according to changing oxygen, stress or chemical gradient to meet the metabolic needs of stem cells and maintain their niche is still an urgent problem.

3.5.3 Hydrogels for Organoid

Organoid mainly evolved from the development principle, which refers to the three-dimensional multicellular tissue self-organized by stem cells or organ-specific progenitor cells. It is a unique *in vitro* system that simulates organ development, function and diseases, and can reproduce the complex structure and function of internal organs [121]. In recent years, breakthrough progress has been made in organ-like technology, and a variety of human organs have been successfully

generated, such as brain, intestine, liver, kidney, lung, etc. [122, 123]. These close-to-physiology 3D organs are gaining momentum because of their potential applications in human organ development, disease modeling, drug screening and regenerative medicine [124].

A huge number of culture systems are employed to produce various organs. These methods include suspension culture system, crypt separation method, gas-liquid interface method, embryo model, bioreactor or two-dimensional monolayer culture method [125, 126]. The successful culture of organoid depends on various physical and chemical characteristics of microenvironment, among which functional and structural molecules such as protein, glycosaminoglycan and glycoconjugates form ECM, and play a decisive role by forming complex networks to support cells in all tissues or organs [127].

Natural and synthetic hydrogels provide a new method to promote cell expansion, differentiation and organ tissue by precisely controlling the composition of protein (such as collagen, fibrin and synthetic peptide), and can replace natural ECM to promote the formation of specific organ-like. For example, Broguiere et al. [128] developed fibrin-based hydrogel, which can support the formation and long-term expansion of epithelial organs. They found that fibrin hydrogel supplemented with laminin-111 contributed to the formation and expansion of epithelial organs in mice and humans. It is worth noting that RGD adhesion domain naturally existing in fibrin hydrogel is essential for proliferation and organoid formation of intestinal stem cells. In addition, laminin was identified as the main biological signal factor in ECM required for organ-like growth [128] (Fig. 3.37a).

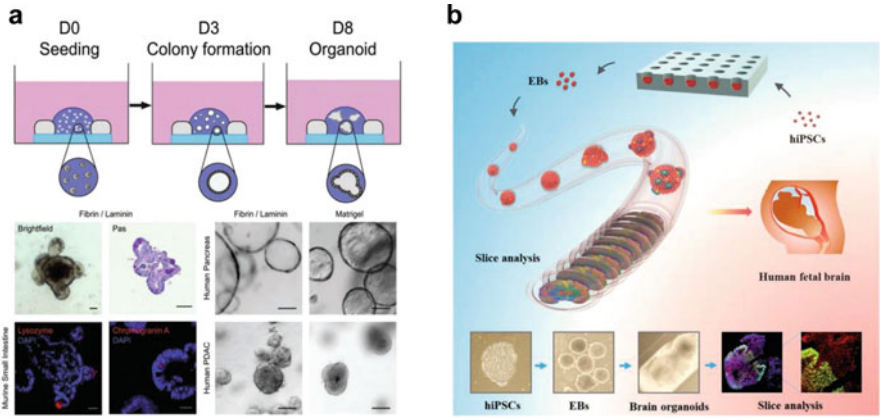

Fig. 3.37 Hydrogels used in engineering and application of organic compounds. (**a**) Chemically modified fibrin-based hydrogels to improve the formation and expansion of epithelial organs in mice and humans (reprinted with permission from Ref. [128]. Copyright 2018, Wiley-VCH); (**b**) synthesizing hollow microfibers based on alginate to promote the generation of brain organs through extension and expansion (Reprinted with permission from Ref. [129]. Copyright 2017 by Royal Society of Chemistry)

In addition, hydrogels can also produce organ-like bodies with specific morphology by regulating specific internal structures, in which passive mechanical stimulation from the hydrogel boundary can regulate tissue morphology and promote condensation and multicell interaction. Zhu et al. [129] have made a hollow alginate gel microfiber by microfluidic technology to produce brain organs that can be imaged in real time during development [129] (Fig. 3.37b). In this work, neuroectodermal spheres from human-induced pluripotent stem cells (hiPSCs) were encapsulated in confined hydrogel microfibers, and then differentiated and produced a large number of brain organs in an expandable manner.

However, despite its infusive potential in new biomedical applications, the existing organoid cultures still have significant shortcomings. First of all, the derivation of organoids usually requires ECMs from animals. The ill-defined components of these biomaterials and the differences between batches have problems in basic research and transformation research [130]. Besides, current organ-like systems usually lack the ability to construct vascular systems, thus hindering their application in biological modeling of adult tissues/organs [131]. In the future, we can combine other bioengineering methods, such as *in vivo* imaging, genome editing and single cell genomics, fusion of biomaterials, engineering and stem cell biology, to solve the problems of constructing high-fidelity tissues and their translation applications.

3.5.4 Hydrogels for Delivering Exosomes

Exosomes (Exos) are nano-sized vesicles secreted by almost all types of cells through paracrine pathway, which can carry protein, RNA/miRNA and other molecules [132], and play a vital role in cell-to-cell communication. Because exosomes have good biocompatibility and immune stability, treatment based on exosomes shows greater potential in chronic wound healing than other biological therapies (such as stem cell transplantation), and has great prospects in clinical treatment of chronic wounds.

Up to now, most hydrogel drug delivery systems directly embed exosomes in hydrogels, by mixing with polymer solutions and cross-linking agents before gelation of hydrogels, or combining with porous hydrogel scaffolds after cross-linking of hydrogels. With the degradation of hydrogel *in vivo*, the encapsulated exosomes are gradually released. For example, Zou et al. [133] constructed an injectable conductive hydrogel combined with Exo derived from human umbilical cord mesenchymal stem cells. Hyperbranched epoxy macromonomer (EHBPE) grafted with aniline tetramer (AT) was synthesized, and HA-SH and thiol-anchored CP05 peptide were cross-linked by epoxy/thiol "click" reaction to treat myocardial injury after myocardial infarction-ischemia/reperfusion (MI-I/R) (Fig. 3.38). By injecting the Gel@Exo composite system into the injured heart of rats, the retention time of Exo in ischemic myocardium can be effectively prolonged, which plays a significant role in promoting cell proliferation, angiogenesis and MI-I/R treatment [133].

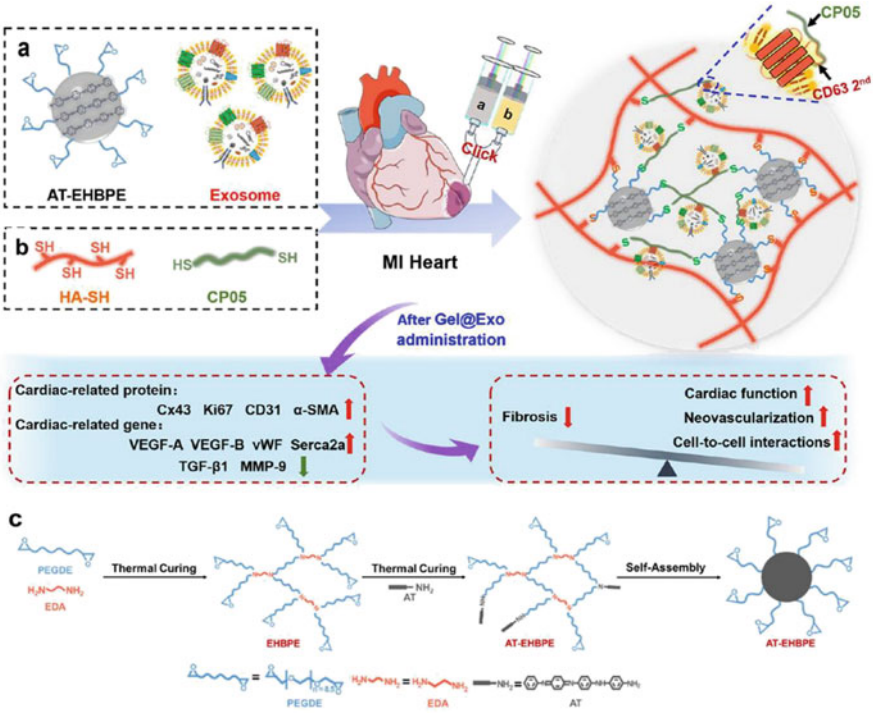

Fig. 3.38 Schematic diagram of injectable conductive hydrogel combined with human umbilical cord mesenchymal stem cell exosome (hUC-MSCs-Exo) for restoring heart function after MI-I/R, and the acquisition of AT-EHBPE macromonomer. (**a**) Precursor solution of AT-EHBPE combined with Exo; (**b**) precursor solution of HA-SH and CP05 peptide; (**c**) the synthetic method of AT-EHBPE (Reprinted with permission from Ref. [133]. Copyright 2021 by ACS Publications)

3.5.5 Effect of Hydrogels on Cells

The interaction between cells and hydrogel is complex and dynamic, and it has an important influence on the physiological processes (such as cell diffusion, proliferation, migration, stem cells, differentiation, etc.) and the pathological process of cells (such as apoptosis, fibrosis, immune rejection, etc.). Generally, once exposed to an external hydrogel, cells will react according to the static physical and chemical properties of the hydrogel (hardness, pore size, viscoelasticity, microstructure, degradability, chemical surface, etc.) [11, 108–111], and then convert these clues into biochemical signals to adjust its biology and homeostasis. More and more evidence shows that cells can sense the changes of the microenvironment caused by external stimuli in real time and respond in time and space.

3.5.5.1 Effect of Mechanical Force and Stiffness of Hydrogels on Cells

Hydrogel matrix generates various mechanical forces that can actively regulate the growth, morphology and movement of cells and the formation and dispersion of biofilm. When cells are encapsulated in hydrogel matrix, dense nanofiber ECM components (such as collagen fibers) connect with biological macromolecules, and has many cell adhesion motifs to enhance cell rigidity. Attached cells can provide the traction needed for cell function, including division, diffusion and migration. Previous studies have reported that local hardening of 2D hydrogel matrix can promote the development of cell adhesion structure and cell diffusion [134].

In a 3D hydrogel environment, the dynamic hydrogel cross-linked by weak and reversible physical interaction enhances 3D diffusion and mechanical sensing ability of encapsulated cells in the matrix. Bian et al. [135] proved that photocross-linked silica nanoparticles (NPs) based on acryl nanoparticles locally strengthened hydrogel network in gelatin host–guest (GHG) hydrogels to produce a regionally rigid network structure, which could significantly accelerate the diffusion of encapsulated stem cells and enhance the osteogenic differentiation induced by stem cells in 3D hydrogel (Fig. 3.39). It is proved that the dynamic hydrogel with local hardening network can accelerate the *in situ* regeneration of bone defects and can be used as an excellent carrier material for stem cell therapy.

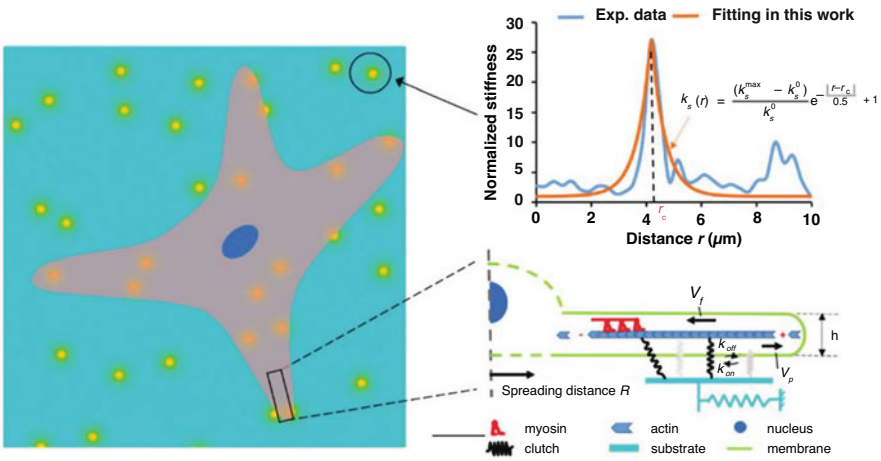

Fig. 3.39 A schematic diagram simulating the enhancement of cell diffusion caused by local hydrogel network stiffening. Orange points represent stiffened locations (i.e., nanoparticle positions) on the substrate where the nearby stiffness distribution is assumed to follow the exponential decay shown in the above illustration. The lower inset: near the edge of the protrusion, the polymerized actin bundle can be connected with the substrate through the clutch (Reprinted with permission from Ref. [135]. Copyright 2021 by Royal Society of Chemistry)

3.5.5.2 Microstructure

The structural characteristics of ECM network *in vivo* (such as fiber diameter and fiber arrangement) show the relationship with tissue type, and meantime determine how cells interact with the surrounding environment. Hydrogel structure may affect cell activity, signal cascade and cell morphology. It is reported that cells can evolve into spindle-shaped morphology on microfibers or aligned fibers, and spontaneously transform into round morphology on nanofibers or randomly oriented fibers [136]. In addition, fiber diameter and fiber arrangement in different cell types can induce different immune responses. In a word, different cell behaviors, intracellular actin and protein expression profiles show that cell biology with fiber diameter and direction dependence follows a mechanical adjustment process. For example, it has been found that compared with randomly oriented fiber scaffolds, neural stem cells (NSCs) tend to be cultured into neuron cells on oriented fiber scaffolds [137].

Besides, porous ECM network can exert different degrees of physical space constraint effects on the resident or mobile cells by changing the pore size, and then affect the behavior of single cells and multicellular tissues. For example, cancer cells can overcome the restriction of primary tumor matrix with 1–30 μm pores and move to the distance [138]. In addition, hydrogel scaffolds have porous structures with different pore sizes, which is also an important physical characteristic. As porous channels are transport channels for nutrients, metabolites and other substances, this unstable porous structure can determine the quality of embedded cells in various pathological applications by regulating physiological activities. On the molecular level, cell constraints in hydrogel will affect cytoskeleton rearrangement, organelle distribution, nuclear membrane proteins, and chromatin recombination by activating various mechanical transduction signals, all of which will ultimately affect cell morphology, migration, invasion, differentiation [139] and so on (Fig. 3.40).

3.5.5.3 Viscoelasticity

It is generally believed that tissues have viscoelastic properties. In addition, hydrogel biomaterials, including ECM-derived components (such as collagen, fibronectin (FN), etc.) and non-ECM-derived materials (such as alginate, chitosan, etc.) also show viscoelastic properties, showing stress relaxation behavior [141]. These viscoelastic properties regulate the interaction between the embedded cells and the surrounding matrix, which can cause differences in cell proliferation, proliferation and differentiation compared with the nonembedded cells. There are many factors that will affect the viscoelasticity of hydrogels, including the composition and concentration of precursors, the flexibility of hydrogels, the cross-linking density or cross-linking methods, etc. The traction of cells on viscoelastic hydrogel matrix changes dynamically with time via Rho and Rac signals (Fig. 3.41a). At first, due to the rigidity of hydrogel scaffold, the traction and tension caused by cell movement and diffusion or deformation on the surrounding hydrogel matrix are offset. As time goes on, these forces gradually decrease due to various dissipation events.

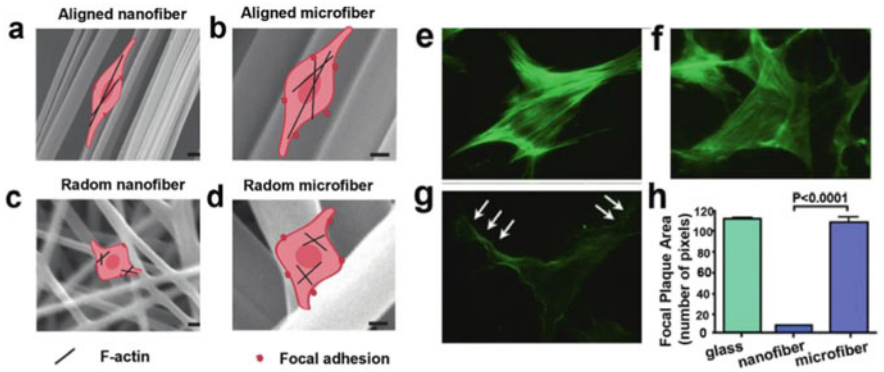

Fig. 3.40 Influence of hydrogel structure exerted on cell activity. (**a**–**d**) Schematic diagram of the interaction between cells and hydrogel scaffolds with different morphologies. Cells generally show spindle-shaped morphology on microfibers (**b**, **d**) or aligned fibers (**a**, **b**), while on nanofibers or randomly oriented fibers (**c**) change into a round shape (Reprinted with permission from Ref. [112]. Copyright 2021 by Springer Nature); (**e**–**h**) F-actin staining (green) of fibroblasts attached on glass (**e**), microfiber (**f**), and nanofiber (**g**), and the quantitative analysis of focal plaque area (**h**). Arrows represent membrane protrusions ("cork-screw" ruffles) (Reprinted with permission from Ref. [140]. Copyright 2011 by American Society of Plastic Surgeons)

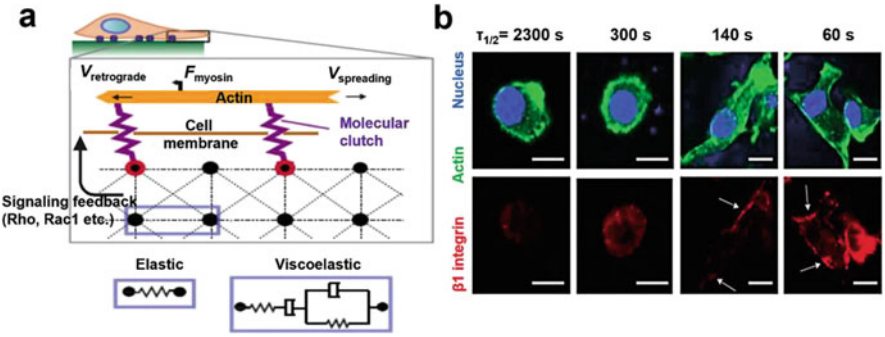

Fig. 3.41 Clarification of viscoelastic regulation of cell biology by hydrogel. (**a**) Schematic diagram of activating Rho and Rac1 signaling pathways to regulate the interaction between cells and elastic/viscoelastic hydrogels (Reprinted with permission from Ref. [142]. Copyright 2015 by Springer Nature); (**b**) A case shows how hydrogel with rapid stress relaxation can induce stem cell proliferation and β1 expression and promote integrin aggregation (Reprinted with permission from Ref. [143]. Copyright 2015 by Springer Nature)

Stress relaxation rate is a sign of viscoelasticity. Compared with alginate with high molecular weight (MW 280 kDa, 3300+/−800 s), alginate with low molecular weight (35 kda) showed a faster relaxation rate (170+/−20 s) [144]. This rapid relaxation rate is beneficial to mechanical matrix remodeling induced by cell contractility, which also allows the aggregation of increased RGD ligands in hydrogels, and further enhances the expression of β1 integrin, FA formation and YAP nuclear translocation in cells (Fig. 3.41b). Thereby regulating the interaction between the

embedded cells and the surrounding matrix, and causing the difference of cell diffusion, proliferation and differentiation compared with the nonembedded cells. For example, some studies have shown that the rapid relaxation of alginate matrix without RGD can significantly promote the formation of cartilage matrix and maintain cell phenotype with less interleukin (IL)-1β secretion [145].

3.5.5.4 Degradation

In addition to the above physical parameters, matrix degradation has also been confirmed to greatly affect cell behavior (such as cell diffusion and contact) and functional characteristics, such as cancer cell invasiveness, multicell aggregation formation and stem cell lineage commitment [146] (Fig. 3.42a). Therefore, the degradation of hydrogel can be controlled by enzyme catalysis, ester hydrolysis or photolysis. The degradation of hydrogel has also been confirmed to affect stem cell lineage commitment [148]. For example, Khetan et al. [149] pointed out that the unique fate of stem cells is regulated by degradation-specific traction stress. In their research, when degradable peptides are incorporated into hydrogels, stem cells cultured in HA hydrogels will differentiate into bone cells. However, it will be

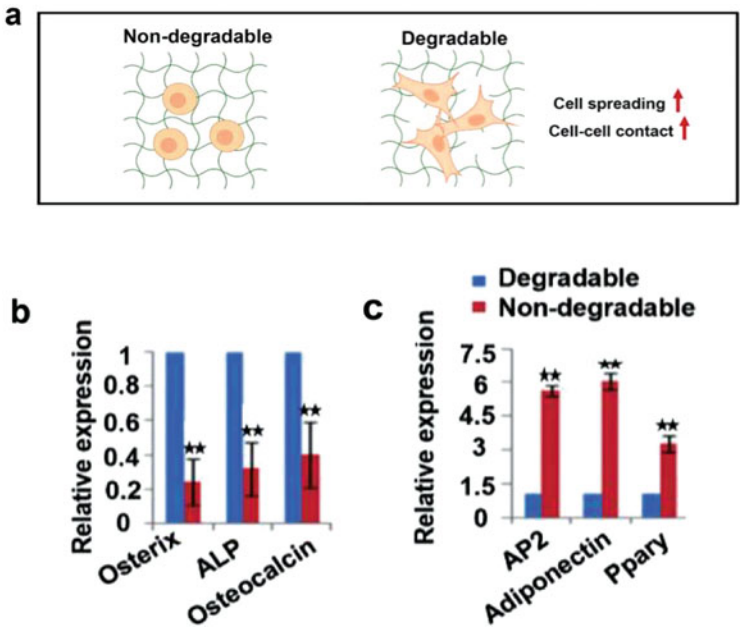

Fig. 3.42 Influence of the degradability of hydrogel on cell biology. (**a**) Schematic diagram illustrating the interaction between trapped cells and degradable/nondegradable hydrogels (Reprinted with permission from Ref. [112]. Copyright 2021 by Springer Nature); (**b**, **c**) osteogenesis and adipogenesis analysis in degradable and nondegradable hydrogel, respectively. $^{**}p < 0.01$ (Reprinted with permission from Ref. [147]. Copyright 2013 by Elsevier)

converted into fat when it is embedded into nondegradable hydrogel through delayed secondary cross-linking process (Fig. 3.42b, c). Specifically, they showed that the degradation of hydrogel can rearrange the cytoskeleton structure of cells, resulting in high diffusion and traction [150].

In another study, researchers [151] showed that the biodegradable hydrogel based on PEG can promote the proliferation and differentiation of stem cells and has great application potential in bone repair. First of all, in the initial stage, degradable bone-like soft hydrogel is helpful to the proliferation and pluripotency support of stem cells. After that, the cells migrated to the surface of the simulated bone defect and differentiated into osteoblasts.

3.5.5.5 Effect of Attachment of Hydrogels on Cells

Cell survival depends on the attachment of cells to the matrix, and without proper attachment, the cells may potentially undergo anoikis. The attachment sites of cells to hydrogels are determined by cell adhesion molecules (CAMs) on cell membranes. CAMs mainly includes integrins (such as α2β1, etc.), proteoglycans (such as CD44) and receptor tyrosine kinases (such as DDR1,2) can specifically interact with some ligands chelated by scaffold matrix [152]. Therefore, hydrogel materials will exert a strong influence on cell fate by regulating the signal cascade induced by cell adhesion. The extracellular domains exposed by different integrins allow cells to specifically recognize ECM proteins, such as FN, collagen, laminin and other ECM components, thus regulating cell adhesion, migration, differentiation, and apoptosis through different signal pathways [153].

Stephanie et al. [154] investigated the interaction between human mesenchymal stem cells (hMSCs) and PEG hydrogel functionalized with cell adhesion peptide (RGD). The interface between RGD peptide-functionalized hydrogel and hMSCs was used as a model system. 8-arm PEG-norbornene (20 kDa) was cross-linked with nondegradable PEG-dithiol (1 kDa), as well as enchained 6.8 mM cell-adhesive RGD peptide (CGGRGDSP) or nonadhesive RDG scrambled peptide (CGGRDGSP) (Fig. 3.43a), in which RGD sequence was found in fibronectin and some other extracellular matrix proteins combined with multiple cell surface receptors. It is revealed that the concentration of RGD has great influence on the short-term binding of hMSCs, and the increase of integrin aggregation at hydrogel-cell interface is related to the decrease of available RGD binding sites, which is crucial for cell adhesion and movement (Fig. 3.43b, c).

3.5.6 Effect of Cells on Hydrogels

3.5.6.1 Effect on Hydrogel Remodeling

Bioactive hydrogel can interact with cells. Hydrogel can not only coordinate the fate of cells, but also determine the “fate” of hydrogel. Cells have the ability to reorganize

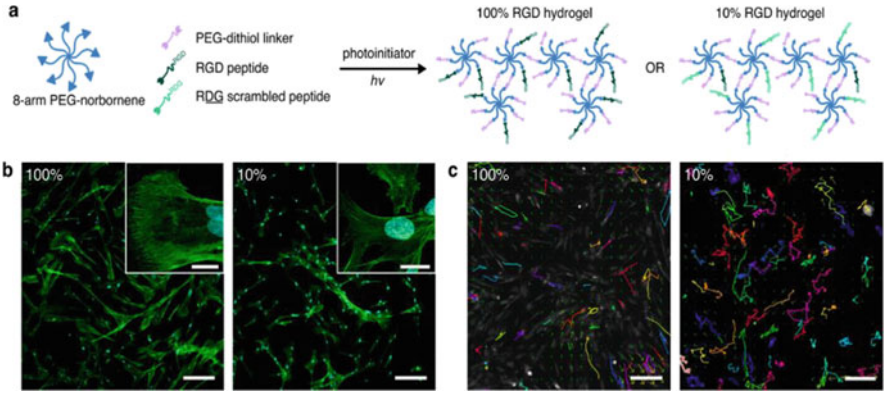

Fig. 3.43 Schematic diagram of stem cell-hydrogel interface and migration analysis of hMSCs on RGD hydrogels. (**a**) Under the action of photoinitiator and 365 nm light, 8-arm PEG-norbornene (20 kDa) was cross-linked with nondegradable PEG-dithiol (1 kDa), tethered 6.8 mM cell adhesive RGD peptide (CGGRGDSP) or nonadhesive RDG coding peptide (CGGRDGSP), resulting in 3D photocross-linked hydrogel network; (**b**) the representative confocal image of hMSCs combined in hydrogel, labeling actin (green) and nucleus (blue). Scale bar = 200 μm main image, 20 μm inset; (**c**) the representative image of the hMSC trajectories marked by orange on the cell tracker on the hydrogel, which was tracked for more than 6 h. Scale bar = 200 μm (Reprinted with permission from Ref. [154]. Copyright 2020 by ACS Publications)

and redesign the surrounding environment through multiple mechanical and chemical actions to make cells embedded in hydrogels reshaping these hydrogels into tissue-like structures. It is one of the key mechanisms used by contracting cells to reshape the surrounding environment. For example, in collagen hydrogel, fibroblasts bind and release through α2β1 integrin, and use the periodic movement of "hand in hand" to pull themselves along collagen fibers [155]. But lacking sufficient strength to bear the applied force, these fibers will bend, leading to the shrinkage and remodeling of the hydrogel (Fig. 3.44).

3.5.6.2 Effect on the Hydrogel Mechanical Properties

The 3D mechanical environment of hydrogel is perceived by cell surface receptors (called integrins), which mediates mechanical transduction pathways [157]. The mechanical interactions between cells and their surrounding hydrogels involves three key mechanisms and related sensing components: focal adhesion complex, stress fiber contraction and filipodia growth (Fig. 3.45). Sensing begins with the adhesive compound, in which the mechanically sensitive integrin can self-organize in a larger compound according to the force exerted (or resisted) by the environment. When integrin directly binds to the cell adhesion site on the polymer chain in the hydrogel, the cell exerts force on the hydrogel to induce the deformation and structural change of the hydrogel. Focal adhesion connected with actin cytoskeleton produces this force, and the hardness of hydrogel matrix, the density of cell adhesion

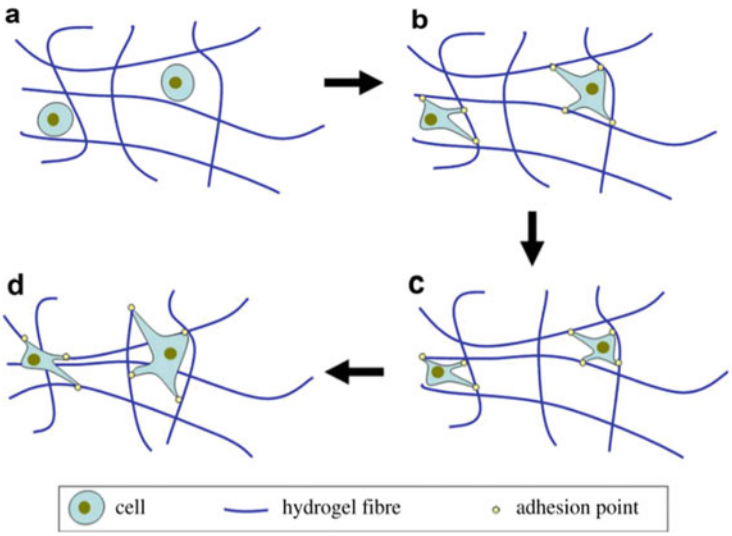

Fig. 3.44 Schematic diagram of the contraction process of a cell-inoculated hydrogel. (**a**) cells are embedded in a hydrogel matrix; (**b**) cells elongate and attach to fibers; (**c**) cells stretch fibers, which leads to the bending of the fiber; (**d**) cells are attached to the new fibers after being released, resulting in the contraction of the hydrogel (Reprinted with permission from Ref. [156]. Copyright 2014 by The Royal Society)

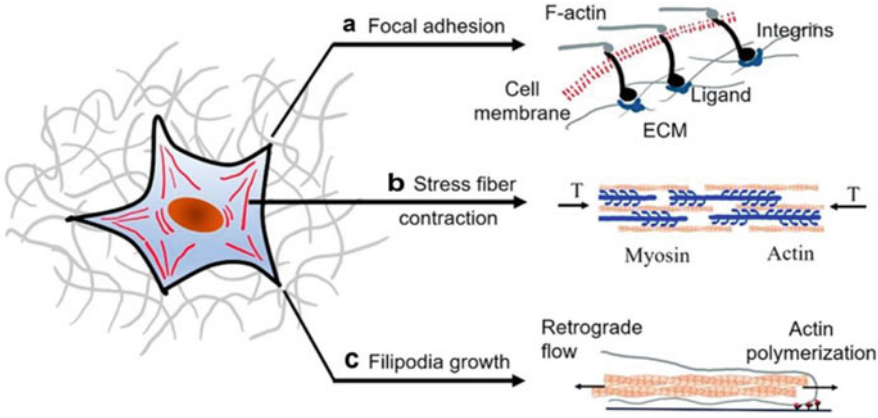

Fig. 3.45 Schematic diagram of main components and mechanisms of cell mechanical sensation. (**a**) Integrin-ligand complexes lead to adhesion between cells and their environment, and the lifetime of which is mediated by different forces. In a suitable mechanical environment, integrins can polymerize into large adhesive spot complexes; (**b**) stress fiber is a part of contractile actin, which can stretch across two adhesion spot complexes. Their combination and separation are restricted by their internal tension; (**c**) in a 3D environment, the spreading of cells is ensured by the extension of filaments, and the dynamics is maintained by the balance between the front actin polymerization and the reverse flow powered by actin contraction (Reprinted with permission from Ref. [157]. Copyright 2021 by American Chemical Society)

sites and specific integrin-ligand bonds will affect the degree of traction [157]. In addition, since the cell process is usually about 1 μm [158] in diameter, and flexible hydrogels generally have a mesh size in the range of 10–100 nm, which indicates that cells need to forcibly deform and/or degrade hydrogels to prolong their process and change their shape [159].

3.5.6.3 Effect on Hydrogel Degradation

The degradation of hydrogel matrix can be induced and regulated by microorganisms. For one thing, a large number of microbial cells will deform the hydrogel, and local cell growth and death may affect the mechanical stability of the hydrogel, resulting in the mechanical deformation of the hydrogel. For another thing, cells will stimulate the chemical degradation of hydrogel matrix. For example, fibroblasts in collagen hydrogel matrix can release matrix metalloproteinases (MMP) (such as collagenase and gelatinase [157]) to digest the matrix and produce other extracellular matrix proteins, which enable cells to recombine their surroundings and form a new matrix.

Scarul et al. [160] found that hydrogels sensitive to enzymes will degrade locally near cells. When the enzyme diffuses in the hydrogel, it can act as a catalyst for polymer degradation, thus reducing the cross-linking density of the hydrogel. After that, the hydrogel network expands, and when the reverse gelation point is reached, the network will eventually dissolve. Due to the competition between diffusion and degradation rates, local reverse gelation was achieved, which led to the degradation front being far away from the cell surface. The tightly cross-linked hydrogel showed local degradation kinetics, in which the network remained intact at the distance away from the particles, while the closer area was completely degraded (Fig. 3.46a). Finally, the degradation front speed was obtained as a function of hydrogel cross-linking density, which could be characterized by width W and speed V (Fig. 3.46b).

3.5.7 Outlook

The unique and customizable function of hydrogel makes it an attractive substitute for tissue engineering scaffolds to reduce or eliminate the need for tissues and organs. These favorable hydrogel matrix can provide molecular customized biological functions, adjustable mechanical properties and an environment very similar to ECM, so as to better adjust stem cell growth and tissue repair. By discussing the characteristics of hydrogel, including three-dimensional, hydrogel structure, biodegradability and dynamic characteristics, we can know how to regulate the function and fate of cells, and how cells can in turn guide the remodeling, mechanical properties and degradability of hydrogel, so as to achieve specific hydrogel-cell phenotype and function.

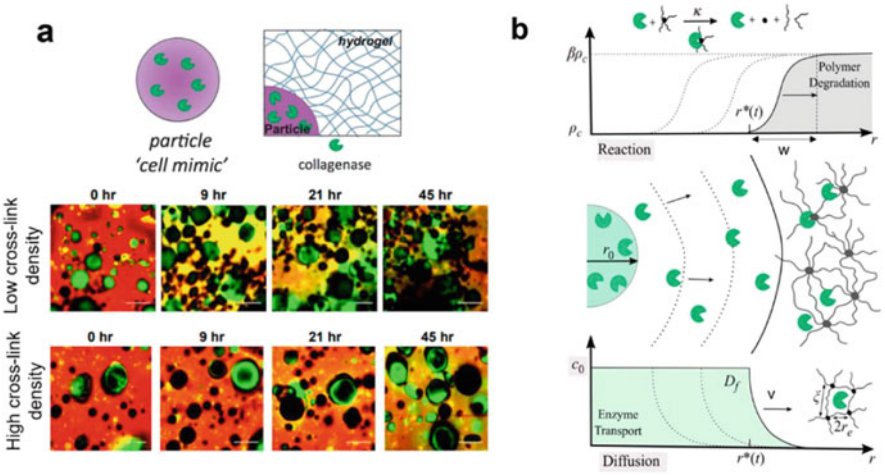

Fig. 3.46 (**a**) Confocal microscope images of spatiotemporal degradation patterns of hydrogels, including enzyme-sensitive covalently cross-linked PEG hydrogels and collagenase-loaded particles in hydrogels [collagenase (green) and PEG hydrogel (red)] (Reprinted with permission from Ref. [157]. Copyright 2021 by American Chemical Society); (**b**) the schematic showing the propagation of a fuzzy interface caused by enzyme diffusion and degradation within an enzyme-sensitive hydrogel. The figure shows the evolution of cross-linking density ρ (ρc is the cross-linking density during reverse gelation) and enzyme concentration. The highlighted parameters κ, c0, and Dg are the key features of the model (Reprinted with permission from Ref. [161]. Copyright 2018 American Physical Society)

However, there is still a lot of work to be done before this hydrogel can guide stem cell groups to repeatedly assemble and differentiate themselves into fully functional tissues. One of the main problems is to effectively summarize the highly complex stem cell niche [112]. Although many studies on hydrogel regulation focus on the influence of a single clue (such as mechanical rigidity or ligand density) on stem cell differentiation, the behavior of stem cells *in vivo* is influenced by various chemical and physical factors. Therefore, in order to fully understand the possible impact of every signal on the fate of stem cells, it is necessary to study the synergistic or antagonistic effects of competitive signals. In the design of hydrogel, the combination method is used to clearly define the effects of solubility, insolubility and mechanical signals on stem cell population, which can supply a response for the specific instructions of cells in their matrix. Combining with the progress of stem cell research, it aims to explore the mechanism of stem cell's specific destiny, and design hydrogel to imitate the guiding clue of natural ECM. In the future, it is expected to create a renewable source of transplanted tissue with ideal tissue regeneration characteristics to better serve clinical application and regenerative medicine.

3.6 Injectable Hydrogels and Their Applications

3.6.1 The Brief Introduction of Injectable Hydrogels

A novel hydrogel system known as injectable hydrogel has been introduced in recent times. This system is designed to fill any irregular defect areas by injecting a material with certain fluidity into the body, which subsequently forms a solid hydrogel. Injectable hydrogels are being increasingly demanded in various biomedical applications owing to their ability to introduce drugs and minimally invasive deployment in the body. These applications include drug delivery, wound repair, and tissue engineering, among others [162, 163]. The advent of technological and scientific advancements has brought about an era of personalized and intelligent medicine. The primary objective of personalized medicine is to diagnose and treat illnesses on a patient-specific basis. This is facilitated by the availability of genomics, proteomics, and metabolomics measurements and the increasing affordability of wearable devices and biosensors, which enable real-time data collection for personalized diagnosis and monitoring of individual patients [164–166]. Injectable hydrogel materials with designable properties that mimic natural ECM can be used as special artificial cellular microenvironments and are important for the large-scale implementation of personalized medicine [167].

Chemically and/or physically cross-linked hydrogels are often utilized for the fabrication of injectable hydrogels. Injectable hydrogel networks can take on a variety of physical forms and spatial structures, such as monolithic hydrogels, fibrous hydrogels, colloidal and granular hydrogels, particle cross-linked hydrogels, and particle-filled hydrogels, depending on their composition and preparation methods [168]. Different structures and types of injectable hydrogels have different distinctions. But the ideal injectable hydrogel should meet the following conditions: (1) it should have good biocompatibility with precursor solutions; (2) the injectable hydrogel solution needs to flow at a moderate pressure and quickly form a gel at the desired site; (3) the process of gel formation should not generate excessive amounts of heat or release harmful small molecules; (4) the mechanical properties must be rapidly enhanced after injection; (5) it has to keep sufficient integrity and strength [169–174]. Injectable hydrogels are often characterized by their *in situ* formability, *in situ* drug delivery, high targeting, and uniform incorporation into therapeutic molecules and/or cells without the need for surgery. Additionally, these hydrogels are biocompatible and biodegradable, which reduces the risk of inducing rejection reactions. These attributes have made injectable hydrogels a highly attractive option in the field of regenerative medicine, garnering significant attention from researchers and clinicians alike.

3.6.2 Injectable Hydrogels for Various Tissue Restoration

3.6.2.1 Injectable Hydrogel for Cardiac Tissue

The heart is a crucial organ in the human body and serves as a core component of the circulatory system by pumping blood. Myocardial infarction (MI) is one of the most serious heart-related illnesses and leads to significant myocardial cell death, microenvironmental changes, loss of electrical communication through fibrotic scarring, and insufficient blood supply to the infarcted myocardium. This results in millions of deaths annually. In response, researchers have explored numerous approaches to address these challenges and proposed several promising treatments. Major clinical strategies include drugs, cardiac assist devices, and heart transplants. Injectable hydrogels have several advantages over traditional methods, including local and targeted delivery via a narrow syringe, which is minimally invasive and does not require surgery [168].

Recently, injectable hydrogels have been widely developed to repair damaged cardiac tissue, with some notable breakthroughs. Wang et al. synthesized a microenvironment-responsive multifunctional hydrogel loaded with anti-inflammatory nanoparticles and custom recombinant type III humanized collagen (rhCol III), which was able to release the anti-inflammatory drugs curcumin (Cur) and rhCol III on demand at the site of heart failure (acidic environment and high ROS). *In vitro* and *in vivo* experiments both confirmed the efficacy of the responsive hydrogel with multiple functions in repairing damaged myocardial tissue. The hydrogel was also found to notably enhance the expression of myocardial markers, such as α-actinin and Connexin 43 (Cx43). This study has promising potential to expedite heart repair and pave the way for treating heart failure [175]. Another case in point, Li et al. explored the application of a combined "anti-inflammatory-provascular" therapeutic strategy in the treatment of infarcted heart. By constructing a symptom-responsive injectable hydrogel system for the responsive delivery of mesoporous silica nanoparticles (MSN), that reshapes macrophage function and modulates the inflammatory microenvironment, while small molecule nucleic acids (microRNA-21) are delivered to endothelial cells via MSN to promote microvascular formation. The dual effects of anti-inflammation and provasculature were observed to promote the recovery of ischemic myocardium in an inflammatory environment in a porcine model of MI. Furthermore, these effects effectively improved cardiac function after the onset of infarction [176]. Li et al. developed a novel approach to address the limitations of immature phenotype and function of cardiomyocytes as well as poor electrical coupling, by encapsulating human-induced pluripotent stem cell-derived cardiomyocytes (hiPS-CM) within a hybrid gold nanoparticle (AuNP)-HA hydrogel matrix. The hiPS-CMs administered through the hydrogel exhibited a stronger angiogenic effect, thereby contributing to the recovery process. Therefore, insights into the development of injectable bionics for repairing the structural and functional damage of the heart are provided by this study [177].

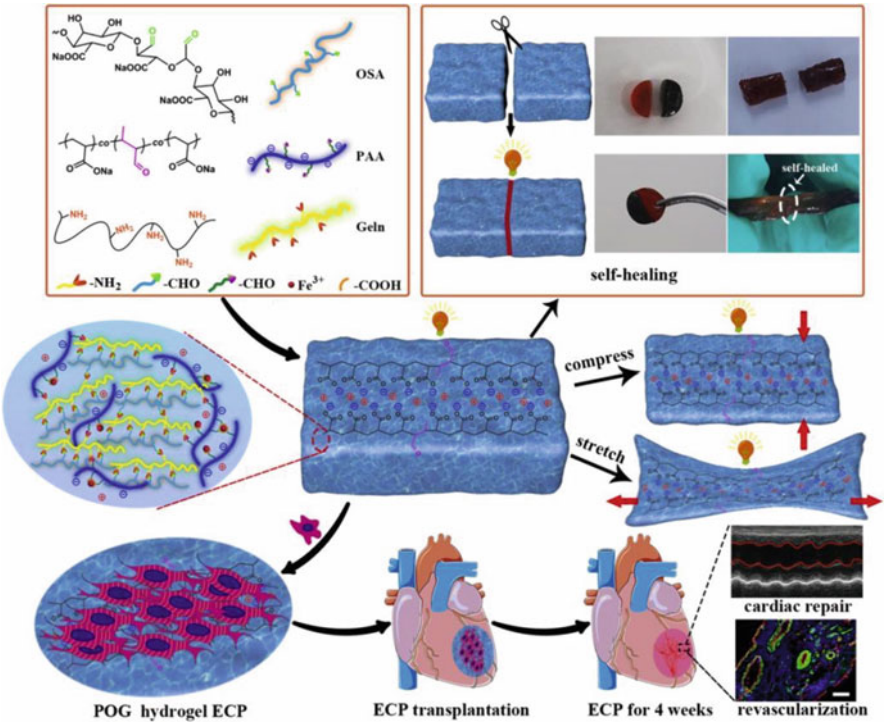

Fig. 3.47 Schematic illustration about the manufacturing process of the adjustable self-healing POG1 hydrogel and its implementation in repairing myocardial infarction (Reprinted with permission from Ref. [179]. Copyright 2021 Elsevier Ltd)

The treatment of MI through microRNA (miRNA)-based therapies, which specifically targeted the proliferation of CM, hold immense promise. Wang et al. have successfully developed an injectable hydrogel, comprising of HA, that facilitates the local and sustained delivery of miR-302 mimics to the heart. The resulting injectable gel effectively promoted local clonal proliferation and significantly increases the number of CMs within the boundary region of a Confetti mouse model. This study provided compelling evidence for the feasibility of a biomaterial-based miRNA delivery system that utilizes injectable hydrogel for the regeneration of the heart postinfarction [178]. A conductive hydrogel has been identified as a promising therapeutic tool for treating damaged myocardium in cases of MI. Song et al. devised an adaptable self-regenerating ion hydrogel (POG 1) by incorporating FDA-sanctioned biocompatible PAA into the oxidized sodium alginate (OA)/gelatin (Geln) hydrogel framework, as depicted in Fig. 3.47. By adjusting the PAA concentration (ranging from 0 to 16.6 mg/mL), PAA nanochannels were established within POG 1, rendering the hydrogels with microscopic, super-homogeneous conductivity, thereby allowing the ionic conductivity of POG hydrogels to be effortlessly fine-tuned to fulfill the necessities of heart tissue. Furthermore, the POG1 hydrogels

created had desirable tensile (> 500% strain) and compressive (> 85% strain) properties. Their mechanical attributes were comparable to those of mammalian hearts (30–500 kPa, Young's modulus), featuring self-regeneration and high deformability. POG 1 hydrogel-contained CM exhibited a more marked directed sarcomere than electron conductor-embedded hydrogels. Subsequently, it was administered via injection into the damaged area of the heart, playing a potent role in reducing left ventricular remodeling and reinstating cardiac function [179].

Despite so many advances in the field of injectable hydrogels for cardiac tissue engineering, there remain significant obstacles to their widespread use in humans. For instance, the mechanisms behind cardiac injury are not yet fully understood, and parameters such as hydrogel dose, injection timing, and material deployment are not yet well-defined. Moreover, the vast majority of hydrogels lack the necessary characteristics to accurately replicate the properties of native cardiac tissue [180].

3.6.2.2 Injectable Hydrogel for Bone Tissue

Due to traumatic injuries, defects, and diseases, cartilage and bone tissue may lose its ability to repair itself, often requiring clinical intervention. Transplantation is currently the most commonly used method for bone regeneration in clinical practice. However, bone transplant materials are a challenge to be solved in the field of bone defect repair. Four basic properties must be considered as materials for bone defect repair: (1) biocompatibility; (2) mechanical resistance; (3) biodegradability; and (4) induced regeneration [181]. Published in recent years are multiple accounts of injectable hydrogels for bone defect filling and facilitating healing. By teaming up with medications, ions, growth factors, stem cells, or microRNA, these hydrogels can trigger bone regeneration in a noninvasive way, deviating from conventional invasive methodologies and serving as a crucial factor in bone repair [168]. For example, Zheng et al. created a flexible composite hydrogel system, consisting of silk protein/mesoporous bioglass/sodium alginate (SMS), which enables seamless filling of bone defects and is reactive to both Ca^{2+} concentrations and inflammatory-like pH in the deficient bone microenvironment. It has the ability to promote new bone formation and angiogenesis by regulating the polarization of macrophages from proinflammatory (M1) to proregenerative (M2) and creating a specific, advantageous environment [182]. The combination of diagnosis and treatment is currently a hot development trend of injectable hydrogels. Li et al. developed a "diagnostic" and therapeutic dual-logic hydrogel that could be used for bone regeneration in diabetes mellitus (DM) by designing a dual-network hydrogel that was electrostatically assembled from phenylboric acid cross-linked and gelatin nanoparticles, as shown in Fig. 3.48. When exposed to high glucose or reactive oxygen species, the polyvinyl alcohol network can be reversibly disrupted, whereas the gelatin network contains biologically active motifs that promote cell affinity and can be degraded by matrix metalloproteinases (MMP). As a result, the biomaterial could determine the timing of drug release in the microenvironment of diabetes mellitus, based on its dynamic nature. Furthermore, it provides therapeutic logic for programming

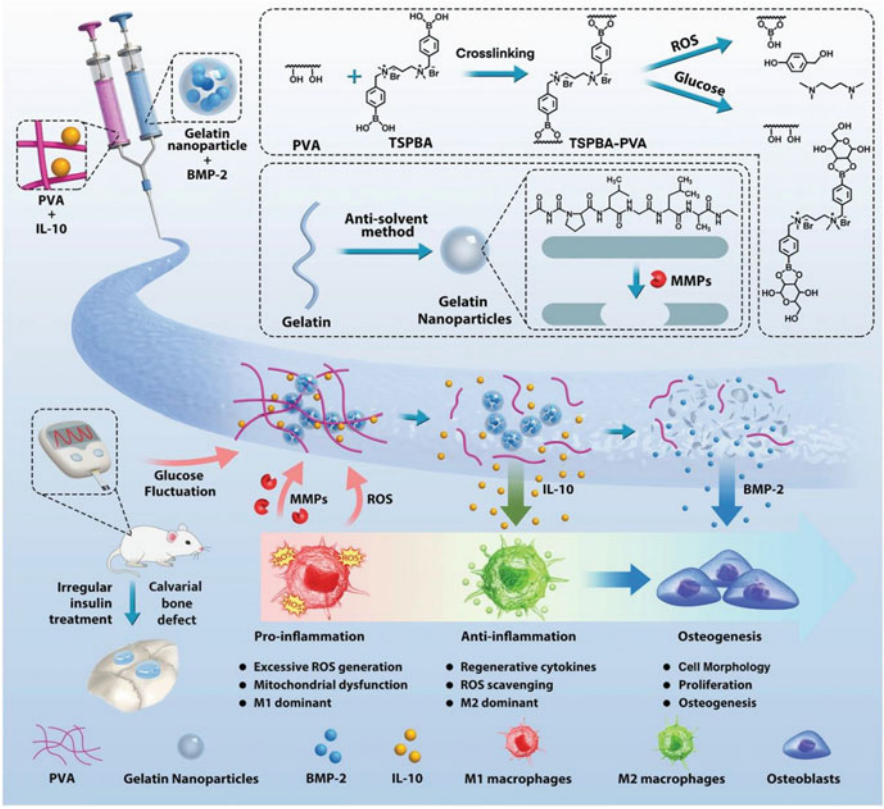

Fig. 3.48 Schematic diagram showing the design principle for "diagnostic" and therapeutic logic-based hydrogel and the mechanism of BMP-2 (HIB)-induced diabetic bone regeneration by reprogramming immune-osteo cascade (Reprinted with permission from Ref. [183]. Copyright 2022 Wiley)

different cargo to align with the immune bone cascade, facilitating better tissue regeneration upon release. *In vivo*, the osteogenic potential of the interleukin hydrogel—which contained interleukin 10 (IL-10) and bone morphogenetic protein 2 (BMP-2)—was assessed, followed by RNA sequencing and bioinformatics analysis in a diabetic rat model. Additionally, the hydrogel was demonstrated to be capable of adapting mechanically to the intricate nature of local bone defects. In addition, this study investigated the biological responses of macrophages and osteoblast precursor cells *in vitro* to reveal the potential regenerative mechanism of bone immune regulation, explained the logic-based cargo release that regulated macrophage polarization by remodeling the mitochondrial-associated antioxidant system, leading to osteogenic enhancement in diabetic bone defects. Additionally, it offered valuable insights into dual-logic-based tissue engineering approaches and the underlying biological mechanisms [183].

Apart from this, cartilage damage remains a threat to humans, but there is no treatment that can fully restore cartilage function. Lu et al. utilized a natural cross-linking agent known as genipin to attach biocompatible carbon dot nanoparticles to collagen, resulting in the formation of injectable hydrogels termed CGN (collagen–genipin–carbon dot nanoparticles). The fusion of carbon dot-altered hydrogel injection and PDT therapy is an innovative tactic for repairing cartilage defects with minimal invasion [184].

There are still a number of obstacles that need to be overcome in order to attain optimal cartilage and bone regeneration through injectable hydrogels. In the future, injectable hydrogels for bone repair could continue to be investigated in the following areas: (1) the creation of biologically active biomaterials suitable for the production of novel injectable hydrogels; (2) the need for more advanced methods to prepare hydrogels that improve mechanical properties and reduce toxicity and other adverse effects; and (3) the design of an optimal hydrogel for widespread use in the clinic [185].

3.6.2.3 Injectable Hydrogel for Muscle Tissue

The muscular tissue is a well-structured tissue made up of numerous unidirectional multinucleated muscle fibers, playing a critical role in the overall movement of the system. Intense physical activity, traumatic injuries, or other external factors can cause severe harm to the muscular tissue that surpasses its natural self-healing capabilities, leading to the development of scar tissue and the impairment of functionality. Autologous transplantation of healthy muscular tissue remains the conventional clinical approach for treating significant muscular injuries, yet it is restricted due to issues such as inadequate donor tissue, loss of donor site function, and donor site morbidity. One promising alternative is the development of tissue-engineered constructs that can be designed and prepared *in vitro* before being transplanted *in vivo*. This is followed by mechanical, chemical and/or electrical stimulation and pretreatment with growth factors, which can promote *in vivo* construct maturation and thus postimplantation survival [186].

As a new material in the field of muscular tissue engineering, injectable hydrogels have garnered significant interest. As an example, Ge et al. demonstrated the use of an injectable conductive antioxidant antibacterial nanocomposite hydrogel scaffold called FPAu. This scaffold was developed using aldehyde-modified Pluronic micelle cross-linked by polydopamine nanoparticles and ultrasmall AuNPs decorated with branched polyethyleneimine (PEI). The FPAu scaffold was used to regenerate and enhance the structural and functional capabilities of whole skeletal muscle tissue. In a rat model with tibialis anterior muscle deficiency, the FPAu scaffold was able to effectively promote the growth of skeletal muscle tissue and restore its mechanical and electrophysiological function [187]. In addition to conductive hydrogels, magnetic injectable hydrogels also enable the repair of muscle tissue. In Fig. 3.49a, Wang et al. utilized a coaxial electrospinning cycle cutting approach to produce monodisperse magnetic short nanofibers (MSNF) with high yield. An injectable

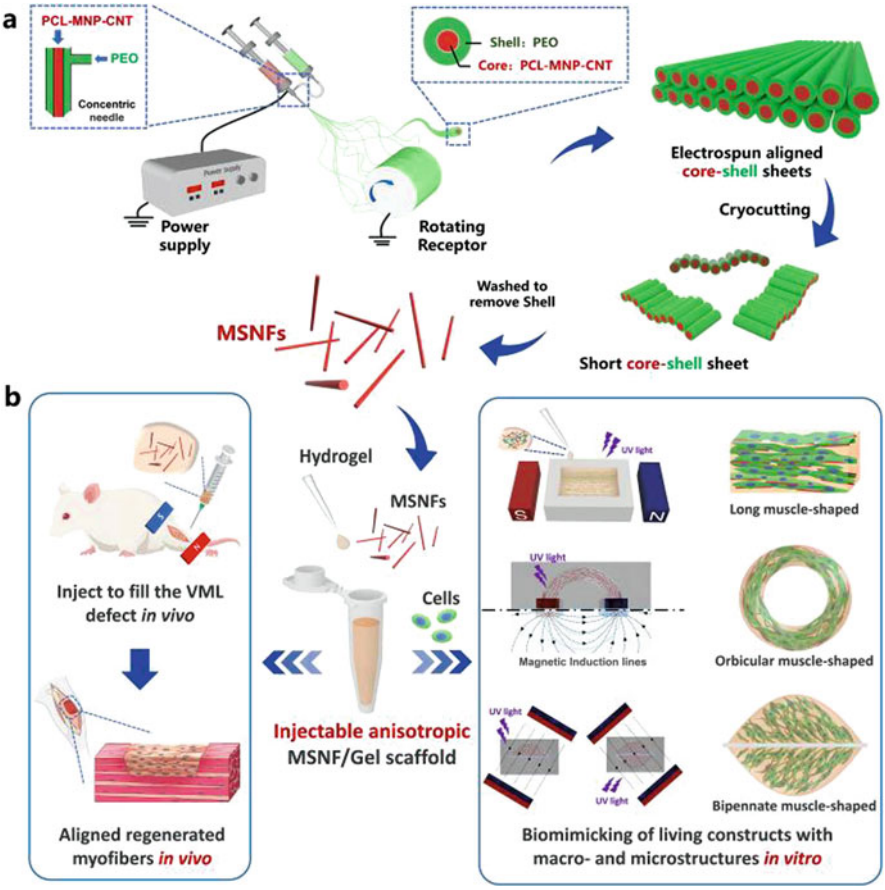

Fig. 3.49 Schematic illustration of injectable anisotropic MSNF/Gel scaffold for biomimicking of living constructs with macro- and microstructures *in vitro* and aligned regenerated myofibers *in vivo*. (**a**) Schematic process of MSNF preparation via a coaxial electrospinning-cyrocutting method. Electrospun core-shell sheets were cryocutted into short core-shell sheets and then washed to remove the shell to obtain dispersed MSNFs; (**b**) injectable MSNF/Gel scaffolds were prepared by encapsulating MSNFs within GelMA hydrogel to promote cell 3D alignment for biomimicking of living constructs with macro- and microstructures *in vitro* or to repair VML defect with aligned regenerated myofibers *in situ* under magnetic field (Reprinted with permission from Ref. [188]. Copyright 2022 Elsevier Ltd)

anisotropic MSNF/gel nanofiber/hydrogel scaffold was then created by incorporating the MSNF into a photocurable GelMA hydrogel using remote magnetic control, which allowed for precise microarchitecture control and the ability to guide three-dimensional cell arrays and tissues. When injected into animal models with volumetric muscle loss (VML) defects under the influence of a magnetic field, the scaffold mimicked the macro- and microtopographic characteristics of the rhombus and biceps brachii in their anatomical positions. This significantly enhanced the

formation of aligned muscle fibers *in vivo* and improved the functional recovery of damaged muscles in the VML model, as demonstrated in Fig. 3.49b. The prepared scaffold not only promoted the formation of muscle fibers in skeletal muscle, but also could biologically produce living structures containing complex anisotropy *in vitro* [188]. The concept of using remote magnetic replication to incorporate the 3D micro- and macrostructures of natural cell tissue represents a highly promising approach for achieving functional anisotropic skeletal muscle regeneration *in situ*.

Despite numerous attempts to identify a secure and efficient treatment to facilitate muscular tissue healing, the existing treatments have not resulted in any significant clinical advancements [189]. Furthermore, the existing studies' utilization of a solitary model does not translate to clinically significant muscular injuries. Thus, future research should employ more intricate and severe injury models to comprehensively assess the effectiveness of injectable hydrogels [190].

3.6.2.4 Injectable Hydrogel for Nerve Tissue

Injuries to organs and tissues are often accompanied by nerve damage, which affects people's normal physiological functions, such as chronic pain, nerve disorders, paralysis or disability. The process of nerve repair is lengthy and requires surgery and medication, together with electrical stimulation and acupuncture. Injectable hydrogels can be used to treat neurological deficiencies and offer desirable advantages. Conductive injectable hydrogels have the ability to promote nerve regeneration. Xu et al. developed self-healing hydrogels and scaffolds capable of shape restoration and conductivity. They employed N-carboxyethyl chitosan (CEC), chitosan-modified polypyrrole (DCP) nanoparticles, and an exclusive aldehyde-capped bifunctional polyurethane (DFPU) as cross-linking agents. CEC was combined with DCP through electrostatic interactions, and DFPU was utilized to cross-link the hydrogel and scaffold materials via a dynamic Schiff base reaction, resulting in a cross-linked network. The lyophilized hydrogels were used to create shape recoverable scaffolds. The scaffold demonstrated exceptional strain/motion sensing properties *in vitro* and ex vivo while being biodegradable and biocompatible *in vivo*. The scaffold also promoted the adhesion, proliferation, and differentiation of neural stem cells (NSCs). The neuroregenerative capacity of conductive hydrogels or cell-filled conductive hydrogels was well demonstrated in a zebrafish brain injury model by restoring motor function, with a functional recovery rate of approximately 53% and 80%, respectively [191]. Xu et al. developed an injectable hydrogel composed of conductive and biodegradable germanium phosphide (GeP) nanosheets combined with a hyaluronic acid graft dopamine (HA-DA) hydrogel matrix, as illustrated in Fig. 3.50a. This hydrogel was successful in repairing spinal cord nerves and accelerating the differentiation of neural stem cells (NSCs) into neurons. Figure 3.50b showed that dopamine molecules were grafted onto HA biomolecules to produce a hyaluronic acid grafted dopamine hydrogel with excellent tissue adhesion capabilities. GeP nanosheets were coated with polydopamine (PDA) to enhance their biological stability and biocompatibility, resulting in GeP@PDA. The

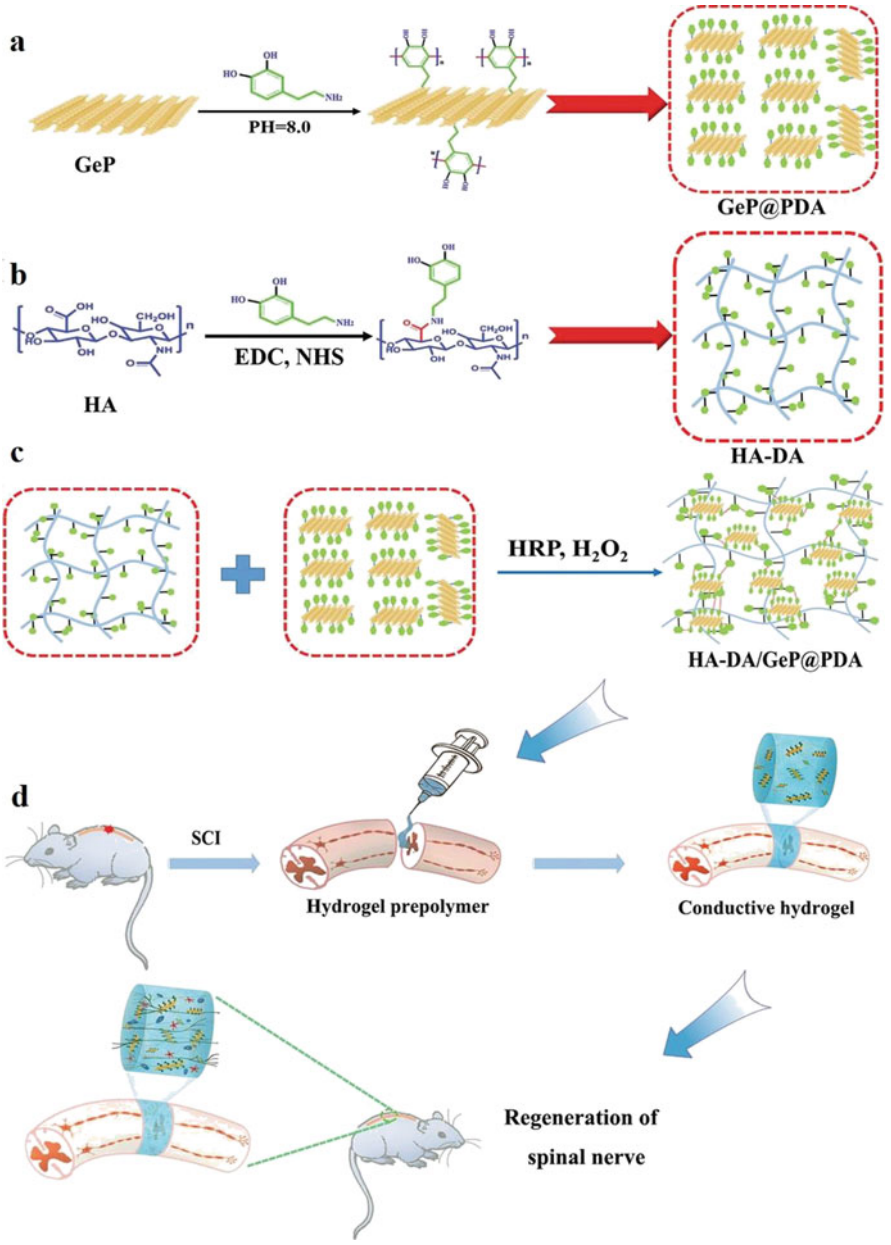

Fig. 3.50 Preparation scheme of (**a**) GeP@PDA nanosheets; (**b**) HA-DA polymers; and (**c**) HA-DA/GeP@PDA conductive hydrogels; (**d**) schematic diagram of the application of injectable and conductive HA-DA/GeP@PDA biohybrid hydrogels in the spinal cord injury repair (Reprinted with permission from Ref. [192]. Copyright 2022 Wiley)

GeP@PDA were added to the HA-DA hydrogel matrix using horseradish peroxidase (HRP)/H_2O_2 as the initiator system, as shown in Fig. 3.50c, significantly increasing the hydrogel's conductivity and enhancing NSC differentiation into neurons *in vitro*. In a rat model of complete transection of the crestal medullary injury, the *in vivo* implanted HA-DA/GeP@PDA hydrogel promoted immunomodulation, endogenous angiogenesis, and neurogenesis of NSCs, significantly improving motor function recovery, as depicted in Fig. 3.50d. This provided a novel approach for developing materials that could be used to repair crestal medullary injuries [192].

Although injectable hydrogels have been studied as scaffolds for neurological repair for many years, there are still some limitations and high risks for injection at different sites *in vivo*, such as the brain. Additionally, the discovery of mechanisms of stimulation of neural tissue growth is still insufficient, such as the frontal lobe connection mechanism between the hydrogel and the axon; therefore, efforts should be focused on exploring the mechanisms behind it for better repair results [193].

3.6.2.5 Injectable Hydrogel for Wound Healing

People all over the world suffer from minor or major injuries every day. The correct management and treatment of some serious wounds are of great life and economic value to individuals and societies. For quick healing of wounds to ensure the health of human, the wound needs to be kept clean, with an adequate blood supply, free of necrotic tissue and in a suitable moisture environment. Medical dressings are supplies to cover the damaged area and are available in natural gauze, synthetic fiber dressings, polymorphic dressings, foamed polymorphic auxiliaries, hydrocolloid dressings, alginate dressings, nanosilver dressings, etc., which can be divided into dry and wet types. It may prevent bacterial overgrowth, control wound exudation, and maintain proper fluid balance. There are several dressing options that are accessible for purchase, including polyurethane films, fibers, and hydrogels, and these have been employed for the purpose of wound management. Hydrogels are an especially advantageous type of dressing due to their ability to create a moist environment, absorb wound exudate, facilitate oxygen flow, and cool the surface of the wound [194–196]. Injectable hydrogels belong to wet type dressings with good hydrophilicity and biocompatibility, facilitating the elimination of metabolic products without affecting the metabolism of the living body. Consequently, wound management heavily relies on the utilization of hydrogel-based dressings, which are commonly employed in a range of medical contexts, from minor to severe tissue injuries. The demand for injectable self-repairing hydrogel dressings that possess diverse attributes is particularly high in relation to wound healing applications. Therefore, there is a pressing need for injectable self-repairing hydrogel dressings with multifunctional properties in the field of wound healing. Zhao et al. have created a range of injectable conductive self-repairing hydrogels, which consist of quaternized chitosan-g-polyaniline (QCSP) and benzaldehyde-based functionalized poly(ethylene glycol)-poly(glycerol sebacate) (PEGS-FA). These hydrogels have been engineered to function as antibacterial and antioxidant agents, as well as

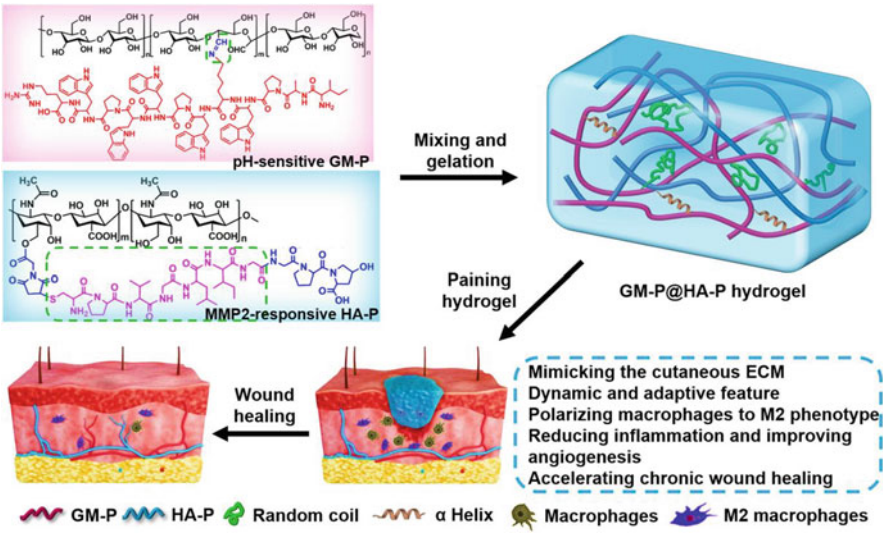

Fig. 3.51 Schematic diagram for the formation and application of biomimetic GM-P@HA-P glycopeptide hydrogel as a multifunctional dressing for MRSA-infected chronic skin wound healing (Reprinted with permission from Ref. [198]. Copyright 2022 Springer)

electroactive dressings for skin wound healing purposes. In comparison to quaternized chitosan/PEGS-FA hydrogels and Tegaderm™ films, this hydrogel has been found to demonstrate superior *in vivo* blood coagulation efficacy at a 5% weight concentration, and also significantly enhances the *in vivo* wound healing process in a complete skin defect model by increasing the expression of various growth factors, including platelet-derived growth factor (VEGF), epidermal growth factor (EGF), and transforming growth factor (TGF-β). Since natural materials are characterized by good biocompatibility and low toxicity, and proteins are crucial components of all tissues, hydrogels based on proteins have a promising future in the field of bioengineering [197]. Liu et al. have developed a glycopeptide heterogeneous hydrogel that is responsive to the tissue environment and antimicrobial, with a focus on its application in chronic wound healing, as shown in Fig. 3.51. Inspired by the composition, structure, and function of natural extracellular matrix (ECM), the researchers coupled dextran (GM) with an endogenous antibiotic peptide using a dynamic and acid-sensitive imine bond (designated as GM-P). This bond mediated the polarization of macrophages toward the M2 type, which can effectively regulate inflammation at the wound site. Another glycopeptide, hyaluronic acid, was prepared by grafting a MMP-2/9 response peptide with a collagen tripeptide (GPHyp) (HA-P), which could mimic the structural support for cell adhesion, migration, natural ECM proliferation, and provide essential amino acids for collagen reconstitution during ECM assembly. The two glycopeptides were mixed together in water to create GM-P@HA-P heterogeneous hydrogels, which had a porous structure of artificial ECM cross-linked by laminar fibers ranging from nano to micron in

diameter. The outcomes indicated that this hydrogel that mimics the extracellular matrix was able to increase cell proliferation, induce macrophage polarization toward the M2 phenotype, and exhibit potent antibacterial activity against both Gram-negative and Gram-positive bacteria. Moreover, it expedited the regeneration of methicillin-resistant *Staphylococcus aureus* (MRSA), reduced inflammation, and stimulated angiogenesis by coordinating a proregenerative response guided by abundant M2 phenotype macrophages derived from infected homozygous diabetic and scalded skin [198].

To enhance the effectiveness of wound management, it is imperative to devise novel materials and uncomplicated methods to develop high-performance injectable hydrogels with enhanced capabilities, such as antibacterial and anti-inflammatory characteristics, antioxidant traits, the promotion of regeneration, and the elimination of scarring.

3.6.2.6 Injectable Hydrogels for Other Tissues

Along with the tissue repairs outlined previously, injectable hydrogels have the potential to treat various other biological tissues, including the lungs, stomach, and intervertebral discs. To this end, Peng and colleagues have created a PEI/PAA powder with self-gelling and adhesive properties. As a result of the robust physical interaction between the polymers, the powder can quickly absorb interfacial water to generate a physically cross-linked hydrogel within a mere 2 s. This hydrogel is capable of efficiently sealing damaged pig stomachs and intestines [199]. Xu et al. have efficiently biosynthesized injectable microspheres composed of gelatin methacrylate (GMs) with controlled and uniform particle sizes via a low-cost electrospray technique. This method has been used to minimize the *in vivo* degeneration of rat intervertebral discs, maintain the integrity of nucleus pulposus tissue, and expedite the synthesis of ECM [200].

To sum up, injectable hydrogels hold tremendous potential for multiple tissue regeneration techniques. The primary obstacle in the near term will be to validate these findings in preclinical and clinical investigations, and ultimately transform them into secure and efficient therapeutic alternatives that comply with regulatory requirements and can be commercialized on a broad scale [168].

3.6.3 Injectable Hydrogel for Tissue Adhesive

Existing bio-adhesives tend to slip when it applied in the complex and humid environment of the human body. The methods like suture fixation and expandable microneedles are invasive and not very user friendly [201]. As a result, it is crucial from a clinical standpoint to develop an adhesive that can securely bond to moist tissue and resist dynamic mechanical movements to support tissue regeneration throughout the healing process at the site of injury. A number of injectable hydrogels

is available that have extremely strong adhesion and can be designed to alleviate the onset of superficial tissue inflammation due to their high permeability and moisturizing properties, which by design can lead to therapeutic results.

A case in point, He et al. have produced a sequence of injectable pH-responsive self-repairing adhesive hydrogels using acryloyl-6-aminohexanoic acid and AA-N-hydroxysuccinimide (AA-NHS). The addition of AA-NHS as a micro-cross-linker led to a rise in the adhesive strength of the hydrogels. When tested on a porcine gastric hemorrhage *in vivo* model, the hydrogels demonstrated excellent hemostatic characteristics by halting acute arterial bleeding and avoiding delayed bleeding. The hydrogel also had a strong therapeutic effect on a gastric wound model, which included significant promotion of wound healing through increased deposition of type I collagen, expression of α-smooth muscle actin (α-SMA), and angiogenesis. These results demonstrate the potential of injectable self-repairing mucoadhesive hydrogels for treating gastric wounds following endoscopic procedures [173]. Liang et al. developed a biocompatible sprayable conductive hydrogel by means of Fe^{3+}—initiated *in situ* polymerization of pyrrole (Ppy) and dopamine, in combination with the complexation of gelatin. A two-step Michael addition reaction was employed to create hyperbranched polymers, with dopamine and pyrrole groups introduced sequentially, as illustrated in Fig. 3.52. Initially, dopamine hydrochloride, pentaerythritol triacrylate, and poly(ethylene glycol) diacrylate were reacted according to a stepwise "A2 + B3 + C2" polymerization mechanism, with the ratio of double bonds to reactive hydrogen set at 1.5:1, forming a hyperbranched poly(amino ester) (HPAE) with acrylate end groups. In the second stage, an excess of pyrrole moiety ends was added to fully envelop this hyperbranched polymer that contained dopamine, leading to the formation of the HPAE-Py polymer. To enhance the biocompatibility of the hydrogel patch, Gelatin was introduced into the precursor solution, along with the purified HPAE-Py polymer, while Fe^{3+} was selected as a multifunctional curing agent that was oxidized during *in situ* polymerization. As a result of the formation of the dopamine-Fe^{3+} complex, the proposed adhesive hydrogel was able to swiftly attach to the wet pulsating surface of the heart, without any unwanted fluid seepage. This consequently enhanced heart function and aided in the restoration of electrophysiological signal conduction and hemodynamics within the infarcted myocardium. This research presents a novel approach for the production of suture-free patches that can be translated into clinical practice [202].

While numerous hydrogels possessing tissue adsorption capabilities have been highlighted for their benefits, certain challenges must be acknowledged and resolved prior to their use in clinical settings. One significant factor to consider is the regulation of their degradation rate based on the proportion and temperature of the precursor. To ensure practicality, further investigation into this area is required, with significant potential for advancement in the future [203].

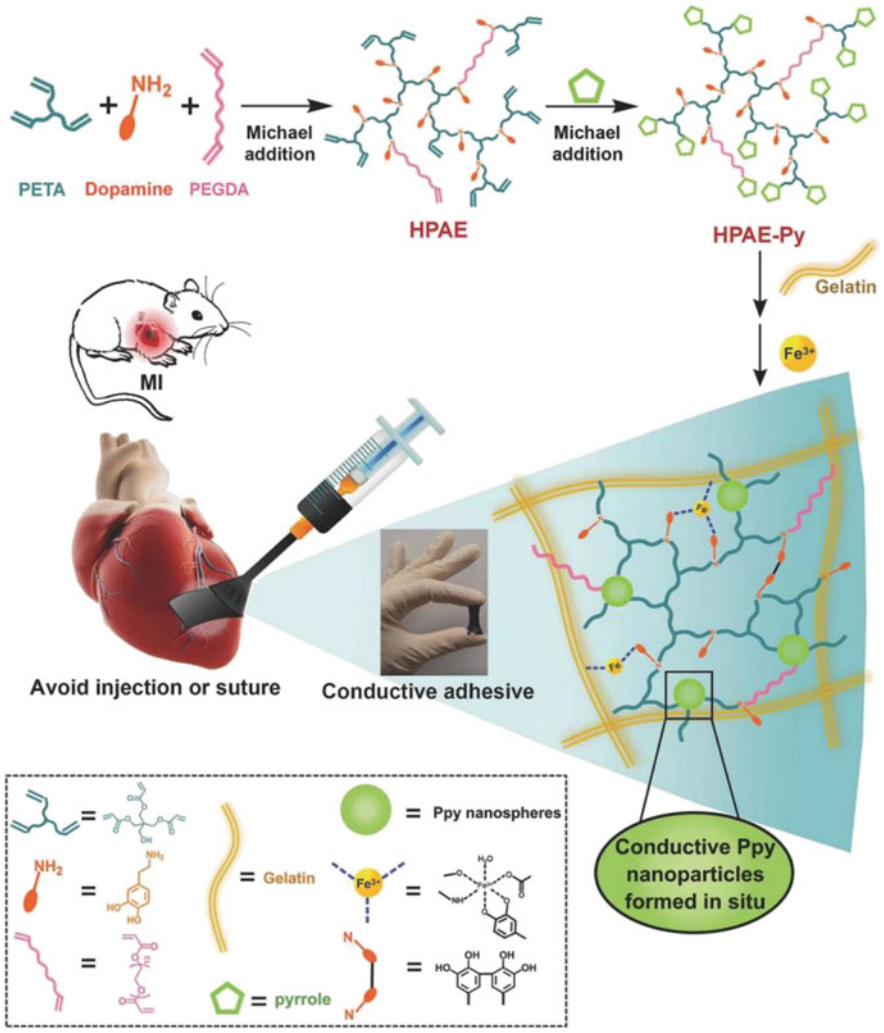

Fig. 3.52 Schematic illustration of the formation of a conductive and adhesive hydrogel, and its application by painting directly on the surface of MI heart in SD rats (Reprinted with permission from Ref. [202]. Copyright 2018 Wiley)

3.6.4 Injectable Hydrogel for 3D Printing

The field of biomedicine and biotechnology has shown significant interest in 3D bioprinting, a technology capable of printing biodegradable materials infused with cells, resulting in the production of 3D tissues. Injectable hydrogels have emerged as a particularly promising material for use in 3D printing due to their dynamic nature, ability to maintain stable rheology, and further stability provided by cross-linking

after secondary printing. As a result of these unique properties, injectable hydrogels have enormous potential for application in the field of 3D printing.

In the study conducted by Shin et al., an injectable, gently conductive granular hydrogel was created utilizing gallic acid redox and *in situ* metal reduction reactions. The granular hydrogel, in which metal nanoparticles were synthesized *in situ*, demonstrated superior electrical conductivity (approximately 0.05 S cm^{-1}) compared to the bulk hydrogel. This conductive particulate hydrogel allowed 3D printing and extrusion to create a free-form three-dimensional configuration on a polymer film with conductivity, forming a conductive microgel that restored electrical conductivity by connecting two separated muscle tissues [204]. Loebel et al. introduced a new type of HA hydrogels formed through noncovalent guest–host interactions, as depicted in Fig. 3.53. Upon injection via a syringe, these hydrogels underwent shear thinning followed by self-healing within seconds when the shear force was eliminated. In this paper, the authors also outlined how to modify HA derivatives with methacrylates for secondary covalent cross-linking and fluorophore reactions for *in vitro* and *in vivo* imaging. HA polymers were carefully designed using relatively low molecular weight raw materials, with precise modification degree and guest-to-body stoichiometry ratios, resulting in hydrogels with specific properties that took 3–4 weeks to complete. The fast self-healing capability of this hydrogel system holds great promise for applications such as *in vivo* injection (including cells and therapeutic molecules) and 3D printing, overcoming the challenge of developing printable hydrogel bioinks that are printable and mechanically stable enough to support printed structures [205].

Despite the rapid development of 3D printing technology in the field of biological tissue engineering, research in this area remains significantly constrained. Ink formulation and print setup are key, and specific rheological benchmarks will subsequently need to be established to determine printability. The intricate nature of materials and structures utilized in 3D printing within this field renders it challenging for any one discipline to fully accommodate its development. As such, a combination of multidisciplinary and interdisciplinary approaches are necessary to enable the printing of increasingly lifelike tissues and organs. This, in turn, lays the foundation for disease research, drug screening, and advancements in tissue engineering [168].

3.6.5 Injectable Hydrogel for Bioelectronics

With the progressive advancement of technology, there is a growing awareness that bioelectronic signals can convey more information to people and provide a good way to understand and solve problems. Hydrogels are much in demand for minimally invasive biomedical treatments. As therapeutic functions alone are no longer adequate, injectable hydrogels have increasingly found use in bioelectronic devices over the past few years, demonstrating substantial progress and enabling diverse monitoring and treatment modalities.

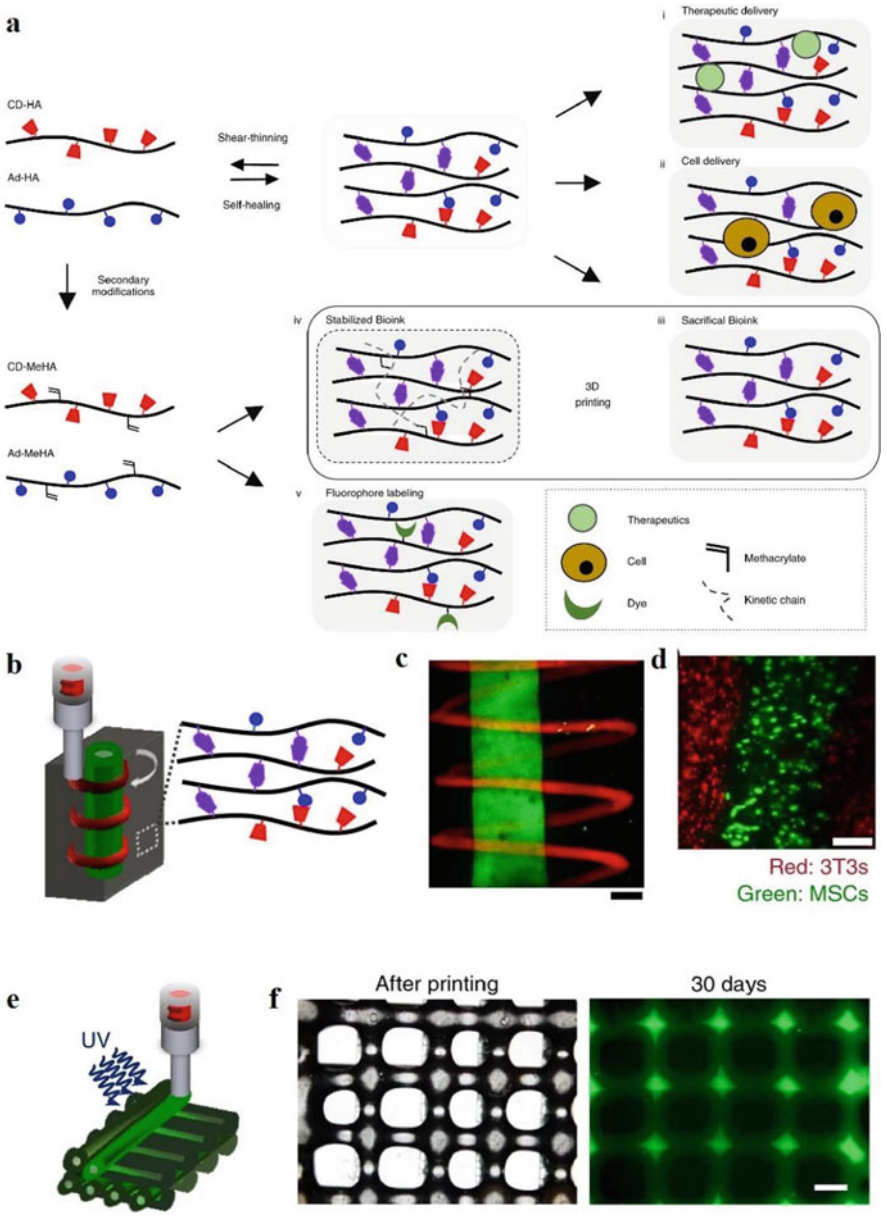

Fig. 3.53 (**a**) Overview of the guest–host hydrogel platform. (Top left) Schematic illustration of HA modified with β-cyclodextrin (CD-HA, red) and adamantane (Ad-HA, blue) with the assembly (self-healing, purple) and disassembly (shear-thinning) of the guest–host complex. (Top right) Encapsulation and delivery of (1) therapeutics (e.g., proteins and therapeutic molecules) and (2) cells (e.g., endothelial progenitor cells) for *in vivo* delivery. (Bottom) Methacrylation of CD-HA and Ad-HA to obtain CD-MeHA and Ad-MeHA polymers, which facilitate hydrogel formation by both (3) physical cross-linking and (4) secondary cross-linking of methacrylate upon UV light exposure (10 mW cm^{-2}, 365 nm), including toward 3D printing applications. CD-MeHA derivatives can also be used for (5) additional peptide-conjugated fluorophore coupling

Zhang et al. have developed an injectable, conductive hydrogel comprised of poly (3,4-ethylenedioxythiophene):poly(styrenesulfonate) (PEDOT:PSS), as demonstrated in Fig. 3.54a. The hydrogel exhibits exceptional biocompatibility and stability due to the physical cross-linking of the $PEDOT^+$ polymer chains, allowing it to spontaneously form hydrogels at room temperature upon injection of the suspension at the desired location. By mixing the PEDOT:PSS suspension with 4-dodecylbenzenesulfonic acid (DBSA), the researchers were able to obtain room temperature-formed PEDOT:PSS (RT-PEDOT:PSS) hydrogels, which possess a high volume expansion rate and can be used in water-repairable hydrogel bioelectronics. Additionally, they proposed a technique to create PEDOT:PSS hydrogel fibers, facilitating the development of soft and self-healing hydrogel bioelectronic devices, as depicted in Fig. 3.54b, which has the potential for use in a range of biomedical applications [206].

The future development is expected to focus on assembling and integrating injectable conductive hydrogels that possess excellent biocompatibility, high electrical conductivity, and water stability with diverse bioelectronic devices and interfaces of biological tissues.

3.7 Clinical Applications of Hydrogels

Over the past few decades, hydrogel items have been implemented in clinical settings. The medical application of hydrogels has considerably broadened, extending from conventional wound dressings to contact lenses, and, more recently, to live-cell therapies [18]. Collagen or gelatin is the most prevalent biomolecule utilized in protein-based hydrogels. Collagen is a vital component of the ECM found in articular cartilage and holds considerable potential in the regeneration of cartilage. Gelatin is a modified form of collagen and shares many of its properties. It exhibits excellent biodegradability and compatibility, which is conducive to the adherence, migration, and proliferation of cells. The most commonly used material to generate hydrogels is nontoxic, low-fouling PEG, which has been sanctioned by the FDA for biomedical purposes [207]. According to Table 3.6, regulatory clearance has been

Fig. 3.53 (continued) to track hydrogel degradation; (**b**) schematic illustration of the extrusion of two differently labeled guest–host hydrogel inks (red and green) into an unlabeled guest–host support hydrogel (gray); (**c**) confocal images show a filament of a fluorescein-labeled ink with a continuous spiral of a second, rhodamine-labeled ink extruded into an unlabeled support gel; (**d**) the printing process enables the patterning of multicellular structures shown by printing MSCs (green) into a support gel containing 3 T3 fibroblasts (red); scale bars, 200 μm; (**e**) schematic illustration of the extrusion of methacrylated GH hydrogel ink and subsequent stabilization with UV exposure in the presence of Irgacure 2959; (**f**) the UV-stabilization process allows for printing of multilayered structures with high spatial fidelity—as shown by the phase-contrast top view image (left)—which maintains the grid structure (right) for more than 30 days in aqueous culture medium. Scale bar, 500 μm (Reprinted with permission from Ref. [205]. Copyright 2017 Springer)

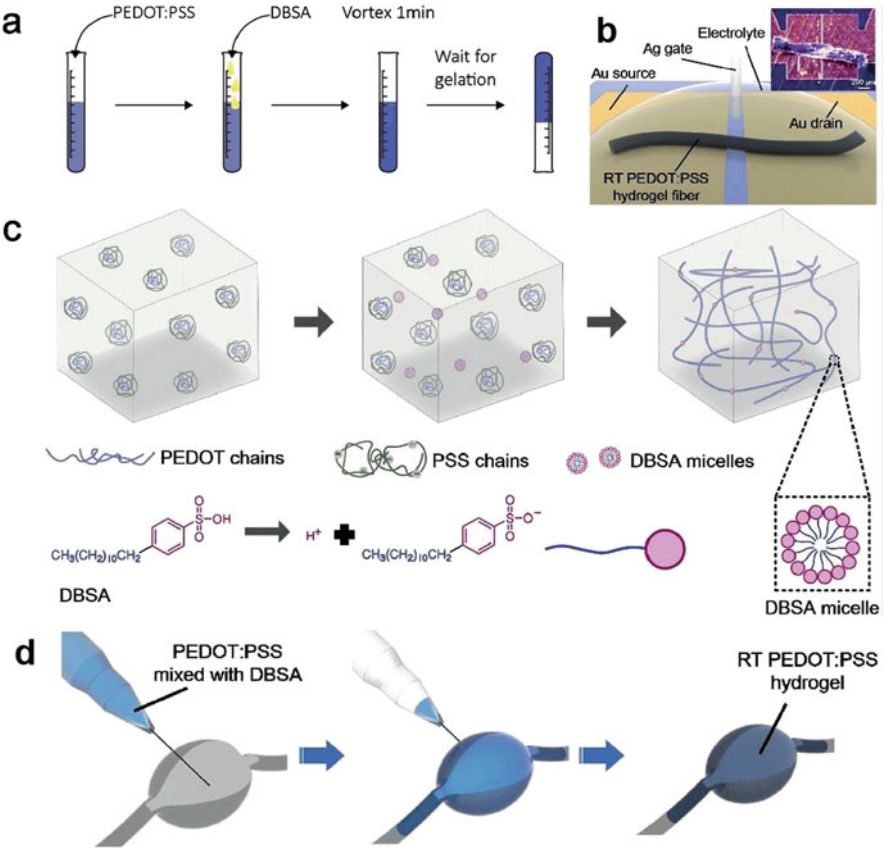

Fig. 3.54 (**a**) Schematic illustration of gelation processes of RT-PEDOT: PSS hydrogel; (**b**) schematic of the fabricated OECTs with injected RT-PEDOT: PSS hydrogel fiber; (**c**) cross-linking mechanism of our RT-PEDOT: PSS hydrogel. The addition of the DBSA into the suspension weakens electrostatic attraction between $PEDOT^+$ and PSS^-, exposing the $PEDOT^+$ chains to water. The exposed $PEDOT^+$ chains undergo a conformational change from a confined-coiled to an expanded-linear structure and subsequently physically cross-linked due to π–π stacking and hydrophobic attractions; (**d**) schematic of injectable RT-PEDOT: PSS hydrogels: Puncturing the soft tissue with syringe (Reprinted with permission from Ref. [206]. Copyright 2022 Elsevier Ltd)

granted for various other constituents of hydrogel technologies for healthcare uses, such as cancer therapy, wound healing, tissue regeneration, and other areas. There are 25 approved hydrogel products in Table 3.6, and we classified clinical trials by relevant disease, material source (i.e. natural, synthetic, or unknown) , and approval date. The source of the material is based on a clinical trial description or a U. S. patent for the device.

Table 3.6 Clinically approved injectable hydrogels [18, 208]

Name	Hydrogel material/payload (gelation mechanism)	Injection type	Approved indication	Company	Approval (year)
Heart					
Algisyl-LVR® hydrogel implant	Alginate (physical interaction)	Percutaneous	Advanced heart failure	LoneStar heart, Inc.	EMA (2014)
Bone					
Durolane	Hyaluronic acid (HA) and hydroxyl versus epoxy (BDDE)	Intra-articular injection	For alleviating discomfort caused by knee osteoarthritis	Bioventus LLC	CE mark (2001) PMA P170007 (2017)
INFUSE® bone graft	Collagen and synthetic human bone morphogenetic protein-2 (physical association)	Spinal injection	Spinal fusion, and spine, oral-maxillofaci and orthopedic trauma surgeries	Medtronic Sofamor Danek USA, Inc.	FDA (2002 for first indication)
INFUSE bone graft	Collagen and imine ligation (formaldehyde)	Implantation via an anterior open or an anterior laparoscopic approach	Containing rhBMP-2, for spinal fusion procedures in skeletally mature patients with degenerative disc disease at one level from L4-S1	Medtronic Sofamor Danek USA, Inc.	P000058 (2002) PMA P000054 (2004)
EUFLEXXA®	HA (physical interaction)	Intra-articular	Knee osteoarthritis	Ferring Pharmaceuticals Inc.	FDA (2004) EMA (2005)
Monovisc	HA and carboxyl versus Carbodiimides (BCDI)	Intra-articular injection	For alleviating discomfort caused by knee osteoarthritis	Anika Therapeutics, Inc.	PMA P090031 (2014)
GelrinC®	PEGDA with denatured fibrinogen	Injected after microfracture cross-linked using UVA light	Osteoarthritis regeneration	Regentis Biomat.	EMA FDA
Kinex bioactive gel	Bioglass, collagen and HA	Injectable solution	Bone void filler	Globus Medical	FDA

Cartilage					
NovoCart inject plus	Maleimide functionalized human albumin and HA cross-linked with bisthio PEG, and autologous chondrocytes	Arthroscopic injectable autologous chondrocyte transplant	Cartilage defects of the knee	Tetec AG	FDA phase III trials (2017)
ChonDux	Chondroitin Sulfates/PEG and Amine aldehyde/radical polymerization	Implantation following the microfracture	Cartilage adhesive	Zimmer Biomet	NCT01110070
Dressing					
Sepragel ENT	HA and hydroxyl versus vinyl Sulfone (DVS)	Surgical application	Occupying space within a dressing and/or stent designed to prevent the formation of adhesions during surgery of the nasal/sinus, middle ear, and external ear canal	Sanofi GENZYME CORP	510 (k) K043035 (2005)
Collagen wound dressing	Collagen and EDC	Topical applications	For management of partial and full-thickness wounds	Dalim Tissen Co., Ltd	510 (k) K112580 (2012)
Bio-ConneKt wound	Collagen and imine	Topical applications	Wound dressing	MLM biologics, Inc.	510 (k) K140456 (2014)
Premvia	Hyaluronan, gelatin, PEG diacrylate (thiol-Michael addition)	Topical/surgical applications	For the management of wounds	BioTime, Inc.	510 (k) K134037 (2014)
Apis	Gelatin and EDC	Topical/surgical applications	For use in management of wounds	SweetBio, Inc.	510 (k) K182725 (2019)
Adhesion					
BioGlue	Bovine serum albumin and imine ligation (glutaraldehyde)	Surgical applications	Surgical adhesive (for use as a supplementary aid to conventional methods of achieving hemostasis in the surgical repair of large blood vessels)	CryoLife Inc.	HDE H990007 (1999) PMA P010003 (2001)

(continued)

Table 3.6 (continued)

Name	Hydrogel material/payload (gelation mechanism)	Injection type	Approved indication	Company	Approval (year)
Tissue					
INCERT-S	HA and carboxyl versus Carbodiimides (BCDI)	Surgical applications	To avoid the formation of tissue adhesions and scarring after spinal surgeries	Anika therapeutics, Inc.	CE Mark (2004)
TenoGlide (tendon wrap)	Collagen, glycosaminoglycan and imine ligation (glutaraldehyde)	Implantation	To manage and protect tendon injury with no substantial loss of tendon tissue	Integra LifeSciences Corporation	510 (k) K053655 (2006)
OrthADAPT	Collagen and EDC/NHS (1,6-hexane diamine and suberic acid)	Surgical applications	For implantation to reinforce soft tissue	Pegasus Biologies, Inc.	K071065 (2007) 510 (k) K090288 (2009)
TraceIT® hydrogel tissue marker	Polyethylene glycol (chemical reaction)	Percutaneous	Enhanced alignment of soft tissue for image-guided therapy	Augmenix, Inc.	FDA (2013)
SpaceOAR® hydrogel	Polyethylene glycol (chemical reaction)	Percutaneous	For protecting vulnerable tissues during prostate cancer radiotherapy	Augmenix, Inc.	EMA (2010) FDA (2015)
Other products					
Hylasine Sepragel sinus	HA and hydroxyl versus vinyl sulfone (DVS)	Surgical application	Space-occupying gel stent to separate and prevent adhesions between mucosal surfaces in the nasal cavity	Sanofi GENZYME CORP	510 (k) K012532 (2001)
Supprelin LA®	Histrelin acetate, poly (2-hydroxyethyl methacrylate) (chemical reaction)	Subcutaneous	Central precocious puberty	Indevus Pharmaceuticals, Inc.	EMA (2005) FDA (2007)

NeuraGen 3D nerve guide matrix	Collagen, glycosaminoglycan and imine ligation (glutaraldehyde)	Implantation	For the repair of peripheral nerve discontinuities	Integra LifeSciences Corporation	K130557 (2014) 510 (k) K163457 (2017)
Chitogel endoscopic sinus surgery kit	Chitosan and dextran Aldehyde and imine ligation	Surgical application	For use in patients undergoing nasal/sinus surgery as a space occupying packing	Chitogel Ltd	510 (k) K172179

3.7.1 Products for Heart Repair

Following a cardiac arrest, scar tissue may develop, impairing the muscle and leading to cardiac insufficiency. And there is no clear treatment option to address the heart tissue damage caused by a heart attack. Current cell delivery techniques have been ineffective, resulting in inadequate engraftment, retention, and viability of transplanted cells in cardiac tissue [209]. Hydrogels as a biomaterial, have been realized in clinical trials and used to treat cardiac injuries. He et al. conducted a study to investigate the safety and feasibility of intracardiac administration of collagen hydrogels combined with human umbilical cord-derived mesenchymal stromal cells (hUC-MSCs) in patients with chronic ischemic heart disease (CIHD) who underwent coronary artery bypass grafting (CABG). Due to variations in evaluation criteria and patient characteristics across previous studies, it is challenging to compare the effectiveness of cell therapy, biomaterial patches, and hydrogels across different investigations. Nevertheless, clinical trials of cardiac repair using hUC-MSCs plus CABG, collagen/cells plus CABG, and CABG alone have been designed. The outcomes of this study confirmed the safety and feasibility of intracardial injection of collagen hydrogel containing hUC-MSCs for the treatment of myocardial infarction in patients undergoing CABG [209]. In addition, there are other clinical hydrogels that can be used for heart repair, such as Algisyl-LVRTM, IK-5001, and VentriGel.

Ventrix, a subsidiary of the University of California, San Diego, has developed a hydrogel product, which conducted the first human clinical trial from 2019 as shown in Fig. 3.55. VentriGel is a catheter-deliverable hydrogel created from porcine decellularized myocardial ECM that can be stored in a lyophilized form and reconstituted with sterile water to form a liquid. The FDA has approved a trial aimed at restoring heart function and repairing damage in patients with heart failure who have previously experienced a heart attack. The gel is safely administered via catheter to patients who have had a heart attack within the past 2 to 36 months and will solidify into porous and fibrous scaffolds within the myocardium, promoting endogenous cell infiltration and cardiac repair. During a clinical phase 1 trial, 15 patients, including 12 men, with moderate damage to the left ventricle of the heart after a heart attack were evaluated. Each patient was administered 15–18 injections into the affected area and was monitored for up to 6 months. The final trial findings demonstrated that the gel could be injected in a minimally invasive manner via a catheter without the need for surgery or general anesthesia. Furthermore, it was found to stimulate a typical remodeling response in the region of the heart injury instead of triggering an inflammatory reaction. However, the Phase 1 trial also had some limitations, for example, it was an uncontrolled monaural trial and efficacy could not be assessed in a small number of patients. As a result of the successful initial human trial, Ventrix is now gearing up for a Phase 2 clinical trial. They plan to conduct a larger randomized trial to assess the effectiveness of VentriGel in enhancing cardiac function and improving the quality of life of heart failure patients [210].

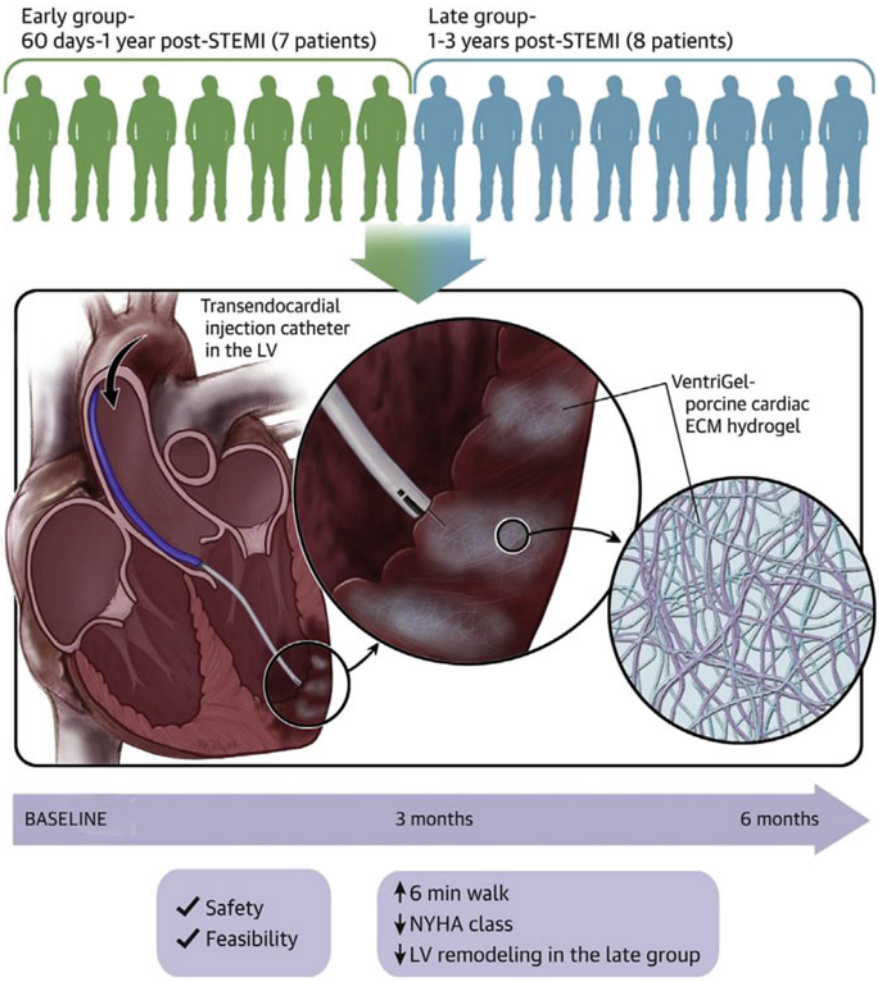

Fig. 3.55 Schematic illustration of VentriGel's clinical trial (Reprinted with permission from Ref. [210]. Copyright 2019 Elsevier Ltd)

3.7.2 Products for Spinal Fusion

With nearly 100 years of development, spinal fusion is a common orthopedic procedure to reduce pain and prevent spinal cord injury. The procedure involves making an incision, inserting a cage, mechanically regaining the spacing between the vertebrae, and then stimulating bone growth with a bone graft to fuse the two bones together. As science and medical technology advanced, spinal fusion began to introduce the concept of minimally invasive surgery and then gradually progressed

to injectable solutions, such as hydrogel. Stryker's OP-1® implant was among the first FDA-approved (2001) products to promote bone growth. However, the OP-1 surgical putty, which contains OP-1 protein and collagen, was categorized as a "Humanitarian device" in 2014 for the treatment of rare ailments. As a result, it was unable to demonstrate its effectiveness [208]. Demineralized bone matrix (DBM) has been clinically approved for spinal applications. Grafton® DBM was clinically tested in 120 patients who underwent posterior lateral spinal fusion. Stryker's OP-1® implant was among the first FDA-approved (2001) products to promote bone growth. However, the OP-1 surgical putty, which contains OP-1 protein and collagen, was categorized as a "Humanitarian device" in 2014 for the treatment of rare ailments. As a result, it was unable to demonstrate its effectiveness [211].

3.7.3 Products for Cartilage Treatment

EUFLEXXA®, developed by Ferring, received FDA approval in 2004 for treating knee pain due to osteoarthritis. However, no synthetic hydrogel has been approved for recycling in the market, possibly due to its low biocompatibility [208]. At present, many hydrogels have been used in the clinical experimental research of cartilage defect repair. NOVOCART® Inject plus is a clinical trial designed to assess the effectiveness and safety of hydrogel-based autologous chondrocyte implantation (ACI) in treating patients with substantial cartilage defects of the knee, such as the medial or lateral femoral condyle or tibial plateau, trochlea or patella. The trial will enroll a total of 96 patients across roughly 20 clinical study sites in Europe, including both adult patients between the ages of 18 and 65 and pediatric patients with closed epiphyses between the ages of 14 and 17. The trial will consist of three phases: screening, treatment, and follow-up, with a maximum duration of 5 years and 4 months. The complete treatment comprised two procedures: the first was the arthroscopic harvesting of autologous chondrocytes for graft production, and the second procedure involved NOVOCART® inject plus transplantation. Autologous chondrocyte implantation was performed on 100 patients who had full-thickness cartilage defects ranging from 4 to 12 cm [2]. Following 2 years of ACI treatment, 93% of the patients experienced an improvement of at least 10 points in their knee injury and osteoarthritis outcome scores compared to preoperative levels. This trial demonstrated that hydrogel-based ACI is an effective treatment option for individuals suffering from significant cartilage defects in the knee joint [212].

3.7.4 Other Products

Thus far, the FDA has approved roughly 200 drugs that utilize a hydrogel dosage form for clinical use. Alongside the products mentioned earlier, other

hydrogel-based medications have been developed to provide various therapeutic benefits, including transdermal, ophthalmic, vaginal, and rectal administration [18]. Hydrogels made from HA are similar in design to dermal fillers and are commonly administered through intra-articular injection, also known as viscose supplementation. This treatment is utilized to alleviate pain and enhance joint function in osteoarthritis patients by replicating the properties of synovial fluid [213]. Both unmodified and cross-linked HA products can be utilized for similar indications and are approved by the FDA under the same product code [213, 214]. TenoGlide (K053655) is a sterile, porous sheet made of bovine collagen I and glycosaminoglycan that has been cross-linked with glutaraldehyde for clinical use. Its intended purpose is to function as a protective shell and sliding surface for damaged tendons, reducing adhesion to the tendon sheath or nearby tissue [18]. Emdogain® has been demonstrated to regenerate a diverse range of periodontal tissues, including bone-like tissue, decellularized dental bone, and alveolar bone, as well as connective tissues like periodontal ligaments [215]. The Contura-funded PAAG-OA was evaluated in 2020 for its effectiveness in inducing symptoms in subjects with osteoarthritis of the knee and compared to the hyaluronic acid Synvisc-One. Clinical trials have demonstrated that Algisyl-LVR, a product of LoneStar Heart, Inc., has the ability to enhance cardiac function among individuals diagnosed with ischemic or nonischemic dilated cardiomyopathy as shown in Table 3.6. The drug has been thoroughly tested, and its effectiveness and safety have been confirmed through clinical trials. Currently, there are indeed many hydrogel products that meet clinical needs, but there are still some shortcomings in terms of quantity and quality. Subsequent research in this area still needs to continue, and it is hoped that more and more comprehensive materials can be developed for the preparation of hydrogels to expand clinical applications.

3.7.5 Conclusion and Outlook

Due to the fact that hydrogel is implanted and has long-term contact with human tissue, it is classified as a Class III device (the highest risk level). As a result, it must undergo extensive clinical investigation before it can be marketed to the public. Risk classification varies from country to country and region to region as it depends on the product equipment group. In the event that the hydrogel solution is categorized as a drug, it will result in a heightened need for documentation and market entry requirements, necessitating more costly and lengthier clinical trials when compared to medical devices. The diagram illustrates the steps involved in the development of hydrogel, its clinical approval, and postmarket surveillance. When hydrogel is classified as a drug, it must be described in detail with scientific evidence. The biocompatibility of the material must be demonstrated according to the relevant ISO 10993 standard, and the manufacturer must specify what aspects of the standard are applicable to their product. Prior to preclinical testing, it is crucial to have a clear understanding of the clinical claims that need to be supported during the animal

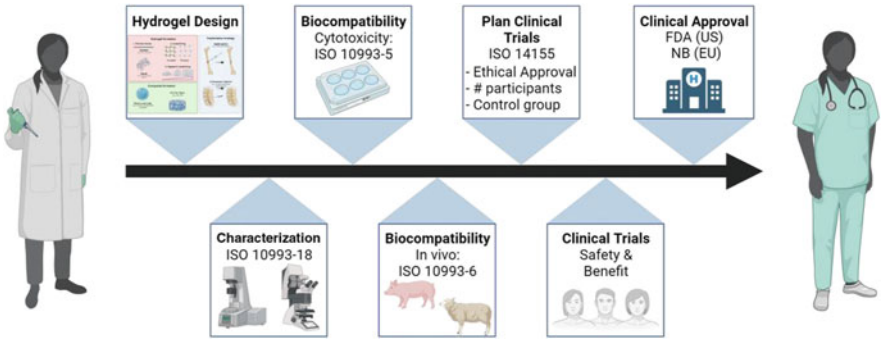

Fig. 3.56 Schematic illustrating the main stages involved in the clinical translation of injectable hydrogels (Reprinted with permission from Ref. [215]. Copyright 2022 Wiley)

model phase, as depicted in Fig. 3.56. Additionally, it is important to select an appropriate animal and implant site that accurately reflect the clinical pathophysiology and load during preclinical trials. The Declaration of Helsinki, along with GCP and ISO 14155:2020, are excellent guidelines for meeting ethical standards [215].

The application of hydrogel in clinical settings is still a significant distance away from academic research. To create hydrogel materials that are capable of clinical use, several specific performance requirements must be met, including mechanical durability, therapeutic agent loading and release, and bioactivity. Additionally, the development of hydrogel delivery technology is a significant challenge, which includes concerns such as chemistry, manufacturing, control, regulatory guidelines, and practical adaptations. After the above vertical problems are well surmounted, we can also gradually expand the horizontal research of injectable hydrogels in different fields by combining multiple disciplines, such as cancer treatment, tissue repair, medical aesthetic industry, 3D/4D printing technology and bioelectronic devices, etc., to achieve the goal of simple, convenient, multifunctional, and multitherapeutic effects (Table 3.6).

3.8 Conclusion and Outlook

Extensive research on hydrogels has demonstrated their potential as highly effective materials for various applications in regenerative medicine. With their straightforward preparation methods and remarkable treatment efficiency, hydrogels have emerged as ideal candidates for diverse therapeutic purposes. These include but are not limited to bone repair, cardiac patches, wound dressings, nerve regeneration, and the treatment of cerebral infarctions. As highlighted in this chapter, hydrogels are still a hotpot in regenerative medicine field, such as drug delivery hydrogels and cell delivery hydrogel. Typical examples such as injectable hydrogels have already faced the clinic step, but related breakthroughs have yet to be investigated.

Despite the advancements in hydrogel development, there are several challenges that remain. Primarily, hydrogels, as primary scaffolds, require sufficient mechanical strength and stiffness. However, the current strength of hydrogels is generally limited. Synthetic polymer hydrogels possess high strength but lack degradability, while natural polymer hydrogels offer good biocompatibility and biodegradability but are prone to rapid degradation due to weak interactions. Consequently, there is a need to design hydrogels that enhance biocompatibility while ensuring high strength. And injectable properties and high strength are still needed to be explored with injectable hydrogel is widely applied. Second, the introduction of bioactive factors in hydrogel requires further test evaluation. Efficient introduction efficiency and release rate without affecting the functional development of hydrogel itself are the problems to be solved. Also, it is a hotpot that realizing intelligent and adaptive drug delivery that scientists have been exploring. Third, scientists have proposed many methods such as radiolabeling methods to monitor the degradation behavior of hydrogels so far, but the real mechanism needs more research, especially in complicated organisms. The controlled degradation behavior of hydrogel is also a problem that has been exploring, now and future. Finally, for the real practical applications of hydrogels, stability, sterilization, storage, transportation and packaging should be accomplished. In addition, hydrogels should be approved as drugs or medical devices have been a controversial topic all the time.

The development and application of hydrogels still have a considerable journey ahead. However, significant progress has already been achieved in utilizing hydrogels within the field of regenerative medicine. In fact, the real repair mechanism of hydrogels and the mechanism of tissue repair (e.g., at the cellular level) are rarely studied. More work is needed in this area for better control and maximum utilization. At the same time, in the shift to larger scale production, more advanced processing equipment is needed. With the popularization of intelligent society, personalized medicine for patients with hydrogels (such as carrying rapid customized treatment for patients of different weight and race) is also worth exploring.

In conclusion, as the need for advanced biomedical materials grows and hydrogel research continues to progress, the potential applications of hydrogels in the field of biomedical materials can expand to include clinical usage. However, it is important to acknowledge that the introduction of novel materials into clinical practice requires collaboration among interdisciplinary teams. The collective expertise of professionals from various fields such as chemistry, biology, medicine, materials science, and mechanical engineering is crucial for successful advancements in this field. By leveraging the combined efforts of these experts, we can anticipate further significant achievements in the future.

Acknowledgments This work was supported by National Key Research and Development Program (Grant No. 2021YFE0105400) and the National Natural Science Foundation of China (Grant No. 31870965).

References

1. Do NHN, Truong QT, Le PK, Ha AC. Recent developments in chitosan hydrogels carrying natural bioactive compounds. Carbohydr Polym. 2022;294:119726. https://doi.org/10.1016/j.carbpol.2022.119726.
2. Spang MT, Christman KL. Extracellular matrix hydrogel therapies: in vivo applications and development. Acta Biomater. 2018;68:1–14. https://doi.org/10.1016/j.actbio.2017.12.019.
3. Zhang YS, Khademhosseini A. Advances in engineering hydrogels. Science. 2017;356:eaaf3627. https://doi.org/10.1126/science.aaf3627.
4. Kirschner CM, Anseth KS. Hydrogels in healthcare: from static to dynamic material microenvironments. Acta Mater. 2013;61:931–44. https://doi.org/10.1016/j.actamat.2012.10.037.
5. Wichterle O, Lim D. Nature 1960;185:117. https://doi.org/10.1038/185117a0.
6. Yannas IV, Lee E, Orgill DP. Synthesis and characterization of a model extracellular matrix that induces partial regeneration of adult mammalian skin. Proc. Nati. Acad. Sci. 1989;86:933–7. https://doi.org/10.1073/pnas.86.3.933.
7. Yang D. Recent advances in hydrogels. Chem Mater. 2022;34:1987–9. https://doi.org/10.1021/acs.chemmater.2c00188.
8. Engler AJ, Sen S, Sweeney HL, Discher DE. Matrix elasticity directs stem cell lineage specification. Cell. 2006;126:677–89. https://doi.org/10.1016/j.cell.2006.06.044.
9. Wang W, Zhang Y, Liu W. Bioinspired fabrication of high strength hydrogels from non-covalent interactions. Prog Polym Sci. 2017;71:1–25. https://doi.org/10.1016/j.progpolymsci.2017.04.001.
10. Huebsch N, et al. Harnessing traction-mediated manipulation of the cell/matrix interface to control stem-cell fate. Nat Mater. 2010;9:518–26. https://doi.org/10.1038/nmat2732.
11. Guvendiren M, Burdick JA. Stiffening hydrogels to probe short- and long-term cellular responses to dynamic mechanics. Nat Commun. 2012;3:792. https://doi.org/10.1038/ncomms1792.
12. Yang C, et al. Spatially patterned matrix elasticity directs stem cell fate. Proc Natl Acad Sci U S A. 2016;113:E4439–45. https://doi.org/10.1073/pnas.1609731113.
13. Walker BW, et al. Rational design of microfabricated electroconductive hydrogels for biomedical applications. Prog Polym Sci. 2019;92:135–57. https://doi.org/10.1016/j.progpolymsci.2019.02.007.
14. Muir VG, Burdick JA. Chemically modified biopolymers for the formation of biomedical hydrogels. Chem Rev. 2020;121:10908–49. https://doi.org/10.1021/acs.chemrev.0c00923.
15. Zhao X, et al. Soft materials by design: unconventional polymer networks give extreme properties. Chem Rev. 2021;121:4309–72. https://doi.org/10.1021/acs.chemrev.0c01088.
16. Wang BX, Xu W, Yang Z, Wu Y, Pi F. An overview on recent progress of the hydrogels: from material resources, properties, to functional applications. Macromol Rapid Commun. 2022;43:e2100785. https://doi.org/10.1002/marc.202100785.
17. Zheng J, et al. Directed self-assembly of herbal small molecules into sustained release hydrogels for treating neural inflammation. Nat Commun. 2019;10:1604. https://doi.org/10.1038/s41467-019-09601-3.
18. Gao Y, Peng K, Mitragotri S. Covalently crosslinked hydrogels via step-growth reactions: crosslinking chemistries, polymers, and clinical impact. Adv Mater. 2021;33:e2006362. https://doi.org/10.1002/adma.202006362.
19. Nykanen A, Nuopponen M, Laukkanen A, Hirvonen S-P, Rytela M, Turunen O, Tenhu H, Mezzenga R, Ikkala O, Ruokolainen J. Phase behavior and temperature-responsive molecular filters based on self-assembly of polystyrene-block-poly(N-isopropylacrylamide)-block-polystyrene. Macromolecules. 2007;40:5827–34.
20. Hassan CM, Peppas NA. Structure and morphology of freeze/thawed PVA hydrogels. Macromolecules. 2000;33:2472–9.
21. Sorlier P, Denuzière A, Viton C, Domard A. Relation between the degree of acetylation and the electrostatic properties of chitin and chitosan. Biomacromolecules. 2001;2:765–72.

22. Cai J, et al. Novel fibers prepared from cellulose in NaOH/urea aqueous solution. Macromol Rapid Commun. 2004;25:1558–62. https://doi.org/10.1002/marc.200400172.
23. Ye D, et al. Deformation drives alignment of nanofibers in framework for inducing anisotropic cellulose hydrogels with high toughness. ACS Appl Mater Interfaces. 2017;9:43154–62. https://doi.org/10.1021/acsami.7b14900.
24. O'Leary LE, Fallas JA, Bakota EL, Kang MK, Hartgerink JD. Multi-hierarchical self-assembly of a collagen mimetic peptide from triple helix to nanofibre and hydrogel. Nat Chem. 2011;3:821–8. https://doi.org/10.1038/nchem.1123.
25. Itagaki H, Fukiishi H, Imai T, Watase M. Molecular structure of agarose chains in thermoreversible hydrogels revealed by means of a fluorescent probe technique. J Polym Sci B Polym Phys. 2005;43:680–8. https://doi.org/10.1002/polb.20374.
26. Dai X, et al. A mechanically strong, highly stable, thermoplastic, and self-healable supramolecular polymer hydrogel. Adv Mater. 2015;27:3566–71. https://doi.org/10.1002/adma.201500534.
27. Li X, et al. Mesoscale bicontinuous networks in self-healing hydrogels delay fatigue fracture. Proc Natl Acad Sci U S A. 2020;117:7606–12. https://doi.org/10.1073/pnas.2000189117.
28. Zhang X, et al. Role of a high calcium ion content in extending the properties of alginate dual-crosslinked hydrogels. J Mater Chem A. 2020;8:25390–401. https://doi.org/10.1039/d0ta09315g.
29. Takashima Y, et al. Expansion-contraction of photoresponsive artificial muscle regulated by host-guest interactions. Nat Commun. 2012;3:1270. https://doi.org/10.1038/ncomms2280.
30. Liu YH, Zhang YM, Yu HJ, Liu Y. Cucurbituril-based biomacromolecular assemblies. Angew Chem Int Ed Engl. 2021;60:3870–80. https://doi.org/10.1002/anie.202009797.
31. Tuncaboylu DC, Sari M, Oppermann W, Okay O. Tough and self-healing hydrogels formed via hydrophobic interactions. Macromolecules. 2011;44:4997–5005. https://doi.org/10.1021/ma200579v.
32. Ma L, et al. Full-textile wireless flexible humidity sensor for human physiological monitoring. Adv Funct Mater. 2019;29:1904549. https://doi.org/10.1002/adfm.201904549.
33. Bao R, et al. A pi-pi conjugation-containing soft and conductive injectable polymer hydrogel highly efficiently rebuilds cardiac function after myocardial infarction. Biomaterials. 2017;122:63–71. https://doi.org/10.1016/j.biomaterials.2017.01.012.
34. Liu X, et al. Power generation from ambient humidity using protein nanowires. Nature. 2020;578:550–4. https://doi.org/10.1038/s41586-020-2010-9.
35. Qiao Y, et al. Gelatin templated polypeptide co-cross-linked hydrogel for bone regeneration. Adv Healthc Mater. 2019;9:e1901239. https://doi.org/10.1002/adhm.201901239.
36. Du YQ, et al. Chirality from d-guanosine to l-guanosine shapes a stable gel for three-dimensional cell culture. Chem Commun. 2021;57:12936–9. https://doi.org/10.1039/c9cc09911e.
37. Wang B, et al. Flexible and stretchable metal oxide nanofiber networks for multimodal and monolithically integrated wearable electronics. Nat Commun. 2020;11:2405. https://doi.org/10.1038/s41467-020-16268-8.
38. Yu Q, Song Y, Shi X, Xu C, Bin Y. Preparation and properties of chitosan derivative/poly (vinyl alcohol) blend film crosslinked with glutaraldehyde. Carbohydr Polym. 2011;84:465–70. https://doi.org/10.1016/j.carbpol.2010.12.006.
39. Hoyle CE, Bowman CN. Thiol-ene click chemistry. Angew Chem Int Ed Engl. 2010;49:1540–73. https://doi.org/10.1002/anie.200903924.
40. Nair DP, et al. The Thiol-Michael addition click reaction: a powerful and widely used tool in materials chemistry. Chem Mater. 2013;26:724–44. https://doi.org/10.1021/cm402180t.
41. Mohanty S, et al. 3D printed silicone-hydrogel scaffold with enhanced physicochemical properties. Biomacromolecules. 2016;17:1321–9. https://doi.org/10.1021/acs.biomac.5b01722.

42. Zhao J, et al. Novel coaxial fiber-shaped sensing system integrated with an asymmetric supercapacitor and a humidity sensor. Energy Stor Mater. 2018;15:315–23. https://doi.org/10.1016/j.ensm.2018.06.007.
43. Ni C, Chen D, Zhang Y, Xie T, Zhao Q. Autonomous shapeshifting hydrogels via temporal programming of photoswitchable dynamic network. Chem Mater. 2021;33:2046–53. https://doi.org/10.1021/acs.chemmater.0c04375.
44. Cai C, et al. Self-healing hydrogel embodied with macrophage-regulation and responsive-gene-silencing properties for synergistic prevention of peritendinous adhesion. Adv Mater. 2022;34:e2106564. https://doi.org/10.1002/adma.202106564.
45. Liang Y, Li Z, Huang Y, Yu R, Guo B. Dual-dynamic-bond cross-linked antibacterial adhesive hydrogel sealants with on-demand removability for post-wound-closure and infected wound healing. ACS Nano. 2021;15:7078–93. https://doi.org/10.1021/acsnano.1c00204.
46. Yao X, Cui Y. A PEDOT:PSS functionalized capacitive sensor for humidity. Measurement. 2020;160:107782. https://doi.org/10.1016/j.measurement.2020.107782.
47. Chen Q, et al. Active and stable alcohol dehydrogenase-assembled hydrogels via synergistic bridging of triazoles and metal ions. Nat Commun. 2023;14:2117. https://doi.org/10.1038/s41467-023-37921-y.
48. Miyata T, Asami N, Uragami T. Structural design of stimuli-responsive bioconjugated hydrogels that respond to a target antigen. J Polym Sci B Polym Phys. 2009;47:2144–57. https://doi.org/10.1002/polb.21812.
49. Norioka C, Okita K, Mukada M, Kawamura A, Miyata T. Biomolecularly stimuli-responsive tetra-poly(ethylene glycol) that undergoes sol–gel transition in response to a target biomolecule. Polym Chem. 2017;8:6378–85. https://doi.org/10.1039/c7py01370a.
50. Rodriguez-Rivera GJ, Post A, John M, Buchan S, Wancura M, Chwatko M, Waldron C, Kalkunte N, Zoldan J, Arseneault M, Razavi M, Cosgriff-Hernandez E. Towards prevention of re-entrant arrhythmias: injectable hydrogel electrodes enable direct capture of previously inaccessible cardiac tissues. bioRxiv. 2021;1:2021. https://doi.org/10.1101/2021.11.03.467102.
51. Zhao T, et al. Macroscopic layered organogel-hydrogel hybrids with controllable wetting and swelling performance. Adv Funct Mater. 2018;28:1. https://doi.org/10.1002/adfm.201800793.
52. Si Y, et al. Ultrahigh-water-content, superelastic, and shape-memory nanofiber-assembled hydrogels exhibiting pressure-responsive conductivity. Adv Mater. 2017;29:24. https://doi.org/10.1002/adma.201700339.
53. Liu X, et al. Ingestible hydrogel device. Nat Commun. 2019;10:493. https://doi.org/10.1038/s41467-019-08355-2.
54. Nakajima T, Kurokawa T, Ahmed S, Wu W-L, Gong JP. Characterization of internal fracture process of double network hydrogels under uniaxial elongation. Soft Matter. 2013;9:1955–66. https://doi.org/10.1039/c2sm27232f.
55. Han S, et al. A multiparameter pressure-temperature-humidity sensor based on mixed ionic-electronic cellulose aerogels. Adv Sci (Weinh). 2019;6:1802128. https://doi.org/10.1002/advs.201802128.
56. Liang JG, et al. Preparation of ultrasensitive humidity-sensing films by aerosol deposition. ACS Appl Mater Interfaces. 2018;10:851–63. https://doi.org/10.1021/acsami.7b14082.
57. Gong JP, Katsuyama Y, Kurokawa T, Osada Y. Double-network hydrogels with extremely high mechanical strength. Adv Mater. 2003;15:1155–8. https://doi.org/10.1002/adma.200304907.
58. Zheng SY, et al. Molecularly engineered zwitterionic hydrogels with high toughness and self-healing capacity for soft electronics applications. Chem Mater. 2021;33:8418–29. https://doi.org/10.1021/acs.chemmater.1c02781.
59. Jiang P, et al. 3D printing of dual-physical cross-linking hydrogel with ultrahigh strength and toughness. Chem Mater. 2020;32:9983–95. https://doi.org/10.1021/acs.chemmater.0c02941.

60. Yu X, et al. Fast-recoverable, self-healable, and adhesive nanocomposite hydrogel consisting of hybrid nanoparticles for ultrasensitive strain and pressure sensing. Chem Mater. 2021;33:6146–57. https://doi.org/10.1021/acs.chemmater.1c01595.
61. Wei H, et al. Ultrastretchable, highly transparent, self-adhesive, and 3D-printable ionic hydrogels for multimode tactical sensing. Chem Mater. 2021;33:6731–42. https://doi.org/10.1021/acs.chemmater.1c01246.
62. Shin SR, et al. Cell-laden microengineered and mechanically tunable hybrid hydrogels of gelatin and graphene oxide. Adv Mater. 2013;25:6385–91. https://doi.org/10.1002/adma.201301082.
63. Li P, et al. A polycationic antimicrobial and biocompatible hydrogel with microbe membrane suctioning ability. Nat Mater. 2011;10:149–56. https://doi.org/10.1038/nmat2915.
64. Huang W, et al. Noncompressible hemostasis and bone regeneration induced by an absorbable bioadhesive self-healing hydrogel. Adv Funct Mater. 2021;31:2009189. https://doi.org/10.1002/adfm.202009189.
65. Hoare TR, Kohane DS. Hydrogels in drug delivery: progress and challenges. Polymer. 2008;49:1993–2007. https://doi.org/10.1016/j.polymer.2008.01.027.
66. Homayun B, Lin X, Choi HJ. Challenges and recent progress in oral drug delivery systems for biopharmaceuticals. Pharmaceutics. 2019;11:129. https://doi.org/10.3390/pharmaceutics11030129.
67. Li J, Mooney DJ. Designing hydrogels for controlled drug delivery. Nat Rev Mater. 2016;1:1–17. https://doi.org/10.1038/natrevmats.2016.71.
68. Bernhard S, Tibbitt MW. Supramolecular engineering of hydrogels for drug delivery. Adv Drug Deliv Rev. 2021;171:240–56. https://doi.org/10.1016/j.addr.2021.02.002.
69. Gačanin J, Synatschke CV, Weil T. Biomedical applications of DNA-based hydrogels. Adv Funct Mater. 2019;30:1906253. https://doi.org/10.1002/adfm.201906253.
70. Jiang Y, Wang J, Zhang H, Chen G, Zhao Y. Bio-inspired natural platelet hydrogels for wound healing. Sci Bull. 2022;67:1776–84. https://doi.org/10.1016/j.scib.2022.07.032.
71. Vazquez-Gonzalez M, Willner I. Stimuli-responsive biomolecule-based hydrogels and their applications. Angew Chem Int Ed Engl. 2020;59:15342–77. https://doi.org/10.1002/anie.201907670.
72. Nguyen MK, Alsberg E. Bioactive factor delivery strategies from engineered polymer hydrogels for therapeutic medicine. Prog Polym Sci. 2014;39:1236–65. https://doi.org/10.1016/j.progpolymsci.2013.12.001.
73. Sun W, et al. Strong dual-crosslinked hydrogels for ultrasound-triggered drug delivery. Nano Res. 2018;12:115–9. https://doi.org/10.1007/s12274-018-2188-4.
74. Fu M, et al. Interpenetrating polymer network hydrogels formed using antibiotics as a dynamic crosslinker for treatment of infected wounds. Adv Healthc Mater. 2022;11:e2200902. https://doi.org/10.1002/adhm.202200902.
75. Hoang HT, et al. Dual cross-linked chitosan/alginate hydrogels prepared by Nb-Tz 'click' reaction for pH responsive drug delivery. Carbohydr Polym. 2022;288:119389. https://doi.org/10.1016/j.carbpol.2022.119389.
76. Picchioni F, Muljana H. Hydrogels based on dynamic covalent and non covalent bonds: a chemistry perspective. Gels. 2018;4:21. https://doi.org/10.3390/gels4010021.
77. Song X, et al. Facile preparation of drug-releasing supramolecular hydrogel for preventing postoperative peritoneal adhesion. ACS Appl Mater Interfaces. 2021;13:56881–91. https://doi.org/10.1021/acsami.1c16269.
78. Olate-Moya F, Palza H. Effect of graphene oxide on the pH-responsive drug release from supramolecular hydrogels. J Appl Polym Sci. 2021;139:51420. https://doi.org/10.1002/app.51420.
79. Abune L, Wang Y. Affinity hydrogels for protein delivery. Trends Pharmacol Sci. 2021;42:300–12. https://doi.org/10.1016/j.tips.2021.01.005.

80. Skopinska-Wisniewska J, De la Flor S, Kozlowska J. From supramolecular hydrogels to multifunctional carriers for biologically active substances. Int J Mol Sci. 2021;22:7402. https://doi.org/10.3390/ijms22147402.
81. Lin CC, Metters AT. Hydrogels in controlled release formulations: network design and mathematical modeling. Adv Drug Deliv Rev. 2006;58:1379–408. https://doi.org/10.1016/j.addr.2006.09.004.
82. Peret BJ, Murphy WL. Controllable soluble protein concentration gradients in hydrogel networks. Adv Funct Mater. 2008;18:3410–7. https://doi.org/10.1002/adfm.200800218.
83. DuBose JW, Cutshall C, Metters AT. Controlled release of tethered molecules via engineered hydrogel degradation: model development and validation. J Biomed Mater Res A. 2005;74:104–16. https://doi.org/10.1002/jbm.a.30307.
84. Karamzadeh Y, Ansari Asl A, Rahmani S. PCL microsphere/PEG-based composite hydrogels for sustained release of methadone hydrochloride. J Appl Polym Sci. 2020;137:48967. https://doi.org/10.1002/app.48967.
85. Gupta P, Purwar R. Influence of cross-linkers on the properties of cotton grafted poly (acrylamide-co-acrylic acid) hydrogel composite: swelling and drug release kinetics. Iran Polym J. 2021;30:381–91. https://doi.org/10.1007/s13726-020-00897-3.
86. Serra L, Domenech J, Peppas NA. Drug transport mechanisms and release kinetics from molecularly designed poly(acrylic acid-g-ethylene glycol) hydrogels. Biomaterials. 2006;27:5440–51. https://doi.org/10.1016/j.biomaterials.2006.06.011.
87. Narayanaswamy R, Torchilin VP. Hydrogels and their applications in targeted drug delivery. Molecules. 2019;24:603. https://doi.org/10.3390/molecules24030603.
88. Mo C, Luo R, Chen Y. Advances in the stimuli-responsive injectable hydrogel for controlled release of drugs. Macromol Rapid Commun. 2022;43:e2200007. https://doi.org/10.1002/marc.202200007.
89. Koetting MC, Peters JT, Steichen SD, Peppas NA. Stimulus-responsive hydrogels: theory, modern advances, and applications. Mater Sci Eng R Rep. 2015;93:1–49. https://doi.org/10.1016/j.mser.2015.04.001.
90. Zong S, et al. Intelligent hydrogel with both redox and thermo-response based on cellulose nanofiber for controlled drug delivery. Carbohydr Polym. 2022;278:118943. https://doi.org/10.1016/j.carbpol.2021.118943.
91. Pua ML, Yoshitomi T, Chonpathompikunlert P, Hirayama A, Nagasaki Y. Redox-active injectable gel using thermo-responsive nanoscale polyion complex flower micelle for noninvasive treatment of local inflammation. J Control Release. 2013;172:914–20. https://doi.org/10.1016/j.jconrel.2013.10.009.
92. Yu H, et al. Nanoarchitectonics of cartilage-targeting hydrogel microspheres with reactive oxygen species responsiveness for the repair of osteoarthritis. ACS Appl Mater Interfaces. 2022;14:40711–23. https://doi.org/10.1021/acsami.2c12703.
93. Liang Y, et al. pH/glucose dual responsive metformin release hydrogel dressings with adhesion and self-healing via dual-dynamic bonding for athletic diabetic foot wound healing. ACS Nano. 2022;16:3194–207. https://doi.org/10.1021/acsnano.1c11040.
94. Chen D, Chen C, Huang C, Chen T, Liu Z. Injectable hydrogel for NIR-II photo-thermal tumor therapy and dihydroartemisinin-mediated chemodynamic therapy. Front Chem. 2020;8:251. https://doi.org/10.3389/fchem.2020.00251.
95. Chen T, et al. Cellulose nanocrystals reinforced highly stretchable thermal-sensitive hydrogel with ultra-high drug loading. Carbohydr Polym. 2021;266:118122. https://doi.org/10.1016/j.carbpol.2021.118122.
96. Mai BT, Conteh JS, Gavilan H, Di Girolamo A, Pellegrino T. Clickable polymer ligand-functionalized iron oxide nanocubes: a promising nanoplatform for 'local hot spots' magnetically triggered drug release. ACS Appl Mater Interfaces. 2022;14(43):48476. https://doi.org/10.1021/acsami.2c14752.
97. Smith AD, et al. Resistive graphene humidity sensors with rapid and direct electrical readout. Nanoscale. 2015;7:19099–109. https://doi.org/10.1039/c5nr06038a.

98. Husseini GA, Pitt WG. Micelles and nanoparticles for ultrasonic drug and gene delivery. Adv Drug Deliv Rev. 2008;60:1137–52. https://doi.org/10.1016/j.addr.2008.03.008.
99. Liu X, et al. Functionalized carbon nanotube and graphene oxide embedded electrically conductive hydrogel synergistically stimulates nerve cell differentiation. ACS Appl Mater Interfaces. 2017;9:14677–90. https://doi.org/10.1021/acsami.7b02072.
100. Qu J, Zhao X, Ma PX, Guo B. Injectable antibacterial conductive hydrogels with dual response to an electric field and pH for localized "smart" drug release. Acta Biomater. 2018;72:55–69. https://doi.org/10.1016/j.actbio.2018.03.018.
101. Leganes Bayon J, et al. On-demand hydrophobic drug release based on microwave-responsive graphene hydrogel scaffolds. Chemistry. 2020;26:17069–80. https://doi.org/10.1002/chem.202001429.
102. Nawaz A, Wong TW. Microwave as skin permeation enhancer for transdermal drug delivery of chitosan-5-fluorouracil nanoparticles. Carbohydr Polym. 2017;157:906–19. https://doi.org/10.1016/j.carbpol.2016.09.080.
103. Li W, et al. Clinical translation of long-acting drug delivery formulations. Nat Rev Mater. 2022;7:406–20. https://doi.org/10.1038/s41578-021-00405-w.
104. Kim H, et al. Visible light-triggered on-demand drug release from hybrid hydrogels and its application in transdermal patches. Adv Healthc Mater. 2015;4:2071–7. https://doi.org/10.1002/adhm.201500323.
105. Dreiss CA. Hydrogel design strategies for drug delivery. Curr Opin Colloid Interface Sci. 2020;48:1–17. https://doi.org/10.1016/j.cocis.2020.02.001.
106. Kesharwani P, Bisht A, Alexander A, Dave V, Sharma S. Biomedical applications of hydrogels in drug delivery system: an update. J Drug Deliv Sci Technol. 2021;66:102914. https://doi.org/10.1016/j.jddst.2021.102914.
107. Ma P, et al. The translational application of hydrogel for organoid technology: challenges and future perspectives. Macromol Biosci. 2021;21:e2100191. https://doi.org/10.1002/mabi.202100191.
108. Caliari SR, et al. Stiffening hydrogels for investigating the dynamics of hepatic stellate cell mechanotransduction during myofibroblast activation. Sci Rep. 2016;6:21387. https://doi.org/10.1038/srep21387.
109. Ondeck MG, et al. Dynamically stiffened matrix promotes malignant transformation of mammary epithelial cells via collective mechanical signaling. Proc Natl Acad Sci U S A. 2019;116:3502–7. https://doi.org/10.1073/pnas.1814204116.
110. Rape AD, Zibinsky M, Murthy N, Kumar S. A synthetic hydrogel for the high-throughput study of cell–ECM interactions. Nat Commun. 2015;6:8129. https://doi.org/10.1038/ncomms9129.
111. Yang B, et al. Enhanced mechanosensing of cells in synthetic 3D matrix with controlled biophysical dynamics. Nat Commun. 2021;12:3514. https://doi.org/10.1038/s41467-021-23120-0.
112. Cao H, Duan L, Zhang Y, Cao J, Zhang K. Current hydrogel advances in physicochemical and biological response-driven biomedical application diversity. Signal Transduct Target Ther. 2021;6:426. https://doi.org/10.1038/s41392-021-00830-x.
113. Ballios BG, et al. A hyaluronan-based injectable hydrogel improves the survival and integration of stem cell progeny following transplantation. Stem Cell Reports. 2015;4:1031–45. https://doi.org/10.1016/j.stemcr.2015.04.008.
114. An G, et al. Functional reconstruction of injured corpus cavernosa using 3D-printed hydrogel scaffolds seeded with HIF-1alpha-expressing stem cells. Nat Commun. 2020;11:2687. https://doi.org/10.1038/s41467-020-16192-x.
115. Wu S, Xu R, Duan B, Jiang P. Three-dimensional hyaluronic acid hydrogel-based models for in vitro human iPSC-derived NPC culture and differentiation. J Mater Chem B. 2017;5:3870–8. https://doi.org/10.1039/C7TB00721C.
116. Daly AC, Riley L, Segura T, Burdick JA. Hydrogel microparticles for biomedical applications. Nat Rev Mater. 2020;5:20–43. https://doi.org/10.1038/s41578-019-0148-6.

117. Praveschotinunt P, et al. Engineered E. coli Nissle 1917 for the delivery of matrix-tethered therapeutic domains to the gut. Nat Commun. 2019;10:5580. https://doi.org/10.1038/s41467-019-13336-6.
118. Johnston TG, et al. Compartmentalized microbes and co-cultures in hydrogels for on-demand bioproduction and preservation. Nat Commun. 2020;11:563. https://doi.org/10.1038/s41467-020-14371-4.
119. Rodrigo-Navarro A, Sankaran S, Dalby MJ, del Campo A, Salmeron-Sanchez M. Engineered living biomaterials. Nat Rev Mater. 2021;6:1175–90. https://doi.org/10.1038/s41578-021-00350-8.
120. An B, et al. Programming living glue systems to perform autonomous mechanical repairs. Matter. 2020;3:2080–92. https://doi.org/10.1016/j.matt.2020.09.006.
121. Rossi G, Manfrin A, Lutolf MP. Progress and potential in organoid research. Nat Rev Genet. 2018;19:671–87. https://doi.org/10.1038/s41576-018-0051-9.
122. Yin X, et al. Engineering stem cell organoids. Cell Stem Cell. 2016;18:25–38. https://doi.org/10.1016/j.stem.2015.12.005.
123. Clevers H. Modeling development and disease with organoids. Cell. 2016;165:1586–97. https://doi.org/10.1016/j.cell.2016.05.082.
124. Dutta D, Heo I, Clevers H. Disease modeling in stem cell-derived 3D organoid systems. Trends Mol Med. 2017;23:393–410. https://doi.org/10.1016/j.molmed.2017.02.007.
125. Ashok A, Choudhury D, Fang Y, Hunziker W. Towards manufacturing of human organoids. Biotechnol Adv. 2020;39:107460. https://doi.org/10.1016/j.biotechadv.2019.107460.
126. Aisenbrey EA, Murphy WL. Synthetic alternatives to matrigel. Nat Rev Mater. 2020;5:539–51. https://doi.org/10.1038/s41578-020-0199-8.
127. Gjorevski N, et al. Designer matrices for intestinal stem cell and organoid culture. Nature. 2016;539:560–4. https://doi.org/10.1038/nature20168.
128. Broguiere N, et al. Growth of epithelial organoids in a defined hydrogel. Adv Mater. 2018;30:1801621. https://doi.org/10.1002/adma.201801621.
129. Zhu Y, et al. A hollow fiber system for simple generation of human brain organoids. Integr Biol. 2017;9:774–81. https://doi.org/10.1039/c7ib00080d.
130. Huch M, Knoblich JA, Lutolf MP, Martinez-Arias A. The hope and the hype of organoid research. Development. 2017;144:938–41. https://doi.org/10.1242/dev.150201.
131. Liu H, et al. Advances in hydrogels in organoids and organs-on-a-chip. Adv Mater. 2019;31:1902042. https://doi.org/10.1002/adma.201902042.
132. de Abreu RC, et al. Native and bioengineered extracellular vesicles for cardiovascular therapeutics. Nat Rev Cardiol. 2020;17:685–97. https://doi.org/10.1038/s41569-020-0389-5.
133. Zou Y, et al. Restoring cardiac functions after myocardial infarction-ischemia/reperfusion via an exosome anchoring conductive hydrogel. ACS Appl Mater Interfaces. 2021;13:56892–908. https://doi.org/10.1021/acsami.1c16481.
134. Doyle AD, Carvajal N, Jin A, Matsumoto K, Yamada KM. Local 3D matrix microenvironment regulates cell migration through spatiotemporal dynamics of contractility-dependent adhesions. Nat Commun. 2015;6:8720. https://doi.org/10.1038/ncomms9720.
135. Yuan W, et al. Microscopic local stiffening in a supramolecular hydrogel network expedites stem cell mechanosensing in 3D and bone regeneration. Mater Horiz. 2021;8:1722–34. https://doi.org/10.1039/d1mh00244a.
136. Lee S, Kim HS, Yoo HS. Electrospun nanofibrils embedded hydrogel composites for cell cultivation in a biomimetic environment. RSC Adv. 2017;7:54246–53. https://doi.org/10.1039/c7ra08595h.
137. Abbasi N, et al. Influence of oriented nanofibrous PCL scaffolds on quantitative gene expression during neural differentiation of mouse embryonic stem cells. J Biomed Mater Res A. 2016;104:155–64. https://doi.org/10.1002/jbm.a.35551.
138. Liu X, Inda ME, Lai Y, Lu TK, Zhao X. Engineered living hydrogels. Adv Mater. 2022;34:e2201326. https://doi.org/10.1002/adma.202201326.

139. Lo YP, et al. Three-dimensional spherical spatial boundary conditions differentially regulate osteogenic differentiation of mesenchymal stromal cells. Sci Rep. 2016;6:21253. https://doi.org/10.1038/srep21253.
140. Hsia HC, Nair MR, Mintz RC, Corbett SA. The fiber diameter of synthetic bioresorbable extracellular matrix influences human fibroblast morphology and fibronectin matrix assembly. Plast Reconstr Surg. 2011;127:2312–20. https://doi.org/10.1097/PRS.0b013e3182139fa4.
141. Li L, Eyckmans J, Chen CS. Designer biomaterials for mechanobiology. Nat Mater. 2017;16:1164–8. https://doi.org/10.1038/nmat5049.
142. Chaudhuri O, et al. Substrate stress relaxation regulates cell spreading. Nat Commun. 2015;6:6364. https://doi.org/10.1038/ncomms7365.
143. Chaudhuri O, et al. Hydrogels with tunable stress relaxation regulate stem cell fate and activity. Nat Mater. 2016;15:326–34. https://doi.org/10.1038/nmat4489.
144. Farooque TM, et al. Measuring stem cell dimensionality in tissue scaffolds. Biomaterials. 2014;35:2558–67. https://doi.org/10.1016/j.biomaterials.2013.12.092.
145. Lee HP, Gu L, Mooney DJ, Levenston ME, Chaudhuri O. Mechanical confinement regulates cartilage matrix formation by chondrocytes. Nat Mater. 2017;16:1243–51. https://doi.org/10.1038/nmat4993.
146. Parmar PA, et al. Temporally degradable collagen-mimetic hydrogels tuned to chondrogenesis of human mesenchymal stem cells. Biomaterials. 2016;99:56–71. https://doi.org/10.1016/j.biomaterials.2016.05.011.
147. Tang Y, et al. MT1-MMP-dependent control of skeletal stem cell commitment via a β1-integrin/YAP/TAZ signaling axis. Dev Cell. 2013;25:402–16. https://doi.org/10.1016/j.devcel.2013.04.011.
148. Madl CM, et al. Maintenance of neural progenitor cell stemness in 3D hydrogels requires matrix remodelling. Nat Mater. 2017;16:1233–42. https://doi.org/10.1038/nmat5020.
149. Feng Q, Zhu M, Wei K, Bian L. Cell-mediated degradation regulates human mesenchymal stem cell chondrogenesis and hypertrophy in MMP-sensitive hyaluronic acid hydrogels. PLoS One. 2014;9:e99587. https://doi.org/10.1371/journal.pone.0099587.
150. Khetan S, et al. Degradation-mediated cellular traction directs stem cell fate in covalently crosslinked three-dimensional hydrogels. Nat Mater. 2013;12:458–65. https://doi.org/10.1038/nmat3586.
151. Wei Q, et al. Soft hydrogels for balancing cell proliferation and differentiation. ACS Biomater Sci Eng. 2020;6:4687–701. https://doi.org/10.1021/acsbiomaterials.0c00854.
152. Zhang X, et al. Physically and chemically dual-crosslinked hydrogels with superior mechanical properties and self-healing behavior. New J Chem. 2020;44:9903–11. https://doi.org/10.1039/d0nj00348d.
153. Chen JW, et al. Controlling the surface chemistry of a hydrogel for spatially defined cell adhesion. ACS Appl Mater Interfaces. 2019;11:15411–6. https://doi.org/10.1021/acsami.9b04023.
154. Maynard SA, et al. Nanoscale molecular quantification of stem cell-hydrogel interactions. ACS Nano. 2020;14:17321–32. https://doi.org/10.1021/acsnano.0c07428.
155. Meshel AS, Wei Q, Adelstein RS, Sheetz MP. Basic mechanism of three-dimensional collagen fibre transport by fibroblasts. Nat Cell Biol. 2005;7:157–64. https://doi.org/10.1038/ncb1216.
156. Ahearne M. Introduction to cell-hydrogel mechanosensing. Interface Focus. 2014;4:20130038. https://doi.org/10.1098/rsfs.2013.0038.
157. Vernerey FJ, Lalitha Sridhar S, Muralidharan A, Bryant SJ. Mechanics of 3D cell-hydrogel interactions: experiments, models, and mechanisms. Chem Rev. 2021;121:11085–148. https://doi.org/10.1021/acs.chemrev.1c00046.
158. Parsons JT, Horwitz AR, Schwartz MA. Cell adhesion: integrating cytoskeletal dynamics and cellular tension. Nat Rev Mol Cell Biol. 2010;11:633–43. https://doi.org/10.1038/nrm2957.
159. Bracher M, et al. Cell specific ingrowth hydrogels. Biomaterials. 2013;34:6797–803. https://doi.org/10.1016/j.biomaterials.2013.05.057.

160. Skaalure SC, Akalp U, Vernerey FJ, Bryant SJ. Tuning reaction and diffusion mediated degradation of enzyme-sensitive hydrogels. Adv Healthc Mater. 2016;5:432–8. https://doi.org/10.1002/adhm.201500728.
161. Sridhar SL, Vernerey FJ. Localized enzymatic degradation of polymers: physics and scaling laws. Phys Rev Appl. 2018;9:031001.
162. Piantanida E, Alonci G, Bertucci A, De Cola L. Design of nanocomposite injectable hydrogels for minimally invasive surgery. Acc Chem Res. 2019;52:2101–12. https://doi.org/10.1021/acs.accounts.9b00114.
163. Tu Y, et al. Advances in injectable self-healing biomedical hydrogels. Acta Biomater. 2019;90:1–20. https://doi.org/10.1016/j.actbio.2019.03.057.
164. Tayler IM, Stowers RS. Engineering hydrogels for personalized disease modeling and regenerative medicine. Acta Biomater. 2021;132:4–22. https://doi.org/10.1016/j.actbio.2021.04.020.
165. Teoh JH, et al. 3D printing personalized, photocrosslinkable hydrogel wound dressings for the treatment of thermal burns. Adv Funct Mater. 2021;31:2105932. https://doi.org/10.1002/adfm.202105932.
166. Li M, et al. Flexible accelerated-wound-healing antibacterial MXene-based epidermic sensor for intelligent wearable human-machine interaction. Adv Funct Mater. 2022;32:2208141. https://doi.org/10.1002/adfm.202208141.
167. Unruh RM, Bornhoeft LR, Nichols SP, Wisniewski NA, McShane MJ. Inorganic-organic interpenetrating network hydrogels as tissue-integrating luminescent implants: physicochemical characterization and preclinical evaluation. Macromol Biosci. 2022;22:e2100380. https://doi.org/10.1002/mabi.202100380.
168. Bertsch P, Diba M, Mooney DJ, Leeuwenburgh SCG. Self-healing injectable hydrogels for tissue regeneration. Chem Rev. 2022;123:834–73. https://doi.org/10.1021/acs.chemrev.2c00179.
169. Mealy JE, et al. Injectable granular hydrogels with multifunctional properties for biomedical applications. Adv Mater. 2018;30:e1705912. https://doi.org/10.1002/adma.201705912.
170. Guo H, et al. Injectable and self-healing hydrogels with double-dynamic bond tunable mechanical, gel-sol transition and drug delivery properties for promoting periodontium regeneration in periodontitis. ACS Appl Mater Interfaces. 2021;13:61638–52. https://doi.org/10.1021/acsami.1c18701.
171. Zhang M, et al. Super-ductile, injectable, fast self-healing collagen-based hydrogels with multi-responsive and accelerated wound-repair properties. Chem Eng J. 2021;405:126756. https://doi.org/10.1016/j.cej.2020.126756.
172. Wang B, et al. Mussel-inspired bisphosphonated injectable nanocomposite hydrogels with adhesive, self-healing, and osteogenic properties for bone regeneration. ACS Appl Mater Interfaces. 2021;13:32673–89. https://doi.org/10.1021/acsami.1c06058.
173. He J, et al. Injectable self-healing adhesive pH-responsive hydrogels accelerate gastric hemostasis and wound healing. Nanomicro Lett. 2021;13:80. https://doi.org/10.1007/s40820-020-00585-0.
174. Thambi T, Li Y, Lee DS. Injectable hydrogels for sustained release of therapeutic agents. J Control Release. 2017;267:57–66. https://doi.org/10.1016/j.jconrel.2017.08.006.
175. Hu C, et al. Regeneration of infarcted hearts by myocardial infarction-responsive injectable hydrogels with combined anti-apoptosis, anti-inflammatory and pro-angiogenesis properties. Biomaterials. 2022;290:121849. https://doi.org/10.1016/j.biomaterials.2022.121849.
176. Li Y, et al. Injectable hydrogel with MSNs/microRNA-21-5p delivery enables both immunomodification and enhanced angiogenesis for myocardial infarction therapy in pigs. Sci Adv. 2021;7:eabd6740.
177. Li H, et al. Injectable AuNP-HA matrix with localized stiffness enhances the formation of gap junction in engrafted human induced pluripotent stem cell-derived cardiomyocytes and promotes cardiac repair. Biomaterials. 2021;279:121231. https://doi.org/10.1016/j.biomaterials.2021.121231.

178. Wang LL, et al. Local and sustained miRNA delivery from an injectable hydrogel promotes cardiomyocyte proliferation and functional regeneration after ischemic injury. Nat Biomed Eng. 2017;1:983–92. https://doi.org/10.1038/s41551-017-0157-y.
179. Song X, et al. A tunable self-healing ionic hydrogel with microscopic homogeneous conductivity as a cardiac patch for myocardial infarction repair. Biomaterials. 2021;273:120811. https://doi.org/10.1016/j.biomaterials.2021.120811.
180. Pena B, et al. Injectable hydrogels for cardiac tissue engineering. Macromol Biosci. 2018;18:e1800079. https://doi.org/10.1002/mabi.201800079.
181. Seeman E, Delmas PD. Bone quality—the material and structural basis of bone strength and fragility. N Engl J Med. 2006;354:2250–61.
182. Zheng A, et al. Promoting lacunar bone regeneration with an injectable hydrogel adaptive to the microenvironment. Bioact Mater. 2023;21:403–21. https://doi.org/10.1016/j.bioactmat.2022.08.031.
183. Li D, et al. A logic-based diagnostic and therapeutic hydrogel with multistimuli responsiveness to orchestrate diabetic bone regeneration. Adv Mater. 2022;34:e2108430. https://doi.org/10.1002/adma.202108430.
184. Lu Z, et al. An injectable collagen-genipin-carbon dot hydrogel combined with photodynamic therapy to enhance chondrogenesis. Biomaterials. 2019;218:119190. https://doi.org/10.1016/j.biomaterials.2019.05.001.
185. Liu M, et al. Injectable hydrogels for cartilage and bone tissue engineering. Bone Res. 2017;5:17014. https://doi.org/10.1038/boneres.2017.14.
186. Jana S, Levengood SKL, Zhang M. Anisotropic materials for skeletal-muscle-tissue engineering. Adv Mater. 2016;28:10588–612. https://doi.org/10.1002/adma.201600240.
187. Ge J, et al. Engineering conductive antioxidative antibacterial nanocomposite hydrogel scaffolds with oriented channels promotes structure-functional skeletal muscle regeneration. Chem Eng J. 2021;425:130333. https://doi.org/10.1016/j.cej.2021.130333.
188. Wang L, et al. Injectable remote magnetic nanofiber/hydrogel multiscale scaffold for functional anisotropic skeletal muscle regeneration. Biomaterials. 2022;285:121537. https://doi.org/10.1016/j.biomaterials.2022.121537.
189. Xu X, et al. A novel injectable fibromodulin-releasing granular hydrogel for tendon healing and functional recovery. Bioeng Transl Med. 2022;8(1):e10355. https://doi.org/10.1002/btm2.10355.
190. Han WM, Mohiuddin M, Anderson SE, Garcia AJ, Jang YC. Co-delivery of Wnt7a and muscle stem cells using synthetic bioadhesive hydrogel enhances murine muscle regeneration and cell migration during engraftment. Acta Biomater. 2019;94:243–52. https://doi.org/10.1016/j.actbio.2019.06.025.
191. Xu J, Wong C-W, Hsu S-H. An injectable, electroconductive hydrogel/scaffold for neural repair and motion sensing. Chem Mater. 2020;32:10407–22. https://doi.org/10.1021/acs.chemmater.0c02906.
192. Xu C, et al. Two-dimensional-germanium phosphide-reinforced conductive and biodegradable hydrogel scaffolds enhance spinal cord injury repair. Adv Funct Mater. 2021;31:2104440. https://doi.org/10.1002/adfm.202104440.
193. Sun H, et al. Injectable hydrogels in repairing central nervous system injuries. Adv Mater Sci Eng. 2021;2021:1–11. https://doi.org/10.1155/2021/7381980.
194. Liang Y, He J, Guo B. Functional hydrogels as wound dressing to enhance wound healing. ACS Nano. 2021;15:12687. https://doi.org/10.1021/acsnano.1c04206.
195. Zeng Q, Qi X, Shi G, Zhang M, Haick H. Wound dressing: from nanomaterials to diagnostic dressings and healing evaluations. ACS Nano. 2022;16:1708–33. https://doi.org/10.1021/acsnano.1c08411.
196. Fan Y, et al. Nanogel encapsulated hydrogels as advanced wound dressings for the controlled delivery of antibiotics. Adv Funct Mater. 2020;31:2006453. https://doi.org/10.1002/adfm.202006453.

197. Zhao X, et al. Antibacterial anti-oxidant electroactive injectable hydrogel as self-healing wound dressing with hemostasis and adhesiveness for cutaneous wound healing. Biomaterials. 2017;122:34–47. https://doi.org/10.1016/j.biomaterials.2017.01.011.
198. Liang Y, Xu H, Li Z, Zhangji A, Guo B. Bioinspired injectable self-healing hydrogel sealant with fault-tolerant and repeated thermo-responsive adhesion for sutureless post-wound-closure and wound healing. Nanomicro Lett. 2022;14:185. https://doi.org/10.1007/s40820-022-00928-z.
199. Zhou X, et al. Injectable thermosensitive hydrogel containing erlotinib-loaded hollow mesoporous silica nanoparticles as a localized drug delivery system for NSCLC therapy. Adv Sci. 2020;7:2001442. https://doi.org/10.1002/advs.202001442.
200. Xu H, et al. Growth differentiation factor-5-gelatin methacryloyl injectable microspheres laden with adipose-derived stem cells for repair of disc degeneration. Biofabrication. 2020;13:015010. https://doi.org/10.1088/1758-5090/abc4d3.
201. Sayed JE, Kamperman M. Ultra-sounding out a technique that sticks. Science. 2022;377:707.
202. Liang S, et al. Paintable and rapidly bondable conductive hydrogels as therapeutic cardiac patches. Adv Mater. 2018;30:e1704235. https://doi.org/10.1002/adma.201704235.
203. Cha GD, et al. Multifunctional injectable hydrogel for in vivo diagnostic and therapeutic applications. ACS Nano. 2022;16(1):554. https://doi.org/10.1021/acsnano.1c07649.
204. Shin M, Song KH, Burrell JC, Cullen DK, Burdick JA. Injectable and conductive granular hydrogels for 3D printing and electroactive tissue support. Adv Sci. 2019;6:1901229. https://doi.org/10.1002/advs.201901229.
205. Loebel C, Rodell CB, Chen MH, Burdick JA. Shear-thinning and self-healing hydrogels as injectable therapeutics and for 3D-printing. Nat Protoc. 2017;12:1521–41. https://doi.org/10.1038/nprot.2017.053.
206. Zhang S, et al. Room-temperature-formed PEDOT:PSS hydrogels enable injectable, soft, and healable organic bioelectronics. Adv Mater. 2020;32:e1904752. https://doi.org/10.1002/adma.201904752.
207. Menees SB, Lembo AJ, Chey WD. Six-month efficacy of polyethylene glycol (PEG) 3350 in the treatment of chronic idiopathic constipation: analysis using FDA endpoints. Am J Gastroenterol. 2020;115:S230.
208. Mandal A, Clegg JR, Anselmo AC, Mitragotri S. Hydrogels in the clinic. Bioeng Transl Med. 2020;5:e10158. https://doi.org/10.1002/btm2.10158.
209. He X, et al. Effect of intramyocardial grafting collagen scaffold with mesenchymal stromal cells in patients with chronic ischemic heart disease: a randomized clinical trial. JAMA Netw Open. 2020;3:e2016236. https://doi.org/10.1001/jamanetworkopen.2020.16236.
210. Traverse JH, et al. First-in-man study of a cardiac extracellular matrix hydrogel in early and late myocardial infarction patients. JACC Basic Transl Sci. 2019;4:659–69. https://doi.org/10.1016/j.jacbts.2019.07.012.
211. Cammisa FP, et al. Two-year fusion rate equivalency between Grafton® DBM gel and autograft in posterolateral spine fusion. Spine. 2004;29:660–6.
212. Niemeyer P, et al. Treatment of large cartilage defects in the knee by hydrogel-based autologous chondrocyte implantation: two-year results of a prospective, multicenter, single-arm phase III trial. Cartilage. 2022;13:19476035221085146. https://doi.org/10.1177/19476035221085146.
213. Evans CH, Kraus VB, Setton LA. Progress in intra-articular therapy. Nat Rev Rheumatol. 2014;10:11–22. https://doi.org/10.1038/nrrheum.2013.159.
214. Conrozier T, et al. Standardized follow-up of patients with symptomatic knee osteoarthritis treated with a single intra-articular injection of a combination of cross-linked hyaluronic acid and mannitol. Clin Med Insights Arthritis Musculoskelet Disord. 2016;9:175–9. https://doi.org/10.4137/CMAMD.S39432.
215. Ovrebo O, et al. Design and clinical application of injectable hydrogels for musculoskeletal therapy. Bioeng Transl Med. 2022;7:e10295. https://doi.org/10.1002/btm2.10295.

Chapter 4
Multilayer Microcapsules with Tailored Structures and Properties as Delivery Carriers for Drugs and Growth Factors

Weijun Tong and Changyou Gao

Abstract Multilayer microcapsules fabricated via the layer-by-layer (LbL) assembly method with tailored structures and functionalities are promising candidates as carriers of drugs, growth factors, and other bioactive agents in biomedicine. The capsules loaded with growth factors also can be integrated with scaffolds to form bioactive scaffolds for regenerative medicine. This chapter discusses first the recent progress of the fabrication of LbL microcapsules including manipulation of their properties by chemical cross-linking, microcapsules based on new driving forces, microcapsules with subcompartments, and microcapsules which can transform their shape. Their potential applications as drug delivery carriers, emphasizing on the new encapsulation methods, the fabrication of nanoparticles and nanocapsules, the triggered release of encapsulated substances, and the deformation and recovery behavior of microcapsules, are demonstrated. Finally, the loading of growth factors into multilayer capsules and their incorporation into scaffolds are introduced.

Keywords Layer-by-layer · Polyelectrolytes · Microcapsules · Drug carriers · Growth factors · Loading and release · Scaffolds

4.1 Introductions

Hollow capsules are of great interest due to their potential applications and fundamental importance as new colloidal structures in areas such as medicine, catalysis, cosmetics, as well as biotechnology [1]. One of the promising methods which can fabricate hollow capsules with tailored structures and functions is the layer-by-layer

W. Tong (✉) · C. Gao
MOE Key Laboratory of Macromolecular Synthesis and Functionalization, Department of Polymer Science and Engineering, Zhejiang University, Hangzhou, China
e-mail: tongwj@zju.edu.cn; cygao@zju.edu.cn

C. Gao (ed.), *Polymeric Biomaterials for Tissue Regeneration*,
https://doi.org/10.1007/978-981-99-6948-7_4

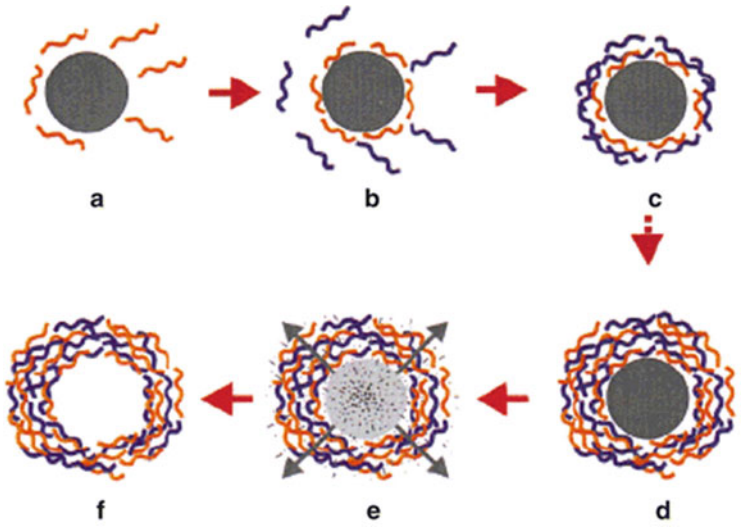

Fig. 4.1 The initial steps (**a-d**) involve step-wise film formation by repeated exposure of the colloids to polyelectrolytes of alternating charge. After the desired number of polyelectrolyte layers are deposited, the core is removed (**e**) to obtain a suspension of polyelectrolyte hollow shells (**f**).

(LbL) assembly [2, 3] of multilayer films onto colloidal particles, followed by core removal (Fig. 4.1) [4, 5]. Through this method, the capsules with well-controlled size and shape, finely tuned wall thickness, and variable wall compositions have been obtained [6]. The LbL microcapsules with integrated multifunctionality have high capacity for loading of a wide range of substances and sensitive response to diverse stimuli and thus are highly attractive for the biorelated applications [7–9]. At the beginning, the studies of LbL multilayer capsules are mainly focused on the fabrication and basic physicochemical properties [6]. However, the past decade has witnessed a rapid increase of researches concerning their functionalization and applications, particularly in the biomedical fields such as drug delivery [10]. In this chapter, we first focus on the recent progress of the LbL microcapsules in our lab with respect to manipulation of their properties by chemical cross-linking and fabrication of the microcapsules based on new driving forces, the capsules with subcompartments, and the capsules which can transform their shape. Then, we will discuss the potential applications of LbL capsules as drug delivery carriers, emphasizing on the new encapsulation methods developed in our lab, the surface modification of smaller particles, as well as the deformation and recovery behavior of microcapsules passing through a model capillary vessel. Finally, the loading of growth factors into multilayer capsules and their incorporation into scaffolds are discussed.

4.2 Multilayer Microcapsules with Tailored Structures, Properties, and Functions

4.2.1 Cross-Linking to Tailor the Properties of Microcapsules

The electrostatic interaction is first used for the fabrication of LbL microcapsules. Although it is generally strong enough to hold the integrity of the microcapsules, in some cases cross-linking is still necessary for the capsules to survive through harsh conditions such as high ionic strength, extreme pH, and strong polar organic solvent [11, 12]. Moreover, cross-linking also can effectively manipulate the permeability and mechanical strength of the capsules [11, 13]. For the multilayer films and capsules based on hydrogen bonding, further stabilization is also required for biomedical applications since most of them will be disassembled at physiological conditions [14, 15]. Many methods have been developed to cross-link the multilayer films and capsules, such as carbodiimide chemistry [16–18], UV irradiation [13], as well as thermal cross-linking [19]. More recently, disulfide [20, 21] and click chemistry [22–28] have also been proved effective for cross-linking the hydrogen-bonded multilayers and microcapsules.

The above mentioned techniques are exclusively based on a reaction between the functional groups of the two components in the multilayers. We demonstrated that the multilayer microcapsules assembled from poly(allylamine hydrochloride) (PAH) and poly(styrene sulfonate) (PSS) could be considerably stabilized by cross-linking of only the PAH component with glutaraldehyde (GA) [29]. After cross-linking, the capsule wall was apparently thicker and with higher folds. The capsules were quite stable in 0.1 M NaOH even after 24 h. The elasticity modulus (680 MPa) of the capsule walls was doubled compared with that of the control. Furthermore, the permeability of the capsule walls was also greatly reduced after cross-linking. We further applied this method to the poly(ethylenimine) (PEI) and poly(acrylic acid) (PAA) weak polyelectrolyte microcapsules [30]. The cross-linked microcapsules can maintain their macroscopic topology at extreme low or high pH while reorganizing their localized microstructure to enable selective permeation or rejection of macromolecules at lower (<pH 4) and higher pH (>pH 6), respectively. Thus, it is possible to produce capsules that are dual-pH responsive and stable over a broad pH range.

4.2.2 Capsules Directly Assembled Based on Nonelectrostatic Interactions

Different driving forces can endow the microcapsules with different physicochemical structures, stimuli response, and thereby their functionality and applicability. At the beginning, the electrostatic interaction was the first driving forces for the LbL assembly [4, 5, 31]; thus, the building blocks were mainly charged species. Then hydrogen bonding has been employed for the assembly of microcapsules. Recently,

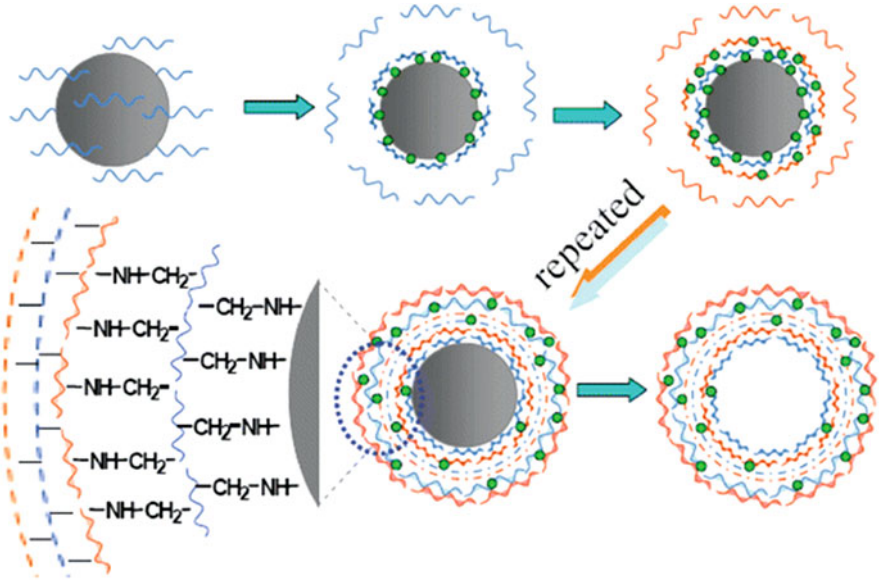

Fig. 4.2 Schematic illustration of the process of direct covalent LbL assembly on a silica particle and fabrication of a hollow capsule by etching out the template core. The *blue lines* represent PGMA, the *red lines* represent PAH, and the *green dots* represent the covalent linkage between layers. (Reprinted with permission from Ref. [33]. Copyright 2007 by Wiley-VCH)

the multilayer hollow microcapsules based on other nonelectrostatic interactions such as covalent bonding, host–guest interaction, and bio-specific interactions have been fabricated, which show unique properties.

Covalent LbL-assembled microcapsule is stable enough to withstand the long-time etching of strong polar organic solvent [32]. We recently fabricated a new structure of microcapsules with high modulus and high stability through the covalent LbL assembly (Fig. 4.2) [33]. Aminosilanized SiO_2 microparticles were used as templates. Poly(glycidyl methacrylate) (PGMA) and PAH were alternately immobilized onto the particle surfaces through a coupling reaction between the epoxides and the amines. Thus, a highly cross-linked structure was produced in this process. The templates were removed by HF etching, resulting in hollow microcapsules. The microcapsules are stable in extreme pHs and elevated temperature. Using the method of osmotic-induced invagination [34, 35], the elastic modulus of the microcapsule walls without any treatments was found to be as high as 910 MPa, which is quite stable even under acid and base treatment.

The reaction between amine and aldehyde is fast and efficient in aqueous solution at room temperature; based on this reaction, single polyelectrolyte component multilayers and microcapsules can be fabricated through direct covalent assembly of PAH with GA [36]. The structure and the cutoff molecular weight of the capsule walls are dependent on the molecular weight of used polymers [37]. This method can be applied not only on biomacromolecules with amine groups such as polypeptides

and proteins but also on polysaccharides, because GA also can readily react with hydroxyl groups at very mild conditions.

However, the main drawback of the abovementioned methods is that the obtained capsules may largely lose their stimuli-responsive properties due to the uncontrollable covalent reactions [36, 37]. One solution to this problem is to carefully control the content of reactive groups in polymer chains, leading to a controllable reaction degree and a number of functional groups [38]. Bovine serum albumin (BSA) is a kind of biocompatible and biodegradable natural protein. It has a high content of aspartic and glutamic acids, lysine, and arginine [39, 40]. Only the amine groups of lysine can be cross-linked by GA [41], while the other amino acids with free carboxylic groups still exist, which can induce the pH response of the resultant capsules. We recently demonstrated that [42] BSA hollow capsules could be obtained by covalent assembly of BSA and GA on a template followed by core removal. The capsules possessed reversible pH-responsive permeability, which can be used to encapsulate macromolecules.

Host–guest interaction is another type of driving forces frequently employed in supramolecular chemistry. It is known that the host–guest interaction is readily mediated by the host and guest molecules with respect to their matching degree and concentration. If charge interaction is further introduced, multiresponsive microcapsules can thus be expected. According to this design, multilayer microcapsules were fabricated by using the interaction between β-cyclodextrin (β-CD) and ferrocene grafted to a weak polyelectrolyte PAH, which can further introduce charge interaction into the capsule walls (Fig. 4.3) [43]. The microcapsules that consist of PAH-g-β-CD and PAH-g-ferrocene indeed show multiresponsiveness to environmental stimuli. For example, they swell and shrink at low and high pH, respectively. Incubation in a salt or β-CD solution can also mediate their swelling and shrinking behaviors. With these smart features, the microcapsules can serve as reservoirs for drugs, DNAs, enzymes, and so on.

The specific interactions between complementary DNA bases are stable enough under physiological conditions in nature, which can be used for the assembly of multilayer films and capsules [44]. Moreover, carbohydrate–protein interaction, which is a combination of multiple hydrogen bonding and hydrophobic interactions and participates in a wide variety of biological events [45–47], is also quite stable at physiological conditions. Therefore, this interaction can be used to assemble microcapsules which simultaneously possess good stability and responsiveness to external stimulus due to its noncovalent nature. Concanavalin A (Con A) can specifically bind to polysaccharides such as dextran and glycogen [48–50]; thus, it can be utilized to fabricate thin films with them through lectin–carbohydrate interactions [51–53]. These films can respond to glucose [50, 53]. Recently, the hollow capsules assembled by Con A and glycogen through LbL method were also obtained. They are stable at physiological pH range due to the relatively strong multiple hydrogen bonding but still can respond to glucose [54]. The sequential multilayer film growth proceeds successfully on both planar and curved substrates when the Con A molecules adopt confirmation of tetramers or more complicated aggregates. The obtained capsules show layer-number-dependent shell shrinkage, distortion, and

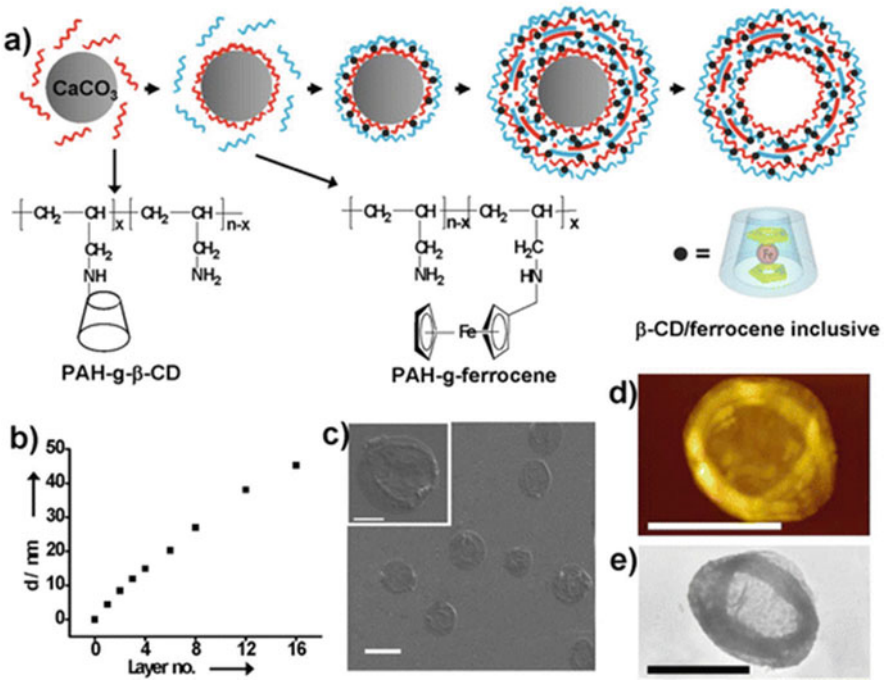

Fig. 4.3 Fabrication process and structure characterization of host–guest microcapsules. (**a**) LbL assembly of same polyelectrolyte on carbonate particles to obtain hollow microcapsules using host–guest interaction. The chemical structure of PAH-g-β-CD, PAH-g-ferrocene, and β-CD/ferrocene inclusive are shown in the second row. (**b**) The thickness of the PAH-g-β-CD/PAH-g-ferrocene multilayers assembled on silicon wafer as a function of layer no. (**c**) SEM, (**d**) SFM, and (**e**) TEM images of the prepared (PAH-g-β-CD/PAH-g-ferrocene)3 microcapsules, respectively; bar is 5 μm. Inset in (**c**) is a higher magnification image of one capsule; bar is 2 μm. (Reprinted with permission from Ref. [43]. Copyright 2008, American Chemical Society)

densification. The capsules are stable in a pH range of 6–9 and show specific responses to glucose, mannose, fructose, and dextran. Triggered by these stimuli, the preloaded cargoes in the capsules can be released.

4.2.3 Capsules with Subcompartments

The multicompartmental micro- and nanostructures can be loaded with multiple cargoes and mimic the structure of cells; thus, they have received tremendous attention recently [55–58]. Hollow capsules with subcompartments are ideal models which resemble the structure of cells. By combining of other techniques, diverse LbL capsules with different subcompartments have been obtained [59]. The

subcompartments can be incorporated through two different ways: wall decoration and interior loading.

Kreft et al. first reported the LbL microcapsules with a shell-in-shell structure for integrated and spatially confined enzymatic reactions [60]. De Geest et al. reported the assembly of multilayers on big hydrogel particles (hundreds of microns) in which tens of hollow LbL microcapsules or microparticles are loaded [57, 61]. Recently, Caruso group incorporated intact liposomes into LbL capsule walls or inside capsules to prepare "capsosomes," which can be then employed as enzymatic reactors and delivery vehicles for hydrophobic cargoes [62–66].

Alternatively, polymeric micelles also can be incorporated into the walls or interiors of LbL capsules as the subcompartments. The micelles possess advantages of sustained release of hydrophobic substances. In particular, polymeric micelles possess a unique core/shell structure and relatively good stability [67]. Thus, the micelle-incorporated microcapsules combine the advantages of both micro- and nanostructures. Polymeric micelles can be loaded into the shell through alternating assembly of poly(styrene-*b*-acrylic acid) (PS-*b*-PAA) micelles and oppositely charged polyelectrolyte on templates [68]. After core removal, the as-prepared microcapsules show extraordinary stability in concentrated HCl (37%) and 0.1 M NaOH. This extraordinary stability against highly acidic or alkaline conditions is possibly due to the hydrophobic interaction between PS cores of the micelles and hydrogen bonding of the PAA chains in adjacent layers and PAH chains. The incorporation of polymeric micelles in LbL capsule interiors has been presented by Li et al. [69] as well as Tong et al. [70]. In the latter method [70], LbL assembly was conducted on $CaCO_3$ microparticles predoped with PS-*b*-PAA micelles, resulting in encapsulation of micelles after core removal. The micelles inside the capsules can form a chain and network-like structure with more micelles near the capsule walls. Hydrophobic drugs as such can be loaded into the hydrophobic cores of micelles, while the negatively charged PAA corona of the micelles can result in spontaneous deposition [71–75] of water-soluble and positively charged drugs. The apparent concentrations of hydrophobic and water soluble are much higher than that of the feeding values. Therefore, capsules with this synergetic feature show their great promise in loading of drugs with different physicochemical properties.

4.2.4 Shape Transformation of Capsules

The smart capsule systems are of high attraction due to their ability to respond to the alteration of environment conditions. LbL-assembled capsules can change their structure and properties intelligently in response to various stimuli. But most of the intelligence of the hollow structures results from controllable swelling and shrinking, accompanying with permeability change [76]. Less concern is paid to shape transformation of the hollow structures, which is only observed in vesicles and hollow silica spheres previously [77–83]. Recently, single-component microcapsules were fabricated in our lab by an in situ reaction of reactive

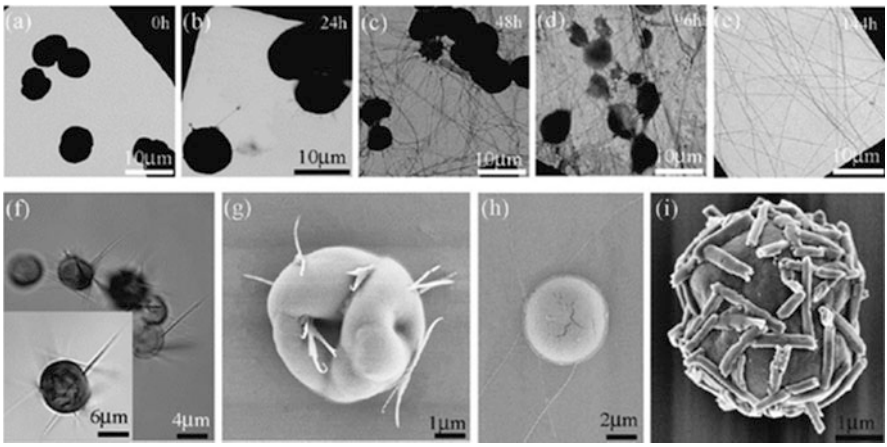

Fig. 4.4 TEM images showing the process of nanotube protruding from the PAH-Py microcapsules incubated in pH 0 HCl for 0(**a**), 24(**b**), 48(**c**), 96(**d**), and 144 h(**e**), respectively. (**f**) Optical images (inset, a higher magnification) showing the protruded nanotubes from the PAH-Py microcapsules incubated in pH 0 HCl for 30 h. SEM images of a microcapsule with nanotubes after treatment in pH 0 HCl for (**g**) 30 h and (**h**) 72 h, respectively. (**i**) SEM image of a microcapsule with nanorods after treatment in pH 2 HCl for 1 h. (Reprinted with permission from Ref. [85]. Copyright 2011, American Chemical Society)

hydrophobic low-molecular-weight molecules with corresponding PE-doped $CaCO_3$ microparticles, followed by core removal [84, 85].

The first example is the capsules made of ferrocenecarboxaldehyde (Fc-CHO) and PAH-doped $CaCO_3$ microparticles [84]. This single-component microcapsule is stabilized by hydrophobic aggregation of Fc moieties. Due to the redox properties of Fc, the PAH-Fc microcapsules can reversibly swell and shrink in response to oxidation and reduction. At the same time, the permeability also can be changed reversibly. PAH-pyrene (Py) microcapsules also can be fabricated through the reaction of pyrenecarboxaldehyde with the doped PAH [85]. When this kind of capsules is incubated in acidic solution, one-dimensional nanotubes (1D-NTs) or nanorods (1D-NRs) are protruded from the microcapsules. The 1D-NTs keep growing with incubation time and eventually form a network. Meanwhile, the microcapsules are degraded gradually and disappear completely after 144 h (Fig. 4.4). The micelles assembled from PAH-Py polymers treated at similar conditions also can be transformed into one-dimensional structures. The one-dimensional nanotubes are formed by 1-pyrenecarboxaldehyde with ordered π–π stacking and exhibit a helical structure and anisotropic property. The final nanostructures are determined by the different hydrolysis rate of Schiff base at different pH values. The linear PAH also can guide the building-up process especially for the nanotubes. Through this mechanism, hollow capsules budded with nanotubes or nanorods mimicking the cellular protrusion of filopodia are successfully fabricated by controlling the incubation time in solutions with different pH (Fig. 4.4).

By chemical cross-linking and surface modification, 1D-NR growth state from the PAH-Py microcapsules can be well controlled [86]. The 1D-NRs also can grow in the LbL-assembled capsules in a controllable manner [87]. For this purpose, PSS/PAH multilayers were assembled on the surface of $CaCO_3$ (PAH-Py) microparticles, yielding PAH-Py and (PSS/PAH)n double-shell capsules. By incubation of the obtained capsules in pH 2 solution, the 1D-NRs grow within the PSS/PAH multilayer capsules in three dimensions. The fluorescence emission intensity of Py NRs inside the capsules can be tuned by a charge-transfer pair. This novel composite structure with PAH-Py NRs inside PE multilayer microcapsules provides a creative strategy for in situ nanomaterials fabrication, illuminating the trend for controllable properties and functions of smart nanodevices. The modulation of the protrusion of NRs also can be achieved by addition of small molecules such as 1-pyrenesulfonic acid sodium salt ($PySO_3Na$) [88], demonstrating the tunable properties of such kind of nanostructures.

Inspired by the above results, PAH-Py NRs consisting of a Py-CHO core and PAH shell can be prepared by surface grafting of PAH onto Py-CHO NRs [89]. After coated with PAH, The NRs become more curved and flexible as a result of partial loss of Py-CHO from the NRs. The PAH-Py NRs with a hydrophilic and charged PAH layer can be suspended stably in water for at least 3 months. Because of the charge attraction and coordination effect of amino groups, Au NPs can be either adsorbed or in situ synthesized on the PAH-Py NR surface. The initial fluorescence emission of Py is largely remained due to the excellent isolation effect of PAH, which avoids direct contact between Py and the Au NPs. Using the similar process, other hybrid organic–inorganic functional nanomaterials with controlled physicochemical structures can be synthesized, such as tetraphenylethylene (TPE) nanoparticles [90]. TPE-substituted poly(allylamine hydrochloride) (PAH-g-TPE) was synthesized by a Schiff base reaction between PAH and TPE-CHO. The PAH-g-TPE forms micelles in water at pH 6, which are further transformed into pure TPE-CHO nanoparticles (NPs) with a diameter of ~300 nm after incubation in a solution of low pH value. In contrast, only amorphous precipitates are obtained when TPE-CHO methanol solution is incubated in water. The aggregation-induced emission feature of the TPE molecule is completely retained in the TPE NPs, which can be internalized into cells and show blue fluorescence. Formation mechanism of the TPE NPs is proposed by taking into account the guidance effect of linear and charged PAH molecules and the propeller-stacking manner between the TPE-CHO molecules.

4.3 Microcapsules as Drug Delivery Carriers

The LbL-assembled capsules with tailored structures and functions are versatile platforms for encapsulation, storage, and delivery of diverse substances. Thus, the LbL-assembled capsules are ideal advanced drug carriers for the delivery of diverse drugs and growth factors. There are already several excellent reviews which

summarized the very recent progress in this field [21, 91–99]. The following sections will mainly focus on the recent advances in this field.

4.3.1 Controlled Loading of Low-Molecular-Weight Drugs

Many applications of the multilayer capsules must face a challenge of efficient loading of the desired substances. This is particularly difficult for loading of low-molecular-weight and water-soluble substances because small molecules can freely diffuse through the capsule walls [100]. We developed the "spontaneous deposition" method, which is based on a mechanism of high affinity of the preloaded substances in the capsules with the cargoes that will be loaded. Gao et al. first found that positively charged molecules such as dextran labeled with tetramethylrhodamine isothiocyanate (TRITC-dextran) could deposit into the aged "hollow" microcapsules templated on melamine formaldehyde (MF) particles with a large amount [71]. The strong fluorescence emitted from the interior of capsules could prove the existence of considerable high concentration of dextran in the capsule interiors (the so-called spontaneous deposition) (Fig. 4.5a). Many other water-soluble substances with positive charges such as polyelectrolytes [71], proteins [71], enzymes [72], and low-molecular-weight dyes and anticancer drugs (Fig. 4.5b, c) [73] can be spontaneously deposited with a large quantity. Moreover, the deposition still occurs even if the molecules have very few positive charges such as the TRITC-dextran (Fig. 4.5a), which gets positive charges from a few pendent TRITC groups. The driving force for this phenomenon is the electrostatic interaction between the negatively charged complex (PSS/MF) within the capsule interior and the loaded molecules. The PSS/MF complex is formed by the dissociated PSS from the very initial layer and the positively charged MF degradation product.

The spontaneously deposited low-molecular-weight drugs in the LbL microcapsules templated on MF colloidal particles can be released in a sustained manner [73, 74]. The amount of the loaded drugs can be controlled through changing the feeding concentration of the drugs, temperature, as well as salt concentration. This tailorable deposition behavior is crucial for control release applications. The loaded drugs can be released in a sustained manner. The release profile can be tuned by changing the interaction between the drugs and the PSS/MF complex. The presence of anticancer drug-loaded capsules can effectively kill HL-60 cells, a kind of human leukemia cell [73].

For better control of the spontaneous deposition property, the capsules can be preloaded with charged polyelectrolyte using a polyelectrolyte-doped template [75, 101–104]. At higher drug feeding concentration and higher salt concentration, large amount of daunorubicin (DNR) and DOX can be loaded [75, 103]. The drug concentration within the microcapsules is hundreds of times higher than the feeding concentration. The drug can be released from the capsules through a diffusion-controlled release mechanism at the initial stage (4 h). The in vitro experiments demonstrate that the encapsulated drug can effectively induce the apoptosis of

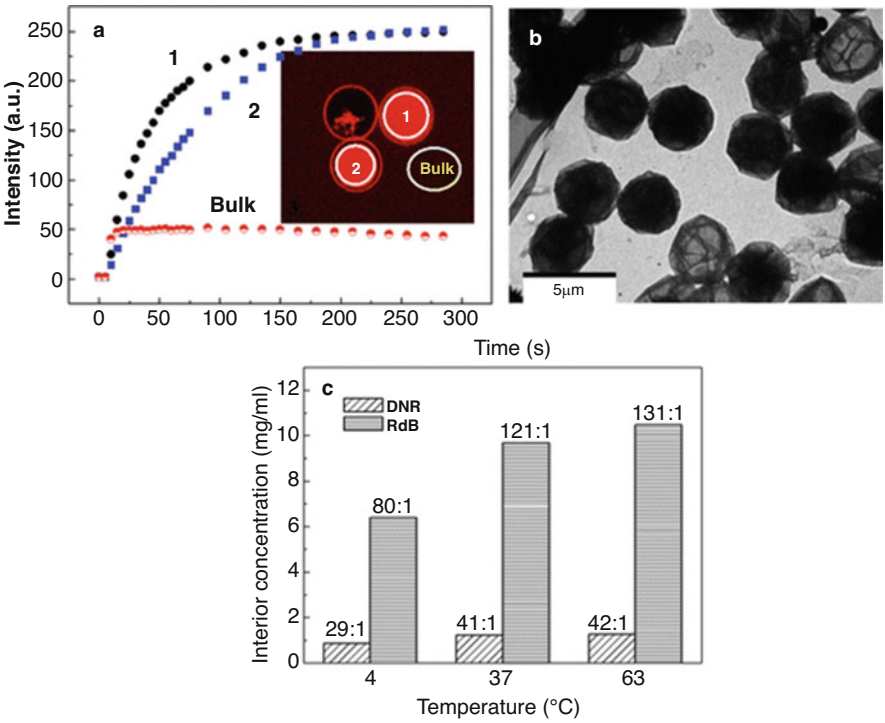

Fig. 4.5 (**a**) Fluorescence intensity averaged from inside the *circles* as a function of incubation time. TRITC-dextran (M_w ~65 kDa) and preformed MF-(PSS/PAH)5 capsules were used. (**b**) TEM images of daunorubicin (DNR) deposited MF-(PSS/PAH)5 capsules. (**c**) DNR and rhodamine B (*RdB*) concentrations in the capsule interior as a function of temperature. MF-(PSS/PAH)4 (PSS/PDADMAC)5 capsules were used for DNR with a feeding concentration of 30 mg/ml and MF-(PSS/PAH)5 capsules for RdB, 80 mg/ml. The *numbers* in the figure represent the concentration ratios of capsule interior and bulk. *PDADMAC* poly(diallyldimethylammonium chloride). (Reprinted with permission from Ref. [73]. Copyright 2005 by Wiley-VCH)

HepG2 tumor cells. The encapsulated DOX also has better efficacy than that of the free drug in terms of tumor inhibition in a 4-week in vivo culture period [104].

Nonetheless, challenge is still remained to better maintain the drugs inside the capsules and then control their release profile. Previous studies demonstrate that poly (diallyldimethylammonium chloride) (PDADMAC)/PSS capsules with PSS as the outmost layer can shrink dramatically at elevated temperature [105, 106], resulting in a thicker and denser capsule wall. So dextran (Mw from 10 to 70 kDa) can be effectively encapsulated with a slightly higher concentration than the feeding value [107]. The loading of water-soluble small molecular drugs also can be achieved using this method [108]. In our recent work [109], spontaneous deposition and heat-induced shrinkage were combined to fabricate a drug carrier system, showing a high drug loading efficiency and more controllable release profile. Through this strategy,

photosensitizers also can be encapsulated, and most of them are stably retained for a long time and protected by capsule wall against reductive enzyme [110].

Encapsulation of low-molecular-weight drugs through the attractions between the drugs and the preloaded substances in the multilayer capsules also can be applied to different systems via specific interactions besides the electrostatic interactions. For example, Sukhorukov and coworkers reported that low-molecular-weight doxycycline could be encapsulated in LbL microcapsules via attraction to dextran sulfate (DS) in the microcapsule core because doxycycline molecules can penetrate the shells and react with DS to form a complex within the microcapsule [111]. The specific and sustained activity of doxycycline is well maintained. If the capsules are further coated with a lipid layer, the release and sustained activity of encapsulated drug can be enhanced because its leakage is greatly prohibited. This method could provide a long-term delivery system of low-molecular-weight drugs from multilayer capsules. Kharlampieva and coworkers reported a facile method for the efficient encapsulation of a wide range of hydrophilic substances with molecular weight less than 1000 and different charges [112]. The capsules are fabricated via LbL assembly of poly(methacrylic acid) (PMAA) and poly(*N*-vinylpyrrolidone) (PVPON) on silica templates. After cross-linking of the PMAA multilayers, PVOPN is entrapped in the shell to form an interpenetrated network. The capsules show reversible variation in diameter upon pH changes, and thus encapsulation of low-molecular-weight substances could be achieved at pH = 7.5 followed by sealing the capsule wall with high-molecular-weight DS at pH = 5.5. It is interesting that the negatively charged molecules can be entrapped within the capsule cavity, while the positively charged molecules are encapsulated within the negatively charged capsule shell. This approach allows the simultaneous loading of different low-molecular-weight substances at different positions in the capsules; thus, the capsules can deliver multiple drugs. Furthermore, the pH-responsiveness of the capsule also can achieve the controlled release of the drugs.

Normal LbL assembled microcapsules fail to encapsulate low-molecular-weight drugs because of the semipermeable nature of the shell. Sukhorukov and coworkers reported a new method to fabricate poly-L-arginine hydrochloride (PARG)/DS/silica (SiO_2) composite capsules [113]. The inorganic SiO_2 layer is in situ formed to seal the capsules; thus, low-molecular-weight drug can be effectively encapsulated inside. The cell experiments demonstrate that the PARG/DS/silica capsules can be degraded into fragments and the release of encapsulated molecules is achieved in a relatively short time (2 h), while the capsules with a similar structure using nonbiodegradable polyelectrolytes remain intact even after 3 days.

4.3.2 LbL Assembly on Nanoparticles

Most of the LbL capsules have a diameter of a few micrometers, which are too large for intravenous injection. One possible solution is to assemble multilayers on particles with a smaller size. De Koker et al. have reviewed the progress of LbL

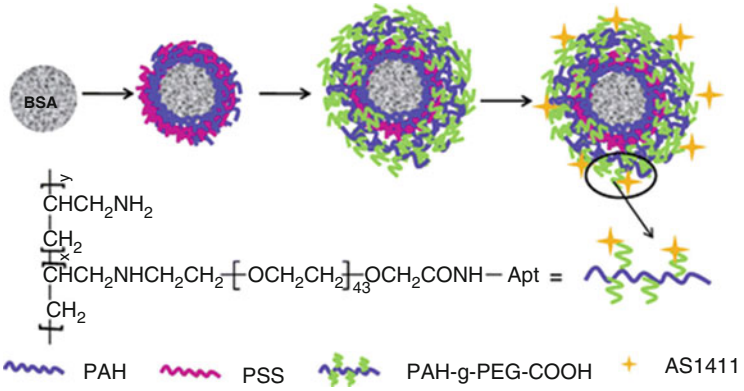

Fig. 4.6 Schematic illustration to show the preparation process of BSA nanoparticles coated with PAH/PSS multilayers and coupled with aptamer AS1411. (Reprinted with permission from Ref. [119]. Copyright 2012 by RSC)

assembly on ultrasmall (sub-100 nm) particles, which are mainly gold NPs [98]. In our lab, surface modification of biodegradable and nontoxic polyester, poly(lactide-*co*-glycolide) (PLGA) NPs with a size around 200–300 nm using LbL assembly have been extensively investigated. PLGA is one of the commonly used polymers for drug delivery [114, 115]. These particles with such a size can be injected into the blood vessel and may accumulate in cancerous tissues through the well-known enhanced permeability and retention (EPR) effect. Modification of NP surface with targeting molecules can enhance the drug concentration in the targeted organs or tissues and reduce the dosage and toxic side effects. In order to effectively immobilize the ligands, the NPs should possess enough number of active groups and are stable enough for following reactions. The LbL assembly can endow the NPs with uniform surface charge density, numerous active groups, and excellent stability in various mediums. For example, PAA/PEI and chitosan (CS)/alginate (CS/ALG) can be used to build multilayers on the PLGA NPs for further immobilization of PEG and folic acid aiming at long-time circulation and targeting [116, 117]. The surface charge and the thickness of the assembled multilayers can greatly influence the release profile of loaded dyes [118]. The surface with negative charges or PEG also can reduce protein adsorption, whereas surface modified with folic acid can enhance the NP uptake by human hepatoma cells.

The multilayers also can be assembled on the NPs before drug loading, and then different drugs can be loaded into the preformed multilayer-coated particles for different applications. In our recent work [119], BSA NPs with a size about 200 nm were coated with PAH/PSS multilayers, onto which a layer of PAH-*g*-PEG-COOH was further adsorbed. By carbodiimide chemistry, aptamer-AS1411 molecules were immobilized (Fig. 4.6). Aptamer-AS1411 can target to overexpressed nucleolin on cancer cell membrane [120, 121]. The PEGylated multilayer-coated BSA NPs have enhanced colloidal stability even in serum-containing medium [122]. DOX can be effectively loaded into the preformed BSA

NPs through electrostatic interaction between negative charges in BSA and positive charges in DOX. The encapsulation efficiency (98.6%) and loading percentage (9%) are both very high. The loaded drugs can be released faster at pH 5.5 than at pH 7.4. In vitro cell culture demonstrates that the as-prepared BSA NPs can specifically bind to liver cancer cells, leading to higher cellular uptake and cytotoxicity.

Except of the solid nanosize templates, the multilayers also can be assembled on emulsion droplets. For example, Szczepanowicz and coworkers reported the preparation of nanoparticles via direct coating on the emulsion droplets with polyelectrolyte multilayer shells [123]. The oil cores containing paclitaxel can be first stabilized by docusate sodium salt/poly-L-lysine surface complex (AOT/PLL) and are further coated in multilayers formed by the LbL assembly of poly-L-glutamic acid (PGA) and PLL up to five or six layers. Their surfaces can be further modified through the assembly of the pegylated polyelectrolyte, resulting in prolonged persistence of the nanocarriers in the circulation. The obtained nanoparticles can be stabilized in cell culture medium and the encapsulated hydrophobic anticancer drug can be released to kill cancer cells. Due to the dynamic nature of the emulsion droplets and the surfactants, the emulsion-based templates generally have relatively limited colloidal stability and broad size distribution. Cheng and coworkers used crystallized miniemulsion droplets as templates for the fabrication of multilayer nanocapsules [124]. Compared with normal emulsions, the miniemulsions are kinetically more stable and the crystallization of the inside oil phase can result in their higher colloidal stability due to the surface-anchored surfactant molecules. Polyelectrolytes with opposite charges can be alternatively assembled on this kind of templates and the crystallized oil phase can be dissolved by using proper organic solvent, resulting in hollow nanocapsules with well-defined structures and controlled size.

In order to obtain hollow nanocapsules, the nanosize templates should be removed under mild conditions. For example, Cui and coworkers reported the LbL assembly of multilayers on Cu_2O nanoparticles [125]. Cu_2O particles are cheap and can be easily fabricated. After the assembly of multilayers, they can be removed in $Na_2S_2O_3$ solution at neutral pH. During this process, no toxic reagents are needed. Furthermore, Cu_2O nanoparticles with tunable morphologies and sizes can be synthesized via tuning the preparation conditions. Thus, the nanocapsules with different shapes could be obtained by using Cu_2O nanoparticles with different shapes as templates. In addition, the capsule shape significantly influences their interaction with cells. The association of cubic capsules to HeLa cells are significantly increased compared with their tetradecahedral and spherical counterparts. This kind of nanocapsules with tunable morphologies can provide an ideal model system for the investigation of bio–nano interactions.

Although the LbL method have been proved to be a versatile approach for the preparation of multilayer nanocapsules with engineered structure and properties by using diverse building blocks and templates, the fabrication of nanocapsules through this method at large scale is still challenging and time-consuming. The traditional LbL assembly process needs several washing and centrifugation steps before each assembly of polyelectrolyte layer, resulting in a very long preparation time and accumulated particle loss after multiple centrifugation steps. In order to solve this

problem, Elizarova and coworkers reported a continuous method to the preparation of nanosize multilayer capsules using calcium phosphate nanoparticles as templates [126]. This method uses a tubular flow type reactor which can fabricate tens of milligrams of nanocapsules in 1 h. In the fabrication process, the template nanoparticles and polyelectrolyte solution are first mixed in the tubing to form the first layer on the templates. Then the modified nanoparticles pass into the next segment of tubing, where they meet the second polyelectrolyte with opposite charges. After mixing, the second layer is assembled on the particles. These steps can be continuously repeated until the required number of layers is assembled. The key point for the successful fabrication of nanocapsules via this method is to avoid the presence of any excess polyelectrolyte in the tubing, otherwise severe coagulation may happen. Thus, the careful control of the added amount of polyelectrolyte in the tubing is critical. The results demonstrate that slightly under dosing the amount of added polyelectrolyte can ensure the negligible free polyelectrolyte in solution. During the alternative assembly steps, the typical charge reversal can be observed and the relatively strong surface charges can make the particles stable during the fabrication process. Finally, after the required number of layers are assembled, the calcium phosphate templates can be facilely removed by incubation in mild acidic solution to obtain the hollow nanocapsules.

4.3.3 Capsules Squeeze Through a Confined Capillary

Compared with their nanometer-sized counterparts, the LbL microcapsules can be fabricated in an easier way [127]. However, microcapsules are difficult for intravenous injection. But in human blood, the circulation cells have a size of several microns. One example is red blood cell (RBC), which has extreme reversible deformability under physiological flow, so that it can easily pass through the smallest blood capillary vessel (~3 μm). One can imagine that if the capsules have proper shape and flexibility, they may easily squeeze through narrow capillary as natural RBC. This kind of capsules may have great potential applications as drug carriers. The deformability of polymeric microparticles (mainly hydrogel microparticles) with different shapes and sizes through a narrow constriction has been studied under flow conditions. For example, RBC-mimicking particles, which are flexible enough to flow through narrow glass capillaries and able to recover to discoidal shape, have been successfully fabricated [128]. Hayashi et al. demonstrated that 3.5 μm biconcave disk-shaped particles fabricated by electrospraying of cellulose derivative polymers can maintain RBC-like shape after filtrated through a membrane with a pore size of 1 μm [129]. Haghgooie et al. synthesized PEG hydrogel particles with different shapes including disks, rings, crosses, and S-shapes and demonstrated the modes of particles' passage through poly(dimethyl siloxane) (PDMS) channels [130]. However, little is known about the deformation behaviors of multilayer microcapsules with a size similar to RBC under flow in a smaller microchannel

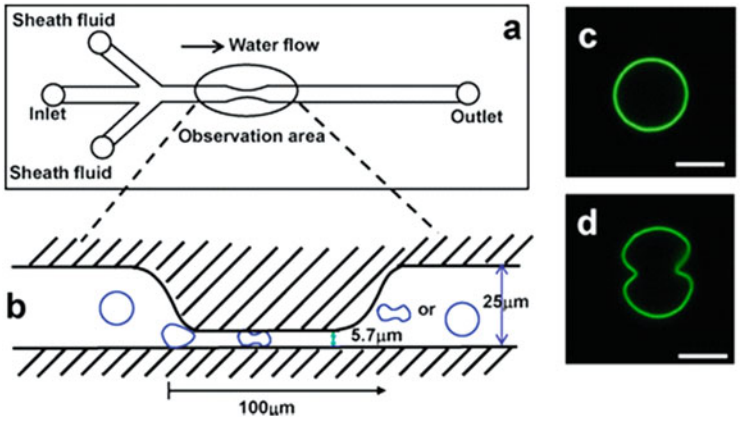

Fig. 4.7 Scheme drawing to show the structure of the microchannel device by (**a**) *top view* and (**b**) *side view*. CLSM images of the 6.8 μm (**c**) and 8.6 μm (**d**) (PAH/PSS)5 microcapsules after being squeezed through the microchannel with a height of 5.7 μm. The former can recover its original spherical shape (**c**), while the latter keeps its deformed shape (**d**). (Adapted with permission from Ref. [133]. Copyright 2012, American Chemical Society)

[131], although the static deformation behaviors have been systematically studied under the press of a colloidal probe [132] or osmotic pressure [34, 35].

Recently, the deformability of multilayer microcapsules under flow in a confined microchannel was studied in our lab (Fig. 4.7) [133]. The influences of capsule size, wall thickness, cross-linking, and the filling of PSS inside on the deformation and recovery behaviors of the capsules were systematically investigated. The recovery ability of capsules is dependent on the deformation extent but not mechanical strength. The squeezed hollow microcapsules can recover their original spherical shape when the deformation extent is smaller than 16%, whereas permanent physical deformation takes place at a larger deformation extent such as 34%. In a sharp contrast, all the intact capsules prefilled with PSS can recover their original shape even when the deformation extent is as large as 47%. The spontaneously loaded dyes can be well maintained after the deformation and recovery process. It is the first time to disclose the alteration of drug amount in multilayer microcapsules after flowing through a constriction.

Furthermore, the RBC-like multilayer microcapsules also have been successfully fabricated by templating on $Ca(OH)_2$ particles with an RBC-like shape through covalent LbL method. The capsules can preserve their RBC-like morphology well in water after template removal. When the RBC-like capsules (6.7 μm) are trapped in a microcapillary with a smaller size (5 μm), they deform only in the areas in contact with the capillary wall. After they are forced to pass through, 90% of the RBC-like capsules recover their original discoidal shape. By assembling additional hemoglobin layers on the RBC-like capsules, they can be endowed with oxygen-binding and release capacity [134].

Yet, this is only the first step toward the fabrication of RBC-mimicking multilayer capsules. Nonetheless, the current results are important not only for understanding of capsule properties but also for their practical applications as drug delivery carriers. For example, the capsules for injection application should have a smaller size, soft wall structure, and RBC-like shape, while those for embolization should have a stiff wall which can clog the blood vessels with higher efficiency.

4.3.4 Anisotropic Capsules Interact with Cells

As drug carriers, multilayer capsules should interact with different cells and may be internalized, which is of practical important for delivery of cargoes into cells. Thus, their interactions with cells draw much attention recently. It is well known that the physicochemical properties of colloidal particles can strongly influence their interactions with biological systems [135, 136]. Especially, the small differences on their physicochemical characteristics may strongly influence the interactions between particles and cells and further affect their cellular uptake, intracellular distribution, and ultimate cellular fate [137]. Recently, the shape of particles has been found to play a crucial role in the interactions between cells and particles and is regarded as a new important parameter for designing materials to realize specific biological functions [138, 139]. Smith and coworkers [140] demonstrated that the polystyrene particles with three shapes (spheres, prolate ellipsoids, and oblate ellipsoids) could manipulate different attachment and internalization of macrophages. Mitragotri and coworkers [141] found that compared with rods, the spherical polystyrene particles with identical total volumes exhibited significant perinuclear accumulation. When ovalbumin is used as a model antigen conjugated to particle surfaces, the regulation of immune response could be achieved by changing sizes and shapes of nanoparticles [142]. Moreover, in a model microvascular network, elongated particles exhibited higher adhesion and binding probability than spheres [143, 144]. In an in vivo experiment, the hydrogel microparticles mimicking the shape of red blood cells could possess the increased blood circulation and enhanced adhesion ability [145].

Polyelectrolyte multilayer microcapsules with tailored structures and properties have gained much interest in biomedical field especially for drug loading and release [10, 91–99]. However, researches about the interactions between anisotropic polyelectrolyte microcapsules and cells are rare [146, 147], and the mechanism of shape-induced difference in interactions between capsules and cells needs further investigation. For example, Caruso and coworkers [146] reported the fabrication of rod-shaped hydrogel capsules with tunable aspect ratios by a templating method. With increasing of the aspect ratios, slower and less cellular internalization of capsules was observed. Kharlampieva and coworkers [147] obtained polymer capsules with hemispherical geometry by drying poly(*N*-vinyl pyrrolidone)/tannic acid (PVPON/TA)n multilayer capsules and found that compared with their spherical and

cubic counterparts, the hemispherical capsules are taken up in a greater extent. However, the mechanism behind is not very clear.

More recently, bowl-like microcapsules were fabricated by osmotic-induced invagination of microcapsule in concentrated PSS solution [148]. Both the bowl-like and spherical capsules maintained their colloidal stability and shape in cell culture medium up to 7 days. The bowl-like microcapsules could be internalized with a faster rate and higher number by SMCs and macrophages than their spherical counterparts. Preferential attachment onto the cell membrane from the bend side and easier enwrapping by cell membranes are likely the major reasons enabling the uptake of the bowl-like capsules in priority than their spherical counterparts. Such results may help people to understand the role of capsule shape in the interaction with cells and provide useful guidance for further design of more efficient carriers.

4.3.5 Triggered Release of Encapsulated Substances from the Capsules

Although encapsulation of active substances into multilayer capsules can protect them from the influence of the environment, the encapsulated substances should be released in a triggered way at desired positions. Among various triggers, the remote stimuli-light and ultrasound (US) have the advantages of high temporal and spatial resolution and controllable power without direct contact. Thus in the following part, we will focus on these two methods.

The LbL method can integrate light-responsive building blocks into the shells of multilayer capsules. For example, Zapotoczny and coworkers incorporated a relatively small amount of multiwalled carbon nanotubes (MWCNTs) into the shells of multilayer capsules, leading to an almost 20-fold increase of the apparent elastic modulus of the obtained capsules [149]. Due to their absorption in the near-infrared region and specific arrangement of MWCNTs in the shells, the capsules can show a light-triggered enhancement of permeability in a reversible, nondestructive manner. Using this feature, durability and facile encapsulation/release of desired substances into/from microcapsules can be achieved, which is crucial for their practical applications.

US imaging has the advantages of low cost, fast real-time visualization, deep penetration in tissues, and noninvasiveness. More important, the US can trigger drug release via inertial cavitation-caused mechanical damage to the capsules, and also can achieve spatiotemporal controllable drug release. Compared with light, the penetration depth in tissues is much higher. By choosing proper functional building blocks during the assembly of multilayer capsules, the capsules can be endowed with US-sensitive properties. For example, integration of metal and metal oxide nanoparticles in multilayer capsules can improve their US sensitivity because of the increased shell density [150]. Fe_3O_4 nanoparticles-modified capsules can be broken into pieces after 60 s sonication at an energy density of 377 W/cm^2

[151]. ZnO nanoparticles-modified capsules also can be totally ruptured by US after 9 s at an energy density of 30 W/cm^2 [152]. However, the higher-power US used in these studies may result in tissue damage and other side effects. Kharlampieva and coworkers reported high US imaging contrast and low-power diagnostic or high-power therapeutic US-triggered drug release from hydrogen-bonded TA and PVPON multilayer capsules [153]. The capsules possess good and long-term US imaging contrast. Upon low-power diagnostic US irradiation, the encapsulated drug can be gradually released, while its fast release can be achieved via high-power therapeutic US irradiation. Furthermore, the US imaging contrast of capsules can be regulated by changing the number of layers, and the type and molecular weight of used polymers.

The integration of functional building blocks into the shells of multilayer capsules not only can increase the US sensitivity but also can endow the capsules with other specific functionalities. For example, Sukhorukov and coworkers developed an method to the in situ fabrication and assembly of fluorescent carbon dots (CDs) into the shells of multilayer capsules [154]. CDs are synthesized in situ in capsule shells by carbonization of dextran molecules via hydrothermal treatment. The obtained nanocomposite capsules have luminescence which can be used for imaging. The heat treatment also can encapsulate low-molecular-weight drug into the capsules. The in situ formation of CDs in capsule shells endows with US responsiveness; thus, the loaded drug can be released upon US treatment. The shells of multilayer capsules also can be functionalized with radionuclide for imaging via positron emission tomography (PET) [155]. The capsules are prepared via LbL assembly of TA and deferoxamine (DFO)-functionalized PVPON. DFO can chelate the 89Zr radionuclide. The in vivo PET imaging can track the capsules in vivo and reveal their biodistribution. The encapsulated hydrophilic anticancer drug can be released upon the irradiation of therapeutic US to the Zr-functionalized capsules. Similarly, multilayer capsules with iron oxide nanoparticles-incorporated shells also possess magnetic resonance imaging (MRI) and US-triggered drug release abilities and thus can achieve real-time tracking and targeted delivery in vivo [156]. Such kinds of capsules with imaging ability as well as US-triggered drug release should have broad applications in the biomedical field.

In order to better control the release of encapsulated substances, the multilayer capsules which can respond to multistimuli have been developed. For example, iron oxide and graphene oxide (GO) are assembled with polysaccharides through the LbL method to form the shells of multilayer capsules. The capsules can be loaded with drugs through pH control, while the iron oxide and GO empower the capsules with magnetic and light responsiveness. Thus, the alternative magnetic field and near-infrared laser can trigger the release of drugs on demand [157]. Sukhorukov and coworkers also designed triple-responsive inorganic–organic hybrid microcapsules for the controlled release of encapsulated drugs [158]. The UV light and US responses are endowed by the in situ deposited TiO_2 and SiO_2 nanostructures in the capsule shells through a sol–gel process. This process also can reduce the permeability of the capsules, leading to the encapsulation of low-molecular-weight drugs. The enzymatic response is achieved by using biodegradable polypeptides and

polysaccharides for the fabrication of capsules. Upon employing different stimuli, the encapsulated drug can be released according to different mechanisms at desired times. This work demonstrates that the multilayer capsules are ideal platforms for the design of multimodal-responsive drug carriers.

4.4 Microcapsules as Growth Factor Carriers and Their Incorporation into Scaffold

Spatial- and temporal-controlled delivery of growth factors is crucial for the efficient repair upon tissue injury or failure in tissue engineering. But delivery of growth factors to the site of tissue regeneration is challenging since these proteins have short half-lives, high molecular weight, and slow tissue penetration. Thus, the generally used strategy to enhance in vivo efficacy of growth factors is the use of growth factor-loaded delivery systems, which release growth factors in a controlled way. Due to the tailored structures, multiple functionalities, as well as controlled permeability, the multilayer capsules are promising candidates as growth factor carriers.

Several methods have been successfully developed to load different growth factors into multilayer capsules. Akashi and coworkers first developed biodegradable multilayer capsules to encapsulate basic fibroblast growth factor (bFGF) as a cytokine release carrier [159]. The multilayer capsules were fabricated via the layer-by-layer (LbL) assembly of chitosan and dextran sulfate. The bFGF was encapsulated into the capsules by reversibly controlling the capsule permeability. At pH $<$ 8.0, the capsule shell was nonpermeable for macromolecules. However, FITC-dextran with a molecular weight as high as 250 kDa could easily penetrate the capsules at pH $>$ 8.0. Using the pH-controlled reversible shell permeability, bFGF was successfully encapsulated into the capsules. Release of the encapsulated bFGF was sustained over 70 h. Due to the local and sustained release of bFGF, mouse L929 fibroblast cells proliferated well for 2 weeks. Antipina and coworker used a coprecipitation-based layer-by-layer encapsulation method to load bFGF into the microcapsules [160]. In this method, bFGF was first protected by heparin and bovine serum albumin and then coprecipitated into $CaCO_3$ microparticles. Low cytotoxic and biodegradable polyelectrolytes dextran sulfate and poly-L-arginine were used for capsule shell assembly on the $CaCO_3$ microparticles. The encapsulation efficiency was greatly influenced by the shell thickness. Under optimized conditions, a maximum encapsulation efficiency of 42% could be achieved. The controlled release of FGF2 from the microcapsules was helpful to enhance the proliferation of L929 cells. De Geest and coworkers introduced a postloading approach by engineering the capsules in such a way that they acted as growth factor-binding "microsponges" [161]. In this method, $CaCO_3$ microparticles doped with heparin were first fabricated by a coprecipitation method. Subsequently, these microparticles were coated with heparin/poly-L-arginine multilayers, followed by decomposition of the $CaCO_3$ core. In this way, hollow capsules were obtained with

heparin both as membrane component and being suspended in their hollow void. Heparin is well known to have a high affinity for several growth factors. Therefore, the engineered microcapsules with high heparin content will enhance their growth factor-binding capacity. Transforming growth factor-beta 1 (TGF-beta 1) could be loaded and released from such kind of heparin-engineered microcapsules without affecting its biological activity. The growth factor-loaded multilayer capsules could be easily incorporated within a gelatin tissue engineering scaffold without affecting the properties of this scaffold.

Benkirane-Jessel and coworkers first demonstrated that a hydrogel scaffold incorporated with the growth factor-loaded multilayer capsules could induce bone formation in vivo [162]. In this research, bone morphogenetic proteins (BMP_2) and TGF-beta 1 were assembled into the shell of biodegradable multilayer microcapsules. The stem cells were differentiated into bone cells when cocultured with growth factor-loaded multilayer capsules. More importantly, when such kind of capsules were integrated with alginate gel and implanted into mice, inducing bone formation in vivo was observed. The in vivo results demonstrate the promising application potential of multilayer microcapsules as growth factor carriers in the field of tissue engineering and regenerative medicine.

4.5 Conclusions and Outlooks

The LbL assembly technique is a highly versatile and powerful platform for the fabrication of capsules with tailored structures and functions. They have already shown their great promise of applications in many areas, especially in the field of controlled release. Recently, much attention has been paid on the multilayer capsules assembled by new driving forces and those with highly sophisticated structures for biomedical applications, such as drug and growth factor carriers, as highlighted in this chapter.

Although the significant advances have been made in this area, there are still some key obstacles which should be overcome. First, for the real practical applications of multilayer capsules, rapid, scalable, and efficient new preparation methods should be developed. One recent example is the microcapsule preparation technique utilizing a fluidized bed for the LbL assembly of polymers [163]. The properties of obtained microcapsules are in close agreement with conventionally prepared LbL capsules. The technique provides a new way to rapidly generate microcapsules, while being also amenable to scale-up and mass production. Furthermore, a fully flow-based technique using tangential flow filtration (TFF) for LbL assembly on particles was developed [164]. Multilayered particles and capsules with size ranging from micrometers to submicrometers can be assembled on different templates using diverse polymers. The well-controlled, integrated, and automatable nature of the TFF LbL system provides significant progress of the practical applications of LbL systems. Second, the in vivo behaviors of LbL capsules such as degradation and toxicity are largely unexplored. For intravenous injection, the LbL capsules are

required to circulate in the bloodstream and have good hemocompatibility. Several recent researches have shown that coating of blood-compatible multilayers on the ultrasmall (~20 nm) [165, 166] and submicron (~500 nm) [167] particles is beneficial to obtain injectable capsule drug delivery systems. Therefore, particles with a submicron size are attractive for preparation of LbL capsules, which may accumulate in cancerous tissues through EPR effect.

The LbL capsules with tailed structures and functions can be loaded with both drugs and imaging agents within a single system to form theranostic carriers, which can selectively accumulate in diseased tissues and simultaneously report their biochemical and morphological characteristics. At the same time, the synergistic carriers which carry chemo-, radio-, and gene therapeutics can enhance the treatment efficacy [168, 169].

For successful tissue regeneration, it is extremely important to provide cells with a local environment using biomaterials which enable them to proliferate and differentiate efficiently and correctly, resulting in cell-induced tissue regeneration. For this purpose, capsules or spheres can be integrated into different scaffolds to provide for prolonged, site-specific delivery of loaded growth factors, drugs, as well as other bioactive species. The capsules should be well designed with properly controlled release profile as well as surface properties, so that they can act as an integral part of the porous three-dimensional scaffolds, and their incorporation does not significantly affect the scaffold properties but can release their cargoes to meet the needs of cells.

The researches and applications of LbL multilayer capsules are highly multidisciplinary. With the efforts afforded by the experts from fields of chemistry, materials science, mechanical engineering, biology, and so on, the abovementioned obstacles will be overcome sooner or later, and more achievements in this field can be expected in the future.

Acknowledgments The research is financially supported by the Natural Science Foundation of China (51120135001 and 21374101, 21174130, 20804036), Ph.D. Programs Foundation of the Ministry of Education of China (20110101130005), and Zhejiang Provincial Natural Science Foundation of China (Y4110064).

References

1. Caruso F. Hollow capsule processing through colloidal templating and self-assembly. Chem Eur J. 2000;6:413–9.
2. Decher G, Hong JD. Buildup of ultrathin multilayer films by a self-assembly process.1. Consecutive adsorption of anionic and cationic bipolar amphiphiles on charged surfaces. Makromol Chem Macromol Symp. 1991;46:321–7.
3. Decher G. Fuzzy nanoassemblies: toward layered polymeric multicomposites. Science. 1997;277:1232–7.
4. Caruso F, Caruso RA, Mohwald H. Nanoengineering of inorganic and hybrid hollow spheres by colloidal templating. Science. 1998;282:1111–4.
5. Donath E, Sukhorukov GB, Caruso F, Davis SA, Mohwald H. Novel hollow polymer shells by colloid-templated assembly of polyelectrolytes. Angew Chem Int Ed. 1998;37:2202–5.

6. Peyratout CS, Dahne L. Tailor-made polyelectrolyte microcapsules: from multilayers to smart containers. Angew Chem Int Ed. 2004;43:3762–83.
7. Tong WJ, Gao CY. Multilayer microcapsules with tailored structures for bio-related applications. J Mater Chem. 2008;18:3799–812.
8. Sukhorukov GB, Rogach AL, Garstka M, Springer S, Parak WJ, Munoz-Javier A, Kreft O, Skirtach AG, Susha AS, Ramaye Y, Palankar R, Winterhalter M. Multifunctionalized polymer microcapsules: novel tools for biological and pharmacological applications. Small. 2007;3: 944–55.
9. Sukhorukov GB, Mohwald H. Multifunctional cargo systems for biotechnology. Trends Biotechnol. 2007;25:93–8.
10. Tong WJ, Song XX, Gao CY. Layer-by-layer assembly of microcapsules and their biomedical applications. Chem Soc Rev. 2012;41(18):6103–24.
11. Pastoriza-Santos I, Scholer B, Caruso F. Core-shell colloids and hollow polyelectrolyte capsules based on diazoresins. Adv Funct Mater. 2001;11:122–8.
12. Mauser T, Dejugnat C, Sukhorukov GB. Reversible ph-dependent properties of multilayer microcapsules made of weak polyelectrolytes. Macromol Rapid Commun. 2004;25:1781–5.
13. Zhu HG, McShane MJ. Macromolecule encapsulation in diazoresin-based hollow polyelectrolyte microcapsules. Langmuir. 2005;21:424–30.
14. Sukhishvili SA, Granick S. Layered, erasable, ultrathin polymer films. J Am Chem Soc. 2000;122:9550–1.
15. Sukhishvili SA, Granick S. Layered, erasable polymer multilayers formed by hydrogen-bonded sequential self-assembly. Macromolecules. 2002;35:301–10.
16. Yang SY, Rubner MF. Micropatterning of polymer thin films with ph-sensitive and cross-linkable hydrogen-bonded polyelectrolyte multilayers. J Am Chem Soc. 2002;124:2100–1.
17. Yang SY, Lee D, Cohen RE, Rubner MF. Bioinert solution-cross-linked hydrogen-bonded multilayers on colloidal particles. Langmuir. 2004;20:5978–81.
18. Kozlovskaya V, Ok S, Sousa A, Libera M, Sukhishvili SA. Hydrogen-bonded polymer capsules formed by layer-by-layer self-assembly. Macromolecules. 2003;36:8590–2.
19. Tong WJ, Gao CY. Stable microcapsules assembled stepwise from weak polyelectrolytes followed by thermal crosslinking. Polym Adv Technol. 2005;16:827–33.
20. Zelikin AN, Quinn JF, Caruso F. Disulfide cross-linked polymer capsules: En route to biodeconstructible systems. Biomacromolecules. 2006;7:27–30.
21. Such GK, Johnston APR, Caruso F. Engineered hydrogen-bonded polymer multilayers: from assembly to biomedical applications. Chem Soc Rev. 2011;40:19–29.
22. Connal LA, Kinnane CR, Zelikin AN, Caruso F. Stabilization and functionalization of polymer multilayers and capsules via thiol-ene click chemistry. Chem Mater. 2009;21:576–8.
23. Kinnane CR, Such GK, Antequera-Garcia G, Yan Y, Dodds SJ, Liz-Marzan LM, Caruso F. Low-fouling poly(n-vinyl pyrrolidone) capsules with engineered degradable properties. Biomacromolecules. 2009;10:2839–46.
24. Ochs CJ, Such GK, Yan Y, van Koeverden MP, Caruso F. Biodegradable click capsules with engineered drug-loaded multilayers. ACS Nano. 2010;4:1653–63.
25. Leung MKM, Such GK, Johnston APR, Biswas DP, Zhu ZY, Yan Y, Lutz JF, Caruso F. Assembly and degradation of low-fouling click-functionalized poly(ethylene glycol)-based multilayer films and capsules. Small. 2011;7:1075–85.
26. Ng SL, Such GK, Johnston APR, Antequera-Garcia G, Caruso F. Controlled release of DNA from poly(vinylpyrrolidone) capsules using cleavable linkers. Biomaterials. 2011;32:6277–84.
27. Ochs CJ, Such GK, Caruso F. Modular assembly of layer-by-layer capsules with tailored degradation profiles. Langmuir. 2011;27:1275–80.
28. Liang K, Such GK, Zhu ZY, Yan Y, Lomas H, Caruso F. Charge-shifting click capsules with dual-responsive cargo release mechanisms. Adv Mater. 2011;23:H273–7.
29. Tong WJ, Gao CY, Mohwald H. Manipulating the properties of polyelectrolyte microcapsules by glutaraldehyde cross-linking. Chem Mater. 2005;17:4610–6.

30. Tong WJ, Gao CY, Mohwald H. Stable weak polyelectrolyte microcapsules with ph-responsive permeability. Macromolecules. 2006;39:335–40.
31. Sukhorukov GB, Donath E, Lichtenfeld H, Knippel E, Knippel M, Budde A, Mohwald H. Layer-by-layer self assembly of polyelectrolytes on colloidal particles. Colloids Surf A Physicochem Eng Asp. 1998;137:253–66.
32. Zhang YJ, Yang SG, Guan Y, Cao WX, Xu J. Fabrication of stable hollow capsules by covalent layer-by-layer self-assembly. Macromolecules. 2003;36:4238–40.
33. Feng ZQ, Wang ZP, Gao CY, Shen JC. Direct covalent assembly to fabricate microcapsules with ultrathin walls and high mechanical strength. Adv Mater. 2007;19:3687–91.
34. Gao C, Donath E, Moya S, Dudnik V, Mohwald H. Elasticity of hollow polyelectrolyte capsules prepared by the layer-by-layer technique. Eur Phys J E Soft Matter Biol Phys. 2001;5:21–7.
35. Gao CY, Leporatti S, Moya S, Donath E, Mohwald H. Stability and mechanical properties of polyelectrolyte capsules obtained by stepwise assembly of poly(styrenesulfonate sodium salt) and poly(diallyldimethyl ammonium) chloride onto melamine resin particles. Langmuir. 2001;17:3491–5.
36. Tong WJ, Gao CY, Mohwald H. Single polyelectrolyte microcapsules fabricated by glutaraldehyde-mediated covalent layer-by-layer assembly. Macromol Rapid Commun. 2006;27:2078–83.
37. Tong WJ, Gao CY, Mohwald H. Poly(ethyleneimine) microcapsules: glutaraldehyde-mediated assembly and the influence of molecular weight on their properties. Polym Adv Technol. 2008;19:817–23.
38. Such GK, Tjipto E, Postma A, Johnston APR, Caruso F. Ultrathin, responsive polymer click capsules. Nano Lett. 2007;7:1706–10.
39. Peters T. Serum-albumin. Adv Protein Chem. 1985;37:161–245.
40. Carter DC, Ho JX. Structure of serum-albumin. Adv Protein Chem. 1994;45:153–203.
41. Rubino OP, Kowalsky R, Swarbrick J. Albumin microspheres as a drug-delivery system – relation among turbidity ratio, degree of cross-linking, and drug-release. Pharm Res. 1993;10: 1059–65.
42. Tong WJ, Gao CY, Moehwald H. Ph-responsive protein microcapsules fabricated via glutaraldehyde mediated covalent layer-by-layer assembly. Colloid Polym Sci. 2008;286:1103–9.
43. Wang ZP, Feng ZQ, Gao CY. Stepwise assembly of the same polyelectrolytes using host-guest interaction to obtain microcapsules with multiresponsive properties. Chem Mater. 2008;20: 4194–9.
44. Johnston APR, Read ES, Caruso F. DNA multilayer films on planar and colloidal supports: sequential assembly of like-charged polyelectrolytes. Nano Lett. 2005;5:953–6.
45. Quiocho FA. Carbohydrate-binding proteins – tertiary structures and protein-sugar interactions. Annu Rev Biochem. 1986;55:287–315.
46. Lee YC, Lee RT. Carbohydrate-protein interactions – basis of glycobiology. Acc Chem Res. 1995;28:321–7.
47. Nelson RM, Venot A, Bevilacqua MP, Linhardt RJ, Stamenkovic I. Carbohydrate-protein interactions in vascular biology. Annu Rev Cell Dev Biol. 1995;11:601–31.
48. Lis H, Sharon N. Lectins: carbohydrate-specific proteins that mediate cellular recognition. Chem Rev. 1998;98:637–74.
49. Becker JW, Reeke GN, Cunningham BA, Edelman GM. New evidence on location of saccharide-binding site of concanavalin-a. Nature. 1976;259:406–9.
50. Goldstein IJ, Hollerman CE, Smith EE. Protein-carbohydrate interaction. 2. Inhibition studies on interaction of concanavalin a with polysaccharides. Biochemistry. 1965;4:876–83.
51. Lvov Y, Ariga K, Ichinose I, Kunitake T. Layer-by-layer architectures of concanavalin a by means of electrostatic and biospecific interactions. J Chem Soc Chem Commun. 1995;22: 2313–4.

52. Lvov Y, Ariga K, Ichinose I, Kunitake T. Molecular film assembly via layer-by-layer adsorption of oppositely charged macromolecules (linear polymer, protein and clay) and concanavalin a and glycogen. Thin Solid Films. 1996;284:797–801.
53. Sato K, Imoto Y, Sugama J, Seki S, Inoue H, Odagiri T, Hoshi T, Anzai J. Sugar-induced disintegration of layer-by-layer assemblies composed of concanavalin a and glycogen. Langmuir. 2005;21:797–9.
54. Zhu Y, Tong WJ, Gao CY. Molecular-engineered polymeric microcapsules assembled from concanavalin a and glycogen with specific responses to carbohydrates. Soft Matter. 2011;7: 5805–15.
55. Walker SA, Kennedy MT, Zasadzinski JA. Encapsulation of bilayer vesicles by self-assembly. Nature. 1997;387:61–4.
56. Lutz JF, Laschewsky A. Multicompartment micelles: has the long-standing dream become a reality? Macromol Chem Phys. 2005;206:813–7.
57. De Geest BG, De Koker S, Immesoete K, Demeester J, De Smedt SC, Hennink WE. Self-exploding beads releasing microcarriers. Adv Mater. 2008;20:3687–91.
58. Zhang Y, Ruder WC, Leduc PR. Artificial cells: building bioinspired systems using small-scale biology. Trends Biotechnol. 2008;26:14–20.
59. Delcea M, Yashchenok A, Videnova K, Kreft O, Mohwald H, Skirtach AG. Multicompartmental micro- and nanocapsules: hierarchy and applications in biosciences. Macromol Biosci. 2010;10:465–74.
60. Kreft O, Prevot M, Mohwald H, Sukhorukov GB. Shell-in-shell microcapsules: a novel tool for integrated, spatially confined enzymatic reactions. Angew Chem Int Ed. 2007;46:5605–8.
61. De Geest BG, McShane MJ, Demeester J, De Smedt SC, Hennink WE. Microcapsules ejecting nanosized species into the environment. J Am Chem Soc. 2008;130:14480–2.
62. Stadler B, Chandrawati R, Price AD, Chong SF, Breheney K, Postma A, Connal LA, Zelikin AN, Caruso F. A microreactor with thousands of subcompartments: enzyme-loaded liposomes within polymer capsules. Angew Chem Int Ed. 2009;48:4359–62.
63. Hosta-Rigau L, Stadler B, Yan Y, Nice EC, Heath JK, Albericio F, Caruso F. Capsosomes with multilayered subcompartments: assembly and loading with hydrophobic cargo. Adv Funct Mater. 2010;20:59–66.
64. Chandrawati R, Stadler B, Postma A, Connal LA, Chong SF, Zelikin AN, Caruso F. Cholesterol-mediated anchoring of enzyme-loaded liposomes within disulfide-stabilized polymer carrier capsules. Biomaterials. 2009;30:5988–98.
65. Hosta-Rigau L, Chung SF, Postma A, Chandrawati R, Stadler B, Caruso F. Capsosomes with "free-floating" liposomal subcompartments. Adv Mater. 2011;23:4082–7.
66. Stadler B, Chandrawati R, Goldie K, Caruso F. Capsosomes: subcompartmentalizing polyelectrolyte capsules using liposomes. Langmuir. 2009;25:6725–32.
67. Gohy JF. Block copolymer micelles. In: Block copolymers ii. Berlin: Springer; 2005. p. 65–136.
68. Zhu Y, Tong WJ, Gao CY, Mohwald H. Assembly of polymeric micelles into hollow microcapsules with extraordinary stability against extreme ph conditions. Langmuir. 2008;24:7810–6.
69. Li XD, Lu T, Zhang JX, Xu JJ, Hu QL, Zhao SF, Shen JC. A study of properties of "micelle-enhanced" polyelectrolyte capsules: structure, encapsulation and in vitro release. Acta Biomater. 2009;5:2122–31.
70. Tong WJ, Zhu Y, Wang ZP, Gao CY, Mohwald H. Micelles-encapsulated microcapsules for sequential loading of hydrophobic and water-soluble drugs. Macromol Rapid Commun. 2010;31:1015–9.
71. Gao CY, Donath E, Mohwald H, Shen JC. Spontaneous deposition of water-soluble substances into microcapsules: phenomenon, mechanism, and application. Angew Chem Int Ed. 2002;41:3789–93.

72. Gao CY, Liu XY, Shen JC, Mohwald H. Spontaneous deposition of horseradish peroxidase into polyelectrolyte multilayer capsules to improve its activity and stability. Chem Commun. 2002;17:1928–9.
73. Liu XY, Gao CY, Shen JC, Mohwald H. Multilayer microcapsules as anti-cancer drug delivery vehicle: deposition, sustained release, and in vitro bioactivity. Macromol Biosci. 2005;5: 1209–19.
74. Mao ZW, Ma L, Gao CY, Shen JC. Preformed microcapsules for loading and sustained release of ciprofloxacin hydrochloride. J Control Release. 2005;104:193–202.
75. Zhao QH, Zhang SA, Tong WJ, Gao CY, Shen JC. Polyelectrolyte microcapsules templated on poly(styrene sulfonate)-doped $CaCO_3$ particles for loading and sustained release of daunorubicin and doxorubicin. Eur Polym J. 2006;42:3341–51.
76. He Q, Song WX, Moehwald H, Li JB. Hydrothermal-induced structure transformation of polyelectrolyte multilayers: from nanotubes to capsules. Langmuir. 2008;24:5508–13.
77. Wang JG, Xiao Q, Zhou HJ, Sun PC, Yuan ZY, Li BH, Ding DT, Shi AC, Chen TH. Budded, mesoporous silica hollow spheres: hierarchical structure controlled by kinetic self-assembly. Adv Mater. 2006;18:3284–8.
78. Yu K, Zhang L, Eisenberg A. Novel morphologies of "crew-cut" aggregates of amphiphilic diblock copolymers in dilute solution. Langmuir. 1996;12:5980–4.
79. Tung PH, Kuo SW, Chan SC, Hsu CH, Wang CF, Chang FC. Micellization and the surface hydrophobicity of amphiphilic poly(vinylphenol)-*block*-polystyrene block copolymers. Macromol Chem Phys. 2007;208:1823–31.
80. Sha K, Li D, Li Y, Zhang B, Wang J. The chemoenzymatic synthesis of a novel cbabc-type pentablock copolymer and its self-assembled "crew-cut" aggregation. Macromolecules. 2007;41:361–71.
81. Menger FM, Seredyuk VA. Internally catalyzed separation of adhered lipid membranes. J Am Chem Soc. 2003;125:11800–1.
82. Zhou YF, Yan DY. Real-time membrane fission of giant polymer vesicles. Angew Chem Int Ed. 2005;44:3223–6.
83. Zhou YF, Yan DY. Real-time membrane fusion of giant polymer vesicles. J Am Chem Soc. 2005;127:10468–9.
84. Wang ZP, Mohwald H, Gao CY. Preparation and redox-controlled reversible response of ferrocene-modified poly(allylamine hydrochloride) microcapsules. Langmuir. 2011;27:1286–91.
85. Wang ZP, Mohwald H, Gao CY. Nanotubes protruding from poly(allylamine hydrochloride)-graft-pyrene microcapsules. ACS Nano. 2011;5:3930–6.
86. Wang ZP, Xie Y, Gao CY. Repeated protrusion of fluorescent pyrene nanorods on the surface of crosslinked poly(allylamine hydrochloride) microcapsules. RSC Adv. 2012;2:11354–8.
87. Wang ZP, Liu MY, Xie Y, Gao CY. In situ fabrication of pyrene derivative nanorods inside polyelectrolytes microcapsules with tunable fluorescent properties. J Mater Chem. 2012;22: 2855–8.
88. Guan EJ, Wang TX, Wang ZP, Gao CY. Modulating the nanorods protrusion from poly (allylamine hydrochloride)-*g*-pyrene microcapsules by 1-pyrenesulfonic acid sodium salt. J Colloid Interface Sci. 2013;405:10–6.
89. Wang ZP, Skirtach AG, Xie Y, Liu MY, Mohwald H, Gao CY. Core-shell poly(allyamine hydrochloride)-pyrene nanorods decorated with gold nanoparticles. Chem Mater. 2011;23: 4741–7.
90. Wang TX, Cai YB, Wang ZP, Guan EJ, Yu DH, Qin AJ, Sun JZ, Tang BZ, Gao CY. Decomposition-assembly of tetraphenylethylene nanoparticles with uniform size and aggregation-induced emission property. Macromol Rapid Commun. 2012;33:1584–9.
91. De Geest BG, De Koker S, Sukhorukov GB, Kreft O, Parak WJ, Skirtach AG, Demeester J, De Smedt SC, Hennink WE. Polyelectrolyte microcapsules for biomedical applications. Soft Matter. 2009;5:282–91.

92. De Geest BG, Sukhorukov GB, Mohwald H. The pros and cons of polyelectrolyte capsules in drug delivery. Expert Opin Drug Deliv. 2009;6:613–24.
93. Johnston APR, Such GK, Ng SL, Caruso F. Challenges facing colloidal delivery systems: from synthesis to the clinic. Curr Opin Colloid Interface Sci. 2011;16:171–81.
94. Johnston APR, Such GK, Caruso F. Triggering release of encapsulated cargo. Angew Chem Int Ed. 2010;49:2664–6.
95. De Cock LJ, De Koker S, De Geest BG, Grooten J, Vervaet C, Remon JP, Sukhorukov GB, Antipina MN. Polymeric multilayer capsules in drug delivery. Angew Chem Int Ed. 2010;49: 6954–73.
96. Yan Y, Such GK, Johnston APR, Lomas H, Caruso F. Toward therapeutic delivery with layer-by-layer engineered particles. ACS Nano. 2011;5:4252–7.
97. De Koker S, Lambrecht BN, Willart MA, van Kooyk Y, Grooten J, Vervaet C, Remon JP, De Geest BG. Designing polymeric particles for antigen delivery. Chem Soc Rev. 2011;40:320–39.
98. De Koker S, Hoogenboom R, De Geest BG. Polymeric multilayer capsules for drug delivery. Chem Soc Rev. 2012;41:2867–84.
99. Ariga K, McShane M, Lvov YM, Ji QM, Hill JP. Layer-by-layer assembly for drug delivery and related applications. Expert Opin Drug Deliv. 2011;8:633–44.
100. Sukhorukov GB, Brumen M, Donath E, Mohwald H. Hollow polyelectrolyte shells: exclusion of polymers and donnan equilibrium. J Phys Chem B. 1999;103:6434–40.
101. Tong WJ, Dong WF, Gao CY, Mohwald H. Charge-controlled permeability of polyelectrolyte microcapsules. J Phys Chem B. 2005;109:13159–65.
102. Tong WJ, Song HQ, Gao CY, Mohwald H. Equilibrium distribution of permeants in polyelectrolyte microcapsules filled with negatively charged polyelectrolyte: the influence of ionic strength and solvent polarity. J Phys Chem B. 2006;110:12905–9.
103. Zhao QH, Mao ZW, Gao CY, Shen JC. Assembly of multilayer microcapsules on $CaCO_3$ particles from biocompatible polysaccharides. J Biomater Sci Polym Ed. 2006;17:997–1014.
104. Zhao QH, Han BS, Wang ZH, Gao CY, Peng CH, Shen JC. Hollow chitosan-alginate multilayer microcapsules as drug delivery vehicle: doxorubicin loading and in vitro and in vivo studies. Nanomed Nanotechnol Biol Med. 2007;3:63–74.
105. Kohler K, Shchukin DG, Mohwald H, Sukhorukov GB. Thermal behavior of polyelectrolyte multilayer microcapsules. 1. The effect of odd and even layer number. J Phys Chem B. 2005;109:18250–9.
106. Kohler K, Mohwald H, Sukhorukov GB. Thermal behavior of polyelectrolyte multilayer microcapsules: 2. Insight into molecular mechanisms for the pdadmac/pss system. J Phys Chem B. 2006;110:24002–10.
107. Sadasivan S, Kohler K, Sukhorukov GB. Fabrication of organized porphyrin-nanotube-attached heat-sensitive polyelectrolyte capsules. Adv Funct Mater. 2006;16:2083–8.
108. Song WX, He Q, Mohwald H, Yang Y, Li JB. Smart polyelectrolyte microcapsules as carriers for water-soluble small molecular drug. J Control Release. 2009;139:160–6.
109. Tong WJ, She SP, Xie LL, Gao CY. High efficient loading and controlled release of low-molecular-weight drugs by combination of spontaneous deposition and heat-induced shrinkage of multilayer capsules. Soft Matter. 2011;7:8258–65.
110. Han YY, Bu J, Zhang YY, Tong WJ, Gao CY. Encapsulation of photosensitizer into multilayer microcapsules by combination of spontaneous deposition and heat-induced shrinkage for photodynamic therapy. Macromol Biosci. 2012;12:1436–42.
111. Luo D, Gould DJ, Sukhorukov GB. Local and sustained activity of doxycycline delivered with layer-by-layer microcapsules. Biomacromolecules. 2016;17:1466–76.
112. Kozlovskaya V, Chen J, Zavgorodnya O, Hasan MB, Kharlampieva E. Multilayer hydrogel capsules of interpenetrated network for encapsulation of small molecules. Langmuir. 2018;34: 11832–42.

113. Gao H, Goryacheva OA, Tarakina NV, Sukhorukov GB. Intracellularly biodegradable polyelectrolyte/silica composite microcapsules as carriers for small molecules. ACS Appl Mater Interfaces. 2016;8:9651–61.
114. Hans ML, Lowman AM. Biodegradable nanoparticles for drug delivery and targeting. Curr Opin Solid State Mater Sci. 2002;6:319–27.
115. Uhrich KE, Cannizzaro SM, Langer RS, Shakesheff KM. Polymeric systems for controlled drug release. Chem Rev. 1999;99:3181–98.
116. Zhou J, Romero G, Rojas E, Ma L, Moya S, Gao CY. Layer by layer chitosan/alginate coatings on poly(lactide-*co*-glycolide) nanoparticles for antifouling protection and folic acid binding to achieve selective cell targeting. J Colloid Interface Sci. 2010;345:241–7.
117. Zhou J, Romero G, Rojas E, Moya S, Ma L, Gao CY. Folic acid modified poly(lactide-*co*-glycolide) nanoparticles, layer-by-layer surface engineered for targeted delivery. Macromol Chem Phys. 2010;211:404–11.
118. Zhou J, Moya S, Ma L, Gao CY, Shen JC. Polyelectrolyte coated plga nanoparticles: templation and release behavior. Macromol Biosci. 2009;9:326–35.
119. Xie L, Tong W, Yu D, Xu J, Li J, Gao C. Bovine serum albumin nanoparticles modified with multilayers and aptamers for ph-responsive and targeted anti-cancer drug delivery. J Mater Chem. 2012;22:6053–60.
120. Kim JK, Choi KJ, Lee M, Jo MH, Kim S. Molecular imaging of a cancer-targeting theragnostics probe using a nucleolin aptamer- and microrna-221 molecular beacon-conjugated nanoparticle. Biomaterials. 2012;33:207–17.
121. Iwasaki H, Nabeshima K, Nishio J, Jimi S, Aoki M, Koga K, Hamasaki M, Hayashi H, Mogi A. Pathology of soft-tissue tumors: daily diagnosis, molecular cytogenetics and experimental approach. Pathol Int. 2009;59:501–21.
122. Xie LL, Tong WJ, Xu JQ, Gao CY. Multilayers and poly(allylamine hydrochloride)-graft-poly (ethylene glycol) (pah-g-peg) modified bovine serum albumin nanoparticles: improved stability and ph-responsive drug delivery. Chin J Polym Sci. 2012;30:719–26.
123. Szczepanowicz K, Bzowska M, Kruk T, Karabasz A, Bereta J, Warszynski P. Pegylated polyelectrolyte nanoparticles containing paclitaxel as a promising candidate for drug carriers for passive targeting. Colloids Surf B. 2016;143:463–71.
124. Jafari A, Sun HT, Sun BY, Mohamed MA, Cui HG, Cheng C. Layer-by-layer preparation of polyelectrolyte multilayer nanocapsules via crystallized miniemulsions. Chem Commun. 2019;55:1267–70.
125. Pei HY, Bai YY, Guo JM, Gao ZL, Dai Q, Yu Q, Cui JW. Tunable morphologies of polymer capsules templated from cuprous oxide particles for control over cell association. Chin Chem Lett. 2020;31:505–8.
126. Elizarova IS, Luckham PF. Fabrication of polyelectrolyte multilayered nano-capsules using a continuous layer-by-layer approach. J Colloid Interface Sci. 2016;470:92–9.
127. Schneider G, Decher G. Functional core/shell nanoparticles via layer-by-layer assembly. Investigation of the experimental parameters for controlling particle aggregation and for enhancing dispersion stability. Langmuir. 2008;24:1778–89.
128. Doshi N, Zahr AS, Bhaskar S, Lahann J, Mitragotri S. Red blood cell-mimicking synthetic biomaterial particles. Proc Natl Acad Sci U S A. 2009;106:21495–9.
129. Hayashi K, Ono K, Suzuki H, Sawada M, Moriya M, Sakamoto W, Yogo T. Electrosprayed synthesis of red-blood-cell-like particles with dual modality for magnetic resonance and fluorescence imaging. Small. 2010;6:2384–91.
130. Haghgooie R, Toner M, Doyle PS. Squishy non-spherical hydrogel microparticles. Macromol Rapid Commun. 2010;31:128–34.
131. Prevot M, Cordeiro AL, Sukhorukov GB, Lvov Y, Besser RS, Mohwald H. Design of a microfluidic system to investigate the mechanical properties of layer-by-layer fabricated capsules. Macromol Mater Eng. 2003;288:915–9.
132. Dubreuil F, Elsner N, Fery A. Elastic properties of polyelectrolyte capsules studied by atomic-force microscopy and ricm. Eur Phys J E Soft Matter Biol Phys. 2003;12:215–21.

133. She S, Xu C, Yin X, Tong W, Gao C. Shape deformation and recovery of multilayer microcapsules after being squeezed through a microchannel. Langmuir. 2012;28:5010–6.
134. She S, Li Q, Shan B, Tong W, Gao C. Fabrication of red-blood-cell-like polyelectrolyte microcapsules and their deformation and recovery behavior through a microcapillary. Adv Mater. 2013;25:5814–8.
135. Toy R, Peiris PM, Ghaghada KB, Karathanasis E. Shaping cancer nanomedicine: the effect of particle shape on the in vivo journey of nanoparticles. Nanomedicine. 2014;9:121–34.
136. Albanese A, Tang PS, Chan WC. The effect of nanoparticle size, shape, and surface chemistry on biological systems. Annu Rev Biomed Eng. 2012;14:1–16.
137. Nel AE, Maedler L, Velegol D, Xia T, Hoek EMV, Somasundaran P, Klaessig F, Castranova V, Thompson M. Understanding biophysicochemical interactions at the nano-bio interface. Nat Mater. 2009;8:543–57.
138. Huang X, Teng X, Chen D, Tang F, He J. The effect of the shape of mesoporous silica nanoparticles on cellular uptake and cell function. Biomaterials. 2010;31:438–48.
139. Alexander JF, Kozlovskaya V, Chen J, Kuncewicz T, Kharlampieva E, Godin B. Cubical shape enhances the interaction of layer-by-layer polymeric particles with breast cancer cells. Adv Healthc Mater. 2015;4:2657–66.
140. Sharma G, Valenta DT, Altman Y, Harvey S, Xie H, Mitragotri S, Smith JW. Polymer particle shape independently influences binding and internalization by macrophages. J Control Release. 2010;147:408–12.
141. Kolhar P, Mitragotri S. Polymer microparticles exhibit size and shape dependent accumulation around the nucleus after endocytosis. Adv Funct Mater. 2012;22:3759–64.
142. Kumar S, Anselmo AC, Banerjee A, Zakrewsky M, Mitragotri S. Shape and size-dependent immune response to antigen-carrying nanoparticles. J Control Release. 2015;220:141–8.
143. Doshi N, Prabhakarpandian B, Rea-Ramsey A, Pant K, Sundaram S, Mitragotri S. Flow and adhesion of drug carriers in blood vessels depend on their shape: a study using model synthetic microvascular networks. J Control Release. 2010;146:196–200.
144. Shah S, Liu Y, Hu W, Gao J. Modeling particle shape-dependent dynamics in nanomedicine. J Nanosci Nanotechnol. 2011;11:919–28.
145. Merkel TJ, Jones SW, Herlihy KP, Kersey FR, Shields AR, Napier M, Luft JC, Wu H, Zamboni WC, Wang AZ, Bear JE, DeSimone JM. Using mechanobiological mimicry of red blood cells to extend circulation times of hydrogel microparticles. Proc Natl Acad Sci U S A. 2011;108:586–91.
146. Shimoni O, Yan Y, Wang Y, Caruso F. Shape-dependent cellular processing of polyelectrolyte capsules. ACS Nano. 2013;7:522–30.
147. Chen J, Kozlovskaya V, Goins A, Campos-Gomez J, Saeed M, Kharlampieva E. Biocompatible shaped particles from dried multilayer polymer capsules. Biomacromolecules. 2013;14:3830–41.
148. Li HY, Zhang WB, Tong WJ, Gao CY. Enhanced cellular uptake of bowl-like microcapsules. ACS Appl Mater Interfaces. 2016;8:11210–4.
149. Chojnacka-Gorka K, Wolski K, Zapotoczny S. Durable polyelectrolyte microcapsules with near-infrared-triggered loading and nondestructive release of cargo. ACS Appl Mater Interfaces. 2021;13:1562–72.
150. Skirtach AG, De Geest BG, Mamedov A, Antipov AA, Kotov NA, Sukhorukov GB. Ultrasound stimulated release and catalysis using polyelectrolyte multilayer capsules. J Mater Chem. 2007;17:1050–4.
151. Shchukin DG, Gorin DA, Möhwald H. Ultrasonically induced opening of polyelectrolyte microcontainers. Langmuir. 2006;22:7400–4.
152. Kolesnikova TA, Gorin DA, Fernandes P, Kessel S, Khomutov GB, Fery A, Shchukin DG, Möhwald H. Nanocomposite microcontainers with high ultrasound sensitivity. Adv Funct Mater. 2010;20:1189–95.

153. Chen J, Ratnayaka S, Alford A, Kozlovskaya V, Liu F, Xue B, Hoyt K, Kharlampieva E. Theranostic multilayer capsules for ultrasound imaging and guided drug delivery. ACS Nano. 2017;11:3135–46.
154. Gao H, Sapelkin AV, Titirici MM, Sukhorukov GB. In situ synthesis of fluorescent carbon dots/polyelectrolyte nanocomposite microcapsules with reduced permeability and ultrasound sensitivity. ACS Nano. 2016;10:9608–15.
155. Kozlovskaya V, Alford A, Dolmat M, Ducharme M, Caviedes R, Radford L, Lapi SE, Kharlampieva E. Multilayer microcapsules with shell-chelated Zr-89 for PET imaging and controlled delivery. ACS Appl Mater Interfaces. 2020;12:56792–804.
156. Alford A, Rich M, Kozlovskaya V, Chen J, Sherwood J, Bolding M, Warram J, Bao YP, Kharlampieva E. Ultrasound-triggered delivery of anticancer therapeutics from MRI-visible multilayer microcapsules. Adv Therap. 2018;1:1800051.
157. Deng L, Li Q, Al-Rehili S, Omar H, Almalik A, Alshamsan A, Zhang JF, Khashab NM. Hybrid iron oxide-graphene oxide-polysaccharides microcapsule: a micro-matryoshka for on-demand drug release and antitumor therapy in vivo. ACS Appl Mater Interfaces. 2016;8:6859–68.
158. Timin AS, Muslimov AR, Lepik KV, Saprykina NN, Sergeev VS, Afanasyev BV, Vilesov AD, Sukhorukov GB. Triple-responsive inorganic-organic hybrid microcapsules as a biocompatible smart platform for the delivery of small molecules. J Mater Chem B. 2016;4:7270–82.
159. Itoh Y, Matsusaki M, Kida T, Akashi M. Locally controlled release of basic fibroblast growth factor from multilayered capsules. Biomacromolecules. 2008;9(8):2202–6.
160. She Z, Wang CX, Li J, Sukhorukov GB, Antipina MN. Encapsulation of basic fibroblast growth factor by polyelectrolyte multilayer microcapsules and its controlled release for enhancing cell proliferation. Biomacromolecules. 2012;13(7):2174–80.
161. De Cock LJ, De Wever O, Van Vlierberghe S, Vanderleyden E, Dubruel P, De Vos F, Vervaet C, Remon JP, De Geest BG. Engineered (hep/pARG)(2) polyelectrolyte capsules for sustained release of bioactive TGF-beta 1. Soft Matter. 2012;8(4):1146–54.
162. Facca S, Cortez C, Mendoza-Palomares C, Messadeq N, Dierich A, Johnston APR, Mainard D, Voegel JC, Caruso F, Benkirane-Jessel N. Active multilayered capsules for in vivo bone formation. Proc Natl Acad Sci U S A. 2010;107(8):3406–11.
163. Richardson JJ, Teng D, Bjornmalm M, Gunawan ST, Guo J, Cui JW, Franks GV, Caruso F. Fluidized bed layer-by-layer microcapsule formation. Langmuir. 2014;30(33):10028–34.
164. Bjornmalm M, Roozmand A, Noi KF, Guo JL, Cui JW, Richardson JJ, Caruso F. Flow-based assembly of layer-by-layer capsules through tangential flow filtration. Langmuir. 2015;31(33):9054–60.
165. Poon Z, Chang D, Zhao XY, Hammond PT. Layer-by-layer nanoparticles with a ph-sheddable layer for in vivo targeting of tumor hypoxia. ACS Nano. 2011;5:4284–92.
166. Poon Z, Lee JB, Morton SW, Hammond PT. Controlling in vivo stability and biodistribution in electrostatically assembled nanoparticles for systemic delivery. Nano Lett. 2011;11:2096–103.
167. Yu L, Gao YG, Yue XL, Liu SQ, Dai ZF. Novel hollow microcapsules based on iron-heparin complex multilayers. Langmuir. 2008;24:13723–9.
168. Chen X, Gambhir SS, Cheon J. Theranostic nanomedicine. Acc Chem Res. 2011;44:841.
169. Lammers T, Aime S, Hennink WE, Storm G, Kiessling F. Theranostic nanomedicine. Acc Chem Res. 2011;44:1029–38.

Part II
Biomaterials Surfaces/Interfaces and Bio-interactions

Chapter 5
Interactions of Biomaterial Surfaces with Proteins and Cells

Zhonglin Lyu, Yi Zou, Qian Yu, and Hong Chen

Abstract The interactions of material surfaces with proteins and cells play a vital role in various biological phenomena and determine the ultimate biofunctionality of a given material in contact with a given biological environment. In this chapter, we used the gold nanoparticle layer (GNPL) with three-dimensional micro- and nano-sized structures as an example to discuss the interactions of material surfaces with proteins and cells. GNPL is deposited onto a variety of substrates such as gold surface and enzyme-linked immunosorbent assay (ELISA) plate; the amount and activity of the absorbed proteins, as well as cell behaviors including attachment, proliferation, and differentiation on GNPL-modified surfaces, are systematically investigated. In addition, the synthetic effects of surface topography and surface chemistry are also studied. The results show that GNPL improves protein adsorption, favors the maintenance of their conformation and bioactivity, and further enhances cell adhesion. After modification with protein-resistant polymers and specific ligands, GNPL selectively binds certain proteins and cells from protein and cell mixtures, including the highly complex environment of serum. Moreover, under laser irradiation, GNPL shows the ability for the delivery of various macromolecules to different cell types (including hard-to-transfect cell types) and the ability for high-efficiency eradication of pathogenic bacteria. It is concluded that GNPLs hold great promise in many biomedical fields such as protein detection, regulation of cell behaviors, capture of circulating cancer cells, macromolecular delivery to living cells, and antibacterial application.

Keywords Gold nanoparticle layer · Topography · Surface modification · Protein adsorption · Cell behavior · Antibacterial application

Z. Lyu · Y. Zou · Q. Yu · H. Chen (✉)
State and Local Joint Engineering Laboratory for Novel Functional Polymeric Materials, College of Chemistry, Chemical Engineering and Materials Science, Soochow University, Suzhou, China
e-mail: chenh@suda.edu.cn

C. Gao (ed.), *Polymeric Biomaterials for Tissue Regeneration*,
https://doi.org/10.1007/978-981-99-6948-7_5

The interactions of material surfaces with proteins and cells play a vital role in various biological phenomena and determine the ultimate biofunctionality of a given material in contact with a given biological environment [1]. The effects of surface topography and roughness (especially at the nanometer scale) on protein and cell behavior have attracted increasing attention since topographic features may have dimensions similar to those of proteins and cell membrane receptors [2–4]. For example, gold nanoparticle layers (GNPLs) consist of nanoparticle aggregates with a distribution of sizes and three-dimensional micro- and nano-sized porous structures [5–11]. GNPLs hold great promise in biomedical applications, for example, biosensors and tissue engineering, due to their large surface-to-volume ratio, efficient electron transfer, good stability, and high loading capacity [8, 12, 13]. Formation of GNPL on material surfaces is usually achieved by reduction of tetrachloroauric (III) acid either through surface-bonded reducing groups or reducing agents [5, 6, 12, 14]. For example, Zhang and coworkers used the Si-H reducing group in the residual curing agent (silicone resin solution) in poly(dimethylsiloxane) (PDMS) matrix to reduce $HAuCl_4$ in the preparation of a PDMS–gold nanoparticle composite film. Wang and coworkers have also reported a method for fabricating PDMS-GNPs films [12]. In another report, chitosan, used as a reducing and stabilizing agent, was coated on PDMS; the coated PDMS was then immersed in $HAuCl_4$ solution to form a layer of GNPs [14]. In our research, stable GNPL were prepared on a variety of materials via a facile and low-cost glucose reduction method [5, 6]. The applications of GNPL for control of protein adsorption and regulation of cell behavior are discussed in the following sections.

5.1 Control of Protein Adsorption

The interaction of biomaterials with proteins is of crucial importance in various applications including biochips [15], biosensors [16], medical device coatings [17], and drug delivery [18]. Controlling the adsorption of proteins (e.g., antibodies, enzymes) on material surfaces and conserving their activity are essential in the design of functional surfaces [19]. In this section, protein adsorption on GNPL-modified enzyme-linked immunosorbent assay (ELISA) plates is discussed in detail. The combined effects of the micro-/nanostructures of the GNPL and the chemistry of polymer brushes grafted on GNPL on protein adsorption are highlighted. The modification of GNPL with pH-responsive polymers for controllable capture and release of proteins is also explored in this discussion.

5.1.1 Protein Adsorption on GNPL-Modified ELISA Plates

ELISA is widely used in clinical diagnosis due to its relative simplicity, low cost, and high sensitivity [20, 21]. A major limitation is low binding affinity of antigens

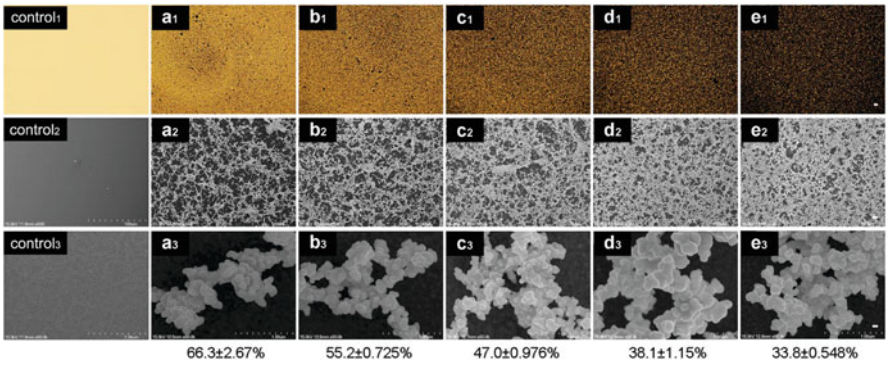

Fig. 5.1 Characterization of unmodified (control) and GNPL-modified ELISA plates. The volumes of plating solution for GNPL (**a**–**e**) were 50, 100, 150, 200, and 250 μL, respectively. (**a1**–**e1**) are visible light micrographs (bar: 100 μm); (**a2**–**e2**) are field emission scanning electron microscopy (FESEM) images (*bar*: 10 μm); (**a3**–**e3**) are high-magnification FESEM images (*bar*: 100 nm); the numbers under the columns are the respective porosity values for GNPL (**a**–**e**). (Reprinted from Ref. [5] with permission. Copyright 2011 American Chemical Society)

and antibodies; in addition, the accessibility of adsorbed proteins on a standard "two-dimensional" microplate surface for the recognition and binding of antigens and antibodies may be limited [22]. To improve accessibility and sensitivity, we have investigated modification of ELISA plates with GNPL to give surfaces that may be described as "three dimensional" [5].

GNPL exhibits three-dimensional porous structures that are composed of gold nanoparticle aggregates with thickness in the micrometer range. By adjusting the volume of the plating solution in the wells, a series of GNPLs with different porosity rates were obtained. With increasing solution volume, the micro- and nano-sized porous structures became more densely aggregated and the porosity value decreased gradually (Fig. 5.1) [5]. It was found that the quantity of proteins (lysozyme (LYZ), human serum albumin (HSA), and fibrinogen (Fg), used as model proteins of different size) adsorbed on GNPL-modified ELISA plates increased significantly with increasing solution volume; e.g., for GNPL prepared with the highest solution volume, the adsorbed quantities of LYZ, HSA, and Fg were, respectively, 2.76-, 2.34-, and 3.26-fold higher than on the unmodified plate. Moreover, due to the micro- and nanostructures of the GNPL, the activity of LYZ absorbed on GNPL was found to be at least 2.65-fold higher than on the unmodified plate. The GNPL-modified plate was shown to amplify the ELISA signals for carcinoembryonic antigen (CEA) and antithrombin (AT) and to increase the limits of detection (LOD) of these antigens significantly. Useful ELISA signals were obtained on GNPL-modified plates when the quantity of CEA was above 2 ng/well; in contrast, no useful signal was obtained on the pristine high-binding ELISA plate even for quantities greater than 10 ng/well. The LOD for AT in buffer solution with GNPL-modified plate was two orders of magnitude lower than for the unmodified plate.

To overcome the limitation of indirect ELISA to selectively bind a specific target from a multiprotein fluid such as serum or plasma, we proposed a GNPL-based ELISA in sandwich format [6]. Sandwich ELISA is widely used in various commercially available kits. In "traditional" sandwich ELISA, the captured (adsorbed) antibody (Ab) binds to the ELISA plate by physical adsorption, resulting in random orientation of the Ab molecules and thus in decreased performance. We hypothesized that an optimum orientation of Ab on the ELISA plate by covalent attachment might improve performance [23]. Accordingly, we immobilized goat anti-rabbit IgG (IgG-alkaline phosphatase (ALP)) on GNPL using 1-ethyl-3-(3-dimethylaminopropyl) carbodiimide hydrochloride (EDC)/*N*-hydroxysuccinimide (NHS) conjugation chemistry. We showed that the activity of IgG covalently immobilized on the GNPL plate was 61% higher than that of IgG physically adsorbed on the unmodified plate.

This result may be attributed, in part, to the improved binding efficiency of the GNPL-modified, compared to the unmodified, ELISA plate; more importantly, the GNPL-modified plate may favor an Ab orientation that facilitates the binding of the IgG substrate to the enzyme. The GNPL-modified ELISA plate showed a lower LOD and higher sensitivity for rabbit IgG in buffer and CEA in plasma. For IgG in buffer, the detection limit of the GNPL-modified ELISA was 0.0512 ng/mL, two orders of magnitude lower than that of the unmodified plate (1.28 ng/mL). For CEA in plasma, the GNPL-modified plate gave a stronger ELISA signal than the unmodified, high-binding ELISA plate as indicated by the deeper color. This was especially true for CEA concentrations greater than 8 ng/mL. The LOD for the GNPL-modified ELISA plate was 2 ng/mL compared to 4 ng/mL for a typical commercial ELISA kit (Linc-Bio Co.).

5.1.2 Controlling Protein Adsorption on GNPL Modified with Hydrophilic Polymer Brushes

Surfaces with micro-/nanostructures adsorb greater quantities of protein than smooth surfaces on a nominal area basis. On the other hand, surfaces modified with hydrophilic polymers such as poly[oligo(ethylene glycol) methacrylate] (POEGMA) tend to resist nonspecific protein adsorption [7, 9]. It was of interest, therefore, to investigate the combined effects of micro-/nanostructures and hydrophilic polymers on protein adsorption. GNPL were modified with POEGMA by surface-initiated atom transfer radical polymerization (SI-ATRP) [7, 9]. Protein adsorption was measured using radiolabeled protein. It was found for human serum albumin (HSA, one of the most abundant proteins in the body) that adsorption on the GNPL surface was about 5.8-fold higher than on smooth Au (sAu) (Fig. 5.2). After modification with POEGMA, adsorption was reduced by about 97%. Adsorption on GNPL-POEGMA and sAu-POEGMA was similar (Fig. 5.2) indicating the strong protein resistance of POEGMA.

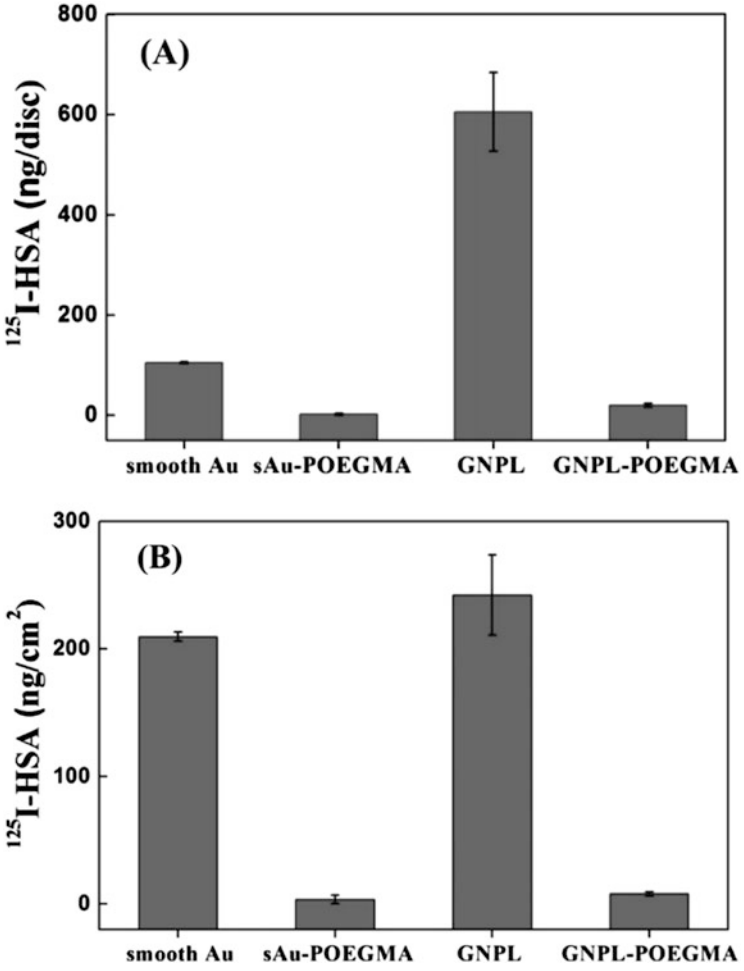

Fig. 5.2 The adsorption of 1 mg/mL HSA measured using ^{125}I radiolabeling method, as expressed in (**a**) nanograms/disc or (**b**) nanograms/cm^2. Data are means ± SD ($n = 3$). (Reprinted from Ref. [9] with permission. Copyright 2012 American Chemical Society)

5.1.3 Capture and Release of Proteins on Multifunctional GNPL

In recent years, various functional surfaces modified with different functional proteins have emerged as novel and active biomaterials due to their numerous applications such as disease therapy, molecular diagnostics, and tissue engineering [24–26]. For these surfaces, to achieve tunable surface bioactivity is vital. An ideal multifunctional surface of this kind should be able to highly regulate the amount of proteins adsorbed on and released from the surface. It should also be able to

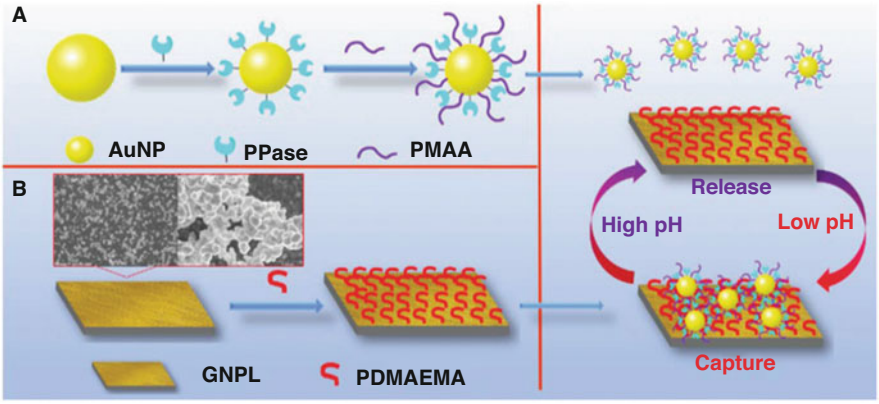

Fig. 5.3 Synthesis of (**a**) AuNP-PPase-PMAA conjugates and (**b**) GNPL-PDMAEMA surfaces; the reversible capture/release of AuNP-PPase-PMAA conjugates on GNPL-PDMAEMA surfaces at different pH values is shown in (**c**). (Reprinted from Ref. [27] with permission. Copyright 2017 Royal Society of Chemistry)

regulate the available bioactivity of the surface. To develop such a multifunctional system, we used pH-sensitive polymers, gold nanoparticles (AuNPs), and GNPLs [27]. pH-sensitive polymers have been proven efficient in responding in real time to pH changes through regulating their chemical and physical properties to achieve protein capture and release [28, 29]. AuNPs and GNPLs were used to introduce nanostructures to the system with the goal to increase the amount of proteins that can be modulated. In detail, this novel system contains (1) AuNPs comodified with an enzyme and poly(methacrylic acid) (PMAA), e.g., AuNP-pyrophosphatase (PPase)-PMAA, as nanostructured protein carriers; (2) GNPLs modified with poly (2-(dimethylamino)ethyl methacrylate) (PDMAEMA), i.e., GNPL-PDMAEMA, as a micro-/nanostructured support platform for surface bioactivity regulation (Fig. 5.3).

PDMAEMA and PMAA were synthesized by RAFT polymerization and functionalized with a thiol group via aminolysis reaction to form PDMAEMA-SH and PMAA-SH. With the free thiol group, PDMAEMA-SH was easily conjugated to GNPLs and PMAA was conjugated AuNPs. It was found that the maximum protein adsorption on the surface occurred at pH 7.0 and the amount of PPase is 359.9 ± 4.2 ng cm^{-2}. The adsorption decreased with increasing pH value. At pH 8.0 and 9.0, the adsorption values were about 65% and 33%, respectively. At pH 10.0, the GNPL-PDMAEMA surface could completely release the AuNP-PPase-PMAA conjugates and only less than 4% protein remained on the surfaces. The pH-dependent protein capture and release mechanism is mainly attributed to the interaction between the two pH responsive polymers: PDMAEMA and PMAA. The pKa of PDMAEMA is between 7.5 and 8.0 [30, 31]. Therefore, it is positively charged at pH 7.0 and negatively charged at pH 10.0. PMAA is negatively charged in the pH range of 6.0–10.0 due to fact that the PMAA carboxylic acid groups are in

the anionic form of –COO– [32]. We also showed that this "capture/release" effect is reversible by cyclic adjustment of the pH value between 7.0 and 10.0 for at least three times.

5.2 Regulation of Cell Behavior

It has been demonstrated that the surfaces on which cells reside and interact in vivo are rough and are composed of diverse three-dimensional micro-/nanostructures which are essential in maintaining cellular functions [33]. For example, extracellular matrix (ECM) and the inner surfaces of blood vessels are rough, with topographical features that affect protein adsorption and cellular responses [34, 35]. Lensen et al. found that poly(ethylene glycol) (PEG) hydrogel surfaces, which are intrinsically cell repellent, support the growth of L929 cells after introducing micro-/nanotopographical features in the surface [36]. Nanotopography has been shown to regulate the properties and behavior of human embryonic stem cells (hESCs), including cell morphology, adhesion, proliferation, and self-renewal [35]. Cardiovascular stents with micro-/nanotopographical surfaces were also found to endothelialize more effectively than those with smooth surfaces [37]. In addition, nanostructured surfaces modified with cell-specific ligands were significantly more efficient in the capture and isolation of circulating tumor cells [38, 39].

5.2.1 Maintaining the Pluripotency of ESCs on GNPLs with Nanoscale Surface Roughness

The influence of surface nanoscale features on the function of ESCs is attracting increasing attention because the features resemble those of the natural ECM where cells reside and interact [40]. Using photolithography Chen and coworkers prepared glass substrates with patterned surface roughness features of 70 and 150 nm and investigated the behavior of hESCs on these surfaces. They found that smooth glass was conducive to maintaining the self-renewal and pluripotency of hESCs in long-term culture; in contrast, the nanorough surfaces promoted spontaneous differentiation and loss of pluripotency [35]. In general, however, the influence of sub-microscale and microscale roughness on the maintenance of ESC pluripotency has not been much explored and remains unclear.

To address this question, we investigated the influence of surface roughness from nano- to submicro- to microscale on the maintenance of mouse ESC (mESC) pluripotency in long-term culture under feeder-free conditions [8]. GNPLs with nano-, sub-micro-, and microscale roughness were prepared by adjusting the volume of the gold plating solution (designated GL-1, GL-2, GL-3, GL-4, and GL-5 with increasing surface roughness). Undifferentiated ESCs can express the Oct-4 gene,

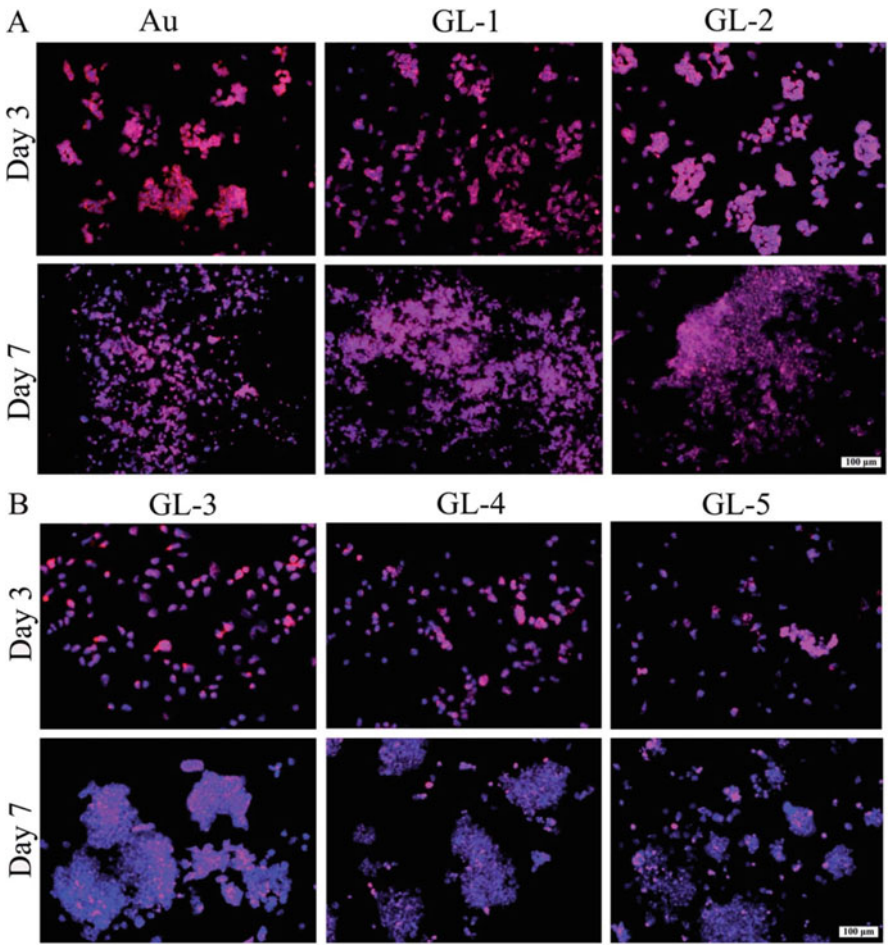

Fig. 5.4 Immunofluorescence images of mESCs cultured for 3 and 7 days on various surfaces. The cells were costained for Oct-4 (*red*) and nuclei (DAPI; *blue*). Undifferentiated mESCs were positively immunolabeled for Oct-4 and were stained *red*. DAPI (*blue* counterstain) labels all cells in the population; therefore, differentiated cell types appear *blue*. (**a**) *Au*, *GL-1*, and *GL-2*; (**b**) *GL-3*, *GL-4*, and *GL-5*. Bar, 100 μm. (Reprinted from Ref. [8] with permission. Copyright 2014 Royal Society of Chemistry)

which is essential for maintaining the cells in the undifferentiated state. Decreases in Oct-4 immunoreactivity signify cell differentiation. The majority of mESCs seeded on sAu, GL-1, and GL-2, whose surface roughness is less than 392 nm, retained their "stemness" after culture for 3 and 7 days, as shown by expression of the Oct-4 gene (Fig. 5.4a). In contrast, the pluripotency of cells cultured on GL-3, GL-4, and GL-5, with surface roughness greater than 573 nm, decreased from day 3; loss of pluripotency was greater after 7 days, particularly on microrough GL-5 (Fig. 5.4b). These results are consistent with data from quantitative polymerase

chain reaction (qPCR) analysis of Oct-4 expression: no significant loss of Oct-4 gene expression was observed in cells grown on nanorough GL-1 (~84%) compared with those on sAu. In contrast, Oct-4 gene expression decreased strongly on GL-3 (~73%) and GL-5 (~52%), with roughness greater than 573 nm. In sum these results show that sAu and GNPLs with low sub-microscale roughness (R_q less than 392 nm) supported very well the long-term pluripotency of mESC. However, GNPLs with sub-microscale surface roughness (R_q) greater than 573 nm and microscale surface roughness of 1205 nm decreased the pluripotency of the cells and accelerated their spontaneous differentiation, especially on microrough GNPL.

The signaling cascades engaged in topological sensing by mESCs were investigated by analyzing the expression of proteins related to E-cadherin-mediated cell–cell adhesion and the formation of integrin-mediated focal adhesions (FAs). It was found that mESCs cultured on sAu and nanorough GNPL (R_q, 106 nm) tended to form larger colonies with cells tightly connected with each other than cells on microrough GNPL. Also the cells maintained much stronger expression of E-cadherin than cells on microrough GNPL. In contrast, the ability of the cells cultured on microrough GNPL to form colonies was significantly decreased, and cells were distributed randomly with much weaker expression of E-cadherin (Fig. 5.5a, b). In addition, β-catenin was expressed exclusively in cells cultured on sAu and nanorough GNPLs, indicating the presence of strong adherens junctions that support E-cadherin-mediated cell–cell adhesions in mESC colonies. In comparison, the cells cultured on microrough GNPL showed much weaker expression of β-catenin (Fig. 5.5c). In focal adhesion (FA) analysis, mESCs exhibited much stronger expression of vinculin (a FA protein) on sAu and nanorough GNPL than on microrough GNPL. These results suggest that nanorough GNPL is conducive to the formation of FAs in mESCs, while microrough GNPL strongly inhibits FA formation, possibly resulting in faster spontaneous differentiation of the mESCs.

5.2.2 *Controlling Cell Behavior on GNPL Grafted with Protein-Resistant Polymers*

Despite much effort devoted to the investigation of the interactions between topography and cell behavior, cellular responses to topography are not well understood and results are contradictory in different experimental systems [41]. Many studies have shown that topographical surfaces increase cell adhesion and cell proliferation by affecting the distribution of ECM proteins adsorbed from the cell culture medium [42, 43] and by increasing protein adsorption [44]. Others believe that cellular responses do not rely only on the cell adhesion proteins or ligands in the local environment, that the topographical structure of the surface itself is important, and that protein adsorption alone does not determine cell behavior. For example, on a surface patterned with grooves overlaid with an orthogonal fibronectin pattern, osteoblasts were aligned predominantly with the grooves, regardless of the

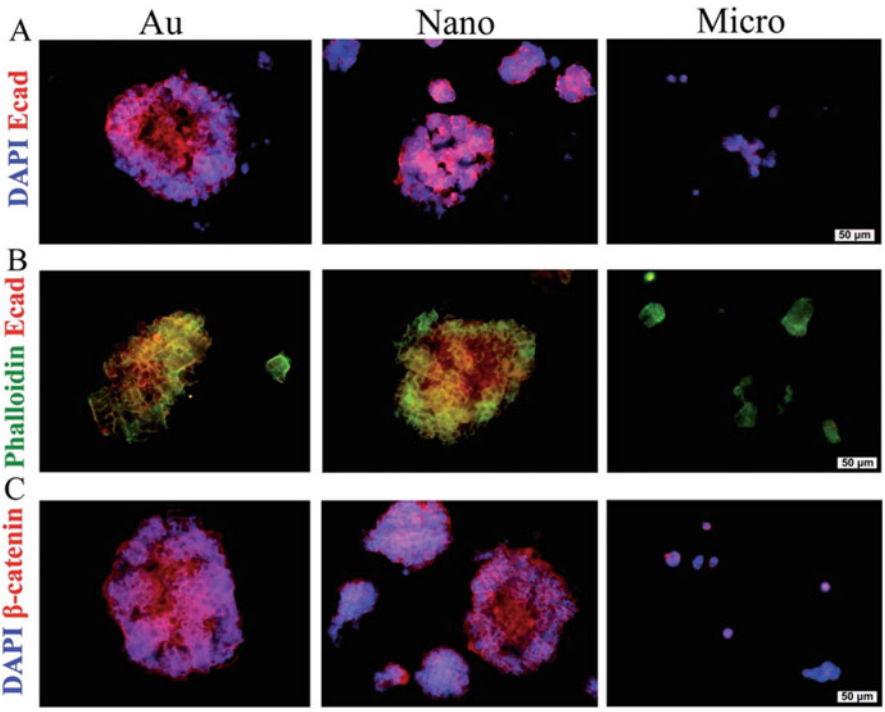

Fig. 5.5 Immunofluorescence images of mESCs on smooth Au and GNPLs with nanoscale and microscale surface roughness after culture for 3 days. (**a**) Cells costained for nuclei (*DAPI*, *blue*) and E-cadherin (*red*); (**b**) cells costained for cytoskeleton (phalloidin, *green*) and E-cadherin (*red*); (**c**) cells costained for nuclei (*DAPI*, *blue*) and *β-catenin* (*red*). Scale bar, 50 μm. (Reprinted from Ref. [8] with permission. Copyright 2014 Royal Society of Chemistry)

distribution of fibronectin (Fn), implying that the topography influenced the cell behavior independently of protein adsorption [45]. Dalby and coworkers showed that cell adhesion was quite different on 10 nm and 50 nm nanoscale islands on poly (*n*-butyl methacrylate)/poly(styrene) blend films [46].

To investigate the role of surface topology independent of other factors on cell behavior, we modified GNPL with POEGMA using SI-ATRP to obtain a topological surface having minimal protein adsorption [9]. Cell adhesion experiments were carried out using two cell types, human L02 hepatocytes and human hepatocellular carcinoma BEL-7402 cells. The cell density on GNPL was higher than on sAu, and after modification with POEGMA cell adhesion was reduced on both surfaces. However, whereas cell adhesion was greatly decreased on sAu, it was reduced by only ~50% for GNPL-POEGMA, and the density on GNPL-POEGMA was an order of magnitude higher than on sAu-POEGMA. L02 and BEL-7402 adhesion on sAu-POEGMA was lower by 92.8% and 97.7%, respectively, compared to sAu. For GNPL-POEGMA surface, the decrease in adhesion compared to GNPL was only 51.5% for L02 and 38.4% for BEL-7402 cells. These data showed that surface

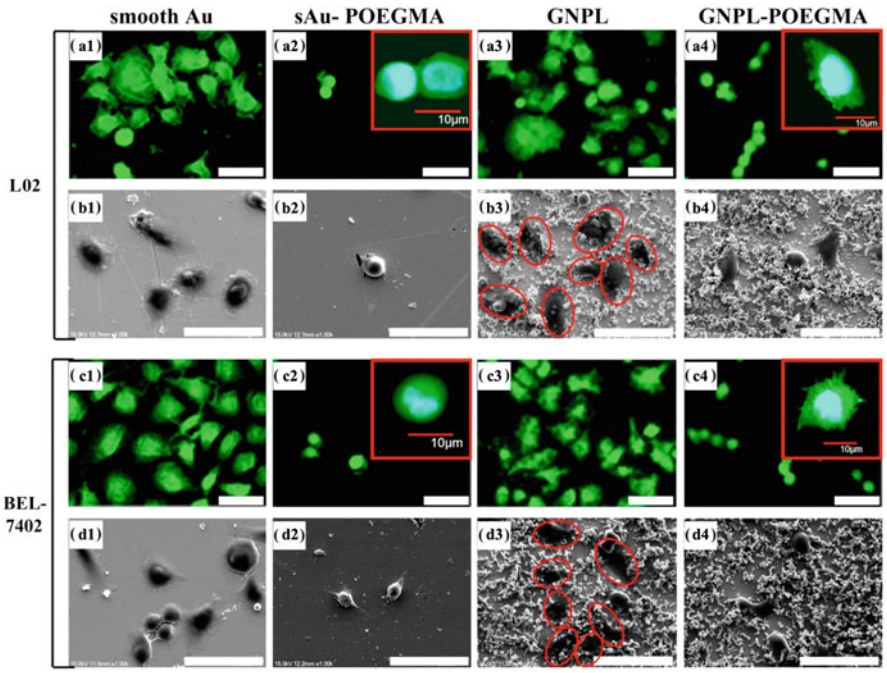

Fig. 5.6 Fluorescence images (**a1**-**a4**) and SEM images (**b1**-**b4**) of L02 cells and fluorescence images (**c1**-**c4**) and SEM images (**d1**-**d4**) of BEL-7402 cells on different surfaces. Spread cells on the GNPL surface are indicated by red ovals in **b3** and **d3**. The scale bar in all images is 50 μm. The shape and filopodia of the cells on POEGMA-modified surfaces were observed by confocal microscopy and are shown as insets in **a2**, **a4**, **c2**, and **c4**. Scale bar, 10 μm

topography is an important determinant of cell adhesion on protein-resistant POEGMA surfaces.

The combined effects of topography and protein resistance on cell–surface interactions were also investigated. Cell spreading was evaluated using fluorescent staining with Alexa Fluor 488 phalloidin (Fig. 5.6a, c). Spreading occurred on the sAu and GNPL surfaces. On the POEGMA-modified surfaces, cell spreading appeared to be constrained to some extent based on the spherical shape of the cells. However, spreading was quite different on the GNPL-POEGMA and sAu-POEGMA surfaces, as shown in the confocal microscopy images (Fig. 5.6 insets). Cells on GNPL-POEGMA showed small lamelipodia and short cell filopodia (Fig. 5.6a4, c4), whereas cells on sAu-POEGMA did not (Fig. 5.6a2, c2). Similar trends were found in SEM images (Fig. 5.6b, d). These results demonstrate that although cell spreading on protein-resistant surfaces was constrained, presumably because of the lack of adsorbed proteins, the cells on topographical surfaces were more firmly attached compared to those on smooth surfaces. In general, it was concluded that topography is more important than protein-resistant polymers for cell adhesion on a protein-resistant surface.

5.2.3 *Controlling Cell Behavior on GNPL Modified with Cell-Binding Ligands*

As well as surface topography, surface chemical modification has been shown to be effective in regulating cell behavior [47, 48]. To promote specific interactions between cells and material surfaces, cell-binding ligands such as arginine–glycine–aspartic acid (RGD) peptide have often been used [49, 50]. However, nonspecific adsorption of serum proteins can interfere with specific cell–ligand interactions. To avoid nonspecific adsorption of serum proteins, Causa and coworkers investigated cell-specific interactions with surfaces in serum-free medium [50]. However, serum contains many proteins and hormones that are vital for the maintenance of cell function. Therefore, studies under serum-free conditions cannot accurately reflect cell-specific interactions. To address this issue, we used protein-resistant polymer brushes (POEGMA) to modify GNPL via SI-ATRP and further modified the POEGMA with glycine–arginine–glycine–aspartic acid–tyrosine (GRGDY) peptide, a typical ligand that binds integrins and triggers specific cell responses [7]. It was found that the cell density on sAu was significantly higher than on GNPL (Fig. 5.7), suggesting that L929 fibroblasts prefer to adhere and proliferate on smooth surfaces. This observation is consistent with previously reported research [51]. We speculated that GNPL surface alters the native conformations of the adsorbed cell-adhesive proteins [52], thereby resulting in poor recognition and binding between the membrane integrins of L929 and those proteins. Hence, it is

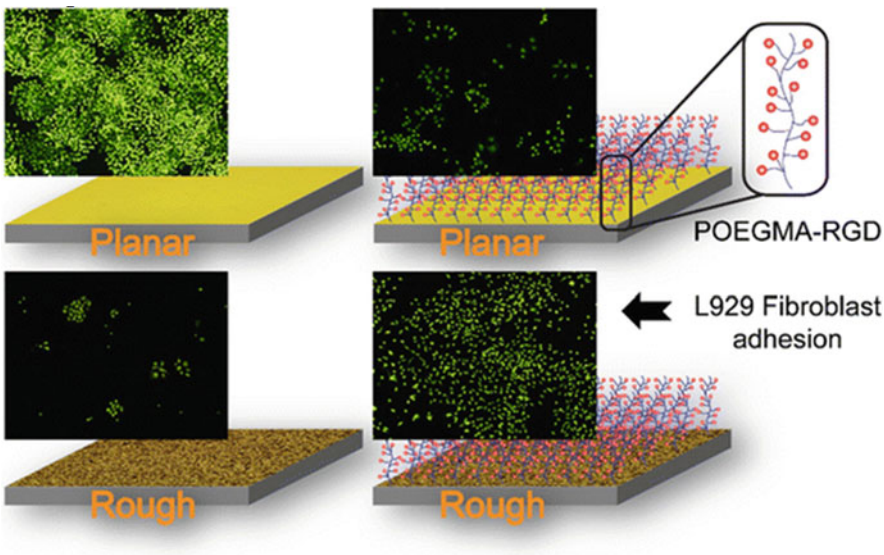

Fig. 5.7 Regulating the behavior of L929 fibroblasts on GNPL modified with POEGMA and cell-binding ligand GRGDY. (Reprinted from Ref. [7] with permission. Copyright 2012 Wiley-VCH)

difficult for L929 cells to form mature focal adhesions on GNPL surfaces, thereby further hindering cell adhesion, spreading, and proliferation.

The cell densities on all of the surfaces modified with POEGMA were significantly reduced and most adherent cells did not spread. A few cells aggregated to form small clusters, indicating that the surfaces were unfavorable for cell adhesion. However, after modification with GRGDY peptide, the cellular responses were totally reversed. The specific binding between cells and GRGDY greatly improved cell adhesion (Fig. 5.7). Cell densities on the GNPL-POEGMA-GRGDY surface were at least 131 ± 13 cells/mm^2 at 120 h. This value was much higher than on the unmodified and POEGMA-modified GNPLs and even higher than on sAu after the same treatment. Thus, it appeared that although the increased surface roughness was unfavorable for the adhesion of L929 cells, the much higher surface-to-volume ratio of the GNPL surface resulted in a higher density of surface immobilized molecules, and the enhanced specific interactions between cells and GRGDY peptides counteracted the negative effect of the roughness, resulting in improved cell adhesion and proliferation.

The cell density on GNPL with lower surface roughness (GNPL (a)) was higher than on the two GNPLs with higher surface roughness (GNPL (c) and GNPL (b); roughness: GNPL (c) > GNPL (b)), and it was the only GNPL that supported cell growth. It appears that surface roughness and cell-specific binding, having opposite effects, reached an optimal balance on GNPL (a). The densities of GRGDY peptide on GNPL (b) and (c) were higher than on GNPL (a) due to their higher surface-to-volume ratios. However, according to a study reported by Mann and West, a very high density of cell-binding ligands immobilized on surfaces is unfavorable for the proliferation of certain mesenchymal-derived cell types [53]. A similar phenomenon was observed by Bellis and coworkers [54, 55]. In our work [6], although the cell density on sAu-POEGMA-GRGDY surface also increased to 83 ± 8 cells/mm^2, it was still lower than on unmodified Au surface (310 ± 25 mm^2) (Fig. 5.7). This could be due to lower specific binding on the modified sAu surface compared to the modified GNPL surface; in addition, the POEGMA spacer reduced the adsorption of serum proteins including that of cell-adhesive proteins such as Fn.

5.2.4 *Capture of Circulating Cancer Cells Using Aptamer-Modified GNPL*

The measurement and analysis of circulating tumor cells (CTCs) can be regarded as a "liquid biopsy" of the tumor, providing insight into tumor biology in the critical window where intervention could actually make a difference [56]. However, CTCs are present in extremely low numbers in the bloodstream: typically one CTC cell per 10^5–10^7 normal blood cells [57]. Therefore, enrichment of CTCs is a prerequisite for CTC analysis. Over the past few decades, a diverse suite of technologies has been developed for isolating and counting CTCs in patient blood samples [58, 59]. The

known enhancement of cell–surface interactions, including cell adhesion, by micro-/nanostructuring can [60] be exploited for the enrichment and separation of CTCs. Aptamers (APTs), which may be considered as nucleic acid forms of traditional antibodies, can be designed to have specific affinity for given cell types. Moreover, APTs have been designed as efficient diagnostic probes for tumors both in vitro and in vivo [61]. Based on this knowledge, we modified GNPLs, first with POEGMA as an antifouling spacer using SI-ATRP; TD05 APT with high specific affinity for Ramos cells was then linked to the terminal hydroxyl groups of POEGMA by *N*, *N*′-disuccinimidyl carbonate (DSC) activation to give Au-POEGMA-APT and GNPL-POEGMA-APT surfaces. The B leukemia CTC cell, Ramos cell, was selected as a target to study the selective capture ability of cell-specific APT-modified GNPLs of varying surface roughness (designated GNPL1, GNPL2, and GNPL3 with increasing surface roughness) in cell mixtures containing Ramos and CEM cells (CL1014, T-cell line, human ALL) under serum-containing cell culture conditions [10].

The number of Ramos cells on the APT-modified GNPL surfaces increased with increasing surface roughness while the CEM cell number decreased, albeit slowly. The density of Ramos cells on the sAu, GNPL1, GNPL2, and GNPL3 surfaces were, respectively, 1.3-, 1.9-, 1.9-, and 2.2-fold greater than those of CEM cells. In contrast, after aptamer modification, the proportion of Ramos cells increased significantly with increasing surface roughness, with densities on the sAu, GNPL1, GNPL2, and GNPL3 surfaces, respectively, 2.2-, 2.8-, 3.0-, and 2.7-fold greater than those of CEM cells. We concluded that in serum-containing conditions, the roughness of the GNPLs enhanced the selectivity of the APT for Ramos cells. However, compared with serum-free conditions, the selectivity was still much weaker.

Serum is a highly complex fluid that contains many types of proteins which adsorb to surfaces nonspecifically and may “hide” the surface-immobilized APT to some extent, thereby further inhibiting the binding of cell receptors to the immobilized APT. This effect may be responsible, in large part, for the observed decrease in selectivity in serum compared to buffer. To improve the Ramos selectivity of the APT-modified surfaces in serum-containing conditions, we introduced POEGMA as a protein-resistant element. After POEGMA modification, the numbers of cells on Au-POEGMA and GNPL(1–3)-POEGMA were significantly reduced compared to the unmodified surfaces in serum-containing conditions. In addition, there was no observable difference in the numbers of Ramos and CEM cells. With the introduction of APT on the POEGMA, the density of Ramos cells increased significantly, whereas the density of CEM cells did not change. The density of Ramos cells on the four (sAu, GNPL1, GNPL2, and GNPL3) POEGMA surfaces modified with APT were, respectively, 0.9-, 1.5-, 3.5-, and 6.6-fold greater than those of CEM (Fig. 5.8).

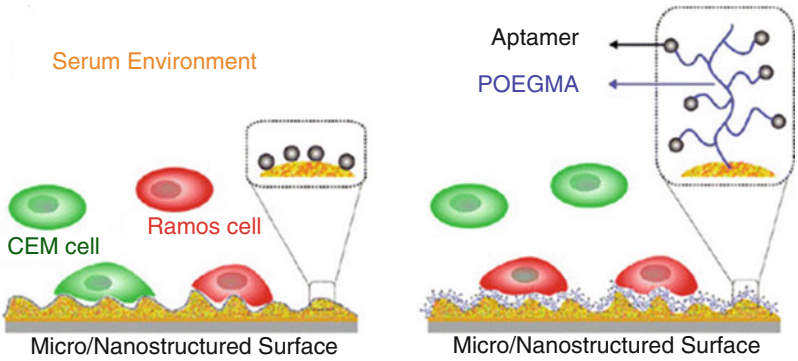

Fig. 5.8 Selective capture of Ramos cells in serum-containing conditions on GNPL surface modified with POEGMA and APT. (Reprinted from Ref. [10] with permission. Copyright 2013 American Chemical Society)

5.2.5 *Macromolecular Delivery to Cells Using GNPL via the Photoporation Effect*

Gold nanoparticle (GNP)-mediated photoporation has garnered increasing attention as a promising approach for macromolecular delivery to living cells [62–65]. When exposed to laser light of particular wavelengths, the membrane-associated GNPs convert the absorbed laser energy into heat, leading to increased membrane permeability and the transport of normally cell-impermeable macromolecules directly into the cytosol [66]. Additionally, by tuning the laser energy, the size of the pores created in the cell membrane by the GNPs can be varied, allowing control of the quantity and size of the molecules delivered [67]. Compared with traditional photoporation, in which cell membrane permeability is achieved by focusing high-intensity femtosecond (fs) laser pulses onto individual cells, GNP-mediated photoporation can be achieved at a lower laser energy with unfocused laser light that can irradiate a large number of cells, leading to greatly increased throughput [62]. Moreover, GNPs have superior chemical and biological properties including easy surface modification for molecular attachment and improved biocompatibility. Although effective, this method relies on complex and expensive equipment to generate laser light in short pulses [67]. Moreover, concerns remain because the extreme heating of the GNPs during irradiation may cause them to distort and fragment, resulting in high cytotoxicity [68, 69]. To solve these problems, we developed a new platform for macromolecular delivery that retains the photothermal properties of GNPs while avoiding the side effects caused by their entry into the cells. Instead of free GNPs, we used GNPLs as the photoporation "reagent." GNPLs, composed of numerous GNPs with nano- and microtopography, provide multiple sites for contact between cell membranes and the GNPs. We therefore hypothesized that GNPLs may serve as a novel and versatile macromolecular delivery platform upon irradiation with continuous-wave (CW) laser light (Fig. 5.9) [70].

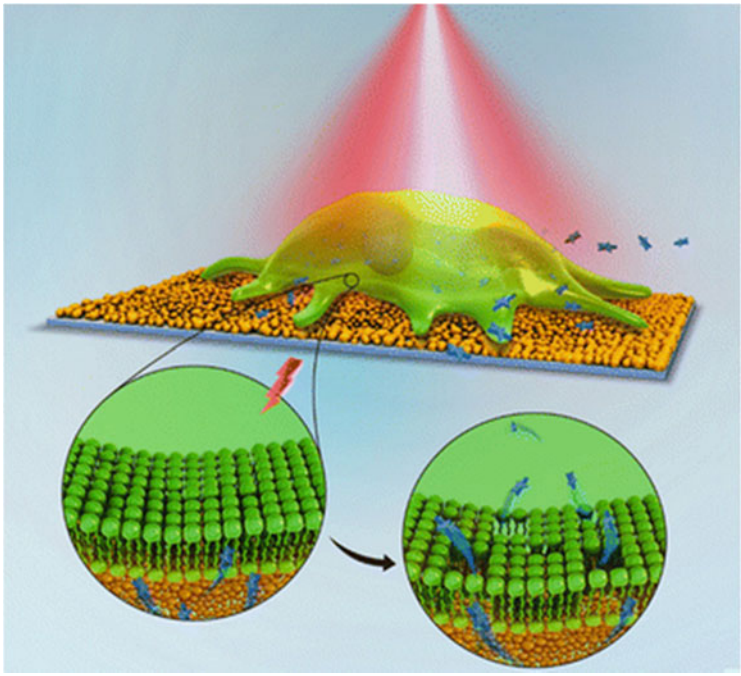

Fig. 5.9 A novel platform for macromolecular delivery into cells using gold nanoparticle layers via the photoporation effect. (Reprinted from Ref. [70], copyright 2016, WILEY-VCH Verlag GmbH & Co)

We first tried delivery of dextran to cells using this approach. Tetramethylrhodamine isothiocyanate (TRITC)-labeled dextran (red fluorescence), with a molecular weight of 4.4 kDa, was used as a model macromolecule and HeLa cells as model cells. It was found that without laser irradiation, dextran did not enter the cells efficiently; no red fluorescence was observed. Strong red fluorescence began to be observed at 3.2 W cm^{-2}/45 s, and the fluorescence intensity increased further at 5.1 W cm^{-2}/30 s. Decrease in irradiation time to 20 s at 5.1 W cm^{-2} failed to give high fluorescence intensity. The delivery efficiency in presence of sAu under those conditions was much lower. To further demonstrate the efficient delivery of TRITC-dextran to HeLa cells, we obtained confocal microscopy images using the Z-stack mode to view the distribution of TRITC-dextran. Scans were taken from top to bottom of the cell membrane. The images indicated that macromolecules entered the interior of the cells and were not merely attached to the cell membrane. Moreover, cell viability experiments demonstrated that vitality was maintained under these conditions.

Plasmid DNA (pDNA) is a commonly used gene carrier and its efficient delivery to living cells is essential for gene therapy. However, due to its large size and the necessity for transport into the nucleus, transfection is more difficult with pDNA than with dextran or RNA. In our work, the applicability of GNPL-laser irradiation

for the delivery of pDNA encoding green fluorescent protein (GFP), a widely used pDNA model that can easily transfect HeLa cells, was assessed. Lipofectamine 2000 (Lipo2000) complexed with pDNA was used as a standard cell transfection agent (positive control) because Lipo2000 is a widely used, commercially available transfection reagent for delivery of pDNA and RNA into cells [71]. It was found that under irradiation conditions 3.2 W cm^{-2}/45 s and 5.1 W cm^{-2}/30 s, virtually 100% of the HeLa cells gave a green fluorescence signal, suggesting the successful delivery and expression of pDNA in the cells. These results are in line with data from flow cytometry. Compared with 3.2 W cm^{-2}/45 s, the transfection efficiency at 5.1 W cm^{-2}/30 s was significantly higher; the cells showed stronger green fluorescence, similar to that obtained using Lipo2000. These results show that under laser irradiation, our platform based on GNPLs achieved direct and efficient delivery of pDNA to HeLa cells without compromising cell viability. Moreover, the transfection efficiency of this vector-free system was comparable to that of Lipo2000.

Gene delivery to different cell types has resulted in advances in the understanding of gene function and the development of genetic therapies [72–74]. Although Lipo2000 is effective for the transfection of many cell types, it is ineffective for the transfection of hard-to-transfect cell types such as primary cells including mouse embryonic fibroblasts (mEFs) used widely in stem cell research and human umbilical vein endothelial cells (HUVECs), which are used for endothelial cell physiology and pathology studies. Therefore, we investigated the delivery of pDNA to hard-to-transfect mEFs and HUVECs. Efficient intracellular delivery to mEFs has previously been challenging. For example, the transfection efficiencies of mEFs with pDNA using pDNA/magnetic nanoparticles and optimized electroporation were reported as ~11% [75] and ~40% [76], respectively. It was shown that pDNA was delivered to and expressed in mEFs under irradiation conditions of 3.2 W cm^{-2}/45 s with a transfection efficiency of approximately 39%, much higher than the ~19% using Lipo2000 ($p < 0.001$). At 5.1 W cm^{-2}/30 s, the transfection efficiency was further enhanced to 53% ($p < 0.001$, vs Lipo2000), and the fluorescence intensity was much higher than for Lipo2000 ($p < 0.001$). In addition, cell viability both immediately after and 24 h after laser irradiation was higher than 95% under both conditions. For HUVECs, sufficient intracellular delivery of pDNA could not be achieved using GNPL along probably because of the differences in cell type and size. The average size of HUVECs is only about 35% of the average size of mEFs meaning there are more sites for the contact between mEFs and GNPL surfaces than that between HUVECs and GNPL surfaces. To address this problem, we combined Lipo2000 and GNPL where pDNA was complexed with Lipo2000 before exposure to laser irradiation. At 5.1 W cm^{-2}/30 s, we achieved a transfection efficiency of ~44%, much higher than ~8% from using Lipo2000 alone ($p < 0.001$). Altogether, these data demonstrate that this system is effective for the pDNA transfection of hard-to-transfect cell types with an efficiency much higher than for Lipo2000 alone.

5.2.6 *Macromolecular Delivery to "Recalcitrant" Cells Using PEI and GNPL via the Photoporation Effect*

Using GNPL-assisted photoporation, we have achieved relatively high delivery efficiency of pDNA to hard-to-transfect mEFs (~53%) and HUVECs (~44%). However, there is still room to further improve the delivery efficiently. Polyethylenimine (PEI) is a representative synthetic nonviral gene carrier with superior transfection efficiency due to its unique "proton sponge effect" for endosomal escape of the gene payload [77]. The commercially available 25 kDa branched PEI (bPEI) in particular has been widely considered as the "gold standard" carrier for gene delivery [78]. Unfortunately, such high molecular weight (MW) PEI (HPEI) is generally cytotoxic, thus limiting its application. Low MW PEI (LPEI, MW <2 kDa) is acceptable with respect to cytotoxicity but has low transfection efficiency. Considerable efforts have been made to prepare novel PEI derivatives to overcome these limitations [79–81]. However, safe and efficient delivery systems for hard-to-transfect primary cell lines have rarely been reported. After confirming the potential of GNPL to serve as a universal macromolecular delivery platform [70], here we explored the possibility of combing LPEI with GNPL for safe and high-efficient pDNA delivery specifically to hard-to-transfect primary cell lines (mEFs and HUVECs) (Fig. 5.10). In this platform, LPEI serves as a carrier of pDNA to protect it from degradation. Laser-activated GNPL serves as a membrane disruption agent [82].

We achieved a very high pDNA transfection efficiency of 94.0 ± 6.3% to HUVECs when we added LPEI/pDNA complexes with a N/P of 20 to cells growing on GNPL under laser irradiation. Cell viability under this condition was very well

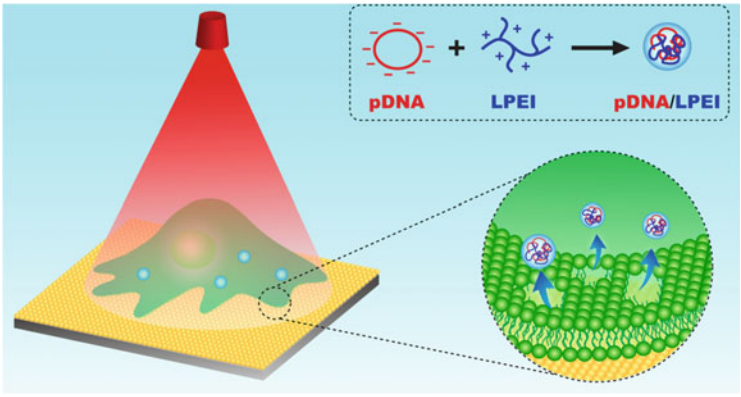

Fig. 5.10 LPEI/pDNA complex is formed by electrostatic interactions. Targeted cells are cultured on the GNPL, and then exposed to laser irradiation to enhance the permeability of the cell membrane, thereby assisting the diffusion of LPEI/pDNA complex from the surrounding medium into the cell. (Reprinted from Ref. [82] with permission. Copyright 2017 American Chemical Society)

maintained at ~100%, 48 h after transfection. The transfection value is higher than the value achieved using 25k PEI (75.1 ± 18.6%). Moreover, cell viability 48 h after transfection using 25k bPEI decreased to less than 5%, much lower than the viability of our system ($p < 0.001$). These results showed that LPEI/GNPL collaborative delivery system significantly outperformed the golden standard-25k bPEI for the delivery of pDNA to HUVECs. It is worth noting that this efficiency is also much higher than the efficiency achieved by complexing pDNA with Lipo2000 before exposure to GNPL-assisted laser irradiation (~44%).

We further investigated the delivery of pDNA to mEFs. Similar to HUVECs, our system gave high transfection efficiency (88.5 ± 9.2%) and high cell viability (99.8 ± 4.1%, 48 h after transfection) for mEFs. Last, we used our platform to deliver functional pDNA to illustrate its potential for endothelialization of artificial blood [83]. For this purpose, ZNF580 gene, which codes for a zinc finger protein, was chosen. This protein plays a critical role in alleviating atherosclerosis and has been shown to promote the proliferation and migration of endothelial cells [84]. Our data indicated that 48 h after transfection, the relative ZNF580 microRNA (mRNA) content was ~1.3 times higher than that of the negative control group. Moreover, transfection with pZNF580 resulted in an increase in initial attachment and a significant increase in long-term proliferation of HUVECs. In particular, after 48 h culture, the density of adherent pZNF580 transfected cells was about twice that of nontransfected cells ($p < 0.05$). These data suggest that our transfection method can effectively deliver pZNF580 to HUVECs such that proliferation for revascularization purposes may be enhanced. Together, we showed that our LPEI/GNPL collaborative delivery system provides a highly efficient and relatively simple approach for intracellular delivery, especially for hard-to-transfect cell lines that are difficult to treat using more traditional methods.

5.2.7 *GNPL-Based Regenerable Smart Antibacterial Surfaces*

Attachment and subsequent colonization by bacteria on the surfaces of synthetic materials and devices pose serious problems in both human healthcare and industrial applications [85, 86]. Antibacterial surfaces with capability to prevent bacterial attachment and biofilm formation have been a longstanding focus of research [87–91]. However, conventional antibacterial surfaces are becoming less effective due to the emergence of multidrug resistant bacteria [92]. Photothermal therapy using strong light absorbers to generate local heat for physical destruction of bacteria provides a promising approach for circumventing the problem of antibiotic resistance [93–98]. However, these photothermal antibacterial coatings suffer from the same inherent drawbacks as traditional antibacterial surfaces based on contact-killing mechanisms, and even if they show high bactericidal efficiency, they remain contaminated by dead bacteria and other debris, which not only provide nutrients for

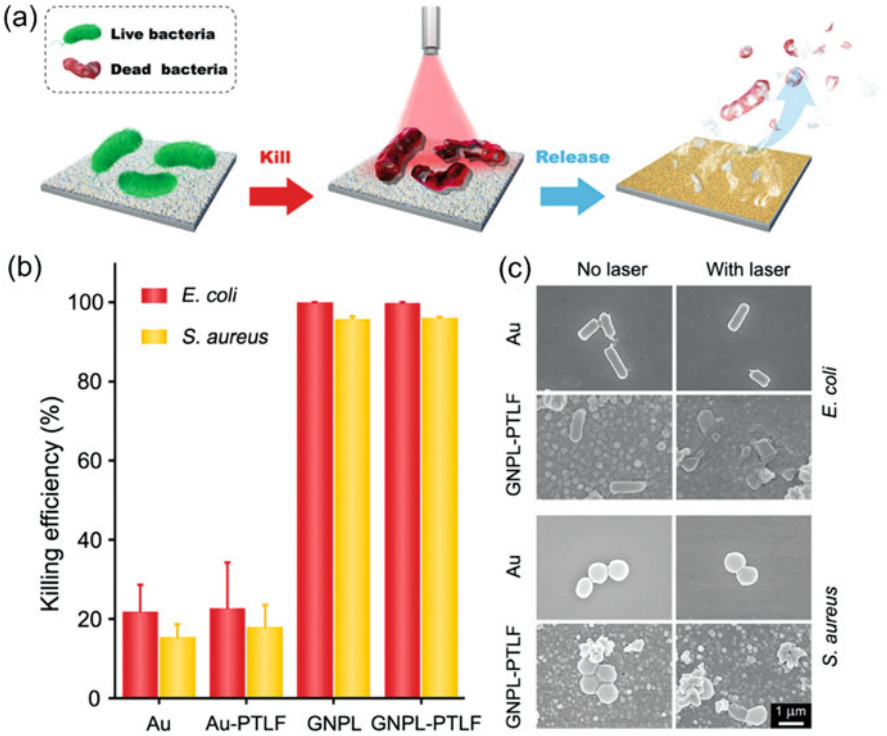

Fig. 5.11 (**a**) Schematic illustration of a smart antibacterial surface based on a GNPL-PTLF hybrid film with photothermal bacteria-killing capability and Vc-triggered bacteria-releasing ability. (**b**) Photothermal bactericidal activity of surfaces against *E. coli* and *S. aureus* under NIR laser irradiation (2.3 W/cm^2, 5 min) evaluated using a colony counting assay. Error bars represent the standard deviation of the mean ($n = 3$). (**c**) Typical SEM images of attached bacteria on Au and GNPL-PTLF surfaces with/without NIR laser irradiation. (Reprinted from Ref. [103] with permission. Copyright 2018 Royal Society of Chemistry)

subsequent bacterial interactions, but may also trigger severe immune responses and inflammation [99]. To circumvent the problem of dead bacteria, a promising "kill-and-release" strategy has been proposed for the development of smart antibacterial surfaces with the capability of not only killing the attached bacteria but also releasing dead bacteria and debris "on demand" under an appropriate stimulus [100–102]. To the best of our knowledge, smart photothermal antibacterial surfaces have not been developed yet. To fill this gap, we developed the first smart photothermal antibacterial surfaces with bacteria-releasing properties [103].

This smart coating is composed of two functional layers (Fig. 5.11a). The first is a gold nanoparticle layer (GNPL) composed of GNP aggregates which serve as the photothermal bactericidal agent. Compared with dispersed GNPs, the aggregated GNPs exhibit a more efficient photothermal effect due to the redshifted absorption [104]. In addition, the GNPL possesses a unique micro-nanotopography that provides multiple sites for contact with bacteria and facilitates local hyperthermia

induced by NIR laser irradiation. We anticipate that the GNPL can also be used as an effective antibacterial material on which attached bacteria can be destroyed photothermally. In addition, the GNPL was coated with a thin phasetransitioned lysozyme film (PTLF) as a contamination releasing layer. PTLF was recently developed in our previous works as a novel biocompatible two-dimensional (2D) proteinaceous nanofilm with versatile applications. For substrates immersed in phase-transitioned lysozyme solution, a PTLF composed of densely aggregated oligomers within amyloid-like structures was shown to form on the surface in a few minutes. Such PTLFs are transparent and exhibit strong substrate bonding even in extreme pH conditions or under gas plasma treatment [105, 106].

It is thus expected that the addition of PTLF will not affect the light-to-heat conversion capability of the GNPL or the bactericidal efficacy of the GNPL. Our results showed that more than 99% of attached Gram-positive *S. aureus* or Gram-negative *E. coli* were killed under near infrared laser radiation at 2.3 W/cm^2 for 5 min (Fig. 5.11b, c). we also showed that the degradation of PTLF can be triggered in a closely controlled manner by treatment with vitamin C (Vc). Almost all of the killed bacteria could be removed by incubating the surface in Vc solution for a short time period of 10 min due to the degradation of the topmost layer of PTLF. Moreover, the GNPL-PTLF coating can be used repeatedly over at least three "kill-and-release" cycles, which is of particular importance for long-term usage.

5.3 Summary and Outlook

Gold nanoparticle layers, as a representative material with surface topological structures, have a direct influence on protein adsorption/activity and cell behavior including adhesion, spreading, proliferation, and differentiation. Compared to smooth gold surfaces, GNPLs, due to their "three-dimensional" structure, offer better access for the binding of biomacromolecules such as proteins, antigens, and antibodies and favor the maintenance of their conformation and bioactivity, thereby improving cell adhesion further. In combination with protein-resistant polymers and specific ligands for certain types of proteins or cells, modified GNPL can selectively bind certain proteins and cells from protein and cell mixtures, including the highly complex environment of serum. In combination with stimuli-responsive polymers such as pH-sensitive polymers, modified GNPL can achieve multifunction such as recyclable protein capture and release. In addition, under laser irradiation, GNPLs show excellent photothermal property. This feature endows GNPLs with the ability to serve as a novel and efficient platform for the delivery of various macromolecules to different cell types including hard-to-transfect cell types. It also provides GNPLs with the opportunity to serve as an efficient and antibiotic-free antibacterial coating with the potential to kill and remove adherent bacteria, particularly multidrug resistant bacteria, on the surfaces of medical devices. It is concluded that GNPLs hold great promise in many biomedical fields such as protein detection, regulation of

protein and cell behavior, capture of circulating cancer cells, macromolecular delivery to living cells, and antibacterial applications.

Acknowledgments This work was supported by the National Natural Science Foundation of China (21774086, 22175125, and 21935008) and the Natural Science Foundation of the Jiangsu Higher Education Institutions of China (21KJA150008). We thank Prof. John Brash for the helpful discussion.

References

1. Yuan L, Yu Q, Li D. Chen H surface modification to control protein/surface interactions. Macromol Biosci. 2011;11:1031–40.
2. Gittens RA, McLachlan T, Olivares-Navarrete R, Cai Y, Berner S, Tannenbaum R, Schwartz Z, Sandhage KH. Boyan B D the effects of combined micron-/submicron-scale surface roughness and nanoscale features on cell proliferation and differentiation. Biomaterials. 2011;32:3395–403.
3. Chen W, Weng S, Zhang F, Allen S, Li X, Bao L, Lam RH, Macoska JA, Merajver SD. Fu J Nanoroughened surfaces for efficient capture of circulating tumor cells without using capture antibodies. ACS Nano. 2013;7:566–75.
4. Yu Q, Ista LK, Gu R, Zauscher S, Lopez GP. Nanopatterned polymer brushes: conformation, fabrication and applications. Nanoscale. 2016;8:680–700.
5. Zhou F, Yuan L, Wang H, Li D, Chen H. Gold nanoparticle layer: a promising platform for ultra-sensitive cancer detection. Langmuir. 2011;27:2155–8.
6. Zhou F, Wang M, Yuan L, Cheng Z, Wu Z, Chen H. Sensitive sandwich ELISA based on a gold nanoparticle layer for cancer detection. Analyst. 2012;137:1779–84.
7. Zhou F, Li D, Wu Z, Song B, Yuan L, Chen H. Enhancing specific binding of L929 fibroblasts: effects of multi-scale topography of GRGDY peptide modified surfaces. Macromol Biosci. 2012;12:1391–400.
8. Lyu Z, Wang H, Wang Y, Ding K, Liu H, Yuan L, Shi X, Wang M, Wang Y, Chen H. Maintaining the pluripotency of mouse embryonic stem cells on gold nanoparticle layers with nanoscale but not microscale surface roughness. Nanoscale. 2014;6:6959–69.
9. Shi X, Wang Y, Li D, Yuan L, Zhou F, Wang Y, Song B, Wu Z, Chen H, Brash JL. Cell adhesion on a POEGMA-modified topographical surface. Langmuir. 2012;28:17011–8.
10. Wang Y, Zhou F, Liu X, Yuan L, Li D, Wang Y, Chen H. Aptamer-modified micro/nanostructured surfaces: efficient capture of Ramos cells in serum environment. ACS Appl Mater Interfaces. 2013;5:3816–23.
11. Wu J, Qu Y, Yu Q, Chen H. Gold nanoparticle layer: a versatile nanostructured platform for biomedical applications. Mater Chem Front. 2018;2:2175–90.
12. Zhang Q, Xu JJ, Liu Y, Chen HY. In-situ synthesis of poly(dimethylsiloxane)-gold nanoparticles composite films and its application in microfluidic systems. Lab Chip. 2008;8:352–7.
13. Bai HJ, Shao ML, Gou HL, Xu JJ, Chen HY. Patterned au/poly(dimethylsiloxane) substrate fabricated by chemical plating coupled with electrochemical etching for cell patterning. Langmuir. 2009;25:10402–7.
14. Wang B, Chen K, Jiang S, Reincke F, Tong W, Wang D, Gao C. Chitosan-mediated synthesis of gold nanoparticles on patterned poly(dimethylsiloxane) surfaces. Biomacromolecules. 2006;7:1203–9.
15. Drummond TG, Hill MG, Barton JK. Electrochemical DNA sensors. Nat Biotechnol. 2003;21:1192–9.

16. Nam JM, Thaxton CS, Mirkin CA. Nanoparticle-based bio-bar codes for the ultrasensitive detection of proteins. Science. 2003;301:1884–6.
17. Webster TJ, Schadler LS, Siegel RW, Bizios R. Mechanisms of enhanced osteoblast adhesion on nanophase alumina involve vitronectin. Tissue Eng. 2001;7:291–301.
18. Brigger I, Dubernet C, Couvreur P. Nanoparticles in cancer therapy and diagnosis. Adv Drug Deliv Rev. 2012;64:24–36.
19. Roach P, Farrar D, Perry CC. Surface tailoring for controlled protein adsorption: effect of topography at the nanometer scale and chemistry. J Am Chem Soc. 2006;128:3939–45.
20. Eteshola E, Leckband D. Development and characterization of an ELISA assay in PDMS microfluidic channels. Sens Actuators, B. 2017;18:129–33.
21. Jia CP, Zhong XQ, Hua B, Liu MY, Jing FX, Lou XH, Yao SH, Xiang JQ, Jin QH, Zhao JL. Nano-ELISA for highly sensitive protein detection. Biosens Bioelectron. 2009;24:2836–41.
22. Park JS, Cho MK, Lee EJ, Ahn KY, Lee KE, Jung JH, Cho Y, Han SS, Kim YK, Lee JA. Highly sensitive and selective diagnostic assay based on virus nanoparticles. Nat Nanotechnol. 2009;4:259–64.
23. Dixit CK, Vashist SK, O'Neill FT, O'Reilly B, BD MC, O'Kennedy R. Development of a high sensitivity rapid Sandwich ELISA procedure and its comparison with the conventional approach. Anal Chem. 2010;48:7049–52.
24. Jonkheijm P, Weinrich D, Schroder H, Niemeyer CM, Waldmann H. Chemical strategies for generating protein biochips. Angew Chem Int Ed. 2008;47:9618–47.
25. Xu FJ, Neoh KG, Kang ET. Bioactive surfaces and biomaterials via atom transfer radical polymerization. Prog Polym Sci. 2009;34:719–61.
26. Sproule TL, Alex Lee J, Li H, Lannutti JJ, Tomasko DL. Bioactive polymer surfaces via supercritical fluids. J Supercrit Fluids. 2004;28:241–8.
27. Li Z, Liu F, Yuan Y, Wu J, Wang H, Yuan L, Chen H. Multifunctional gold nanoparticle layers for controllable capture and release of proteins. Nanoscale. 2017;9:15407–15.
28. Sundaram HS, Ella-Menye J-R, Brault ND, Shao Q, Jiang S. Reversibly switchable polymer with cationic/zwitterionic/anionic behavior through synergistic protonation and deprotonation. Chem Sci. 2014;5:200–5.
29. Kumar S, Tong X, Dory YL, Lepage M, Zhao YA. CO_2-switchable polymer brush for reversible capture and release of proteins. Chem Commun. 2013;49:90–2.
30. Qiu X, Hu S. "Smart" materials based on cellulose: a review of the preparations, properties, and applications. Materials. 2013;6:738–81.
31. Qiao Y, Huang Y, Qiu C, Yue X, Deng L, Wan Y, Xing J, Zhang C, Yuan S, Dong A, Xu J. The use of PEGylated poly[2-(*N*,*N*-dimethylamino)ethyl methacrylate] as a mucosal DNA delivery vector and the activation of innate immunity and improvement of HIV-1-specific immune responses. Biomaterials. 2010;31:115–23.
32. Lu W, Ma W, Lu J, Li X, Zhao Y, Chen G. Microwave-assisted synthesis of glycopolymer-functionalized silver nanoclusters: combining the bioactivity of sugar with the fluorescence and cytotoxicity of silver. Macromol Rapid Commun. 2014;35:827–33.
33. Ross AM, Jiang Z, Bastmeyer M, Lahann J. Physical aspects of cell culture substrates: topography, roughness, and elasticity. Small. 2012;8:336–55.
34. Dolatshahi-Pirouz A, Jensen T, Kraft DC, Foss M, Kingshott P, Hansen JL, Larsen AN, Chevallier J, Besenbacher F. Fibronectin adsorption, cell adhesion, and proliferation on nanostructured tantalum surfaces. ACS Nano. 2010;4:2874–82.
35. Chen W, Villa-Diaz LG, Sun Y, Weng S, Kim JK, Lam RH, Han L, Fan R, Krebsbach PH, Fu J. Nanotopography influences adhesion, spreading, and self-renewal of human embryonic stem cells. ACS Nano. 2012;6:4094–103.
36. Schulte V, Dıéz M, Möller M, Lensen M. Surface topography induces fibroblast adhesion on intrinsically nonadhesive poly(ethylene glycol) substrates. Biomacromolecules. 2009;10:2795–801.

37. Loya MC, Brammer KS, Choi C, Chen LH, Jin S. Plasma-induced nanopillars on bare metal coronary stent surface for enhanced endothelialization. Acta Biomater. 2010;6:4589–95.
38. Chen L, Liu X, Su B, Li J, Jiang L, Han D, Wang S. Aptamer-mediated efficient capture and release of T lymphocytes on nanostructured surfaces. Adv Mater. 2011;23:4376–80.
39. Sekine J, Luo SC, Wang S, Zhu B, Tseng HR, Yu HH. Functionalized conducting polymer nanodots for enhanced cell capturing: the synergistic effect of capture agents and nanostructures. Adv Mater. 2011;23:4788–92.
40. Lee MR, Kwon KW, Jung H, Kim HN, Suh KY, Kim K, Kim KS. Direct differentiation of human embryonic stem cells into selective neurons on nanoscale ridge/groove pattern arrays. Biomaterials. 2010;31:4360–6.
41. Cretel E, Pierres A, Benoliel AM, Bongrand P. How cells feel their environment: a focus on early dynamic events. Cell Mol Bioeng. 2008;1:5–14.
42. Chen H, Song W, Zhou F, Wu Z, Huang H, Zhang J, Lin Q, Yang B. The effect of surface microtopography of poly(dimethylsiloxane) on protein adsorption, platelet and cell adhesion. Colloids Surf B Biointerfaces. 2009;71:275–81.
43. Yamamoto S, Tanaka M, Sunami H, Arai K, Takayama A, Yamashita S, Morita Y, Shimomura M. Relationship between adsorbed fibronectin and cell adhesion on a honeycomb-patterned film. Surf Sci. 2006;600:3785–91.
44. Rechendorff K, Hovgaard MB, Foss M, Zhdanov VP, Besenbacher F. Enhancement of protein adsorption induced by surface roughness. Langmuir. 2006;22:10885–8.
45. Charest JL, Eliason MT, Garcia AJ, King WP. Combined microscale mechanical topography and chemical patterns on polymer cell culture substrates. Biomaterials. 2006;27:2487–94.
46. Dalby MJ, Riehle MO, Johnstone HJ, Affrossman S, Curtis AS. Nonadhesive nanotopography: fibroblast response to poly(*n*-butyl methacrylate)-poly(styrene) demixed surface features. J Biomed Mater Res A. 2003;67:1025–32.
47. Marcon L, Spriet C, Coffinier Y, Galopin E, Rosnoblet C, Szunerits S, Heliot L, Angrand PO, Boukherroub R. Cell adhesion properties on chemically micropatterned boron-doped diamond surfaces. Langmuir. 2010;26:15065–9.
48. Lagunas A, Comelles J, Martinez E, Samitier J. Universal chemical gradient platforms using poly(methyl methacrylate) based on the biotin-streptavidin interaction for biological applications. Langmuir. 2010;26:14154–61.
49. Li B, Chen J, Wang JH. RGD peptide-conjugated poly(dimethylsiloxane) promotes adhesion, proliferation, and collagen secretion of human fibroblasts. J Biomed Mater Res A. 2006;79:989–98.
50. Causa F, Battista E, Della Moglie R, Guarnieri D, Iannone M, Netti PA. Surface investigation on biomimetic materials to control cell adhesion: the case of RGD conjugation on PCL. Langmuir. 2010;26:9875–84.
51. Kunzler TP, Drobek T, Schuler M, Spencer ND. Systematic study of osteoblast and fibroblast response to roughness by means of surface-morphology gradients. Biomaterials. 2007;28:2175–82.
52. Lord MS, Cousins BG, Doherty PJ, Whitelock JM, Simmons A, Williams RL, Milthorpe BK. The effect of silica nanoparticulate coatings on serum protein adsorption and cellular response. Biomaterials. 2006;27:4856–62.
53. Mann BK, West JL. Cell adhesion peptides alter smooth muscle cell adhesion, proliferation, migration, and matrix protein synthesis on modified surfaces and in polymer scaffolds. J Biomed Mater Res. 2002;60:86–93.
54. Sawyer AA, Weeks DM, Kelpke SS, McCracken MS, Bellis SL. The effect of the addition of a polyglutamate motif to RGD on peptide tethering to hydroxyapatite and the promotion of mesenchymal stem cell adhesion. Biomaterials. 2005;26:7046–56.
55. Sawyer AA, Hennessy KM, Bellis SL. The effect of adsorbed serum proteins, RGD and proteoglycan-binding peptides on the adhesion of mesenchymal stem cells to hydroxyapatite. Biomaterials. 2007;28:383–92.

56. Wang S, Liu K, Liu J, Yu ZT, Xu X, Zhao L, Lee T, Lee EK, Reiss J, Lee YK, Chung LW, Huang J, Rettig M, Seligson D, Duraiswamy KN, Shen CK, Tseng HR. Highly efficient capture of circulating tumor cells by using nanostructured silicon substrates with integrated chaotic micromixers. Angew Chem Int Ed. 2011;50:3084–8.
57. Alunni-Fabbroni M, Sandri MT. Circulating tumour cells in clinical practice: methods of detection and possible characterization. Methods. 2010;50:289–97.
58. Nagrath S, Sequist LV, Maheswaran S, Bell DW, Irimia D, Ulkus L, Smith MR, Kwak EL, Digumarthy S, Muzikansky A, Ryan P, Balis UJ, Tompkins RG, Haber DA, Toner M. Isolation of rare circulating tumour cells in cancer patients by microchip technology. Nature. 2007;450:1235–9.
59. Adams AA, Okagbare PI, Feng J, Hupert ML, Patterson D, Gottert J, McCarley RL, Nikitopoulos D, Murphy MC, Soper SA. Highly efficient circulating tumor cell isolation from whole blood and label-free enumeration using polymer-based microfluidics with an integrated conductivity sensor. J Am Chem Soc. 2008;130:8633–41.
60. Fischer KE, Aleman BJ, Tao SL, Hugh Daniels R, Li EM, Bunger MD, Nagaraj G, Singh P, Zettl A, Desai TA. Biomimetic nanowire coatings for next generation adhesive drug delivery systems. Nano Lett. 2009;9:716–20.
61. Medley CD, Bamrungsap S, Tan W, Smith JE. Aptamer-conjugated nanoparticles for cancer cell detection. Anal Chem. 2011;83:727–34.
62. Qin Z, Bischof JC. Thermophysical and biological responses of gold nanoparticle laser heating. Chem Soc Rev. 2012;41:1191–217.
63. Sapsford KE, Algar WR, Berti L, Gemmill KB, Casey BJ, Oh E, Stewart MH, Medintz IL. Functionalizing nanoparticles with biological molecules: developing chemistries that facilitate nanotechnology. Chem Rev. 2013;113:1904–2074.
64. Qu Y, Zhang Y, Yu Q, Chen H. Surface-mediated intracellular delivery by physical membrane disruption. ACS Appl Mater Interfaces. 2020;12:31054–78.
65. Qu Y, Lu K, Zheng Y, Huang C, Wang G, Zhang Y, Yu Q. Photothermal scaffolds/surfaces for regulation of cell behaviors. Bioact Mater. 2022;8:449–77.
66. Delcea M, Sternberg N, Yashchenok AM, Georgieva R, Baumler H, Mohwald H, Skirtach AG. Nanoplasmonics for dual-molecule release through nanopores in the membrane of red blood cells. ACS Nano. 2012;6:4169–80.
67. Xiong R, Raemdonck K, Peynshaert K, Lentacker I, De Cock I, Demeester J, De Smedt SC, Skirtach AG, Braeckmans K. Comparison of gold nanoparticle mediated photoporation: vapor nanobubbles outperform direct heating for delivering macromolecules in live cells. ACS Nano. 2014;8:6288–96.
68. Baumgart J, Humbert L, Boulais E, Lachaine R, Lebrun JJ, Meunier M. Off-resonance plasmonic enhanced femtosecond laser optoporation and transfection of cancer cells. Biomaterials. 2012;33:2345–50.
69. Vogel A, Noack J, Hüttman G, Paltauf G. Mechanisms of femtosecond laser nanosurgery of cells and tissues. Appl Phys B Lasers Opt. 2005;81:1015–47.
70. Lyu Z, Zhou F, Liu Q, Xue H, Yu Q, Chen HA. Universal platform for macromolecular Deliveryinto cells using gold nanoparticle layers via the photoporation effect. Adv Funct Mater. 2016;26:5787–95.
71. Katas H, Alpar HO. Development and characterisation of chitosan nanoparticles for siRNA delivery. J Control Release. 2006;115:216–25.
72. Wang L, Wu J, Hu Y, Hu C, Pan Y, Yu Q, Chen H. Using porous magnetic iron oxide nanomaterials as a facile photoporation nanoplatform for macromolecular delivery. J Mater Chem B. 2018;6:4427–36.
73. Zheng Y, Wu Y, Zhou Y, Wu J, Wang X, Qu Y, Wang Y, Zhang Y, Yu Q. Photothermally activated electrospun nanofiber Mats for high-efficiency surface-mediated gene transfection. ACS Appl Mater Interfaces. 2020;12:7905–14.

74. Lu K, Qu Y, Lin Y, Li L, Wu Y, Zou Y, Chang T, Zhang Y, Yu Q, Chen HA. Photothermal nanoplatform with sugar-triggered cleaning ability for high-efficiency intracellular delivery. ACS Appl Mater Interfaces. 2022;14:2618–28.
75. Fouriki A, Dobson J. Nanomagnetic gene transfection for non-viral gene delivery in NIH 3T3 mouse embryonic fibroblasts. Materials. 2013;6:255–64.
76. Okita K, Nakagawa M, Hyenjong H, Ichisaka T, Yamanaka S. Generation of mouse induced pluripotent stem cells without viral vectors. Science. 2008;322:949–53.
77. Yue Y, Jin F, Deng R, Cai J, Chen Y, Lin MC, Kung HF, Wu C. Revisit complexation between DNA and polyethylenimine—effect of uncomplexed chains free in the solution mixture on gene transfection. J Control Release. 2011;155:67–76.
78. Kircheis R, Wightman L, Wagner E. Design and gene delivery activity of modified polyethylenimines. Adv Drug Deliv Rev. 2001;53:341–58.
79. Teo PY, Yang C, Hedrick JL, Engler AC, Coady DJ, Ghaem-Maghami S, George AJ, Yang YY. Hydrophobic modification of low molecular weight polyethylenimine for improved gene transfection. Biomaterials. 2013;34:7971–9.
80. Tian H, Guo Z, Chen J, Lin L, Xia J, Dong X, Chen X. PEI conjugated gold nanoparticles: efficient gene carriers with visible fluorescence. Adv Healthc Mater. 2012;1:337–41.
81. Peng Q, Hu C, Cheng J, Zhong Z, Zhuo R. Influence of disulfide density and molecular weight on disulfide cross-linked polyethylenimine as gene vectors. Bioconjug Chem. 2009;20:340–6.
82. Wu J, Xue H, Lyu Z, Li Z, Qu Y, Xu Y, Wang L, Yu Q, Chen H. Intracellular delivery platform for "recalcitrant" cells: when polymeric carrier marries photoporation. ACS Appl Mater Interfaces. 2017;9:21593–8.
83. Yang J, Feng Y, Zhang L. Biodegradable carrier/gene complexes to mediate the transfection and proliferation of human vascular endothelial cells. Polym Adv Technol. 2015;26:1370–7.
84. Feng Y, Guo M, Liu W, Hao X, Lu W, Ren X, Shi C, Zhang W. Co-self-assembly of cationic microparticles to deliver pEGFP-ZNF580 for promoting the transfection and migration of endothelial cells. Int J Nanomedicine. 2017;12:137–49.
85. Wu MC, Deokar AR, Liao JH, Shih PY, Ling YC. Graphene-based photothermal agent for rapid and effective killing of bacteria. ACS Nano. 2013;7:1281–90.
86. Lin D, Qin T, Wang Y, Sun X, Chen L. Graphene oxide wrapped SERS tags: multifunctional platforms toward optical labeling, photothermal ablation of bacteria, and the monitoring of killing effect. ACS Appl Mater Interfaces. 2014;6:1320–9.
87. Tan SY, Chew SC, Tan SY, Givskov M, Yang L. Emerging frontiers in detection and control of bacterial biofilms. Curr Opin Biotechnol. 2014;26:1–6.
88. Hadjesfandiari N, Yu K, Mei Y, Kizhakkedathu JN. Polymer brush-based approaches for the development of infection-resistant surfaces. J Mater Chem B. 2014;2:4968–78.
89. Wei T, Yu Q, Chen H. Responsive and synergistic antibacterial coatings: fighting against bacteria in a smart and effective way. Adv Healthc Mater. 2019;8:1801381.
90. Zou Y, Zhang Y, Yu Q, Chen H. Dual-function antibacterial surfaces to resist and kill bacteria: painting a picture with two brushes simultaneously. J Mater Sci Technol. 2021;70:24–38.
91. Zou Y, Zhang Y, Yu Q, Chen H. Photothermal bactericidal surfaces: killing bacteria using light instead of biocides. Biomater Sci. 2021;9:10–22.
92. Bassetti M, Merelli M, Temperoni C, Astilean A. New antibiotics for bad bugs: where are we? Ann Clin Microbiol Antimicrob. 2013;12:22.
93. Wilson M. Photolysis of oral bacteria and its potential use in the treatment of caries and periodontal disease. J Appl Bacteriol. 1993;75:299–306.
94. Ray PC, Khan SA, Singh AK, Senapati D, Fan Z. Nanomaterials for targeted detection and photothermal killing of bacteria. Chem Soc Rev. 2012;41:3193–209.
95. Wang Y, Wei T, Qu Y, Zhou Y, Zheng Y, Huang C, Zhang Y, Yu Q, Chen H. Smart, photothermally activated, antibacterial surfaces with thermally triggered bacteria-releasing properties. ACS Appl Mater Interfaces. 2020;12:21283–91.
96. Wang Y, Zou Y, Wu Y, Wei T, Lu K, Li L, Lin Y, Wu Y, Huang C, Zhang Y, Chen H, Yu Q. Universal antifouling and photothermal antibacterial surfaces based on multifunctional

metal–phenolic networks for prevention of biofilm formation. ACS Appl Mater Interfaces. 2021;13:48403–13.
97. Li L, Li G, Wu Y, Lin Y, Qu Y, Wu Y, Lu K, Zou Y, Chen H, Yu Q, Zhang Y. Dual-functional bacterial cellulose modified with phase-transitioned proteins and gold nanorods combining antifouling and photothermal bactericidal properties. J Mater Sci Technol. 2022;110:14–23.
98. Lin Y, Zhang H, Zou Y, Lu K, Li L, Wu Y, Cheng J, Zhang Y, Chen H, Yu Q. Superhydrophobic photothermal coatings based on candle soot for prevention of biofilm formation. J Mater Sci Technol. 2023;132:18–26.
99. Mi L, Jiang S. Integrated antimicrobial and nonfouling zwitterionic polymers. Angew Chem Int Ed. 2014;53:1746–54.
100. Wei T, Tang Z, Yu Q, Chen H. Smart antibacterial surfaces with switchable bacteria-killing and bacteria-releasing capabilities. ACS Appl Mater Interfaces. 2017;9:37511–23.
101. Wei T, Qu Y, Zou Y, Zhang Y, Yu Q. Exploration of smart antibacterial coatings for practical applications. Curr Opin Chem Eng. 2021;34:100727.
102. Yu Q, Chen H. Smart antibacterial surfaces with switchable function to kill and release bacteria. Acta Polym Sin. 2020;51:319–25.
103. Qu Y, Wei T, Zhao J, Jiang S, Yang P, Yu Q, Chen H. Regenerable smart antibacterial surfaces: full removal of killed bacteria via a sequential degradable layer. J Mater Chem B. 2018;6:3946–55.
104. Burda C, Chen X, Narayanan R, El-Sayed MA. Chemistry and properties of nanocrystals of different shapes. Chem Rev. 2005;105:1025–102.
105. Wang D, Ha Y, Gu J, Li Q, Zhang L, Yang P. 2D protein supramolecular nanofilm with exceptionally large area and emergent functions. Adv Mater. 2016;28:7414–23.
106. Gu J, Miao S, Yan Z, Yang P. Multiplex binding of amyloid-like protein nanofilm to different material surfaces. Colloid Interface Sci Commun. 2018;22:42–8.

Chapter 6
Surface Modification of Tissue Engineering Scaffolds

Zuyong Wang, Feng Wen, and Mark Seow Khoon Chong

Abstract Scaffolds in tissue engineering provide a substrate for cells to grow on, in order to form functional, organised tissue. The ideal scaffold thus possesses mechanical properties to cope with physiological loads, degradation profiles to match the rate of tissue regeneration, while also eliciting favourable host responses. There is, however, often a trade-off between having optimal bulk or surface properties. To address this, various strategies to perform surface modification have been developed to tailor scaffolds for specific applications. These strategies are discussed in this chapter and may be broadly categorised under modification based largely on physical mechanisms (employed largely to induce changes in topography, roughness or wettability) or chemical modification (employed largely to introduce new functional groups on a surface). Subsequently, the characterisation of the modified surface is necessary, in order to facilitate design for use as scaffolds. These evaluations are similarly discussed in this chapter as physical, chemical and biological characterisation methods. The latter, in particular, is unique to materials used in medical applications (including tissue engineering scaffolds) and the section discussed the use of the ISO 10993 set of standards.

Keywords Surface modification · Scaffolds · Tissue engineering · Surface characterisation · Biocompatibility

Z. Wang
Hunan University, Changsha, China

F. Wen
Wenzhou Institute, University of Chinese Academy of Sciences, Wenzhou, China

M. S. K. Chong (✉)
National University of Singapore, Singapore, Singapore
e-mail: markchong@nus.edu.sg

C. Gao (ed.), *Polymeric Biomaterials for Tissue Regeneration*,
https://doi.org/10.1007/978-981-99-6948-7_6

6.1 Introduction

A wide range of biomaterials, both synthetic and biologically derived, are used widely in biomedical applications, including utility as scaffolds in tissue engineering. These materials are largely selected on their bulk properties, such as mechanical strength and degradation properties, in order to meet structural requirements [1, 2]. However, host responses are largely mediated by interactions with the material surfaces [3], and there emerges a need to tailor these surface properties to elicit appropriate biological responses, while retaining the bulk properties on which the materials were selected [4]. To meet these needs, much research has been dedicated toward the development of surface modification technologies. This chapter discusses the common technologies being used, as well as some methods employed to characterise the modified surfaces.

6.2 Surface Modification Techniques

6.2.1 Physical Surface Modification

The focus of biomaterials is shifting from bioinert implants to bioactive designs, in order to manipulate the interactions between cell physiologic systems and material properties, including physical cues. Physical surface modification refers to processes that apply physical methods to effect change in physical properties (such as roughness and wettability), biochemical properties (biochemical components, functional groups and/or the distribution of them) or topographic structure (lattice structure, pore size and micropatterns) of the surface. Through the physical, biochemical or topographic cues conferred by these modification methods, the adhesion, proliferation, alignment and intracellular physiological activities of cells on modified surface can be controlled. More recently, physical modification methods have also been shown to elicit antimicrobial effects [5, 6] and even retard blood coagulation [7–9].

6.2.1.1 Topographical Engineering

Scaffolds in tissue engineering are analogous to the extracellular matrix (ECM) in that they provide the mechanical substrate for cell growth. Besides structural support, it has become evident that physical cues, in the form of topographical microstructures, are capable of guiding cell alignment and migration in the microenvironment [10, 11]. This phenomenon was described in as early as 1912 by Harrison in the direction of cell motion on spider web and was later defined as ‘contact guidance’ by Weiss [12, 13]. Presently, biological reactions triggered by biomaterial topography have been demonstrated on parenchymal cells, inflammatory cells and bacteria.

Cell Attachment, Growth, Morphogenesis and Differentiation In earlier studies, fibroblasts seeded on quartz slides with parallel ridge-groove structures showed alignment and elongation along the direction of gratings, reflecting contact guidance. Such effects have been shown to be dependent on topographical parameters, such as groove depth [14]. In a study on PMMA substrates with similar patterns, larger depth and width were found to be effective in restricting the lateral movement of fibroblasts across groove structures, smaller widths restricted the longitudinal movement along the ridges [15]. These observations indicate that cells can recognise the dimension of a surface topography both at microscales (cellular sizes) and nanoscales (near the sizes of filopodia and lamellipodia) [16], believed to be mediated by patterning of focal adhesions and filopodial sensing [17, 18]. Focal adhesions (FA) are multi-protein complexes mechanically linking intracellular actin to extracellular substrates via integrin-ligand bundles. It has been evidenced from multiple studies that matured FA result in elongated morphology, aligned in the direction of actin filaments and subject to forces correlating with the main axis of FA elongation [19], and cells adhered on the interface of dual microstructured films have been demonstrated to acquire 'half-cell' alignments [20]. These highlight the utility of topographical engineering in generating the specific anisotropy found in connective, mechano-sensitive, electro-active and shear-responsive tissues [16].

Topographic cues also have mechanical effects on cells by causing deformation of cytoskeleton and adjusting intracellular tension, with accordant changes in nuclear structure, epigenetic signals and expression profiles. These biochemical signals and mechanical signals may in turn further modulate cellular responses and influence cell physiological activities in a cascade of events, influencing cell motility, apoptosis [21], proliferation [22, 23] and differentiation [23–26]. Additionally, the formed focal adhesions serve as biochemical signal sensors to allow transmembrane signal transduction, such as focal adhesion kinase pathways, by activation of integrin receptors [27–29]. Wang et al. reported significant up-regulation of myogenic genes in human mesenchymal stem cells (hMSCs) [24, 25] and tenogenic genes in human tendon cells [26, 30], when these cells were cultured on anisotropic poly(ε-caprolactone) (PCL) surfaces with aligned topographies. In nerve regeneration applications, up-regulation of neural markers at mRNA and protein levels was observed in hMSCs on aligned PCL nanofibre scaffold when compared with that on polystyrene (PS) plate, indicating an enhanced commitment of MSCs into neural cells [31]. Considering, however, that elongated morphologies may have concomitant downstream effects [26] and noting that gene expression triggered by topographies lack tissue specificity [23–25, 32], it would be too simplistic to assume that topographical engineering (or any other single approach) can be used in isolation in therapeutic tissue regeneration.

Immuno-Regulation While generally an important factor in biocompatibility, the immune response is particularly critical in determining the long-term outcome of implants, through the mediation of host responses such as chronic inflammation, fibrosis or integration. For example, neutrophils and macrophages serve both phagocytic and signalling roles, and materials with defined surface structural and

topographical features were reported to favourably modulate the innate immune response, leading to improved healing outcomes. TiO_2 honeycomb-like structures at a minimal scale of 90 nm were reported to facilitate macrophage filopodia formation and up-regulate the Rho family of guanosine triphosphatases (*RhoA*, *Rac1* and *CDC42*), in turn reinforcing the polarisation of macrophages through the activation of the RhoA/Rho-associated protein kinase signalling pathway [33] Similarly, osseointegration events on controlled nanotopographical structures were found to be heavily influenced by microscale features and nanopatterns on implant in vivo, through modulation of inflammatory responses [34]. In a study on breast implants with different surface topographies (average roughness from 0 to 90 μm) in mice and rabbits, an average roughness of 4 μm was found to result in the least amount of inflammation and foreign body response [35]. These observations may be due in part to macrophage polarisation, as demonstrated by Wang et al. [36]. In the latter, the nanotopography of hydroxyapatite disks was shown to influence tissue inflammation, up-regulate gene expression of M2 phenotypic marker and raise the fraction of ARG+ M2 macrophages in vivo. Such findings may be extended to applications beyond implants for tissue engineering, and more generally to modulating immune responses in vivo. In a recent study, heparin-doped polypyrrole (PPy/Hep) electrodes of different surface roughness, with surface roughness values from 5.5 to 17.6 nm, demonstrated different degrees of macrophage recruitment, inflammatory polarisation and fibrotic tissue formation, and could successfully record electrocardiographic signals for up to 10 days without substantial decreases in sensitivity [37]. Such studies indicate that an improved understanding of the relationship between material features and its immunomodulatory potential may help in the design of implantable materials.

Anti-bacterial Effects Following colonisation by bacteria, the formation of a biofilm is typically detrimental for medical devices; endotoxic effects aside, biofilms formed also impede the device performance. It has been shown that bacteria adhere preferentially to topographies that maximise their contact area to surface [38], in accordance with adhesion point theories [39]. When organisms are smaller than topographical structures, the available contact area for bacteria is large; thus, it is able to obtain adhesive strength. Secondarily, the stiffness of a cell wall limits the ability of bacteria to adapt freely to the surface topographies at very small sizes [40]. Such reasoning is supported by studies showing bacteria prefer to adhere at square corners, convex features rather than on flat or concave walls. Yang et al. [41] have proposed a contact-based effect involving energetically favourable adhesion sites and physical confinement. The preferential adhesion points can also influence bacteria motility, thereby interfering with bacterial adhesion. Specifically, surface topographies with line structures decrease bacteria attachment compared to flat surfaces [42], modulated by the elongated morphology and up-regulation of flagellar genes. Meanwhile, bacteria deposits on different surface topographies may confer mechanical stretch to the bacterial cell surface. This can cause the rupture of bacterial cell membrane, leading to bacteria lysis and death. Such bactericidal properties have also been described on pillar topographies, regardless of material surface chemistry.

The killing effect can be enhanced further by multiscale roughness, for example, nano- and microstructures for a highly biocide-free bactericidal property [43].

Physical Modification Methods In order to modify the topographical structure of tissue engineering scaffold, materials are often either added onto substrate surface by methods like nanofibre coating [23, 44] and plasma deposition [45] or ablated by methods like chemical etching and laser corrosion [46, 47]. Li et al. modified the surface of a flexible PCL film with fibres and demonstrated improved deposition efficacy on rougher surfaces [44]. A further study by Guo et al. reported post-fabrication processing by single-axial drawing that induced a coating of highly aligned fibrous topography, leading to enhanced adhesion to substrate and possible application in rotator cuff tendon repair [23, 30]. Similarly, mechanical techniques like stretching may also be applied directly to polymer materials to avoid weight loss and change in material composition while creating new microstructures. After uniaxial stretching, for example, hierarchically and heterologously oriented ridge-groove structures that mimicked ECM more are observed on PCL films and successfully guided human bone marrow MSC elongation and alignment with a preferential orientation determined by the topographical anisotropy [24]. The elongation and alignment of MSC could be observed as soon as 12 h post seeding and demonstrated to last as long as 15 days in vitro. More specifically, altered cell morphology, cytoskeletal reorientation and nucleus elongation were pointed out in the following studies, with increased expression of myogenic genes in MSCs [24, 25] and tenogenic genes in tenocytes [26] following extended culture on the stretched PCL films. The topographical features of stretched PCL films can be further controlled by alkaline hydrolysis [46]. Small concaved features formed at the edge of ridges after soaking in aqueous NaOH solution for longer than 10 days that developed into parallel grooves across the ridges and finally split the ridges into small parallel islands after 30 days of soaking. With declined ridge height and aspect ratio between ridges and grooves resulted from hydrolysis, the guidance effect of topographies on MSC alignment and elongation may be compromised. In addition, the ridge-groove topographies can be further augmented with femtosecond laser microperforation to create secondary microfeatures [20, 32]. Thus, engineered scaffolds were used to generate hybrid cell-material sheet, for example, when MSCs and human umbilical vein endothelial cells were seeded separately on each face of the stretched PCL film. This construct allowed heterotypic cell-cell contacts across the film and mimicked the myoendothelial communication between tunica media and intima. In a recent study, Luo et al. applied a femtosecond laser to write micro-grooves on PCL film, where laser engineering was found to influence both surface wettability and 3D cell morphology [47]. Even with precise laser engineering, physical alterations are coupled with chemical changes on the biomaterials surface (such as polymerisation and chain scission), and these effects must be considered in rational design and selection of processing methods.

6.2.1.2 Wettability Engineering

Wettability refers to the interaction at the two-phase interface between fluid and solid. Solid surface with a greater wettability is more favourable for the fluid to spread over or adhere to it, so that the contact angle between solid–fluid interface and vapour–fluid interface is smaller. Wettability presents as one of the primary concerns in scaffold material design, for its influence on both initial cell attachment and migration on scaffold surfaces via adsorption of proteins from culture medium in vitro or from extracellular fluid in vivo and then binding to cell adhesion molecules on cell surface. The preferable range of wettability varies according to the kind of cells. For example, a range of water contact angles for cell adhesion and growth was suggested to be from 50° to 60° [48], but a more hydrophilic surface with the water contact angle between 20° and 40° was more suitable for cell attachment of NIH 3T3 fibroblasts [49]. When inherent surface wettability is not favourable for cell growth, surface modification may be necessary. For example, PCL fibres from electrospinning are considered too hydrophobic for direct cell adhesion, with a typical water contact angle of 100–130° [23]. By depositing the PCL fibres on a substrate, subjecting to single-axial drawing, or blending with bioactive tricalcium phosphate particles, the contact angles of the fibres can be further adjusted. Coating with polymers such as poly(vinyl phosphonic acid-*co*-acrylic acid) (PVPA), can also render a surface hydrophilic, with water contact angles dropping to 43.3 ± 1.2° [50]. After 14 days in vitro culture, osteoblasts on PCL/PVPA scaffold generated a better-defined cytoskeleton than those on uncoated PCL scaffold, indicating a better cell spreading due to improved wettability of PCL fibre. Such methods reflect the classical approach of modifying the surface of a bulk material that possesses desirable physical properties, in order to confer the preferred properties of the surface material (which typically has inadequate bulk properties).

Alkaline hydrolysis is one of the mature techniques to modify surface wettability for polyester biomaterials such as PCL [51], PLA [52, 53] and PLGA [54, 55] and already has been applied in industry. After treatment with alkaline agent (usually mild NaOH solution), the ester bonds on the surface of polyester materials break and form carboxyl and hydroxyl end-groups. As observed in the previous section, hydrolysis may also alter topographies of the surface, resulting in an improved roughness. The increased surface energy results in greater affinity to water molecules, resulting in the higher hydrophilicity favoured by specific cell types. More controlled and targeted approaches using laser-assisted techniques have been well investigated to modify biomaterial surface wettability by making the controllable topographical roughness for implants and bioelectronic applications [16, 56]. Based on the Wenzel equation, the increase in roughness of a solid surface can either increase the hydrophilicity in a hydrophilic system in which the water contact angle is smaller than 90° or increase the hydrophobicity in a hydrophobic system where the water contact angle is larger than 90°. Thus, by changing the surface roughness, the wettability of biomaterials can be optimised for a better cytocompatibility. Extreme ultraviolet (EUV) irradiation is another approach for roughness optimisation for

polymeric materials. For instance, polyether ether ketone (PEEK) commonly used in reconstructive surgery has unique mechanical and physicochemical properties, but lack polar surface chemical groups, and has an inherently low surface energy. To modify extremely stable materials such as the PEEK surface, EUV irradiation in the presence of oxygen and nitrogen gases were used [57], which made significant changes to surface topography with increased surface roughness, formation of conical structures and incorporation of nitrogen and oxygen atoms. As a result, the PEEK surface demonstrated non-cytotoxic properties and an enhancement in adhesion of human osteoblast-like MG63. Nanofibre deposition or nanoparticle deposition onto the surface of biomaterials is another approach to change surface roughness [44]. On PLA films incorporated with magnetic nanoparticles, enhanced adhesion and proliferation of cardiac-like rat myoblasts H9c2 was found on the film with the highest amount of embedded nanoparticles and hence the largest surface roughness with the largest water contact angle [58]. It is noteworthy that in this study, with the increase of surface roughness, film surface turned from being hydrophilic to hydrophobic, which looks contrary to abovementioned conclusion from the Wenzel equation. This is because surface wettability is influenced by complex factors including not only the roughness but also other aspects like electrical and chemical nature, which should also be taken into account at the design of material surface.

Other techniques for surface roughening are still under exploration. Borrowing ideas from micromanipulation, carving the surface of polymer materials or moving polymer chains at a microlevel and even nano-level high precision for surface modification may be realised under two-photon polymerisation (TPP), atomic force microscope (AFM) or scanning tunnelling microscope (STM) with manipulator and tip of scanning probe. As yet, such approaches are limited by high costs and availability of such facilities; these are further exacerbated by the demand for specialised cross-linking agents and material systems for TPP techniques, while only electrically conductive polymers can be processed under STM.

6.2.1.3 Physical Deposition

Physical deposition is a commonly-employed method to produce a functional coating layer on substrate material so as to grant the material with more desirable surface properties. In particular, bioactive components including inorganic particles, synthetic polymers, lipids, polysaccharides, peptides, proteins as well as cell receptor ligands [59, 60] are deposited onto scaffold materials for enhanced initial cell attachment and proliferation or to regulate intracellular protein synthesis and induce cell differentiation [61]. For the combination of functional materials with substrates, weak forces such as van der Waals forces, hydrogen bond force and electrostatic attraction force are formed during deposition. Based on the existing form of coating materials, physical deposition can be classified into solution deposition, vapour and sputtering deposition. The last two share a similar process that deposition of a material starts as a solid and transports to the substrate surface to build up a film slowly. Compared to chemical conjugation, physical modification might be less

stable which leads to gradual loss of the coating layer [62]. On the other hand, physical deposition has a broader application with the multitude of materials as substrate or as coating layer regardless of their chemical composition.

Solution deposition methods may be further subcategorised into immersion and adsorption, casting, dip coating and electrophoretic deposition. These methods are based on allowing the substrate to contact and adsorb the functional molecules dissolved in a liquid phase, followed by removal of the solvent by evaporation. Immersion and adsorption are the simplest methods by which substrate stands in a solution and spontaneously adsorbs the functional molecules uniformly dispersed in this solution. In applied electric field, deposition of coating molecules can be accelerated by electrophoretic motion of these molecules in solution toward the substrate placed at a corresponding electrode. This technique for physical deposition is named as electrophoretic deposition. Besides, the thickness of coating layer is determined by the time length of deposition and/or electric field strength. The technique as casting for modification of smooth and flat surface is developed from the same principle as immersion. Other than a static contact between substrate and solution, solution containing functional molecules is sprayed onto the substrate and subsequently spreads over the surface at high-speed spinning and thereby forms a thin liquid layer that leaves the functional molecules as a film covering the substrate after evaporation. The thickness of this coating film is controllable depending on both the speed of centrifuging and the viscosity of the solution. Dip coating is another popular low-cost technique for deposition on monolithic three-dimensional scaffolds. The process is completed by partially or fully inserting the substrate into coating solution followed by removal from the solution. For example, polypropylene (PP) has a remarkably low surface energy and poor surface functions [63]. By dip-coating of the PP surface with functional molecules, the surface segregation of these moieties yields a low-fouling surface. In addition, the process of dip coating can be repeated to obtain multiple coating layers, which is named as ‘layer-by-layer’ fabrication. Unlike simple immersing or spin casting, dip coating enables oriented alignment of coating layers formed by amphiphilic molecules like phospholipid and further affects surface properties of scaffold materials. Amphiphilic molecules refer to the kind of molecules that possesses both hydrophilic groups and lipophilic groups. In a solution, these molecules float on the surface of the solvent, keep the part of the molecule compatible with the solvent under liquid level and expose the other part above liquid level. Through different operating procedures consisted of dipping and removing, specific moieties on the amphiphilic molecules can be connected to the substrate surface or the previous coating layer. Especially on polymer substrates, entrapment of coating molecules in the surface may occur at the same time with physical adsorption due to the space created at swelling of polymers in the solvent, resulting in added amount of coating molecules deposited on polymer substrate [64].

Physical vapour deposition (PVD) is a surface coating method in which the coating material is vaporised in a cell at high temperature, often in the presence of gaseous plasma. The vapour is subsequently transported to the substrate surface and condenses to generate a thin film on it. Based on the methods applied to generate and

deposit material, PVD is further classified into vacuum evaporation deposition [65] pulsed laser deposition [66], electron beam deposition [67], cathodic arc deposition [68] and (most commonly for tissue engineering scaffolds) sputtering deposition [69]. In order to create gaseous coating material, inert gas (typically argon) is transferred into plasma and accelerated under a high-voltage electric field. Bombardment from this high-energy plasma at cathodic target frees coating molecules from solid source into a vapour phase through momentum transfer. These active molecules deposit on all surfaces inside a chamber to release energy and rebuild thermodynamic equilibrium, therefore forming a thin film on the substrate surface. Compared to evaporation deposition, sputtering deposition is superior in surface coating, being amenable to materials with relatively low melting points and forming a more sturdy coating on the substrate.

6.2.2 Chemical Modification

While biomaterials are primarily selected on their bulk properties, host responses are largely governed by the cell-material interactions at interface. It follows that synthetic materials, ranging from polymers to ceramics and metals, usually lack appropriate biological surface cues to elicit or direct desirable cellular and tissue responses such as adhesion, proliferation and immune response [1, 70–72]. To this end, chemical surface modifications may be performed to introduce biochemical cues onto material surfaces, while retaining the existing bulk material properties. These modification methods are summarised in Table 6.1, of which plasma-, gamma-, UV-, hydrolysis- and aminolysis-induced chemical modifications are the most common and are discussed in further detail.

6.2.2.1 Plasma-Induced Modification

Plasma-induced modification is useful for the selective creation of chemistry and topography on biomaterial surface with an excellent retention of the bulk

Table 6.1 Physical and chemical surface modification methods

Methods	References
Radiation (electron beam and gamma)	[73, 74]
Plasma (RF, microwave, acoustic, corona discharge)	[75–77]
Photo (UV and visible sources)	[78]
Ion beam (sputtering, etching, implantation)	[79, 80]
Gas phase deposition	[71, 81, 82]
Silanisation	[83]
Coating (with or without covalent bonding)	[84, 85]
Chemical reaction (oxidation, reduction, hydrolysis, aminolysis)	[70, 86, 87]

characteristics for specific biomedical applications [88–91]. Plasma, the fourth state of matter after solid, liquid and gas, is typically generated by applying high voltages to gases, under which the gas molecules or atoms will be ionised by the electrical discharge and therefore split up into electrons and ions [92]. The effectiveness of the ionisation process is dependent on operating parameters such as gas flow rate, pressure and constituents, as well as the distance between the discharge electrodes. Plasma can be further characterised with an energy distribution in the range of 10–20 eV to effectively modify most materials. The interaction between ionised gas species with surface substrates contacted in plasma could produce tailored physical and chemical modifications on substrate surface through ionic activity in plasma and functionalities (functional groups or free radicals) formation on the surface. As described earlier, in physical modification, the bombardment of ionic species powered by an electrical field can increase substrate surface roughness and promote interfacial adhesion of depositions [89]. Additionally, chemical modification can be achieved by controlling the (1) functional groups or free radicals which are generated on substrate surfaces by interaction between charged particles and surface molecules of the substrate [75] and (2) desirable monomer polymerisation and deposition on the surface of the substrate [93]. The functionalities formation on substrate surfaces may be altered by proper selection of the nature of the gaseous medium in plasma. Plasma generated in oxygen, ammonia and carbon dioxide gases can be used to introduce functionalities such as hydroperoxide, amino and carboxylic groups on substrate surface, respectively. Additionally, inert gases such as argon lead to the generation of free radicals on the polymer backbone, which are transformed into hydroperoxide bridges in the presence of oxygen and water vapour [1, 94]. Biomaterials with functionalities formation on their surface are either directly used for biomedical applications or continuously conjugated with following various desirable molecules for specific biomedical applications while those functionalities will be used as anchorage points. It has been reported that polyvinylidene fluoride membrane exposed to plasma resulted in grafting of quaternary ammonium compounds successfully [95]. This was performed via electron transfer for atom-transfer radical-polymerization; the thus-modified surface demonstrated a high inhibition rate ~98.3% of *E. coli* and ~98.5% of *S. aureus*, respectively. Control of plasma parameters and conjugants provides great versatility in the tailoring and customisation of surfaces of biomaterials. It is important to note here the process of plasma surface modification often leads to the formation of a layer of polymer on the surface and is coupled with physical alterations to the topography (discussed earlier in the preceding section) [1, 96, 97].

PCL and poly(lactide-*co*-caprolactone) (PLCL) have been used as bioresorbable polymers in numerous bioelectronics [95], medical devices [98] as well as for tissue engineering applications [23, 26, 30]. Biomolecule such as monomeric acrylic acid was conjugated on the surface of PCL and PLCL to optimise their bioactivities through plasma-induced surface modification [1, 75]. The exposure to argon/oxygen plasma under a UV irradiation resulted in formation of peroxide and hydroperoxide groups, which further initiated the addition polymerisation of acrylic acid to the PCL and PLCL membranes by decomposition of hydroperoxides. The degree of

polymerisation of acrylic acid on membrane surfaces is considerably influenced by the plasma exposure parameters, such as plasma power, pressure, exposure time and the reaction conditions involving monomer concentration and reaction time. Collagen and Jagged-1 peptides were then immobilised on the modified PCL and PLCL surface through carbodiimide coupling.

These technologies may be readily adapted toward other biomolecules, in order to tailor specific responses. Hyaluronic acid (HA), for example, is a biopolymer possessing numerous functions to be involved in wound repair, cell migration and cell signalling within the body [99, 100]. It is largely considered to be non-toxic, non-immunogenic, enzymatically degradable and relatively non-adhesive to cells and proteins [101]. Additionally, HA is involved in several physiological processes, including angiogenesis, extracellular matrix homeostasis, wound healing and the mediation of long-term inflammation. This versatile nature of HA has led to many studies not only on the preparation of HA alone but also on the subsequent usage for surface modification of biomaterials for specific medical applications. While HA can be applied as a physical coating, they get displaced easily, and covalent bonding of HA is necessary for use in biomedical applications. For example, HA covalently bonded on polydimethylsiloxane surface through oxygen plasma surface modification resulted in the decrease in the protein adsorption and significant cell growth and neural differentiation [96]; biomolecular binding to HA can further modulate biological activity, particularly for wound healing applications.

In performing plasma modifications, several parameters may be controlled in order to maximise polymerisation yield. Plasma treatment time, for example, significantly influences the formation of free radicals, and titration may be performed to establish the optimum plasma treatment time required for maximal free radical generation. Overexposure may also lead to the loss of free radicals that are otherwise responsible for peroxidation during exposure to oxygen [75, 102]. Additionally, the polymerisation conditions, such as spacer-monomer concentration, have profound impact on the yield of polymerisation. Without UV irradiation (typically at elevated temperatures), the yield initially increases with monomer concentration, reaches a maximum and then tends to decrease beyond a critical concentration [76], whereby extensive autocatalysis leads to homopolymerisation of the solution phase. In contrast, with UV irradiation and controlled temperatures, the yield typically increases continuously with the increase of the monomer concentration [1].

6.2.2.2 Ultraviolet (UV)-Induced Modification

UV irradiation is a simple, efficient and economic method widely used for surface modification of biomaterials [103, 104]. UV light is generally classified in four sub-bands: UVA (315–400 nm), UVB (280–315 nm), UVC (100–280 nm) and EUV (10–124 nm). At the wavelengths from 180 to 400 nm, UV light provides sufficient energy to disrupt molecular bonds on biomaterial surfaces, leading to a series of photo-physical, thermal and photochemical processes. However, this influence is often not limited only to superficial layer of the material but potentially alters the

material bulk properties [105]. As such, initiators are commonly used, which can reduce the dosage of UV irradiation in the surface modification process [91, 106, 107].

UV light irradiation has been extensively studied for surface modification of low- (LDPE) and high-density (HDPE) polyethylene membranes. For example, when HDPE was treated with selected active compounds and a photo-initiator under 254 nm UV excitation, the surface chemistry of HDPE was altered [107]. Functional moieties conjugated on the surface of HDPE via specific bonds resulted in increased wettability of the innately hydrophobic HDPE surface. However, the surface modification by UV irradiation could induce photodegradation and aging effect on the bulk polymer [108, 109].

In another example of UV-induced surface modification, irradiation of polyethylene terephthalate (PET) in formation of nano- and microstructures on the polymer surfaces, leading to more hydrophobic surfaces [110]. In contrast, when PET films were functionalised through conjugation with both RGD peptide and galactose ligands, enhanced cell adhesion and synergistic functions were also observed [91]. Plasma and UV irradiation can also be combined, by first irradiating the PET films with argon plasma (at power output of 40 W for 1 min) and then exposure to air (for 10 min) to induce the formation of peroxides and hydroperoxides on its surface. This is followed by UV irradiation to induce surface polymerisation of degassed monomeric solutions. Alternatively, this step could be replaced by the addition of some agents such as sodium periodate, which helps in oxygen depletion to ensure polymerisation efficiently. For example, exposure to UV (365 nm) may be performed to initiate the formation of a poly(acrylic acid) (pAAc) on the PET surface. Subsequently, RGD peptide and galactose ligands can be coupled to the pAAc layer using carbodiimide chemistry. This approach led to successful grafting of pAAc on PET films, with carboxyl-group density of 78.57 nmol/cm^2 available for subsequent conjugation of RGD peptides and galactose ligands.

More recently, extreme UV (EUV) radiation has been used as a source of high-energy ultraviolet radiation. The main advantage of the EUV irradiation is preservation of bulk properties of irradiated material due to its photon energy which is capable of breaking more molecular bonds at the upper surface of the material as compared to common UV light [111]. For the same reason, however, EUV radiation propagates only in vacuum, and hence, irradiation of materials in gaseous environment requires a special arrangement. Similar to plasma etching, EUV radiation is also used to produce nano-/microsized pattern on the surface of polymers [112].

6.2.2.3 Gamma-Induced Modification

Gamma radiation is an extremely high-frequency electromagnetic radiation and comprises high-energy photons generally above 110 keV. Gamma-induced modification is a well-established technique to modify biomaterial properties by gamma ray irradiation-induced modifications (grafting, cross-linking or gel formation). Cobalt-60 and cesium-137 are common sources used in gamma-induced

modifications. This technique has been intensively used for applications in the medical field for surface modification of materials to control blood-material interactions and conjugation of molecules in polymeric matrices to form specific chemical moieties or drug carriers. The major advantages of gamma-induced modification are as follows: (1) Due to its high-energy nature, initiators are not required in the process. Therefore, the purity of products may be maintained, as free radicals are formed on the polymer/monomer backbone. (2) Deep penetration of gamma rays through the polymer matrix enables rapid and uniform generation of free radicals and therefore could initiate the modification process throughout the entire material. (3) The gamma-induced modification can be performed at room temperatures. (4) It generates less environmental pollution than chemical methods. Several studies have been devoted to the development of biomaterials based on the radiation surface modification process [113–117].

As described earlier, surface chemistry is critical in mediating host and cellular responses. Additionally, functional groups on the surface can be exploited as chemically reactive sites for coupling other function molecules for specific biomedical applications. In this context, gamma irradiation may be useful for the introduction of functional moieties to the material surface. For example, polystyrene (PS) has many attractive features for medical applications but is a typically inert polymer which lacks functional groups. Exposure to gamma radiation yielded carbonyl and ether functional groups on the surface. Carbonyl groups were presented below the top few molecular layers of ester. Unsaturated carbonyl/acid groups formed a higher proportion of the total carbonyls with increasing depth, and the extent of interior oxidation was linear with gamma dosage [118]. In another study, polyethersulfone (PES) was subjected to gamma radiation for the purpose of changing the material's innate hydrophobicity, in order to make render the surface less susceptible to fouling [119]; this process was shown to be remarkable for homogeneity of the modified surface. One of the main challenges in designing blood-contacting biomaterials lies in the need to prevent thrombus formation. Proper tailoring of the biomaterial surface is aimed at reducing the adsorption of clot-initiating proteins and the adhesion of platelets. In one study, polyethylene glycol methacrylate (PEG-MA) with different molecular weights was conjugated on the surface of PE films by gamma irradiation, and results showed less adsorption of proteins and adhesion of platelets on PE film surfaces after modification [120]. The degree of grafting is found to be strongly dependent on the reaction conditions, as well as the storage time and temperature of the irradiated film prior to the reaction. Additionally, reaction temperatures can be controlled to keep segmental mobility low such that the free radicals that are produced during the irradiation remain trapped within the matrix.

6.2.2.4 Hydrolysis- and Aminolysis-Induced Modification

Many polyesters such as poly(lactic-glycolic acid) (PLGA), PET, poly(ester urethane) (PU), PLLA and PCL have been used for wide biomedical applications such as drug delivery and medical devices due to their well controllable degradation rate

and mechanical properties [87, 121–123]. As mentioned earlier, surface modification of these polymers is necessary to improve their biocompatibility. Among those surface modification methods available, wet-chemical methods of hydrolysis and aminolysis are used most frequently due to their (1) simple steps, (2) ease of control (3) and scalability to three-dimensional structures. Through hydrolysis and aminolysis, carboxylic acid and amine groups could be produced on the surface of polymer in a highly controlled manner, with minimal erosion.

Hydrolysis of polyesters can be driven by either acidic or basic conditions [86, 124]. However, under acidic conditions, hydrolysis of esters is achieved via electrophilic attack by hydrogen ions on the carbonyl oxygen which requires very strongly acidic conditions and may target the bulk material, instead of being limited to surface hydrolysis. In contrast, under basic conditions, hydrolysis is achieved by nucleophilic attack by hydroxide ions on the carbonyl carbon, which is surface-oriented and results in less bulk hydrolysis. For example, PCL films subjected to alkaline hydrolysis obtained rapid increase in surface wettability, while the surface topography was less changed at microscales and accompanied by little mass loss [46]. However, alkaline hydrolysis typically results in bulk degradation of the PCL film and accelerated loss of structure. In the same study, hydrolysis was limited to the superficial layer of uniaxially drawn PCL, highlighting the effects of post-processing.

Aminolysis is driven by nucleophilic attack on the carbonyl carbon to generate a positively charged tetrahedral intermediate. Aminolysis may be performed either in basic solutions or in an aprotic, polar solvent. Unlike base hydrolysis, the overall activation energy for the aminolysis is low and even negative in organic solvents, resulting in reduced or inverse dependence of aminolysis on the reaction temperature. It has been previously reported that aminolysis rates typically reach a plateau at pH values just above the pKa of the amine in aqueous solutions [125]. In a study on PCL scaffolds for vascular tissue engineering applications, aminolysis was performed to introduce amino groups through reaction surface of PCL with 1,6-hexanediamine [121]. It was found that there was a direct correlation between the amount of amino groups generated on the PCL film surface and the concentrations of 1,6-hexanediamine concentrations (0–14%). The amount of amino groups also increased with a prolonged exposure duration, reaching a maximum value at 1 h. Incubation beyond that resulted in a decrease in free amine groups, possibly due to auto-polymerisation with terminal carboxyl groups or degradation of the superficial layer. The exposed amino groups could subsequently be used as anchor sites for the conjugation of protein such as gelatin, chitosan and collagen. The follow-up endothelial cell culture proved that the cell attachment and proliferation ratios were obviously improved, and the cells showed a similar morphology to those cultured on tissue culture polystyrene surfaces.

6.3 Techniques for Analysing Modified Surfaces

Surface characterisation of a modified material is an essential step in determining whether the surface modification is successful and whether the modified surface can satisfy the requirements of its intended application [75, 88, 126]. There are various techniques to characterise the surface properties of a material, and they are broadly categorised into physical, chemical and biological techniques based on the nature of the information intended to be elicited out. In general, physical techniques focus on the surface tension, topography and weight variation, and chemical techniques provide information on the chemical structure and chemical composition of the surface, and biological techniques assess the biocompatibility and cellular responses to the surface. The most common techniques used in the characterisation of polymeric biomaterial surfaces for tissue engineering applications are summarised in Table 6.2 and presented in the following sections.

6.3.1 Physical Characterisation

6.3.1.1 Contact Angle Measurement

As most of polymeric biomaterials will apply in an aqueous environment during their applications in vitro or in vivo. Therefore, it is important to study the interaction between water and the surface of the material, also known as material surface wettability. This reactivity of water with material surface is central in molecular

Table 6.2 Most common techniques for characterising polymeric biomaterial surfaces

Technique	Category	Probe	Information	Requirement
Contact angle	Physical	Liquid drop	Surface energy	Clean, homogeneous, non-porous surface
SEM	Physical	Electrons	Surface topography	Vacuum, conductive sample surface
AFM	Physical	Cantilever	Surface topography, composition, roughness	Clean
QCM	Physical	Quartz crystal resonator.	Mass change	Polymer need to be pre-coated on resonator surface
FTIR	Chemical	Infrared light	Surface composition, binding state	Bulk phase having no overlapping IR absorption with surface molecules
XPS	Chemical	X-ray/ electrons	Chemical composition, binding state	Vacuum, separate elemental analysis for hydrogen
TOF-SIMS	Chemical	Ions	Surface composition	Vacuum, samples stored in aluminium foil or clean glass containers

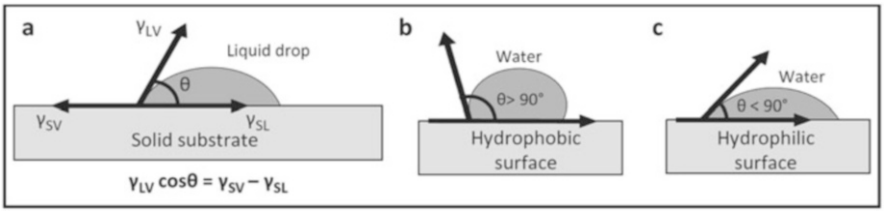

Fig. 6.1 Schematic representation of (**a**) the relation between the contact angle θ and the surface tensions at the three interfaces, (**b**) a drop of water on a hydrophobic surface and (**c**) a drop of water on a hydrophilic surface. (Reprinted from [129], with permission from Springer)

self-association of water at the interface, leading to the formation of water structure that governs the selective adsorption of proteins on the material surface [127]. The wettability of a surface is typically revealed by placing a drop of liquid onto the surface and measuring the contact angle – the angle between the liquid–vapour interface and the solid surface [128]. The contact angle θ is related to the surface tensions at the liquid–vapour, solid–vapour and solid–liquid interfaces (represented by γ_{LV}, γ_{SV} and γ_{SL}) in Young's equation given in Fig. 6.1a [129, 130]. In general, a stronger attraction between the liquid and the surface leads to a lower contact angle. For biomaterials, deionised water is typically used as the probe liquid. Surfaces with a contact angle of more than 90° are generally defined as hydrophobic (Fig. 6.1b), whereas surfaces with a contact angle of less than 90° are generally defined as hydrophilic (Fig. 6.1c). In surface modification experiments, comparing the contact angle value before the modification with the value after the modification can be used to examine the effectiveness of the modification process [1].

Contact angle measurements are typically done on a goniometer, an instrument used for precise measurements of angles. A modern goniometer is equipped with a camera and a software where the researcher can define the solid–liquid interface (also known as drop baseline) and set the fitting method to fit the drop shape. Beside static measurements, dynamic contact angle measurements can also be performed to enhance sensitivity. Dynamic techniques include increasing and decreasing the drop volume and tilting the surface to determine the advancing and receding contact angles. While contact angle measurement is valuable for assessing surface wettability, it is not reliable for heterogeneous surfaces where the wettability differs at various parts of the sample and porous samples where the drop is absorbed into the material [131]. Contact angle measurements also do not offer information on the surface chemistry and topography changes after surface modification. Hence, other characterisation techniques are often performed paralleling with contact angle measurements to provide a full evaluation on the result of a surface modification process [1, 88]. In Fig. 6.2, it shows the contact angle of PEEK is 100.3°. After the sulphonation and hydrothermal treatment, the surface contact angle changes to 70.1° with improved hydrophilicity due to the porous structures on the surface. The contact angle of SPEEK-Sr becomes 25.7°, which is more hydrophilic due to the presence of dopamine on the surface [128].

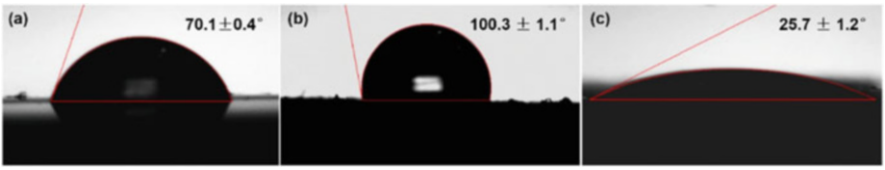

Fig. 6.2 Contact angles of PEEK surface with different treatments. (**a**) PEEK; (**b**) SPEEK-H; (**c**) SPEEK-Sr. (Reprinted from Hu et al. [128] with permission from Springer)

6.3.1.2 Scanning Electron Microscopy (SEM)

Information on the surface morphology and topography of a polymeric biomaterial can be obtained by various microscopic techniques, depending on the dimension of the surface, the desired lateral resolution, the depth of the surface and the sample environment. While optical microscopy is the easiest to use and least invasive among the techniques, its lateral resolution is limited to the wavelength of light, which is around 300 nm. Hence, SEM, which reveals surface features at nanometre lateral resolutions, is often the preferred technique to visualise the surface topography of a biomaterial [132–135]. In SEM, a beam of electrons is directed onto the sample under vacuum, and the resultant interaction between the electrons and the sample surface causes an emission of secondary electrons, which are collected by the detector to produce an electron micrograph. Samples that are not electrically conductive need to be sputter-coated with a thin metallic coating to prevent electrical charging (the accumulation of electrons) on the sample. As the analysis takes place under vacuum to prevent scattering of electrons by air molecules, samples containing cells and biological tissues have to be fixed and dried to ensure that the biological components remain stable in vacuum [133, 136]. Figure 6.3 shows that the cells adhered and spread on the surface of substrates and displayed characteristic star/slayed-shaped morphologies on day 3. The cells reached around 80% confluency on day 7, and the cells formed confluent monolayer sheets for all groups on day 28 [133].

Some samples, such as hydrated polymers and surfaces modified with adsorbed molecules, may not be suitable for SEM due to their instability in vacuum. As the SEM operates in a dry environment, the information obtained may not truly represent the actual surface topography in physiological conditions. Nevertheless, the ease of operation and the ease of interpreting the images make SEM one of the most universal techniques to analyse surface topography of a biomaterial at the nanometre scale. The development of the environmental SEM (ESEM) permits wet, uncoated specimens to be studied; however, beside high cost of equipment, the restricted possible minimum magnification may limit its applications as well [137].

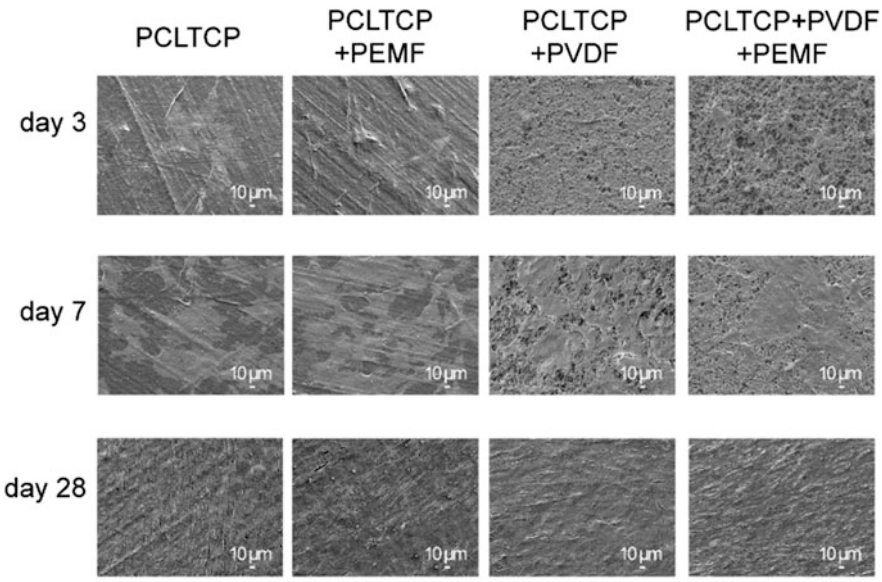

Fig. 6.3 Fixed cell morphology on PCL-TCP without (PCL-TCP) and with pulsed electromagnetic field (PEMF) (PCL-TCP + PEMF) and on PVDF-coated PCL-TCP without (PCL-TCP + PVDF) and with PEMF (PCL-TCP + PVDF+PEMF) observed using SEM on day 3, 7 and 28. (Reprinted from Dong et al. [133], with permission from MDPI)

6.3.1.3 Atomic Force or Scanning Force Microscopy (AFM or SFM)

AFM (SFM) offers three dimensional (3D) and high resolution information at the sample surface and is capable of detecting surface features of several nanometres in depth or height, unlike SEM which offers two dimensional information and limited to tens of nanometres scale only. In fact, AFM can be used to resolve molecules or even single atoms adsorbed on a smooth surface, and its sensitivity allows researchers to obtain images of delicate biological features [130, 138]. An AFM consists of a sharp tip attached to a flexible microscale cantilever (Fig. 6.4). When the tip is scanned across the sample surface, attractive and repulsive forces between the tip and sample cause the cantilever to deflect vertically. The deflection is detected by a photodiode via a laser beam reflected off the top of the cantilever, and the signal is processed into a topographical image. Depending on the scan mode, a constant force or constant height between the tip and the sample is maintained by a feedback loop, which controls the movement of the piezoelectric scanner holding the sample [139].

Depending on the sample's properties and the application, the AFM can be operated in a number of modes. One frequently used mode is the contact mode, where the tip is in constant contact with the sample. While the contact mode offers the highest resolution, the shear forces applied by the tip may damage soft samples and surfaces with weakly adsorbed molecules. Another frequently used mode is the

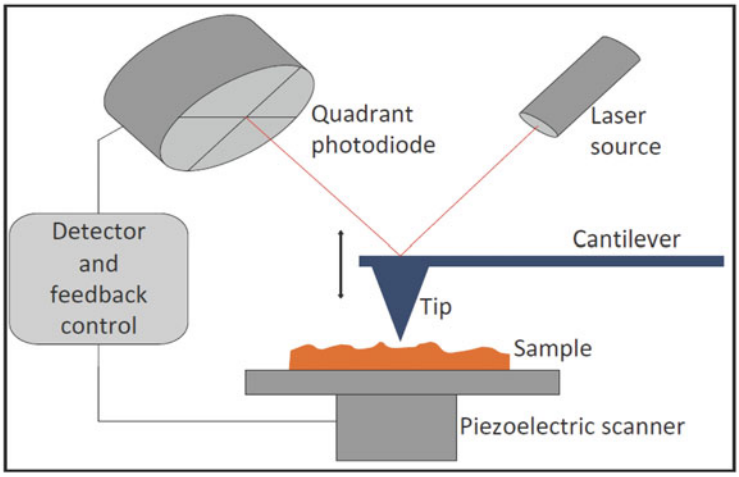

Fig. 6.4 Schematic representation of the working principle of AFM

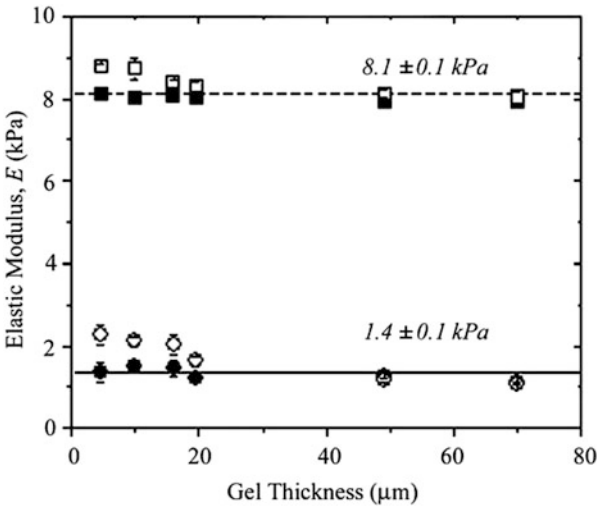

Fig. 6.5 The elasticities of polyacrylamide thin films (5% acrylamide solutions were mixed with either 0.3% (squares) or 0.03% (circles) bis-acrylamide crosslinker and polymerised). (Reprinted from Engler et al. [141], with permission from Elsevier)

tapping mode, where the cantilever is oscillating above the moving sample and the changes in amplitude and phase are tracked. Since the tip is not in contact with the sample, the tapping mode is suitable for soft samples. Besides high resolutions, other advantages of the AFM include its ability to operate in a variety of environments including air and aqueous solutions, its ability to measure interaction forces between a surface and adsorbed molecules and its ability to measure electrical properties (e.g., charge density) of a surface [75]. In addition, the AFM can also be used to obtain the mechanical (modulus, stiffness, viscoelastic, frictional) and magnetic properties [140, 141]. Figure 6.5 shows that the elasticities of polyacrylamide are independent of thickness as measured by AFM indentation.

On the other hand, limiting characteristics of the AFM are a much slower scanning speed, small scanning area (less than 100 μm wide), sample damage or sample movement caused by shear forces from the tip and probe damage caused by hard samples with steep features.

6.3.1.4 Quartz Crystal Microbalance (QCM)

A quartz crystal microbalance (QCM), is also known as quartz microbalance (QMB), or quartz crystal nanobalance (QCN)), which measures a mass variation per unit area through measuring the change in frequency of a quartz crystal resonator. The QCM takes advantage of the piezoelectric effect of the quartz crystal, converts the surface mass change of the quartz crystal into the frequency change of the output electrical signal of the quartz crystal oscillation circuit and then obtains the high-precision data through the computer and other auxiliary equipment [142]. The measurement accuracy can be nanogram level and theoretically can measure the mass change equivalent to a single molecular layer or atomic layer of a fraction. QCM was used to determine the affinity of molecules (proteins, in particular) to surfaces functionalised with recognition sites and interactions between biomolecules [143, 144]. For example, the capture ability of heparin on cellulose nanocrystals surface was evaluated with QCM by measuring changes in resonance frequency shifts (Δf) and energy dissipation (ΔD) as a function of time under constant flows [145]. Larger entities such as bacteria, viruses and polymers are investigated as well [146]. With the rapid development of science and technology, QCM has also been greatly updated, and in combination with other instruments, QCM can also be used in more areas [142, 147, 148]. For example, combined with light microscopes, cells behaviour could be observed on the chip's surface; combined with electrochemical cell chamber, the changes of electrochemical properties could be detected. While the QCM is a direct and sensitive method to characterise surface of material, it should be noted that the adsorption protein obtained using QCM test is a 'wet protein', which includes information about the water molecules associated with the protein. Therefore, the QCM will result in a much greater amount of adsorption protein than that of surface plasmon resonance (SPR) test [149]. Figure 6.6 shows the fibrinogen adsorbed on the surface of SAM-OEG membrane by both QCM and SPR. The adsorption protein obtained from the QCM is 19.5 ng/cm^2, while the adsorption protein obtained from the SPR test is 0.93 ng/cm^2. It can be seen that the adsorption of fibrinogen on the membrane surface measured by QCM is 20 times higher than that obtained by SPR.

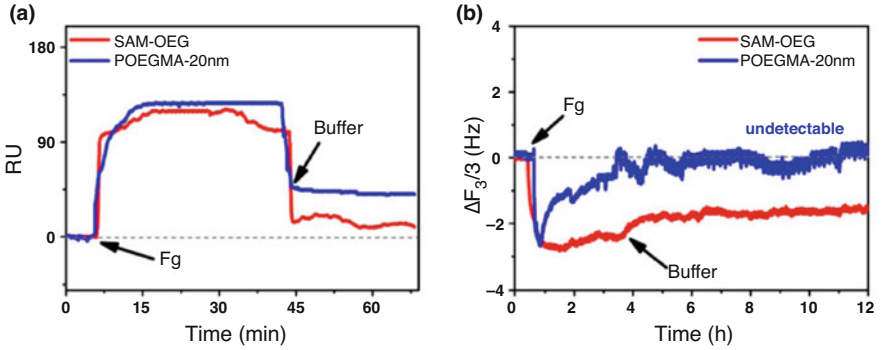

Fig. 6.6 Fibrinogen adsorption (0.1 mg/mL) on SAM-OEG and POEGMA membranes surface measured by (**a**) SPR and (**b**) QCM-D. (Reprinted with permission from Luan et al. [149], with permission from American Chemical Society)

6.3.2 Chemical Characterisation

6.3.2.1 Attenuated Total Reflectance Fourier Transform Infrared Spectroscopy (FTIR)

The surface chemistry of polymeric biomaterials can be investigated by various spectroscopic techniques, and ATR-FTIR is one spectroscopic technique that is widely used [1, 75, 150]. The principle behind Fourier transform infrared spectroscopy (FTIR) is that various organic functional groups absorb light at specific wavelengths in the infrared (IR) spectrum that are characteristic of their vibrational modes [151]. Hence, FTIR allows quantitative determination of a sample's chemical composition and is a powerful tool to track the chemical changes that occur after a chemical reaction. FTIR is typically performed by passing a beam of IR light through a solid sample blended with a salt transparent to IR or a liquid sample sandwiched between two salt discs. However, since most polymeric biomaterials are opaque to IR light and cannot be homogeneously blended with salt, they are analysed in the attenuated total reflection mode, where the surface of the sample is pressed onto an inorganic crystal (e.g., ZnSe or Ge) and a beam of IR light is directed toward the crystal–sample interface. Despite total reflection at the interface, the incident IR beam penetrates the sample in the form of an evanescent wave. After the sample absorbs light at specific wavelengths, the reflected beam leaves the crystal and is converted to an IR spectrum by the FTIR system [152]. Figure 6.7 shows that two distinct bands were observed at 1560 and 3419 cm^{-1} in P-JAG scaffolds spectrum. The band observed at 1560 cm^{-1} is assigned to the N–H bend of primary amines in JAG peptides and the broad band at 3419 cm^{-1} corresponds to N–H stretch of primary and secondary amines in JAG peptides. Therefore, the spectrum suggested that the Jagged-1 peptides were successfully immobilised onto the surface of scaffolds [75].

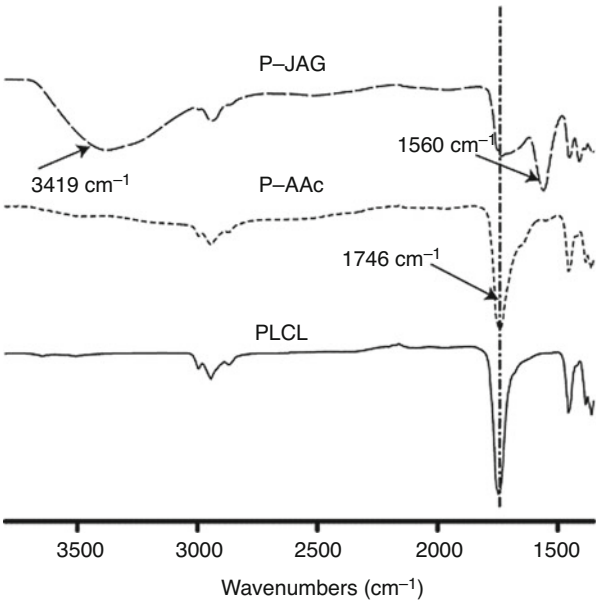

Fig. 6.7 ATR-FTIR spectra of PLCL (continuous line), P-AAc (short-dashed line) and P-JAG (long-dashed line) scaffolds. (Reprinted with permission from Wen et al. [75], with permission from American Chemical Society)

While the ATR-FTIR is fast and easy to use, it is not a very surface-specific technique because the probe depth ranges from several hundred nanometres to several micrometres. In contrast, a layer of immobilised molecules (e.g., proteins) on a surface may only be several to tens of nanometres thick. For polymeric biomaterials, the bulk phase's IR absorption may mask the peaks of the immobilised molecules, making it impossible to detect the presence of the immobilised molecules [126]. Because of this reason, ATR-FTIR is limited to the analysis of homogeneous samples or thin layers of organic molecules on inorganic substrates, where the IR absorptions of the inorganic phase do not overlap with that of the organic molecules.

6.3.2.2 X-Ray Photoelectron Spectroscopy (XPS)

XPS is a more powerful and more surface-specific technique than ATR-FTIR for analysing the surface chemical composition of polymeric biomaterial, with a sampling depth of less than 10 nm [126]. In XPS, X-rays are radiated onto the sample to excite the electrons in the atoms, causing the electrons at the surface of the sample to eject. The quantity of the ejected electrons is measured as a function of the incident energy by the photoelectron spectrometer. As each chemical element has a characteristic spectrum, the overall spectrum can be used to quantitatively determine the elemental composition in the sample surface. Although the incident X-ray can penetrate far into the sample surface, only the electrons within 10 nm of the surface can escape from the sample surface without obstruction [153]. This explains the high surface specificity of XPS. The sampling depth and surface sensitivity can be further

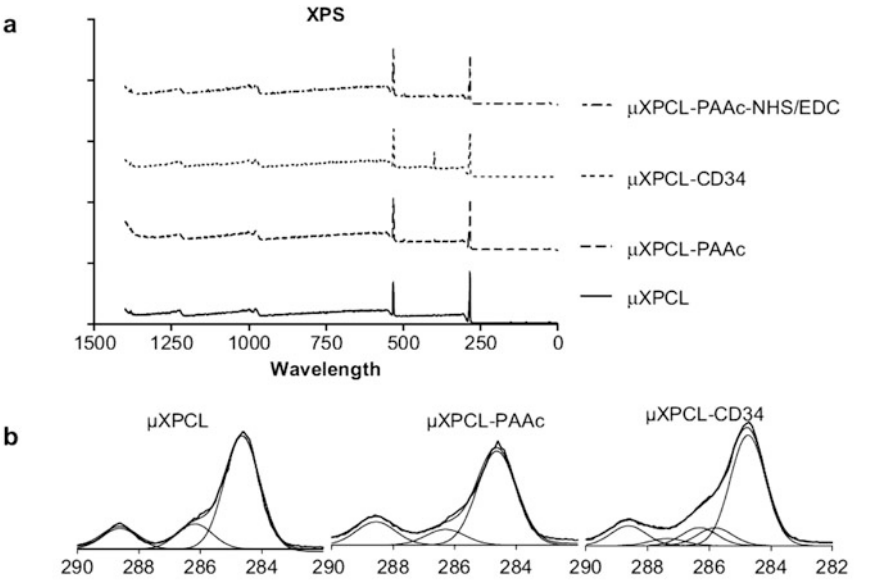

Atomic Ratio (%)					
Binding Energy (eV)	-C-H ~284.6	-C-O ~286.2	-O-C=O ~288.6	-C-N ~285.8	-O-C-N ~287.4
Pristine	71.2	15.8	13.0	-	-
μXPCL-PAAc	70.7	11.8	17.5	-	-
μXPCL-CD34	63.7	10.4	11.5	10.3	4.1

Fig. 6.8 XPS survey of material surfaces. (**a**) XPS can be used to obtain a wide survey spectra of material surfaces. Here, polycaprolactone (*PCL*) films were modified with polyacrylic acid (*pAAc*) to allow conjugation of a protein (CD34 antibody), as identified by the peak at 286.4 eV. (**b**) Relative intensity of the deconvoluted C1S spectra can also be used to show increase in carboxyl groups following PAAc engraftment, followed by introduction of peptide groups following CD34 antibody conjugation. (Reprinted with permission from Chong et al. [88], with permission from Elsevier)

controlled by changing the angle between incident X-ray and the sample surface. As XPS is surface specific, it is a useful tool to detect the presence of immobilised molecules on the surface of a modified biomaterial. For example, protein molecules grafted onto an aliphatic polymer can be detected and quantified by the N1 peaks, since nitrogen atoms are present in the protein molecules but not in the polymer [1, 75, 88] (Fig. 6.8). Besides elemental quantification, chemical state information can also be obtained from XPS, as the chemical environment around an atom can influence the binding energy of the ejected electrons and cause a chemical shift. One example is carbon, which exhibits different binding energy in various functional groups. As a result, the chemical shift of the C1 peak can be used to identify certain functional groups [70, 88]. However, one major limitation of XPS is its inability to

detect hydrogen or helium, which can lead to inaccurate information on the elemental composition of a hydrogen-containing sample. While XPS is sensitive, it requires a vacuum environment to prevent scattering of ejected electrons by gas molecules. This means that, similar to SEM, XPS is only suitable for dry samples and may not be suitable for surfaces with adsorbed molecules. In addition, caution has to be taken for polymers and biomolecules as they can degrade under X-ray radiation, leading to altered chemical properties.

6.3.2.3 Time-of-Flight Secondary Ion Mass Spectroscopy (TOF-SIMS)

TOF-SIMS is a spectroscopy technique for obtaining information on the chemical composition of a solid surface. With a sampling depth of 1–2 nm, it has an even higher surface specificity than XPS. Originally developed for the analysis of inorganic materials, TOF-SIMS has progressed into a versatile tool for the analysis of organic molecules, biomolecules and polymers, and it has an advantage over XPS for being able to identify hydrogen [126, 154]. In TOF-SIMS, a beam of energetic primary ions, usually argon or gallium, bombard onto the sample surface, generating a collision cascade where the primary ions transfer energy to the sample. The collision causes atoms and molecules to sputter from the sample surface. A small portion of the sputtered particles are ionised to produce secondary ions, which are accelerated via an electric field and then made to travel a distance in a field-free drift region before reaching the detector. As the speed of the ions depends on their masses, the time of flight of an ion provides information on its mass and eventually its identity. As each chemical structure has its characteristic mass spectrum, analysis of the final spectrum can provide significant information on the chemical composition of the sample surface [155]. TOF-SIMS can be operated in two modes – static and dynamic. Static TOF-SIMS scans the sample surface with a low-energy primary ion beam to produce a static analysis of the topmost layer of the sample. Dynamic TOF-SIMS uses a high-energy primary ion beam to erode the sample surface continuously and record the real-time signal simultaneously, producing a depth profile of the chemical compositions layer by layer into the bulk. While TOF-SIMS is highly sensitive for surface analysis, it can also be sensitive to contamination. Common contaminants include plasticisers found in plastic containers and silicones found in double-sided tape used to secure samples [154]. Because of this reason, TOF-SIMS samples should be stored in aluminium foil or clean glass containers. Like SEM and XPS, TOF-SIMS is performed in a high-vacuum environment, so samples should be dry and stable in vacuum. Another limitation of TOF-SIMS is the huge quantity of data generated, as every pixel of a two-dimensional image contains a full mass spectrum. Analysis of the data can be extremely time-consuming and complicated if one does not know the sample well. To simplify data analysis and maximise the amount of meaningful information, computational multivariate analysis methods are developed to process TOF-SIMS images [156].

6.4 Characterisation of Biocompatibility

Having discussed the physical and chemical characterisation methods, this section focuses on the biological characterisation of surface-modified biomaterials. In general, the ISO 10993 provides an extensive set of guidelines to evaluate the safety and efficacy of devices and may be applied toward material testing. It also provides an opportunity for the investigator to better understand the safety profiles of the material used, which may be helpful in guiding the rational selection of materials for design of medical products. Many of these tests are contextual and need to be appropriately selected for use in specific applications. The ISO 10993-4, for example, deals with material interactions with blood and provides the basis for selection and design of appropriate tests for blood-contacting surfaces, such as engineered blood vessels. Similarly, the ISO 10993-5 provides basic guidelines for cytocompatibility testing. At this point, it should be noted, for eventual translation into the market, that the European Committee (EC) adopts this standard and makes it part of their technical review in regulatory evaluation of safety of medical devices.

6.4.1 A Note on the Use of the ISO 109993

In continuing this discussion, it is important to stress that any given material cannot be declared to be 'universally biocompatible'; biocompatibility can only defined only in the context of application. Correspondingly, regulatory bodies such as the US FDA are unable to provide a blanket approval for any group or type of polymers for medical applications. Instead, the selection and use of material for a device, along with appropriate tests to demonstrate safety for use in the identified medical application will need to be carefully designed. For regulatory submissions, the control and documentation of this process is covered as part of a quality system, in accordance with good manufacturing practices. Discussion of design controls is beyond the scope of this chapter and readers are instead directed to Section 4 of the ISO 13485, as well as the US FDA guidance document on design controls. In the subsequent sections, the following will be discussed:

ISO 109993-1: Evaluation and testing within a risk management process Part 1 provides background and overview on the approach toward biocompatibility testing.

ISO 10993-4: Selection of Tests for Interactions with Blood, ISO 10993-5: Tests for in vitro Cytotoxicity Discussion of Part 4 and Part 5 will provide examples of the development and use of assays for the evaluation of specific aspects of biocompatibility.

6.4.2 ISO 10993-1: Evaluation and Testing Within a Risk Management Process

The ISO 10993-1 is an important document as it provides a starting point toward developing a plan for the evaluation of biological responses to a medical device. It includes a description of the general principles applying to biological evaluation of medical devices, followed by a framework to categorise medical devices according to the nature and duration of contact with the body. Accordingly, appropriate data sets and / or relevant parts of the ISO 10993 may be selected to guide testing, in order to address identified gaps in knowledge about the device and material being used.

The general principles provide useful insight into the thought process behind the risk-based approach to biological evaluation. A critical consideration is that testing should only be performed where there is insufficient information to perform an adequate risk assessment (the process of doing so may be accessed in the ISO 10993-2). A flow chart is also provided in this section to guide users through considerations in categorising a given device, including whether the patient contact is involved, formulation used, manufacturing processes, geometry and physical properties, as well as the nature of use.

Subsequently, the medical device may be categorised as a surface medical device, externally communicating device or implant medical device, and further sub-categorised on the type of tissue contact. Following further consideration of the contact duration (limited, prolonged or long-term), relevant endpoints of biological evaluation are identified, that can indicate the data sets needed to assess biological safety. Following data gap analysis, a list of required data sets may then be identified, which can be generated in conformance with appropriate standards. For example, a scaffold being used in vascular tissue engineering, may be seen as an implant medical device that comes in contact with blood, with long term duration of more than 30 days. Accordingly, the typical biological evaluation endpoints will typically include Haemocompatibility and In Vitro Cytotoxicity (discussed later).

6.4.3 ISO 10993-4: Selection of Tests for Interactions with Blood

The ISO 10993-4 deals with studying interactions with blood. It includes a framework to categorise blood-contacting materials (based on intended use and duration of contact), an overview of governing principles in studying interactions with blood and selected tests, including the rationale behind use of data generated from such tests.

6.4.3.1 Categorisation of Device Types

Blood contacting devices, in the context of this document, do not include devices in which the contacted blood does not return to or reside in the body. Accordingly, blood contacting devices may be broadly represented as external communicating devices or implants (such as heart valves. External communicating devices may be further categorised as devices that serve as an indirect blood path (such as blood collection devices) or those that directly contact circulating blood (such as atherectomy devices). It should be noted that the context of application impacts the level of risk significantly – intravascular catheters may be used for a variety of applications and may be categorised as indirectly or directly contacting circulating blood, depending on the use. It is thus the intended use or site of application that dictates the level of risks, rather than the material used or surface modifications employed.

6.4.3.2 Characterisation of Blood Interactions

Similar to ISO 10993-1, a decision tree can be used to decide whether testing for interactions with blood should be performed. Additionally, a table is provided to identify the category of tests for consideration; these include haemolysis (material-induced or mechanically induced) and thrombosis (coagulation, platelet activation, complement, haematology and ex vivo/in vivo. While not prescriptive nature, the standard provides rationale for the selection of these tests and essential considerations in the design of such tests. Some recommended tests include PTT assays and thrombosis and are performed in the context of the device (discussed later).

6.4.3.3 Types of Tests

The recommended tests in 10993-5 are divided into categories based on the primary process being measured. Taking the example of a vascular graft, in order to evaluate thrombosis in vivo, common measures include percentage occlusion of the graft following a period of implantation. The standards do not dictate testing protocols due to the diverse nature of devices being evaluated and that blood interactions tend to be context-specific. It is also not possible to include target numbers that qualify a given material to be 'haemocompatible'. Rather, a set of principles are provided, suggesting the rationalisation necessary to justify the choice and design of tests. Some examples are discussed as follows:

In Vitro Tests In vitro testing typically involves exposure of the material to blood and may include bench tops models (such as the Chandler loop test model [157]) that simulate physiological conditions, particularly that of an 'anticipated worst case scenario'. In such a set-up, materials to be tested are exposed to collected blood and the interactions with blood are studied through the use of assays in bench top

settings. Partial Thromboplastin Time (PTT) is one such assay in which the time taken to induce clotting of recalcified citrated plasma is measured, following the addition of partial thromboplastin. To perform coagulation testing of medical devices and materials, exposure to the device or material serves to activate the coagulation. By measuring the change in PTT following exposure, a relative measure of surface coagulability may be established for a range of modified surfaces. The PTT and other in vitro tests provide repeatable settings, avoid the use of animals and also provide a cost-effective way to perform initial evaluations. They are, however, limited in their ability to replicate physiological settings and longer-term studies typically involved the use of animals. For more detailed discussion on blood compatibility testing, the following review provides further elaboration of testing methodology [158].

Ex Vivo Tests Ex vivo testing involves directing circulating blood to contact with a test material. These include 'open' systems such as the Dudley clotting test, where a tube is inserted into a test subject via a catheter and the time taken for blood to stop dripping from the open end of the tube can be compared. Popular 'closed' systems include AV shunts, where the test material is directly exposed to circulating blood. Typically, tests involving AV shunts may be continued for extended durations and more information may be derived. For example, retrieved shunts may be examined for presence of thrombi on the surface, or changes in patency may be measured to indicate thrombogenic responses. Luminal surfaces may also be studied for platelet adhesion, while downstream vasculature may be monitored for embolic events.

In Vivo Tests In vivo testing of devices typically involves implantation of a device in the intended site of use, to more closely mimic clinical application. These typically require greater planning and can provide more data temporally and across a range of diverse tests. For instance, serial monitoring of implanted vascular grafts by arteriograms provide vital information on the development of thrombi and changes in patency over time. In testing of modified surfaces (not necessarily in the specific context of a device), the non-anticoagulated venous implant (NAVI) or anticoagulated venous implant (AVI) models are used. These involve inserting of device materials formed into catheter shapes into the veins of animals for up to 4 h, followed by gross assessment of amount of thrombus on the material/catheter surface. The technique faces several shortcomings, including limited time exposures, variability of results and operator dependence. Perhaps more critically, the high flow environments lead to very low levels of surface-associated thrombus. Particularly in AVI settings, this results in most material surfaces being labelled non-thrombogenic (even if it is not the case).

6.4.4 ISO 10993-5: Tests for In Vitro Cytotoxicity

The ISO 10993-5 deals primarily with the evaluation of cytotoxicity or, more accurately in this case, the lack thereof. Broadly, it involves exposing test cells to

Table 6.3 Summary of cytotoxicity tests and their corresponding cell lines

Test name	Suitable cell lines
Neutral red uptake	BALB/c 3T3 cells, clone 31 CRB 9005
Colony-forming cytotoxicity	V79
MTT cytotoxicity	L-929
XTT cytotoxicity	L-929

Referenced from ISO 10993-5:2009, Annexes A–D. Copyright remains with ISO

the material, either directly or indirectly, followed by evaluation of viability. Some tests available for such evaluations are listed in Table 6.3.

In general, a numerical grade of >2 in qualitative scoring is considered cytotoxic. For qualitative testing, reduction of cell viability by $>30\%$ shall indicate cytotoxic effects. Under these conditions, significant considerations shall be given to the surface modification procedure, which could include but is not limited to (1) use of cross-linking agents, (2) chemical alteration of biomaterial molecular structure and (3) surface-modified coating chemistry and its cytotoxicity effects.

At this point, it is critical to highlight that the evaluation of cytocompatibility alone is not a direct measure of surface modification efficacy (except where the modification is performed specifically to improve cytocompatibility). It does, however, provide important indications on the safety profile of the surface coating process, in order to flag out unexpected cytotoxic events arising from the modification process.

6.4.4.1 Direct Contact

Direct contact methods involve the direct exposure of cells to the material surface, followed by evaluation of cell viability. One important test requirement would be to ensure that there is at least one flat surface (no specific requirement on roughness is provided). In addition, if the biomaterial is meant to be used sterile, then it shall be sterilised accordingly before testing is done. Otherwise, the basic principles of aseptic handling during testing shall apply. The selection of cell lines to be used for testing shall, in principle, follows the requirements of the standard. However, concession is also given to situations where a specific response to a selected cell line is desired; in this case, cell line reproducibility and accuracy of response need to be demonstrated. Testing the material involves culturing the cells to subconfluency on standard plates and subsequently placing the material directly on the cells. Cell viability is then tracked over multiple days and may also be morphologically observed under microscope. Important test requirements are that appropriate experimental controls (both positive and negative) should be included and that the biomaterial shall only cover one-tenth of the exposed surface area of the cell layer.

Determination of cytotoxicity may be performed using qualitative and quantitative measurements although it is preferred that quantitative measurements are taken.

Table 6.4 Reactivity grades for direct contact test

Grade	Reactivity	Description of reactivity zone
0	None	No detectable zone around or under specimen
1	Slight	Some malformed or degenerated cells under specimen
2	Mild	Zone limited to area under specimen
3	Moderate	Zone extending specimen size up to 10 cm
4	Severe	Zone extending farther than 10 cm beyond specimen

Adapted from ISO 10993-5:2009, Section 8.5. Copyright remains with ISO

If qualitative measurements are taken, the following table (Table 6.4) provides the guidelines to which cytotoxicity shall be measured.

6.4.4.2 Exposure to Liquid Extracts

This process involves the incubation of the modified material in an extraction fluid medium, to which the cells are subsequently exposed. Extraction conditions generally follow the principle of simulating or exaggerating clinical use conditions without causing significant changes in the biomaterial. For this purpose, the extraction vehicle can be culture medium, physiological saline or any other justifiable medium. Importantly, to fulfil the requirements of the standard, the extraction vehicle(s) should allow extraction of polar and non-polar elements.

The extraction conditions shall be conducted without causing significant changes in the biomaterial and therefore should be chosen carefully. Generally, normal cell culture condition of 37 °C for a period of 24 ± 2 h is applied. However, raised temperatures and durations of extraction may be applied provided that the chemistry of the biomaterial is unaffected, and the intended use of the biomaterial justifies the extraction conditions. Additionally, in situations where the cumulative contact of the biomaterial is less than 4 h and is in contact with intact skin or mucosa surfaces, the extraction times shall be at least 4 h.

6.4.4.3 Indirect Contact

Indirect methods are concerned with measuring the leachables from a material. Two methods are most commonly performed. In the agar diffusion method, selected cell lines are grown to subconfluency, and 0.5–2 mass per cent of melted agar is casted over the cells, with a fresh culture medium change. The sample is then placed on top of the agar, followed by a predefined period of incubation (24–74 h) before evaluation. In the filter diffusion method, a surfactant-free filter of pore size 0.45 μm is used. Briefly, an aliquot of a continuously stirred cell suspension is added onto the surfactant-free filter and incubated until subconfluency is achieved. The filters are then transferred onto a layer of solidified agar (cell side facing down) before the biomaterial is placed onto the acellular side of the filter (top side).

6.5 Conclusion

In this chapter, the modification of tissue engineering scaffold surfaces was discussed. Surface modification seeks to confer desirable surface properties, while retaining bulk properties. In tissue engineering scaffolds, this is often difficult to achieve due to the susceptibility of degradable scaffolds to bulk alterations. This has led to innovative approaches that range from physical to chemical approaches, yielding modified surfaces with varied physical, chemical and biological properties. To characterise these changes, various assays have been developed that can help develop a deeper understanding of the effect of surface modification. Particularly for implant applications, the characterisation of biological responses is important toward establishing the safety profile of modified surfaces; these were discussed using the ISO 10993 standards to illustrate how the selection and design of testing methodology is as important as the choice of surface modification techniques in the development of tissue engineering scaffolds.

References

1. Cheng Z, Teoh S-H. Surface modification of ultra thin poly(ε-caprolactone) films using acrylic acid and collagen. Biomaterials. 2004;25(11):1991–2001.
2. Huebsch N, Mooney DJ. Inspiration and application in the evolution of biomaterials. Nature. 2009;462(7272):426–32.
3. Anjum N, et al. Radiation effects on polymers for biological use, vol. 162. Springer; 2003.
4. Mitragotri S, Lahann J. Physical approaches to biomaterial design. Nat Mater. 2009;8(1): 15–23.
5. Erakovic S, et al. Novel bioactive antimicrobial lignin containing coatings on titanium obtained by electrophoretic deposition. Int J Mol Sci. 2014;15(7):12294–322.
6. Gour N, Ngo KX, Vebert-Nardin C. Anti-infectious surfaces achieved by polymer modification. Macromol Mater Eng. 2014;299(6):648–68.
7. Ren X, et al. Surface modification and endothelialization of biomaterials as potential scaffolds for vascular tissue engineering applications. Chem Soc Rev. 2015;44(15):5680–742.
8. Rudolph A, et al. Surface modification of biodegradable polymers towards better biocompatibility and lower thrombogenicity. PLoS One. 2015;10(12):e0142075.
9. Milleret V, et al. Influence of the fiber diameter and surface roughness of electrospun vascular grafts on blood activation. Acta Biomater. 2012;8(12):4349–56.
10. Provenzano PP, et al. Contact guidance mediated three-dimensional cell migration is regulated by Rho/ROCK-dependent matrix reorganization. Biophys J. 2008;95(11):5374–84.
11. Flemming RG, et al. Effects of synthetic micro-and nano-structured surfaces on cell behavior. Biomaterials. 1999;20(6):573–88.
12. Zhou F, et al. Phenomenon of contact guidance on the surface with nano-micro-groove-like pattern and cell physiological effects. Chin Sci Bull. 2009;54(18):3200–5.
13. Weiss P. Experiments on cell and axon orientation in vitro: the role of colloidal exudates in tissue organization. J Exp Zool. 1945;100:353–86.
14. Britland S, et al. Synergistic and hierarchical adhesive and topographic guidance of BHK cells. Exp Cell Res. 1996;228(2):313–25.
15. Sun F, et al. Geometric control of fibroblast growth on proton beam-micromachined scaffolds. Tissue Eng. 2004;10(1–2):267–72.

16. Wang Z, et al. Reliable laser fabrication: the quest for responsive biomaterials surface. J Mater Chem B. 2018;6(22):3612–31.
17. Driscoll MK, et al. Contact guidance of amoeboid cells via nanotopography. ACS Nano. 2014;8(4):3546–55.
18. Bettinger CJ, Langer R, Borenstein JT. Engineering substrate topography at the micro-and nanoscale to control cell function. Angew Chem Int Ed. 2009;48(30):5406–15.
19. Balaban NQ, et al. Force and focal adhesion assembly: a close relationship studied using elastic micropatterned substrates. Nat Cell Biol. 2001;3(5):466.
20. Wang Z, et al. Dual-microstructured porous, anisotropic film for biomimicking of endothelial basement membrane. ACS Appl Mater Interfaces. 2015;7(24):13445–56.
21. Cao H, et al. The effects of nanofiber topography on astrocyte behavior and gene silencing efficiency. Macromol Biosci. 2012;12(5):666–74.
22. Zhang W, et al. Effects of integrated bioceramic and uniaxial drawing on mechanically-enhanced fibrogenesis for bionic periosteum engineering. Colloids Surf B: Biointerfaces. 2022;214:112459.
23. Guo T, et al. Engineering of tenogenic patch scaffold with fibrous microtopography and reinforcement via uniaxial cold-drawing. Mater Des. 2022;217:110609.
24. Wang Z-Y, et al. Biomimetic three-dimensional anisotropic geometries by uniaxial stretch of poly (ε-caprolactone) films for mesenchymal stem cell proliferation, alignment, and myogenic differentiation. Tissue Eng Part C Methods. 2013;19(7):538–49.
25. Wang Z-Y, et al. Enhancing mesenchymal stem cell response using uniaxially stretched poly (ε-caprolactone) film micropatterns for vascular tissue engineering application. J Mater Chem B. 2014;2(35):5898–909.
26. Wang Z, et al. Functional regeneration of tendons using scaffolds with physical anisotropy engineered via microarchitectural manipulation. Sci Adv. 2018;4(10):eaat4537.
27. Goodman SL, Sims PA, Albrecht RM. Three-dimensional extracellular matrix textured biomaterials. Biomaterials. 1996;17(21):2087–95.
28. Ozaki I, et al. Regulation of TGF-β1-induced pro-apoptotic signaling by growth factor receptors and extracellular matrix receptor integrins in the liver. Front Physiol. 2011;2:78.
29. Teo BKK, et al. Nanotopography modulates mechanotransduction of stem cells and induces differentiation through focal adhesion kinase. ACS Nano. 2013;7(6):4785–98.
30. Zhu S, et al. An engineered tenogenic patch for the treatment of rotator cuff tear. Mater Des. 2022;224:111402.
31. Chew SY, et al. Aligned protein–polymer composite fibers enhance nerve regeneration: a potential tissue-engineering platform. Adv Funct Mater. 2007;17(8):1288–96.
32. Wang Z, et al. Direct laser microperforation of bioresponsive surface-patterned films with through-hole arrays for vascular tissue-engineering application. ACS Biomater Sci Eng. 2015;1(12):1239–49.
33. Zhu Y, et al. Regulation of macrophage polarization through surface topography design to facilitate implant-to-bone osteointegration. Sci Adv. 2021;7(14):eabf6654.
34. Karazisis D, et al. The effects of controlled nanotopography, machined topography and their combination on molecular activities, bone formation and biomechanical stability during osseointegration. Acta Biomater. 2021;136:279–90.
35. Doloff JC, et al. The surface topography of silicone breast implants mediates the foreign body response in mice, rabbits and humans. Nat Biomed Eng. 2021;5(10):1115–30.
36. Wang M, et al. Regulation of macrophage polarization and functional status by modulating hydroxyapatite ceramic micro/nano-topography. Mater Des. 2022;213:110302.
37. Lee S, et al. High-performance implantable bioelectrodes with immunocompatible topography for modulation of macrophage responses. ACS Nano. 2022;16(5):7471–85.
38. Li W, et al. Surface design for antibacterial materials: from fundamentals to advanced strategies. Adv Sci. 2021;8(19):2100368.
39. Scardino AJ, Guenther J, Nys R. Attachment point theory revisited: the fouling response to a microtextured matrix. Biofouling. 2008;24(1):45–53.

40. Rodriguez V, et al. Bacterial response to spatially organized microtopographic surface patterns with nanometer scale roughness. Colloids Surf B Biointerfaces. 2018;169:340–7.
41. Yang M, et al. Control of bacterial adhesion and growth on honeycomb-like patterned surfaces. Colloids Surf B Biointerfaces. 2015;135:549–55.
42. Gu H, et al. How Escherichia coli lands and forms cell clusters on a surface: a new role of surface topography. Sci Rep. 2016;6:14.
43. Hasan J, et al. Multi-scale surface topography to minimize adherence and viability of nosocomial drug-resistant bacteria. Mater Des. 2018;140:332–44.
44. Li D, et al. Mechanically-enhanced fibre topography via electrospinning on a poly (-ε-caprolactone) film for tendon tissue-engineering application. Mater Technol. 2021;37:1–9.
45. Flamm DL, Auciello O. Plasma deposition, treatment, and etching of polymers: the treatment and etching of polymers. Elsevier; 2012.
46. Wang ZY, et al. Biomimetic three-dimensional anisotropic geometries by uniaxial stretching of poly(ε-caprolactone) films: degradation and mesenchymal stem cell responses. J Biomed Mater Res A. 2014;102(7):2197–207.
47. Luo F-F, et al. Effects of femtosecond laser micropatterning on the surface properties and cellular response of biomedical tantalum-blended composites. J Cent South Univ. 2022;29 (10):3376–84.
48. Kim SH, et al. Correlation of proliferation, morphology and biological responses of fibroblasts on LDPE with different surface wettability. J Biomater Sci Polym Ed. 2007;18(5):609–22.
49. Webb K, Hlady V, Tresco PA. Relative importance of surface wettability and charged functional groups on NIH 3T3 fibroblast attachment, spreading, and cytoskeletal organization. J Biomed Mater Res. 1998;41(3):422–30.
50. Bassi A, et al. The chemical and physical properties of poly (ε-caprolactone) scaffolds functionalised with poly (vinyl phosphonic acid-co-acrylic acid). J Tissue Eng. 2011;2011: 615328.
51. Lei T, et al. Silicon-incorporated nanohydroxyapatite-reinforced poly (ε-caprolactone) film to enhance osteogenesis for bone tissue engineering applications. Colloids Surf B: Biointerfaces. 2020;187:110714.
52. Siddiqui MN, et al. Depolymerization of PLA by phase transfer catalysed alkaline hydrolysis in a microwave reactor. J Polym Environ. 2020;28(6):1664–72.
53. Mistry AN, et al. Rapid biodegradation of high molecular weight semi-crystalline polylactic acid at ambient temperature via enzymatic and alkaline hydrolysis by a defined bacterial consortium. Polym Degrad Stab. 2022;202:110051.
54. Partikel K, et al. Effect of nanoparticle size and PEGylation on the protein corona of PLGA nanoparticles. Eur J Pharm Biopharm. 2019;141:70–80.
55. Machatschek R, Lendlein A. Fundamental insights in PLGA degradation from thin film studies. J Control Release. 2020;319:276–84.
56. Zhong F, et al. Piezoresistive design for electronic skin: from fundamental to emerging applications. Opto-Electron Adv. 2022;5:210029-1–210029-32.
57. Czwartos J, et al. Effect of extreme ultraviolet (EUV) radiation and EUV induced, N_2 and O_2 based plasmas on a PEEK surface's physico-chemical properties and MG63 cell adhesion. Int J Mol Sci. 2021;22(16):8455.
58. Ventrelli L, et al. Influence of nanoparticle-embedded polymeric surfaces on cellular adhesion, proliferation, and differentiation. J Biomed Mater Res A. 2014;102(8):2652–61.
59. Pan H, et al. Effects of functionalization of PLGA-[Asp-PEG] n copolymer surfaces with Arg-Gly-Asp peptides, hydroxyapatite nanoparticles, and BMP-2-derived peptides on cell behavior in vitro. J Biomed Mater Res A. 2014;102(12):4526–35.
60. Jaganathan SK, et al. Radiation-induced surface modification of polymers for biomaterial application. J Mater Sci. 2015;50(5):2007–18.
61. Hersel U, Dahmen C, Kessler H. RGD modified polymers: biomaterials for stimulated cell adhesion and beyond. Biomaterials. 2003;24(24):4385–415.

62. Katti DS, Vasita R, Shanmugam K. Improved biomaterials for tissue engineering applications: surface modification of polymers. Curr Top Med Chem. 2008;8(4):341–53.
63. Hara M, et al. Surface-functionalization of isotactic polypropylene via dip-coating with a methacrylate-based terpolymer containing perfluoroalkyl groups and poly(ethylene glycol). Polym J. 2019;51(5):489–99.
64. Xie Z, et al. Electrospun poly (D, L)-lactide nonwoven mats for biomedical application: surface area shrinkage and surface entrapment. J Appl Polym Sci. 2011;122(2):1219–25.
65. Mamidi N, et al. Carbonaceous nanomaterials incorporated biomaterials: the present and future of the flourishing field. Compos Part B. 2022;243:110150.
66. Liu Z, Liu X, Ramakrishna S. Surface engineering of biomaterials in orthopedic and dental implants: strategies to improve osteointegration, bacteriostatic and bactericidal activities. Biotechnol J. 2021;16(7):2000116.
67. Hamdi M, Ektessabi A-I. Calcium phosphate coatings: a comparative study between simultaneous vapor deposition and electron beam deposition techniques. Surf Coat Technol. 2006;201(6):3123–8.
68. Parau AC, et al. Comparison of 316L and Ti6Al4V biomaterial coated by ZrCu-based thin films metallic glasses: structure, morphology, wettability, protein adsorption, corrosion resistance, biomineralization. Appl Surf Sci. 2022;612:155800.
69. Kumar S, Roy DN, Dey V. A comprehensive review on techniques to create the anti-microbial surface of biomaterials to intervene in biofouling. Colloid Interface Sci Commun. 2021;43:100464.
70. Du Y, et al. Synthetic sandwich culture of 3D hepatocyte monolayer. Biomaterials. 2008;29(3):290–301.
71. Yang Z, et al. The covalent immobilization of heparin to pulsed-plasma polymeric allylamine films on 316L stainless steel and the resulting effects on hemocompatibility. Biomaterials. 2010;31(8):2072–83.
72. Xie Y, et al. Preparation and in vitro evaluation of plasma-sprayed Mg_2SiO_4 coating on titanium alloy. Acta Biomater. 2009;5(6):2331–7.
73. Mastalerz C, et al. Effects of electron beam irradiation on 3D-printed biopolymers for bone tissue engineering. J Compos Sci. 2021;5(7):182.
74. Rizwan A, et al. Simulation of light distribution in gamma irradiated UHMWPE using Monte Carlo model for light (MCML) transport in turbid media: analysis for industrial scale biomaterial modifications. Polymers. 2021;13(18):3039.
75. Wen F, et al. Induction of myogenic differentiation of human mesenchymal stem cells cultured on notch agonist (Jagged-1) modified biodegradable scaffold surface. ACS Appl Mater Interfaces. 2014;6(3):1652–61.
76. Gupta B, et al. Plasma-induced graft polymerization of acrylic acid onto poly(ethylene terephthalate) films. J Appl Polym Sci. 2001;81(12):2993–3001.
77. Kim S-W. Surface modification of polypropylene in an impulse corona discharge. Korean J Chem Eng. 1996;13(1):97–100.
78. Szustakiewicz K, et al. Cytotoxicity study of UV-laser-irradiated PLLA surfaces subjected to bio-ceramisation: a new way towards implant surface modification. Int J Mol Sci. 2021;22(16):8436.
79. Ensinger W, Müller H. Surface modification and coating of powders by ion beam techniques. Mater Sci Eng A. 1994;188(1–2):335–40.
80. Shen Z, et al. Material surface modification by pulsed ion beam. J Mater Sci. 1990;25(7):3139–41.
81. Saini G, et al. Two-silane chemical vapor deposition treatment of polymer (nylon) and oxide surfaces that yields hydrophobic (and superhydrophobic), abrasion-resistant thin films. J Vac Sci Technol A. 2008;26(5):1224–34.
82. Shafi HZ, et al. Surface modification of reverse osmosis membranes with zwitterionic coating for improved resistance to fouling. Desalination. 2015;362:93–103.

83. Egghe T, et al. Silanization of plasma-activated hexamethyldisiloxane-based plasma polymers for substrate-independent deposition of coatings with controlled surface chemistry. ACS Appl Mater Interfaces. 2022;14(3):4620–36.
84. Engler AJ, et al. Matrix elasticity directs stem cell lineage specification. Cell. 2006;126(4): 677–89.
85. Özçam AE, et al. Multipurpose polymeric coating for functionalizing inert polymer surfaces. ACS Appl Mater Interfaces. 2016;8(8):5694–705.
86. Chong M, Lee C, Teoh S. Characterization of smooth muscle cells on poly(ε-caprolactone) films. Mater Sci Eng C. 2007;27(2):309–12.
87. Wen F, et al. Development of poly (lactic-co-glycolic acid)-collagen scaffolds for tissue engineering. Mater Sci Eng C. 2007;27(2):285–92.
88. Chong MS, et al. Development of cell-selective films for layered co-culturing of vascular progenitor cells. Biomaterials. 2009;30(12):2241–51.
89. Laschke MW, et al. Surface modification by plasma etching impairs early vascularization and tissue incorporation of porous polyethylene (Medpor®) implants. J Biomed Mater Res B Appl Biomater. 2016;104(8):1738–48.
90. Moraczewski K, et al. Comparison of some effects of modification of a polylactide surface layer by chemical, plasma, and laser methods. Appl Surf Sci. 2015;346:11–7.
91. Du Y, et al. 3D hepatocyte monolayer on hybrid RGD/galactose substratum. Biomaterials. 2006;27(33):5669–80.
92. Khelifa F, et al. Free-radical-induced grafting from plasma polymer surfaces. Chem Rev. 2016;116(6):3975–4005.
93. Löpez GP, et al. Glow discharge plasma deposition of tetraethylene glycol dimethyl ether for fouling-resistant biomaterial surfaces. J Biomed Mater Res. 1992;26(4):415–39.
94. Cai EZ, et al. Bio-conjugated polycaprolactone membranes: a novel wound dressing. Arch Plast Surg. 2014;41(06):638–46.
95. Ping M, et al. Surface modification of polyvinylidene fluoride membrane by atom-transfer radical-polymerization of quaternary ammonium compound for mitigating biofouling. J Membr Sci. 2019;570–571:286–93.
96. Yue Z, et al. Bio-functionalisation of polydimethylsiloxane with hyaluronic acid and hyaluronic acid–collagen conjugate for neural interfacing. Biomaterials. 2011;32(21): 4714–24.
97. Chong MSK, et al. Beyond cell capture: antibody conjugation improves hemocompatibility for vascular tissue engineering applications. Tissue Eng A. 2010;16(8):2485–95.
98. Zhang W, et al. Scaffold with micro/macro-architecture for myocardial alignment engineering into complex 3D cell patterns. Adv Healthc Mater. 2019;8(22):1901015.
99. Graça MFP, et al. Hyaluronic acid—based wound dressings: a review. Carbohydr Polym. 2020;241:116364.
100. Dovedytis M, Liu ZJ, Bartlett S. Hyaluronic acid and its biomedical applications: a review. Eng Regener. 2020;1:102–13.
101. Ruiz A, Rathnam KR, Masters KS. Effect of hyaluronic acid incorporation method on the stability and biological properties of polyurethane–hyaluronic acid biomaterials. J Mater Sci Mater Med. 2014;25(2):487–98.
102. Suzuki M, et al. Graft copolymerization of acrylamide onto a polyethylene surface pretreated with glow discharge. Macromolecules. 1986;19(7):1804–8.
103. Schnyder B, et al. UV-irradiation induced modification of PDMS films investigated by XPS and spectroscopic ellipsometry. Surf Sci. 2003;532:1067–71.
104. Praschak D, Bahners T, Schollmeyer E. PET surface modifications by treatment with monochromatic excimer UV lamps. Appl Phys A Mater Sci Process. 1998;66(1):69–75.
105. Eve S, Mohr J. Study of the surface modification of the PMMA by UV-radiation. Procedia Eng. 2009;1(1):237–40.
106. Cho JD, Kim SG, Hong JW. Surface modification of polypropylene sheets by UV-radiation grafting polymerization. J Appl Polym Sci. 2006;99(4):1446–61.

107. Daniloska V, et al. UV light induced surface modification of HDPE films with bioactive compounds. Appl Surf Sci. 2010;256(7):2276–83.
108. Ainali NM, Bikiaris DN, Lambropoulou DA. Aging effects on low- and high-density polyethylene, polypropylene and polystyrene under UV irradiation: an insight into decomposition mechanism by Py-GC/MS for microplastic analysis. J Anal Appl Pyrolysis. 2021;158:105207.
109. Fairbrother A, et al. Temperature and light intensity effects on photodegradation of high-density polyethylene. Polym Degrad Stab. 2019;165:153–60.
110. Ahad I, et al. Extreme ultraviolet surface modification of polyethylene terephthalate (PET) for surface structuring and wettability control. Acta Phys Pol A. 2016;129(2):241–3.
111. Bartnik A, et al. Simultaneous treatment of polymer surface by EUV radiation and ionized nitrogen. Appl Phys A Mater Sci Process. 2012;109(1):39–43.
112. Reisinger B, et al. EUV micropatterning for biocompatibility control of PET. Appl Phys A Mater Sci Process. 2010;100(2):511–6.
113. Schulze A, et al. Permanent surface modification by electron-beam-induced grafting of hydrophilic polymers to PVDF membranes. RSC Adv. 2013;3(44):22518–26.
114. Rahman N, et al. The effect of hot DMSO treatment on the γ-ray-induced grafting of acrylamide onto PET films. Polym J. 2014;46(7):412–21.
115. da Cunha L, et al. Surface modification of styrene-divinylbenzene copolymers by polyacrylamide grafting via gamma irradiation. Polym Bull. 2008;61(3):319–30.
116. Velo-Gala I, et al. Surface modifications of activated carbon by gamma irradiation. Carbon. 2014;67:236–49.
117. Onyiriuka E, Hersh L, Hertl W. Surface modification of polystyrene by gamma-radiation. Appl Spectrosc. 1990;44(5):808–11.
118. Johnson S. Pulsed laser deposition of hydroxyapatite thin films. Georgia Institute of Technology; 2005.
119. Lou D, et al. Antifouling membranes prepared from polyethersulfone grafted with poly (ethylene glycol) methacrylate by radiation-induced copolymerization in homogeneous solution. ACS Omega. 2020;5(42):27094–102.
120. Kwon OH, et al. Graft copolymerization of polyethylene glycol methacrylate onto polyethylene film and its blood compatibility. J Appl Polym Sci. 1999;71(4):631–41.
121. Zhu Y, et al. Surface modification of polycaprolactone membrane via aminolysis and biomacromolecule immobilization for promoting cytocompatibility of human endothelial cells. Biomacromolecules. 2002;3(6):1312–9.
122. Liu Y, He T, Gao C. Surface modification of poly (ethylene terephthalate) via hydrolysis and layer-by-layer assembly of chitosan and chondroitin sulfate to construct cytocompatible layer for human endothelial cells. Colloids Surf B: Biointerfaces. 2005;46(2):117–26.
123. Wen F, et al. Development of dual-compartment perfusion bioreactor for serial coculture of hepatocytes and stellate cells in poly (lactic-co-glycolic acid)-collagen scaffolds. J Biomed Mater Res B. 2008;87(1):154–62.
124. Jung JH, Ree M, Kim H. Acid-and base-catalyzed hydrolyses of aliphatic polycarbonates and polyesters. Catal Today. 2006;115(1–4):283–7.
125. Croll TI, et al. Controllable surface modification of poly(lactic-*co*-glycolic acid) (PLGA) by hydrolysis or aminolysis I: physical, chemical, and theoretical aspects. Biomacromolecules. 2004;5(2):463–73.
126. Ma Z, Mao Z, Gao C. Surface modification and property analysis of biomedical polymers used for tissue engineering. Colloids Surf B Biointerfaces. 2007;60(2):137–57.
127. Vogler EA. Structure and reactivity of water at biomaterial surfaces. Adv Colloid Interf Sci. 1998;74(1):69–117.
128. Hu L, et al. Strontium-modified porous polyetheretherketone with the triple function of osteogenesis, angiogenesis, and anti-inflammatory for bone grafting. Biomater Adv. 2022;143:213160.
129. Grundke K. Characterization of polymer surfaces by wetting and electrokinetic measurements—contact angle, interfacial tension, zeta potential. In: Stamm M, editor. Polymer surfaces and interfaces: characterization, modification and applications. Berlin: Springer; 2008. p. 103–38.

130. Murthy NS. Techniques for analyzing biomaterial surface structure, morphology and topography. In: Surface modification of biomaterials: methods analysis and applications. Elsevier Inc.; 2011. p. 232–55.
131. Hawker MJ, Pegalajar-Jurado A, Fisher ER. Innovative applications of surface wettability measurements for plasma-modified three-dimensional porous polymeric materials: a review. Plasma Process Polym. 2015;12(9):846–63.
132. Iandolo D, et al. Development and characterization of organic electronic scaffolds for bone tissue engineering. Adv Healthc Mater. 2016;5(12):1505–12.
133. Dong Y, et al. Synergistic effect of PVDF-coated PCL-TCP scaffolds and pulsed electromagnetic field on osteogenesis. Int J Mol Sci. 2021;22(12):6438.
134. Merrett K, et al. Surface analysis methods for characterizing polymeric biomaterials. J Biomater Sci Polym Ed. 2002;13(6):593–621.
135. Li H, et al. Human mesenchymal stem-cell behaviour on direct laser micropatterned electrospun scaffolds with hierarchical structures. Macromol Biosci. 2013;13(3):299–310.
136. Wang Y, et al. Hybrid hydrogel composed of hyaluronic acid, gelatin, and extracellular cartilage matrix for perforated TM repair. Front Bioeng Biotechnol. 2021;9(1333):811652.
137. Danilatos GD. Figure of merit for environmental SEM and its implications. J Microsc. 2011;244(2):159–69.
138. Variola F. Atomic force microscopy in biomaterials surface science. Phys Chem Chem Phys. 2015;17(5):2950–9.
139. Eaton P, West P. Atomic force microscopy. Oxford University Press; 2010.
140. Li T, Zeng K. Nanoscale piezoelectric and ferroelectric behaviors of seashell by piezoresponse force microscopy. J Appl Phys. 2013;113(18):187202.
141. Engler AJ, et al. Surface probe measurements of the elasticity of sectioned tissue, thin gels and polyelectrolyte multilayer films: correlations between substrate stiffness and cell adhesion. Surf Sci. 2004;570(1):142–54.
142. John J, et al. An electrochemical quartz crystal microbalance study of a prospective alkaline anion exchange membrane material for fuel cells: anion exchange dynamics and membrane swelling. J Am Chem Soc. 2014;136(14):5309–22.
143. Kusakawa Y, Yoshida E, Hayakawa T. Protein adsorption to titanium and zirconia using a quartz crystal microbalance method. Biomed Res Int. 2017;2017:1521593.
144. Pang D, et al. Preparation of a beta-tricalcium phosphate nanocoating and its protein adsorption behaviour by quartz crystal microbalance with dissipation technique. Colloids Surf B: Biointerfaces. 2018;162:1–7.
145. Liu Q, et al. Cationic cellulose nanocrystals for fast, efficient and selective heparin recovery. Chem Eng J. 2021;420:129811.
146. Shen Z, et al. Nonlabeled quartz crystal microbalance biosensor for bacterial detection using carbohydrate and lectin recognitions. Anal Chem. 2007;79(6):2312–9.
147. Ju J, et al. Electrochemistry at bimetallic Pd/Au thin film surfaces for selective detection of reactive oxygen species and reactive nitrogen species. Anal Chem. 2020;92(9):6538–47.
148. Shpigel N, et al. In situ hydrodynamic spectroscopy for structure characterization of porous energy storage electrodes. Nat Mater. 2016;15(5):570–5.
149. Luan Y, et al. "Hearing loss" in QCM measurement of protein adsorption to protein resistant polymer brush layers. Anal Chem. 2017;89(7):4184–91.
150. Luan P, Oehrlein GS. Characterization of ultrathin polymer films using p-polarized ATR-FTIR and its comparison with XPS. Langmuir. 2019;35(12):4270–7.
151. Müller M. Vibrational spectroscopic and optical methods. In: Stamm M, editor. Polymer surfaces and interfaces: characterization, modification and applications. Berlin: Springer; 2008. p. 47–70.
152. Chittur KK. FTIR/ATR for protein adsorption to biomaterial surfaces. Biomaterials. 1998;19(4):357–69.

153. Pleul D, Simon F. X-ray photoelectron spectroscopy. In: Stamm M, editor. Polymer surfaces and interfaces: characterization, modification and applications. Berlin: Springer; 2008. p. 71–89.
154. Yang J, Alexander MR. 8—Techniques for analysing biomaterial surface chemistry. In: Williams R, editor. Surface modification of biomaterials. Woodhead Publishing; 2011. p. 205–32.
155. Pleul D, Simon F. Time-of-flight secondary ion mass spectrometry. In: Stamm M, editor. Polymer surfaces and interfaces: characterization, modification and applications. Berlin: Springer; 2008. p. 91–102.
156. Tyler BJ, Rayal G, Castner DG. Multivariate analysis strategies for processing ToF-SIMS images of biomaterials. Biomaterials. 2007;28(15):2412–23.
157. Chandler AB. In vitro thrombotic coagulation of the blood; a method for producing a thrombus. Lab Investig. 1958;7(2):110–4.
158. Weber M, et al. Blood-contacting biomaterials: in vitro evaluation of the hemocompatibility. Front Bioeng Biotechnol. 2018;6:99.

Chapter 7
Gradient Biomaterials and Their Impact on Cell Migration

Zhengwei Mao, Shan Yu, Tanchen Ren, and Changyou Gao

Abstract Cell migration participates in a variety of physiological and pathological processes such as embryonic development, cancer metastasis, blood vessel formation and remolding, tissue regeneration, immune surveillance, and inflammation. Cell migration regulation is of paramount importance to achieving the recruitment of specific cells for tissue regeneration. The cells specifically migrate up along gradually varying concentrations (gradient) of soluble signaling factors and/or ligands bound into the extracellular matrix (ECM) in the body during the wound-healing process. Therefore, creating artificial microenvironments by incorporating physical, chemical, and biological signal gradients within engineered biomaterials is a potential solution to promote tissue regeneration. In this chapter, the gradients existing in vivo and their influences on cell migration are firstly described. Recent progress in the fabrication of gradient biomaterials is then discussed. The impact of gradient biomaterials on cell responses, especially cell migration, is discussed, highlighting their potential application in regenerative medicine. The future trends in gradient biomaterials and programmed cell migration in context with tissue regeneration are prospected.

Keywords Gradient biomaterials · Cell migration · Material–cell interaction · Tissue regeneration · Regenerative medicine

7.1 Introduction

Regenerative medicine is proposed to study transformations of cells and extracellular matrix during tissue repair for perspective regenerative therapies. An important step is to recruit nearby somatic or stem cells to wound sites with the assistance of biomaterials [1]. Within this process, cell migration, especially directionally moving

Z. Mao (✉) · S. Yu · T. Ren · C. Gao (✉)
MOE Key Laboratory of Macromolecular Synthesis and Functionalization, Department of Polymer Science and Engineering, Zhejiang University, Hangzhou, China
e-mail: zwmao@zju.edu.cn; cygao@zju.edu.cn

C. Gao (ed.), *Polymeric Biomaterials for Tissue Regeneration*,
https://doi.org/10.1007/978-981-99-6948-7_7

toward the wound site under the guidance of spatiotemporal signals, plays a paramount role [2]. Therefore, it is very important to study the cell migration behavior with the presence of physical, chemical, and biological cues to get in-depth understanding of tissue regeneration process and thereby provide guidance principles for designing advanced biomaterials.

Cells migrate in response to gradients of stimuli such as dissolved chemoattractants (chemotaxis) or surface-attached molecules (haptotaxis) as well as biophysical contact cues (durotaxis or mechanotaxis) in vivo [3, 4]. Ramón Cajal (1892) first proposed that gradients of attractive molecules could guide growing axons to their targets [5]. Since then, in vivo gradients of chemical signals have been proved to exist, and their roles in guiding the translocation of cells have been widely recognized. Mechanical guidance (mechanotaxis), which exists widely in extracellular matrix, is also thought to drive processes of cell migration in tissue regeneration [6, 7].

The "gradient biomaterials" offer an ideal model, enabling the studies of cell behaviors in a complicate and precisely regulated microenvironment. Over the past 20 years, a lot of techniques have been developed to generate spatiotemporal gradients and advanced functional biomaterials [8, 9]. The gradient biomaterials have been adopted to systematically study the cell responses to biomaterials including cell adhesion, distribution, and alignment [10]. Recently, cell migration induced by gradient biomaterials [11] and their potential applications in tissue regeneration [12, 13] are attracting more and more attentions.

In this chapter, we focus on the design of the gradient biomaterials and their impact on cell migration. Firstly, the knowledge obtained from nature: biological gradients existing in vivo and their influences on cell migration will be introduced. Methodologies for preparing the gradient materials will be summarized, followed by the directed migration behaviors of cells. Finally, the chapter concludes with current challenges and future perspectives.

7.2 Cell Migration

Cell migration in vivo is a very significant process on both physiological and pathological aspects. During embryonic development in mammal, cells migrate beneath ectoderm to create different germ layers, which are required for proper tissue formation [14]. Cell migration is also prominent in numerous tissue regeneration processes in adults, such as morphogenesis, angiogenesis, wound healing, and immune response [15–17]. For example, when wound occurs, immune cells and subsequently fibroblasts invade into the temporarily formed clots to fill the defect under the guidance of inflammatory factors. Meanwhile, the epidermal cells proliferate and migrate to cover the surface [15]. Migration of mesenchymal progenitor cells induced by biological signals is important to tissue reprogramming during bone repair [18].

More importantly, undesired cell migration will cause diseases or improper regeneration of tissues such as atherosclerosis, a chronic inflammatory disease of arterial wall [19]. During atherosclerosis, endothelium, composed of endothelial cells (ECs), is damaged, and subsequent migration of vascular smooth muscle cells (SMCs), which naturally move much faster than ECs to the impaired vessels, is stimulated by various inflammatory factors [20], leading to further damage of the vasculature. In-stent restenosis (ISR), a particular refractory form of neointimal hyperplasia [21], is another example. Stent implantation has become the main method to treat coronary artery diseases. However, the implantation may induce a series of pathological processes such as thrombosis and abnormal release of cytokines. These pathological events subsequently trigger the migration and proliferation of SMCs and thereby induce ISR [22]. Therefore, it is of great importance to understand the mechanism of cell migration especially under correct physiological conditions.

7.2.1 The Biological Processes of Cell Migration

The migration of single cell is the best-studied model of cell movement in vitro, and the newly developed fluorescent tagging technology also makes it possible to visualize the cell migration in vivo [23–25]. Cell migration is a complex process requiring work cooperation of cytoskeleton, membrane, and signaling systems (Fig. 7.1) [26]. Responding to the external topographic or chemical stimuli, cells protrude their leading edge [27]. The directional extension of active membrane, including both lamellipodia (sheetlike protrusions) and filopodia (spikelike protrusions), brings on attachment and thus traction force to the substrate, resulting in a counterforce on the cell to promote cell migration [28]. The contraction of cytoskeleton filaments pulls the cell body toward the leading edge, with a consequent release of attachment at the rear to allow the tail to retract, then the cell moves forward. All these steps involve the assembly and disassembly of the cytoskeleton filaments, especially actin fibers, producing forward movement of cells. Herein, moderate adhesion strength provided by the supporting matrix is essential for dynamic cell protrusion and contraction [29].

The cell migration process also involves the spatiotemporal transition of intracellular signaling, such as focal adhesion kinase (FAK), mitogen-activated protein kinases (MAPKs), and Rho GTPases [24, 30–32]. Rho family GTPases, including Cdc42, Rac, and Rho, act as molecular switches of actin polymerization, actomyosin contraction, and cell mobility. Cdc42 and Rac regulate actin polymerization and membrane protrusion, while Rho generates the contraction and retraction forces required in the cell body and at the rear [33]. MAPKs, including ERK, p38MAPK, and JNK, can promote cell migration by regulating actin dynamics. For example, ERK1 and ERK2 can phosphorylate MLCK and increase MLC phosphorylation to enhance cell migration [34–36]. In addition, many downstream signal molecules participate in the migration process. For example, the Ser/Thr kinase p65PAK

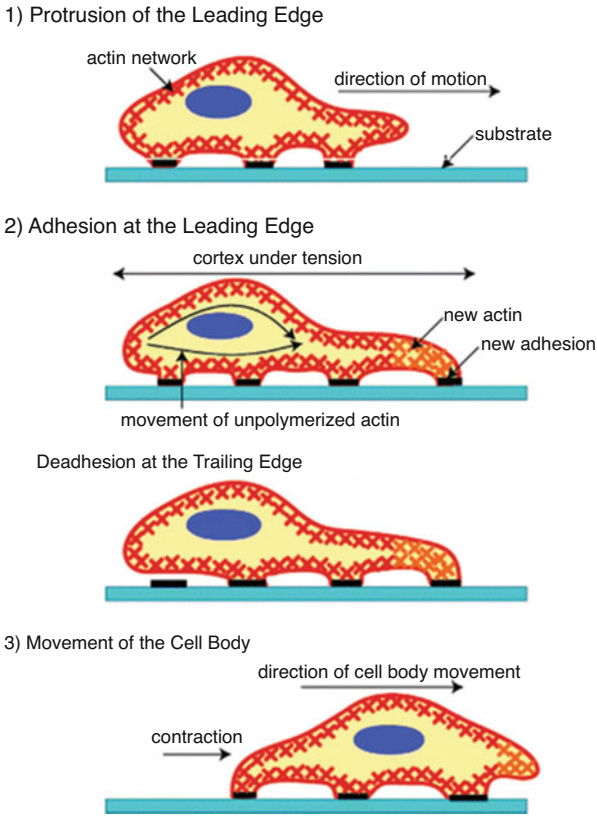

Fig. 7.1 A schematic of the three stages of cell movement: after determining its direction of motion, the cell extends a protrusion in this direction by actin polymerization at the leading edge. It then adheres its leading edge to the surface where it is moving and deadheres at the cell body and rear. Finally, it pulls the whole cell body forward by contraction force generated on the cell body and rear of the cell. (Reprinted from [26] with permission. Copyright Ivyspring International Publisher)

controls focal adhesion (FA) turnover since the integrin adhesion complexes should be dynamically changed, allowing the cells to adhere and pass [37].

Among all intracellular signals, one of the most well-studied long-term modifications, driven by mechanical cues, is the activation and localization of the Yes-associated protein (YAP) [38]. YAP is a family of transcriptional cofactors whose translocation to the nucleus is known to be controlled by mechanical cues of the environment, such as ECM rigidity, strain, shear stress, adhesive area, or force [39]. Interestingly, YAP nuclear translocation is itself a short-term modification, but the effects of this translocation have long-term transcriptional effects. Once in the nucleus, YAP binds to TEAD transcription factors and induces the transcription of genes associated with proliferation and inhibition of differentiation or cell migration and invasion in cancer cells [40].

In the process of durotaxis stimulating, externally or internally generated gradients sensed by FA, actomyosin network or plasma membrane, the serial mechanotransductions which are related to above spatiotemporal transition of intracellular signaling [41]. Cells undergoing chemotaxis normally adjust the distribution of guidance cues with enzymes (e.g., by degradation with MMPs or ADAMs) [42], or by endocytosing them with its receptors, while still responding to them [43],

which suggests that the responding cells are actively involved in shaping the gradient. During haptotaxis, cells sense differences in ECM concentration or engagement across a single cell, and then react by polarizing their cytoskeletal and motility machinery to enable them to protrude and migrate up the gradient toward fixed substrate-bound cues. Hence, many of the molecules identified as important for this type of migration are like those of chemotaxis and durotaxis [44]. The precise mechanisms for galvanotaxis are largely unknown.

Collective migration is the second principal mode of cell movement [45, 46]. This mode differs from single cell migration since cells remain connected as they move, resulting in migrating cohorts and varying degrees of tissue organization [47, 48]. Some collective cell migrations under gradients stimuli were found even though no single cell migration could be observed under the same stimuli. Collective migration of cohesive cell groups in vivo is particularly prevalent during embryogenesis and drives the formation of many complex tissues and organs. Raimon et al. reported their findings in collective cell durotaxis emerging from long-range intercellular force transmission [49]. This emergent mode of directed collective cell migration applied to a variety of epithelial cell types, required the action of myosin motors, and originated from the supracellular transmission of contractile physical forces. Recent discoveries also show that durotaxis and dynamic stiffness gradients exist in vivo, and gradients of chemical and mechanical signals cooperate to achieve efficient directional cell migration [50, 51].

Collective cell migration can be defined by three hallmarks. Firstly, the cells remain physically and functionally connected because the cell–cell junctions are well preserved during movement [52, 53]. Secondly, multicellular polarity and organization of the actin networks generate traction and protrusion forces for migration and maintain cell–cell junctions. Isolated cells are more sensitive to environmental fluctuations, whereas cell clusters can counteract the effects of fluctuations by cell–cell interactions [54]. Thirdly, in most modes of collective migration, moving cells structurally modify the tissue along the migration path, leading to the modification of ECM [55]. Depending on the context, collective movement can occur by two-dimensional sheet migration across a planar surface or by multicellular strands or groups moving through a three-dimensional scaffold.

7.2.2 Gradient Signals In Vivo

Although cells migration patterns are diverse, gradient stimuli play an important role in different patterns. Most cells are surrounded by extracellular matrix (ECM), which is a complex network consisting of proteins, polysaccharides, and signaling molecules. Physical cues such as pore size, topography, stiffness and viscoelasticity as well as chemical cues including the composition of ECM and concentration of signal molecules are the main guiding cues for cell migration in vivo, inducing cell polarity and thus controlling the migration rate and direction.

7.2.2.1 Physical Gradients and Their Influence on Cell Migration

Physical gradients are defined as the gradual varying physical properties such as porosity, stiffness, and morphology. Native bones have physical gradients formed with its density distribution diversity. The dense cortical bone locates in the outer layer and low-density "trabecular" bone locates inside. The pore size decreases from inside to outside. Such structures provide great permeability and excellent mechanical support [56]. Particularly, the mechanical strength or modulus is inversely dependent on the porosity and the pore volume [57]. Therefore, the bimodal structure of bone (cortical and cancellous) gives rise to the gradient of mechanical properties in the nature bone. In addition to the porosity, the bone stiffness and elasticity can also be determined by the variability of mineralization or mineral density, cell type, and cytokine gradient features [58]. The compression strength differs from 133 MPa in midfemoral to 6.8 MPa in proximal femoral, while the modulus of elasticity decreases from 17 to 0.4 GPa [59]. Therefore, biomaterials with similar physical gradients consist of structural diversity could potentially induce osteointegration to facilitate biological ligament–bone fixation for bone repair [60]. Teeth also contain gradients in composition and mineral density, which give rise to gradients in mechanical properties [61].

Cells can guide their movement by probing the substrate stiffness. Endothelial cells (ECs) and smooth muscle cells (SMCs) can move into tumor tissues due to higher stiffness inside, leading to fast angiogenesis. Fibroblasts also can move into scar tissues because of their higher stiffness and speed up the wound-healing process [62]. After the injury, the migration of muscle stem cells would be enhanced by elevated muscle stiffness for further regeneration [63].

As shown in Fig. 7.2 [64], increase in substrate stiffness can cause an increase in traction force, which would then pull the region forward and trigger a bias in movement direction and an increase in spreading. Such force-induced cytoskeletal contractility was also suggested by studies that adopted magnetic twisting force or dragging force onto integrin-bound beads. The cells responded by increasing the resistive forces and/or reinforcing the integrin-cytoskeleton linkages [65, 66]. Based on these observations, Sheetz et al. speculated that stiffness of the ECM might function as an environmental cue to orient the direction of cell movement [67].

The changes of protein conformation under the action of force are often accompanied by enzyme catalysis. Many enzyme catalytic activities are also associated with force action [68]. The mechanical response process is usually a positive feedback loop mechanism. Myosin traction opens the active sites of structural proteins, activating more structural proteins, skeleton proteins, force acting proteins, etc. The transcription regulation under the action of force also promotes the expression of related proteins, allowing cells to recruit more proteins [69]. The expression and activation of related proteins further promote the generation of intracellular forces. A deep understanding of the cell's recognition of the mechanical properties of the microenvironment can enable a deep analysis of the loading of intracellular forces on the cell microenvironment interface.

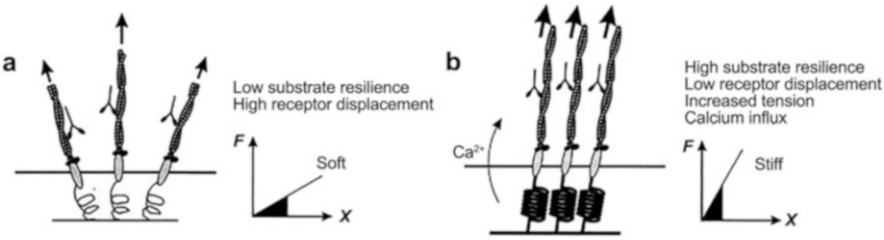

Fig. 7.2 Model for the signal detection of substrate stiffness. The initial probing forces are generated by actin–myosin interactions associated with cell–substrate adhesion sites. (**a**) On a soft substrate, the receptor–ligand complex is mobile and the tension at the anchorage site is weak. With a given energy input (*black area* under the force-displacement graph), the complex can move over a long distance (*x axis*). (**b**) On a stiff substrate, equivalent energy consumption (shown as an equivalent *black area* under the force-displacement graph) causes a higher tension (*y axis*) and lower displacement of the receptor–ligand complex (*x axis*). The increase in tension may induce an influx of extracellular calcium through the stress-activated channels. (Reprinted from [64] with permission. Copyright 2000 The Biophysical Society)

It is unclear how cells actually translate substrate stiffness into downstream responses. One possibility is that cells can directly sense the distance of receptor movement as a result of exerted probing forces. Alternatively, the rigidity of the substrate could be determined by monitoring the magnitude of counterforces upon the consumption of a given amount of energy. On the stiff substrate, strong mechanical feedback from the substrate occurs after a small receptor displacement. Because elastic energy is the integration of forces along the distance, with the same amount of energy consumption, the soft substrate can generate only a weaker mechanical feedback but a larger displacement. The stronger mechanical feedback on stiff substrate may then lead to the activation of stress-sensitive ion channels [70] or conformational changes of other tension-sensitive proteins. These responses in turn may regulate the extent of protein tyrosine phosphorylation, the stability of focal adhesions, and the strength of contractile forces [71]. Therefore, an effective navigating system emerges, in which cells send out local protrusions to probe the mechanical properties nearby. Those receiving strong feedback from the environment are amplified and become the primary leading edge, whereas those receiving weak feedback become unstable and may be further weakened because of the reorganization of the cytoskeleton. These coordinated responses would be a powerful means to direct cell movement in response to mechanical gradient [64]. By utility of step-rigidity micropost arrays, cells are proved to sense substrate rigidity locally to induce an asymmetrical intracellular traction force distribution to contribute to durotaxis [72].

Recent works have revealed that matrix viscoelasticity regulates cell migration that is not observed in previous studies with elastic hydrogels in both two- and three-dimensional culture microenvironments. Ovijit et al. found with rigid or elastic pores, matrix degradation was required for the cells to overcome confinement and migrate. However, given sufficient viscoelasticity or viscoplasticity, cells can

overcome confinement to grow in size, deposit matrix, change their morphology as they spread or undergo mitosis, and migrate [73, 74].

7.2.2.2 Chemical Gradients

Biomolecules including cell factors and microenvironment changes caused by metabolism are two main styles of chemical gradients in nature in living body. One is the biomolecules bound in extracellular matrix, including chemokines, hormones, and proteins. The dominating proteins are ECM proteins such as collagen, fibronectin (Fn), and laminin and growth factors such as fibroblast growth factor family (FGFs), vascular epidermal growth factor (VEGF), and so on. They can initiate multiple intracellular signaling pathways after binding to the receptors on cell surface, regulating various cell responses. For example, bone morphogenetic protein (BMP) concentration gradient in zebrafish is responsible for guiding bone formation [75–77]. Semaphoring Sema 2a concentration gradient is also known for guiding neuron outgrowth [78]. Expression of laminin-2 decreases from the base of the villus to the top in the epithelium of the small intestine, while the expression of laminin-1 increases. Stem cells are guided by this signal gradient and proliferate and undergo differentiation while moving upward to the tip of the villus in vivo.

The other kinds of gradients are made of soluble biomolecules, formed through diffusion and convection (larger molecules) when they are released from the cells and the matrix [79, 80]. The cells respond to the gradients in a diffusion speed and distance-dependent manner [81]. Tumor cells, for example, are known to secrete an array of chemokines (e.g., IL8, CCL21, SDF-1α) and growth factors (e.g., EGF) to form a tight control of their microenvironments and to enhance their ability to migrate to a distant site [82, 83]. Immune cells are another kind of cells that utilize molecular gradients within their surrounding as guidance cues to migrate [84, 85]. Dendritic cells, for instance, are known to migrate up lymphoidal chemokine gradients (CCL21 and CCL19) toward lymphatic vessels [86].

The second example of the molecular gradient formation is the oxygen concentration, pH, and reactive oxygen species gradient as a result of cellular metabolic activities [87–90]. Tumor cells have a high metabolic rate and thus a high oxygen consumption rate. Tumor cells initially grow with a mature vascular structure until the tumor body reaches a critical size, where the cells in the center become hypoxic due to limited oxygen supply from their surrounding tissues by diffusion. As a result, an oxygen concentration gradient with the highest concentration at the tumor edge is generated. In a vascularized tumor, blood vessels are oxygen suppliers to the tumor cells. Due to tumor metabolic activities, there is an oxygen and pH gradient adjacent to the blood vessel. As a result, tumor cells can sense the oxygen concentration gradient and pH gradient and then move toward blood vessels, which is a key step of tumor metastasis [82, 87]. In contrast, endothelial cells migrate toward the acidic end of an extracellular pH gradient, because cell membrane protrusion stability and actin–integrin adhesion complex formation are increased in acidic pH, which could contribute to the preferential polarization toward acidic pH and favor

directional cell migration [91]. During wound healing, extracellular pH-gradients work as pivotal governors of keratinocyte cell migrations to impact epidermal barrier repair [92]. ROS is also proved involved in regulating wound healing by altering epithelial cytoskeletal dynamics at the leading edge and directing cell migration [93].

These two kinds of gradients also coordinate with each other to complete biological activities. For example, during angiogenesis, the soluble VEGF gradient increases the vessel caliber, while the gradient of matrix-bound VEGF promotes the vessel branch sprouting [94]. Hypoxia could also induce directed migration of human monocytes accompanied the function of chemokine C motif chemokine ligand 26 (CCL 26) [95].

7.2.3 Possible Mechanism of Gradient-Dominated Cell Migration

In nature, an object always travels randomly in an environment without an asymmetric cue, which has been recognized as Brownian movement. In an anisotropic system, a driving force is imposed to the object due to the asymmetric interactions with surrounding environment. The directional transport of liquid and particles based on the gradients of surface energy has been reported [9, 96].

The first response of cells to the gradient is to polarize, by redistributing chemosensory signaling receptors on their surface [97–99]. Chan et al. reported that the cells reoriented and positioned toward the direction of higher ligand density when they were seeded on a ligand density gradient [100]. Arnold and Hirschfeld-Warneken et al. prepared an RGD density gradient to control the spatial distribution of integrin receptors on cell membrane, leading to the cell polarization and subsequent migration [101, 102]. Directional cell migration can be achieved when cellular polarization is kept in one direction due to the presence of the external gradient signaling. Another explanation of gradient-guided cell migration is attributed to the adhesiveness between the cell and the underlying substrate. Cells attach to the substrate stronger at one end. The imbalance of adhesive force leads to forward movement toward the direction of increasing adhesiveness. The rear of the cells contracts to diminish the cellular polarization extent, and the movement is paused until the cells polarize again [97, 98]. Smith et al. found that the cells move faster on the gradient with a larger slope, but had no difference in cell polarization [103]. So the increase of migration speed is attributed to the higher frequency of cellular polarization, gradient recognition, and/or more stable polarization state.

For long and complex migration environments in vivo is different. Cells can create gradients that are tailored to their own optima for responsiveness. This is true whether the gradients are 100% self-generated—made newly from a homogeneous environment—or reshaped by attractant breakdown from a higher-concentration and less sharply focused imposed gradient [104, 105]. Self-generated chemotaxis, a process in which cells create their own local, dynamic gradients by breaking down

an attractant in their environment. Self-generated chemoattractant gradients allow cells to navigate complex paths with great efficiency. Diffusion and attractant breakdown allow cells to obtain detailed information about their surroundings that could not be provided by simple attractant gradients [106].

7.3 Methods to Prepare Gradient Biomaterials

Since cells migrate in response to signal gradients in vivo, it would be of interest to prepare gradient biomaterials to mimic the signal and study material–cell interactions and/or guide cell directional movement for tissue regeneration. So far many methods have been developed to prepare gradient biomaterials. Abundant 2D gradients have been developed due to their easy fabrication and controlled structures. In the past, biological effect of 2D gradient biomaterials and structure design has been studied. The functions to regulate cell migrations of 2D gradient biomaterials were tailored by controlled structure precisely. There are two categories of techniques for producing gradient surfaces: "bottom-up" and "top-down." The former technique constructs patterns by continuously introducing building blocks on the surface, such as silane, thiol, and macromolecules without destroying the bulk materials [107]. The latter one is deconstruction and modification of surfaces gradually via external stimuli such as light, electron, plasma, etching solution, and so on [108]. As a result, the structures and properties of the surface will be altered.

Besides these technologies that are initially designed for the modification of material surface, another category of technologies has been developed to construct gradients in 3D matrix. Although it is much more difficult to elucidate the cell responses in 3D gradient biomaterial, the complicated and favorable biological effects raised wide interests in development of 3D gradient biomaterials.

7.3.1 Bottom-Up Approaches

The bottom-up technologies are valid for various functional molecules and are feasible to control their grafting density, chain length, and spatial organization. By changing the chemical structures, the surface properties can be gradually switched from hydrophilic to hydrophobic [109], from soft to stiff, and from cell resistant to cell adhesive [110]. The gradient surfaces can be prepared based on kinetic and spatial controlled reaction (Fig. 7.3).

7.3.1.1 Infusion

By gradually elevating or lowering the solution level, surfaces can be decorated with organic monolayer with a gradient pattern [114, 115]. The method is so simple and

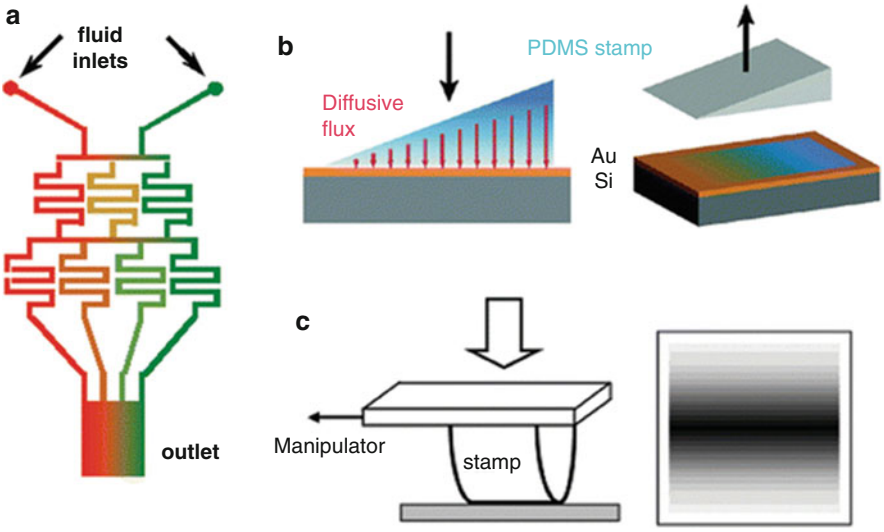

Fig. 7.3 (**a**) Schematic design of a representative gradient-generating microfluidic network. Solutions containing different chemicals are introduced from the *top* inlets and allowed to flow through the network. When all the branches are recombined, a concentration gradient is established across the outlet channel. (Reprinted from [111] with permission. Copyright 2001 American Chemical Society). (**b**) Thiol diffuses into the stamp from an ink pad. It leaves the stamp because of adsorption to the gold surface and creates a partially covered surface. (Reprinted from [112] with permission. Copyright 2005 American Chemical Society). (**c**) Symmetrical lateral gradients are generated using hemicylindrical stamps. The contact area increases under increased compression. The *darker areas* indicate the more hydrophobic region where the contact time is longer. The sketch is not to scale. (Reprinted from [113] with permission. Copyright 2003 American Chemical Society)

convenient that neither special instrument nor rigorous condition is required. Furthermore, it is feasible to generate gradients of a variety of chemical functionalities on the micrometer to centimeter scale.

By controlling the injection speed, the position on the gradient corresponds directly to the immersion time. The slope of the gradient also can be tuned by adjusting the injection speed: higher infusion speed will make a smaller slope [116]. Also, the slopes and the lengths of the gradients can be tailored by changing the feeding concentration [117]. The concentration of molecules or the molecular weight of polymers on the gradient decreases linearly with its maximum at the bottom end which reacts for the longest time. Yu et al. fabricated a gradient from superhydrophobicity to superhydrophilicity by slowly adding the $HS(CH_2)_{11}CH_3$ solution to the container holding the gold substrate and then backfilling $HS(CH_2)_{10}CH_2OH$ [118]. In a further step, the gradients can be backfilled either in a contrary direction (head-to-tail method) or by fully immersing it into the complementary solution (full immersion method). Obviously, the head-to-tail method produces a steeper gradient [119].

Recently, some novel methods based on infusion were developed to fabricate gradient surface on the micrometer scale. Huang et al. report a facile and robust way to fabricate a surface with gradient topography of porous structure in one direction, based on the breath figure (BF) method [120]. In a classic BF method, a polymer solution, prepared with a volatile solvent, is cast onto a substrate and dries under a humid environment for BF structure fabrication. Different from the traditional way, the polymer solution was separated into polymer substrate and solvent. The polymer substrate was immersed into the solvent and dried under a humid environment to obtain BF pores. The separation of the polymer substrate and the solvent provided a possible condition of gradient growth of water droplets on one BF sample which caused the formation of the gradient BF pore structure.

7.3.1.2 Diffusion

The molecular diffusion and transportation can be achieved in solution, vapor, or gel. The chemical gradient pattern is generated by imprinting the molecules onto the surface. Chaudhury et al. evaporated silane molecules, which were deposited more on the substrate end closer to the vapor source, and achieved the silane density gradient [121]. The steepness of the gradient can be easily adjusted by controlling the diffusion time, the silane molecules, and environment conditions such as humidity and temperature [122–124]. Mougin et al. prepared a thiol concentration gradient by diffusing into a gel matrix and then transferred the gradient to gold substrates [125, 126].

Claussen et al. presented a straightforward experimental method for fabrication of a gradient in mechanical properties on the centimeter scale based on a poly(dimethyl siloxane) (PDMS) system. Compositional gradients are realized by using three syringe pumps feeding different prepolymers capable to undergo thermal crosslinking. Within the gradient samples, the stiffness between the hard and soft part can be varied up to a factor of four. This method can be expanded to other polyaddition systems including polyurethanes and others based on photopolymerizable acrylates and thiol-ene click chemistry [127–129]. However, there is a common problem called “fingering” when two diffusion streams meet. As a result, an inhomogeneity will inevitably exist in the direction perpendicular to the gradient [110]. Qiu et al. reported a facile method for generating a mineral gradient in a biodegradable polymer scaffold. The gradient is achieved by swelling a composite film made of polycaprolactone (PCL) and hydroxyapatite (HAp) nanoparticles with a PCL solution. During the swelling process, the solvent and PCL polymer chains diffuse into the composite film, generating a gradient in HAp density at their interface. The thickness of the mineral gradient can be tuned by varying the extent of swelling to match the length scale of the natural tendon-to-bone attachment (20−60 μm). When patterned with an array of funnel-shaped channels, the mineral gradient presents stem cells with spatial gradations in both biochemical cues (e.g., osteoinductivity and conductivity associated with the HAp nanoparticles)

and mechanical cues (e.g., substrate stiffness) to stimulate their differentiation into a graded distribution of cell phenotypes [130].

7.3.1.3 Microfluidic Lithography (μFL)

Microfluidic system offers a simple and fast way of generating dynamic chemical gradients of growth factors, ECM proteins, enzymes, drugs, or other functional molecules (Fig. 7.3a). Gradient patterns are formed by injecting multiple solutions simultaneously into a channel network, after which the fluid streams repeatedly split, mix, recombine, and branch. Finally, a chemical gradient is established in a single large channel that is perpendicular to the flow and combines all individual branches of fluids. By designing the microchannel network, the slope and shape of the gradients are precisely controlled [111, 131].

Gunawan et al. injected laminin and collagen solutions into a microfluidic system where the streams containing the highest concentration of laminin or collagen were in the farthest channel, respectively [14]. Finally, a concentration gradient with laminin and collagen in converse direction was formed. The microfluidic system also can be used to generate physical gradients. For example, a roughness gradient was fabricated on a silicon wafer after etching by an HF concentration gradient generated by microfluidic assay. By mixing solutions of unifunctional monomers and bifunctional monomers in the microchannels and irradiated under the UV light, a stiffness gradient is created [132]. Kilb et al. used microfluidic devices to build stable interleukin-8 (CXCL8) gradients with resolutions in the range of microns and confirmed THP-1 cells directed migration [133]. Competing gradients could also be realized by microfluidic method. Murugesan et al. fabricated an opposing and aligned gradients of chemoeffectors (1 mM sorbitol as an attractant and 1 mM $NiSO_4$ as an inhibitor) and temperature to detect cell migration under complicated environment [134]. The two-dimensional channel system limits itself to continuous patterns within relative small size.

To overcome this limitation, 3D microfluidic technique is developed using several layers of interconnecting channels [135]. It provides a unique platform to generate complicate and discontinuous gradients and incorporates multiple biomolecules on one gradient [136]. Takahashi et al. proposed the use of novel microfluidic devise produced gradients of pH and oxygen concentration in the extracellular medium [137].

7.3.1.4 Lithography Techniques

The microcontact printing (μCP), developed by Whitesides and his coworkers, has been widely used for generating self-assembled monolayers (SAMs) for its versatility and highly accurate in nanoscale. Recently, a series of technologies have been developed based on μCP, such as decal transfer microlithography (DTM) [138], nanotransfer printing (nTP) [125], and metal transfer printing (MTP)

[139, 140]. Kraus et al. produced a chemical gradient by the mass transfer microcontact printing because the ink mass transported to the substrate was controlled by the thickness of the stamp (Fig. 7.3b) [112]. Jeon et al. found that the surface density of octadecyltrichlorosilane (OTS) was increased by prolongation of the reaction time [141]. Inspired by Jeon's finding, Choi et al. developed a method to prepare chemical gradients by changing the contact time. Gradually or stepwisely increasing the pressure upon the half ball-shaped elastic stamp results in the increase of contact area and correspondingly decreases the contact time from the center to the edge. Subsequently, density gradients of OTS were generated. The gradient length and slope were easily tuned by the radius and curvature of the elastic stamp (Fig. 7.3c) [113]. Lang et al. prepared a microfluidic network into a silicon wafer to deliver protein solutions containing different concentrations of an axonal guidance molecule ephrinA5 onto a silicone stamp. In a subsequent μCP step, the protein was transferred onto a polystyrene culture dish. In this way, stepwise substrate-bound concentration gradients of ephrinA5 were fabricated, spanning a total distance of 320 μm [142]. Although the patterns generated by μCP are complex and facile, the μCP technologies are limited to planar surface [135].

A series of surface patterning techniques which utilize an ultrasharp scanning tip (or an array of tips in some examples) have been developed for the fabrication of 3D nanostructures on surfaces. For example, Zheng et al. developed dip-pen nanodisplacement lithography (DNL), a high-resolution, program controllable, solution-free, and diffusion-limited lithography tool for construction of molecules on a surface at the nanometer scale [135, 143]. Briefly, an AFM tip inked with initiator molecules ω-mercaptoundecyl bromoisobutyrate (MUDBr) was used to shave Au surfaces which had been modified with an inert SAM of 16-mercaptohexadecanoic acid (MHA) at a contact mode. At high load (typically larger than 100 nN), MHA molecules were removed by the tip, where simultaneously MUDBr molecules were transferred onto the same area of Au surface. Finally, poly(2-(methacryloyloxy)ethyl-trimethylammonium chloride) (PMETAC) brushes were prepared via SI-ATRP method (Fig. 7.4a, b). This technique can be used to project a 2D feature density array into a 3D surface morphology with polymer brushes [144]. For instance, the authors fabricated polymer gradients of different shapes. A grayscale image with gradual change of brightness was first converted into a bitmap image, where the density of white/black pixels is proportional to the brightness/darkness. Then the bitmap was used as a blueprint for DNL patterning, yielding an initiator pattern comprising arrays of initiator nanodots. After SI-ATRP, PMETAC brushes were grown from the as-made initiator "bitmap" to generate a Mona Lisa's face (Fig. 7.4c). Xue et al. proposed a novel fabrication strategy to introduce ordered nanopattern arrays into gradient biomaterials, through combining SI−ATRP and inclined reactive ion etching (RIE) based on colloidal lithography [145]. Zhang et al. introduced micropatterns gradient via lithography techniques into the inner wall of nerve guidance conduits can effectively regulate the behavior of Schwann cells, the elongation of axons, and the phenotype of macrophages, thereby aiding the regeneration of injured nerve. The micropatterns were created on the PLCL films by a "double replicating template method" [146, 147].

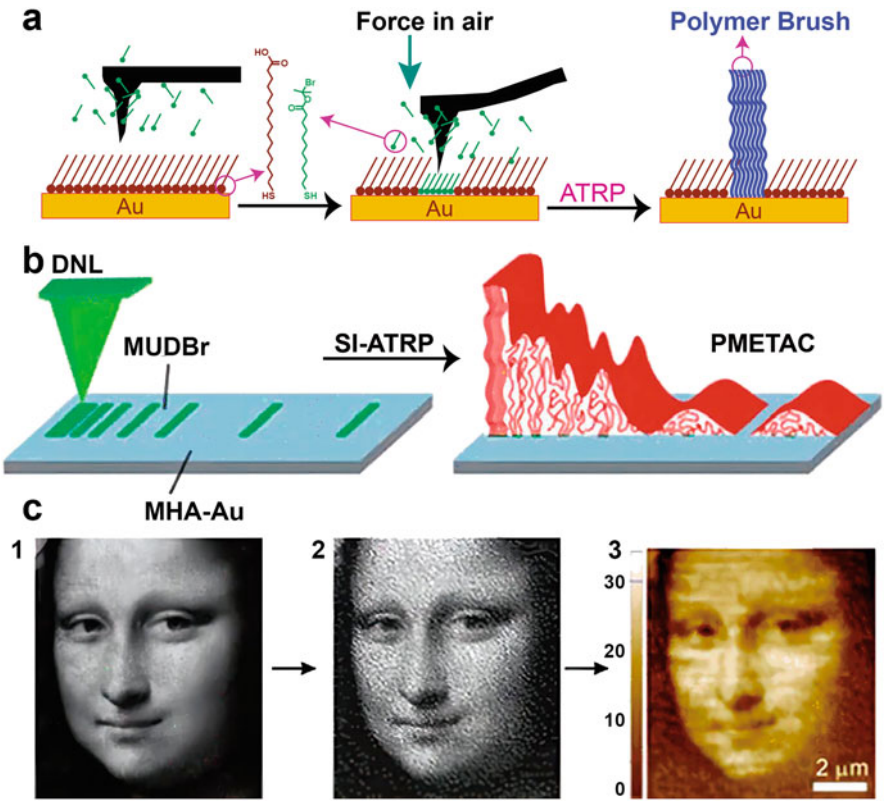

Fig. 7.4 3D PMETAC brushes fabricated by DNL. (**a**) Schematic illustration of the DNL process. (**b**) Schematic illustration of obtained nanopatterning of polymer brushes. (**c**) 3D Mona Lisa portrait fabricated by the feature density method. *1* Grayscale image of Mona Lisa's face. (*2*) Bitmap image converted from (*1*). (*3*) AFM topographic view of PMETAC brushes fabricated with DNL and SI-ATRP using (*2*) as guild map. (Reprinted from [144] with permission. Copyright 2011 WILEY-VCH Verlag GmbH)

7.3.1.5 Electrochemical Method

The isoelectric focusing (IEF) technology has been used to develop a concentration gradient of charged molecules and then transferred to a desired substrate [148]. In the IEF technique, the ampholytes migrate directionally due to the presence of the electric field. For instance, positively charged polylysine accumulates around the cathode and forms a concentration gradient accordingly. The gradient can be transferred to a substrate with the assistant of soaked PDMS stamp. This method can be applied to various polyelectrolytes including proteins, peptides, and

polysaccharides. The slope of the gradients can be adjusted by both electrical field and pH value which determines the charge property of the molecules [149].

Electrochemical techniques based on the oxidation–reduction reaction have also been used to prepare thiol gradients immobilized on the gold surface. By applying an external electric field, the thiols are reduced and detached from the substrate on the region close to the cathode, whereas the thiols are oxidized and remained onto the substrate on the region close to the anode [100, 150].

7.3.2 Top-Down Technologies

The top-down approaches are widely used to introduce active sites on inert surface. For the inert materials without reactive groups, such as polyethylene (PE), polytetrafluoroethylene (PTFE), and polyesters, surface modifications can be performed under high-energy sources such as plasma, corona, and UV light (Fig. 7.5). They provide a destructive process on the surfaces and generate a lot of reactive residues. Chemical gradients can be prepared by spatially altering the exposure time or the power of the energy sources.

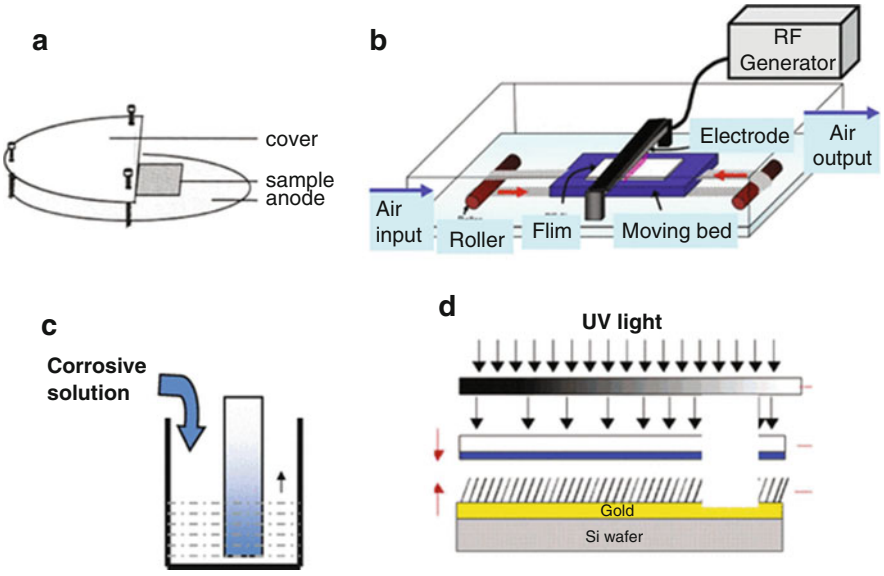

Fig. 7.5 (**a**) Schematic presentation (*side view*) of the glow-discharge reactor chamber, with the electrodes, sample cover, and sample position. (Reprinted from [151] with permission. Copyright 1999 Elsevier Science B.V.) (**b**) Schematic diagram of apparatus for preparation of a gradient on PE surfaces by corona discharge. (Reprinted from [152] with permission. Copyright 2008 Elsevier B. V.) (**c**) Scheme of the preparation process of the gradient by a chemical degradation method. (**d**) Remote photocatalytic oxidation of a thiol SAM under a gradient of UV illumination. (Reprinted from [153] with permission. Copyright 2007 American Chemical Society)

7.3.2.1 Plasma Treatment

The plasma changes substrate by bombarding the surface with high-energy particulates such as electrons, atoms, ions, and radicals. The etching extent is gradually reduced by partly shielding off the reactive particles. Spijker et al. generated a gradient surface by using an aluminum shield on the sample, with its slope conveniently tunable by changing the distance between the mask and the sample [151]. Mangindaan et al. created a wettability gradient on hydrophobic polypropylene film by plasma treatment under a mask [154]. Various functional groups such as amino groups, carboxyl groups, hydroxyl groups, and sulfonic acid groups can be introduced onto the substrate by applying nitrogen, ammonia, oxygen, and sulfur dioxide plasma, respectively [155, 156]. Polymer gradients can also be created on the surface under a shield during plasma polymerization process [157]. Ravi et al. fabricated continuous composition gradients in both 2D hydrogels and 3D thermoplastic scaffolds with atmospheric pressure plasma jet systems [158]. An improvement in mechanical properties of continuous gradients compared to discrete gradients in the 3D scaffolds, and the ability to selectively enhance cell adhesion were demonstrated.

7.3.2.2 Corona Discharge

The corona discharge treatment is a relative simple and cheap technology to generate gradient on the surfaces, as the samples are treated in air instead of in vacuum during the plasma treatment. Lee et al. adopted this technology to create various gradient surfaces [152, 159–162]. For example, polymer sheets were placed under a knife-type electrode which was connected to a radio-frequency generator. Carbon radicals were produced on the polymer surfaces, forming hydroperoxides, and then decomposed into polar oxygen-based groups such as hydroxyl, ether, aldehyde, and carboxylic acid group [160]. Gradients with increasing density of functional groups can be produced by gradually enhancing power while moving the sample with a motorized drive [163]. The radicals also can serve as initiators to trigger the surface-initiated polymerization and active sites to immobilize proteins and peptides [164, 165].

7.3.2.3 UV Irradiation

Peroxides can be generated on the surfaces under strong UV irradiation [166]. Bin et al. produced a gradient with increasing density of carboxyl groups by slowly moving the photomask between a UV lamp and polymer substrates [167, 168]. This process is efficient and simple which only requires a light source. Besides, multicomponent can be immobilized simultaneously. Photolithography is another example using light to prepare gradient materials [96, 153, 169]. For instance, the

substrate is firstly covered with a thiol or silane self-assembled monolayer (SAM) and then irradiated by a UV light to destroy the organic layer. Blondiaux et al. developed a technique by combining a mask with grayscale gradient and titanium dioxide (TiO_2) remote photocatalytic lithography [153]. The TiO_2 layer was placed under the mask and the region exposed to UV irradiation produced radicals, which diffused vertically and thus locally degraded the organic SAM on the gold surface underneath. As a result, a chemical gradient was created with tunable shape and length dependent on the masks.

Ding et al. generated a cell-laden gradient hydrogel with preprogrammable deformation by simply photocrosslinking a mixed solution of a photocrosslinkable polymer macromer, photoinitiator (PI), UV absorber, and live cells. Gradient formation was demonstrated in various polymers including poly(ethylene glycol) (PEG), alginate, and gelatin derivatives using various UV absorbers that present overlap in UV spectrum with that of the PI UV absorbance spectrum. Moreover, this simple and effective method was used as a universal platform to integrate with other hydrogel-engineering techniques such as photomask-aided microfabrication, photopatterning, ion-transfer printing, and 3D bioprinting to fabricate more advanced cell-laden scaffold structures [170]. Hao et al. developed a combinatorial surface-modified platform with biochemical gradients through thiol-ene "click" chemistry by adjusting the intensity of ultraviolet (UV) irradiation [171]. The multistep attachment of different molecules onto substrates is archived via the multistep UV-initiated thiol-ene "click" reaction. The high-throughput arrays with the gradient density of single ligand and the orthogonal gradient density of two ligands were rapidly fabricated via the one-step UV gradient irradiation and the two-step orthogonal UV gradient-initiated thiol-ene "click" reaction.

7.3.2.4 Wet Chemistry Etching

This method was normally applied to the degradable polymers such as polyesters. Gao et al. developed an aminolysis technology to introduce amino groups on the surface of polyesters, which act as active sites for further functionalization [172–175]. Using this method, polymers are degraded progressively by continuously immersing into the reactive solution or injecting the reactive solution into a tube containing the substrates via a microinjection pump [176]. Tan et al. used this technology to construct an amine density gradient on poly(L-lactic acid) (PLLA) film [177, 178]. Besides polyesters, the wet chemistry can also be applied to etch the polyelectrolyte multilayers which are assembled by the alternative adsorption of polycations and polyanions via electrostatic attraction. Generally, etching the multilayers in a salt solution with a critical high ionic strength will reorganize the charge and structure of the multilayers, leading to swell, soften, and even dissolve of the multilayers [179, 180]. The chemical composition and related structure of the modified multilayers are determined by the salt concentration, which provides a simple method to generate gradient multilayers. Han et al. posttreated the polyelectrolytes multilayers in a gradient NaCl solution with a concentration ranging

from 3 to 5 M, yielding the gradient multilayers with a similar chemistry composition and surface charge but gradually changed swelling ratio [181].

However, the top-down technologies in general are limited to the types of functional surfaces generated and unsuitable to process surfaces with unstable biomacromolecules such as ECM proteins and growth factors. Thus, recently the bottom-up methods are more widely used or adopted to further functionalize the surfaces after introduction of active sites on inert surfaces by the top-down approaches.

7.3.3 3D Gradient Generation Technologies

The gradients in a 3D matrix are more important because they are more similar to the situation in vivo and have the potential application of inducing cell migration in the tissue regeneration process. However, the "top-down" and the "bottom-up" technologies are usually applied to manufacture gradients on material surfaces, not suitable or at least needing major modification in a 3D matrix. Up to present, only limited technologies have been developed to generate 3D gradients in porous scaffolds or hydrogels.

Several techniques have been developed for fabricating physical gradient with gradually changing pore size or porosity in scaffolds, to mimic the graded tissue morphology in vivo [112, 113, 141]. For example, Tampieri et al. developed a multiple and differentiated impregnation procedure to prepare porosity-gradient HA scaffolds [57]. Roy et al. [182] and Woodfield et al. [183] used a 3D printing technology to create polymer scaffolds with gradually changing porosity and pore size, respectively. Oh et al. developed a centrifugation method to fabricate a polycaprolactone (PCL) scaffold with gradually increasing pore size and porosity along a cylindrical axis via directional phase separation [184]. Additionally, gradients with gradually changing microstructure can be fabricated using a temperature gradient, based on the heat-induced phase separation [185, 186]. Polyurethane copolymers with different block compositions are also good candidates for this method, resulted in diverse microphase separation and gradient of microstructure [187].

It is relatively easier to prepare 3D chemical gradients in hydrogels due to their similarity to the solutions. Delong et al. prepared hydrogels with a bFGF gradient by diffusing two types of hydrogel precursor solutions (with/without bFGF) [188]. In brief, the PEG solution with bFGF was persistently injected into a container having PEG solution without bFGF. The two solutions were mixed together and finally pumped into a mold where they were exposed to UV light to crosslink the polymer network and stabilize the gradient [10, 189]. Xu et al. prepared a semaphorin 3A density gradient on MatriGel through diffusion method [190]. Microfluidic and diffusion technologies can also be applied to fabricate gradient hydrogels [12–16, 191]. The 3D stiffness gradient can be generated by spatially controlling the crosslinking degree. Wong et al. prepared polyacrylamide hydrogels with gradually

changing modulus by applying a photomask with a grayscale gradient to control the polymerization degree under a UV light [192]. Hansen et al. fabricated arrays of 84 polymer gradients on a single glass microscope slide by inkjet printing, allowing a combination of high-throughput and true combinatorial methods. The gradual change of composition within the polymer gradients is achieved by using two different monomers and a crosslinker [193]. Hubka et al. designed a versatile multichannel gradient maker device and created gradients of HS proteoglycan-derived perlecan/HSPG2 domain I in hyaluronic hydrogels [194].

In contrast to hydrogels, preparation of gradients in porous scaffolds is a bit more difficult and usually not precisely controllable. Charu et al. put a droplet of EDC-activated protein solution under fibrin scaffolds. Along with the protein solution diffused upward to the top, a protein concentration gradient was generated and covalently immobilized within the 3D scaffolds. This kind of diffusion-based method offers good control of gradient slopes by changing reaction time and can be extended to conjugate a variety of proteins on different materials [177]. Oh et al. prepared PCL/Pluronic F127 scaffolds with gradually increasing growth factor density from top to bottom by centrifugation of fibril-like PCL and subsequent surface immobilization of growth factors (Fig. 7.6) [195]. Several kinds of growth factors such as VEGF165, BMP-7, and transforming growth factor-β2 (TGF-β2) were immobilized on the surfaces via heparin binding and reached a density gradient due to gradually increasing surface area along the longitudinal direction. The released amount of VEGF165 from the cylindrical scaffolds gradually decreased along the longitudinal direction in a sustained manner, which allows for a controlled spatial distribution of growth factors in a 3D environment. Barry et al. used plasma-induced polymerization method to deposit a thicker layer of polymer on the scaffold periphery than that in the scaffold core, leading to functional scaffolds containing a gradient [196]. Hsu et al. proposed an adaptable microporous hydrogel (AMH) through microfluidic fabrication based on a unique type of microsized building block that spontaneously forms interconnected pores, propagates the gradients of neuron growth factors [197]. Li et al. demonstrated a facile method for fabrication of continuous gradients of stromal-cell-derived factor-1α (SDF1α) embedded in the radially aligned electrospun collagen/poly (ε-caprolactone) mats which showed great potential for guiding nerve regeneration [198].

7.4 Influences of Gradient Biomaterials on Cell Migration

Gradient materials are widely considered as an engine to drive orient movement of objects such as droplets, particles, and living cells [199, 200]. Whitesides et al. presented the first study of a gradient of surface free energy, which drives water drop to move uphill. The motion of water droplet was the result of an imbalance in the forces due to surface tension acting on the liquid-solid contact line on the two opposite sides (“uphill” or “downhill”) of the drop [121]. Although many investigations are taken to correlate cell responses such as adhesion, proliferation,

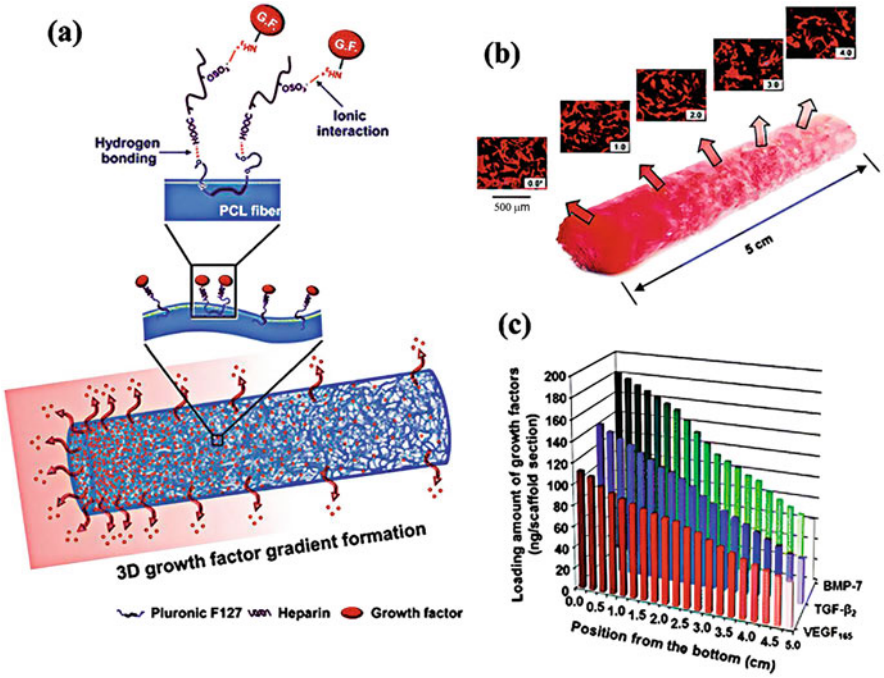

Fig. 7.6 (**a**) Schematic diagrams of the successive binding of heparin and growth factor onto the fibril surface of the PCL/F127 cylindrical scaffold and the formation of 3D growth factor gradient on the scaffold. (**b**) Gross appearance and fluorescence microscopy images showing the rhodamine-labeled VEGF165 gradient along the longitudinal direction of the PCL/F127 cylindrical scaffold. The VEGF165 immobilized on the cylindrical scaffold is expressed as a *red color*. (**c**) Loading amount of growth factors (BMP-7, TGF-β2, and VEGF165) immobilized onto the PCL/F127/heparin scaffold sections. The scaffolds show the gradually decreasing concentration of growth factors along the longitudinal direction from the *bottom* position to the *top* position (growth factor concentration gradient scaffolds). (Reprinted from [195] with permission. Copyright 2011 Elsevier Ltd)

differentiation, and migration [201–203] to the physical and chemical cues, much less studies have been carried out to elucidate the cell migration patterns on gradient materials. According to the forms of gradients, there are in general two categories of gradients: (1) simple gradients with one dominating signal and one direction and (2) complicate gradients with several signals and/or several directions.

7.4.1 The Effect of Simple Gradients on Cell Migration

The simple gradients can be divided into two categories as well: (1) physical gradients with gradually changing physical properties including modulus and

topography and (2) chemical gradients with the spatially changing chemical compositions including the density and species of the functional molecules.

7.4.1.1 Physical Gradients

Matrix stiffness has been found to have a severe influence on cell adhesion and mobility. Nadia et al. found that cells attached to a rigid substrate exhibited better defined cytoskeleton and filament structure [132]. Pelham et al. confirmed that cells exhibited higher lamellipodia activity and motility on soft surface due to the destabilized adhesion [204]. Cheung et al. used microfluidic-based lithography to pattern cell-adhesive hydrogel substrates with microvariations in stiffness. The micropatterns are generated by feeding PEG-fibrinogen and various amounts of poly(ethylene glycol diacrylate) (PEGDA) into the microfluidic channel. Human foreskin fibroblasts respond to the patterned stiffness heterogeneity by migrating toward the stiffer regions along the discrete stiffness gradients [205]. Hopp et al. gradually immersed poly(allylamine hydrochloride)/poly(acrylic acid) (PAH/PAA) polyelectrolyte multilayers into 1-ethyl-3-(3-dimethylaminopropyl) carbodiimide (EDC) solution and obtained the gradient multilayers which had an elastic modulus ranging from 0.5 MPa at the noncrosslinked end to 110 MPa at the end of the substrate crosslinked for 4 h. Human dermal fibroblasts attach better to the stiffer regions of the gradient initially and subsequently a higher proliferation rate and stronger cytoskeletal development [206]. Thus, the stiffness gradient is expected to guide cell migration [192, 207]. Vascular smooth muscle cells were found to undergo direct migration on a radial gradient-compliant substrate from soft to stiff regions, leading to accumulation of cells in the stiff regions after 24 h. Hartman developed and characterized a polyacrylamide hydrogel culture platform featuring highly tunable gradients in mechanical stiffness. The results found that vascular smooth muscle cells durotaxis relied on the substrates coating proteins, e.g., extracellular matrix composition [208]. Cai et al. reported the strategy of bioinspired mechanotactic hybrids taking advantage of underlying 3D printed microstructures to remotely manipulate the apparent mechanical attributes of the planar surface of the superficial layer, to establish a mechanistic coupling of epithelial migration with ECM stiffness alone (Fig. 7.7). The results demonstrated that ECM stiffness alone played a key role in manipulating collective cell migration, which was important for studying diverse physiology processes including wound healing or cancer metastasis [209].

Keller et al. prepared photosensitive multilayers and then a continuous surface gradient of modulus by photocrosslinking. A7r5 smooth muscle cells exhibited the greater sensitivity to both shallow and steep modulus gradients by elongating and orienting along the shallow gradient and durotaxing up the steep gradient. U2OS osteoblast-like cells only spread and adhered well to the stiffer part of the gradient, but did not show obvious directional migration along the gradient [210]. Kuo et al. casted polyacrylamide gels on a stiff support with controlled topography, resulting in a thin gel layer of variable height. The topographical profiles projected a stiffness

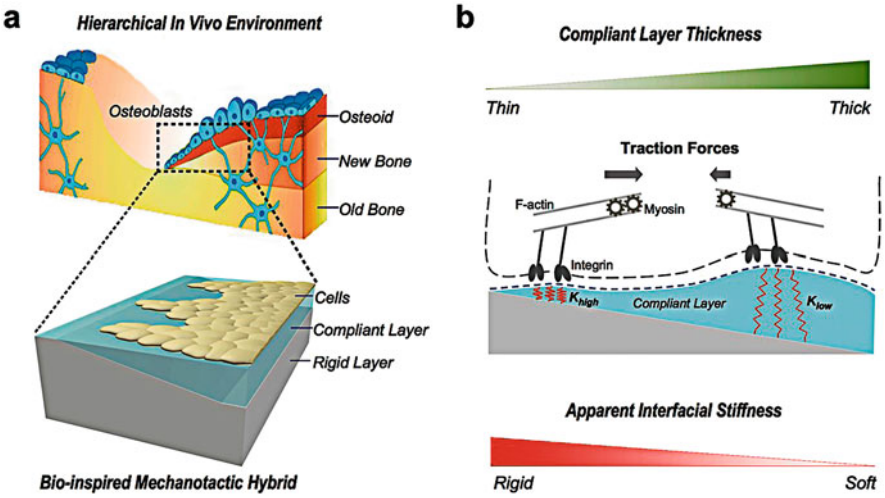

Fig. 7.7 Bioinspired mechanotactic hybrids based on cellular tactile mechanosensation. (**a**) Bioinspired mechanotactic hybrids (lower) comprising the microstructured rigid layer and superficial compliant layer are hypothesized to resemble a physiologically effective interface for modulating cell physiology, such as that of the bone remodeling process (upper). (**b**) Adherent cells translate the gradient thickness of the compliant layer into gradient apparent interfacial stiffness based on traction-mediated mechanosensing through actomyosin interaction via focal adhesions. The blue dashed line depicts the homogeneous topographical and compositional cues at the interface [209]. (Copyright 2016 WILEY-VCH Verlag GmbH)

map onto the gel, resulting in controlled linear and nonlinear 2D stiffness gradients. Fibroblasts, which migrate toward stiffer substrates, accumulated in areas with a gel thickness below 15 μm [211].

Lo et al. studied the mechanism of cell response [64, 212]. Focal adhesion kinase (FAK) plays an important role in mechanical stimulation. For an equal amount of energy, the counterforce provided by the soft substrate is smaller compared to the rigid one. The stronger feedback makes cell adhere stronger and spread better on the tough region. Thus, cells migrate directionally through dynamic detecting the imbalance in forces from the front to the back [70]. Besides, cell–cell interaction also plays an important role in cell migration. Han et al. posttreated the polyelectrolyte multilayers in a gradient NaCl solution with a concentration ranging from 3 to 5 M, yielding the gradient multilayers with a similar chemistry composition but gradually changing swelling ratio [181]. Compared to the random migration with a lower speed at a smaller cell density, the vascular smooth muscle cells migrated directionally to the low hydration side with higher modulus at an appropriate cell density ($\sim 1.5 \times 10^4/\text{cm}^2$) under the assistance of cell–cell interactions. The cell migration rates on the gradient surface were significantly larger than those on the corresponding uniform surfaces with the similar chemical structure and mechanical

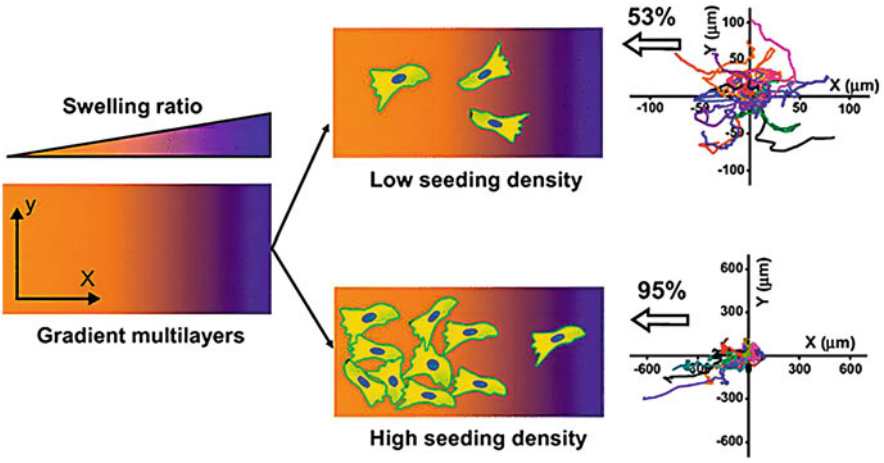

Fig. 7.8 Schematic illustration of cell migration on gradient PSS/PDADMAC PEMs with gradually changing swelling ratio at different cell density. (Reprinted with permission from [181] Copyright 2012, Elsevier Ltd)

property. Both the gradient cues and cell–cell interaction address important influences on the directional cell migration (Fig. 7.8).

Topography, the configuration of a surface, can largely affect the cell migration behaviors. Kim et al. created a model substrate of anisotropic micro- and nanotopographic pattern arrays with variable local density using UV-assisted capillary force lithography (CFL). They found that fibroblasts attached on the denser pattern areas aligned and elongated stronger along the direction of ridges, while those on the sparser areas showed a biphasic dependence of the migration speed on the pattern density. In addition, cells responded to local variations in topography by altering morphology and preferably migrating along the direction of grooves, i.e., direction of pattern and increasing pattern density [213, 214]. Mak et al. created microchannels with gradually narrowing spaces to study the metastasis process of cancer cells penetrating tight spaces within the ECM and during intravasation and extravasation through the vascular wall. The highly metastatic breast cancer cells (MDA-MB-231) showed a more invasive nature since 87% of the cells migrated into the spatially confining region. In contrast, most of the nonmetastatic breast epithelial cells (MCF-10A) (75%) were turning around by repolarization [215].

Han et al. prepared multilayers with gradually changing stiffness on air-plasma-treated poly(dimethylsiloxane) membranes, with the pattern direction parallel to the gradient. The synergetic effects of the surface topography and swelling gradient can effectively guide the unidirectional migration of single smooth muscle cells without impairment of their migration rate [216, 217].

Although durotaxis—cell migration toward increasing substrate stiffness—is well established, it remains unknown whether individual cells can migrate toward softer environments. Isomursu et al. used microfabricated stiffness gradients to

demonstrate the directed migration of U-251MG glioma cells toward less stiff regions. This "negative durotaxis" does not coincide with changes in canonical mechanosensitive signaling or actomyosin contractility. Instead, as predicted by the motor–clutch-based model, migration occurs toward areas of "optimal stiffness," where cells can generate maximal traction [218].

7.4.1.2 Chemical Gradients

Since gradients of extracellular matrix proteins, growth factors, and other signaling molecules have already been acknowledged in vivo, many chemical gradients are created and used to study their influences on cell migration behaviors in vitro. Gradients of synthetic polymers in terms of density, chain length, and chemical composition are constructed, in order to provide gradually alteration of hydrophilicity, charge, and eventually cell responses on different positions. Many gradients can efficiently regulate cell adhesion, elongation, and polarization; they are in general not effective enough to guide directional cell migration.

The gradients of biological molecules have a stronger influence on cell migration, depending on both the absolute concentration and the slope of the concentration gradient [219]. As there are two kinds of chemical gradients in vivo, i.e., one bound to ECM and the other soluble, the gradient materials are also divided into two categories:

Immobilized Gradients

The immobilized gradients can be further divided into three subcategories: synthetic molecules, ECM proteins (including related peptides), and growth factors. Zelzer et al. presented a new diffusion-controlled method to easily prepare chemical gradients by plasma polymerization. Surface chemical gradients from hydrophobic plasma-polymerized hexane to a more hydrophilic plasma-polymerized allylamine, with a water contact angle range of 60–93° over a length of 8 mm, were formed on glass coverslips. Fibroblasts adhered and proliferated preferentially on hydrophilic end, showing a gradual decrease of cell density toward the hydrophobic end [220]. Wu et al. prepared surfaces with various densities of methoxy poly(ethylene glycol) (mPEG) brushes to modulate the cell adhesion force: cell adhesion force gradually decreases on the surfaces with a higher mPEG density. The migration rate of vascular smooth muscle cells increased initially and then decreased along with the increase of mPEG grafting mass. The fastest rate appeared on the mPEG brushes with moderate grafting mass of 300–500 ng/cm^2 [29]. Ren et al. prepared hydrophilic poly(2-hydroxyethyl methacrylate) (PHEMA) brushes with a gradient increase of the molecular weight, which provided a precise control over the density of hydrophilic units along the gradient. The gradients were proved to provide a gradient of cell adhesion force, which in turn tuned the directional cell migration [221].

Collagen is one of the major proteins in ECM, which can significantly improve the cell adhesion and spreading. Fibronectin and laminin are able to mediate the communication and movement of cells. These proteins have certain structure domains which can bind to the corresponding receptors on cell plasma membrane. For example, both collagen and fibronectin contain the peptide sequence of RGD (Arg-Gly-Asp), which can bind to integrin subfamily, a kind of transmembrane receptors [222, 223]. The specific interaction between the integrin and the receptors conveys the external stimuli and transition into cells. Rajagopalan et al. studied the effect of Fn and RGD on spreading and motility of fibroblasts [224]. Although the migration speed is similar, fibroblasts on Fn-modified surface have higher traction force that is directly related to the size of focal adhesion, indicating that Fn has a higher affinity toward fibroblasts. Thus, ECM protein density gradients are supposed to carry the increasing strength of signal, making the cells polarized and subsequently directional migration. Smith et al. prepared fibronectin density gradients on gold surface to increase the migration speed of bovine aortic endothelial cells along the gradient direction [225]. The same group also reported that human microvascular endothelial cells (hMEC) migrated faster on a fibronectin gradient with a larger slope in the range of 0.34–1.23 ng Fn/mm^3 [103]. Gunawan et al. created linear density gradients of laminin by the microfluidic method. Rat IEC-6 intestinal crypt-like cells migrated up the gradients with similar rate compared to that on the same local laminin concentration on uniform surface. However, cell directedness decreased significantly at high laminin densities [14]. Cai et al. prepared a collagen gradient on PLLA surface. Endothelial cells on the gradient areas with low and moderate collagen surface densities displayed a strong motility tendency, whereas the cells grew on the gradient area with a high collagen density demonstrating a reverse response to the collagen gradient. The results suggest that cell motility is regulated by the collagen gradient in a surface-density-dependent manner [226]. Yu et al. prepared an amino group density gradient on poly(e-caprolactone) (PCL) membrane surface by a gradient aminolysis method, which was transferred into gelatin density gradient by covalent linking with glutaraldehyde. The resulted gelatin density gradient ranged from 0.49 to 1.57 μg/cm^2 on the PCL membrane. Human vein endothelial cells showed preferred orientation and directional migration toward the gradient direction with an enhanced gelatin density at the proper position (gelatin density), forwarding a new step toward the preparation of applicable gradient biomaterials in tissue regeneration [227].

Usually, a peptide with a functional amino acid sequence of specific proteins can be used as an alternative in gradient preparation because of its high stability and low molecular weight [228]. Adams et al. placed chick embryo dorsal root ganglia (DRG) in the middle of a grid pattern containing gradients of IKVAV peptide, the functional sequence in laminin. DRG growth cones followed a peptide path to the perpendicularly oriented gradients, and most of the growth cones could turn and climb up the gradients [229]. Delong et al. cultured human dermal fibroblasts on hydrogels with surface gradients of RGD peptide and found that the cells aligned with the gradients and tended to migrate up the gradients [10]. Guarnieri et al. also demonstrated that mouse fibroblasts prefer to migrate to the direction of an RGD

gradient on hydrogel surfaces with higher migration rate than that on uniform RGD surfaces and increased along with slope of the RGD density gradient [230]. Hirschfeld-Warneken et al. found that cells elongated along the ligand density gradient with a larger distance [102]. The migration speed of a single cell in response to a linear ligand density gradient on a solid substrate as a function of gradient slope was theoretically predicted based on a 1D continuum viscoelastic model. The model predicts a biphasic dependence of cell migration speed on gradient slope, with a maximum speed at an intermediate gradient slope [231].

Besides ECM proteins and their derived peptides, various growth factors are used to prepare gradients and study their effect on cell migration. DeLong et al. synthesized hydrogels with bFGF density gradients and observed that smooth muscle cells migrated directionally up the gradients toward increasing bFGF concentration [188]. Liu et al. found the density gradient of VEGF can induce the directional migration of endothelial cells. This guidance effect is further enhanced on the combinational gradients of VEGF and FN [232]. Masters et al. found that keratinocytes exhibited almost tenfold directional migration on an optimal concentration at EGF gradient compared to that on EGF free surfaces. Immobilization of IGF-1 (insulin-like growth factor 1) gradients also accelerated and directed keratinocytes migration; however, no difference in migration was found when combining EGF and IGF-1 gradients [233]. Schwarz et al. introduced an in vitro system allowing to track migratory responses of dendritic cells to precisely controlled immobilized gradients of CCL21, and the findings suggested that stable, tissue-bound CCL21 gradients as sustainable "roads" ensure optimal guidance in vivo [234].

Selective cell migration is required for many important physiological processes. For example, unnatural migration and proliferation of smooth muscle cells (SMCs) from media to the intima after the damage of endothelium eventually leads to atherosclerosis, the leading cause of death and disability. Thus, a Cys-Ala-Gly (CAG) peptide density gradient is generated on homogeneous cell-resisting poly (2-hydroxyethyl methacrylate-*co*-glycidyl methacrylate) brushes by immersing the brushes in a complementary gradient solution of CAG and competitive mercapto-terminated methoxyl poly(ethylene glycol) [235]. Furthermore, Yu et al. developed a universal modification method for biomaterials based on polydopamine and hyaluronic acid, and then REDV peptide was further added onto the MA-HA layer via a thiol-ene reaction in a gradient manner [236]. Selective endothelial cell adhesion and migration were found on the specific peptide gradient and even collective migration could be observed.

Gradients of Soluble Factors

Soluble factor concentration gradients which are commonly existed in natural 3D environment are also widely used to guide cell migration. For example, Frevert et al. developed a gradient of interleukin-8 (IL-8). Single neutrophils preferably migrated to the direction of higher concentration of IL-8 at the local concentration up to

200 ng/mL [237]. Besides, bFGF, stromal cell-derived factor-1 alpha (SDF-1α), EGF, and VEGF are also used as chemotactic agents [188, 238–240]. Wang et al. found that metastatic breast cancer cells could migrate up EGF gradient of nonlinear polynomial profile toward a higher EGF concentration [241]. However, there are some factors that can inhibit the cell mobility such as transforming growth factor β-1 (TGF β-1) [242] and angiotensin 1 [243].

7.4.2 The Effect of Complicate Gradients on Cell Migration

Besides the simple gradients with one dominating factor and/or one direction, there are always more complicate gradients exist in nature and generated on biomaterials. As expected, these gradients may have different impact on cell migration compared to their simpler counterparts. Study of the cell motility on a complicate gradient will provide insight into the complex physiological environment that guides and directs cell migration.

7.4.2.1 Gradients with Complicate Shape

Kidoaki et al. developed custom designed equipment for reduction projection-type photolithographic microelasticity patterning. By using the system, they prepared microelasticity-patterned gels with square hard domains within a softer surrounding gel. The jump in elasticity across the boundary was adjusted by regulating the photogelation conditions by varying the photoirradiation power and duration, and the boundary width was regulated by controlling the focus on reduction-projected images of photomasks (Fig. 7.9) [244]. The effects of the elasticity jump and boundary width were assessed systematically. As a result, the conditions required to induce mechanotaxis were found to be a jump in elasticity of a certain threshold magnitude (30–40 kPa) and a sufficiently narrow width of the elasticity boundary (50 μm), comparable to the adhesion area of a single cell. On the other hand, smaller boundary conditions of 3–20 kPa/50 μm did not induce mechanotaxis. Levchenko et al. presented a 2D topographically patterned substrate of variable local densities and anisotropy in a single substrate as a platform for studying the organization and migration of adherent cells. The patterns were fabricated by UV-assisted capillary force lithography, which provides a simple and efficient way to construct micropatterns with controlled geometry over a large area. They demonstrated that fibroblasts can recognize the topographic pattern density gradient, resulting in directional migration toward the denser area. The cell shape and velocity were largely dependent on the degree of the local anisotropy of the substrate, indicating that cells could integrate orthogonally directed mechanical cues on the scale comparable to that of the sizes of the native ECM networks [214]. The same group prepared a mountain-like fibronectin density gradient and found that Chinese

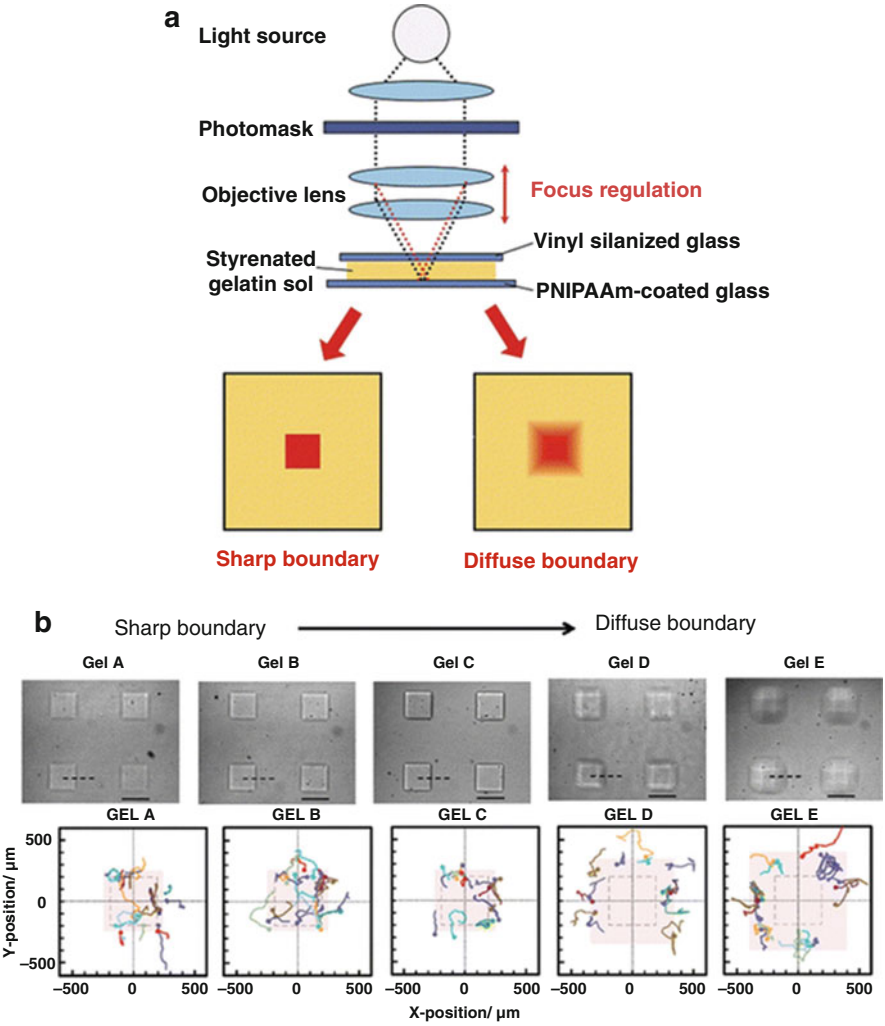

Fig. 7.9 (**a**) Schematic representation of the reduction projection-type photolithographic microelasticity patterning of styrenated gelatin gel. The resulting gel sample is attached to the *top* of vinyl-silanized glass, and photomask patterns are copied on the *bottom* of the gel surface covered with PNIPAAm-coated glass. The boundary conditions of the elasticity gradient can be controlled by raising the lens position and focusing out from the gel surface. (**b**) *Upper photos*: phase-contrast microscopic images of micropatterned *square* hard domains with elasticity gradients of different boundary conditions. *Lower graphs* show cell trajectories observed around elasticity boundaries with different gradient conditions. The starting positions of each trajectory are indicated by a dot. (Reprinted from [244] with permission. Copyright 2011 Elsevier Ltd)

hamster ovary (CHO) cells moved from both edges toward the center areas of the gradient with a higher fibronectin surface density [245].

7.4.2.2 Gradients with Complicate Signals

Several gradient signals with synergetic or opposite guidance on cell migration may merge together. Therefore, it would be interesting and also important to know how cell moves under such a complicate environment. Hale et al. designed a polyacrylamide hydrogel with a 100 μm interfacial region where the chemical and mechanical properties were gradually varied in opposing directions: the stiffer side has a low collagen concentration, whereas the softer side has a high collagen concentration. The mouse fibroblasts either migrated preferentially toward the high collagen density and soft side on the gradient or remained on the high collagen density region, suggesting that chemical gradient is more powerful than stiffness gradient in directing fibroblasts' movement [246]. Rao et al. studied cell movement in response to an epidermal growth factor (EGF) gradient in a gradually tapered space, imposing mechanical stresses. The chemoattractant drives cell migration into the narrow confines of the tapered channels, while the mechanical gradient clearly alters the migration of cells. PC-3 cells, a prostate cancer cell line, prefer to enter the channels from the wider to the narrow end. In contrast, PNT1A cells, a normal prostate epithelial cell, do not like to enter. The results indicate that the impact of physical stress on cell migration patterns may be cell type specific [247]. Mao et al. developed a special microfluidic device which has six channels, each with separate inlets for cell seeding and cytokine infusion. This device enables the competitive recruitment of cells that are simultaneously exposed to multiple cytokine gradients under real-time imaging, to identify the most chemotactic factors on bone marrow mesenchymal stem cells [248].

Wu et al. designed a PEG density gradient surface to drive the directional cell migration through the continuously increasing cell adhesion force along the reduced mPEG density axis, together with striped patterns at the same direction. The cells elongated along the direction of the stripes and the gradient and were separated by spacing stripes grafted with dense mPEG brushes. The cell orientation guided by striped patterns and polarization imitated by the chemical gradient have a synergetic effect on cell movement, leading to a more effective directional migration [249]. Ren et al. developed complementary density gradients consist of hydrophilic PHEMA brushes and cell anchoring peptides: both gradients provide the same direction guidance on cell migration, leading to fivefold increase of cell mobility and very high directionality [250]. Chiang developed a microfluidic cell culture device which was capable of reliably generating perpendicular chemical and oxygen gradients for cell migration studies [251]. Takahashi et al. demonstrated heterogeneous migration of the cells into the wound space in such a way that MDA-MB-231 cells preferentially migrated in the direction of higher pH/oxygen concentration [137].

7.4.3 *Cell Migration in 3D Matrix and Possible Application in Tissue Regeneration*

The cell migration behaviors as a function of gradients in 3D scaffolds and hydrogels have also been demonstrated. Dodla et al. cast dorsal root ganglia in agarose gels and prepared laminin gradient by photochemistry after diffusion. The presence of laminin gradients significantly enhanced the rate of neurite extension from the cells [252]. Moore et al. prepared PHEMA gels containing concentration gradients of NGF and neurotrophin 3 (NT-3), which were immobilized during photocrosslinking of the PHEMA [253]. Dorsal root ganglia cells only showed extended neurites along gradients of both factors rather than the ones with one factor alone, suggesting a synergistic effect. Musoke-Zawedde et al. used UV light micropatterning to fabricate RGD peptide density gradients in hyaluronan gels. The gradients were able to guide neurite outgrowth from primary neural cells [254].

Tampieri et al. [57] prepared ceramic scaffolds containing a gradient in porosity and applied them for rabbit femur defects repair. New bone formation was accelerated in the scaffolds at the region with higher porosity. Roy et al. [182] implanted polymer/ceramic composite scaffolds containing porosity gradient in rabbit calvarial defects. More new bone formation was observed in the high porosity zones than in the low porosity zones. Hoffman et al. [255] demonstrated that silk scaffolds containing pore size gradients have better performance to induce formation of a tissue with a graded morphology. Oh et al. studied the cell/tissue responses to the scaffolds with a pore size/porosity gradient in vitro and in vivo. The chondrocytes and osteoblasts prefer to migrate in large pore/high porosity part, while the fibroblasts prefer to proliferate in smaller pores/lower porosity part of the scaffolds in vitro. The best bone formation was found from midrange pore/porosity scaffolds after implantation into rabbit calvarial defects [184]. Based on electrospinning technique, Sundararaghavan et al. prepared gradients of increasing stiffness and RGD peptides' density along the thickness of fibrous HA scaffolds. The chick aortic arch explants had significantly greater cell infiltration into the scaffolds toward increasing RGD density gradient than that in the scaffolds with uniform RGD distribution [256].

7.5 Conclusions and Future Perspectives

Various top-down and bottom-up technologies have been developed to produce 2D and 3D gradient materials with gradually changing physical, chemical, and biological properties, mimicking the microenvironments in vivo and proving the possibility to guide cell directional migration in vitro. Complicate gradients consist of multiple signal gradients, and/or complicate gradient shapes have also been prepared to mimic the real environment in vivo. The majority of the current literatures are focused on single cell/cell sheet migration on planar gradient surfaces. It is of

importance to study the migration behaviors of cells encapsulated in 3D matrix, more closely mimicking the situation in vivo. The gradients in 3D scaffolds or gels are somewhat more complicate to fabricate and characterize. More importantly, measuring the migration of cells (usually a group of cells rather than single cell or cell sheet) encapsulated in 3D matrix is also more challenging.

Selective cell migration plays an essential role in many physiological processes. Undesired cell migration at the wrong time or place can lead to serious problems [19, 257]. For example, after nerve damage, Schwann cells (SCs), the principle glial cells that support the survival and function of neurons in the peripheral nervous system [258], are required to migrate out and form a tunnel which is able to lead damaged neuron to sprout and grow, thus guiding the regeneration of nerves [259]. However, fibroblasts in the connective tissue around usually have stronger mobility and form scar tissues by secreting collagen-based ECM after injury [260]. This will impede the migration of Schwann cells and thus regeneration of functional nerve tissue [261, 262]. Therefore, it is very important to design gradient biomaterials that are able to specifically guide the directional migration of cells required in tissue regeneration.

Last but not the least, material synthesis techniques should be sufficiently advanced to create physiologically relevant gradient materials to fit complex spatio-temporal phenomena such as tissue morphogenesis. Smart biomaterials incorporated with multiple gradient cues inside scaffolds, which mimic the timely cellular and structural characteristics of native tissues, could then be created for the regeneration of tissues having complex and multiple types of cells.

References

1. Godwin JW, Brockes JP. Regeneration, tissue injury and the immune response. J Anat. 2006;209(4):423–32.
2. Jagur-Grodzinski J. Polymers for tissue engineering, medical devices, and regenerative medicine. Concise general review of recent studies. Polym Adv Technol. 2006;17(6):395–418.
3. Redd MJ, et al. Imaging macrophage chemotaxis in vivo: studies of microtubule function in zebrafish wound inflammation. Cell Motil. 2006;63(7):415–22.
4. Cara DC, et al. Role of p38 mitogen-activated protein kinase in chemokine-induced emigration and chemotaxis in vivo. J Immunol. 2001;167(11):6552.
5. Cajal SR. La Rétine des Vertébrés. Cellule. 1892;9:119–257.
6. Roca-Cusachs P, et al. Mechanical guidance of cell migration: lessons from chemotaxis. Curr Opin Cell Biol. 2013;25(5):543–9.
7. Hartman CD, et al. Extracellular matrix type modulates cell migration on mechanical gradients. Exp Cell Res. 2017;359(2):361–6.
8. Keenan TM, Folch A. Biomolecular gradients in cell culture systems. Lab Chip. 2008;8(1):34–57.
9. Genzer J, Bhat RR. Surface-bound soft matter gradients. Langmuir. 2008;24(6):2294–317.
10. DeLong SA, et al. Covalent immobilization of RGDS on hydrogel surfaces to direct cell alignment and migration. J Control Release. 2005;109(1):139–48.
11. Chung S, et al. Microfluidic platforms for studies of angiogenesis, cell migration, and cell–cell interactions. Ann Biomed Eng. 2010;38(3):1164–77.

12. Mimura T, et al. A novel exogenous concentration-gradient collagen scaffold augments full-thickness articular cartilage repair. Osteoarthr Cartil. 2008;16(9):1083–91.
13. Singh M, et al. Strategies and applications for incorporating physical and chemical signal gradients in tissue engineering. Tissue Eng Part B Rev. 2008;14(4):341–66.
14. Gunawan RC, et al. Cell migration and polarity on microfabricated gradients of extracellular matrix proteins. Langmuir. 2006;22(9):4250–8.
15. Martin P. Wound healing—aiming for perfect skin regeneration. Science. 1997;276(5309): 75–81.
16. Bernstein LR, Liotta LA. Molecular mediators of interactions with extracellular matrix components in metastasis and angiogenesis. Curr Opin Oncol. 1994;6(1):106–13.
17. Barriga EH, et al. Tissue stiffening coordinates morphogenesis by triggering collective cell migration in vivo. Nature. 2018;554(7693):523–7.
18. Xu J, et al. NGF-p75 signaling coordinates skeletal cell migration during bone repair. Sci Adv. 2022;8(11):eabl5716.
19. Ceradini DJ, et al. Progenitor cell trafficking is regulated by hypoxic gradients through HIF-1 induction of SDF-1. Nat Med. 2004;10(8):858–64.
20. Tedgui A, Mallat Z. Cytokines in atherosclerosis: pathogenic and regulatory pathways. Physiol Rev. 2006;86(2):515–81.
21. Casscells W. Migration of smooth muscle and endothelial cells. Critical events in restenosis. Circulation. 1992;86(3):723–9.
22. Galis ZS, et al. Targeted disruption of the matrix metalloproteinase-9 gene impairs smooth muscle cell migration and geometrical arterial remodeling. Circ Res. 2002;91(9):852–9.
23. Ahmed F, et al. GFP expression in the mammary gland for imaging of mammary tumor cells in transgenic mice. Cancer Res. 2002;62(24):7166–9.
24. Ridley AJ, et al. Cell migration: integrating signals from front to back. Science. 2003;302 (5651):1704–9.
25. Friedl P, Weigelin B. Interstitial leukocyte migration and immune function. Nat Immunol. 2008;9(9):960–9.
26. Ananthakrishnan R, Ehrlicher A. The forces behind cell movement. Int J Biol Sci. 2007;3(5): 303–17.
27. Raftopoulou M, Hall A. Cell migration: Rho GTPases lead the way. Dev Biol. 2004;265(1): 23–32.
28. Mitchison TJ, Cramer LP. Actin-based cell motility and cell locomotion. Cell. 1996;84(3): 371–9.
29. Wu J, et al. Controlling the migration behaviors of vascular smooth muscle cells by methoxy poly(ethylene glycol) brushes of different molecular weight and density. Biomaterials. 2012;33(3):810–20.
30. Wehrle-Haller B, Imhof BA. Actin, microtubules and focal adhesion dynamics during cell migration. Int J Biochem Cell Biol. 2003;35(1):39–50.
31. Hall A. Rho GTPases and the control of cell behaviour. Biochem Soc Trans. 2005;33(5): 891–5.
32. Wong K, et al. Signal transduction in neuronal migration: roles of GTPase activating proteins and the small GTPase Cdc42 in the Slit-Robo pathway. Cell. 2001;107(2):209–21.
33. Manabe RI, et al. GIT1 functions in a motile, multi-molecular signaling complex that regulates protrusive activity and cell migration. J Cell Sci. 2002;115(7):1497–510.
34. Klemke RL, et al. Regulation of cell motility by mitogen-activated protein kinase. J Cell Biol. 1997;137(2):481–92.
35. Cheresh DA, et al. Regulation of cell contraction and membrane ruffling by distinct signals in migratory cells. J Cell Biol. 1999;146(5):1107–16.
36. Nguyen DHD, et al. Myosin light chain kinase functions downstream of Ras/ERK to promote migration of urokinase-type plasminogen activator-stimulated cells in an integrin-selective manner. J Cell Biol. 1999;146(1):149–64.

37. Obermeier A, et al. PAK promotes morphological changes by acting upstream of Rac. EMBO J. 1998;17(15):4328–39.
38. Halder G, et al. Transduction of mechanical and cytoskeletal cues by YAP and TAZ. Nat Rev Mol Cell Biol. 2012;13(9):591–600.
39. Dasgupta I, McCollum D. Control of cellular responses to mechanical cues through YAP/TAZ regulation. J Biol Chem. 2019;294(46):17693–706.
40. Rocha AS, et al. The angiocrine factor Rspondin3 is a key determinant of liver zonation. Cell Rep. 2015;13(9):1757–64.
41. Espina JA, et al. Durotaxis: the mechanical control of directed cell migration. FEBS J. 2022;289(10):2736–54.
42. Muinonen-Martin AJ, et al. Melanoma cells break down LPA to establish local gradients that drive chemotactic dispersal. PLoS Biol. 2014;12(10):e1001966.
43. Wright PD, et al. Terbinafine is a novel and selective activator of the two-pore domain potassium channel TASK3. Biochem Biophys Res Commun. 2017;493(1):444–50.
44. Shellard A, Mayor R. All roads lead to directional cell migration. Trends Cell Biol. 2020;30 (11):852–68.
45. Vaughan RB, Trinkaus JP. Movements of epithelial cell sheets in vitro. J Cell Sci. 1966;1(4): 407–13.
46. Friedl P, et al. Collective cell migration in morphogenesis and cancer. Int J Dev Biol. 2004;48 (5-6):441–9.
47. Friedl P. Prespecification and plasticity: shifting mechanisms of cell migration. Curr Opin Cell Biol. 2004;16(1):14–23.
48. Montell DJ. Morphogenetic cell movements: diversity from modular mechanical properties. Science. 2008;322(5907):1502–5.
49. Sunyer R, et al. Collective cell durotaxis emerges from long-range intercellular force transmission. Science. 2016;353(6304):1157–61.
50. Shellard A, Mayor R. Collective durotaxis along a self-generated stiffness gradient in vivo. Nature. 2021;600(7890):690–4.
51. Clark AG, et al. Self-generated gradients steer collective migration on viscoelastic collagen networks. Nat Mater. 2022;21(10):1200–10.
52. Carmona-Fontaine C, et al. Contact inhibition of locomotion in vivo controls neural crest directional migration. Nature. 2008;456(7224):957–61.
53. Friedl P, Wolf K. Proteolytic interstitial cell migration: a five-step process. Cancer Metastasis Rev. 2009;28(1):129–35.
54. Liu Y, et al. Rotational constraint contributes to collective cell durotaxis. Appl Phys Lett. 2020;117:213702.
55. Friedl P, Gilmour D. Collective cell migration in morphogenesis, regeneration and cancer. Nat Rev Mol Cell Biol. 2009;10(7):445–57.
56. Lin S, et al. Influence of physical properties of biomaterials on cellular behavior. Pharm Res. 2011;28(6):1422–30.
57. Tampieri A, et al. Porosity-graded hydroxyapatite ceramics to replace natural bone. Biomaterials. 2001;22(11):1365–70.
58. Karageorgiou V, Kaplan D. Porosity of 3D biomaterial scaffolds and osteogenesis. Biomaterials. 2005;26(27):5474–91.
59. Cullinane DM, Einhorn TA. Biomechanics of bone. Princ Bone Biol. 2002;1:17–32.
60. He J, et al. Microfiber-reinforced nanofibrous scaffolds with structural and material gradients to mimic ligament-to-bone interface. J Mater Chem B. 2017;5(43):8579–90.
61. Ho SP, et al. The tooth attachment mechanism defined by structure, chemical composition and mechanical properties of collagen fibers in the periodontium. Biomaterials. 2007;28(35): 5238–45.
62. Lange JR, Fabry B. Cell and tissue mechanics in cell migration. Exp Cell Res. 2013;319(16): 2418–23.

63. Silver JS, et al. Injury-mediated stiffening persistently activates muscle stem cells through YAP and TAZ mechanotransduction. Sci Adv. 2021;7(11):eabe4501.
64. Lo C-M, et al. Cell movement is guided by the rigidity of the substrate. Biophys J. 2000;79(1): 144–52.
65. Wang N, et al. Mechanotransduction across the cell surface and through the cytoskeleton. Science. 1993;260(5111):1124–7.
66. Choquet D, et al. Extracellular matrix rigidity causes strengthening of integrin–cytoskeleton linkages. Cell. 1997;88(1):39–48.
67. Sheetz MP, et al. Cell migration: regulation of force on extracellular-matrix-integrin complexes. Trends Cell Biol. 1998;8(2):51–4.
68. Sun Q, et al. How do the cells sense and respond to the microenvironment mechanics? Chin Sci Bull. 2020;65.
69. Saini K, Discher DE. Forced unfolding of proteins directs biochemical cascades. Biochemistry. 2019;58(49):4893–902.
70. Lee J, et al. Regulation of cell movement is mediated by stretch-activated calcium channels. Nature. 1999;400(6742):382–6.
71. Pelham RJ, Wang YL. High resolution detection of mechanical forces exerted by locomoting fibroblasts on the substrate. Mol Biol Cell. 1999;10(4):935–45.
72. Breckenridge MT, et al. Substrates with engineered step changes in rigidity induce traction force polarity and durotaxis. Cell Mol Bioeng. 2014;7(1):26–34.
73. Chaudhuri O, et al. Effects of extracellular matrix viscoelasticity on cellular behaviour. Nature. 2020;584(7822):535–46.
74. Lou J, et al. Stress relaxing hyaluronic acid-collagen hydrogels promote cell spreading, fiber remodeling, and focal adhesion formation in 3D cell culture. Biomaterials. 2018;154:213–22.
75. Myers DC, et al. BMP activity gradient regulates convergent extension during zebrafish gastrulation. Dev Biol. 2002;243(1):81–98.
76. Jones CM, Smith JC. Establishment of a BMP-4 morphogen gradient by long-range inhibition. Dev Biol. 1998;194(1):12–7.
77. Piccolo S, et al. The head inducer Cerberus is a multifunctional antagonist of Nodal, BMP and Wnt signals. Nature. 1999;397(6721):707–10.
78. Isbister CM, et al. Gradient steepness influences the pathfinding decisions of neuronal growth cones in vivo. J Neurosci. 2003;23(1):193.
79. Zhou S, et al. Nutrient gradients in engineered cartilage: metabolic kinetics measurement and mass transfer modeling. Biotechnol Bioeng. 2008;101(2):408–21.
80. Swartz MA, Fleury ME. Interstitial flow and its effects in soft tissues. Annu Rev Biomed Eng. 2007;9(1):229–56.
81. Lühmann T, Hall H. Cell guidance by 3D-gradients in hydrogel matrices: importance for biomedical applications. Materials. 2009;2(3):1058–83.
82. Kim BJ, Wu M. Microfluidics for mammalian cell chemotaxis. Ann Biomed Eng. 2012;40(6): 1316–27.
83. Roussos ET, et al. Chemotaxis in cancer. Nat Rev Cancer. 2011;11(8):573–87.
84. Herzmark P, et al. Bound attractant at the leading vs. the trailing edge determines chemotactic prowess. Proc Natl Acad Sci U S A. 2007;104(33):13349–54.
85. Servant G, et al. Polarization of chemoattractant receptor signaling during neutrophil chemotaxis. Science. 2000;287(5455):1037–40.
86. Haessler U, et al. Dendritic cell chemotaxis in 3D under defined chemokine gradients reveals differential response to ligands CCL21 and CCL19. Proc Natl Acad Sci U S A. 2011;108(14): 5614–9.
87. Carmeliet P, Jain RK. Angiogenesis in cancer and other diseases. Nature. 2000;407(6801): 249–57.
88. Choi NW, et al. Phosphorescent nanoparticles for quantitative measurements of oxygen profiles in vitro and in vivo. Biomaterials. 2012;33(9):2710–22.

89. Helmlinger G, et al. Interstitial pH and pO2 gradients in solid tumors in vivo: high-resolution measurements reveal a lack of correlation. Nat Med. 1997;3(2):177–82.
90. Verbridge SS, et al. Oxygen-controlled three-dimensional cultures to analyze tumor angiogenesis. Tissue Eng Part A. 2010;16(7):2133–41.
91. Paradise RK, et al. Directional cell migration in an extracellular pH gradient: a model study with an engineered cell line and primary microvascular endothelial cells. Exp Cell Res. 2013;319(4):487–97.
92. Schreml S, et al. Luminescent dual sensors reveal extracellular pH-gradients and hypoxia on chronic wounds that disrupt epidermal repair. Theranostics. 2014;4(7):721–35.
93. Khoshnevisan R, et al. nox1 regulates collective and planktonic cell migration: insights from patients with pediatric-onset IBD and NOX1 deficiency. Inflamm Bowel Dis. 2020;26(8): 1166–76.
94. Ruhrberg C, et al. Spatially restricted patterning cues provided by heparin-binding VEGF-A control blood vessel branching morphogenesis. Genes Dev. 2002;16(20):2684–98.
95. Hummitzsch L, et al. Hypoxia directed migration of human naïve monocytes is associated with an attenuation of cytokine release: indications for a key role of CCL26. J Transl Med. 2020;18 (1):404.
96. Ito Y, et al. The movement of a water droplet on a gradient surface prepared by photodegradation. Langmuir. 2007;23(4):1845–50.
97. Singer SJ, Kupfer A. The directed migration of eukaryotic cells. Annu Rev Cell Biol. 1986;2 (1):337–65.
98. Lauffenburger DA, Horwitz AF. Cell migration: a physically integrated molecular process. Cell. 1996;84(3):359–69.
99. Sullivan SJ, et al. Asymmetric distribution of the chemotactic peptide receptor on polymorphonuclear leukocytes. J Cell Biol. 1984;99(4):1461–7.
100. Chan EWL, Yousaf MN. A photo-electroactive surface strategy for immobilizing ligands in patterns and gradients for studies of cell polarization. Mol Biosyst. 2008;4(7):746–53.
101. Arnold M, et al. Induction of cell polarization and migration by a gradient of nanoscale variations in adhesive ligand spacing. Nano Lett. 2008;8(7):2063–9.
102. Hirschfeld-Warneken VC, et al. Cell adhesion and polarisation on molecularly defined spacing gradient surfaces of cyclic RGDfK peptide patches. Eur J Cell Biol. 2008;87(8):743–50.
103. Smith JT, et al. Directed cell migration on fibronectin gradients: Effect of gradient slope. Exp Cell Res. 2006;312(13):2424–32.
104. Tweedy L, Insall RH. Self-generated gradients yield exceptionally robust steering cues. Front Cell Dev Biol. 2020;8:00133.
105. Tweedy L, et al. Self-generated chemotactic gradients—cells steering themselves. Curr Opin Cell Biol. 2016;42:46–51.
106. Tweedy L, et al. Seeing around corners: cells solve mazes and respond at a distance using attractant breakdown. Science. 2020;369(6507):eaay9792.
107. Tu RS, Tirrell M. Bottom-up design of biomimetic assemblies. Adv Drug Deliv Rev. 2004;56 (11):1537–63.
108. Morgenthaler S, et al. Surface-chemical and -morphological gradients. Soft Matter. 2008;4(3): 419–34.
109. Wang L, et al. Tunable wettability and rewritable wettability gradient from superhydrophilicity to superhydrophobicity. Langmuir. 2010;26(14):12203–8.
110. Riepl M, et al. Molecular gradients: an efficient approach for optimizing the surface properties of biomaterials and biochips. Langmuir. 2005;21(3):1042–50.
111. Dertinger SKW, et al. Generation of gradients having complex shapes using microfluidic networks. Anal Chem. 2001;73(6):1240–6.
112. Kraus T, et al. Printing chemical gradients. Langmuir. 2005;21(17):7796–804.
113. Choi S-H, Zhang Newby BM. Micrometer-scaled gradient surfaces generated using contact printing of octadecyltrichlorosilane. Langmuir. 2003;19(18):7427–35.

114. Tomlinson MR, Genzer J. Formation of grafted macromolecular assemblies with a gradual variation of molecular weight on solid substrates. Macromolecules. 2003;36(10):3449–51.
115. Matyjaszewski K, et al. Polymers at interfaces: using atom transfer radical polymerization in the controlled growth of homopolymers and block copolymers from silicon surfaces in the absence of untethered sacrificial initiator. Macromolecules. 1999;32(26):8716–24.
116. Li L, et al. Fabrication of thermoresponsive polymer gradients for study of cell adhesion and detachment. Langmuir. 2008;24(23):13632–9.
117. Venkataraman NV, et al. Order and composition of methyl-carboxyl and methyl-hydroxyl surface-chemical gradients. Langmuir. 2006;22(9):4184–9.
118. Yu X, et al. Surface gradient material: from superhydrophobicity to superhydrophilicity. Langmuir. 2006;22(10):4483–6.
119. Morgenthaler S, et al. A simple, reproducible approach to the preparation of surface-chemical gradients. Langmuir. 2003;19(25):10459–62.
120. Huang J, et al. Gradient porous structure templated by breath figure method. Langmuir. 2021;37(19):6016–21.
121. Chaudhury MK, Whitesides GM. How to make water run uphill. Science. 1992;256(5063): 1539–41.
122. Zhao B. A combinatorial approach to study solvent-induced self-assembly of mixed poly (methyl methacrylate)/polystyrene brushes on planar silica substrates: effect of relative grafting density. Langmuir. 2004;20(26):11748–55.
123. Wu T, et al. Combinatorial study of the mushroom-to-brush crossover in surface anchored polyacrylamide. J Am Chem Soc. 2002;124(32):9394–5.
124. Genzer J, et al. Formation mechanisms and properties of semifluorinated molecular gradients on silica surfaces. Langmuir. 2006;22(20):8532–41.
125. Liedberg B, Tengvall P. Molecular gradients of omega-substituted alkanethiols on gold: preparation and characterization. Langmuir. 1995;11(10):3821–7.
126. Mougin K, et al. Construction of a Tethered poly(ethylene glycol) surface gradient for studies of cell adhesion kinetics. Langmuir. 2005;21(11):4809–12.
127. Karpiak JV, et al. Density gradient multilayer polymerization for creating complex tissue. Adv Mater. 2012;24(11):1466–70.
128. Claussen KU, et al. Learning from nature: synthesis and characterization of longitudinal polymer gradient materials inspired by mussel byssus threads. Macromol Rapid Commun. 2012;33(3):206–11.
129. Cai L, et al. Lubricated biodegradable polymer networks for regulating nerve cell behavior and fabricating nerve conduits with a compositional gradient. Biomacromolecules. 2012;13(2): 358–68.
130. Qiu J, et al. Biomimetic scaffolds with a mineral gradient and funnel-shaped channels for spatially controllable osteogenesis. Adv Healthc Mater. 2022;11(9):2100828.
131. Irimia D, et al. Universal microfluidic gradient generator. Anal Chem. 2006;78(10):3472–7.
132. Zaari N, et al. Photopolymerization in microfluidic gradient generators: microscale control of substrate compliance to manipulate cell response. Adv Mater. 2004;16(23-24):2133–7.
133. Kilb MF, et al. Immobilisation of CXCL8 gradients in microfluidic devices for migration experiments. Colloids Surf B Biointerfaces. 2021;198:111498.
134. Murugesan N, et al. Interplay of chemical and thermal gradient on bacterial migration in a diffusive microfluidic device. Biomicrofluidics. 2017;11(2):024108.
135. Chiu DT, et al. Patterned deposition of cells and proteins onto surfaces by using three-dimensional microfluidic systems. Proc Natl Acad Sci U S A. 2000;97(6):2408–13.
136. Wigenius JA, et al. Limits to nanopatterning of fluids on surfaces in soft lithography. Adv Funct Mater. 2008;18(17):2563–71.
137. Takahashi E, et al. A relatively small gradient of extracellular pH directs migration of MDA-MB-231 cells in vitro. Int J Mol Sci. 2020;21(7):2565.
138. Childs WR, Nuzzo RG. Decal transfer microlithography: a new soft-lithographic patterning method. J Am Chem Soc. 2002;124(45):13583–96.

139. Wang Z, et al. Metal transfer printing and its application in organic field-effect transistor fabrication. Adv Mater. 2003;15(12):1009–12.
140. Bhangale SM, et al. Biologically active protein gradients via microstamping. Adv Mater. 2005;17(7):809–13.
141. Jeon NL, et al. Structure and stability of patterned self-assembled films of octadecyltrichlorosilane formed by contact printing. Langmuir. 1997;13(13):3382–91.
142. Lang S, et al. Growth cone response to ephrin gradients produced by microfluidic networks. Anal Bioanal Chem. 2008;390(3):809–16.
143. Liu X, et al. Programming nanostructures of polymer brushes by dip-pen nanodisplacement lithography (DNL). Nanoscale. 2010;2(12):2614–8.
144. Zhou X, et al. Fabrication of arbitrary three-dimensional polymer structures by rational control of the spacing between nanobrushes. Angew Chem Int Ed. 2011;50(29):6506–10.
145. Xue P, et al. Graded protein/PEG nanopattern arrays: well-defined gradient biomaterials to induce basic cellular behaviors. ACS Appl Mater Interfaces. 2019;11(1):1595–603.
146. Zhang D, et al. Micropatterns and peptide gradient on the inner surface of a guidance conduit synergistically promotes nerve regeneration in vivo. Bioact Mater. 2022;9:134–46.
147. Zhang D, et al. Surface-anchored graphene oxide nanosheets on cell-scale micropatterned poly (d,l-lactide-co-caprolactone) conduits promote peripheral nerve regeneration. ACS Appl Mater Interfaces. 2020;12(7):7915–30.
148. Righetti PG, Bossi A. Isoelectric focusing in immobilized pH gradients: an update. J Chromatogr B Biomed. 1997;699(1):77–89.
149. Venkateswar RA, et al. An electrophoretic method for microstamping biomolecule gradients. Biomed Microdevices. 2000;2(4):255–64.
150. Plummer ST, et al. Electrochemically derived gradients of the extracellular matrix protein fibronectin on gold. Langmuir. 2003;19(18):7528–36.
151. Spijker HT, et al. Protein adsorption on gradient surfaces on polyethylene prepared in a shielded gas plasma. Colloids Surf B Biointerfaces. 1999;15(1):89–97.
152. Shin YN, et al. Adhesion comparison of human bone marrow stem cells on a gradient wettable surface prepared by corona treatment. Appl Surf Sci. 2008;255(2):293–6.
153. Blondiaux N, et al. Fabrication of multiscale surface-chemical gradients by means of photocatalytic lithography. Langmuir. 2007;23(7):3489–94.
154. Mangindaan D, et al. Experimental and numerical modeling of the controllable wettability gradient on poly(propylene) created by SF6 plasma. Plasma Processes Polym. 2010;7(9-10): 754–65.
155. Pitt WG. Fabrication of a continuous wettability gradient by radio frequency plasma discharge. J Colloid Interface Sci. 1989;133(1):223–7.
156. Gölander CG, Pitt WG. Characterization of hydrophobicity gradients prepared by means of radio frequency plasma discharge. Biomaterials. 1990;11(1):32–5.
157. Whittle JD, et al. A method for the deposition of controllable chemical gradients. Chem Commun. 2003;14:1766–7.
158. Sinha R, et al. A hybrid additive manufacturing platform to create bulk and surface composition gradients on scaffolds for tissue regeneration. Nat Commun. 2021;12(1):500.
159. Lee JH, et al. Interaction of different types of cells on polymer surfaces with wettability gradient. J Colloid Interface Sci. 1998;205(2):323–30.
160. Lee JH, et al. Platelet adhesion onto chargeable functional group gradient surfaces. J Biomed Mater Res. 1998;40(2):180–6.
161. Khang G, et al. The effect of fluid shear stress on endothelial cell adhesiveness to modified polyurethane surfaces. Polymers. 2000;8:179–85.
162. Kim MS, et al. Gradient polymer surfaces for biomedical applications. Prog Polym Sci. 2008;33(1):138–64.
163. Jin Ho L, Hai Bang L. A wettability gradient as a tool to study protein adsorption and cell adhesion on polymer surfaces. J Biomat Sci Polym Ed. 1993;4(5):467–81.

164. Kim MS, et al. First preparation of biotinylated gradient polyethylene surface to bind photoactive caged Streptavidin. Langmuir. 2005;21(9):4066–70.
165. Lee JH, et al. Preparation and characterization of functional group gradient surfaces. J Polym Sci Pt A Polym Chem. 1994;32(8):1569–79.
166. Gijsman P, et al. Comparison of the UV-degradation chemistry of polypropylene, polyethylene, polyamide 6 and polybutylene terephthalate. Polym Degrad Stab. 1999;65(3):433–41.
167. Li B, et al. A technique for preparing protein gradients on polymeric surfaces: effects on PC12 pheochromocytoma cells. Biomaterials. 2005;26(13):1487–95.
168. Li B, et al. Influence of carboxyl group density on neuron cell attachment and differentiation behavior: gradient-guided neurite outgrowth. Biomaterials. 2005;26(24):4956–63.
169. Ding Y-X, et al. Spatial variation of the charge and sulfur oxidation state in a surface gradient affects plasma protein adsorption. Langmuir. 2010;26(14):12140–6.
170. Ding A, et al. 4D biofabrication via instantly generated graded hydrogel scaffolds. Bioact Mater. 2022;7:324–32.
171. Hao H, et al. Rapid buildup arrays with orthogonal biochemistry gradients via light-induced Thiol–Ene "Click" chemistry for high-throughput screening of peptide combinations. ACS Appl Mater Interfaces. 2020;12(18):20243–52.
172. Zhu Y, et al. Immobilization of biomacromolecules onto aminolyzed poly(L-lactic acid) toward acceleration of endothelium regeneration. Tissue Eng. 2004;10(1-2):53–61.
173. Zhu Y, et al. Endothelium regeneration on luminal surface of polyurethane vascular scaffold modified with diamine and covalently grafted with gelatin. Biomaterials. 2004;25(3):423–30.
174. Zhu Y, et al. Endothelial cell functions in vitro cultured on poly(L-lactic acid) membranes modified with different methods. J Biomed Mater Res Pt A. 2004;69A(3):436–43.
175. Li CY, et al. PCL film surfaces conjugated with P(DMAEMA)/gelatin complexes for improving cell immobilization and gene transfection. Bioconjug Chem. 2011;22(9):1842–51.
176. Ueda-Yukoshi T, Matsuda T. Cellular responses on a wettability gradient surface with continuous variations in surface compositions of carbonate and hydroxyl groups. Langmuir. 1995;11(10):4135–40.
177. Tan H, et al. Microscale control over collagen gradient on poly(l-lactide) membrane surface for manipulating chondrocyte distribution. Colloids Surf B Biointerfaces. 2008;67(2):210–5.
178. Wu J, et al. Covalently immobilized gelatin gradients within three-dimensional porous scaffolds. Chin Sci Bull. 2009;54(18):3174–80.
179. Han L, et al. Modulating the structure and properties of poly(sodium 4-styrenesulfonate)/poly (diallyldimethylammonium chloride) multilayers with concentrated salt solutions. Langmuir. 2012;28(1):193–9.
180. Kunzler TP, et al. Systematic study of osteoblast and fibroblast response to roughness by means of surface-morphology gradients. Biomaterials. 2007;28(13):2175–82.
181. Han L, et al. Directional cell migration through cell–cell interaction on polyelectrolyte multilayers with swelling gradients. Biomaterials. 2013;34(4):975–84.
182. Roy TD, et al. Performance of degradable composite bone repair products made via three-dimensional fabrication techniques. J Biomed Mater Res Pt A. 2003;66A(2):283–91.
183. Woodfield TBF, et al. Polymer scaffolds fabricated with pore-size gradients as a model for studying the zonal organization within tissue-engineered cartilage constructs. Tissue Eng. 2005;11(9-10):1297–311.
184. Oh SH, et al. In vitro and in vivo characteristics of PCL scaffolds with pore size gradient fabricated by a centrifugation method. Biomaterials. 2007;28(9):1664–71.
185. Meredith J. Advances in combinatorial and high-throughput screening of biofunctional polymers for gene delivery, tissue engineering and anti-fouling coatings. J Mater Chem. 2009;19: 34–45.
186. Meredith JC, et al. Combinatorial characterization of cell interactions with polymer surfaces. J Biomed Mater Res Pt A. 2003;66A(3):483–90.
187. Sormana J-L, Meredith JC. High-throughput discovery of structure−mechanical property relationships for segmented poly(urethane−urea)s. Macromolecules. 2004;37(6):2186–95.

188. DeLong SA, et al. Covalently immobilized gradients of bFGF on hydrogel scaffolds for directed cell migration. Biomaterials. 2005;26(16):3227–34.
189. Kapur TA, Shoichet MS. Immobilized concentration gradients of nerve growth factor guide neurite outgrowth. J Biomed Mater Res Pt A. 2004;68A(2):235–43.
190. Xu Z, et al. Regeneration of cortical tissue from brain injury by implantation of defined molecular gradient of semaphorin 3A. Biomaterials. 2018;157:125–35.
191. Luo Y, Shoichet MS. A photolabile hydrogel for guided three-dimensional cell growth and migration. Nat Mater. 2004;3(4):249–53.
192. Wong JY, et al. Directed movement of vascular smooth muscle cells on gradient-compliant hydrogels. Langmuir. 2003;19(5):1908–13.
193. Hansen A, et al. Fabrication of arrays of polymer gradients using inkjet printing. Macromol Rapid Commun. 2012;33(13):1114–8.
194. Hubka KM, et al. Perlecan domain I gradients establish stable biomimetic heparin binding growth factor gradients for cell migration in hydrogels. Acta Biomater. 2019;97:385–98.
195. Oh SH, et al. Creating growth factor gradients in three dimensional porous matrix by centrifugation and surface immobilization. Biomaterials. 2011;32(32):8254–60.
196. Barry JJA, et al. Using a core–sheath distribution of surface chemistry through 3D tissue engineering scaffolds to control cell ingress. Adv Mater. 2006;18(11):1406–10.
197. Hsu R-S, et al. Adaptable microporous hydrogels of propagating NGF-gradient by injectable building blocks for accelerated axonal outgrowth. Adv Sci. 2019;6(16):1900520.
198. Li X, et al. Radially aligned electrospun fibers with continuous gradient of SDF1α for the guidance of neural stem cells. Small. 2016;12(36):5009–18.
199. Macner AM, et al. Condensation on surface energy gradient shifts drop size distribution toward small drops. Langmuir. 2014;30(7):1788–98.
200. Hernández SC, et al. Chemical gradients on graphene to drive droplet motion. ACS Nano. 2013;7(6):4746–55.
201. Maheshwari G, et al. Cell adhesion and motility depend on nanoscale RGD clustering. J Cell Sci. 2000;113(10):1677–86.
202. Bhat RR, et al. Tailoring cell adhesion using surface-grafted polymer gradient assemblies. Adv Mater. 2005;17(23):2802–7.
203. Borkenhagen M, et al. Three-dimensional extracellular matrix engineering in the nervous system. J Biomed Mater Res. 1998;40(3):392–400.
204. Pelham RJ, Wang YL. Cell locomotion and focal adhesions are regulated by substrate flexibility. Proc Natl Acad Sci U S A. 1997;94(25):13661–5.
205. Cheung YK, et al. Microscale control of stiffness in a cell-adhesive substrate using microfluidics-based lithography. Angew Chem Int Ed. 2009;48(39):7188–92.
206. Hopp I, et al. The influence of substrate stiffness gradients on primary human dermal fibroblasts. Biomaterials. 2013;34(21):5070–7.
207. Liang GB, et al. Dynamic changes in focal adhesion kinase during cell migration induced by bFGF and the significance. Sheng Li Xue Bao. 2004;56(4):509–14.
208. Hartman CD, et al. Vascular smooth muscle cell durotaxis depends on extracellular matrix composition. Proc Natl Acad Sci U S A. 2016;113(40):11190–5.
209. Cai P, et al. Bio-inspired mechanotactic hybrids for orchestrating traction-mediated epithelial migration. Adv Mater. 2016;28(16):3102–10.
210. Martinez JS, et al. Cell durotaxis on polyelectrolyte multilayers with photogenerated gradients of modulus. Biomacromolecules. 2013;14(5):1311–20.
211. Kuo C-HR, et al. Complex stiffness gradient substrates for studying mechanotactic cell migration. Adv Mater. 2012;24(45):6059–64.
212. Wang H-B, et al. Focal adhesion kinase is involved in mechanosensing during fibroblast migration. Proc Natl Acad Sci U S A. 2001;98(20):11295–300.
213. Kim D-H, et al. Mechanosensitivity of fibroblast cell shape and movement to anisotropic substratum topography gradients. Biomaterials. 2009;30(29):5433–44.

214. Kim D-H, et al. Guided cell migration on microtextured substrates with variable local density and anisotropy. Adv Funct Mater. 2009;19(10):1579–86.
215. Mak M, et al. Microfabricated physical spatial gradients for investigating cell migration and invasion dynamics. PLoS One. 2011;6(6):e20825.
216. Han L, et al. Unidirectional migration of single smooth muscle cells under the synergetic effects of gradient swelling cue and parallel groove patterns. Colloids Surf B Biointerfaces. 2013;111:1–6.
217. Han L, et al. Polyelectrolyte multilayer patterns created by capillary force and their impact on cell migration. Chin J Chem. 2014;32(1):66–72.
218. Isomursu A, et al. Directed cell migration towards softer environments. Nat Mater. 2022;21(9): 1081–90.
219. Peret BJ, Murphy WL. Controllable soluble protein concentration gradients in hydrogel networks. Adv Funct Mater. 2008;18(21):3410–7.
220. Zelzer M, et al. Investigation of cell–surface interactions using chemical gradients formed from plasma polymers. Biomaterials. 2008;29(2):172–84.
221. Ren T, et al. Directional migration of vascular smooth muscle cells guided by a molecule weight gradient of poly(2-hydroxyethyl methacrylate) brushes. Langmuir. 2013;29(21): 6386–95.
222. Zhu X, Evans JP. Analysis of the roles of RGD-binding integrins, α4/α9 integrins, α6 integrins, and CD9 in the interaction of the Fertilin β (ADAM2) disintegrin domain with the mouse egg membrane 1. Biol Reprod. 2002;66(4):1193–202.
223. Chan BMC, et al. In vitro and in vivo consequences of VLA-2 expression on rhabdomyosarcoma cells. Science. 1991;251(5001):1600–2.
224. Rajagopalan P, et al. Direct comparison of the spread area, contractility, and migration of balb/c 3T3 fibroblasts adhered to fibronectin- and RGD-modified substrata. Biophys J. 2004;87(4): 2818–27.
225. Smith JT, et al. Measurement of cell migration on surface-bound fibronectin gradients. Langmuir. 2004;20(19):8279–86.
226. Cai K, et al. Regulation of endothelial cells migration on poly(d, l-lactic acid) films immobilized with collagen gradients. Colloids Surf B Biointerfaces. 2010;79(1):291–7.
227. Yu S, et al. Preparation of gelatin density gradient on poly(ε-caprolactone) membrane and its influence on adhesion and migration of endothelial cells. J Colloid Interface Sci. 2015;451: 177–83.
228. Wu J, et al. Gradient biomaterials and their influences on cell migration. Interface Focus. 2012;2(3):337–55.
229. Adams DN, et al. Growth cones turn and migrate up an immobilized gradient of the laminin IKVAV peptide. J Neurobiol. 2005;62(1):134–47.
230. Guarnieri D, et al. Covalently immobilized RGD gradient on PEG hydrogel scaffold influences cell migration parameters. Acta Biomater. 2010;6(7):2532–9.
231. Sarvestani AS, Jabbari E. Analysis of cell locomotion on ligand gradient substrates. Biotechnol Bioeng. 2009;103(2):424–9.
232. Liu L, et al. Endothelial Cell migration on surface-density gradients of fibronectin, VEGF, or both proteins. Langmuir. 2007;23(22):11168–73.
233. Stefonek-Puccinelli TJ, Masters KS. Co-immobilization of gradient-patterned growth factors for directed cell migration. Ann Biomed Eng. 2008;36(12):2121–33.
234. Schwarz J, et al. Dendritic cells interpret haptotactic chemokine gradients in a manner governed by signal-to-noise ratio and dependent on GRK6. Curr Biol. 2017;27(9):1314–25.
235. Du W, Gao C. Selective adhesion and directional migration of endothelial cells guided by Cys-Ala-Gly peptide density gradient on antifouling polymer brushes. Macromol Biosci. 2019;19 (11):1900292.
236. Yu S, et al. Preparation of an Arg-Glu-Asp-Val peptide density gradient on hyaluronic acid-coated poly(ε-caprolactone) film and its influence on the selective adhesion and directional migration of endothelial cells. ACS Appl Mater Interfaces. 2016;8(43):29280–8.

237. Frevert CW, et al. Measurement of cell migration in response to an evolving radial chemokine gradient triggered by a microvalve. Lab Chip. 2006;6(7):849–56.
238. Bernal A, et al. L-selectin and SDF-1 enhance the migration of mouse and human cardiac mesoangioblasts. Cell Death Differ. 2012;19(2):345–55.
239. Cornejo M, et al. Effect of NRG1, GDNF, EGF and NGF in the migration of a Schwann cell precursor line. Neurochem Res. 2010;35(10):1643–51.
240. De Simone R, et al. NGF promotes microglial migration through the activation of its high affinity receptor: modulation by TGF-β. J Neuroimmunol. 2007;190(1):53–60.
241. Wang S-J, et al. Differential effects of EGF gradient profiles on MDA-MB-231 breast cancer cell chemotaxis. Exp Cell Res. 2004;300(1):180–9.
242. Sutton AB, et al. The response of endothelial cells to TGF beta-1 is dependent upon cell shape, proliferative state and the nature of the substratum. J Cell Sci. 1991;99(4):777–87.
243. Ennett AB, Mooney DJ. Tissue engineering strategies for in vivo neovascularisation. Expert Opin Biol Ther. 2002;2(8):805–18.
244. Kawano T, Kidoaki S. Elasticity boundary conditions required for cell mechanotaxis on microelastically-patterned gels. Biomaterials. 2011;32(11):2725–33.
245. Park J, et al. Simple haptotactic gradient generation within a triangular microfluidic channel. Lab Chip. 2010;10(16):2130–8.
246. Hale NA, et al. Cell migration at the interface of a dual chemical-mechanical gradient. ACS Appl Mater Interfaces. 2010;2(8):2317–24.
247. Rao SMN, et al. The migration of cancer cells in gradually varying chemical gradients and mechanical constraints. Micromachines. 2014;5(1):13–26.
248. Mendelson A, et al. Competitive stem cell recruitment by multiple cytotactic cues. Lab Chip. 2013;13(6):1156–64.
249. Wu J, et al. Directional migration of vascular smooth muscle cells guided by synergetic surface gradient and chemical pattern of poly(ethylene glycol) brushes. J Bioact Compat Polym. 2013;28(6):605–20.
250. Ren T, et al. Complementary density gradient of poly(hydroxyethyl methacrylate) and YIGSR selectively guides migration of endotheliocytes. Biomacromolecules. 2014;15(6):2256–64.
251. Chiang HJ, et al. Polydimethylsiloxane-polycarbonate microfluidic devices for cell migration studies under perpendicular chemical and oxygen gradients. J Vis Exp. 2017;(120):55292.
252. Dodla MC, Bellamkonda RV. Anisotropic scaffolds facilitate enhanced neurite extension in vitro. J Biomed Mater Res Pt A. 2006;78A(2):213–21.
253. Moore K, et al. Immobilized concentration gradients of neurotrophic factors guide neurite outgrowth of primary neurons in macroporous scaffolds. Tissue Eng. 2006;12(2):267–78.
254. Musoke-Zawedde P, Shoichet MS. Anisotropic three-dimensional peptide channels guide neurite outgrowth within a biodegradable hydrogel matrix. Biomed Mater. 2006;1(3):162.
255. Hofmann S, et al. Control of in vitro tissue-engineered bone-like structures using human mesenchymal stem cells and porous silk scaffolds. Biomaterials. 2007;28(6):1152–62.
256. Sundararaghavan HG, Burdick JA. Gradients with depth in electrospun fibrous scaffolds for directed cell behavior. Biomacromolecules. 2011;12(6):2344–50.
257. Kunkel EJ, Butcher EC. Chemokines and the tissue-specific migration of lymphocytes. Immunity. 2002;16(1):1–4.
258. Taniuchi M, et al. Induction of nerve growth factor receptor in Schwann cells after axotomy. Proc Natl Acad Sci U S A. 1986;83(11):4094–8.
259. Fields RD, Stevens-Graham B. New insights into neuron-glia communication. Science. 2002;298(5593):556–62.
260. Richard L, et al. Endoneurial fibroblast-like cells. J Neuropathol Exp Neurol. 2012;71(11):938–47.
261. Atkins S, et al. Scarring impedes regeneration at sites of peripheral nerve repair. Neuroreport. 2006;17(12):1245.
262. Dreesmann L, et al. Nerve fibroblast impact on Schwann cell behavior. Eur J Cell Biol. 2009;88(5):285–300.

Chapter 8
Stem Cell Differentiation Mediated by Biomaterials/Surfaces

Hongyan He and Changsheng Liu

Abstract Directing the differentiation of stem cells into a specific stromal lineage such as adipocyte, chondrocyte, fibroblast, myocyte, and osteoblast cell is a key and important step for medical uses. However, the uncontrolled and inefficient proliferative and differentiation behaviors of stem cells are still the significant challenges. Since the stem cell fate is strongly determined by the characteristics of the microenvironment in vitro, the biomaterials/surfaces constructs in two-dimensional or three-dimensional (3D) artificial structures could offer the several biological, mechanical, and chemical cues to modulate the cellular proliferation, and most importantly lineage particular differentiation. Besides these regulation cues, adding growth components existing in the ECM also holds the potential for guiding the stem cell fate in vitro. Therefore, this chapter aims to provide an update on the influencing cues that are being explored to govern stem cell fate, with a focus on the differentiation of bone marrow-derived mesenchymal stem cells (MSCs). The factors discussed here include topography, porosity and pore size, stiffness, hierarchy structure, chemical properties, and genetic factors.

Keywords Stem cells · Bone marrow-derived stem cells · Differentiation · Artificial extracellular matrix · Growth factors

8.1 Introduction

As one of the greatest discoveries in the biomedical field over the last century, stem cells have the remarkable potential to develop into different cell/tissue types in the body under the proper conditions during early life and growth [1, 2]. In addition, stem cells are capable of serving as a sort of internal regenerating/repair system in many tissues, dividing essentially without limit to replenish other cells as long as the

H. He · C. Liu (✉)
School of Material Science and Engineering, East China University of Science and Technology, Shanghai, P.R. China
e-mail: liucs@ecust.edu.cn

C. Gao (ed.), *Polymeric Biomaterials for Tissue Regeneration*,
https://doi.org/10.1007/978-981-99-6948-7_8

person or animal is still alive [3]. Because of these unique capabilities, stem cells have absorbed a great interest for regenerative medicine and tissue engineering [4, 5]. Typically, stem cells are divided into embryonic stem cells (ESCs) and adult stem cells (ASCs). ESCs are pluripotent stem cells derived from the inner cell mass of blastocysts, and able to differentiate to generate primitive ectoderm, which ultimately differentiates into all derivatives of the three primary germ layers: ectoderm, endoderm, and mesoderm [6, 7]. Meanwhile, ASCs are multipotent cells derived from adult somatic tissues with the potential to differentiate into many specific cell types [8]. In comparison with ASCs, ESCs can generate all cell types in the body and have long-term self-renewal capacity. In another words, ESCs are capable of propagating themselves indefinitely in an undifferentiated state under defined conditions, and generating almost all mature cell phenotypes [9], allowing ESCs as useful resources for basic research and clinical applications [7]. Recently, human ESCs have been produced and approved for use in a very small number of early clinical trials. However, ESC research still needs to face the challenges including ethical considerations, safety issue of ESCs, and a higher risk of tumorigenicity [10].

With the development of cell biology and biotechnologies, many researchers have tended to develop ASC-based therapies for regenerative medicine and tissue-engineered applications. Generally, ASCs can be isolated from several sources including body itself (i.e., brain, bone marrow, blood vessels, and other organs and tissues), amniotic fluid, pluripotent stem cells, and other ASCs [11]. Over the last decade, it has become essential to better understand how to direct the differentiation fates of stem cells into a specific stromal lineage. However, the uncontrolled and inefficient proliferative and differentiation behaviors of stem cells are still the significant challenges for medical uses. Since the stem cell fate is strongly determined by the characteristics of the microenvironment in vitro, the biomaterials/surfaces constructs in two-dimensional or three-dimensional (3D) artificial structures could offer the several biological, mechanical and chemical cues to modulate the cellular proliferation, and most importantly lineage particular differentiation. Besides these regulation cues, adding growth components existing in the ECM also holds the potential for guiding the stem cell fate in vitro. Therefore, this chapter aims to provide an update on the influencing cues that are being explored to govern stem cell fate, with a focus on the differentiation of bone marrow-derived mesenchymal stem cells (MSCs). The factors discussed here include topography, porosity and pore size, stiffness, hierarchy structure, chemical properties, and genetic factors. The emphasis of discussion will be placed on the influence of these factors to govern stem cell fate. This chapter aims to highlight the successful strategies and the mechanisms to control stem cells fate for regenerative medicine and tissue engineering.

8.2 Mesenchymal Stem Cells and Alternatives

Mesenchymal stem cell (MSCs), or marrow stromal cell, are the most popular types of ASCs for medical research and clinic uses. These types of stem cells are usually isolated from bone marrow, and also derived from nonmarrow tissues, such as placenta, umbilical cord blood, adipose tissue, adult muscle, corneal stroma, or the dental pulp of deciduous baby teeth [12, 13]. MSCs are multipotent stromal cells that can differentiate into a variety of cell types, including osteoblast, chondrocytes, myocytes, and adipocytes [8, 14]. Numerous studies have demonstrated that MSCs have great differentiation capacity and immunomodulatory functions [15]. For cell-based therapies, MSCs indeed display several advantages over embryonic or induced pluripotent stem cells: easier isolation via autologous ways, don't require rigorous conditions in vitro, a low risk of tumorigenicity [16]. Summing up the increasing research activities over the last decade, MSCs have the clinic perspectives to replace cell tissue that has been damaged or destroyed in treating cancers, neurological disorder, autoimmune disease, and orthopedic applications [17, 18].

8.3 Biomaterials as an Artificial Extracellular Matrix

8.3.1 Extracellular Matrix

The integration of material science and molecular cell biology has shed new light to the interaction and communications between cells and materials, from a more extensive and profound perspective [19–21]. Over the past decades, scientists have noticed the bidirectional relations between cells and materials. Cells can alter the physical or chemical properties of materials through secreting cytokines or other chemical cues. In addition aspect, surrounding materials (especially the surface of materials) can determine the temporal and spatial coordination of numerous cell fates by inducing a myriad of signals [19, 22]. Particularly, in the field of tissue engineering or regenerative medicine, it is of great interest to utilize the close interaction between cells and materials to design materials that may facilitate the ingrowth and differentiation of cells or induce morphogenesis in constructed tissues. Among all materials, extracellular matrix (ECM) can serve as the best candidate due to its high similarity to original organs or tissues, biocompatibility and bioactivities. The main advantage of ECM as a scaffolding material is its realization for so-called constructive remodeling, that is, it supports and encourages specific tissue formation at the implantation site rather than forming inferior and less functional scar tissue [23].

Naturally, extracellular matrix is a combination of macromolecules that are synthesized and secreted by cells. Such macromolecules are usually distributed on the surface of cells or around different cells, comprising a delicate and complicated network to support and connect the tissue structure and adjust the physiological behaviors among cells. Typically, extracellular matrix could be classified into three

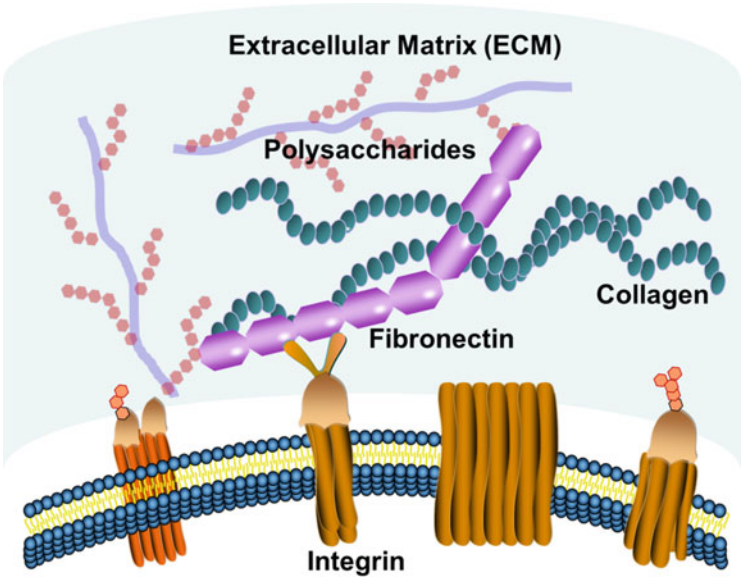

Fig. 8.1 Schematic structure of extracellular matrix

groups: glycosaminoglycans, structural proteins, and adhesives (shown in Fig. 8.1) [24]. Glycosaminoglycans or proteoglycan can form hydrogels, encapsulating various matrix components. Structural proteins, such as collagen and elastin, can ensure the strength and flexibility of ECM. Meanwhile, the adhesives including fibronectin and laminin can promote the adhesion of cells onto ECM.

ECM provides the foremost function as structural support to cells, it also bestows an optimized environment by providing sites for cell adhesion, creating soluble factor gradients and forming interfaces between different cell types within a tissue. Take an example, three-dimensional ECMs in tissue engineering are employed to construct new natural tissues from isolated cells (i.e., stem cells). The ECMs encapsulating stem cells can facilitate the inflow of nutrients, and ensure the mechanical stability of the local environment for the seeded cells to form specific gene expression [25].

Many researchers have revealed that tissue formation, function and regeneration depend on the interaction of numerous individual cell-fate processes, each of which is induced by an array of signals originating from the extracellular environment. Thus, the cell-fate processes would be directed or guided by controlling the ECMs surrounding each cells and comprising the molecular signals. The important components in ECMs include: (1) insoluble natural matrix molecule (collagen, laminin, elastin, or fibronectin), (2) soluble macromolecules (growth factors, chemokines, and cytokines), and (3) proteins on surfaces of neighboring cells (cadherins) [19]. The ultimate fate of a cell to proliferate, differentiate, migrate, apoptose, or perform other specific functions is a coordinated response to the molecular interactions with these ECM components. For stem cell, cell fate is influenced by such

coordinated interaction of soluble factors, extracellular matrix and signals from neighboring cells. Specific binding of signal molecules with cell–surface receptors induces complex intracellular signaling pathways with subsequent effect on gene expression, self-renewal, morphogenesis, and differentiation [25].

8.3.2 Natural ECM and Artificial ECM

According to the material sources, extracellular matrix could be classified into two categories: natural derived ones and synthetic ECMs [26]. Take a natural example, collagens are purified protein components separated from animal or human tissues. Such biologically derived materials can be desired carriers to embed cells, and then be grafted into tissue defects or induce regeneration and remodeling due to potential advantages of specific cell interactions. Since natural ECM-derived biomaterials are highly biocompatible, a number of them have been already approved by FDA for clinical applications. Apart from the compatibility, natural-derived ones still preserve inherent properties of biological recognition originated from the animal source, such as receptor-binding ligands and susceptibility to cell-triggered proteolytic degradation and remodeling. Those cell-recognizable receptors are able to improve integrin-dependent interaction, and some of them (i.e., carbohydrates) can act as the specific ligands to recognize the surface molecules of the cells (e.g., galactose, a specific ligand for asialoglycoprotein receptor on hepatocytes) [27]. However, there still exist limitations for natural ECM-derived materials. First, the quality of the natural products depends on the animal source and the manufacturing process. They might have instable properties and suffer from batch-to-batch variations. The quantities of the natural ECM materials are not enough to meet the application needs because of the complexities associated with purification. Secondly, the natural ECM-derived materials cannot meet the mechanical requirements for some specific clinical applications. Commonly, such materials show lower mechanical strength and are only suitable for soft-tissue repairing. Moreover, natural biomaterials might have potential risks in immunogenicity issues and pathogen transmission.

In order to solve these issues above, synthetic biomaterials are designed and prepared to meet the requirements chemically and biologically. The past few years have witnessed the rapid development of synthesized biomaterials as artificial extracellular matrix for biomedical applications and clinical use. Compared to naturally-derived ones, synthetic biomaterials can be manufactured reproducibly on a large scale and have great flexibility in tuning their microstructure, mechanical properties and physiological properties. However, synthetic materials show poor capability of cell recognition in general. Therefore, the biomaterials as artificial ECMs for engineering tissues have to follow several criterions. The materials should facilitate the localization and delivery of imbedded cells to the specific sites in the body, while maintaining the structural stability. Moreover, the material should possess molecular cues, mimicking different aspects of natural extracellular matrix and guiding the cell behaviors. To achieve these favorable effects, different

functional components should be introduced on/into the artificial ECMs. The most important components could be integrin-dependent ligands (i.e., collagen, laminin, or fibronectin), cell–cell adhesion molecules (i.e., cadherins or ICAM), binding sites for growth factor proteins (i.e., BMP-2, HGF, and VEGF) or small molecules (i.e., drugs or hormones), which allows the easy accessibility to cells and ligands for endocytosis.

Nowadays, a wide range of synthesized materials have been developed to mimic extracellular matrix with many functions including cellular 3D architecture, mechanical integrity to the new tissue, and the space for the diffusion of nutrients and metabolites. In general, such biomaterials could be divided into synthesized hydrogels, degradable polymers, or polypeptides and recombinant artificial ECM.

8.3.2.1 Synthesized Hydrogels

Typically, synthesized hydrogels have similar characteristics with natural ECM in biocompatibility and suitability for cells to survive. These useful materials have already gained much attention in the field of biological application and clinical use. The crosslinked and hydrophilic polymers with controllable microstructures can be beneficial for tissue-like viscoelasticity, oxygen transportation and nutrients flow. Rape et al. [28] have prepared light-modulated hyaluronic acid hydrogels that enables imposition of mutually independent and spatially continuous gradients of ligand density and substrate stiffness, which facilitated the MSCs for mechanosensitive differentiation. Another study from Yosi Navaro [29] reveals that modification of matrix stiffness will have great influence on the ability of cultured stem cells to proliferate, survive, and differentiate into mature cells.

In particular, when cells are encapsulated in three-dimensional hydrogels, the whole biomaterial is highly similar to extracellular matrix in our body. It has been reported that photopolymerizable polyethylene glycol (PEG) derivatives have been used as tissue engineering scaffolds for synthetic ECM analogs by Brenda K. Mann and his colleagues [30]. The materials highly resembled the natural ECMs and demonstrated the excellent performance for biocompatibility. However, most synthesized hydrogels lack essential biological cues to induce favorable cell behaviors and cannot be biodegradable. Therefore, a number of biological sites are incorporated in the hydrogels, such as cell adhesion ligands, proteolytic susceptible ligands, and growth factors. Meanwhile, proteolytically degradable peptides or enzymatic degradable groups are also introduced to improve the degradability. As reported by Elena Cambria, sortase-mediated ligation was used to conjugate human epidermal growth factor grafted to a GGG ligation motif (GGG-EGF) to PEG hydrogels containing the sortase LPRTG substrate, promoting biological activity [31]. It is noted that the cell-containing hydrogels must be prepared under mild conditions so as not to cause the loss in cell viability or subsequent cell behaviors such as cell adhesion, migration and differentiation.

8.3.2.2 Degradable Polymers

Degradable polymers are also widely used as artificial ECMs. Since the physical and chemical properties of biodegradable polymers can be easily turned by controlling the synthesized conditions, or choosing the functional monomers, the degradable polymers can be designed to match the requirements of many medical applications. Compared to other materials, degradable polymers can be easily modified on surfaces for further functionalization through grafting or anchoring.

Polyesters are one of the degradable polymers that are commonly employed as artificial ECMs, including polyglycolic acid (PGA), poly(L-lactic acid) (PLLA) and copolymers of poly(lactic-*co*-glycolic acid) (PLGA). All of these materials have already been approved by FDA for various biomedical applications and clinical use. The ester bonds in the polymers enable them to degrade through hydrolysis and the degradation rate could also be adjusted by changing the number of ester bonds during synthesis process. Meanwhile, polyesters have better mechanical strength than hydrogels or naturally-derived ECMs and thus can be applied in hard tissue repairing. For instance, nanofibrous PLLA scaffolds have been reported to show the similarity to the structure of natural collagen fibers and create a more favorable microenvironment for cells to survive [32]. Beside the advantages above, typical degradable polymers further need the introduction of biomedical cues stimulating or responding to the cells. Therefore, growth factors or bioactive domains have been incorporated in/onto polymers to endow the materials with ability to recapitulate natural ECMs. For instance, RGD peptides (three letters which stand for arginine, glycine and aspartic acid respectively), are widely employed in the modification of polymers to promote cell adhesion, since the surface density, spatial arrangement as well as integrin affinity and selectivity of RGD peptide influenced cells responses like adhesion and migration [33].

Amino-acid-based polymers are also degradable polymers employed as artificial extracellular matrix. With the development of the synthesized poly(amino-acid), such new biomaterials have been increasingly used for medical uses in recent years. Compared to other polymers that need further modification or functionalization for biomedical cues, amino-acid-based polymers naturally preserve the ability to build the interactions with cells. It is worth noting that certain manipulations on subsequent cell behaviors could be achieved by precisely determining the amino-acid orders and well-defined molecular architecture. For example, Girotti and coworkers incorporated elastin domains, lysines, and fibronectin CS5 domains containing well-known cell attachment sequence REDV into one single polymer, promoting cell proliferation activity, angiogenesis and other bioactivities of interest for tissue growing, repairing and healing [34]. Yihua Loo and his group reported a novel peptide bioinks for 3D printing in tissue repairing applications [35]. The artificial ECM contained lysine hexapeptides, which could self-assemble into stable, nanofibrous three-dimensional hydrogels with excellent stiffness of up to 40 kPa. These biocompatible scaffolds supported the three-dimensional culture of human

stem cells and differentiation of primary cells into organotypic (gastrointestinal and skin) structures.

8.3.2.3 Recombinant Artificial ECM

Hydrogels and degradable polymers have showed unique properties although some mechanical limitations. Most inorganic materials such as ceramics possess great mechanical property, but are limited in terms of fragility, poor degradability and lack of bioactive sites. Recently, recombinant artificial ECM materials have been developed to combine the advantages of degradable polymers, natural saccharides and even inorganic materials. For example, sericin-loaded electrospun nanofibrous composite scaffold composing cationic gelatin, hyaluronan and chondroitin sulfate and selected glycosaminoglycans (GAGs) were developed to mimic the extracellular microenvironment for dermal tissue applications [36]. Within the composite, the gelatin functioned as the structural support, hyaluronan, chondroitin sulfate and GAGs as naturally-derived ECM composites for cell adhesion and proliferation, while sericin served as promoter for subsequent differentiation of hMSCs. Moreover, it was revealed that the electrospun scaffold with multiple compositions could promote epithelial differentiation of hMSC in terms of several protein markers and gene expression of some dermal proteins.

With the deep understanding about the signals and the underlying pathways regulating stem cell fate, adult stem cells have been demonstrated the residence within specific extracellular regulatory microenvironments, consisting of a complex mixture of soluble and insoluble, short- and long-range ECM signals. These multiple, local environmental cues are integrated by cells that respond by choosing self-renewal or a pathway of differentiation. Synthesized artificial ECMs could facilitate the formation of damaged tissues, homeostasis and regeneration by offering suitable stem cell niches for stem cells to differentiate to favorable lineages. As we can see, great emphasis could be placed on the precise control of stem cell fate through the careful regulation of synthesized artificial ECM materials. The design of synthetic materials mimicking natural stem cell microenvironments may be a potentially powerful tool to understand and control stem cell function. A great number of artificial ECMs have been developed to explore the interaction between the materials and stem cell fate control. Synthetic extracellular matrix either made hyaluronic acid (HA) [37] and gelatin or HA hydrogels [38] showed the improved differentiation of MSCs and superior integration of the repair tissue. Kraehenbuehl's group also demonstrated that the synthetic three-dimensional ECM based on metalloproteinase-sensitive PEGs could direct differentiation of pluripotent cardioprogenitors [39].

With certain biological cues incorporated into the material, together with the stem cells, the artificial ECMs could mimic the natural ECM while possessing better performance in mechanical and degradable properties, reproducible large-scale production, and good processability. Therefore, great challenges still remain in the control over dynamics and spatial organization of presentation of multiple signals

due to the intricate and complicated structure of natural ECMs. As to the signals, the number of molecules that may have great impact on the cell behaviors is still underexploited. As for the materials, novel materials that have better spatial and hierarchical orders are still needed to upgrade the current materials. Hopefully, with the joint efforts from the scientists of different fields, new generation of artificial ECMs will soon appear and bring benefits to tissue engineering and regenerative medicine.

8.4 The Influence of Biomaterials/Surfaces on Stem Cell Differentiation

8.4.1 Surface Topography

Cell interactions with the surrounding extracellular matrix (ECM) play an important role in regulating cellular behaviors. It has widely appreciated that the properties of this cell–ECM interface—chief of all is surface topography—must mimic those of native ECM to appropriately guide cell function. Recent advances in biomaterial surface engineering have shown that surface biomechanical, spatial and topographical properties can elicit control over fundamental biological processes such as cell shape, proliferation [40, 41] and differentiation [42–44]. The modification of topology is critical in controlling cellular functions by designing surfaces as well as creating different topological cues to control cell adhesion and hence differentiation.

8.4.1.1 Surface Structure and Two-Dimensional Organization

Currently, several surface topographical cues in scaffolds with two-dimensional structure, such as surface roughness or various kinds of micro/nanoscale topographies of materials, have been shown in vitro or in vivo to guide marrow stem cell differentiation toward osteogenesis and sustain bone ingrowth. For example, Ana B. et al. [45] prepared surface roughness gradients of average roughness (Ra) varying from the submicron to the micrometer range (~0.5–4.7 μm), and mean distance between peaks (RS_m) gradually varying from ~214 μm to 33 μm. Their study demonstrated that optimal surface roughness (Ra ~2.1–3.1 μm/RS_m ~71.1–48.1 μm) promoting faster osteogenic commitment and strongest osteogenic expression. It has also been suggested from in vivo studies that controlling surface roughness is one of the most important parameters governing osteointegration [46]. In that regard, roughness topography may mimic the physical cues left by osteoclast activity on bone surface morphology during bone resorption [47]. Furthermore, the surface roughness increases the surface area of the implant material, allowing greater initial matrix deposition and earlier bone ingrowth [48].

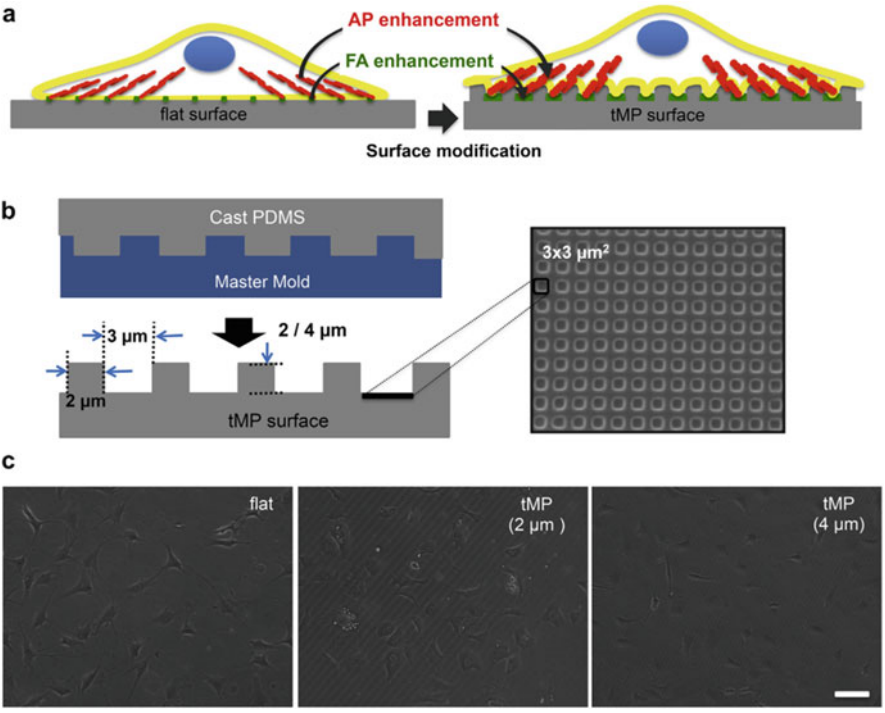

Fig. 8.2 (**a**) Schematic showing the strategy of the tMP bioactive surfaces which are intended to enhance focal adhesion (FA) and actin polymerization (AP) by the surface modification; (**b**) schematic showing preparation of the tMP surfaces which are intended to enhance FA and AP; (**c**) phase contrast images of cells cultured on the prepared substrates 24 h after seeding [50]. (Reprinted with permission from Elsevier Ltd. 2013)

Apart from surface roughness, there are a variety of micro- or submicrosurface topologies. Liu and his group [49] reported that biomaterial microtopography induced indirect mechanotransduction and thus osteoblast differentiation. As shown in Fig. 8.2, Chang Ho Seo et al. [50] upregulated the osteogenic differentiation of mMSC by culturing on the tailor-made micropit (tMP, 3×3 mm^2) surfaces that enhanced focal adhesion (FA) and (actin polymerization) AP of the cells. As shown in Fig. 8.2c, the cell on the flat surface was spread with broad lamellipodium and little traction force. On the contrary, the cell on the tMP surface significantly shrank and had a relatively strong traction force in the central direction which is important for signaling activation correlated with the cell differentiation. Wang et al. [51] investigated the effects of grooved topography on the differentiation of MSCs into osteoblasts, adipocytes and myoblasts regarding the late markers. In their study, a series of submicron-grooved surfaces with groove-to-ridge ratio of 1-to-1 (groove width/depth (nm): 450/100, 450/350, 900/100, and 900/550) was fabricated, the result of differentiation of MSCs into different lineages, especially osteogenesis is that the two deep grooved substrates (450/350 and 900/550) were increased to a level

compared to that on the flat surface, and significantly higher than those on the shallow surfaces (450/100 and 900/100).

These methods of controlling cell attachment, shape and then differentiation by surface topography have shown that MSCs have the remarkable ability to switch between becoming fat and bone cells based just on their ability to spread on a surface and contract against it. Well-spread cells express calcifying bone proteins common in osteoblasts in a manner that is dependent on the cell's ability to apply traction to the material. On the other hand, poorly-spread cells develop large lipid deposits typical of adipocytes and are limited in their spreading and tension generation. Besides traction force, another distinct impact of these micropit/micron-grooved substrates on cell behavior is formation of focal adhesions and F-actin. Several studies indicated that micropit or submicron-grooved substrates enhanced the formation of actin filaments and focal contacts compared with plain surfaces, and the enhancement was positively correlated with pit/groove depth [52]. It has been suggested that both the formation of focal adhesions and F-actin is correlated to the differentiation of MSCs [53–55].

8.4.1.2 Designing Surface Topology for the Third Dimension

Inspired by these previous investigations in two-dimensional biomaterials, surface topology in three-dimensional scaffold with hierarchical structures and its distribution should also have direct or indirect effects on osteoblast maturation as well as MSC osteogenic differentiation, presenting different effect from two-dimensional surface. Due to the restriction and difficulties of fabrication of surface topologies with uniform distribution and different morphology on the highly interconnected hole wall of the three-dimensional material, majority existing surface modification in metal or polymer materials stayed in two-dimensional level rather than in three-dimensional scaffold. Thus, subsequent smart designs should incorporate 3D structures, which more closely mimic native ECM and may guide cell shape and differentiation to improve the generative function of an engineered tissue.

To mimic the hierarchical porous architecture and specific biological cues of natural bone, Wei Tang et al. [56] developed a trimodal macro/micro/nanoporous scaffold (Fig. 8.3) with the mesoporous bioglass (MBG). Comparing with the BMS (2D MBG), the TMS (3D MBG) exhibited inspiring properties in terms of osteoconductivity, osteoinductivity, recombinant human bone morphogenetic protein-2 (rhBMP-2) delivery, and biodegradability.

Gwendolen et al. [57] analyzed the reason why stem cells are liable to differentiate on substrate in 3D microenvironment. The cell "feels" the structural properties of the biomaterial surrounding it depending strongly on biomaterial structure. As shown in Fig. 8.4, a microporous foam where the pore size greatly exceeds the cell, effectively presents a flat or slightly curved substrate to the cell as it adheres to a strut (Fig. 8.4a, top). By only attaching its basal surface to the material, mechanotransduction mechanisms of the cell may be similar to those already elucidated on planar substrates where large forces are observed on stiff strut

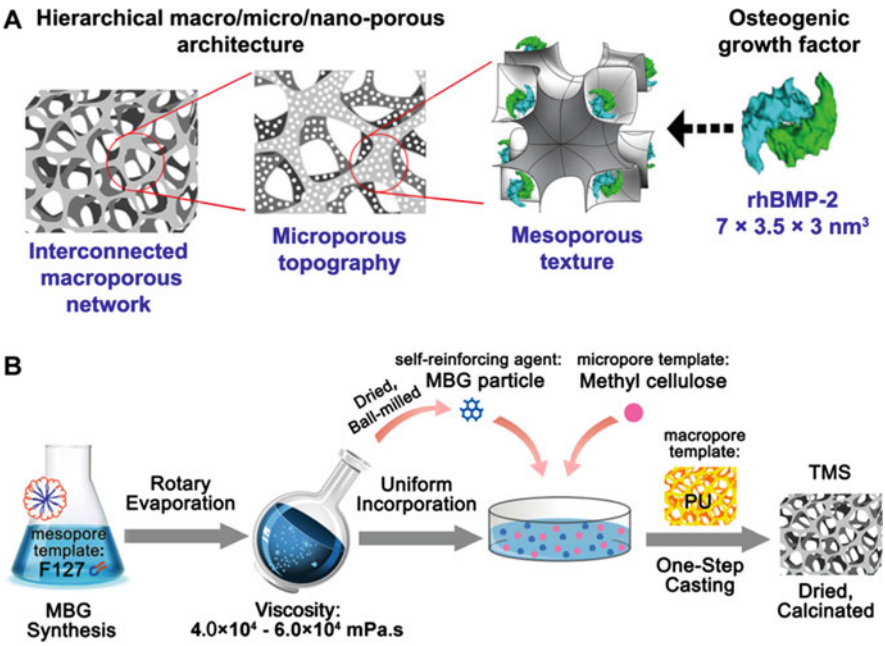

Fig. 8.3 (**a**) Design of trimodal macro/micro/nanoporous scaffold loaded with rhBMP-2; (**b**) Schematic illustration of preparing trimodal MBG scaffold (TMS) [56]. (Reprinted with permission from Elsevier Ltd. 2015)

materials (Fig. 8.4b, large arrows). Intriguingly, micropatterns that induce cell curvature on surfaces as well as micropores of varying size within a scaffold appear to directly regulate force production in stem cells, indicating that there may exist a gradual transition from a highly tensed, spread cell to a low tension, more rounded cell that contacts the material in all dimensions (Fig. 8.4a, b, bottom). If the pore size is too large the cell can only spread on a strut of the scaffold in a manner similar to planar materials, the cell's environment is then dominated by the scaffold's stiff mechanical properties and forces are large (big arrows). On the other hand, when porosity is small and the cell can attach in three dimensions, the force developed will be smaller (smaller arrows), more likely resulting in differentiation.

8.4.1.3 Regulation of Stem Cells by Surface Nanotopography

As discussed earlier, the microenvironment that cells contact with can be a potent regulator of adhesion and differentiation. In addition to macroscale surface topology all of the above, cells also have the ability to sense nanoscale geometric cues from their environment. Recent findings show that mammalian cells do respond to nanoscale features on synthetic surfaces [58, 59]. In the respect of stem cells adhesion, Yim et al. [60] demonstrated that nanotopography alone can upregulate

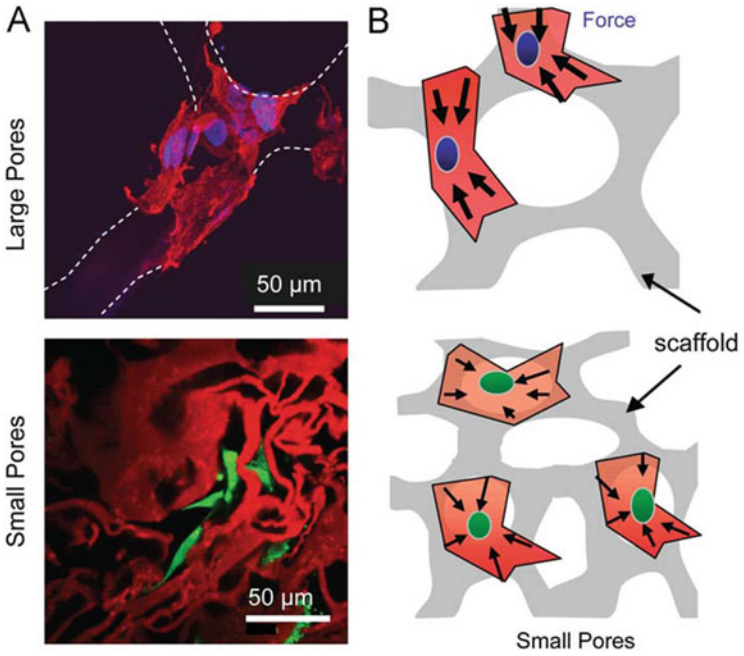

Fig. 8.4 3D Scaffold parameters influence stem cell contractility and differentiation [57]. (Reprinted with permission from Elsevier Ltd. 2009)

the neuronal markers of hMSCs. Another group has also demonstrated the important roles of topography in one-dimensional and three-dimensional cell migration [61]. Evelyn Yim et al. [53] designed a type of nanotopography as shown in Fig. 8.5 that modulated cell behavior by changing the integrin clustering and focal adhesion (FA) assembly, leading to changes in cytoskeletal organization and cell mechanical properties.

In terms of stem cells differentiation, one impressive report from Dalby et al. [62] demonstrates that the use of nanoscale disorder with a diameter of 120 nm are able to induce hMSCs to produce bone mineral and osteogenic differentiation in vitro, in the absence of osteogenic supplements. This approach of scaffold materials stimulating stem cell differentiation had similar efficiency to that of stem cells cultured with osteogenic media. Zhao et al. designed series of hierarchical micro/nanotextured topographies (MNTs) combined with micropitted and nanotubes topography (as shown in Fig. 8.6). They provided that the combined topography was more similar to the extracellular matrix (ECM) of natural bone and exhibited more pronounced effects on MSC osteogenic differentiation as well as osteoblast maturation [63, 64].

The micro- and nanoscale surface topographical modification is widely applied to enhance properties of biomaterials and regulate cell osteogenic differentiation. the underlying mechanism is also widely explored. Liu et al. [49] propose that the

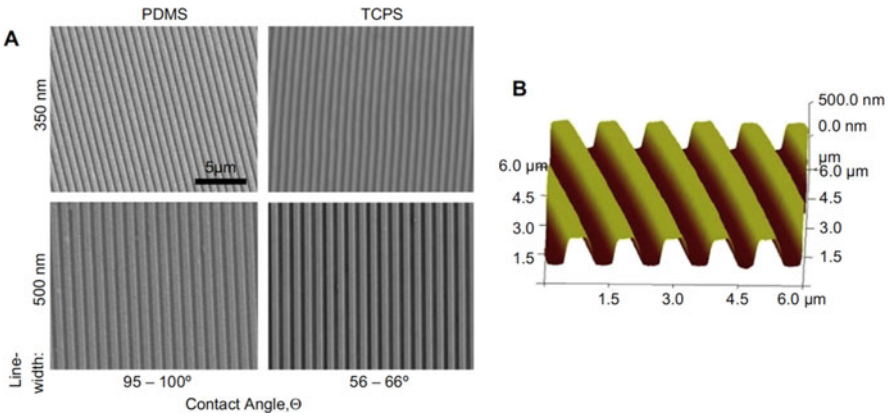

Fig. 8.5 (**a**) Scanning electron micrographs of gratings with 350 nm line width and 700 nm pitch (350 nm gratings), and 500 nm line width and 1 mm pitch (500 nm gratings); (**b**) Atomic force micrograph (AFM) of 350 nm gratings on TCPS [53]. (Reprinted with permission from Elsevier Ltd. 2009)

surface topography modulates cell differentiation via mechanotransduction of direct and indirect. As shown in Fig. 8.7, N-cadherin may be important in the process of topography inducing indirect mechanotransduction as well as regulating the β-catenin signaling. In Fig. 8.7a, the microtopography downregulates the N-cadherin expression leading to higher β-catenin signaling and consequently osteoblast differentiation, whereas the nanotopography significantly upregulates the N-cadherin expression resulting in reduced β-catenin signaling activity and thus depressed differentiation. As shown in Fig. 8.7b, N-cadherin can cut down the β-catenin at the cell–cell adhesion site and interact with the Wnt coreceptor LRP5/6. Inhibiting the Wnt/β-catenin signaling results in negative regulation of the β-catenin.

In this regard, the control of surface topography in engineered constructs has proven to be a valuable tool in guiding the commitment and development of stem cells. Importantly, the ability to modulating variety of surface topologies that, through physical as well as molecular interactions, enable undirected or directed control of stem cell behavior may further enhance our capabilities in engineering functional tissue substitutes. By controlling the nanotopography and microtopography of tissue engineering scaffolds in two/three dimension, we may further improve the regulation of stem cell fate in bioartificial systems. Such significant advances shown in these in vitro studies emphasize the importance of a multidisciplinary approach for the use of stem cells in the development of engineered tissue substitutes, and may lead to enhanced biomaterial clinical performance.

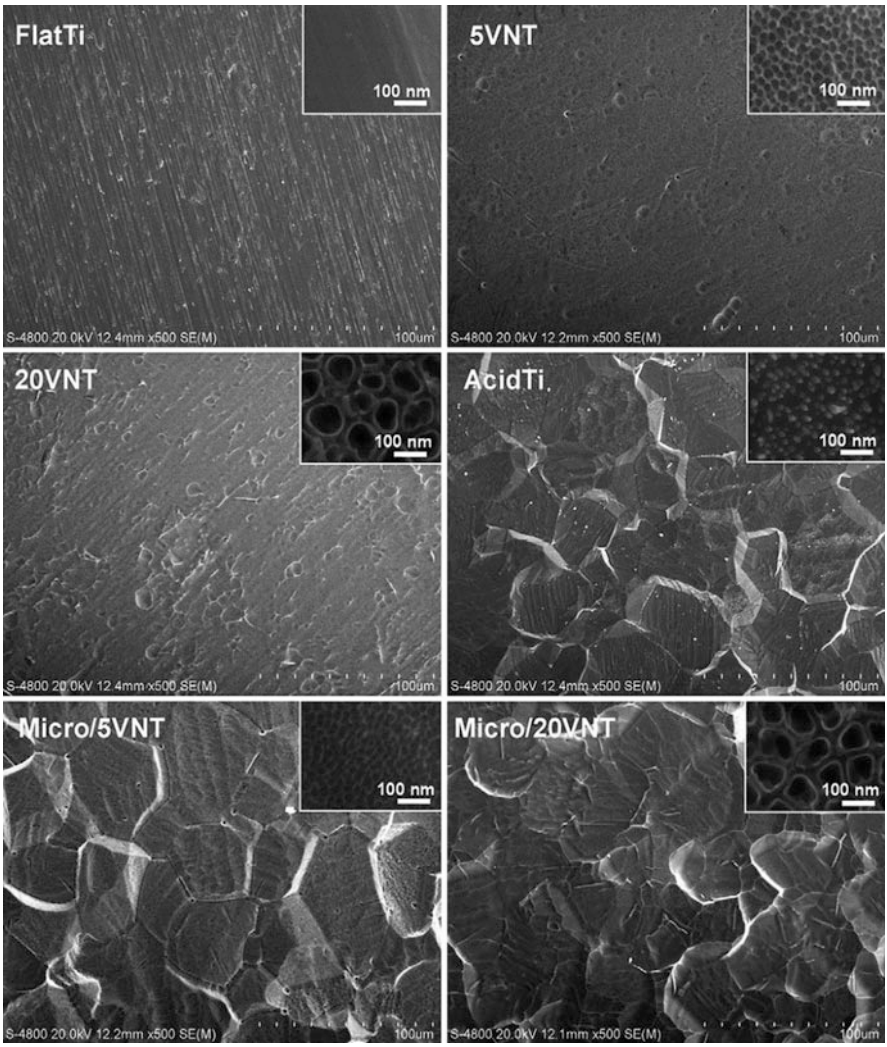

Fig. 8.6 SEM pictures showing the morphology of the fabricated samples [63]. (Reprinted with permission from Elsevier Ltd. 2014)

8.4.2 Porosity and Pore Size

Porosity is a parameter that refers to fraction of the gel volume filled with liquid phase, which is the volume of voids around matrix scaffold molecules per unit volume of the gel. Pore size is a very different parameter, which, unlike porosity, directly refers to geometry of pores. Cell adhesion and motility depend on size of the pores, rather than porosity. Mean pore size has correlation with porosity for many synthetic polymers of simple composition. However, for natural polymers like

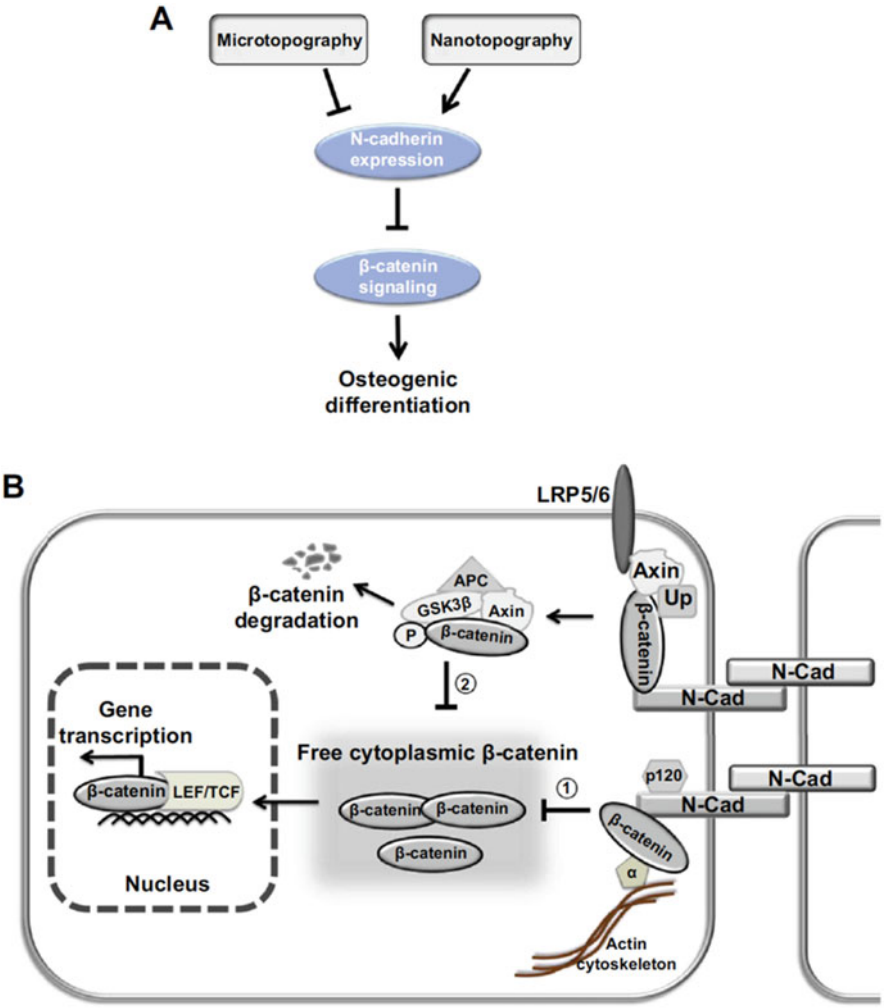

Fig. 8.7 Illustration of the detailed N-cadherin/b-catenin signaling in the micro/nanotopography-induced mechanotransduction [49]. (Reprinted with permission from Elsevier Ltd. 2011)

collagenous gels, there is no direct correlation, since the diameter of collagen fibrils can vary from few nanometers to a few hundred nanometers [65].

Porosities of scaffolds are the prerequisite for permeability in vitro and in vivo. Scaffolds matrix act mostly as media for fluid flow, diffusion, and cell migration [66]. Permeability of ECM defines accessibility of small molecules (nutrients, hormones, and oxygen), large molecules (e.g., that is function of basement membranes), cell processes (e.g., axons), or cells (vascularization). Permeability of ECM to cell migration is important for regenerative processes. Poor permeability for cells, such as in scarred tissues, results in poor regeneration. Therefore, permeability for

fluid flows and molecular diffusion is important for cell survival, since low permeability may result in lack of nutrients and ischemia.

Interconnected porous structures provide nutrients to the cells growing into the pores and allow for optimal interaction of the scaffold with cells. The aspects that are taken under consideration include pore size, size distribution, porous morphology, interconnectivity and surface area to volume ratio [67]. Each of these factors influences biological response, notably, cell migration, proliferation, and thus tissue regeneration. Substrate porosity seems to be an important factor as it can vary the length between two adjacent anchoring points, to which cell can adhere [68]. According to the IUPAC, the porous size of dense materials is classified in three different types: micropores (<2 nm), mesopores (2–50 nm), and macropores (>50 nm). Nevertheless, for tissue engineering, a slightly different description of the pore sizes is commonly applied. In the following part, we will adopt the nomenclature used by biomaterial scientists to describe the pore sizes of tissue engineering scaffolds, which classify pore sizes as: macropores (>50 μm), micropores (0.1–50 μm) and mesopores (2–50 nm). Therefore, we will distinguish these three different types of pores throughout this section and will not consider the pore ranges established by IUPAC.

8.4.2.1 Macropores

Scaffold macroporosity plays a critical role in the regeneration of damaged tissues, allowing cell penetration, which is essential for the later integration with the host tissue and increase the chances for key processes to take place, including tissue matrix and blood vessel ingrowth. It is generally acknowledged that the optimum pore size for scaffolds lies in the range between 100 and 400 μm [69]. Specifically, macropore size determines the efficiency at which cells seed into the scaffold. Small pores prevent the cells from penetrating the scaffold, while large pores prevent cell attachment due to a reduced area and, therefore, available ligand density [70]. The scaffold should have an adequate porosity in terms of the magnitude of the porosity, the pore size distribution, and its interconnectivity. This also will allow cell in-growth and vascularization and promote metabolite transport. A scaffold with an open and interconnected pore network and a high degree of porosity (>90%) is ideal for the scaffold to interact and integrate with the host tissue [71].

Macroporous scaffolds were observed to be potentially promising toward wound healing in relation to nonporous. Porous hydroxyapatite (HAp) scaffolds fabricated by additive manufacturing methods indicated significant bone formation when the pore diameter was in the range of ~400–1200 and ~300–800 μm [72]. As mentioned before, the extent of bone ingrowth was observed to depend on pore size. Pores of diameter ~20–50 μm are expected to provide favorable functionality from the viewpoint of physiological liquid exchange, while pores of diameter ~100–350 μm are suitable for cell colonization and vascularization, leading to penetration of tissue into the biomaterial structure [73]. This size range facilitated migration of cells in porous scaffolds and was appropriate for increased bone regeneration.

The degree of macropore interconnectivity is considered to be critically important in a manner similar to pore size. In biodegradable porous ceramics, the degree of interconnectivity was noted to be seemingly more important than the pore size, while in nonbiodegradable materials, interconnectivity and pore size were observed to be equally important. Under in vivo conditions, the penetration of cells and chondroid tissue formation inside macropores occurred when the interconnectivity dimensions were greater than ~20 μm, while mineralized bone formation occurred when the interconnectivity size exceeded 50 μm [74]. The interconnectivity of pores ensures availability of higher surface area for enhanced cell adhesion and proliferation.

The range of the optimum macropore size differs with different materials. For example, the effect of 3D silk fibroin scaffolds on cell proliferation and migration of human foreskin fibroblast showed that pore sizes of 200 to 250 μm and porosity of approximately 86% enabled better cell proliferation [75]. However, cell proliferation of these scaffolds with smaller pore sizes of 100 to 150 μm can be improved by having higher porosity of approximately 91%. Hence, by altering the pore size, porosity, or both parameters, the cell viability and proliferation can be enhanced [76]. Besides affecting the cell proliferation capability, it has been shown that the amount of ECM produced, that is, the amount of GAG secretion and the expression of collagen gene markers are also affected by the pore size of scaffolds [77]. The study by Lien et al. demonstrated that chondrocytes showed preferential proliferation and ECM production for scaffolds with pore sizes between 250 and 500 μm [78]. This pore size range was observed to be capable of maintaining the phenotype of cells, while pores ranging from 50 to 200 μm resulted in cell dedifferentiation [79]. Thus, the role of porosity and interconnectivity in scaffolds is also to facilitate cell migration within the porous structure such that cell growth is enabled while overcrowding is avoided.

Therefore, for bone tissue engineering, the optimal pore size for osteoblast activity in tissue engineered scaffolds is still controversial. In general, scaffolds with pore sizes of about 20 to 1500 μm have been used. Akay et al. studied the behavior of osteoblasts in PolyHIPE polymer (PHP), a type of highly porous polymeric foam [80]. The osteoblasts were shown to populate more in smaller pores (40 μm) when they were grown in scaffolds with different pore sizes, but larger pore sizes (100 μm) facilitated cell migration. However, the different pore sizes did not have any effect on extent of mineralization or cell penetration depth. Collagen–GAG (CG) scaffolds were also studied to determine its optimal pore size for bone tissue engineering purposes and the effect of pore size on a preosteoblastic cell line, MC3T3-E1 [81]. From the results, optimal cell proliferation and infiltration was found in CG scaffolds with mean pore sizes greater than 300 μm. In addition, the ability of larger pores to facilitate cell infiltration was shown to override the beneficial effect of greater initial cell attachment surface areas provided by smaller pores. Hence, this study supported previous reports that suggested the importance of having pore sizes greater than 300 μm for osteogenesis to occur. However, it should be noted that cell differentiation is also dependent on the cell type, scaffold material, and fabrication conditions.

The pore size has also been shown to have an effect on the proliferation and differentiation of cells for cartilage tissue engineering. Adipose stem cells were seeded on PCL scaffolds prepared with different pore sizes (100, 200 and 400 μm) and were placed under chondrogenic differentiation conditions for 21 days. The results showed that proliferation was higher for the 100 and 200 μm pore sizes, whereas cells tended to agglomerate in the 400 μm pore size scaffolds. Nevertheless, proteoglycan production as well as chondrogenic markers was significantly higher for the 400 μm pore size scaffolds compared to the 100 and 200 μm pore sizes [82]. Cell aggregation and cell–cell contact is known to be the most significant step for chondrogenic differentiation. Hence, the higher pore size allows the allocation of higher number of cells in the pores, which tend to agglomerate once they encounter other cells in the bigger pores showing higher markers of chondrogenesis. In the smaller pores, the number of cells is more limited and therefore preferentially attach to the substrates rather than surrounding cells since there is no proper space to accommodate more cells.

Another effective system to determine the optimum pore size is through the use of gradient scaffolds. In general, results show a cell-dependent behavior, presenting osteoblast and chondrocytes preferentially in the bigger pore sizes after 56 days, whereas fibroblasts are mainly present in the smaller ones [83]. Furthermore, adipose stem cells grown in the gradient pore size (90–400 μm) scaffolds were shown to have the highest chondrogenic differentiation but lowest proliferation in the biggest pore size (400 μm) [84]. This further confirms the previous hypothesis, showing that when cells encounter bigger pore sizes, enough number of cells can be allocated to allow the cell–cell contact and hence present higher markers of chondrogenic differentiation.

8.4.2.2 Micropores

While macropores with pore sizes and pore interconnections in the range of hundreds of microns are relevant for cells to migrate and proliferate, micropores with pore sizes in a smaller range also play pivotal roles in tissue engineering. These pores are usually few microns in size and are involved mainly on the initial adsorption of proteins on the surface of the materials. Cells interact with biomaterials through cell–protein interactions through the transmembrane proteins. Therefore, it is believed that the increase in protein concentration may significantly affect cell fate. Besides the ability to adsorb proteins, these small sized pores are also known to allow the regulation of cell behavior, playing key roles in directing stem cell fate.

The role of macroporosity has been mainly associated with the ability of a scaffold to allow proper bone ingrowth and bone regeneration, while having in general slight effects on cell proliferation and differentiation. Nevertheless, the porosity in the range of nanometers up to several microns has tremendous effects on the ability of cells to proliferate and differentiate and hence play a key role in the overall bone regeneration. Not only it is able to regulate the phenotype of cells to

induce higher cell mineralization, but also increase the protein adsorption, which in turn can increase the osteoinductive capacity of a material.

Microporosity can be incorporated into ceramic and polymeric scaffolds with different techniques. For example, a microporous foam material, wherein the pore size greatly exceeds the cell, displays a slightly curved substrate to the cell. As the basal surface of the cell attaches to the material, mechanotransduction mechanisms may be similar to those already elucidated on planar substrates. Microscopic pores of about cell size lead to a low tension, more grounded cell contacts with the material in all dimensions. There may exist a gradual transition from first variant to the last for intermediate pore sizes [85].

Surface microporosity of a material plays a very important role on cell behavior. The influence of pore sizes on cell behavior was determined by culturing MG-63 osteoblast-like cells on polycarbonate membranes designed with different pore sizes. Lee et al. [86] has reported that the cells spread and adhered better on membranes with smaller micropores (0.2 μm diameter) than on those with larger micropores (3.0–8.0 μm). Moreover, the cells cultured on larger micropores produced increased levels of ALP and osteocalcin. In another study, the different microporosity and topography of CDHA materials (total porosity of 35 vol.%, pores of 5 μm) was partially responsible for the different patterns of proliferation and differentiation observed for osteoblast cells [87]. Materials with smaller CDHA crystals stimulated differentiation, whereas those with bigger crystals enhanced proliferation.

Habibovic et al. performed an elegant experiment to determine the role of microporosity in two families of chemically identical porous ceramics: HAp and biphasic calcium phosphate (BCP) [88]. Sintering temperatures between 1100 and 1200 °C allowed modifying the microporosity (within a pore diameter range of 2 μm) while not altering their macroporosity (249 ± 38 μm). The results showed that the implantation into the back muscles of Dutch milk goats for 6 and 12 weeks allowed bone formation in the presence of micropores but failed when the amount of micropores remained low (HAp sintered at 1250 °C). The higher amount of adsorbed/entrapped proteins in the microporous walls enhanced bone formation [89], which was essential to provide the biomaterial with osteoinductive capacity. It is thus speculated that the microporosity modifies the dynamic interface of materials and consequently triggered the differentiation of relevant cells toward the osteogenic lineages. It has been pointed out that a higher microporosity was inherently linked with a higher specific surface area and hence could cause a major dissolution of ions [88]. The higher ion dissolution would facilitate the apatite formation in vivo, causing the coprecipitation of endogenous proteins (e.g., BMPs) that could in turn trigger the differentiation of recruited undifferentiated cells toward the osteogenic lineage [90]. Another hypothesis suggested that the inflammatory response triggered after the implantation of a biomaterial, which causes the release of cytokines that promote the differentiation of circulating MSCs into osteoblasts, would induce osteoinductivity [91]. In experiments by Peyton et al. [92], on MSCs motility in 3D PEG scaffolds, pore diameter has been varied from 7 to 17 μm (i.e., from significantly smaller than the spherical cell diameter to approximately cell diameter). Cell speed is the highest compared to

larger pores, but net displacement of the cells within matrix is maximal for intermediate pore sizes, probably because of difficulty in finding straight way in the large-pore scaffold.

Micropores also play a key role in controlling protein adsorption as well as cell–material interactions. Nevertheless, these pores may also be efficient systems for the loading and release of specific biological molecules with regenerative potential. These pores which are usually in the range of tens microns have been shown to be ideal for growth factor allocation that have enhanced bone regeneration [93]. These promotions in bone regeneration by micropores have been collectedly defined as an "initial micropore-acceleration" at the early stage of regeneration [56, 94]. Combining previous literatures with the results, Tang et al. speculated several possible reasons for this acceleration as follows. By providing a larger surface area, the microporosities could facilitate the coprecipitation of endogenous cytokines and growth factor, which indirectly stimulate stem cells recruitment to the defect site [95]. After then, surfaces with microporous topologies could significantly enhance biomineralization and were beneficial for protein adsorption and cell attachment. During cartilage formation, newly formed collagen fibers mineralized and wrapped in the micropores forming tight interlock between material and tissue, resulting in a bone/scaffold composite with no "dead space." Due to this "initial micropore-acceleration," the healing progresses of trimodal macro-/micro-/nanoporous and bimodal macro-/microporous scaffolds were in ahead of bimodal macro-/nanoporous scaffolds.

8.4.2.3 Mesopores/Nanopores

Mesoporous materials refer to as mesostructured materials or simply mesophases, and belong to the class of nanomaterials, whose properties can be tuned at the nanometrical scale. Specifically, according to IUPAC nomenclature, mesoporous materials refer to materials with pore sizes ranging within 2–50 nm. These materials are generally obtained by coupling a sol–gel method that is very effective to prepare glasses and ceramics at room temperature, with a supramolecular self-assembling process. This particular approach is possible by taking advantage of hydrophobic/hydrophilic features of some molecules (i.e., surfactants) to prepare supramolecular aggregates (micelle). The first successful synthesis of pure-silica mesostructured materials was performed in the early 1990s, when surfactants as structure-directing agents were used by Mobil Oil researchers [96]. Since then, many classes of mesoporous materials with different pore features have been synthesized.

With regard to the biomedical field, mesoporous materials, being characterized by an ordered texture of nano-sized pores, can easily host drug molecules and, therefore, are good candidates for designing and producing systems for controlled drug delivery. In addition, the silanol groups located on the walls of silica mesoporous materials may not only be useful to functionalize the walls for enhancing the drug adsorption ability of the materials, but can also react with biological fluids to produce HAp or apatite-like nanocrystals [97]. In vitro bioactivity studies, carried out by soaking SBA-15, MCM-41, and MCM-48 in SBF, revealed that an

apatite-like layer was formed on the surface of SBA-15 and MCM-48 materials after 30 and 60 days of immersion, respectively [98]. This behavior is quite surprising as these mesophases, being constituted by pure silica, should not exhibit bioactive properties. In fact, according to Hench's definition of bioactivity [99], bioactive mechanisms can occur only if particular ion-exchange phenomena take place between the material and surrounding fluids. On the other hand, it is obvious that mesoporous materials are nontraditional materials, and therefore, their mesoporous texture can impart them unexpected and fascinating properties. MCM-41 also exhibited a bioactive behavior when its walls were doped with phosphorus, or by adding small quantities of bioactive glasses.

MBG scaffolds exhibited greatly enhanced bone-forming properties, when compared with traditional bioactive glass (BG) scaffold of the same composition [100]. Besides its higher surface area and pore volume, the effects of mesopores reported by literatures are described. Drug release studies by using gentamicin have been reported [101]. The drug uptake ability of MBG scaffolds was over twofold higher than that of the BG scaffold; in addition, as far as drug delivery is concerned, during the whole release period in SBF, gentamicin was delivered from the MBG scaffold at a much lower release rate when compared with that from BG scaffolds.

Since entrapment in mesopores has turned out to be a promising strategy in the fields of enzymatic biocatalysis and biosensors etc., and some researchers have reported that the mesoporous support with comparable porous size to the protein molecule is beneficial for higher loading, preserved activity and sustained release. Motivated by these previous investigations, Tang et al. [56] proposed the concept of "size-matched mesoporous entrapment" for rhBMP-2 delivery and endeavored to investigate the possibility of matching the mesoporous dimension with the size of rhBMP-2 molecule ($7 \times 3.5 \times 3$ nm^3) to achieve a desirable immobilization, and further realize optimal bone regeneration by cooperation of multiscale structure and rhBMP-2.

Cells respond to their surrounding structure and with nanostructures exhibit unique proliferative and differentiation properties. Since the early 1970s, bioactive glasses are known to be able to chemically bond to living bone without the formation of fibrous tissue around the implant due to the growth of a bone-like apatite layer on its surface [102, 103]. It was demonstrated that HAp formation on the sol–gel glass surface is related both to the structure and to the composition of the material, whereas melt-derived bioactive glasses show a direct dependence only from the composition. An increase of the pore volume and specific area (up to 200 m^2/g) in sol–gel glasses highly accelerates the deposition of HAp, thus enhancing the bonding of the material to bone tissue [104]. Ordered mesoporous silica possess a very high surface area and an ordered system of generally open mesopores but are not properly suitable as filling materials for bone repair because of their almost complete lack of bioactivity [105]. Some authors reported a weak bioactive behavior of SBA-15 and MCM-48, but only after relevant times of contact with biological fluids (>30 days) [106]. On the contrary, MBGs belonging to the SiO_2-CaO-P_2O_5 ternary system were found to exhibit a faster and higher bioactivity also in comparison with sol–gel glasses, thanks to their textural and structural properties (specific surface area

up to 500 m^2/g) [107]. Therefore, considering their superior bioactivity, MBGs may be a very promising material for bone tissue regeneration and exhibit the potential of mediate the fate of stem cells by immobilization of growth factors and its inherent osteoinductive properties.

8.4.3 Surface Stiffness

Matrix stiffness is an important regulator of cellular responses (such as migration, proliferation and collagen deposition) mediating interface integration. As cells lay down extracellular matrix (mainly collagen) within a cell sheet or biomaterial sheet scaffold during in vitro culture or in vivo postimplantation, matrix density and stiffness increase. Increasing matrix stiffness would, in turn, be expected to affect the integration process by regulating critical cell behavior. It has been suggested that identification of variations in matrix stiffness could provide a useful tool for assessing interface integrity at step-off edges during cartilage repair [108].

Cell behavior and mechanical properties of the extracellular environment are intimately related. Cells can translate the stiffness of the microenvironments to which they are attached into biological signals (mechanotransduction) by a series of transmembrane receptors. These receptors comprise an intracellular domain (interacting with cytoplasmic proteins including the cytoskeleton) and an extracellular domain that specifically binds to adhesion partners. Tension forces expose active sites in these receptors with kinase activity, which allow the transformation of mechanical stimulation in chemical signals [109].

Matrix stiffness has been shown to play an important role in cell survival, proliferation and differentiation. For example, the stiffness of different matrices (0.1–1 kPa, 8–17 kPa, and 25–40 kPa) on which native mesenchymal stem cells were cultured was demonstrated to determine the lineage of the cells during differentiation (neurogenic, myogenic and osteogenic respectively) in vitro [110]. These experiments show that mechanical properties of the ECM induce not only cell spreading and changes in cell morphology, but also stimulate or repress the synthesis of specific transcription factors, inducing the establishment of special phenotypes concordant with the organ where the cells come from, or defining their fate in case of stem-cell differentiation.

Stiffness of the adjacent tissue affects stem cell fate in vivo when the cell exits its niche and starts to participate in regenerative process [111–113]. Stem cells tend to proliferate, migrate toward the injured site, and differentiate to the relevant cell type, adoptive to stiffness of the substrate. Stiffness of ECM has been shown to be crucial for maintenance of satellite stem cells in vivo [112]. Collagen VI has been proved to be the major regulator of stiffness in the stem cell niche in this case. For instance, experimental models that allow control over physical properties of ECM such as stiffness typically employ small adhesion molecules (i.e., short peptides) instead of natural full-size multidomain matrix molecules. Short peptides immobilized on abnormally stiff surfaces are also a standard approach to study effect of spatial

placement of epitopes. Biologically relevant full-size ECM adhesion molecules, such as niche-specific laminin isoforms, fibronectin, or vitronectin, are often immobilized on flat and abnormally stiff plastic or glass surfaces [85].

To date several hundreds of research papers are dedicated to dependence of stem cell fate on stiffness of their substrates in vitro. Similar results are obtained with different materials used as substrates: MSCs tend to differentiate to the cell type relevant to stiffness of the substrate as long as the other parameters (such as different substrate geometries or adhesion ligands) are not limiting for cell attachment and spreading [114]. These elastic materials include polyacrylamide gels, PEG hydrogels, and HA gels. MSCs are cultured on substrates of different stiffness in differentiation media specific for the particular cell lineage and expression of specific cell markers is monitored.

Briefly, the MSCs differentiate into neuronal or glial cells on the soft matrices that resemble soft brain tissue [115]. They differentiate into adipocytes on twofold stiffer substrates [116], into myoblasts on 10-fold stiffer substrates [117], and into osteocytes on harder matrices that mimic premineralized bone [118]. MSCs differentiation tendency with respect to substrate stiffness is summarized in Table 8.1.

MSCs have weaker cell adhesion to soft substrates, but anchor more strongly to stiff substrates. The level of adhesion strength correlates with commitment of the MSC to specific cell lineage. Suppression of adhesion strength for a cell on hard substrates imitates cell behavior on soft substrates in terms of the lineage marker expression. Alterations in the number, stability, and strength of the developing cell adhesions lead to reorganization of the cytoskeleton and change in cell morphology. On stiffer substrates stem cells tend to spread more and tend to assemble their cytoskeleton, such as build long actin-myosin stress fibers [43]. Majority of MSCs develop branched morphology with multiple filopodia on soft gels that mimic elasticity of brain (0.1–1 kPa) [119]. MSCs acquire rather spheroid shape on matrices resembling adipose tissue (4 kPa) [116]. Spindle-shaped cells appear on stiffer matrices that mimic elasticity of striated muscle (8–17 kPa). Spreading on even more stiff matrices (25–40 kPa) yields polygonal MSCs similar in morphology to osteoblasts.

Also stiffer hydrogels generally promote acceleration of stem cell proliferation compared to softer gels. It has been established for human bone marrow stem cells on polyvinyl alcohol gels of 1 kPa to 24 kPa stiffness [120] and for rat bone marrow stem cells on polyacrylamide (PAA) substrates of 6.1 kPa and 46.7 kPa [121]. The human MSC proliferation rate increases up to 10-fold with the increase of stiffness from 0.7 kPa to 80 kPa on the polyacrylamide (PAA) substrates [122]. The murine embryonic stem cells (ESC) proliferation accelerates as stiffness increases from 41 kPa to 2.3 MPa on the polydimethylsiloxane (PDMS) substrates [123].

Cells are not only sensitive to ECM adhesion but also to its rigidity and elasticity. It was observed that there is an inverse correlation between matrix density or rigidity and cell migration. Discher and collaborators demonstrated the importance of matrix elasticity on stem cell fate [124]. Depending on the elasticity of the surface on which the MSCs were grown, they could differentiate into lineages that corresponded to the stiffness of the native environment which was resembled. For example, MSCs

Table 8.1 Summary of MSC differentiation dependence on substrate stiffness [85] (open access)

Lineage	Matrix stiffness, *E*	Material	Testing method
Neurogenic	0.1–1 kPa	2D polyacrylamide gels, collagen coated	Nanoindentation using atomic force microscopy
	~1 kPa	2D polyvinyl alcohol hydrogel	Compression test
	1 kPa	3D type I collagen gel and hyaluronic acid gel	Compression test
	~1–2 kPa	2D gelatin-hydroxyphenylpropionic acid gel	Dynamic shear deformation 1%, 1 Hz using rheometer
	6.1 kPa	2D polyacrylamide gel (PAA)	Compression test
Gliogenic	10 kPa	3D type I collagen gel and hyaluronic acid gel	Compression test
Vascular endothelial cells	2–3 kPa	3D polyethylene glycol dimethacrylate (PEGdma) nanofiber hydrogel	Tensile test
Adipogenic	2.5–5 kPa	3D alginates-agarose hydrogel with RGD	Compression test
	4 kPa	2D polyacrylamide gel(PAA)	Nanoindentation using atomic force microscopy
	1.5 kPa, 6 kPa	2D polydimethylsiloxane (PDMS)	Tensile and macroscopic indentation tests
Myogenic	7–17 kPa	2D polyacrylamide gels(PAA), collagen coated	Nanoindentation using atomic force microscopy
	12–15 kPa	3D polyethylene glycol dimethacrylate (PEGdma) nanofiber hydrogel	Tensile test
	~30 kPa	2D gelatin-hydroxyphenylproplonic acid gel	Dynamic shear deformation 1%, 1 Hz using rheometer
	>9 kPa:25 kPa, 80 kPa	2D polyacrylamide gel, coated with collagen, fibronectin	Dynamic mechanical analysis
Cardiomyocytes	45 and 65 kPa	3D thermosensitive hydrogel (PAA and HEMA-PTMC)	Tensile test
Osteogenic	11–30 kPa	3D alginates-agarose hydrogel with RGD	Compression test
	15–100 kPa	2D polydimethylsiloxane (PDMS)	Tensile and macroscopic indentation tests
	24 kPa	2D polyvinyl alcohol hydrogel	Compression test
	25–40 kPa	2D polyacrylamide gels, collagen coated	Nanoindentation using atomic force microscopy
	30 kPa	2D polyacrylamide gel(PAA)	Nanoindentation using atomic force microscopy

(continued)

Table 8.1 (continued)

Lineage	Matrix stiffness, *E*	Material	Testing method
	42 kPa	2D polyacrylamide gel (PAA) collagen coated	Tensile test
	46.7 kPa	2D polyacrylamide gel (PAA)	Compression test
	~60 kPa	2D gelatin-hydroxy-phenylpropionic acid	Dynamic shear deformation 1%, 1 Hz using rheometer
	80 kPa	2D polyacrylamide gel coated with collagen, fibronectin	Dynamic mechanical analysis
	190 kPa ~3.1 MPa	2D polydimethylsiloxane (PDMS)	Nanoindentation

cultured on soft gels (0.1–1 kPa), to mimic brain elasticity, developed a neuronal morphology, with filopodia branching and spreading including expressing genes related to neuronal differentiation pattern. Furthermore, medium stiffness gels (8–17 kPa), which mimic striated muscle elasticity, promoted differentiation to myogenic cells, and the gels with the highest stiffness (25–40 kPa) to mimic bone elasticity, enhanced osteogenic differentiation.

A recent study based on an ECM composed of hyaluronan and fibronectin, found that adult human dermal fibroblasts migrate faster on softer substrates and demonstrate more dynamic lamellipodial activity [125]. Perhaps more significantly, in addition to having an effect on the speed of migration, substrate stiffness has also been implicated in controlling the direction of cell movement. A previous report suggested that cells migrate preferentially toward stiffer surfaces, a phenomenon termed durotaxis [126].

As matrix stiffness is proved to affect significantly formation of focal adhesions, it is crucial to investigate the epitope cluster effect with respect to substrate stiffness. Stem cells express specific integrins, which connect cytoskeleton to the ECM. The level of cell surface integrins appears to be significantly lower on soft substrates than that on stiff substrates [127]. Different types of integrins are responsible for adhesions at different stiffness levels. Thus, integrin α2 is upregulated in the course of osteogenic induction of MSCs on stiff matrices [128]. Integrin α5 is downregulated on soft gels, but its overexpression had no effect on cell spreading [129]. Activation of integrin α1 in bone marrow MSCs is induced by soft substrate to a significantly greater degree than by stiff substrate [127, 130]. α1-integrin signaling in the niche is involved in the maintenance of epidermal stem cells or neural stem/progenitors in a stem cell state. Proliferation of MSC is mediated by activation of integrin α1 and selectin. Later, we shall discuss in detail the biochemistry of integrin interaction with the specific matrix molecules.

Moreover, stiffer matrices made of the same material have lower pore size and permeability. Polymer substrates of the same stiffness but variable pore sizes can be produced [113]. It is important to note that solute permeability of the matrix is enhanced under dynamic deformations due to increased fluid flow

[131]. Permeability for the cells also is affected by substrate stiffness and viscoelasticity, because cells can deform actively more pliable matrices to move through. These aspects are still to be investigated.

8.4.4 Chemical Properties

Incorporation of well-defined chemical properties in/onto biomaterials/scaffold also enhances the adhesion and growth of stem cells, and then directs specific differentiation to induce certain biological functions. Briefly, the cell–biomaterial interaction is a very complex process which involves many cytokines and ECM proteins. The surface chemical characteristics of biomaterials/scaffold can affect the adsorption of such cytokines and ECM proteins, and this in turn influences the subsequent cellular response. Chemical properties of biomaterials, mainly including substrate elemental composition, surface functional groups, biochemical functionalization, have significant influences on regulating stem cell activities. In this section, we will provide an interpretation of how the above chemical cues can affect stem cell response and direct stem cells fate in vitro.

8.4.4.1 Physiological Processes of Cell–Material Interaction

Understanding the mechanism of the physiological processes that control cell–biomaterial interaction is fundamental to investigate the influence of chemical properties on stem cell adhesion and phenotype. As the first step, adhesion of stem cells onto the biomaterial matrix is essential for its viability, proliferation and differentiation. The adhesion of stem cells on biomaterials is primarily mediated by specific recognition and binding of cellular receptors on cell membrane to cytokines/ECM proteins adsorbed on the material surfaces. Among all the transmembrane receptors in stem cells, integrin, a widely expressed family of heterodimeric receptors [132], have turned out to exert principal role in anchoring cells to ECM. By binding to its extracellular ligand, an Arg-Gly-Asp (RGD) peptide found in several ECM proteins, integrins can activate the formation of the focal adhesion (FA) complex and cytoskeleton reorganization in stem cell [133, 134]. Through integrin-ECM protein mediated focal adhesions, stem cells are able to sense the underlying material substrate, and react to its chemical properties (Fig. 8.8). For example, focal adhesion kinase (FAK) and vinculin are major players in the focal adhesion processes activated by integrin-fibronectin (Fn) interactions [135–137]. In particular, vinculin transduces integrin-mediated intracellular signaling molecules that promote cell migration [133, 138].

Importantly, it was testified that the initial adhesion and morphology of stem cells at the material surface can influence the subsequent long-term function of stem cell lineage [139]. Cell–material and cell–cell interactions activate specific intracellular signal pathways that regulate stem cell fate. Thus, the enhancement in early cellular

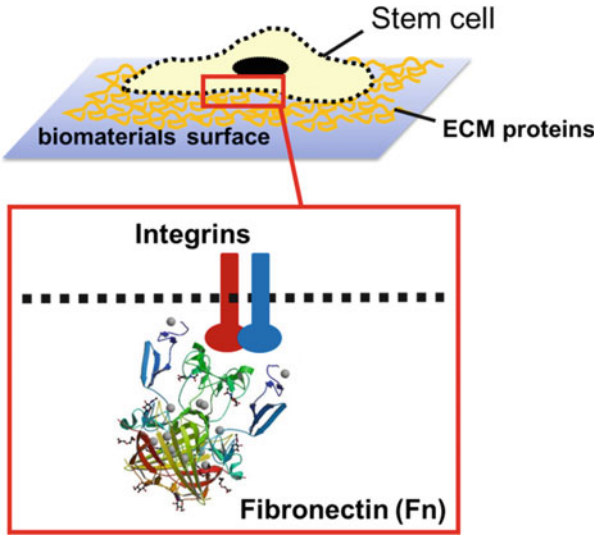

Fig. 8.8 Schematic illustration of the integrins' function in cell–material interaction

response including adhesion and cytoskeleton changes is prerequisite to stimulating subsequent stem cell differentiation, and ultimately, to achieving a specific cell phenotype and certain biological functions. Specifically, many reports demonstrated that the substrate-induced intracellular FA formation and actin polymerization could stimulate the osteogenic differentiation of MSCs [140–143]. In the following, we will mainly discuss the effects of biomaterial chemical properties on MSCs adhesion, viability and osteogenic differentiation.

8.4.4.2 Effects of Elemental Composition on Stem Cell Behaviors

The effects of chemical elemental characteristics on stem cell responses have been investigated extensively. It is noteworthy that some divalent ions have been found to participate in the bioprocess of cells adhesion [144]. Some functions of integrins are dependent on interaction with divalent cations such as calcium, magnesium, and manganese through a metal ion-dependent adhesion site (MIDAS) and MIDAS-like motives [144, 145]. Among divalent cations, magnesium increases the affinity of integrins for ligands including ECM in a millimolar concentration, and while calcium reverses the increased affinity in some cases [144, 146]. Magnesium is a vital and widely used component for the bone substitutes. Zhang et al. [147] systematically studied the effects of the magnesium in calcium phosphate cement (CPC) on the initial responses and the ultimate differentiation of MSCs, as well as the mechanism involved. The magnesium precursor (MPC) consisted of Ca $(H_2PO_4)_2 \cdot H_2O$ and MgO in a molar ratio of 1:2 was incorporated into CPC to obtain the MPC-modified CPC (MCPC). By regulating the weight percentage of MPC in the range from 0% to 20% in MCPC, MCPCs surfaces with different magnesium

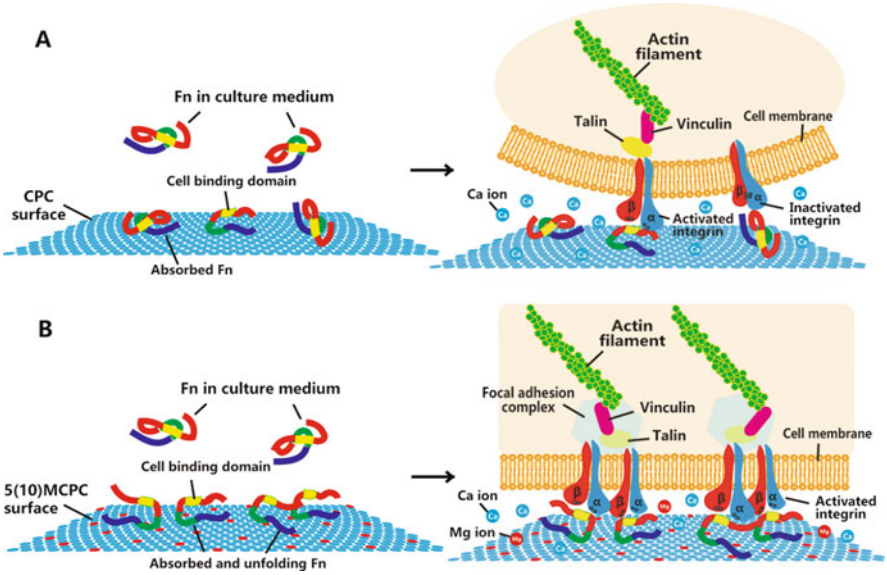

Fig. 8.9 Schematic diagram of the adsorption-induced changes in the structural orientation of the binding domain in Fn and the ensuing interaction between Fn and integrin α5β1 on (**a**) CPC and (**b**) 5(10) MCPC

density were obtained. The Fn adsorption and the availability of the cell-binding domains on the synthesized surfaces were determined by immunofluorescence staining and quartz crystal microbalance with dissipation (QCM-D) analysis. The attachment, morphology, focal adhesion formation, actin filaments assembly, and the expression of integrin subunits of MSCs on different cements were assayed. The results indicated that the incorporation of certain content of MPC into CPC could not only enhance the adhesion and spread but also promote the osteogenic differentiation of MSCs in vitro. And the desirable efficacy was achieved on the 5MCPC (with 5% MPC) with moderate proportion of Mg. As the schematic diagram (Fig. 8.9) shows, 5MCPC were believed to effectively modulate the orientation of the adsorbed Fn for enhanced cell binding affinity, and upregulate the integrin α5β1 expression of MSCs. Based on these results, it can be inferred that the Mg element concentration had predominant effect on the interaction of Fn and integrin α5β1, which mediated the MCPC-induced enhanced cellular response in MSCs.

Besides, some research has shown that the existence of silicon may stimulate the proliferation of MSCs and activate cells to produce transforming growth factors. For example, Ding et al. found that the Si/Ca ratio of calcium silicate cements could modulate attachment and proliferation of MSCs [148]. Calcium silicate cements with a higher Si content promoted cell attachment and triggered greater total integrin, pFAK and collagen type I expression compared to the cement with a higher Ca content. Integrin expression profiles changed accordingly, with higher levels of α2β1 and αvβ3 subintegrin in the cells on the Si-rich and Ca-rich cements, respectively,

which were ascribed to the collagen-binding and Fn-binding subintegrin on human primary cells, respectively. MAPK/ERK and MAPK/p38 signaling pathways were activated in MSCs cultured on these cement substrates, and their inhibition significantly attenuated cell adhesion, proliferation and differentiation as assessed according to total DNA and alkaline phosphatase (ALP) activity. Si component of calcium silicate materials can induce upregulation of MAPK/ERK and MAPK/p38 signaling pathway more effectively than Ca component.

8.4.4.3 Effects of Functional Groups on Stem Cell Behaviors

Many functional groups, for example, $–CH_3$, $–NH_2$, –SH, –OH, and –COOH, can influence the self-renewal and lineage commitment of MSCs directly or through interacting with specific ECM proteins. Using self-assembled monolayers (SAMs) of alkanethiols on gold as model surfaces, Keselowsky [137] et al. investigated the effects of surface chemistry on Fn adsorption, integrin binding, and cell adhesion. SAMs presenting terminal $–CH_3$, –OH, –COOH, and $–NH_2$ functionalities modulated adsorbed Fn conformation as determined through differences in the binding affinities of monoclonal antibodies raised against the central cell-binding domain ($–OH > –COOH = –NH_2 > –CH_3$). Binding of integrin α5β1 to adsorbed Fn was controlled by SAM surface chemistry in a manner consistent with antibody binding ($–OH > –COOH = –NH_2 > –CH_3$), whereas integrin αV binding followed the trend: –COOH much greater than $–OH = –NH_2 = –CH_3$, demonstrating integrin α5β1 specificity for Fn adsorbed onto the NH_2 and OH SAMs. Cell adhesion strength to Fn-coated SAMs correlated with integrin α5β1 binding ($–OH > –COOH = –NH_2 > –CH_3$), and experiments with function-perturbing antibodies demonstrated that this receptor provides the dominant adhesion mechanism.

Curran [149] et al. examined the behavior of MSCs cultured on a range of silane-modified surfaces to determine the effects of the surface functional groups on the early differentiation potential of MSCs in vitro. Cells were cultured for 1 and 7 days in direct contact with glass which had been functionalized by surface treatment to provide a range of different surfaces: $–CH_3$, $–NH_2$, –SH, –OH, and –COOH modified surfaces and a clean glass reference (TAAB). Viable cell adhesion was quantified by Lactate Dehydrogenase assay, and morphology and viability was qualitatively evaluated using calcein AM, ethidium homodimer, cytoskeletal (F-Actin), ECM (Fn and vitronectin), and Hoechst staining (nucleus). The expression of selected differentiation markers, Collagen type II (chondrocytes), CBFA1 (bone transcription factor), Collagen type I (MSC marker), and TGF-β3 (extracellular matrix production) was determined using real time polymerase chain reaction. The expression of ornithine decarboxylase was evaluated as a marker of proliferation. Surfaces of the $–NH_2$ group demonstrated the greatest level of cell adhesion by the 7-day period, and mRNA expression profiles indicated osteogenic differentiation, increased CBFA1 and decreased Collagen type II expression. Cells cultured in contact with the –COOH surfaces displayed different cell morphologies, Fn and vitronectin spatial distributions compared with the cells in contact with the $–NH_2$

surfaces, in addition to an increase in Collagen type II expression, indicative of chondrogenic differentiation. The modifications to the surface chemistry of glass did affect cell behavior, both in terms of viable cell adhesion, morphology and profiles of mRNA expression, providing the means to alter the differentiation potential of the MSCs.

Using high internal phase emulsion (HIPE) templating method, Viswanathan [150] et al. fabricated a 3D scaffold with amphiphilic block copolymers polystyrene-b-poly(ethylene oxide) (PS-PEO) and/or polystyrene-b-poly(acrylic acid) (PS-PAA), which exhibited both cell inert (PEO) and adhesive (PAA) domains. The results demonstrate how Fn and MSCs adhere in a domain specific manner: an optimal balance between concentration and spatial distribution of PAA domains may be contributing toward the preferential adhesive behavior of the stem cells, which means not only the type, but also the spatial distribution (pattern) of the functional groups that directing the stem cell growth and fate.

8.4.4.4 Effects of Biochemical Functionalization on Stem Cell Behaviors

Another approach toward the control of stem cell behavior on biomaterials is the biochemical incorporation of adhesion-promoting oligopeptides or oligosaccharides. Stem cell adhesion to traditional biomaterials is based upon recognition of short peptides of ECM proteins from the body fluids adsorbing specifically or nonspecifically to the material surface by the corresponding adhesion receptors, which means the cell–material interaction is indirect. As a more direct approach, several investigators have explored the covalent or physicochemical incorporation of adhesion-promoting oligopeptides and oligosaccharides onto the biomaterial surface.

Extensive research has been performed by anchoring oligopeptides representing the ECM binding sites onto the biomaterial surfaces. The most commonly used peptide for surface modification is RGD, the signaling domain derived from fibronectin and laminin. A number of materials including glass [151], quartz [152], metal oxide [153], and polymers [154] have been modified with these peptides and characterized for cellular interaction with their surfaces. Different coupling techniques have also been employed to ensure covalent binding of the peptides to the surface of the materials. For example, the reactive moieties on the model surface, usually $–NH_2$, were chemically reacted with certain functional groups, usually –COOH, that are present within the bioactive peptide. A bi-functional crosslinker that has a long spacer arm can be used for the immobilization of the peptide to the surface, which can enable the immobilized peptide to move flexibly in the biological environment [152]. For polymer substrates lacking appropriate functional groups for a coupling reaction, a photochemical immobilization method [155] has been utilized to graft cell-binding peptides. In order to examine that any cellular responses to the modified substrates are mediated solely by the immobilized peptides, the experiment has often been performed under serum-free conditions.

Designing materials that can selectively interact with cell-binding peptides while minimizing nonspecific adsorption of ECM proteins is also challenging. Immobilization of poly(ethylene glycol) (PEG) [156] or its derivative [157] on the surface has been effective to limit cell adhesion. The interpenetrating polymer network (IPN) that consists of both the hydrophilic chain that can limit nonspecific adsorption of proteins and the reactive chain that allows for peptide immobilization may be desirable for this application [158]. With RGD covalently incorporated into poly (ethylene glycol) diacrylate (PEODA) hydrogel, Yang [159] et al. demonstrated that RGD-conjugated PEGDA hydrogel system promotes the osteogenesis of bone marrow-derived MSCs. RGD-tethered hydrogel stimulated the production of bone marker proteins, such as ALP and osteocalcin, in a dose-dependent manner, with 2.5 mM being the optimal concentration.

Cao [160] et al. synthesized a series of charged or neutral oligopeptide motifs coupled with RGD using quartz substrates as model. MSCs behaviors on the modified surfaces with different charged oligopeptide motifs were studied. It was found that these different charged oligopeptide motifs coupled with RGD were biocompatible for cell proliferation and adhesion. Moreover, it was demonstrated that the positively charged oligopeptide motif could inhibit osteogenic differentiation, while the negatively charged and neutral oligopeptide motifs could enhance osteogenic differentiation in the presence of RGD.

Chien [161] et al. determined the effects of surface bioadhesive signals on self-renewal and osteogenic differentiation of MSCs using a low-fouling platform. Cell-resistant poly(carboxybetaine) hydrogel was conjugated with 5 μM or 5 mM of cell-adhesive RGD peptides in order to control the cells' affinity to the substrate. MSCs were cultured on the RGD-modified poly(carboxybetaine) hydrogel and then the cells' states of stemness and osteogenic differentiation were evaluated. The MSCs formed 3D spheroids on the 5 μM RGD substrate, while exhibited spreading morphology on the 5 mM RGD substrate. Furthermore, MSCs on the 5 μM RGD hydrogel maintained a better stemness phenotype, while the hMSCs on the 5 mM RGD hydrogel proliferated faster and underwent osteogenic differentiation. In conclusion, the stemness of hMSCs was best maintained on a low RGD surface, while osteogenic differentiation of hMSCs was enhanced on a high RGD surface. Wang [162] et al. investigated MSCs behaviors on micro/nanopatterns with RGD nanoarrays of nanospacings 46 and 95 nm, and with micropans of side lengths 35 and 65 μm (four groups in total). The osteogenic and adipogenic differentiation of MSCs was conducted, and the potential effect of RGD nanospacing and the effect of cell spreading size on cell differentiation were decoupled for the first time. The results reveal that RGD nanospacing, independent of cell spreading size, acts as a strong regulator of cell tension and stem cell differentiation.

8.4.5 Multiscale Hierarchical Structure

Hierarchical structures was first proposed in 1994 in order to develop novel processing technologies to fabricate hierarchically structured materials with proper control on an industrial scale [163]. In 2005, Hollister proposed a clear definition stating hierarchical structure refers to the features at scales from the nanometer to millimeter that are able to determine how well the bioscaffold meets the conflicts between mechanical function and mass-transport needs [164].

Almost all types of biomaterials, such as metals, polymers, ceramics, hybrids and composites, can be machined into biomedical scaffolds for the purpose of tissue engineering. For example, by employing a liquid foaming method and subsequent chemical treatments, three-dimensionally hierarchical porous structures can be successfully achieved in titanium scaffolds with pore size ranging from the nanometer to micrometer scale. This scaffold also has a sufficient compressive strength to meet the requirements of implantation [165]. Woodard et al. revealed that the micropores in porous hierarchical HAp bone scaffolds are quite important to maintain the mechanical satiability of the scaffolds, as the newly formed bone in the scaffolds supported the load after a fracture. The mechanical failure stress was significantly less than that of the scaffolds with pure macropores. Furthermore, evidence also suggested that bone could arrest crack propagation in hierarchical HAp scaffolds [166]. Practically, hierarchical bimodal or multimodal porous architectures with macro-, micro-, and nanopores, simultaneously, are also important in modulating the permeability and compliance of polymeric scaffolds that favor various applications in tissue engineering.

8.4.5.1 Hierarchical Pore Sizes Structure

Actually, sol–gel glass scaffolds can be considered the precursors of the hierarchically structured macro-/mesoporous glass scaffolds [167]. In the last couple of years, some attempts for fabricating multiscale glass-based scaffolds have been carried out by using properly mesostructured materials, in which the nanoporous size and arrangement can be carefully controlled and designed. The purpose of such scaffolds is twofold, as they combine the properties of traditional glass-derived scaffolds, i.e., mechanical support in the defect zone, bioactivity, favored osteointegration, and bone tissue regeneration, with the unique features supplied by mesoporous materials, such as enhanced bioactivity and controlled drug adsorption/ release ability for drug therapy in situ.

Yun et al. [168] synthesized hierarchically porous 3D MBG scaffolds with good in vitro bioactivity by using a combination of sol–gel, double polymers templating, and rapid prototyping techniques. Li et al. [169] reported the synthesis of multiscale porous MBG scaffolds by using the block copolymer EO20PO70EO20 (P123) and a PU macroporous sponge as cotemplates and demonstrated that a HAp layer was formed on the scaffold surface after soaking in SBF for 4 h. Zhu et al. [170]

successfully prepared 3D porous MBG scaffolds by a combination of PU sponge and P123 surfactant as cotemplates and evaporation-induced self-assembly (EISA) process. Apart from MBG, inorganic nanostructures based on calcium phosphates are also compounds of great interest in scaffold development since they are the major inorganic constituent (69 wt%) of naturally occurring mineralized bone.

Of special interests are the scaffolds that are able to present a bimodal pore size distribution, mainly having macropores for cells penetration and micropores for protein adsorption/delivery. Interestingly, the micropores also present some roles in the overall mechanical properties of scaffolds. For instance, HAp scaffolds were prepared with two different micropore sizes, mainly 5.96 and 16.2 μm, showing higher bending and compression strength in the presence of smaller micropores [93]. Microporous (54–80 vol.%) bioactive glass scaffolds with hierarchical porosity have been recently developed with the aim to satisfy the macroporosity needed for bone ingrowth while maintaining adequate mechanical properties (12–20 MPa) [93].

Inspired by the impressive property of natural bone, 3D hierarchical porous scaffolds have attracted significant attentions since they can provide transportation "highways" on various scales during osteoregeneration, and promote the innate regenerative mechanisms of the human body. In recent years, synthetic scaffolds with hierarchical macro/micro- or macro/nanoarchitectures are being rapidly developed and have evolved various biomaterials, including biodegradable polymers (Tyrosine-derived polycarbonate, PLGA), ceramics (hydroxyapatite, bioglass, calcium carbonate) and metals (stainless steel and titanium), etc. Numerous studied have concluded that interconnected macroporosity with diameter larger than 100 μm is a prerequisite for bone ingrowth, cellular infiltration and nutrient/waste transportation [171]; and micro- and nanotopologies on the material surface play a critical role on cell attachment, biomineralization and full-scale osteointegration in vivo. Based on these previous researches, Tang et al. [56] have successfully incorporated trimodal macro/micro/nanoscale structures into one scaffold to achieve optimal osteogenic properties.

8.4.5.2 Hierarchical Porosity Structure

Natural bone is a classic case of a functionally graded structure with an outer highly dense region (cortical bone) having an elastic modulus of ~18 GPa, the inner porous region (cancellous bone) having an elastic modulus of ~1 GPa, and the bone marrow cavity in the central region [172]. Thus, there is a gradual increase in porosity as well as modulus variation from cortical to cancellous transition, especially at the end of long bones. Thus, to replicate the architecture of natural bone, 3D scaffolds with graded porosity are preferred. In this context, Ti–6Al–4V rod was fabricated with central foam core (density ~0.6 g/cm^3) and outer foam structure with relatively higher density (~1.1 g/cm^3) as shown in Fig. 8.10 [173]. The inner and outer foam characterized by a stiffness of 0.3 and 2.2 GPa, respectively. Also, a porous cylinder of Ti–6Al–4V alloy was fabricated using the electron beam melting (EBM) method, characterized by a lower density inner foam, surrounded by a foam with relatively

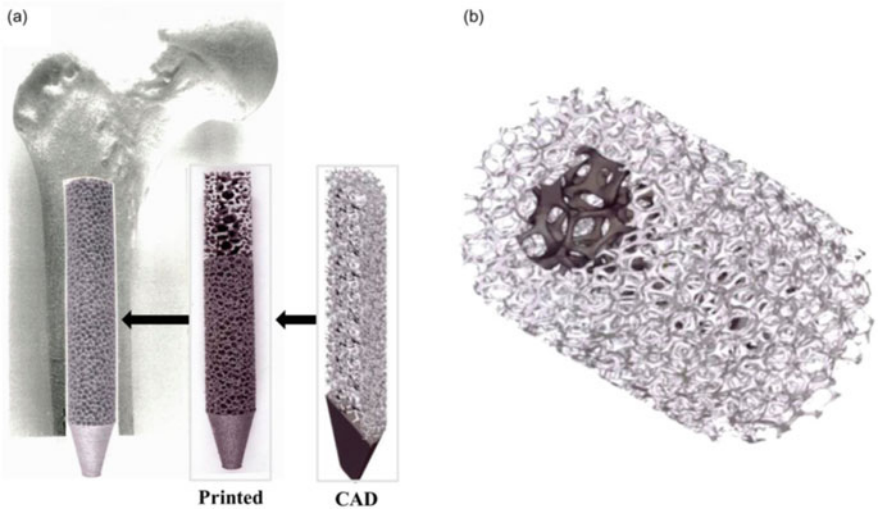

Fig. 8.10 A conceptual view of intramedullary stem of Ti–6Al–4V foam built by EBM using the CAD model and cylindrical foam with dense outer region and low-density inner core [173] (Open access)

higher density (Fig. 8.10b). Generally, porous materials with a specific pore size facilitate growth of one particular cell. For example, pore sizes of ~5–15 μm were considered suitable for fibroblast, ~70–120 μm for chondrocytes, and ~100–400 μm for osteoblast ingrowth. In contrast, gradient porous materials can simultaneously repair and reconstruct two or more different tissues, since the different regions provide different microenvironments for multiple tissues.

8.4.5.3 Hierarchical Surface Structure

Cells are innately receptive of their surroundings, typically to a broad spectrum of feature sizes from the macro down to molecular level, between 100 μm and 10 nm. It is through an elaborate and dynamic feedback mechanism of signal transfer between the ECM and the cells, that the behavior of the latter is coordinated into complex functional tissues. Hence, engineering these dynamic ECM mechanisms into biomaterials is the key to control cell behavior.

It is already circumstantiated that both micrometer and nanometer scale features of a material have marked influence on cell behavior. Additionally, materials organized on multiple length scales have better conformity to biological matrices than those with single scale features and are hence more propitious for all kinds of biomedical applications. The effects of microscale surface topography on cellular responses have been investigated over the years. Currently, nanostructuring of surfaces have garnered immense interest in view of their structural similitude to the native ECM of cells. Undeniably, nanotopography plays a cardinal role in

modulating cell functionality. Recent research by Gentile et al. manifests the potentiality of moderately rough nanostructured surfaces with large fractal dimensions in promoting stable cell adhesion, growth and proliferation [174].

Literature is replete with evidences on topographic sensitivity of cells (i.e., interplay of cells with surface features) to nanoscale as well as micrometer-range features like grooves, ridges and wells. Nanoscale alterations in topography evoke multifarious cell responses, including changes in cell adhesion, cell orientation, cell motility, surface antigen display, cytoskeletal condensation, activation of tyrosine kinases, and modulation of intracellular signaling pathways, which in turn coordinate transcriptional activity and gene expression. Notwithstanding the feature size, cell behavior is also administered by the nature of ordered topography (e.g., ridges, grooves, steps, pits, pillars, channels) and their symmetry (e.g., orthogonal or hexagonal packing).

In vivo, the basement membrane, composed of ECM components, is a complex network of pores, fibers, ridges, and other features of nanometer sized dimensions. Topographical cues generated by the ECM, independent of biochemistry, have direct effects on cell behavior such as adhesion, migration, cytoskeletal arrangements, and differentiation. Cells are inherently sensitive to local microscale, mesoscale, and nanoscale topographic and molecular patterns in the ECM environment, a phenomenon called "contact guidance" [175]. The development of microfluidics and micro-/nanofabrication methods to analyze the cellular response to substrate topography has provided new insights into the interactions of cells with their microenvironments.

Grooves and pillars are the most common feature types employed in the study of the effects of surface structures on cells. The influence of groove patterns on the behavior of cell has been extensively investigated by using various cell types such as fibroblast, osteoblast, epithelial, myoblast, etc. A large number of studies revealed that cells tend to align to the long axis of the grooves. Kaiser et al. defined the role of groove/ridge dimensions on fibroblast cell migration [176]. They found that surface structures significantly influenced cell orientation, migration direction, as well as migration speed in the directions parallel and perpendicular to the grooves/ridge in a surface structure-dependent way. Uttayarat et al. investigated the combination of flow shear stress and groove guidance on endothelial cell migration [177]. When flow direction was oriented parallel to microgrooves, the cells migrated along the microgrooves. When microgrooves were oriented perpendicular to the flow, most cells migrated orthogonal to the grooves and downstream with the flow. Lee et al. reported that the nanoscale ridge/groove pattern arrays alone can effectively and rapidly induce the differentiation of human embryonic stem cells into a neuronal lineage without the use of any differentiation-inducing agents, indicating the significant role of topography in determining cell fates [178].

The influence of pillar patterns on the behavior of cells has also been extensively studied. MSCs preferentially differentiated and osteosarcoma cancer cells increased their malignant transformation due to the micropillar geometry. In particular, increase of pillar heights from 1 to 10 μm affected the in vitro adhesion and guide morphology of fibroblasts by laminin expression enhancement [179]. Furthermore, the spacing between 5 and 10 μm of pillars was shown to rearrange the actin

cytoskeleton and govern fibroblast migration in vitro [180]. Nanotopography alone can induce the differentiation of MSCs into neuronal lineage and induced a more significant upregulation of neuronal markers compared to microtopography, highlighting the importance of feature size in topography induced differentiation.

Other micro-/nano-sized features, such as nodes, pits, pores, and so forth have been reported to influence the behavior of cells. The topography of the cell substratum plays an important role in regulating cellular behavior, and micro-/nanofabrication techniques provide useful tools for manipulating cells in both fundamental cell biology research and tissue engineering.

8.5 Delivery of Bioactive Agents

To enhance the interactions between the materials and host cells/tissues and directs the differentiation of MSCs, one of the useful strategies is the introduction of the bioactive components in extracellular matrix components within/onto the material structures. These components usually include ECM peptides/polypeptides, cytokines, growth factors, and DNAs. In the view of the osteoinductive potential, osteogenic growth factors such as Fibroblast Growth Factor 2 (FGF-2), TGF-β2, and BMP-2 have been extensively used to improve the material osteoinductivity.

8.5.1 Growth Factors

Growth factors were initially discovered as a result of their ability to motivate continuous mitosis of quiescent cells in a nutritionally complete medium without serum. While nutrients and growth factors are both essential for mitosis, only growth factors know how to initiate mitosis of quiescent cells. A variety of cellular processes need growth factors as regulatory agents. The biology of these factors differs from the classical hormones as neither their site(s) of synthesis nor site(s) of action is limited to defined tissues.

Growth factors are polypeptides that transmit signals to modulate cellular activities. It is known that growth factors play crucial roles in communication and information transfer between cells and their microenvironment [181]. Moreover, growth factors are soluble-secreted signaling polypeptides capable of instructing specific cellular responses in a biological environment. The specific cellular response trigged by growth factor signaling can result in a very wide range of cell actions, including cell survival, and control over migration, differentiation or proliferation of a specific subset of cells. Prior to addressing strategic delivery of growth factors, understanding the biological functions and roles of these proteins in the extracellular matrix is first of all required because the extracellular matrix contain numerous components such as adhesive molecules, notch signaling molecules, traction-enabling adhesion molecules and proteoglycan molecules to bind and modulate

the activity of a number of growth factors. The signal transmission mechanism initiates with growth factor secretion by the producer cell. The growth factor instructs cell behavior through binding to specific transmembrane receptors on the target cells. The machinery that transduces the growth factor-binding signal to the cell nucleus involves a complex array of events involving cytoskeleton protein phosphorylation, ion fluxes, changes in metabolism, gene expression, protein synthesis and ultimately an integrated biological response.

Growth factors differ from other oligo-/polypeptide molecules, such as insulin and hormones, in the mode of delivery and response elicited. Typically, growth factors do not act in an endocrine fashion; they exhibit short-range diffusion through the extracellular matrix and act locally owing to their short half-lives and slow diffusion [182]. The ability of a growth factor to deliver a particular message to a distinct subpopulation of cells is not exclusively determined by the identity of the growth factor and its ability to diffuse through the ECMs; it is also determined by the target cell number, type of receptors and the intracellular signal transduction subsequent to factor binding. The same growth factor can convey different instructions depending on the receptor type to which it binds, and on the cell type to which it binds. Moreover, the same receptor can translate different messages depending on the intracellular transduction pathways. The ultimate response of a target cell to a particular soluble growth factor can also be governed by external factors, including the ability of the factors to bind to ECM, ECM degradation and growth factor concentration and cell target location [183].

Growth factors are involved in the regulation of a variety of cellular processes and typically act as signaling molecules between cells [184]. They promote cell proliferation, differentiation and maturation, which vary in growth factors. As a result, they play important roles in wound healing and tissue regeneration. However, most growth factors act in a diffusible manner and are generally unstable in a tissue environment. This prolonged retention is considered to maintain the activity of growth factors in cells or in their environment (i.e., the ECM or artificial implant scaffolds), until the repair process is initiated or even completed. Thus, many attempts have been made to improve the performance of growth factors (e.g., their active period and stability). In addition, it is very important to add biofunctionality such as the regulation of cell functions to biomaterials used for artificial organs. Modification of growth factors for immobilization on, or for high-affinity binding to cells or scaffold biomaterials has been performed by various researchers [185].

Most growth factors which act in a diffusible manner, interact with their cognate receptor on the cell membrane, and form a complex. This interaction induces phosphorylation of the receptor and triggers signal transduction in the cell. These complexes are then internalized, partially decomposed by lysosomes, and partially recycled to the cell membrane [186]. Thus, internalization of the receptor/growth factor complexes leads to the desensitization of cells (downregulation), and to the reduction of excessive responses and overstimulation. In contrast, some growth factors are known to act in a nondiffusible manner by being present at the cell surface (juxtacrine) or by associating with specific substances, such as the ECM (matricrine). The nondiffusible mechanism was elucidated by the discovery of cell

membrane-bound growth factors in the 1990s, which include heparin-binding EGF-like growth factor (HB-EGF), transforming growth factor-β (TGF-β), tumor necrosis factor-α (TNF-α), colony-stimulating factor 1 (CSF-1), and the c-kit ligand [187]. These growth factors are barely internalized even after binding to their receptors but exhibit long-term activity without downregulation. This point suggests the possibility of designing binding growth factors with specific activities.

There are several characteristic properties of growth factors. Many cell types can produce the same growth factor and the same growth factor can act on many cell types (pleitropism) with the same or different effects. Furthermore, different growth factors can share the same biological effect (redundancy). Growth factors can influence the secretion of other growth factor (antagonize or enhance). Growth factors are not stored as preformed molecules but their secretion is a brief self-limited event and their synthesis is initiated by new gene transcription, transient transcriptional activation, and their mRNAs are unstable [188]. There is transient synthesis, rapid release with activity controlled by posttranscriptional mechanisms such as proteolytic release of an active product from an inactive precursor. Most cellular responses to growth factors require new mRNA and protein synthesis.

The availability of growth factors from the conditioned medium of cultured human cells, their expansion through recombinant technologies, and improved understanding of their functions and clinical applications has increased the need for pharmaceutical forms. Unfortunately, the short half-lives of growth factors, their relatively large size, slow tissue penetration, their potential toxicity at systemic levels all leading to a long time for tissue to respond, obviates conventional routes of administration.

All vascularization processes involve a series of interactions among cytokines, growth factors, various types of cells, and enzymes. The onset of vascularization begins with the binding of biological agents to the surface receptors of endothelial or endothelial progenitor cells, and a resulting cascade of agents act in the subsequent processes of vascularization. Numerous growth factors involved in vasculogenesis, angiogenesis, and arteriogenesis have been identified and characterized, including vascular endothelial growth factor (VEGF), fibroblast growth factor (FGF), placenta growth factor (PIGF), hepatocyte growth factor (HGF), platelet-derived growth factor (PDGF), Angiopoietin-1 and Angiopoietin-2, insulin-like growth factor (IGF), granulocyte macrophage colony-stimulating factor (GM-CSF), and monocyte chemoattractant protein-1 (MCP-1). Growth factors are often chosen as drug candidates for rebuilding networks of blood vessels for therapeutic angiogenesis or for tissue engineering.

Members of the transforming growth factor-β (TGF-β) superfamily are secreted multifunctional growth factors that determine the development, maintenance and regeneration of tissues and organs. Their importance in the development of multicellular organisms is clear from their presence in all vertebrates and invertebrate animals. On the basis of their phylogenetic and functional relationships, the TGFβ/BMPs can be subdivided into four subgroups, which also highlight mechanistic differences in receptor binding and activation or the differences found in modulatory mechanisms [189]. These subgroups are the TGFβs, the bone

morphogenetic proteins (BMPs) and growth and differentiation factors (GDFs), activin/inhibins, and the so-called outsider subgroup.

8.5.2 Brief Introduction of BMPs

Bone morphogenetic proteins belong to the large transforming growth factor-beta (TGF-β) superfamily of structurally related signaling proteins which are disulfide-linked dimers composed of two 12 to 15 kD monomers. To date, more than 20 members have been identified in humans with varying functions during developmental and physiological processes [190] such as embryogenesis, skeletal formation, hematopoiesis, and neurogenesis. Among these growth factors, BMP-2, BMP-4, and BMP-7 (also called osteogenic protein-1) have been largely used as recombinant proteins for their ability to repair bone defects in different animal models [191, 192]. Liu et al. [193] have elucidated the exact mechanism by which BMPs affect MSCs. These proteins generate the transcription factor Smads by combining with type I or II serine/threonine receptor on the MSC membrane to activate 203 gene loci which control the osteoblast differentiation of MSCs.

BMP-2 is a FDA-approved growth factor and can induce ectopic bone and cartilage formation in adult vertebrates and is involved in central steps in early embryonal development. A cDNA encoding mature human BMP-2 could be efficiently expressed in *Escherichia coli*, and after renaturation, a dimeric BMP-2 protein of Mr 25000 was prepared with a purity greater than 98%. Fernando Lecanda et al. [194] have proved that BMP-2 has profound effects on the proliferation, expression of most of the bone matrix proteins and the mineralization of both relatively immature human bone marrow stromal preosteoblasts and mature human osteoblasts. However, combined with clinical challenges such as limited efficacy, excessive doses, side effects, and high costs, efforts have focused on optimizing the carrier of BMP-2, as well as improving BMP-2 half-life and/or sustaining and localizing its release [195].

8.5.3 Mass Production of rhBMP-2

Because of the limited source of natural BMP-2, and the risk of infection by pathogens, BMP-2 molecules with high activity expressed via eukaryotic cells has been introduced in the market by Medtronic. However, it has the disadvantages of complicated process, high production cost, and low output. Meanwhile, the *E. coli* expression system holds great potential because of simple process and low production cost. The recombinant proteins expressed in *E. coli* system often form inclusion bodies, especially when they are expressed at high levels. How to achieve the proper renaturation of recombinant proteins from inclusion bodies would become the key issue for the process. By optimizing the gene codon, expression vector and host

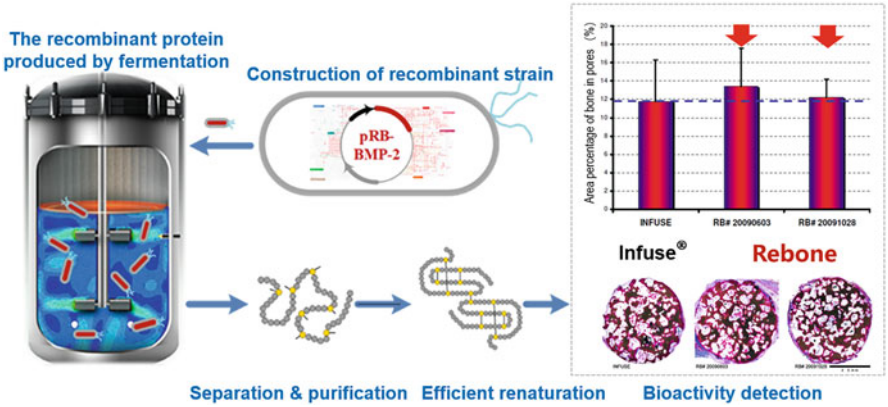

Fig. 8.11 Mass production of rhBMP-2 by recombinant *E. coli*

bacteria, the ECUST team developed the recombinant *E. coli* strains with intellectual property (shown in Fig. 8.11). The reduction environment at low temperature and special aggregation inhibitor were utilized in the renaturation of recombinant proteins from inclusion bodies to efficiently reach a native conformation. The rhBMP-2 molecules with over 95% purity and homodimer structure were successfully obtained. According to the detection report by a research institution, the bioactivity of our rhBMP-2 could reach the best level abroad (Infuse, USA).

On the basis of small-scale manufacturing, the engineering magnification of fermentation, protein purification, renaturation and refinement of recombinant protein have been investigated, which the technology has already been transferred to Shanghai Rebone Biomaterials Co., Ltd. After solving the issues of engineering amplification affecting protein activity, the suitable and detection indexes were determined to screen the factors affecting the yield and activity of rhBMP-2. Moreover, the optimization of the manufacturing process allows the integration of the whole system. It is also realized for the establishment of the mass production in accordance with GMP standard and the stable mass production of rhBMP-2 with high-activity. The products have been used in over 30 provinces national wide and achieved satisfactory performances in bone defect treatment, trauma repairing and spine surgery. Therefore, the ECUST team has acquired the reputation from our international counterparts as “the frontier of bone repairing technology.”

8.5.4 Immobilization of Growth Factors

8.5.4.1 Immobilization Approach of Growth Factors

Growth factors typically act as signaling molecules to regulate a variety of cellular processes. For example, BMPs stimulate bone cell differentiation and improve the cell proliferation, whereas FGF and VEGF enhance angiogenesis. BMPs have been

integrated on/into the implantable materials to significantly enhance a wide variety of biological functions including stimulating osteogenesis and angiogenesis [196, 197]. Upregulation of BMP-2 has been observed during the first three weeks of osteogenesis [198]. Moreover, the growth factors released during the inflammatory phase have the potential of attracting undifferentiated mesenchymal stem cells to the injured site [199]. On the basis of these findings and the nature of BMP-2, this growth factor must be delivered in a sustained fashion that emulates the natural release profile of BMP-2 in vivo.

There are several methods for immobilizing biological molecules including BMPs on inorganic/organic surfaces. Physisorption is the easiest method of surface modification. The direct immobilization of growth factors by physisorption is easily disrupted by desorption and the growth factors will diffuse into the surrounding medium, losing their ability to exert a sustained effect [200]. Growth factors have also been chemically immobilized on surfaces by covalent bonding or by biologically anchoring. Some linkers have also been used as intermediaries to chemically immobilized growth factors, including coupling agents, polyphenols, and dopamine. Meanwhile, the covalent binding usually requires nonphysiological conditions [201]. Many researchers have also developed layer-by-layer self-assembly and biomimetic/electrochemical deposition approaches for immobilizing growth factors [202]. However, either time consuming or poor controlling of the coating properties limit their applications. To achieve the high loading efficiency and maintain the biological stability of BMP-2, the immobilization techniques require the fast operation, mild conditions, as well as the well-controlled coating. Among different techniques, the electrostatic spray deposition (ESD) has shown the great potential for biomolecule incorporation on/into metallic materials because of simple and low-cost, fast deposition rate, protein-friendly, well-controlled, and easy coating for complex geometries [203]. To date, this technology has been successfully applied to deposit many inorganic/organic materials on the metallic surfaces. Our group also used this technique to codeposit BMP-2 and chitosan on metallic surface for enhancing the proliferation and osteogenic differentiation of bone MSCs [204].

Growth factors are often added to the scaffold surface via electrostatic interaction and ionic complexation, and the corresponding release depends on protein–surface interactions that are governed by surface charge, surface roughness, and surface energetics. For more sustained release, bioactive molecules can be physically encapsulated within the scaffolding material and in microparticles. Covalent immobilization methods must be assessed in terms of gradients, spatial distribution and density, conjugation efficiency, dose dependence, downstream signaling, heparin/affinity-based delivery, dual delivery, and cleavable linkers [205]. For the purpose of this point, 100% or less delivery over the course of 30 days is considered successful sustained release, based on the timescale required for repairing different tissues.

8.5.4.2 The Influence of Surface Properties on the Activity of Growth Factors

As an important member of transforming growth factor beta superfamily, BMP-2 molecule has been shown to have prominent functions in inducing osteogenic differentiation and promoting osteogenesis [206]. BMP-2 not only participates in the development of various organs and the directional differentiation of cells in the early embryonic period, but also causes undifferentiated mesenchymal stem cell and osteoblast precursor cells to undergo chemotaxis, division and differentiation after birth. Since 2002, BMP-2 molecule has been approved for spinal fusion, tibial fracture, and dental transplantation by the FDA and the European Medical Regulatory Agency. Our group has also investigated the effects of the composition and surface/interface on the structure and biological activity of rhBMP-2, elucidating the nanoeffects during the regulatory processes.

On the typical zero-dimensional material-silica nanoparticles (SNPs), Tian et al. [207] prepared SNPs with different sizes of 20 nm, 60 nm and 100 nm, respectively, and evaluated the secondary structure and biological activity of rhBMP-2 with the change of SNPs size. It was found that there was a rapid adhesion stage, the rhBMP-2 loading on the surface of SNPs increased linearly with the time from 0 to 15 min. Subsequently, there was a saturated adsorption stage, in 20 to 30 min, the rhBMP-2 loading on the SNPs surface increased slowly with time until it reached the equilibrium adsorption. In contrast, the outer surface of SNPs at 60 nm showed a distinct rhBMP-2 protein coating, and the interface is very distinct. Infrared and circular dichroism spectra showed the unfolding effect of rhBMP-2. SNPs with different particle sizes could decrease the β-rotation/folding and α-helix structure in rhBMP-2. Compared with free rhBMP-2, although the bioactivity of rhBMP-2 adsorbed on the surface of SNPs was reduced, however, the biological activity of rhBMP-2 in SNP60 samples was higher than that in SNP100 and SNP20 samples. Therefore, the surface curvature of 60 nm nanoparticles is beneficial to the maintenance of the structure and activity of rhBMP-2.

As a typical one-dimensional material, single-walled carbon nanotubes (SWNTs) can promote the maintenance of protein secondary structure and biological activity. Li et al. [208] investigated the effects of hydrophilic carbon nanotubes (SWNTS-COOH) and hydrophobic carbon nanotubes (SWNTs-CH_3) on the adsorption properties, secondary structure and activity of rhBMP-2. The single-beam SWNTs-COOH or SWNTs-CH_3 with a diameter of about 6 to 8 nm is similar to the three-dimensional size of rhBMP-2, and has a strong affinity for rhBMP-2. It took only 10 min for rhBMP-2 to reach saturation adsorption (>90%). The α-helix structure and β-fold structure of rhBMP-2 adsorbed on SWNTs-COOH surface decreased obviously. Compared with the rhBMP-2 in solution, rhBMP-2 molecules adsorbed on SWNTs-CH_3 and SWNTs-COOH significantly increased the osteogenic activity by 51% and 23%, respectively. However, compared with free rhBMP-2, the biological activity of rhBMP-2 released from SWNTs-CH_3 decreased by about 30%, while that of rhBMP-2 released from SWNTs-COOH had no significant

difference. When rhBMP-2 nonspecifically adsorbed to SWNTs-COOH or SWNTs-CH3 surfaces, its intramolecular folded structure might partially fold in order to contact the SWNTs surface to a greater extent; therefore, the secondary structure of rhBMP-2 was changed. Considering the molecular size of rhBMP-2, it is hypothesized that rhBMP-2 molecules might bind on the surface of SWNTs vertically or parallelly.

The two-dimensional surface properties of the materials significantly affect the adsorption kinetics of proteins. For this purpose, the hydroxylapatite (HAP) with different surface roughness HAP (5.2 ± 0.3 nm), HAP-pol (17.4 ± 0.3 nm) and HAP-sin (7.7 ± 0.2 nm) were prepared [209]. To study the effect of rhBMP-2 on the adsorption capacity, Huang et al. investigated molecular dynamics behavior and biological activity of rhBMP-2. The mass of rhBMP-2 adsorbed on HAP, HAP-pol and HAP-sin were 115.8 ± 3.7 ng, 176.9 ± 4.9 ng and 123.4 ± 3.3 ng, respectively. The results of osteogenic activity showed that the ALP value of HAP-Pol/BMP-2 was significantly higher than that of HAP/rhBMP-2 and HAP-sin/rhBMP-2. SMAD1/5/8 signaling pathway is the most important and classical signaling pathway of rhBMP-2 in mediating osteogenic differentiation of C2C12 cells. Western blot analysis showed that the expression of SMAD1/5/8 of C2C12 was higher in all groups, but the expression of p-Smad1/5/8 of C2C12 was significantly different. In the order of HAP-sin < HAP < HAP-pol, the expression level of SMAD1/5/8 increased significantly ($p < 0.05$), indicating that rhBMP-2 adsorbed on HAP-pol had the highest osteoinductive activity.

Mesoporous materials with pore sizes close to those of protein molecules could facilitate protein immobilization, activity retention, and sustained-release effects [210, 211]. Therefore, the MBG materials with different mesoporous sizes were designed and prepared. The effects of mesoporous sizes on the loading, adsorption, slow release and bioactivity of BMP-2 were studied. The pore diameters of MBG-4 and MBG-8 were 4.30 nm and 7.67 nm, respectively. And their pore orifices were slightly smaller than the pore diameters, which were 3.63 nm and 5.48 nm, respectively. The pore diameter of MBG-40 (44.03 nm) was much larger than that of MBG-4 and MBG-8, but its pore orifices was relatively small (5.93 nm), which was close to that of MBG-8. The size of BMP-2 protein was close to the pore diameter of MBG-4, and the BMP-2 protein molecules could enter the mesoporous interior, at the same time, the internal diameter of the pore was close to the size of the protein molecule, so the adsorption mainly took place in the pore. The circular dichroism data confirmed that the change rate of the secondary structure of BMP-2 released from MBG was only 2% to 3% compared with that of free BMP-2 released from MBG. The structural change rate of MBG-8 was the lowest (2%), while the structural change rate of BMP-2 released from nonmesoporous BG was relatively high. These results indicated that the mesopore could protect the secondary structure of the protein, and the protein loaded in the mesopore could maintain its biological activity after slow release. The results of ALP activity test confirmed that MBG had no significant effect on the activity of BMP-2 protein, and the BMP-2 released from MBG-8 had the highest level of ALP activity. In another words, the mesoporous pore size contributes to the activity maintenance of immobilized BMP-2 molecules.

8.5.5 *Influence of Ions on rhBMP-2 and Stem Cell Differentiation*

8.5.5.1 The Influence of Various Ions on the Activity of rhBMP-2 to Induce the Osteogenic Differentiation

As has been discussed, rhBMP-2 is a widely-used, potent osteogenic growth factor and can induce osteogenic differentiation of multipotent mesenchymal cells and induce bone formation in both animals and humans. Various matrixes have been and are currently being adopted to carry rhBMP-2 [212–215]. However, due to the hydrogen/ionic/hydrophobic interaction with the substrates, or the environmental factors such as pH, ionic strength, temperature in vitro and in vivo, highly efficient delivery of rhBMP-2 remains a challenge till now. Therefore, fundamental understanding of the conformational behavior of rhBMP-2 during its application in vitro and in vivo would be very significant to design and fabrication of the rhBMP-2-based orthopedic implants/scaffolds. Recent studies reveal that metal cations play a decisive role in the regulation of protein folding, conformation, stability, and bioactivity of protein. Zinc (Zn^{2+}), copper (Cu^{2+}), calcium (Ca^{2+}), magnesium (Mg^{2+}), manganese (Mn^{2+}), or strontium (Sr^{2+}) have been reported as modulators for protein conformation and biofunctions [216–218]. Thus, the interaction between cations and rhBMP-2 was systematical elucidated in this section.

Considering the fact that Ca^{2+} is the most pervasive component of the bone matrix/scaffold and is abundant in cell culture medium and the physiological environment, the "hormesis" phenomenon was observed for the influence of calcium on the bioactivity of rhBMP-2. Briefly, low concentration of Ca^{2+} (0.18 mM) enhanced rhBMP-2-induced osteogenic differentiation, while high Ca^{2+} concentration ($>$1.80 mM) exerted negative effect. In vivo ectopic bone formation exhibited similar trend. Further studies by circular dichroism spectroscopy, fluorescence spectroscopy, together with cell culture experiments revealed at low concentration, weak interaction of Ca^{2+} and rhBMP-2 slightly increased β-sheet/-turn content and facilitated recognition of BMP-2 and BMPRIA. But, high Ca^{2+} concentration ($>$1.8 mM) induced formation of Ca-rhBMP-2 complex and markedly increased content of β-sheet/-turn, which led to inhibition binding of rhBMP-2 and BMPRIA and thus suppression of downstream Smad1/5/8, ERK1/2, and p38 mitogen-associated protein kinase signaling pathways (as shown in Fig. 8.12). Those results suggested osteogenic bioactivity of BMP-2 can be adjusted via extracellular Ca^{2+}, which should provide guide and assist for development of BMP-2-based materials for bone regeneration [219].

Strontium (Sr^{2+}) has pronounced effects on stimulating bone formation and inhibiting bone resorption in bone regeneration. The interaction between Sr^{2+} and rhBMP-2 was further discussed in this part. Sr^{2+} could bind rhBMP-2 rapidly, even in the presence of Ca^{2+} and Mg^{2+}, and inhibited rhBMP-2-induced osteogenic differentiation in vitro and osteogenetic efficiency in vivo. Further studies demonstrated that Sr^{2+} treatment undermined the binding capacity of rhBMP-2 with its

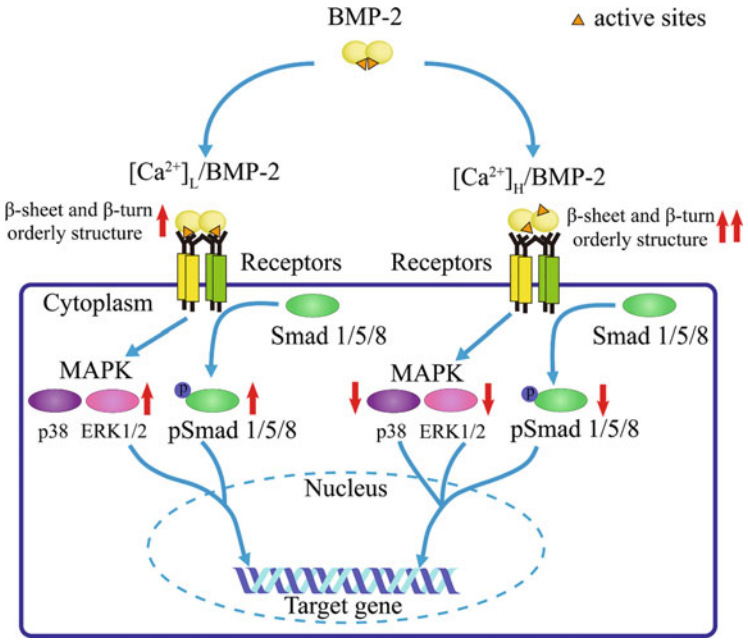

Fig. 8.12 Schematic depiction of the effect of Ca^{2+} on the conformation and bioactivity of rhBMP-2. Effect of Ca^{2+} on the rhBMP-2-induced osteogenic differentiation. Ca^{2+} ion at low concentration facilitated for the binding capacity of BMP-2 with its receptors on cell membrane and thus enhanced Smad1/5/8, and MAPK signaling transduction, which further stimulated expression of osteogenic marker genes and the ALP activity. Additionally, increasing Ca^{2+} attenuated the binding capacity to BMPR-IA, downregulated the signaling transductions of Smad1/5/8, MAP Kinases, and consequently reduced the rhBMP-2-induced gene expression and ALP activity [219]. (Copyright 2015 Changsheng Liu, et al.)

receptor BMPRIA and thus attenuated Smad 1/5/8 phosphorylation without affecting their dephosphorylation in C2C12 cells. Furthermore, circular dichroism spectroscopy, fluorescence spectroscopy and X-ray photoelectron spectroscopy all revealed that the inhibitory effect of Sr^{2+} on the rhBMP-2 osteogenic activity was associated with the formation of Sr-rhBMP-2 complex and ensuing enhancement of β-sheet structure (as shown in Fig. 8.13). Our work suggests the activity of rhBMP-2 to induce osteogenic differentiation was decreased by directly interaction with free Sr ions in solution, which should provide guide and assist for development of BMP-2-based materials for bone regeneration [220].

Moreover, magnesium is a vital and widely used component for the bone substitutes. Mg^{2+} plays a vital role to modulate the conformation and bioactivity of rhBMP-2. However, possibly due to the weak bonding of Mg^{2+} with rhBMP-2, low concentration of Mg^{2+} has no obvious effect on the osteogenic activity of rhBMP-2.

However, those results mentioned above were analyzed using C2C12, a pluripotent skeletal muscle myogenic progenitor cell line, which can differentiate toward an osteoblastic lineage in the presence of BMP-2 and thus is considered as a useful

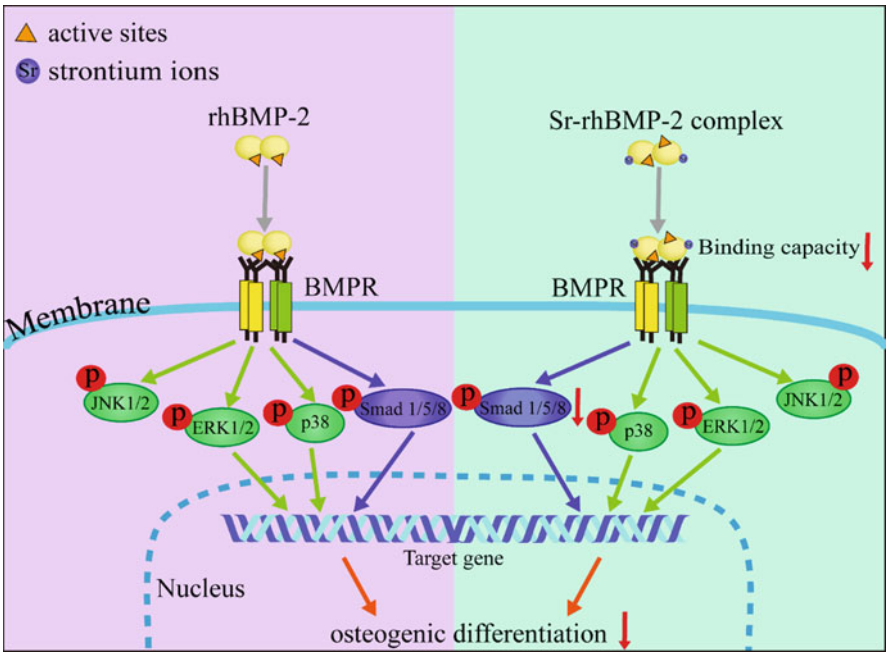

Fig. 8.13 Schematic depiction of the effect of Sr^{2+} on the conformation and bioactivity of rhBMP-2. Compared with free rhBMP-2, the Sr-rhBMP-2 complex, facilitated by the interaction of rhBMP-2 and Sr^{2+} ion, attenuated the binding capacity to BMPR-IA, consequently downregulated the Smad signaling transduction cascades and eventually reduced the rhBMP-2-induced osteogenic differentiation in vitro (including ALP activity and bone-related protein and gene expression) and osteogenetic efficiency in vivo [220]. (Reprinted with permission from Elsevier Ltd. 2016)

model for analyzing both the common and specific signaling mechanisms of BMPs [221]. Although the rhBMP-2-induced ALP activity in rat mesenchymal stem cells showed a same trend, the influence of cations on the rhBMP-2 in stem cells still unknown.

Furthermore, Lithium (Li^+) ions, which are widely used as a long-term mood stabilizer in the treatment of depressive disorders, are known to affect embryonic development by altering cell fate determination and pattern formation. Li^+ activates the canonical Wnt signaling pathway through inhibition of the β-catenin degradation kinase, glycogen synthase kinase-3 (GSK3) to mimic the canonical WNT signaling. Analogous to WNT, lithium prevents GSK3-mediated phosphorylation of cytosolic transcription factor β-catenin and its subsequent degradation by the proteasome complex. Although stabilization of β-catenin in osteoblasts has been shown to promote bone mass accrual in a mouse model, several studies reported inhibitory effects of lithium supplements on the osteogenic differentiation of cultured mesenchymal stem cells. One possible explanation for these apparent contradictory findings might be that lithium affects the differentiation of osteoblast progenitors

through additional signaling events, which independently or in concert with WNT signaling, affect the bone resorption activities in vivo. In murine MC3T3-E1 preosteoblasts and a pluripotent mesenchymal cell line C2C12, lithium inhibits BMP-2 signaling to affect osteogenic differentiation on account to reduction of BMP-2-induced Smad 1/5/8 phosphorylation without affecting their dephosphorylation. Additionally, in MC3T3-E1 cells, lithium attenuates BMP-2-induced osteogenic differentiation through GSK3 inhibition; while in C2C12 cells, these negative effects of lithium ions on BMP-2 signaling do not rely on GSK3 inhibition or activation of canonical WNT signaling [222].

8.5.5.2 Influence of Various Ions on the Osteogenic Differentiation of Stem Cells

Due to the excellent biocompatibility and bioactivity, CaP-based biomaterials have been attracting great attention in the bone regeneration. The dynamic dissolution/precipitation of CaP minerals from the mineralized matrices dictates the concentrations of Ca^{2+} and PO_4^{3-} in the extracellular milieu. The previous investigation has proposed the role for inorganic ions in stimulating osteogenic differentiation.

The response of osteoprogenitors to calcium (Ca^{2+}), which created an in vitro environment with high extracellular Ca^{2+}, is of primary interest for both normal bone homeostasis and the clinical field of bone regeneration. It reported that Ca^{2+} enhanced proliferation and morphological changes in human bone marrow-derived mesenchymal stromal cells (hMSCs) with the upregulated expression level of osteogenic genes including ECM proteins (osteopontin, bone sialoprotein, and osteocalcin) and BMP-2. This means hMSCs will develop an osteoblastic phenotype due to increased [Ca^{2+}] in the culture medium. Ca^{2+} is a ligand for several G-protein-coupled receptors (GPCRs), can enter the cell via gap junction hemichannels or activate the Notch signaling pathway in the chick embryo during left-right organ asymmetry acquisition. The best described GPCR involved in Ca^{2+} sensing is the Calcium Sensing receptor (CaSR), as well as metabotropic glutamate receptors (mGluRs), gamma-aminobutyric acid (GABA), GABAB, and GPRC6A. Furthermore, ion channels such as voltage-gated Ca^{2+} channels (VGCCs), acid sensing ion channels (ASIC)-ASIC1a/ASIC1b, and human ether-à-go-go related gene (HERG) K^+ channels open in response to variations in [Ca^{2+}]. The analysis of signal transduction pathways with GPCR agonists and antagonists, targeting the CaSR and mGluR1 respectively, suggests that these receptors are not involved in BMP-2 expression, but cannot exclude the possibility of an unknown GPCR mediating hMSCs BMP-2 expression in response to [Ca^{2+}]. Type L voltage-gated calcium channels are involved in mediating the signaling pathway between extracellular Ca^{2+} and BMP-2 expression, but not exclusively. Moreover, in other cell line such as osteoblasts, Ca^{2+} treatment results in phosphorylation of extracellular signal regulated kinases 1 and 2 (ERK1/2), and ERK1/2 phosphorylation also occurred when MC3T3-E1 cells were treated with Ca^{2+}. In addition, biphasic CaP crystals failed to induce expression of a characteristic set of genes in mouse embryonic fibroblasts

when upstream activators of ERKs were blocked. In hMSCs, MEK1/2 activity is essential for the effect of Ca^{2+}, probably via Fos expression and AP-1 formation that in turn binds to the AP-1 binding domain of the BMP-2 promoter region [223].

Phosphate ions have generated excitement in the field of vascular biology due to an increased propensity for intravascular calcification with hyperphosphatemia seen in chronic renal disease. The mechanism behind phosphate-induced osteogenesis has been partially elucidated to involve the ubiquitous sodium phosphate cotransporter SLC20A1, adenosine signaling, and ERK1/2 phosphorylation. Extracellular PO_4^{3-} enters the cells through SLC20a1 and subsequently into the mitochondria, which serves as a substrate for ATP synthesis. ATP is then secreted and metabolized into adenosine, which subsequently promotes osteogenic differentiation of hMSCs through the A2b adenosine receptor via autocrine and/or paracrine signaling. Another possibility is that intracellular transport of calcium or phosphate ions inhibits negative regulators of the Smad signaling pathway such as Smad 6 or Smad 7 [224, 225].

Due to the pronounced effects for stimulating bone formation and inhibiting bone resorption, strontium (Sr^{2+}) has been incorporated into biomaterials/scaffold to improve the bioactivity for bone-regeneration applications. It has reported that Sr^{2+} promotes osteoblast differentiation including upregulating expression of the endogenous BMP-2 probably via calcium sensing receptor (CaR)-dependent mechanism or modulation of the Wnt/β-catenin and MAPK pathways [226–231].

The further studies aimed to investigate the possible effects of strontium on MSCs and signaling pathways possibly involved. The increased phosphorylation of mitogen-activated protein kinase (MAPK) ERK1/2 and p38 was detected in strontium-treated MSCs. PD98059 and SB203580, selective inhibitors of ERK1/2 kinase and p38, attenuated the effect of strontium on osteogenesis. Furthermore, it was demonstrated that Rat Sarcoma viral oncogene homolog (RAS), an upstream regulator of ERK1/2 and p38, was activated by strontium treatment and siRNA-mediated Ras knockdown inhibited strontium stimulated expression of osteogenic markers. Finally, the transcriptional activity and phosphorylation level of Runx2 was significantly increased in response to strontium treatment in MSCs. PD98059 and Ras siRNA inhibited the effect of strontium on Runx2 activation. Taken together, strontium can promote osteogenic differentiation of MSCs through activating the Ras/MAPK signaling pathway and the downstream transcription factor Runx2 [232].

Wnt/β-catenin signaling is involved in almost every aspect in embryonic development and plays a central role in bone development and homeostasis. β-Catenin signaling also plays an important role in regulating the commitment of the differentiation of pluripotent stem cell into osteoblast lineage during fracture healing. The canonical Wnt signaling could regulate osteogenesis of MSCs and improve the efficiency of bone tissue engineering. The in vivo data demonstrated the expression of β-catenin and Frizzed receptor was significantly increased by strontium, thus transducing signals that activated the downstream osteogenic transcriptional factors and enhancing osteoblastic differentiation; on the other hand, strontium could also

inhibit the expression of Wnt pathway inhibitors, prevent the degradation of β-catenin, and promote osteogenic differentiation.

8.5.6 Influences of Other Molecules on rhBMP-2 and Stem Cell Differentiation

8.5.6.1 Interactions Between GAG Sugars and BMP-2

Recent evidence suggests that BMP-2 kinetics can be improved by complexing the growth factor with glycosaminoglycan (GAG) sugars [233]. GAGs are long-chain compounds composed of repeating disaccharide units with a carboxyl group and one or more sulfates, in which one sugar is N-acetylgalactosamine or N-acetylglucosamine [234]. These highly anionic, linear polysaccharides form important constituents of the extracellular matrix and are noted for their ability to bind, stabilize and protect various growth and adhesive factors [235]. Heparin, heparan sulfate (HS), keratan sulfate, dermatan sulfate, chondroitin sulfate, and hyaluronic acid are well known as endogenous GAGs.

Heparin, a hyper-sulfated glycosaminoglycan (GAG) sugar harvested from mast cell-rich tissues, has been investigated extensively and shown great promise in this regard. Heparin can bind to and modulate various extracellular molecules including growth factors, adhesion molecules, and receptors. Rainer Ruppert et al. [236] identified the basic N-terminal domains of dimeric BMP-2 as heparin-binding sites that are not obligatory for receptor activation but modulate its biological activity. Some studies have reported that heparin enhances the bioactivities of BMP-2 through binding to and stabilizing BMP-2, protecting BMP-2 from degradation and inhibition by BMP antagonists [233, 237], or acting as a BMP-2 coreceptor by facilitating ligand-induced receptor hetero-oligomerization [238], thereby improving BMP-2 efficacy. In contrast, some researchers have found that heparin inhibits BMP-2 osteogenic bioactivity in vitro by binding to both BMP-2 and BMPR [239], or sequestering BMP-2 on the cell surface and mediating the internalization of BMP-2 [233]. In addition, Shin Kanzaki et al. [240] found that heparin decreased the phosphorylation of Smad1/5/8 after 0.5 h culture, while prolonged periods of culture with heparin enhanced the Smad phosphorylation in BMP-2-stimulated MC3T3 cells. These findings indicate biphasic effects of heparin on BMP-2 activity and suggest that heparin has complex effects on the BMP-2 osteogenic bioactivities. Thus, the mechanism by which heparin regulates bone metabolism induced by BMP-2 remains unclear.

Despite promising results, the use of heparin to augment BMP-2 therapy may pose unwanted effects due to heparin's affinity for a wide range of proteins. For instance, heparin's ability to interact and activate antithrombin III promotes its wide use in anticoagulant therapy [241]. As the fracture hematoma acts as a reservoir for cytokines and growth factors important for bone repair [235], the use of anticoagulant compounds like heparin may be counter-productive. Furthermore, heparin

treatment is known to reduce bone density and has been linked to the development of osteoporosis [242] through its pro-osteoclastic actions in vitro [243] and in vivo [242].

Like heparin, HS is a GAG sugar with repeating disaccharide units of N-glucosamine and uronic acid. Importantly however, HS is less sulfated (40%–60%) compared to heparin (>80%), and has a greater variability in its sulfation pattern that is critical for binding specific signaling molecules [244]. This specificity is of major biomedical significance, because HS retains the advantageous bioactivity of heparin without the adverse effects associated with its pleiotropic protein affinity.

Christian Dombrowski et al. [245] found that exogenous application of HS to cultures of primary rat MSCs could stimulate their proliferation, leading to increased expression of osteogenic markers and enhanced bone nodule formation. Studies from Bramono et al. [246] have demonstrated that marrow-derived HS (HS5) is an effective adjuvant of BMP-2 which sustains BMP-2-dependent osteogenic activity in a similar pattern to heparin and minimizes side effects by (1) prolonging BMP-2 half-life, (2) reducing interactions between BMP-2 with its antagonist noggin, and (3) modulating BMP-2 distribution on the cell surface. The sulfated polysaccharides could enhance the biological activity of both homodimers and heterodimers of BMPs by continuously serving the ligands to their signaling receptors expressed on cell membranes [247]. In addition, not only the total amounts of sulfur but also its position and/or structure is important to modify the stimulatory capacity of BMP activity.

Marie-Christelle Degat et al. [248] explored the binding capacity of synthetic heparin-like dextran derivatives to BMP-2. Affinity electrophoresis analysis provided evidence that carboxy-methylated dextran polymers grafted with high amounts of benzylamide groups (named DMCB) interact with BMP-2. In vitro, DMCB dose-dependently promoted osteoblast differentiation induced by BMP-2 in C2C12 myoblasts more efficiently than heparin. In rats in vivo, DMCB also stimulated ectopic calcification mediated by BMP-2. These data indicate that dextran-based polysaccharides prolong the half-life of the growth factor and promote its biological activity.

Dose-dependent effects on BMP bioactivity were observed in both sulfated chitosan and heparin. Compared with native heparin, 2-N, 6-O-sulfated chitosan (26SCS) showed much stronger simultaneous effects on the BMP-2 bioactivity at low dose. Stimulated secreted Noggin protein failed to block the function of BMP-2 in the presence of 26SCS. The BMP-2 ligand bound to its receptor was enhanced by low dose of 26SCS, whereas weakened by the increasing amounts of 26SCS. Furthermore, simultaneous administration of BMP-2 and 26SCS in vivo dose-dependently induced larger amounts of ectopic bone formation compared with BMP-2 alone. These findings indicated that 26SCS could be used as the synergistic factor of BMP-2 for bone regeneration [249]. Marianne Buttner et al. [250] have reported that over-sulfated CS derivatives themselves are able to induce osteogenic differentiation of hMSC, probably independent of BMP-2 and TGF-β1 signaling and offer therefore an interesting approach for the improvement of bone healing. The enzymatic disruption of HS and CS chains on cell surface proteoglycans alters BMP

and Wnt activity so as to enhance the lineage commitment and osteogenic differentiation of hMSCs [251].

Hyaluronic acid is a long polysaccharide consisting of repeating disaccharide units of N-acetylglucosamine and D-glucuronic acid, and a major component of extracellular matrix (ECM) proteins in mammalian tissues. Michinao Kawano et al. [252] found that HA enhanced BMP-2 osteogenic bioactivity in MG63 cells via downregulation of BMP-2 antagonists and ERK phosphorylation. Also Jungju Kim et al. [253] found that during bone regeneration in vivo, there was a synergetic effect of bone formation with HA-based hydrogel with hMSCs and BMP-2 in the histological and immunohistochemical analysis.

8.5.6.2 Dexamethasone/Ascorbic Acid/Glycerolphosphate (DAG)

Dexamethasone/ascorbic acid/glycerolphosphate (DAG) and BMP-2 are potent agents in cell proliferation and differentiation pathways. Dexamethasone (DEX) is a synthetic glucocorticoid that has been used clinically as an anti-inflammatory drug, although long-term administration of DEX or other steroids may cause or exacerbate osteoporosis. However, DEX has also been used for decades to differentiate MSCs into adipogenic [254], chondrogenic [255], and osteogenic lineages [256]. DEX affected not only the proliferation rate but also the subpopulation composition of BMSCs and MuSCs, and subsequently augmented their osteogenic capacity during osteogenic differentiation. During osteogenic induction by BMP-2, DEX also markedly affected cell proliferation in both BMSCs and MuSCs. In an in vivo ectopic bone formation model, bone formation in muscle-implanted scaffolds containing dexamethasone and BMP-2 was more than two fold higher than that in scaffolds containing BMP-2 alone. These results suggest that DEX potently enhances the osteogenic capability of BMP-2 and may thus decrease the quantity of BMP-2 required for clinical application, thereby reducing the complications caused by excessive doses of BMP-2 [257].

In Langenbach and Handschel's review [258], it has been concluded that Dex induces Runx2 expression by FHL2/β-catenin-mediated transcriptional activation and that Dex enhances Runx2 activity by upregulation of TAZ and MKP1. Ascorbic acid leads to the increased secretion of collagen type I (Col1), which in turn leads to increased Col1/α2β1 integrin-mediated intracellular signaling. The phosphate from β-Gly serves as a source for the phosphate in hydroxylapatite and in addition influences intracellular signaling molecules. Treatment with β-glycerolphosphate can result in nonosteogenic dystrophic mineralization.

Marcus et al. [259] found that DAG induced collagen I secretion from MSCs, which was further increased by the combination of DAG + BMP-2. In comparison, the collagen scaffold and the control samples showed no significant influence on collagen I secretion of MSCs. DAG stimulation of MSCs led also to a steady but not significant increase of BMP-2 level. A DAG and more, a DAG+BMP-2, stimulation increased the number of mesenchymal cells ($CD105^+/CD73^+$). To be summarized, BMP-2 enhances DAG-induced osteogenic differentiation in mesenchymal bone

marrow cells. Both agents interact in various ways and can modify osteoblastic bone formation.

8.5.6.3 Extracellular Antagonists of BMP-2

BMP antagonists were found in the Spemann organizer of Xenopus embryos as a molecule to inhibit BMP binding to their receptors. They are designated as noggin and chordin. After the first discovery of the BMP antagonists, numerous BMP antagonists, which are secretory proteins with cysteine arrangement structure, were found. The extracellular BMP antagonists represent a number of secreted peptides, which bind BMPs with high affinity and prevent their interaction with their specific receptors. Antagonists such as Noggin, Chordin, Gremlin (Grem1), and twisted gastrulation-1 (Twsg1) have been shown to inhibit BMP action in a range of different cell types and developmental stage-specific contexts.

Noggin binds to BMP-2 and BMP-4 with high affinity and to BMP-6 and BMP-7 with low affinity to prevent further action of BMP action. Chao Chen's study [253] showed that noggin suppression significantly decreased human MSC metabolism and DNA content on Days 3 and 6, and decreased total protein amount on Day 14. Noggin suppression also reduced the expression levels of osteoblastic genes, ALP, integrin-binding sialoprotein (IBSP), muscle segment homeobox gene (MSX2), osteocalcin (OC), osteopontin (OPN), and runt-related transcription factor-2 (RUNX2). Significantly decreased enzymatic ALP activity in noggin-suppressed group was evident. Moreover, noggin suppression decreased calcium deposits by BMP-2-induced osteoblasts. Collectively, this study showed that noggin suppression decreased viability and BMP-2-induced osteogenic differentiation of human MSCs, suggesting that noggin is stimulatory to osteogenesis of human MSCs. It has also been reported that endogenous signaling by BMP-2 controls the differentiation of embryonic stem cells into this lineage. Treatment of embryonic stem cell cultures with BMP antagonist noggin blocks this form of differentiation and induces the appearance of a novel cell type that can give rise to neural precursors [260].

Chordin as well as noggin binds BMPs and modulates BMP action. Using fluorescent labeling, BMP-2 was found to be internalized in HeLa cells via a clathrin-dependent pathway, with Noggin and Grem1 increasing BMP-2 uptake. By contrast, chordin decreased BMP-2 uptake, suggesting that BMP ligand and receptor interactions on the cell surface involve cooperative binding of BMP antagonists such as Noggin and Grem1 as well as other proteins such as the Endoglin CD105 coreceptor [261]. Francois NK Kwong [262] demonstrated that chordin knockdown accelerated early osteogenesis of MSCs and led to increased deposition of mineral at late time points. The suppression of chordin led to an increase in the bioavailability of endogenously produced BMP-2 to drive the differentiation of osteoprogenitors.

Twisted gastrulation (TSG) is expressed in lung, thymus, and kidney, and binds to BMPs to inhibit BMP action in osteoblasts. The action of TSG may be determined in cell-specific manner. Recent studies using TSG overexpression system in stromal/

preosteoblasts supported antagonistic activity of TSG on BMP signaling [257]. The mechanism for agonist activity of TSG is explained by indirect action: TSG promotes cleavage of coassociator chordin to enhance to BMP activity.

Gremlin is a glycoprotein that binds and antagonizes the actions of BMPs-2, -4, and -7. Gremlin appears to activate the extracellular regulated kinase (ERK) pathway in endothelial and tumor cells, and as a consequence to have direct cellular effects. Gremlin antagonizes BMP actions on the differentiation of marrow stromal cells and on osteoblastic function in vitro. Targeted osteoblast gremlin overexpression in vivo leads to spontaneous fractures and osteopenia. The reduction in bone volume is due to a decrease in osteoblast function and in number, confirming a possible effect of this BMP antagonist in the regulation of cell growth. Gremlin and other members of the differential screening-selected gene aberrative in neuroblastoma family, such as cerberus, coco, and sclerostin, inhibit BMP as well as Wnt activity, suggesting additional potential mechanisms of action for this group of BMP antagonists [263].

8.5.6.4 Interplay Between BMP-2 and Other Cytokines

Currently, commercially available rhBMP-2 is impregnated in an absorbable collagen sponge (ACS), which is used to retain rhBMP-2 at wound sites and to permit a slow release into the extracellular milieu. In the clinic, trauma, contamination, degradation of the ACS, and exogenous BMP-2 [264, 265], can trigger an exaggerated inflammatory environment, which is characterized by the recruitment of inflammatory cells and stem cells to the implantation site and the secretion of various inflammatory cytokines in serium, such as TNF-α, IL-1β, IL-8, and IL-6 [266]. Recently, the use of anti-inflammatory drugs such as bone morphogenetic protein-binding peptide [267], triptolide-micelles [268], and corticosteroids [269] was proved to reduce the inflammatory response and subsequently enhance the osteoinductive capacity of BMP-2. These results indicate that the low osteoinductive efficacy of BMP-2 may be a result of the exaggerated inflammatory environment. Huang's group has reported that TNF-α/IL-1β- and BMP-2-activated p38 and ERK1/2 signaling have opposing roles that converge on Runx2 to regulate osteoblastic differentiation [270]. The elucidation of these mechanisms may hasten the development of new strategies and improve the osteoinductive efficacy of BMP-2 in the clinic to enhance osteoblastic differentiation and bone formation. Their recent studies have demonstrated that synergy between IL-6 and sIL-6R promotes the cell surface translocation of BMPRIA and maintains the stability of BMPRI A expression, leading to enhanced BMP-2/ACS-induced bone regeneration [271].

In addition, the combined release of stromal cell-derived factor-1 (SDF-1) and BMP-2 enhanced the recruitment of osteogenic cells and angiogenesis, resulting in the synergistic effect on bone regeneration [272]. Kerstin Kleinschmidt et al. [273] produced a mutant growth and differentiation factor-5 (GDF-5) protein BB-1 which enhanced heterotopic bone formation in mice. Rabbit radius defects treated with a BB-1-coated collagen carrier healed earlier and with increased bone volume compared to BMP-2 and GDF-5 according to in vivo micro-CT follow-up. While BMP-2

callus often remained spongy, BB-1 supported earlier corticalis and marrow cavity formation, showing no pseudojoint persistence like with GDF-5. Thus, by combining positive angiogenic and osteogenic features of GDF-5 and BMP-2, only BB-1 restored the natural bone architecture within 12 weeks, rendering this promising growth factor variant especially promising for long bone regeneration.

TGF-βs and FGF-2, -4, and -6 have been proven to be inducers of osteoblast proliferation (a higher extent for TGF-β and FGF-2) and inhibitors of ALP activity and osteoblast mineralization, indicating potential application for in vitro bone growth induction in bone tissue engineering. To determine how fibroblast growth factor-2 (FGF-2) affects the BMP signaling pathway during BMP-induced ectopic bone formation, Yokio Nakamura et al. [274] implanted type I collagen disks containing constant amounts of BMP-2 (5 μg) onto the back muscles of adult male mice and confirmed that low doses of FGF-2 increased ectopic bone formation in vivo and high doses inhibited bone formation. Northern and/or Western blots of recovered muscle from the in vivo experiment and treated muscle-derived primary culture cells from the in vitro experiment revealed that low doses of FGF-2, but not high doses, increased the expression BMP receptor (BMPR)-1B, phosphorylated Smad1, Noggin, and Osteocalcin. Further indicated that low-dose FGF-2 may facilitate BMP-2-induced ectopic bone formation by altering the expression of BMPRs on the surface of bone forming progenitor cells.

In a summary, there is accumulating evidence to demonstrate that stem cell fate could be regulated by the chemical/mechanical properties of matrix materials, topography, geometry and hierarchy structure, and genetic clues delivered. It is obvious that stem cells have the ability to sense the microenvironment and give the response to the surroundings in a different manner. By well regulating the factors discussed above, the stem cells fates could be potentially directed to the desirable way for medical applications. However, the microenvironments surrounding the stem cells in vivo are integrated and complicated. Besides the factors we have discussed in this chapter, MSCs in vivo are also composed of microenvironmental cells that nurture stem cells and enable them to maintain tissue homeostasis, such as potential of hydrogen (pH), ionic concentration, cytokines secreted by immune cells, oxygen, and biomechanics introduced by implants. Numerous attempts have been made to reveal the interaction between the stem cells and microenvironment in vivo [275–277]. However, this field of research is still developing but there is great promise that stem cell fate could be controlled by designing advanced biomaterials and intelligent surfaces, which are responsive to their environment to fulfill bone healing demands.

8.6 Future Perspectives

Nanotopography and micro-/nanohierarchy structure have shown to offer important clues for controlling specific stem cell responses. Using these nanoscale features of biomaterials to guide stem cell fate holds great promise for bone repair and

regeneration. Furthermore, micro-/nanohierarchy structure could be designed on a single biomaterial to induce different stem cell responses by creating gradient pores, matching further scope for therapeutic applications. The main challenges in using these nanoscale features in the clinic applications are the precise control of nanostructures for large scale production. Therefore, it is necessary to make more attempts for the feasible and affordable technologies for large-scale production.

The immobilization of growth factors (i.e., rhBMP-2) or other bioactive agents to biomaterials has been confirmed to be a successful strategy in directing stem cell differentiation. it is highly desirable to study the effects of nanomaterials on protein structure and cell behavior and the regulatory mechanisms qualitatively and quantitatively. Many strategies have been applied for investigating material-cell interactions and directing stem cell fate, despite the current series of studies in which material surface physicochemical properties contribute to stem cell properties, including adhesion, spreading, migration, proliferation, and differentiation; however, the effects of bulk and surface topology on cellular properties, multicell interactions, and multicell self-assembly in 3D and complex environments need more investigation. Further studies are also required for successful clinical translation. A better control of the bioactivity, orientation and spacing, stability of the growth factors will realize the desired control of stem cell differentiation, enrich the connotation of material biology, and guide the design of new materials.

Another important issue is the long-term effects of biomaterials, the growth factors, and functional groups on the response of the stem cells/microenvironment in vivo. There is a great need to determine the better regulation of the inductive chemical clues for the desired response in a specific application. Since the cells other than stem cells in vivo would response to these material clues, further investigation need to be done to ensure the wanted functionalities without negative effects in vivo.

Many studies have investigated the effect of different factors on stem cell behavior. However, it becomes a big challenge to take into account more factors and even all possible parameters for guiding the stem cell fate. Advanced technology and more testing model systems need to develop for mimicking the microenvironments including stem cells, other surrounding cells, biomaterials, etc. All these knowledge and results allow us to better understand the intrinsic function and reparative properties of the stem cells and offer the great potential for more economical and clinically effective cell therapies for future medical applications.

References

1. Thomson JA, Itskovitz-Eldor J, Shapiro SS, Waknitz MA, Swiergiel JJ, Marshall VS, Jones JM. Blastocysts embryonic stem cell lines derived from human. Science. 1998;282(5391): 1145–7.
2. Becker AJ, McCulloch EA, Till JE. Cytological demonstration of the clonal nature of spleen colonies derived from transplanted mouse marrow cells. Nature. 1963;197:452–4.
3. http://stemcells.nih.gov/staticresources/info/basics/.

4. Sundelacruza S, Kaplana DL. Stem cell- and scaffold-based tissue engineering approaches to osteochondral regenerative medicine. Semin Cell Dev Biol. 2009;20(6):646–55.
5. Dawson JI, Oreffo ROC. Bridging the regeneration gap: stem cells, biomaterials and clinical translation in bone tissue engineering. Arch Biochem Biophys. 2008;473:124–31.
6. Rao BM, Zandstra PW. Culture development for human embryonic stem cell propagation: molecular aspects and challenges. Curr Opin Biotechnol. 2005;16:568–76.
7. Moore KA, Lemischka IR. Stem cells and their niches. Science. 2006;311:1880–5.
8. Pittenger MF, Mackay AM, Beck SC, Jaiswal RK, Douglas R, Mosca JD, Moorman MA, Simonetti DW, Craig S, Marshak DR. Multilineage potential of adult human mesenchymal stem cells. Science. 1999;284:143–7.
9. Ying QL, Nichols J, Chambers I, Smith A. BMP induction of Id proteins suppresses differentiation and sustains embryonic stem cell self-renewal in collaboration with STAT3. Cell. 2003;115(3):281–92.
10. Knoepfler PS. Deconstructing stem cell tumorigenicity: a roadmap to safe regenerative medicine. Stem Cells. 2009;27:1050–6.
11. Lodi D, Iannitti T, Palmieri B. Stem cells in clinical practice: applications and warnings. J Exp Clin Cancer Res. 2011;30(1):9.
12. Wang S, Qu X, Zhao R. Clinical applications of mesenchymal stem cells. J Hematol Oncol. 2012;5(19):1–9.
13. Branch MJ, Hashmani K, Dhillon P, Jones DR, Dua HS, Hopkinson A. Mesenchymal stem cells in the human corneal limbal stroma. Invest Ophthalmol Vis Sci. 2012;53(9):5109–16.
14. Brighton CT, Hunt RM. Early histologic and ultrastructural changes in microvessels of periosteal callus. J Orthop Trauma. 1997;11(4):244–53.
15. Gebler A, Zabel O, Seliger B. The immunomodulatory capacity of mesenchymal stem cells. Trends Mol Med. 2012;18(2):128–34.
16. Zaman WS, Makpol S, Sathapan S, Chua KH. Long-term in vitro expansion of human adipose-derived stem cells showed low risk of tumourigenicity. J Tissue Eng Regen Med. 2014;8:67–76.
17. Murphy MB, Moncivais K, Caplan AI. Mesenchymal stem cells: environmentally responsive therapeutics for regenerative medicine. Exp Mol Med. 2013;45:e54.
18. Tanna T, Sachan V. Mesenchymal stem cells: potential in treatment of neurodegenerative diseases. Curr Stem Cell Res Ther. 2014;9(6):513–21.
19. Lutolf MP, Hubbell JA. Synthetic biomaterials as instructive extracellular microenvironments for morphogenesis in tissue engineering. Nat Biotechnol. 2005;23(1):47–55.
20. Langer R, Tirrell DA. Designing materials for biology and medicine. Nature. 2004;428(6982):487–92.
21. Bao G, Suresh S. Cell and molecular mechanics of biological materials. Nat Mater. 2003;2(11):715–25.
22. Moghaddam MJ, Matsuda T. Molecular design of three-dimensional artificial extracellular matrix: photosensitive polymers containing cell adhesive peptide. J Polym Sci Pt A Polym Chem. 1993;31(6):1589–97.
23. Badylak SF. Xenogeneic extracellular matrix as a scaffold for tissue reconstruction. Transpl Immunol. 2004;12:367–77.
24. Freeman S. Biological science. 2nd ed. Hoboken, NJ: Pearson Prentice Hall; 2005.
25. Trappmann B, Gautrot JE, Connelly JT, et al. Extracellular-matrix tethering regulates stem-cell fate. Nat Mater. 2012;11(7):642–9.
26. Badylak SF, Freytes DO, Gilbert TW. Reprint of: extracellular matrix as a biological scaffold material: structure and function. Acta Biomater. 2015;23:S17–26.
27. Grazyna K, Victoria K-B. Galactose-specific receptors on liver cells. I. Hepatocyte and liver macrophage receptors differ in their membrane anchorage. Biochim Biophys Acta. 1985;847(1):108–14.
28. Rape AD, Zibinsky M, Murthy N, Kumar S. A synthetic hydrogel for the high-throughput study of cell-ECM interactions. Nat Commun. 2015;6:8129.

29. Navaro Y, Bleich-Kimelman N, Hazanov L, et al. Matrix stiffness determines the fate of nucleus pulposus–derived stem cells. Biomaterials. 2015;49:68–76.
30. Mann BK, Gobin AS, Tsai AT, et al. Smooth muscle cell growth in photopolymerized hydrogels with cell adhesive and proteolytically degradable domains: synthetic ECM analogs for tissue engineering. Biomaterials. 2001;22(22):3045–51.
31. Cambria E, Renggli K, Ahrens CC, et al. Covalent modification of synthetic hydrogels with bioactive proteins via sortase-mediated ligation. Biomacromolecules. 2015;16(8):2316–26.
32. Woo KM, Chen VJ, Ma PX. Nano-fibrous scaffolding architecture selectively enhances protein adsorption contributing to cell attachment. J Biomed Mater Res A. 2003;67(2):531–7.
33. Hersel U, Dahmen C, Kessler H. RGD modified polymers: biomaterials for stimulated cell adhesion and beyond. Biomaterials. 2003;24(24):4385–415.
34. Girotti A, Reguera J, Rodríguez-Cabello JC, et al. Design and bioproduction of a recombinant multi (bio) functional elastin-like protein polymer containing cell adhesion sequences for tissue engineering purposes. J Mater Sci Mater Med. 2004;15(4):479–84.
35. Loo Y, Lakshmanan A, Ni M, et al. Peptide bioink: self-assembling nanofibrous scaffolds for three-dimensional organotypic cultures. Nano Lett. 2015;15(10):6919–25.
36. Bhowmick S, Scharnweber D, Koul V. Co-cultivation of keratinocyte-human mesenchymal stem cell (hMSC) on sericin loaded electrospun nanofibrous composite scaffold (cationic gelatin/hyaluronan/chondroitin sulfate) stimulates epithelial differentiation in hMSCs: in vitro study. Biomaterials. 2016;88:83–96.
37. Liu Y, Shu XZ, Prestwich GD. Osteochondral defect repair with autologous bone marrow-derived mesenchymal stem cells in an injectable, in situ, cross-linked synthetic extracellular matrix. Tissue Eng. 2006;12(12):3405–16.
38. Khetan S, Guvendiren M, Legant WR, et al. Degradation-mediated cellular traction directs stem cell fate in covalently crosslinked three-dimensional hydrogels. Nat Mater. 2013;12(5): 458–65.
39. Kraehenbuehl TP, Zammaretti P, Van der Vlies AJ, et al. Three-dimensional extracellular matrix-directed cardioprogenitor differentiation: systematic modulation of a synthetic cell-responsive PEG-hydrogel. Biomaterials. 2008;29(18):2757–66.
40. Geiger B, Bershadsky A, Pankov R, Yamada KM. Transmembrane crosstalk between the extracellular matrix–cytoskeleton crosstalk. Nat Rev Mol Cell Biol. 2001;2:793–805.
41. Huang S, Ingber DE. The structural and mechanical complexity of cell-growth control. Nat Cell Biol. 1999;1:E131–8.
42. Reilly GC, Engler AJ. Intrinsic extracellular matrix properties regulate stem cell differentiation. J Biomech. 2010;43:55–62.
43. Discher DE, Mooney DJ, Zandstra PW. Growth factors, matrices, and forces combine and control stem cells. Science. 2009;324:1673–7.
44. Vogel V, Sheetz M. Local force and geometry sensing regulate cell functions. Nat Rev Mol Cell Biol. 2006;7:265–75.
45. Ana BF, Stefanie GL, Markus R, Mirren C, Tolga G, Katharina MW, Nicholas DS, Rui LR, Marcus T, Nuno MN. Differential regulation of osteogenic differentiation of stem cells on surface roughness gradients. Biomaterials. 2014;35:9023–32.
46. Elias CN, Oshida Y, Lima JHC, Muller CA. Relationship between surface properties (roughness, wettability and morphology) of titanium and dental implant removal torque. J Mech Behav Biomed Mater. 2008;1(3):234–42.
47. Hefti T, Frischherz M, Spencer ND, Hall H, Schlottig F. A comparison of osteoclast resorption pits on bone with titanium and zirconia surfaces. Biomaterials. 2010;31(28):7321–31.
48. Yeo A, Wong WJ, Khoo HH, Teoh SH. Surface modification of PCL-TCP scaffolds improve interfacial mechanical interlock and enhance early bone formation: an in vitro and in vivo characterization. J Biomed Mater Res A. 2010;92(1):311–21.
49. Liu Q, Wang W, Zhang L, Zhao L, Song W, Duan X, Zhang Y. Involvement of N-cadherin/b-catenin interaction in the micro/nanotopography induced indirect mechanotransduction. Biomaterials. 2014;35:6206–18.

50. Seo C, Jeong H, Feng Y, et al. Micropit surfaces designed for accelerating osteogenic differentiation of murine mesenchymal stem cells via enhancing focal adhesion and actin polymerization. Biomaterials. 2014;35:2245–52.
51. Wang PY, Li WT, Yu J, Tsai WB. Modulation of osteogenic, adipogenic and myogenic differentiation of mesenchymal stem cells by submicron grooved topography. J Mater Sci Mater Med. 2012;23(12):3015–28.
52. Wang P-Y, Yu J, Lin J-H, Tsai W-B. Modulation of alignment, elongation and contraction of cardiomyocytes through a combination of nanotopography and rigidity of substrates. Acta Biomater. 2011;7:3285–93.
53. Yim EK, Darling EM, Kulangara K, Guilak F, Leong KW. Nanotopography- induced changes in focal adhesions, cytoskeletal organization, and mechanical properties of human mesenchymal stem cells. Biomaterials. 2010;31:1299–306.
54. Kilian KA, Bugarija B, Lahn BT, Mrksich M. Geometric cues for directing the differentiation of mesenchymal stem cells. Proc Natl Acad Sci U S A. 2010;107:4872–7.
55. Salasznyk RM, Klees RF, Williams WA, Boskey A, Plopper GE. Focal adhesion kinase signaling pathways regulate the osteogenic differentiation of human mesenchymal stem cells. Exp Cell Res. 2007;313:22–37.
56. Tang W, Lin D, Yu YM, Niu HY, Guo H, Yuan Y, Liu CS. Bioinspired trimodal macro/micro/nano-porous scaffolds loading rhBMP-2 for complete regeneration of critical size bone defect. Acta Biomater. 2016;32:309–23.
57. Gwendolen CR, Adam JE. Intrinsic extracellular matrix properties regulate stem cell differentiation. J Biomech. 2010;43:55–62.
58. Dalby MJ, Gadegaard N, Riehle MO, Wilkinson CDW, Curtis ASG. Investigating filopodia sensing using arrays of defined nano-pits down to 35 nm diameter in size. Int J Biochem Cell Biol. 2004;36(10):2005–15.
59. Yim EK, Reano RM, Pang SW, Yee AF, Chen CS, Leong KW. Nanopattern induced changes in morphology and motility of smooth muscle cells. Biomaterials. 2005;26(26):5405–13.
60. Yim EK, Pang SW, Leong KW. Synthetic nanostructures inducing differentiation of human mesenchymal stem cells into neuronal lineage. Exp Cell Res. 2007;313(9):1820–9.
61. Doyle AD, Wang FW, Matsumoto K, Yamada KM. One-dimensional topography underlies three-dimensional fibrillar cell migration. J Cell Biol. 2009;184(4):481–90.
62. Dalby MJ, Gadegaard N, Tare R, Andar A, Riehle MO, Herzyk P, et al. The control of human mesenchymal cell differentiation using nanoscale symmetry and disorder. Nat Mater. 2007;6:997–1003.
63. Zhao L, Liu L, Wu Z, Zhang Y, Chu PK. Effects of micropitted/nanotubular titania topographies on bone mesenchymal stem cell osteogenic differentiation. Biomaterials. 2012;33:2629–41.
64. Zhao L, Mei S, Chu PK, Zhang Y, Wu Z. The influence of hierarchical hybrid micro/nano-textured titanium surface with titania nanotubes on osteoblast functions. Biomaterials. 2010;31:5072–82.
65. Liu Y, Manjubala I, Roschger P, Epari DR, Schell H, Lienau J, Bail HJ, Duda GN, Fratzl P. Characteristics of mineral particles in the callus during fracture healing in a sheep model. Calcif Tissue Int. 2008;82:S69–70.
66. Ramanujan S, Pluen A, McKee TD, Brown EB, Boucher Y, Jain RK. Diffusion and convection in collagen gels: implications for transport in the tumor interstitium. Biophys J. 2002;83:1650–60.
67. Sabetrasekh R, Tiainen H, Lyngstadaas SP, Reseland J, Haugen H. A novel ultra-porous titanium dioxide ceramic with excellent biocompatibility. J Biomater Appl. 2011;25(6):559–80.
68. Wen JH, Vincent LG, Fuhrmann A, Choi YS, Hribar KC, Taylor-Weiner H, Chen S, Engler AJ. Interplay of matrix stiffness and protein tethering in stem cell differentiation. Nat Mater. 2014;13:979–87.

69. Cyster L, Grant D, Howdle S, Rose F, Irvine D, Freeman D, Scotchford C, Shakesheff K. The influence of dispersant concentration on the pore morphology of hydroxyapatite ceramics for bone tissue engineering. Biomaterials. 2005;26:697–702.
70. Edwards SL, Werkmeister JA. Mechanical evaluation and cell response of woven polyetheretherketone scaffolds. J Biomed Mater Res A. 2012;100(12):3326–31.
71. Freyman TM, Yannas IV, Gibson LJ. Cellular materials as porous scaffolds for tissue engineering. Prog Mater Sci. 2001;46:273–82.
72. Kumara A, Nunea KC, Murra LE, Misra RDK. Biocompatibility and mechanical behavior of three-dimensional scaffolds for biomedical devices: process–structure–property paradigm. Int Mater Rev. 2016;16(1):20–40.
73. Sun T, Donoghue PS, Higginson JR, Gadegaard N, Barnett SC, Riehle MO. The interactions of astrocytes and fibroblasts with defined pore structures in static and perfusion cultures. Biomaterials. 2011;32(8):2021–31.
74. Lu JX, Flautre B, Anselme K, Hardouin P, Gallur A, Descamps M, Thierry B. Role of interconnections in porous bioceramics on bone recolonization in vitro and in vivo. J Mater Sci Mater Med. 1999;10(2):111–20.
75. Mandal BB, Kundu SC. Cell proliferation and migration in silk fibroin 3D scaffolds. Biomaterials. 2009;30(15):2956–65.
76. Berger M, Probst F, Schwartz C, Cornelsen M, Seitz H, Ehrenfeld M, Otto S. A concept for scaffold-based tissue engineering in alveolar cleft osteoplasty. J Craniomaxillofac Surg. 2015;43(6):830–6.
77. Nam J, Johnson J, Lannutti JJ, Agarwala S. Modulation of embryonic mesenchymal progenitor cell differentiation via control over pure mechanical modulus in electrospun nanofibers. Acta Biomater. 2011;7(4):1516–24.
78. Lien SM, Ko LY, Huang TJ. Effect of pore size on ECM secretion and cell growth in gelatin scaffold for articular cartilage tissue engineering. Acta Biomater. 2009;5(2):670–9.
79. Loh QL, Choong C. Three-dimensional scaffolds for tissue engineering applications: role of porosity and pore size. Tissue Eng Part B Rev. 2013;19(6):485–502.
80. Akay G, Birch MA, Bokhari MA. Microcellular polyHIPE polymer supports osteoblast growth and bone formation in vitro. Biomaterials. 2004;25(18):3991–4000.
81. Ahn G, Kim Y, Lee S-W, Jeong Y, Son H, Lee D. Effect of heterogeneous multi-layered gelatin scaffolds on the diffusion characteristics and cellular activities of preosteoblasts. Macromol Res. 2014;22:99–107.
82. Im GI, Ko JY, Lee JH. Chondrogenesis of adipose stem cells in a porous polymer scaffold: influence of the pore size. Cell Transplant. 2012;21(11):2397–405.
83. Carlier A, van Gastel N, Geris L, Carmeliet G, Van Oosterwyck H. Size does matter: an integrative in vivo-in silico approach for the treatment of critical size bone defects. PLoS Comput Biol. 2014;10(11):e1003888.
84. Mygind T, Stiehler M, Baatrup A, et al. Mesenchymal stem cell ingrowth and differentiation on coralline hydroxyapatite scaffolds. Biomaterials. 2007;28:1036–104.
85. Akhmanova M, Osidak E, Domogatsky S, Rodin S, Domogatskaya A. Physical, spatial, and molecular aspects of extracellular matrix of in vivo niches and artificial scaffolds relevant to stem cells research. Stem Cells Int. 2015;2015:167025.
86. Lee JH, Lee SJ, Khang G, Lee HB. Interaction of fibroblasts on polycarbonate membrane surfaces with different micropore sizes and hydrophilicity. J Biomater Sci Polym Ed. 1999;10 (3):283–94.
87. Guo H, Su J, Wei J, Kong H, Liu C. Biocompatibility and osteogenicity of degradable Ca-deficient hydroxyapatite scaffolds from calcium phosphate cement for bone tissue engineering. Acta Biomater. 2009;5(1):268–78.
88. Habibovic P, Yuan H, van der Valk CM, Meijer G, van Blitterswijk CA, de Groot K. 3D microenvironment as essential element for osteoinduction by biomaterials. Biomaterials. 2005;26(17):3565–75.

89. Kruyt MC, Wilson CE, de Bruijn JD, van Blitterswijk CA, Oner CF, Verbout AJ, Dhert WJ. The effect of cell-based bone tissue engineering in a goat transverse process model. Biomaterials. 2006;27(29):5099–106.
90. Chan CK, Kumar TS, Liao S, Murugan R, Ngiam M, Ramakrishnan S. Biomimetic nanocomposites for bone graft applications. Nanomedicine (Lond). 2006;1(2):177–88.
91. Prall WC, Haasters F, Heggebö J, Polzer H, Schwarz C, Gassner C, Grote S, Anz D, Jäger M, Mutschler W, Schieker M. Mesenchymal stem cells from osteoporotic patients feature impaired signal transduction but sustained osteoinduction in response to BMP-2 stimulation. Biochem Biophys Res Commun. 2013;440(4):617–22.
92. Peyton SR, Kalcioglu ZI, Cohen JC, Runkle AP, Van Vliet KJ, Lauffenburger DA, Griffith LG. Marrow-derived stem cell motility in 3D synthetic scaffold is governed by geometry along with adhesivity and stiffness. Biotechnol Bioeng. 2011;108(5):1181–93.
93. Perez RA, Mestres G. Role of pore size and morphology in musculo-skeletal tissue regeneration. Mater Sci Eng C Mater Biol Appl. 2016;61:922–39.
94. Kim JS, Cha JK, Cho AR, Kim MS, Lee JS, Hong JY, Choi SH, Jung UW. Acceleration of bone regeneration by BMP-2-loaded collagenated biphasic calcium phosphate in rabbit sinus. Clin Implant Dent Relat Res. 2015;17(6):1103–13.
95. Lan Levengood SK, Polak SJ, Poellmann MJ, et al. The effect of BMP-2 on micro- and macroscale osteointegration of biphasic calcium phosphate scaffolds with multiscale porosity. Acta Biomater. 2010;6(8):3283–91.
96. Yanagisawa T, Tsuneo S, Shimizu T, Kuroda K, Kato C. The preparation of alkyltrimethylammonium-kanemite complexes and their conversion to microporous materials. Bull Chem Soc Jpn. 1990;63:988–92.
97. Simovic S, Ghouchi-Eskandar N, Sinn AM, Losic D, Prestidge CA. Silica materials in drug delivery applications. Curr Drug Discov Technol. 2011;8(3):269–76.
98. Izquierdo-Barbaa I, Ruiz-Gonzálezb L, Doadrioa JC. Tissue regeneration: a new property of mesoporous materials. Solid State Sci. 2005;8:983–9.
99. Gough JE, Notingher I, Hench LL. Osteoblast attachment and mineralized nodule formation on rough and smooth 45S5 bioactive glass monoliths. J Biomed Mater Res A. 2004;68(4):640–50.
100. Yun HS, Kim SH, Khang D, Choi J, Kim HH, Kang M. Biomimetic component coating on 3D scaffolds using high bioactivity of mesoporous bioactive ceramics. Int J Nanomedicine. 2011;6:2521–31.
101. Zhu Y, Kaskel S. Comparison of the in vitro bioactivity and drug release property of mesoporous bioactive glasses (MBGs) and bioactive glasses (BGs) scaffolds. Microporous Mesoporous Mater. 2009;118(1-3):176–82.
102. Termine JD, Eanes ED. Comparative chemistry of amorphous and apatitic calcium phosphate preparations. Calcif Tissue Res. 1972;10(3):171–97.
103. Xia W, Chang J. Preparation, in vitro bioactivity and drug release property of well-ordered mesoporous 58S bioactive glass. J Non Crystall Solids. 2008;354(12):1338–41.
104. Kaur G, Pickrell G, Sriranganathan N, Kumar V, Homa D. Review and the state of the art: sol-gel and melt quenched bioactive glasses for tissue engineering. J Biomed Mater Res B Appl Biomater. 2016;104:1248. https://doi.org/10.1002/jbm.b.33443.
105. Horcajada P, Ramila A, Boulahya K, Gonzalez-Calbet J, Vallet-Regi M. Bioactivity in ordered mesoporous materials. Solid State Sci. 2004;X6:1295–300.
106. Aghaeia H, Nourbakhshb AA, Karbasic S, et al. Investigation on bioactivity and cytotoxicity of mesoporous nano-composite MCM-48/hydroxyapatite for ibuprofen drug delivery. Ceram Int. 2014;40(5):7355–62.
107. Yan X, Deng H, Huang X, et al. Mesoporous bioactive glasses. I. Synthesis and structural characterization. J Non Crystall Solids. 2015;10:3209–17.
108. Bae WC, Law AW, Amiel D, Sah RL. Sensitivity of indentation testing to step-off edges and interface integrity in cartilage repair. Ann Biomed Eng. 2004;32(3):360–9.

109. Zhang H, Landmann F, Zahreddine H, et al. A tension-induced mechanotransduction pathway promotes epithelial morphogenesis. Nature. 2011;471(7336):99–103.
110. Okolicsanyi RK, Griffiths LR, Haupt LM. Mesenchymal stem cells, neural lineage potential, heparan sulfate proteoglycans and the matrix. Dev Biol. 2014;388(1):1–10.
111. Eroshenko N, Ramachandran R, Yadavalli VK, Rao RR. Effect of substrate stiffness on early human embryonic stem cell differentiation. J Biol Eng. 2013;7(1):7.
112. Hosseinkhani M, Shirazi R, Rajaei F, Mahmoudi M, Mohammadi N, Abbasi M. Engineering of the embryonic and adult stem cell niches. Iran Red Crescent Med J. 2013;15(2):83–92.
113. Zhao W, Li X, Liu X, Zhang N, Wen X. Effects of substrate stiffness on adipogenic and osteogenic differentiation of human mesenchymal stem cells. Mater Sci Eng C Mater Biol Appl. 2014;40:316–23.
114. Yilgor P, Sousa RA, Reis RL, et al. 3D plotted PCL scaffolds for stem cell based bone tissue engineering. Macromol Symp. 2008;269:92–9.
115. Her GJ, Wu HC, Chen MH, Chen MY, Chang SC, Wang TW. Control of three-dimensional substrate stiffness to manipulate mesenchymal stem cell fate toward neuronal or glial lineages. Acta Biomater. 2013;9(2):5170–80.
116. Wen JH, Vincent LG, Fuhrmann A, et al. Interplay of matrix stiffness and protein tethering in stem cell differentiation. Nat Mater. 2014;13(10):979–87.
117. Wang L-S, Boulaire J, Chan PPY, Chung JE, Kurisawa M. The role of stiffness of gelatin-hydroxyphenylpropionic acid hydrogels formed by enzyme-mediated crosslinking on the differentiation of human mesenchymal stem cell. Biomaterials. 2010;31(33):8608–16.
118. Wang P-Y, Tsai W-B, Voelcker NH. Screening of rat mesenchymal stem cell behaviour on polydimethylsiloxane stiffness gradients. Acta Biomater. 2012;8(2):519–30.
119. Flanagan LA, Ju YE, Marg B, et al. Janmey Neurite branching on deformable substrates. Neuroreport. 2002;13:2411–5.
120. Kim TH, An DB, Oh SH, et al. Creating stiffness gradient polyvinyl alcohol hydrogel using a simple gradual freezing-thawing method to investigate stem cell differentiation behaviors. Biomaterials. 2015;40:51–60.
121. Li Z, Gong Y, Sun S, et al. Differential regulation of stiffness, topography, and dimension of substrates in rat mesenchymal stem cells. Biomaterials. 2013;34(31):7616–25.
122. Rowlands AS, George PA, Cooper-White JJ. Directing osteogenic and myogenic differentiation of MSCs: interplay of stiffness and adhesive ligand presentation. Am J Physiol Cell Physiol. 2008;295(4):C1037–44.
123. Evans ND, Minelli C, Gentleman E, et al. Substrate stiffness affects early differentiation events in embryonic stem cells. Eur Cell Mater. 2009;18:1–13.
124. Tse JR, Engler AJ. Stiffness gradients mimicking in vivo tissue variation regulate mesenchymal stem cell fate. PloS One. 2011;6(1):e15978.
125. Ghosh K, Pan Z, Guan E, et al. Cell adaptation to a physiologically relevant ECM mimic with different viscoelastic properties. Biomaterials. 2007;28(4):671–9.
126. Isenberg BC, Dimilla PA, Walker M, Kim S, Wong JY. Vascular smooth muscle cell durotaxis depends on substrate stiffness gradient strength. Biophys J. 2009;97(5):1313–22.
127. Du J, Chen X, Liang X, et al. Integrin activation and internalization on soft ECM as a mechanism of induction of stem cell differentiation by ECM elasticity. Proc Natl Acad Sci U S A. 2011;108(23):9466–71.
128. Shih YR, Tseng KF, Lai HY, Lin CH, Lee OK. Matrix stiffness regulation of integrin-mediated mechanotransduction during osteogenic differentiation of human mesenchymal stem cells. J Bone Miner Res. 2011;26(4):730–8.
129. Yeung T, Georges PC, Flanagan LA, et al. Effects of substrate stiffness on cell morphology, cytoskeletal structure, and adhesion. Cell Motil Cytoskeleton. 2005;60:24–34.
130. Jiang L, Sun Z, Chen X, et al. Cells sensing mechanical cues: stiffness influences the lifetime of cell-extracellular matrix interactions by affecting the loading rate. ACS Nano. 2016;10(1):207–17.

131. Albro MB, Chahine NO, Li R, Yeager K, Hung CT, Ateshian GA. Dynamic loading of deformable porous media can induce active solute transport. J Biomech. 2008;41:3152–7.
132. García AJ. Get a grip: integrins in cell-biomaterial interactions. Biomaterials. 2005;26:7525–9.
133. Berrier AL, Yamada KM. Cell-matrix adhesion. J Cell Physiol. 2007;213:565–73.
134. Hynes RO. Integrins: bidirectional, allosteric signaling machines. Cell. 2002;110:673–87.
135. García AJ, Boettiger D. Integrin-fibronectin interactions at the cell-material interface: initial integrin binding and signaling. Biomaterials. 1999;20:2427–33.
136. Dumbauld DW, Michael KE, Hanks SK, García AJ. Focal adhesion kinasedependent regulation of adhesive forces involves vinculin recruitment to focal adhesions. Biol Cell. 2010;102: 203–13.
137. Keselowsky BG, Collard DM, Garcia AJ. Surface chemistry modulates fibronectin conformation and directs integrin binding and specificity to control cell adhesion. J Biomed Mater Res A. 2003;66:247–59.
138. Galbraith CG, Yamada KM, Sheetz MP. The relationship between force and focal complex development. J Cell Biol. 2002;159:695–705.
139. ter Brugge PJ, Torensma R, De Ruijter JE, Figdor CG, Jansen JA. Modulation of integrin expression on rat bone marrow cells by substrates with different surface characteristics. Tissue Eng. 2002;8:615–26.
140. Khang D, Kim SY, Liu-Snydera P, Palmore GT, Durbinc SM, Webster TJ. Enhanced fibronectin adsorption on carbon nanotube/poly(carbonate) urethane: independent role of surface nano-roughness and associated surface energy. Biomaterials. 2007;28:4756–68.
141. Rodriguez JP, Gonzalez M, Rios S, Cambiazo V. Cytoskeletal organization of human mesenchymal stem cells (MSC) changes during their osteogenic differentiation. J Cell Biochem. 2004;93:721–31.
142. Engler AJ, Sen S, Sweeney HL, Discher DE. Matrix elasticity directs stem cell lineage specification. Cell. 2006;126:677–89.
143. Khang D, Choi J, Im YM, Kim YJ, Jang JH, Park JW, et al. Role of subnano-, nano and submicron-surface features on osteoblast differentiation of bone marrow mesenchymal stem cells. Biomaterials. 2012;33:5997–6007.
144. Leitinger B, McDowall A, Stanley P, Hogg N. The regulation of integrin function by Ca^{2+}. Biochim Biophys Acta. 2000;1498:91–8.
145. Baneres JL, Roquet F, Martin A, Parello J. A minimized human integrin alpha 5 beta 1 that retains ligand recognition. J Biol Chem. 2000;275:5888–903.
146. Grzesiak J, Davis G, Kirchhofer D, Pierschbacher M. Regulation of alpha 2 beta 1-mediated fibroblast migration on type I collagen by shifts in the concentrations of extracellular Mg^{2+} and Ca^{2+}. J Cell Biol. 1992;117(5):1109–17.
147. Zhang J, MaXY LD, Shi HS, Yuan Y, Tang W, Zhou HJ, Guo H, Qian JC, Liu CS. Magnesium modification of a calcium phosphate cement alters bone marrow stromal cell behavior via an integrin-mediated mechanism. Biomaterials. 2015;53:251–64.
148. Shie MY, Ding SJ. Integrin binding and MAPK signal pathways in primary cell responses to surface chemistry of calcium silicate cements. Biomaterials. 2013;34:6589–606.
149. Curran JM, Chen R, Hunt JA. Controlling the phenotype and function of mesenchymal stem cells in vitro by adhesion to silane-modified clean glass surfaces. Biomaterials. 2005;34:7057–67.
150. Viswanathan P, Chirasatitsin S, Ngamkham K, Engler AJ, Battaglia G. Cell instructive microporous scaffolds through interface engineering. J Am Chem Soc. 2012;134(49): 20103–9.
151. Dee KC, Anderson TT, Bizios R. Design and function of novel osteoblast-adhesive peptides for chemical modification of biomaterials. J Biomed Mater Res. 1998;40:371–7.
152. Rezania A, Johnson R, Lefkow AR, Healy KE. Bioactivation of metal oxide surfaces. 1. Surface characterization and cell response. Langmuir. 1999;15:6931–9.
153. Xiao S-J, Textir M, Spencer ND. Covalent attachment of celladhesive (Arg-Gly-Asp)-containing peptides to titanium surface. Langmuir. 1998;14:5507–16.

154. Massia SP, Hubbell JA. Covalently attached GRGD on polymer surfaces promotes biospecific adhesion of mammalian cells. Ann N Y Acad Sci. 1990;589:261–70.
155. Sugawara T, Matsuda T. Photochemical surface derivatization of a peptide containing Arg-Gly-Asp (RGD). J Biomed Mater Res. 1995;29:1047–52.
156. Houseman BT, Mrksich M. The microenvironment of immobilized Arg-Gly-Asp peptides is an important determinant of cell adhesion. Biomaterials. 2001;22:943–55.
157. Bearinger JP, Castner DG, Healy KE. Biomolecular modification of p(AAm-co-EG/AA) IPNs supports osteoblast adhesion and phenotypic expression. J Biomater Sci Polym Ed. 1998;9:629–52.
158. Kao WJ, Lee D, Schense JC, Hubbell JA. Fibronectin modulates macrophage adhesion and FBGC formation: the role of RGD, PHSRN, and PRRARV domains. J Biomed Mater Res. 2000;55:79–88.
159. Yang F, Williams CG, Wang DA, Lee H, Manson PN, Elisseeff J. The effect of incorporating RGD adhesive peptide in polyethylene glycol diacrylate hydrogel on osteogenesis of bone marrow stromal cells. Biomaterials. 2005;26(30):5991–8.
160. Cao FY, Yin WN, Fan JX, Tao L, Qin SY, Zhuo RX, Zhang XZ. Evaluating the effects of charged oligopeptide motifs coupled with rgd on osteogenic differentiation of mesenchymal stem cells. ACS Appl Mater Interfaces. 2015;7(12):6698–705.
161. Chien HW, Fu SW, Shih AY, Tsai WB. Modulation of the stemness and osteogenic differentiation of human mesenchymal stem cells by controlling RGD concentrations of poly (carboxybetaine) hydrogel. Biotechnol J. 2014;9(12):1613–23.
162. Wang X, Li SY, Yan C, Liu P, Ding JD. Fabrication of RGD micro/nanopattern and corresponding study of stem cell differentiation. Nano Lett. 2015;15(3):1457–67.
163. Brandt K, Wolff MF, Salikov V, Heinrich S, Schneider GA. A novel method for a multi-level hierarchical composite with brick-and-mortar structure. Sci Rep. 2013;3:2322.
164. Thiagarajan G, Deshmukh K, Wang Y, Misra A, Katz JL, Spencer P. Nano finite element modeling of the mechanical behavior of biocomposites using multi-scale (virtual internal bond) material models. J Biomed Mater Res A. 2007;83(2):332–44.
165. Dhandayuthapani B, Yoshida Y, Maekawa T, Kumar DS. Polymeric scaffolds in tissue engineering application: a review. Int J Polym Sci. 2011;2011:290602.
166. Kim K, Yeatts A, Dean D, Fisher JP. Stereolithographic bone scaffold design parameters: osteogenic differentiation and signal expression. Tissue Eng Part B Rev. 2010;16(5):523–39.
167. Cabanas-Polo S, Philippart A, Boccardi E, et al. Facile production of porous bioactive glass scaffolds by the foam replica technique combined with sol-gel/electrophoretic deposition. Ceram Int. 2016;42(5):5772–7.
168. Yun HS, Kim SE, Hyeon YT. Design and preparation of bioactive glasses with hierarchical porenetworks. Chem Commun. 2007;21:2139–41.
169. Li X, Wang X, Chen H, Shi J. Hierarchically porous bioactive glass scaffolds synthesized with a PUF and P123 contemplated approach. Chem Mater. 2007;19(17). https://doi.org/10.1021/cm0708564.
170. Zhu M, Zhang J, Zhou Y, et al. Preparation and characterization of magnetic mesoporous bioactive glass/carbon composite scaffolds. J Chem. 2013;2013:893479.
171. Dorozhkin SV. Biocomposites and hybrid biomaterials based on calcium orthophosphates. Biomatter. 2011;1(1):3–56.
172. Esen S, Bor ET, Bor S. Characterization of loose powder sintered porous titanium and Ti6Al4V alloy. Turk J Eng Environ Sci. 2009;33:207–19.
173. Murr LE, Gaytan SM, Martinez E, Medina F, Wicker RB. Next generation orthopaedic implants by additive manufacturing using electron beam melting. Int J Biomater. 2012;2012:245727.
174. Mitra J, Tripathi G, Sharmaaand A, Basu B. Scaffolds for bone tissue engineering: role of surfacepatterning on osteoblast response. RSC Adv. 2013;3:11073–94.
175. Zheng W, Zhang W, Jiang X. Precise control of cell adhesion by combination of surface chemistry and soft lithography. Adv Healthc Mater. 2013;2(1):95–108.

176. Kim DH, Han K, Gupta K, et al. Mechanosensitivity of fibroblast cell shape and movement to anisotropic substratum topography gradients. Biomaterials. 2009;30(29):5433–44.
177. Uttayarat P, Chen M, Li M, et al. Microtopography and flow modulate the direction of endothelial cell migration. Am J Physiol Heart Circ Physiol. 2008;294(2):H1027–35.
178. Lee MR, Kwon KW, Jung H, et al. Direct differentiation of human embryonic stem cells into selective neurons on nanoscale ridge/groove pattern arrays. Biomaterials. 2010;31(15): 4360–6.
179. Baker DW, Liu X, Weng H, Luo C, Tang L. Fibroblast/fibrocyte: surface interaction dictates tissue reactions to micropillar implants. Biomacromolecules. 2011;12(4):997–1005.
180. Ng CK, Yu KN. Proliferation of epithelial cells on PDMS substrates with micropillars fabricated with different curvature characteristics. Biointerphases. 2012;7:21.
181. Nimni ME. Polypeptide growth factors: targeted delivery systems. Biomaterials. 1997;18(18): 1201–25.
182. Amsden B. Novel biodegradable polymers for local growth factor delivery. Eur J Pharm Biopharm. 2015;97(Pt B):318–28.
183. Lee K, Silva EA, Mooney DJ. Growth factor delivery-based tissue engineering: general approaches and a review of recent developments. J R Soc Interface. 2011;8(55):153–70.
184. Werner S, Grose R. Regulation of wound healing by growth factors and cytokines. Physiol Rev. 2003;83:835–70.
185. Xiao Y, Reis LA, Zhao Y, Radisic M. Modifications of collagen-based biomaterials with immobilized growth factors or peptides. Methods. 2015;84:44–52.
186. Tada S, Kitajima T, Ito Y. Design and synthesis of binding growth factors. Int J Mol Sci. 2012;13(5):6053–72.
187. Iwamoto R, Mekada E. Heparin-binding EGF-like growth factor: a juxtacrine growth factor. Cytokine Growth Factor Rev. 2000;11(4):335–44.
188. Pagès G, Pouysségur J. Transcriptional regulation of the vascular endothelial growth factor gene—a concert of activating factors. Cardiovasc Res. 2005;65(3):564–73.
189. Yadin D, Knaus P, Mueller TD. Structural insights into BMP receptors: specificity, activation and inhibition. Cytokine Growth Factor Rev. 2016;27:13–34.
190. Yoon BS, Lyons KM. Multiple functions of BMPs in chondrogenesis. J Cell Biochem. 2004;93:93–103.
191. Sellers RS, Peluso D, Morris EA. The effect of recombinant human bone morphogenetic protein-2 (rhBMP-2) on the healing of full-thickness defects of articular cartilage. J Bone Joint Surg Am. 1997;79:1452–63.
192. Louwerse RT, Heyligers IC, Klein-Nulend J, et al. Use of recombinant human osteogenic protein-1 for the repair of subchondral defects in articular cartilage in goats. J Biomed Mater Res. 2000;49:506–16.
193. Liu H, Peng H, Wu Y, et al. The promotion of bone regeneration by nanofibrous hydroxyapatite/chitosan scaffolds by effects on integrin-BMP/Smad signaling pathway in BMSCs. Biomaterials. 2013;34:4404–17.
194. Lecanda F, Avioli LV, Cheng S-L. Regulation of bone matrix protein expression and induction of differentation of human osteoblasts and human bone marrow stromal cells by bone morphogenetic protein-2. J Cell Biochem. 1997;67:386–9.
195. Nauth A, Ristiniemi J, McKee MD, Schemitsch EH. Bone morphogenetic proteins in open fractures: past, present, future. Injury. 2009;40(Suppl. 3):S27–31.
196. Kanczler JM, Oreffo ROC. Osteogenesis and angiogenesis: the potential for engineering bone. Eur Cell Mater. 2008;15:110–4.
197. La WG, Park S, Yoon HH. Delivery of a therapeutic protein for bone regeneration from a substrate coated with graphene oxide. Small. 2013;9(23):4051–60.
198. Dimitriou R, Tsiridis E, Giannoudis PV. Current concepts of molecular aspects of bone healing. Injury. 2005;36:1392–404.

199. Chappard D, Aguado E, Hure G, et al. The early remodeling phases around titanium implants: a histomorphometric assessment of bone quality in a 3 and 6 months study in sheep. Int J Oral Maxillofac Implants. 1999;14:189–96.
200. Hall J, Sorensen RG, Wozney JM, Wikesjo UM. Bone formation at rhBMP-2-coated titanium implants in the rat ectopic model. J Clin Periodontol. 2007;34:444–51.
201. Kim D, Herr AE. Protein immobilization techniques for microfluidic assays. Biomicrofluidics. 2013;7(4):41501(1-47).
202. Hong J, Shah NJ, Drake AC, DeMuth PC, Lee JB, Chen J, Hammond PT. Graphene multilayers as gates for multi-week sequential release of proteins from surfaces. ACS Nano. 2012;6(1):81–8.
203. Rosario C, Rodriguez-Evora M, Reyes R. valuation of nanostructure and microstructure of bone regenerated by BMP-2-porous scaffolds. Biomed Mater. 2015;103(9):2998–3011.
204. Qin J, He H, Zhang W, Chen F, Liu C. Effective incorporation of rhBMP-2 on implantable titanium disks with microstructures by using electrostatic spraying deposition. RSC Adv. 2016;6:51914–23.
205. Reed S, Wu B. Sustained growth factor delivery in tissue engineering applications. Ann Biomed Eng. 2014;42(7):1528–36.
206. Foldbjerg R, Dang D, AAutrup H. Cytotoxicity and genotoxicity of silver nanoparticles in the human lung cancer cell line, a549. Arch Toxicol. 2011;85:743–50.
207. Tian Y, Li Z, Zhang W, et al. Size-mediated adsorption dynamics, conformation and bioactivity of bone morphogenetic protein-2 onto silica nanoparticles. J Nanosci Nanotechnol. 2016;16:5528–36.
208. Li ZY, Gan Q, Zhang WJ, et al. Surface-induced conformational and functional changes of bone morphogenetic protein-2 adsorbed onto single-walled carbon nanotubes. Biochem Biophys Res Commun. 2013;440:215–21.
209. Huang B, Yuan Y, Ding S, et al. Nanostructured hydroxyapatite surfaces-mediated adsorption alters recognition of bmp receptor IA and bioactivity of bone morphogenetic protein-2. Acta Biomater. 2015;27:275–85.
210. Lin D, Chai Y, Ma Y, et al. Rapid initiation of guided bone regeneration driven by spatiotemporal delivery of IL-8 and BMP-2 from hierarchical MBG-based scaffold. Biomaterials. 2017;196:122–37.
211. Cai L, Lin D, Chai Y, et al. MBG scaffolds containing chitosan microspheres for binary delivery of IL-8 and BMP-2 for bone regeneration. J Mater Chem B. 2018;6:4453–65.
212. Kang Y, Kim S, Khademhosseini A, Yang Y. Creation of bony microenvironment with CaP and cell-derived ECM to enhance human bone-marrow MSC behavior and delivery of BMP-2. Biomaterials. 2011;32:6119–30.
213. Jeon O, Song SJ, Kang SW, Putnam AJ, Kim BS. Enhancement of ectopic bone formation by bone morphogenetic protein-2 released from a heparin-conjugated poly(L-lactic-co-glycolic acid) scaffold. Biomaterials. 2007;28:2763–71.
214. Mercado AE, Ma J, He X, Jabbari E. Release characteristics and osteogenic activity of recombinant human bone morphogenetic protein-2 grafted to novel self-assembled poly (lactide-co-glycolide fumarate) nanoparticles. J Control Release. 2009;140:148–56.
215. Shen H, Hu X, Yang F, Bei J, Wang S. The bioactivity of rhBMP-2 immobilized poly(lactide-co-glycolide) scaffolds. Biomaterials. 2009;30:3150–7.
216. Hoang QQ, Sicheri F, Howard AJ, Yang DS. Bone recognition mechanism of porcine osteocalcin from crystal structure. Nature. 2003;425:977–80.
217. Mi L, Giarmarco MM, Shao Q, Jiang S. Divalent cation-mediated polysaccharide interactions with zwitterionic surfaces. Biomaterials. 2012;33:2001–6.
218. Zhang Y, Jiang T, Zheng Y, Zhou P. Interference of EGCG on the Zn(II)-induced conformational transition of silk fibroin as a model protein related to neurodegenerative diseases. Soft Matter. 2012;8:5543–9.

219. Zhang W, He H, Tian Y, Gan Q, Zhang J, Yuan Y, et al. Calcium ion-induced formation of beta-sheet/-turn structure leading to alteration of osteogenic activity of bone morphogenetic protein-2. Sci Rep. 2015;5:12694–700.
220. Zhang W, Tian Y, He H, et al. Strontium attenuates rhBMP-2-induced osteogenic differentiation via formation of Sr-rhBMP-2 complex and suppression of Smad-dependent signaling pathway. Acta Biomater. 2016;33:290–300.
221. Lee K-S, Kim H-J, Li Q-L, Chi X-Z, Ueta C, Komori T, et al. Runx2 is a common target of transforming growth factor β1 and bone morphogenetic protein 2, and cooperation between Runx2 and Smad5 induces osteoblast-specific gene expression in the pluripotent mesenchymal precursor cell line C2C12. Mol Cell Biol. 2000;20:8783–92.
222. Li J, Khavandgar Z, Lin S-H, Murshed M. Lithium chloride attenuates BMP-2 signaling and inhibits osteogenic differentiation through a novel WNT/GSK3- independent mechanism. Bone. 2011;48:321–31.
223. Barradas AM, Fernandes HA, Groen N, Chai YC, Schrooten J, van de Peppel J, van Leeuwen JP, van Blitterswijk CA, de Boer J. A calcium-induced signaling cascade leading to osteogenic differentiation of human bone marrow-derived mesenchymal stromal cell. Biomaterials. 2012;33(11):3205–15.
224. Shih Y-RV, Hwang Y, Phadke A, Kang H, Hwang NS, Caro EJ, et al. Calcium phosphate-bearing matrices induce osteogenic differentiation of stem cells through adenosine signaling. Proc Natl Acad Sci U S A. 2014;111:990–5.
225. Ren X, Bischoff D, Weisgerber DW, Lewis MS, Tu V, Yamaguchi DT, et al. Osteogenesis on nanoparticulate mineralized collagen scaffolds via autogenous activation of the canonical BMP receptor signaling pathway. Biomaterials. 2015;50:107–14.
226. Verberckmoes SC, De Broe ME, D'Haese PC. Dose-dependent effects of strontium on osteoblast function and mineralization. Kidney Int. 2003;64:534–43.
227. Xin Y, Jiang J, Huo K, Hu T, Chu PK. Bioactive $SrTiO_3$ nanotube arrays: strontium delivery platform on Ti-based osteoporotic bone implants. ACS Nano. 2009;3:3228–34.
228. Andersen OZ, Offermanns V, Sillassen M, Almtoft KP, Andersen IH, Sørensen S, et al. Accelerated bone ingrowth by local delivery of strontium from surface functionalized titanium implants. Biomaterials. 2013;34:5883–90.
229. Zhao L, Wang H, Huo K, Zhang X, Wang W, Zhang Y, et al. The osteogenic activity of strontium loaded titania nanotube arrays on titanium substrates. Biomaterials. 2013;34:19–29.
230. Bonnelye E, Chabadel A, Saltel F, Jurdic P. Dual effect of strontium ranelate: stimulation of osteoblast differentiation and inhibition of osteoclast formation and resorption in vitro. Bone. 2008;42:129–38.
231. Yang F, Yang D, Tu J, Zheng Q, Cai L, Wang L. Strontium enhances osteogenicdifferentiation of mesenchymal stem cells and in vivo bone formation by activating Wnt/catenin signaling. Stem Cells. 2011;29:981–91.
232. Peng S, Zhou G, Luk KD, Cheung KM, Li Z, Lam WM, et al. Strontium promotes osteogenic differentiation of mesenchymal stem cells through the Ras/MAPK signaling pathway. Cell Physiol Biochem. 2009;23:165–74.
233. Takada T, Katagiri T, Ifuku M, Morimura N, Kobayashi M, Hasegawa K, et al. Sulfated polysaccharides enhance the biological activities of bone morphogenetic proteins. J Biol Chem. 2003;278:43229–35.
234. Bellows CG, Aubin JE, Heersche JN, Antosz ME. Mineralized bone nodules formed in vitro from enzymatically released rat calvaria cell populations. Calcif Tissue Int. 1986;38:143–54.
235. Rai B, Nurcombe V, Cool SM. Heparan sulfate-based treatments for regenerative medicine. Crit Rev Eukaryot Gene Expr. 2011;21:1–12.
236. Ruppert R, Hoffmann E, Sebald W. Human bone morphogenetic protein 2 contains a heparin-binding site which modifies its biological activity. Rur J Biochem. 1996;237:295–302.
237. Zhao B, Katagiri T, Toyoda H, Takada T, Yanai T, Fukuda T, Chung UI, et al. Heparin potentiates the in vivo ectopic bone formation induced by bone morphogenetic protein-2. J Biol Chem. 2006;281:23246–53.

238. Kuo WJ, Digman MA, Lander AD. Heoaran sulfate acts as a bone morphogenetic protein coreceptor by facilitating ligand-induced receptor hetero-oligomerization. Mol Biol Cell. 2010;21:4028–41.
239. Kanzaki S, Takahashi T, Kanno T, et al. Heparin inhibits BMP-2 osteogenic bioactivity by binding to both BMP-2 and BMP receptor. J Cell Physiol. 2008;216:844–50.
240. Kanzaki S, Ariyoshi W, Takahashi T, et al. Dual effects of heparin on BMP-2-induced ostrogenic activity in MC3T3-E1 cells. Pharmacol Rep. 2011;63:1222–30.
241. Atha DH, Stephens AW, Rosenberg RD. Evaluation of critical groups required for the binding of heparin to antithrombin. Proc Natl Acad Sci U S A. 1984;81(4):1030–4.
242. Muir JM, Andrew M, Hirsh J, Weitz JI, Young E, Deschamps P, Shaughnessy SG. Histomorphometric analysis of the effects of standard heparin on trabecular bone in vivo. Blood. 1996;88(4):1314–20.
243. Goldhaber P. Heparin enhancement of factors stimulating bone resorption in tissue culture. Science. 1965;147:407–8.
244. Esko JD, Selleck SB. Order out of chaos: assembly of ligand binding sites in heparan sulfate. Annu Rev Biochem. 2002;71:435–71.
245. Dombroeski C, Song SJ, Chuan P, et al. Heparan sulfate mediates the proliferation and differentiation of rat mesenchymal stem cells. Stem Cells Dev. 2009;18(4):661–70.
246. Bramono DS, Murali S, Rai B, et al. Bone marrow-derived heparan sulfate potentiates the osteogenic activity of bone morphogenetic protein-2 (BMP-2). Bone. 2012;50(4):954–64.
247. Takada T, Katagiri T, Ifuku M, et al. Sulfated polysaccharides enhance the biological activities of bone morphogenetic proteins. J Biol Chem. 2003;278(44):43229–35.
248. Degat MC, Dubreucq G, Meunier A. Enhancement of the biological activity of BMP-2 by synthetic dextran derivatives. J Biomed Mater Res A. 2009;88A(1):174–83.
249. Zhou H, Qian J, Wang J, et al. Enhanced bioactivity of bone morphogenetic protein-2 with low dose of 2-N, 6-O-sulfated chitosan in vitro and in vivo. Biomaterials. 2009;30:1715–24.
250. Buttner M, Moller S, Keller M, et al. Over-sulfated chondroitin sulfate Derivatives induce osteogenic differentiation of hMSC independent of BMP-2 and TGF-β1 signaling. J Cell Physiol. 2013;228(2):330–40.
251. Manton KJ, Leong DF, Cool SM, Nurcombe V. Disruption of heparan and chondroitin sulfate signaling enhances mesenchymal stem cell-derived osteogenic differentiation via bone morphogenetic protein signaling pathways. Stem Cells. 2007;25:2845–54.
252. Kawano M, Ariyoshi W, Iwanaga K, et al. Mechanism involved in enhancement of osteoblast differentiation by hyaluronic acid. Biochem Biophys Res Commun. 2011;405(4):575–80.
253. Kim J, Kim IS, Cho TH, et al. Bone regeneration using hyaluronic acid-based hydrogel with bone morphogenic protein-2 and human mesenchymal stem cells. Biomaterials. 2007;28(10):1830–7.
254. Pittenger MF, Mackay AM, Beck SC, Jaiswal RK, Douglas R, et al. Multilineage potential of adult human mesenchymal stem cells. Science. 1999;284:143–7.
255. Derfoul A, Perkins GL, Hall DJ, Tuan RS. Glucocorticoids promote chondrogenic differentiation of adult human mesenchymal stem cells by enhancing expression of cartilage extracellular matrix genes. Stem Cells. 2006;24:1487–95.
256. Haynesworth SE, Goshima J, Goldberg VM, Caplan AI. Characterization of cells with osteogenic potential from human marrow. Bone. 1992;13:81–8.
257. Yuasa M, Yamada T, Taniyama T, et al. Dexamethasone enhances osteogenic differentiation of bone marrow- and muscle-derived stromal cells and augments ectopic bone formation induced by bone morphogenetic protein-2. PloS One. 2015;10(2):e0116462.
258. Lanqenbach F, Handschel J. Effects of dexamethasone, ascorbic acid and β-glycerophosphate on the osteogenic differentiation of stem cells in vitro. Stem Cell Res Ther. 2013;4:117.
259. Marcus J, Johannes F, Wiebke D, et al. Dexamethasone modulates BMP-2 effects on mesenchymal stem cells in vitro. J Orthop Res. 2008;26(11):1440–8.
260. Pera MF, Andrade J, Houssami S, et al. Regulation of human embryonic stem cell differentiation by BMP-2 and its antagonist noggin. J Cell Sci. 2004;117:1269–80.

261. Alborzinia H, Schmidt-Glenewinkel H, Ilkavets I, Breitkopf-Heinlein K, Cheng X, Hortschansky P, Dooley S, Wölfl S. Quantitative kinetics analysis of BMP2 uptake into cells and its modulation by BMP antagonists. J Cell Sci. 2013;126:117–27.
262. Kwong FN, Richardson SM, Evans CH. Chordin knockdown enhances the osteogenic differentiation of human mesenchymal stem cells. Arthritis Res Ther. 2008;10:R65.
263. Gazzerro E, Pereira RC, Jorgetti V, Olson S, Economides AN, Canalis E. Skeletal overexpression of gremlin impairs bone formation and causes osteopenia. Endocrinology. 2005;146:655–65.
264. Schett G. Effects of inflammatory and anti-inflammatory cytokines on the bone. Eur J Clin Invest. 2011;41:1361–6.
265. Ritting AW, Weber EW, Lee MC. Exaggerated inflammatory response and bony resorption from BMP-2 use in a pediatric forearm nonunion. J Hand Surg Am. 2012;37:316–21.
266. Robin BN, Chaput CD, Zeitouni S, Rahm MD, Zerris VA, Sampson HW. Cytokine-mediated inflammatory reaction following posterior cervical decompression and fusion associated with recombinant human bone morphogenetic protein-2: a case study. Spine (Phila Pa 1976). 2010;35:E1350–4.
267. Lee KB, Murray SS, Taghavi CE, Song KJ, Brochmann EJ, Johnson JS, et al. Bone morphogenetic protein-binding peptide reduces the inflammatory response to recombinant human bone morphogenetic protein-2 and recombinant human bone morphogenetic protein-7 in a rodent model of soft-tissue inflammation. Spine J. 2011;11:568–76.
268. Ratanavaraporn J, Furuya H, Tabata Y. Local suppression of pro-inflammatory cytokines and the effects in BMP-2-induced bone regeneration. Biomaterials. 2012;33:304–16.
269. Tan Y, Montgomery SR, Aghdasi BG, Inoue H, Kaner T, Tian H, et al. The effect of corticosteroid administration on soft-tissue inflammation associated with rhBMP-2 use in a rodent model of inflammation. Spine (Phila Pa 1976). 2013;38:806–13.
270. Huang RL, Yuan Y, Tu J, Zou GM, Li Q. Opposing TNF-α/IL-1β- and BMP-2-activated MAPK signaling pathways converge on Runx2 to regulate BMP-2-induced osteoblastic differentiation. Cell Death Dis. 2014;5:e1187.
271. Huang R-L, Chen G, Wang W, et al. Synergy between IL-6 and soluble IL-6 receptor enhances bone morphogenetic protein-2/absorbable collagen sponge-induced bone regeneration via regulation of BMPRIA distribution and degradation. Biomaterials. 2015;67:308–22.
272. Ratanavaraporn J, Furuya H, Kohara H, et al. Synergistic effects of the dual release of stromal cell-derived factor-1 and bone morphogenetic protein-2 from hydrogels on bone regeneration. Biomaterials. 2011;32(11):2797–811.
273. Kleinschmidt K, Ploeger F, Nickel J, et al. Enhanced reconstruction of long bone architecture by a growth factor mutant combining positive features of GDF-5 and BMP-2. Biomaterials. 2013;34(24):5926–36.
274. Nakamura Y, Tensho K, Nakaya H, et al. Low dose fibroblast growth factor-2 (FGF-2) enhances bone morphogenetic protein-2 (BMP-2)-induced ectopic bone formation in mice. Bone. 2005;36(3):399–407.
275. Wuertz K, Urban J, Klasen J, Ignatius A, Wilke HJ, Claes L, et al. Influence of extracellular osmolarity and mechanical stimulation on gene expression of intervertebral disc cells. J Orthop Res. 2007;25:1513–22.
276. Hoppe A, Güldal NS, Boccaccini AR. A review of the biological response to ionic dissolution products from bioactive glasses and glass-ceramics. Biomaterials. 2011;32:2757–74.
277. Jiang C, Liu J, Zhao J, Xiao L, An S, Gou Y, et al. Effects of hypoxia on the immunomodulatory properties of human gingiva–derived mesenchymal stem cells. J Dental Res. 2015;94:69–77.

Part III
Regeneration of Some Clinic-Targeted Tissues

Chapter 9
Cartilage Regeneration

Yuankun Dai and Changyou Gao

Abstract The treatment of damage to cartilage represents one of the most challenging clinical tasks due to the limited spontaneous healing and regenerative capability of cartilage. Clinically applied protocols for cartilage regeneration are still faced with various obstacles. The cartilage tissue engineering combines scaffolds, cells, and bioactive molecules, achieving cartilage engineering in vitro and cartilage regeneration in vivo. More recently, the controversy and difficulty in regulatory application of various cells and bioactive molecules gradually push forward the emergence of in situ inductive cartilage regeneration by recruiting endogenous regenerative cells. With these perspectives, we aim to present an overview of existing cartilage regeneration technologies with emphasis of recent progresses, development, and major steps taken toward the structure and functional regeneration of cartilage. In this chapter, essential elements of various protocols and their advantages and disadvantages and challenges and future perspectives of cartilage regeneration are discussed.

Keywords Tissue engineering · Cartilage regeneration · Scaffolds · Chondrocytes · Stem cells · In situ inductivity

9.1 Introduction

Articular cartilage is a highly developed connective tissue for weight-bearing and friction-reducing. Chondrocyte is the only type of cells in mature articular cartilage, occupying 1–10% of the tissue volume. Seventy to 80% of weight of articular cartilage is water. Collagen, proteoglycans, matrix glycoproteins, and small amount

Y. Dai (✉)
Marine Biomedical Research Institute of Qingdao, Ocean University of China, Qingdao, China
e-mail: daiyuankun1234@126.com

C. Gao (✉)
MOE Key Laboratory of Macromolecular Synthesis and Functionalization, Department of Polymer Science and Engineering, Zhejiang University, Hangzhou, China
e-mail: cygao@zju.edu.cn

C. Gao (ed.), *Polymeric Biomaterials for Tissue Regeneration*,
https://doi.org/10.1007/978-981-99-6948-7_9

of elastin and phospholipids contribute the other 20–30% of the weight [1, 2]. Figure 9.1a shows the composition and structure of articular cartilage [3]. Cells and extracellular matrix (ECM) in cartilage distribute laterally in the superficial, randomly in the middle, and vertically in the deep layers of cartilage, respectively.

The avascular structure in the articular cartilage determines that the chondrocytes can only get nutrients from the synovial fluid [4]. After maturation of cartilage, chondrocytes have low ability to migrate and proliferate. Hence, articular cartilage has low possibility of self-healing when lesion occurs. The intrinsic migration of bone marrow mesenchymal stem cells (BMSCs) into cartilage defect always leads to the formation of fibrocartilage [4].

Articular cartilage defects caused by arthritis and trauma severely affect the healthy life of human being. In order to treat cartilage defects, different protocols such as autologous chondrocyte implantation (ACI), mosaicplasty, microfracture, autologous matrix-induced chondrogenesis (AMIC), and cartilage tissue engineering have been developed, as shown in Fig. 9.1b [5].

ACI utilizes autologous chondrocytes grown in culture, which are reimplanted in a second-stage procedure to repair large chondral defects [6]. Mosaicplasty is indicated for the treatment of smaller defects, less than 2–4 cm^2 in size, primarily on the femoral condyles. The treatment of larger lesions is limited by donor site morbidity, and the use in the patellofemoral joint is controversial [7]. To overcome these challenges, cartilage tissue engineering has been developed to realize the structural and functional regeneration of damaged cartilage [8]. As shown in Fig. 9.2a, the cells, scaffolds, and bioactive molecules are defined as three essential elements for the traditional cartilage tissue engineering [9, 10]. Various chondrogenetic cell sources are available for the cartilage tissue engineering. The chondrogenesis capability of these cells can be induced or enhanced with many biochemical or biomechanical stimulation in vitro. After culture in vitro, scaffold-based or scaffold-free engineered cartilage could be obtained and implanted for cartilage regeneration in vivo. Hence, cartilage tissue engineering involves direct intra-articular delivery of progenitor cells, progenitor cell delivery on scaffolds, or cell-free scaffolds coated with biological factors to recruit endogenous cells for articular cartilage defect repair [10]. The implantation of biomaterials or cartilage constructs is always accompanied by injury through the surgical procedures.

Inflammatory response takes a pivotal role in tissue repair and regeneration, since injury to the tissue always initiates an inflammatory response to the biomaterials. Moreover, the implantation of engineered cell–material hybrids elicits an adaptive immune reaction toward the cellular component, which in turn influences the host response to the material component [11]. When degradable biomaterials are applied, the immune response is additionally affected by the degradation products and surface changes of the biomaterials. Chronic inflammation in osteoarthritis develops as inflammatory stimuli persist at the implant site with macrophages, representing the driving force in perpetuating immune responses. Monocytes arriving at the implantation site undergo a phenotypic change to differentiate into macrophages. Their activation leads to further dissemination of chemo-attractants. Macrophages

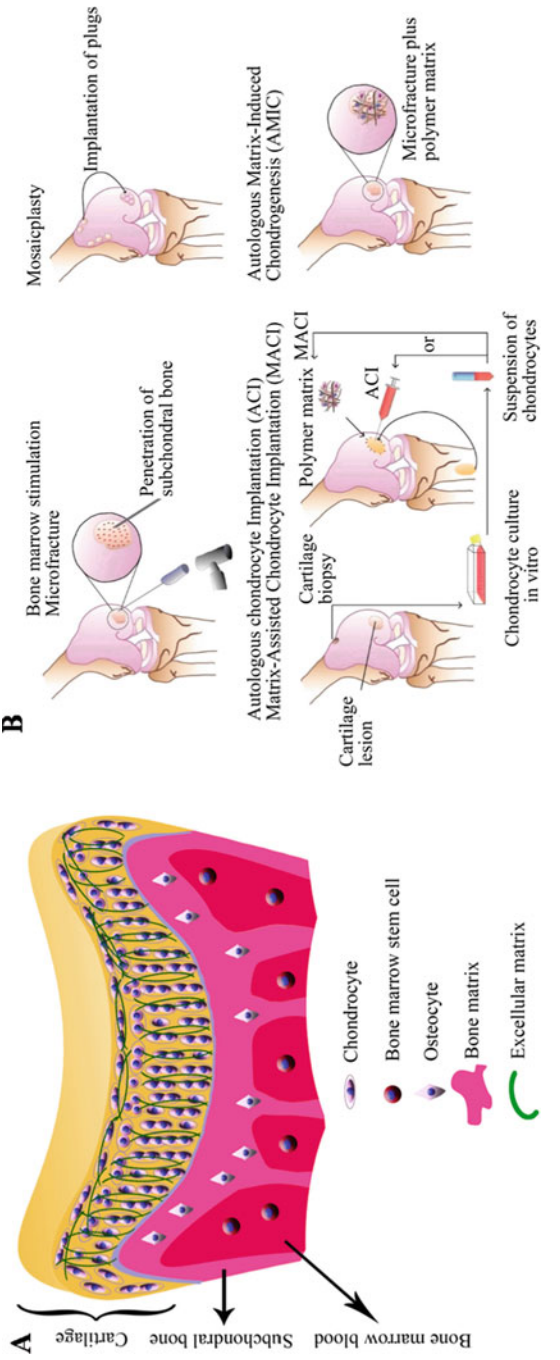

Fig. 9.1 (**a**) Composition and structure of articular cartilage and (**b**) various clinical strategies for regeneration of cartilage. (Reprinted from [5] with permission)

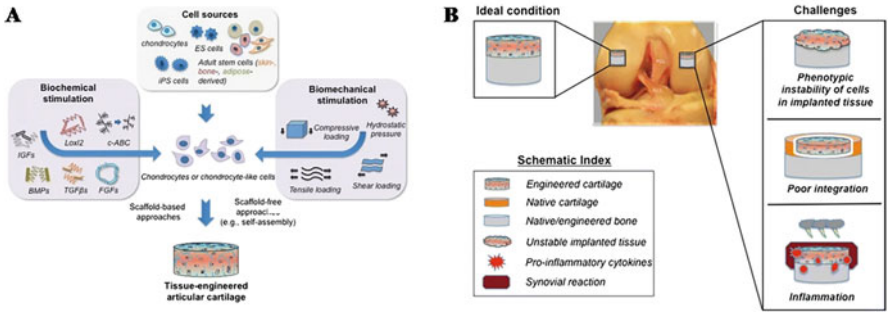

Fig. 9.2 (**a**) Articular cartilage tissue engineering involving the formation of three-dimensional tissues in vitro by seeding cells into scaffolds or through scaffold-free approaches in the presence of biochemical and biomechanical stimuli. (**b**) Challenges in cartilage tissue engineering. (Reprinted from [10] with permission)

attached to the biomaterials can foster invasion of additional inflammatory cells by secreting chemokines [12]. Taking these concerns into consideration, challenges of articular cartilage tissue engineering are shown in Fig. 9.2b. In summary, difficulty in the regulation and maintenance of cell chondrogenetic phenotype, poor integration between the implanted and the host tissues, and immunoregulation of the implanted biomaterials are the main issues that impede the development of cartilage tissue engineering [10].

9.2 Traditional Cell-Loaded Constructs for Cartilage Regeneration

9.2.1 Biomaterials for Cartilage Regeneration

An ideal cartilage tissue engineering scaffold should preserve the following characteristics: biocompatible, biodegradable, highly porous, suitable for cell attachment, proliferation and differentiation, osteoconductive, noncytotoxic, flexible and elastic, and nonantigenic. Generally, biomaterials used for cartilage tissue engineering can be divided into two categories: natural polymers and synthetic polymers. Each kind of these materials has their own advantages and shortcomings [13]. The natural materials are hydrophilic and bioactive, which enhance the cell–material interactions and facilitate the cells' chondrogenesis to the same extent. Collagen [14–21], fibrin [22–27], silk fibrin [28–32], hyaluronic acid (HA) [33–46], alginate [47–51], gelatin [40, 52–57], chitosan [58–64], etc. have been broadly invested in tissue engineering. The scaffolds based on these natural polymers are usually in a format of hydrogels, either with single or multicomponents. Examples of cartilage tissue engineering scaffolds based on native materials are shown in Fig. 9.3.

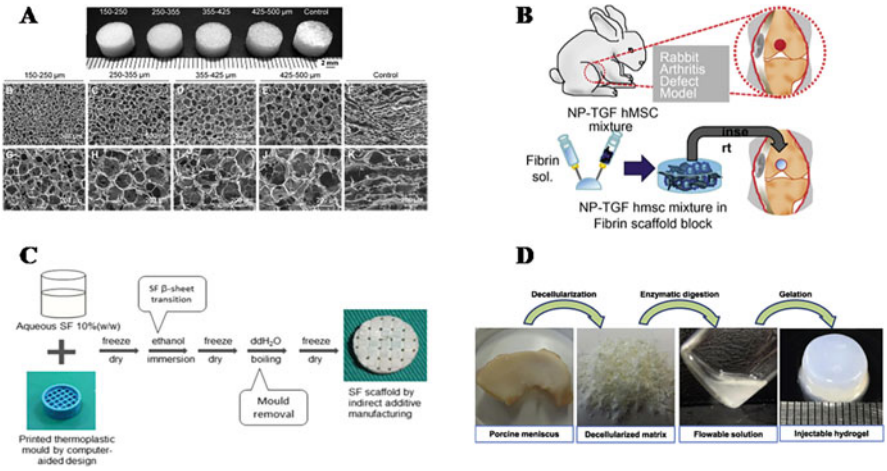

Fig. 9.3 Examples of cartilage tissue engineering scaffolds based on native materials. (**a**) Collagen porous scaffold. (**b**) BMSCs-loaded fibrin glue. (**c**) Silk fibroin scaffold. (**d**) Acellular cartilage matrix. (Reprinted from [29, 65–67] with permission)

9.2.1.1 Natural Materials

Collagen, which constitutes the major part of the extracellular matrix (ECM) and is the essential component and mechanical building block of various physiological systems including cartilage, is highly recommended in cartilage tissue engineering. Collagen has many advantages including favorable biocompatibility and high density of the RGD sequences and other sequences facilitating cell adhesion and cell differentiation [19]. Macroporous scaffolds of collagen can be fabricated conveniently by freeze-drying and chemical cross-linking (Fig. 9.3a) [67]. Vickers et al. prepared a chemically cross-linked collagen type II and glycosaminoglycan (GAG) scaffold with a low cross-linking density. Culture of bone marrow stem cells in the scaffold for 4 weeks in vitro found cell-mediated contraction, increased cell number density, and a greater degree of chondrogenesis [68]. Levingstone et al. fabricated a multilayer scaffold consisting of a bone layer composed of collagen type I and hydroxyapatite, an intermediate layer composed of collagen type I and type II and hydroxyapatite, and a superficial layer composed of collagen type I and HA [69]. The scaffolds were implanted into osteochondral defects created in the medial femoral condyle of the knee joint of New Zealand white rabbits, resulting in tissue regeneration with a zonal organization, repair of the subchondral bone, formation of an overlying cartilaginous layer, and evidence of an intermediate tidemark.

Fibrin gel has several features including biocompatibility and biodegradability. The fibronectin-rich fibrin glue is an essential protein in cartilage matrix for chondrocytes-ECM interaction [26]. Fibrin gel could serve as a delivery system for chondrogenetic cells and/or bioactive molecules to facilitate cartilage regeneration (Fig. 9.3b) [65]. Fibrin gel loaded with human bone marrow-derived

mesenchymal stem cells (hMSCs) and growth factor could realize full regeneration of cartilage defects in rabbits [65]. Park et al. fabricated a hybrid hydrogel composed of fibrin and HA, into which chondrocytes were implanted for culture in vivo [23]. Cartilage-like tissues were formed in the hybrid hydrogel, showing higher amounts of the ECM components, GAG, and collagen.

Hyaluronic acid (HA) is one of the most extensively studied natural materials for cartilage tissue engineering. HA is a linear polysaccharide found natively in adult articular cartilage that is involved in many cellular processes, including proliferation, morphogenesis, inflammation, and wound repair. Furthermore, HA is also important to cartilage formation and is differentially regulated during limb bud formation and mesenchymal cell condensation. HA hydrogels support chondrocyte matrix deposition and chondrogenic differentiation of mesenchymal stem cells (MSCs) [70]. HA is widely used to functionalize hydrogels or scaffolds for regeneration of cartilage defects. Sheu et al. fabricated a hydrogel based on oxidized HA and resveratrol, into which chondrocytes were implanted for culture in vitro, resulting in upregulated expression of collagen type II, aggrecan, and Sox9 genes and downregulated inflammatory factors [39].

Alginate is a natural anionic and hydrophilic polymer obtained primarily from brown seaweed and bacteria. It is composed of β-D-mannuronate and α-L-guluronate residues [71] and has been widely applied in many biomedical fields due to its excellent biocompatibility, low toxicity, and the mild gelation condition required to form a cross-linked structure [49]. Alginate can be easily modified through chemical and physical reactions to obtain derivatives and can be processed into three-dimensional scaffolds such as hydrogels, microspheres, microcapsules, sponges, foams, and fibers. Studies prove that the alginates would support the chondrogenesis [72, 73]. The cells-alginate constructs are widely used for the regeneration of articular cartilage defects, and some of the researches demonstrate quite positive results. Igarashi et al. delivered BMSCs in an ultra-purified alginate gel into articular cartilage defects in rabbit knees, resulting in complete regeneration of the defects [74].

Gelatin is a denatured collagen, but has relatively low antigenicity compared with collagen. Recently, gelatin-based biomaterials have been widely studied in tissue engineering. However, it is difficult to use pure gelatin scaffold for hard-tissue regeneration such as bone and cartilage due to its weaker mechanical strength. Hence, many studies focus on preparing pure gelatin scaffolds by using proper cross-linking methods [75] or hybrid scaffolds based on gelatin [40, 54, 55, 76]. Some natural materials such as HA, fibrin, chitosan, and synthetic materials have been extensively incorporated to obtain hybrid scaffolds, which not only preserve higher mechanical property but also retain the bioactivity of natural materials.

Chitosan is obtained by deacetylation of chitin which is an abundant natural material. The positive charge in the molecular chain may protect GAGs from hydrolysis [61]. However, the positive charge may also limit the proliferation of chondrocytes. Meanwhile, weaker mechanical property of wet chitosan also limits its application in cartilage tissue engineering [62]. Therefore, the hybrids of one or

more materials are always adopted for the application of chitosan in tissue engineering.

Silk fibroin extracted from silkworm cocoons is composed of fibrous protein (fibroin), containing amino acids and glue-like protein (sericin). Silk fibroin is widely used natural material for tissue regeneration taking into consideration of their excellence in biocompatibility, degradability, and mechanical properties [77, 78]. Scaffolds based on silk fibroin for cartilage regeneration can be fabricated through a template/solution-casting method as reported (Fig. 9.3c) [29]. Biphasic scaffolds with a cartilage phase constituting of bovine cartilage matrix biofunctionalized fibroin and differentiated autologous prechondrocytes, and a bone phase (decellularized bovine bone) has been fabricated to promote cartilage regeneration in a model of joint damage in pigs [79]. Cao et al. developed a multifunctional silk-based hydrogel incorporated with metal-organic framework nanozymes, which showed enhanced cell viability as well as antioxidant and antibacterial properties. In the full-thickness osteochondral defect model of rabbit, the hydrogel displayed successful regeneration of osteochondral defect [80].

ECM materials have become more popular because the matrices retain the structure of native cartilage, which preserve mechanical and chemical signals that can induce cell differentiation and recruitment without additional biologic additives. Cartilage ECM can be obtained from either cell-derived matrices secreted during culture in vitro or from native cartilage (Fig. 9.3d) [66]. Decellularization is an effective way to fully remove all cellular components and nucleic acids or to kill the remnant cells within the matrix [79–84]. The scaffolds based on the decellularized cartilage ECM regenerate hyaline cartilage when combined with rabbit MSCs after transplantation into weight-bearing area of patellar grooves in rabbits for 12 weeks [85]. Dai et al. prepared an acellular bone matrix scaffold using iliac bone of pigs [86]. The scaffold implantation combined with microfracture was used to treat full-thickness articular defects (9 mm in diameter) without destroying the subchondral bone of pigs. 24 weeks after surgery, the defects were repaired with hyaline-like neocartilage which has the similar mechanical properties to the normal cartilage. Ayariga et al. developed a decellularized ECM scaffolds from avian articular cartilage [87]. The obtained scaffolds registered an interconnected and porous architecture, as well as stiffness comparable to the native cartilage tissues. Meanwhile, human chondrocytes survived, proliferated, and interacted with the scaffolds, showing that the decellularized scaffolds are suitable for cartilage regeneration. Das et al. prepared a cartilaginous ECM-derived biomaterial from goat ears [88]. MSCs showed obvious chondrogenic differentiation with increasing amount collagen and GAGs in the decellularized scaffolds. Upon implantation of the IGF-1-loaded cell-free scaffolds in rabbits' osteochondral defects for 3 months, the histological and micro-CT evaluation revealed significant enhancement and regeneration of neocartilage and subchondral bone. Oh et al. prepared full-thickness porcine cartilage-derived ECM, and then fabricated mechanically reinforced ECM scaffolds by combining salt-leaching and crosslinking methods [89]. Chondrocytes showed higher levels of cartilage-specific markers in the scaffolds compared to that in the ECM scaffolds prepared by simple freeze-drying [90]. Antler decellularized

cartilage-derived matrix (AdCDM) rich in collagen and GAGs was prepared by combining freezing-thawing and enzymatic degradation. Treatment of osteochondral defects with the AdCDM showed a flat and smooth surface of the neocartilage at the surgery site. Meanwhile, compared to porcine decellularized cartilage-derived matrix, AdCDM could lead to better osteochondral regeneration with higher international cartilage repair society scores (ICRS). Decellularized ECM bioinks, derived from specific native tissues or organs, have been used to fabricate 3D-printed tissues and organs. Zhang et al. developed a crosslinker-free bioink with silk fibroin and decellularized articular cartilage extracellular matrix of goat [91]. The silk fibroin and decellularized ECM interconnect with each other through physical crosslinking and entanglement, which bypass the toxicity inherent in the chemical crosslinking process of most bioinks. In vitro test proved that BMSCs highly expressed chondrogenesis-specific genes in the 3D-printed scaffold using this bioink.

9.2.1.2 Synthetic Materials

Synthetic polymers are also widely applied in cartilage tissue engineering, but the relatively low cell adhesive ability limits their applications. The widely used synthetic materials include poly(lactide-*co*-glycolide) acid (PLGA) [40, 57, 92–94], polycaprolactone (PCL) [95–99], poly(ethylene glycol) (PEG) [34, 100–108], etc. The scaffolds composted of solely synthetic materials can hardly realize good tissue regeneration. Therefore, the natural materials such as collagen, gelatin, fibrin, HA, and acellular ECMs, as mentioned before, can be compounded or incorporated into the synthetic polymeric scaffolds. Examples of cartilage tissue engineering scaffolds based on synthetic materials are shown in Fig. 9.4.

PCL is a semicrystalline polymer. It belongs to a family of poly α-hydroxyl esters and is one of the most widely used biodegradable polyesters for medical applications because of its biocompatibility, biodegradability, and flexibility [111]. It is widely used to prepare scaffolds for cartilage tissue engineering as well [40, 46, 47, 92, 112–114]. For example, Kim et al. prepared a PCL scaffold constructed with layers of electrospun and salt-leaching PCL membrane, into which chondrocytes were seeded by using an injectable heparin-based hydrogel (Fig. 9.4a). In vivo transplantation of the construct into partial-cartilage defects demonstrates significant cartilage formation with good integration to the surrounding cartilage [95]. Lebourg et al. modified PCL scaffolds with cross-linked HA to grant PCL more hydrophilic and biomimetic microenvironment. Complete regeneration of chondral defects in rabbits in vivo was confirmed by implanting the scaffolds for 24 weeks [38].

PLAG is usually synthesized via ring-opening copolymerization of lactide and glycolide, which has prominent advantages such as adjustable molecular weight and degradation rates, good mechanical properties especially toughness, and excellent processability [115]. It has been widely used to prepare scaffolds to engineer tissues including cartilage, bone, nerve, etc. [116–121]. Chang et al. seeded endothelial progenitor cells into a highly porous PLGA scaffold and implanted into the

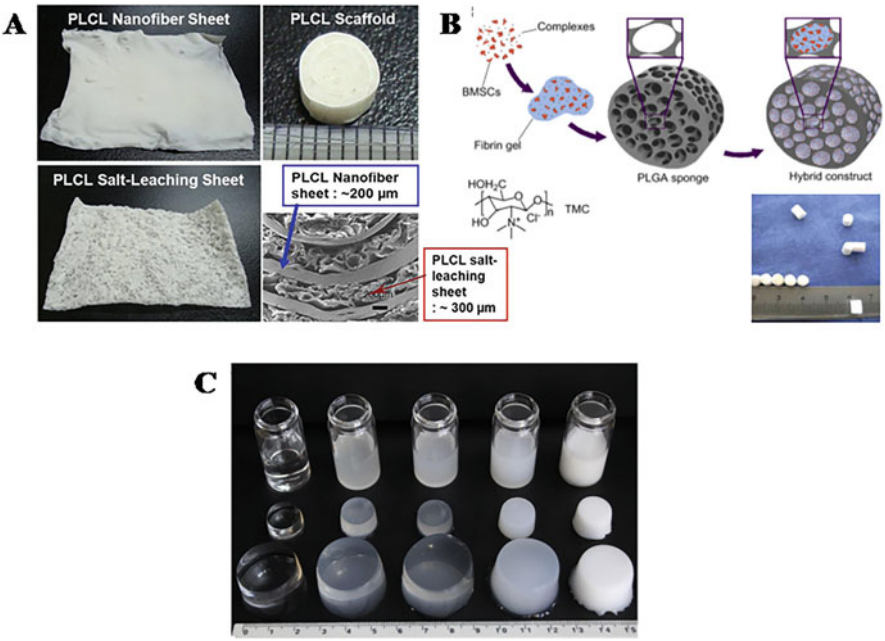

Fig. 9.4 Examples of cartilage tissue engineering scaffolds based on synthetic materials. (**a**) PLCL scaffold. (**b**) PLGA scaffold. (**c**) PEG hydrogel. (Reprinted from [95, 109, 110] with permission)

osteochondral defect in the medial femoral condyle of rabbits. After 12 weeks, the defects were regenerated with hyaline cartilage, showing a normal columnar chondrocyte arrangement, higher Sox9 expression, and greater contents of GAG and collagen type II [122]. In order to enhance the bioactivity of PLGA scaffolds, bioactive materials such as HA, gelatin, collagen, and fibrinogen can be usually incorporated. PLGA/fibrin gel-based constructs combined with MSCs and TGF-β1 chondrogenic genes could facilitate the in vivo regeneration of full-thickness cartilage defects in a rabbit model (Fig. 9.4b) [109, 123, 124]. The PLGA scaffold is fabricated by a gelatin porogen leaching method, into which fibrinogen containing cells and plasmid TGF-β1 gene complexes is infiltrated and then gelated. The chondrocytes cultured in vitro distribute evenly and maintain a round morphology in the hybrid scaffold as that in the normal cartilage [125]. The implantation of PLGA/fibrin gel/N,N,N-trimethyl chitosan chloride (TMC)/pDNA-TGF-β1 construct into osteochondral defects for 12 weeks in vivo results in regenerated cartilage with smooth surface and well integration with its surrounding tissue and subchondral bone [109].

PEG hydrogel has received wide attention due to its injectability, noncell-adhesive property, cell compatibility, and low immunogenicity. Meanwhile, PEG hydrogel could be prepared for cartilage regeneration (Fig. 9.4c) [110]. The nondegradability of PEG in physiological environment limits its application in tissue

engineering, although the PEG molecules of lower molecular weight, like PEG-400, have been proved to metabolize via renal or intestine pathways [126]. Biodegradable segments such as oligo(lactic acid), oligo(ε-caprolactone), oligo(trimethylene carbonate), and phosphate groups have been introduced into the PEG-based macromers. Fan et al. developed a microcavitary hydrogel via photopolymerization of biodegradable oligo(trimethylene carbonate)-poly(ethylene glycol)-oligo(trimethylene carbonate) diacrylate macromers [106]. The cavitary structure in the hydrogel would accelerate degradation of the hydrogel. Compared with noncavitary hydrogel, the cell density and total contents of collagen and GAG are significantly higher. The hydrolytically biodegradable PEG hydrogels offer a promising platform for chondrocyte encapsulation and for tuning degradation of cartilage tissue engineering scaffolds. Skaalure et al. prepared a semi-interpenetrating network of bioactive HA and oligo(lactic acid)-PEG hydrogel, into which chondrocytes were encapsulated and cultured for 4 weeks. In this way, the contents of collagen and GAG are significantly increased [34].

9.2.2 Cells for Cartilage Regeneration

Chondrocytes in the cartilage produce cartilage ECMs and therefore have been the first choice for cartilage tissue engineering [127]. They are isolated from various sources such as articular cartilage, nasal septum, ribs, and ear cartilage and are extensively used for the study of cartilage regeneration in vitro and in vivo. However, one of the major limitations of chondrocytes is their instability in the culture in vitro, leading to the loss of expression of cartilage matrices such as collagen type II and aggrecan. Recently, multipotent MSCs have been gained increasing interest in cartilage tissue engineering as an alternative to autologous chondrocytes due to their ease in isolation and high expansion capacity in vitro. MSCs exhibit the potential to differentiate into chondrocytes [128], tenocytes [129], ligament cells [130], neuronal cells [131, 132], cardiomyocyte [133, 134], osteoblasts [135], and other cell types [136]. In particular, bone marrow-derived stem cells (BMSCs), adipose-derived stem cells (ADSCs), and embryonic stem cells (ESCs) are most widely applied in cartilage tissue engineering.

9.2.2.1 Chondrocytes

Chondrocytes are metabolically active cells that synthesize a large spectrum of ECM components such as collagen, glycoproteins, proteoglycans, and HA [127]. Since the chondrocytes are the only type of cells in articular cartilage, they are used for the regeneration of cartilage defects in priority both in vitro and in vivo [127, 137–144]. It is believed that the use of chondrocytes would lead to the formation of neotissue with exactly the same ECMs with the native cartilage [145]. The activity of chondrocytes is altered by many factors present within their chemical and

mechanical environment. However, the use of chondrocytes for cartilage repair suffers from chondrocyte dedifferentiation. A proper culture and delivery of chondrocytes, including the use of chondrogenetic culture medium, growth factors, and mesenchymal stem cells, need to be well adjusted in order to keep the phenotype of chondrocytes [140]. Three-dimensional scaffolds can better mimic the native microenvironment of chondrocytes in cartilage tissue, promoting cell–cell and cell–matrix interactions and enforcing round chondrogenetic cell morphology and thereby maintaining their phenotype. Xu et al. encapsulated chondrocytes in alginate gel beads and cultured in spinner flasks in chondrogenic and chondrocyte growth medium and then subcutaneously implanted the cells-loaded beads to evaluate the ectopic chondrogenesis [142]. The results prove high deposition of glycosaminoglycan and expression of cartilage-specific genes. Lohan et al. precultured chondrocytes in polyglycolide (PGA) scaffolds for 3 weeks, which were then implanted into critical-sized osteochondral defect of rabbit knee femoropatellar groove [138, 141]. Twelve weeks after implantation, neocartilage was formed in vivo in the PGA constructs seeded with chondrocytes. The results are significantly better than those of the cell-free PGA scaffolds and empty defects.

9.2.2.2 Bone Marrow-Derived Stem Cells (BMSCs)

BMSCs have been extensively used for chondrogenesis in a three-dimensional culture in vitro with addition of chondrogenetic factors and regeneration of cartilage defects in animal models in vivo [33, 146–149]. BMSCs can be isolated via plastic adhesion or negative selection from bone marrow aspirate that includes a highly heterogeneous cell population such as hematopoietic cells, endothelial cells, and adipocytes [150]. However, there are some limitations of BMSCs. The relative number of BMSCs in the marrow blood is rather small, and their differentiation ability decreases significantly with age [151]. Meanwhile, the constructs of cartilage containing BMSCs can raise many problems such as fibrosis, vascularization, the "hollow" phenomenon, and shrinkage likely due to the incomplete differentiation of BMSCs, deterring the clinical translation of tissue-engineered cartilage [149]. Hence, chondrogenetic bioactive factors are always applied to promote chondrogenesis differentiation of BMSCs. Li et al. fabricated a bilayered poly (vinyl alcohol)/gelatin/vanillin (PVA/Gel/V) and nanohydroxyapatite/polyamide-6 (n-HA/PA6) scaffold, into which BMSCs were implanted. The obtained constructs were used for the regeneration of cartilage and subchondral bone defects in rabbits in vivo [152]. With BMSCs loading, the two different layers of the composite biomimetic scaffolds provide a suitable microenvironment for cells to form respective tissues.

9.2.2.3 Adipose-Derived Stem Cells (ADSCs)

ADSCs are becoming more and more attractive because they can be easily isolated from adipose tissues and cultured in vitro for an extended period of time with stable expansion and low levels of senescence [153]. Adipose tissue contains a large proportion of MSCs and is easily accessible in all individuals. Compared with BMSCs, the ADSCs are relatively abundant and can be easily available. In vitro and in vivo studies confirm the chondrogenetic ability of ADSCs and the ability of cartilage regeneration [154–160]. In the presence of platelet-rich plasma (PRP) and cartilage-specific extracellular molecules, the expression of collagen type II and aggrecan can be significantly upregulated [159, 160]. Wang et al. proved different chondrogenic degrees of ADSCs being cultured in hydrogels composed of chondroitin sulfate, HA, and heparin sulfate, respectively [157]. This chondrogenetic potential of ADSCs makes them a promising candidate for restoration of cartilage defects in vivo. Wang et al. implanted ADSCs into acellular cartilage matrices and used the cell-loading constructs to restore the articular cartilage defects of rabbits [158]. After 12 weeks of implantation, the defects are filled with neotissues, showing a smooth surface, highly expressed collagen type II and GAG, and chondrocyte-like cells in the recesses. TEM analysis confirms plenty of secretary matrix particles in the neotissue.

9.2.2.4 Embryonic Stem Cells (ESCs)

Recently, several studies have demonstrated the regeneration of cartilage defects in vivo by using ESC progenitor cells [161–164]. ESCs can be obtained from the blastocyst and are able to self-renew for a prolonged period of time without differentiation and, most importantly, can be differentiated into a large variety of tissues derived from all three germ layers. Although the application of ESCs would bring problems such as immunologic incompatibility, possible development of teratomas, and ethical issues in human, the in-depth study of ESCs would promote their applications in healing human diseases. For the cartilage regeneration, ESCs are also a promising choice [161, 163, 165–167]. Pilichi et al. demonstrated a positive result of application of nondifferentiated ESCs in vivo for osteochondral regeneration without tumorigenic and teratoma formation [164]. They treated osteochondral defects in a sheep model with ESCs for 24 weeks, proving the regeneration of articular cartilage defects with hyaline cartilage, without signs of immune rejection or teratoma. Toh et al. used TGF-β1 to induce chondrogenic differentiation of ESCs, explored the potential of these ESC-derived chondrogenic cells to produce an ECM-enriched cartilaginous tissue construct when cultured in HA hydrogel, and further investigated the cartilage regenerative ability in an osteochondral defects in a rat model [162]. Twelve weeks after implantation, a hyaline-like neocartilage layer is formed, showing good surface regularity and complete integration with the adjacent host cartilage and a regenerated subchondral bone.

9.2.2.5 Induced Pluripotent Stem Cells (iPSCs)

iPSCs may be generated from somatic cells through reprogramming, enabling them to possess embryonic-like properties. Shinya Yamanaka's group initially derived the iPSCs in 2006 by reprogramming mouse fibroblasts, and human fibroblasts in the following year [168, 169]. iPSC may differentiate into other cell linages and be maintained in a nondifferentiated state for an extended period of time to cultivate cells, known as the self-renewal process. The iPSCs are similar to ESCs but less of an ethical dilemma [170]. Nam et al. obtained human iPSCs from cord blood mononuclear cells using the Sendai virus [171]. The iPSCs were differentiated into chondrogenic lineage with pellet culture and maintained for 30 days. The generated pellets showed high expression of chondrogenic gene and deposition of cartilage extracellular matrix proteins. Yamashita et al. reported that differentiation of iPSCs into hyaline cartilaginous particles and implantation of the particles into joint surface defects realized the repair of cartilage defects, and neither tumor nor ectopic tissue formation was observed [172]. Kotaka et al. labeled iPSCs magnetically with nanoscale iron particles, and delivered the cells specifically into cartilage defects in nude rats using a magnetic field [173]. The histological grading proved useful and safe for cartilage repair using the mentioned iPSCs. Liu et al. fabricated a polycaprolactone/gelatin scaffold using two separate electrospinning processes [174]. After seeded with mouse iPSCs derived from mouse dermal fibroblasts, the iPSCs-scaffolds were implanted into osteochondral defects of rabbits, resulting in an enhanced gross appearance and histological improvement, higher cartilage-specific gene expression and protein levels as well as subchondral bone regeneration.

9.2.2.6 Dental Pulp Stem Cells (DPSCs)

DPSCs are a type of self-renewal MSCs residing within the perivascular niche of the dental pulp [175]. DPSCs are a promising source of stem cells for tissue-engineering therapies because of their low cost and easy accessibility. DPSCs can differentiate into several different cell types, including neurons, odontoblasts, osteoblasts, adipocytes and chondrocytes [176]. Mata et al. cultured DPSCs in 3% alginate hydrogel, and implanted the hydrogel in a rabbit model of cartilage damage [177]. Three months post surgery, the cartilage defects were well regenerated. Yanasse et al. reported a successful regeneration of full-thickness articular cartilage defects in rabbits using DPSCs-loaded platelet-rich plasma scaffolds [178].

9.2.2.7 Umbilical Cord Mesenchymal Stem Cells (UCMSCs)

Human UCMSCs can be derived from various parts of human umbilical cord, including Wharton's jelly, cord lining, and the perivascular region [179]. hUCMSCs are advantageous because of their high expansion capacity, noninvasive harvesting,

and hypoimmunogenicity. hUCMSCs possess the same potential of chondrogenic differentiation regardless of the portion of the umbilical cord from which they are isolated [180]. According to the research of Fong et al., the chondrogenic potential of hUCMSCs is thrice that of BMSCs in producing collagen [181]. Zheng et al. fabricated polycaprolactone/hydroxyapatite (PCL-HA) scaffolds using fused deposition modeling 3D-printing technology [182]. Furthermore, rabbit UCMSCs and chondrocytes with a ratio of 3:1 were seeded on the prepared PCL/HA scaffolds. After 8 weeks of implantation into rabbits' femoral trochlear defects, the ICRS scores of the repaired defects for the UCMSCs and chondrocyte-seeded PCL-HA scaffolds were significantly higher than the unseeded PCL/HA scaffolds. 125 patients were included in a clinical study to evaluate cartilage regeneration by implanting allogenic hUCMSCs with concomitant high tibial osteotomy (HTO) [183]. Second-look arthroscopy and ICRS grade evaluation proved the effectiveness of this treatment for patients with medial compartment osteoarthritis and various deformities. Another clinical research including 176 patients also confirmed that implantation of allogenic hUCMSCs with concomitant HTO could provide clinical outcomes in terms of pain relief, functional scores, and quality of life [184].

9.2.2.8 Other Cells

Besides BMSCs, ADSCs, ESCs, iPSCs, DPSCs, UCMSCs, other types of stem cells from muscle, synovium, and periosteum can also be used for the cartilage regeneration [185–188].

Several works report that synovium-derived MSCs (SMSCs) show a higher colony-forming efficiency than BMSCs. Because the SMSCs display a great potential to differentiate into chondrocytes, they are one of the best candidates for the repair of cartilage defects [189]. SMSCs have the potential for both cartilage tissue engineering in vitro and cartilage regeneration in vivo. With appropriate stimulation, SMSCs are capable of migrating into articular cartilage defects and differentiating to chondrocytes [189–194]. Fan et al. explored therapeutic chondrogenesis of rabbit SMSCs encapsulated in photopolymerized hydrogels with the treatment of TGF-β1, resulting in positive SMSC chondrogenesis. Meanwhile, SMSCs may be a type of tissue-specific stem cells, because they can respond to signaling in the joint and promote cartilage defect regeneration [195]. Pei et al. isolated SMSCs from synovial tissue of rabbit knee joints and mixed SMSCs with fibrin glue, followed by seeding into a nonwoven PGA mesh. After the constructs were prematured for 1 month in vitro, they were implanted into rabbit knees to repair osteochondral defects. Six months later, the cartilage defects were full of smooth hyaline-like cartilage with high expressions of collagen type II and GAG and were well integrated with the surrounding native cartilage. No detectable collagen type I and macrophages were found [196].

9.2.3 *Bioactive Signals for Cartilage Regeneration*

The cell growth factors are typical bioactive molecules, which can stimulate or inhibit cellular proliferation, differentiation, migration, and gene expression [198]. There are a number of essential growth factors that have regulatory effects on chondrocytes or stem cells in terms of chondrocyte maturation and cartilage formation. The candidate growth factors include transforming growth factor β (TGF-β), insulin-like growth factor-1 (IGF-1), bone morphogenic proteins (BMPs), fibroblast growth factor (FGF), platelet-derived growth factor (PDGF), etc. [199]. Each growth factor plays a different role in the migration, proliferation, and differentiation of cells as summarized in Fig. 9.5. However, it is difficult to precisely define the function of each growth factor due to the functional overlaps in temporal scale [197].

9.2.3.1 TGF-β

So far four types of TGF-β superfamily, namely, TGF-β1, TGF-β2, TGF-β3, and BMP, have been found in cartilage [198]. Activated TGF-β not only increases the synthesis of proteoglycan but also prevents degradation of cartilage ECM by inhibiting matrix metalloproteinase (MMP). These TGF-β isomers play an important role in the late stage of chondrocyte differentiation and may participate in bone formation as well. TGF-β1 induces early stage of chondrogenesis and increases

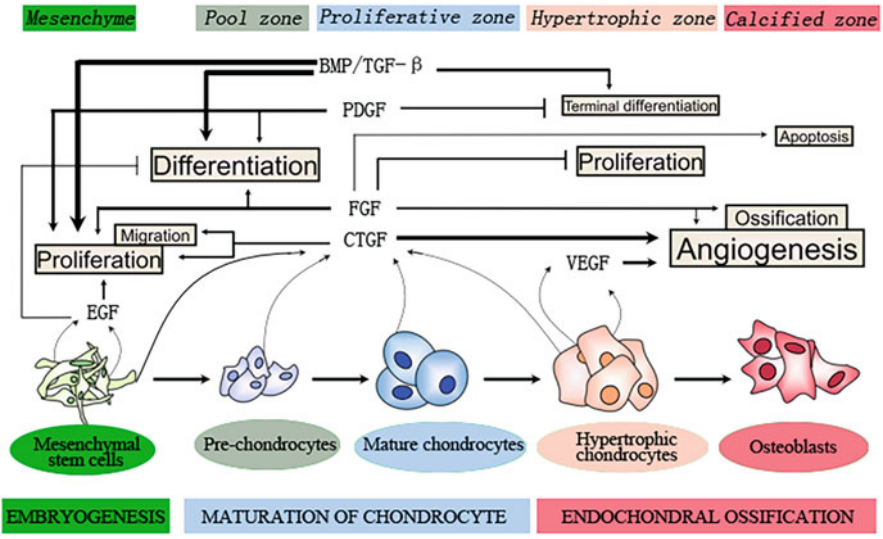

Fig. 9.5 Schematic overview of the role of growth factors at different stages of chondrogenesis. (Reprinted from [197] with permission)

the production of aggrecan and collagen type II [200]. TGF-β3 plays a role in the maturation of chondrocytes [201]. The TGF-β has been extensively used for the regeneration of cartilage defects in vitro and in vivo [122, 202–211]. For example, Yin et al. fabricated a TGF-β1-immobilized scaffold by incorporating TGF-β1-loaded gelatin microspheres into PLGA framework and evaluated the ADSC differentiation in the scaffold in vitro and regenerative ability of cartilage defect in vivo. The cell proliferation and GAG deposition in the TGF-β1-immobilized scaffold are significantly increased, and the cartilage regeneration is promoted in the defective articular cartilage in vivo [211]. Lu et al. engineered ADSCs with a baculovirus system that confers prolonged and robust TGF-β3/BMP-6 expression. Culture for 2 weeks in vitro in a porous scaffold leads to the formation of cartilaginous constructs with improved maturity and mechanical properties. After implantation into full-thickness articular cartilage defects in rabbits, these engineered constructs regenerate neocartilages that resemble native hyaline cartilage in terms of cell morphology, matrix composition, and mechanical properties. The neocartilages also have cartilage-specific zonal structures without signs of hypertrophy and degeneration and integrate well with the native cartilages [187].

9.2.3.2 IGFs

IGFs have a polypeptide sequence similar to proinsulin that allows cells to communicate with their physiologic environment. IGF-1 is well known to promote cell proliferation and inhibit apoptosis. IGF-1 is expressed in developing cartilage, mature cartilage, and synovial fluid of the joint. Both of in vitro and in vivo studies confirm that IGF-1 can induce chondrocyte differentiation and proliferation of MSCs and enhance proteoglycan and collagen type II synthesis [212–219]. Spiller et al. encapsulated IGF-1 in degradable PLGA microparticles and embedded the particles in PVA hydrogel. The PGA fiber scaffolds with chondrocytes were wrapped around the hydrogels and were implanted subcutaneously in athymic mice. Histology analysis proves enhanced cartilage formation in the layers surrounding the hydrogel with increased content of ECMs, mechanical properties, and integration between the cartilage layers and the hydrogels [218]. The regeneration of cartilage and subchondral bone in vivo was confirmed by injecting IGF-1 suspended HA solution to the temporomandibular in a rabbit model. Twelve and twenty-four weeks after the injection, the defects were well repaired, and nearly normal microarchitectural properties of the subchondral cancellous bone were found in the defects [217].

9.2.3.3 BMPs

BMPs are able to induce the formation of the cartilage and bone, which are required for the formation of prechondrogenic condensation and differentiation into chondrocytes. Meanwhile, they can increase the expression of the specific chondrocyte markers such as type X collagen [139, 205, 220–227]. BMP-2, a potent

regulator of chondrogenic expression, has received considerable attention in cartilage and osteochondral tissue engineering. Jeong et al. investigated the influence of BMP-2 on the production of cartilage matrix and subsequent bone matrix by using primary chondrocytes seeded on designed three-dimensional PCL scaffolds with chemically conjugated BMP-2. The chemically conjugated BMP-2/PCL scaffolds can significantly promote better cartilage regeneration without particularly accelerating endochondral ossification both in vitro and in vivo compared with those non-BMP-2-treated scaffolds [139].

9.2.3.4 FGF-2

FGF-2 is known as a chondrocyte mitogen found in normal cartilage and has great potential for clinical applications. It can stimulate chondrocytes to synthesize cartilaginous matrix [228–233]. Maehara et al. impregnated a porous hydroxyapatite/collagen scaffold with FGF-2 and used the scaffolds to repair large osteochondral defects in a rabbit model. With the addition of FGF-2, the neotissue in the defects displays not only the most abundant bone regeneration but also cartilage regeneration with hyaline-like appearance [232].

9.2.3.5 PDGF

PDGF is a glycolytic protein released by platelets and other cells, which stimulates the growth of cells of mesenchymal origin, for example, the cartilage [234–237]. Meanwhile, the released PDGF-AA from hydrogel being filled in the full-thickness cartilage defects greatly promotes BMSC recruitment into the hydrogel. This confirms the ability of PDGF to recruit BMSCs besides promotion of cell proliferation [237].

9.2.3.6 Exosomes (Exos)

Exos are extracellular vesicles with 30–150 nm in diameter that are produced by cells through the paracrine pathway, which contain various types of nucleic acids and proteins [238]. Recently, Exos have been regarded as important carriers for transmitting biological signals between cells instead of waste products of cells. Exos derived from stem cells are considered as ideal substitutes for stem cells in "cell-free" cartilage regeneration [239]. Jiang et.al. combined Exos derived from human Wharton's jelly-derived MSCs with scaffold of acellular porcine articular cartilage [240]. 6 months' experiment in vivo proved that the Exos can promote osteochondral regeneration in a "cell-free" condition. Shao et. al. revealed that Exos derived from infrapatellar fat pad MSCs can significantly promote the proliferation as well as the expression of Sox-9, Aggrecan, and Collagen II relative genes of chondrocytes in vitro [241]. Furthermore, Shao et.al. created a rabbit articular cartilage defect

with 4 mm in diameter and 1.5 mm in depth, and then treated with the Exos suspension. 12 weeks after the treatment, the defected cartilage was effectively regenerated with a hyaline morphology. In spite of these positive results using Exos to facilitate the regeneration of articular cartilage defect, the underlying mechanism of action remains unknown. Additionally, the low yield of Exos leads to a higher cost of Exos therapy than stem cell therapy, which might be the potential limitation to move the Exos therapy forward from bench to bedside [242].

9.2.3.7 Platelet-Rich Plasma (PRP)

PRP is a kind of autologous derivative of the whole blood, which is rich in growth factors. PRP could stimulate the migration and chondrogenic differentiation of human subchondral progenitor cells [243]. Meanwhile, PRP would counteract effects of an inflammatory environment on genes regulating matrix degradation and formation in human chondrocytes [244, 245]. Recently, PRP has commonly been utilized in the repair and regeneration of damaged articular cartilage. Lu et al. prepared an injectable hydrogel with hyaluronic acid (HA), fucoidan (FD) and gelatin (GLT), which was further cross-linked with genipin (GP) [246]. The PRP-loaded injectable hydrogel was prepared by adding PRP in the hydrogel before gelation. It could facilitate the sustained release of PRP growth factors, and promote cartilage regeneration in rabbits. Singh et al. developed a hybrid scaffold by embedding PRP/alginate-based hydrogel in porous 3D scaffold of chitosan/chondroitin sulfate/silk fibroin [247]. The hybrid construct could provide PRP-based cocktails of growth factors, which facilitates chondrogenic ECM deposition and enhanced expression of cartilage tissue-specific collagen type II and aggrecan. Autologous chondrocytes-loaded hybrid scaffolds possess the superior potential to regenerate hyaline cartilage defect of thickness around 1.10 ± 0.36 mm and integrate with surrounding tissue at the defect site.

9.2.4 Methods for Cartilage Tissue Engineering

9.2.4.1 Preculture In Vitro for Cartilage Tissue Engineering

Functional repair of focal cartilage defects requires filling the space with neotissue that has compressive properties comparable to native tissue and integration with adjacent host cartilage. One of the main issues in cartilage tissue engineering is represented by the ideal maturation of the construct before implantation in vivo, in order to optimize matrix quality and integration [248]. Considerable progress has been made toward the in vitro tissue engineering of neocartilage with compressive properties approaching native levels [249–253]. In 1997, Cao et al. reported a human ear-shaped tissue-engineered construct by using bovine articular chondrocytes and a nonwoven PGA scaffold [254]. Deponti et al. studied the difference of cartilage

maturation with or without preculture. Articular chondrocytes were embedded in fibrin glue with preculture in vitro for 1 week and implanted subcutaneously in rat, proving better tissue maturation compared with the constructs without preculture [249]. Pei et al. mixed synovium-derived stem cells with fibrin glue, which were then seeded into nonwoven PGA mesh. After 1-month incubation with growth factors, the premature construct was used to repair osteochondral defects in a rabbit model. Six months later, the defects were full of smooth hyaline-like cartilage with high expression of collagen type II and GAG, which integrated well with the surrounding tissue too [196].

Culture of constructs in a dynamic environment involving fluid flow or agitation is beneficial for cartilage synthesis compared to the static culture conditions [255]. Therefore, various bioreactors have been applied for cartilage tissue engineering, offering advantages such as better control over culture conditions, reduced diffusional limitations for delivery of nutrients and metabolites, enhanced oxygen transfer, and exertion of mechanical and hydrodynamic forces influencing cell and tissue development [256]. Shahin et al. precultured chondrocytes in PGA scaffold for 5 weeks within a bioreactor, confirming improved GAG retention in the scaffolds [257].

9.2.4.2 Regeneration of Cartilage Defects In Situ

With the deep acknowledge of cell behavior regulation and bioactive molecule functions, the in situ regeneration of cartilage defects with direct implantation of cartilage tissue engineering constructs based on biomaterials, cells, and bioactive growth factors has been extensively studied. The scaffolds based on native and/or synthetic materials play a role in supporting the viability of cells and deposition of neo-ECMs, while the bioactive growth factors regulate cell differentiation and physiological activity. Numerous studies give positive regenerative results by using the bioactive constructs in repair of articular cartilage defects. As described early, cells (chondrocytes, BMSCs, ADSCs, ESCs, etc.) and bioactive growth factors (TGF-β, IGF-1, BMPs, FGF, PDGF, etc.) are loaded into scaffolds (hydrogels, porous scaffolds, etc.), which are then implanted into the cartilage defects without prematuring. Li et al. implanted a PLGA scaffold filled with fibrin gel, mesenchymal stem cells (MSCs), and poly(ethylene oxide)-b-poly(L-lysine) (PEO-b-PLL)/pDNA-TGF-β1 complexes into osteochondral defects, resulting in full in situ regeneration of the defect [123]. However, the application of constructs containing cells and bioactive molecules is still faced with obstacles like source, amount, and phenotype maintenance of MSCs during culture, immune reaction against foreign cells, as well as feasibility of clinical translation considering the ratio of performance to price [258].

Injectable hydrogels have a greater potential to promote articular cartilage regeneration considering their tailorable structural and mechanical capabilities. Importantly, the free-flowing property makes it convenient for the loading of drugs, growth factors and cells into the injectable hydrogel by simple dissolution procedures

[38]. Zheng et.al. fabricated an injectable hydrogel based on silk fibroin, chitosan and thermal-sensitive glycerophosphate [259]. With the incorporation of TGF-β1 and BMSCs, the prepared injectable hydrogel could promote the regeneration of partial-thickness cartilage defect on knees of SD rats. Dong et.al. developed a physiochemical dual crosslinking injectable hydrogel using catechol-modified gelatin, dopamine-modified oxidized hyaluronic acid, and dendritic mesoporous organic silica nanoparticles with Fe^{3+} layers for the encapsulation of dexamethasone [260]. The obtained hydrogel was injected into osteochondral defects of 3.5 mm in diameter and 5 mm in thickness of SD rats. Post implantation for 8 weeks revealed the efficacy of the treatment on cartilage defects by the effective removal of the ROS and the inhibition of TNF-α and IL-6. Dong et.al. fabricated an injectable chitosan/silk fibroin hydrogel containing SDF-1 and PLGA microspheres loaded with Kartogenin [261]. The SDF-1 released from the hydrogel facilitated the recruitment of BMSCs in vivo, and the slowly released Kartogenin promoted the chondrogenesis of MSCs. After the hydrogel was injected into the cartilage defects (4 mm in diameter and 1.5 mm in depth) of rabbits combined with microfracture for 12 weeks, the subchondral bones and superficial cartilage were reconstructed, which were similar to the natural tissues.

9.3 Cell-Free Constructs for Cartilage Regeneration In Situ

Based upon the principles of tissue engineering, the stem cells and chondrocytes are usually used for cartilage regeneration. However, the controversy of using cells in tissue engineering still exists because of the uncertainty of dose, time point, as well as side effects [262]. In fact, stem cells are abundant in bone marrow and adult organs such as the brain, peripheral blood, skin, teeth, etc. Once tissues get damaged, endogenous stem/progenitor cells will migrate to the injured site through peripheral blood by responding to the immune cell-secreted biochemical signals [263, 264]. Therefore, homing of endogenous cells for tissue regeneration in situ would be a promising new therapeutic option to bypass the controversial of cell usage. Compared to that of the traditional cartilage tissue engineering, the recruitment of cells into cartilage defect to realize the regeneration in situ still remains rare [265]. Nonetheless, the cell-free scaffolds combined with anti-inflammatory molecules and BMSC-attractive chemokines would have positive influence on the regenerative outcome of cartilage defects. For example, Park et al. studied the in situ recruitment of BMSCs into cartilage defects by transplantation of polylactide/β-tricalcium phosphate (PLA/β-TCP) scaffolds containing IL-8 or MIP-3α [8]. Compared to those scaffolds without chemokines, the scaffolds with IL-8 or MIP-3α can highly facilitate the restoration of cartilage with a smoother surface and higher deposition of collagen. Wang et al. fabricated an anti-inflammatory scaffold composed of resveratrol-grafted polyacrylic acid and atelocollagen [266]. The scaffolds were transplanted into osteochondral defects without the employment of cells. After implantation for 12 weeks, the

proinflammation genes such as IL-1, MMP13, and COX-2 were downregulated, while the cartilage-related genes were upregulated, leading to efficient regeneration of cartilage defects. For the sake of easier application clinically, a widely accepted biomaterial instead of a brand-new one would be the best choice for fabricating the scaffold. Dai et al. fabricated a macroporous fibrin scaffold with high Fg content and mechanical strength through a porogen leaching method by using PCL microspheres as the porogen. Together with the excellent bioactivity of Fg, the cell-free fibrin scaffold could efficiently regenerate full-thickness cartilage defects in rabbit knees, resulting in neocartilage with a smooth surface, well integrity with surrounding tissue, highly deposited GAGs and collagen type II, and higher expression of cartilage-related genes and proteins, which ensure the great potential for clinical application of Fg scaffold to achieve in situ inductive cartilage regeneration [267]. A PLGA scaffold with oriented pores in its radial direction was implanted into rabbit articular osteochondral defect for 12 weeks, confirming obvious tide mark formation, and abundant chondrocytes distributing regularly with obvious lacunas in the cartilage layer [268]. A scaffold with oriented pores in radial direction can be prepared by using methacrylated hyaluronic acid via controlled directional cooling, and followed with structure-stabilization via post photocrosslinking, and further infiltrated with PLGA to enhance the mechanical strength [269]. In vivo test proved that the composite without loading cells can facilitate simultaneous regeneration of both cartilage and subchondral bone. Meanwhile, the cell-free scaffolds can facilitate cartilage regeneration in clinic too. Roessler et al. implanted a cell-free collagen type I matrix for the treatment of large cartilage defects (mean defect size 3.71 ± 1.93 cm^2, range 1.20–9.00) of the knee and conducted a short-term follow-up after the implantation. Significant pain reduction was achieved after implantation for 6 weeks, while the activity of patients was highly improved and nearly reached to preoperative value after 12 months [270].

9.4 Simultaneous Regeneration of Cartilage and Subchondral Bone

Articular cartilage defects can be divided into two forms, full-thickness cartilage defects without subchondral bone damage and osteochondral defects involving both the cartilage and the underlying subchondral bone [271]. Subchondral bone plays a pivotal role in supporting cartilage and will suffer from deterioration once cartilage is damaged. When damage of subchondral bone occurs, the neocartilage has poor integration with the subchondral bone, leading to negative regeneration of the articular cartilage defects [272]. Hence, the regeneration of structure and functions of the articular cartilage defects can be realized only if both cartilage and subchondral bone are simultaneously regenerated with good interface binding [273]. There are several problems that should be overcome for the regeneration of osteochondral defects, including the construction of different layers of scaffolds,

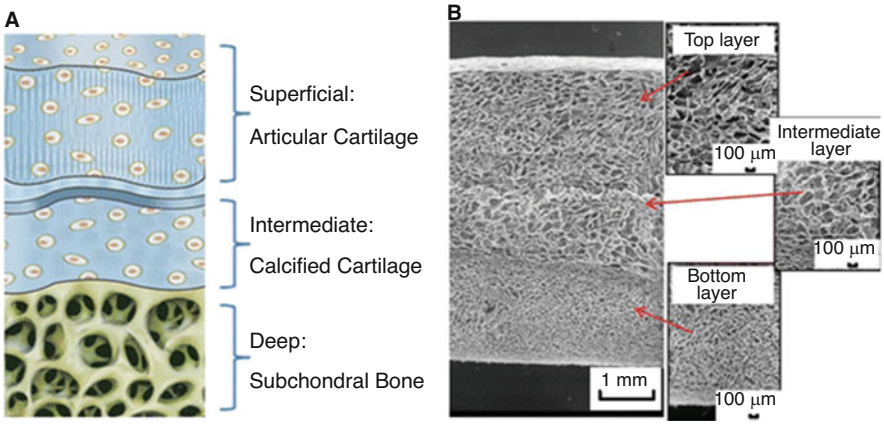

Fig. 9.6 (**a**) Schematic design of multilayered scaffolds for osteochondral defect regeneration. (**b**) Three-layered collagen scaffolds. (Reprinted from [69] with permission)

well integration of the neoformed tissues with native tissues, and the effective binding of neoformed cartilage and subchondral bone [274]. Schematic design of multilayered scaffolds for osteochondral defect regeneration and typical multilayered collagen scaffolds is shown in Fig. 9.6 [69]. Osteochondral tissues encompass cartilage layer, calcified cartilage, and subchondral bone layers in the spatial scale (Fig. 9.6a). The scaffolds with a biphasic structure based on different materials and different chemical or mechanical properties are designed for the regeneration of cartilage and subchondral bone, respectively (Fig. 9.6b) [275–279]. The evaluation of the regenerative ability of the scaffolds in vivo has found some positive results [280–283]. For example, the biphasic PEG/hydroxyapatite scaffold with cartilage- and subchondral bone-like hierarchical nanoroughness, microstructure, and spatiotemporal bioactive cues can be prepared by the 3D-printing technology. In vitro culture proves osteochondral differentiation of BMSCs in the scaffold [284]. The bilayered scaffold composed of PLCL, PLGA, and β-tricalcium phosphate (β-TCP) has been prepared by a sintering method and a gel pressing method. The PLGA/β-TCP layer has osteoconduction activity for bone regeneration, while the elastic PLCL scaffold has mechanoactive properties for cartilage regeneration [285]. The biphasic scaffold composed of aragonite-hyaluronic acid (Ar-HA) layers shows full regenerative ability of osteochondral defects with a critical size of 6 mm in diameter and 10 mm in depth in the load-bearing femoral condyle of goats [286].

Recently, 3D-printing technology has emerged as a promising strategy to fabricate scaffolds for osteochondral defects. 3D-printing provides many advantages, including well-controlled architecture (size, shape, interconnectivity, and orientation). The 3D-printed scaffold would provide structural and mechanical support, and sufficient nutrient supply, leading to regeneration of functional cartilage akin to native tissue. Depending on the biomaterials, 3D-printed scaffolds for cartilage regeneration can be classified as natural, synthetic, and inorganic scaffolds.

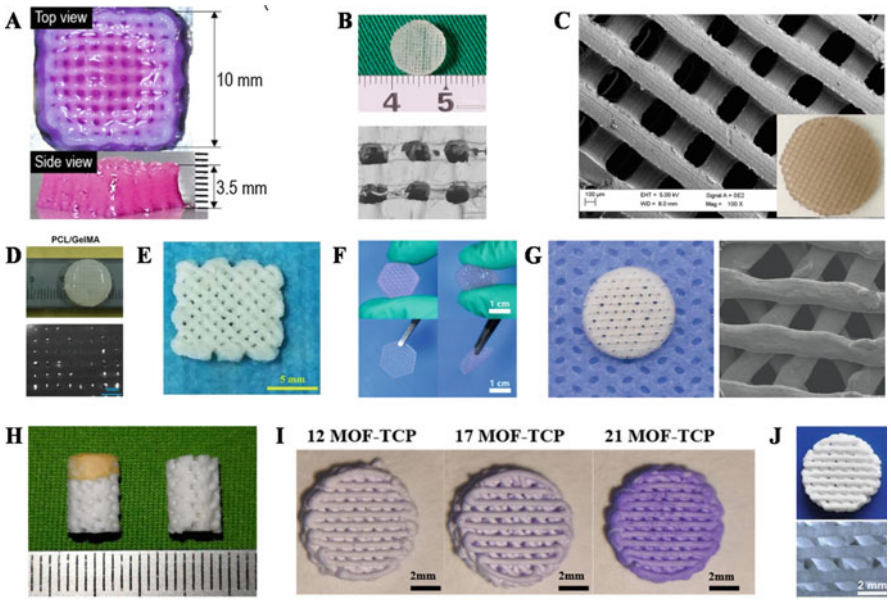

Fig. 9.7 3D-printed scaffolds of (**a**) cell-laden collagen, (**b**) modified PEG and gelatin, (**c**) modified PEG and gelatin incorporating with graphene, (**d**) polycaprolactone and modified gelatin, (**e**) short electrospinning gelatin/PLGA fibers and cartilage decellularized matrix, (**f**) gellan gum with Li-Mg-Si bioceramics, (**g**) polycaprolactone and hydroxyapatite, (**h**) bone layer (polycaprolactone / hydroxyapatite) and cartilage layer (chitosan/silk firoin), (**i**) Zn/Co-MOF-β-TCP, **(j)** Mo-doped bioactive glass ceramic. (Reprinted from [287, 291, 296, 299, 295, 303, 182, 302, 316, 317] with permission)

The natural 3D-printed scaffold is mainly designed in a form of hydrogel, by using proteins (collagen (Fig. 9.7a) [287–289], gelatin (Fig. 9.7b) [290–301], fibrin [292], and silk fibroin [298, 302]), polysaccharides (gellan gum [303], cellulose [303], chitosan [302], hyaluronic acid [294, 304, 305], alginate [290, 297, 303, 306–309], chondroitin sulfate [291]), and acellular matrix [295, 310, 311]. Compared with the traditional hydrogel with submicro- or nano-sized gel network, the 3D-printed hydrogel could be granted with macropores which facilitate the supply of oxygen and nutrients and the proliferation and differentiation of encapsulated cells. Li et al. fabricated a macroporous hydrogel with silk fibroin and tyramine-substituted gelatin by extrusion-based low temperature 3D printing [292]. The internal structure of the hydrogel could be well designed to improve the retention of stem cell aggregates and promote the articular cartilage repair. A bilayered hydrogel was fabricated using gellan gum, cellulose and sodium alginate [303]. Bioceramic particles were incorporated into the lower part of the hydrogel to mimic the subchondral bone. The hydrogel loaded with stem cells in the lower part, and with chondrocytes in the upper part could facilitate simultaneous regeneration of both cartilage and subchondral bone. Hydrogel with interpenetrating polymer network could be fabricated by 3D-printed technology using polyethylene

glycol diacrylate, gelatin methacryloyl, and chondroitin sulfate methacrylate through photocrosslinking [291]. The designed hydrogel possessed not only adequate mechanical strength but also maintained a suitable 3D microenvironment for differentiation, proliferation and extracellular matrix production of stem cells.

Compared with natural biomaterials, synthetic biomaterials are favored by researchers because of their strong controllability and mechanical properties. Up to now, several biodegradable synthetic polymers, including polyethylene glycol (PEG) (Fig. 9.7c) [291, 296], polyvinyl alcohol (PVA) [312], polyurethane [304, 311, 313], poly (lactic-*co*-glycolic acid) (PLGA) (Fig. 9.7e) [295], and polycaprolactone (PCL) (Fig. 9.7d) [182, 299, 302, 308, 309, 314, 315], have been used in 3D-printed scaffolds for cartilage regeneration. For instance, Zhou et al. developed a graphene oxide-doped, gelatin methacrylate and poly (ethylene glycol) diacrylate (PEGDA)-based 3D-printing ink, in which the PEGDA could greatly improve the printability performance of the ink [296]. Because of the strong hydrogen bonding interaction in the PEGDA solution, there exists severe extrusion swelling of the pure PEGDA solution during the most common nozzle printing process, which greatly restricts the development of 3D printing of PEGDA hydrogel. Meng et al. improved the printing accuracy of PEGDA solution by adding graphene oxide and hydroxyapatite, and realized the 3D printing of a PEGDA-based hydrogel with a biomimetic pore size gradient [312]. Inspired by the architecture of collagen fibers in native cartilage tissue, Cao et al. fabricated a tri-layered scaffold with pore size gradient based on polycaprolactone and methacrylated alginate hydrogel encapsulating stem cells [308]. The stem cells-loaded gradient 3D-printed scaffolds showed excellent cell survival, proliferation and morphology, collagen II deposition, and hopeful chondrogenic differentiation.

Moreover, the scaffolds for osteochondral repair based on bioresorbable ceramic, including hydroxyapatite (Fig. 9.7g, h) [182, 288, 297, 301, 302, 307], β-tricalcium phosphate(β-TCP) [316], and bioactive glass ceramic (Fig. 9.7f) [303, 317] can be fabricated by 3D-printing technology. Hydroxyapatite is one of the essential inorganic components from bones and teeth, which is widely applied in biomedical engineering due to their excellent biocompatibility, bioactivity, osteointegrity, and osteoconductive properties [318]. Hsieh et al. prepared a biomimetic scaffold consisting of hydroxyapatite/polycaprolactone and glycidyl-methacrylate-hyaluronic acid for healing osteochondral defects [319]. The scaffolds were implanted in the knees of a miniature pig for a period of 12 months, and realized the regeneration of hyaline cartilage. β-TCP is a typical bioresorbable ceramic for bone tissue regeneration [320]. Shu et al. prepared a 3D-printed β-TCP scaffold, which was further functionalized with zinc-cobalt bimetallic organic framework (Zn/Co-MOF) (Fig. 9.7i) [316]. The hybrid scaffolds preserve excellent antioxidative and anti-inflammatory properties to protect cells from reactive oxygen species invasion, and induce the osteogenic and chondrogenic differentiation simultaneously in vitro. Moreover, in vivo studies prove that the Zn/Co-MOF-TCP scaffolds could accelerate the integrated regeneration of cartilage and subchondral bone in severe osteochondral defects induced by osteoarthritis. Dang et al. prepared a series of molybdenum-doped bioactive glass ceramic through combining a sol-gel

method with 3D-printing technology (Fig. 9.7j) [317]. The scaffold not only significantly stimulated the proliferation and differentiation of both chondrocytes and stem cells in vitro, but also showed bi-lineage bioactivities for regeneration of articular cartilage and subchondral bone tissues in vivo.

9.5 Histological Grading of Cartilage

Histological quality of repaired cartilage is one of the most important evaluations of success in cartilage regeneration. Up to present, various histological scoring systems are used to evaluate the quality of cartilage tissues. Basically, a scoring system should be comprehensive but also applicable to researchers with limited knowledge of cartilage histology. In summary, the systems are divided into three categories to describe the osteoarthritic, in vivo repaired, and in vitro engineered cartilage, respectively [321].

Scoring systems for osteoarthritic cartilage focus on the degenerative features of healthy or diseased cartilage. Histological-Histochemical Grading System (HHGS) is the first system for the evaluation of osteoarthritic cartilage [322]. It evaluates the cartilage structure, cell distribution, Safranin-O staining, and tidemark integrity to classify the level of cartilage damage. HHGS is applied in the grading of both human and animal cartilages [323, 324]. Although widely used, HHGS is not efficient to evaluate the specific extent of cartilage deterioration [325]. Osteoarthritis Research Society International (OARSI) developed an Osteoarthritis Cartilage Histopathology Assessment System for better evaluation of the severity and the extent of cartilage surface damage during the arthritic process [326]. The OARSI system is more adequate for the assessment of mild osteoarthritis and could be more conveniently used by less experienced observers [325].

Many scoring systems are developed to evaluate the regeneration of cartilage defect in vivo. O'Driscoll score, Pineda scale, Wakitani score, OsScore, Knutsen score, and International Cartilage Repair Society (ICRS) score are widely used [321]. O'Driscoll is the first scoring system to assess the repaired cartilage in vivo and is frequently used for cartilage analysis in animal studies [327]. However, many different subitems make it a bit lengthy and complicated to use. Pineda scale is developed to simplify the assessment and is applied to evaluate the self-healing ability of cartilage defect in rabbit at the first beginning [328]. After that, Wakitani introduced a modified scoring system based on Pineda scale, which is extensively applied to evaluate animal cartilage repair in vivo [329]. O'Driscoll, Pineda scale, and Wakitani score are mainly used to evaluate cartilage repair in animal models. In contrast to the animal studies, the study of cartilage repair in human is hard to evaluate due to the infeasible harvest of large biopsy. Considering that, Robert et al. proposed a scoring system for small biopsy of repaired human cartilage, which is named as OsScore [330]. Moreover, ICRS introduced ICRS I and ICRS II scoring systems for more easy and reliable histological evaluation of repaired cartilage [331, 332]. ICRS scoring systems are based on a catalogue of repaired cartilage as

a reference for scoring. Distinguished from other systems, ICRS scoring enables discrimination of each subitem, instead of summarizing all the subitems to create a total score. Compared with the ICRS I, the ICRS II contains additional categories, making it more comprehensive. Especially when a scaffold is used in cartilage repair, a category of inflammation can be included to the ICRS II [333].

Scoring system for engineered cartilage should focus on the quality of newly generated cartilage after engineering in vitro. Few histological scoring systems are available for the evaluation of engineered cartilage. O'Driscoll introduced a simple scoring system to evaluate the density of GAGs in the engineered cartilage [334]. This system is not sufficient since many other characteristics, for example, cell morphology, are not included. Another grading system, Bern score, was validated for the evaluation of engineered cartilage [335]. In contrast to O'Driscoll score, Bern score has a broader score range, which gives more information about the characteristics of tissue [336].

9.6 Challenges and Perspectives

Although the cartilage tissue engineering has been investigated for over two decades, rather limited success is achieved to develop clinically relevant outcomes. Nonetheless, significant strides have been made to select optimal cell sources; to identify suitable chemistry, morphology, and compliance of scaffold materials; and to optimize culture conditions and dose and delivery of soluble factors, which are of great importance to develop models of cartilage development in vitro and regeneration of cartilage defects in vivo. Meanwhile, many efforts have been made to overcome the limitations in cell harvesting and to establish culture and implantation techniques in vitro. Novel methods of manufacture such as 3D printing have opened new horizons for constructing personalized constructs for cartilage regeneration. A thorough understanding of the biological processes at both cellular and molecular levels will ensure the safety and effectiveness of these innovations. With the deep understanding of pathological and healing principles under cartilage defects, cell homing and in situ inductive regeneration of both cartilage and subchondral bone are also full of prospects. All these developments, taken together, may in the future lead to the successful and cost-effective translation from the bench top to the bedside by using novel cell/biomaterial constructs in cartilage regeneration.

References

1. McDevitt CA, Marcelino J. Composition of articular cartilage. Sports Med Arthrosc Rev. 1994;2:1–12.

2. Poole AR, Kojima T, Yasuda T, Mwale F, Kobayashi M, Laverty S. Composition and structure of articular cartilage: a template for tissue repair. Clin Orthop Relat Res. 2001;391: S26–33.
3. Umlauf D, Frank S, Pap T, Bertrand J. Cartilage biology, pathology, and repair. Cell Mol Life Sci. 2010;67:4197–211.
4. Kay P, Freemont A, Davies D. The aetiology of multiple loose bodies. Snow storm knee. Bone Joint J. 1989;71:501–4.
5. Jeuken RM, Roth AK, Peters RJ, van Donkelaar CC, Thies JC, van Rhijn LW, et al. Polymers in cartilage defect repair of the knee: current status and future prospects. Polymers. 2016;8: 219.
6. Gomoll AH, Farr J. Autologous chondrocyte implantation (ACI). Cartilage restoration. New York: Springer; 2014. p. 143–52.
7. Gomoll AH, Farr J, Osteochondral autograft transfer. Cartilage restoration. New York: Springer; 2014. p. 123–9.
8. Park MS, Kim YH, Jung Y, Kim SH, Park JC, Yoon DS, et al. In situ recruitment of human BMSCs using chemokines for articular cartilage regeneration. Cell Transplant. 2014;24(6): 1067–83.
9. Bhardwaj N, Devi D, Mandal BB. Tissue-engineered cartilage: the crossroads of biomaterials. Cells and stimulating factors. Macromol Biosci. 2015;15:153–82.
10. Kwon H, Paschos NK, Hu JC, Athanasiou K. Articular cartilage tissue engineering: the role of signaling molecules. Cell Mol Life Sci. 2016;73:1173–94.
11. Babensee JE, Anderson JM, McIntire LV, Mikos AG. Host response to tissue engineered devices. Adv Drug Deliv Rev. 1998;33:111–39.
12. Badylak SF, Gilbert TW. Immune response to biologic scaffold materials. Semin Immunol. 2008;20:109–16.
13. Puppi D, Chiellini F, Piras AM, Chiellini E. Polymeric materials for bone and cartilage repair. Prog Polym Sci. 2010;35:403–40.
14. Zheng L, Fan HS, Sun J, Chen XN, Wang G, Zhang L, et al. Chondrogenic differentiation of mesenchymal stem cells induced by collagen-based hydrogel: an in vivo study. J Biomed Mater Res A. 2010;93A:783–92.
15. Cheng H-W, Luk KDK, Cheung KMC, Chan BP. In vitro generation of an osteochondral interface from mesenchymal stem cell-collagen microspheres. Biomaterials. 2011;32:1526–35.
16. Bian W, Li D, Lian Q, Li X, Zhang W, Wang K, et al. Fabrication of a bio-inspired beta-tricalcium phosphate/collagen scaffold based on ceramic stereolithography and gel casting for osteochondral tissue engineering. Rapid Prototyp J. 2012;18:68–80.
17. Park S-H, Song T, Bae TS, Khang G, Choi BH, Park SR, et al. Comparative analysis of collagens extracted from different animal sources for application of cartilage tissue engineering. Int J Precis Eng Manuf. 2012;13:2059–66.
18. Zhang Q, Lu H, Kawazoe N, Chen G. Preparation of collagen scaffolds with controlled pore structures and improved mechanical property for cartilage tissue engineering. J Bioact Compat Polym. 2013;28:426–38.
19. Zheng L, Lu HQ, Fan HS, Zhang XD. Reinforcement and chemical cross-linking in collagen-based scaffolds in cartilage tissue engineering: a comparative study. Iran Polym J. 2013;22: 833–42.
20. Yuan T, Zhang L, Li K, Fan H, Fan Y, Liang J, et al. Collagen hydrogel as an immunomodulatory scaffold in cartilage tissue engineering. J Biomed Mater Res B Appl Biomater. 2014;102:337–44.
21. Zheng L, Jiang X, Chen X, Fan H, Zhang X. Evaluation of novel in situ synthesized nano-hydroxyapatite/collagen/alginate hydrogels for osteochondral tissue engineering. Biomed Mater. 2014;9(6):065004.
22. Silverman RP, Passaretti D, Huang W, Randolph MA, Yaremchuk M. Injectable tissue-engineered cartilage using a fibrin glue polymer. Plast Reconstr Surg. 1999;103:1809–18.

23. Park SH, Park SR, Chung SI, Pai KS, Min BH. Tissue-engineered cartilage using fibrin/hyaluronan composite gel and its in vivo implantation. Artif Organs. 2005;29:838–45.
24. Ahmed TAE, Giulivi A, Griffith M, Hincke M. Fibrin glues in combination with mesenchymal stem cells to develop a tissue-engineered cartilage substitute. Tissue Eng Part A. 2011;17:323–35.
25. Singh K, Moyer H, Williams JK, Schwartz Z, Boyan BD. Fibrin glue a scaffold for cellular-based therapy in a critical-sized defect. Ann Plast Surg. 2011;66:301–5.
26. Hong HJ, Lee JS, Choi JW, Min BH, Lee HB, Kim CH. Transplantation of autologous chondrocytes seeded on a fibrin/hyaluronan composite gel into tracheal cartilage defects in rabbits: preliminary results. Artif Organs. 2012;36:998–1006.
27. Cakmak O, Babakurban ST, Akkuzu HG, Bilgi S, Ovali E, Kongur M, et al. Injectable tissue-engineered cartilage using commercially available fibrin glue. Laryngoscope. 2013;123:2986–92.
28. Bhardwaj N, Kundu SC. Chondrogenic differentiation of rat MSCs on porous scaffolds of silk fibroin/chitosan blends. Biomaterials. 2012;33:2848–57.
29. Chen C-H, Liu JM-J, Chua C-K, Chou S-M, Shyu VB-H, Chen J-P. Cartilage tissue engineering with silk fibroin scaffolds fabricated by indirect additive manufacturing technology. Materials. 2014;7:2104–19.
30. Han K-S, Song JE, Tripathy N, Kim H, Moon BM, Park CH, et al. Effect of pore sizes of silk scaffolds for cartilage tissue engineering. Macromol Res. 2015;23:1091–7.
31. Yan L-P, Silva-Correia J, Oliveira MB, Vilela C, Pereira H, Sousa RA, et al. Bilayered silk/silk-nanoCaP scaffolds for osteochondral tissue engineering: in vitro and in vivo assessment of biological performance. Acta Biomater. 2015;12:227–41.
32. Yodmuang S, McNamara SL, Nover AB, Mandal BB, Aganwal M, Kelly T-AN, et al. Silk microfiber-reinforced silk hydrogel composites for functional cartilage tissue repair. Acta Biomater. 2015;11:27–36.
33. Snyder TN, Madhavan K, Intrator M, Dregalla RC, Park D. A fibrin/hyaluronic acid hydrogel for the delivery of mesenchymal stem cells and potential for articular cartilage repair. J Biol Eng. 2014;8:10.
34. Skaalure SC, Dimson SO, Pennington AM, Bryant SJ. Semi-interpenetrating networks of hyaluronic acid in degradable PEG hydrogels for cartilage tissue engineering. Acta Biomater. 2014;10:3409–20.
35. Mintz BR, Cooper JA. Hybrid hyaluronic acid hydrogel/poly(epsilon-caprolactone) scaffold provides mechanically favorable platform for cartilage tissue engineering studies. J Biomed Mater Res A. 2014;102:2918–26.
36. Magalhaes J, Crawford A, Hatton PV, Blanco FJ, Roman JS. Poly(2-ethyl-(2-pyrrolidone) methacrylate) and hyaluronic acid-based hydrogels for the engineering of a cartilage-like tissue using bovine articular chondrocytes. J Bioact Compat Polym. 2014;29:545–59.
37. Levett PA, Hutmacher DW, Malda J, Klein TJ. Hyaluronic acid enhances the mechanical properties of tissue-engineered cartilage constructs. PloS One. 2014;9:e113216.
38. Lebourg M, Martinez-Diaz S, Garcia-Giralt N, Torres-Claramunt R, Ribelles JLG, Vila-Canet G, et al. Cell-free cartilage engineering approach using hyaluronic acid-polycaprolactone scaffolds: a study in vivo. J Biomater Appl. 2014;28:1304–15.
39. Sheu SY, Chen WS, Sun JS, Lin FH, Wu T. Biological characterization of oxidized hyaluronic acid/resveratrol hydrogel for cartilage tissue engineering. J Biomed Mater Res A. 2013;101:3457–66.
40. Chang NJ, Jhung YR, Yao CK, Yeh ML. Hydrophilic gelatin and hyaluronic acid-treated PLGA scaffolds for cartilage tissue engineering. J Appl Biomater Funct Mater. 2013;11:45–52.
41. Toh WS, Lim TC, Kurisawa M, Spector M. Modulation of mesenchymal stem cell chondrogenesis in a tunable hyaluronic acid hydrogel microenvironment. Biomaterials. 2012;33:3835–45.

42. Matsiko A, Levingstone TJ, O'Brien FJ, Gleeson JP. Addition of hyaluronic acid improves cellular infiltration and promotes early-stage chondrogenesis in a collagen-based scaffold for cartilage tissue engineering. J Mech Behav Biomed Mater. 2012;11:41–52.
43. Erickson IE, Kestle SR, Zellars KH, Farrell MJ, Kim M, Burdick JA, et al. High mesenchymal stem cell seeding densities in hyaluronic acid hydrogels produce engineered cartilage with native tissue properties. Acta Biomater. 2012;8:3027–34.
44. Tan HP, Chu CR, Payne KA, Marra KG. Injectable in situ forming biodegradable chitosan-hyaluronic acid based hydrogels for cartilage tissue engineering. Biomaterials. 2009;30:2499–506.
45. Park SJ, Yu SM, Chun MH, Chun HJ, Kim CH. Effect of hyaluronic acid on attachment and proliferation of chondrocyte on chitosan/hyaluronic acid bead scaffolds. Tissue Eng Regen Med. 2009;6:438–44.
46. Jung SH, Jang JW, Kim SH, Hong HH, Oh AY, Rhee JM, et al. Articular cartilage regeneration using hyaluronic acid loaded PLGA scaffold by emulsion freeze-drying method. Tissue Eng Regen Med. 2008;5:643–9.
47. Choi SW, Moon SK, Chu JY, Lee HW, Park TJ, Kim JH. Alginate hydrogel embedding poly (D, L-lactide-co-glycolide) porous scaffold disks for cartilage tissue engineering. Macromol Res. 2012;20:447–52.
48. Kim HM, Park JY, Kim EY, Song JE, Kwon SY, Chung JW, et al. Tissue engineered cartilage reconstruction with alginate sponge containing demineralized bone particles. Polym Korea. 2014;38:278–85.
49. Park H, Lee KY. Cartilage regeneration using biodegradable oxidized alginate/hyaluronate hydrogels. J Biomed Mater Res A. 2014;102:4519–25.
50. Fan CJ, Wang DA. Potential use of alginate beads as a chondrocyte delivery vehicle and stepwise dissolving porogen in a hydrogel scaffold for cartilage tissue engineering. RSC Adv. 2015;5:80688–97.
51. Reppel L, Schiavi J, Charif N, Leger L, Yu H, Pinzano A, et al. Chondrogenic induction of mesenchymal stromal/stem cells from Wharton's jelly embedded in alginate hydrogel and without added growth factor: an alternative stem cell source for cartilage tissue engineering. Stem Cell Res Ther. 2015;6:260.
52. Xue JX, Feng B, Zheng R, Lu Y, Zhou GD, Liu W, et al. Engineering ear-shaped cartilage using electrospun fibrous membranes of gelatin/polycaprolactone. Biomaterials. 2013;34:2624–31.
53. Levett PA, Melchels FPW, Schrobback K, Hutmacher DW, Malda J, Klein TJ. A biomimetic extracellular matrix for cartilage tissue engineering centered on photocurable gelatin, hyaluronic acid and chondroitin sulfate. Acta Biomater. 2014;10:214–23.
54. Zheng R, Duan HC, Xue JX, Liu Y, Feng B, Zhao SF, et al. The influence of gelatin/PCL ratio and 3-D construct shape of electrospun membranes on cartilage regeneration. Biomaterials. 2014;35:152–64.
55. Kuo CY, Chen CH, Hsiao CY, Chen JP. Incorporation of chitosan in biomimetic gelatin/chondroitin-6-sulfate/hyaluronan cryogel for cartilage tissue engineering. Carbohydr Polym. 2015;117:722–30.
56. Miao T, Miller EJ, McKenzie C, Oldinski RA. Physically crosslinked polyvinyl alcohol and gelatin interpenetrating polymer network theta-gels for cartilage regeneration. J Mater Chem B. 2015;3:9242–9.
57. Yin F, Cai JF, Zen W, Wei YH, Zhou W, Yuan F, et al. Cartilage regeneration of adipose-derived stem cells in the TGF-beta 1-immobilized PLGA-gelatin scaffold. Stem Cell Rev Rep. 2015;11:453–9.
58. Breyner NM, Hell RCR, Carvalho LRP, Machado CB, Peixoto Filho IN, Valerio P, et al. Effect of a three-dimensional chitosan porous scaffold on the differentiation of mesenchymal stem cells into chondrocytes. Cells Tissues Organs. 2010;191:119–28.

59. Ragetly GR, Slavik GJ, Cunningham BT, Schaeffer DJ, Griffon DJ. Cartilage tissue engineering on fibrous chitosan scaffolds produced by a replica molding technique. J Biomed Mater Res A. 2010;93A:46–55.
60. Bi L, Cao Z, Hu Y, Song Y, Yu L, Yang B, et al. Effects of different cross-linking conditions on the properties of genipin-cross-linked chitosan/collagen scaffolds for cartilage tissue engineering. J Mater Sci Mater Med. 2011;22:51–62.
61. Oliveira JT, Crawford A, Mundy JL, Sol PC, Correlo VM, Bhattacharya M, et al. Novel melt-processable chitosan-polybutylene succinate fibre scaffolds for cartilage tissue engineering. J Biomater Sci Polym Ed. 2011;22:773–88.
62. Whu SW, Hung K-C, Hsieh K-H, Chen C-H, Tsai C-L, S-h H. In vitro and in vivo evaluation of chitosan-gelatin scaffolds for cartilage tissue engineering. Mater Sci Eng C Mater Biol Appl. 2013;33:2855–63.
63. Garcia-Lopez J, Garciadiego-Cazares D, Melgarejo-Ramirez Y, Sanchez-Sanchez R, Solis-Arrieta L, Garcia-Carvajal Z, et al. Chondrocyte differentiation for auricular cartilage reconstruction using a chitosan based hydrogel. Histol Histopathol. 2015;30:1477–85.
64. Muzzarelli RAA, El Mehtedi M, Bottegoni C, Aquili A, Gigante A. Genipin-crosslinked chitosan gels and scaffolds for tissue engineering and regeneration of cartilage and bone. Mar Drugs. 2015;13:7314–38.
65. Park JS, Yang HN, Woo DG, Jeon SY, Park K-H. Chondrogenesis of human mesenchymal stem cells in fibrin constructs evaluated in vitro and in nude mouse and rabbit defects models. Biomaterials. 2011;32:1495–507.
66. Wu J, Ding Q, Dutta A, Wang Y, Huang Y-h, Weng H, et al. An injectable extracellular matrix derived hydrogel for meniscus repair and regeneration. Acta Biomater. 2015;16:49–59.
67. Zhang Q, Lu H, Kawazoe N, Chen G. Pore size effect of collagen scaffolds on cartilage regeneration. Acta Biomater. 2014;10:2005–13.
68. Vickers SM, Gotterbarm T, Spector M. Cross-linking affects cellular condensation and chondrogenesis in Type II collagen-GAG scaffolds seeded with bone marrow-derived mesenchymal stem cells. J Orthop Res. 2010;28:1184–92.
69. Levingstone TJ, Thompson E, Matsiko A, Schepens A, Gleeson JP, O'Brien FJ. Multi-layered collagen-based scaffolds for osteochondral defect repair in rabbits. Acta Biomater. 2016;32:149–60.
70. Kim IL, Mauck RL, Burdick JA. Hydrogel design for cartilage tissue engineering: a case study with hyaluronic acid. Biomaterials. 2011;32:8771–82.
71. Sun JC, Tan HP. Alginate-based biomaterials for regenerative medicine applications. Materials. 2013;6:1285–309.
72. Steinert A, Weber M, Dimmler A, Julius C, Schütze N, Nöth U, et al. Chondrogenic differentiation of mesenchymal progenitor cells encapsulated in ultrahigh – viscosity alginate. J Orthop Res. 2003;21:1090–7.
73. Paige KT, Cima LG, Yaremchuk MJ, Schloo BL, Vacanti JP, Vacanti CA. De novo cartilage generation using calcium alginate-chondrocyte constructs. Plast Reconstr Surg. 1996;97:168–78. discussion 79–80.
74. Igarashi T, Iwasaki N, Kasahara Y, Minami A. A cellular implantation system using an injectable ultra-purified alginate gel for repair of osteochondral defects in a rabbit model. J Biomed Mater Res A. 2010;94A:844–55.
75. Lien SM, Li WT, Huang TJ. Genipin-crosslinked gelatin scaffolds for articular cartilage tissue engineering with a novel crosslinking method. Mater Sci Eng C Biomim Supramol Syst. 2008;28:36–43.
76. Kim DH, Heo SJ, Shin JW, Mun CW, Park KM, Park KD, et al. Preparation of thermosensitive gelatin-pluronic copolymer for cartilage tissue engineering. Macromol Res. 2010;18:387–91.
77. Shin EY, Park JH, Shin ME, Song JE, Carlomagno C, Khang G. Evaluation of chondrogenic differentiation ability of bone marrow mesenchymal stem cells in silk fibroin/gellan gum hydrogels using miR-30. Macromol Res. 2019;27(4):369–76.

78. Farokhi M, Mottaghitalab F, Fatahi Y, et al. Silk fibroin scaffolds for common cartilage injuries: possibilities for future clinical applications. Eur Polym J. 2019;115:251–67.
79. Perez-Silos V, Moncada-Saucedo NK, Pena-Martinez V, et al. A cellularized biphasic implant based on a bioactive silk fibroin promotes integration and tissue organization during osteochondral defect repair in a porcine model. Int J Mol Sci. 2019;20(20):5145.
80. Cao Z, Wang H, Chen J, et al. Silk-based hydrogel incorporated with metal-organic framework nanozymes for enhanced osteochondral regeneration. Bioact Mater. 2023;20:221–42.
81. Sutherland AJ, Beck EC, Dennis SC, Converse GL, Hopkins RA, Berkland CJ, et al. Decellularized cartilage may be a chondroinductive material for osteochondral tissue engineering. PloS One. 2015;10:e0121966.
82. Fermor HL, Russell SL, Williams S, Fisher J, Ingham E. Development and characterisation of a decellularised bovine osteochondral biomaterial for cartilage repair. J Mater Sci Mater Med. 2015;26:186.
83. Chen Y-C, Chen R-N, Jhan H-J, Liu D-Z, Ho H-O, Mao Y, et al. Development and characterization of acellular extracellular matrix scaffolds from porcine menisci for use in cartilage tissue engineering. Tissue Eng Part C Methods. 2015;21:971–86.
84. Benders KEM, van Weeren PR, Badylak SF, Saris DBF, Dhert WJA, Malda J. Extracellular matrix scaffolds for cartilage and bone regeneration. Trends Biotechnol. 2013;31:169–76.
85. Yang Z, Shi Y, Wei X, He J, Yang S, Dickson G, et al. Fabrication and repair of cartilage defects with a novel acellular cartilage matrix scaffold. Tissue Eng Part C Methods. 2009;16:865–76.
86. Dai L, He Z, Jiang Y, et al. One-step strategy for cartilage repair using acellular bone matrix scaffold based in situ tissue engineering technique in a preclinical minipig model. Am J Transl Res. 2019;11(10):6650–9.
87. Ayariga JA, Huang H, Dean D. Decellularized avian cartilage, a promising alternative for human cartilage tissue regeneration. Materials. 2022;15(5):1974.
88. Das P, Mishra R, Devi B, et al. Decellularized xenogenic cartilage extracellular matrix (ECM) scaffolds for the reconstruction of osteochondral defects in rabbits. J Mater Chem B. 2021;9(24):4873–94.
89. Oh HJ, Kim SH, Cho J-H, Park S-H, Min B-H. Mechanically reinforced extracellular matrix scaffold for application of cartilage tissue engineering. Tissue Eng Regener Med. 2018;15(3):287–99.
90. Chu W, Hu G, Peng L, Zhang W, Ma Z. The use of a novel deer antler decellularized cartilage-derived matrix scaffold for repair of osteochondral defects. J Biol Eng. 2021;15(1):23.
91. Zhang X, Liu Y, Luo C, et al. Crosslinker-free silk/decellularized extracellular matrix porous bioink for 3D bioprinting-based cartilage tissue engineering. Mater Sci Eng C. 2021;118:111388.
92. Fan HB, Hu YY, Zhang CL, Li XS, Lv R, Qin L, et al. Cartilage regeneration using mesenchymal stem cells and a PLGA-gelatin/chondroitin/hyaluronate hybrid scaffold. Biomaterials. 2006;27:4573–80.
93. He X, Lu H, Kawazoe N, Tateishi T, Chen G. A novel cylinder-type poly(L-lactic acid)-collagen hybrid sponge for cartilage tissue engineering. Tissue Eng Part C Methods. 2010;16:329–38.
94. Andreas K, Zehbe R, Kazubek M, Grzeschik K, Sternberg N, Baumler H, et al. Biodegradable insulin-loaded PLGA microspheres fabricated by three different emulsification techniques: investigation for cartilage tissue engineering. Acta Biomater. 2011;7:1485–95.
95. Kim M, Hong B, Lee J, Kim SE, Kang SS, Kim YH, et al. Composite system of PLCL scaffold and heparin-based hydrogel for regeneration of partial-thickness cartilage defects. Biomacromolecules. 2012;13:2287–98.
96. Perez Olmedilla M, Lebourg M, Escobar Ivirico JL, Nebot I, Garcia Giralt N, Gallego Ferrer G, et al. In vitro 3D culture of human chondrocytes using modified epsilon-caprolactone scaffolds with varying hydrophilicity and porosity. J Biomater Appl. 2012;27:299–309.

97. Cai Y, Li J, Poh CK, Tan HC, Thian ES, Fuh JYH, et al. Collagen grafted 3D polycaprolactone scaffolds for enhanced cartilage regeneration. J Mater Chem B. 2013;1:5971–6.
98. Chen C-H, Shyu VB-H, Chen J-P, Lee M-Y. Selective laser sintered poly-epsilon-caprolactone scaffold hybridized with collagen hydrogel for cartilage tissue engineering. Biofabrication. 2014;6:015004.
99. Kundu J, Shim J-H, Jang J, Kim S-W, Cho D-W. An additive manufacturing-based PCL-alginate-chondrocyte bioprinted scaffold for cartilage tissue engineering. J Tissue Eng Regen Med. 2015;9:1286–97.
100. Hwang YS, Sangaj N, Varghese S. Interconnected macroporous poly(ethylene glycol) cryogels as a cell scaffold for cartilage tissue engineering. Tissue Eng Part A. 2010;16: 3033–41.
101. Zhang C, Sangaj N, Hwang YS, Phadke A, Chang CW, Varghese S. Oligo(trimethylene carbonate)-poly(ethylene glycol)-oligo(trimethylene carbonate) triblock-based hydrogels for cartilage tissue engineering. Acta Biomater. 2011;7:3362–9.
102. Rennerfeldt DA, Renth AN, Talata Z, Gehrke SH, Detamore MS. Tuning mechanical performance of poly(ethylene glycol) and agarose interpenetrating network hydrogels for cartilage tissue engineering. Biomaterials. 2013;34:8241–57.
103. Roberts JJ, Bryant SJ. Comparison of photopolymerizable thiol-ene PEG and acrylate-based PEG hydrogels for cartilage development. Biomaterials. 2013;34:9969–79.
104. Yu F, Cao XD, Li YL, Zeng L, Yuan B, Chen XF. An injectable hyaluronic acid/PEG hydrogel for cartilage tissue engineering formed by integrating enzymatic crosslinking and Diels-Alder “click chemistry”. Polym Chem. 2014;5:1082–90.
105. Yu F, Cao XD, Li YL, Zeng L, Zhu JH, Wang G, et al. Diets-Alder crosslinked HA/PEG hydrogels with high elasticity and fatigue resistance for cell encapsulation and articular cartilage tissue repair. Polym Chem. 2014;5:5116–23.
106. Fan CJ, Wang DA. A biodegradable PEG-based micro-cavitary hydrogel as scaffold for cartilage tissue engineering. Eur Polym J. 2015;72:651–60.
107. Skaalure SC, Chu S, Bryant SJ. An enzyme-sensitive PEG hydrogel based on aggrecan catabolism for cartilage tissue engineering. Adv Healthc Mater. 2015;4:420–31.
108. Sridhar BV, Brock JL, Silver JS, Leight JL, Randolph MA, Anseth KS. Development of a cellularly degradable PEG hydrogel to promote articular cartilage extracellular matrix deposition. Adv Healthc Mater. 2015;4:702–13.
109. Wang W, Li B, Li Y, Jiang Y, Ouyang H, Gao C. In vivo restoration of full-thickness cartilage defects by poly (lactide-co-glycolide) sponges filled with fibrin gel, bone marrow mesenchymal stem cells and DNA complexes. Biomaterials. 2010;31:5953–65.
110. Sharifi S, Blanquer SBG, van Kooten TG, Grijpma DW. Biodegradable nanocomposite hydrogel structures with enhanced mechanical properties prepared by photo-crosslinking solutions of poly(trimethylene carbonate)–poly(ethylene glycol)–poly(trimethylene carbonate) macromonomers and nanoclay particles. Acta Biomater. 2012;8:4233–43.
111. Kim H-J, Lee J-H, Im G-I. Chondrogenesis using mesenchymal stem cells and PCL scaffolds. J Biomed Mater Res A. 2010;92A:659–66.
112. Munirah S, Kim SH, Ruszymah BHI, Khang G. The use of fibrin and poly(lactic-co-glycolic acid) hybrid scaffold for articular cartilage tissue engineering: an in vivo analysis. Eur Cell Mater. 2008;15:41–51.
113. Quinlan E, Lopez-Noriega A, Thompson E, Kelly HM, Cryan SA, O’Brien FJ. Development of collagen-hydroxyapatite scaffolds incorporating PLGA and alginate microparticles for the controlled delivery of rhBMP-2 for bone tissue engineering. J Control Release. 2015;198:71–9.
114. Sato T, Chen GP, Ushida T, Ishii T, Ochiai N, Tateishi T. Tissue-engineered cartilage by in vivo culturing of chondrocytes in PLGA-collagen hybrid sponge. Mater Sci Eng C Biomim Supramol Syst. 2001;17:83–9.
115. Pan Z, Ding J. Poly(lactide-co-glycolide) porous scaffolds for tissue engineering and regenerative medicine. Interface Focus. 2012;2:366–77.

116. Chang N-J, Lin C-C, Shie M-Y, Yeh M-L, Li C-F, Liang P-I, et al. Positive effects of cell-free porous PLGA implants and early loading exercise on hyaline cartilage regeneration in rabbits. Acta Biomater. 2015;28:128–37.
117. Jose MV, Thomas V, Johnson KT, Dean DR, Nyalro E. Aligned PLGA/HA nanofibrous nanocomposite scaffolds for bone tissue engineering. Acta Biomater. 2009;5:305–15.
118. Kim SS, Park MS, Jeon O, Choi CY, Kim BS. Poly(lactide-co-glycolide)/hydroxyapatite composite scaffolds for bone tissue engineering. Biomaterials. 2006;27:1399–409.
119. Lee JY, Bashur CA, Goldstein AS, Schmidt CE. Polypyrrole-coated electrospun PLGA nanofibers for neural tissue applications. Biomaterials. 2009;30:4325–35.
120. Oh SH, Kim JH, Song KS, Jeon BH, Yoon JH, Seo TB, et al. Peripheral nerve regeneration within an asymmetrically porous PLGA/Pluronic F127 nerve guide conduit. Biomaterials. 2008;29:1601–9.
121. Uematsu K, Hattori K, Ishimoto Y, Yamauchi J, Habata T, Takakura Y, et al. Cartilage regeneration using mesenchymal stem cells and a three-dimensional poly-lactic-glycolic acid (PLGA) scaffold. Biomaterials. 2005;26:4273–9.
122. Chang NJ, Lam CF, Lin CC, Chen WL, Li CF, Lin YT, et al. Transplantation of autologous endothelial progenitor cells in porous PLGA scaffolds create a microenvironment for the regeneration of hyaline cartilage in rabbits. Osteoarthr Cartil. 2013;21:1613–22.
123. Li B, Yang J, Ma L, Li F, Tu Z, Gao C. Fabrication of poly(lactide-co-glycolide) scaffold filled with fibrin gel, mesenchymal stem cells, and poly(ethylene oxide)-b-poly(L-lysine)/TGF-beta 1 plasmid DNA complexes for cartilage restoration in vivo. J Biomed Mater Res A. 2013;101: 3097–108.
124. Wang W, Li B, Yang J, Xin L, Li Y, Yin H, et al. The restoration of full-thickness cartilage defects with BMSCs and TGF-beta 1 loaded PLGA/fibrin gel constructs. Biomaterials. 2010;31:8964–73.
125. Wang W, Li D, Wang M-c, Li Y-l. A hybrid scaffold of poly (lactide-co-glycolide) sponge filled with fibrin gel for cartilage tissue engineering. Chin J Polym Sci. 2011;29:233–40.
126. Robinson GM, Orrego H, Israel Y, Devenyi P, Kapur BM. Low-molecular-weight polyethylene-glycol as a probe of gastrointestinal permeability after alcohol ingestion. Dig Dis Sci. 1981;26:971–7.
127. Akkiraju H, Nohe A. Role of chondrocytes in cartilage formation, progression of osteoarthritis and cartilage regeneration. J Dev Biol. 2015;3:177–92.
128. Mackay AM, Beck SC, Murphy JM, Barry FP, Chichester CO, Pittenger MF. Chondrogenic differentiation of cultured human mesenchymal stem cells from marrow. Tissue Eng. 1998;4: 415–28.
129. Wang Q-W, Chen Z-L, Piao Y-J. Mesenchymal stem cells differentiate into tenocytes by bone morphogenetic protein (BMP) 12 gene transfer. J Biosci Bioeng. 2005;100:418–22.
130. Lee IC, Wang J-H, Lee Y-T, Young T-H. The differentiation of mesenchymal stem cells by mechanical stress or/and co-culture system. Biochem Biophys Res Commun. 2007;352:147–52.
131. Dezawa M, Kanno H, Hoshino M, Cho H, Matsumoto N, Itokazu Y, et al. Specific induction of neuronal cells from bone marrow stromal cells and application for autologous transplantation. J Clin Invest. 2004;113:1701–10.
132. Tropel P, Platet N, Platel J-C, Noel D, Albrieux M, Benabid A-L, et al. Functional neuronal differentiation of bone marrow-derived mesenchymal stem cells. Stem Cells. 2006;24:2868–76.
133. Li HW, Yu B, Zhang Y, Pan ZW, Wei XA, Li HL. Jagged1 protein enhances the differentiation of mesenchymal stem cells into cardiomyocytes. Biochem Biophys Res Commun. 2006;341:320–5.
134. Li L, Zhu J, Tian J, Liu X, Feng C. A role for Gcn5 in cardiomyocyte differentiation of rat mesenchymal stem cells. Mol Cell Biochem. 2010;345:309–16.
135. Jaiswal N, Haynesworth SE, Caplan AI, Bruder SP. Osteogenic differentiation of purified, culture-expanded human mesenchymal stem cells in vitro. J Cell Biochem. 1997;64:295–312.

136. Chamberlain G, Fox J, Ashton B, Middleton J. Concise review: mesenchymal stem cells: their phenotype, differentiation capacity, immunological features, and potential for homing. Stem Cells. 2007;25:2739–49.
137. Kim M, Kim SE, Kang SS, Kim YH, Tae G. The use of de-differentiated chondrocytes delivered by a heparin-based hydrogel to regenerate cartilage in partial-thickness defects. Biomaterials. 2011;32:7883–96.
138. Lohan A, Marzahn U, El Sayed K, Haisch A, Kohl B, Mueller RD, et al. In vitro and in vivo neo-cartilage formation by heterotopic chondrocytes seeded on PGA scaffolds. Histochem Cell Biol. 2011;136:57–69.
139. Jeong CG, Zhang H, Hollister SJ. Three-dimensional polycaprolactone scaffold-conjugated bone morphogenetic protein-2 promotes cartilage regeneration from primary chondrocytes in vitro and in vivo without accelerated endochondral ossification. J Biomed Mater Res A. 2012;100A:2088–96.
140. Hubka KM, Dahlin RL, Meretoja VV, Kasper FK, Mikos AG. Enhancing chondrogenic phenotype for cartilage tissue engineering: monoculture and coculture of articular chondrocytes and mesenchymal stem cells. Tissue Eng Part B Rev. 2014;20:641–54.
141. Lohan A, Marzahn U, El Sayed K, Haisch A, Mueller RD, Kohl B, et al. Osteochondral articular defect repair using auricle-derived autologous chondrocytes in a rabbit model. Ann Anat. 2014;196:317–26.
142. Xu F, Xu L, Wang Q, Ye Z, Zhou Y, Tan W-S. 3D dynamic culture of rabbit articular chondrocytes encapsulated in alginate gel beads using spinner flasks for cartilage tissue regeneration. Biomed Res Int. 2014;2014:539789.
143. Li G, Fu N, Xie J, Fu Y, Deng S, Cun X, et al. Poly(3-hydroxybutyrate-co-4-hydroxybutyrate) based electrospun 3D scaffolds for delivery of autogeneic chondrocytes and adipose-derived stem cells: evaluation of cartilage defects in rabbit. J Biomed Nanotechnol. 2015;11:105–16.
144. Omobono MA, Zhao X, Furlong MA, Kwon C-H, Gill TJ, Randolph MA, et al. Enhancing the stiffness of collagen hydrogels for delivery of encapsulated chondrocytes to articular lesions for cartilage regeneration. J Biomed Mater Res A. 2015;103:1332–8.
145. Bryant SJ, Bender RJ, Durand KL, Anseth KS. Encapsulating chondrocytes in degrading PEG hydrogels with high modulus: engineering gel structural changes to facilitate cartilaginous tissue production. Biotechnol Bioeng. 2004;86:747–55.
146. Xue JX, Gong YY, Zhou GD, Liu W, Cao Y, Zhang WJ. Chondrogenic differentiation of bone marrow-derived mesenchymal stem cells induced by acellular cartilage sheets. Biomaterials. 2012;33:5832–40.
147. Deng J, She R, Huang W, Dong Z, Mo G, Liu B. A silk fibroin/chitosan scaffold in combination with bone marrow-derived mesenchymal stem cells to repair cartilage defects in the rabbit knee. J Mater Sci Mater Med. 2013;24:2037–46.
148. Lim CT, Ren X, Afizah MH, Tarigan-Panjaitan S, Yang Z, Wu Y, et al. Repair of osteochondral defects with rehydrated freeze-dried oligo poly(ethylene glycol) fumarate hydrogels seeded with bone marrow mesenchymal stem cells in a porcine model. Tissue Eng Part A. 2013;19:1852–61.
149. Xue K, Qi L, Zhou G, Liu K. A two-step method of constructing mature cartilage using bone marrow-derived mesenchymal stem cells. Cells Tissues Organs. 2013;197:484–95.
150. Wang L, Tran I, Seshareddy K, Weiss ML, Detamore MS. A comparison of human bone marrow-derived mesenchymal stem cells and human umbilical cord-derived mesenchymal stromal cells for cartilage tissue engineering. Tissue Eng Part A. 2009;15:2259–66.
151. Li C, Wei G, Gu Q, Wen G, Qi B, Xu L, et al. Donor Age and cell passage affect osteogenic ability of rat bone marrow mesenchymal stem cells. Cell Biochem Biophys. 2015;72:543–9.
152. Li X, Li Y, Zuo Y, Qu D, Liu Y, Chen T, et al. Osteogenesis and chondrogenesis of biomimetic integrated porous PVA/gel/V-n-HA/pa6 scaffolds and BMSCs construct in repair of articular osteochondral defect. J Biomed Mater Res A. 2015;103:3226–36.
153. Zuk PA, Zhu M, Mizuno H, Huang J, Futrell JW, Katz AJ, et al. Multilineage cells from human adipose tissue: implications for cell-based therapies. Tissue Eng. 2001;7:211–28.

154. Yoon HH, Bhang SH, Shin J-Y, Shin J, Kim B-S. Enhanced cartilage formation via three-dimensional cell engineering of human adipose-derived stem cells. Tissue Eng Part A. 2012;18:1949–56.
155. Jung M-S, Jang HB, Lee S-E, Park J-H, Hwang Y-S. In vitro micro-mineralized tissue formation by the combinatory condition of adipose-derived stem cells, macroporous PLGA microspheres and a bioreactor. Macromol Res. 2014;22:47–57.
156. Veronesi F, Maglio M, Tschon M, Aldini NN, Fini M. Adipose-derived mesenchymal stem cells for cartilage tissue engineering: state-of-the-art in in vivo studies. J Biomed Mater Res A. 2014;102:2448–66.
157. Wang T, Lai JH, Han L-H, Tong X, Yang F. Chondrogenic differentiation of adipose-derived stromal cells in combinatorial hydrogels containing cartilage matrix proteins with decoupled mechanical stiffness. Tissue Eng Part A. 2014;20:2131–9.
158. Wang ZJ, An RZ, Zhao JY, Zhang Q, Yang J, Wang JB, et al. Repair of articular cartilage defects by tissue-engineered cartilage constructed with adipose-derived stem cells and acellular cartilaginous matrix in rabbits. Genet Mol Res. 2014;13:4599–606.
159. Shen J, Gao Q, Zhang Y, He Y. Autologous platelet-rich plasma promotes proliferation and chondrogenic differentiation of adipose-derived stem cells. Mol Med Rep. 2015;11:1298–303.
160. Tang X-B, Dong P-L, Wang J, Zhou H-Y, Zhang H-X, Wang S-Z. Effect of autologous platelet-rich plasma on the chondrogenic differentiation of rabbit adipose-derived stem cells in vitro. Exp Ther Med. 2015;10:477–83.
161. Cheng A, Kapacee Z, Peng J, Lu S, Lucas RJ, Hardingham TE, et al. Cartilage repair using human embryonic stem cell-derived chondroprogenitors. Stem Cells Transl Med. 2014;3:1287–94.
162. Toh WS, Lee EH, Guo X-M, Chan JKY, Yeow CH, Choo AB, et al. Cartilage repair using hyaluronan hydrogel-encapsulated human embryonic stem cell-derived chondrogenic cells. Biomaterials. 2010;31:6968–80.
163. Hwang NS, Varghese S, Elisseeff J. Cartilage tissue engineering—directed differentiation of embryonic stem cells in three-dimensional hydrogel culture. In: Vemuri MC, editor. Methods in molecular biology. New York: Humana Press; 2007. p. 351–73.
164. Pilichi S, Rocca S, Pool RR, Dattena M, Masala G, Mara L, et al. Treatment with embryonic stem-like cells into osteochondral defects in sheep femoral condyles. BMC Vet Res. 2014;10:301.
165. Wakitani S, Aoki H, Harada Y, Sonobe M, Morita Y, Mu Y, et al. Embryonic stem cells form articular cartilage, not teratomas, in osteochondral defects of rat joints. Cell Transplant. 2004;13:331–6.
166. Hwang NS, Varghese S, Elisseeff J. Derivation of chondrogenically-committed cells from human embryonic cells for cartilage tissue regeneration. PloS One. 2008;3:e2498.
167. Toh WS, Lee EH, Cao T. Potential of human embryonic stem cells in cartilage tissue engineering and regenerative medicine. Stem Cell Rev Rep. 2011;7:544–59.
168. Takahashi K, Tanabe K, Ohnuki M, et al. Induction of pluripotent stem cells from adult human fibroblasts by defined factors. Cell. 2007;131(5):861–72.
169. Takahashi K, Yamanaka S. Induction of pluripotent stem cells from mouse embryonic and adult fibroblast cultures by defined factors. Cell. 2006;126(4):663–76.
170. Lach MS, Rosochowicz MA, Richter M, Jagiello I, Suchorska WM, Trzeciak T. The induced pluripotent stem cells in articular cartilage regeneration and disease modelling: are we ready for their clinical use? Cell. 2022;11(3):529.
171. Nam Y, Rim YA, Jung SM, Ju JH. Cord blood cell-derived iPSCs as a new candidate for chondrogenic differentiation and cartilage regeneration. Stem Cell Res Ther. 2017;8:16.
172. Yamashita A, Morioka M, Yahara Y, et al. Generation of scaffoldless hyaline cartilaginous tissue from human iPSCs. Stem Cell Rep. 2015;4(3):404–18.
173. Kotaka S, Wakitani S, Shimamoto A, et al. Magnetic targeted delivery of induced pluripotent stem cells promotes articular cartilage repair. Stem Cells Int. 2017;2017:9514719.

174. Liu J, Nie HR, Xu ZL, et al. The effect of 3D nanofibrous scaffolds on the chondrogenesis of induced pluripotent stem cells and their application in restoration of cartilage defects. PloS One. 2014;9(11):111566.
175. Gronthos S, Mankani M, Brahim J, Robey PG, Shi S. Postnatal human dental pulp stem cells (DPSCs) in vitro and in vivo. Proc Natl Acad Sci U S A. 2000;97(25):13625–30.
176. Dai J, Wang J, Lu J, et al. The effect of co-culturing costal chondrocytes and dental pulp stem cells combined with exogenous FGF9 protein on chondrogenesis and ossification in engineered cartilage. Biomaterials. 2012;33(31):7699–711.
177. Mata M, Milian L, Oliver M, et al. In vivo articular cartilage regeneration using human dental pulp stem cells cultured in an alginate scaffold: a preliminary study. Stem Cells Int. 2017;2017:8309256.
178. Yanasse R, De Labio R, Marques L, et al. Xenotransplantation of human dental pulp stem cells in platelet-rich plasma for the treatment of full-thickness articular cartilage defects in a rabbit model. Exp Ther Med. 2019;17(6):4344–56.
179. Ding DC, Chang YH, Shyu WC, Lin SZ. Human umbilical cord mesenchymal stem cells: a new era for stem cell therapy. Cell Transplant. 2015;24(3):339–47.
180. Mennan C, Wright K, Bhattacharjee A, Balain B, Richardson J, Roberts S. Isolation and characterisation of mesenchymal stem cells from different regions of the human umbilical cord. Biomed Res Int. 2013;2013:916136.
181. Fong CY, Gauthaman K, Cheyyatraivendran S, Lin HD, Biswas A, Bongso A. Human umbilical cord Wharton's jelly stem cells and its conditioned medium support hematopoietic stem cell expansion ex vivo. J Cell Biochem. 2012;113(2):658–68.
182. Zheng P, Hu X, Lou Y, Tang K. A rabbit model of osteochondral regeneration using three-dimensional printed polycaprolactone-hydroxyapatite scaffolds coated with umbilical cord blood mesenchymal stem cells and chondrocytes. Med Sci Monit. 2019;25:7361–9.
183. Song J-S, Hong K-T, Kong C-G, et al. High tibial osteotomy with human umbilical cord blood-derived mesenchymal stem cells implantation for knee cartilage regeneration. World J Stem Cells. 2020;12(6):514–26.
184. Yang H-Y, Song E-K, Kang S-J, Kwak W-K, Kang J-K, Seon J-K. Allogenic umbilical cord blood-derived mesenchymal stromal cell implantation was superior to bone marrow aspirate concentrate augmentation for cartilage regeneration despite similar clinical outcomes. Knee Surg Sports Traumatol Arthrosc. 2022;30(1):208–18.
185. Chang H, Tate MLK. Concise review: the periosteum: tapping into a reservoir of clinically useful progenitor cells. Stem Cells Transl Med. 2012;1:480–91.
186. De Bari C, Dell'Accio F, Tylzanowski P, Luyten FP. Multipotent mesenchymal stem cells from adult human synovial membrane. Arthritis Rheum. 2001;44:1928–42.
187. Liu Y, Buckley CT, Downey R, Mulhall KJ, Kelly DJ. The role of environmental factors in regulating the development of cartilaginous grafts engineered using osteoarthritic human infrapatellar fat pad–derived stem cells. Tissue Eng Part A. 2012;18:1531–41.
188. Richter W. Mesenchymal stem cells and cartilage in situ regeneration. J Intern Med. 2009;266: 390–405.
189. Ogata Y, Mabuchi Y, Yoshida M, Suto EG, Suzuki N, Muneta T, et al. Purified human synovium mesenchymal stem cells as a good resource for cartilage regeneration. PloS One. 2015;10:e0129096.
190. Alegre-Aguaron E, Sampat SR, Xiong JC, Colligan RM, Bulinski JC, Cook JL, et al. Growth factor priming differentially modulates components of the extracellular matrix proteome in chondrocytes and synovium-derived stem cells. PloS One. 2014;9:e88053.
191. Chang CB, Han SA, Kim EM, Lee S, Seong SC, Lee MC. Chondrogenic potentials of human synovium-derived cells sorted by specific surface markers. Osteoarthr Cartil. 2013;21:190–9.
192. Chang C-H, Chen C-C, Liao C-H, Lin F-H, Hsu Y-M, Fang H-W. Human acellular cartilage matrix powders as a biological scaffold for cartilage tissue engineering with synovium-derived mesenchymal stem cells. J Biomed Mater Res A. 2014;102:2248–57.

193. Jones BA, Pei M. Synovium-derived stem cells: a tissue-specific stem cell for cartilage engineering and regeneration. Tissue Eng Part B Rev. 2012;18:301–11.
194. Suzuki S, Muneta T, Tsuji K, Ichinose S, Makino H, Umezawa A, et al. Properties and usefulness of aggregates of synovial mesenchymal stem cells as a source for cartilage regeneration. Arthritis Res Ther. 2012;14:R136.
195. Fan J, Ren L, Liang R, Gong Y, Cai D, Wang D-A. Chondrogenesis of synovium-derived mesenchymal stem cells in photopolymerizing hydrogel scaffolds. J Biomater Sci Polym Ed. 2010;21:1653–67.
196. Pei M, He F, Boyce BM, Kish VL. Repair of full-thickness femoral condyle cartilage defects using allogeneic synovial cell-engineered tissue constructs. Osteoarthr Cartil. 2009;17:714–22.
197. Demoor M, Ollitrault D, Gomez-Leduc T, Bouyoucef M, Hervieu M, Fabre H, et al. Cartilage tissue engineering: molecular control of chondrocyte differentiation for proper cartilage matrix reconstruction. Biochim Biophys Acta Gen Subj. 2014;1840:2414–40.
198. Lee S-H, Shin H. Matrices and scaffolds for delivery of bioactive molecules in bone and cartilage tissue engineering. Adv Drug Deliv Rev. 2007;59:339–59.
199. Angel MJ, Sgaglione NA, Grande DA. Clinical applications of bioactive factors in sports medicine—current concepts and future trends. Sports Med Arthrosc Rev. 2006;14:138–45.
200. Kawamura K, Chu CR, Sobajima S, Robbins PD, Fu FH, Izzo NJ, et al. Adenoviral-mediated transfer of TGF-β1 but not IGF-1 induces chondrogenic differentiation of human mesenchymal stem cells in pellet cultures. Exp Hematol. 2005;33:865–72.
201. Bian L, Zhai DY, Tous E, Rai R, Mauck RL, Burdick JA. Enhanced MSC chondrogenesis following delivery of TGF-β3 from alginate microspheres within hyaluronic acid hydrogels in vitro and in vivo. Biomaterials. 2011;32:6425–34.
202. Han Y, Wei Y, Wang S, Song Y. Cartilage regeneration using adipose-derived stem cells and the controlled-released hybrid microspheres. Joint Bone Spine. 2010;77:27–31.
203. Hildner F, Albrecht C, Gabriel C, Redl H, van Griensven M. State of the art and future perspectives of articular cartilage regeneration: a focus on adipose-derived stem cells and platelet-derived products. J Tissue Eng Regen Med. 2011;5:E36–51.
204. Lu C-H, Lin K-J, Chiu H-Y, Chen C-Y, Yen T-C, Hwang S-M, et al. Improved chondrogenesis and engineered cartilage formation from TGF-beta 3-expressing adipose-derived stem cells cultured in the rotating-shaft bioreactor. Tissue Eng Part A. 2012;18:2114–24.
205. Re'em T, Witte F, Willbold E, Ruvinov E, Cohen S. Simultaneous regeneration of articular cartilage and subchondral bone induced by spatially presented TGF-beta and BMP-4 in a bilayer affinity binding system. Acta Biomater. 2012;8:3283–93.
206. Pretzel D, Linss S, Ahrem H, Endres M, Kaps C, Klemm D, et al. A novel in vitro bovine cartilage punch model for assessing the regeneration of focal cartilage defects with biocompatible bacterial nanocellulose. Arthritis Res Ther. 2013;15:R59.
207. Lu C-H, Yeh T-S, Yeh C-L, Fang Y-HD, Sung L-Y, Lin S-Y, et al. Regenerating cartilages by engineered ASCs: prolonged TGF-beta 3/BMP-6 expression improved articular cartilage formation and restored zonal structure. Mol Ther. 2014;22:186–95.
208. Elmallah RK, Cherian JJ, Jauregui JJ, Pierce TP, Beaver WB, Mont MA. Genetically modified chondrocytes expressing TGF-beta 1: a revolutionary treatment for articular cartilage damage? Expert Opin Biol Ther. 2015;15:455–64.
209. Kim SH, Kim SH, Jung Y. TGF-beta(3) encapsulated PLCL scaffold by a supercritical CO2-HFIP co-solvent system for cartilage tissue engineering. J Control Release. 2015;206:101–7.
210. Murphy MK, Huey DJ, Hu JC, Athanasiou KA. TGF-beta 1, GDF-5, and BMP-2 stimulation induces chondrogenesis in expanded human articular chondrocytes and marrow-derived stromal cells. Stem Cells. 2015;33:762–73.

211. Zhang N, Lock J, Sallee A, Liu H. Magnetic nanocomposite hydrogel for potential cartilage tissue engineering: synthesis, characterization, and cytocompatibility with bone marrow derived mesenchymal stem cells. ACS Appl Mater Interfaces. 2015;7:20987–98.
212. Capito RM, Spector M. Collagen scaffolds for nonviral IGF-1 gene delivery in articular cartilage tissue engineering. Gene Ther. 2007;14:721–32.
213. Singh NK, Singh GR, Amarpal, Kinjavdekar P, Sharma AK, Mohanty TR. Articular cartilage repair with autografting under the influence of insulin-like growth factor-1 in rabbits. J Vet Med Ser A Physiol Pathol Clin Med. 2007;54:210–8.
214. Davies LC, Blain EJ, Gilbert SJ, Caterson B, Duance VC. The potential of IGF-1 and TGF beta 1 for promoting "Adult" articular cartilage repair: an in vitro study. Tissue Eng Part A. 2008;14:1251–61.
215. Bastiaansen-Jenniskens YM, Koevoet W, Feijt C, Bos PK, Verhaar JAN, Van Osch GJVM, et al. Proteoglycan production is required in initial stages of new cartilage matrix formation but inhibits integrative cartilage repair. J Tissue Eng Regen Med. 2009;3:117–23.
216. An C, Cheng Y, Yuan Q, Li J. IGF-1 and BMP-2 induces differentiation of adipose-derived mesenchymal stem cells into chondrocytes-like cells. Ann Biomed Eng. 2010;38:1647–54.
217. Liu XW, Hu J, Man C, Zhang B, Ma YQ, Zhu SS. Insulin-like growth factor-1 suspended in hyaluronan improves cartilage and subchondral cancellous bone repair in osteoarthritis of temporomandibular joint. Int J Oral Maxillofac Surg. 2011;40:184–90.
218. Spiller KL, Liu Y, Holloway JL, Maher SA, Cao Y, Liu W, et al. A novel method for the direct fabrication of growth factor-loaded microspheres within porous nondegradable hydrogels: controlled release for cartilage tissue engineering. J Control Release. 2012;157:39–45.
219. Joos H, Wildner A, Hogrefe C, Reichel H, Brenner RE. Interleukin-1 beta and tumor necrosis factor alpha inhibit migration activity of chondrogenic progenitor cells from non-fibrillated osteoarthritic cartilage. Arthritis Res Ther. 2013;15:R119.
220. Henson FMD, Vincent T. Chondrocyte outgrowth into a gelatin scaffold in a single impact load model of damage/repair—effect of BMP-2. BMC Musculoskelet Disord. 2007;8:120.
221. Kuo AC, Rodrigo JJ, Reddi AH, Curtiss S, Grotkopp E, Chiu M. Microfracture and bone morphogenetic protein 7 (BMP-7) synergistically stimulate articular cartilage repair. Osteoarthr Cartil. 2006;14:1126–35.
222. Matsumoto T, Cooper GM, Gharaibeh B, Meszaros LB, Li G, Usas A, et al. Cartilage repair in a rat model of osteoarthritis through intraarticular transplantation of muscle-derived stem cells expressing bone morphogenetic protein 4 and soluble Flt-1. Arthritis Rheum. 2009;60:1390–405.
223. Menendez MI, Clark DJ, Carlton M, Flanigan DC, Jia G, Sammet S, et al. Direct delayed human adenoviral BMP-2 or BMP-6 gene therapy for bone and cartilage regeneration in a pony osteochondral model. Osteoarthr Cartil. 2011;19:1066–75.
224. Nochi H, Sung JH, Lou J, Adkisson HD, Maloney WJ, Hruska KA. Adenovirus mediated BMP-13 gene transfer induces chondrogenic differentiation of murine mesenchymal progenitor cells. J Bone Miner Res. 2004;19:111–22.
225. Shi J, Zhang X, Zhu J, Pi Y, Hu X, Zhou C, et al. Nanoparticle delivery of the bone morphogenetic protein 4 gene to adipose-derived stem cells promotes articular cartilage repair in vitro and in vivo. Arthroscopy. 2013;29:2001–U182.
226. Yang HS, La W-G, Bhang SH, Kim H-J, Im G-I, Lee H, et al. Hyaline cartilage regeneration by combined therapy of microfracture and long-term bone morphogenetic protein-2 delivery. Tissue Eng Part A. 2011;17:1809–18.
227. Zhang Y, Tang CL, Chen WJ, Zhang Q, Wang SL. Dynamic compression combined with exogenous SOX-9 promotes chondrogenesis of adipose-derived mesenchymal stem cells in PLGA scaffold. Eur Rev Med Pharmacol Sci. 2015;19:2671–8.
228. Kaul G, Cucchiarini M, Arntzen D, Zurakowski D, Menger MD, Kohn D, et al. Local stimulation of articular cartilage repair by transplantation of encapsulated chondrocytes overexpressing human fibroblast growth factor 2 (FGF-2) in vivo. J Gene Med. 2006;8:100–11.

229. Takafuji H, Suzuki T, Okubo Y, Fujimura K, Bessho K. Regeneration of articular cartilage defects in the temporomandibular joint of rabbits by fibroblast growth factor-2: a pilot study. Int J Oral Maxillofac Surg. 2007;36:934–7.
230. Ellman MB, An HS, Muddasani P, Im H-J. Biological impact of the fibroblast growth factor family on articular cartilage and intervertebral disc homeostasis. Gene. 2008;420:82–9.
231. Kuroda Y, Akiyama H, Kawanabe K, Tabata Y, Nakamura T. Treatment of experimental osteonecrosis of the hip in adult rabbits with a single local injection of recombinant human FGF-2 microspheres. J Bone Miner Metab. 2010;28:608–16.
232. Maehara H, Sotome S, Yoshii T, Torigoe I, Kawasaki Y, Sugata Y, et al. Repair of large osteochondral defects in rabbits using porous hydroxyapatite/collagen (HAp/Col) and fibroblast growth factor-2 (FGF-2). J Orthop Res. 2010;28:677–86.
233. Kim JH, Lee MC, Seong SC, Park KH, Lee S. Enhanced proliferation and chondrogenic differentiation of human synovium-derived stem cells expanded with basic fibroblast growth factor. Tissue Eng Part A. 2011;17:991–1002.
234. Yuan L-J, Niu C-C, Lin S-S, Chan Y-S, Yang C-Y, Chen W-J, et al. Additive effects of hyperbaric oxygen and platelet-derived growth factor-BB in chondrocyte transplantation via up-regulation expression of platelet-derived growth factor-beta receptor. J Orthop Res. 2009;27:1439–46.
235. Shin SH, Song HY, Kim MY, Do EK, Kim KH, Kim JH. Platelet-activating factor receptor mediates oxidized low density lipoprotein-induced migration of bone marrow-derived mesenchymal stem cells. Cell Physiol Biochem. 2010;26:689–98.
236. Howard D, Shepherd JH, Kew SJ, Hernandez P, Ghose S, Wardale JA, et al. Release of growth factors from a reinforced collagen GAG matrix supplemented with platelet rich plasma: influence on cultured human meniscal cells. J Orthop Res. 2014;32:273–8.
237. Lee JM, Ryu JH, Kim EA, Jo S, Kim B-S, Lee H, et al. Adhesive barrier/directional controlled release for cartilage repair by endogenous progenitor cell recruitment. Biomaterials. 2015;39:173–81.
238. Liu X, Yang Y, Li Y, et al. Integration of stem cell-derived exosomes with in situ hydrogel glue as a promising tissue patch for articular cartilage regeneration. Nanoscale. 2017;9(13):4430–8.
239. Wu X, Wang Y, Xiao Y, Crawford R, Mao X, Prasadam I. Extracellular vesicles: potential role in osteoarthritis regenerative medicine. J Orthop Transl. 2020;21:73–80.
240. Jiang S, Tian G, Yang Z, et al. Enhancement of acellular cartilage matrix scaffold by Wharton's jelly mesenchymal stem cell-derived exosomes to promote osteochondral regeneration. Bioact Mater. 2021;6(9):2711–28.
241. Shao J, Zhu J, Chen Y, et al. Exosomes from Kartogenin-pretreated infrapatellar fat pad mesenchymal stem cells enhance chondrocyte anabolism and articular cartilage regeneration. Stem Cells Int. 2021;2021:6624874.
242. Chen J, Huang T, Liu R, Wang C, Jiang H, Sun H. Congenital microtia patients: the genetically engineered exosomes released from porous gelatin methacryloyl hydrogel for downstream small RNA profiling, functional modulation of microtia chondrocytes and tissue-engineered ear cartilage regeneration. J Nanobiotechnol. 2022;20(1):164.
243. Krueger JP, Hondke S, Endres M, Pruss A, Siclari A, Kaps C. Human platelet-rich plasma stimulates migration and chondrogenic differentiation of human subchondral progenitor cells. J Orthop Res. 2012;30(6):845–52.
244. van Buul GM, Koevoet WLM, Kops N, et al. Platelet-rich plasma releasate inhibits inflammatory processes in osteoarthritic chondrocytes. Am J Sports Med. 2011;39(11):2362–70.
245. Sancho-Tello M, Martorell S, Mata Roig M, et al. Human platelet-rich plasma improves the nesting and differentiation of human chondrocytes cultured in stabilized porous chitosan scaffolds. J Tissue Eng. 2017;8:2041731417697545.
246. Lu H-T, Chang W-T, Tsai M-L, Chen C-H, Chen W-Y, Mi F-L. Development of injectable fucoidan and biological macromolecules hybrid hydrogels for intra-articular delivery of platelet-rich plasma. Mar Drugs. 2019;17(4):236.

247. Singh BN, Nallakumarasamy A, Sinha S, et al. Generation of hybrid tissue engineered construct through embedding autologous chondrocyte loaded platelet rich plasma/alginate based hydrogel in porous scaffold for cartilage regeneration. Int J Biol Macromol. 2022;203: 389–405.
248. Scotti C, Mangiavini L, Boschetti F, Vitari F, Domeneghini C, Fraschini G, et al. Effect of in vitro culture on a chondrocyte-fibrin glue hydrogel for cartilage repair. Knee Surg Sports Traumatol Arthrosc. 2010;18:1400–6.
249. Deponti D, Di Giancamillo A, Mangiavini L, Pozzi A, Fraschini G, Sosio C, et al. Fibrin-based model for cartilage regeneration: tissue maturation from in vitro to in vivo. Tissue Eng Part A. 2012;18:1109–22.
250. Erickson IE, Kestle SR, Zellars KH, Dodge GR, Burdick JA, Mauck RL. Improved cartilage repair via in vitro pre-maturation of MSC-seeded hyaluronic acid hydrogels. Biomed Mater. 2012;7:024110.
251. Jeon JE, Schrobback K, Meinert C, Sramek V, Hutmacher DW, Klein TJ. Effect of preculture and loading on expression of matrix molecules, matrix metalloproteinases, and cytokines by expanded osteoarthritic chondrocytes. Arthritis Rheum. 2013;65:2356–67.
252. Sabatino MA, Santoro R, Gueven S, Jaquiery C, Wendt DJ, Martin I, et al. Cartilage graft engineering by co-culturing primary human articular chondrocytes with human bone marrow stromal cells. J Tissue Eng Regen Med. 2015;9:1394–403.
253. Zhao X, Bichara DA, Zhou L, Kulig KM, Tseng A, Bowley CM, et al. Conditions for seeding and promoting neo-auricular cartilage formation in a fibrous collagen scaffold. J Craniomaxillofac Surg. 2015;43:382–9.
254. Cao Y, Vacanti JP, Paige KT, Upton J, Vacanti CA. Transplantation of chondrocytes utilizing a polymer-cell construct to produce tissue-engineered cartilage in the shape of a human ear. Plast Reconstr Surg. 1997;100:297–302.
255. Freyria A-M, Cortial D, Ronzière M-C, Guerret S, Herbage D. Influence of medium composition, static and stirred conditions on the proliferation of and matrix protein expression of bovine articular chondrocytes cultured in a 3-D collagen scaffold. Biomaterials. 2004;25:687–97.
256. Darling EM, Athanasiou KA. Articular cartilage bioreactors and bioprocesses. Tissue Eng. 2003;9:9–26.
257. Shahin K, Doran PM. Strategies for enhancing the accumulation and retention of extracellular matrix in tissue-engineered cartilage cultured in bioreactors. PloS One. 2011;6:e23119.
258. Gaissmaier C, Koh JL, Weise K, Mollenhauer JA. Future perspectives of articular cartilage repair. Injury. 2008;39(Suppl 1):S114–20.
259. Zheng D, Chen T, Han L, et al. Synergetic integrations of bone marrow stem cells and transforming growth factor-beta 1 loaded chitosan nanoparticles blended silk fibroin injectable hydrogel to enhance repair and regeneration potential in articular cartilage tissue. Int Wound J. 2022;19(5):1023–38.
260. Dong X, Li C, Zhang M, et al. Multifunctional injectable hydrogel for effective promotion of cartilage regeneration and protection against osteoarthritis: combined chondroinductive, antioxidative and anti-inflammatory strategy. Sci Technol Adv Mater. 2022;23(1):361–75.
261. Dong Y, Liu Y, Chen Y, et al. Spatiotemporal regulation of endogenous MSCs using a functional injectable hydrogel system for cartilage regeneration. NPG Asia Mater. 2021;13 (1):71.
262. Bauge C, Boumediene K. Use of adult stem cells for cartilage tissue engineering: current status and future developments. Stem Cells Int. 2015;2015:438026.
263. Fioretta ES, Fledderus JO, Burakowska-Meise EA, Baaijens F, Verhaar MC, Bouten CV. Polymer–based scaffold designs for in situ vascular tissue engineering: controlling recruitment and differentiation behavior of endothelial colony forming cells. Macromol Biosci. 2012;12:577–90.
264. Vanden Berg-Foels WS. In situ tissue regeneration: chemoattractants for endogenous stem cell recruitment. Tissue Eng. 2013;45:e57.

265. Kon E, Roffi A, Filardo G, Tesei G, Marcacci M. Scaffold-based cartilage treatments: with or without cells? A systematic review of preclinical and clinical evidence. Arthroscopy. 2015;31:767–75.
266. Wang W, Sun L, Zhang P, Song J, Liu W. An anti-inflammatory cell-free collagen/resveratrol scaffold for repairing osteochondral defects in rabbits. Acta Biomater. 2014;10:4983–95.
267. Dai Y, Liu G, Ma L, Wang D, Gao C. Cell-free macro-porous fibrin scaffolds for in situ inductive regeneration of full-thickness cartilage defects. J Mater Chem B. 2016;4:4410–9.
268. Dai Y, Shen T, Ma L, Wang D, Gao C. Regeneration of osteochondral defects in vivo by a cell-free cylindrical poly(lactide-co-glycolide) scaffold with a radially oriented microstructure. J Tissue Eng Regen Med. 2018;12(3):1647–61.
269. Dai Y, Gao Z, Ma L, Wang D, Gao C. Cell-free HA-MA/PLGA scaffolds with radially oriented pores for in situ inductive regeneration of full thickness cartilage defects. Macromol Biosci. 2016;16(11):1632–42.
270. Roessler PP, Pfister B, Gesslein M, Figiel J, Heyse TJ, Colcuc C, et al. Short-term follow up after implantation of a cell-free collagen type I matrix for the treatment of large cartilage defects of the knee. Int Orthop. 2015;39:2473–9.
271. Madry H, van Dijk CN, Mueller-Gerbl M. The basic science of the subchondral bone. Knee Surg Sports Traumatol Arthrosc. 2010;18:419–33.
272. Gelse K, Klinger P, Koch M, Surmann-Schmitt C, von der Mark K, Swoboda B, et al. Thrombospondin-1 prevents excessive ossification in cartilage repair tissue induced by osteogenic protein-1. Tissue Eng Part A. 2011;17:2101–12.
273. Ghosh S, Viana J, Reis R, Mano J. Bi-layered constructs based on poly (L-lactic acid) and starch for tissue engineering of osteochondral defects. Mater Sci Eng C. 2008;28:80–6.
274. Nukavarapu SP, Dorcemus DL. Osteochondral tissue engineering: current strategies and challenges. Biotechnol Adv. 2013;31:706–21.
275. Chen GP, Sato T, Tanaka J, Tateishi T. Preparation of a biphasic scaffold for osteochondral tissue engineering. Mater Sci Eng C Biomim Supramol Syst. 2006;26:118–23.
276. Jiang C-C, Chiang H, Liao C-J, Lin Y-J, Kuo T-F, Shieh C-S, et al. Repair of porcine articular cartilage defect with a biphasic osteochondral composite. J Orthop Res. 2007;25:1277–90.
277. Yang Q, Peng J, Lu S-b, Guo Q-y, Zhao B, Zhang L, et al. Evaluation of an extracellular matrix-derived acellular biphasic scaffold/cell construct in the repair of a large articular high-load-bearing osteochondral defect in a canine model. Chin Med J (Engl). 2011;124:3930–8.
278. Duan X, Zhu X, Dong X, Yang J, Huang F, Cen S, et al. Repair of large osteochondral defects in a beagle model with a novel type I collagen/glycosaminoglycan-porous titanium biphasic scaffold. Mater Sci Eng C Mater Biol Appl. 2013;33:3951–7.
279. Liu S, Wu J, Liu X, Chen D, Bowlin GL, Cao L, et al. Osteochondral regeneration using an oriented nanofiber yarn-collagen type I/hyaluronate hybrid/TCP biphasic scaffold. J Biomed Mater Res A. 2015;103:581–92.
280. Jeon JE, Vaquette C, Klein TJ, Hutmacher DW. Perspectives in multiphasic osteochondral tissue engineering. Anat Rec Adv Integr Anat Evol Biol. 2014;297:26–35.
281. Jang K-M, Lee J-H, Park CM, Song H-R, Wang JH. Xenotransplantation of human mesenchymal stem cells for repair of osteochondral defects in rabbits using osteochondral biphasic composite constructs. Knee Surg Sports Traumatol Arthrosc. 2014;22:1434–44.
282. Filardo G, Kon E, Perdisa F, Balboni F, Marcacci M. Autologous osteochondral transplantation for the treatment of knee lesions: results and limitations at two years' follow-up. Int Orthop. 2014;38:1905–12.
283. Zhang S, Chen L, Jiang Y, Cai Y, Xu G, Tong T, et al. Bi-layer collagen/microporous electrospun nanofiber scaffold improves the osteochondral regeneration. Acta Biomater. 2013;9:7236–47.
284. Castro NJ, Patel R, Zhang LG. Design of a novel 3D printed bioactive nanocomposite scaffold for improved osteochondral regeneration. Cel Mol Bioeng. 2015;8:416–32.
285. Kim SH, Kim SH, Jung Y. Bi-layered PLCL/(PLGA/beta-TCP) composite scaffold for osteochondral tissue engineering. J Bioact Compat Polym. 2015;30:178–87.

286. Kon E, Filardo G, Shani J, Altschuler N, Levy A, Zaslav K, et al. Osteochondral regeneration with a novel aragonite-hyaluronate biphasic scaffold: up to 12-month follow-up study in a goat model. J Orthop Surg Res. 2015;10:81.
287. Koo Y, Choi E-J, Lee J, Kim H-J, Kim G, Do SH. 3D printed cell-laden collagen and hybrid scaffolds for in vivo articular cartilage tissue regeneration. J Ind Eng Chem. 2018;66:343–55.
288. Parisi C, Salvatore L, Veschini L, et al. Biomimetic gradient scaffold of collagen-hydroxyapatite for osteochondral regeneration. J Tissue Eng. 2020;11:2041731419896068.
289. Gostynska N, Krishnakumar GS, Campodoni E, et al. 3D porous collagen scaffolds reinforced by glycation with ribose for tissue engineering application. Biomed Mater. 2017;12(5): 055002.
290. Kankala RK, Lu F-J, Liu C-G, Zhang S-S, Chen A-Z, Wang S-B. Effect of Icariin on Engineered 3D-printed porous scaffolds for cartilage repair. Materials. 2018;11(8):1390.
291. Guan J, Yuan F-z, Mao Z-m, et al. Fabrication of 3D-printed interpenetrating hydrogel scaffolds for promoting chondrogenic differentiation. Polymers. 2021;13(13):2146.
292. Li Q, Xu S, Feng Q, et al. 3D printed silk-gelatin hydrogel scaffold with different porous structure and cell seeding strategy for cartilage regeneration. Bioact Mater. 2021;6(10): 3396–410.
293. Nelson M, Li S, Page SJ, et al. 3D printed silica-gelatin hybrid scaffolds of specific channel sizes promote collagen type II, Sox9 and Aggrecan production from chondrocytes. Mater Sci Eng C. 2021;123:111964.
294. Posniak S, Chung JHY, Liu X, et al. Bioprinting of chondrocyte stem cell co-cultures for auricular cartilage regeneration. Acs Omega. 2022;7(7):5908–20.
295. Chen W, Xu Y, Li Y, et al. 3D printing electrospinning fiber-reinforced decellularized extracellular matrix for cartilage regeneration. Chem Eng J. 2020;382:122986.
296. Zhou X, Nowicki M, Cui H, et al. 3D bioprinted graphene oxide-incorporated matrix for promoting chondrogenic differentiation of human bone marrow mesenchymal stem cells. Carbon. 2017;116:615–24.
297. Yang Y, Yang G, Song Y, Xu Y, Zhao S, Zhang W. 3D bioprinted integrated osteochondral scaffold-mediated repair of articular cartilage defects in the rabbit knee. J Med Biol Eng. 2020;40(1):71–81.
298. Deng C, Yang J, He H, et al. 3D bio-printed biphasic scaffolds with dual modification of silk fibroin for the integrated repair of osteochondral defects. Biomater Sci. 2021;9(14):4891–903.
299. Cao Y, Cheng P, Sang S, et al. 3D printed PCL/GelMA biphasic scaffold boosts cartilage regeneration using co-culture of mesenchymal stem cells and chondrocytes: in vivo study. Mater Des. 2021;210:110065.
300. Levato R, Webb WR, Otto IA, et al. The bio in the ink: cartilage regeneration with bioprintable hydrogels and articular cartilage-derived progenitor cells. Acta Biomater. 2017;61:41–53.
301. Ding X, Gao J, Yu X, et al. 3D-printed porous scaffolds of hydrogels modified with TGF-beta 1 binding peptides to promote in vivo cartilage regeneration and animal gait restoration. ACS Appl Mater Interfaces. 2022;14(14):15982–95.
302. Thunsiri K, Pitjamit S, Pothacharoen P, Pruksakorn D, Nakkiew W, Wattanutchariya W. The 3D-printed bilayer's bioactive-biomaterials scaffold for full-thickness articular cartilage defects treatment. Materials. 2020;13(15):3417.
303. Qin C, Ma J, Chen L, et al. 3D bioprinting of multicellular scaffolds for osteochondral regeneration. Mater Today. 2021;49:68–84.
304. Shie M-Y, Chang W-C, Wei L-J, et al. 3D printing of cytocompatible water-based light-cured polyurethane with hyaluronic acid for cartilage tissue engineering applications. Materials. 2017;10(2):136.
305. Fu Y, Zoetebier B, Both S, Dijkstra PJ, Karperien M. Engineering of optimized hydrogel formulations for cartilage repair. Polymers. 2021;13(9):1526.
306. Gorronogoitia I, Urtaza U, Zubiarrain-Laserna A, Alonso-Varona A, Zaldua AM. A study of the printability of alginate-based bioinks by 3D bioprinting for articular cartilage tissue engineering. Polymers. 2022;14(2):354.

307. Zhang H, Huang H, Hao G, et al. 3D printing hydrogel scaffolds with nanohydroxyapatite gradient to effectively repair osteochondral defects in rats. Adv Funct Mater. 2021;31(1): 2006697.
308. Cao Y, Cheng P, Sang S, et al. Mesenchymal stem cells loaded on 3D-printed gradient poly (epsilon)-caprolactonelimethacrylated alginate composite scaffolds for cartilage tissue engineering. Regener Biomater. 2021;8(3):rbab019.
309. Olubamiji AD, Zhu N, Chang T, et al. Traditional invasive and synchrotron-based noninvasive assessments of three-dimensional-printed hybrid cartilage constructs in situ. Tissue Eng Part C Methods. 2017;23(3):156–68.
310. Ryu J, Brittberg M, Nam B, et al. Evaluation of three-dimensional bioprinted human cartilage powder combined with micronized subcutaneous adipose tissues for the repair of osteochondral defects in Beagle dogs. Int J Mol Sci. 2022;23(5):2743.
311. Chen M, Li Y, Liu S, et al. Hierarchical macro-microporous WPU-ECM scaffolds combined with microfracture promote in situ articular cartilage regeneration in rabbits. Bioact Mater. 2021;6(7):1932–44.
312. Meng Y, Cao J, Chen Y, Yu Y, Ye L. 3D printing of a poly(vinyl alcohol)-based nanocomposite hydrogel as an artificial cartilage replacement and the improvement mechanism of printing accuracy. J Mater Chem B. 2020;8(4):677–90.
313. Chen Y-W, Shie M-Y, Chang W-C, Shen Y-F. Approximate optimization study of light curing waterborne polyurethane materials for the construction of 3D printed cytocompatible cartilage scaffolds. Materials. 2021;14(22):6804.
314. Camacho P, Behre A, Fainor M, Seims KB, Chow LW. Spatial organization of biochemical cues in 3D-printed scaffolds to guide osteochondral tissue engineering. Biomater Sci. 2021;9 (20):6813–29.
315. Li S, Tallia F, Mohammed AA, Stevens MM, Jones JR. Scaffold channel size influences stem cell differentiation pathway in 3-D printed silica hybrid scaffolds for cartilage regeneration. Biomater Sci. 2020;8(16):4458–66.
316. Shu C, Qin C, Chen L, et al. Metal-organic framework functionalized bioceramic scaffolds with antioxidative activity for enhanced osteochondral regeneration. Adv Sci. 2023;10: 2206875.
317. Dang W, Wang X, Li J, et al. 3D printing of Mo-containing scaffolds with activated anabolic responses and bi-lineage bioactivities. Theranostics. 2018;8(16):4372–92.
318. Han YT, Wei QQ, Chang PB, et al. Three-dimensional printing of hydroxyapatite composites for biomedical application. Crystals. 2021;11(4):353.
319. Hsieh Y-H, Shen B-Y, Wang Y-H, Lin B, Lee H-M, Hsieh M-F. Healing of osteochondral defects implanted with biomimetic scaffolds of poly(epsilon-Caprolactone)/Hydroxyapatite and Glycidyl-Methacrylate-modified hyaluronic acid in a minipig. Int J Mol Sci. 2018;19(4): 1125.
320. Bohner M, Santoni BLG, Dobelin N. Beta-tricalcium phosphate for bone substitution: synthesis and properties. Acta Biomater. 2020;113:23–41.
321. Rutgers M, van Pelt MJP, Dhert WJA, Creemers LB, Saris DBF. Evaluation of histological scoring systems for tissue-engineered, repaired and osteoarthritic cartilage. Osteoarthr Cartil. 2010;18:12–23.
322. Mankin HJ, LIPPIELLO L. Biochemical and metabolic abnormalities in articular cartilage from osteo-arthritic human hips. J Bone Joint Surg Am. 1970;52:424–34.
323. Lahm A, Uh M, Erggelet C, Haberstroh J, Mrosek E. Articular cartilage degeneration after acute subchondral bone damage—an experimental study in dogs with histopathological grading. Acta Orthop Scand. 2004;75:762–7.
324. Pearson RG, Kurien T, Shu KSS, Scammell BE. Histopathology grading systems for characterisation of human knee osteoarthritis—reproducibility, variability, reliability, correlation, and validity. Osteoarthr Cartil. 2011;19:324–31.
325. Custers RJH, Creemers LB, Verbout AJ, van Rijen MHP, Dhert WJA, Saris DBF. Reliability, reproducibility and variability of the traditional histologic/histochemical grading system vs the

new OARSI osteoarthritis cartilage histopathology assessment system. Osteoarthr Cartil. 2007;15:1241–8.
326. Pritzker K, Gay S, Jimenez S, Ostergaard K, Pelletier J-P, Revell P, et al. Osteoarthritis cartilage histopathology: grading and staging. Osteoarthr Cartil. 2006;14:13–29.
327. O'Driscoll SW, Keeley FW, Salter RB. Durability of regenerated articular cartilage produced by free autogenous periosteal grafts in major full-thickness defects in joint surfaces under the influence of continuous passive motion. A follow-up report at one year. J Bone Joint Surg Am. 1988;70:595–606.
328. Pineda S, Pollack A, Stevenson S, Goldberg V, Caplan A. A semiquantitative scale or histologic grading of articular cartilage repair. Cells Tissues Organs. 1992;143:335–40.
329. Wakitani S, Goto T, Pineda SJ, Young RG, Mansour JM, Caplan AI, et al. Mesenchymal cell-based repair of large, full-thickness defects of articular cartilage. J Bone Joint Surg Am. 1994;76:579–92.
330. Roberts S, McCall IW, Darby AJ, Menage J, Evans H, Harrison PE, et al. Autologous chondrocyte implantation for cartilage repair: monitoring its success by magnetic resonance imaging and histology. Arthritis Res Ther. 2002;5:1.
331. Mainil-Varlet P, Aigner T, Brittberg M, Bullough P, Hollander A, Hunziker E, et al. Histological assessment of cartilage repair. J Bone Joint Surg Am. 2003;85:45–57.
332. Mainil-Varlet P, Van Damme B, Nesic D, Knutsen G, Kandel R, Roberts S. A new histology scoring system for the assessment of the quality of human cartilage repair: ICRS II. Am J Sports Med. 2010;38:880–90.
333. Hoemann CD, Tran-Khanh N, Chevrier A, Chen G, Lascau-Coman V, Mathieu C, et al. Chondroinduction is the main cartilage repair response to microfracture and microfracture with BST-CarGel: results as shown by ICRS-II histological scoring and a novel zonal collagen type scoring method of human clinical biopsy specimens. Am J Sports Med. 2015;43:2469–80.
334. O'Driscoll SW, Marx RG, Beaton DE, Miura Y, Gallay SH, Fitzsimmons JS. Validation of a simple histological-histochemical cartilage scoring system. Tissue Eng. 2001;7:313–20.
335. Grogan SP, Barbero A, Winkelmann V, Rieser F, Fitzsimmons JS, O'Driscoll S, et al. Visual histological grading system for the evaluation of in vitro-generated neocartilage. Tissue Eng. 2006;12:2141–9.
336. Bonasia DE, Marmotti A, Mattia S, Cosentino A, Spolaore S, Governale G, et al. The degree of chondral fragmentation affects extracellular matrix production in cartilage autograft implantation: an in vitro study. Arthroscopy. 2015;31:2335–41.

Chapter 10
Skin Regeneration

Xiaowen Zheng, Qian Li, Lie Ma, and Changyou Gao

Abstract The engineering of skin substitutes and their applications on the regeneration of damaged skin have advanced dramatically in the past decades. However, scientists are still struggling with the generation of full-thickness skin with native structure and completed functions. In this chapter, classified by sources, recent developments of biomaterials for skin regeneration have been summarized. Then the most common formats of the engineering skin substitutes are introduced. The strategies of the biological functionalization in the design of skin substitutes are further summarized. Some important challenges in the field of skin substitutes such as angiogenesis, scarring, and appendages loss, and the advanced strategies including endogenous stem cells-based therapy and on-demand therapy are particularly focused on. Finally, a brief conclusion and some perspectives are given in terms of the future trend of biomaterials for skin regeneration.

Keywords Skin · Scaffold · Biofunctionalization · In situ regeneration · Regenerative medicine

10.1 Introduction

The skin, the largest organ of the human body, provides a protective barrier against physical, chemical, and biological pathogens to support and maintain human health. In addition, the skin also has the function of temperature regulation, external insult protection, and detoxing. Typically, the skin has hierarchical structures including the upper epidermal layer, interlayer dermis, and subcutaneous tissue. The epidermis

X. Zheng · Q. Li · L. Ma (✉) · C. Gao
MOE Key Laboratory of Macromolecular Synthesis and Functionalization, Department of Polymer Science and Engineering, Zhejiang University, Hangzhou, China
e-mail: liema@zju.edu.cn; cygao@zju.edu.cn

C. Gao (ed.), *Polymeric Biomaterials for Tissue Regeneration*,
https://doi.org/10.1007/978-981-99-6948-7_10

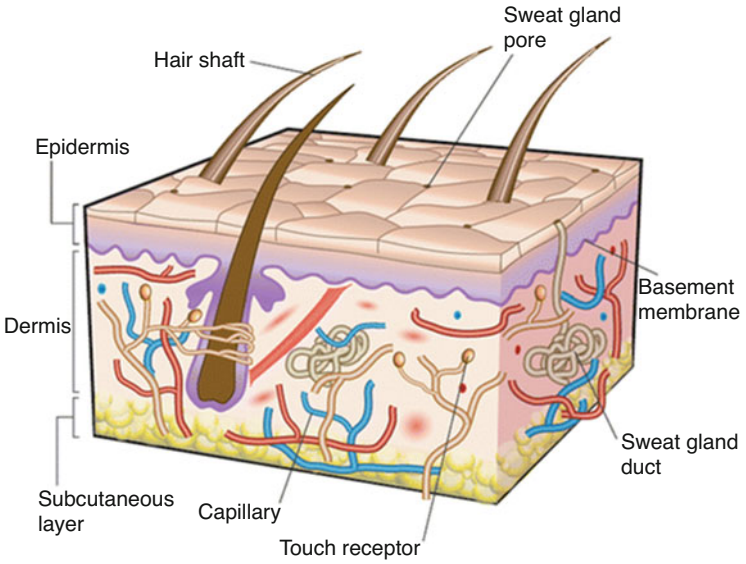

Fig. 10.1 The structure of the human skin. (Reprinted from Ref. [1] with permission. Copyright 2007, Rights Managed by Nature Publishing Group)

whose thickness is 0.1–0.2 mm consists mainly of keratinocytes derived from the capillary network. The dermis layer composes of fibroblasts and extracellular matrix (ECM) including collagen, glycosaminoglycans (GAGs), and elastin. Skin appendages such as hair follicles, sweat glands, and sebaceous glands are from the subcutaneous tissue and play a great role in the sensation, temperature regulation, and detoxing (Fig. 10.1) [1].

Burn, trauma, or chronic diseases frequently cause the loss of the skin, leading to descent of nonspecific immunity and bacterial infection, which is one of the most severe problems affecting human life quality. Thus, skin regeneration has become a major aim in the field of wound healing. In the past several decades, surgical therapies including skin transplantation have been applied to treat the loss of the skin and have achieved great success in skin regeneration. Autologous skin graft is the "gold standard" for clinical treatment of skin defect, and allograft plays a big role in the early period of skin repair as a temporary cover until a permanent skin graft is available. However, skin autograft and allograft are limited by the timely availability and donor sites. In addition, current skin grafts often suffer from a range of problems including incomplete biological functions, scar formation, and bacterial or virus infection during surgical therapies [2]. Thus, it has been becoming more and more urgent to find effective therapy strategies for the treatment of skin loss facing with the increasing clinical need and a vast patient resource.

Recently, skin substitute based on tissue engineering is being rapidly developed to bypass the limitations of conventional tissue transplantation and provide new therapeutic strategy to restore skin function [3]. Tissue engineering combines

scaffold, cells, and biofactors to remodel the target tissue or organ in vitro, followed by in vivo transplantation according to the principles of materials, medicine, and biology. Skin tissue substitutes based on tissue engineering have been fabricating over the past several decades to provide more suitable therapeutic schemes for skin loss, and some commercial products are available in clinical application. For example, Dermagrafts®, a dermal skin substitute consists of poly(glycolic acid) (PGA), poly(lactic acid) (PLA), and fibroblasts, has been used to treat diabetic ulcers [4]. However, the fully functional skin regeneration is still a big challenge for skin tissue engineering. Better tissue engineering strategy in the aspect of exploitation of new biomaterials and novel design of biomaterial scaffolds should be developed to fulfill the increasing demand of skin regeneration.

This chapter focuses on the application of tissue engineering and regenerative medicine approach for the fabrication of bioengineered constructs for skin regeneration. First of all, the materials and the design of material scaffold for skin regeneration are summarized. Then the biofunctionalization of biomaterial scaffold is reviewed by using proteins, genes, and cytokines. Finally, some important challenges for skin regeneration including angiogenesis, scarring, appendages regeneration, and in situ tissue regeneration are discussed.

10.2 Materials for Skin Regeneration

10.2.1 Natural Materials

Collagen, one of the most important components of ECM and composed of a triple helix, is widely used in skin regeneration due to its good biocompatibility, biodegradability, flexibility, and structural and functional similarity to ECM [5]. Besides the collagen derived from animal, plant-derived human collagen has been shown to be a promising biomaterial for skin tissue engineering because of its low risk of an allergic response or disease transmission [6]. However, the poor mechanical properties of collagen limit its application in skin substitute. A variety of methods including cross-linking and blending with other substances have been established to improve the mechanical properties of collagen-based scaffold [7]. For example, synthetic human elastin/collagen composite scaffolds were fabricated by electrospinning for tissue engineering dermis [8]. The scaffold supported fibroblast infiltration, de novo collagen deposition, and new capillary formation. Recently, a full-thickness skin equivalent consists of collagen and silk was prepared to study skin biology [9]. In our lab, a collagen/chitosan scaffold cross-linked with glutaraldehyde has been fabricated to promote the growth of fibroblasts and dermis regeneration. The cross-linking of glutaraldehyde and introduction of chitosan can enhance the biostability of the scaffold [10, 11]. Wang et al. used PLGA-knitted mesh to integrate with collagen/chitosan scaffold to improve the mechanical strength of the scaffolds [12]. Some commercial products based on collagen have been applied in clinical practice. For example, Integra® fabricated by cross-linked bovine

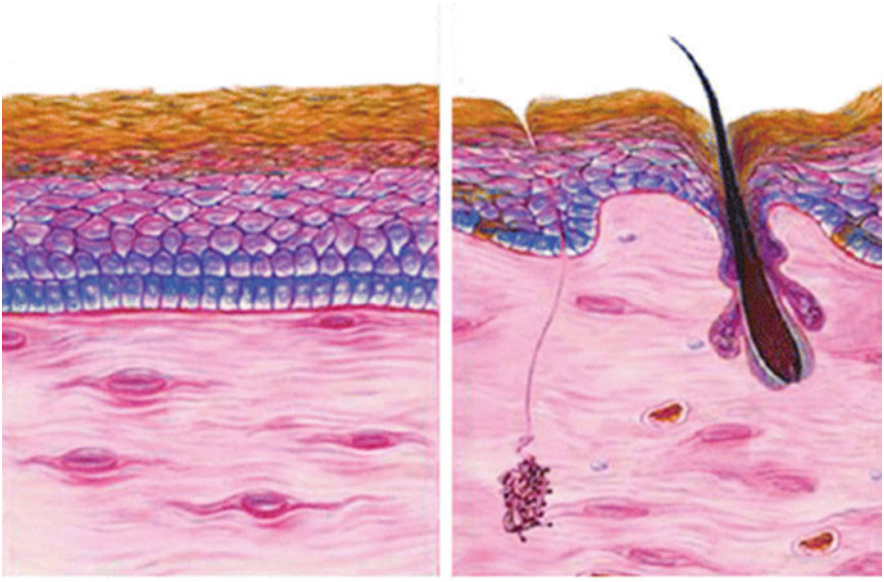

Fig. 10.2 Histology of Apligraf compared with normal human skin. (Reprinted from Ref. [13] with permission. Copyright 2010 John Wiley & Sons, Inc.)

collagen and chondroitin-6-sulfate was employed for dermal regeneration. Apligraf®, a collagen-based hydrogel seeded with dermal fibroblasts and epidermal cells, has been widely applied to treat burns and several kinds of ulcers in the clinic (Fig. 10.2) [13, 14]. But it remains a challenge to regenerate the skin with complete appendages.

Chitosan, the deacetylated derivative of chitin, is a linear polysaccharide consisting of glucosamine and N-acetyl glucosamine [15]. Chitosan can be tailored with various molecular weights (50–2000 kDa) as well as degrees of deacetylation (30–95%), allowing wide adjustment of mechanical and biological properties [16]. Cross-linking is usually made to control the degradation rate and enhance the mechanical properties of chitosan matrix for skin tissue engineering as well [17]. Chitosan can be applied to deliver bioactive molecules. For example, the human epidermal growth factor (EGF) and basic fibroblast growth factor (bFGF) were encapsulated in chitosan scaffold to promote wound healing [18, 19]. In addition, membranes based on chitosan are widely used as wound dressings because of the antibacterial capacity of chitosan [20]. However, the most extensive application of chitosan for skin regeneration is serving as a three-dimensional matrix. Tchemtchoua et al. prepared chitosan nanofibrillar scaffold for skin repair. Compared to chitosan sponge, the chitosan nanofibrillar scaffold induced a faster regeneration of both the epidermis and dermis (Fig. 10.3) [21]. Kiyozumi et al. fabricated a photo-cross-linkable chitosan hydrogel containing DMEM/F12 medium

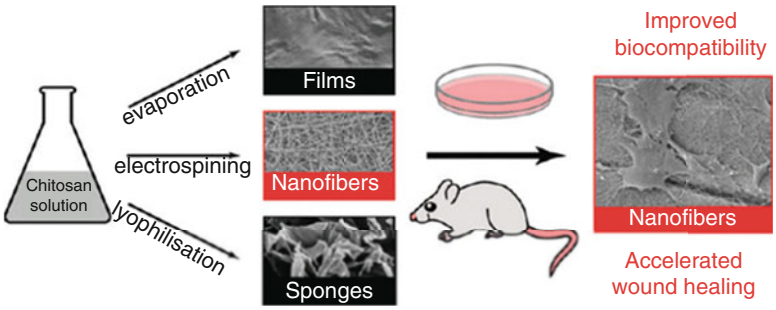

Fig. 10.3 Compared with chitosan films and sponges, the nanofibrillar structure strongly improved cell adhesion and proliferation in vitro. When used as a dressing covering full-thickness skin wounds in mice, chitosan nanofibrils induced a faster regeneration of both the epidermis and dermis compartments. (Reprinted from [21] with permission. Copyright 2011 American Chemical Society)

(medium-Az-CH-LA) for skin regeneration [22]. The hydrogel promoted re-epithelialization, vascularization, and wound repair. Moreover, compared to collagen sponge, thicker granulation tissue and earlier neovascularization were found in medium-Az-CH-LA [23].

Other natural biomaterials for skin regeneration including gelatin, hyaluronan, and fibrin are widely used as well. Shevchenko et al. designed a gelatin scaffold with attached silicone pseudo-epidermal layer for wound repair using a cryogelation technique [24]. The mechanical properties of the scaffold were comparable to the clinical product Integra®. In vivo test showed that the gelatin scaffold supports wound healing by allowing host cellular infiltration, biointegration, and remodeling. Monteiro et al. utilized a spray-assisted layer-by-layer assembly technique to fabricate a multilayer film composed of poly-L-lysine (the epidermal component) and porous hyaluronic acid scaffold (the dermal component) in a rapid and controlled manner for skin tissue engineering [25]. The multilayer film enhances cell adhesion and regeneration of the epidermal barrier functions. Losi et al. prepared a fibrin-based scaffold with incorporated VEGF- and bFGF-loaded nanoparticles to stimulate wound healing [26]. The scaffold induces re-epithelialization and enhances granulation tissue formation/maturity and collagen deposition in genetically diabetic mice. Acellular dermal matrix (ADM) is used to obtain scaffolds with similar components and structure of ECM of the natural skin. For instance, AlloDerm® made of ADM by LifeCell® Corporation is extensively employed for full-thickness skin regeneration.

10.2.2 Synthetic Polymers

The mechanical property is the biggest drawback of natural materials for skin regeneration: thus, natural materials usually need to be cross-linked or combined with other materials. On the contrary, synthetic polymers with predictable and

flexible physical and chemical properties including mechanical properties, functional groups, and degradation rate can be obtained under controlled conditions with mature techniques. Besides, synthetic polymers are biodegradable, are less expensive, and have lower immunological response than natural materials [27]. Furthermore, synthetic polymers such as PGA, PLA, poly(lactide-*co*-glycolide) (PLGA), and polycaprolactone (PCL) have been approved by the Food and Drug Administration (FDA) of the USA.

Synthetic polymers are important materials for skin regeneration. TransCyte® developed by the Advanced Tissue Science Company consisting of PLA scaffold and fibroblasts has been approved by the FDA for the healing of degree III burns [28]. PLGA matrices with fiber diameters varying from 150 to 6000 nm were fabricated via electrospinning [29]. Human skin fibroblasts acquire a well-spreading morphology and show significant growth on fiber matrices in the 350–1100 nm diameter range. Fibrous scaffolds composed of PLA and poly(ethylene glycol) (PEG) were prepared by electrospinning for skin tissue engineering [30]. The scaffold containing 30% PEG exhibited most beneficial properties including wettability, and adaptable bulk biodegradation, and promoted the penetration and growth of human dermal fibroblasts. However, synthetic polymers are usually hydrophobic, and their lack of functional groups leads to limited capacity to combine with biomolecules. To enforce the bioactivity of synthetic polymers, natural materials are widely applied with synthetic polymers to design hybrid scaffolds. Chen et al. fabricate a hybrid scaffold composed of knitted PLGA and weblike collagen microsponges to facilitate cell seeding and distribution and rapid formation of the dermal tissue [31]. A porous polycaprolactone (PCL)/collagen membrane was designed by Venugopal et al. via electrospinning. The well-defined nanostructure can well promote the growth and adhesion of cells [32]. The postmodification of synthetic polymers is another important method for the enhancement of bioactivity. Yang et al. used anhydrous ammonia plasma treatment to modify surface properties to improve the cell affinity of a PLA/PLGA scaffold [33]. The modified scaffold facilitated the growth of fibroblasts. Nanofibrous PCL/gelatin scaffolds were modified by collagen type I grafting [34]. The diameter of the fiber and porosity decreased with the increase of grafted collagen, and the collagen-modified nanofibrous PCL/gelatin scaffolds can maintain characteristic shape and promote proliferation of fibroblasts.

10.3 Scaffold Design for Skin Regeneration

The scaffold plays a vital role for skin regeneration by serving as a three-dimensional matrix for maintaining cell activities and promoting extracellular matrix formation, delivering biofactors, preserving tissue volume, and providing temporary mechanical function. As the skin is complicated with a multilayer structure, how to design a scaffold mimicking the hierarchical structure and ultrastructure of ECM of the skin is an issue of great importance. So far different formats of scaffolds have been designed

to treat different kinds of damaged skins. For example, chitosan/poly(vinyl alcohol) (PVA) nanofibrous membrane has been prepared by electrospinning as a wound dressing [35]. However, for dermal or even full-thickness skin regeneration, the most common scaffold formats are porous scaffolds and hydrogels.

10.3.1 Porous Scaffolds

The porous scaffold is the most common format for skin regeneration. Typically a porous scaffold possesses unique microstructures similar to native ECM, showing high surface area which facilitates cell attachment and growth. Both natural and synthetic polymers can be fabricated into the porous scaffolds with controlled three-dimensional structures by methods such as gas foaming, freeze-drying, and electrospinning.

A novel porous scaffold composed of collagen, hyaluronic acid, and gelatin was fabricated by freeze-drying for skin repair [36]. The average pore diameter of the scaffold was 132.5 ± 8.4 μm, which is beneficial for cell attachment and infiltration. The in vivo histological results revealed that the scaffold promoted wound healing compared to the group without treatments. Lu et al. fabricated a funnel-like porous PLLA–collagen and PLLA–gelatin hybrid scaffolds by forming collagen or gelatin sponge on a woven PLLA mesh for skin tissue engineering [37]. PLLA–collagen and PLLA–gelatin porous scaffolds promoted the regeneration of the dermal tissue and reduced contraction during the formation of new tissues. In our lab, Ma et al. have developed a collagen/chitosan hybrid porous scaffold which was cross-linked by glutaraldehyde (GA) to improve their biostability for skin regeneration [11]. Collagen and chitosan are evenly distributed in the scaffolds with high porosity and good interconnectivity. In vitro culture suggested that the porous scaffold could maintain the original good cytocompatibility of collagen and effectively accelerate infiltration and proliferation of human dermal fibroblasts. In vivo test revealed that the scaffold could induce the fibroblast infiltration from the surrounding tissues. Besides, collagen/chitosan-silicone membrane bilayer dermal equivalent (BDE) was designed, in which the silicone membrane covers the hybrid scaffold to prevent water evaporation and infection (Fig. 10.4) [38]. The porous BDE can be functionalized by plasmid DNA to form a gene-activated scaffold for more complicated reconstruction of the damaged skin. For example, the porous BED combined with *N*,*N*,*N*-trimethyl chitosan chloride (TMC)/pDNA-VEGF complexes can significantly enhance the expression of VEGF, which in turn facilitates the regeneration of full-thickness incisional wounds [39]. To inhibit the scar formation during wound healing, TMC/siRNA-TGF-β1 complexes were incorporated into the BDE to interfere in transforming growth factor-β1 (TGF-β1) signal pathway and suppress the expression of TGF-β1 [40]. The functionalized porous BDE can inhibit scar formation compared to the normal BDE. These results indicate that the porous BDE holds great promise for skin regeneration in clinical application.

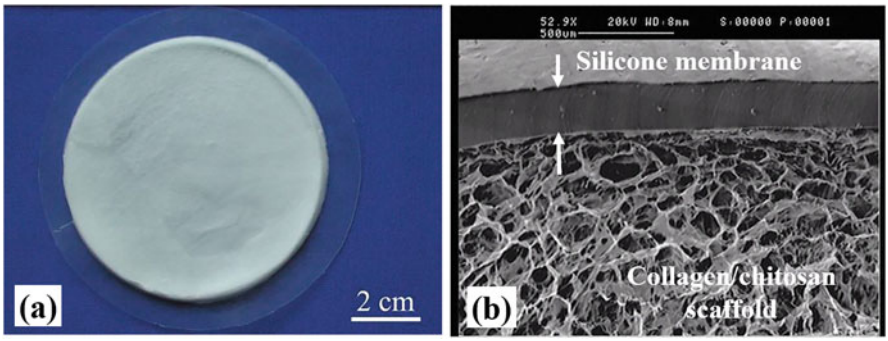

Fig. 10.4 (**a**) A view of the scaffold after being combined with a silicone membrane with a thickness of about 0.14 mm. (**b**) The microstructures of the scaffold observed under a scanning electron microscope. (Reprinted from Ref. [38] with permission. Copyright 2006 John Wiley & Sons, Ltd)

10.3.2 Hydrogel

Hydrogels are three-dimensional cross-linked polymer networks that are capable of absorbing large amount of water, which is important for the absorption of the excess of wound exudates [41]. In addition, hydrogels can protect the wound site from infection and promote the healing process by providing a moisturized environment. Moreover, hydrogels can preserve the bioactivity of growth factors, antibiotics, cytokines, and cells, making them ideal carriers for the delivery of biomolecules to realize complete skin regeneration. Many studies have been focused on the applications of hydrogel for skin regeneration [42–45].

Chitosan hydrogel is well known as a wound dressing, showing good biocompatibility, anti-infective activity, and the ability to accelerate wound healing. Thermo-responsive hydrogel was developed by using chitosan and agarose for skin regeneration [46]. The hydrogel prevented water loss and wound dehydration and was in favor of cell internalization and proliferation. A bilayer physical hydrogel of chitosan without any external cross-linking agent was used to induce inflammatory cell migration and angiogenesis [47]. A hydrogel sheet composed of alginate, chitin/chitosan, and fucoidan (ACF-HS) has been developed for wound dressing (Fig. 10.5) [48]. The hydrogel can provide a moist environment for rapid wound healing. Significantly advanced granulation tissue was observed in the healing-impaired wounds being treated with the hydrogel. Wong et al. fabricated a pullulan–collagen composite hydrogel by using a salt-induced phase inversion technique, which can recapitulate the reticular structure of human dermal ECM [49]. The hydrogel promoted wound closure due to the increased recruitment of stromal cells as well as the formation of the granulation tissue. A versatile, nontoxic, in situ cross-linkable biodegradable dextran hydrogel loaded with chitosan microparticles containing VEGF and EGF was designed for skin regeneration. In vivo results showed that the hydrogel improved the physical, chemical, and biological protection

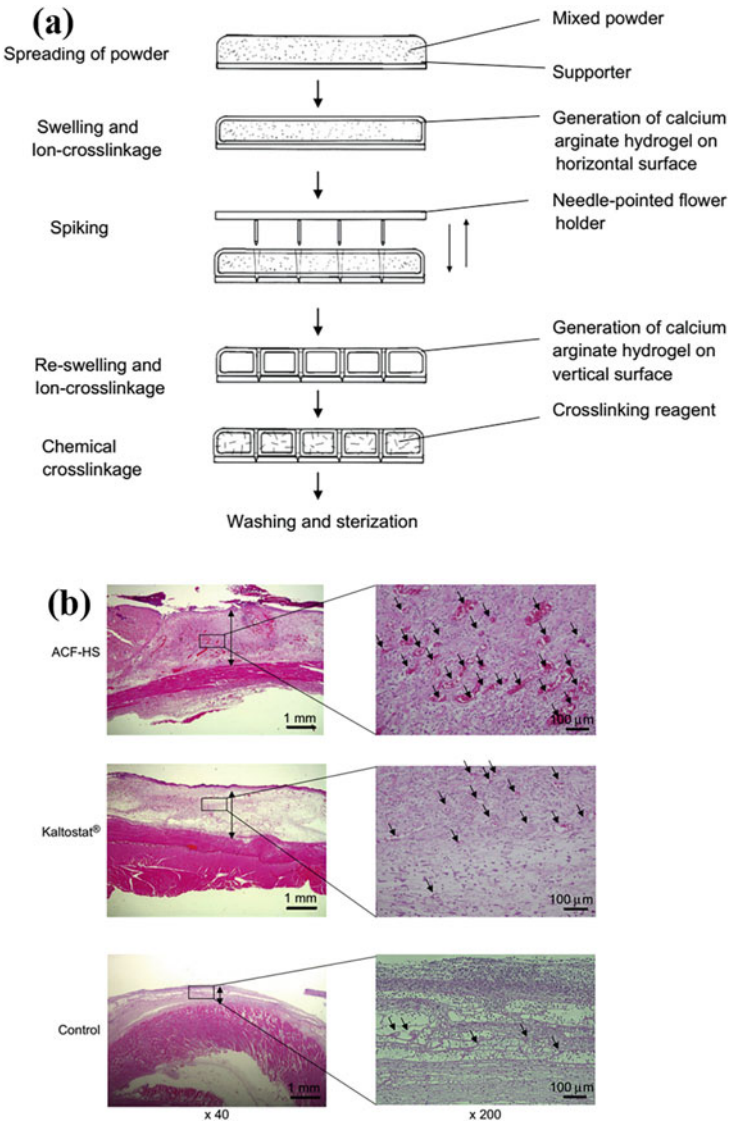

Fig. 10.5 (**a**) Preparative procedures for ACF-HS. (**b**) Histological examination of wounds covered with ACF-HS or Kaltostat® and controls (uncovered). In the *left panel*, *black arrows* show formed granulation tissues. In the *right panel*, *squares* show the sites for microphotographs, and *black arrows* show blood vessels containing erythrocytes. (Reprinted from Ref. [48] with permission. Copyright 2009 Published by Elsevier Ltd)

of the damaged skin [50]. Besides, the spatiotemporally controlled release of VEGF- and EGF-enhanced angiogenesis and re-epithelialization are crucial for the reconstruction of the native skin. More excitingly, a recent study shows that dextran-based

hydrogels supported the infiltration of inflammatory cells, resulting in its rapid degradation and promoted infiltration of angiogenic cells and endothelial cells into the healing wounds [51]. In addition, the remarkable neovascularization and regeneration with hair follicles and sebaceous glands were observed after 21 days, and new hair was observed 5 weeks later. These results indicate that dextran-based hydrogel alone without bioactive factors can promote complete skin regeneration with appendages.

10.4 Biofunctionalization of Skin Regeneration Scaffolds

Skin repair is the result of synergistic effect of different kinds of cells whose proliferation, migration, differentiation, and ECM secretion are well regulated by bioactive factors such as growth factors, genes, and cytokines. Combining bioactive factors with scaffolds is a promising way to promote the efficiency and quality of the regenerated skin.

10.4.1 Growth Factors

Growth factors are capable of stimulating cellular growth, cellular proliferation, and cellular differentiation. Usually they are proteins or steroid hormones regulating a variety of cellular processes. Growth factors typically act as signaling molecules between cells to promote cell differentiation or maturation and have been widely used in tissue engineering skin constructs. Some growth factors are promising mediators of wound healing, such as the epidermal growth factor (EGF), fibroblast growth factor (FGF), vascular endothelial growth factors (VEGF), platelet-derived growth factor (PDGF), insulin-like growth factor-1 (IGF-1), transforming growth factors α and β (TGF-α and TGF-β), and hepatocyte growth factor (HGF). Site-specific delivery of growth factors in microdevices could provide an efficient means of stimulating localized recruitment to the cell transplants and would ensure cell survival and functions. By combining growth factors with microvehicles, bioactive skin scaffolds can be constructed. Richardson et al. incorporated VEGF and PDGF into a porous PLGA scaffold to realize a controlled dose and rate of delivery, pioneering the research of a vehicle delivering multiple angiogenic factors with distinct kinetics [52]. Perets et al. incorporated bFGF-loaded microspheres with three-dimensional porous alginate scaffolds, achieving enhanced vascularization in vivo [53]. Tabata et al. combined FGF, HGF, and VEGF with collagen gels to promote the regeneration of hair follicles after implantation [54]. Mao et al. combined FGF on a substrate via a layer-by-layer technique to fabricate bioactive films, on which fibroblasts proliferated better and secreted more ECM [55]. Regarding to hair follicle regeneration, HGF, a mitogen, motogen, and morphogen for lots of different organs, is expressed by the cells in human hair follicles and involved in the

cycle of hair growth. Uijtdewilligen et al. incorporated insulin-like growth factor-2 (IGF-2) and sonic hedgehog (SHH) into a collagen type I heparin scaffold to form an embryonic-like scaffold which could help to repair the skin without contraction or scar formation [56].

10.4.2 Genes

As summarized above, with the ability to modulate and direct cells efficiently, the growth factors have been extensively used as bioactive factors to combine with tissue engineering scaffolds. However, the most challenging limitation is their short half-lives. The emerging gene technique provides an optional method to make cells produce growth factors constantly. Hence, functional genes can be incorporated into scaffolds as bioactive factors and are locally expressed to encode specific growth factors at wound site. Specific examples of application of gene therapy in skin tissue engineering will be introduced below.

Shea et al. incorporated plasmid DNA encoding platelet-derived growth factor (PDGFB) into a three-dimensional PLGA sponge, implantation of which in a rat dermis showed enhancement of granulation tissue and vascularization [57]. Other types of matrices such as collagen and PVA sponges loaded with genes are also developed and used to treat cutaneous wounds, resulting in improvement of flap survival, granulation tissue formation, angiogenesis, and re-epithelialization [39, 58].

Alternatively, the nucleic acids (e.g., plasmid, siRNA) are complexed with cationic polymers or lipids, with the design of these transfection reagents depending upon the nucleic acid properties, such as size [59]. Complexation with polymers or lipids protects against degradation, creates a less negative particle relative to naked plasmid, and facilitates internalization and intracellular trafficking [60].

10.4.3 Cytokines

Cytokines, a family of small molecules of approximately 8–10 kDa in size, are key regulators of cell migration, immune responses, and wound healing [61]. Proinflammatory cytokines, particularly IL-1 and IL-6 and TNF-α, are upregulated during the inflammatory phase of wound healing.

IL-1 is produced by monocytes, neutrophils, macrophages, and keratinocytes and is immediately released by keratinocytes during wound healing. IL-1 activates fibroblasts and promotes the secretion of FGF [62]. IL-6 is secreted by neutrophils and monocytes and has been shown to be involved in healing response. Evidence shows that IL-6 is closely related with wound healing by regulating leukocyte infiltration, angiogenesis, and collagen accumulation [63]. TNF-α can promote the

expression of FGF-7, indicating that it can favor the process of re-epithelialization [64].

Stromal cell-derived factor-1α (SDF-1α, CXCL12) chemokine is a member of the CXC family and works via the CXCR4 receptor. It plays a role in the inflammatory response by recruiting lymphocytes to the wound and promoting angiogenesis. Endothelial cells, myofibroblasts, and keratinocytes express SDF-1. A number of researches have proved that SDF-1α plays a pivotal role in the recruitment of stem cells. For example, PLGA scaffolds incorporated with SDF-1α can recruit more stem cells, which favors angiogenesis and decreases fibrotic and inflammatory responses. More interestingly, mechanical stretch can upregulate SDF-1α in the skin tissue and promote migration of circulating bone marrow-derived mesenchymal stem cells (BMSCs) [65]. The application of SDF-1α provides an avenue for the recruitment of stem cells, which is crucial for the in situ skin regeneration. For example, Nakamura et al. used mesenchymal stem cells (MSCs) genetically engineered with (SDF-1α) to heal skin wounds [66]. SDF-1α-engineered MSCs (SDF-MSCs) expressed more SDF-1α and enhanced the migration of MSCs and dermal fibroblasts and promoted skin wound closure.

10.5 Important Challenges and Strategies

Although many significant milestones of bioengineered skin have been reached for clinical therapies of full-thickness defects, challenges still remain to fulfill the criteria of "regenerated skin" with complete structural, esthetic, and functional properties as the nature of the skin. How to achieve rapid angiogenesis, inhibited scarring, and regeneration of appendages is a key issue related to the quality of the regenerated skin. In addition, in situ regeneration, which should be particularly concerned, would be less costly and complex than those approaches that require ex vivo cell manipulation.

10.5.1 Angiogenesis

One of the most critical issues for most bioengineered tissues is the rapid and appropriate angiogenesis of the constructs, since a tissue beyond a certain size generally cannot survive without the supply of nutrients and oxygen, and removal of waste products of cells [67]. For materials with a thickness larger than 0.4 mm, new blood vessels are not able to penetrate rapidly [68]. The delayed or poor angiogenesis of the reconstructed skin will hinder the nourishment of the overlaying epidermal layer and result in the failure of the graft. Moreover, if the transplantation of split-thickness skin grafts is delayed, the timely healing of the damaged skin will be hampered and the risk of death will increase [69]. It is clear that the blood supply is essential to realize the long-term integration of the reconstructed skin with the host

tissue. Therefore, acceleration of the angiogenesis rate to achieve rapid formation of new blood capillaries is urgently required, whereas still remains a research focus for improvement of existing skin substitutes.

Suitable pore size of tissue-engineered scaffold plays an important role in improving permeability, facilitating cell migration, and enhancing angiogenesis. Yannas et al. found that a pore size ranging from 90 to 150 μm and porosity larger than 90% promote vessel formation [70]. Pruitt et al. reported that only when pore size of scaffold is larger than 80 μm it can be conducive to the ingrowth of connective tissue and neovascularization [71]. Another possible approach to enhance the angiogenesis of the tissue-engineered skin is to combine the prefabricated vessels with some special kinds of cells to achieve better initial onset of revascularization for early anastomoses between graft and bed vessels. As one example, human dermal microvascular endothelial cells were incorporated into collagen or fibrin hydrogels. Three-dimensional capillaries were formed after transplantation of the prevascularized substitutes [72]. The engineered capillaries were further stabilized by pericytes and smooth muscle cells and ultimately connected to the microvessels of the wound ground. It is also found some glycosaminoglycans have angiogenetic effect. Pieper et al. reported that the incorporation of glycosaminoglycans could increase angiogenesis degree in vivo [73]. However, a sufficient vasculature still takes more than 4 weeks to develop.

The most powerful approach to induce angiogenesis in the engineered tissues is to use angiogenetic growth factors such as bFGF, VEGF, and PDGF. So far many efforts have been made to enhance angiogenesis by incorporation of angiogenic growth factors into tissue engineering scaffolds. With the loading of bFGF, the fibrin and collagen scaffolds show enhanced angiogenesis when applied to the rabbit ear ulcers, therefore greatly improving the healing of full-thickness skin defects [74]. Wissink et al. used heparin to realize a controlled release of bFGF through specific binding, which is effective in promoting the growth of endothelial cells within the collagen scaffold in vitro [75]. Perets et al. encapsulated bFGF into PLGA microspheres and then loaded the microspheres into a porous sodium alginate scaffold [53]. The formation of large mature vessels was greatly promoted by the bFGF-loaded scaffold in a rat peritoneal model.

However, delivery of the growth factors faces some challenges due to their sensitivity and instability, and their half-lives are only on the order of minutes in serum. In addition, the high cost of growth factors also limits their trial in practice. The gene technique has been considered as an alternative way in order to overcome the drawbacks of growth factors. By loading of more stable and functional genes into the scaffolds, the gene-activated matrix (GAMs) can be generated to locally transfect cells and constantly produce targeted growth factors at wound site. Endowed with the advantages of localized treatment, maintenance of effective amount of bioactive DNAs, and protection of DNAs against immune responses and nuclease degradation, the GAMs have shown great promise for the enhanced angiogenesis of the engineered skin. Mao et al. used TMC as a cationic gene delivery vector to carry plasmid DNA encoding VEGF (pDNA-VEGF) and constructed a gene-activated collagen scaffold for skin repair [76]. The in vivo application to Sprague-Dawley

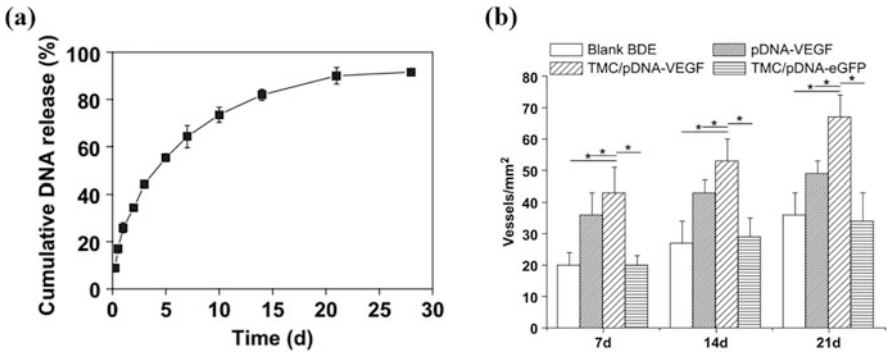

Fig. 10.6 (**a**) Cumulative release of DNA from the scaffolds as a function of time. (**b**) TMC/pDNA-VEGF group had a significantly higher number of newly formed and mature blood vessels. (Reprinted from Ref. [77] with permission. Copyright 2010 Elsevier Ltd)

mice demonstrated that the TMC/pDNA-VEGF complexes remarkably promoted the in vivo expression of VEGF and thus enhanced the angiogenesis of the scaffolds. Recently, a gene-activated collagen-chitosan/silicone membrane bilayer dermal equivalent (BDE) has been prepared and evaluated for treatment of the full-thickness incisional wounds in terms of histology, immunohistochemistry, immunofluorescence, real-time quantitative PCR, and Western blotting analysis in a porcine model [39]. The TMC/pDNA-VEGF group shows highest level of VEGF expression at both mRNA and protein levels, resulting in the highest densities of newly formed and mature vessels. After 112 days of ultrathin skin graft transplantation, the healing skin has a similar structure and ~80% tensile strength of the normal skin. Exploitation of the gene-activated BDE for the healing of full-thickness burns was also performed, showing very positive angiogenesis and repair results similar to those for incisional wounds (Fig. 10.6) [77].

10.5.2 Scarring

Although skin substitutes based on principle of regeneration have achieved important progresses, scarring still remains a problem which results in issues such as disfiguration, itching, and local ulceration [78]. Prevention of scarring is therefore a major challenge to be addressed for the repair and regeneration of skin defects, and antiscarring technologies should be incorporated for the new generation of the skin constructs.

Scars are the outcome of postnatal healing process of normal acute mammalian tissue repair including integration of bioengineered skins [79]. Scarring is a rapid tissue repairing process driven by an evolutionarily devised mechanism, allowing rapid recover of tissue integrity to fill tissue voids. Scarring involves a series of

cellular events related to tissue repair including inflammation, migration/proliferation and ECM deposition, and also the inputs of numerous cell types, matrix components, and signaling molecules. Essentially, the excessive and disordered accumulation of ECM such as collagen, as well as the imbalance of new deposition and destruction of collagen, directly leads to the scar formation. By contrast, the scar-free regeneration should have features including complete restoration of skin structure, normal collagen deposition, and regular distribution of hair follicles, capillaries, and glands, which reflects a focus of interest for the emerging fields of regenerative medicine. Central to a material-based approach for skin regeneration is to build a suitable environment where cells are exposed to a complex pattern of bioactive molecules, which direct desired cell behaviors and right tissue regeneration.

Fetal wound repair is essentially a scar-free regenerative process. It has been extensively studied and confirmed that embryonic scarless wound repair exhibits reduced fibrin clots and platelet degranulation, and suppressed inflammatory response, which has provided therapeutic strategies for scar-free repair. Most importantly, the growth factor profile is also quite different for embryonic wound and adult wound. The large family of TGF-β protein, which can be secreted by multiple cell types such as platelets, macrophages, and fibroblasts, is one of the most important biosignal molecules during the wound healing process. It acts as a chemokine for fibroblasts, induces differentiation of myofibroblasts, regulates the collagen synthesis, and modulates the matrix turnover. Recent investigations have confirmed that the level of TGF-β1 and TGF-β2 in fetal skin injuries is lower than that in adult skin, while the level of TGF-β3 is elevated [80]. Inspired by these findings, successful reduction of scarring of adult skin wounds has been reported by interrupting TGF-β1 and TGF-β2 signaling pathway through neutralization with antibodies, inactivation by proteoglycan-like decorin, and blockage of function by exogenous receptors, as well as exogenous addition of the TGF-β3 isoforms. Samuels et al. [81] found that hypertrophic scar was induced in a rabbit embryos subcutaneous model by injecting the TGF-β1 and TGF-β2, while the addition of their polyclonal neutralizing antibody could inhibit scarring and generate a normal tensile strength and more physical dermal architecture. A recent research proves that after infected by adenovirus encoding a truncated TGF-β receptor II, normal dermal fibroblasts could result in wounds with an average of 49% reduction of the scar area and less inflammatory reaction in the full-thickness incisional wounds in rats [82].

The recently emerging biomolecular cues of RNA interference (RNAi) offer a fascinating and prospective alternative to specifically silence targeted genes and downregulate targeted protein levels [83]. Delivery of exogenous small interfering RNA (siRNA) mediated by three-dimensional scaffolding materials is right now at the frontier of current research. Compared with other strategies, the RNAi not only shows higher efficiency and specificity during a long duration time but also avoids risks of immunogenicity and inactivation in the antibody method. In a recent research in our lab, TMC/siRNA complexes targeting TGF-β1 were incorporated into the collagen-chitosan/silicone membrane bilayer dermal equivalent (BDE) to fabricate an RNAi functionalized bioengineered skin (RNAi-BDE), aiming to

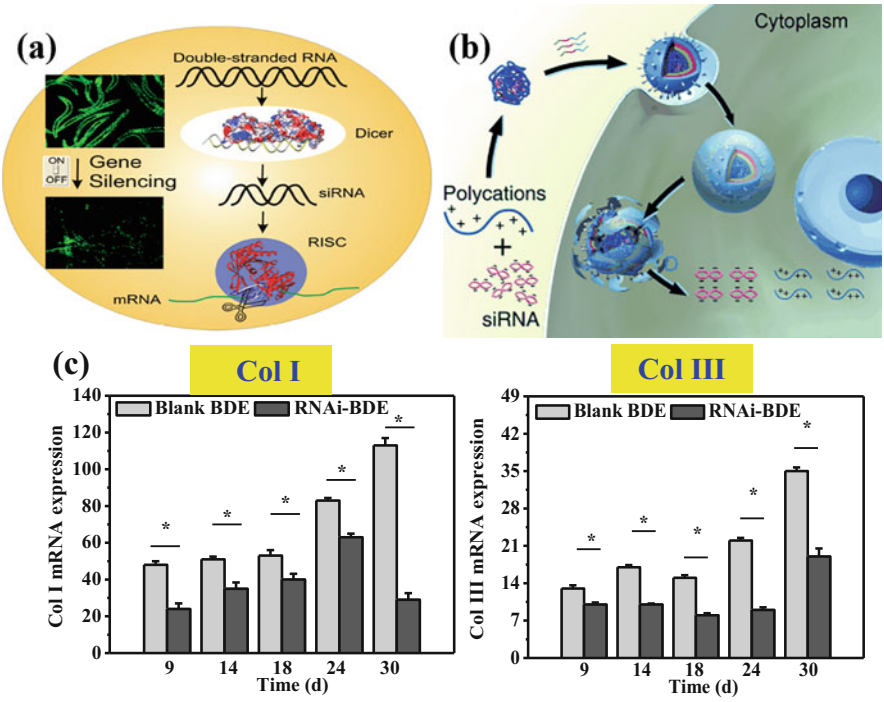

Fig. 10.7 (**a**) The siRNA could silence special gene expression. (**b**) Combination of polycations TMC with siRNA to form complexes which could be transfected into cells. Wound formation is mainly caused by massive and disordered deposition of Col I and Col III. (**c**) TMC/siRNA can suppress the expression of both Col I and Col III significantly. (Reprinted from Ref. [40] with permission. Copyright 2012 Elsevier Ltd)

interfere TGF-β1 signal pathway, directing cell behaviors, and ultimately inhibiting scarring (Fig. 10.7). The RNAi-BDE functioned as a reservoir for the incorporated TMC/siRNA complexes, enabling a prolonged siRNA release. Application of the RNAi-BDE on the full-thickness skin defects of pig backs confirmed the in vivo inhibition of TGF-β1 expression by immunohistochemistry, real-time quantitative PCR, and Western blotting during 30 days postsurgery. The levels of other scar-related factors such as collagen type I, collagen type III, and α-smooth muscle actin (α-SMA) were also downregulated. In combination with the ultrathin skin graft transplantation for 73 days, the regenerated skin by RNAi-BDE had an extremely similar structure to that of the normal one with significant scar inhibition.

10.5.3 Appendages

Skin appendages such as hair follicle, sweat gland, sebaceous gland make skin functions well in touch, temperature sensation, excretion, perspiration, and thermoregulation. Regeneration of skin appendages is an important symbol of skin recovery and functionalization. Although some commercial artificial skin substitutions can achieve a structural repair in the epidermis and the dermis, it remains a challenge to regenerate the skin with complete appendages [13]. Hence, regenerated skin cannot fully replace normal skin in function.

Hair follicle is a mini-organ which produces hair. It is composed of hair papilla, matrix, root sheath, hair fiber, bulge, and so on. There are three stages in hair growth: the growth phase (anagen), the regressing phase (catagen), and the quiescent phase (telogen). Growth cycles are controlled by chemical signals like epidermal growth factor. Efforts of reconstructing hair follicles have been made decades ago. Lin et al. combined epidermal stem cells in collagen/gelatin scaffold with fibroblasts; hair follicle-like structure was formed after implantation. It is also reported that the interaction between epidermal cells and mesenchymal cells contributes to the formation of hair follicles. More recently, MSCs are induced into hair papilla-like cells [84]. Moreover, polysaccharide, as one main component of dermal ECM, is reported to induce the regeneration of hair follicles on a mice model [51]. Recently, it was reported that hair growth was promoted by adipose-derived stem cell (ASC) transplantation in animal experiments, and a conditioned medium of ASCs (ASC-CM) induced the proliferation of hair-compositing cells in vitro. Jin et al. introduced some ASC stimulators in preconditioning to enhance hair regeneration [85]. They also highlighted the functional role of ASCs in hair cycle progression and concluded the advantages and disadvantages of their application in hair regeneration.

Sweat glands are small tubular structures of the skin that can produce sweat. There are two kinds of sweat glands. Eccrine sweat glands are distributed all over the body (except for the lips, tip of the penis, and the clitoris), although their density varies a lot from region to region, while apocrine sweat glands are larger, having different mechanisms of secretion, and are limited to axilla (armpits) and perianal areas. Sweat glands play a key role in thermoregulation and inner balance. Therefore, it is vital to reconstruct sweat glands especially for large-area burns. Fu et al. cultured sweat gland cells (SGCs) on gelatin microspheres containing EGF and delivered the SGCs-microspheres complex into an engineered skin construct mainly composed of a fibroblast-embedded collagen-based matrix [86]. This engineered skin construct was then transplanted onto full-thickness cutaneous wound in an athymic murine model. Remarkably, sweat gland-like structure can be achieved in vitro within the hybrid matrix. Huang Sha et al. designed a functional in vitro cell-laden three-dimensional extracellular matrix mimics (3D-ECM) with composite hydrogels based on gelatin and sodium alginate. It provides the spatial inductive cues for enhancing specific differentiation of epidermal lineages to regenerate sweat glands [87].

Sebaceous glands are kind of microscopic glands in the skin that secrete an oily/waxy matter, called sebum, to lubricate and waterproof the skin and hair of mammals. In human beings, they are found in greatest abundance on the face and scalp, though distributed throughout all skin sites except the palms and soles. Compared with hair follicles and sweat glands, sebaceous glands are later to be studied. But exciting progress has been made related to reconstruction of sebaceous glands. Hair bulge cells have been reported to possess the potential of differentiating into sebaceous glands. Horsley et al. firstly found a kind of progenitor cells that can secret factor Blimp1, which can stimulate the regeneration of sebaceous glands when they get hurt [88].

Appendages do have a firm interaction rather than separate growth, although most researches are still confined to one certain appendage. With further study of biology of appendages, and clarifying the interaction of materials and related cells (specifically stem cells) and appendages themselves, it is quite possible to functionalize skin constructs by reconstructing different appendages together in the future.

10.5.4 In Situ Skin Regeneration

Along with the advancement of science and technology in biology, medicine, and material science, the insight mechanism of wound healing is better understood. Diverse methods for skin repair and regeneration have also been developed. Stem cell-based therapy, which is a promising cure for a multitude of diseases and disorders, has been one of the best documented approaches in regenerative medicine. However, the ex vivo expansion of stem cells and their in vivo delivery are restricted by the low survival rate and the limited availability of stem cell sources.

It has been demonstrated that endogenous stem cells can be actively attracted to sites of injury [3]. Thus, recruiting sufficient endogenous stem cells to the wound area and inducing them to repair the structure and functions of skin become a key challenge. This technique, known as in situ regeneration, has the potential to provide new therapeutic options for all kinds of tissues and organs. The in situ tissue regeneration method relies on endogenous stem cell homing, proliferation, differentiation, and rebuilding functional skins. Such options would be less costly and complex than the traditional approaches which require substantial ex vivo cell manipulation.

Microenvironment, which could be changed by cytokines, surface topology, and so on, could influence stem cell recruiting. Some cytokines can enhance tissue regeneration by facilitating cell homing. Chen et al. fabricated a radially oriented scaffold which could effectively promote BMSCs migration, whose effect was further enhanced by addition of stromal cell-derived factor-1 (SDF-1) (Fig. 10.8) [89]. It is reported that the migration abilities of PDMSCs exposed to hypoxic conditions are significantly increased. Interestingly, decreased integrin alpha4 in PDMSCs under hypoxia increases PDMSC migration ability [90]. In addition, bone morphogenetic protein-7 (BMP-7) is another cell homing factor [3]. Shao et al.

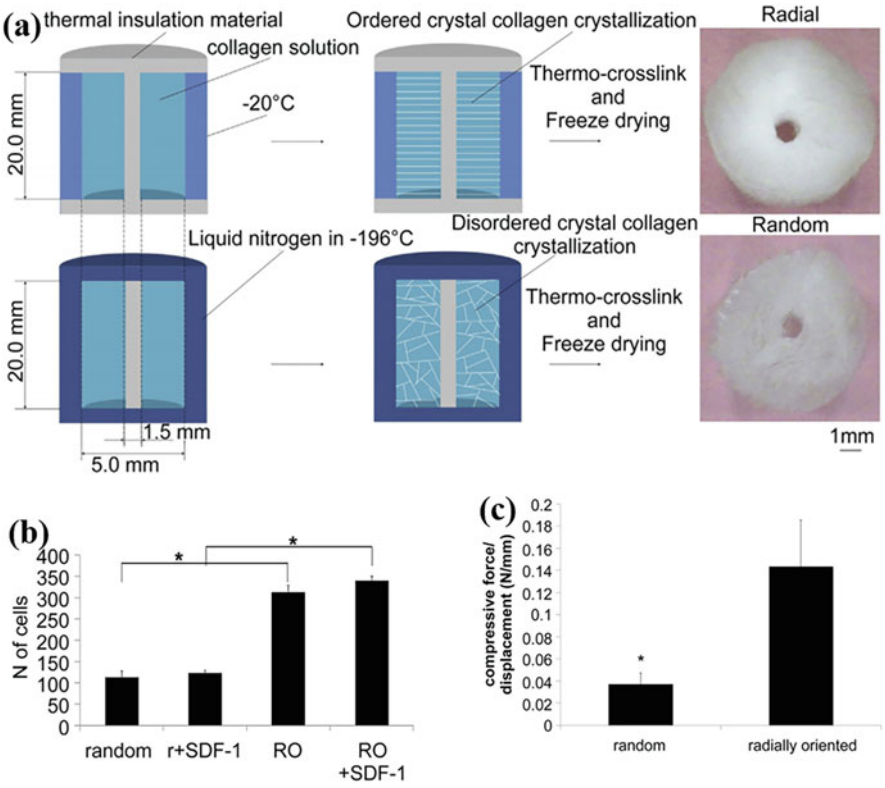

Fig. 10.8 (**a**) Fabrication of the radially oriented (RO) and random collagen scaffolds. (**b**) The radially oriented scaffolds had significantly better mechanical property compared with the random scaffolds. (**c**) The cell number was quantified at low magnification and the radially oriented scaffolds accelerated cell infiltration. (Reprinted from Ref. [89] with permission. Copyright 2014 Elsevier Ltd)

found that a peptide sequence (E7, EPLQLKM) with seven amino acids has a high specific affinity to bone marrow-derived MSCs [91]. In the subsequent work, E7 peptide was immobilized to a collagen scaffold via a collagen-binding domain (CBD) to construct a functional collagen scaffold, which could enhance the speed of healing process [92]. It is reported that E7-modified scaffolds incorporated with rhTGF-β1 could maintain a sustained release and bioactivity. A series of analyses indicate that the E7 peptide promotes BMSC initial adhesion and that the scaffolds containing both E7 and rhTGF-β1 are the most favorable for BMSC survival (Fig. 10.9) [93].

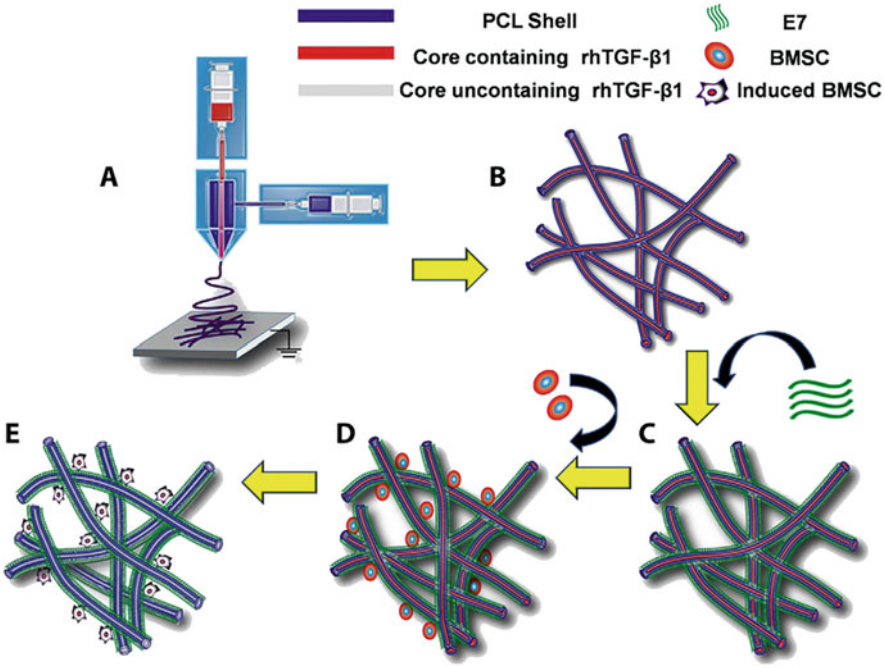

Fig. 10.9 The preparation process for coaxial electrospun fiber scaffolds. (**a**) The process of coaxial electrospinning: the spinneret is composed of two concentric needles; the outer needle is used to deliver the shell solution (*blue*, PCL), while the inner needle is used to eject the core solution (*red*, rhTGF-β 1). (**b**) Scaffold composed of electrospun coaxial fibers, with core (*red*) and shell (*blue*) structure. (**c**) Scaffold conjugated with the BMSC-specific affinity peptide (E7) (*green*). (**d**) E7-modified scaffold facilitates adhesion of BMSCs onto the surface. (**e**) The E7-modified surface and sustained release of rhTGF-β 1 in the core of the coaxial fibers promote adhesion and differentiation of BMSCs [93]. (Reprinted from Ref. [93] with permission. Copyright 2014 Elsevier Ltd)

10.5.5 On-Demand Therapy of Skin Defect

The "Black Box" status of skin regeneration caused by the passive management of traditional materials makes it difficult to obtain the real status of skin defect and provide on-demand treatment in time. Therefore, the development of next-generation skin regeneration system with the abilities of real-time monitoring, diagnosis at an early stage, and on-demand therapy is of great significance. By the integration of flexible electronics with wound dressing, a pioneer wearable skin regeneration system, which can collect physiological signals from wound sites and diagnose healing status real time, was proposed [94, 95]. On the other hand, providing therapy in time to match wound pathological need, i.e., on-demand therapy, is another designing requisite for next-generation skin regeneration system [96]. Therefore, some studies developed advanced wound dressings to provide

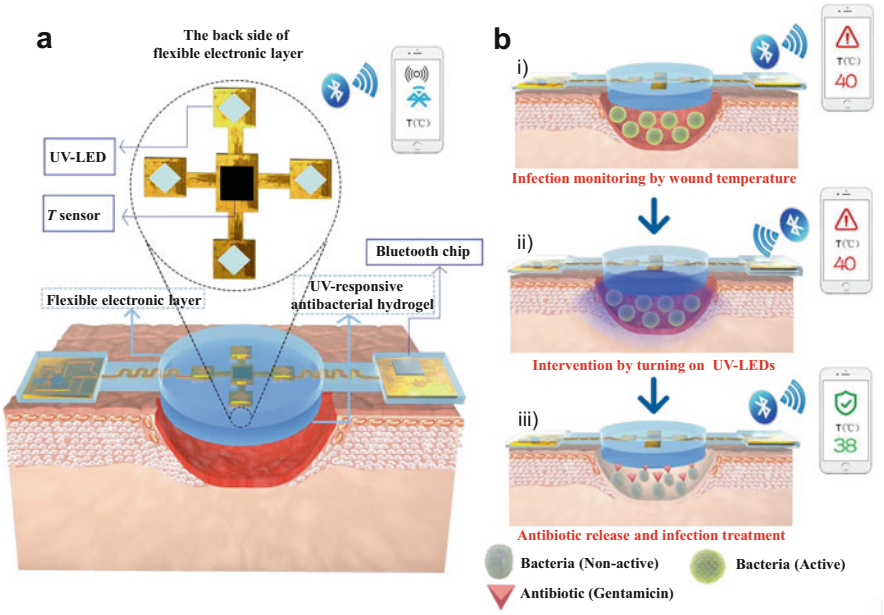

Fig. 10.10 Schematics of the structures and working principles of the smart flexible electronic-integrated wound dressing. (**a**) The integrated system consists of a polydimethylsiloxane-encapsulated flexible electronic layer and an UV-responsive antibacterial hydrogel. The flexible electronic device is integrated with a sensor for monitoring temperature and four UV-LEDs for emitting UV light (365 nm) to trigger the release of antibiotic from the UV-responsive antibacterial hydrogel when needed; a Bluetooth chip is also integrated for wireless data transmission in real time. (**b**) Conceptual view of the integrated system for infected-wound monitoring and on-demand treatment: (**i**) real-time monitoring of wound temperature and providing an alert of hyperthermia caused by infection; (**ii**) turning on UV-LEDs to trigger the release of antibiotics; (**iii**) infection inhibition by the released antibiotics, resulting in decreased wound temperature [99]. (Reprinted from Ref. [99] with permission. Copyright 2020 John Wiley & Sons, Ltd)

on-demand therapy by combining responsive drug-delivery system [97, 98]. Pang et al. reported a novel flexible electronic-integrated skin regeneration system (Fig. 10.10). It was capable of monitoring wound temperature in real-time to provide early diagnosis of pathological infection. By integrating a responsive antibacterial hydrogel into the healing system, antibiotics were released to wound sites controllably to realize on-demand therapy. Wound temperature was collected by the integrated sensor and transmitted via Bluetooth. Once wound temperature was higher than a preset value, infection would be diagnosed, and antibiotics were released responsively to kill bacteria as required [99].

10.6 Conclusions and Future Perspectives

Skin regeneration is one of the most serious problems in clinical medicine. The use of skin grafts is still an important therapy for damaged skin. So far decades of efforts have focused on the development of the tissue-engineered skin based on material technologies, chemistry, biology, and medicine. Bioengineered skins for epidermal, dermal, and full-thickness defects have been fabricated, and some of them are currently commercially available. However, most of them are not sufficient to regenerate new skin similar with native skin.

To realize the regeneration of the skin with a complicated structure and complete functions, it is becoming increasingly popular to design "smart biomaterial system" to provide instructive signals to stimulate target cell responses in the processes of skin regeneration. "Smart biomaterials" can be obtained by adjusting the properties of biomaterials including physical properties, chemical compositions, and biofunctions. Meanwhile, the application of flexible electronic devices into skin regeneration system is able to monitor the wound status in real time, and provide on demand therapy on the basis of need during the skin regeneration process. Moreover, by the combination of stem cells or in situ recruitment of endogenous stem cells, the stem cell hybrid material has attracted more and more interest for the in situ skin regeneration with appendages. We believe that with the development of biomaterial science and regenerative medicine, the skin with a complicated structure and multifunction similar to those of the native skin can be regenerated sooner or later.

Acknowledgment We acknowledge financial support by the Key Science Technology Innovation Team of Zhejiang Province (2013TD02), the Natural Science Foundation of China (51322302, 20934003), and the National Key Research Program of China (2016YFC1101001).

References

1. MacNeil S. Progress and opportunities for tissue-engineered skin. Nature. 2007;445:874–80.
2. Tabata Y. Biomaterial technology for tissue engineering applications. J R Soc Interface. 2009;6 (35):S311–24.
3. Chen FM, Wu LA, Zhang M, et al. Homing of endogenous stem/progenitor cells for in situ, tissue regeneration: promises, strategies, and translational perspectives. Biomaterials. 2011;32 (12):3189–209.
4. Marston WA. Dermagraft, a bioengineered human dermal equivalent for the treatment of chronic nonhealing diabetic foot ulcer. Expert Rev Med Devices. 2004;1(1):21–31.
5. Parenteau-Bareil R, Gauvin R, Berthod F. Collagen-based biomaterials for tissue engineering applications. Materials. 2010;3:1863–87.
6. Willard JJ, Drexler JW, Das A, et al. Plant-derived human collagen scaffolds for skin tissue engineering. Tissue Eng Part A. 2013;19(13–14):1507–18.
7. Cao H, Chen MM, Liu Y, et al. Fish collagen-based scaffold containing PLGA microspheres for controlled growth factor delivery in skin tissue engineering. Colloids Surf B Biointerfaces. 2015;136:1098–106.

8. Rnjak-Kovacina J, Wise SG, Zhe L, et al. Electrospun synthetic human elastin: collagen composite scaffolds for dermal tissue engineering. Acta Biomater. 2012;8(10):3714–22.
9. Bellas E, Seiberg M, Garlick J, et al. In vitro 3D full-thickness skin-equivalent tissue model using silk and collagen biomaterials. Macromol Biosci. 2012;12(12):1627–36.
10. Ma L, Gao C, Mao Z, et al. Thermal dehydration treatment and glutaraldehyde cross-linking to increase the biostability of collagen-chitosan porous scaffolds used as dermal equivalent. J Biomater Sci Polym Ed. 2003;14(8):861–74.
11. Ma L, Gao C, Mao Z, et al. Collagen/chitosan porous scaffolds with improved biostability for skin tissue engineering. Biomaterials. 2003;24(26):4833–41.
12. Wang X, You C, Hu X, et al. The roles of knitted mesh-reinforced collagen-chitosan hybrid scaffold in the one-step repair of full-thickness skin defects in rats. Acta Biomater. 2013;9(8): 7822–32.
13. Zhong SP, Zhang YZ, Lim CT. Tissue scaffolds for skin wound healing and dermal reconstruction. Wiley Interdiscip Rev Nanomed Nanobiotechnol. 2010;2:510–25.
14. Edmonds M. Apligraf in the treatment of neuropathic diabetic foot ulcers. Int J Lower Extrem Wounds. 2009;8(1):11–8.
15. Montembault A, Viton C, Domard A. Physico-chemical studies of the gelation of chitosan in a hydroalcoholic medium. Biomaterials. 2005;26(8):933–43.
16. Ribeiro MP, Ana E, Daniela S, et al. Development of a new chitosan hydrogel for wound dressing. Wound Repair Regen. 2009;17(6):817–24.
17. Adekogbe I, Ghanem A. Fabrication and characterization of DTBP-crosslinked chitosan scaffolds for skin tissue engineering. Biomaterials. 2005;26(35):7241–50.
18. Hong JP, Kim YW, Lee SK, et al. The effect of continuous release of recombinant human epidermal growth factor (rh-EGF) in chitosan film on full thickness excisional porcine wounds. Ann Plast Surg. 2008;61(4):457–62.
19. Mizuno K, Yamamura K, Yano K, et al. Effect of chitosan film containing basic fibroblast growth factor on wound healing in genetically diabetic mice. J Biomed Mater Res A. 2003;64 (1):177–81.
20. Abdelgawad AM, Hudson SM, Rojas OJ. Antimicrobial wound dressing nanofiber mats from multicomponent (chitosan/silver-NPs/polyvinyl alcohol) systems. Carbohydr Polym. 2014;100 (100):166–78.
21. Tchemtchoua VT, Atanasova G, Aqil A, et al. Development of a chitosan nanofibrillar scaffold for skin repair and regeneration. Biomacromolecules. 2011;12(9):3194–204.
22. Kiyozumi T, Kanatani Y, Ishihara M, Saitoh D, Shimizu J, Yura H, et al. Medium (DMEM/F12)-containing chitosan hydrogel as adhesive and dressing in autologous skin grafts and accelerator in the healing process. J Biomed Mater Res B Appl Biomater. 2006;79:129–36.
23. Kiyozumi T, Kanatani Y, Ishihara M, et al. The effect of chitosan hydrogel containing DMEM/F12 medium on full-thickness skin defects after deep dermal burn. Burns. 2007;33(5):642–8.
24. Shevchenko RV, Eeman M, Rowshanravan B, et al. The in vitro characterization of a gelatin scaffold, prepared by cryogelation and assessed in vivo as a dermal replacement in wound repair. Acta Biomater. 2014;10(7):3156–66.
25. Monteiro IP, Shukla A, Marques AP, et al. Spray-assisted layer-by-layer assembly on hyaluronic acid scaffolds for skin tissue engineering. J Biomed Mater Res A. 2015;103(1): 330–40.
26. Losi P, Briganti E, Errico C, et al. Fibrin-based scaffold incorporating VEGF- and bFGF-loaded nanoparticles stimulates wound healing in diabetic mice. Acta Biomater. 2013;9(8):7814–21.
27. Rezwan K, Chen QZ, Blaker JJ, et al. Biodegradable and bioactive porous polymer/inorganic composite scaffolds for bone tissue engineering. Biomaterials. 2006;27(18):3413–31.
28. Amani H, Dougherty WR, Blome S. Use of Transcyte® and dermabrasion to treat burns reduces length of stay in burns of all size and etiology. Burns J Int Soc Burn Injuries. 2006;32(7): 828–32.
29. Kumbar SG, Nukavarapu SP, James R, et al. Electrospun poly(lactic acid-*co*-glycolic acid) scaffolds for skin tissue engineering. Biomaterials. 2008;29(30):4100–7.

30. Cui W, Zhu X, Yang Y, et al. Evaluation of electrospun fibrous scaffolds of poly(dl-lactide) and poly(ethylene glycol) for skin tissue engineering. Mater Sci Eng C. 2009;29(6):1869–76.
31. Chen G, Sato T, Ohgushi H, et al. Culturing of skin fibroblasts in a thin PLGA-collagen hybrid mesh. Biomaterials. 2005;26(15):2559–66.
32. Venugopal JR, Zhang Y, Ramakrishna S. In vitro culture of human dermal fibroblasts on electrospun polycaprolactone collagen nanofibrous membrane. Artif Organs. 2006;30(6): 440–6.
33. Yang J, Shi G, Bei J, Wang S, Cao Y, Shang Q, et al. Fabrication and surface modification of macroporous poly(L-lactic acid) and poly(L-lactic-*co*-glycolic acid) (70/30) cell scaffolds for human skin fibroblast cell culture. J Biomed Mater Res. 2002;62:438–46.
34. Gautam S, Chou CF, et al. Surface modification of nanofibrous polycaprolactone/gelatin composite scaffold by collagen type I grafting for skin tissue engineering. Mater Sci Eng C Mater Biol Appl. 2014;34(1):402–9.
35. Zhou Y, Yang D, Chen X, et al. Electrospun water-soluble carboxyethyl chitosan/poly(vinyl alcohol) nanofibrous membrane as potential wound dressing for skin regeneration. Biomacromolecules. 2008;9(1):349–54.
36. Wang HM, Chou YT, Wen ZH, et al. Novel biodegradable porous scaffold applied to skin regeneration. PLoS One. 2013;8(6):e56330.
37. Lu H, Oh HH, Kawazoe N, et al. PLLA-collagen and PLLA-gelatin hybrid scaffolds with funnel-like porous structure for skin tissue engineering. Sci Technol Adv Mater. 2012;13(6): 64210–8.
38. Shi Y, Ma L, Zhou J, et al. Collagen/chitosan-silicone membrane bilayer scaffold as a dermal equivalent. Polym Adv Technol. 2005;16(11–12):789–94.
39. Rui G, Xu S, Ma L, et al. Enhanced angiogenesis of gene-activated dermal equivalent for treatment of full thickness incisional wounds in a porcine model. Biomaterials. 2010;31(28): 7308–20.
40. Liu X, Liang J, Zhang B, et al. RNAi functionalized collagen-chitosan/silicone membrane bilayer dermal equivalent for full-thickness skin regeneration with inhibited scarring. Biomaterials. 2013;34(8):2038–48.
41. Vlierberghe SV, Dubruel P, Schacht E. Biopolymer-based hydrogels as scaffolds for tissue engineering applications: a review. Biomacromolecules. 2011;12(5):1387–408.
42. Yanchun Liu MD, Cai S, Xiao ZS, et al. Release of basic fibroblast growth factor from a crosslinked glycosaminoglycan hydrogel promotes wound healing. Wound Repair Regen. 2007;15(2):245–51.
43. Shepherd J, Sarker P, Rimmer S, et al. Hyperbranched poly(NIPAM) polymers modified with antibiotics for the reduction of bacterial burden in infected human tissue engineered skin. Biomaterials. 2011;32(32):258–67.
44. Peattie RA, Nayate AP, Firpo MA, et al. Stimulation of in vivo angiogenesis by cytokine-loaded hyaluronic acid hydrogel implants. Biomaterials. 2004;25(14):2789–98.
45. Lee PY, Cobain E, Huard J, et al. Thermosensitive hydrogel PEG-PLGA-PEG enhances engraftment of muscle-derived stem cells and promotes healing in diabetic wound. Mol Ther J Am Soc Gene Ther. 2007;15(6):1189–94.
46. Miguel SP, Ribeiro MP, Brancal H, et al. Thermoresponsive chitosan-agarose hydrogel for skin regeneration. Carbohydr Polym. 2014;111(20):366–73.
47. Boucard N, Viton C, Agay D, et al. The use of physical hydrogels of chitosan for skin regeneration following third-degree burns. Biomaterials. 2007;28(24):3478–88.
48. Murakami K, Aoki H, Nakamura S, et al. Hydrogel blends of chitin/chitosan, fucoidan and alginate as healing-impaired wound dressings. Biomaterials. 2010;31(1):83–90.
49. Wong VW, Rustad KC, Galvez MG, et al. Engineered pullulan-collagen composite dermal hydrogels improve early cutaneous wound healing. Tissue Eng Part A. 2011;17(5–6):631–44.
50. Ribeiro MP, Morgado PI, Miguel SP, et al. Dextran-based hydrogel containing chitosan microparticles loaded with growth factors to be used in wound healing. Mater Sci Eng C. 2013;33(5):2958–66.

51. Sun G, Zhang X, Shen YI, et al. Dextran hydrogel scaffolds enhance angiogenic responses and promote complete skin regeneration during burn wound healing. Proc Natl Acad Sci U S A. 2011;108(52):20976–81.
52. Richardson TP, Peters MC, Ennett AB, et al. Polymeric system for dual growth factor delivery. Nat Biotechnol. 2001;19(11):1029–34.
53. Perets A, Baruch Y, Weisbuch F, et al. Enhancing the vascularization of three-dimensional porous alginate scaffolds by incorporating controlled release basic fibroblast growth factor microspheres. J Biomed Mater Res A. 2003;65:489–97.
54. Ozeki M, Tabata Y. In vivo promoted growth of mice hair follicles by the controlled release of growth factors. Biomaterials. 2003;24(13):2387–94.
55. Mao Z, Ma L, Zhou J, et al. Bioactive thin film of acidic fibroblast growth factor fabricated by layer-by-layer assembly. Bioconjug Chem. 2005;16(5):1316–22.
56. Uijtdewilligen PJE, Versteeg EMM, Gilissen C, et al. Towards embryonic-like scaffolds for skin tissue engineering: identification of effector molecules and construction of scaffolds. J Tissue Eng Regen Med. 2013;10(1):E34–44.
57. Shea LD, Smiley E, Bonadio J, et al. DNA delivery from polymer matrices for tissue engineering. Nat Biotechnol. 1999;17(6):551–4.
58. Hijjawi J, Mogford JE, Chandler LA, et al. Platelet-derived growth factor B, but not fibroblast growth factor 2, plasmid DNA improves survival of ischemic myocutaneous flaps. Arch Surg. 2004;139(2):142–7.
59. Putnam D, Doody A. RNA-interference effectors and their delivery. Crit Rev Ther Drug Carrier Syst. 2006;23(2):137–64.
60. Laporte LD, Rea JC, Shea LD. Design of modular non-viral gene therapy vectors. Biomaterials. 2006;27(7):947–54.
61. Vanden BergFoels WS. In situ tissue regeneration: chemoattractants for endogenous stem cell recruitment. Tissue Eng Part B Rev. 2014;20(1):28–39.
62. Tang A, Gilchrest BA. Regulation of keratinocyte growth factor gene expression in human skin fibroblasts. J Dermatol Sci. 1996;11(1):41–50.
63. Lin ZQ, Kondo T, Ishida Y, et al. Essential involvement of IL-6 in the skin wound-healing process as evidenced by delayed wound healing in IL-6-deficient mice. J Leukoc Biol. 2003;73 (6):713–21.
64. Barrientos S, Stojadinovic O, Golinko MS, et al. Growth factors and cytokines in wound healing. Wound Repair Regen. 2008;16(5):333.
65. Zhou SB, Wang J, Chiang CA, et al. Mechanical stretch upregulates SDF-1α in skin tissue and induces migration of circulating bone marrow-derived stem cells into the expanded skin. Stem Cells. 2013;31(12):2703–13.
66. Nakamura Y, Ishikawa H, Kawai K, et al. Enhanced wound healing by topical administration of mesenchymal stem cells transfected with stromal cell-derived factor-1. Biomaterials. 2013;34 (37):9393–400.
67. Zhang B, Liu X, Wang C, et al. Chapter 52—bioengineering skin constructs. In: Stem cell biology and tissue engineering in dental sciences. London: Academic; 2015. p. 703–19.
68. Black AF, Berthod F, L'Heureux N, et al. In vitro reconstruction of a human capillary-like network in a tissue-engineered skin equivalent. FASEB J. 1998;12(13):1331–40.
69. O'Ceallaigh S, Herrick SE, Bluff JE, et al. Quantification of total and perfused blood vessels in murine skin autografts using a fluorescent double-labeling technique. Plast Reconstruct Surg. 2006;117(1):140–51.
70. O'Brien FJ, Harley BA, Yannas IV, et al. The effect of pore size on cell adhesion in collagen-GAG scaffolds. Biomaterials. 2005;26(4):433–41.
71. Pruitt B Jr, Levine NS. Characteristics and uses of biologic dressings and skin substitutes. Arch Surg. 1984;119(3):312–22.
72. Böttcher-Haberzeth S, Biedermann T, Klar AS, et al. Tissue engineering of skin: human tonsil-derived mesenchymal cells can function as dermal fibroblasts. Pediatr Surg Int. 2014;30(2): 213–22.

73. Pieper JS, Wachem PBV, Luyn MJAV, et al. Attachment of glycosaminoglycans to collagenous matrices modulates the tissue response in rats. Biomaterials. 2000;21(16):1689–99.
74. Pandit AS, Feldman DS, Caulfield J. In vivo wound healing response to a modified degradable fibrin scaffold. J Biomater Appl. 1998;12(3):222–36.
75. Wissink MJB, Beernink R, Poot AA, et al. Improved endothelialization of vascular grafts by local release of growth factor from heparinized collagen matrices. J Control Release. 2000;64 (1–3):103–14.
76. Mao Z, Shi H, Rui G, et al. Enhanced angiogenesis of porous collagen scaffolds by incorporation of TMC/DNA complexes encoding vascular endothelial growth factor. Acta Biomater. 2009;5(8):2983–94.
77. Guo R, Xu S, Ma L, et al. The healing of full-thickness burns treated by using plasmid DNA encoding VEGF-165 activated collagen-chitosan dermal equivalents. Biomaterials. 2011;32(4): 1019–31.
78. Costa AMA, Desmoulire A. Mechanisms and factors involved in development of hypertrophic scars. Eur J Plast Surg. 1998;21(1):19–23.
79. Lappert PW. Scarless fetal skin repair: “unborn patients” and “fetal material”. Plast Reconstr Surg. 1996;98(6):1125.
80. Chalmers RL. The evidence for the role of transforming growth factor-beta in the formation of abnormal scarring. Int Wound J. 2011;8(3):218–23.
81. Samuels P, Tan AK. Fetal scarless wound healing. J Otolaryngol. 1999;28(5):296–302.
82. Liu W, Chua C, Wu X, et al. Inhibiting scar formation in rat wounds by adenovirus-mediated overexpression of truncated TGF-beta receptor II. Plast Reconstr Surg. 2005;115(3):860–70.
83. Monaghan M, Pandit A. RNA interference therapy via functionalized scaffolds. Adv Drug Deliv Rev. 2011;63:197–208.
84. Yoo BY. Application of mesenchymal stem cells derived from bone marrow and umbilical cord in human hair multiplication. J Dermatol Sci. 2010;60(2):74–83.
85. Jin SE, Sung JH. Hair regeneration using adipose-derived stem cells. Histol Histopathol. 2015;31:249–56.
86. Huang S, Xu Y, Wu C, et al. In vitro, constitution and in vivo, implantation of engineered skin constructs with sweat glands. Biomaterials. 2010;31(21):5520–5.
87. Huang S, Yao B, Xie J, et al. 3D bioprinted extracellular matrix mimics facilitate directed differentiation of epithelial progenitors for sweat gland regeneration. Acta Biomater. 2015;32: 170–7.
88. Horsley V, O’Carroll D, Tooze R, et al. Blimp1 defines a progenitor population that governs cellular input to the sebaceous gland. Cell. 2006;126(3):597–609.
89. Chen P, Tao J, Zhu S, et al. Radially oriented collagen scaffold with SDF-1 promotes osteochondral repair by facilitating cell homing. Biomaterials. 2015;39:114–23.
90. Ho CJ, Mook LS, In YY, et al. Microenvironmental interaction between hypoxia and endothelial cells controls the migration ability of placenta-derived mesenchymal stem cells via alpha4 integrin and rho signaling. J Cell Biochem. 2015;117(5):1145–57.
91. Shao Z, Zhang X, Pi Y, et al. Polycaprolactone electrospun mesh conjugated with an MSC affinity peptide for MSC homing in vivo. Biomaterials. 2012;33(12):3375–87.
92. Wang H, Yan X, Shen L, et al. Acceleration of wound healing in acute full-thickness skin wounds using a collagen-binding peptide with an affinity for MSCs. Burns Trauma. 2014;2(4): 181–6.
93. Man Z, Yin L, Shao Z, et al. The effects of co-delivery of BMSC-affinity peptide and rhTGF-β1 from coaxial electrospun scaffolds on chondrogenic differentiation. Biomaterials. 2014;35: 5250–60.
94. Rogers J, Takao S, Huang Y. Materials and mechanics for stretchable electronics. Science. 2010;327:1603.
95. Gao W, Ota H, Kiriya D, et al. Flexible electronics toward wearable sensing. Acc Chem Res. 2019;52:523–33.

96. Kiaee G, Mostafalu P, Samandari M, et al. A pH-mediated electronic wound dressing for controlled drug delivery. Adv Healthc Mater. 2018;7:e1800396.
97. Mostafalu P, Tamayol A, Rahimi R, et al. Smart bandages: smart bandage for monitoring and treatment of chronic wounds. Small. 2018;14:e1703509.
98. Gong M, Wan P, Ma D, et al. Flexible breathable nanomesh electronic devices for on-demand therapy. Adv Funct Mater. 2019;29:1902127.
99. Pang Q, Lou D, Li S, et al. Smart flexible electronic-integrated wound dressing for real-time monitoring and on-demand treatment of infected wounds. Adv Sci. 2020;7:1902673.

Chapter 11
Regeneration of Blood Vessels

Muhammad Rafique, Yongzhen Wei, Adam C. Midgley, Kai Wang, Qiang Zhao, and Deling Kong

Abstract Regeneration of damaged, diseased, or resected blood vessels can be achieved using vascular grafts. Additionally, vascular grafts can be used for bypass surgeries and as arteriovenous graft construction for hemodialysis access. These tubular structures are derived from either living donor vessels, decellularized vascular tissues, artificially constructed polymeric scaffolds, or biomimetic tissue-engineered blood vessels. Numerous factors can influence the performance of vascular grafts, their regenerative capacity, and their long-term patency and functionality. These factors can include the choice of polymer scaffold, the polymer degradation rate and elasticity, the physical and biomechanical structure of the scaffold, and whether functional modifications have been made to the scaffolds. This chapter introduces the commonly utilized polymers for vascular graft construction, the fabrication techniques, functional modifications of vascular grafts, and the *in vivo* applicability and clinical relevance of vascular grafts.

Keywords Vascular grafts · Polymers · Fabrication · Degradation · Tissue regeneration

Muhammad Rafique and Yongzhen Wei contributed equally with all other contributors.

M. Rafique · Y. Wei · A. C. Midgley (✉) · K. Wang · Q. Zhao · D. Kong (✉)
Key Laboratory of Bioactive Materials for the Ministry of Education, College of Life Sciences, Nankai University, Tianjin, China
e-mail: midgleyac@nankai.edu.cn; kongdeling@nankai.edu.cn

C. Gao (ed.), *Polymeric Biomaterials for Tissue Regeneration*,
https://doi.org/10.1007/978-981-99-6948-7_11

11.1 Introduction: Overview of Vascular Grafts and Key Challenges

Blood vessels have the imperative role of transporting blood around the body, delivering oxygen and nutrients to tissues. Vascular diseases such as atherosclerosis may result in obstruction of blood flow and tissue ischemia [1]. Vascular grafts have proven effective tools for the treatment of vascular diseases [2]. In the United States, an estimated 450,000 vascular grafts are used for bypass surgery each year, most of which are autologous venous and arterial grafts. However, autologous grafts are limited by availability due to prior use of autologous donor grafts or existing comorbidities in approximately 30% of cases, which necessitates the requirement for artificial vascular grafts [3]. Artificial blood vessels have become an indispensable necessity for cardiovascular surgeries. Some products have been successfully commercialized, such as polytetrafluoroethylene (PTFE; Teflon), expanded PTFE (ePTFE; Gore-Tex), and poly(ethylene terephthalate) (Dacron). Both Teflon and Dacron have been effectively employed as large-diameter (>6 mm internal diameter) vascular grafts, wherein blood flow rate is high, yet these materials yield disappointing clinical results when used as small-diameter (<6 mm internal diameter) coronary artery grafts [4]. In addition, nondegradation of Teflon and Dacron grafts often leads to calcification in the long term [5]. In this regard, development of vascular grafts with relatively slow biodegradation and controlled tissue regenerative processes has emerged as an important concept and direction. These grafts are designed to provide a favorable tissue microenvironment for the recruitment of autologous vascular cells and vascular progenitor cells. A key ideal is that following the complete degradation of the polymer scaffold, a native tissue-like "neoartery" is generated [6].

Despite recent advancements in knowledge and technologies for the fabrication of small-diameter vascular grafts, there are still many scientific questions that remain to be addressed. At the forefront of the questions being asked are how to: enhance vascular regeneration while avoiding pathogenesis; attain long-term patency; and achieve native tissue-like functionality. The current SDVG strategic landscape and approaches to meet clinical requirements are summarized below (Fig. 11.1).

11.1.1 Endothelialization of Vascular Grafts

The endothelium is a smooth luminal cell monolayer that facilitates laminar blood flow through the blood vessel, and it is also a dynamic organ with active roles in coagulation homeostasis, the sensing and transduction of the hemodynamic forces of circulation, and the cellular metabolism of the vascular wall [2]. A major focus of vascular graft research is the promotion of endothelialization. Within many general functions, the endothelium is a physiological barrier equipped with multiple mechanisms to prevent thrombus formation and maintain patency and homeostasis, by

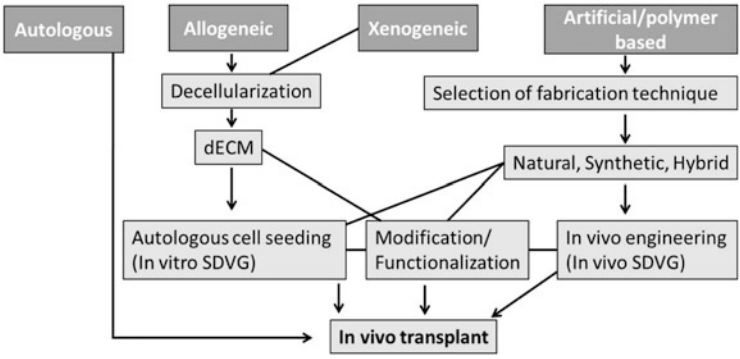

Fig. 11.1 Schematic representation of current landscape of small-diameter vascular grafts (SDVG)

harboring factors that interrupt the coagulation cascade, such as antithrombin III, the protein C receptor thrombomodulin, and tissue factor pathway inhibitor. The endothelium prevents platelet activation by the production of nitric oxide, prostacyclin, ectonucleotidases, and surface heparan sulfates [7]. A vascular graft that resists thrombosis by forming a confluent luminal endothelium *in vivo* is a key objective in vascular tissue engineering.

11.1.2 Restenosis of Vascular Grafts

A common shortcoming in the transplantation of small-diameter vascular grafts is the occurrence of short- and mid-term restenosis. Short-term restenosis is driven by platelet adhesion, activation, and aggregation, which results in thrombus formation. Mid-term restenosis is promoted by the overproliferation of vascular smooth muscle cells (VSMCs), resulting in neointimal hyperplasia. In general terms, the occurrence of restenosis could be ascribed to poor hemocompatibility of artificial vascular grafts [8]. In addition, physical forces have been associated with vascular graft intimal hyperplasia [9]. Prominently, compliance mismatches between the graft and surrounding host artery results in adverse local hemodynamic effects at the anastomosis sites with consequent intimal thickening and eventual graft failure [10]. Development of more compliant sutures, suturing techniques, mechanical clips, biological glue, and laser-based solder techniques have taken precedent [11], with the shared aim to improve pulsatile laminar blood flow in arterial propagation across the anastomosis sites and to reduce damage to the surrounding endothelium [10]. Evidence supports that the timely formation of a confluent endothelial cell monolayer is crucial in preventing the initiation and progression of VSMC overgrowth. The endothelium prevents contact of blood components with the subendothelial matrix of the arterial wall, thereby avoiding activation of the coagulation cascade. This is imperative, as early events in the cascade, such as platelet degranulation following contact with

type-I collagen, have been shown to induce mitogenic factors such as transforming growth factor (TGF)-β [2]. Animal models of endothelial injury have demonstrated that loss of an intact endothelium results in VSMC phenotypic change to a proliferative state. Indeed, it is widely accepted that increased proliferation of terminally differentiated VSMCs contribute significantly to neointima formation [2, 12]. Therefore, construction of vascular grafts with hemocompatible luminal surfaces or blood–material interfaces with antithrombogenic properties is a key consideration during the design process.

11.1.3 Anticoagulation Functions of Vascular Grafts

Several different antithrombotic agents have been evaluated experimentally with the shared aim of reducing the occurrence of thrombotic occlusion in small-diameter vascular grafts [13]. Heparin, a ubiquitously expressed mucopolysaccharide, inhibits thrombin and activated factors IX, X, XI, and XII, which participate in the conversion of prothrombin to thrombin. Thus, heparin functions to reduce thrombin formation. In addition, heparin has a potent antiproliferative effect on VSMCs, independent of its anticoagulant activity, and mediated through interactions with cell receptors, growth factors, adhesion molecules, and protease inhibitors [14]. The systemic administration required to achieve therapeutic levels of antithrombotic drugs at the graft site is expensive and impacted by association with serious hemorrhagic complications. An alternative approach is the immobilization of antithrombotic agents on the graft material. This strategy offers advantages of inhibiting the localized thrombotic process while avoiding systemic side effects [15]. Enzyme prodrug therapy (EPT) is a technique that has been employed in the fabrication of anticoagulant vascular grafts [16]. The versatility of EPT allows the production of bioactive drug molecules by immobilized enzymes at the graft site, in response to the systemic administration of caged prodrugs. In addition to targeted and localized drug delivery, the advantage of EPT also includes the fine tuning of drug dosage, duration, and administration [17].

11.1.4 Calcification of Vascular Grafts

The calcification of cardiovascular implants has been extensively described, and prevention of calcification has remained an important challenge for researchers and industry for decades [18]. The presence of cardiovascular calcification significantly predicts patient morbidity and mortality. Calcific mineral deposition within the soft cardiovascular tissues disrupts the normal biomechanical function of these tissues, leading to complications such as heart failure, myocardial infarction, and stroke [19]. The realization that calcification results from active cellular processes offers hope that the design strategies, choice of materials with favorable biomechanics, and

functional modification of vascular grafts can help to prevent the disease process. The underlying mechanism of vascular calcification includes the migration of VSMCs toward intima, resulting in intimal thickening and endovascular stenosis. One source of intimal hyperplasia and calcification has been suggested to be the unmitigated differentiation of stem cell antigen-1 $(Sca\text{-}1)^+$ stem/progenitor cells into hyperproliferative VSMCs expressing the osteogenic genes, thus leading to mid- or late-term graft failure. To circumvent this, multiple approaches have been employed. For example, the sustained release of nitric oxide (NO) from engineered vascular grafts has shown benefits in attenuating the formation of calcification, which may in part be due to regulation of NO over stem cell biology [20–22]. In addition, the use of natural biomaterials has proven to be a promising strategy to reduce the risk of calcification, which has been suggested to be dependent on an improved rate of vascular tissue regeneration by implanted cardiovascular biomaterials [23].

11.1.5 Animal Models for the Assessment of Vascular Grafts

To assess the capacity of the new conduits to maintain physiologic function in the circulatory system and to determine the response of both the host and the conduits to implantation, evaluation of the grafts in preclinical animal studies is required [24]. Preclinical assessment of vascular grafts using appropriate animal models is essential to determine the clinical potential of engineered tissues. Advancement of knowledge and technologies used in vascular graft fabrication has led to multiple criteria that are utilized in the assessment of clinical potential. Each of these criteria may be best analyzed in different experimental settings. At first, the selection of an appropriate animal model needs to include criteria relevant to the vascular graft, such as implantation site, vascular diameter and length, and period of implantation. Equally important are criteria relevant to the animal species selected such as cost, availability, ease of handling, animal response to surgical procedures, target vessel diameter and length, and target physiology. Optimally, an animal model needs to be selected that meets most of these criteria. It is best to match site and diameter to test the hemodynamics and implantability; use longer grafts (>4 cm) to test patency; select the type of anastomosis (end to end, end to side) to test shear stress; or select species that exhibit similar immunogenicity and thrombogenicity mechanisms as those at work in humans.

The type of analysis, for example, serial imaging or monitoring versus a single measurement at the end of the experiment, is also important in determining the choice of animal model. Secondly, similarity to human physiology is one major factor that is considered when assessing criteria specifically related to translational studies. For example, ovine and nonhuman primate models show greater similarity to humans in terms of thrombogenicity mechanisms as compared to canine or porcine models. On the other hand, dogs exhibit lack of spontaneous endothelialization of vascular grafts, and they tend to be hyperthrombogenic, akin to observations made in humans. These two features make the canine model more

stringent for vascular grafts testing. By contrast, lack of similarity in vascular dimensions and hemodynamics makes small animals, like murine models, poor choices for long-term grafts evaluation. However, the plethora of transgenic mice presents a very useful resource to dissect molecular mechanisms related to immune response, remodeling under pathogenic conditions, vascular reactivity, and other aspects of graft physiology. Age and gender should be considered. Age may affect the microenvironmental factors that are critical for successful grafting and long-term tissue regeneration. As the concerns of animal rights and limitations on the use of nonhuman primates increase, the porcine and ovine models have become more widely used in recent years. In addition to the ethical considerations, cost is also a factor, making the porcine and ovine choice models. There is no absolute ideal regarding animal model selection or international consensus on standards associated with the development and testing of vascular grafts. The lack of standardized models makes it difficult to compare results among different investigators. To best evaluate the implantation of vascular grafts in such a variety of animal models, there is a requirement for optimal model selection and use of proper internal controls [25].

In comparison to small animal models, safety and efficacy parameters in preclinical settings are closer to humans in large animal models, which exhibit similar coagulation systems, hemodynamics, and hematological profiles. For example, minipigs possess a similar anatomy, physiology, immune system, and life span to humans, which makes them a suitable large animal model for the evaluation of human-derived tissue engineered products for transplantation. Itoh et al. developed an immunodeficient pig model (IODP) by removing the spleen and thymus in combination with the administration of immunosuppressive drugs. The developed IOPD was employed for arteriovenous shunt grafting of human-origin three dimensional (3D)-bioprinted tubes (HOBPT) and long-term implantation, which exemplifies the extent of steps required to move toward appropriate evaluations of preclinical cell regeneration approaches and regenerative medicine applications [26]. Grajciarová et al. analyzed tissue-engineered vascular grafts (TEVGs) implanted in ovine and porcine common carotid arteries. The research team found that ovine and porcine common carotid arteries were not equivalent in most parameters to human carotid or internal thoracic arteries. Furthermore, left and right ovine common carotid arteries did not have the same histological composition, suggesting limitations for sham-operated controls within the same animal. The team concluded that the middle and distal segments, but not the proximal segments, of ovine and porcine common carotid arteries served as the better sites for vascular graft implantation and graft testing, indicating that implantation location can influence graft evaluation [27].

11.2 Selection of Polymers for Vascular Grafts

In this section, we discuss other factors that influence vascular regeneration and their long-term patency and function. Among these factors, we focus on the selection of suitable polymers, their degradation and mechanical properties, the scaffolds' structure, and examples of functional modification to scaffolds.

11.2.1 Synthetic Polymers

11.2.1.1 ePTFE

Initial vascular prostheses used nondegradable polymers such as PTFE (Teflon) or ePTFE (Gore-Tex). ePTFE is very stable *in vivo* with no reported failures due to degradation of the graft. The process of ePTFE manufacture is by heating, stretching, and extrusion that results in a nontextile porous tube [25], with an electronegative luminal surface that is antithrombotic. A 5-year patency of 91–95% was achieved with ePTFE arterial substitutes, with neither trans-anastomotic nor transmural endothelialization. Decreased patency (45%) was observed in femoropopliteal bypass surgeries [28]. Surgeons have used nondegradable synthetic Teflon or Dacron as medium-to-large-diameter grafts, which can provide 10 years of symptom-free lifestyle. However, these materials have inferior performance in replacement of small-diameter (<6 mm) blood vessels due to high rates of neointimal hyperplasia and thrombosis [29]. Several attempts have been adopted to improve the patency of ePTFE grafts. An early study showed that preseeding ePTFE grafts with autologous endothelial cells (ECs) gave adequate ECs coverage and considerably improved patency of the grafts in canine models, compared to unseeded ePTFE grafts [30]. Compared with biodegradable materials, the chronic immune responses that can be induced by nondegradable properties and the stiffness of the nondegradable polymer materials themselves limit their wider applicability in the current clinical practice.

11.2.1.2 PCL

Poly (ε-caprolactone) (PCL) is a versatile polymer that shows strong promise for the construction of small-diameter vascular grafts due to its good biocompatibility, suitable mechanical strength, and slow biodegradation rate. Walpoth's group [5] reported that electrospun PCL grafts were degraded to 20% of original molecular weight at 18 months of postimplantation, without dilatation and significant increase in compliance. PCL does not undergo plastic deformation when exposed to long cyclic strain. Therefore, it possesses elastic properties suitable for vascular graft application [31].

The mechanical performance of PCL vascular grafts can be readily tuned by facile blending of PCL with other polymeric materials. Sang et al. indicated that PCL/collagen composite grafts, with fiber diameters of approximately 520 nm, possessed appropriate tensile strength (4.0 ± 0.4 MPa) and adequate elasticity (2.7 ± 1.2 MPa) [32]. The burst pressure of these composite grafts was 4912 ± 155 mmHg, which was much greater than that of the pure PCL grafts (914 ± 130 mmHg) and native vessels. Mercado-Pagán et al. [33] synthesized biocompatible and biodegradable PCL-urethane macromers to fabricate hollow fiber membranes of varied sizes as small-diameter vascular graft candidates. Their tensile stiffness ranged from 0.09 to 0.11 N/mm and maximum tensile force from 0.86 to 1.03 N, with minimum failure strains of approximately 130% and burst pressures from 1158 to 1468 mmHg. In another study, grafts were prepared by using the PLA and PCL physical blends in the ratios of 75:25 and 25:75 with the dimension of (40 × 0.2 × 4) millimeter by electrospinning [34]. Hydrophobicity and tensile stress were significantly higher in PLA-PCL (75:25), whereas tensile strain and fiber density were significantly higher in PLA-PCL (25:75). Cell viability and proliferation were rationally influenced by the aligned nanofibers. Gene expression revealed the grafts' thromboresistivity, elasticity, and aided neovascularization. Thus, these scaffolds could be an ideal candidate for small-diameter blood vessel engineering.

A 24-week comparison of the performance of electrospun PCL grafts and ePTFE grafts (2 mm diameter) as rat abdominal aorta replacement grafts was performed by Pektok et al. [35]. The research team found that PCL grafts showed enhanced tissue regeneration characteristics compared to ePTFE grafts. Faster endothelialization and extracellular matrix (ECM) formation in tandem with degradation of the PCL graft fibers were attributed as the major advantages of using PCL as a vascular graft material. Walpoth's group [5] implanted electrospun PCL vascular grafts into rat abdominal aorta. Results showed no aneurysmal dilation, perfect patency, excellent structural integrity, and limited intimal hyperplasia throughout the study. Endothelialization, cell invasion, and neovascularization of the graft wall rapidly increased until 6 months. However, from 6 to 18 months, regression of cell number and capillary density and severe calcification were observed within the graft wall. The calcification was suggested to be linked to hypoxia, oxidative stress, and provocation of inflammation, due to the grafts' dense fibrous structure or the local low compliance.

Given that prolonged presence of synthetic polymer implants *in vivo* may provoke chronic inflammatory responses from macrophages, leading to increased risk of calcification in long-term implantation, various approaches have been employed to adapt the properties of PCL grafts to alleviate persistent inflammation at graft sites. Kong's group [6] fabricated macroporous electrospun PCL grafts with thicker fibers (5–6 μm) and larger pores (~30 μm). They demonstrated that thicker fiber electrospun PCL vascular grafts enhanced vascular regeneration and the remodeling process by mediating macrophage polarization into the "proregenerative" M2 phenotype, whereas the porosity facilitated enhanced cellular infiltration. Gao et al. sought to accelerate graft degradation rates by blending PCL with the fast degrading

synthetic polymer, poly(lactic-*co*-glycolic acid) (PLGA). Electrospun PCL/PLGA (60:40) scaffolds demonstrated more cellular infiltration after 4 weeks of subcutaneous implantation, owing to enhanced degradation of the PLGA component by hydrolysis [36]. Agarwal et al. constructed grafts with core fibers sealed by PCL/poly-L-lactic acid (PLLA), demonstrating that *in vitro* degradation was accelerated by blending PCL/PLLA, compared to PCL. Similarly, *in vivo* implantation in murine inferior vena cava replacement models showed higher degradation occurred in scaffolds containing PCL/PLLA blends [37]. Rafique et al. employed an alternative approach to mitigate prolonged inflammation. They incorporated dimethyloxalylglycine (DMOG), a competitive inhibitor of hypoxia-inducible factor (HIF)-hydroxylated prolyl hydroxylase, into electrospun PCL vascular grafts. DMOG-loaded PCL grafts were implanted in rat abdominal aorta replacement models for 1 month. The grafts remained patent and supported improved functional vascular regeneration, endothelialization, VSMC layer regeneration, and anti-inflammatory responses, compared to unloaded PCL grafts [38].

11.2.1.3 PLCL

Poly(L-lactide-*co*-ε-caprolactone) (PLCL) copolymers have been applied as a biomaterial for the construction of vascular grafts due to the high elastic properties and relatively long-term implantation duration. Kurobe et al. [39] have shown that the PLCL coating completely degrades 4 months after implantation in a mouse model. In previous reports, PLCL vascular grafts were fabricated by an extrusion-particulate leaching technique, but there were a few problems for extruded PLCL grafts in cell seeding efficiency, cell ingrowth, and mechanical strength. Sang-Heon et al. [40] fabricated and characterized a new tubular, macroporous, fibrous PLCL (5:5) graft using gel spinning. Compared to extruded PLCL scaffolds, the fibrous PLCL scaffold showed improved biological activities, such as cell seeding efficiency and proliferation, and improved mechanical properties, such as tensile strength and viscoelastic properties. Shafiq et al. [41] fabricated scaffolds by mixing appropriate proportions of linear PLCL and substance P (SP)-immobilized PLCL, using electrospinning to develop vascular grafts. PLCL-SP showed significantly higher host cell infiltration, blood vessel formation, and mesenchymal stem cells (MSCs) recruitment *in vivo*. Mun et al. [42] seeded VSMCs onto electrospun PLCL scaffolds to construct a three-dimensional network. The vascular grafts constructed using cell–matrix engineering were similar to the native vessels in their mechanical properties, such as tensile strength, tensile strain, and elastic-modulus.

Adjustments to graft degradation rates can serve as a suitable strategy to rate-match degradation to new tissue formation. Fukunishi et al. evaluated PLCL blended with polydioxanone (PDO) to form composite vascular grafts with improved performances [43]. Fast and slow degrading vascular grafts were prepared by varying the ratio of PDO:PLCL. A 9:1 ratio showed the fastest degradation, and a 1:1 ratio showed the slowest degradation rate. Following *in vivo* implantation in rat abdominal aorta, the fast-degrading grafts produced more ECM crosslinking enzymes,

including tissue transglutaminase (TG2) and lysly oxidase (LOX), and resulted in a well-organized ECM with mechanical properties similar to native artery. This study highlighted the importance of achieving rates of polymer degradability that can support the timely formation of new ECM and vascular tissue, while providing mechanical and functional support until the neoartery forms and can takeover mechanical and functional roles.

11.2.1.4 PGA

The poly(glycolic acid) (PGA) is a highly biocompatible and bioresorbable polyester that demonstrates rapid biodegradability. Therefore, PGA is often used in vascular grafts to provide elevated and/or partial degradability. Cho et al. [44] fabricated a hybrid biodegradable polymer scaffold from PLCL copolymer reinforced with PGA fibers. The PGA/PLCL vascular patches were seeded with ECs and VSMCs differentiated from bone marrow stromal cells (BMSCs) and implanted in the inferior vena cava (IVC) of bone marrow donor dogs. Compared with PLCL scaffolds, PGA/PLCL scaffolds exhibited tensile mechanical properties more similar to those of dog inferior vena cava. Eight weeks after implantation, the vascular patches remained patent with no sign of thrombosis, stenosis, or dilatation. Rapoport et al. [45] utilized electrospinning technique to form tubular scaffold composites with structural features reminiscent of the corrugated laminae seen in blood vessels. This tubular scaffold was fabricated with complex "J"-shaped behavior using elastic polyurethane (PU) and reinforcing PGA woven mesh. The mechanical behavior of this tubular scaffold achieved from a low-stiffness highly elastic zone giving rise to a high-stiffness zone, and the value of burst pressures and toughness was 3095 ± 1016 mmHg and 6.3 ± 1.9 MJ/m^3, respectively. Another study incorporated a polyethylene terephthalate (PET) fiber core layer with a PGA fiber layer sheath to achieve grafts with partial degradability. After implantation, the PGA component rapidly degraded and was replaced by host tissue containing a mixture of α-smooth muscle actin $(\alpha\text{-SMA})^+$ cells and other host cells. The grafts showed unified structure with the adjoined aortic tissues. The adhesion strength between the graft and aortic wall was significantly enhanced in the grafts that used PET/PGA layers, and there was demonstratable histologic and mechanical integration with the surrounding native aortic tissues [46]. Fukunishi et al. described the *in vitro* and *in vivo* degradation of nanofibrous PGA/PLCL vascular grafts. *In vitro* evaluation showed that PGA/PLCL vascular grafts were degraded completely after 12 weeks and lost 100% of their strength. Long-term (6-months) *in vivo* evaluation in rat and sheep models of vascular transplantation showed that the grafts were fully degraded and remodeled into neoarteries in the sheep model, but were still present in the rat model, which indicated that *in vivo* degradation rates of vascular grafts should be more widely assessed in larger animal models to better predict degradation behavior in preclinical studies [47].

The Niklason lab utilized the relatively fast biodegradability of PGA scaffolds to generate bioreactor-grown tissue engineered vascular grafts and evaluated their

performance as arteriovenous access point for hemodialysis in baboon models, and as coronary artery bypass grafts in canine models. The grafts were seeded with human or canine vascular cells and incubated in a bioreactor that delivered cyclic radial strain to allow the production and deposition of a collagenous ECM. The grafts were subsequently decellularized, revealing ECM grafts free from PGA that were then used for *in vivo* implantation. In the animal models, the grafts remained patent without any dilatation, calcification, or intimal hyperplasia. This approach demonstrated that allogeneic cell sources can be effectively used with PGA scaffolds to produce readily available or "off-the-shelf" tissue engineered vascular grafts [48].

11.2.1.5 PGS

Polycondensation of glycerol and sebacic acid forms the elastomeric poly(glycerol sebacate) (PGS). PGS shows appreciable mechanical properties and biocompatibility and degrades within 2 months *in vivo* [49]. Ye et al. [50] described that PGS elastomer was used to construct the microvessel framework. *In vivo* studies of scaffolds implanted subcutaneously and intraperitoneally, without or with exogenous cells, into nude rats demonstrated biodegradation of the membrane interface and host blood cell infiltration of the microvessels. This modular, implantable scaffold could serve as a basis for building tissue constructs of increasing scale and clinical relevance.

In vitro hemocompatibility evaluation of PGS-based biphasic scaffolds were shown to be nonthrombogenic compared to other synthetic grafts [51]. Single-layered three-dimensional microfluidic PGS scaffolds also achieved biomimetic fluid properties [52]. Wang's group investigated the effect of pore size in PGS porous scaffold on VSMCs organization. They found that pores of 25–32 μm increased VSMCs alignment, elastin, and collagen production [53]. A shortcoming of PGS is its low mechanical strength, thereby increasing the risk of graft rupture or deformation. Thus, Wang's group fabricated a PGS porous tube with an average pore size of 21.2 ± 0.79 μm enveloped by a dense nonwoven PCL fiber sheath to provide enhanced mechanical and structural stability to meet the demands of arterial blood pressure [54]. After implanting the cell-free biodegradable PGS/PCL elastomeric grafts into rat abdominal aorta, they found that the PGS graft cores degraded rapidly to yield neoarteries free of foreign materials at 3 months postimplantation in rat models. Based on this success, Khosravi et al. [55] developed a novel method for electrospinning smaller grafts composed of a PGS microfibrous core enveloped by a thin PCL outer sheath. Electrospun PGS-PCL composites were implanted as infrarenal aortic interposition grafts in mice and remained patent up to the 12-month endpoint without rupture, thrombosis, or stenosis.

Further work by the Wu lab prepared PGS/PCL composite grafts by varying the time of electrospinning of the PCL nanofiber sheath wrapped around the PGS fiber core. Increasing density of PCL nanofibers was shown to be beneficial for enhancing the mechanical strength of the vascular graft. After 3–12 months of *in vivo* implantation in rat abdominal aorta, PCL reinforced PGS grafts were found to be superior in

patency rate, wall thickness, endothelial and smooth muscle cell remodeling, elevated ECM remodeling of collagen, elastin and glycosaminoglycans and enhanced mechanical characteristics including tough and complaint mechanics. The fast degradation of PGS led to timely neoartery formation while PCL ensured maintained mechanical strength [56].

11.2.2 Natural Polymers

11.2.2.1 Collagen

Collagen is a major structural component of ECM essential for mechanical integrity and is found in the majority of tissues. Collagen gels have long been used as tubular scaffolds for vascular graft engineering [57, 58]. Wu et al. [59] cocultured ECs and VSMCs onto collagen membranes, resulting in TEVGs that possessed sufficient tensile strength, favorable biocompatibility, and promoted vascular regeneration. Collagen-based scaffolds have been a choice platform for exploratory clinical trials for the repair of substantial tissue damage. Hirai et al. [60] developed collagen-based constructs for use in low-pressure-loaded venous systems. A solution of type-I collagen containing a suspension of bovine aortic VSMCs was poured into a tubular glass mold with a Dacron mesh support. After 24 weeks of *in vitro* culture, the resultant vascular constructs could tolerate luminal pressures up to 100 mmHg [61]. Kumar et al. [62] fabricated tubular conduits comprising collagen fiber networks and elastin-like protein polymers to mimic native tissue structure and function. These conduits compared favorably to the ultimate tensile strength (UTS) and a Young's modulus of native blood vessels (1.4–11.1 MPa and 1.5 ± 0.3 MPa, respectively). The dense fibrillar collagen networks exhibited an UTS of 0.71 ± 0.06 MPa, strain to failure of 37.1 ± 2.2%, and Young's modulus of 2.09 ± 0.42 MPa.

11.2.2.2 Elastin

The elastin protein provides flexibility and elasticity to tissues and organs. Elastin is found in abundance within artery walls, facilitating high strain and efficient elastic energy storage, which ensures pulsatile blood flow for tissue perfusion. Elastin scaffolds are typically brittle and exhibit lower mechanical parameters than native elastin-rich tissues. Elastin scaffolds have less stress relaxation than intact or decellularized aorta, which has stress relaxation rates that are linearly dependent on initial stress levels. The rate of stress relaxation for elastin increases linearly at stress levels below ~60 kPa [63]. Therefore, scaffolds that combine elastin with other macromolecules can maintain elasticity while improving mechanical strength. Buijtenhuijs et al. [64] lyophilized insoluble type-I collagen and elastin to produce porous scaffolds comprised of interspersed collagen and elastin fibers, which

improved mechanical performance. Smith et al. [65] fabricated cross-linked suture-reinforced polydioxanone (PDO)-elastin tubes that exhibited compliance matching native arteries. Tropoelastin (TE) is the soluble polypeptide precursor of elastin. Thus, TE can be more readily fabricated into scaffolds using techniques that can enhance scaffold performance. McKenna et al. [66] fabricated a tubular construct using electrospun recombinant human TE (rhTE). The fabricated scaffolds had elastic moduli in the range of 0.15–0.91 MPa and ultimate tensile strengths of approximately 0.36 MPa. The results of *in vitro* studies demonstrated that the fabricated electrospun rhTE scaffolds supported the growth of an EC monolayer with typical cobblestone morphology after 48 h culture time.

11.2.2.3 Fibrin

Fibrin is the product of fibrinogen cleavage and is an insoluble protein with prominent roles in the blood clotting cascade. In 2000, Ye et al. [67] prepared 3D fibrin gel matrices for cardiovascular tissue engineering and reported uniform cell growth and collagen deposition into the gel. Syedain et al. [68] fabricated TEVGs based on entrapment of human dermal fibroblasts in fibrin gel. The vascular grafts possessed circumferential fiber alignment characteristic of native arteries, which was essential for graft mechanical performance. The same team confirmed that hypoxia coupled with insulin supplementation improved collagen deposition and strength of fibrin-based TEVGs [69]. Elsayed et al. [70] devised the fabrication of novel, electrospun, multilayer, gelatin fiber scaffolds, with controlled fiber layer orientation and optimized gelatin cross-linking to achieve not only compliance equivalent to that of coronary artery but also for the first time strength of the wet tubular acellular scaffold (swollen with absorbed water) same as that of the tunica media of coronary artery in both circumferential and axial directions. Most importantly, the suture retention strength of gelatin scaffolds firstly achieved in the range of 1.8–1.94 N for wet acellular scaffolds and was same or better than that for fresh saphenous vein.

11.2.2.4 Hyaluronic Acid

Hyaluronic acid (HA) is a nonsulfated glycosaminoglycan (GAG) comprised of linear, unbranching, polyanionic disaccharide units of D-glucuronic acid and N-acetyl-D-glucosamine. Zhu et al. [71] demonstrated that collagen/HA scaffolds with interconnected porous networks provided appropriate mechanical properties and biocompatibility for use as an intimal layer scaffold for endothelialization. Joo et al. [72] reported that bioactive HA could be chemically modified into HA-catechol using a single-step method, which benefited *in vitro* endothelialization. Esterified HA (HYAFF) is routinely used for clinical tissue engineering applications. The problems associated with HA-based biopolymers are related to poor mechanical properties and rapid degradation rates. In efforts to increase mechanical properties of HA biomaterials, Arrigoni et al. [73] added sodium ascorbate (SA) to VSMC

cultures seeded in HYAFF nonwoven sheets. The SA facilitated the cross linking of VSMC-synthesized ECM with the HYAFF sheets, and when reformed into vascular grafts, provided improved mechanical properties, lower stiffness, and increased tensile strength.

Emerging data continue to reveal differential physiological and pathological functions attributable to different molecular weight (MW) HA [74]. Qin et al. explored whether low MW (LMW) or high MW (HMW) HA was beneficial in vascular remodeling of biomimetic vascular grafts [75]. The team prepared electrospun vascular grafts from native artery ECM with biodegradable polyesters such as PLCL and PCL, in combination with either HMW or LMW HA. Incorporation of LMW (15–40 kDa) HA into electrospun vascular grafts enhanced endothelialization and migration of vascular stem/progenitor cells into the graft. At the same time, VSMCs demonstrated enhanced migration and subsequent elastin-enriched neoartery tissue formation after 6 months of implantation time. The beneficial VSMC responses were dependent on HA interactions with its principal cell-surface receptor CD44, which is a receptor known to govern a diverse array of cellular functions and growth mechanisms [76].

11.2.2.5 Chitosan

Chitosan is the deacetylated product of the natural structural polysaccharide chitin, which is the main component of fungal cell walls, insect exoskeletons, and crustacean carapaces. Chitosan is biodegradable, biocompatible, and bacteriostatic, among other attributed functions; and is widely used in the food, textile, agriculture, environmental protection, cosmetic, and biomedical industries. Chupa et al. [77] demonstrated that porous chitosan scaffolds could be generated by freezing and lyophilization. Ling et al. [78] employed a freeze-dried mesh of knitted chitosan fibers coated in a chitosan/gelatin. A next generation version of the scaffold possessed hydrophilic swelling, a burst strength of almost 4000 mmHg, and high suture retention strength [79], suggesting suitability for vascular graft fabrication.

11.2.2.6 Silk Fibroin

Silk fibers are obtained from various invertebrates such as insects and spiders. The *Bombyx mori* silkworm larvae are a major source of silk used in biomedical applications, such as implantable devices, retinal replacements, sutures, ligatures, and skin repair materials, among others. Silk fibers are composed of structural silk fibroin (SF) core filaments surrounded by a layer of sericin β-sheet crystals. SF is extracted from silk by a process known as degumming, wherein the sticky hydrophilic sericin layers are removed [80]. SF possesses several advantages including *in vivo* proteolytic degradation, biocompatibility, and elevated cellular affinity. Double-raschel SF vascular grafts containing SF sponge were evaluated in animal models of arterial replacements, wherein an 85% patency rate was demonstrated in

rat abdominal aorta replacement models after 1 year of implantation. An early infiltration of ECs and VSMCs into the SF grafts promoted rapid endothelialization and vascular media regeneration, respectively [81]. Kiritani et al. used SF-based venous vascular grafts as replacements for rat inferior vena cava. The performance of SF grafts was compared to ePTFE implants, and after 4 weeks of implantation, SF grafts exhibited patency with superior endothelialization and collagen fiber remodeling compared to ePTFE grafts [82].

11.2.2.7 Extracellular Matrix-Based Vascular Grafts

The extracellular matrix (ECM) is a 3D network of extracellular polymeric macromolecules, such as collagen, elastin, fibrin, and HA, among others, which provide structural and biochemical support to cells. Thus, ECM-based scaffolds can provide a biologically active substrate on which cells can adhere, migrate, and infiltrate. It is increasingly recognized that biomimetic, natural polymers mimicking the ECM have low thrombogenicity and functional motifs that regulate cell–matrix interactions, with these factors being critical for TEVGs, especially small-diameter grafts. Popularized methods for generating acellular ECM-based vascular grafts include: the *ex vivo* decellularization of vascular or elastic tissues [83]; *in vitro* seeding of vascular cells onto polymer scaffolds, culture, and subsequent decellularization [48]; *in vivo* implantation of polymer scaffolds, and subsequent explant and decellularization [84]; and the incorporation of powdered ECM into vascular graft fabrication techniques [85].

11.2.3 Synthetic-Natural Polymer Hybrid Grafts

Synthetic-natural hybrid materials aim to recapitulate the bioactivity provided by natural polymers, while benefiting from the mechanical advantages borne from synthetic polymers. Over recent years, there has been an evident trend in the published literature suggesting a preference for synthetic-natural hybrid vascular graft fabrication and their evaluation in preclinical studies.

11.2.3.1 Synthetic Polymer Sheath-Reinforced Grafts

Synthetic polymers can be used as supporting sheaths or stents to symmetrically reinforce living and decellularized vascular tissues, preventing collapse when used for vascular grafting. Jeremy et al. studied the effect of external synthetic stents and sheaths in pig models of vein-into-artery interposition grafting and showed a profound effect on vein graft remodeling and thickening [86]. These outcomes appear to be mediated by the promotion of angiogenesis due to the accumulation of proangiogenic factors, inflammatory cells, ECs, and VSMCs in the space between

the graft and sheath/stent. Decellularization of allogeneic vascular grafts may damage the ECM and impair the associated biomechanics (e.g., accelerate elastin deformation and degradation), and may result in vascular graft overexpansion and aneurysm formation. To address these problems, Gong et al. combined PCL nanofiber sheaths with decellularized small-diameter vessels, forming hybrid tissue-engineered vascular grafts (HTEVs) [87]. The luminal surfaces of HTEVs were coated with heparin before allograft transplantation. The electrospun PCL nanofiber sheaths significantly enhanced the biomechanics of decellularized vessels, facilitating patency and preventing vasodilation or aneurysm over the 6 weeks implantation time in rat models. Hemodynamic factors play major roles in intimal hyperplasia development and subsequent bypass failure. Longchamp et al. developed *ex vivo* models for the perfusion of human saphenous vein segments under arterial shear stress [88]. The data showed that the incorporation of external supporting scaffolds decreased dilatation and intimal hyperplasia while maintaining vein media layer integrity, via increases in shear stress and decreases in wall tension and VSMC apoptosis. At the molecular level, external meshes prevented the upregulation of matrix metalloproteinases (MMP-2, MMP-9) and plasminogen activator type I (PAI-1), which participate in the degradation and remodeling of ECM. Yang et al. fabricated a rapamycin-loaded HTEVs by using decellularized rat aorta as supported by an outer sheath of electrospun rapamycin-loaded PCL [89]. After 12 weeks of implantation time in rat abdominal aorta replacement models, the grafts exhibited improved mechanical properties and prolonged bioactivity, compared to decellularized rat aorta alone. The grafts remained functional for up to 8 weeks and intimal hyperplasia was reduced across the 12 weeks implantation time, compared to HTEV without rapamycin.

11.2.3.2 Synthetic-Natural Polymer Blends and Layered Grafts

Gelatin and Collagen Blends and Layers

Combination of synthetic and natural polymers at the fabrication stage can result in hybrid vascular grafts that outperform grafts consisting of singular polymer materials. Shi et al. prepared hybrid grafts containing PCL and gelatin. Bioinert PCL benefitted from the addition of gelatin owing to its bioactivity and biocompatibility. The lumens were heparinized to reduce the incidence of thrombosis. These hybrid grafts efficiently promoted endothelialization and VSMC layer regeneration *in vivo* [90]. In a very recent study, Ma et al. evaluated heparinized PCL/collagen hybrid vascular grafts. The grafts were biocompatible, possessed biomechanics similar to natural artery, and promoted cell proliferation of ECs to enhance timely vascular tissue regeneration [91]. Ju et al. coelectrospun PCL/collagen bilayer scaffolds with a high porosity outer layer and lower porosity inner layer [92]. The outer layer enhanced VSMC infiltration and the inner layer facilitated EC attachment. The microstructure and mechanical properties of the PCL/collagen grafts were controlled by adjusting fiber diameter. Stitzel et al. discovered that controlling the ratio of

collagen, elastin, and PLGA improved the electrospinning process and overall physical strength of the scaffolds, which were capable of resisting rupture at approximately 12-fold normal systolic pressure [93]. Kobayashi et al. produced composite nanofiber vascular grafts composed of PGA/collagen, which could accomplish the recruitment of host cells and timely cellular infiltration without incorporation of other bio-derived matter-like growth factors [94]. Recently, the Wu group fabricated PGS core and PCL/collagen sheath small-diameter vascular grafts by coelectrospinning [95]. The grafts were coloaded with rapamycin and 3-methyladenine (3-MA) and demonstrated sustained release to regulate macrophage autophagy, which in-turn polarized macrophages to M2-like phenotypes, promoted endothelialization, and drove the myogenic differentiation of vascular progenitor cells within the graft walls.

Fibrin Blends

Fibrin alone has poor mechanical strength. Therefore, a combination of mechanically strong materials with fibrin can offer improved outcomes. Yang et al. prepared electrospun vascular grafts by blending varying ratios of PU:fibrin (0:100, 5:95, 15:85, 25:75) [96]. The 15:85 blend demonstrated superior resistance to thrombosis and possessed appropriate mechanical properties. The hydrophilicity of fibrin elevated cell proliferation and adhesion *in vitro*, which ultimately translated to augmented vascular regeneration and remodeling *in vivo*, after 3 months of implantation.

Chitosan Blends and Layers

The poor mechanical properties of chitosan are a limitation that can be mitigated by its combination with synthetic polymers. Equivalent blends of chitosan and PCL demonstrate an ultimate strength two-fold that of chitosan alone [97]. Chen et al. [98] fabricated electrospun chitosan/poly(L-lactide-*co*-ε-caprolactone) (PLLA-CL) nanofibrous scaffolds that functionally and structurally resembled native ECM. The mechanical properties of the scaffolds were further improved (two-fold) by cross-linking of the randomly orientated fibers. Nanofibrous chitosan/PCL vascular grafts were fabricated by sequential coelectrospinning [99], before further modification with heparin and immobilization of vascular endothelial growth factor (VEGF) to form VEGF-gradient scaffold layers. The resultant grafts successfully prevented thrombosis and promoted neoartery formation. Similarly, Yin et al. fabricated bilayered PLCL and polyethylene glycosylated (PEGylated)-chitosan [100]. A blend of 1:6 PEGylated-chitosan to PLCL was cast on a metal rod by drip feeding and PLCL and water soluble PEG was electrospun to form the outer layer. The composite grafts demonstrated the excellent hemocompatibility, structural integrity, blood vessel formation, EC, and VSMC layer regeneration in canine femoral artery replacement models. An elevated expression of angiogenesis related genes and negligible calcification were observed 24 weeks postimplantation.

Silk Fibroin Blends and Layers

Recently, Caldiroli et al. prepared three-layered hybrid SF/PU vascular grafts by sequential electrospinning stages [101]. The hybrid graft contained a PU middle layer, with SF inner and outer layers. The SF/PU hybrid grafts implanted in rat abdominal aorta replacement and femoral shunt models, wherein they maintained patent blood flow after 3 months of implantation time. Kuang et al. fabricated composite vascular grafts based on PLCL core and heparin/SF shell nanofibers by using electrospinning and freeze-drying [102]. The grafts could maintain long-term patency for up to 8 months implantation time in rabbit carotid artery replacement models.

11.2.3.3 Synthetic Polymer-Reinforced Biotubes

Alternatively, synthetic polymers can be used to fabricate scaffolds upon which cells or tissue can grow and integrate with the scaffold, depositing ECM between the synthetic polymer fibers, therein producing polymer-reinforced neotissue, or "biotubes" when scaffolds have cylindrical or tubular structures [103]. The biocompatibility and relatively low immunogenicity of PCL lends to the diversity of strategies that can be employed to develop vascular grafts with enhanced tissue regeneration and long-term performance. In a more recent innovative study, Zhi et al. used an *in vivo* bioengineering strategy to develop PCL reinforced biotubes (PBs) by implanting melt spun PCL based fibrous skeletons (PS) into the dorsal subcutaneous tissue [104]. After 1 month of subcutaneous implantation, PS were enriched with autologous extracellular matrix (ECM) and infiltrated host cells. The resultant PBs were evaluated as rat abdominal aorta replacements, canine carotid arterial replacements, and as ovine arteriovenous grafts for hemodialysis access. The developed PBs demonstrated superior mechanical characteristics, attenuation of intimal hyperplasia, rapid hemostasis, repeated needle puncture tolerance, long-term patency and vascular regeneration in all three of the evaluated animal models.

11.3 Fabrication of Polymeric Vascular Graft Scaffolds

To date, numerous techniques have been employed to fabricate vascular grafts from synthetic and natural polymer materials. Each of these methods has its own unique advantages and disadvantages. The microstructures of the vascular grafts formed by these methods have a large influence on their regenerative and remodeling capacity. An important factor in vascular grafts is pore size. If pores are too small, it will hinder cell infiltration, but if pores are too large, problems such as blood leakage can occur. Current studies tend to fabricate vascular grafts using combination of two or more approaches. The following are some typical techniques usually applied in fabrication of polymer-based vascular grafts.

11.3.1 Electrospinning

Electrospinning is one of the most commonly employed techniques to fabricate vascular grafts. It is a simple and effective way to produce fibers ranging from 50 nm to 10 μm. The electrospinning apparatus consists of a syringe pump, a high-voltage power supply, a grounded iron rod, and a spinneret. Fibers are spun onto a collecting platform (typically a cylinder or mandrel), and fiber properties can be modified by regulating parameters such as rod rotating speed, voltage, flow velocity, and solution concentration. As discussed in greater detail above, a number of synthetic and natural polymers have been explored for the fabrication of nanofibers [105]. The Walpoth group have extensively studied electrospinning and PCL vascular graft fabrication for long-term implantation models. Electrospun PCL grafts showed excellent structural integrity and patency over 18 months of implantation time in rat models, with no aneurysmal dilation or thrombosis, and minimal intimal hyperplasia. However, calcification and a cellular regression were observed at 12 months postimplantation [5]. To prevent blood leakage but retain cell infiltrability, bilayered grafts have been prepared by electrospinning a high-porosity internal layer with a low-porosity external layer. It was previously identified that implanted bilayered grafts were occupied by cells that migrated from the anastomosis sites rather than cells captured and recruited from the circulating blood [106, 107]. This phenomenon represents an important directive with significance for the fabrication of biodegradable vascular grafts. Limited cell infiltration into grafts hampers regeneration and remodeling. To circumvent this issue, macroporous electrospun PCL grafts with thicker fibers (5–6 μm) and larger pores (30 μm) were implanted in rat abdominal aorta replacement models. The macroporous grafts markedly improved cell infiltration, ECM secretion/deposition between the graft fibers, and functional regeneration. Analysis of the cellularization process revealed that the thicker-fiber scaffolds induced many M2 macrophages to infiltrate into the graft wall, which further promoted cellular infiltration and vascularization [6] (Fig. 11.2).

Regeneration of VSMCs with circumferential orientation within the grafts is crucial for functional vascular reconstruction *in vivo*. Thus, the Kong lab fabricated a bilayered vascular graft with a circumferentially aligned microfiber internal layer by wet spinning, and an external layer composed of random nanofibers was prepared by electrospinning. The internal circumferentially aligned microfibers provided topographic guidance for *in vivo* regeneration of VSMCs, and the external random nanofibers offered enhanced mechanical properties and prevented leakage and rupture after graft implantation. The results demonstrated that circumferentially oriented VSMCs and longitudinally-aligned ECs were present in the neoartery, which was capable of exhibiting contraction and relaxation properties in response to vasoactive agents [108] (Fig. 11.3).

Electrospinning has also been employed to generate sacrificial scaffolds that can later be used as substrates to grow cells or tissues, before removing the polymer template with polymer leaching methods to create patterned biologically derived scaffolds. Zhu et al. reported an example of this technique, wherein they fabricated

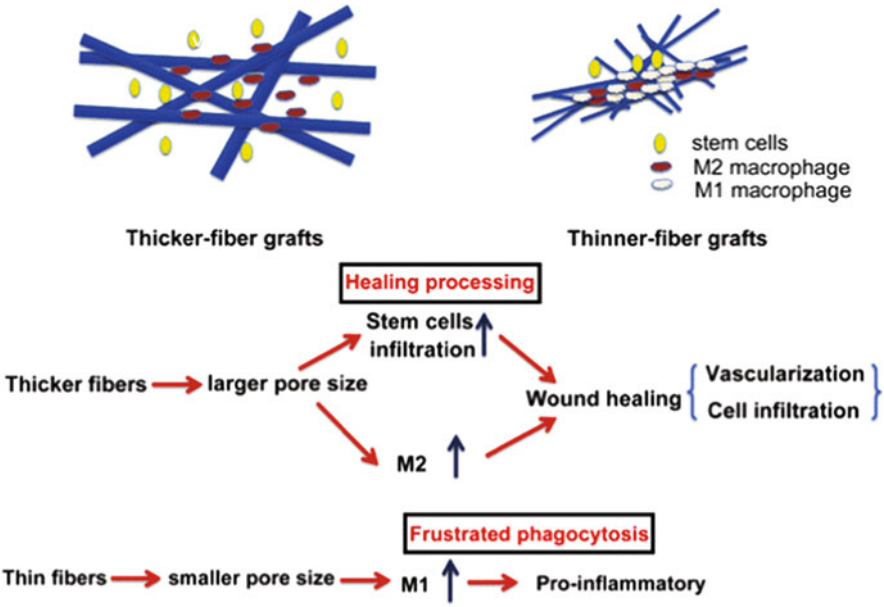

Fig. 11.2 Schematic illustrates that the pore size of electrospun PCL grafts may modulate the polarization of macrophages phenotype (Reprinted from Ref. [6] with permission, Copyright 2014 Elsevier Ltd.)

parallelly aligned PCL microfibers membranes by electrospinning. These membranes were implanted in the subcutaneous pouch of rats for 4 weeks. The interfiber spaces of explanted membranes were filled with infiltrated cells, which had secreted a collagenous ECM. The PCL template was then removed by leaching and the scaffold decellularized to yield ECM membrane scaffolds containing microchannels where the PCL fibers had previously occupied. The broad applicability of ECM microchannel scaffolds included rat abdominal artery replacement models, wherein it promoted cellularization, vascularization, and favorably modulated the inflammatory response. This approach was proposed to be suitable for developing "off-the-shelf" ECM based scaffolds for augmenting tissue regeneration and integration after *in vivo* implantation [84].

11.3.2 Melt Spinning

Melt spinning deposits thin fibers on the collecting mandrel by melting the polymer solution in the absence of electric field. The obtained fibers typically exhibit an aligned orientation with insignificant variation in fiber diameter. Parameters such as fiber angle and interfiber spacing can be stringently controlled. Therefore, fiber morphological parameters are more reproducible and predictable. In recent studies,

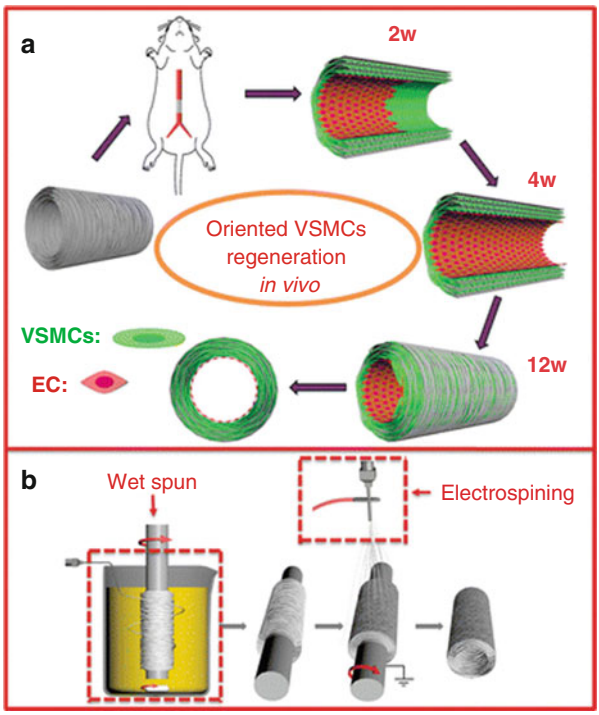

Fig. 11.3 (**a**) Schematic illustration shows the circumferentially aligned microfibers of the grafts which guide VSMCs' regeneration in circumferential orientation. (**b**) The bilayered grafts are prepared by wet spinning and electrospinning method (Reprinted from Ref. [108] with permission. Copyright 2015 Elsevier Ltd.)

melt spinning has been used to prepare core-shell fiber scaffolds with enhanced mechanical characteristics [109]. Zhi et al. employed melt spinning to produce PCL fiber skeletons (PS). The tight, consistent fiber angles allowed for heat treatment to create precision bonds between intersecting fibers. The prepared PS were implanted subcutaneously in the dorsum of rats and large animal models for subsequent enrichment with host cells and ECM components, thereby producing *in vivo* tissue engineered PS-reinforced biotubes (PBs). These PBs were evaluated in rat abdominal aorta, canine carotid artery and sheep arteriovenous graft (AVG) models wherein the heat-treated medium fiber angle biotubes (hMPBs) demonstrated suitable mechanical strength, patency, rapid hemostasis and vascular regeneration, without aneurysmal dilatation [104].

11.3.3 Mold Pouring

One of the earliest polymer-based grafts that entered clinical application was a hybrid biodegradable synthetic polymer vascular graft, fabricated by pouring a solution of PCL-PLA (50:50) copolymer onto PGA woven fabric sheets, followed by lyophilization [110]. Twenty-five patients received graft implants and no graft-related mortalities were reported. There was no evidence of aneurysm formation,

graft infection, graft rupture, or ectopic calcification [111, 112]. Since then, mold pouring has become a popularized method to obtain coated scaffolds with desirable shapes. Polymer solutions are casted in specifically shaped molds with or without supporting meshes or structures. Upon solidification of the polymer solution, the mold is removed to leave the shaped scaffold. It can be used to construct tubular vascular grafts as well as branching blood vessels. In the fabrication of vascular grafts, usually injection molding is applied, wherein polymer solution is initially poured into a device possessing an inner rod relevant to desired luminal. Injection molding also allows integration of pore-forming methodologies such as gas foaming, salt leaching and phase separation. Molding can be achieved using singular polymers, around inserted polymer mesh supports, molded with micropatterned surface topology, and using sacrificial polymers for the fabrication of mesochannels for ingrowth of vasculature [113].

11.3.4 3D Bioprinting

Gaining increasing attention in recent years, 3D-bioprinting technology has promising potential in multiple tissue engineering and regenerative medicine applications due to its extended applicability in bridging the divergence between artificial constructs and natural body tissues. The integration of biological and nanobiological sciences has further extended 3D-bioprinting applications to transplantation, drug screening, clinical treatment and toxicological research. There are three common methods of 3D bioprinting, including extrusion, material jetting, and vat polymerization. In the field of tissue engineering of native body tissues including bone, cartilage, skin tissue, heart, neural tissues, and vascular grafts, the role of 3D bioprinting is becoming indispensable. Cui et al. constructed microvessels by thermal ink-jet printing of human ECs and fibrin and observed rapid EC proliferation and microvasculature formation. In addition, vascular chips fabricated by using 3D-bioprinting technology have been successfully utilized for *in vitro* studies [114]. Duarte et al. engineered vascular chip platforms by using elastin bio-ink hydrogels extruded with human umbilical vein ECs, resulting in the formation of vascular networks that closely resembled native tissue [115]. Huang et al. fabricated triple layered vascular grafts using E-jet 3D printing in combination with electrospinning and electrospraying. The prepared grafts had an internal aligned fibrous layer, a middle electrospun dense fibrous layer, and an external layer composed of mixed fibers obtained by coelectrospraying. The grafts were implanted and exhibited suitable mechanical strength due to aligned inner layer fibers, which also offered a suitable substrate for EC proliferation, migration, and cell infiltration into the graft walls via the porous outer layer [116].

11.3.5 Particle Leaching

Particle leaching methods have been utilized in vascular graft fabrication to induce elevated porosity to scaffolds. Wang's lab developed bilayered vascular grafts composed of PGS layer fabricated by salt leaching method and PCL sheath generated by electrospinning which increased graft strength and prevented bleeding. Three months' postimplantation in rat abdominal aorta, the neoarteries resembled native arteries in several aspects: a confluent endothelium and contractile smooth muscle layers and regular, strong, and synchronous pulsation [54]. The long-term study showed that the neoarteries contained nerves and had the same amount of mature elastin as native arteries and responded to vasomotor agents, although with smaller magnitude than native aortas [117]. A study by the Wu lab confirmed that the thickness and density of PCL sheath in bilayered grafts could affect the vascular remodeling and regeneration [56]. Sugar spheres can also be used as porogen to produce highly interconnected vascular graft by several steps. Polymer solution was firstly cast into an assembled sugar template under a mild vacuum. The polymer-sugar composite was phase separated at low temperature overnight and then immersed into cyclohexane to exchange Tetrahydrofuran (THF). The consequential composites were freeze-dried, and the sugar spheres were leached out in distilled water and freeze-dried again. *In vivo* subcutaneous implantation studies indicated VSMCs differentiation and host tissue infiltration in the scaffolds [118]. A thin dense layer needed to prevent leakage of blood after this kind of macroporous vascular graft was implanted *in vivo*.

11.3.6 Phase Separation

Phase separation can generate macroporous scaffolds which can increase cell migration and cell seeding efficiency. Polymer dissolution is processed by liquid-liquid phase separation and polymer gelation to generate a nanofibrous sponge. Then the solvent is extracted, and the foam is freeze-dried. Many parameters such as gelation temperature, polymer concentration, solvent characteristics, and thermal treatment can affect scaffolds morphology, Young's modulus, and tensile strength. Ma's lab developed a porous vascular graft with biodegradable PLLA through thermally induced phase-separation (TIPS) techniques. The grafts with oriented gradient microtubular structures in the axial or radial direction can be produced by utilizing different thermal conductivities of the mold materials and using benzene as the solvent. The porosity, tubular size, and the orientational direction of the microtubules can be regulated by the TIPS temperature, the polymer concentration, and by utilizing materials of different thermal conductivities [119]. Bilayered vascular grafts of poly(ester urethane) urea (PEUU) were fabricated by electrospinning and TIPS and implanted *in vivo* after seeded with pericytes. Cell-seeded TEVGs showed extremely higher patency rate than the unseeded control. The remodeled vascular

grafts consisted of multiple layers of α-SMA$^+$ and calponin$^+$ cells and a von Willebrand factor (VWF)$^+$ EC monolayer on the lumen [120, 121]. Sugiura et al. developed a novel bioresorbable vascular graft with a porous PLCL sponge-type scaffold reinforced by PLA nanofibers, which was fabricated by phase-separation and electrospinning. The animal experiments showed promise for application as small-diameter arterial grafts [122].

11.3.7 Solution Blow Spinning

Akentjew et al. developed a new protocol for the construction of mechanically stable and biologically active nanofibrous vascular grafts that structurally mimicked human coronary artery ECM [123]. They employed dip spinning and solution blow spinning (SBS) technology to introduce suitably angled nanofibers with partial fiber waviness in graft scaffolds. To achieve it, initially the PCL fibers were deposited on a spinning rod by solution blow spinning in which the rod moved vertically by dip spinning system (Fig. 11.4). Then cell laden methacryloyl gelatin alginate (GEAL) sublayers were made by vertical dipping of fiber coated rod into GEAL solution followed by exposure to UV light. The developed small-diameter vascular grafts were mechanically and biologically stable owing to the spatial deposition of fibers in required angles and fibers arrangements and loading of BM-MSCs in the wall of graft. It proved that cell encapsulated GEAL sublayer reinforced with PCL fibers was an effective strategy for the development of small-diameter vascular grafts mimicking the mechanics of human coronary artery, which can regulate the long-term patency and remodeling in the *in vivo* settings.

11.4 Functional Modification of Vascular Grafts

11.4.1 Nitric Oxide-Releasing Materials

Nitric oxide (NO) is a critical regulator of vascular homeostasis and serves as an excellent candidate for improving the thromboresistance of cardiovascular biomaterials. NO is endogenously produced by nitric oxide synthases: endothelial (eNOS); inducible (iNOS); and neuronal (nNOS) isoforms [124]. A reduction in the generation and bioavailability of NO occurs in several disorders, including platelet activation, arterial thrombosis, and atherosclerosis [125]. It was reported that endothelial NO production is closely related to 5-year graft patency in patients receiving coronary artery bypass grafting [126]. Several studies have proven that the lower levels of NO produced by saphenous veins, compared to arterial conduits, may contribute to early graft failure [127, 128]. In this regard, molecular modification of blood-contacting devices with NO-generating compounds is one of the most direct and effective approaches to mimic the functions of the endothelium and thus reduce

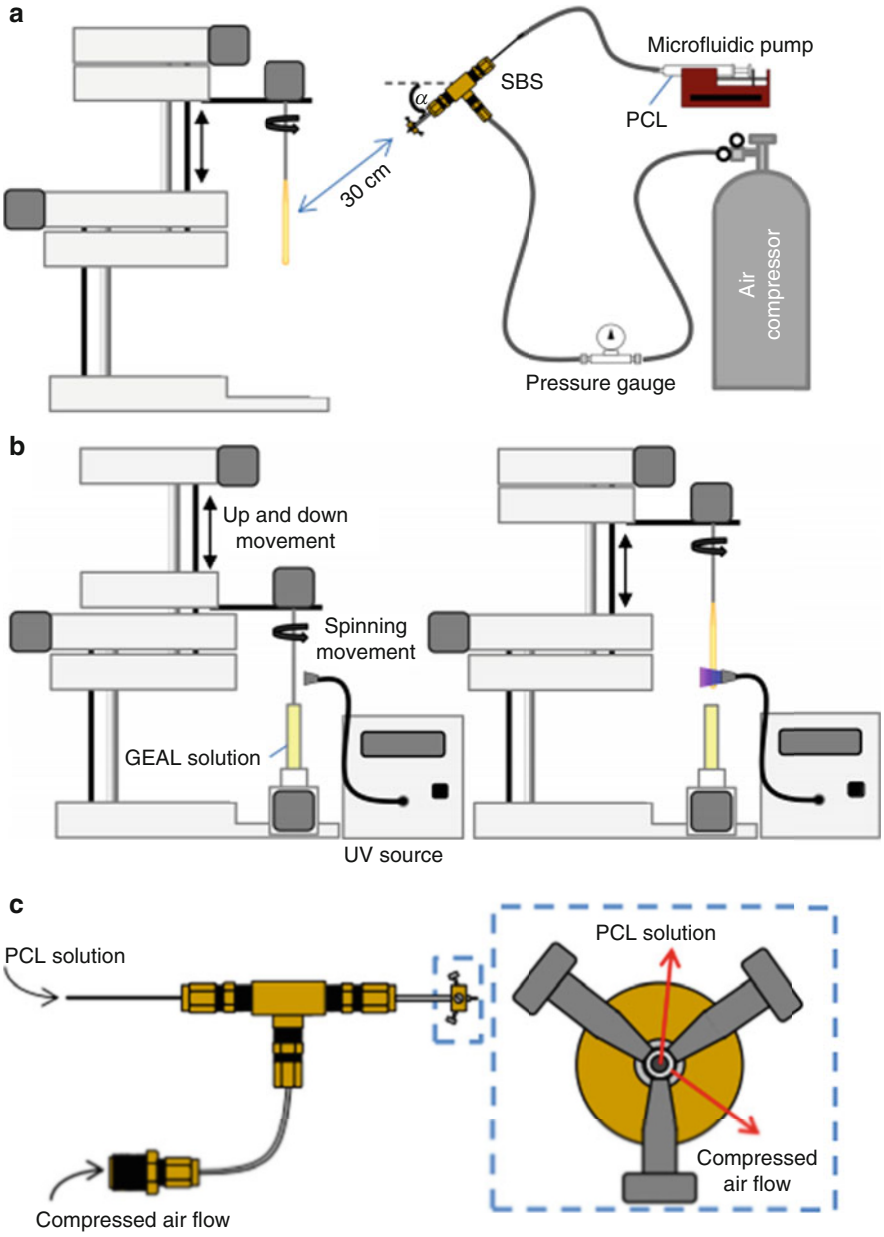

Fig. 11.4 (**a**) Schematic of angled solution blow spinning technique showing deposition of PCL fibers into a spinning rod to create a sublayer of PCL fibers. (**b**) Fabrication of GEAL sublayers through rotating retraction and exposure to ultraviolet (UV) radiation after vertical dipping of an oriented fiber-coated rod into GEAL solution. (**c**) Solution blow-spinning (SBS) equipment with a concentric outer nozzle for compressed air delivery and a central inner nozzle for the extrusion of PCL solution (right, end view) (Reprinted from Ref. [123] with permission. Copyright 2015 Elsevier Ltd.)

thrombogenicity. However, the short half-life of NO (<1 s in the presence of oxygen and hemoglobin) and its radial influence are limited to a few micrometers [129]. Several chemical strategies for NO-release and NO-generation have been developed to recapitulate the pharmacological potential of NO-releasing biomaterials [130, 22].

NO-releasing materials were first reported by Smith et al. in 1996 [131], wherein covalent attachment of NO donors directly to the ePTFE polymer backbone was utilized to functionalize bypass grafts and provided enhanced antithrombotic performance. Fleser et al. [132] implanted small-diameter (5 mm) PU vascular grafts coated with a polymer containing NO donors (dialkyl hexanediamine diazeniumdiolate) in sheep arteriovenous bridge-graft models for 21 days. Approximately 80% of the NO-eluting grafts remained patent, compared with only 50% of control grafts. Despite a lack of statistical significance in patency rate differences, the control grafts contained adherent thrombi and fibrin matrices containing inflammatory and red blood cells, whereas these were absent in NO-releasing grafts.

In recent years, emergent roles in the regulation of VSMC proliferation, migration, and differentiation have made NO attractive for incorporation into degradable tissue engineering vascular grafts. Enayati et al. designed vascular grafts that supported long-term *in situ* release of bioactive NO by blending PCL with S-nitroso-human-serum-albumin (S-NO-HSA), an NO donor with a prolonged half-life. PCL-S-NO-HSA supported rapid endothelialization, whereas VSMC proliferation was attenuated in the early phase [133]. The Zhao lab designed nitrate-functionalized vascular grafts based on a design concept that utilized blends of LMW nitrate-functionalized PCL polymers with HMW PCL. In rat abdominal aorta replacement models, transplant of PCL/NO small-diameter vascular grafts demonstrated therapeutic efficacy, including maintenance of vessel patency, and enhanced vascular regeneration, as characterized by earlier regeneration of endothelium and organized VSMC layer, compared to PCL small-diameter vascular grafts [20]. The same group went on to fabricate biohybrid vascular grafts by combining decellularized porcine veins and a nitrate-functionalized polymer sheath. The nitrate sheath provided sustained NO-release that mimicked native endothelium; thereby inhibiting intimal hyperplasia and vascular calcification in both rabbit and mouse models of right common carotid artery replacement. The underlying mechanism was revealed to involve a promotion of vascular stem/progenitor cell contribution to repopulation of vascular cell lineages and the subsequent enhancement of vascular regeneration and remodeling [21].

In addition to immobilization of NO donors on polymer matrix, there are many studies on modification of polymers by catalysts for promoting the transfer of NO from exogenous or endogenous NO donors in blood. Wang et al. [16] constructed a functional vascular graft by immobilization of β-galactosidase on vascular graft surface for catalyzing exogenous prodrug to release NO locally and sustainably (Fig. 11.5). The functional vascular grafts were implanted into the rat abdominal aorta with a 1-month monitoring period. The *in vivo* results showed effective inhibition of thrombus formation and enhancement of vascular tissue regeneration and remodeling of the grafts. However, nonspecific release of NO from these prodrugs was also evident because of the widespread distribution of endogenous

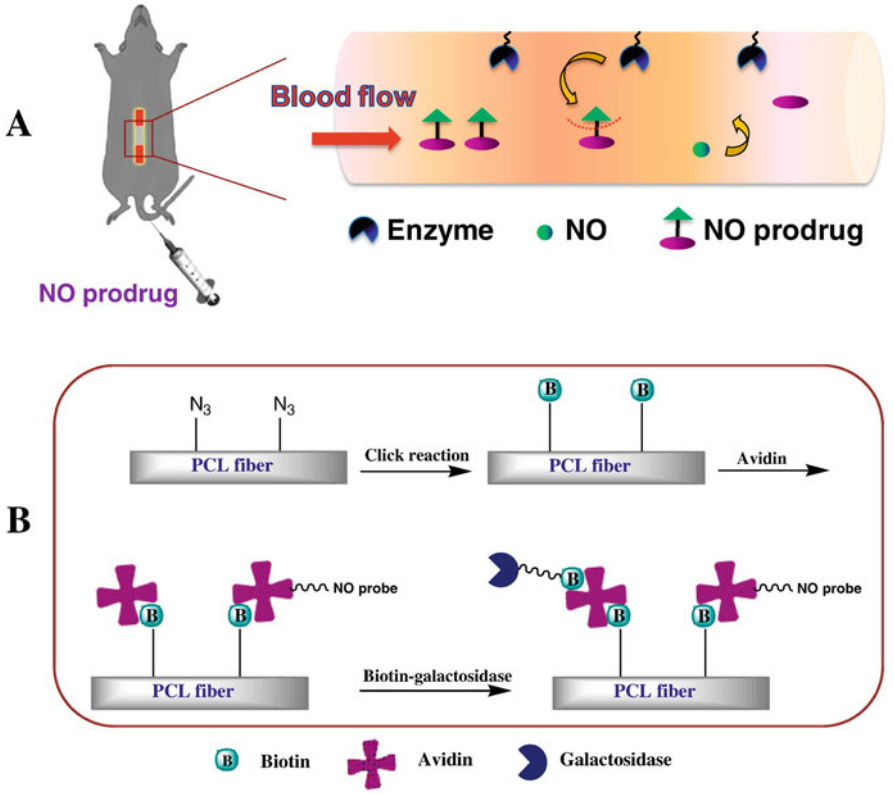

Fig. 11.5 Illustration for the enzyme immobilized on the vascular grafts to catalyze the decomposition of exogenously administrated NO prodrug to release NO. (**a**) Pathway for the surface enzyme functionalization of PCL vascular grafts (**b**) (Reprinted from Ref. [16] with permission. Copyright 2015 Elsevier B.V)

glycosidases in blood and specific tissues, which limits the therapeutic efficacy. Hou et al. reported a solution using a "bump-and-hole" strategy to modify an NO delivery system based on an enzyme-prodrug pair of galactosidase-Gal-NO [134]. Further studies are necessary to assess the use of engineered galactosidase-Gal-NO for NO delivery on blood-contacting devices.

The endogenous NO donors, S-nitrosothiols (RSNOs), are present in circulating blood and offer opportunities to generate localized synthesis of NO at a continuous rate. Glutathione peroxidases (GPx) and selinium or copper ions with GPx-like catalytic activity can catalyze the decomposition of RSNOs into NO *in vivo* [130]. The Huang and Yang labs have published a series of studies that used selenocystamine or copper ions incorporated onto cardiovascular stents [135–137]. The NO release rates could mimic the natural endothelium rate (0.5 to 4×10^{-10} mol $\times$ cm^{-2} $\times$ min^{-1}) by adjusting the dose of incorporated catalytic

substances. *In vivo* data showed that modified stents promoted re-endothelialization while reducing neointimal formation. Recently, the same group developed NO-eluting organoselenium/alginate hydrogel coatings for vascular stents. The NO hydrogels coatings tolerated balloon dilation during angioplasty, prevented thrombosis, inhibited intimal hyperplasia, and effectively promoted the rapid restoration of native endothelium [138].

The Niklason group demonstrated that local delivery of NO increased Fas receptor cell–surface expression and enhanced the potential VSMC-targeted apoptosis by Fas ligand (FasL) delivered to the same region. The group developed FasL-NO donor-releasing ethylene-vinyl acetate copolymer (EVAc)-coated stents. The stents were deployed into pig coronary arteries and cultured in a perfusion bioreactor for 1 week. The resultant FasL-NO donor-releasing EVAc-coated stents prevented the occurrence of intimal hyperplasia and in-stent restenosis, without harming endothelial restoration [139]. Kushwaha et al. [140] developed a nanofibrous matrix, which is formed by self-assembly of peptide amphiphiles (PAs), containing NO donating residues and Tyr-Ile-Gly-Ser-Arg (YIGSR) peptide sequence, a laminin-derived cell-adhesive peptide sequence. The NO-releasing nanofibrous matrix demonstrated a significantly enhanced proliferation of ECs but reduced VSMCs proliferation and platelet attachment. Andukuri et al. [141] reported a similar design in which electrospun PCL nanofibers were coated with NO-releasing PAs containing cell-adhesive ligands (YIGSR and KKKKK) by a solvent evaporation technique. The presence of YIGSR ligands and release of NO promoted the adhesion and proliferation of ECs while simultaneously limiting the adhesion and proliferation of VSMCs and the adhesion and activation of platelets. Yang et al. modified vascular stents with two vasoactive moieties (NO-generating organoselenium and endothelial progenitor cell-targeting peptide). These surface modified stents demonstrated superior inhibition of in-stent restenosis, thrombosis, and VSMC migration and proliferation, while promoting endothelial progenitor cell recruitment, adhesion, and proliferation [142].

11.4.2 Antibody and Peptide Modification

Surface modification of blood-contacting devices with antibodies, functional proteins or polypeptides has emerged as a popular strategy to maintain long-term homeostasis. Currently, research on antibody and polypeptide modification has two directions: improving hemocompatibility and enhancing endothelialization.

Multiple approaches have been developed to diminish coagulation while promoting endothelialization of ePTFE grafts. For example, Badv et al. developed ePFTE with endothelial cell specific anti-CD34 antibodies modified onto the luminal surface. This modification hindered nonspecific adhesion of proteins, bacteria, and blood cells while promoting EC adhesion [143, 144]. Lu et al. used anti-CD133 antibody to coat the ePTFE grafts [144]. After adsorption of polyethylenimine (PEI), dipped alternately in heparin solution and collagen solution, synthetic ePTFE grafts

coated with five bilayers of heparin/collagen were prepared. Then the multilayers were immersed in glutaraldehyde to promote cross-linking and to immobilize the anti-CD133 antibody. Finally, they implanted the graft into the carotid artery of pig. The results demonstrated that these synthetic ePTFE grafts coated with anti-CD133 antibody-functionalized heparin/collagen multilayer may achieve rapid endothelialization. Zhao's group developed a functional vascular graft by surface immobilization of stem cell antigen-1 (Sca-1) antibody on an electrospun PCL graft. Anti-Sca-1 antibody presentation significantly increased Sca-1^+ vascular stem/progenitor cell capture and retention in cell-free PCL scaffolds, which led to effective and enhanced vascular regeneration [145].

Various polypeptides have been developed to minimize thrombogenicity and to improve the hemocompatibility of vascular grafts. In a study by Xing et al. ePTFE vascular grafts were modified with polydopamine (PDA) coating to enhance surface hydrophilicity, bivalirudin (BVLD) to provide antithrombogenic functionality and REDV tetrapeptides, which facilitated specific binding and capture of α4β1 integrin-expressing ECs. The combination of these modifications resulted in improved patency and endothelialization of grafts after 12 weeks of implantation in porcine carotid artery replacement models [146].

C-type natriuretic peptides (CNPs) are endothelium-derived peptides shown to inhibit VSMC migration, constrictive remodeling, and thrombus formation after vascular injury [147]. Li et al. loaded CNPs into PCL grafts by electrospinning and confirmed improved hemocompatibility and vascular regeneration of artificial vascular grafts [148]. The Kong lab designed RGD (arginine-glycine-aspartic acid)-containing amphiphilic molecule (Nap-FFGRGD) that self-assembled into a functional coating on the surface of electrospun PCL fibers. Nap-FFGRGD coated PCL grafts provided a hydrophilic surface that exhibited prominent anticoagulation and enhanced cell adhesion *in vitro* [149], and enhanced *in vivo* patency rates and vascular regeneration after implantation in rabbit carotid arterial implantation models, compared to uncoated PCL grafts [150]. Hashi et al. conjugated the polypeptide hirudin, a derivative of *Hirudo medicinalis* leech saliva to PLLA vascular grafts through an intermediate PEG linker [49]. The PEG linker layer assisted in the reduction of platelet adhesion/aggregation, whereas immobilized hirudin suppressed thrombin activity, which led to improved graft patency rates. Mahara et al. modified ultrahigh hydrostatic pressure (UHP)-decellularized ostrich carotid arteries with a heterobifunctional peptide composed of a collagen-binding region $(Pro\text{-}Hyp\text{-}Gly)_n$, $(POG)_n$, and the REDV peptide. The modified graft was transplanted into minipig femoral arteries and was observed over the course of 20 days, without the administration of anticoagulant medication. Five grafts remained patent and no thrombogenesis could be observed on the luminal surface. In contrast, all unmodified grafts became occluded with severe thrombosis [151].

Cell-specific peptides can be identified by phage display technology, which allows the identification of specific ligands for a particular cell surface protein even without prior knowledge of the particular cell-surface molecules [152]. Using this technique, Veleva et al. identified TPSLEQRTVYAK (TPS), a peptide ligand specific to endothelial outgrowth cells [153]. Subsequently, several studies have

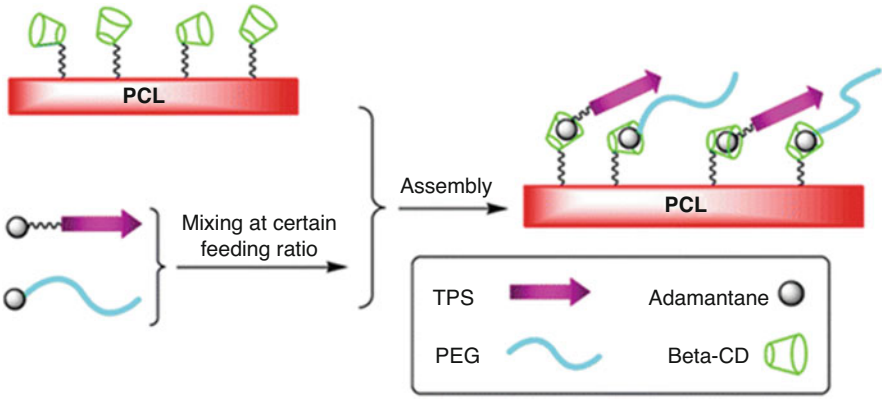

Fig. 11.6 Schematic illustration for the supramolecular assembly of functional molecules on the surface of PCL-CD film (Reprinted from Ref. [156] with permission. Copyright 2013 American Chemical Society)

attempted to incorporate TPS into biomaterials to capture endothelial progenitor cells in the blood. A fusion protein, TPS-linker-HGFI (TLH), which was composed of HGFI that originated from *Grifola frondosa* and functional peptide TPS, was expressed by *Pichia pastoris* expression system. PCL scaffolds were incubated overnight in a sterilized aqueous TLH solution, followed by blowing off the excess protein solution and drying in a super clean bench. Cell adhesion test showed that the TLH-modified PCL could specially enhance the adhesion of ECs and EPCs [154, 155]. This work presented a new perspective to apply hydrophobins in tissue engineering and regenerative medicine and provided an alternative approach in surface modification. However, one major challenge is to prevent nonspecific protein adsorption, which could mask the effects of TPS and hence require strategies such as passivation using PEG. Ji et al. developed a method for the dual functionalization of a PCL surface through the supramolecular assembly technology [156]. Functionalization of PCL-cyclodextrin (PCL-CD) through host–guest inclusion complexation was performed in aqueous medium. PEG can decrease protein adsorption, and TPSLEQRTVYAK (TPS) peptide can specifically bind EPCs. The two kinds of functional molecules were immobilized on the PCL surface through host–guest inclusion complexation. Aqueous solution of adamantine (AD) conjugated guest compounds (PEG-AD and TPS-AD) alone or in combination was prepared (Fig. 11.6). Typically, the total concentration of guest compounds was kept at 1 mg/mL irrespective of the composition. Then PCL-CD films were put into the solutions, incubated, and dried. The relative composition of the PEG and TPS could be further fine-tuned by adjusting the feeding ratio. The PEG functionalization significantly inhibited the adsorption of fibrinogens and the adhesion of platelets, thus reducing the possibility of thrombus formation. Moreover, the TPS-functionalized surface showed enhanced attachment toward EPCs compared with the surface without TPS functionalization. The dual functions provided by the

corresponding functional molecules were well preserved, which indicated that the host–guest supramolecular assembly technology is particularly useful for covalent immobilization of bioactive molecules onto polymeric scaffolds.

Another phage display derived peptide is CRRETAWAC. This sequence is specific to ECs and has a low affinity for platelets. It has been shown that this sequence can also bind to porcine ECs [157], hence facilitating future animal studies. Although some efficient progress on the technique for polypeptide modification has been reported, the clinical translation of these strategies remains constrained by the limited therapeutic duration afforded by a finite reservoir of bioactive agents, as well as by the degradation or denaturation of surface components by oxidation, hydrolysis and proteolysis when exposed over time to a physiological environment [158, 159]. Chaikof's group developed an orthogonal ligation scheme that enables repeated covalent assembly and disassembly of surface bound biomolecular constituents *in vitro* and *in vivo* [159]. This group selectively immobilized thrombin-inhibitor, thrombomodulin (TM) on ePTFE vascular grafts *in situ* via this feasible strategy [160]. Reversible transpeptidation, a laboratory evolved *Staphylococcus aureus* sortase A (eSrtA) enabled the rapid immobilization of a recombinant TM fragment, containing an eSrtA recognition peptide (LPETG) motif, onto the vascular graft and permitted multiple cycles of bonding and stripping of engineered TM *in vivo* while preserving biological activity [161]. In addition, β-peptide polymers are designed to address the shortcomings of native peptides and have superior advantages of resistance to proteolysis [162]. Zhou et al. synthesized a series of amphiphilic β-peptide polymers with variable compositions of β-amino acid residues and tunable amphiphilicity. The results show that varying the composition of β-peptide polymers can tune the adhesion of EC and SMC in different trends. The optimal β-peptide polymer displays superior EC vs. SMC selectivity than EC-selective peptides regarding cell adhesion, proliferation, and migration. Moreover, β-peptide polymer-modification on material surface results in a complete *in situ* endothelialization of implanted materials and a significant reduction in intimal hyperplasia [163].

11.4.3 Incorporation of Growth Factors

Vascular regeneration is a complex process that is tightly regulated by a variety of growth factors. Many researchers have committed to investigating how to modify artificial vascular grafts with growth factors to recapitulate vascular growth, repair, and regenerative processes.

VEGF is an important angiogenic cytokine that exerts an effect on angiogenesis, is the most common growth factor used for promoting endothelialization [164]. A prospective cohort study showed that increased soluble vascular endothelial growth factor receptor-1 (sVEGFR-1) levels, a recently defined cytokine that reduces the amount of VEGF available to interact with their transmembrane receptors, are associated with arteriovenous fistula stenosis in hemodialysis patients [165]. These

results provide strong evidence that VEGF signaling is important in the prevention of vascular stenosis. VEGF acts directly on ECs or EPCs, promoting cell functions such as proliferation, migration, and differentiation. Taborska et al. developed a fibrin/heparin mesh to coat ePTFE vascular grafts. The meshes were further enriched with the growth factors, VEGF and fibroblast growth factor (FGF). The controlled release of heparin and growth factors prevented thrombus formation after implantation of ePTFE/fibrin graft that were preseeded with autologous ECs, thereby accelerating the formation of a cohesive endothelial monolayer [166]. The Kong lab prepared fusion proteins of hydrophobic HGFI linked to VEGF, which formed a self-assembled layer on the surface of hydrophobic PCL vascular grafts [167]. After implantation in rat abdominal aorta replacement models, the VEGF-HGFI complex-modified grafts exhibited superior endothelialization and tissue regeneration compared to control grafts [168]. The Swartz and Andreadis groups developed acellular TEVGs from small intestinal submucosa with immobilized heparin and VEGF, and showed that following implantation into ovine arteries, the grafts underwent complete endothelialization and remained patent for 1-month [169]. Recently, the same group identified that VEGF captured blood circulating monocytes with high specificity and directed their differentiation toward a mixed EC- and macrophage-like phenotype [170].

The Breuer group examined the role of vasculogenic platelet-derived growth factor (PDGF)-B in TEVG neotissue development using myeloid cell-specific PDGF-B knockout-mice. Results showed that myeloid cell-derived PDGF contributes to vascular neotissue formation by regulating VSMC proliferation and ECM deposition [171]. Han et al. prepared multilayered small-diameter vascular scaffolds dual loaded with VEGF and PDGF [172]. The multilayered grafts including inner, middle and outer layers were prepared by dual-source and dual-power electrospinning. The inner PEG-b-PLCL (PELCL)/gelatin was loaded with VEGF. The middle PLGA/gelatin layer was loaded with PDGF. The outer PCL/gelatin layer provided mechanical strength. The results suggested that dual-loading VEGF and PDGF enhanced vascular regeneration and maintained patency in rabbit left common carotid artery replacement models over the course of 8 weeks. However, growth factor therapies have led to concerns of overstimulation of VSMC proliferation that may induce neointimal hyperplasia in long-term implantations. Recently, the Owens group provided evidence that VSMC-to-myofibroblast transition was induced by PDGF and TGF-β and was dependent on aerobic glycolysis, whereas endothelial-to-mesenchymal transition (EndoMT) was induced by interleukin (IL)-1β and TGF-β [173]. Moreover, endothelial-derived TGF-β signaling was shown to be a primary driver of atherosclerosis-associated vascular inflammation [174, 175]. Thus, these studies suggest that application and loading of growth factors into vascular grafts requires careful consideration, and techniques that benefit from controlled spatio-temporal release may be preferred.

Recent studies have suggested an important role for recipient resident stem/progenitor cells in TEVG regeneration [176, 177]. After graft implantation, inflamed vascular cells might release cytokines such as stem cell factor (SCF) to recruit recipient stem/progenitor cells to vascular grafts and take part in the regeneration

and remodeling of vascular grafts [178]. Zhao's group found that an HDAC7-derived peptide can mobilize vascular adventitial stem/progenitor cells and promote their differentiation into endothelial cells, thus accelerating the endothelialization of vascular grafts. This group incorporated dickkopf-3 (DKK-3) into tissue engineering vascular grafts and evaluated the functionalized vascular grafts in a rat model. Dkk3-loaded tissue-engineered vessel grafts showed efficient endothelization and recruitment of vascular progenitor cells, which had acquired characteristics of mature smooth muscle cells [179]. Stromal cell-derived factor-1α (SDF-1α) is considered to be a potent factor for EPCs homing and neovascularization. Yu et al. [180] cross-linked heparin to PLLA scaffold surfaces before incubating SDF-1α with the scaffolds to generate heparin-SDF-1α-treated PLLA scaffolds. These were implanted into the left common carotid artery of rats and demonstrated an enhanced self-regeneration capability of the grafts by recruiting endothelial progenitor cells and smooth muscle progenitor cells, contributing to endothelialization and the remodeling of the vascular wall, respectively.

To determine whether functional blood vessels could be formed *in situ* through recruitment of circulating cells, Talacua et al. [181] utilized Gore-Tex sheets and PCL/fibrin conduits loaded with monocyte chemoattractant protein-1 (MCP-1). Following implantation into the abdominal aorta of rats, an end-to-end anastomosis was made to a 4 × 10 mm^2 impenetrable Gore-Tex strip using 10–0 interrupted sutures distally and proximally of the electrospun tube. Then, Gore-Tex was wrapped around the PCL in samples, creating an impenetrable outer layer. The results demonstrated that Gore-Tex shielding led to a significant reduction of cell ingrowth from neighboring tissues, whereas MCP-1 was beneficial to endothelialization and tissue formation via the recruitment of circulating cells.

11.4.4 Incorporation of Nucleic Acids

Gene therapy, supplementation, and regulation are potential treatment options for acquired and inherited cardiovascular diseases. In the 1980s, direct intra-arterial gene transfer with endovascular catheters demonstrated the potential of cardiovascular gene therapy [182]. Currently, the potential targets for cardiovascular gene therapy include severe cardiac and peripheral ischemia, heart failure, vein graft failure, and some forms of dyslipidemias [183].

E2F transcription factor antisense decoys have been tested in clinical settings, but the results were disappointing [184]. However, these trials established the clinical feasibility of using a 30-min intraoperative window to functionalize graft tissues *ex vivo* with prophylactic therapies [185]. Akowuah et al. [186] engineered vascular grafts with genetically modified BMSCs on poly(propylene carbonate) graft, which delivered the tissue inhibitor of metalloproteinase 3 (TIMP-3) plasmid to the saphenous vein graft *in vitro* by ultrasound exposure in the presence of echo contrast microbubbles. In porcine carotid artery transplantation models, at 28 days postgrafting, lumen and total vessel area were significantly greater in TIMP-3

group than in the untransfected and control groups. Meng et al. [187] developed a receptor-targeted nanocomplex (RTN) vector system. The RTN vector was composed of cationic liposome lipofectin, a peptide (Peptide-Y: K16GACYGLPHKFCG), and plasmid DNA encoding iNOS. Vein grafts were transfected with RTN before engraftment into rabbit carotid arteries. The majority of ECs and macrophages remained positively transfected at 7-days. Morphometric analysis of vein graft samples at 28-day postimplantation showed an approximate 50% reduction in neointimal thickness and 64% reduction in neointimal area in iNOS-treated groups compared with control groups. Zhong et al. [188] developed a novel recombinant lentivirus for the delivery of hepatocyte growth factor (HGF) and Bax in a rabbit vein graft model of bypass grafting. Rabbit vein segments were dissected and HGF and Bax cDNA were introduced by lentivirus vectors. Then, vein segments were interposed into the rabbit carotid arteries. The results showed that vein graft thickening was markedly reduced in HGF/Bax-treated rabbits compared to controls. Jiang's group designed plasmid DNA encoding TIMP-3 and lyophilized it on the inner surface of a flexible, biodegradable, and conductive external metal-polymer conductor stents (MPCS) to overexpress TIMP-3 in the adventitia and the middle layers of vein grafts. The engineered MPCS significantly inhibited intimal hyperplasia of vein grafts in rabbit models [189].

Electrospun fibers can be easily gene functionalized by encapsulating plasmids, siRNAs, and microRNAs [190]. Yuan's group developed a bioactive trilayered electrospun graft encapsulating both microRNA (miR)-126 and miR-145 for rationally modulating vascular regeneration. The rapid release of miR-126 from the inner layer could promote the proliferation and intracellular NO production of ECs. Meanwhile, the slow release of miR-145 from the middle layer was in favor of modulating the contractile SMC phenotype by targeting KLF4 and upregulating the protein expression of myocardin and myosin [191].

Genetically modified cells may be beneficial in fabricating TEVGs. They are generated by the introduction of genetic material into cells to: (1) replace a disease-causing gene; (2) inactivate a mutated gene; (3) transdifferentiate some specific cell lineages; and (4) express growth factors for cell expansion [192]. Zhang et al. created small-diameter vessels by seeding and culturing eNOS-modified MSCs onto a synthetic polymer scaffold produced by an electrospinning technique [193]. The results showed that the seeded cells integrated with the microfibers of the scaffold to form a three-dimensional cellular network, indicating a favorable interaction between this synthetic scaffold and MSCs. High transduction efficiency was obtained with the use of concentrated retrovirus in the gene transfection of MSCs. The use of MSCs and therapeutic genes in tissue engineering of blood vessels could be helpful in improving vessel regeneration and patency.

References

1. Li S, Sengupta D, Chien S. Vascular tissue engineering: from in vitro to in situ. Wiley Interdiscip Rev Syst Biol Med. 2014;6:61–76.
2. Yow KH, Ingram J, Korossis SA, Ingham E, Homer-Vanniasinkam S. Tissue engineering of vascular conduits. Br J Surg. 2006;93:652–61.
3. Moore MJ, Tan RP, Yang N, Rnjak-Kovacina J, Wise SG. Bioengineering artificial blood vessels from natural materials. Trends Biotechnol. 2022;40:693–707.
4. Baguneid MS, Seifalian AM, Salacinski HJ, Murray D, Hamilton G, Walker MG. Tissue engineering of blood vessels. J Cell Mol Med. 2006;11:945–57.
5. Valence SD, Tille JC, Mugnai D, Mrowczynski W, Gurny R, Möller M, Walpoth BH. Long term performance of polycaprolactone vascular grafts in a rat abdominal aorta replacement model. Biomaterials. 2012;33:38–47.
6. Wang Z, Cui Y, Wang J, Yang X, Wu Y, Wang K, Gao X, et al. The effect of thick fibers and large pores of electrospun poly(ε-caprolactone) vascular grafts on macrophage polarization and arterial regeneration. Biomaterials. 2014;35:5700–10.
7. Hinsbergh VWMV. The endothelium: vascular control of haemostasis. Eur J Obstet Gynecol Reprod Biol. 2001;95:198–201.
8. Yao Y, Wang J, Cui Y, Xu R, Wang Z, Zhang J, Wang K, et al. Effect of sustained heparin release from PCL/chitosan hybrid small-diameter vascular grafts on anti-thrombogenic property and endothelialization. Acta Biomater. 2014;10:2739–49.
9. Sarkar S, Salacinski HJ, Hamilton G, Seifalian AM. The mechanical properties of infrainguinal vascular bypass grafts: their role in influencing patency. Eur J Vasc Endovasc Surg. 2006;31:627–36.
10. Tiwari A, Cheng KS, Salacinski H, Hamilton G, Seifalian AM. Improving the patency of vascular bypass grafts: the role of suture materials and surgical techniques on reducing anastomotic compliance mismatch. Eur J Vasc Endovasc Surg. 2003;25:287–95.
11. Salacinski HJ, Goldner S, Giudiceandrea A, Hamilton G, Seifalian AM, Edwards A, Carson RJ. The mechanical behavior of vascular grafts: a review. J Biomater Appl. 2001;15:241–78.
12. Tang Z, Wang A, Yuan F, Yan Z, Liu B, Chu JS, Helms AJ, et al. Differentiation of multipotent vascular stem cells contributes to vascular diseases. Nat Commun. 2012;3:875–87.
13. Oltrona L, Eisenberg PR, Abendschein DR, Rubin BG. Efficacy of local inhibition of procoagulant activity associated with small-diameter prosthetic vascular grafts. J Vasc Surg. 1996;24:624–31.
14. Lin PH, Chen C, Bush RL, Yao Q, Lumsden AB, Hanson SR. Small-caliber heparin-coated ePTFE grafts reduce platelet deposition and neointimal hyperplasia in a baboon model. J Vasc Surg. 2004;39:1322–8.
15. Letourneur D, Caleb BL, Castellot JJ. Heparin binding, internalization, and metabolism in vascular smooth muscle cells: II. Degradation and secretion in sensitive and resistant cells. J Cell Physiol. 1995;165:676–86.
16. Wang Z, Lu Y, Qin K, Wu Y, Tian Y, Wang J, Zhang J, et al. Enzyme-functionalized vascular grafts catalyze in-situ release of nitric oxide from exogenous NO prodrug. J Control Release. 2015;210:179–88.
17. Mendes AC, Zelikin AN. Enzyme prodrug therapy engineered into biomaterials. Adv Funct Mater. 2014;24:5202–10.
18. Levy RJ, Schoen FJ, Anderson HC, Harasaki H, Koch TH, Brown W, Lian JB, et al. Cardiovascular implant calcification: a survey and update. Biomaterials. 1991;12:707–14.
19. Hutcheson JD, Goettsch C, Rogers MA, Aikawa E. Revisiting cardiovascular calcification: a multifaceted disease requiring a multidisciplinary approach. Semin Cell Dev Biol. 2015;46:68–77.

20. Yang S, Zheng X, Qian M, Wang H, Wang F, Wei Y, Midgley AC, et al. Nitrate-functionalized poly(ε-caprolactone) small-diameter vascular grafts enhance vascular regeneration via sustained release of nitric oxide. Front Bioeng Biotechnol. 2021;9:770121.
21. Wang F, Qin K, Wang K, Wang H, Liu Q, Qian M, Chen S, et al. Nitric oxide improves regeneration and prevents calcification in bio-hybrid vascular grafts via regulation of vascular stem/progenitor cells. Cell Rep. 2022;39:110981.
22. Midgley AC, Wei Y, Li Z, Kong D, Zhao Q. Nitric-oxide-releasing biomaterial regulation of the stem cell microenvironment in regenerative medicine. Adv Mater. 2020;32:e1805818.
23. Liu J, Li B, Jing H, Wu Y, Kong D, Leng X, Wang Z, et al. Swim bladder as a novel biomaterial for cardiovascular materials with anti-calcification properties. Adv Healthc Mater. 2022;11:e2102688.
24. Swartz DD, Andreadis ST. Animal models for vascular tissue-engineering. Curr Opin Biotechnol. 2013;24:916–25.
25. Chlupac J, Filova E, Bačáková L. Blood vessel replacement: 50 years of development and tissue engineering paradigms in vascular surgery. Physiol Res. 2009;58(Suppl 2):119–39.
26. Itoh M, Mukae Y, Kitsuka T, Arai K, Nakamura A, Uchihashi K, Toda S, et al. Development of an immunodeficient pig model allowing long-term accommodation of artificial human vascular tubes. Nat Commun. 2019;10:1–8.
27. Grajciarová M, Turek D, Malečková A, Pálek R, Liška V, Tomášek P, Králičková M, et al. Are ovine and porcine carotid arteries equivalent animal models for experimental cardiac surgery: a quantitative histological comparison. Ann Anat. 2022;242:151910.
28. Deutsch M, Meinhart J, Zilla P, Howanietz N, Gorlitzer M, Froeschl A, Stuempflen A, et al. Long-term experience in autologous in vitro endothelialization of infrainguinal ePTFE grafts. J Vasc Surg. 2009;49:352–62.
29. Seifu DG, Purnama A, Mequanint K, Mantovani D. Small-diameter vascular tissue engineering. Nat Rev Cardiol. 2013;10:410–21.
30. Budd JS, Allen KE, Hartley G, Bell PRF. The effect of preformed confluent endothelial cell monolayers on the patency and thrombogenicity of small calibre vascular grafts. Eur J Vasc Surg. 1991;5:397–405.
31. Lu XL, Sun ZJ, Cai W, Gao ZY. Study on the shape memory effects of poly(l-lactide-co-ε-caprolactone) biodegradable polymers. J Mater Sci Mater Med. 2008;19:395–9.
32. Lee SJ, Liu J, Oh SH, Soker S, Atala A, Yoo JJ. Development of a composite vascular scaffolding system that withstands physiological vascular conditions. Biomaterials. 2008;29:2891–8.
33. Mercado-Pagán ÁE, Stahl AM, Ramseier ML, Behn AW, Yang Y. Synthesis and characterization of polycaprolactone urethane hollow fiber membranes as small diameter vascular grafts. Mater Sci Eng C Mater Biol Appl. 2016;64:61–73.
34. Sankaran KK, Krishnan UM, Sethuraman S. Axially aligned 3D nanofibrous grafts of PLA–PCL for small diameter cardiovascular applications. J Biomater Sci Polym Ed. 2014;25:1791–812.
35. Pektok E, Nottelet B, Tille JC, Gurny R, Kalangos A, Moeller M, Walpoth BH. Degradation and healing characteristics of small-diameter poly(ε-caprolactone) cascular grafts in the rat systemic arterial circulation. Circulation. 2008;118:2563–70.
36. Gao J, Chen S, Tang D, Jiang L, Shi J, Wang S. Mechanical properties and degradability of electrospun pcl/plga blended scaffolds as vascular grafts. Transact Tianjin Univ. 2019;25:152–60.
37. Agarwal R, Blum KM, Musgrave A, Onwuka EA, Yi T, Reinhardt JW, Best CA, et al. Degradation and in vivo evaluation of polycaprolactone, poly(ε-caprolactone-co-L-lactide), and poly-L-lactic acid as scaffold sealant polymers for murine tissue-engineered vascular grafts. Regen Med. 2019;14:627–37.
38. Rafique M, Wei T, Sun Q, Midgley AC, Huang Z, Wang T, Shafiq M, et al. The effect of hypoxia-mimicking responses on improving the regeneration of artificial vascular grafts. Biomaterials. 2021;271:120746.

39. Kurobe H, Tara S, Maxfield MW, Rocco KA, Bagi PS, Yi T, Udelsman BV, et al. Comparison of the biological equivalence of two methods for isolating bone marrow mononuclear cells for fabricating tissue-engineered vascular grafts. Tissue Eng C Methods. 2015;21:597–604.
40. Sang-Heon K, Jae Hyun K, Sub CM, Eunna C, Youngmee J, Soo Hyun K, Kim YH. Fabrication of a new tubular fibrous PLCL scaffold for vascular tissue engineering. J Biomater Sci Polym Ed. 2006;17:1359–74.
41. Shafiq M, Jung Y, Kim SH. In situ vascular regeneration using substance P-immobilised poly (L-lactide-co-ε-caprolactone) scaffolds: stem cell recruitment, angiogenesis, and tissue regeneration. Eur Cell Mater. 2015;30:282–302.
42. Mun CH, Jung Y, Kim SH, Lee SH, Kim HC, Kwon IK, Kim SH. Three-dimensional electrospun poly(lactide-co-ε-caprolactone) for small-diameter vascular grafts. Tissue Eng Part A. 2012;18:1608–16.
43. Fukunishi T, Ong CS, He YJ, Inoue T, Zhang H, Steppan J, Matsushita H, et al. Fast-degrading tissue-engineered vascular grafts lead to increased extracellular matrix cross-linking enzyme expression. Tissue Eng Part A. 2021;27:1368–75.
44. Cho SW, Jeon O, Lim JE, Gwak SJ, Kim SS, Choi CY, Kim DI, et al. Preliminary experience with tissue engineering of a venous vascular patch by using bone marrow–derived cells and a hybrid biodegradable polymer scaffold. J Vasc Surg. 2006;44:1329–40.
45. Rapoport HS, Fish J, Basu J, Campbell J, Genheimer C, Payne R, Jain D. Construction of a tubular scaffold that mimics J-shaped stress/strain mechanics using an innovative electrospinning technique. Tissue Eng Part C Methods. 2012;18:567–74.
46. Takeuchi M, Kuratani T, Miyagawa S, Shirakawa Y, Shimamura K, Kin K, Yoshida T, et al. Tissue-engineered stent-graft integrates with aortic wall by recruiting host tissue into graft scaffold. J Thorac Cardiovasc Surg. 2014;148:1719–25.
47. Fukunishi T, Ong CS, Yesantharao P, Best CA, Yi T, Zhang H, Mattson G, et al. Different degradation rates of nanofiber vascular grafts in small and large animal models. J Tissue Eng Regen Med. 2020;14:203–14.
48. Dahl SL, Kypson AP, Lawson JH, Blum JL, Strader JT, Li Y, Manson RJ, et al. Readily available tissue-engineered vascular grafts. Sci Transl Med. 2011;3:68ra9.
49. Hashi CK, Derugin N, Janairo RRR, Lee R, Schultz D, Lotz J, Li S. Antithrombogenic modification of small-diameter microfibrous vascular grafts. Arterioscler Thromb Vasc Biol. 2010;30:1621–7.
50. Ye X, Lu L, Kolewe ME, Park H, Larson BL, Kim ES, Freed LE. A biodegradable microvessel scaffold as a framework to enable vascular support of engineered tissues. Biomaterials. 2013;34:10007–15.
51. Motlagh D, Yang J, Lui KY, Webb AR, Ameer GA. Hemocompatibility evaluation of poly (glycerol-sebacate) in vitro for vascular tissue engineering. Biomaterials. 2006;27:4315–24.
52. McClure MJ, Sell SA, Simpson DG, Bowlin GL. Electrospun polydioxanone, elastin, and collagen vascular scaffolds: uniaxial cyclic distension. J Eng Fibers Fabr. 2009;4:18–25.
53. Lee KW, Stolz DB, Wang Y. Substantial expression of mature elastin in arterial constructs. Proc Natl Acad Sci. 2011;108:2705–10.
54. Wu W, Allen RA, Wang Y. Fast-degrading elastomer enables rapid remodeling of a cell-free synthetic graft into a neoartery. Nat Med. 2012;18:1148–53.
55. Khosravi R, Best CA, Allen RA, Stowell CET, Onwuka E, Zhuang JJ, Lee YU, et al. Long-term functional efficacy of a novel electrospun poly(glycerol sebacate)-based arterial graft in mice. Ann Biomed Eng. 2016;44:2402–16.
56. Yang X, Wei J, Lei D, Liu Y, Wu W. Appropriate density of PCL nano-fiber sheath promoted muscular remodeling of PGS/PCL grafts in arterial circulation. Biomaterials. 2016;88:34–47.
57. Weinberg CB, Bell E. A blood vessel model constructed from collagen and cultured vascular cells. Science. 1986;231:397–400.
58. Achilli M, Lagueux J, Mantovani D. On the effects of UV-C and pH on the mechanical behavior, molecular conformation and cell viability of collagen-based scaffold for vascular tissue engineering. Macromol Biosci. 2010;10:307–16.

59. Wu HC, Wang TW, Kang PL, Tsuang YH, Sun JS, Lin FH. Coculture of endothelial and smooth muscle cells on a collagen membrane in the development of a small-diameter vascular graft. Biomaterials. 2007;28:1385–92.
60. Hirai J, Matsuda T. Venous reconstruction using hybrid vascular tissue composed of vascular cells and collagen: tissue regeneration process. Cell Transplant. 1996;5:93–105.
61. Offeddu GS, Ashworth JC, Cameron RE, Oyen ML. Structural determinants of hydration, mechanics and fluid flow in freeze-dried collagen scaffolds. Acta Biomater. 2016;41:193–203.
62. Kumar VA, Caves JM, Haller CA, Dai E, Liu L, Grainger S, Chaikof EL. Acellular vascular grafts generated from collagen and elastin analogs. Acta Biomater. 2013;9:8067–74.
63. Zou Y, Zhang Y. The orthotropic viscoelastic behavior of aortic elastin. Biomech Model Mechanobiol. 2010;10:613–25.
64. Buijtenhuijs P, Buttafoco L, Poot AA, Daamen WF, Van Kuppevelt TH, Dijkstra PJ, De Vos RA, et al. Tissue engineering of blood vessels: characterization of smooth-muscle cells for culturing on collagen-and-elastin-based scaffolds. Biotechnol Appl Biochem. 2004;39:141–9.
65. Smith MJ, McClure MJ, Sell SA, Barnes CP, Walpoth BH, Simpson DG, Bowlin GL. Suture-reinforced electrospun polydioxanone–elastin small-diameter tubes for use in vascular tissue engineering: a feasibility study. Acta Biomater. 2008;4:58–66.
66. McKenna KA, Hinds MT, Sarao RC, Wu PC, Maslen CL, Glanville RW, Babcock D, et al. Mechanical property characterization of electrospun recombinant human tropoelastin for vascular graft biomaterials. Acta Biomater. 2011;8:225–33.
67. Ye Q, Zünd G, Benedikt P, Jockenhoevel S, Hoerstrup SP, Sakyama S, Hubbell JA, et al. Fibrin gel as a three dimensional matrix in cardiovascular tissue engineering. Eur J Cardiothorac Surg. 2000;17:587–91.
68. Syedain ZH, Meier LA, Bjork JW, Lee A, Tranquillo RT. Implantable arterial grafts from human fibroblasts and fibrin using a multi-graft pulsed flow-stretch bioreactor with noninvasive strength monitoring. Biomaterials. 2010;32:714–22.
69. Bjork JW, Meier LA, Johnson SL, Syedain ZH, Tranquillo RT. Hypoxic culture and insulin yield improvements to fibrin-based engineered tissue. Tissue Eng Part A. 2012;18:785–95.
70. Elsayed Y, Lekakou C, Labeed F, Tomlins P. Fabrication and characterisation of biomimetic, electrospun gelatin fibre scaffolds for tunica media-equivalent, tissue engineered vascular grafts. Mater Sci Eng C. 2015;61:473–83.
71. Zhu C, Fan D, Wang Y. Human-like collagen/hyaluronic acid 3D scaffolds for vascular tissue engineering. Mater Sci Eng C Mater Biol Appl. 2014;34C:393–401.
72. Joo H, Byun E, Lee M, Hong Y, Lee H, Kim P. Biofunctionalization via flow shear stress resistant adhesive polysaccharide, hyaluronic acid-catechol, for enhanced in vitro endothelialization. J Ind Eng Che. 2016;34:14–20.
73. Arrigoni C, Camozzi D, Imberti B, Mantero S, Remuzzi A. The effect of sodium ascorbate on the mechanical properties of hyaluronan-based vascular constructs. Biomaterials. 2006;27:623–30.
74. Midgley AC, Bowen T. Analysis of human hyaluronan synthase gene transcriptional regulation and downstream hyaluronan cell surface receptor mobility in myofibroblast differentiation. Methods Mol Biol. 2022;2303:453–68.
75. Qin K, Wang F, Simpson RM, Zheng X, Wang H, Hu Y, Gao Z, et al. Hyaluronan promotes the regeneration of vascular smooth muscle with potent contractile function in rapidly biodegradable vascular grafts. Biomaterials. 2020;257:120226.
76. Midgley AC, Zhao Q. CD44 receptor diversity and potential in preventative and regenerative therapies. Clin Transl Discov. 2022;2:e78.
77. Chupa JM, Foster AM, Sumner SR, Madihally SV, Matthew HWT. Vascular cell responses to polysaccharide materials:: in vitro and in vivo evaluations. Biomaterials. 2000;21:2315–22.
78. Zhang L, Ao Q, Wang A, Lu G, Kong L, Gong Y, Zhao N, et al. A sandwich tubular scaffold derived from chitosan for blood vessel tissue engineering. J Biomed Mater Res A. 2006;77A:277–84.

79. Zhu C, Fan D, Duan Z, Xue W, Shang L, Chen F, Luo Y. Initial investigation of novel human-like collagen/chitosan scaffold for vascular tissue engineering. J Biomed Mater Res A. 2009;89:829–40.
80. Zizhou R, Wang X, Houshyar S. Review of polymeric biomimetic small-diameter vascular grafts to tackle intimal hyperplasia. ACS Omega. 2022;7:22125–48.
81. Enomoto S, Sumi M, Kajimoto K, Nakazawa Y, Takahashi R, Takabayashi C, Asakura T, et al. Long-term patency of small-diameter vascular graft made from fibroin, a silk-based biodegradable material. J Vasc Surg. 2010;51:155–64.
82. Kiritani S, Kaneko J, Ito D, Morito M, Ishizawa T, Akamatsu N, Tanaka M, et al. Silk fibroin vascular graft: a promising tissue-engineered scaffold material for abdominal venous system replacement. Sci Rep. 2020;10:1–9.
83. Tosun Z, McFetridge PS. Improved recellularization of ex vivo vascular scaffolds using directed transport gradients to modulate ECM remodeling. Biotechnol Bioeng. 2013;110: 2035.
84. Zhu M, Li W, Dong X, Yuan X, Midgley AC, Chang H, Wang Y, et al. In vivo engineered extracellular matrix scaffolds with instructive niches for oriented tissue regeneration. Nat Commun. 2019;10:4620.
85. Edgar L, Altamimi A, García Sánchez M, Tamburrinia R, Asthana A, Gazia C, Orlando G. Utility of extracellular matrix powders in tissue engineering. Organogenesis. 2018;14:172–86.
86. Jeremy JY, Gadsdon P, Shukla N, Vijayan V, Wyatt M, Newby AC, Angelini GD. On the biology of saphenous vein grafts fitted with external synthetic sheaths and stents. Biomaterials. 2007;28:895–908.
87. Gong W, Lei D, Li S, Huang P, Qi Q, Sun Y, Zhang Y, et al. Hybrid small-diameter vascular grafts: anti-expansion effect of electrospun poly ε-caprolactone on heparin-coated decellularized matrices. Biomaterials. 2016;76:359–70.
88. Longchamp A, Alonso F, Dubuis C, Allagnat F, Berard X, Meda P, Saucy F, et al. The use of external mesh reinforcement to reduce intimal hyperplasia and preserve the structure of human saphenous veins. Biomaterials. 2014;35:2588–99.
89. Yang Y, Lei D, Zou H, Huang S, Yang Q, Li S, Qing FL, et al. Hybrid electrospun rapamycin-loaded small-diameter decellularized vascular grafts effectively inhibit intimal hyperplasia. Acta Biomater. 2019;97:321–32.
90. Shi J, Chen S, Wang L, Zhang X, Gao J, Jiang L, Tang D, et al. Rapid endothelialization and controlled smooth muscle regeneration by electrospun heparin-loaded polycaprolactone/gelatin hybrid vascular grafts. J Biomed Mater Res Part B Appl Biomater. 2019;107:2040–9.
91. Ma W, Wang L, Zhang Q, Dong X, Zhu T, Lu S. Electrospun PCL/collagen hybrid nanofibrous tubular graft based on post-network bond processing for vascular substitute. Biomater Adv. 2022;139:213031.
92. Ju YM, Choi JS, Atala A, Yoo JJ, Lee SJ. Bilayered scaffold for engineering cellularized blood vessels. Biomaterials. 2010;31:4313–21.
93. Stitzel J, Liu J, Lee SJ, Komura M, Berry J, Soker S, Lim G, et al. Controlled fabrication of a biological vascular substitute. Biomaterials. 2006;27:1088–94.
94. Kobayashi H, Terada D, Yokoyama Y, Moon DW, Yasuda Y, Koyama H, Takato T. Vascular-inducing poly(glycolic acid)-collagen nanocomposite-fiber scaffold. J Biomed Nanotechnol. 2013;9:1318–26.
95. Chen W, Xiao W, Liu X, Yuan P, Zhang S, Wang Y, Wu W. Pharmacological manipulation of macrophage autophagy effectively rejuvenates the regenerative potential of biodegrading vascular graft in aging body. Bioactive Mater. 2022;11:283–99.
96. Yang L, Li X, Wu Y, Du P, Sun L, Yu Z, Song S, et al. Preparation of PU/fibrin vascular scaffold with good biomechanical properties and evaluation of its performance in vitro and in vivo. Int J Nanomedicine. 2020;15:8697.
97. Sarasam A, Madihally SV. Characterization of chitosan–polycaprolactone blends for tissue engineering applications. Biomaterials. 2005;26:5500–8.

98. Chen F, Su Y, Mo X, He C, Wang H, Ikada Y. Biocompatibility, alignment degree and mechanical properties of an electrospun chitosan–p(lla-cl) fibrous scaffold. J Biomater Sci Polym Ed. 2009;20:2117–28.
99. Du F, Wang H, Zhao W, Li D, Kong D, Yang J, Zhang Y. Gradient nanofibrous chitosan/poly ε-caprolactone scaffolds as extracellular microenvironments for vascular tissue engineering. Biomaterials. 2011;33:762–70.
100. Yin A, Zhuang W, Liu G, Lan X, Tang Z, Deng Y, Wang Y. Performance of PEGylated chitosan and poly (L-lactic acid-co-ε-caprolactone) bilayer vascular grafts in a canine femoral artery model. Colloids Surf B Biointerfaces. 2020;188:110806.
101. Caldiroli A, Pederzani E, Pezzotta M, Azzollini N, Fiori S, Tironi M, Rizzo P, et al. Hybrid fibroin/polyurethane small-diameter vascular grafts: from fabrication to in vivo preliminary assessment. Biomed Mater. 2022;17:055015.
102. Kuang H, Wang Y, Shi Y, Yao W, He X, Liu X, Mo X, et al. Construction and performance evaluation of hep/silk-PLCL composite nanofiber small-caliber artificial blood vessel graft. Biomaterials. 2020;259:120288.
103. Nakayama Y, Ishibashi-Ueda H, Takamizawa K. In vivo tissue-engineered small-caliber arterial graft prosthesis consisting of autologous tissue (biotube). Cell Transplant. 2004;13: 439–49.
104. Zhi D, Cheng Q, Midgley AC, Zhang Q, Wei T, Li Y, Wang T, et al. Mechanically reinforced biotubes for arterial replacement and arteriovenous grafting inspired by architectural engineering. Sci Adv. 2022;8:eabl3888.
105. Hasan A, Memic A, Annabi N, Hossain M, Paul A, Dokmeci MR, Dehghani F, et al. Electrospun scaffolds for tissue engineering of vascular grafts. Acta Biomater. 2014;10:11–25.
106. Valence SD, Tille JC, Giliberto JP, Mrowczynski W, Gurny R, Walpoth BH, Möller M. Advantages of bilayered vascular grafts for surgical applicability and tissue regeneration. Acta Biomater. 2012;8:3914–20.
107. Wu Y, Zhi D, Midgley A, Zhao Q, Kong D, Wang K. The cell source in tissue regeneration of vascular grafts. Sci Sin Vitae. 2019;49:1100–8.
108. Zhu M, Wang Z, Zhang J, Wang L, Yang X, Chen J, Fan G, et al. Circumferentially aligned fibers guided functional neoartery regeneration in vivo. Biomaterials. 2015;61:85–94.
109. van Kampen KA, Fernández-Pérez J, Baker M, Mota C, Moroni L. Fabrication of a mimetic vascular graft using melt spinning with tailorable fiber parameters. Biomater Adv. 2022;139: 212972.
110. Hibino N, Imai Y, Shin-Oka T, Aoki M, Watanabe M, Kosaka Y, Watanabe T, et al. First successful clinical application of tissue engineered blood vessel. Kyobu Geka. 2002;55:368–73.
111. Shin'oka T, Matsumura G, Hibino N, Naito Y, Watanabe M, Konuma T, Takahiko S, et al. Midterm clinical result of tissue-engineered vascular autografts seeded with autologous bone marrow cells. J Thorac Cardiovasc Surg. 2005;129:1330–8.
112. Hibino N, McGillicuddy E, Matsumura G, Ichihara Y, Naito Y, Breuer C, Shinoka T. Late-term results of tissue-engineered vascular grafts in humans. J Thorac Cardiovasc Surg. 2010;139:431–6.
113. Wang Z, Mithieux SM, Weiss AS. Fabrication techniques for vascular and vascularized tissue engineering. Adv Healthc Mater. 2019;8:1900742.
114. Tan B, Gan S, Wang X, Liu W, Li X. Applications of 3D bioprinting in tissue engineering: advantages, deficiencies, improvements, and future perspectives. Mater Chem B. 2021;9: 5385–413.
115. Duarte Campos DF, Lindsay CD, Roth JG, LeSavage BL, Seymour AJ, Krajina BA, Ribeiro R, et al. Bioprinting cell- and spheroid-laden protein-engineered hydrogels as tissue-on-chip platforms. Front Bioeng Biotechnol. 2020;8:374.
116. Huang R, Gao X, Wang J, Chen H, Tong C, Tan Y, Tan Z. Triple-layer vascular grafts fabricated by combined e-jet 3d printing and electrospinning. Ann Biomed Eng. 2018;46: 1254–66.

117. Allen RA, Wu W, Yao M, Dutta D, Duan X, Bachman TN, Champion HC, et al. Nerve regeneration and elastin formation within poly(glycerol sebacate)-based synthetic arterial grafts one-year post-implantation in a rat model. Biomaterials. 2014;35:165–73.
118. Hu J, Sun X, Ma H, Xie C, Chen YE, Ma PX. Porous nanofibrous PLLA scaffolds for vascular tissue engineering. Biomaterials. 2010;31:7971–7.
119. Ma H, Hu J, Ma PX. Polymer scaffolds for small-diameter vascular tissue engineering. Adv Funct Mater. 2010;20:2833–41.
120. Soletti L, Hong Y, Guan J, Stankus JJ, El-Kurdi MS, Wagner WR, Vorp DA. A bilayered elastomeric scaffold for tissue engineering of small diameter vascular grafts. Acta Biomater. 2010;6:110–22.
121. He W, Nieponice A, Soletti L, Hong Y, Gharaibeh B, Crisan M, Usas A, et al. Pericyte-based human tissue engineered vascular grafts. Biomaterials. 2010;31:8235–44.
122. Sugiura T, Tara S, Nakayama H, Kurobe H, Yi T, Lee YU, Lee AY, et al. Novel bioresorbable vascular graft with sponge-type scaffold as a small-diameter arterial graft. Ann Thorac Surg. 2016;102:720–7.
123. Akentjew TL, Terraza C, Suazo C, Maksimcuka J, Wilkens CA, Vargas F, Zavala G, et al. Rapid fabrication of reinforced and cell-laden vascular grafts structurally inspired by human coronary arteries. Nat Commun. 2019;10:1–15.
124. de Mel A, Murad F, Seifalian AM. Nitric oxide: a guardian for vascular grafts? Chem Rev. 2011;111:5742–67.
125. Loscalzo J. Nitric oxide insufficiency, platelet activation, and arterial thrombosis. Circ Res. 2001;88:756–62.
126. Suvorava T, Dao VT, Bas M, Kojda G. Nitric oxide and the CABG patient. Curr Opin Pharmacol. 2012;12:195–202.
127. Gaudino M, Antoniades C, Benedetto U, Deb S, Di Franco A, Di Giammarco G, Fremes S, et al. Mechanisms, consequences, and prevention of coronary graft failure. Circulation. 2017;136:1749–64.
128. Liu ZG, Ge ZD, He GW. Difference in endothelium-derived hyperpolarizing factor-mediated hyperpolarization and nitric oxide release between human internal mammary artery and saphenous vein. Circulation. 2001;104:344–9.
129. Nichols SP, Storm WL, Koh A, Schoenfisch MH. Local delivery of nitric oxide: targeted delivery of therapeutics to bone and connective tissues. Adv Drug Deliv Rev. 2012;64:1177–88.
130. Rao J, Pan Bei H, Yang Y, Liu Y, Lin H, Zhao X. Nitric oxide-producing cardiovascular stent coatings for prevention of thrombosis and restenosis. Front Bioeng Biotechnol. 2020;24:578.
131. Smith DJ, Chakravarthy D, Pulfer S, Simmons ML, Hrabie JA, Citro ML, Saavedra JE, et al. Nitric oxide-releasing polymers containing the [N(O)NO]- group. J Med Chem. 1996;39:1148–56.
132. Fleser PS, Nuthakki VK, Malinzak LE, Callahan RE, Seymour ML, Reynolds MM, Merz SI, et al. Nitric oxide-releasing biopolymers inhibit thrombus formation in a sheep model of arteriovenous bridge grafts. J Vasc Surg. 2004;40:803–11.
133. Enayati M, Schneider KH, Almeria C, Grasl C, Kaun C, Messner B, Rohringer S, et al. S-nitroso human serum albumin as a nitric oxide donor in drug-eluting vascular grafts: biofunctionality and preclinical evaluation. Acta Biomater. 2021;134:276–88.
134. Hou J, Pan Y, Zhu D, Fan Y, Feng G, Wei Y, Wang H, et al. Targeted delivery of nitric oxide via a 'bump-and-hole'-based enzyme-prodrug pair. Nat Chem Biol. 2019;15:151–60.
135. Yang Z, Yang Y, Zhang L, Xiong K, Li X, Zhang F, Wang J, et al. Mussel-inspired catalytic selenocystamine-dopamine coatings for long-term generation of therapeutic gas on cardiovascular stents. Biomaterials. 2018;178:1–10.
136. Zhang F, Zhang Q, Li X, Huang N, Zhao X, Yang Z. Mussel-inspired dopamine-cu (II) coatings for sustained in situ generation of nitric oxide for prevention of stent thrombosis and restenosis. Biomaterials. 2019;194:117–29.

137. Lyu N, Du Z, Qiu H, Gao P, Yao Q, Xiong K, Tu Q, et al. Mimicking the nitric oxide-releasing and glycocalyx functions of endothelium on vascular stent surfaces. Adv Sci. 2020;7:2002330.
138. Chen Y, Gao P, Huang L, Tan X, Zhou N, Yang T, Qiu H, et al. A tough nitric oxide-eluting hydrogel coating suppresses neointimal hyperplasia on vascular stent. Nat Commun. 2021;12:7079.
139. Kural MH, Wang J, Gui L, Yuan Y, Li G, Leiby KL, Quijano E, et al. Fas ligand and nitric oxide combination to control smooth muscle growth while sparing endothelium. Biomaterials. 2019;212:28–38.
140. Kushwaha M, Anderson JM, Bosworth CA, Andukuri A, Minor WP, Lancaster JR, Anderson PG, et al. A nitric oxide releasing, self assembled peptide amphiphile matrix that mimics native endothelium for coating implantable cardiovascular devices. Biomaterials. 2010;31:1502–8.
141. Andukuri A, Kushwaha M, Tambralli A, Anderson JM, Dean DR, Berry JL, Sohn YD, et al. A hybrid biomimetic nanomatrix composed of electrospun polycaprolactone and bioactive peptide amphiphiles for cardiovascular implants. Acta Biomater. 2011;7:225–33.
142. Yang Z, Zhao X, Hao R, Tu Q, Tian X, Xiao Y, Xiong K, et al. Bioclickable and mussel adhesive peptide mimics for engineering vascular stent surfaces. Proc Natl Acad Sci U S A. 2020;117:16127–37.
143. Badv M, Alonso-Cantu C, Shakeri A, Hosseinidoust Z, Weitz JI, Didar TF. Biofunctional lubricant-infused vascular grafts functionalized with silanized bio-inks suppress thrombin generation and promote endothelialization. ACS Biomater Sci Eng. 2019;5:6485–96.
144. Lu S, Zhang P, Sun X, Gong F, Yang S, Shen L, Huang Z, et al. Synthetic ePTFE grafts coated with an anti-CD133 antibody-functionalized heparin/collagen multilayer with rapid in vivo endothelialization properties. ACS Appl Mater Interfaces. 2013;5:7360–9.
145. Wang H, Xing M, Deng W, Qian M, Wang F, Wang K, Midgley AC, et al. Anti-Sca-1 antibody-functionalized vascular grafts improve vascular regeneration via selective capture of endogenous vascular stem/progenitor cells. Bioact Mater. 2022;16:433–50.
146. Xing Z, Wu S, Zhao C, Bai Y, Jin D, Yin M, Liu H, et al. Vascular transplantation with dual-biofunctional ePTFE vascular grafts in a porcine model. J Mater Chem B. 2021;9:7409–22.
147. Rotmans JI, Verhagen HJ, Velema E, de Kleijn DP, van den Heuvel M, Kastelein JJ, Pasterkamp G, et al. Local overexpression of C-type natriuretic peptide ameliorates vascular adaptation of porcine hemodialysis grafts. Kidney Int. 2004;65:1897–905.
148. Li J, Zhuo N, Zhang J, Sun Q, Si J, Wang K, Zhi D. The loading of C-type natriuretic peptides improved hemocompatibility and vascular regeneration of electrospun poly(ε-caprolactone) grafts. Acta Biomater. 2022;151:304–16.
149. Zheng W, Gao J, Song L, Chen C, Guan D, Wang Z, Li Z, et al. Surface-induced hydrogelation inhibits platelet aggregation. J Am Chem Soc. 2013;135:266–71.
150. Zheng W, Wang Z, Song L, Zhao Q, Zhang J, Li D, Wang S, et al. Endothelialization and patency of RGD-functionalized vascular grafts in a rabbit carotid artery model. Biomaterials. 2012;33:2880–91.
151. Mahara A, Somekawa S, Kobayashi N, Hirano Y, Kimura Y, Fujisato T, Yamaoka T. Tissue-engineered acellular small diameter long-bypass grafts with neointima-inducing activity. Biomaterials. 2015;58:54–62.
152. Mousavizadeh A, Jabbari A, Akrami M, Bardania H. Cell targeting peptides as smart ligands for targeting of therapeutic or diagnostic agents: a systematic review. Colloids Surf B Biointerfaces. 2017;158:507–17.
153. Veleva AN, Heath DE, Cooper SL, Patterson C. Selective endothelial cell attachment to peptide-modified terpolymers. Biomaterials. 2008;29:3656–61.
154. Niu B, Huang Y, Zhang S, Wang D, Xu H, Kong D, Qiao M. Expression and characterization of hydrophobin HGFI fused with the cell-specific peptide TPS in Pichia pastoris. Protein Expr Purif. 2012;83:92–7.
155. Huang Y, Zhang S, Niu B, Wang D, Wang Z, Feng S, Hu H, et al. Poly(ε-caprolactone) modified with fusion protein containing self-assembled hydrophobin and functional peptide

for selective capture of human blood outgrowth endothelial cells. Colloids Surf B Biointerfaces. 2013;101:361–9.
156. Ji Q, Zhang S, Zhang J, Wang Z, Wang J, Cui Y, Pang L, et al. Dual functionalization of poly (ε-caprolactone) film surface through supramolecular assembly with the aim of promoting in situ endothelial progenitor cell attachment on vascular grafts. Biomacromolecules. 2013;14: 4099–107.
157. Dudash LA, Kligman FL, Bastijanic JM, Kottke-Marchant K, Marchant RE. Cross-reactivity of cell-selective CRRETAWAC peptide with human and porcine endothelial cells. J Biomed Mater Res A. 2014;102:2857–63.
158. Banerjee I, Pangule RC, Kane RS. Antifouling coatings: recent developments in the design of surfaces that prevent fouling by proteins, bacteria, and marine organisms. Adv Mater. 2011;23: 690–718.
159. Ham HO, Qu Z, Haller CA, Dorr BM, Dai E, Kim W, Liu DR, et al. In situ regeneration of bioactive coatings enabled by an evolved Staphylococcus aureus sortase a. Nat Commun. 2016;7:11140.
160. Ham HO, Haller CA, Su G, Dai E, Patel MS, Liu DR, Liu J, et al. A rechargeable anti-thrombotic coating for blood-contacting devices. Biomaterials. 2021;276:121011.
161. Jiang R, Weingart J, Zhang H, Ma Y, Sun XL. End-point immobilization of recombinant thrombomodulin via sortase-mediated ligation. Bioconjug Chem. 2012;23:643–9.
162. Liu R, Chen X, Gellman SH, Masters KS. Nylon-3 polymers that enable selective culture of endothelial cells. J Am Chem Soc. 2013;135:16296–9.
163. Zhou R, Wu Y, Chen K, Zhang D, Chen Q, Zhang D, She Y, et al. A polymeric strategy empowering vascular cell selectivity and potential application superior to extracellular matrix peptides. Adv Mater. 2022;34:e2200464.
164. Apte RS, Chen DS, Ferrara N. VEGF in signaling and disease: beyond discovery and development. Cell. 2019;176:1248–64.
165. Eroglu E, Kocyigit I, Kahriman G, Karakukcu C, Tuncay A, Zararsiz GE, Eren D, et al. Soluble vascular endothelial growth factor receptor-1 as a novel marker of arteriovenous fistula stenosis in hemodialysis patients. Hemodial Int. 2021;25:164–72.
166. Táborská J, Riedelová Z, Brynda E, Májek P, Riedel T. Endothelialization of an ePTFE vessel prosthesis modified with an antithrombogenic fibrin/heparin coating enriched with bound growth factors. RSC Adv. 2021;11:5903–13.
167. Zhao L, Ma S, Pan Y, Zhang Q, Wang K, Song D, Wang X, et al. Functional modification of fibrous pcl scaffolds with fusion protein VEGF-HGFI enhanced cellularization and vascularization. Adv Healthc Mater. 2016;18:2376–85.
168. Wang K, Zhang Q, Zhao L, Pan Y, Wang T, Zhi D, Ma S, et al. Functional modification of electrospun poly(ε-caprolactone) vascular grafts with the fusion protein VEGF-HGFI enhanced vascular regeneration. ACS Appl Mater Interfaces. 2017;9:11415–27.
169. Koobatian MT, Row S, Smith RJ, Koenigsknecht C, Andreadis ST, Swartz DD. Successful endothelialization and remodeling of a cell-free small-diameter arterial graft in a large animal model. Biomaterials. 2016;76:344–58.
170. Smith RJ, Nasiri B, Kann J, Yergeau D, Bard JE, Swartz DD, Andreadis ST. Endothelialization of arterial vascular grafts by circulating monocytes. Nat Commun. 2020;11:1622.
171. Onwuka E, Best C, Sawyer A, Yi T, Heuer E, Sams M, Wiet M, et al. The role of myeloid cell-derived PDGF-B in neotissue formation in a tissue-engineered vascular graft. Regen Med. 2017;12:249–61.
172. Han F, Jia X, Dai D, Yang X, Zhao J, Zhao Y, Fan Y, et al. Performance of a multilayered small-diameter vascular scaffold dual-loaded with VEGF and PDGF. Biomaterials. 2013;34: 7302–13.
173. Newman AA, Serbulea V, Baylis RA, Shankman LS, Bradley X, Alencar GF, Owsiany K, et al. Multiple cell types contribute to the atherosclerotic lesion fibrous cap by PDGFRβ and bioenergetic mechanisms. Nat Metab. 2021;3:166–81.

174. Chen PY, Qin L, Li G, Wang Z, Dahlman JE, Malagon-Lopez J, Gujja S, et al. Endothelial TGF-β signalling drives vascular inflammation and atherosclerosis. Nat Metab. 2019;1:912–26.
175. Chen PY, Qin L, Baeyens N, Li G, Afolabi T, Budatha M, Tellides G, et al. Endothelial-to-mesenchymal transition drives atherosclerosis progression. J Clin Invest. 2015;125:4514–28.
176. Zhang L, Issa Bhaloo S, Chen T, Zhou B, Xu Q. Role of resident stem cells in vessel formation and arteriosclerosis. Circ Res. 2018;122:1608–24.
177. Wang D, Li LK, Dai T, Wang A, Li S. Adult stem cells in vascular remodeling. Theranostics. 2018;8:815–29.
178. Ni Z, Deng J, Potter CMF, Nowak WN, Gu W, Zhang Z, Chen T, et al. Recipient c-kit lineage cells repopulate smooth muscle cells of transplant arteriosclerosis in mouse models. Circ Res. 2019;125:223–41.
179. Pan Y, Yang J, Wei Y, Wang H, Jiao R, Moraga A, Zhang Z, et al. Histone deacetylase 7-derived peptides play a vital role in vascular repair and regeneration. Adv Sci (Weinh). 2018;5:1800006.
180. Yu J, Wang A, Tang Z, Henry J, Lee BL, Zhu Y, Yuan F, et al. The effect of stromal cell-derived factor-1α/heparin coating of biodegradable vascular grafts on the recruitment of both endothelial and smooth muscle progenitor cells for accelerated regeneration. Biomaterials. 2012;33:8062–74.
181. Talacua H, Smits AI, Muylaert DE, van Rijswijk JW, Vink A, Verhaar MC, Molet AD, et al. In situ tissue engineering of functional small-diameter blood vessels by host circulating cells only. Tissue Eng Part A. 2015;21:2583–94.
182. Nabel EG, Plautz G, Nabel GJ. Site-specific gene expression in vivo by direct gene transfer into the arterial wall. Science. 1990;249:1285–8.
183. Ylä-Herttuala S, Baker AH. Cardiovascular gene therapy: past, present, and future. Mol Ther. 2017;25:1095–106.
184. Alexander JH, Hafley G, Harrington RA, Peterson ED, Ferguson TB, Lorenz TJ, Goyal A, et al. Efficacy and safety of edifoligide, an E2F transcription factor decoy, for prevention of vein graft failure following coronary artery bypass graft surgery: PREVENT IV: a randomized controlled trial. JAMA. 2005;294:2446–54.
185. Evans BC, Hocking KM, Osgood MJ, Voskresensky I, Dmowska J, Kilchrist KV, Brophy CM, et al. MK2 inhibitory peptide delivered in nanopolyplexes prevents vascular graft intimal hyperplasia. Sci Transl Med. 2015;7:291ra95.
186. Akowuah EF, Gray C, Lawrie A, Sheridan PJ, Su CH, Bettinger T, Gunn J, et al. Ultrasound-mediated delivery of TIMP-3 plasmid DNA into saphenous vein leads to increased lumen size in a porcine interposition graft model. Gene Ther. 2005;12:1154–7.
187. Meng QH, Irvine S, Tagalakis AD, McAnulty RJ, McEwan JR, Hart SL. Inhibition of neointimal hyperplasia in a rabbit vein graft model following non-viral transfection with human iNOS cDNA. Gene Ther. 2013;20:979–86.
188. Zhong JT, Chang Q, Sun Y, Gao HB, Xu P. Lentiviral vector mediated expression of Bax and hepatocyte growth factor inhibits vein graft thickening in a rabbit vein graft model. Pharmazie. 2014;69:809–13.
189. Ding L, Hang C, Cheng S, Jia L, Mou L, Tang L, Zhang C, et al. A soft, conductive external stent inhibits intimal hyperplasia in vein grafts by electroporation and mechanical restriction. ACS Nano. 2020;14:16770–80.
190. Rujitanaroj PO, Wang YC, Wang J, Chew SY. Nanofiber-mediated controlled release of siRNA complexes for long term gene-silencing applications. Biomaterials. 2011;32:5915–23.
191. Wen M, Zhi D, Wang L, Cui C, Huang Z, Zhao Y, Wang K, et al. Local delivery of dual micrornas in trilayered electrospun grafts for vascular regeneration. ACS Appl Mater Interfaces. 2020;12:6863–75.

192. Sung YK, Kim SW. Recent advances in the development of gene delivery systems. Biomater Res. 2019;23:8.
193. Zhang J, Qi H, Wang H, Hu P, Ou L, Guo S, Li J, et al. Engineering of vascular grafts with genetically modified bone marrow mesenchymal stem cells on poly (propylene carbonate) graft. Artif Organs. 2006;30:898–905.

Chapter 12
Myocardial Tissue Repair and Regeneration

Kai Wang, Shuqin Wang, Yuchen Miao, Yuwen Lu, Houwei Zheng, Kaicheng Deng, Liang Song, Shifen Li, Yang Zhu, and Changyou Gao

Abstract Heart failure caused by myocardial infarction (MI) remains a major threat to human health. After MI, a series of pathological events take place, including apoptosis of cardiac cells, arrhythmia, inflammation, fibrosis, and adverse remodeling of infarcted myocardium. To repair the damaged heart, researchers have done a lot to find out effective methods for the MI treatment. Recent progress in the field of biomaterials engineering for disease treatment mainly focused on tuning the physicochemical properties for better therapeutic effect based on tissue–biomaterial interaction. Among them, biomaterials have been developed to increase oxygen supply, salvage cardiac cells, maintain electroconductivity, mediate microenvironment, and regenerate cardiomyocytes in the infarct and border zone, in order to preserve cardiac function and morphology. Strategies for controlling these properties include chemical modification, type and degree of crosslinking, and incorporation of bioactive molecules. This chapter focuses on the advances and clinical translation of various biomaterials for repair and regeneration of cardiac tissue after MI.

Keywords Myocardial infarction · Oxygen supply · Mechanical support · Electrical signal conduction · Anti-inflammation · Regeneration

K. Wang · S. Wang · Y. Miao · Y. Lu · H. Zheng · K. Deng · L. Song · S. Li · C. Gao (✉)
MOE Key Laboratory of Macromolecular Synthesis and Functionalization, Department of Polymer Science and Engineering, Zhejiang University, Hangzhou, China
e-mail: cygao@zju.edu.cn

Y. Zhu (✉)
MOE Key Laboratory of Macromolecular Synthesis and Functionalization, Department of Polymer Science and Engineering, Zhejiang University, Hangzhou, China

State Key Laboratory of Transvascular lmplantation Devices, Zhejiang University, Hangzhou, China
e-mail: zhuyang@zju.edu.cn

C. Gao (ed.), *Polymeric Biomaterials for Tissue Regeneration*,
https://doi.org/10.1007/978-981-99-6948-7_12

12.1 Introduction

Heart failure (HF) remains one of the leading causes of mobility and mortality worldwide. HF is the end stage of various cardiovascular diseases, and adversely impacts cardiac function [1]. Myocardial infarction (MI) resulted from the occlusion of coronary arteries is the major cause of HF. Irreversible cardiomyocyte necrosis and apoptosis caused by myocardial ischemia would lead to electrical signal disorder, inflammation and fibrosis in infarcted area and border zone, which all contribute to the development of HF [2].

The focus of clinical interventions including percutaneous coronary intervention (PCI) and coronary artery bypass grafting (CABG) for MI can restore blood perfusion in ischemic myocardium [3, 4]. In addition, medications including angiotensin-converting enzyme inhibitors, angiotensin II receptor blockers, beta-blockers, diuretics, and inotropes are commonly applied in the early and middle stages of MI to increase blood supply. In the end stage, the ultimate option is heart transplantation, yet the high cost and the shortage of suitable donors make it not suitable as a universal choice [5]. Another prospective approach for MI or HF treatment is stem cell-based therapy. The therapeutic potential of mesenchymal stem cells (MSCs) and endothelial progenitor cells (EPCs) has been demonstrated in terms of attenuating left ventricular remodeling and promoting angiogenesis [6, 7]. However, promoting retention and proliferation of implanted stem cells are highly challenging [7]. Therefore, there is a need to develop more efficient and comprehensive therapies to repair heart function and promote cardiac tissue regeneration [8].

Numerous biomaterials have been developed to treat MI. These biomaterials not only offer mechanical support temporarily to inhibit LV dilation, but also serve as carriers to deliver bioactive payloads such as cells, exosomes, bioactive factors and drugs with improved retention [9, 10]. CorPatch, a cardiac patch device derived from decellularized porcine intestine, has been approved by FDA for treating HF [11]. The patients received CABG and fibrin patch implantation with human ESC-derived cardiac progenitor cells showed a substantial increase in left ventricular ejection fraction (LVEF) [12, 13]. Meanwhile, a Phase I clinical trial on VentriGel, an intramyocardially injected extracellular matrix hydrogel, has demonstrated its safety and feasibility of transendocardial injection [14]. A calcium–alginate hydrogel, named Algisyl-LVR, has been administered to dilated cardiomyopathy patients. The LV size was reduced, and no adverse events were reported after 24-months follow-up [15].

This chapter summarized recent advances in research and clinical translation of biomaterials for HF or MI treatment, with the focuses on alleviating ischemia, inhibiting LV dilatation, restoration of electric signal conduction, mediation of inflammation, and promoting cardiac regeneration (Scheme 12.1).

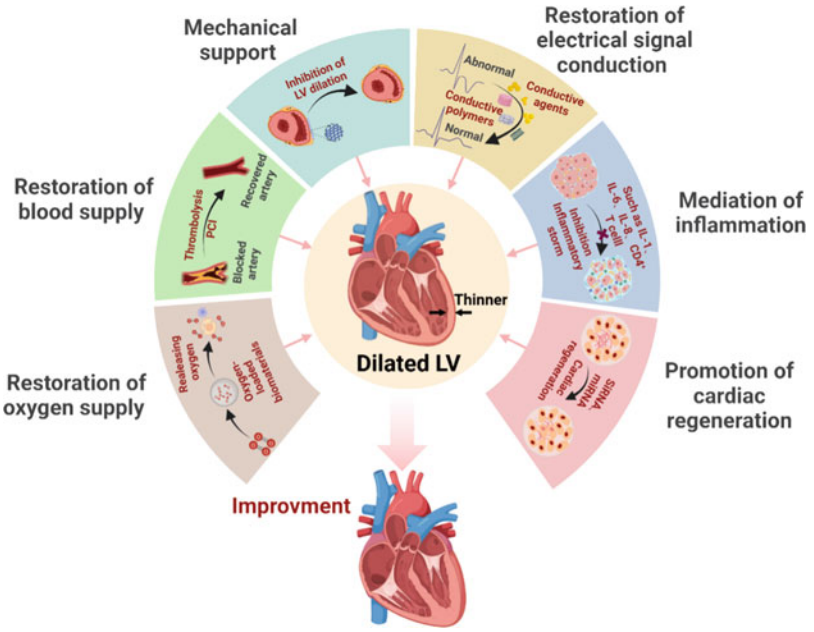

Scheme 12.1 Methods and beneficial effects of biomaterials treatment for myocardial infarction and heart failure

12.2 Restoration of Oxygen Supply

12.2.1 Oxygen Production In Situ

In myocardial infarction, the occlusion of coronary artery causes acute ischemia of the myocardium, leading to the unbalanced consumption of oxygen and adenosine triphosphate and ultimate ischemic necrosis of the myocardium [16]. Oxygen therapy has been continuously improved since it was pioneered by Beddoes in 1978, as numerous studies have demonstrated their positive therapeutic effect on different types of ischemic diseases [17–19]. Current oxygen therapy for myocardial infarction focuses on systemic oxygen enrichment, but the efficacy needs to be improved. Moreover, the results of clinical trials and preclinical studies are inconsistent, and clinical data are scarce to demonstrate the efficacy of oxygen inhalation in MI patients [20, 21]. This may be a result of the mismatch between the systemic oxygen supplement and the disease characteristics of local hypoxic environment in the ischemic myocardium [16].

Biocompatible oxygen-carrying biomaterials (OCB) have been applied on myocardial tissue repairment attributed to their reversible binding and on-demand release of oxygen. Hemoglobin-based oxygen carriers (HBOC) containing natural hemoglobin or myoglobin have been widely studied [22–25]. For example, Caswell et al.

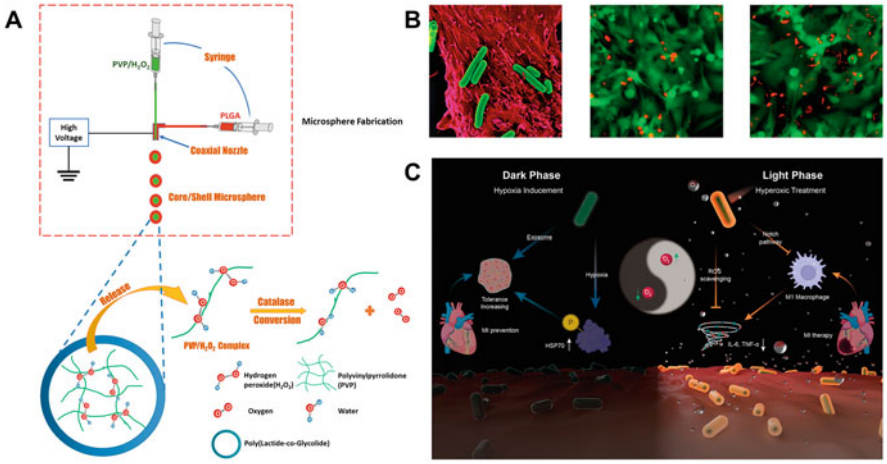

Fig. 12.1 Oxygen-generating biomaterials. (**a**) Fabrication and oxygen release mechanism of oxygen releasing microspheres [28]. (Reprinted from [28] with permission, copyright 2021 Elsevier). (**b**) False-colored scanning electron micrograph of multiple *S. elongatus* cyanobacteria (green) with a single rat cardiomyocyte (red) (left). Representative images of a live/dead assay of cardiomyocytes alone (middle) and cardiomyocytes cocultured with *S. elongatus* (right) [35]. (Reprinted from [35] with permission, copyright 2020 American Chemical Society). (**c**) Schematic illustration for the synthesis of UCCy@Gel for acute MI prevention (dark phase) and therapy (light phase) [37] (Reprinted from [37] with permission, copyright 2022 Wiley)

used HBOC-201 to reduce myocardial infarct size in a canine model of acute coronary artery occlusion and reperfusion [22]. Besides HBOC, perfluorocarbons have been applied to improve cardiac performance due to their high oxygen solubility, chemical and biological inertness, and ease of sterilization [26, 27].

As another kind of oxygen therapy materials, oxygen-generating biomaterials (OGB) are also employed in treating myocardial disease [28–38]. One category of OGB is based on the decomposition of peroxides to generate oxygen, of which the peroxides are usually combined with polymers to build oxygen releasing materials. As shown in Fig. 12.1a, Fan et al. developed an injectable, oxygen-releasing core/shell microspheres with poly (lactide-*co*-glycolic acid) as shell and poly (N-vinylpyrrolidone)/H_2O_2 complex as core to augment cell survival and promote cardiac repair after myocardial infarction [28]. The system can be easily injected and retained at the infarction site. The system can release oxygen continuously for 4 weeks which is significantly longer than the traditional oxygen system [29, 30], while avoiding the generation of excessive reactive oxygen species (ROS) induced by high oxygen concentration, thereby achieving heart repair as evidenced by echocardiographic and immunohistological analysis.

Taking into account both oxygen production and consumption of metabolites, a photosynthetic OGB system was developed, which can form a small *in situ* ecosystem where the metabolic products can be reused by photosynthetic organisms to produce O_2 [31–33]. As shown in Fig. 12.1b, Haraguchi et al. created an *in vitro*

"symbiotic recycling system" composed of mammalian cells and algae, which can increase the dissolved oxygen concentration in the medium and decrease glucose consumption and lactate production, resulting in thicker cardiac tissues [34]. Cohen et al. developed an innovative approach to correct myocardial ischemia by directly applying photosynthetic *S. elongatus* to infarcts and inducing *in situ* photosynthesis [35]. With the help of *S. elongatus* and local light irradiation, the photosynthesis system can provide oxygen and nutrients to ischemic myocardium, thereby alleviating the pathological conditions. Compared to that in the control ischemic myocardium, the oxygenation level in *S. elongatus*-treated hearts increased by 25 times after 10 min irradiation, and the cardiac output increased by 60% after 45 min treatment. In addition, *S. elongatus* can sustainably improve ventricular function after transient ischemia, as demonstrated by echocardiography and cardiac magnetic resonance imaging 4 weeks after treatment. However, without physical support after injection, local retention of the cyanobacteria in the myocardium is limited. Stapleton et al. used bioengineered hydrogel particles to extend the retention and further enhance the therapeutic effect of *S. elongatus* [36]. A mixture of aqueous calcium–ethylenediaminetetraacetic acid (Ca-EDTA) complex solution and aqueous alginate–*S. elongatus* solution was emulsified into microgels (50 μm–80 μm in diameter) using a microfluidic t-junction device. The encapsulation of *S. elongatus* into alginate microgels as delivery vehicles sustained local photosynthetic O_2 delivery to ischemic myocardium. Moreover, as shown in Fig. 12.1c, Liu et al. developed a photoresponsive upconversion cyanobacterium nanocapsule (UCCy@Gel) to achieve near-infrared-induced respiration and photosynthesis [37]. *In vitro* experiments demonstrated that the encapsulated cyanobacteria in UCCy@Gel maintained high activity. The MI mice injected with UCCy@Gel and treated with 980 nm NIR for 3 days showed significant improvement in cardiac function. It is hypothesized that oxygen therapy activates the Notch pathway to suppress macrophage polarization to the inflammatory M1 type, and the upregulation of HSP70 activates the Wnt/β-catenin pathway to downregulate caspase-3 in dark.

The studies of oxygen releasing materials for myocardial infarction treatment currently remain at the rodent level, while large animal models are needed to further substantiate their corresponding efficacy and safety. In addition, due to the risk of oxidative damage from hyperoxia and metabolic death from hypoxia, local oxygen concentration needs to be controlled in an appropriate range to achieve the recovery of cardiac function in infarcted hearts [39]. Nakada et al. discovered that ~7% oxygen for 2 weeks is effective in improving cardiomyocyte proliferation [40]. Optimal target spatial and temporal profiles of oxygen concentration in infarct and border zone tissue are yet to be determined.

12.2.2 Increasing Blood Supply

When coronary arteries are occluded, the blood supply would be insufficient at the infarcted myocardium [41]. The pharmaceuticals, primary percutaneous coronary

intervention (PCI), and fibrinolytic therapy are mainstream modalities for treating ischemic cardiomyopathy, reducing infarct size and preserving cardiomyocytes via rapid dredging of the blocked vessels and restoring the structural integrity of the downstream vascular system [42]. When there are blockages in most of tiny blood vessels, or a large scale of cardiomyocyte death after MI, the PCI treatment seems not to work that well [43]. Therefore, it is necessary to find out additional cardioprotective strategies to rebuild vessels to increase blood supply after MI without bringing side effects. Using bioactive molecules such as genes, proteins or cells to promote angiogenesis is an appropriate method for restoring blood supply. Biomaterials such as hydrogels, scaffolds, patches, nanocarriers and liposomes are the ideal carriers for to shelter and deliver these bioactive molecules to the treating site, which have become promising treatments for ischemic cardiomyopathy [44].

Growth factors including vascular endothelial growth factor (VEGF), basic fibroblast growth factor (bFGF), hepatocyte growth factor (HGF), insulin-like growth factor 1 (IGF-1), and stromal cell-derived factor 1 (SDF-1) have shown the ability of promoting angiogenesis in infarcted hearts [45]. Biomaterials have been used as carriers to extend the retention and control the release of the growth factors. For instance, Rufaihah et al. used polyethylene glycol and fibrinogen to prepare an injectable composite hydrogel to load and deliver VEGF-A in a sustained and controlled manner. The VEGF-loaded hydrogel significantly improves the angiogenesis and cardiac function compared to MI control [46]. In addition, angiogenic effects can be further enhanced by combined use of growth factors. Coulombe et al. prepared a collagen-based hydrogel incorporated with proteins-loaded alginate microspheres, where the alginate microspheres loaded single, double and triple combinations of bFGF, VEGF and sonic hedgehog (SHH), which were then applied in a rat ischemia/reperfusion model. VEGF and bFGF together could promote 2D vascularization, and SHH could further encourage the growth of blood vessels in a 3D-modified experiment of aortic ring vascularization. Altogether, the cocktail of growth factors outperforms single proteins in angiogenesis [47]. Exerting comprehensive therapeutic effects on the infarction site at the same time via cardiac patches is another promising therapeutic approach for MI treatment. Ye et al. designed a multifunctional device that included an elastic patch, microchannel networks and a therapeutic-agents-delivering system through a subcutaneously implanted pump. When applied in a rat MI model, the delivery system assisted by the pump is able to release the loaded platelet-derived growth factor-BB sustainably, which helps to further decrease ventricular remodeling, and facilitate angiogenesis and achieve a better cardiac function finally [48].

The emergence of stem cell therapies and their efficacy in animal experiments have brought great hope to restoration of blood supply in MI patients. Two main possible mechanisms of boosting angiogenesis by stem cells are direct cardiomyogenic/vasculogenic differentiation and indirect stimulation of the reparative response through paracrine effects [49]. Human induced pluripotent stem cells (hiPSCs), as an important cell therapy choice, are widely used in experimental or clinical treatment for various ischemic diseases [50]. Multiple researches have demonstrated that hiPSCs are able to reduce the infarct size, inhibit tissue fibrosis,

improve cardiac function and increase ejection fraction. For example, Zhang et al. prepared a 3D fibrin patch combined with three kinds of hiPSCs-derived cells (cardiomyocytes, smooth muscle cells, endothelial cells) loaded with IGF1, which was injected into infarcted porcine hearts. There are significant improvements in myocardial contractile quality, wall stress and metabolism, demonstrating that the hiPSC treatment can promote myocardial repair and enhance heart function [51]. Likewise, Cheng et al. injected a hydrogel containing iPSCs-derived cardiac progenitor cells into a porcine MI model via intrapericardial injection, which was then formed a patch-like mold in the pericardial cavity, leading to a desirable cardiac regeneration and repair after 4 weeks of treatment [52].

MicroRNAs (miRNA) are a class of noncoding single-stranded RNAs of about 22 nucleotides in length encoded by endogenous genes, which can regulate gene expression, cell cycle, and developmental timing of organisms. Some miRNAs can alleviate important pathological consequences of MI [53]. Recent progresses have shown the potential of miRNA in MI treatment by stimulating neovascularization. For example, Yang et al. used functionalized mesoporous silica nanoparticles (MSNs) loaded with microRNA-21-5p, which were loaded into an injectable hydrogel to prepare a miRNA delivery system. In response to the local acidic microenvironment, a sustained release of microRNA-21 to the injection site was achieved. In a porcine MI model, microRNA-21-5p delivery to endothelial cells via MSNs remarkably promoted local neovascularization and decreased cardiomyocytes apoptosis [54].

12.3 Mechanical Support

In some patients, left ventricular wall will become thin and dilate, forming a ventricular aneurysm [55]. According to Laplace theorem [56], the stress of the ventricular wall is inversely proportional to the thickness of the cardiac wall; thus, the dilatation and thinning of the left ventricular wall further increase the stress in the ventricular wall. This vicious cycle leads to expansion of necrosis and fibrosis [57].

Mechanical signals during ventricular remodeling are sensed by cardiac cells including cardiomyocytes and fibroblasts, and converted into transcriptional responses [58]. Transcriptional levels of mechanosensing genes including Piezo1 and Piezo2 are significantly increased in patients with ischemic cardiomyopathy compared to control. Correspondingly, the expression of cardiac contraction genes is down-regulated [44]. Therefore, the mechanical environment in the myocardium needs to be fixed to fully repair the infarcted heart.

12.3.1 Decreasing Mechanical Load

As the LV dilates and LV wall becomes thinner, the stress and mechanical load in the infarct areas significantly increase [59]. Injectable hydrogels implanted into the myocardium and cardiac patches placed on epicardial surface could increase the thickness of myocardium, hence decrease the stress, strain, and mechanical load in the LV myocardium, and break the aforementioned vicious cycle.

Decreasing mechanical load in myocardial infarct regions is desirable for heart with thinning left ventricular walls. The range of the stiffness for the native myocardium is ~20–100 kPa [60]. When stretched at 30% strain along the circumferential direction of the myocardium, the strain in the acute infarct region is higher than the strains in remote healthy regions. Biomaterials including hydrogels and cardiac patches for decreasing mechanical load of myocardial tissue must fulfill specific mechanical requirements of native myocardium to prevent mechanical mismatches that may impair heart function [61]. Wall et al. simulated the mechanical effects of injecting a noncontractile material into ovine LV myocardium with an anteroapical infarct using a finite element model [62]. The injectate reduces pathological wall stress in a volume, stiffness, and position-dependent manner, particularly in the border zone myocardium. Lin et al. studied how viscoelastic patch with different stiffness and viscosity affected the heart cycle on a simplified left ventricle [63]. At working frequency, the stroke volume dropped promptly as the order of magnitude of G''/G' (the ratio between the loss and storage modulus) approached 10^{-1}. When G''/G' is near 10^{-1}, the ventricle has a longer exposure to the lowered stroke volume under initial prestretch during the equilibration process. It is desirable to have $G''/G' \sim 1$ for a wider frequency range, which can be satisfied at the gel point [64]. A material near the gel point can not only provide necessary fluidity, but also avoid excessive dissipation.

As shown in *in vitro* tensile experiments, injectable hydrogels and cardiac patches significantly reduce the stress and strain in both longitudinal and circumferential directions of LV wall [65, 66]. Cardiac function and geometry are preserved in hydrogel- or patch-treated hearts compared to untreated ones. In addition, the expression of mechanosensing genes including Piezo1/2 and Angiotensin II is significantly lowered down, whereas the decreased expression level of cardiac contraction genes is also restored [67]. These results confirm the key role of mechanical effects in the progression of pathological LV remodeling, and the mechanical support from biomaterials can mediate such effects.

The hydrogel materials are desirable to be stiff, degradable, and compatible with minimally invasive injection approaches [68]. Some common natural hydrogels made from collagen [69], fibrin [70], decellularized extracellular matrix (ECM) [71], chitosan [72], and alginate [73] are used for cardiac tissue engineering. Potential drawbacks for these materials include rapid degradation, long gelation time, and poor mechanical properties [74]. By altering the compositions, structures, and processing of hydrogels, their mechanical strength, porosity, degradation rate, gelation rate, and other properties can be modulated. Polyethylene glycol (PEG) is a

synthetic polymer, and its mechanical properties can be more easily modulated compared to natural polymers. Chow et al. [75] copolymerized PEG acrylate with PEG dithiol to develop a degradable hydrogel with mechanical properties similar to the normal infarcted myocardium. Poly(N-isopropylacrylamide) (PNIPAAm), a thermosensitive water-soluble homopolymer, has been used in conjunction with carbon nanotubes (CNTs), an attractive combination for cardiac engineering in particular due to the conductive abilities and strong mechanical properties of CNTs [76]. GelMA hydrogels can be tailored by modifying the amount of methacrylic anhydride, which can provide the hydrogels with considerable strength and stiffness [77].

Injectable hydrogels have been tested in clinical trials. In one clinical study used IK-5001 device, injectable acellular alginate-based hydrogels were tested in 27 MI patients. All patients were treated with the hydrogel and all tolerated the procedure, with no adverse events. Moreover, echocardiographic results demonstrate that the left ventricular (LV) indices and the LVEF are preserved [78]. Hydrogel with alginate as the main component has been applied in clinical trials. Its therapeutic potential of inhibiting the injury process after MI has been proved in phase I and Phase II clinical trials, and the safety of implantation has been effectively verified [79–81]. Injection of Algisyl-LVR [82] was used for the first time in patients who had symptomatic heart failure. In all patients, the cardiac function of the left ventricle (LV) was improved significantly, as manifested by consistent reduction of the LV volume and wall stress through finite element method [83]. Zhu et al. [52] demonstrated the feasibility of minimally-invasive intrapericardial injection in a clinically-relevant porcine model to deliver therapeutic-bearing hydrogels to the heart for cardiac repair.

Biomaterials-based cardiac patches can be categorized into two types according to the sources of materials including natural materials and synthetic materials. The natural materials for cardiac patches include proteins (collagen, fibrin, and gelatin), polysaccharides (alginate, chitosan, and hyaluronic acid), and decellularized tissues. Some groups adopted natural tissues such as peritoneum and muscle tissue to prepare cardiac patches. Fibrin materials have a nanometric fibrous structure similar to native ECM [84]. A clinical trial was performed to investigate the feasibility of the surgical procedure, revealing the effectiveness of the fibrin patch loaded with human ESC-derived cardiac progenitor cells in clinical applications [85]. Instead of open-chest surgery, Tang et al. [86] explored a way to apply cardiac patches by spray-painting platelet and fibrin *in situ* onto the heart. The spray method is beneficial in reducing fibrosis and improving cardiac function. With divalent and trivalent ions such as Ca^{2+}, the cohesive nature of alginate allows it to be compressed into the form of patch [87]. The decellularized tissue-based patches showed a high integration with host cardiac tissues, as characterized by the observation of neovascularization in the host myocardium [88]. The stiffness of most natural materials ranges in tens of Pa, so patches are hard to tolerate the stress exerted by ventricle. Mechanical properties of synthetic materials are usually higher, and batch-to-batch variability is usually lower compared to natural materials [89]. Among the synthetic materials, polyurethane (PU) and poly(glycerol sebacate) (PGS) have relatively higher

biocompatibility. Wagner et al. [90, 91] studied biodegradable polyester urethane urea (PEUU) patches. After being applied onto the infarcted myocardium, the PEUU patches promoted the formation of smooth muscle, induce muscle cellularization, attenuate LV adverse remodeling, and improve contractile function. Chen et al. [66] found that the Young's modulus of PGS synthesized at 110, 120, and 130 °C ranges from tens of kPa to several MPa, which well meets the mechanical requirements of the materials applied for cardiac patches. Cardiac patches can be fixed to the myocardium by suturing [92], adhesion [93], and microneedles [59]. Compared to suturing and adhesion, the microneedle fixation is a facile and safe suture-free technology for patch implantation. Lu et al. [59] developed a self-interlocking patch which provides a mechanical support close to sutured patch. The circumferential and longitudinal strains in the infarct are reduced to 12.3% and -3.5%, respectively.

12.3.2 Assisting Cardiac Output

As a result of myocardial infarction, the cardiac output is impaired, leading to disproportion between blood supply and demand [94, 95]. Drugs including sodium nitroprusside [96], dobutamine [97], milrinone [98], sacubitril/valsartan [99], and levosimendan [100, 101] are employed to increase cardiac output, but with consequent side effects. For instance, cyanide toxicity is a complication of sodium nitroprusside administration [102], calcitropes such as dobutamine may increase myocardial oxygen demand and cause arrhythmias [98]. Mechanical devices are widely used as alternatives to enhance cardiac output, and the physical mechanisms vary depending on the type of devices.

Temporary circulatory support (TCS) devices are used to enhance cardiac output in treatment for heart failure after myocardial infraction. Current commercially available devices include intra-aortic balloon pump (IABP), Impella, and TandemHeart. IABP has been widely used for five decades. First, the balloon is placed in the descending thoracic aorta. The balloon inflates and increases the volume in the aorta during diastole, causing the peak diastolic pressure to rise and coronary blood flow to increase. Subsequently, the balloon deflates during systole, the aortic volume decreases and results in reduction in the afterload with subsequent improved unloading of the left ventricle (Fig. 12.2) [103]. However, some passive clinical results, including a failure to significantly reduced 30-day mortality in patients with AMI complicated by cardiogenic shock [104], cause the recommendations for an IABP guideline downgrading in treating acute myocardial infarction.

Impella is a kind of percutaneous temporary circulatory support device that is mainly composed of a motor pump and a pigtail catheter. It is inserted via the femoral artery, and the pigtail catheter is positioned across the aortic valve in a retrograde way, where left ventricular blood is delivered to the proximal aorta by the pump. This device works by decreasing left ventricular size, pressure, wall tension, and oxygen consumption [105].

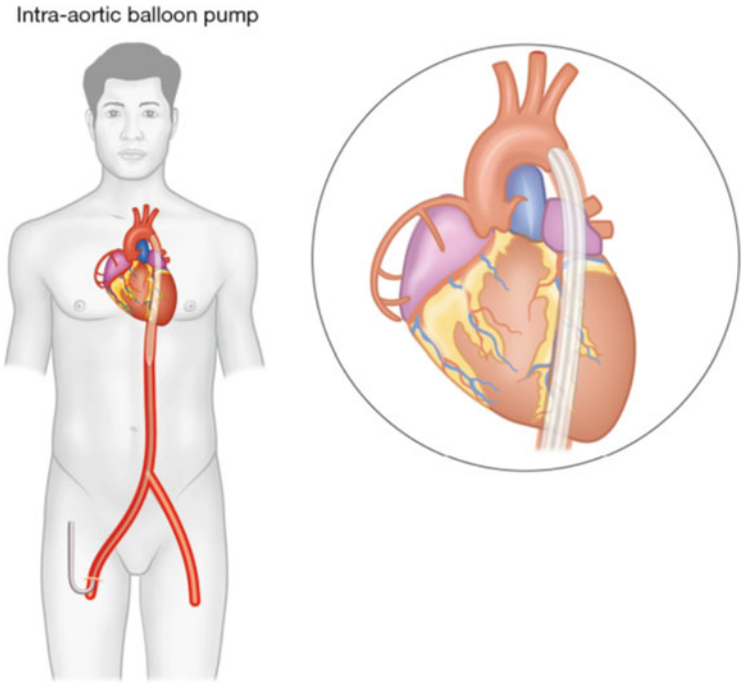

Fig. 12.2 Intra-aortic balloon pump schematic [106] (Reprinted from [106] with permission, copyright 2020 AME PUBL CO)

Similar to Impella, TandemHeart is a percutaneous ventricular assisting device (VAD) consisting of drainage and return cannulas, a centrifugal pump, and a console regulating the pump. The drainage catheter is usually inserted via the femoral vein into the right atrium and placed in the left atrium by using a trans-septal approach [106]. The TandemHeart increases cardiac output and mean arterial pressure, and decreases cardiac filling pressure by venting the left atrium [107]. However, retrograde aortic blood flow increases left ventricular afterload, potentially diminishing the beneficial effects of this device [108].

LVAD (left ventricular assist device) is employed for extended mechanical circulatory support, which has two basic patterns of perfusion, including the pulsatile and continuous-flow devices. The development of LVAD can be divided into three stages. The first-generation devices simulate the natural perfusion by using pulsatile pumps, but have significant limitations including limited durability, extensive surgery for implantation, large external lead, and audible pump [109, 110]. The second-generation devices replace the pulsatile pumps with axial-flow pumps to provide continuous blood flow, thereby providing better organ perfusion and superior durability than the first generation. Continuous-flow LVADs have several basic components including the inflow cannula, outflow cannula, internal pump, percutaneous driveline, controller, and power source. The inflow cannula placed in the LV delivers

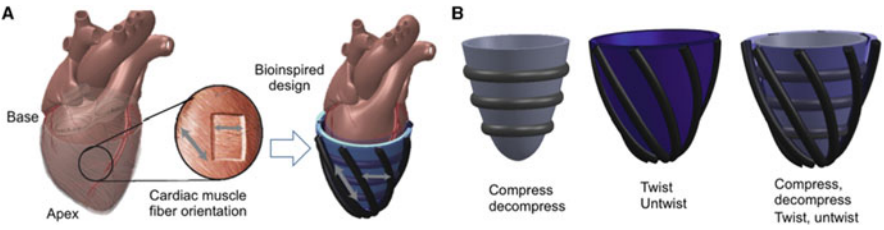

Fig. 12.3 (**a**) The muscle fiber orientations of the outer two layers of the myocardium of the heart inspire the design of the VAD. (**b**) Individual active layers composed of fluidic actuator contractile elements arranged and embedded in soft matrices can compress and decompress, twist and untwist, or simultaneously perform both actions [113] (Reprinted from [113] with permission, copyright 2017 Science)

blood from the LV cavity to the pumping chamber and subsequently carries blood from the pump chamber to the aorta. The primary difference between the third-generation and the second-generation devices is the design of pump. The third-generation devices use centrifugal pumps instead of axial-flow pumps to deliver blood based on centrifugal mechanism. Compared to the second generation, the third-generation LVADs have a noncontact bearing design, thereby are better at durability. It is known that excessive shear stress activates platelets. The centrifugal pumps allow lower shear in working process, and substantially reduce the chance of stroke and pump thrombosis [111].

The LVADs contact with blood, thus continuously activate the coagulation system, posing risks of embolization. Therefore, devices that do not contact with blood are highly desirable. The concept of DCC (direct cardiac compression device) was introduced more than 50 years ago to prevent any contact with blood by compressing the failing heart from its external surface (the epicardium) [112].

Walsh et al. [113] designed a tethered implantable sleeve (Fig. 12.3) based on soft robotic techniques that can provide circulatory support for patients with impaired heart function. Normally, myocardium simultaneously undergoes twisting and compressive motions. Soft pneumatic artificial muscles (PAMs) are oriented in helical and circumferential patterns to simulate the two outer layers of the myocardial fibers of the heart to replicate cardiac motion. Silicone and thermoplastic polyurethane (TPU) are used to fabricate PAMs, and alginate polyacrylamide hydrogel is introduced between device and tissue as a protective layer which can minimize inflammation and reduce friction when the device moves over the heart. The cardiac output is reduced to about 45% of baseline when acute heart failure happens in a porcine model induced by fusing esmolol, then recovers to about 97% of baseline when the soft robotic sleeve is initiated. This study demonstrates the potential for soft robotic techniques applied in supporting heart function, but long-term safety and efficacy are yet to be verified.

Gu et al. [114] combined permanent magnets and patches to provide powerful actuation assisting native heart pumping inside a magnetic actuation system (Fig. 12.4). Each magnetically active cardiac patch (MACP) is composed of an NdFeB magnet, a magnet housing, and a 3D-printed patch to fix on the epicardial

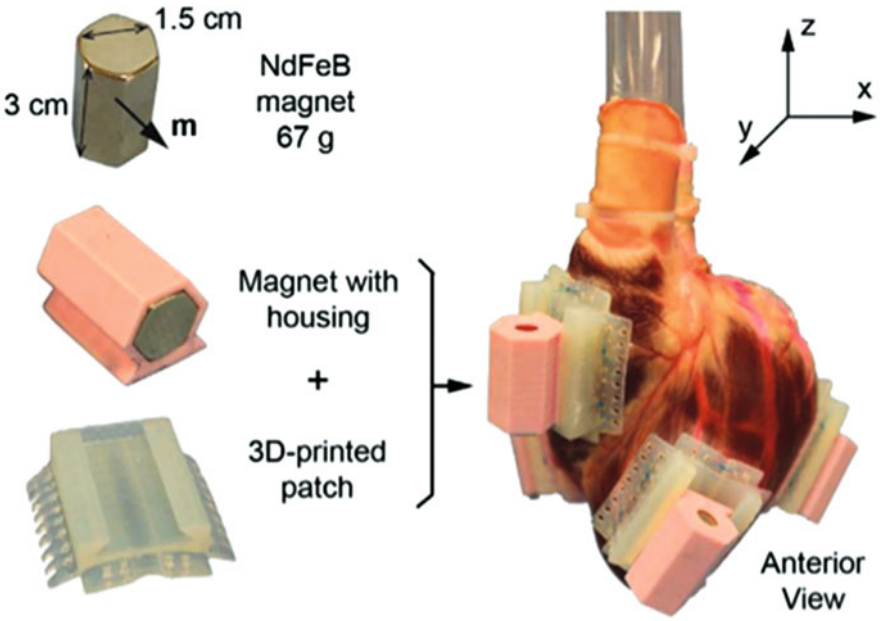

Fig. 12.4 Schematic illustration of functioning MACP [114] (Reprinted from [114] with permission, copyright 2021 Wiley)

surface. The magnet housing and patch are made of polylactic acid (PLA) and durable resin (FLDUCL02), respectively. When preprogrammed dynamic magnetic fields are applied to the MACPs, the patches will compress the heart in a predetermined way. It is shown that EFs reach 37% in the left ventricle and 63% in the right ventricle on a healthy pig's heart *in vitro*. However, this system could be further optimized, for example, exploring phase differences to increase the volumetric output of the heart, and developing new methods to adhere the patches on the heart in a less invasive way instead of surgical sutures.

Zhou et al. developed an active hydraulic ventricular attaching support system (ASD) to overcome the major limitations of prior devices by combination and optimization of existing treatment means [115]. As shown in Fig. 12.5, ASD is a net cover composed of interconnected hollow flexible tubules. Apertures on the side facing the epicardium can be introduced into the tubules to release the therapeutic materials filled in hollow tubules. In addition, ASD tubules can be packed with fluid and connected to external pneumatic pump for exerting continuous pressure on the ventricles to provide physical pressure. ASD is implanted via a median-sternotomy and pericardiotomy, and placed over the heart to entirely enclose both ventricles and to protect the atrioventricular (AV) groove from interrupted sutures [116]. The latest experiments in a rat heart failure model indicate that the ASD can improve cardiac function and prevent ventricular remodeling [117]. However, further experiments

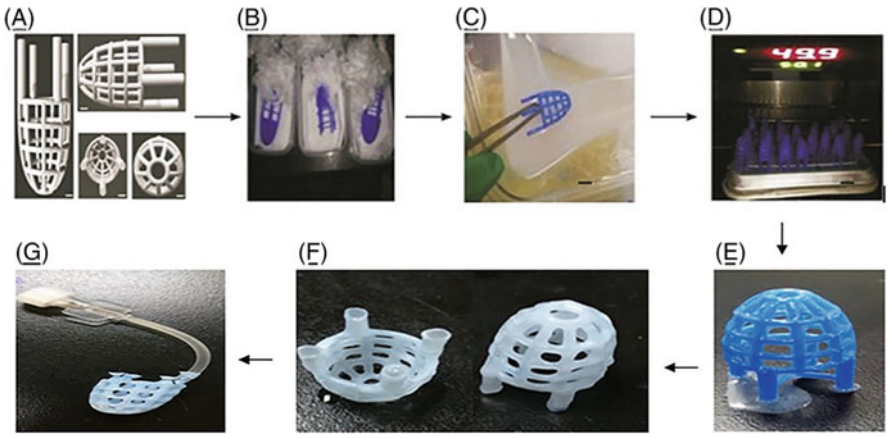

Fig. 12.5 The ASD device. (**a**) 3D model of ASD, (**b**) 3D blue wax model, (**c**) wax model of ASD was plunge into liquid silicon, (**d**) model put into oven for 1 h at 50 °C, (**e**) blue wax start melting from the ASD model at 100 °C for 30 min, (**f**) ASD from pure silicon, and (**g**) ASD connected with implantable catheter, scale bar 100 μm [118] (Reprinted from [118] with permission, copyright 2019 Wiley)

should also be conducted to study whether the pathologic remodeling persists or not after the termination of restraint therapy.

12.4 Restoration of Electrical Signal Conduction

Due to the limited regenerative capacity of myocardial cells [119], heterogeneous fibrous tissue will gradually replace the infarcted myocardium after suffering MI, including the embedded cardiac conduction system. In many patients, the infarct is structurally featured with scattered clusters of surviving myocardial cells in the scar tissue, leading to reentrant and low conduction velocity of electrical singal. As a result, the infarcted myocardium could not maintain normal excitation-contraction coupling and electrical signal transduction, causing arrhythmia impairment in cardiac pumping function, which is a major short-term risk in MI patients. Therefore, reconstructing cardiac conduction in the infarct is highly desirable and may generate synergic effect together with mechanical support.

At present, the main method of clinical treatment for arrhythmia is radiofrequency catheter ablation (RFCA). RFCA is a minimally invasive therapy that sends the mapping and ablation electrode catheter into the heart through blood vessel, release the controllable radiofrequency current locally, and dehydrate the myocardial tissue causing tachycardia and dry necrosis, thus blocking the abnormal electrical activity to achieve the therapeutic purpose [120]. However, the above methods can not directly improve the electrical conductivity of myocardial infarction area. A promising strategy to reduce the risk of arrhythmia is to use conductive biomaterials to

assist electrical signal propagation and synchronize discrete myocardial tissue. There are two main strategies to implant conductive biomaterials, which are direct injection of biomaterials into the MI area and fixation of biomaterials on the surface of the myocardium.

Common conductive biomaterials mainly include intrinsic conductive polymers, carbon-based nanomaterials, and metal nanomaterials. Intrinsically conductive polymers are synthetic polymers with conductive properties. The delocalized electrons move along their conjugated main chains, forming a large number of movable charge carriers (electrons or holes) in the molecular chains to achieve conductivity. The intrinsic conductive polymers in cardiac tissue engineering include polypyrrole (PPy), polyaniline (PANi), polythiophene (PTh), and their derivatives [121–123]. The carbon-based nanomaterials are a kind of biomaterials with unique structure and physical and chemical properties. Graphene, carbon nanotubes (CNTs), fullerenes and carbon dots [124–126] are the most popular carbon materials in cardiac repair. The metal nanomaterials have remarkable conductivity, and their high surface free energy allows them to be easily modified. Gold, silver and their related alloys are also commonly used as conductive biomaterials in biomedical applications. They are usually in nanometer size, such as nanotubes/nanowires [127], nanorods [128], and nanoparticles [129].

12.4.1 Conductive Injectates

Injectable hydrogels have received extensive attention in the field of MI treatment and cardiac tissue engineering, because they can provide mechanical support and be functionalized to reduce necrosis, suppress inflammation and fibrosis, and promote angiogenesis [130]. Conductive hydrogels, cardiac patches, conductive nanofibrous membrane and porous conductive scaffold have been developed so far [131] to transmit electrical signals across the necrotic zones and connect the remaining contractile myocardium in the infarct.

The conductive hydrogels are mainly fabricated by mixing conductive components into hydrogel substrate such as carbon-based nanomaterials or metal nanoparticles. Nikkhah et al. fabricated UV-crosslinkable gold nanorods (GNR)-incorporated gelatin methacrylate (GelMA) hybrid hydrogels for myocardial regeneration and repair (Fig. 12.6a). The conductive structure of hybrid hydrogels promoted intercellular signal transmission and electrical signal transmission, which increased the expression of Cx43 gap junction and synchronous calcium signal transmission in myocardial cells. Notably, compared to pure GelMA hydrogel, cardiomyocytes grown on hybrid hydrogels showed more robust synchronized contraction behavior [128]. Ramezani et al. added carbon nanofibers into collagen to make the Col-CNF nanocomposite. The Col-CNF can significantly improve the repair of damaged cells without causing inflammation or toxic reaction, because the Col-CNF is a conductive, biocompatible material that can lead to new blood vessels [132]. Li et al. incorporated activated-graphene oxide (GO) into silk fiber hydrogel

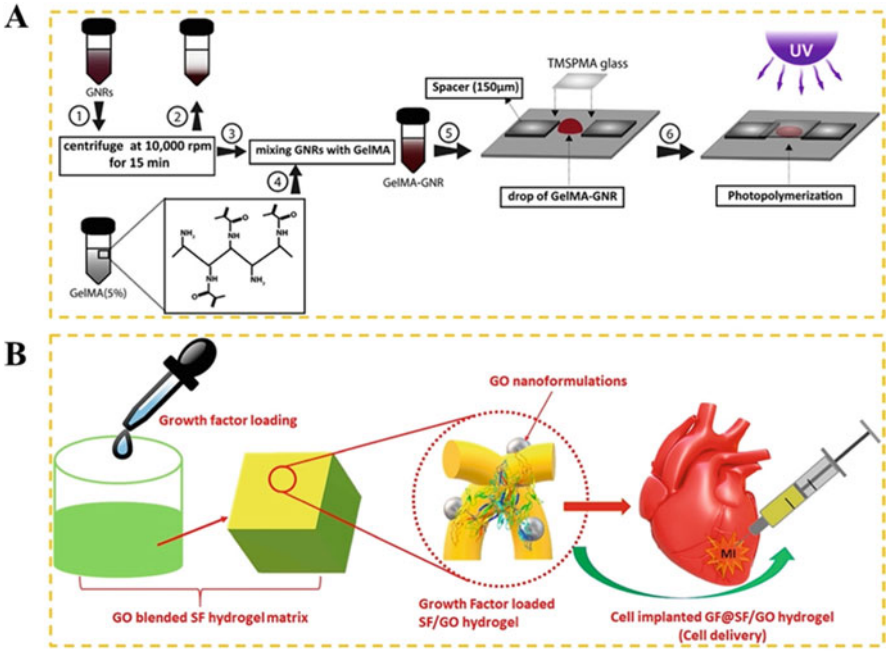

Fig. 12.6 (**a**) Schematic illustration of the fabrication procedure of GelMA-GNR hybrid hydrogel construct [128]. (Reprinted from [128] with permission, copyright 2016 Elsevier). (**b**) Schematic representation of the structure of hydrogel network with GO nanoformulations and growth factors and its application in MI [133] (Reprinted from [133] with permission, copyright 2020 Elsevier)

and combined the composite with stem cells (Fig. 12.6b). The conductive scaffold not only improved cell survival and LV wall thickness, but also decreased scar area [133].

Another method of preparing conductive hydrogel is combining conductive components with hydrogel substrate through chemical and/or physical crosslinking [134], where the conductive components mainly include intrinsically conducting polymers, piezoelectric polymers and conjugated conductive polymers. Li et al. grafted pyrrole onto chitosan by chemical oxidative polymerization to prepare the polypyrrole (PPy)-chitosan conductive hydrogel (Fig. 12.7a) [135]. Compared to chitosan alone, neonatal rat cardiomyocytes on the PPy-chitosan hydrogel exhibited enhanced Ca^{2+} signal transduction. The hydrogel can also improve the electrical coupling between skeletal muscles, indicating that PPy-chitosan can electrically connect the contraction cells. Electrocardiogram results showed that the QRS interval of rats injected with the PPy-chitosan polymer is shortened, and the lateral activation rate was increased, proving that the conductivity was improved. Also, echocardiography proved that the index of cardiac function (ejection fraction and fraction shortening) is improved 8 weeks after injection. Wang et al. successfully synthesized biodegradable poly(L-lactide)-b-poly(ethylene glycol)-b-poly

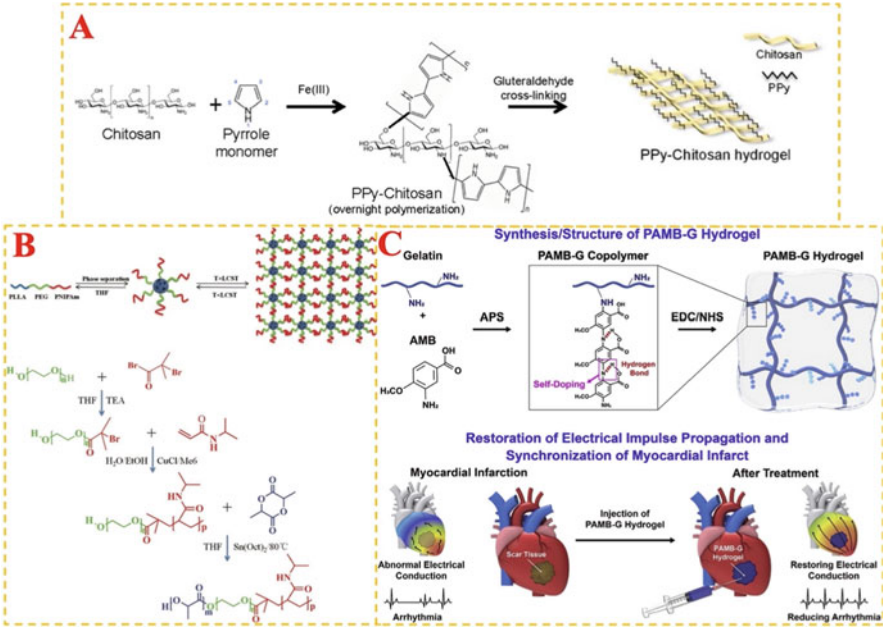

Fig. 12.7 (**a**) Schematic outlining the grafting of PPy monomers to chitosan and subsequent cross-linking to form a hydrogel [135]. (Reprinted from [135] with permission, copyright 2015 Lippincott Williams & Wilkins). (**b**) Triblock PLLA-PEG-PNIPAm copolymers and nanofibrous gelling microspheres (NF-GMS) [136]. (Reprinted from [136] with permission, copyright 2020 Wiley). (**c**) Synthesis and structure of PAMB hydrogel and mechanism of its restoring electrical impulse propagation and synchronizing myocardial contraction following a myocardial infarction [137] (Reprinted from [137] with permission, copyright 2020 Elsevier)

(N-isopropyl acrylamide) (PLLA-PEG-PNIPAm), a kind of piezoelectric polymer that could form a hydrogel (NF-GMS) *in vivo* after injection (Fig. 12.7b) [136]. Animal experiments proved that the NF-GMS with CM can significantly reduce infarct area, stimulate angiogenesis in the infarct, and restore the cardiac function. Li et al. synthesized a conductive polymer, poly-3-amino-4-methoxybenzoic acid (PAMB), which was grafted onto nonconductive gelatin (PAMB-G) (Fig. 12.7c) [137]. Microelectrode array (MEA) analysis showed that the hearts placed on PAMB-G hydrogel had a higher field potential amplitude compared to the hearts placed on gelatin, and can transfer current from one heart to another in the distance. After MI in the rat heart, PAMB-G hydrogel injected into the infarct area significantly promoted the transmission of current in the scar area, and enhances the synchronous contractility of the myocardium, thus protecting ventricular function and reducing arrhythmia.

12.4.2 Conductive Epicardial Bridges

The conduction of electrical signals in myocardium is directional and anisotropic. Hydrogels, particularly injectable hydrogels, usually do not have anisotropic features alike native myocardium and thus are intrinsically limited in fully restoring both speed and direction of myocardial conduction. In contrast, conductive cardiac patches prepared by electrospinning, film casting, 3D printing and other technologies can be endowed with anisotropy [138]. Although only fixed to epicardium, the patches are more continuous, cover a larger area, and have less damage to the myocardium. The conductive cardiac patches can bypass the abnormal area with conduction failure or slowness in the damaged myocardium, prevent arrhythmia, and restore normal electrical conduction [139].

Similar to conductive hydrogels, the common conductive components used to fabricate conductive patches are intrinsically conductive polymers, carbon-based nanomaterials and metal nanomaterials. Zhang et al. deposit reduced graphene oxide (rGO) on electrospun silk fibroin fiber to prepare conductive cardiac patches (rGO/silk$_{A/R}$) with anisotropic conductivity (Fig. 12.8a) [140]. The anisotropic conductive rGO/silk$_{A/R}$ patch was efficient in repairing the infarcted myocardium compared to the nonconductive silk and the isotropic conductive silk. The conductive patch can significantly improve the cardiac function, survival rate of functional myocardial cells, and resistance to ventricular fibrillation to reduce the myocardial remodeling after infarction. This study proved that effective biomimetic myocardial microenvironment reconstruction based on anisotropic conductive patch biomaterials is a promising choice to promote the repair post MI. Santos et al. combined poly (glycerol sebacate) (PGS), collagen, and PPy to prepare composite cardiac patch by an evaporation method (Fig. 12.8b). In addition, the conductive patches showed higher blood wettability and faster drug release, and can induce cell signal transduction [141].

The mechanical and conductive anisotropy of conductive patches can also be realized through the design of micro patterns. Steven et al. used excimer laser micro cutting to micropattern honeycomb structure on chitosan films with PAN coating (AuxCP) [142]. The obtained conductive cardiac patches had a negative Poisson's ratio. A broad range of mechanical strength and electrical anisotropy can be achieved, which allows adjustment to match the natural heart tissue. The AuxCP significantly increased the conduction velocity of the infarcted myocardium. Rat MI model results showed that the conductive patch integrated well with natural heart tissue *in vivo*, had negligible adverse effect on cardiac function, and did not cause severe fibrosis reaction [142].

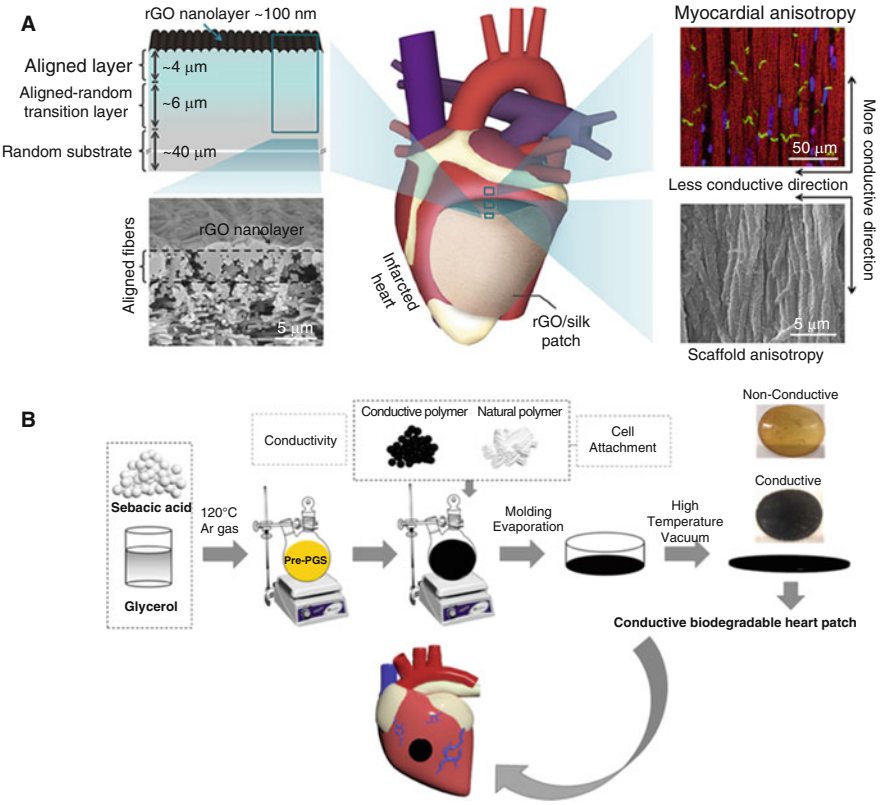

Fig. 12.8 (**a**) Schematics illustrating the fabrication of rGO/silk$_{A/R}$ scaffolds and their application in restoring electrical integrity in infarcted myocardium [140]. (Reprinted from [140] with permission, copyright 2022 Elsevier). (**b**) Schematic illustration of the steps used for the synthesis of conductive and elastic biodegradable cardiac patches by an evaporation method [141] (Reprinted from [141] with permission, copyright 2020 American Chemical Society)

12.5 Mediation of Inflammation, Immune Responses, and Metabolism

Inflammation is the body's natural and fundamental response to signals of tissue damage or pathogenic infection [41]. Sudden cardiomyocyte death caused by myocardial infarction rapidly activates the innate immune pathway, which triggers a strong but transient inflammatory response. Moderate inflammation facilitates the removal of dead cells and extracellular matrix debris and can be suppressed by subsequent repair process [143]. However, excessive inflammation increases the risk of heart failure.

In the early stages of myocardial infarction, danger signals released from damaged cardiomyocytes or pathogens are recognized by innate immune pattern

recognition receptors including Toll-like receptors (TLR) expressed on innate immune cells [144] such as monocytes, macrophages, and neutrophils. Upon binding to extracellular damage-associated molecular patterns (DAMPs), TLR activates cytoplasmic adaptor molecules, which initiates a series of activation pathways, including nuclear factor-κB (NF-κB), interferon regulators, and mitogen-activated protein kinase (MAPK) pathway. It will then lead to the production of proinflammatory cytokines such as tumor necrosis factor (TNF), interleukin-1β (IL-1β) and IL-6 and chemokines through transcriptional and posttranscriptional mechanisms [145]. The upregulation of TLR induces the synthesis of adhesion molecules in endothelial cells and activates leukocyte integrin, which mediates strong adhesion interactions and ultimately leads to the recruitment of inflammatory cells into infarcts [146].

During the inflammation of myocardial infarction, resident immune cells in the myocardium are activated to produce cytokines, chemokines, proteases, growth factors, and free radicals [147]. Circulating immune cells then adhere on the inflammatory site via endothelial cells to enhance the proinflammatory response as mentioned above. If the response is insufficient or excessive, it would disrupt the balance between the innate and adaptive arms of the immune system, leading to late inflammation. This dysregulated immune response leads to a catastrophic cascade characterized by local or systemic tissue damage. In addition to TLR, the immune cells possess NOD-like receptors (NLR) that specifically recognize pathogenic patterns in the cytoplasm, leading to inflammasome-mediated activation of proinflammatory cytokine release. This results in the degradation of cytokines and oxidative damage to cells [148–150]. Macrophages in myocardial infarction are primarily responsible for eliminating apoptotic neutrophils and controlling inflammatory processes through phenotypic transformation. However, due to abnormal differentiation of macrophages and abnormal metabolism of neutrophils, the macrophages remain in the M1 phenotype and release excessive proinflammatory factors, leading to aggravated inflammation [151]. Programmed anti-inflammatory regulation fails, and abnormal neutrophils result in excess production of reactive oxygen and nitrogen species (RONS). RONS, including oxygen and nitrogen radicals such as superoxide anion radicals ($O_2 \cdot^-$), hydroxyl radicals (·OH), and nitric oxide radicals (·NO), are proinflammatory molecules that cause lipid peroxidation and oxidative stress. RONS activate IκB kinase, inhibit phosphotyrosine and phosphoserine/threonine phosphatases, thereby upregulating redox-sensitive NF-κB and further exacerbating inflammation [149]. This leads to poor angiogenesis and insufficient production of desirable growth factors.

In addition, the high demand for oxygen in healing tissues, coupled with persistent and overproduction of ROS, reduces oxygen utilization and micronutrient supply in injured tissues. This also affects cellular metabolism, which is a compilation of enzyme-catalyzed chemical reactions in cells and is essential to all living organisms [152]. The excessive inflammation results in an energy imbalance, oxygen imbalance, and redox imbalance in cellular metabolism.

12.5.1 Suppressing Inflammation

The inflammation can be controlled through ROS and some cell regulations. Concretely, the level of ROS may be regulated by endogenous or exogenous antioxidant mechanisms involving the action of antioxidants by inhibiting the production of ROS, eliminating excess ROS, stimulating various antioxidant enzyme systems, and accelerating the production of nonenzymatic antioxidants or delivering the antioxidants such as superoxide dismutase (SOD), catalase (CAT), and glutathione peroxidase (GPx) [153], ascorbate, α-tocopherol, and glutathione [154]. Fibroblasts and vascular cells, which are abundant in healing infarcts, may also help suppress inflammatory signals [155]. The acquisition of pericyte coating by angiogenic vessels in the infarcted heart may inhibit inflammatory activity, thereby stabilizing the microvasculature and preventing long-term leukocyte recruitment [156, 157].

The inflammation-inhibiting biomaterials mainly work through eliminating ROS, releasing anti-inflammatory agents, and/or providing mechanical support. A biodegradable elastic polyurethane polythioketal (PUTK) patch with ROS-responsive TK units was used for MI treatment in rats, showing myocardial protection effects (Fig. 12.9) [158, 159]. Upgraded PUTK films with antioxidant properties were

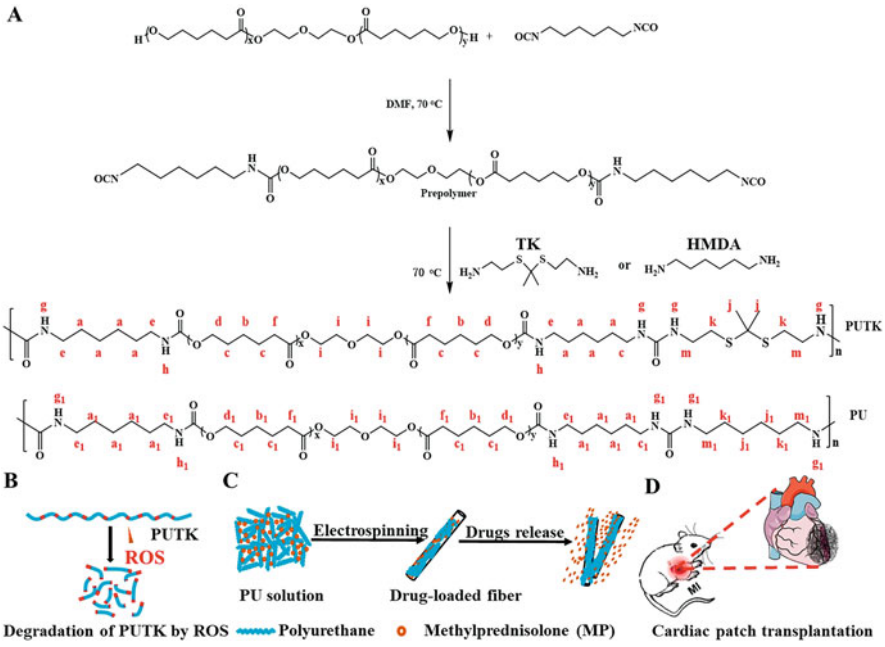

Fig. 12.9 Synthetic scheme for ROS-responsive polyurethane (PUTK) and nonresponsive polyurethane (PU) from poly(ε-caprolactone) diol, 1,6-hexamethylene diisocyanate, and chain extenders of ROS-cleavable thioketal (TK) and 1,6-hexanediamine (HMDA), respectively [158] (Reprinted from [158] with permission, copyright 2020 Elsevier)

synthesized using ascorbic acid (AA) as a chain extender. These patches support proliferation of C2C12 myoblasts and H9C2 cardiomyoblasts, reduce intracellular oxidative stress, scavenge free radicals, and alleviate ischemia-reperfusion injury [160]. A novel hydrogel that can effectively scavenge ROS with TK units and generate O_2 in a hypoxia and inflammatory condition was prepared for MI treatment, which could almost recover fully the important heart functions, as indicated by LVEF, left ventricular fraction shortening (FS), end systolic volume (ESV), and end diastolic velocity (EDV) without difference to those of the sham ones [143]. Together with the patches or hydrogels, anti-inflammatory agents can be delivered to the target site. After injection, the hydrogel can continue to release the therapeutic agents such as stem cells and exosomes to suppress inflammation [52]. In addition, the mechanical support from hydrogels and patches can relieve inflammation in infarcted myocardium by affecting mechanosensing [161].

12.5.2 Mediating Immune Responses

In the late stages of inflammation, the immune cells including regulatory T (Treg) cells and Th2 cells, together with regulatory M2-like macrophages, increase in number and resolve inflammation by producing anti-inflammatory cytokines, including transforming growth factor-β (TGF-β) and IL-10 [162, 163]. In fact, the cells do not need to be viable to mediate immune responses. Vagnozzi et al. reported that injecting freeze-thaw killed cells after ischemia-reperfusion injury resulted in the same functional improvement as injecting putative viable cells, suggesting that the proteins and genetic materials play a key role in promoting cardiac repair via mediation of immune response. On the other hand, the local injection of zymosan, a potent stimulant of innate immune system, is effective in treating cardiovascular diseases. This effect is attributed to the recruitment of $CCR2^+$ and $CX3CR1^+$ (M2-like) macrophages. In heart failure, CAR-T cells targeting activated cardiac fibroblasts and senescent cells reduced cardiac fiber burden [164].

In addition to affecting and recruiting immune cells, biomaterials that mimic immune cell functions also promote heart repair. The polylysine-modified polyurethane has the function of promoting M2 polarization and reducing inflammation *in vitro* and *in vivo* [165]. Tissue inhibitors of metalloproteinases, a family of endogenous MMP inhibitors expressed by immune cells including peripheral blood monocytes, B cells, and T cells, can suppress immune responses and inflammation by reducing immune cell penetration and/or alleviating MMP-induced matrix degradation [166]. Fan et al. prepared a hydrogel by fusing bFGF with glutathione-S-transferase (GST) and MMP-2/9 cleavable peptide PLGLAG (TIMP) to collagen. By inhibiting MMP-2/9 activities, the hydrogel mimics the TIMP secretion function of immune cells, resulting in attenuated ventricular wall thinning [167]. Moreover, polymer grids covered with extracellular matrix or rich in induced cardiomyocyte progenitors were applied in a mouse MI model. The grids promoted macrophage infiltration and polarization to M2 in the epicardium [168]. In addition, nanoparticles

that enhance immune tolerance have been used to modulate immune response. The nanoparticles-delivered antigen and rapamycin to dendritic cells (DC) can induce antigen-presenting tolerogenic dendritic cells (tDC) and antigen-specific Tregs. Intradermal injection of liposomal nanoparticles loaded with MI-associated antigens and rapamycin into MI mice elicited antigen-specific immune tolerance *in vivo* by generating antigen-specific Tregs in the infarct area and modulating macrophage polarization, thereby improving cardiac remodeling and function [169, 170].

12.5.3 Regulating Metabolic Activities

The heart uses energy in the form of adenosine triphosphate (ATP), but the heart muscle stores very little ATP; thus, ATP must be synthesized constantly. Cardiomyocyte metabolism involves the breakdown of nutrients, production of ATP (catabolism), and consumption of energy to synthesize complex molecules needed to perform cellular activities and energy storage (anabolic). Cardiomyocyte energy homeostasis is a cellular process that balances energy production and expenditure. Glycolysis and oxidative phosphorylation (OXPHOS) are two major metabolic processes by which cells convert nutrients into energy in the form of ATP to support biosynthetic activities. Maintaining oxygen homeostasis is essential for the survival and function of most cells because oxygen is required for the OXPHOS process of ATP production [152]. Common treatments of metabolic disorders work by inhibiting glycolysis with drugs such as dichloroacetic acid, metformin, or in the myocardial infarction, by the paracrine effects of stem cells that increase ATP and NADH levels, decrease oxidative stress, and increase phosphorylated -Akt and phosphorylated -GSK-3β [171].

Biomaterials strategies have been developed to balance cardiac metabolism. Dimethyl itaconate (DMI) is an enzyme involved in the metabolic tricarboxylic acid cycle (TCA), which can effectively inhibit mammalian succinate dehydrogenase (SDH), and reverse the electron transport chain in mitochondria [172]. In ischemia-reperfusion injury, accumulated succinate is rapidly oxidized by SDH, which drives the production of massive ROS through reverse electron transport at mitochondrial complex [173]. Due to the inhibitory effect of DMI on SDH, local delivery of DMI by a cardiac patch to the infarct prevented the mitochondrial ROS overproduction and promotes the recovery from pathological conditions. As a result, released DMI reduced infarct size and improved ventricular function by inhibiting inflammation in the early stage and promoting anti-inflammatory activity in the late stage for proper tissue repair.

12.6 Promotion of Cardiac Regeneration

The strategies mentioned above mainly focus on preventing pathological LV remodeling and heart failure [174]. Heart transplantation remains the final option for end-stage heart failure [49]. However, the number of heart donors is small compared to the patient population [175, 176], and the recipients need immunosuppression therapy [177]. On the other hand, it is found that terminally differentiated cardiomyocytes in adult human heart has the ability to proliferate, although highly limited [178, 179]. In addition, exogenous cardiomyocytes can integrate with the host heart. Therefore, heart regeneration becomes a theoretically achievable goal and potentially a viable approach to combat heart failure [40, 49, 180]. In this section, we shall discuss current biomaterials-based treatments to promote cardiac regeneration.

12.6.1 Delivery of Cardiac Cells Using Biomaterials

Noncardiac cells and cardiac-derived cells, including skeletal myoblasts, bone marrow-derived cells, mesenchymal stem cells (MSCs), cardiac stem cells (CSCs), and induced pluripotent stem cells (iPSCs), have been used for cardiac regeneration [174]. For example, skeletal myoblasts were utilized to remuscularize the damaged heart and restore cardiac function. The transplanted skeletal myoblasts can differentiate into a myogenic lineage, and then improve the ejection fraction in ischemic cardiomyopathies [181]. CSCs exhibit self-renewal and multipotent capacity to repair damaged hearts [182]. iPSCs can differentiate into functional cardiomyocytes *in vitro*, and then be transplanted into the heart [183].

However, as early clinical trials suffered from poor engraftment and differentiation, the priority is to improve their early retention and subsequent differentiation. Biomaterials in tissue engineering intends to create an appropriate microenvironment for cell therapies, promoting their survival, migration, proliferation and differentiation for better treatment. Biomaterials can impact cell-based therapies by their spatiotemporal modulation on cell microenvironments, which can direct cell behavior during their migration, differentiation, and regeneration in the microenvironment. Particularly, hydrogel scaffolds are attractive for stem cell delivery because they can improve the survival of transplanted cells or recruited endogenous cells to support cell-based treatment [184]. First, high-water content and tissue-like mechanical properties of hydrogels make them compatible with soft tissue. Furthermore, the porous structures of hydrogels are able to allow cell attachment and growth, as well as the "smart" release of biological agents at the injury site. Recently, Li et al. [185] showed that intrapericardial cavity (IPC) injection of adult mesenchymal stem cells in hydrogel is a promising solution for the low retention issue of MSCs at the infarction site (Fig. 12.10). Immunohistochemistry data reveal better cellular proliferation, less apoptosis, and better vascular regeneration in the myocardium after delivery of MSCs in hydrogel. In addition, they further demonstrated the feasibility

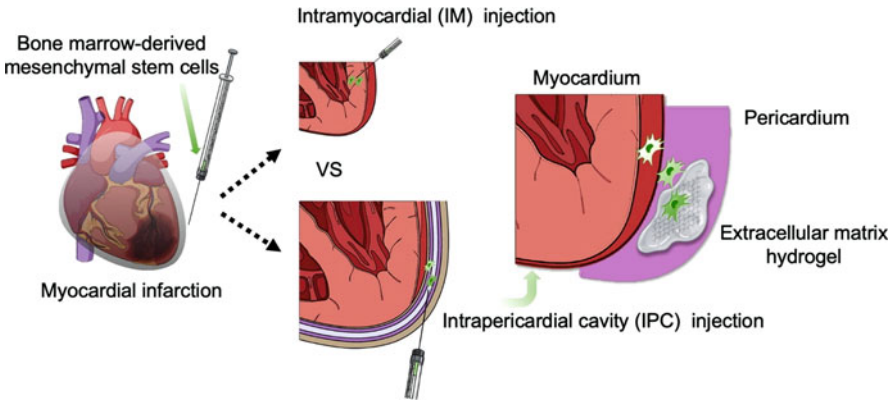

Fig. 12.10 Injection of GFP-MSCs into the pericardial cavity of infarcted mouse hearts is feasible and improves survival [185] (Reprinted from [185] with permission, copyright 2022 Elsevier)

and safety of IPC injection in a porcine model, the retention of MSCs was extended in the infarcted heart.

12.6.2 Delivery of Bioactive Factors

A lot of cellular functions are achieved via cell–cell communications based on bioactive factors including growth factors, microRNAs (miRNAs), and exosomes. Some of these bioactive factors can promote heart regeneration by activating signaling pathways that increase cardiomyocyte proliferation or suppressing signaling pathways that inhibit cardiomyocyte proliferation. For example, growth factor neuregulin 1 (NRG1) and its receptors, receptor tyrosine-protein kinase ERBB2 and ERBB4, play a critical role in cardiac development [186]. After the activation of the NRG1–ERBB2/ERBB4 signaling pathway, cardiomyocyte proliferation can be restarted in injured heart [187, 188]. Incorporating NRG1 and FGF1 within bioresorbable PLGA-MPs maintained growth factor levels in the ischemic myocardium in a rat MI model, leading to induction of tissue revascularization, activation of endogenous regeneration, and improvement in heart function [189].

RNA interference is a promising strategy for cardiac regeneration [190]. They mediate many processes in the damaged heart, including improving cardiomyocyte survival, promoting cardiomyocyte proliferation, inducing angiogenesis, and modulating cardiac repair. Adeno-associated virus 9 (AAV9)-mediated overexpression of mir-199a-3p and mir-590-3p can induce cardiomyocyte proliferation, stimulate cardiac regeneration and improve cardiac function [191]. Cardiomyocyte proliferation and heart regeneration are also induced by a cluster of mir-302/367 [192] via inhibition of Hippo/YAP signaling. Mir-34a [193], which was initially demonstrated to regulate the ageing process, is an important regulator of cardiomyocyte

proliferation and cardiac regeneration, so that inhibition of this miRNA leads to enhanced cardiomyocyte proliferation and cardiac regeneration in response to MI. Mir-26a [194] can promote angiogenesis by targeting relative antiangiogenic genes. Overexpression of mir-126 [195] can stimulate heart repair by improving survival and migration of transplanted mesenchymal stromal cells and proangiogenic bone-marrow-derived cells. Recently, mir-19a/b was proved to protect heart from MI and promote cardiomyocyte proliferation by inhibition of PTEN, a negative regulator of cardiomyocyte survival and proliferation [196]. Burdick et al. [197] developed an injectable supramolecular hydrogel to sustainably deliver mir-302 to the infarcted heart. The local and sustained release of mir-302 from hydrogels *in vitro* promoted cardiomyocyte proliferation over 2 weeks. Their findings suggest that hydrogel-based miRNA delivery systems can lead to improved outcomes via cardiac regeneration after myocardial infarction.

Despite the encouraging results, some preclinical studies revealed the risks associated with miRNA application. Mir-199a in infarcted pig hearts stimulates cardiomyocyte de-differentiation, proliferation and cardiac repair. After delivery of mir-199a, the treated pigs showed marked improvement in both global and regional contractility, increased muscle mass and reduced scar size [198]. However, the subsequent persistent and uncontrolled expression of the microRNA resulted in sudden arrhythmic death of most of the treated pigs. Such events were concurrent with myocardial infiltration of proliferating cells displaying a poorly differentiated myoblastic phenotype. These results show that achieving cardiac repair through stimulation of endogenous cardiomyocyte proliferation is feasible in large animals. However, dosage of this therapy needs to be optimized. There is still a long way for clinical translation. Therefore, to combat heart failure, it may require synergic therapeutic strategies. Li et al. [54] developed a microRNA-21-5p delivery system using functionalized mesoporous silica nanoparticles (MSNs). This system enabled on-demand microRNA-21 delivery in response to acidic microenvironment. The released complexes are able to mediate inflammatory response by inhibiting M1 polarization of macrophages. In addition, microRNA-21-5p delivery by MSNs promotes neovascularization and rescues at-risk cardiomyocytes. The synergy of anti-inflammatory and proangiogenic effects effectively reduce infarct size in a porcine model of myocardial infarction.

12.7 Conclusion

The immense potentials of biomaterials in promoting cardiac repair with respect to alleviating ischemia, providing mechanical support, restoration of electric signal conduction, mediation of inflammation, and promoting cardiac regeneration have attracted tremendous efforts. However, among the aforementioned strategies, only a few have been validated in clinical trials. More studies are required to demonstrate their safety and efficacy. The ultimate goal of regenerating damaged myocardium

and full restoration of cardiac function may be achieved by integrating and balancing the therapeutic effects of biomaterials designs.

Acknowledgments This work was supported by National Key Research and Development Program of China (2019YFE0117400), the National Natural Science Foundation of China (No. 82202328, U22A20155, 51873188), and the Key research and development program of Zhejiang Province (2022C01106).

References

1. Carrillo-Salinas FJ, Ngwenyama N, Anastasiou M, Kaur K, Alcaide P. Heart inflammation: immune cell roles and roads to the heart. Am J Pathol. 2019;189:1482–94.
2. Pascual-Gil S, Garbayo E, Diaz-Herraez P, Prosper F, Blanco-Prieto MJ. Heart regeneration after myocardial infarction using synthetic biomaterials. J Control Release. 2015;203:23–38.
3. Reed GW, Rossi JE, Cannon CP. Acute myocardial infarction. Lancet. 2017;389:197–210.
4. Gong FF, Vaitenas I, Malaisrie SC, Maganti K. Mechanical complications of acute myocardial infarction: a review. JAMA Cardiol. 2021;6:341–9.
5. Chang T, Liu C, Lu K, Wu Y, Xu M, Yu Q, Shen Z, Jiang T, Zhang Y. Biomaterials based cardiac patches for the treatment of myocardial infarction. J Mater Sci Technol. 2021;94:77–89.
6. Karantalis V, Suncion-Loescher VY, Bagno L, Golpanian S, Wolf A, Sanina C, Premer C, Kanelidis AJ, McCall F, Wang B, Balkan W, Rodriguez J, Rosado M, Morales A, Hatzistergos K, Natsumeda M, Margitich I, Schulman IH, Gomes SA, Mushtaq M, DiFede DL, Fishman JE, Pattany P, Zambrano JP, Heldman AW, Hare JM. Synergistic effects of combined cell therapy for chronic ischemic cardiomyopathy. J Am Coll Cardiol. 2015;66:1990–9.
7. Lee SH, Murthy HR, Langburt D. Stem-cell cardiospheres for myocardial regeneration: advancing cell therapy in myocardial infarction and heart failure. J Physiol. 2018;596:3839–40.
8. Heidenreich P. Inflammation and heart failure: therapeutic or diagnostic opportunity? J Am Coll Cardiol. 2017;69:1286–7.
9. Rane AA, Christman KL. Biomaterials for the treatment of myocardial infarction: a 5-year update. J Am Coll Cardiol. 2011;58:2615–29.
10. Stapleton L, Zhu Y, Woo YJ, Appel E. Engineered biomaterials for heart disease. Curr Opin Biotechnol. 2020;66:246–54.
11. Vasanthan V, Biglioli M, Hassanabad AF, Dundas J, Matheny RG, Fedak PW. The cormatrix cor™ patch for epicardial infarct repair. Futur Cardiol. 2021;17:1297–305.
12. Menasché P, Vanneaux V, Hagège A, Bel A, Cholley B, Cacciapuoti I, Parouchev A, Benhamouda N, Tachdjian G, Tosca L, Trouvin J-H, Fabreguettes J-R, Bellamy V, Guillemain R, Suberbielle Boissel C, Tartour E, Desnos M, Larghero J. Human embryonic stem cell-derived cardiac progenitors for severe heart failure treatment: first clinical case report: figure 1. Eur Heart J. 2015;36:2011–7.
13. Menasche P, Vanneaux V, Hagege A, Bel A, Cholley B, Parouchev A, Cacciapuoti I, Al-Daccak R, Benhamouda N, Blons H, Agbulut O, Tosca L, Trouvin JH, Fabreguettes JR, Bellamy V, Charron D, Tartour E, Tachdjian G, Desnos M, Larghero J. Transplantation of human embryonic stem cell-derived cardiovascular progenitors for severe ischemic left ventricular dysfunction. J Am Coll Cardiol. 2018;71:429–38.
14. Traverse JH, Henry TD, Dib N, Patel AN, Pepine C, Schaer GL, DeQuach JA, Kinsey AM, Chamberlin P, Christman KL. First-in-man study of a cardiac extracellular matrix hydrogel in early and late myocardial infarction patients. JACC Basic Transl Sci. 2019;4:659–69.

15. Lee RJ, Hinson A, Bauernschmitt R, Matschke K, Fang Q, Mann DL, Dowling R, Schiller N, Sabbah HN. The feasibility and safety of algisyl-lvr as a method of left ventricular augmentation in patients with dilated cardiomyopathy: initial first in man clinical results. Int J Cardiol. 2015;199:18–24.
16. Heusch G. Myocardial ischemia: lack of coronary blood flow, myocardial oxygen supply-demand imbalance, or what? Am J Physiol Heart Circ Physiol. 2019;316:H1439–46.
17. Cui H, Su Y, Wei W, Xu F, Gao J, Zhang W. How microalgae is effective in oxygen deficiency aggravated diseases? A comprehensive review of literature. Int J Nanomed. 2022;17:3101–22.
18. Zhu Y, Jung J, Anilkumar S, Ethiraj S, Madira S, Tran NA, Mullis DM, Casey KM, Walsh SK, Stark CJ, Venkatesh A, Boakye A, Wang H, Woo YJ. A novel photosynthetic biologic topical gel for enhanced localized hyperoxygenation augments wound healing in peripheral artery disease. Sci Rep. 2022;12:10028.
19. Juan B, Cabello JE, Garcia VR, Burls A. Oxygen therapy for acute myocardial infarction: a web-based survey of physicians' practices and beliefs. Emergencias. 2009;21:7.
20. Cabello JB, Burls A, Emparanza JI, Bayliss SE, Quinn T. Oxygen therapy for acute myocardial infarction. Cochrane Database Syst Rev. 2016;12:CD007160.
21. Loomba RS, Nijhawan K, Aggarwal S, Arora RR. Oxygen in the setting of acute myocardial infarction: is it really a breath of fresh air? J Cardiovasc Pharmacol Ther. 2016;21:143–9.
22. Caswell JE, Strange MB, Rimmer DM 3rd, Gibson MF, Cole P, Lefer DJ. A novel hemoglobin-based blood substitute protects against myocardial reperfusion injury. Am J Physiol Heart Circ Physiol. 2005;288:H1796–801.
23. Estep TN. Haemoglobin-based oxygen carriers and myocardial infarction. Artif Cells Nanomed Biotechnol. 2019;47:593–601.
24. Zhou W, Li S, Hao S, Zhang H, Li T, Li W, Liu J, Wang H, Yang C. Protective effect and mechanism of low p50 haemoglobin oxygen carrier on isolated rat heart. Artif Cells Nanomed Biotechnol. 2022;50:121–9.
25. Spahn DR. Artificial oxygen carriers: a new future? Crit Care. 2018;22:46.
26. Kuzmiak-Glancy S, Covian R, Femnou AN, Glancy B, Jaimes R 3rd, Wengrowski AM, Garrott K, French SA, Balaban RS, Kay MW. Cardiac performance is limited by oxygen delivery to the mitochondria in the crystalloid-perfused working heart. Am J Physiol Heart Circ Physiol. 2018;314:H704–15.
27. Qin X, Zhou Y, Wang Y, Wang Z, Wang Y, Chen J, Zhu L, Quan X, Liu Z, Zhang H, Jiang L, Dong H, Zhang Z. Preparation and characterization of protein-loaded pfc nanoemulsions for the treatment of heart diseases by pulmonary administration. Eur J Pharm Sci. 2021;158:105690.
28. Fan Z, Xu Z, Niu H, Gao N, Guan Y, Li C, Dang Y, Cui X, Liu XL, Duan Y, Li H, Zhou X, Lin PH, Ma J, Guan J. An injectable oxygen release system to augment cell survival and promote cardiac repair following myocardial infarction. Sci Rep. 2018;8:1371.
29. Harrison BS, Eberli D, Lee SJ, Atala A, Yoo JJ. Oxygen producing biomaterials for tissue regeneration. Biomaterials. 2007;28:4628–34.
30. Oh SH, Ward CL, Atala A, Yoo JJ, Harrison BS. Oxygen generating scaffolds for enhancing engineered tissue survival. Biomaterials. 2009;30:757–62.
31. Wang Y, Xue Y, Zhang T, Fang Q, Jin M, Wang X, Wang Z, Hu Y, Zhao W, Lou D, Tan W-Q. Photosynthetic biomaterials: applications of photosynthesis in algae as oxygenerator in biomedical therapies. Bio-Des Manuf. 2021;4:596–611.
32. Chen QW, Qiao JY, Liu XH, Zhang C, Zhang XZ. Customized materials-assisted microorganisms in tumor therapeutics. Chem Soc Rev. 2021;50:12576–615.
33. Khavari F, Saidijam M, Taheri M, Nouri F. Microalgae: therapeutic potentials and applications. Mol Biol Rep. 2021;48:4757–65.
34. Haraguchi Y, Kagawa Y, Sakaguchi K, Matsuura K, Shimizu T, Okano T. Thicker three-dimensional tissue from a "symbiotic recycling system" combining mammalian cells and algae. Sci Rep. 2017;7:41594.

35. Cohen JE, Goldstone AB, Paulsen MJ, Shudo Y, Steele AN, Edwards BB, Patel JB, MacArthur JW Jr, Hopkins MS, Burnett CE, Jaatinen KJ, Thakore AD, Farry JM, Truong VN, Bourdillon AT, Stapleton LM, Eskandari A, Fairman AS, Hiesinger W, Esipova TV, Patrick WL, Ji K, Shizuru JA, Woo YJ. An innovative biologic system for photon-powered myocardium in the ischemic heart. Sci Adv. 2017;3:e1603078.
36. Stapleton LM, Farry JM, Lucian HJ, Wang H, Totherow KP, Paulsen MJ, Agmon G, Cabatu M, Thakore AD, Eskandari AN, Anilkumar SD, Buncom FJ, Appel EA, Woo YJ. Cyanobacteria-alginate microgels for sustained photosynthetic oxygen delivery to rescue cardiomyocytes in an ischemic milieu. Circulation. 2019;140:15828.
37. Liu Y, Zhong D, He Y, Jiang J, Xie W, Tang Z, Qiu J, Luo J, Wang X. Photoresponsive hydrogel-coated upconversion cyanobacteria nanocapsules for myocardial infarction prevention and treatment. Adv Sci. 2022;9:e2202920.
38. Zhu Y, Woo YJ. Photosynthetic symbiotic therapeutics—an innovative, effective treatment for ischemic cardiovascular diseases. J Mol Cell Cardiol. 2022;164:51–7.
39. Wang JZ, Zhang YH, Du WT, Liu G, Zhang XY, Cheng SZ, Guo XH. A post-surgical adjunctive hypoxic therapy for myocardial infarction: initiate endogenous cardiomyocyte proliferation in adults. Med Hypotheses. 2019;125:16–20.
40. Nakada Y, Canseco DC, Thet S, Abdisalaam S, Asaithamby A, Santos CX, Shah AM, Zhang H, Faber JE, Kinter MT, Szweda LI, Xing C, Hu Z, Deberardinis RJ, Schiattarella G, Hill JA, Oz O, Lu Z, Zhang CC, Kimura W, Sadek HA. Hypoxia induces heart regeneration in adult mice. Nature. 2017;541:222–7.
41. Frangogiannis NG. The inflammatory response in myocardial injury, repair, and remodelling. Nat Rev Cardiol. 2014;11:255–65.
42. Kim T, Lemaster JE, Chen F, Li J, Jokerst JV. Photoacoustic imaging of human mesenchymal stem cells labeled with prussian blue-poly(l-lysine) nanocomplexes. ACS Nano. 2017;11: 9022–32.
43. Hausenloy DJ, Yellon DM. Myocardial ischemia-reperfusion injury: a neglected therapeutic target. J Clin Invest. 2013;123:92–100.
44. Li X, Zhang YB, Ren XY, Wang Y, Chen DX, Li Q, Huo MF, Shi JL. Ischemic microenvironment-responsive therapeutics for cardiovascular diseases. Adv Mater. 2021;33: 2105348.
45. Huang K, Hu SQ, Cheng K. A new era of cardiac cell therapy: opportunities and challenges. Adv Healthc Mater. 2019;8:1801011.
46. Rufaihah AJ, Vaibavi SR, Plotkin M, Shen JY, Nithya V, Wang J, Seliktar D, Kofidis T. Enhanced infarct stabilization and neovascularization mediated by vegf-loaded pegylated fibrinogen hydrogel in a rodent myocardial infarction model. Biomaterials. 2013;34:8195–202.
47. Munarin F, Kant RJ, Rupert CE, Khoo A, Coulombe KLK. Engineered human myocardium with local release of angiogenic proteins improves vascularization and cardiac function in injured rat hearts. Biomaterials. 2020;251:120033.
48. Huang SX, Lei D, Yang Q, Yang Y, Jiang CY, Shi HP, Qian B, Long Q, Chen WY, Chen YM, Zhu L, Yang WJ, Wang L, Hai WX, Zhao Q, You ZW, Ye XF. A perfusable, multifunctional epicardial device improves cardiac function and tissue repair. Nat Med. 2021;27:480.
49. Cahill TJ, Choudhury RP, Riley PR. Heart regeneration and repair after myocardial infarction: translational opportunities for novel therapeutics. Nat Rev Drug Discov. 2017;16:699–717.
50. Mei X, Cheng K. Recent development in therapeutic cardiac patches. Front Cardiovasc Med. 2020;7:610364.
51. Ye L, Chang YH, Xiong Q, Zhang PY, Zhang LY, Somasundaram P, Lepley M, Swingen C, Su LP, Wendel JS, Guo J, Jang A, Rosenbush D, Greder L, Dutton JR, Zhang JH, Kamp TJ, Kaufman DS, Ge Y, Zhang JY. Cardiac repair in a porcine model of acute myocardial infarction with human induced pluripotent stem cell-derived cardiovascular cells. Cell Stem Cell. 2014;15:750–61.

52. Zhu DS, Li ZH, Huang K, Caranasos TG, Rossi JS, Cheng K. Minimally invasive delivery of therapeutic agents by hydrogel injection into the pericardial cavity for cardiac repair. Nat Commun. 2021;12:1412.
53. Boon RA, Dimmeler S. Micrornas in myocardial infarction. Nat Rev Cardiol. 2015;12:135–42.
54. Li Y, Chen X, Jin RH, Chen L, Dang M, Cao H, Dong Y, Cai BL, Bai G, Gooding JJ, Liu SY, Zou DH, Zhang ZY, Yang C. Injectable hydrogel with msns/microrna-21-5p delivery enables both immunomodification and enhanced angiogenesis for myocardial infarction therapy in pigs. Sci Adv. 2021;7:eabd6740.
55. Vallabhajosyula S, Kanwar S, Aung H, Cheungpasitporn W, Raphael CE, Gulati R, Singh M. Temporal trends and outcomes of left ventricular aneurysm after acute myocardial infarction. Am J Cardiol. 2020;133:32–8.
56. Nadruz W. Myocardial remodeling in hypertension. J Hum Hypertens. 2015;29:1–6.
57. Bahit MC, Kochar A, Granger CB. Post-myocardial infarction heart failure. JACC Heart Fail. 2018;6:179–86.
58. Saucerman JJ, Tan PM, Buchholz KS, McCulloch AD, Omens JH. Mechanical regulation of gene expression in cardiac myocytes and fibroblasts. Nat Rev Cardiol. 2019;16:361–78.
59. Lu Y, Ren T, Zhang H, Jin Q, Shen L, Shan M, Zhao X, Chen Q, Dai H, Yao L, Xie J, Ye D, Lin T, Hong X, Deng K, Shen T, Pan J, Jia M, Ling J, Li P, Zhang Y, Wang H, Zhuang L, Gao C, Mao J, Zhu Y. A honeybee stinger-inspired self-interlocking microneedle patch and its application in myocardial infarction treatment. Acta Biomater. 2022;153:386–98.
60. Fioretta ES, Fledderus JO, Baaijens FP, Bouten CV. Influence of substrate stiffness on circulating progenitor cell fate. J Biomech. 2012;45:736–44.
61. Liau B, Zhang D, Bursac N. Functional cardiac tissue engineering. Regen Med. 2012;7:187–206.
62. Wall ST, Walker JC, Healy KE, Ratcliffe MB, Guccione JM. Theoretical impact of the injection of material into the myocardium: a finite element model simulation. Circulation. 2006;114:2627–35.
63. Lin X, Liu Y, Bai A, Cai H, Bai Y, Jiang W, Yang H, Wang X, Yang L, Sun N. A viscoelastic adhesive epicardial patch for treating myocardial infarction. Nat Biomed Eng. 2019;3:632–43.
64. Chambon F, Winter HH. Linear viscoelasticity at the gel point of a crosslinking pdms with imbalanced stoichiometry. J Rheol. 1987;31:683–97.
65. Li Z, Guan J. Hydrogels for cardiac tissue engineering. Polymers. 2011;3:740–61.
66. Chen Q-Z, Bismarck A, Hansen U, Junaid S, Tran MQ, Harding SE, Ali NN, Boccaccini AR. Characterisation of a soft elastomer poly(glycerol sebacate) designed to match the mechanical properties of myocardial tissue. Biomaterials. 2008;29:47–57.
67. Zhu Y, Lu Y, Jiang S, Shen T, He C, Gao Y, Shen L, Jin Q, Zhao Y, Hu H, Ling J, He J, Zhuang L. Cardiac patch treatment alleviates ischemic cardiomyopathy correlated with reverting piezo1/2 expression by unloading left ventricular myocardium. bioRxiv. 2022;2022:490841.
68. Matsumura Y, Zhu Y, Jiang H, D'Amore A, Luketich SK, Charwat V, Yoshizumi T, Sato H, Yang B, Uchibori T. Intramyocardial injection of a fully synthetic hydrogel attenuates left ventricular remodeling post myocardial infarction. Biomaterials. 2019;217:119289.
69. Sun H, Zhou J, Huang Z, Qu L, Lin N, Liang C, Dai R, Tang L, Tian F. Carbon nanotube-incorporated collagen hydrogels improve cell alignment and the performance of cardiac constructs. Int J Nanomedicine. 2017;12:3109.
70. Awada H, Long D, Wang Z, Hwang M, Kim K, Wang Y. A single injection of protein-loaded coacervate-gel significantly improves cardiac function post infarction. Biomaterials. 2017;125:65–80.
71. Ungerleider J, Johnson T, Rao N, Christman K. Fabrication and characterization of injectable hydrogels derived from decellularized skeletal and cardiac muscle. Methods. 2015;84:53–9.

72. Shu Y, Hao T, Yao F, Qian Y, Wang Y, Yang B, Li J, Wang C. Roy peptide-modified chitosan-based hydrogel to improve angiogenesis and cardiac repair under hypoxia. ACS Appl Mater Interfaces. 2015;7:6505–17.
73. Hao T, Li J, Yao F, Dong D, Wang Y, Yang B, Wang C. Injectable fullerenol/alginate hydrogel for suppression of oxidative stress damage in brown adipose-derived stem cells and cardiac repair. ACS Nano. 2017;11:5474–88.
74. Asti A, Gioglio L. Natural and synthetic biodegradable polymers: different scaffolds for cell expansion and tissue formation. Int J Artif Organs. 2014;37:187–205.
75. Chow A, Stuckey DJ, Kidher E, Rocco M, Jabbour RJ, Mansfield CA, Darzi A, Harding SE, Stevens MM, Athanasiou T. Human induced pluripotent stem cell-derived cardiomyocyte encapsulating bioactive hydrogels improve rat heart function post myocardial infarction. Stem Cell Rep. 2017;9:1415–22.
76. Koerner H, Price G, Pearce NA, Alexander M, Vaia RA. Remotely actuated polymer nanocomposites—stress-recovery of carbon-nanotube-filled thermoplastic elastomers. Nat Mater. 2004;3:115–20.
77. Klotz BJ, Gawlitta D, Rosenberg AJ, Malda J, Melchels FP. Gelatin-methacryloyl hydrogels: towards biofabrication-based tissue repair. Trends Biotechnol. 2016;34:394–407.
78. Frey N, Linke A, Süselbeck T, Müller-Ehmsen J, Vermeersch P, Schoors D, Rosenberg M, Bea F, Tuvia S, Leor J. Intracoronary delivery of injectable bioabsorbable scaffold (ik-5001) to treat left ventricular remodeling after st-elevation myocardial infarction: a first-in-man study. Circ Cardiovasc Interv. 2014;7:806–12.
79. Anker SD, Coats AJ, Cristian G, Dragomir D, Pusineri E, Piredda M, Bettari L, Dowling R, Volterrani M, Kirwan B-A. A prospective comparison of alginate- nat mat hydrogel with standard medical therapy to determine impact on functional capacity and clinical outcomes in patients with advanced heart failure (augment-hf trial). Eur Heart J. 2015;36:2297–309.
80. Li Y, Yang HY, Lee DS. Advances in biodegradable and injectable hydrogels for biomedical applications. J Control Release. 2021;330:151–60.
81. Ruvinov E, Cohen S. Alginate biomaterial for the treatment of myocardial infarction: progress, translational strategies, and clinical outlook: from ocean algae to patient bedside. Adv Drug Deliv Rev. 2016;96:54–76.
82. Lee LC, Wall ST, Klepach D, Ge L, Zhang Z, Lee RJ, Hinson A, Gorman JH III, Gorman RC, Guccione JM. Algisyl-lvr™ with coronary artery bypass grafting reduces left ventricular wall stress and improves function in the failing human heart. Int J Cardiol. 2013;168:2022–8.
83. Lee LC, Zhihong Z, Hinson A, Guccione JM. Reduction in left ventricular wall stress and improvement in function in failing hearts using algisyl-lvr. J Vis Exp. 2013;74:e50096.
84. Roura S, Gálvez-Montón C, Bayes-Genis A. Fibrin, the preferred scaffold for cell transplantation after myocardial infarction? An old molecule with a new life. J Tissue Eng Regen Med. 2017;11:2304–13.
85. Menasché P, Vanneaux V, Hagège A, Bel A, Cholley B, Parouchev A, Cacciapuoti I, Al-Daccak R, Benhamouda N, Blons H. Transplantation of human embryonic stem cell–derived cardiovascular progenitors for severe ischemic left ventricular dysfunction. J Am Coll Cardiol. 2018;71:429–38.
86. Tang J, Vandergriff A, Wang Z, Hensley MT, Cores J, Allen TA, Dinh P-U, Zhang J, Caranasos TG, Cheng K. A regenerative cardiac patch formed by spray painting of biomaterials onto the heart. Tissue Eng Part C Methods. 2017;23:146–55.
87. Feng J, Wu Y, Chen W, Li J, Wang X, Chen Y, Yu Y, Shen Z, Zhang Y. Sustained release of bioactive igf-1 from a silk fibroin microsphere-based injectable alginate hydrogel for the treatment of myocardial infarction. J Mater Chem B. 2020;8:308–15.
88. Shah M, Kc P, Zhang G. In vivo assessment of decellularized porcine myocardial slice as an acellular cardiac patch. Nat Biomed Eng. 2019;11:23893–900.
89. Wang Z, Hu Q, Zeng Z, Wang X-Z, Guan Y-Q, Zhang Y. Vascular endothelial cells mediated the indirect effect of mpeg-pcl copolymers on blood coagulation. Colloids Interface Sci Commun. 2020;39:100326.

90. Hashizume R, Fujimoto KL, Hong Y, Guan J, Toma C, Tobita K, Wagner WR. Biodegradable elastic patch plasty ameliorates left ventricular adverse remodeling after ischemia-reperfusion injury: a preclinical study of a porous polyurethane material in a porcine model. J Thorac Cardiovasc Surg. 2013;146:391.
91. Fujimoto KL, Tobita K, Guan J, Hashizume R, Takanari K, Alfieri CM, Yutzey KE, Wagner WR. Placement of an elastic biodegradable cardiac patch on a subacute infarcted heart leads to cellularization with early developmental cardiomyocyte characteristics. J Card Fail. 2012;18: 585–95.
92. Yao Y, Li A, Wang S, Lu Y, Xie J, Zhang H, Zhang D, Ding J, Wang Z, Tu C, Shen L, Zhuang L, Zhu Y, Gao C. Multifunctional elastomer cardiac patches for preventing left ventricle remodeling after myocardial infarction in vivo. Biomaterials. 2022;282:121382.
93. Feng J, Shi H, Yang X, Xiao S. Self-adhesion conductive sub-micron fiber cardiac patch from shape memory polymers to promote electrical signal transduction function. Nat Biomed Eng. 2021;13:19593–602.
94. Holmes JW, Borg TK, Covell JW. Structure and mechanics of healing myocardial infarcts. Annu Rev Biomed Eng. 2005;7:223–53.
95. Thygesen K, Alpert JS, White HD. Universal definition of myocardial infarction. J Am Coll Cardiol. 2007;50:2173–95.
96. Franciosa J, Limas C, Guiha N, Rodriguera E, Cohn J. Improved left ventricular function during nitroprusside infusion in acute myocardial infarction. Lancet. 1972;299:650–4.
97. Nandkeolyar S, Ryu R, Mohammad A, Cordero-Caban K, Abramov D, Tran H, Hauschild C, Stoletniy L, Hilliard A, Sakr A. A review of inotropes and inopressors for effective utilization in patients with acute decompensated heart failure. J Cardiovasc Pharmacol. 2021;78:336–45.
98. DesJardin JT, Teerlink JR. Inotropic therapies in heart failure and cardiogenic shock: an educational review. Eur Heart J Acute Cardiovasc Care. 2021;10:676–86.
99. Iskandar MZ, Lang CC. Sacubitril and valsartan fixed combination to reduce heart failure events in post-acute myocardial infarction patients. Drugs Today (Barc). 2017;53:545–51.
100. Zhu JC, Zhang Y, Chen LL, He Y, Qing XM. Levosimendan in patients with low cardiac output syndrome undergoing cardiac surgery: a systematic review and meta-analysis. Anaesth Crit Care Pain Med. 2019;38:243–9.
101. Tumminello G, Cereda A, Barbieri L, Biondi-Zoccai G, Lucreziotti S, Mafrici A, Carugo S. Meta-analysis of placebo-controlled trials of levosimendan in acute myocardial infarction. J Cardiovasc Dev Dis. 2021;8:129.
102. Cheung AT, Cruz-Shiavone GE, Meng QC, Pochettino A, Augoustides JA, Bavaria JE, Ochroch EA. Cardiopulmonary bypass, hemolysis, and nitroprusside-induced cyanide production. Anesth Analg. 2007;105:29–33.
103. de Waha S, Desch S, Eitel I, Fuernau G, Lurz P, Sandri M, Schuler G, Thiele H. Intra-aortic balloon counterpulsation—basic principles and clinical evidence. Vasc Pharmacol. 2014;60: 52–6.
104. Thiele H, Zeymer U, Neumann FJ, Ferenc M, Olbrich HG, Hausleiter J, Richardt G, Hennersdorf M, Empen K, Fuernau G, Desch S, Eitel I, Hambrecht R, Fuhrmann J, Bohm M, Ebelt H, Schneider S, Schuler G, Werdan K, Investigators I-SIT. Intraaortic balloon support for myocardial infarction with cardiogenic shock. N Engl J Med. 2012;367:1287–96.
105. Lusebrink E, Kellnar A, Krieg K, Binzenhofer L, Scherer C, Zimmer S, Schrage B, Fichtner S, Petzold T, Braun D, Peterss S, Brunner S, Hagl C, Westermann D, Hausleiter J, Massberg S, Thiele H, Schafer A, Orban M. Percutaneous transvalvular microaxial flow pump support in cardiology. Circulation. 2022;145:1254–84.
106. Wong ASK, Sin SWC. Short-term mechanical circulatory support (intra-aortic balloon pump, impella, extracorporeal membrane oxygenation, TandemHeart): a review. Ann Transl Med. 2020;8:829.
107. Kar B, Gregoric ID, Basra SS, Idelchik GM, Loyalka P. The percutaneous ventricular assist device in severe refractory cardiogenic shock. J Am Coll Cardiol. 2011;57:688–96.

108. Combes A, Price S, Slutsky AS, Brodie D. Temporary circulatory support for cardiogenic shock. Lancet. 2020;396:199–212.
109. Brady W, Weigand S, Bergin J. Ventricular assist device in the emergency department: evaluation and management considerations. Am J Emerg Med. 2018;36:1295–9.
110. Robertson J, Long B, Koyfman A. The emergency management of ventricular assist devices. Am J Emerg Med. 2016;34:1294–301.
111. Goodman D, Stulak J, Rosenbaum AN. Left ventricular assist devices: a historical perspective at the intersection of medicine and engineering. Artif Organs. 2022;46:343–2360.
112. Bonnemain J, del Nido PJ, Roche ET. Direct cardiac compression devices to augment heart biomechanics and function. Annu Rev Biomed Eng. 2022;24:137–56.
113. Roche ET, Horvath MA, Wamala I, Alazmani A, Song SE, Whyte W, Machaidze Z, Payne CJ, Weaver JC, Fishbein G, Kuebler J, Vasilyev NV, Mooney DJ, Pigula FA, Walsh CJ. Soft robotic sleeve supports heart function. Sci Transl Med. 2017;9:eaaf3925.
114. Gu HR, Bertrand T, Boehler Q, Chautems C, Vasilyev NV, Nelson BJ. Magnetically active cardiac patches as an untethered, non-blood contacting ventricular assist device. Adv Sci. 2021;8:200072.
115. Anonymous, Zhou X, Active hydraulic ventricular attaching support system, Official Gazette of the United States Patent and Trademark Office Patents, US20120059214A1.
116. Naveed M, Mohammad IS, Xue L, Khan S, Gang W, Cao YF, Cheng YJ, Cui XX, Chen DD, Feng Y, Wang ZJ, Zhou XH. The promising future of ventricular restraint therapy for the management of end-stage heart failure. Biomed Pharmacother. 2018;99:25–32.
117. Nawaz W, Naveed M, Zhang J, Noreen S, Saeed M, Sembatya KR, Ihsan AU, Mohammad IS, Wang G, Zhou XH. Cardioprotective effect of silicon-built restraint device (asd), for left ventricular remodeling in rat heart failure model. J Mater Sci Mater Med. 2022;33:1–13.
118. Yasmeen S, Liao XQ, Khan FU, Ihsan AU, Li X, Li CY, Chen DD, Yu F, Wang ZJ, Sembatya KR, Mikrani R, Zhou XH. A novel approach to devise the therapy for ventricular fibrillation by epicardial delivery of lidocaine using active hydraulic ventricular attaching support system: an experimental study in rats. J Biomed Mater Res B Appl Biomater. 2019;107:1722–31.
119. Eng G, Lee BW, Protas L, Gagliardi M, Brown K, Kass RS, Keller G, Robinson RB, Vunjak-Novakovic G. Autonomous beating rate adaptation in human stem cell-derived cardiomyocytes. Nat Commun. 2016;7:10312.
120. Singh A, Shiekh PA, Das M, Seppala J, Kumar A. Aligned chitosan-gelatin cryogel-filled polyurethane nerve guidance channel for neural tissue engineering: fabrication, characterization, and in vitro evaluation. Biomacromolecules. 2019;20:662–73.
121. Feng J, Shi H, Yang X, Xiao S. Self-adhesion conductive sub-micron fiber cardiac patch from shape memory polymers to promote electrical signal transduction function. ACS Appl Mater Interfaces. 2021;13:19593–602.
122. Wang C, Chai Y, Wen X, Ai Y, Zhao H, Hu W, Yang X, Ding M-Y, Shi X, Liu Q, Liang Q. Stretchable and anisotropic conductive composite hydrogel as therapeutic cardiac patches. ACS Mater Lett. 2021;3:1238–48.
123. Zhou X, Rajeev A, Subramanian A, Li Y, Rossetti N, Natale G, Lodygensky GA, Cicoira F. Self-healing, stretchable, and highly adhesive hydrogels for epidermal patch electrodes. Acta Biomater. 2022;139:296–306.
124. Erol O, Uyan I, Hatip M, Yilmaz C, Tekinay AB, Guler MO. Recent advances in bioactive 1d and 2d carbon nanomaterials for biomedical applications. Nanomedicine. 2018;14:2433–54.
125. Ku SH, Lee M, Park CB. Carbon-based nanomaterials for tissue engineering. Adv Healthc Mater. 2013;2:244–60.
126. Maiti D, Tong X, Mou X, Yang K. Carbon-based nanomaterials for biomedical applications: a recent study. Front Pharmacol. 2018;9:1401.
127. Dvir T, Timko BP, Brigham MD, Naik SR, Karajanagi SS, Levy O, Jin H, Parker KK, Langer R, Kohane DS. Nanowired three-dimensional cardiac patches. Nat Nanotechnol. 2011;6:720–5.

128. Navaei A, Saini H, Christenson W, Sullivan RT, Ros R, Nikkhah M. Gold nanorod-incorporated gelatin-based conductive hydrogels for engineering cardiac tissue constructs. Acta Biomater. 2016;41:133–46.
129. Baei P, Jalili-Firoozinezhad S, Rajabi-Zeleti S, Tafazzoli-Shadpour M, Baharvand H, Aghdami N. Electrically conductive gold nanoparticle-chitosan thermosensitive hydrogels for cardiac tissue engineering. Mater Sci Eng C Mater Biol Appl. 2016;63:131–41.
130. Naahidi S, Jafari M, Logan M, Wang Y, Yuan Y, Bae H, Dixon B, Chen P. Biocompatibility of hydrogel-based scaffolds for tissue engineering applications. Biotechnol Adv. 2017;35: 530–44.
131. Baheiraei N, Yeganeh H, Ai J, Gharibi R, Ebrahimi-Barough S, Azami M, Vahdat S, Baharvand H. Preparation of a porous conductive scaffold from aniline pentamer-modified polyurethane/pcl blend for cardiac tissue engineering. J Biomed Mater Res A. 2015;103:3179–87.
132. Tashakori-Miyanroudi M, Rakhshan K, Ramez M, Asgarian S, Janzadeh A, Azizi Y, Seifalian A, Ramezani F. Conductive carbon nanofibers incorporated into collagen bio-scaffold assists myocardial injury repair. Int J Biol Macromol. 2020;163:1136–46.
133. Yuan Z, Qin Q, Yuan M, Wang H, Li R. Development and novel design of clustery graphene oxide formed conductive silk hydrogel cell vesicle to repair and routine care of myocardial infarction: investigation of its biological activity for cell delivery applications. J Drug Deliv Sci Technol. 2020;60:102001.
134. Foyt DA, Norman MDA, Yu TTL, Gentleman E. Exploiting advanced hydrogel technologies to address key challenges in regenerative medicine. Adv Healthc Mater. 2018;7:e1700939.
135. Mihic A, Cui Z, Wu J, Vlacic G, Miyagi Y, Li SH, Lu S, Sung HW, Weisel RD, Li RK. A conductive polymer hydrogel supports cell electrical signaling and improves cardiac function after implantation into myocardial infarct. Circulation. 2015;132:772–84.
136. Zhao C, Tian S, Liu Q, Xiu K, Lei I, Wang Z, Ma PX. Biodegradable nanofibrous temperature-responsive gelling microspheres for heart regeneration. Adv Funct Mater. 2020;30:2000776.
137. Zhang C, Hsieh MH, Wu SY, Li SH, Wu J, Liu SM, Wei HJ, Weisel RD, Sung HW, Li RK. A self-doping conductive polymer hydrogel that can restore electrical impulse propagation at myocardial infarct to prevent cardiac arrhythmia and preserve ventricular function. Biomaterials. 2020;231:119672.
138. Birla RK, Williams SK. 3d bioprinting and its potential impact on cardiac failure treatment: an industry perspective. APL Bioeng. 2020;4:010903.
139. Pedrotty DM, Kuzmenko V, Karabulut E, Sugrue AM, Livia C, Vaidya VR, McLeod CJ, Asirvatham SJ, Gatenholm P, Kapa S. Three-dimensional printed biopatches with conductive ink facilitate cardiac conduction when applied to disrupted myocardium. Circ Arrhythm Electrophysiol. 2019;12:e006920.
140. Zhao G, Feng Y, Xue L, Cui M, Zhang Q, Xu F, Peng N, Jiang Z, Gao D, Zhang X. Anisotropic conductive reduced graphene oxide/silk matrices promote post-infarction myocardial function by restoring electrical integrity. Acta Biomater. 2022;139:190–203.
141. Zanjanizadeh Ezazi N, Ajdary R, Correia A, Makila E, Salonen J, Kemell M, Hirvonen J, Rojas OJ, Ruskoaho HJ, Santos HA. Fabrication and characterization of drug-loaded conductive poly(glycerol sebacate)/nanoparticle-based composite patch for myocardial infarction applications. ACS Appl Mater Interfaces. 2020;12:6899–909.
142. Kapnisi M, Mansfield C, Marijon C, Guex AG, Perbellini F, Bardi I, Humphrey EJ, Puetzer JL, Mawad D, Koutsogeorgis DC, Stuckey DJ, Terracciano CM, Harding SE, Stevens MM. Auxetic cardiac patches with tunable mechanical and conductive properties toward treating myocardial infarction. Adv Funct Mater. 2018;28:1800618.
143. Ding J, Yao Y, Li J, Duan Y, Nakkala JR, Feng X, Cao W, Wang Y, Hong L, Shen L, Mao Z, Zhu Y, Gao C. A reactive oxygen species scavenging and o2 generating injectable hydrogel for myocardial infarction treatment in vivo. Small. 2020;16:e2005038.

144. Vishwakarma A, Bhise NS, Evangelista MB, Rouwkema J, Dokmeci MR, Ghaemmaghami AM, Vrana NE, Khademhosseini A. Engineering immunomodulatory biomaterials to tune the inflammatory response. Trends Biotechnol. 2016;34:470–82.
145. Villarreal-Leal RA, Cooke JP, Corradetti B. Biomimetic and immunomodulatory therapeutics as an alternative to natural exosomes for vascular and cardiac applications. Nanomedicine. 2021;35:102385.
146. Julier Z, Park AJ, Briquez PS, Martino MM. Promoting tissue regeneration by modulating the immune system. Acta Biomater. 2017;53:13–28.
147. Xu Z, Liang B, Tian J, Wu J. Anti-inflammation biomaterial platforms for chronic wound healing. Biomater Sci. 2021;9:4388–409.
148. Mata R, Yao Y, Cao W, Ding J, Zhou T, Zhai Z, Gao C. The dynamic inflammatory tissue microenvironment: signality and disease therapy by biomaterials. Research. 2021;2021: 4189516.
149. El-Kenawi A, Ruffell B. Inflammation, ros, and mutagenesis. Cancer Cell. 2017;32(6):727.
150. Rock KL, Latz E, Ontiveros F, Kono H. The sterile inflammatory response. Annu Rev Immunol. 2010;28:321–42.
151. Mcdonald B, Kubes P. Innate immune cell trafficking and function during sterile inflammation of the liver. Gastroenterology. 2016;151:1087–95.
152. Willemen NGA, Hassan S, Gurian M, Li J, Allijn IE, Shin SR, Leijten J. Oxygen-releasing biomaterials: current challenges and future applications. Trends Biotechnol. 2021;39:1144–59.
153. Yang B, Chen Y, Shi J. Reactive oxygen species (ros)-based nanomedicine. Chem Rev. 2019;119:4881–985.
154. Tejero J, Shiva S, Gladwin MT. Sources of vascular nitric oxide and reactive oxygen species and their regulation. Physiol Rev. 2019;99:311–79.
155. Boddupalli A, Zhu L, Bratlie KM. Methods for implant acceptance and wound healing: material selection and implant location modulate macrophage and fibroblast phenotypes. Adv Healthc Mater. 2016;5:2575–94.
156. Tu Z, Zhong Y, Hu H, Shao D, Haag R, Schirner M, Lee J, Sullenger B, Leong KW. Design of therapeutic biomaterials to control inflammation. Nat Rev Mater. 2022;7:557–74.
157. Zymek PT, Bujak M, Chatila KF, Cieślak A, Thakker GD, Entman ML, Frangogiannis NG. The role of platelet-derived growth factor signaling in healing myocardial infarcts. J Am Coll Cardiol. 2006;48(11):2315–23.
158. Yao Y, Ding J, Wang Z, Zhang H, Xie J, Wang Y, Hong L, Mao Z, Gao J, Gao C. Ros-responsive polyurethane fibrous patches loaded with methylprednisolone (mp) for restoring structures and functions of infarcted myocardium in vivo. Biomaterials. 2020;232: 119726.
159. Xie J, Yao Y, Wang S, Fan L, Ding J, Gao Y, Li S, Shen L, Zhu Y, Gao C. Alleviating oxidative injury of myocardial infarction by a fibrous polyurethane patch with condensed ros-scavenging backbone units. Adv Healthc Mater. 2022;11:e2101855.
160. Shiekh PA, Singh A, Kumar A. Engineering bioinspired antioxidant materials promoting cardiomyocyte functionality and maturation for tissue engineering application. ACS Appl Mater Interfaces. 2018;10:3260–73.
161. Ifkovits JL, Tous E, Minakawa M, Morita M, Robb JD, Koomalsingh KJ, Gorman JH 3rd, Gorman RC, Burdick JA. Injectable hydrogel properties influence infarct expansion and extent of postinfarction left ventricular remodeling in an ovine model. Proc Natl Acad Sci U S A. 2010;107:11507–12.
162. Chiraz A, Fatma G, Dhafer L. Role of human macrophage polarization in inflammation during infectious diseases. Int J Mol Med. 2018;19:1801.
163. Larouche J, Sheoran S, Maruyama K, Martino MM. Immune regulation of skin wound healing: mechanisms and novel therapeutic targets. Adv Wound Care. 2018;7:209–31.
164. Rurik JG, Aghajanian H, Epstein JA. Immune cells and immunotherapy for cardiac injury and repair. Circ Res. 2021;128:1766–79.

165. Duan Y, Zheng H, Li Z, Yao Y, Ding J, Wang X, Nakkala JR, Zhang D, Wang Z, Zuo X, Zheng X, Ling J, Gao C. Unsaturated polyurethane films grafted with enantiomeric polylysine promotes macrophage polarization to a m2 phenotype through pi3k/akt1/mtor axis. Biomaterials. 2020;246:120012.
166. Khokha R, Murthy A, Weiss A. Metalloproteinases and their natural inhibitors in inflammation and immunity. Nat Rev Immunol. 2013;13:649–65.
167. Fan C, Shi J, Zhuang Y, Zhang L, Huang L, Yang W, Chen B, Chen Y, Xiao Z, Shen H, Zhao Y, Dai J. Myocardial-infarction-responsive smart hydrogels targeting matrix metalloproteinase for on-demand growth factor delivery. Adv Mater. 2019;31:e1902900.
168. Tung WT, Maring JA, Xu X, Liu Y, Becker M, Somesh DB, Klose K, Wang W, Sun X, Ullah I, Kratz K, Neffe AT, Stamm C, Ma N, Lendlein A. In vivo performance of a cell and factor free multifunctional fiber mesh modulating p[1] Carrillo-Salinas FJ, Ngwenyama N, Anastasiou M, Kaur K, Alcaide P, heart inflammation: immune cell roles and roads to the heart. Am J Pathol. 2019;189:1482–94.
169. Weissleder R, Nahrendorf M, Pittet MJ. Imaging macrophages with nanoparticles. Nat Mater. 2014;13:125–38.
170. Kwon SP, Hwang BH, Park EH, Kim HY, Lee JR, Kang M, Song SY, Jung M, Sohn HS, Kim E, Kim CW, Lee KY, Oh GC, Choo E, Lim S, Chung Y, Chang K, Kim BS. Nanoparticle-mediated blocking of excessive inflammation for prevention of heart failure following myocardial infarction. Small. 2021;17:e2101207.
171. Arslan F, Lai RC, Smeets MB, Akeroyd L, Choo A, Aguor EN, Timmers L, van Rijen HV, Doevendans PA, Pasterkamp G, Lim SK, de Kleijn DP. Mesenchymal stem cell-derived exosomes increase atp levels, decrease oxidative stress and activate pi3k/akt pathway to enhance myocardial viability and prevent adverse remodeling after myocardial ischemia/reperfusion injury. Stem Cell Res. 2013;10:301–12.
172. Nakkala JR, Yao Y, Zhai Z, Duan Y, Zhang D, Mao Z, Lu L, Gao C. Dimethyl itaconate-loaded nanofibers rewrite macrophage polarization, reduce inflammation, and enhance repair of myocardic infarction. Small. 2021;17:e2006992.
173. Chouchani ET, Pell VR, Gaude E, Aksentijević D, Sundier SY, Robb EL, Logan A, Nadtochiy SM, Ord ENJ, Smith AC, Eyassu F, Shirley R, Hu C-H, Dare AJ, James AM, Rogatti S, Hartley RC, Eaton S, Costa ASH, Brookes PS, Davidson SM, Duchen MR, Saeb-Parsy K, Shattock MJ, Robinson AJ, Work LM, Frezza C, Krieg T, Murphy MP. Ischaemic accumulation of succinate controls reperfusion injury through mitochondrial ros. Nature. 2014;515:431–5.
174. Hashimoto H, Olson EN, Bassel-Duby R. Therapeutic approaches for cardiac regeneration and repair. Nat Rev Cardiol. 2018;15:585–600.
175. Bristow MR, Saxon LA, Boehmer J, Krueger S, Kass DA, De Marco T, Carson P, DiCarlo L, DeMets D, White BG, DeVries DW, Feldman AM, Investigators C. Cardiac-resynchronization therapy with or without an implantable defibrillator in advanced chronic heart failure. NEJM. 2004;350:2140–50.
176. Ferreira J. Long-term use of a left ventricular assist device for end-stage heart failure. Revista Portuguesa de cardiologia: orgao oficial da Sociedade Portuguesa de Cardiologia = Portuguese journal of cardiology: an official journal of the Portuguese society of Cardiology. 2001;20:1279–80.
177. Yacoub M. Cardiac donation after circulatory death: a time to reflect. Lancet. 2015;385:2554–6.
178. Xin M, Olson EN, Bassel-Duby R. Mending broken hearts: cardiac development as a basis for adult heart regeneration and repair. Nat Rev Mol Cell Biol. 2013;14:529–41.
179. van Rooij E. Cardiac repair after myocardial infarction. NEJM. 2016;374:85–7.
180. Porrello ER, Mahmoud AI, Simpson E, Hill JA, Richardson JA, Olson EN, Sadek HA. Transient regenerative potential of the neonatal mouse heart. Science. 2011;331:1078–80.
181. Nowak E, Gawor M, Ciemerych MA, Zimowska M. Silencing of gelatinase expression delays myoblast differentiation in vitro. Cell Biol Int. 2018;42:373–82.

182. Beltrami AP, Barlucchi L, Torella D, Baker M, Limana F, Chimenti S, Kasahara H, Rota M, Musso E, Urbanek K, Leri A, Kajstura J, Nadal-Ginard B, Anversa P. Adult cardiac stem cells are multipotent and support myocardial regeneration. Cell. 2003;114:763–76.
183. Mummery CL, Zhang J, Ng ES, Elliott DA, Elefanty AG, Kamp TJ. Differentiation of human embryonic stem cells and induced pluripotent stem cells to cardiomyocytes a methods overview. Circ Res. 2012;111:344–58.
184. Shim JB, Ankeny RF, Kim H, Nerem RM, Khang G. A study of a three-dimensional plga sponge containing natural polymers co-cultured with endothelial and mesenchymal stem cells as a tissue engineering scaffold. Biomed Mater. 2014;9:045015.
185. Li J, Lv Y, Zhu D, Mei X, Huang K, Wang X, Li Z, Zhang S, Hu S, Popowski KD, Cheng K, Wang J. Intrapericardial hydrogel injection generates high cell retention and augments therapeutic effects of mesenchymal stem cells in myocardial infarction. Chem Eng J. 2022:427.
186. Gassmann M, Casagranda F, Orioli D, Simon H, Lai C, Klein R, Lemke G. Aberrant neural and cardiac development in mice lacking the erbb4 neuregulin receptor. Nature. 1995;378:390–4.
187. D'Uva G, Aharonov A, Lauriola M, Kain D, Yahalom-Ronen Y, Carvalho S, Weisinger K, Bassat E, Rajchman D, Yifa O, Lysenko M, Konfino T, Hegesh J, Brenner O, Neeman M, Yarden Y, Leor J, Sarig R, Harvey RP, Tzahor E. Erbb2 triggers mammalian heart regeneration by promoting cardiorlyocyte dedifferentiation and proliferation. Nat Cell Biol. 2015;17:627.
188. Bersell K, Arab S, Haring B, Kuehn B. Neuregulin1/erbb4 signaling induces cardiomyocyte proliferation and repair of heart injury. Cell. 2009;138:257–70.
189. Garbayo E, Jose Gavira J, Garcia de Yebenes M, Pelacho B, Abizanda G, Lana H, Jose Blanco-Prieto M, Prosper F. Catheter-based intramyocardial injection of fgf1 or nrg1-loaded mps improves cardiac function in a preclinical model of ischemia-reperfusion. Sci Rep. 2016;6:25932.
190. van Rooij E, Olson EN. Microrna therapeutics for cardiovascular disease: opportunities and obstacles. Nat Rev Drug Discov. 2012;11:860–72.
191. Eulalio A, Mano M, Dal Ferro M, Zentilin L, Sinagra G, Zacchigna S, Giacca M. Functional screening identifies mirnas inducing cardiac regeneration. Nature. 2012;492:376.
192. Tian Y, Liu Y, Wang T, Zhou N, Kong J, Chen L, Snitow M, Morley M, Li D, Petrenko N, Zhou S, Lu M, Gao E, Koch WJ, Stewart KM, Morrisey EE. A microrna-hippo pathway that promotes cardiomyocyte proliferation and cardiac regeneration in mice. Sci Transl Med. 2015;7:279ra38.
193. Xu Q, Seeger FH, Castillo J, Iekushi K, Boon RA, Farcas R, Manavski Y, Li Y-G, Assmus B, Zeiher AM, Dimmeler S. Micro-rna-34a contributes to the impaired function of bone marrow-derived mononuclear cells from patients with cardiovascular disease. J Am Coll Cardiol. 2012;59:2107–17.
194. Icli B, Wara AKM, Moslehi J, Sun X, Plovie E, Cahill M, Marchini JF, Schissler A, Padera RF, Shi J, Cheng H-W, Raghuram S, Arany Z, Liao R, Croce K, MacRae C, Feinberg MW. Microrna-26a regulates pathological and physiological angiogenesis by targeting bmp/smad1 signaling. Circ Res. 2013;113:1231.
195. Jansen F, Yang X, Nickenig G, Werner N. Endothelial microparticle-mediated transfer of microrna-126 promotes vascular endothelial cell repair via spred1 and is abrogated in glucose-damaged endothelial microparticles. Circulation. 2013;128:2026–38.
196. Gao F, Kataoka M, Liu N, Liang T, Huang Z-P, Gu F, Ding J, Liu J, Zhang F, Ma Q, Wang Y, Zhang M, Hu X, Kyselovic J, Hu X, Pu WT, Wang JA, Chen J, Wang D-Z. Therapeutic role of mir-19a/19b in cardiac regeneration and protection from myocardial infarction. Nat Commun. 2019;10:1802.

197. Wang LL, Liu Y, Chung JJ, Wang T, Gaffey AC, Lu M, Cavanaugh CA, Zhou S, Kanade R, Atluri P, Morrisey EE, Burdick JA. Sustained mirna delivery from an injectable hydrogel promotes cardiomyocyte proliferation and functional regeneration after ischaemic injury. Nat Biomed Eng. 2017;1:983.
198. Gabisonia K, Prosdocimo G, Aquaro GD, Carlucci L, Zentilin L, Secco I, Ali H, Braga L, Gorgodze N, Bernini F, Burchielli S, Collesi C, Zandona L, Sinagra G, Piacenti M, Zacchigna S, Bussani R, Recchia FA, Giacca M. Microrna therapy stimulates uncontrolled cardiac repair after myocardial infarction in pigs. Nature. 2019;569:418.

Chapter 13
Nerve Regeneration

Kefei Zhao, Weiwei Zheng, Qiaoxuan Wang, Haijun Hu, and Changyou Gao

Abstract Nerve injuries may result in neurological dysfunction or even permanent disability, which poses various challenges to physicians. In the peripheral nervous system (PNS), only small nerve injuries can be regenerated spontaneously in vivo, while larger nerve injuries must be treated surgically with biomaterials or nerve grafts harvested. Attributed to the influence of inhibiting factors such as inflammation and microenvironment changes, a solution to completely repair central nervous system (CNS) injuries has not been discovered. Hence, most bioengineering strategies for PNS have been focused on the guidance of regenerative nerves, whereas the efforts for CNS have been focused on creating a suitable regenerating microenvironment in vivo. Recent advances in neurology, tissue engineering, biomaterials, gene transfection, and multifactor combinations offer optimistic prospects for the development of nerve regeneration. In this chapter, we firstly examine the current understanding of the neurophysiology and factors that are critical for nerve regeneration, and discuss their implications for promoting axon regeneration. Then, the current approaches, challenges, and future perspectives of biomaterials being explored to aid PNS and CNS regeneration are highlighted.

Keywords Nerve physiology · Nerve microenvironment · Biomaterial scaffold · Nerve conduit · Nerve recovery

Kefei Zhao, Weiwei Zheng, Qiaoxuan Wang, and Haijun Hu have contributed equally to this work.

K. Zhao · W. Zheng · Q. Wang · H. Hu · C. Gao (✉)
MOE Key Laboratory of Macromolecular Synthesis and Functionalization, Department of Polymer Science and Engineering, Zhejiang University, Hangzhou, China
e-mail: cygao@zju.edu.cn

C. Gao (ed.), *Polymeric Biomaterials for Tissue Regeneration*,
https://doi.org/10.1007/978-981-99-6948-7_13

13.1 Introduction

Nervous system, composed of neuronal cells, stromal cells, and glial cells, plays a dominant role in regulating physiological activities of the mammalian body, maintaining the homeostasis of the internal environment and coordinating the balance of the external environment [1]. However, nerve injury has emerged as a significant economic burden of the public. In recent decades, the incidence of nerve injuries has been on the rise, with hundreds of thousands of cases reported worldwide [2]. Unfortunately, many of these injuries result in lifelong disability, as the available therapeutic options for repair are often suboptimal, especially for severe nerve lacerations [3].

Nerve injuries not only diminish the quality of life to patients but also present multiple challenges for physicians, ranging from mild discomfort to lifelong impairment [4]. Sunderland [5] provides a classification scheme to effectively discuss nerve pathophysiology via a common language. As shown in Fig. 13.1a, nerve injuries are categorized into five grades based on the extent of damage to the axons, connective tissues, and presence of demyelination [6]. The mildest Grade I is known as neurapraxia and is defined by focal demyelination without damage to the axons or connective tissues. Neurapraxia is commonly caused by mild compression or traction of the nerve, which results in a decrease in conduction velocity and muscle weakness. Grade II, known as axonotmesis, involves direct damage to the axons and focal demyelination while maintaining continuity of the connective tissues. Grades III to V represent various degrees of neurotmesis, all of which involve increasing amounts of connective tissue damage. Grades III and IV typically

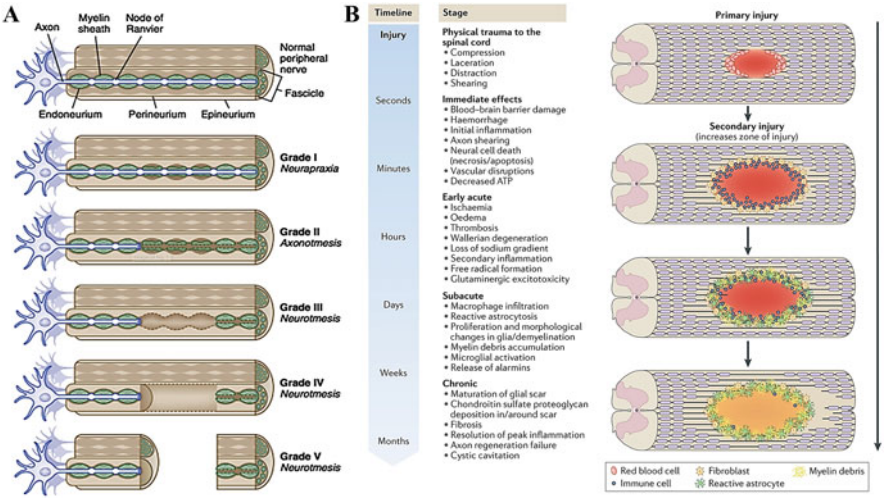

Fig. 13.1 (**a**) Classification of nerve trauma. (Reprinted from [6] with permission. Copyright 2013 Elsevier). (**b**) The pathophysiology of spinal cord injury in the absence of treatments along the timeline. (Reprinted from [7] with permission. Copyright 2020 Springer Nature)

are resulted from acute traumatic compression of a blunt object, which causes damage to the endoneurium and perineurium [8, 9]. The most severe form, Grade V, involves complete transection of axons and connective tissue layers, leading to complete discontinuity of the nerve. In more than 90% of direct axonal injuries (Grades II to V), nerve regeneration is the primary means of recovery [10]. Failure of axons to regenerate and rebuild functional connections with their original targets often results in motor, sensory, and autonomic dysfunctions following nerve injuries.

The process of regenerating injured nerves shares similarities with axon growth during embryonic stages, but is hindered by numerous obstacles. The intrinsic growth capacity and surrounding inflammatory microenvironment play a key role in determining the extent of regeneration, resulting in various injury responses in vivo [11]. For instance, peripheral nerve injuries often result in robust regeneration, leading to functional recovery. However, unlike the PNS, the mammalian CNS typically does not regenerate spontaneously due to the absence of certain regulatory mechanisms [12]. Figure 13.1b shows that primary trauma to the spinal cord without treatment not only inhibits neuronal regeneration significantly but also triggers a secondary cascade of inflammatory, vascular, and biochemical events that exacerbate the impairment of neuronal function [13–15]. Taking these concerns into consideration, a common feature of the studies in recent years is that the application of functional biomaterials can effectively regulate a series of behaviors of cells and contribute positively to several processes of nerve repair and regeneration [16]. With the constant development of both materials science and cell biology, there has been a surge in the creation of carriers, scaffolds, and templates. These novel designs aim to construct intricate, three-dimensional structures consisting of cells, growth factors, and biomaterials, which regulates the injury microenvironments and responses in vivo [17]. In order to identify a clinical treatment that is better suited for patients, researchers must prioritize the regeneration of axons and focus on translating fundamental research into practical clinical applications. In this chapter, we will examine the current understanding of neurophysiology and factors that are critical for nerve regeneration. We will discuss their implications for axon regeneration and highlight current approaches, challenges, and future perspectives of biomaterials being explored to aid PNS regeneration and CNS repair.

13.2 Intrinsic Behavior of Axon Following Nerve Injury

13.2.1 Pathology of Injured Neurons and Their Microenvironment

13.2.1.1 The Pathophysiology of Nerve Injury

The pathophysiology of nerve injury comprises primary and secondary injuries, resulting in a central lesion and an expanded zone of injury, respectively. The main

source of primary injury stems from an initial traumatic event, such as mechanical injury and ischemia-induced glucose and oxygen deprivation in stroke [18, 19]. A secondary injury occurs as a result of a series of biological and immune responses, which expand the initial injury area and ultimately lead to the formation of a glial scar. The timeline of events following spinal cord injury is summarized in Fig. 13.1b [7]. Briefly, the initial physical impact causes mechanical disruption to the structure of the spinal cord, resulting in cellular disruption and apoptosis which is known as primary injury. The release of damage-associated molecular patterns (DAMPs) from apoptotic and necrotic cells triggers the activation of microglia and astrocytes, the resident glial cells. The disruption of tight junctions of endothelial cell happens due to the released matrix metalloproteinase (MMPs) and other enzymes which lead to blood–brain barrier (BBB) damage. Leukocytes thereafter infiltrate into the parenchyma along with the upregulation of cellular adhesion molecules, cytokines, and chemokines, which activate immune response and lead to further tissue injury (secondary injury). The chronic inflammation phase could persist for several months until it is eventually inhibited by the development of a glial scar. However, this scar formation can hinder natural plasticity and tissue regeneration processes [20].

13.2.1.2 Features of Pathological Microenvironments in Nerve Injury

There are several features in the pathophysiology process of nerve injury, which are potential immunomodulatory targets.

Excitotoxicity

Glutamate is the principal neurotransmitter responsible for facilitating rapid synaptic transmission between presynaptic neurons, postsynaptic neurons, and glial cells. It binds to glutamate receptors located on various postsynaptic neurons, thereby playing a vital role in synaptic plasticity, memory, learning, and other cognitive functions. Ionotropic glutamate receptors, including N-methyl-D-aspartate (NMDA), α-amino-3-hydroxy-5-methyl-4-isoxazole-propionicacid (AMPA), and Kainate, require extracellular binding of glutamate to become activated. Even though the concentration of glutamate is 10,000 times higher inside the cell than outside, these receptors remain inactive without extracellular glutamate binding. Large amounts of intracellular neurotransmitters (e.g., glutamate) are released from apoptotic cells caused by the primary injury. The glutamate receptors, encompassing both NMDA and non-NMDA types, become hyperactivated. This results in an excessive influx of Ca^{2+} ions, as well as the accumulation of Na^{+} and chloride (Fig. 13.2). The disrupted osmotic equilibrium finally results in cell lyses [21].

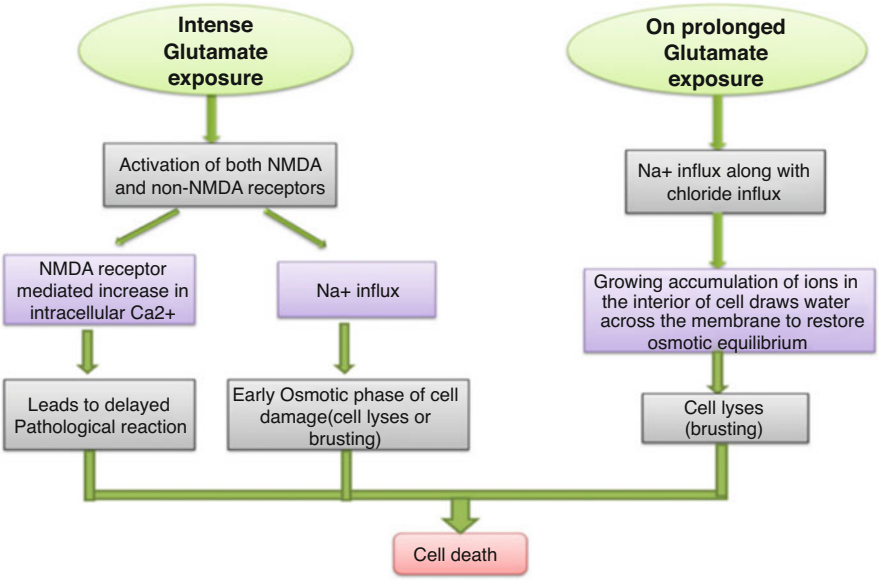

Fig. 13.2 Mechanism of excitotoxicity. (Reprinted from [21] with permission. Copyright 2013 Elsevier)

Oxidative Stress and Inflammatory Response

Similar to other injury, overproduced reactive oxygen and nitrogen species (ROS/RNS) induced oxidative stress and inflammatory response including highly expressed inflammatory cytokines, chemokines, and other mediators are prominent in pathophysiology process of nerve injury. ROS/RNS are produced after injury to eliminate pathogen and infected cells. However, the accumulation of highly reactive ROS/RNS in chronic nerve injury can lead to significant damage to essential cellular components such as DNA and proteins, resulting in the impairment and destruction of normal cells and tissues [21, 22]. The production of inflammatory cytokines, including IL-1β, TNF-α, and IL-6, is initiated by microglia/macrophages with proinflammatory properties as well as immune cells located in the peripheral regions. These cytokines and chemokines recruit immune cells into the injury core after BBB damage and arose intense inflammatory response [23]. For example, TNF-α can arouse enlarged inflammation through mitogen-activated protein kinase (MAPK) signal pathway and activating canonical NF-κB pathway [24–26]. Besides, TNF-α can induce cell apoptosis/necroptosis, in most circumstances, via kinase receptor-interacting serine/threonine-protein kinase1 pathway [25, 27, 28].

Neurogenesis Inhibitor

It is difficult for nerve tissue to regenerate after injury especially for central nervous system. There are mainly two types of barriers that separate nerve bridging and inhibit neurite growth. The first is proteins associated with myelin debris including the myelin-associated glycoprotein, myelin proteins Nogo, and oligodendrocyte myelin glycoprotein. The second deposit is comprised of chondroitin sulfate proteoglycans (CSPGs), which consist of lecticans, phosphacan, transmembrane protein NG2, and small leucine-rich proteoglycans including biglycan and decorin [7]. Dai group identified that several functional regions of Nogo-A including Nogo-66 can promote the differentiation of neural progenitors into glial cells via mTOR-STAT3 pathway [29, 30]. The inhibition of neuronal growth by CSPG involves multiple receptor proteins, such as protein tyrosine phosphatases (PTPσ), leukocyte common antigen-related phosphatase (LAR), NgR1, and NgR3 [31, 32]. Besides, CSPGs might act by hindering the signal pathway of molecules that promote growth, such as laminin and its receptor integrins. RhoA-Rho kinase signaling and Akt and Erk pathways were reported in CSPG inhibition, and more molecular mechanisms are under investigation [33].

13.2.2 Brief Regeneration Process Description

To gain a better understanding of the mechanisms that control intrinsic regenerative ability, it is crucial to comprehend how injury detection occurs and which internal signaling events trigger and coordinate regenerative responses in both axon and soma. In this regard, we will begin by summarizing the general regulatory mechanisms involved in PNS regeneration. Subsequently, we will discuss various manipulations that may be employed to promote axon regeneration in the adult CNS.

13.2.2.1 Growth Cone Formation

Following axonal damage, several cellular processes take place at the injury site such as rupture of the axon's plasma membrane, influx of calcium and iron, and disassembly of the cytoskeleton, among others. However, the recovery of the nerve heavily relies on the reestablishment of growth cone-like structures within a few hours of experiencing a crushing injury. As revealed by in vivo imaging, the formation of growth cone is the first process of axonal regrowth [34]. The motile growth cone in the mammalian PNS undergoes a restructuring of its cytoskeleton, resulting in the formation of a polarized extension that guides its movement. But, affected by the largely disorganized microtubules and unique microenvironment, the injured CNS axonal stumps undergo transformation into a retraction bulb without exhibiting regenerative response [35].

13.2.2.2 Extension of Regenerating Axons

It is possible that the regeneration of damaged nerves involves a process similar to axon growth during embryonic stages, but with additional obstacles to overcome. The injured axons are repaired by the cell body through a process of regeneration that involves bridging the gap between the stumps, starting from the proximal end and extending toward the distal end. During the initial stage of axon regeneration, existing vesicles within the proximal axon segment can merge with the axolemma to repair the membrane and support temporary axonal sprouting. As axonal growth progresses in later stages of regeneration, the requirements of lipids and proteins at extending axonal terminals are more dependent on the local synthesis to sustain regenerative growth [36]. Therefore, a crucial transformation occurs during the regeneration of neurons, which involves a shift in metabolic status from quiescent metabolism observed in mature neurons to an active anabolic metabolism in the regenerating neurons. However, injury in the adult CNS can often impede local synthesis, which can lead to the failure of neuronal regeneration after injury [37].

13.2.2.3 Role of Neural Signals

After a partial injury in the CNS, both animals and humans tend to recover some degree of function spontaneously, which is attributed to the reorganization of surviving axons [37, 38]. However, transected axons exhibit minimal growth responses. Additionally, injured neurons undergo changes such as atrophic cell bodies, decreased axonal transport, and dystrophic growth cones [39]. These changes may cause a decline in the intrinsic regenerative ability of adult CNS neurons. Although damage sensors activate evolutionarily conserved responses, the interpretation of such signals varies greatly among injured axons' cell bodies. Nawabi and colleagues used proteomic methods and gene network analysis on injured mouse retinal ganglion cells to identify a set of injury-induced signaling alterations that included well-known regeneration regulators such as calcium, p53, JAK/STAT, and MAPK, as well as components of mTOR pathway such as Rictor, Raptor, mTOR, and c-myc [11, 40] (Fig. 13.3).

13.3 PNS Therapeutic Strategies

Despite the ability of the peripheral nerves to regenerate, the functional recovery is exceedingly challenging and necessitates the use of artificial techniques for more effective treatment [6, 41]. The most widely utilized form of treatment for peripheral nerve injuries (PNI) is surgery [42, 43]. Neurorrhaphy is typically used to suture together the proximal and distal ends of nerves with short gaps, which are less than 1 cm in length [41]. The gold standard for repairing long peripheral nerve gaps

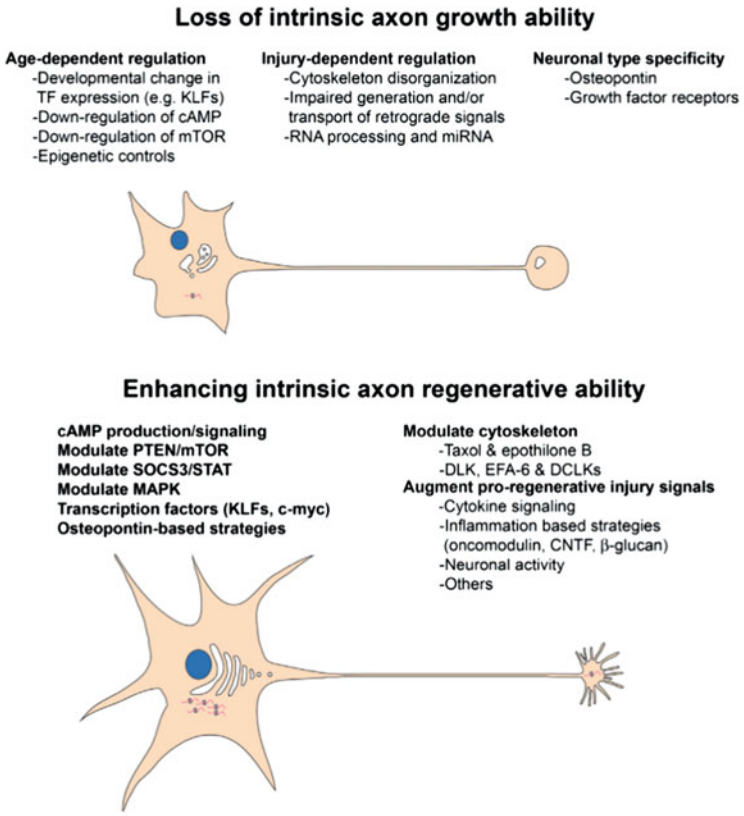

Fig. 13.3 Developing strategies to promote regeneration by targeting various intrinsic control mechanisms involved in the regenerative process. (Reprinted from [11] with permission. Copyright 2022 Elsevier)

(>2 cm) is considered to be nerve autografts, which involve implanting a graft of the patient's own nerve tissue from another part of their body [6, 41, 44, 45]. However, donor-site morbidity, surgical difficulties, tissue availability, and a diameter mismatch between the recipient nerve and the graft limit the application of autologous nerve transplantation [41, 46, 47]. The use of artificial nerve guide conduits is being investigated as an alternative therapy strategy to address the limitations of nerve grafting approaches [45].

The term "nerve guide conduits" (NGCs) refer to nerve guidance channels constructed of natural and/or synthetic biopolymers that are intended to bridge nerve injury sites, which generally have mechanical and physiological properties for neural regeneration. In this chapter, we will discuss the development of different designs and materials utilized in NGCs, along with exploring the manufacturing techniques and cutting-edge technologies employed.

13.3.1 Design of the Nerve Guide Conduits

13.3.1.1 Single Hollow NGCs

The earliest studies on utilizing tubulation to reconnect peripheral nerve gaps appeared in the nineteenth century [48]. In 1879, Neuber created a decalcified bone tube that could be absorbed by the body. This tube was initially used for wound drainage purposes [49]. Later in 1881, Gluck utilized this bone tube as a conduit to guide nerve regeneration [50]. Based on the concept of the single hollow tube, the first-generation NGCs were generally created as single hollow structures, which allow axonal elongation and steer regenerating axons to reconnect with their target neurons [51, 52]. The regenerative development of peripheral injured nerves in a hollow NGC could be succinctly represented in 5 phases (Fig. 13.4) [53, 54]: (1) the fluid phase; (2) the matrix phase; (3) the cellular migration phase; (4) the axonal phase; and (5) the myelination phase. After the injury, plasma exudate from both ends of the nerve fills the conduit which leads to an accumulation of neurotrophic factors and precursor molecules of extracellular matrix (ECM) over a period of several hours. Within the first week, an acellular fibrin cable forms between the injured nerve stumps in the second phase, which usually results in an ECM bridge for the subsequent stage. Then, the cellular migration begins, and Schwann cells (SCs), as well as a few endothelial and fibroblast cells, infiltrate into the gap along this fibrin cable. Following their proliferation and alignment, these SCs create an aligned SC cable—also known as the Büngner glial bands. Following the SCs cable, immature axons begin to regrow in the axonal phase, which occurs 2 weeks after the injury. The biological cues provided by the cable help guide the axons toward their distal targets. Once this process is complete, SCs transform into a myelinating phenotype and generate myelin, which wraps around each axon to produce mature myelinated axons.

The NGCs' hollow structure has been demonstrated that supports regenerative peripheral axons to be separated from fibrotic tissue, protects from mechanical pressures, reduces the growth of extra nerve fibers, and promotes the build-up of a dense concentration of neurotrophic factors. [53, 55, 56]. It also has the merit of simplicity and is easy to manufacture, making it extremely useful in clinical applications [45]. Between 1995 and 2010, the majority of Food and Drug Administration (FDA)-approved NGCs made of different materials have hollow structures and are used extensively in clinical treatment, including the Neurotube®, NeuraGen®, and Neurolac® [57–59].

However, the clinical application of hollow nerve guides that have been approved by the FDA or CE (European Conformity) is currently restricted to bridging nerve defects that are no longer than 3 cm in length [56]. The advantages of a single hollow conduit are outweighed by its limitations, for example, the improper dispersion of regenerative axons and incomplete reinnervation [60], the insufficient levels of regeneration because of the inadequate formation of ECM [61]. Moreover, the stiffness of the conduits is not strong enough to withstand the mechanical strain

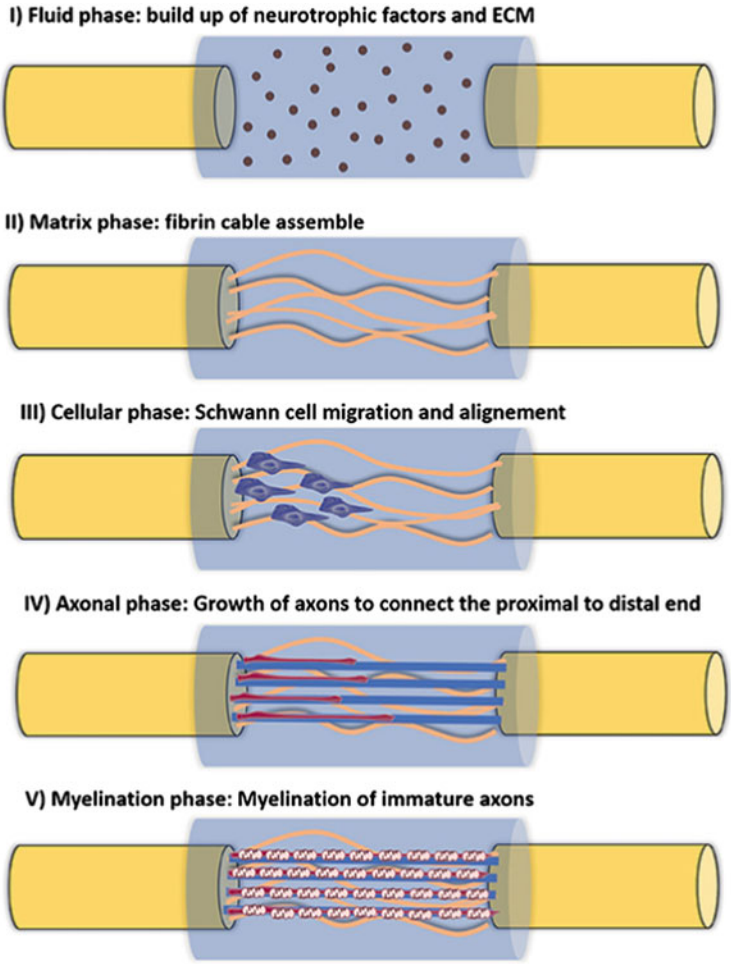

Fig. 13.4 Five different stages of nerve regeneration occur within the hollow NGC. (Reprinted under the terms of the CC-BY 4.0 license [53]. Copyright 2019, The Authors, published by Frontiers)

from the surrounding tissue [59]. A proposal has been made for the further advancement of hollow conduits with more sophisticated structural designs in order to enhance results after repairing nerve gaps that are larger.

13.3.1.2 Optimizing the Hollow NGCs

The insufficient development of fibrin cables as an ECM component results in the inability of the solitary hollow structure in the long nerve gap to sustain sufficient formation of the SC cable. Due to this, the SCs are unable to align through the injury

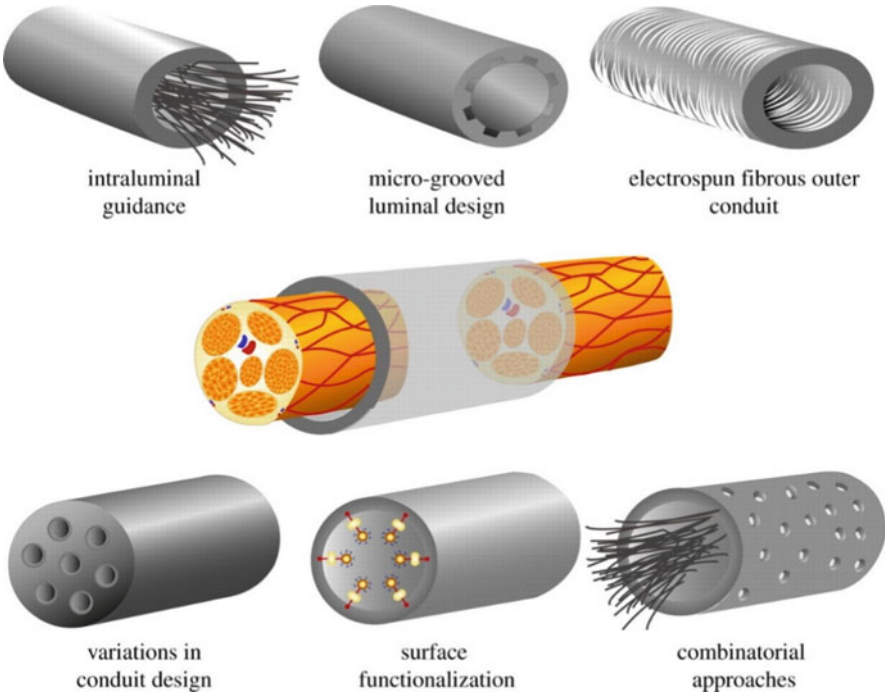

Fig. 13.5 Schematic summary of the structural repair strategies used to improve existing hollow nerve-guided catheters. (Reprinted from [54] with permission. Copyright 2012 The Royal Society)

site, which leads to a decrease in the formation of Bands of Bungner. These structures provide topographical guidance for regrowing axons, and their absence is the primary reason for poor regeneration [62]. Typically, as axons grow and extend, they form specialized structures at their tips called growth cones. These growth cones use filopodia and lamellipodia to explore and interact with the surrounding environment at a very small scale, seeking out specific cues that guide them toward their intended targets [56]. Thus, researchers have focused on how to control the development of axon by adding or manipulating the internal structure of the conduits to improve nerve recovery. These approaches (Fig. 13.5) have been employed to limit the spreading of axons, enhance the exchange of nutrients, and create a peripheral nerve environment that more closely mimics its microarchitecture [54].

Multichannel NGCs

The early version of the improved design introduced multichannels or microchannels into the tube to direct the regeneration of individual nerve fascicles

in a manner that mimics the architecture of the nerve fascicles. The use of multi/micro-channels increases the surface area available for cell attachment and growth factor release, thereby enhancing nerve regeneration. Hadlock et al. fabricated a polymer multichannel conduit with finely controlled diameters and hole positions that simulate both skeletal muscle basal lamina and autograft architecture for bridging peripheral nerve defects in 2004. This unique channel structure increases by up to five times the surface area available for Schwann cell attachment in comparison to a single hollow conduit [63]. Yao et al. found that this design could decrease the overall axonal dispersion/misdirection. A range of collagen conduits, including 1-, 2-, 4-, and 7-channel conduits, were utilized to examine the impact of channel number on axonal regeneration, along with commercially produced single channel conduits (NeuraGen®). Their findings demonstrated that the 1-channel and 4-channel conduits developed in this study showed superior results in terms of axonal regeneration when compared to other conduit types. Additionally, they demonstrated that, compared to a 1-channel conduit, a 2- and a 4-channel conduit dramatically reduces the proportion of motor neurons with double projections [64]. According to this study, the use of multichannel tubes has the potential to prevent axons from being misdirected and improve the success of reinnervation with their corresponding targets. Until now, the multichannel nerve conduits are still a popular study topic, but the present generation of multichanneled NGCs are ill-suited for axon ingrowth because of their low mechanical flexibility, permeability, and tiny cross-sectional area of channels [65–67]. The blunt edges of a multichanneled conduit can cause nerve fascicles to deform, as the outer layer of the conduit is directly sutured to the edge of the nerve segments' epineurium. This presents an immediate concern that may result in surgical complications [68]. A microchannel NGC with a jacket layer designed by Belanger et al. solved this problem commendably, and they found that the mechanical properties could be improved by using multilayer materials [69]. Although huge efforts have been taken on improving the multichannel NGCs, this design cannot avoid the same defect as the single-channel conduit—when the nerve gap is too long, the insufficient formation of the Bungner band will cause deficient nerve regeneration. Therefore, it is still necessary to take the manufacturing complexity into account and make further improvements before applying for clinical translation.

Intraluminal Guidance Structures

The addition of structural intraluminal guide cues or physical lumen fillers is one topical nerve healing technique. These topographical cues could either replace the incomplete or unformed fibrin cable or serve as an extra anchor to help the fibrin cable formation [70], overcoming the limitation of single-channel and multichannel conduits to some extent. The pioneering work to improve the hollow conduits by adding fillers was performed by Lundborg on silicone tubes. A new type of artificial nerve graft was developed in 1997, made up of eight polyamide filaments with a diameter of 250 μm, enclosed within silicone tubes that had an inner diameter of

1.8 mm. This graft was successful in bridging an extended 15 mm gap in the sciatic nerve of rats, whereas conventional silicone tubes were unable to achieve comparable nerve repair results in similar conditions [71]. After that, some researchers bent their efforts to incorporate structural intraluminal guidance cues into the hollow NGCs, which could be concluded in aligned fillers and irregular fillers. The former methods aim to introduce supporting fibers parallel to the axis of the axon to enhance the guidance of regenerating axons [72, 73]. Huang and colleagues developed a compound scaffold using electrospinning poly(ε-caprolactone) (PCL) with directionally frozen orientated collagen-chitosan filler. Their study showed that this scaffold, which had evenly distributed longitudinal guidance fillers, has promising clinical applications, as it promotes nerve regeneration and functional recovery [74]. The latter involves the addition of hydrogel or sponge materials with high porosity to facilitate the exchange of nutrients, offer adequate mechanical qualities, or mimic the natural microenvironment for cell growth [75–77]. The neurotrophic factors or exogenous cells could be added to the hydrogel or sponge materials to further promote nerve regeneration. BD™ PuraMatrix™ peptide hydrogel prepared by BD Biosciences was tested as a carrier within a tubular membrane conduit to promote regeneration across a 10 mm gap after PNI [78]. The double-layer composite hydrogel nerve conduit constructed by injecting conductive hydrogel into the cavity of chitosan conduit significantly promotes sciatic nerve regeneration compared with the chitosan hollow conduit [79]. Bian et al. created an injectable hydrogel using bisphosphonates that provide continuous delivery of Mg^{2+} in combination with a 3D-engineered PCL conduit to facilitate the regeneration of peripheral nerves [80]. However, not only axon-regenerating rate but also nutrient exchange efficiency decline when the fillers have excessive density, inappropriate position, or erratic distribution. According to Ngo et al.'s research, it is crucial to take into account both the "packing density" (or "void fraction") and the distribution of intraluminal structures when incorporating them into hollow NGC [81]. Thus, the impact of the fillers' density, porosity, or distribution on nerves should be investigated before the application of the NGCs with intraluminal Guidance Structures.

Although most clinical NGCs are designed as hollow structures, the tubes with fillers, known as the second-generation axon guidance channels, are gradually taken to the clinical stage. In 2012, a study conducted on rats demonstrated that the incorporation of synthetic collagen basal-lamina matrix along with chondroitin-6-sulfate into the lumen had a significant positive impact on both bridging the nerve gap and improving functional motor recovery [82]. In 2014, Shakhbazau and colleagues suggested that a collagen-glycosaminoglycan (GAG) matrix which mimics the Schwann cell basal lamina could serve as an appropriate and biologically reasonable substrate for nerve regeneration [83]. Recently, the FDA-approved NeuraGen® 3D Nerve Guide Matrix, which is composed of collagen I shell and porous inner collagen matrix with chondroitin-6-sulfate, was launched by Integra Life Sciences Holding Corporation on March 22, 2022. This conduit has been created with the aim of facilitating an ideal healing environment for nerve repair in cases with short to mid-gap injuries.

Luminal Wall Improvement

Numerous regeneration processes, including cell differentiation, survival, and migration, are influenced by the interactions between cells and nerve conduits (cell–ECM, cell–cell). Thus, the scaffold surface is a crucial interface element of NGCs that could be modified and improved to promote the biological conditions for nerve regeneration.

Some approaches are concentrated on physical alterations in the luminal wall, which are other physical guidance signals akin to the intraluminal guidance structure within a hollow NGC. These filaments range from orientated or nonorientated micrometer-scale features to the more biomimetic nanoscale topographies [53]. The ability to aid axonal growth cones in recognizing and reacting appropriately to the surrounding environment, ultimately guiding them toward the distal stump, is a potential function assisting nerve regeneration [84, 85]. Ouyang et al. developed an effective method to electrospun nanofibers with multiple longitudinal nanogrooves into a fibrous NGC, and proved that this ordered structure can considerably enhance nerve regeneration [86]. Gao et al. discovered that an NGC featuring both linear groove micropatterns and peptide gradients can significantly hasten the regeneration of the sciatic nerve, leading to improvements in rate, functional recovery, microstructures, as well as a reduction of fibrosis in muscle tissues [87]. The grooved design of the conduit solves the issues of low cross-sectional area or porosity. The inner layer, which is longitudinally aligned, offers topographical cues that aid in the regeneration of axons and the migration of SCs. Meanwhile, the outer layer provides structural support to the conduit while maintaining its porosity.

Generally, it is not enough to further promote nerve regeneration by altering the structure of the NGCs only, because the materials' surfaces with hydrophobicity are unsuitable for cell adhesion or proliferation [88]. There has been significant research dedicated to enhancing scaffold surfaces with biomolecules, which can be accomplished through several methods including full protein coatings, physical adsorption or covalent conjugation of proteins, and the incorporation of protein mimetics onto material surfaces [54]. For example, introducing ECM proteins as NGC luminal wall coating as a biochemical contact-guidance cue for axonal growth [89], and using the short chain protein peptide mimetics such as RGD and IKVAK et al. can enhance the adhesion and proliferation of neural cells [87, 90, 91].

Combination Strategy

Relying on a certain type of structural design alone cannot completely solve all the problems in the regeneration process of the nerve gap. Recently, research is absorbed in integrating two or more structural transformation methods in NGCs to repair nerve injury. For instance, Wang and Mo et al. fabricated a 3D biomimetic nerve conduit from silk fibroin and adopted a multiscale strategy to conquer the flaw of the low cross-section available for nerve regeneration, which more closely resembles the

natural milieu of the peripheral nerve. By utilizing 3D nanofiber sponges with parallel multichannels, researchers were able to create biomimetic nerve guidance conduits (NGCs) that mimicked the perineurium-like structures found in autografts. Through a series of analyses, it was demonstrated that these NGCs were effective in repairing sciatic nerve defects in vivo and showed similarity to autografts [68]. Park and Jung et al. utilized a nanoporous poly(lactide-*co*-ε-caprolactone) (PLCL) membrane coupled with an inner-aligned gelatin hydrogel to design a nerve guidance conduit (NGC). The gelatin hydrogel possessed a microgrooved surface pattern that acted as a conducting guidance path for axonal regeneration and also served as a reservoir for the incorporation and release of bioactive molecules. This approach resulted in promising outcomes, demonstrating successful axonal regeneration [92]. Gao and Zhang et al. combined the surface topographical features and distribution of biochemical cues to design an NGC with both the micropatterns and functional CQAASIKVAV peptide gradient, demonstrating that the different structures of NGCs play a synergistic role in rat nerve regeneration [87].

13.3.2 Materials of the Nerve Guide Conduits

For the NGCs, the material selection is a crucial factor that should take the rigorous safety, nutrition exchange efficiency, biocompatibility, biodegradability, and mechanical properties et al. into consideration before the NGCs used in the application [93]. It generally can either be natural or synthetic (bioabsorbable or nonabsorbable) [94].

One of the earliest materials utilized for nerve regeneration is synthetic nondegradable silicone, because silicone performs admirably in the healing of peripheral nerve damage, creating an isolated environment for nerve regeneration [52, 56]. The first FDA-approved silicone rubber sheath was invented in 1985 [93]. Several researchers have reported successful nerve repairs utilizing these products [52, 95, 96]. Clinical studies revealed that the silicone chamber could effectively repair nerve gaps between 3 and 5 mm in length [97]. However, the nondegradability, poor mechanical properties, and nonmachinability make the silicon tubes gradually eliminated from the field of peripheral nerve treatment. Now, the silicone tube has been used as a template to evaluate the regenerative effect of other materials [98]. Chen et al. demonstrated that the silicon NGC filled with collagen-, laminin-, and fibronectin-gel could result in further nerve regeneration compared to the empty silicone tubes [99].

Since the widespread use of silicone NGCs in nerve regeneration, researchers have explored a variety of natural, synthetic, and composite biopolymers to create NGCs. Each option has its advantages and disadvantages.

13.3.2.1 Synthetic Materials

Synthetic materials can be fabricated into 3D structures while maintaining regulatable mechanical properties. To avoid the inflammatory response and secondary removal operations associated with the nondegradable conduits, the enhanced NGCs have a tendency to opt for biodegradable materials that break down naturally within a reasonable time frame and provoke only mild foreign body responses. In 1990, the first clinical absorbable NGCs made by polyglycolic acid (PGA) were studied by Mackinnon and Dellon, and the clinical report has determined that utilizing a bioabsorbable PGA tube for the reconstruction of nerve gaps up to 3.0 cm yields clinical outcomes that are at least equivalent to those achieved through the traditional nerve graft procedure, while simultaneously circumventing any potential donor-site morbidity [100]. Then, the PGA conduits were approved by FDA and named Neurotube® in 1995 [58]. Other than PGA, there has been extensive research on the use of aliphatic polyesters such as polycaprolactone (PCL), poly (lactic acid) (PLA), and their copolymers (PLCL) for the fabrication of nerve guidance conduits (NGCs). Indeed, these polymers have been used widely in FDA-approved devices as well [45, 101]. PCL is a biocompatible, biodegradable, cost-effective, and nontoxic semicrystalline biomaterial and has excellent mechanical properties, and electrospun PCL fibers could be similar to those of peripheral nerve ECM [102]. Reid and Luca developed the PCL NGCs, which displayed promising peripheral nerve regeneration in short and long-term studies [103]. PLA fiber-reinforced conduit was used by Lu et al. to repair a 10 mm gap in the rat sciatic nerve, resulting in successful regeneration at 8 weeks after operation [104]. While NGCs have shown superior results, they still face significant limitations such as a fast degradation rate leading to a reduction in short-term mechanical properties, the presence of acidic degradation products and low solubility [58]. These disadvantages could be overcome by tailoring polymeric properties such as copolymerization because the degradation property is regulated by the crystallinity and molecular weight of the synthesized copolymers [45]. Meek et al. synthesized a copolymer NGC from lactide and caprolactone to bridge a 12 mm sciatic nerve gap [105]. Wu altered the proportion of glycolide and lactide monomers to control the degradation rate and rigidity of poly(lactide-*co*-glycolide) (PLGA) copolymers [106]. Besides, there has been some interests in exploring poly(3-hydroxybutyrate) (PHB) [107], poly(phosphoesters) [108], and polyurethanes [109] as possible candidates for NGC materials.

13.3.2.2 Natural Materials

Natural polymers have a wide application in tissue engineering because they are biodegradable and biocompatible, nonimmunogenic, and hydrophilic, favoring the migration of supporting cells [110]. Natural polymers such as laminin, fibronectin, and collagen, as well as proteins such as silk fibroin and keratin, and polysaccharides

including chitosan and alginate have been the primary components of ECM utilized for nerve reconstruction in recent decades [43]. Collagen, as a major constituent of ECM, is widely utilized as a biological material for various purposes, including peripheral nerve regeneration. Current commercially accessible NGCs such as FDA-approved NeuraGen®, NeuroFlex™, NeuroMax™, NeuroWrap™, and NeuroMend™ are mainly made from cross-linked bovine collagen I [58]. Clinical trials utilizing NeuraGen tubes for repairing nerve gaps up to 18 mm within the hand demonstrated encouraging outcomes [111]. In China, clinical trials with nerve grafts made of chitosan have been authorized by China's State Food and Drug Administration (CFDA) [112]. However, to improve the physiochemical properties such as mechanical strength, degradation/swelling, and stability, it is necessary to take into account material modification, since natural polymers have weak mechanical properties and are difficult to fabricate into 3D structures [43].

13.3.2.3 Composite Materials

There are few contemporary single-material NGCs because the biomaterials are usually modified or blended to meet the requirements of ideal NGCs. The composite materials include natural composite NGCs, synthetic composite NGCs, natural and synthetic composite NGCs, and organic-inorganic composite NGCs [93]. These composites have the ability of certain mechanical properties, adjustable degradation rates, and excellent biocompatibility. For example, Matsumine et al. created a biodegradable hybrid nerve conduit comprising of PGA and collagen. The conduit was filled with either adipose-derived stromal cells or stromal vascular fraction. Upon grafted this NGC onto the nerve defects, an excellent nerve regeneration effect was shown at 13 weeks [113]. Yu and Mo et al. developed a nerve guidance conduit using polypyrrole-coated PLCL/silk fibroin nanofibers. The conduit was tested on rats and shown to promote nerve regeneration by inducing proliferation of SCs in the early postsurgery stage and enhancing myelin formation in the later postsurgery stage [114].

13.3.3 Tissue-Engineered Nerve Grafts (TENGs)

Recent developments in tissue engineering have led to the emergence of a subfield dedicated to neural tissue engineering. In this field, tissue-engineered nerve grafts (TENGs), comprised of both artificial and biological nerve grafts, have been developed as a potential substitute for or supplement to autologous nerve grafts [41]. To best direct the regeneration of peripheral axons to their correct destinations and enhance the outcome of utilizing NGCs only, the novel TENGs strategies are not only the varieties of materials or structures of the NGCs but also the combination with drug/gene/growth factors/cells delivery or external stimuli to promote the nerve regeneration [43, 115].

During the process of peripheral nerve regeneration, Schwann cells (SCs) secrete and up-regulate various growth factors such as nerve growth factor (NGF), leukemia inhibitory factor (LIF), glial-derived neurotrophic factor (GDNF), ciliary neurotrophic factor (CNTF), growth-associated protein (GAP-43), brain-derived neurotrophic factor (BDNF), and neurotrophin-4 (NT4), among others. These growth factors play a significant role in axon regeneration. Upon injury to peripheral nerves, the growth factors produced by SCs will gradually decline and cannot be sustained indefinitely. Thus, the continuous supply of growth factors is critically required. Some researches design the TENGs with the ability to control the release of exogenous neurotrophic substances to improve nerve regeneration. A novel technique was devised by Nawrotek et al. to incorporate microspheres containing biologically active nerve growth factor into chitosan/polycaprolactone conduits. This approach has the potential to promote axonal growth and support regrowth of nerves over an extended period [116]. Besides, the structure of the scaffold itself can also be altered to promote sustained delivery. A multilayered fibrous scaffold was developed and fabricated by Koh and Hong et al., which consists of three layers (the first layer is aligned to provide topographical cues, while the following two layers are randomly oriented) and can release multiple growth factors in a controlled manner. This scaffold has potential applications in sciatic nerve regeneration in rats [117]. In addition to delivering growth factors, the delivery methods can also be utilized for delivering medicinal molecules and gene vectors. Gene therapies targeting neurotrophic factors have demonstrated the potential to stimulate peripheral axon regeneration and myelination. For instance, by overexpressing FGF-2 in Schwann cells and grafting them into peripheral nerve lesion sites, Schwann cells have been shown to promote nerve regeneration [118]. Kohn and Schulz-Siegmund et al. established a dual-component hydrogel system (cGEL) combined with an anhydride-containing oligomer. The cGEL was then modified to produce an injectable shear thinning filler for established nerve guidance conduits (NGCs), which included the small molecule LM11A-31. Their research showed that the LM11A-31 functionalized cGEL filler, which possesses extracellular matrix (ECM)-like characteristics and specific biochemical cues, has great potential to support peripheral nerve regeneration (PNR) [119].

In addition to growth factors, nerve regeneration can be aided by the implantation of seed cells, which can produce growth factors and influence the extracellular matrix. In neural tissue engineering, Schwann cells and stem cells (embryonic stem cells (ESC), induced pluripotent stem cells (iPSC), mesenchymal stem cells (MSC), adipose derived stem cells (ADSC), and neural stem cells (NSC)) are frequently employed as preferred seed cells incorporated into the NGCs. The specially manufactured NGC has excellent biocompatibility and a large specific surface, ease for increase the viability and survival rate of the cells [120]. Chen and Li et al. compared three treatment strategies (cell transplantation, multiscale scaffold, and scaffold loading Schwann cell progenitors) with respect to their regeneration efficiency and behavior of peripheral nerves. Their analysis led to the conclusion that using a scaffold treatment is more effective than relying solely on cell grafts. Additionally, preloading the scaffolds with neural crest stem cell-derived

Schwann cell progenitors yielded the most favorable results for promoting nerve regeneration [121]. Exosomes, which are nanosized extracellular vesicles released by almost all cell types, have recently been found to enhance nerve regeneration [122]. There is increasing evidence that exosome miRNAs play a crucial role in vascular regeneration [123], and that miRNAs transported by exosomes from Schwann cells, macrophages, and mesenchymal stem cells (MSCs) promote peripheral nerve regeneration [124].

Although many efforts have been made to improve the TENGs, the ideal nerve conduit should be most similar to transplantation of autologous nerve. The primary objective of future research on nerve guidance conduits (NGCs) is to enhance their functionality through the integration of stem cells, external stimuli, neurotrophic factors, and drugs. Additionally, novel techniques such as Bio 3D printing technology, which has great potential in peripheral nerve regeneration by producing three-dimensional tissue structures using only cells, are being studied and developed [125].

13.4 CNS Therapeutic Strategies

In the last decade, one of the most significant advancements in the field has been the development of various strategies that increase intrinsic regenerative ability. As a result, there is now reproducible and robust axon regrowth in the adult mammalian CNS (Fig. 13.3). The use of combinatorial manipulation of multiple factors has displayed great potential in creating therapeutic strategies for promoting functional recovery of injured axons.

13.4.1 Inflammatory-Regulating Biomaterials

Directed modulation of immune cell function to reduce neuroinflammation and promote tissue homeostasis and/or repair is a developing feasible strategy in nerve regeneration. Proinflammatory cytokines and reactive oxygen species are upregulated in neuroinflammation, leading to the recruitment of immune cells to the injured area in the central nervous system (CNS). This process ultimately promotes unwanted tissue damage [126]. Adaptive biomaterials with physiologically responsive property conjugated and/or encapsulated with active molecules and drugs could regulate the inflammatory through reducing the recruitment and infiltration of immune cells, promoting polarization of M2 macrophage/microglia and lessening the proinflammatory biological molecules (Fig. 13.6). Systemic delivery of small molecules or proteins is used in the early stages of immunotherapy or immunomodulation [128]. For example, fingolimod, an FDA-approved small molecule, can prevent T-cell infiltration by blocking sphingosine 1-phosphate signaling [129]. Unfortunately, systemic delivery of drugs causes rapid excretion or loss and

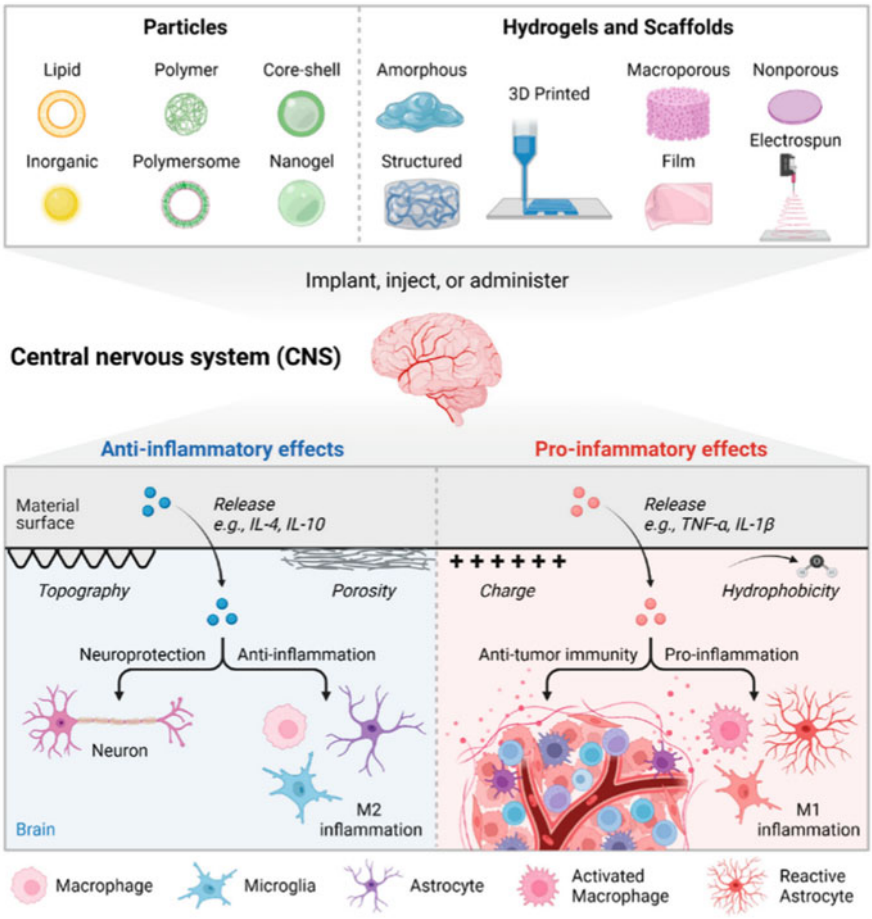

Fig. 13.6 Overview of inflammatory outcomes instructed by engineering material properties. (Reprinted under the terms of the CC-BY 4.0 license [127]. Copyright 2022, The Authors, published by MDPI)

poor targeting. Therefore, it is required to administration of large doses, leading to toxic side effects.

Biomaterials-based scaffolds allow the controlled, targeted, and local delivery of immunomodulatory factors including drugs (e.g., dexamethasone [130], Rolipram [131], minocycline [132]), proteins and growth factors [133], scavengers that can remove unfavorable factors (e.g., ROS), oligonucleotides (e.g., silencing RNA [134]), and endogenous biological signal molecules (e.g., H_2S [135–138], H_2 [139], and NO [140]). Minocycline (MC) is clinically used for antibacteria and anti-inflammation, exhibiting neuroprotective effect in cerebral ischemia, traumatic brain injury, and spinal cord injury [141]. An E-selection-targeting sialic acid-polyethylene glycol-poly (lactic-*co*-glycolic acid) (SAPP) copolymer were used to

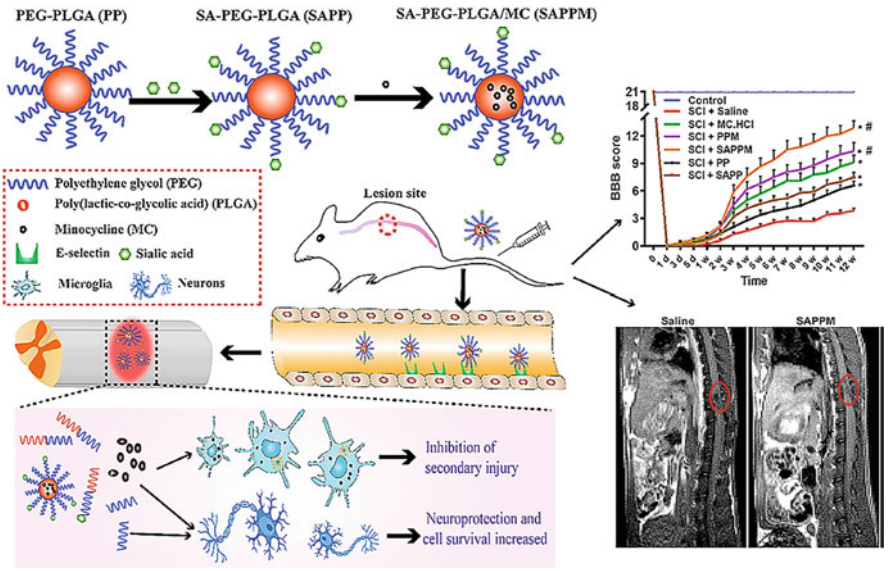

Fig. 13.7 SAPPM micelles injected to injury site inhibit secondary injury and promote functional recovery. (Reprinted from [132] with permission. Copyright 2019 Elsevier)

form micelles carrying MC (SAPPM), which deliver minocycline targeted to the lesion site and released for long time (Fig. 13.7). Such micelles could effectively accumulate in the lesion site of SCI and sustain release of MC over 72 h, inhibiting microglia activation obviously and promoting behavior recovery [132].

Proteins, especially those macromolecular proteins such as fibroblast growth factor 4 (FGF4) can hardly penetrate into blood spinal cord barrier and blood brain barrier. Sulfated glycosaminoglycans (GAGs), for example, heparan sulfate and chondroitin sulfate, are considered as reservoir to bind and stabilize growth factors and chemokines. As shown in Fig. 13.8, a laponite/heparin hydrogel loaded with FGF4 (Lap/Hep@FGF4) was used in SCI rats to reduce astrocyte migration/polarization and promote the axonal generation [133]. RNA interference has become a powerful genetic tool for gene silence in many diseases [142, 143]. However, successful gene delivery requires gene carriers with various essential features, including easy degradation, cellular uptake, and intracellular release. Functionalized curdlan nanoparticles (CMI) carrying NF-kB p65 siRNA (sip65) to knockdown NF-kB p65 in transient middle cerebral artery occlusion result in microglia phenotype conversion from M1 to M2 [134]. Biological signal molecules such as H_2S and NO have been proved to reduce macrophage infiltration and inflammatory cytokines in SCI. H_2 could remove cytotoxic oxygen radicals and activate superoxide dismutase and catalase to accomplish antioxidant purpose [134]. A near-infrared (NIR)-triggered NO release nanosystem could release NO rapidly with stimulation of NIR light, which in turn suppresses gliosis and inflammation, leading neuroregeneration and preventing neurons from apoptosis [140].

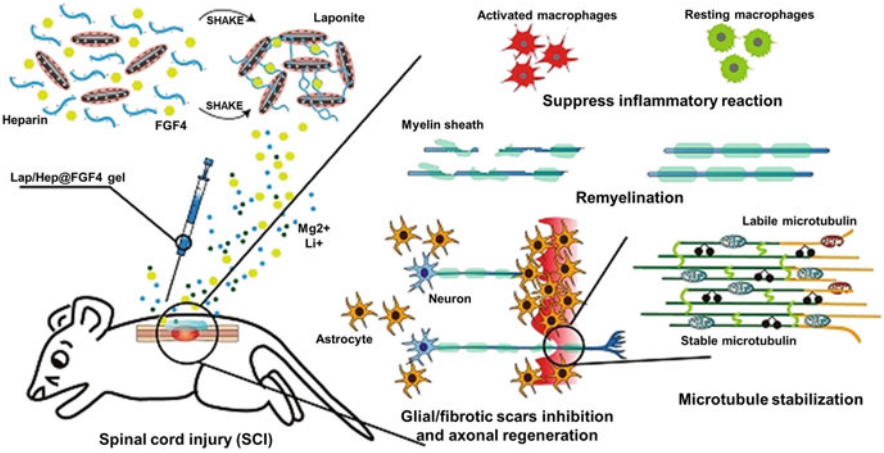

Fig. 13.8 Laponite/heparin hydrogel loaded with FGF4 suppresses inflammation and promotes remyelination and microtube stabilization. (Reprinted under the terms of the CC-BY 4.0 license [133]. Copyright 2022, The Authors, published by Ivyspring)

Recently, many studies focus on scavenging excessive production of ROS to reduce inflammation and protect nerve cells in spinal cord injury, traumatic brain injury or cerebral infraction. As shown in Fig. 13.9, several methods have been developed to scavenge ROS and thereby improve the vile microenvironment after injury, including combined with ROS-responsive unit (e.g., selenium [144], sulfur [145–149], 2,2,6,6-tetramethylpiperidinyloxy [150], thioketal diamine [147, 151], boronic acid benzyl [152]), and carried or directly applied with antioxidant enzymes (e.g., superoxide dismutase (SOD) and catalase (CAT) [153]) or nanoenzymes (e.g., cerium oxide nanoparticles [154, 155], Prussian blue nanozymes [156], Manganese-based nanozymes [157, 158], iron oxide nanoparticles [159], carbon dots nanozymes [160–162], MO-based polyoxometalate nanoclusters [163]). There are many ROS-responsive units applied to biomaterials [164]. Poly(propylene sulfide)120 (PPS120) is a kind of sulfur-containing ROS quencher responding to H_2O_2, showing good anti-inflammatory property. To achieve ROS scavenging and responsive release of curcumin at the lesion site, a hydrogel made of matrix metalloproteinase responsive triglycerol monostearate was utilized to deliver PPS120 and curcumin. This hydrogel reduces the active microglia and reactive astrocyte, and the level of proinflammatory cytokines, leading to nerve regeneration and behavior recovery [148]. Nanomaterials called nanoenzymes have been employed for treating CNS injuries caused by RONS. These materials possess stable enzyme-like activity, powerful antioxidative ability, excellent stability in a physiological environment, and are cost-effective [165, 166]. Prussian blue (PB), an FDA-approved antidote for cesium and thallium intoxication, shows excellent biosafety. Hollow PB nanozymes were used for ischemic stroke treatment, showing great antioxidative, anti-inflammatory and antiapoptotic function [156].

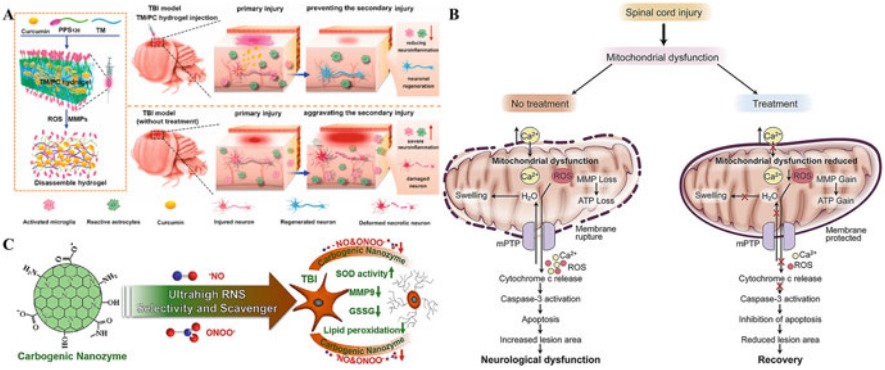

Fig. 13.9 The method to remove ROS. (**a**) Combined with ROS-responsive unit. (Reprinted from [148] with permission. Copyright 2021 Elsevier). (**b**) Supply with SOD and CAT. (Reprinted from [153] with permission. Copyright 2020 Elsevier). (**c**) Nanoenzymes. (Reprinted from [161] with permission. Copyright 2019 American Chemical Society)

In addition, several biomaterials such as chitosan and hyaluronan (HA) show anti-inflammatory properties to some extent. For instance, high molecular weight HA hydrogels could reduce the infiltration of macrophages and microglia cells, and the astrocytic response in SCI. Research has demonstrated that HA reduces microglia activation following stimulation by lipopolysaccharides through the MAPK activation pathway [167, 168]. Additionally, chitosan-NT3 material is capable of inhibiting microglia/macrophage infiltration, indicating a reduction in the immune response [169]. Overall, the inflammatory regulation shows great potential in CNS injury.

13.4.2 Bioactive Protein/Peptide Signals Regulation Biomaterials

As aforementioned, there are several features in the pathophysiology process of nerve injury. For better tissue repair after central nerve system injury, protein/peptide signals are then designed for inhibition or enhancement in different biological process, including removal of inhibitory molecules, increase of neurotrophic factors, addition of cell adhesion molecules, and decrease of glutamate excitotoxicity [170].

13.4.2.1 Removal of Inhibitory Molecules

Chondroitin sulfate proteoglycans (CSPGs) deposit after nerve injury, forming glial scar and inhibiting axonal growth. CSPG are composed of core protein and chondroitin sulfate glycosaminoglycan (CS-GAG) on side chain [20]. Enzymatic

strategies targeting CSPGs with chondroitinase ABC (ChABC) and peptide strategies for inhibiting CSPGS-receptors with intracellular sigma peptide (ISP) are promising approaches to render neuronal plasticity and connectivity.

Chondroitinase ABC (ChABC)

The ChABC derived from bacteria is a depolymerizing lyase, which can cleave a broad range of glycosaminoglycan substrates including CS-GAG. Beneficial effects have been reported for ChABC used in traumatic brain injury (TBI), spinal cord injury (SCI), and stroke, showing enhanced axonal regeneration and improved functional recovery [171–173]. The limitation for ChABC application is its thermal instability. Thus, materials-based long-time control release and gene therapy for long-term ChABC gene expression are studied. Fabrizio Gelain group designed self-assembling peptides (SAPs) hydrogel for sustained release of active ChABC after SCI [174]. The enzymatic activity of ChABC released from SAPs was maintained up to 42 days in both in vitro and in vivo measurements. In chronic SCI rats, enhanced neural regeneration exhibited after local injection of this SAPs hydrogel. Different with traditional gene delivery therapy using adeno-associated virus (AAV) and lentivirus, William L. Murphy group reported mineral-coated microparticles (MCMs) as ChABC mRNA delivery vehicles after SCI (Fig. 13.10) [175]. The

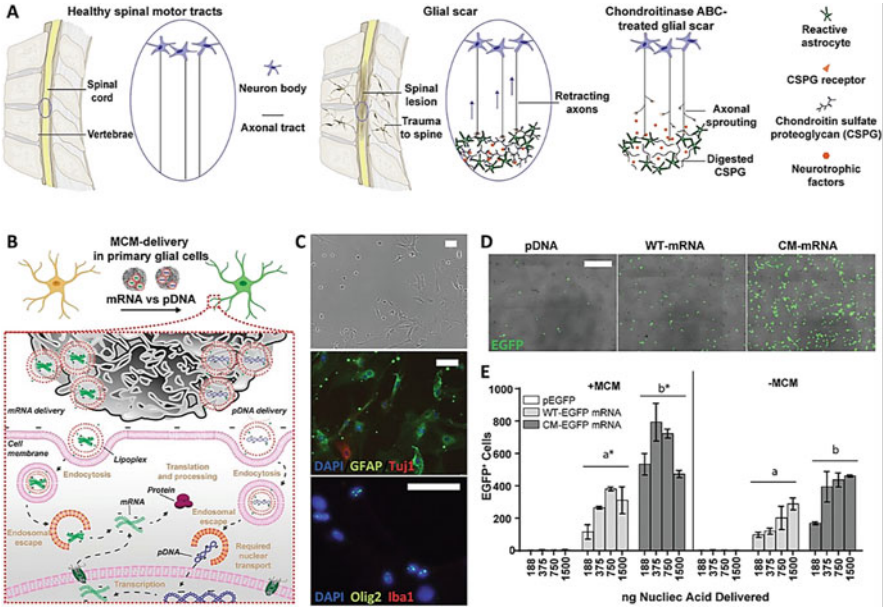

Fig. 13.10 Delivery of both MCMs and mRNA improves transfection efficiency in primary glial cells. (Reprinted under the terms of the CC-BY 4.0 license [175]. Copyright 2022, The Authors, published by Wiley)

production of ChABC was found to reduce the deposition of chondroitin sulfate proteoglycans (CSPGs) in an in vitro model of astrogliosis. ChABC was overexpressed within a glial scar after local microparticles injection, which improved the recovery of motor function seven weeks postinjury. Similar to ChABC, mammalian enzyme arylsulfatase B (ARSB, N-acetylgalatosamine-4-sulfatase), which hydrolyzes C4S moieties from CS-GAGs, has been used as another enzymatic strategy for CSPGs inhibition [20].

Intracellular Sigma Peptide (ISP)

The CSPGs take functions *via* interacting with semaphorins, members of the LAR subfamily, where PTPσ is one of the receptors [31, 176]. Based on the structure of PTPs and related phosphatases, the Jerry Silver group identified a 24-amino-acid intracellular wedge domain that is highly conserved [177]. According to inhibitory regulation mechanism of PTP, they designed ISP, including a novel peptide-mimetic of the PTPs wedge and a TAT domain (GRKKRRQRRRCDMAEHMERLKANDSLKLSQEYESI), to reduce CSPG-mediated axonal inhibition [178]. Rats were subcutaneously treated daily with ISP for 7 consecutive weeks after contusive SCI for 1 day. Enhanced behavioral results and functional recovery were observed after ISP administration. Besides, Yu Luo group performed the same ISP treatment to mouse after middle cerebral artery occlusion (Fig. 13.11), leading to significant behavioral recovery accompanied by neuroprotection, axonal sprouting, and neuroblast migration into the lesion [179]. However, a few biomaterial-based systems are designed with ISP for CNS injury. Similar to ISP, the extracellular LAR peptide (ELP) and the intracellular LAR peptide (ILP) as binding peptides have been used to overcome growth restriction of CSPGs [32, 180].

13.4.2.2 Increasing Neurotrophic Factors

The neurotrophic factors are typical bioactive molecules which are important for cell proliferation, neural differentiation, cell survival, neuronal plasticity, and axonal growth. Neurotrophic factors such as nerve growth factor (NGF), brain-derived neurotrophic factor (BDNF), vascular endothelial growth factor (VEGF), and basic fibroblast growth factor (b-FGF) are utilized for neuroprotection and regeneration due to the challenges associated with axonal regeneration after CNS injury.

Nerve Growth Factor (NGF)

NGF, the first member of the neurotrophin family, was discovered in the 1950s and has since been recognized as a critical factor in neurobiology due to its ability to regulate various important functions such as survival, growth, and differentiation of

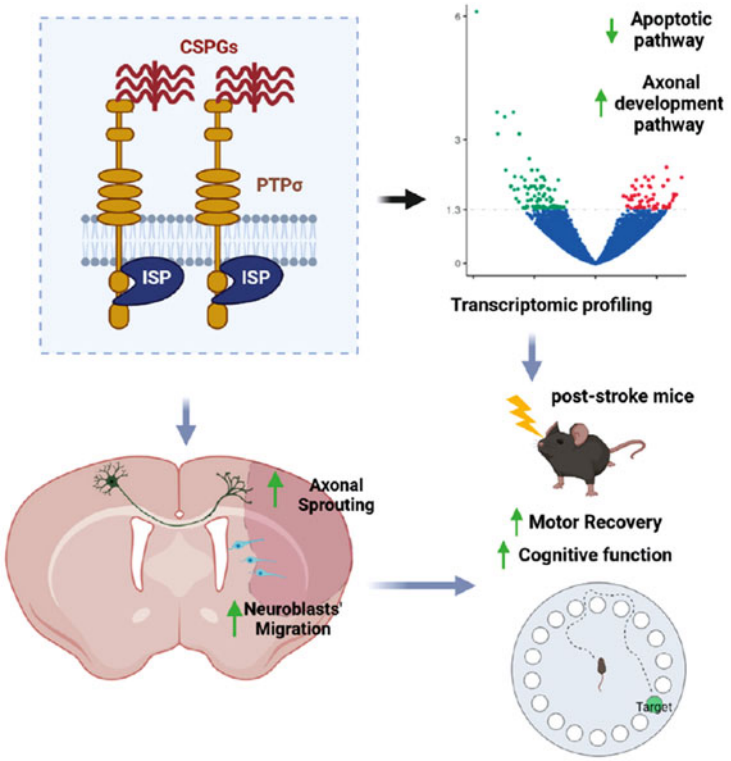

Fig. 13.11 Blocking the CSPG receptor PTPs promotes axonal sprouting, migration of newly born neuroblasts, and recovery from stroke. (Reprinted under the terms of the CC-BY 4.0 license [179]. Copyright 2022, The Authors, published by Elsevier)

nerve cells in both the peripheral and central nervous systems [181]. NGF achieves its biological effects via the tropomyosin kinase receptor A (TrkA)-mitogen-activated protein kinase (MAPK)/extracellular signal-regulated kinase (ERK)/phosphatidylinositol 3-kinase (PI3K)-Akt signaling pathway [182]. Considering the transient half-life of NGF, biocompatible scaffolds and hydrogels are developed with NGF encapsulation for effective long-time controlled release of NGF after CNS injury [183]. David L. Kaplan group reported that a silk fibroin nanofiber (SFN) hydrogel with hierarchical anisotropic microstructures can maintain the bioactivity of NGF and regulate the differentiation of neural stem cells more likely toward neuronal linage. Reduced scar formation and effective recovery of motor functions are achieved in a severe rat long span hemisection SCI model using this hydrogel matrix (Fig. 13.12) [184].

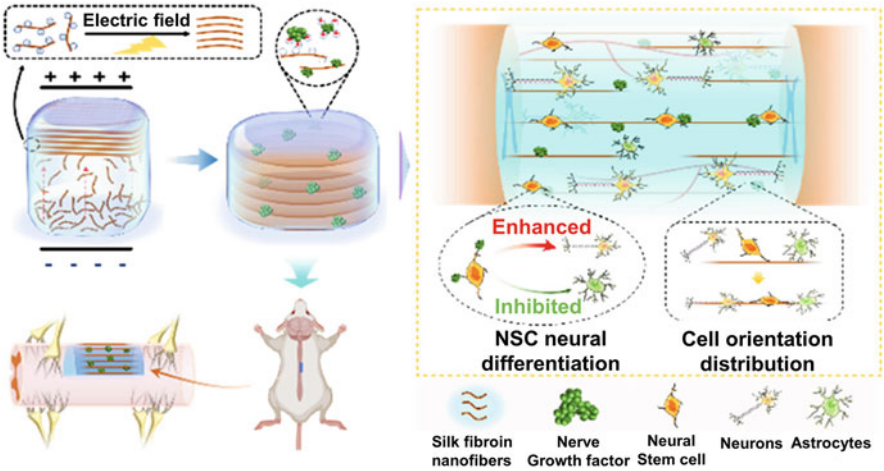

Fig. 13.12 The schematic depicts aligned SFN hydrogels loaded with NGF for long-span spinal cord repair. The aligned topography of SFN promotes neural cell proliferation and migration, whereas the NGFs regulate NSC differentiation. (Reprinted from [184] with permission. Copyright 2022 American Chemical Society)

Brain-Derived Neurotrophic Factor (BDNF)

BDNF is one of the best studied neurotrophins. By interacting with tropomyosin receptor kinase B (TrkB) receptors, BDNF plays an important role in neurogenesis, axonal sprouting, neuroprotection, myelination, and synaptic plasticity [185, 186]. Hydrogels, scaffolds, and nanoparticles are applied for BDNF encapsulation for therapy of CNS injury [187–191]. Li et al. developed a collagen/chitosan scaffold that was integrated with BDNF using low-temperature extrusion 3D printing, which preserved the biological activity of BDNF (Fig. 13.13). After eight weeks of implantation in the transected lesion of the spinal cord, the locomotor function of rats was significantly improved with the use of this scaffold [189]. Virus-based gene therapies are developed for BDNF expression, yet the sustained expression of BDNF may induce neuronal hyperexcitability and spasticity [170].

Vascular Endothelial Growth Factor (VEGF)

Ischemia-induced oxygen and glucose deprivation can lead to cell apoptosis and inflammation response. Thus, using neurotrophic factors such as VEGF to promote blood supply via angiogenesis or vascularization is a promising strategy. Compared to soluble VEGF, VEGF binding to the extracellular matrix enables sustained activation of VEGF receptor-2 (VEGFR-2). According to this mechanism, Tatiana Segura group designed a hydrogel loaded with high cluster VEGF on heparin nanoparticles to improve angiogenesis for regeneration of brain tissue and promotion of neural repair after stroke (Fig. 13.14) [192].

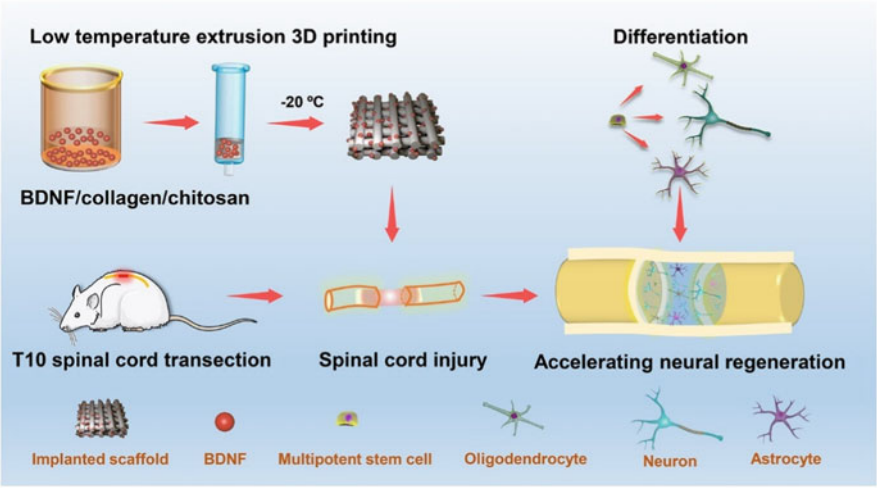

Fig. 13.13 Neural regeneration after spinal cord injury is accelerated by using printed BDNF/collagen/chitosan scaffolds that are integrated with a low-temperature extrusion 3D printer. (Reprinted under the terms of the CC-BY 4.0 license [189]. Copyright 2021, The Authors, published by Oxford University Press)

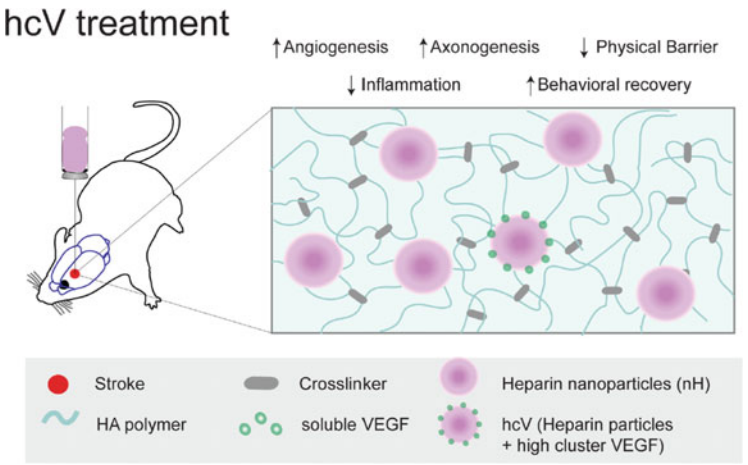

Fig. 13.14 An injectable biomaterial with dual-functionality for angiogenesis in the brain after a stroke. (Reprinted from [192] with permission. Copyright 2018 Springer Nature)

Basic Fibroblast Growth Factor (b-FGF)

The neuroprotective effects of b-FGF have been utilized to facilitate recovery in CNS injuries. Intravenous injection of b-FGF suffers several limitations such as transient half-life, significantly stimulated tumor progression and increased toxic effect especially in high dose [193]. Thus, combination with biomaterial scaffolds

seems a promising strategy for better b-FGF performance. Xiao et al. created a polymer bioactive system that immobilized umbilical cord mesenchymal stem cells (UCMSC) and b-FGF in extracellular matrix (ECM) and heparin-poloxamer (HP) to enhance mitochondrial function and decrease apoptosis (Fig. 13.15) [194].

13.4.3 Biomaterials for Regulating Cells

In most central CNS, neurons and glial cells are lost, and cell replacement occurs in the CNS lesions. However, this method cannot satisfy the function of lost cells [195]. Stem cells could be introduced to new neurons or glia cells to lesson area in CNS, showing great potential for CNS regeneration. There are several cell types that can be utilized for CNS therapy, including neural stem and progenitor cells (NSPCs), olfactory ensheathing cells (OECs), schwann cells, oligodendrocyte precursor cells (OPCs), induced pluripotent stem cells (iPSCs), and mesenchymal stem cells (MSCs) [196]. The mechanisms of action of transplanted cells including neuroprotection, immunomodulation, axon regeneration and sprouting, myelination, and relay formation [197]. Nonetheless, the implanted cell fate is influenced by the microenvironment. For example, NSPCs transplanted into host parenchyma mainly differentiate into oligodendrocytes, while they tend to differentiate to astrocytes in the lesson site [198]. In addition, allogeneic cells, for example, MSCs, have limited survival outside nervous system because of attacking by $CD8^+$ T cells and natural killer cells [199].

Biomaterials can improve cell-based therapeutics by promoting the survival, differentiation, targeting, and integration of transplanted cells, protecting host neural cells, and removing inhibitory substances. In particular, hydrogels or microgels

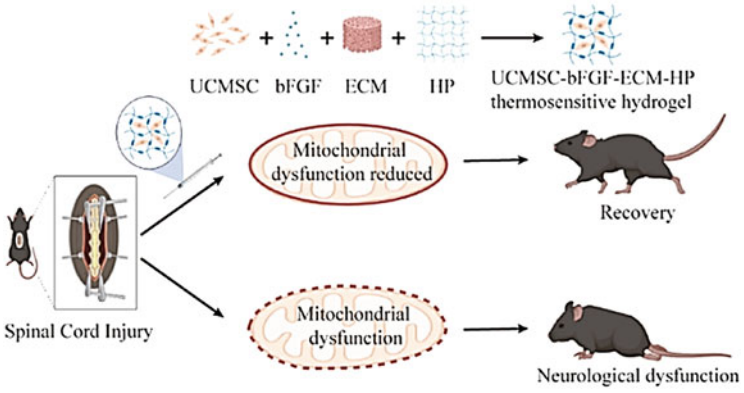

Fig. 13.15 A newly developed thermosensitive hydrogel is capable of promoting spinal cord repair by regulating mitochondrial function. (Reprinted from [194] with permission. Copyright 2022 American Chemical Society)

benefit to the endogenous cells together with transplanted cells surrounding the implant site.

Natural polymers are easily obtainable and have well-studied physical, mechanical, and biological properties. They contain cell adhesion signals and are biodegradable, although they tend to lose their biological activity during sterilization. On the other hand, synthetic biomaterials can be sterilized with ease, and their porosity, structure, stiffness, and degradation rate can be finely tuned to meet specific applications. Hydrogels or microgels have been prepared using various types of natural and synthetic polymers, including hyaluronic acid [200], chondroitin sulfate [201–203], gelatin [204, 205], poly(lactic-*co*-glycolic acid) [206], polyethylene glycol [207], and sodium alginate/collagen [208].

So far the transplanted cells have been mainly focused on bone marrow-derived MSC (BMSC) [151, 157, 205, 208], NPSC [201–203, 209], and iPSCs [200, 204, 210]. BMSC appear to have many unique features such as less immunogenicity, fewer ethical problems and extensive sources. The transplanted BMSCs in the injury site release neurotrophic factors and take part in immunomodulation, and also have a potential to differentiate into neural cells [211]. As shown in Fig. 13.16, a thiokol-containing and ROS-scavenging hydrogel encapsulated with epidermal growth factor, rat-derived basic fibroblast growth factor and BMSC were used to treat SCI. This hydrogel could regulate the hostile pathological microenvironment to protect BMSCs, leading to nerve regeneration to some extent. Besides, extracellular vesicles produced by stem cells, which contain proteins, lipids, nucleic acids, and other biomolecules, are extensively employed in the treatment of CNS injury [212, 213].

For cell therapy, besides transplanting the exogenous stem cells, endogenous repair is another method. However, neurogenesis is scarce or nonexistent in the early stages of spinal cord injury [214, 215]. Nevertheless, early studies of spinal cord injuries suggest that they retain the intrinsic ability of axons to grow. Although axon sprouting may extend beyond the lesion site, only a small number of axons are capable of long-distance regeneration to their original targets [216, 217]. Unexpectedly, recent evidence suggests that endogenous neural stem cells (also known as neural progenitor cells) have the ability to migrate tangentially from the subventricular zone (SVZ) to the neocortex via blood vessels and undergo neurogenesis in situ [218–220].

To improve the neurogenesis after CNS injury, biomaterials are combined with chemoattractants such as stromal cell-derived factor-1α (SDF-1α) [221, 222], which are designed to physical orientation [223] and microgel scaffold to promote the endogenous neural stem cell migration to the injury site [224, 225]. SDF-1α is important for endogenous NSC or neural progenitor cells (NPC) to migrate from SVZ to the injured site in long distance. By combining SDF-1α and bFGF-loaded polyelectrolyte complex nanoparticles (PCNs) with HA matrices, a nanohybrid hydrogel capable of tunable gelation via Schiff base crosslinking can be formed. This hydrogel could effectively promote endogenous NSC migration and neurogenesis, contributing to the size of stroke cavity reduction and functional recovery [221].

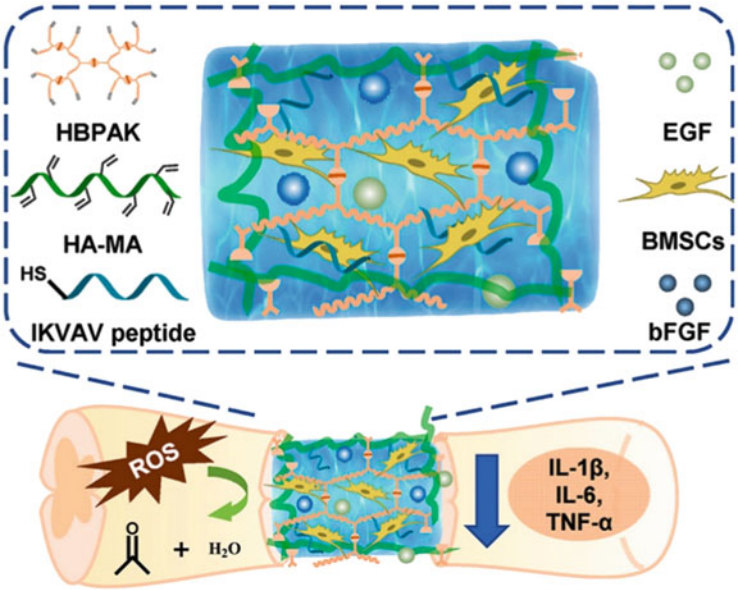

Fig. 13.16 The developed therapy for spinal cord injury involves a hydrogel containing bone marrow-derived mesenchymal stem cells and ROS-scavenging properties. (Reprinted under the terms of the CC-BY-NC-ND 4.0 license [151]. Copyright 2022, The Authors, published by Elsevier)

Radial glial (RG) cells, arranged in parallel during embryonic development of the brain, are capable of guiding neurons to migrate toward areas of brain injury using cerebral cortex RG fibers as a bridge for neuroblast migration [226]. Kawauchi et al. created an aligned fibrin nanofiber hydrogel (AFG) with molecular self-assembly properties using electrospinning. Implantation of the aligned fibrin nanofiber hydrogel in brain can facilitate endogenous neurogenesis through various signaling pathways such as Notch, Wnt, Neurotrophin, Axon guidance, and MAPK [223].

13.5 Challenges and Perspectives

Despite of numerous strategies for regeneration mechanisms and clinical applications, autografts remain the gold standard due to the lack of a viable alternative for long-segment PNS defects. Challenges such as neuron necrosis and precise axon alignment after PNS injury have not been fully addressed. The roles of revascularization in PNS regeneration also need intense research. Nonetheless, there has been notable progress in creating a variety of nerve repair materials that differ in their composition, morphology, and compliance. Notably, the utilization of functional nerve conduits based on biomaterials to bridge nerve gaps and direct PNS regeneration offers renewed optimism for the thousands of individuals affected by PNS

injuries. Based on the understanding of the molecular mechanisms of neural regeneration, novel functionalized nerve conduits have the potential to guide polarized extension, to remove growth-inhibitory substrates, to delivery growth factors, to reduce cells apoptosis, and to improve injured microenvironment on demand. In addition, immunomodulatory therapy representing by promotion of M2 macrophage polarization also shows great promise for the repair of PNS injury.

Repairing damage to the CNS is a daunting challenge due to its limited response to treatment, and effective therapies for CNS injuries have yet to be discovered. Nevertheless, the application of biomaterial scaffolds and a combination of materials and cell therapy has yielded encouraging outcomes in CNS regeneration. Biomaterial scaffolds can mitigate inflammation at injury sites while modifying the microenvironment of lesions. Moreover, they can transport neurotrophic factors and drugs to augment therapeutic effects. Additionally, merging biomaterial scaffolds with cell therapy can facilitate stem cells' survival and differentiation while decreasing the side effects associated with cell therapy. However, there are still several important issues need to be improved, for example, the biodegradability, biocompatibility, and mechanically flexibility of biomaterials, the combination therapy design across cell transplantation, drug delivery, and inflammation modulation, and the correspondence between the rate of biomaterials degradation and the phases of tissue regeneration. Considering the advancements in materials and biology, it is a plausible conjecture that we can attain complete regeneration of the CNS in the foreseeable future.

References

1. Schmidt CE, Leach JB. Neural tissue engineering: strategies for repair and regeneration. Annu Rev Biomed Eng. 2003;5:293–347.
2. Kingham PJ, Terenghi G. Bioengineered nerve regeneration and muscle reinnervation. J Anat. 2006;209:511–26.
3. Brushart TM. Nerve repair. Oxford: Oxford University Press; 2011.
4. Seddon HJ. Three types of nerve injury. Brain. 1943;66:237–88.
5. Sunderland S. A classification of peripheral nerve injuries producing loss of function. Brain. 1951;74:491–516.
6. Menorca RMG, Fussell TS, Elfar JC. Nerve physiology mechanisms of injury and recovery. Hand Clin. 2013;29:317.
7. Lindsay SL, McCanney GA, Willison AG, Barnett SC. Multi-target approaches to CNS repair: Olfactory mucosa-derived cells and heparan sulfates. Nat Rev Neurol. 2020;16:229–40.
8. Dellon AL, Mackinnon SE, Seiler WA. Susceptibility of the diabetic nerve to chronic compression. Ann Plast Surg. 1988;20:117–9.
9. Nishimura T, Hirata H, Tsujii M, Iida R, Hoki Y, Iino T, et al. Pathomechanism of entrapment neuropathy in diabetic and nondiabetic rats reared in wire cages. Histol Histopathol. 2008;23:157–66.
10. Campbell WW. Evaluation and management of peripheral nerve injury. Clin Neurophysiol. 2008;119:1951–65.
11. He Z, Jin Y. Intrinsic control of axon regeneration. Neuron. 2016;90:437–51.

12. Mahar M, Cavalli V. Intrinsic mechanisms of neuronal axon regeneration. Nat Rev Neurosci. 2018;19:323–37.
13. Kwon BK, Tetzlaff W, Grauer JN, Beiner J, Vaccaro AR. Pathophysiology and pharmacologic treatment of acute spinal cord injury. Spine J. 2004;4:451–64.
14. Norenberg MD, Smith J, Marcillo A. The pathology of human spinal cord injury: Defining the problems. J Neurotrauma. 2004;21:429–40.
15. Oyinbo CA. Secondary injury mechanisms in traumatic spinal cord injury: a nugget of this multiply cascade. Acta Neurobiol Exp. 2011;71:281–99.
16. Wang Y, Tan H, Hui X. Biomaterial scaffolds in regenerative therapy of the central nervous system. Biomed Res Int. 2018;2018:7848901.
17. Gyoneva S, Ransohoff RM. Inflammatory reaction after traumatic brain injury: therapeutic potential of targeting cell-cell communication by chemokines. Trends Pharmacol Sci. 2015;36:471–80.
18. Letko Khait N, Ho E, Shoichet MS. Wielding the double-edged sword of inflammation: building biomaterial-based strategies for immunomodulation in ischemic stroke treatment. Adv Funct Mater. 2021;31.
19. Iadecola C, Anrather J. The immunology of stroke: from mechanisms to translation. Nat Med. 2011;17:796–808.
20. Bradbury EJ, Burnside ER. Moving beyond the glial scar for spinal cord repair. Nat Commun. 2019;10:3879.
21. Mehta A, Prabhakar M, Kumar P, Deshmukh R, Sharma PL. Excitotoxicity: Bridge to various triggers in neurodegenerative disorders. Eur J Pharmacol. 2013;698:6–18.
22. Dunnill C, Patton T, Brennan J, Barrett J, Dryden M, Cooke J, et al. Reactive oxygen species (ROS) and wound healing: The functional role of ROS and emerging ROS-modulating technologies for augmentation of the healing process. Int Wound J. 2017;14:89–96.
23. Li ZM, Wang QX, Hu HJ, Zheng WW, Gao CY. Research advances of biomaterials-based microenvironment-regulation therapies for repair and regeneration of spinal cord injury. Biomed Mater. 2021;16.
24. Liu T, Zhang L, Joo D, Sun S-C. NF-kappa b signaling in inflammation. Signal Transduct Target Ther. 2017;2:17023.
25. Annibaldi A, Meier P. Checkpoints in TNF-induced cell death: implications in inflammation and cancer. Trends Mol Med. 2018;24:49–65.
26. Croft M, Siegel RM. Beyond TNF: TNF superfamily cytokines as targets for the treatment of rheumatic diseases. Nat Rev Rheumatol. 2017;13:217–33.
27. Kalliolias GD, Ivashkiv LB. TNF biology, pathogenic mechanisms and emerging therapeutic strategies. Nat Rev Rheumatol. 2016;12:49–62.
28. Blaser H, Dostert C, Mak TW, Brenner D. TNF and ROS crosstalk in inflammation. Trends Cell Biol. 2016;26:249–61.
29. Wang B, Xiao ZF, Chen B, Han J, Gao Y, Zhang J, et al. Nogo-66 promotes the differentiation of neural progenitors into astroglial lineage cells through mtor-stat3 pathway. PloS One. 2008;3:e1856.
30. Gao Y, Xiao ZF, Chen B, Wang B, Han J, Zhao YN, et al. Effect of different regions of Nogo-A on the differentiation of neural progenitors. Neurosci Lett. 2009;458:132–5.
31. Shen YJ, Tenney AP, Busch SA, Horn KP, Cuascut FX, Liu K, et al. PTP sigma is a receptor for chondroitin sulfate proteoglycan, an inhibitor of neural regeneration. Science. 2009;326:592–6.
32. Fisher D, Xing B, Dill J, Li H, Hoang HH, Zhao ZZ, et al. Leukocyte common antigen-related phosphatase is a functional receptor for chondroitin sulfate proteoglycan axon growth inhibitors. J Neurosci. 2011;31:14051–66.
33. Ohtake Y, Li SX. Molecular mechanisms of scar-sourced axon growth inhibitors. Brain Res. 2015;1619:22–35.
34. Ertuerk A, Hellal F, Enes J, Bradke F. Disorganized microtubules underlie the formation of retraction bulbs and the failure of axonal regeneration. J Neurosci. 2007;27:9169–80.

35. Chen L, Wang Z, Ghosh-Roy A, Hubert T, Yan D, O'Rourke S, et al. Axon regeneration pathways identified by systematic genetic screening in C. elegans. Neuron. 2011;71:1043–57.
36. Rishal I, Fainzilber M. Axon-soma communication in neuronal injury. Nat Rev Neurosci. 2014;15:32–42.
37. Bareyre FM, Kerschensteiner M, Raineteau O, Mettenleiter TC, Weinmann O, Schwab ME. The injured spinal cord spontaneously forms a new intraspinal circuit in adult rats. Nat Neurosci. 2004;7:269–77.
38. Rosenzweig ES, Courtine G, Jindrich DL, Brock JH, Ferguson AR, Strand SC, et al. Extensive spontaneous plasticity of corticospinal projections after primate spinal cord injury. Nat Neurosci. 2010;13:1505–U1590.
39. Plunet W, Kwon BK, Tetzlaff W. Promoting axonal regeneration in the central nervous system by enhancing the cell body response to axotomy. J Neurosci Res. 2002;68:1–6.
40. Nawabi H, Belin S, Cartoni R, Williams PR, Wang C, Latremoliere A, et al. Doublecortin-like kinases promote neuronal survival and induce growth cone reformation via distinct mechanisms. Neuron. 2015;88:704–19.
41. Li R, Liu Z, Pan Y, Chen L, Zhang Z, Lu L. Peripheral nerve injuries treatment: a systematic review. Cell Biochem Biophys. 2014;68:449–54.
42. Lien BV, Brown NJ, Ransom SC, Lehrich BM, Shahrestani S, Tafreshi AR, et al. Enhancing peripheral nerve regeneration with neurotrophic factors and bioengineered scaffolds: a basic science and clinical perspective. J Peripher Nerv Syst. 2020;25:320–34.
43. Vijayavenkataraman S. Nerve guide conduits for peripheral nerve injury repair: a review on design, materials and fabrication methods. Acta Biomater. 2020;106:54–69.
44. Terzis J, Faibisoff B, Williams HB. The nerve gap: suture under tension vs graft. Plast Reconstr Surg. 1975;56:166–70.
45. Jiang X, Lim SH, Mao H-Q, Chew SY. Current applications and future perspectives of artificial nerve conduits. Exp Neurol. 2010;223:86–101.
46. Nichols CM, Brenner MJ, Fox IK, Tung TH, Hunter DA, Rickman SR, et al. Effects of motor versus sensory nerve grafts on peripheral nerve regeneration. Exp Neurol. 2004;190:347–55.
47. Moore AM, Ray WZ, Chenard KE, Tung T, Mackinnon SE. Nerve allotransplantation as it pertains to composite tissue transplantation. Hand. 2009;4:239–44.
48. Ijpma FFA, Graaf VDE, RC, Meek MF. The early history of tubulation in nerve repair. J Hand Surg-Eur. 2008;33:581–6.
49. Neuber GA. Ein antiseptischer dauerverband nach grundlicher blutstillung. Archiv Klinische Chirurgie. 1879;24:314–30.
50. Gluck T. Ueber transplantation, regeneration und entzundliche neubildung. Berliner Klinische Wochenschrif. 1881;18:554–7.
51. Lundborg G, Dahlin LB, Danielsen N, Gelberman RH, Longo FM, Powell HC, et al. Nerve regeneration in silicone chambers: influence of gap length and of distal stump components. Exp Neurol. 1982;76:361–75.
52. Du J, Chen H, Qing L, Yang X, Jia X. Biomimetic neural scaffolds: a crucial step towards optimal peripheral nerve regeneration. Biomater Sci. 2018;6:1299–311.
53. Carvalho CR, Oliveira JM, Reis RL. Modern trends for peripheral nerve repair and regeneration: Beyond the hollow nerve guidance conduit. Front Bioeng Biotechnol. 2019;7:337.
54. Daly W, Yao L, Zeugolis D, Windebank A, Pandit A. A biomaterials approach to peripheral nerve regeneration: bridging the peripheral nerve gap and enhancing functional recovery. J R Soc Interface. 2012;9:202–21.
55. Lundborg G, Gelberman RH, Longo FM, Powell HC, Varon S. In vivo regeneration of cut nerves encased in silicone tubes: growth across a six-millimeter gap. J Neuropathol Exp Neurol. 1982;41:412–22.
56. Lundborg G. A 25-year perspective of peripheral nerve surgery: evolving neuroscientific concepts and clinical significance. J Hand Surg. 2000;25:391–414.
57. Kehoe S, Zhang XF, Boyd D. FDA approved guidance conduits and wraps for peripheral nerve injury: a review of materials and efficacy. Injury. 2012;43:553–72.

58. Disumma PG, Kingham PJ, Campisi CC, Raffoul W, Kalbermatten DF. Collagen (neuragen®) nerve conduits and stem cells for peripheral nerve gap repair. Neurosci Lett. 2014;572:26–31.
59. Shin RH, Friedrich PF, Crum BA, Bishop AT, Shin AY. Treatment of a segmental nerve defect in the rat with use of bioabsorbable synthetic nerve conduits: a comparison of commercially available conduits. JBJS. 2009;91:2194–204.
60. Brushart TM, Mathur V, Sood R, Koschorke G-M. Dispersion of regenerating axons across enclosed neural gaps. J Hand Surg. 1995;20:557–64.
61. Koh HS, Yong T, Teo WE, Chan CK, Puhaindran ME, Tan TC, et al. *In vivo* study of novel nanofibrous intra-luminal guidance channels to promote nerve regeneration. J Neural Eng. 2010;7:046003.
62. Hoffman-Kim D, Mitchel JA, Bellamkonda RV. Topography, cell response, and nerve regeneration. Annu Rev Biomed Eng. 2010;12:203–31.
63. Tessa Hadlock CS, Hunter D, Cheney M, Vacanti JP. A polymer foam conduit seeded with Schwann cells promotes guided peripheral nerve regeneration. Tissue Eng. 2000;6:119–27.
64. Yao L, de Ruiter GCW, Wang H, Knight AM, Spinner RJ, Yaszemski MJ, et al. Controlling dispersion of axonal regeneration using a multichannel collagen nerve conduit. Biomaterials. 2010;31:5789–97.
65. Chiono V, Tonda-Turo C. Trends in the design of nerve guidance channels in peripheral nerve tissue engineering. Prog Neurobiol. 2015;131:87–104.
66. De Ruiter GC, Onyeneho IA, Liang ET, Moore MJ, Knight AM, Malessy MJA, et al. Methods for in vitro characterization of multichannel nerve tubes. J Biomed Mater Res A. 2008;84A:643–51.
67. Wang J, Cheng Y, Wang H, Wang Y, Zhang K, Fan C, et al. Biomimetic and hierarchical nerve conduits from multifunctional nanofibers for guided peripheral nerve regeneration. Acta Biomater. 2020;117:180–91.
68. Bender MD, Bennett JM, Waddell RL, Doctor JS, Marra KG. Multi-channeled biodegradable polymer/cultispher composite nerve guides. Biomaterials. 2004;25:1269–78.
69. Belanger K, Schlatter G, Hébraud A, Marin F, Testelin S, Dakpé S, et al. A multi-layered nerve guidance conduit design adapted to facilitate surgical implantation. Health Sci Rep. 2018;1:e86.
70. Kim YT, Haftel VK, Kumar S, Bellamkonda RV. The role of aligned polymer fiber-based constructs in the bridging of long peripheral nerve gaps. Biomaterials. 2008;29:3117–27.
71. Lundborg G, Dahlin L, Dohi D, Kanje M, Terada N. A new type of "bioartificial" nerve graft for bridging extended defects in nerves. J Hand Surg Am. 1997;22:299–303.
72. Newman KD, McLaughlin CR, Carlsson D, Li F, Liu Y, Griffith M. Bioactive hydrogel-filament scaffolds for nerve repair and regeneration. Int J Artif Organs. 2006;29:1082–91.
73. Huang W, Begum R, Barber T, Ibba V, Tee NCH, Hussain M, et al. Regenerative potential of silk conduits in repair of peripheral nerve injury in adult rats. Biomaterials. 2012;33:59–71.
74. Huang L, Zhu L, Shi X, Xia B, Liu Z, Zhu S, et al. A compound scaffold with uniform longitudinally oriented guidance cues and a porous sheath promotes peripheral nerve regeneration in vivo. Acta Biomater. 2018;68:223–36.
75. Yang S, Zhu J, Lu C, Chai Y, Cao Z, Lu J, et al. Aligned fibrin/functionalized self-assembling peptide interpenetrating nanofiber hydrogel presenting multi-cues promotes peripheral nerve functional recovery. Bioact Mater. 2022;8:529–44.
76. Wu X, He L, Li W, Li H, Wong W-M, Ramakrishna S, et al. Functional self-assembling peptide nanofiber hydrogel for peripheral nerve regeneration. Regener Biomater. 2016;4:21–30.
77. Sun B, Zhou Z, Wu T, Chen W, Li D, Zheng H, et al. Development of nanofiber sponges-containing nerve guidance conduit for peripheral nerve regeneration in vivo. ACS Appl Mater Interfaces. 2017;9:26684–96.
78. McGrath AM, Novikova LN, Novikov LN, Wiberg M. Bd™ puramatrix™ peptide hydrogel seeded with schwann cells for peripheral nerve regeneration. Brain Res Bull. 2010;83:207–13.

79. Deng P, Chen F, Zhang H, Chen Y, Zhou J. Multifunctional double-layer composite hydrogel conduit based on chitosan for peripheral nerve repairing. Adv Healthc Mater. 2022;11: 2200115.
80. Yao Z, Yuan W, Xu J, Tong W, Mi J, Ho P-C, et al. Magnesium-encapsulated injectable hydrogel and 3d-engineered polycaprolactone conduit facilitate peripheral nerve regeneration. Adv Sci. 2022;9:2202102.
81. Ngo TTB, Waggoner PJ, Romero AA, Nelson KD, Eberhart RC, Smith GM. Poly(L-lactide) microfilaments enhance peripheral nerve regeneration across extended nerve lesions. J Neurosci Res. 2003;72:227–38.
82. Lee JY, Giusti G, Friedrich PF, Archibald SJ, Kemnitzer JE, Patel J, et al. The effect of collagen nerve conduits filled with collagen-glycosaminoglycan matrix on peripheral motor nerve regeneration in a rat model. J Bone Joint Surg Am. 2012;94A:2084–91.
83. Shakhbazau A, Archibald SJ, Shcharbin D, Bryszewska M, Midha R. Aligned collagen–gag matrix as a 3d substrate for Schwann cell migration and dendrimer-based gene delivery. J Mater Sci Mater Med. 2014;25:1979–89.
84. Goldner JS, Bruder JM, Li G, Gazzola D, Hoffman-Kim D. Neurite bridging across micropatterned grooves. Biomaterials. 2006;27:460–72.
85. Bozkurt A, Deumens R, Beckmann C, Olde Damink L, Schügner F, Heschel I, et al. In vitro cell alignment obtained with a Schwann cell enriched microstructured nerve guide with longitudinal guidance channels. Biomaterials. 2009;30:169–79.
86. Huang C, Ouyang Y, Niu H, He N, Ke Q, Jin X, et al. Nerve guidance conduits from aligned nanofibers: improvement of nerve regeneration through longitudinal nanogrooves on a fiber surface. ACS Appl Mater Interfaces. 2015;7:7189–96.
87. Zhang D, Li Z, Shi H, Yao Y, Du W, Lu P, et al. Micropatterns and peptide gradient on the inner surface of a guidance conduit synergistically promotes nerve regeneration in vivo. Bioact Mater. 2022;9:134–46.
88. Chung HJ, Park TG. Surface engineered and drug releasing pre-fabricated scaffolds for tissue engineering. Adv Drug Deliv Rev. 2007;59:249–62.
89. Zhang XF, Liu HX, Ortiz LS, Xiao ZD, Huang NP. Laminin-modified and aligned poly (3-hydroxybutyrate-co-3-hydroxyvalerate)/polyethylene oxide nanofibrous nerve conduits promote peripheral nerve regeneration. J Tissue Eng Regen Med. 2018;12:e627–36.
90. De Luca AC, Faroni A, Downes S, Terenghi G. Differentiated adipose-derived stem cells act synergistically with RGD-modified surfaces to improve neurite outgrowth in a co-culture model. J Tissue Eng Regen Med. 2016;10:647–55.
91. Hosseinkhani H, Hiraoka Y, Li C-H, Chen Y-R, Yu D-S, Hong P-D, et al. Engineering three-dimensional collagen-IKVAV matrix to mimic neural microenvironment. ACS Chem Nerosci. 2013;4:1229–35.
92. Lee HS, Jeon EY, Nam JJ, Park JH, Choi IC, Kim SH, et al. Development of a regenerative porous PLCL nerve guidance conduit with swellable hydrogel-based microgrooved surface pattern via 3d printing. Acta Biomater. 2022;141:219–32.
93. Zhang X, Qu W, Li D, Shi K, Li R, Han Y, et al. Functional polymer-based nerve guide conduits to promote peripheral nerve regeneration. Adv Mater Interfaces. 2020;7:2000225.
94. Panagopoulos GN, Megaloikonomos PD, Mavrogenis AF. The present and future for peripheral nerve regeneration. Orthopedics. 2017;40:e141–56.
95. Williams LR, Longo FM, Powell HC, Lundborg G, Varon S. Spatial-temporal progress of peripheral nerve regeneration within a silicone chamber: parameters for a bioassay. J Comp Neurol. 1983;218:460–70.
96. Wang-Bennett LT, Coker NJ. Analysis of axonal regeneration through the silicone regeneration chamber: a retrograde tracing study in the rabbit facial nerve. Exp Neurol. 1990;107:222–9.
97. Luo YX, Wang TP. A clinical application of artery-including silicone tubing to peripheral nerve defect. J Tongji Med Univ. 1992;12:247–9.

98. Ciardelli G, Chiono V. Materials for peripheral nerve regeneration. Macromol Biosci. 2006;6: 13–26.
99. Chen Y-S, Hsieh C-L, Tsai C-C, Chen T-H, Cheng W-C, Hu C-L, et al. Peripheral nerve regeneration using silicone rubber chambers filled with collagen, laminin and fibronectin. Biomaterials. 2000;21:1541–7.
100. Mackinnon SE, Dellon AL. Clinical nerve reconstruction with a bioabsorbable polyglycolic acid tube. Plast Reconstr Surg. 1990;85:419–24.
101. Sarker MD, Naghieh S, McInnes AD, Schreyer DJ, Chen X. Regeneration of peripheral nerves by nerve guidance conduits: influence of design, biopolymers, cells, growth factors, and physical stimuli. Prog Neurobiol. 2018;171:125–50.
102. Lee B-K, Ju YM, Cho J-G, Jackson JD, Lee SJ, Atala A, et al. End-to-side neurorrhaphy using an electrospun PCL/collagen nerve conduit for complex peripheral motor nerve regeneration. Biomaterials. 2012;33:9027–36.
103. Reid AJ, de Luca AC, Faroni A, Downes S, Sun M, Terenghi G, et al. Long term peripheral nerve regeneration using a novel PCL nerve conduit. Neurosci Lett. 2013;544:125–30.
104. Lu M-C, Huang Y-T, Lin J-H, Yao C-H, Lou C-W, Tsai C-C, et al. Evaluation of a multi-layer microbraided polylactic acid fiber-reinforced conduit for peripheral nerve regeneration. J Mater Sci Mater Med. 2009;20:1175–80.
105. Meek MF, Van Der Werff JFA, Nicolai J-PA, Gramsbergen A. Biodegradable P(DLLA-ϵ-CL) nerve guides versus autologous nerve grafts: electromyographic and video analysis. Muscle Nerve. 2001;24:753–9.
106. Xueshen W. Synthesis and properties of biodegradable lactic/glycolic acid polymers. In: Encyclopedic handbook of biomaterials and bioengineering, vol. 2; 1995. p. 1015–54.
107. Young RC, Terenghi G, Wiberg M. Poly-3-hydroxybutyrate (PHB): a resorbable conduit for long-gap repair in peripheral nerves. Br J Plast Surg. 2002;55:235–40.
108. Wang S, Wan ACA, Xu X, Gao S, Mao H-Q, Leong KW, et al. A new nerve guide conduit material composed of a biodegradable poly(phosphoester). Biomaterials. 2001;22:1157–69.
109. Hoppen HJ, Leenslag JW, Pennings AJ, van der Lei B, Robinson PH. Two-ply biodegradable nerve guide: basic aspects of design, construction and biological performance. Biomaterials. 1990;11:286–90.
110. Khaing ZZ, Schmidt CE. Advances in natural biomaterials for nerve tissue repair. Neurosci Lett. 2012;519:103–14.
111. Lohmeyer J, Zimmermann S, Sommer B, Machens HG, Lange T, Mailänder P. Überbrückung peripherer nervendefekte durch den einsatz von nervenröhrchen. Chirurg. 2007;78:142–7.
112. Hvistendahl M. China's push in tissue engineering. Science. 2012;338:900–2.
113. Shimizu M, Matsumine H, Osaki H, Ueta Y, Tsunoda S, Kamei W, et al. Adipose-derived stem cells and the stromal vascular fraction in polyglycolic acid-collagen nerve conduits promote rat facial nerve regeneration. Wound Repair Regen. 2018;26:446–55.
114. Sun B, Zhou Z, Li D, Wu T, Zheng H, Liu J, et al. Polypyrrole-coated poly(l-lactic acid-co-ε-caprolactone)/silk fibroin nanofibrous nerve guidance conduit induced nerve regeneration in rat. Mater Sci Eng C. 2019;94:190–9.
115. Manoukian OS, Baker JT, Rudraiah S, Arul MR, Vella AT, Domb AJ, et al. Functional polymeric nerve guidance conduits and drug delivery strategies for peripheral nerve repair and regeneration. J Control Release. 2020;317:78–95.
116. Nawrotek K, Kubicka M, Gatkowska J, Wieczorek M, Michlewska S, Bekier A, et al. Controlling the spatiotemporal release of nerve growth factor by chitosan/polycaprolactone conduits for use in peripheral nerve regeneration. Int J Mol Sci. 2022;23:2852.
117. Hong MH, Hong HJ, Pang H, Lee H-J, Yi S, Koh W-G. Controlled release of growth factors from multilayered fibrous scaffold for functional recoveries in crushed sciatic nerve. ACS Biomater Sci Eng. 2018;4:576–86.
118. Hoyng SA, De Winter F, Gnavi S, De Boer R, Boon LI, Korvers LM, et al. A comparative morphological, electrophysiological and functional analysis of axon regeneration through

peripheral nerve autografts genetically modified to overexpress BDNF, CNTF, GDNF, NGF, NT3 or VEGF. Exp Neurol. 2014;261:578–93.
119. Kohn-Polster C, Bhatnagar D, Woloszyn DJ, Richtmyer M, Starke A, Springwald AH, et al. Dual-component gelatinous peptide/reactive oligomer formulations as conduit material and luminal filler for peripheral nerve regeneration. Int J Mol Sci. 2017;18:1104.
120. Zhang P-X, Han N, Kou Y-H, Zhu Q-T, Liu X-L, Quan D-P, et al. Tissue engineering for the repair of peripheral nerve injury. Neural Regen Res. 2019;14:51–8.
121. Li Y, Lv S, Yuan H, Ye G, Mu W, Fu Y, et al. Peripheral nerve regeneration with 3d printed bionic scaffolds loading neural crest stem cell derived Schwann cell progenitors. Adv Funct Mater. 2021;31:2010215.
122. Qing L, Chen H, Tang J, Jia X. Exosomes and their microrna cargo: new players in peripheral nerve regeneration. Neurorehabil Neural Repair. 2018;32:765–76.
123. Zhang B, Wu X, Zhang X, Sun Y, Yan Y, Shi H, et al. Human umbilical cord mesenchymal stem cell exosomes enhance angiogenesis through the wnt4/β-catenin pathway. Stem Cells Transl Med. 2015;4:513–22.
124. Pegtel DM, Peferoen L, Amor S. Extracellular vesicles as modulators of cell-to-cell communication in the healthy and diseased brain. Philos Trans R Soc Lond B Biol Sci. 2014;369:20130516.
125. Ikeguchi R, Aoyama T, Tanaka M, Noguchi T, Ando M, Yoshimoto K, et al. Nerve regeneration using the bio 3D nerve conduit fabricated with spheroids. J Artif Organs. 2022;25:289. https://doi.org/10.1007/s10047-022-01358-9.
126. DiSabato DJ, Quan N, Godbout JP. Neuroinflammation: the devil is in the details. J Neurochem. 2016;139:136–53.
127. Cornelison C, Fadel S. Clickable biomaterials for modulating neuroinflammation. Int J Mol Sci. 2022;23:8496.
128. Dellacherie MO, Seo BR, Mooney DJ. Macroscale biomaterials strategies for local immunomodulation. Nat Rev Mater. 2019;4:379–97.
129. Chun J, Giovannoni G, Hunter SF. Sphingosine 1-phosphate receptor modulator therapy for multiple sclerosis: differential downstream receptor signalling and clinical profile effects. Drugs. 2021;81:207–31.
130. Jeong DU, Bae S, Macks C, Whitaker J, Lynn M, Webb K, et al. Hydrogel-mediated local delivery of dexamethasone reduces neuroinflammation after traumatic brain injury. Biomed Mater. 2021;16:035002.
131. Papa S, Veneruso V, Mauri E, Cremonesi G, Mingaj X, Mariani A, et al. Functionalized nanogel for treating activated astrocytes in spinal cord injury. J Control Release. 2021;330:218–28.
132. Wang X-J, Shu G-F, Xu X-L, Peng C-H, Lu C-Y, Cheng X-Y, et al. Combinational protective therapy for spinal cord injury medicated by sialic acid-driven and polyethylene glycol based micelles. Biomaterials. 2019;217:119326.
133. Wang C, Gong Z, Huang X, Wang J, Xia K, Ying L, et al. An injectable heparin-laponite hydrogel bridge fgf4 for spinal cord injury by stabilizing microtubule and improving mitochondrial function. Theranostics. 2019;9:7016–32.
134. Ganbold T, Bao Q, Zandan J, Hasi A, Baigude H. Modulation of microglia polarization through silencing of NF-KB p65 by functionalized curdlan nanoparticle-mediated RNAi. ACS Appl Mater Interfaces. 2020;12:11363–74.
135. Wang H, Wu Y, Han W, Li J, Xu K, Li Z, et al. Hydrogen sulfide ameliorates blood-spinal cord barrier disruption and improves functional recovery by inhibiting endoplasmic reticulum stress-dependent autophagy. Front Pharmacol. 2018;9:858.
136. Kamat PK, Kyles P, Kalani A, Tyagi N. Hydrogen sulfide ameliorates homocysteine-induced Alzheimer's disease-like pathology, blood–brain barrier disruption, and synaptic disorder. Mol Neurobiol. 2016;53:2451–67.

137. Campolo M, Esposito E, Ahmad A, Di Paola R, Wallace JL, Cuzzocrea S. A hydrogen sulfide-releasing cyclooxygenase inhibitor markedly accelerates recovery from experimental spinal cord injury. FASEB J. 2013;27:4489–99.
138. Wu J, Chen A, Zhou Y, Zheng S, Yang Y, An Y, et al. Novel H_2S-releasing hydrogel for wound repair via in situ polarization of M2 macrophages. Biomaterials. 2019;222:119398.
139. Wang S, Liu K, Zhou Q, Xu C, Gao J, Wang Z, et al. Hydrogen-powered microswimmers for precise and active hydrogen therapy towards acute ischemic stroke. Adv Funct Mater. 2021;31:2009475.
140. Jiang Y, Fu P, Liu Y, Wang C, Zhao P, Chu X, et al. Near-infrared light-triggered no release for spinal cord injury repair. Sci Adv. 2020;6:e3513.
141. Teng YD, Choi H, Onario RC, Zhu S, Desilets FC, Lan S, et al. Minocycline inhibits contusion-triggered mitochondrial cytochrome c release and mitigates functional deficits after spinal cord injury. Proc Natl Acad Sci U S A. 2004;101:3071–6.
142. McManus MT, Sharp PA. Gene silencing in mammals by small interfering RNAs. Nat Rev Genet. 2002;3:737–47.
143. Dorsett Y, Tuschl T. SiRNAs: Applications in functional genomics and potential as therapeutics. Nat Rev Drug Discov. 2004;3:318–29.
144. Wang W, Huang X, Zhang Y, Deng G, Liu X, Fan C, et al. $Se@SiO_2$ nanocomposites suppress microglia-mediated reactive oxygen species during spinal cord injury in rats. RSC Adv. 2018;8:16126–38.
145. Yoo D, Magsam AW, Kelly AM, Stayton PS, Kievit FM, Convertine AJ. Core-cross-linked nanoparticles reduce neuroinflammation and improve outcome in a mouse model of traumatic brain injury. ACS Nano. 2017;11:8600–11.
146. Tarudji AW, Gee CC, Romereim SM, Convertine AJ, Kievit FM. Antioxidant thioether core-crosslinked nanoparticles prevent the bilateral spread of secondary injury to protect spatial learning and memory in a controlled cortical impact mouse model of traumatic brain injury. Biomaterials. 2021;272:120766.
147. Xu J, Ypma M, Chiarelli PA, Park J, Ellenbogen RG, Stayton PS, et al. Theranostic oxygen reactive polymers for treatment of traumatic brain injury. Adv Funct Mater. 2016;26:4124–33.
148. Qian F, Han Y, Han Z, Zhang D, Zhang L, Zhao G, et al. In situ implantable, post-trauma microenvironment-responsive, ROS depletion hydrogels for the treatment of traumatic brain injury. Biomaterials. 2021;270:120675.
149. Huang X, Ye Y, Zhang J, Zhang X, Ma H, Zhang Y, et al. Reactive oxygen species scavenging functional hydrogel delivers procyanidins for the treatment of traumatic brain injury in mice. ACS Appl Mater Interfaces. 2022;14:33756–67.
150. Zhang Y, Li L, Mu J, Chen J, Feng S, Gao J. Implantation of a functional tempo-hydrogel induces recovery from rat spinal cord transection through promoting nerve regeneration and protecting bladder tissue. Biomater Sci. 2020;8:1695–701.
151. Li Z, Zhao T, Ding J, Gu H, Wang Q, Wang Y, et al. A reactive oxygen species-responsive hydrogel encapsulated with bone marrow derived stem cells promotes repair and regeneration of spinal cord injury. Bioact Mater. 2023;19:550–68.
152. Jiang XC, Xiang JJ, Wu HH, Zhang TY, Zhang DP, Xu QH, et al. Neural stem cells transfected with reactive oxygen species–responsive polyplexes for effective treatment of ischemic stroke. Adv Mater. 2019;31:1807591–8.
153. Andrabi SS, Yang J, Gao Y, Kuang Y, Labhasetwar V. Nanoparticles with antioxidant enzymes protect injured spinal cord from neuronal cell apoptosis by attenuating mitochondrial dysfunction. J Control Release. 2020;317:300–11.
154. Zhang S, Liu Y, Sun S, Wang J, Li Q, Yan R, et al. Catalytic patch with redox Cr/CeO2 nanozyme of noninvasive intervention for brain trauma. Theranostics. 2021;11:2806–21.
155. Kim J-W, Mahapatra C, Hong J-Y, Kim MS, Leong KW, Kim H-W, et al. Functional recovery of contused spinal cord in rat with the injection of optimal-dosed cerium oxide nanoparticles. Adv Sci. 2017;4:1700034.

156. Zhang K, Tu M, Gao W, Cai X, Song F, Chen Z, et al. Hollow prussian blue nanozymes drive neuroprotection against ischemic stroke via attenuating oxidative stress, counteracting inflammation, and suppressing cell apoptosis. Nano Lett. 2019;19:2812–23.
157. Li L, Xiao B, Mu J, Zhang Y, Zhang C, Cao H, et al. A MnO_2 nanoparticle-dotted hydrogel promotes spinal cord repair via regulating reactive oxygen species microenvironment and synergizing with mesenchymal stem cells. ACS Nano. 2019;13:14283–93.
158. Singh N, Savanur MA, Srivastava S, D'Silva P, Mugesh G. A redox modulatory Mn_3O_4 nanozyme with multi-enzyme activity provides efficient cytoprotection to human cells in a Parkinson's disease model. Angew Chem Int Ed. 2017;56:14267–71.
159. Pal A, Singh A, Nag TC, Chattopadhyay P, Mathur R, Jain S. Iron oxide nanoparticles and magnetic field exposure promote functional recovery by attenuating free radical-induced damage in rats with spinal cord transection. Int J Nanomedicine. 2013;8:2259–72.
160. Luo W, Wang Y, Lin F, Liu Y, Gu R, Liu W, et al. Y selenium-doped carbon quantum dots efficiently ameliorate secondary spinal cord injury via scavenging reactive oxygen species. Int J Nanomedicine. 2020;15:10113–25.
161. Mu X, He H, Wang J, Long W, Li Q, Liu H, et al. Carbogenic nanozyme with ultrahigh reactive nitrogen species selectivity for traumatic brain injury. Nano Lett. 2019;19:4527–34.
162. Luo W, Zhang L, Li X, Zheng J, Chen Q, Yang Z, et al. Green functional carbon dots derived from herbal medicine ameliorate blood-brain barrier permeability following traumatic brain injury. Nano Res. 2022;15:9274–85.
163. Li S, Jiang D, Ehlerding EB, Rosenkrans ZT, Engle JW, Wang Y, et al. Intrathecal administration of nanoclusters for protecting neurons against oxidative stress in cerebral ischemia/reperfusion injury. ACS Nano. 2019;13:13382–9.
164. Yao Y, Zhang H, Wang Z, Ding J, Wang S, Huang B, et al. Reactive oxygen species (ROS)-responsive biomaterials mediate tissue microenvironments and tissue regeneration. J Mater Chem B. 2019;7:5019–37.
165. Wei H, Wang E. Nanomaterials with enzyme-like characteristics (nanozymes): next-generation artificial enzymes. Chem Soc Rev. 2013;42:6060–93.
166. Wu J, Wang X, Wang Q, Lou Z, Li S, Zhu Y, et al. Nanomaterials with enzyme-like characteristics (nanozymes): next-generation artificial enzymes (II). Chem Soc Rev. 2019;48:1004–76.
167. Khaing ZZ, Milman BD, Vanscoy JE, Seidlits SK, Grill RJ, Schmidt CE. High molecular weight hyaluronic acid limits astrocyte activation and scar formation after spinal cord injury. J Neural Eng. 2011;8:046033.
168. Austin JW, Gilchrist C, Fehlings MG. High molecular weight hyaluronan reduces lipopolysaccharide mediated microglial activation. J Neurochem. 2012;122:344–55.
169. Hao P, Duan H, Hao F, Chen L, Sun M, Fan KS, et al. Neural repair by NT3-chitosan via enhancement of endogenous neurogenesis after adult focal aspiration brain injury. Biomaterials. 2017;140:88–102.
170. Islam A, Tom VJ. The use of viral vectors to promote repair after spinal cord injury. Exp Neurol. 2022;354:114102.
171. Bradbury EJ, Moon LDF, Popat RJ, King VR, Bennett GS, Patel PN, et al. Chondroitinase ABC promotes functional recovery after spinal cord injury. Nature. 2002;416:636–40.
172. Hettiaratchi MH, O'Meara MJ, Teal CJ, Payne SL, Pickering AJ, Shoichet MS. Local delivery of stabilized chondroitinase ABC degrades chondroitin sulfate proteoglycans in stroke-injured rat brains. J Control Release. 2019;297:14–25.
173. Harris NG, Nogueira MSM, Verley DR, Sutton RL. Chondroitinase enhances cortical map plasticity and increases functionally active sprouting axons after brain injury. J Neurotrauma. 2013;30:1257–69.
174. Raspa A, Carminati L, Pugliese R, Fontana F, Gelain F. Self-assembling peptide hydrogels for the stabilization and sustained release of active Chondroitinase ABC in vitro and in spinal cord injuries. J Control Release. 2021;330:1208–19.

175. Khalil AS, Hellenbrand D, Reichl K, Umhoefer J, Filipp M, Choe J, et al. A localized materials-based strategy to non-virally deliver chondroitinase ABC mRNA improves hindlimb function in a rat spinal cord injury model. Adv Healthc Mater. 2022;11:2200206.
176. Baldwin KT, Giger RJ. Insights into the physiological role of CNS regeneration inhibitors. Front Mol Neurosci. 2015;8:23.
177. Lang BT, Cregg JM, DePaul MA, Tran AP, Xu K, Dyck SM, et al. Modulation of the proteoglycan receptor PTP sigma promotes recovery after spinal cord injury. Nature. 2015;518:404–8.
178. Barr AJ, Ugochukwu E, Lee WH, King ONF, Filippakopoulos P, Alfano I, et al. Large-scale structural analysis of the classical human protein tyrosine phosphatome. Cell. 2009;136:352–63.
179. Luo FC, Wang JP, Zhang Z, You Z, Bedolla A, Okwubido-Williams F, et al. Inhibition of CSPG receptor PTPs promotes migration of newly born neuroblasts, axonal sprouting, and recovery from stroke. Cell Rep. 2022;40:111137.
180. Hosseini SM, Alizadeh A, Shahsavani N, Chopek J, Ahlfors JE, Karimi-Abdolrezaee S. Suppressing CSPG/LAR/PTPa axis facilitates neuronal replacement and synaptogenesis by human neural precursor grafts and improves recovery after spinal cord injury. J Neurosci. 2022;42:3096–121.
181. Rocco ML, Soligo M, Manni L, Aloe L. Nerve growth factor: early studies and recent clinical trials. Curr Neuropharmacol. 2018;16:1455–65.
182. Aloe L, Rocco ML, Bianchi P, Manni L. Nerve growth factor: from the early discoveries to the potential clinical use. J Transl Med. 2012;10:239.
183. Song XL, Xu Y, Wu JM, Shao HX, Gao JF, Feng XJ, et al. A sandwich structured drug delivery composite membrane for improved recovery after spinal cord injury under longtime controlled release. Colloid Surface B. 2021;199:111529.
184. Gao X, Cheng WN, Zhang XY, Zhou ZY, Ding ZZ, Zhou XZ, et al. Nerve growth factor-laden anisotropic silk nanofiber hydrogels to regulate neuronal/astroglial differentiation for scarless spinal cord repair. ACS Appl Mater Interfaces. 2022;14:3701–15.
185. Sims SK, Wilken-Resman B, Smith CJ, Mitchell A, McGonegal L, Sims-Robinson C. Brain-derived neurotrophic factor and nerve growth factor therapeutics for brain injury: the current translational challenges in preclinical and clinical research. Neural Plast. 2022;2022:3889300.
186. Fletcher JL, Murray SS, Xiao J. Brain-derived neurotrophic factor in central nervous system myelination: a new mechanism to promote myelin plasticity and repair. Int J Mol Sci. 2018;19:4131.
187. Cook DJ, Nguyen C, Chun HN, Llorente IL, Chiu AS, Machnicki M, et al. Hydrogel-delivered brain-derived neurotrophic factor promotes tissue repair and recovery after stroke. J Cereb Blood Flow Metab. 2017;37:1030–45.
188. Obermeyer JM, Tuladhar A, Payne SL, Ho E, Morshead CM, Shoichet MS. Local delivery of brain-derived neurotrophic factor enables behavioral recovery and tissue repair in stroke-injured rats. Tissue Eng Part A. 2019;25:1175–87.
189. Liu XY, Chen C, Xu HH, Zhang YS, Zhong L, Hu N, et al. Integrated printed BDNF/collagen/chitosan scaffolds with low temperature extrusion 3D printer accelerated neural regeneration after spinal cord injury. Regen Biomater. 2021;8:rbab047.
190. He Z, Zang H, Zhu L, Huang K, Yi T, Zhang S, et al. An anti-inflammatory peptide and brain-derived neurotrophic factor-modified hyaluronan-methylcellulose hydrogel promotes nerve regeneration in rats with spinal cord injury. Int J Nanomedicine. 2019;14:721–32.
191. Harris NM, Ritzel R, Mancini NS, Jiang Y, Yi X, Manickam DS, et al. Nano-particle delivery of brain derived neurotrophic factor after focal cerebral ischemia reduces tissue injury and enhances behavioral recovery. Pharmacol Biochem Behav. 2016;150-151:48–56.
192. Nih LR, Gojgini S, Carmichael ST, Segura T. Dual-function injectable angiogenic biomaterial for the repair of brain tissue following stroke. Nat Mater. 2018;17:642–51.

193. Goto T, Ueha R, Sato T, Fujimaki Y, Nito T, Yamasoba T. Single, high-dose local injection of bFGF improves thyroarytenoid muscle atrophy after paralysis. Laryngoscope. 2020;130:159–65.
194. Li Y, Yang LL, Hu F, Xu J, Ye JS, Liu SH, et al. Novel thermosensitive hydrogel promotes spinal cord repair by regulating mitochondrial function. ACS Appl Mater Interfaces. 2022;14:25155–72.
195. Horner PJ, Gage FH. Regenerating the damaged central nervous system. Nature. 2000;407:963–70.
196. Tetzlaff W, Okon EB, Karimi-Abdolrezaee S, Hill CE, Sparling JS, Plemel JR, et al. A systematic review of cellular transplantation therapies for spinal cord injury. J Neurotrauma. 2011;28:1611–82.
197. Assinck P, Duncan GJ, Hilton BJ, Plemel JR, Tetzlaff W. Cell transplantation therapy for spinal cord injury. Nat Neurosci. 2017;20:637–47.
198. Piltti KM, Salazar DL, Uchida N, Cummings BJ, Anderson AJ. Safety of epicenter versus intact parenchyma as a transplantation site for human neural stem cells for spinal cord injury therapy. Stem Cells Transl Med. 2013;2:204–16.
199. Nauta AJ, Westerhuis G, Kruisselbrink AB, Lurvink EGA, Willemze R, Fibbe WE. Donor-derived mesenchymal stem cells are immunogenic in an allogeneic host and stimulate donor graft rejection in a nonmyeloablative setting. Blood. 2006;108:2114–20.
200. Lam J, Lowry WE, Carmichael ST, Segura T. Delivery of iPS-NPCs to the stroke cavity within a hyaluronic acid matrix promotes the differentiation of transplanted cells. Adv Funct Mater. 2014;24:7053–62.
201. Liu C, Fan L, Xing J, Wang Q, Lin C, Liu C, et al. Inhibition of astrocytic differentiation of transplanted neural stem cells by chondroitin sulfate methacrylate hydrogels for the repair of injured spinal cord. Biomater Sci. 2019;7:1995–2008.
202. Betancur MI, Mason HD, Alvarado-Velez M, Holmes PV, Bellamkonda RV, Karumbaiah L. Chondroitin sulfate glycosaminoglycan matrices promote neural stem cell maintenance and neuroprotection post-traumatic brain injury. ACS Biomater Sci Eng. 2017;3:420–30.
203. McCrary MR, Jesson K, Wei ZZ, Logun M, Lenear C, Tan S, et al. Cortical transplantation of brain-mimetic glycosaminoglycan scaffolds and neural progenitor cells promotes vascular regeneration and functional recovery after ischemic stroke in mice. Adv Healthc Mater. 2020;9:1900285.
204. Fan L, Liu C, Chen X, Zou Y, Zhou Z, Lin C, et al. Directing induced pluripotent stem cell derived neural stem cell fate with a three-dimensional biomimetic hydrogel for spinal cord injury repair. ACS Appl Mater Interfaces. 2018;10:17742–55.
205. Li J, Zhang D, Guo S, Zhao C, Wang L, Ma S, et al. Dual-enzymatically cross-linked gelatin hydrogel promotes neural differentiation and neurotrophin secretion of bone marrow-derived mesenchymal stem cells for treatment of moderate traumatic brain injury. Int J Biol Macromol. 2021;187:200–13.
206. Ma S, Zhou J, Huang T, Zhang Z, Xing Q, Zhou X, et al. Sodium alginate/collagen/stromal cell-derived factor-1 neural scaffold loaded with BMSCs promotes neurological function recovery after traumatic brain injury. Acta Biomater. 2021;131:185–97.
207. Malinovskaya Y, Melnikov P, Baklaushev V, Gabashvili A, Osipova N, Mantrov S, et al. Delivery of doxorubicin-loaded PLGA nanoparticles into U87 human glioblastoma cells. Int J Pharm. 2017;542:77–90.
208. Lampe KJ, Mooney RG, Bjugstad KB, Mahoney MJ. Effect of macromer weight percent on neural cell growth in 2D and 3D nondegradable PEG hydrogel culture. J Biomed Mater Res Part A. 2010;94A:1162–71.
209. Zhang S, Burda JE, Anderson MA, Zhao Z, Ao Y, Cheng Y, et al. Thermoresponsive copolypeptide hydrogel vehicles for central nervous system cell delivery. ACS Biomater Sci Eng. 2015;1:705–17.
210. Zhu Y, Sun L, Fu X, Liu J, Liang Z, Tan H, et al. Engineering microcapsules to construct vascularized human brain organoids. Chem Eng J. 2021;424:130427.

211. Das M, Mayilsamy K, Mohapatra SS, Mohapatra S. Mesenchymal stem cell therapy for the treatment of traumatic brain injury: progress and prospects. Rev Neurosci. 2019;30:839–55.
212. Xia Y, Hu G, Chen Y, Yuan J, Zhang J, Wang S, et al. Embryonic stem cell derived small extracellular vesicles modulate regulatory t cells to protect against ischemic stroke. ACS Nano. 2021;15:7370–85.
213. Wang C, Wang M, Xia K, Wang J, Cheng F, Shi K, et al. A bioactive injectable self-healing anti-inflammatory hydrogel with ultralong extracellular vesicles release synergistically enhances motor functional recovery of spinal cord injury. Bioact Mater. 2021;6:2523–34.
214. Sabelstrom H, Stenudd M, Reu P, Dias DO, Elfineh M, Zdunek S, et al. Resident neural stem cells restrict tissue damage and neuronal loss after spinal cord injury in mice. Science. 2013;342:637–40.
215. Horky LL, Galimi F, Gage FH, Horner PJ. Fate of endogenous stem/progenitor cells following spinal cord injury. J Comp Neurol. 2006;498:525–38.
216. Fawcett JW. Overcoming inhibition in the damaged spinal cord. J Neurotrauma. 2006;23:371–83.
217. Hill CE, Beattie MS, Bresnahan JC. Degeneration and sprouting of identified descending supraspinal axons after contusive spinal cord injury in the rat. Exp Neurol. 2001;171:153–69.
218. Gregoire C-A, Goldenstein BL, Floriddia EM, Barnabe-Heider F, Fernandes KJL. Endogenous neural stem cell responses to stroke and spinal cord injury. Glia. 2015;63:1469–82.
219. Sun GJ, Zhou Y, Stadel RP, Moss J, Yong JHA, Ito S, et al. Tangential migration of neuronal precursors of glutamatergic neurons in the adult mammalian brain. Proc Natl Acad Sci. 2015;112:9484–9.
220. Kojima T, Hirota Y, Ema M, Takahashi S, Miyoshi I, Okano H, et al. Subventricular zone-derived neural progenitor cells migrate along a blood vessel scaffold toward the post-stroke striatum. Stem Cells. 2010;28:545–54.
221. Jian W-H, Wang H-C, Kuan C-H, Chen M-H, Wu H-C, Sun J-S, et al. Glycosaminoglycan-based hybrid hydrogel encapsulated with polyelectrolyte complex nanoparticles for endogenous stem cell regulation in central nervous system regeneration. Biomaterials. 2018;174:17–30.
222. Addington CP, Heffernan JM, Millar-Haskell CS, Tucker EW, Sirianni RW, Stabenfeldt SE. Enhancing neural stem cell response to SDF-1α gradients through hyaluronic acid-laminin hydrogels. Biomaterials. 2015;72:11–9.
223. Chai Y, Zhao H, Yang S, Gao X, Cao Z, Lu J, et al. Structural alignment guides oriented migration and differentiation of endogenous neural stem cells for neurogenesis in brain injury treatment. Biomaterials. 2022;280:121310.
224. Nih LR, Sideris E, Carmichael ST, Segura T. Injection of microporous annealing particle (MAP) hydrogels in the stroke cavity reduces gliosis and inflammation and promotes NPC migration to the lesion. Adv Mater. 2017;29:1606471.
225. Darling NJ, Sideris E, Hamada N, Carmichael ST, Segura T. Injectable and spatially patterned microporous annealed particle (MAP) hydrogels for tissue repair applications. Adv Sci. 2018;5:1801046.
226. Kawauchi T, Sekine K, Shikanai M, Chihama K, Tomita K, Kubo KI, et al. Rab GTPases-dependent endocytic pathways regulate neuronal migration and maturation through N-cadherin trafficking. Neuron. 2010;67:588–602.